Hiroshi G. Okuno
Moonis Ali (Eds.)

LNAI 4570

New Trends in Applied Artificial Intelligence

20th International Conference on
Industrial, Engineering and Other Applications of
Applied Intelligent Systems, IEA/AIE 2007
Kyoto, Japan, June 2007, Proceedings

Springer

Lecture Notes in Artificial Intelligence 4570

Edited by J. G. Carbonell and J. Siekmann

Subseries of Lecture Notes in Computer Science

Hiroshi G. Okuno Moonis Ali (Eds.)

New Trends in Applied Artificial Intelligence

20th International Conference on
Industrial, Engineering, and Other Applications of
Applied Intelligent Systems, IEA/AIE 2007
Kyoto, Japan, June 26-29, 2007
Proceedings

Springer

Series Editors

Jaime G. Carbonell, Carnegie Mellon University, Pittsburgh, PA, USA
Jörg Siekmann, University of Saarland, Saarbrücken, Germany

Volume Editors

Hiroshi G. Okuno
Kyoto University
Graduate School of Informatics
Yoshida-Hommachi, Sakyo, Kyoto 606-8501, Japan
E-mail: okuno@i.kyoto-u.ac.jp

Moonis Ali
Texas State University – San Marcos
Department of Computer Science
Nueces 247, 601 University Drive, San Marcos, TX 78666-4616, USA
E-mail: ma04@txstate.edu

Library of Congress Control Number: Applied for

CR Subject Classification (1998): I.2, F.1, F.2, I.5, F.4.1, D.2, H.4, H.2.8, H.5.2

LNCS Sublibrary: SL 7 – Artificial Intelligence

ISSN 0302-9743
ISBN-10 3-540-73322-1 Springer Berlin Heidelberg New York
ISBN-13 978-3-540-73322-5 Springer Berlin Heidelberg New York

Typesetting: Camera-ready by author, data conversion by Scientific Publishing Services, Chennai, India
Printed on acid-free paper SPIN: 12082827 06/3180 5 4 3 2 1 0

Preface

Albert Einstein

Applied artificial intelligence researchers have been focusing on developing and employing methods and systems to solve real-life problems in all areas including engineering, science, industry, automation & robotics, business & finance, cyberspace, and man–machine interactions. The 20^{th} International Conference on Industrial, Engineering and Other Applications of Applied Intelligent Systems (IEA/AIE-2007) held in Kyoto, Japan presented such work performed by many scientists worldwide.

The previous IEA/AIE conference held in Japan was the Ninth International Conference on Industrial and Engineering Applications of Artificial Intelligence and Expert systems (IEA/AIE-1996) in Fukuoka in 1996. The duration of 11 years between two conferences demanded drastic changes around applied artificial intelligence research. The main causes are the rapid expansion of the Internet and the deluge of electronic and on-line text data. The Program Committee focused on Asian-originating technologies, such as active mining, integration of the Internet and broadcasting, chance discovery, real-world interactions, and fuzzy logic applications. The first four are from Japan and the last one is from Taiwan and China.

We received 462 papers from all parts of the world. Each paper was sent to at least three Program Committee members for review. Only 116 papers were selected for presentation and publication in the proceedings. We would like to express our sincere thanks to the Program Committee and all the reviewers for their hard work.

The papers in the proceedings cover the following topics: application systems, agent-based system chance discovery and social network, constraint satisfaction, data mining, e-commerce, education, fuzzy logic, fuzzy system applications, heuristic search genetic algorithm machine learning manufacturing, neural network, real-world interaction, robot, speech, text processing, vision, and other applications.

The set of selected papers presented at IEA/AIE-2007, sponsored by the International Society of Applied Intelligence (ISAI) and the Graduate School of Informatics, Kyoto University, is offered in this volume. These papers highlight new trends of applied artificial intelligence and show how new research could lead to new and innovative applications. We hope that you find these papers to be educational, useful in your own research, and stimulating.

In addition to the ISAI and Graduate School of Informatics, Kyoto University, the main sponsors of the conference, our special thanks are due to the Association for the Advancement of Artificial Intelligence (AAAI, former American

Association for Artificial Intelligence), the Association for Computing Machinery (ACM/SIGART), the Canadian Society for the Computational Studies of Intelligence (CSCSI/SCEIO), the European Neural Network Society (ENNS), the Human Interface Society (HIS), the Institute of Electronics, Information and Communication Engineers (IEICE), the International Neural Network Society (INNS), the Information Processing Society of Japan (IPSJ), the Japanese Society for Artificial Intelligence (JSAI), the Robotics Society of Japan (RSJ), the Taiwanese Association for Artificial Intelligence (TAAI), and Texas State University San Marcos.

We wish to thank the members of the Program Committee, especially those who played specific roles: Kazunori Komatani (Publicity Chair), Tokyoaki Nishida (Program Co-chair), Yukio Osama (Program Co-chair), Shyi-Ming Chen and Takayuki Ito (Special Session Organizers), and Tetsuya Ogata (Local Organization Chair).

We would like to thank Secreatari@t Inc. and Miki Nishii for their efficiency in dealing with the registration and management issues. We would also like to thank the Artificial Intelligence Research Promotion Foundation and the Support Center for Advanced Telecommunications Technology Research, Foundations, Google Japan Inc., Honda Research Institute Japan Co., Ltd., and TOME R&D Inc. for their financial support for IEA/AIE-2007. There are many other participants, as well as all the authors, who were critically important in the organization of this conference. The conference would not have been possible without their valuable support.

April 2007

Hiroshi G. Okuno
Moonis Ali

Organization

The IEA/AIE-2007 was organized by the International Society of Applied Intelligence and the Graduate School of Informatics, Kyoto University in cooperation with AAAI, ACM/SIGART, CSCSI/SCEIO, ENNS, HIS, IEICE, INNS, IPSJ, JSAI, RSJ, TAAI, and Texas State University San Marcos.

Chairs

General Chair	Moonis Ali (Texas State University San Marcos, USA)
Program Chair	Hiroshi G. Okuno (Kyoto University, Japan)
Program Co-chairs	Toyoaki Nishida (Kyoto University, Japan)
	Yukio Osawa (The University of Tokyo, Japan)
Publicity Chair	Kazunori Komatani (Kyoto University, Japan)
Local Organization Chair	Tetsuya Ogata (Kyoto University, Japan)

Program Committee

Akutsu, Tatsuya, Japan
Auberge, Veronique, France
Bannister, Peter R., UK
Belli, Fevzi, Germany
Borzemski, Leszek, Poland
Brezillon, Patrick, France
Burke, Edmund K, UK
Chan, C. W., Hong Kong
Chen, Shyi-Ming, Taiwan
Chien, Been-Chian, Taiwan
Chung, Paul, UK
Clifton, David, UK
Correa da Silva, Flavio Soares, Brazil
Dapoigny, Richard, France
Desimone, Roberto, Australia
Dimitriadis, A. Yannis, Spain
Duan, Hai-Bin, China
Esposito, Floriana, Italy
Galichet, Sylvie, France
Guesgen, Hans Werner, New Zealand
Harandi, Mehdi T., USA
Hattori, Hiromitsu, USA
Hendtlass, Tim, Australia
Horvath, Gabor, Hungary
Huget, Marc-Philippe, France
Iida, Fumiya, Switzerland
Ishizuka, Mitsuru, Japan
Ito, Takayuki, Japan
Jacquenet, Francois, France
Jain, Lakhmi, Australia
Jo, Geun Sik, Korea
Kabanza, Froduald, Canada
Kaikhah, Khosrow, USA
Kaneda, Shigeo, Japan
Kim, Jin Hyung, Korea
Kinoshita, Tetsuo, Japan
Krol, Dariusz, Poland
Kumar, Amruth, USA
Kerschberg, Larry, USA
Laurent, Foulloy, France
Lee, Chang-Hwan, Korea
Lee, Chang-Shing, Taiwan
Lee, Huey-Ming, Taiwan
Lee, Seungkeun, France
Liu, Ying, Singapore
Madani, Kurosh, France

Maki, Atsuto, Japan
Matsuo, Tokuro, Japan
Matthews, Manton M., USA
Minato, Shin-ichi, Japan
Mira, Jose, Spain
Monostori, Laszlo, Hungary
Mori, Tatsunori, Japan
Munoz-Avila, Hector, USA
Murphey, Yi Lu, USA
Nakano, Mikio, Japan
Neumann, Bernd, Germany
Nguyen, Ngoc Thanh, Poland
Onoda, Takashi, Japan
Orchard, Robert, Canada
Pellegrini, Christian, Switzerland
Potter, Walter Don, USA
Ramaswamy, Srini, USA
Randall, Marcus Christian, Australia
Rayward-Smith, Victor J., UK
Roche, Christophe, France
Saitta, Lorenza, Italy
Sanchez-Marre, Miquel, Spain
Shimazu, Akira, Japan
Shpitalni, Moshe, IL
Suzuki, Kazuhiko, Japan
Tanaka, Takushi, Japan
Treur, Jan, The Netherlands
Uehara, Kuniaki, Japan
Vadera, Sunil, UK
Valtorta, Marco, USA
Vancza, Jozsef, Hungary
Wang, Xue Z., UK
Washio, Takashi, Japan
Watanabe, Toyohide, Japan
Williams, Graham, Australia
Wittig, Thies, Germany
Yang, Chunsheng, Canada
Yang, Yubin, Australia
Yannis, Karnavas L., Greece
Zaiping, Chen, China

Additonal Reviewers

Asakura, Koichi, Japan
Asano, Futoshi, Japan
Aydin, Kemal, USA
Bai, Ruibin, UK
Biba, Marenglen, Italy
Blachuta, Marian, Poland
Blanco, Ángela, Spain
Bosse, Tibor, The Netherlands
Boukezzoula, Reda, France
Castiello, Ciro, Italy
Cuong, Le Anh, Japan
d'Amato, Claudia, Italy
Egri, Peter, Hungary
Elsalloukh, Hassan, USA
Fanizzi, Nicola, Italy
Ferilli, Stefano, Italy
Fuente, M.J., Spain
Fukumoto, Junichi, Japan
Habe, Hitoshi, Japan
Hanaue, Kouichi, Japan
Hasegawa, Yuji, Japan
Hayashida, Morihiro, Japan
Heuvelink, Annerieke, The Netherlands
Hirayama, Takatsugu, Japan
Hoogendoorn, Mark, The Netherlands
Ikezaki, Masakazu, Japan
Ito, Shinya, USA
Jabir, Shayma, USA
Joshi, Hemant, USA
Kato, Jien, Japan
Kojiri, Tomoko, Japan
Koshizen, Takamasa, Japan
Kukla, Grzegorz, Poland
Kumon, Makoto, Japan
Kuga, Masahiro, Japan
Le, Nguyen Minh, Japan
Li, Jinpeng, UK
Martín-Merino, Manuel, Spain
Mauro, Nicola Di, Italy
McCollum, Barry, UK
Mencar, Corrado, Italy
Mete, Mutlu, USA
Mukai, Naoto, Japan
Nakadai, Kazuhiro, Japan

Nakajima, Hirofumi, Japan
Nakamura, Makoto, Japan
Nishide, Shun, Japan
Nobuhara, Shohei, Japan
Nomiya, Hiroki, Japan
Nowak, Andrzej, Poland
Okabe, Tatsuya, Japan
Orlowski, Cezary, Poland
Overeinder, Benno, The Netherlands
Oyama, Satoshi, Japan
Qu, Rong, UK
Pan, Youlian, Canada
Pilot, Tomasz, Poland
Poland, Jan, Japan
Sainz-Palmero, Gregorio, Spain
Sakurada, Hideki, Japan
Sakurai, Kouichi, Japan
Sakurai, Yuko, Japan
Seki, Kazuhiro, Japan
Serban, R., The Netherlands
Sharpanskykh, Alexei, The Netherlands
Shirahama, Kimiaki, Japan
Singh, Ravi Pratap, Italy
Smith, Brian A., USA
Stegers, Ruud, The Netherlands
Szlachetko, Bogdan, Poland
Tajima, Keishi, Japan
Takai, Takeshi, Japan
Takeuchi, Johane, Japan
Tamura, Takeyuki, Japan
Thai, Nguyen Phuong, Japan
Than, Nguyen Tri, Japan
Tinmar, Trevor, UK
Trawinski, Bogdan, Poland
Vinh, Nguyen Van, Japan
Walkowiak, Tomasz, Poland
Yada, Tetsushi, Japan
Yokoo, Makoto, Japan
Yasumura, Yoshiaki, Japan
Yoshimoto, Hiromasa, Japan
Yuruk, Nurcan, USA
Zatwarnicki, Krzysztof, Poland
Zeugmann, Thomas, Japan
Zhang, Chuanlei, USA
Zheng, Xinliang, USA

Table of Contents

[Special] Real World Interaction

[Special] Fuzzy System Applications II

Vision II

Genetic Algorithm

[Special] Fuzzy System Applications III

Robot

Poster

Genetic Algorithm II

Fuzzy Logic I

Manufacturing

Data Mining I

Neural Network I

Constraint Satisfaction

Data Mining II

Neural Network II

Fuzzy Logic II

Machine Learning I

[Special] Chance Discovery and Social Network I

Education

Machine Learning II

[Special] Chance Discovery and Social Network II

Speech

[Special] E-commerce I

Heuristic Search I

Application System

[Special] E-commerce II

Agent-Based System

Heuristic Search II

Other Applications

Towards New Content Services by Fusion of Web and Broadcasting Contents

Katsumi Tanaka

Department of Social Informatics,
Graduate School of Informatics, Kyoto University
tanaka@dl.kuis.kyoto-u.ac.jp
http://www.dl.kuis.kyoto-u.ac.jp

Abstract. We describe the research on fusion of Web and TV broadcasting contents conducted by Kyoto University 21st COE program and NICT communication/broadcasting contents fusion project. Despite much talk about the fusion of broadcasting and the Internet, no technology has been established for fusing web and TV program content. We proposed several ways to acquire information from diverse information sources of different media types, especially from Web and TV broadcasting. A notable difference between Web contents and TV program contents is that the former is a document-based information media and the latter is a time-based continuous information media, which leads to the difference of information accessing methods. Conventional "Web browsing" is an active manner of accessing information. On the other hand, conventional "TV watching" is a passive way of accessing information. In order to search, integrate and view the information of Web and TV, we explored (1) media conversion between Web and TV contents, (2) watching TV with live chats, (3) dynamic TV-content augmentation by Web, and (4) searching for TV contents with Web.

Keywords: World Wide Web, Broadcasting Contents, Browsing, Search.

1 Introduction

The Internet use is now very widespread, and content such as movies can be easily downloaded from the Internet at home. The increasing popularity of the Internet has coincided with a major change in the broadcasting environment as digital broadcasting has been introduced and data broadcasting services have become available. With these advances, the fusion of broadcasting and the Internet has become a widely discussed topic.

A notable difference between Web contents and TV program contents is that the former is a document-based information media and the latter is a time-based continuous information media, which leads to the difference of information accessing methods. Conventional Web "browsing" is an active manner of accessing information. On the other hand, conventional TV "watching" is a passive way of accessing information. In our research, first, we focused on media conversion between these two media. By the media conversion technologies, users will be able to access information of these two media in their favorite style. For example, it will

H.G. Okuno and M. Ali (Eds.): IEA/AIE 2007, LNAI 4570, pp. 1–11, 2007.

become possible to “watch and listen to Web” in the same way they watch TV, or to “browse TV programs” as if they were browsing the Web.

Recently, Hasegawa et al (E.Hasegawa and Y. Tanaka, NEC tech. report Vol.57, No.6, pp.10-13, 2004) reported that (1) 72% of Japanese people were watching TV concurrently with Web, (2) 52% of Japanese people, who watch TV, accessed Internet just after TV watching, and (3) the number of people who chat while watching TV, was also increasing. In the near future, the fusion of TV and Web media will make the boundaries between them blurred. It will become possible, for example, for consumers to create or annotate TV program contents, which at present are created only by broadcasting companies. This means that content authors, who will include both professionals and consumers, will be able to send information using their favorite media, content style, and environment. As for this, in this paper, we propose a way of watching TV together with user live chats.

Furthermore, it will become possible to obtain TV program content and web content simultaneously; that is, the two forms of content will be blended and their boundaries between them will disappear. With the improvement in the performance of various home appliances, TV content can be recorded or stored by users in various places in their immediate environment. For example, 1-TB hard-disk (HDD) recorders on the market can record more than 1700 hours of video at a certain quality. It is reported that the HDD recorders brought the increase of Japanese TV viewing time (2 hours 9 minutes increase per a day). We regard the fusion of TV and web content as a key factor that will shape next-generation systems for content delivery. This will lead to the change of TV viewing. We propose a new way to watch TV which is augmented by Web. Also, we propose a new search engine that can find TV contents together with Web.

2 Media Conversion from Web to TV

We developed three different prototype systems [1-6]: u-Pav which reads out the entire text of web content and presents image animation, Web2TV which reads out the entire text of web content and presents character agent animation, and Web2Talkshow which presents keyword-based dialogue and character agent animation. These prototype systems enable users to watch web content in the same way as they watch TV.

The u-Pav (Ubiquitous Passive Viewer) system is based on using the text read-out type of the audio component and the image animation type of the visual component. We developed u-Pav for two purposes: (1) to adapt fusion content to a ubiquitous environment, and (2) to communicate the entire content of selected web pages to users accurately and intuitively. The audio component of u-Pav is text, which is articulated using synthesized speech. For the visual component, the title and lines are shown through a ticker, and keywords and images are animated. The program synchronizes the tickers, the animations, and the speech.

Figure 1 shows a display image from u-Pav. The u-Pav can be displayed on a mobile phone screen simply by changing the visual component. The system was designed for use in a business environment. We developed u-Pav using Flash because Flash content can be displayed on mobile phones in Japan.

As shown in Figure 2, our Web2TV prototype system presents audio components using text read-out types and visual components using character agent animation types. Web2TV looks like a headline news program. Character agents are used to read-out the web content and the system presents images synchronized with the character agent reading out the text. The audio component consists of the character agents' lines, which are the entire web page text. The visual component consists of the camera work, lighting, studio set, and the character agents and their actions.

In both of u-Pav and Web2TV, one notable technique is the extraction of images and its corresponding text from Web by HTML page analysis, both of which are synchronized during replay.

Web2Talkshow transforms declarative sentences of a Web page into humorous dialogue based on keywords extracted from the page (see Figure 3). In Japan, there is a traditional form of standup comedy called "manzai". "Manzai" typically consists of two or three comedians participating in a humorous dialogue, rather like American "stand-up comedy", or Chinese "xiang sheng". In the case of two people, one plays the "straight man", and the other plays the "fool". We use this "manzai" style in Web2Talkshow. After parsing sentences extracted from a page, the system generates a topic structure consisting of subject terms and detailing terms based on term frequencies. Several QA dialogue templates of "manzai" style are prepared, and the QA dialogue is generated by filling the templates with the topic structure terms. The comparison and the evaluation of the u-Pav, Web2TV and Web2Talkshow is shown in [3].

Fig. 1. uPav: TV-style Web watching

Fig. 2. Web2TV: TV-style Web watching

Fig. 3. Web2Talkshow: TV-style Web watching

3 Media Conversion from TV to Web

3.1 TV2Web and Webified Video [7-11]

Closed captioning (CC) originally allows deaf and hard of hearing/hearing-impaired people and others to read a transcript or dialogue of the audio portion of a video, film, or other presentation. In Japan, totally 40% TV programs of major private broadcasting companies are associated with CCs. NHK is required to accomplish 100% CCs until 2007. Except live programs, more than 50% TV programs have their CCs in 2004. Closed caption data are regarded as a valuable metadata of TV program contents.

We have developed a system, called TV2Web and Webified Video, that automatically converts TV video streams with closed caption into a Web-page like content (see Figure 4). The generated Web pages include thumbnails of video units and text data generated from their closed caption data.

Users can "browse TV contents" on a normal Web browser. With zooming metaphors, TV2Web can seamlessly alter the level of detail (LOD) of the content being viewed. They can search for favorite TV scenes faster than with analog video equipment. Our experimental result shows 35% improvement for scene search tasks of video streams.

Fig. 4. TV2Web: Browsing TV contents

3.2 Zooming Cross-Media and a Zooming Description Language ZDL [10]

Based on the idea of TV2Web and Webified Video, we proposed the "zooming cross-media" concept that uses zooming to achieve both changes in the level of detail and transitions between media, for contents containing varied media. We proposed a zooming description language (ZDL) based on XML. Unlike existing zooming interfaces, ZDL codes the zooming operation and behavior on the content side. Because ZDL adopts XML coding, we can locate "zooming" as the third interface in the Web document environment after "scrolling" and "anchor clicking."

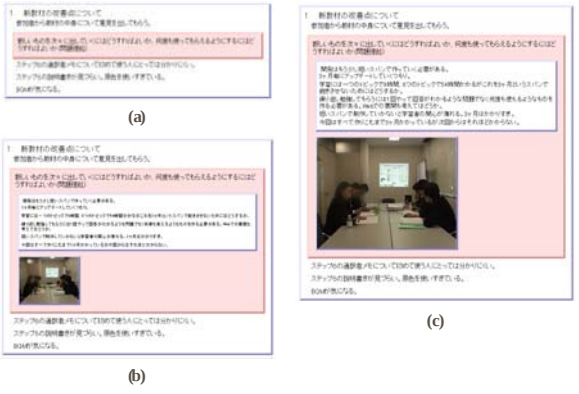

Fig. 5. "Zooming cross-media" applied to multimedia meeting minutes

We applied the idea of the "zooming cross-media" to generation of multimedia meeting minutes). Fig. 5 (a) shows an initial state and the colored part is a selected text. Fig. 5 (b) and (c) show zoomed conditions. As the zooming operation proceeds, a detail text part (the lower part of the selected part) and a still/video image appear ((b) and (c) show the still and the video image, respectively). The still image and video image are a snapshot picture and a recorded video that were captured when the discussion corresponding to the selected text occurred. We also applied the idea to implement a browser for search results, where the both of Web pages and video contents are searched for (see Figure 6). Zooming-in a Web page shows a thumbnail image of the page, and zooming-in a TV program contents shows a video thumbnail.

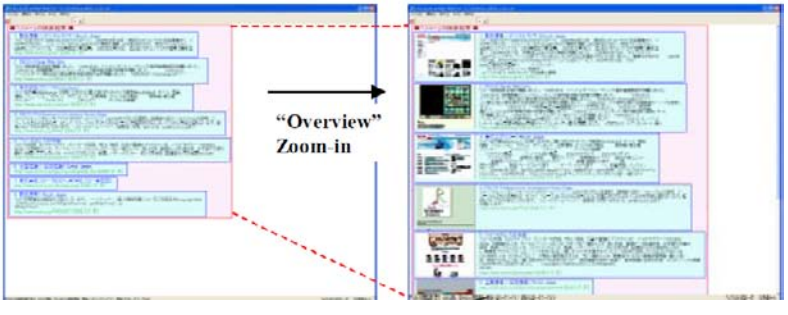

Fig. 6. "Zooming cross-media" applied to browsing search results

The zooming operation and behavior is independently coded from the content structure in ZDL. With ZDL, it is possible to (1) control the zooming of each "zoom object" making up the con-tents, (2) control the degree of zooming by introducing a "zoom rate" parameter, and (3) relate objects mutually and specify zooming propagation between related objects.

Zoom object is a target of zooming operation, and consists of text, images, video, sound, and other media-objects making up the contents. A <template/> tag expresses

a template of zoom objects. The “name” attribute specifies the template name and an attribute “match” specifies the base position of the contained media-objects in the content structure code. The media-objects are specified by <text/>, <video/>, etc. The “select” attribute specifies a relative position of each media-object, with respect to the base (reference) position specified through the “match” attribute. The user selects the desired zooming target and performs the zooming operation (e.g., by pointing to the zooming target by a mouse); however, ZDL does not deal concretely with how zooming targets are selected.

A zoom rate is uniquely defined in a zoom object, and is a continuous value (from 0.0 to 1.0) that specifies the degree of zooming. An attribute “zoomFactor” specifies it. Using the <dispText/>, <dispVideo/> and similar tags, the display state of each zooming object with respect to a given zooming rate is coded. Based on this, it is possible to code the change in the LODs of media-objects, as well as the media transition. Further, the “initZoomFactor” attribute inside the <template/> tag represents the initial zooming rate used to initially display the contents. Zoom rate is determined by the zooming operation performed by the user (e.g., the relationship between the movement of the mouse and the zooming rate); however, the ZDL does not deal concretely with how zooming operations are performed.

Zoom propagation means that when a zoom object (O) is zoomed, other related objects are also zoomed in conjunction with the object (O). For example, when an upper level object in the content structure is zoomed, lower level objects are also zoomed. A <propagation/> tag expresses this behavior. An attribute “destination” specifies a template name of destination objects and an attribute “select” specifies the position of their media-objects in the content structure. An attribute “relation” specifies the ratio between two changing rates of the zoom rate of the source and the destination objects.

4 Watching TV with Live Chats [12][13]

Video indexing is one of the fundamental techniques for achieving such functions. Several conventional indexing methods have been proposed using visual features such as color, camera motion, human faces, texts obtained from closed captions, and classes and volumes of audio information. However, because these methods work based on data provided by broadcast stations, the indices basically reflect only the intentions of TV programmers and stations. Therefore, conventional methods cannot incorporate factors such as the viewpoints and responses of other viewers of a TV program into the functions of scene search, summary presentation, and digest viewing.

The popularity of live chats on the Web is growing. Live chat communities on the Internet are virtual communities where viewers of a TV program congregate, and post messages in real time about their impressions of the program or about the program itself. By engaging in the chats while simultaneously viewing TV programs, users can feel a sense of unity by sharing emotions with other viewers.

We proposed a method of generating views of TV content from the perspectives of viewers’ using live chats on the Web. In the method, metadata related to viewers’ perspectives, such as important scenes in a program or responses by a particular

viewer are efficiently extracted through a combination of statistical analysis of chats data and pattern matching. Then, from the extracted metadata, scenes are chronologically listed (see Figure 7(a)) or ranked (see Figure 7(b)) based on the number of viewer response or the responses of all viewers who have preferences that are similar to those of a particular viewer. In this way, new views of TV content, such as chronological views and ranking views, are created. This method provides a new way of viewing TV that reflects the direct responses and perspectives of viewers.

(a) (b)

Fig. 7. TV viewing with live-chats

5 Dynamic TV-Content Augmentation by Complementary Web Pages [14-18]

A great deal of technology has been developed to help people access the information they require. With advances in the availability of information, information-seeking activities are becoming more sophisticated. This means that information technology must move to the next stage, i.e., enable users to acquire information from multiple perspectives to satisfy diverse needs. For instance, with the spread of digital broadcasting and broadband Internet connection services, infrastructure for the integration of TV programs and the Internet has been developed that enables users to acquire information from different media at the same time to improve information quality and the level of detail.

We proposed a novel content-based join model for data streams (closed captions of videos or TV programs) and Web pages based on the concept of topic structures. We then proposed a mechanism based on this model for retrieving complementary Web pages to augment the content of video or television programs.

One of the most notable features of this complementary retrieval mechanism is that the retrieved information is not just similar to the video or TV program, but also provides additional information.

We developed an application system called WebTelop, which augments TV programs in real time by retrieving complementary Web pages.

To extract the topic structure from a TV scene with closed caption, we define two kinds of co-occurrence relationship: the undirected term co-occurrence ratio and the directed term co-occurrence ratio. We define the notion of "subject degree" to determine whether a keyword has a high probability of being a subject term. The subject degree of word is defined by its directed term co-occurrence ratio with other keywords, and its term frequency. That is, if a keyword has high ratios of directed co-occurrence with other keywords within a topic and its term frequency is higher than that of the other keywords, it is considered the subject term. We also defined the "content degree" to determine the content terms of a topic based on the undirected co-occurrence relationship. The content degree of a keyword within a topic is defined as the sum of its undirected term co-occurrence with the subject terms.

The retrieval of complementary information consists of three phases: extract the topic structure from closed caption data, generate a query using the extracted topic structure to extend the topic structure, and execute the query and rank the retrieved results.

Figure 8 shows a screen image of our WebTelop. Figure 9 shows the Webtelop function incorporated into a multimedia search-result browsing interface, where complementary Web pages are automatically retrieved while viewing a TV program.

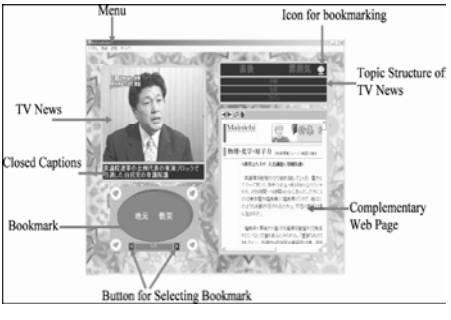

Fig. 8. WebTelop: Automatic search of complementary Web pages by TV closed caption

Fig. 9. Application of WebTelop to integrated search of Web and TV

6 Searching for TV with Web [19]

As a first step towards achieving such a next-generation search engine, we propose a search engine that handles Web content (with hyperlinks) and TV programs (without them), that performs integrated searching of this content, and that performs chain searches for content related to each search result if needed. An integrated search is achieved by generating integrated indices based on keywords obtained from TV programs and Web content and by ranking the content in the indices. Chain searches for related content are achieved by ranking by calculating the similarities between the content in a search result and the other content in the integrated indices. Our search engine can:

- simultaneously search for both Web content and TV programs that match a given keyword query,
- search for TV programs having content related to the Web content being browsed right now,
- search for Web content having content related to the TV program being watched right now.

Preliminary testing of a prototype system (see Figure 9) validated the approach used in our method.

The integrated search of Web content and recorded TV programs is performed based on keyword queries made by the user. Queries of one keyword or more are transformed into a common form using the indices in the integrated index DB. Web content and recorded TV programs are retrieved and ranked in an integrated manner in descending order based on the calculated similarities (integrated ranking). While viewing a Web page or recorded TV program in the integrated search result, users may want to search for related Web pages or recorded TV programs by making the viewed content itself a new query. In this case, a search similar to the integrated search is done by calculating the integrated similarity. This enables chains of searches by making the viewed content the new query (see Figure 8). The interface for displaying the search results works as follows: first, the integrated search results are shown in a list, and then, when a particular result is selected by the user, more details on the result and the top-ranked related content obtained in a chain search will appear according to how the user zooms. First, an integrated search is performed using a given query, followed by a chain search based on each content item in the search result. The result of the integrated search and chain search, written in XHTML, is transformed using a description language ZDL that can control the display appearance using a zooming metaphor, outputting the data in XHTML+JavaScript, which can be displayed at different levels of details according to the user's interest. The output data can be browsed via the zooming operation using a general browser.

One more important remained problem of the integrated search for Web and TV program contents is how to rank the search results. As for Web pages, there are already established ranking methods such as Google's PageRank. PageRank assumes the existence of hyperlinks for pages. On the other hand, TV program contents do not have any hyperlinks. When searching for TV programs and Web pages, we need a ranking algorithm that can handle not only Web pages but also TV program contents. Recently, Kabutoya et al. [20][21] proposed a way to provide a virtual PageRank evaluation to contents without hyperlinks. This is to simulate PageRank algorithm for contents without hyperlinks based on the similarity analysis of TV program contents and Web pages.

7 Concluding Remark

In this paper, we describe our research activities of the research on fusion of the Web and TV broadcasting [22]. Especially, we reported here our technologies for media conversion between TV and Web contents, watching TV with live chats, dynamic TV-content augmentation by complementary Web pages, and a search engine for TV and Web contents.

Acknowledgment

This research was supported in part by Informatics Research Center for Development of Knowledge Society Infrastructure (Kyoto University COE program of the Ministry of Education, Culture, Sports, Science and Technology, Japan) and the research of NICT (National Institute of Information and Communications Technology) Media Interaction Group. The author would like to thank all the COE members, members in Tanaka Lab., Kyoto University and colleagues of NICT Media Interaction Group for their collaboration.

References

1. Tanaka, K., Nadamoto, A., Kusahara, M., Hattori, T., Kondo, H., Sumiya, K.: Back to the TV: Information Visualization Interfaces based on TV-Program Metaphors. In: Proc. of IEEE International Conference on Multimedia and Expo(III), pp. 1229–1232 (2000)
2. Nadamoto, A., Hayashi, M., Tanaka, K.: Web2Talkshow:Transforming Web Content into TV-program-like Content Based on the Creation of Dialogue. In: Proc. of the 14th International World Wide Web Conference (WWW2005), pp. 1144–1145 (May 2005)
3. Nadamoto, A., Tanaka, K.: Complementing your TV-viewing by web content automatically-transformed into TV-program-type content. In: Proc. of the 13th Annual ACM International Conference on Multimedia (ACM Multimedia2005), pp. 41–50 (November 2005)
4. Nadamoto, A., Jatowt, A., Hayashi, M., Tanaka, K.: Web2Talkshow: Web content Transformed into Humorous Dialogue-based TV-program-like Conte. In: Maybury, M., Stock, O., Wahlster, W. (eds.) INTETAIN 2005. LNCS (LNAI), vol. 3814, pp. 253–258. Springer, Heidelberg (2005)
5. Uwada, H., Nadamoto, A., Kumamoto, T., Hamabe, T., Yokozawa, M., Tanaka, K.: Automated Content Transformation with Adjustment for Visual Presentation Related to Terminal Types. In: Zhou, X., Li, J., Shen, H.T., Kitsuregawa, M., Zhang, Y. (eds.) APWeb 2006. LNCS, vol. 3841, pp. 1214–1217. Springer, Heidelberg (2006)
6. Nadamoto, A., Kumamoto, T., Uwada, H., Hamabe, T., Yokozawa, M., Tanaka, K.: u-PaV: Automatic Transformation of Web Content into TV-like Video Content for Ubiquitous Environment. In: Proc. of the IEEE 7th International Conference on Mobile Data Management (MDM'06), p. 61 (May 2006)
7. Sumiya, K., Munisamy, M., Tanaka, K.: TV2Web: Generating and Browsing Web with Multiple LOD from Video Streams and their Metadata. In: Proc. International Conference on Informatics Research for Development of Knowledge Society Infrastructure (ICKS'04), pp. 158–167. IEEE Computer Society Digital Library, Los Alamitos (2004)
8. Sumiya, K., Munisamy, M., Tanaka, K.: TV2Web: Generating and Browsing Web with multiple LOD from Video Streams and Their metadata. In: Proc. of the 13th International World Wide Web Conference (WWW2004), pp. 398–399 (May 2004)
9. Miyamori, H., Tanaka, K.: Webified Video: Media Conversion from TV Program to Web Content and their Integrated Viewing Method. In: Proc. of the 14th International World Wide Web Conference (WWW2005), pp. 946–947 (May 2005)
10. Araki, T., Miyamori, H., Minakuchi, M., Kato, A., Stejic, Z., Ogawa, Y., Tanaka, K.: Zooming Cross-Media: A Zooming Description Language Coding LOD Control and Media Transition. In: Andersen, K.V., Debenham, J., Wagner, R. (eds.) DEXA 2005. LNCS, vol. 3588, pp. 260–269. Springer, Heidelberg (2005)

11. Miyamori, H., Tanaka, K.: Webified Video: Media Conversion from TV Programs to Web Content for Cross-Media Information Integration. In: Andersen, K.V., Debenham, J., Wagner, R. (eds.) DEXA 2005. LNCS, vol. 3588, pp. 176–185. Springer, Heidelberg (2005)
12. Miyamori, H., Nakamura, S., Tanaka, K.: Personal TV Viewing by Using Live Chat as Metadata. In: Proc. of the 14th International World Wide Web Conference (WWW2005), pp. 948–949 (May 2005)
13. Miyamori, H., Nakamura, S., Tanaka, K.: Generation of Views of TV Content Using TV Viewers' Perspectives Expressed in Live Chats on the Web. In: Proc. of the 13th Annual ACM International Conference on Multimedia (ACM Multimedia2005), pp. 853–861 (November 2005)
14. Ma, Q., Tanaka, K.: WebTelop: Dynamic TV-Content augmentation by Using Web Pages. In: Proc. of IEEE International Conference on Multimedia and Expo (ICME2003), vol. 2, pp. 173–176 (2003)
15. Ma, Q., Tanaka, K.: Topic-Structure Based Complementary Information Retrieval for Information Augmentation. In: Yu, J.X., Lin, X., Lu, H., Zhang, Y. (eds.) APWeb 2004. LNCS, vol. 3007, Springer, Heidelberg (2004)
16. Miyamori, H., Ma, Q., Tanaka, K.: WA-TV: Webifying and Augmenting Broadcast Content for Next-Generation Storage TV. In: Proc. of IEEE International Conference on Multimedia & Expo (ICME2005) (July 2005)
17. Ma, Q., Tanaka, K.: Context-Sensitive Complementary Information Retrieval for Text Stream. In: Andersen, K.V., Debenham, J., Wagner, R. (eds.) DEXA 2005. LNCS, vol. 3588, pp. 471–481. Springer, Heidelberg (2005)
18. Ma, Q., Tanaka, K.: Topic-Structure-Based Complementary Information Retrieval and Its Application. ACM Transactions on Asian Language Information Processing 4(4), 476–503 (2005)
19. Miyamori, H., Stejic, Z., Araki, T., Minakuchi, M., Ma, Q., Tanaka, K.: Towards Integration Services for Heterogeneous Resources: An Integrated Search Engine for Web Content and TV Programs. In: Proc. of the 2nd International Conference on Semantics, Knowledge, and Grid (SKG'06), p. 16. IEEE Computer Science Digital Library, Los Alamitos (2006)
20. Kabutoya, Y., Yumoto, T., Oyama, S., Tajima, K., Tanaka, K.: Quality Estimation of Local Contents Based on PageRank Values of Web Pages. In: ICDE Workshops 2006, p. 134 (2006)
21. Kabutoya, Y., Yumoto, T., Oyama, S., Tajima, K., Tanaka, K.: Comparative Quality Evaluation of TV Contents Based on Web Analysis. In: ICDE Workshops 2007 (April 2007)
22. Tanaka, K.: Content Integration from Web and Broadcast Information Sources. In: Proc. International Conference on Informatics Research for Development of Knowledge Society Infrastructure (ICKS'04), pp. 99–106. IEEE Computer Society Digital Library, Los Alamitos (2004)

Pattern Discovery from Graph-Structured Data - A Data Mining Perspective

Hiroshi Motoda

Asian Office of Aerospace Research & Development
Air Force Office of Scientific Research, Tokyo, Japan
hiroshi.motoda@aoard.af.mil

Abstract. Mining from graph-structured data has its root in concept formation. Recent advancement of data mining techniques has broadened its applicability. Graph mining faces with subgraph isomorphism which is known to be NP-complete. Two contrasting approaches of our work on extracting frequent subgraphs are revisited, one using complete search (AGM) and the other using heuristic search (GBI). Both use canonical labelling to deal with subgraph isomorphism. AGM represents a graph by its adjacency matrix and employs an Apriori-like bottom up search algorithm using anti-monotonicity of frequency. It can handle both connected and dis-connected graphs, and has been extended to handle a tree data and a sequential data by incorporating a different bias to each in joining operators. It has also been extended to incorporate taxonomy in labels to extract generalized subgraphs. GBI employs a notion of chunking, which recursively chunks two adjoining nodes, thus generating fairly large subgraphs at an early stage of search. The recent improved version extends it to employ pseudo-chunking which is called chunkingless chunking, enabling to extract overlapping subgraphs. It can impose two kinds of constraints to accelerate search, one to include one or more of the designated subgraphs and the other to exclude all of the designated subgraphs. It has been extended to extract paths and trees from a graph data by placing a restriction on pseudo-chunking operations. GBI can further be used as a feature constructor in decision tree building. The paper explains how both GBI and AGM with their extended versions can be applied to solve various data mining problems which are difficult to solve by other methods.

1 Introduction

Recent advancement of data mining techniques has made it possible to mine from complex structured data. Since structure is represented by proper relations and a graph can easily represent relations, knowledge discovery from graph-structured data (graph mining) poses a general problem for mining from structured data. Some examples amenable to graph mining are finding functional components from their behavior, finding typical web browsing patterns, identifying typical substructures of chemical compounds, finding subsequences of DNA typical to some functions and discovering diagnostic rules from patient history records.

The first example above is also called concept formation and has been a subarea of artificial intelligence research since many years ago. One such work is

H.G. Okuno and M. Ali (Eds.): IEA/AIE 2007, LNAI 4570, pp. 12–22, 2007.

by Yoshida and Motoda[11], where a concept is defined as something that minimizes inference load and the problem is finding a mapping that satisfies this requirement. This can be amenable to graph mining problem. The results of qualitative simulation of a digital circuit was mapped to a set of directed graph from which hierarchical concepts such as "pull down transistor", "exclusive OR" and "carry chain" were extracted. The idea behind the concept formation from a graph-structure data and its application to a digital circuit is schematically shown in Figs. 1 and 2. Similar work is reported in [1].

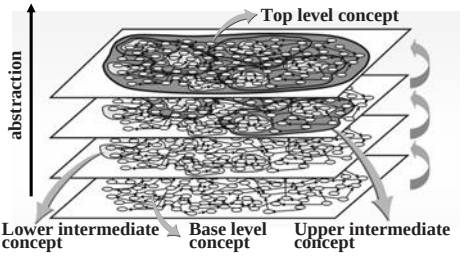

Fig. 1. Hierarchical functional abstraction of a complex object

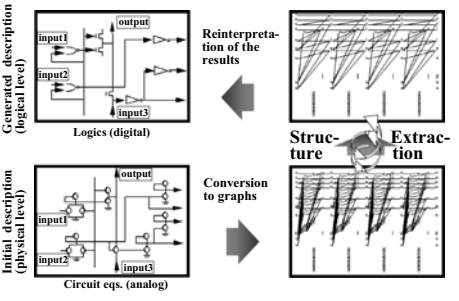

Fig. 2. Concept formation for a digital circuit

Graph mining is based on finding some typicality from a vast amount of graph-structured data. What makes it typical depends on each domain and each task. Most often frequency which has a good property of anti-monotonicity is used to discover typical patterns. Some measure such as information gain or χ^2 are also used but since they are not monotonic with respect to graph subsumption, special care must be taken. Graph mining inevitably faces with subgraph isomorphism which is known to be NP-complete. For example, three subgraphs in Fig. 3 are all isomorphic and it is not easy to find all of them in a huge set of graphs.

Two contrasting approaches have been taken to handle this problem, one searching all possible space efficiently devising a good data structure with an appropriate indexing and the other avoiding exhaustive search using a greedy algorithm with good heuristics. In this paper, our own work on these two approaches is revisited, AGM family for the former and GBI family for the latter, and how these are applied to solve difficult problems which are not easily solved my other approaches is explained. Both approaches use canonical labeling to handle subgraph isomorphism.

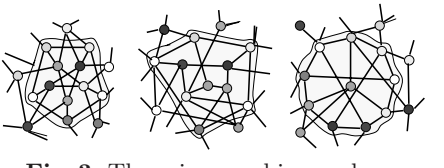

Fig. 3. Three isomorphic graphs

2 AGM Family - Algorithm and Its Applications

AGM [4,3] represents a graph by its adjacency matrix. Labels of nodes and edges are assigned natural numbers. The adjacency matrix is defined as follows. First

node labels are ordered according to their values and grouped according to this order, and a square matrix is formed. An element of the matrix is the edge label if there is an edge between the corresponding node pair and 0 if there is no edge between them. Since the same graph can be represented by multiple adjacency matrices because any permutation of the raw and the column within the same node label represents the same graph, each matrix is given a code and a code which gives a minimum (maximum) is defined as the canonical label.

A code consists of two parts, the first part is the code representing the node label ordering and the second part is the code consisting of the vertically scanned matrix elements. Thus, if the canonical label of two graphs are the same, they are identified as isomorphic. An example is given in Fig. 4. The graph has 5 nodes with 3 node labels and no edge labels. The node labels are ordered as grey (=1), dark-grey (=2) and black (=3). The first part is 11233 and the second part is 1011100011. The four adjacency matrices below represent the same graph. These are different only in the node numbering within the same label. The canonical label is 112331010011101 if the minimum is chosen.

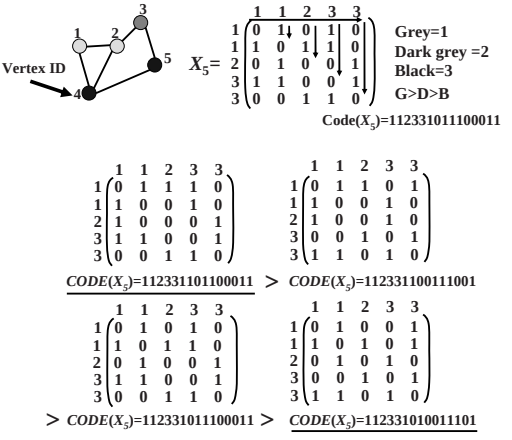

Fig. 4. Adjacency matrix and canonical label

Once we have defined a canonical label, candidate subgraph can be generated and searched using an Apriori-like bottom up search algorithm. In Apriori an itemset P_k of size k can be generated by 2 frequent itemsets of size $k-1$ that share the same $k-2$ items. This is called a join operation. Then it verifies that all the subsets of size $k-1$ in P_k are frequent or not, and if not it discards P_k. Finally the support of P_k is checked to see if it satisfies the min. support condition. The similar procedure can be applied to graphs. Two graphs of size $k-1$ can be joined to generate a graph of size k. Figure 5 shows an example when $k=5$. Here, the first matrix is always a canonical form (matrix with canonical label). What is different is that the generated matrix has missing elements. All the possible alternatives must be considered. If we have β labels for edges, there are $\beta+1$ adjacency matrices for undirected graph and its square for directed graph. Thus, the number of subgraphs rapidly increases with size. AGM

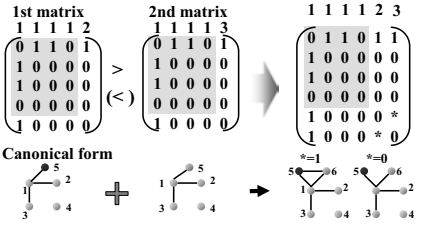

Fig. 5. Join operation of AGM

can handle general graphs, both connected and disconnected, both directed and undirected, and both labeled and unlabeled.

Since AGM is most generic, restricting the types of subgraphs is straightforward. It is easy to place a bias in join operation. B-AGM, biased AGM, can handle connected subgraphs, tree, ordered tree, path and sequence [5]. The conceptual scheme of the AGM family is depicted in Fig. 6.

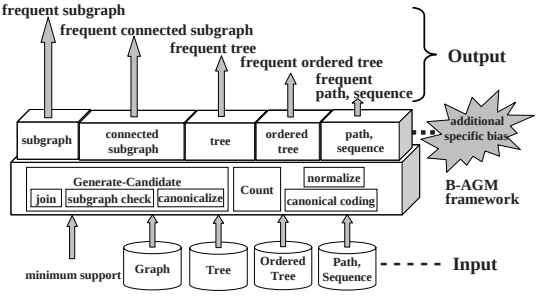

Fig. 6. Mining Various substructures by B-AGM Framework

Performance of AGM was evaluated using PTE dataset and is shown in Figure 7. This is a small dataset (the average graph size is 27). The connected version of B-AGM, AcGM favorably compares with the other later developed graph mining algorithms[10,6]. All do the complete search. If we limit the search to induced subgraphs, B-AGM is most efficient.

AGM family has been applied to many problems, mostly to chemical compound analysis such as mutagenicity, HIV and dopamine, and a few others such as Web browsing history analysis and consumer behavior analysis. In the analysis of mutagenicity of amino acid compounds, AGM was able to find that compounds that have hydrogen next to the nitro substituent in a benzene ring can be active. The results was obtained by using only the topological information of graphs. Later analysis of three dimensional structure of these compounds revealed that in case of hydrogen there is no steric hindrance that destroys the coplanarity to a benzene ring but a more complicated one does destroy the coplanarity. This explains the mining results. When applied to HIV data, AGM was able to find a subgraph which is very close to what is called azido-thymidine (AZT), a well known anti-HIV medicine. The found subgraph is shown in Fig. 8. This is a three class problem and the task is to find all the frequent subgraphs that are greater than the minimum support in the active compounds and less than the maximum support in the inactive compounds.

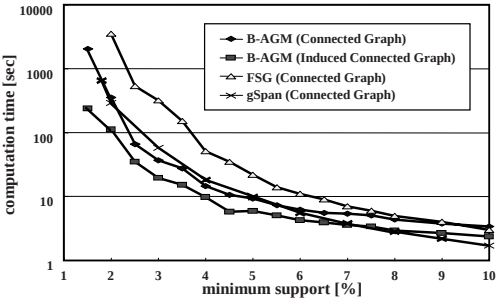

Fig. 7. Performance evaluation of AcGM (PTE data, Average size of graphs=27)

AGM was extended to handle taxonomy in node labels. Use of taxonomy makes it possible to find more abstract concepts even if there are not enough

number of frequent subgraphs at the base level description. The problem is conceptually easy but overgeneralization must be prevented. It is possible to extract the least general subgraph by discarding more general subgraphs that have the same total occurrence where multiple count is allowed if there are more than one occurrence of a subgraph in a graph. This technique was applied to PTE dataset and AGM found more discriminative subgraphs together with the taxonomy itself. AGM was further extended to handle three dimensional structure without modifying the algorithm (3D-AGM). Edge length was discretized into a finite number and was given different labels. With this approach, when applied to classification of dopamine antagonists, 3D-AGM was able to find more discriminative substructures than the standard AGM. An interesting application of AGM is consumer behavior analysis. Each time a person goes to a grocery store, items purchased together are recorded and this can be used for later analysis. The purchase history can be mapped to a directed graph. When applied to a data for a beer market, AGM discovered that a particular brand "Asahi super dry" is sold together with fresh fish and fruit. This hypothesis was tested in collaboration with the grocery store by rearranging the items so that these three are placed close. Interestingly the sales of beer went up more than double and fish sales went up also by 12% during the promotion [9].

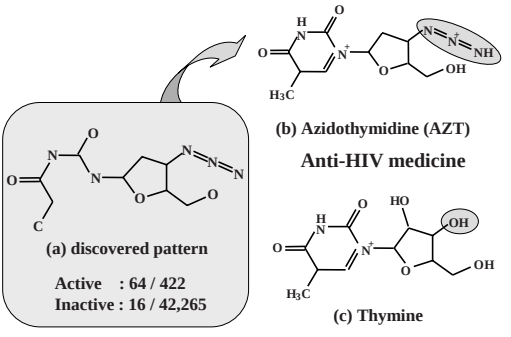

Fig. 8. Discovered subgraph by AcGM for HIV data

3 GBI Family - Algorithm and Its Applications

GBI [7] employs a notion of chunking, which recursively chunks two adjoining nodes, thus generating fairly large subgraphs at an early stage of search. GBI also uses canonical labeling to solve the graph isomorphism problem. Due to the nature of chunking, GBI is able to handle only connected graphs. Instead, GBI can use any criterion that is based on the frequency of paired nodes. However, for finding a subgraph that is of interest any of its subgraphs must be of interest because of the nature of repeated chunking. The frequency measure satisfies this monotonicity property. However, if the criterion chosen does not satisfy this property, repeated chunking may not lead to finding good subgraphs even though the best pair based on the criterion is selected at each iteration. To resolve this issue GBI uses two criteria, one based on frequency measures for chunking and the other for finding discriminative subgraphs after chunking. The latter criterion does not necessarily exhibit the monotonicity property. Any function that is discriminative can be used, such as Information Gain, Gain Ratio, Gini Index and others.

The original GBI contracts graphs after chunking and thus the size of the graphs progressively becomes smaller as chunking proceeds and thus the computational complexity is almost quadratic to the graph size. The basic algorithm is given in Fig. 9. However, the biggest problem with this approach is that it cannot find overlapping subgraphs. Later version introduced a beam search to alleviate this problem (B-GBI), but it was not enough. The recent improved version Cl-GBI extends it to employ pseudo-chunking which is called chunkingless chunking, enabling to extract overlapping subgraphs [8].

GBI(G)
  Enumerate all the pairs P_{all} in G
  Select a subset P of pairs from P_{all} (all the pairs in G) based on typicality criterion
  Select a pair from P_{all} based on chunking criterion
  Chunk the selected pair into one node c
  $G_c :=$ contracted graph of G
  while termination condition not reached
    $P := P \cup$ GBI(G_c)
  return P

Fig. 9. Algorithm of GBI

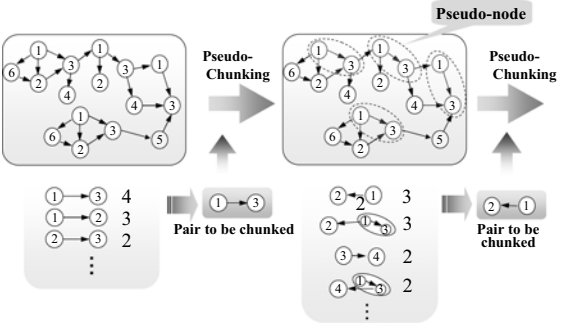

Fig. 10. Pseudo-chunking of Cl-GBI

In Cl-GBI, the selected pairs are registered as new nodes and assigned new labels but are never chunked and the graphs are never "contracted" nor copied into respective states as in B-GBI. In the presence of the pseudo nodes (i.e., newly assigned-label nodes), the frequencies of pairs consisting of at least one new pseudo node are counted. The other is either one of the pseudo nodes including those already created in the previous steps or an original node. The most frequent pairs with the number equal to the beam width specified in advance are selected among the remaining pairs and the new pairs which have just been counted for their frequencies. These steps are repeated for a predetermined number of times, each of which is referred to as a level. Those pairs that satisfy a typicality criterion (e.g., pairs whose information gain exceeds a given threshold) among all the extracted pairs are the output of the algorithm. A frequency threshold is used to reduce the number of pairs being considered to be typical patterns. Another possible method to reduce the number of pairs is to eliminate those pairs whose typicality measure is low even if their frequency count is above the frequency threshold. The two parameters, beam width and number of levels, control the search space. The frequency threshold is another important parameter. The algorithm of Cl-GBI is depicted in Fig. 10. In contrast to GBI and B-GBI graph size remains the same due to pseudo-chunking, and thus, the number of pairs to pseudo-chunk progressively

increases (computational complexity is now exponential to the size). It searches a much larger portion of subgraphs and in fact, search can be complete by setting the beam width and the level large enough. Like B-AGM, the subgraphs to be searched can be limited to paths, acyclic subgraphs and subgraphs (both induced and general) by placing appropriate constraints when chunking the pairs.

Performance of Cl-GBI was evaluated using the same PTE dataset as in AGM. The results are shown in Table 1. The number of beam width and the number of levels to find all the subgraphs are shown. The subgraphs found are confirmed to be the same as what were found by AcGM.

Table 1. Performance evaluation of Cl-GBI (PTE Data)

General subgraphs

Frequency threshold (θ)	30%	20%	10%
No. of freq. patterns	68	190	844
Beam width (b)	10	10	10
No. of levels (N) needed	12	18	84

Induced subgraphs

Frequency threshold (θ)	30%	20%	10%
No. of freq. patterns	49	139	537
Beam width (b)	10	10	10
Number of levels (N) needed	4	7	18

GBI family does not aim to find all the possible subgraphs but rather it attempts to find reasonably good subgraphs at an early stage in the search without searching all the space. To accomplish this, various techniques are introduced to improve its search efficiency. Two of them are mentioned here. The first one is to impose constraints to restrict search. Two kinds of constraints can be conceived. One is to extract only patterns that are of interest to domain experts or related to domain knowledge, and the other is to exclude extracting patterns uninteresting to domain experts or unrelated to domain knowledge. Both are called INpattern constraint and EXpattern constraint. Their implementation is straightforward. However, subgraph isomorphism checking is needed to check these constraints, and thus the number of checking must be reduced as much as possible. For this, necessary conditions for two subgraphs to be isomorphic, e.g. degree of node, node and edge labels, etc. are used. If these conditions are not satisfied, there is no need to compare the two subgraphs. The second one is to use pruning. Frequency satisfies anti-monotonicity but information gain, and χ^2 do not satisfy this constraint. However, they have a nice property of being convex with respect to the arguments. In this case it is possible to set an upperbound to them. Suppose we have a subgraph P and want to chunk it with other subgraph, generating a larger subgraph Q. The information gain of Q is bounded

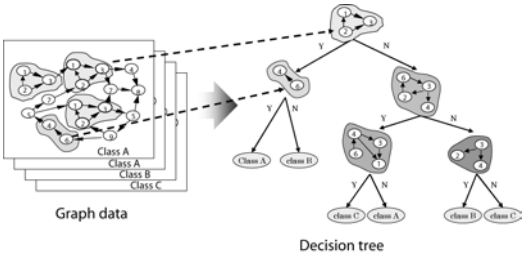

Fig. 11. Using Cl-GBI as a feature constructor in decision tree building

by the maximum of these extreme cases where the input instances containing Q only consists of a single class. If the upperbound for Q is less than or equal to the so far found best information gain or χ^2, then there is no need to pseudo chunk P.

If the final task is classification, graph mining has to be combined with classifier construction. For this task, GBI family can be used as a feature constructor in decision tree building [2] (See Fig. 11). Decision tree constructed this way was named DT-GBI or DT-ClGBI. Each node has a subgraph for which an input data is tested. Cl-GBI is run recursively reusing whatever can be inherited from the previous runs. The beam width and depth level are parameters that can be set at each tree level. The algorithm of DT-ClGBI is given in Fig. 12.

```
DT-GBI(D)
  Create a node DT for D
  if termination condition reached
    return DT
  else
    P := GBI(D) (with the number of
         chunking specified)
    Select a pair p from P
    Divide D into D_y (with p) and D_n (with-
     out p)
    Chunk the pair p into one node c
    D_yc := contracted data of D_y
    for D_i := D_yc, D_n
      DT_i := DT-GBI(D_i)
      Augment DT by attaching DT_i as its
       child along yes(no) branch
  return DT
```

Fig. 12. Algorithm of DT-ClGBI

The performance of DT-ClGBI was evaluated by a synthetic dataset. Directed graphs are randomly generated and equally divided into two classes, active and inactive. Four kinds of basic patterns were embedded in class active with equal probability. The average size of the graphs is changed from 30 to 50.

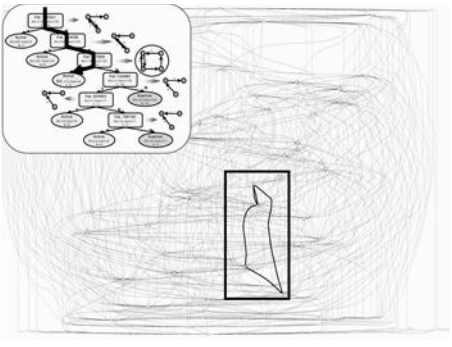

Fig. 13. An example of input graph classified as positive by DT-ClGBI

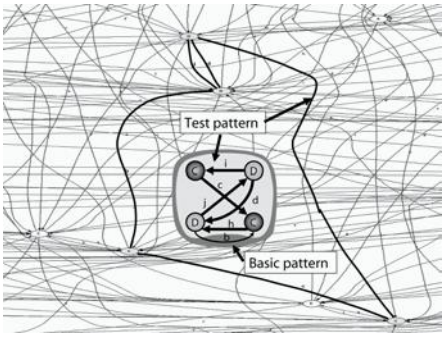

Fig. 14. Test pattern found in the input graph in Fig.13

The expectation was that these basic patterns appear in the test nodes of the decision tree, but the result was not exactly what was expected. The patterns chosen at each node were subgraphs of the basic patterns. Figure 13 shows one of the decision trees obtained and an input graph that failed in the first and the

second tests but passed the third test and classified as positive. A graph of size 50 is not a large graph, but for humans it is complicated enough and not easy to check if it includes the subgraph used for the test.

Both DT-GBI and DT-ClGBI were applied to a medical dataset of chronic hepatitis B and C which has been collected at the medical department of Chiba University over 20 years from 1982 to 2001. It is a large uncleansed time series data and has inconsistent measurements and many missing values. It was hoped that graph mining can extract typical correlation among different tests across time. Figure 15 shows how the time series data of each patient is converted to a directed graph after steps of preprocessing.

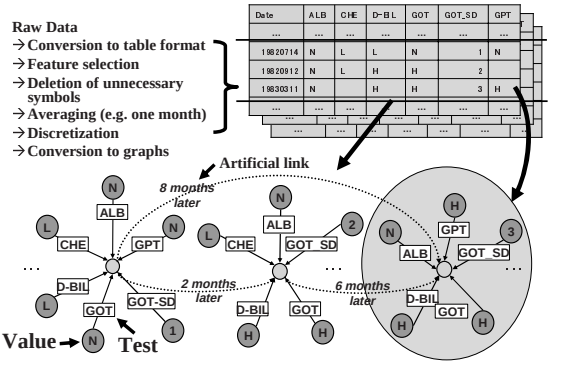

Fig. 15. Data preprocessing and conversion to a directed graph

The star shaped graph represents the various test data that are averaged over two months at a particular time point. These are connected sequentially and artificial links are added up to two years in future to represent possible direct effects of the past to the future. The main task is classifying patients with different fibrosis stages. The data used was 500 days before and after the first biopsy. Feature selection resulted in 32 tests (measurements) as the useful attributes. and the average size of the graphs was about 300. For each experiment 10 fold cross validation was run 10 times. Beam width was set to 15 and the number of levels to 20 at every node of the tree. The average error of distinguishing between F4 stage (liver cirrhosis) and F0+F1 stages (almost healthy) is 12.5% and its standard deviation was 2.12%. The average error of distinguishing between F4 stage and

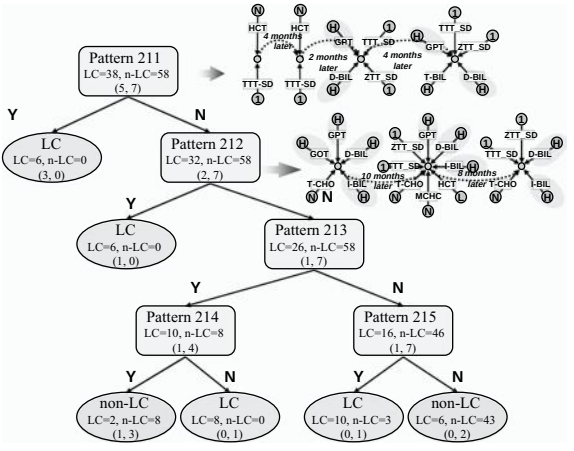

Fig. 16. Optimal decision tree to classify fibrosis progress

F3+F2 stages (not cirrhosis yet but close to it), which is a more difficult task, was 23.5% with the standard deviation of 2.39%. One of the decision trees is shown in Fig. 16. The patterns are fairly complex and these were exactly what we were expecting. However, unfortunately the medical doctors could not interpret these patterns. They thought the techniques interesting but did not accept the results blindly.

Detailed analysis revealed that there are groups of patients whose data behave strangely. This lead to a two stage analysis in which first these abnormal patients were separated from the rest and then a classifier was constructed for each group. The weighted average error of normal and abnormal patients reduced considerably to 7.3% and the tree became very simple and easily interpretable.

4 Conclusion

The paper discussed the use of graph-structured data in data mining perspective. Graph mining is an important area for extracting useful knowledge from structured data. Many interesting and difficult problems can be solved with this approach. However, graph mining is a computationally heavy task. Good algorithm and good data structure are needed. However, what is more important is a right problem setting to produce human understandable solutions. Human's cognitive capability is limited.

References

1. Cook, D.J., Holder, L.B.: Graph-based data mining. IEEE Intelligent Systems 15(2), 32–41 (2000)
2. Geamsakul, W., Yoshida, T., Ohara, K., Motoda, H., Yokoi, H., Takabayashi, K.: Constructing a decision tree for graph-structured data and its applications. Journal of Fundamenta Informatiae, Special issue on Advances in Mining Graphs, Trees and Sequence 66(1-2), 131–160 (2005)
3. Inokuchi, A., Washio, T., Motoda, H.: Complete mining of frequent patterns from graphs: Mining graph data machine learning, 50(3), 321-354 (2003)
4. Inokuchi, A., Washio, T., Motoda, H.: An apriori-based algorithm for mining frequent substructures from graph data. In: Proc. of the 4th European Conference on Principles of Data Mining and Knowledge Discovery, pp. 13–23 (2000)
5. Inokuchi, A., Washio, T., Motoda, H.: General framework for mining frequent subgraphs from labeled graphs. Journal of Fundamenta Informatiae, Special issue on Advances in Mining Graphs, Trees and Sequence 66(1-2), 53–82 (2005)
6. Kuramochi, M., Karypis, G.: An efficient algorithm for discovering frequent subgraphs. IEEE Trans. Knowledge and Data Engineering 16(9), 1038–1051 (2004)
7. Matsuda, T., Motoda, H., Washio, T.: Graph-based induction and its applications. Advanced Engineering Informatics 16(2), 135–143 (2002)
8. Nguyen, P.C., Ohara, K., Motoda, H., Washio, T.: Cl-gbi: A novel approach for extracting typical patterns from graph-structured data. In: Proceedings of the 9th Pacific-Asia Conference on Knowledge Discovery and Data Mining (2005)

9. Yada, K., Motoda, H., Washio, T., Miyawaki, A.: Consumer behavior analysis by graph mining technique. New Mathematics and Natural Computation 2(1), 59–68 (2005)
10. Yan, X., Han, J.: gspan: Graph-based structure pattern mining. In: Proc. of the 2nd IEEE International Conference on Data Mining, pp. 721–724 (2002)
11. Yoshida, K., Motoda, H.: Clip: Concept learning from inference pattern. Journal of Artificial Intelligence 75(1), 63–92 (1995)

A Collocation-Based WSD Model: RFR-SUM

Weiguang Qu[1,2], Zhifang Sui[1], Genlin Ji[2], Shiwen Yu[1], and Junsheng Zhou[2]

[1] Institute of Computational Linguistics, Peking Univ., Beijing 100871, China
{wgqu, szf, yusw}@pku.edu.cn
[2] Department of Computer Science, Nanjing Normal Univ., Nanjing 210097, China
{wgqu, glji, zhoujunsheng}@njnu.edu.cn

Abstract. In this paper, the concept of Relative Frequency Ratio (RFR) is presented to evaluate the strength of collocation. Based on RFR, a WSD Model RFR-SUM is put forward to disambiguate polysemous Chinese word sense. It selects 9 frequently used polysemous words as examples, and achieves the average precision up to 92.50% in open test. It has compared the model with Naïve Bayesian Model and Maximum Entropy Model. The results show that the precision by RFR-SUM Model is 5.95% and 4.48% higher than that of Naïve Bayesian Model and Maximum Entropy Model respectively. It also tries to prune RFR lists. The results reveal that leaving only 5% important collocation information can keep almost the same precision. At the same time, the speed is 20 times higher.

1 Introduction

Word sense disambiguation (WSD) is a central open problem at the lexical level of Natural Language Processing (NLP). Word sense multiplicity is a very general characteristic of natural language. For example, the polysemous word ratio in Modern Chinese Dictionary is 14.8%. In Chinese corpus, the occurrence frequency of polysemous words is around 42%[1]. Ambiguous words pose continuing problems for NLP applications. They can lead to irrelevant document retrieval in Information Retrieval systems and inaccurate translation in Machine Translation systems. For example, the Chinese word "黄色" has two different senses, one of which can be translated into English as "yellow" in "黄色香蕉"(yellow banana), and another as "pornographic" in "黄色小说"(pornographic novel). The aim of WSD is to assign an appropriate sense to an occurrence of word in a given context automatically.

Various approaches have been proposed to deal with the WSD problem, including rule-based approaches, knowledge or dictionary based approaches, corpus-based approaches, and hybrid approaches[2]. Among these approaches, the corpus-based supervised machine learning method is the most successful way, where contextual features have been used mainly to distinguish ambiguous words[3]. The learning algorithms applied include: decision tree, decision list, neural networks, Naïve Bayes, boosting, Winnow, SVM, VSM, maximum entropy. The assumption behind these methods is that it is usually possible to determine the sense

H.G. Okuno and M. Ali (Eds.): IEA/AIE 2007, LNAI 4570, pp. 23–32, 2007.

of an ambiguous word by referring to its context, and thus all of the methods build a classifier using features representing context information[4].

Recently, many researchers realize the importance of collocation and use collocation as WSD resources[3, 5, 6]. In [7], Li uses Naïve Bayesian Classifier as the core algorithm. The primary purpose of using collocation is to improve precision. In [6], Hoa uses maximum entropy approach on WSD and introduces collocation features, syntactic features and semantic features in maximum entropy model. The experiment shows that adding more features from richer levels of linguistic annotation yielded no significant improvement over using only collocation features in Chinese WSD.

Since manual collection of collocation resource is expensive, it is desirable to develop automatic collocation extraction tools. Although some progress has been made in the aspects of automatic collocation extraction[8, 9], the problem of manual selection or collocation proofreading remains unsolved in practice.

In fact, the meaning of a sentence is realized by the composition of every word with a particular order. This means that every word in the sentence other than a particular collocation alone makes contribution to WSD.

In this paper, we propose relative frequency ratio (RFR) of word to evaluate the collocation strength of words in context of each sense, and put forward a model called RFR-SUM, which sums up the RFR value of the words in context of each sense, and makes decision base on the RFR summation. More details will be described in section 2. The main work and innovations in this paper are as follows:

1. Taking Relative Frequency Ratio (RFR) as the measurement of collocation strength, we solve the problem of manual selection or collocation proofreading.

2. Based on RFR, we suggest a collocation-based WSD model: RFR-SUM which sums up the RFR value of the words in context of each sense, and makes decision base on the RFR summation. We compare the model with Naïve Bayesian Model and Maximum Entropy Model. The experimental results verify its feasibility.

3. We try to prune RFR lists. The results reveal that we can get almost the same precision by using only 5% important collocation information. At the same time, the speed is 20 times higher.

The rest of this paper is organized as follows. Section 2 describes the RFR and RFR-SUM Model. Section 3 reports the experiments and the analysis of our result. Section 4 is the conclusions and future work.

2 Relative Frequency Ratio (RFR) and RFR-SUM Model

2.1 Collocation Strength and Relative Frequency Ratio (RFR)

There are actually different definitions of the notion of collocation. Some authors in the computational linguistics and statistical literature define a collocation as two or more consecutive words with a special behavior. But in most linguistically oriented research, a phrase can be a collocation even if it is not consecutive, as

in the example "knock⋯door". Some authors have generalized the notion of collocation even further and included cases of words that are strongly occurred in a common grammatical unit and with a particular order, case like "doctor-nurse" or "plant-airport"[10].

In fact, collocation in this definition is more useful for WSD. If "doctor" occurs with "nurse", it probably denotes doctor vocation. If with "master" or "bachelor", it may have the meaning of Ph.D. degree.

Many researchers realize the importance of collocation, but they think that some words have low discrimination power such as prepositions, conjunctions, articles and pronouns. They don't directly contribute to the content. Therefore, these words are listed in the stop-list and deleted from set of context words before WSD[1]. But in our investigation, even function words can also contribute to WSD[11].

Taken "的 (of)" as an example. If "的" occurs consecutively behind "黄色", i.e. "黄色的", then "黄色" would almost have the sense of yellow color.

We count the distribution of "的" in the sentences with word "黄色" in 23 years' People Daily News (PDN) corpus at two different senses. There are 2137 sentences for yellow color sense and 893 sentences for pornographic sense. We align the sentences by "黄色" and count the distribution of "黄色" at different position. For normalizing the difference of sentence amount between the two senses, the frequency of "的" at different positions for pornographic sense multiplies 2137/893. The result is in Figure 1. The figure shows that when "的" occurs consecutively behind "黄色", the sense will be yellow color at a very high probability.

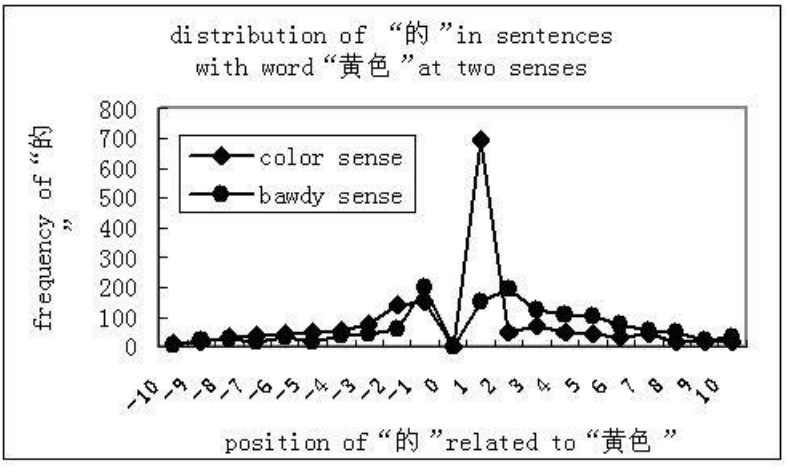

Fig. 1. "的"'s distribution in sentences with "黄色" and aligned by "黄色"

Based on the above-mentioned facts, we believe that every word in context makes contribution to WSD in one way or another. Here we define collocation

as co-occurrence of words in context of target word. We introduce Relative Frequency Ratio (RFR) to evaluate the collocation strength.

Let the context with ambiguous word A be:

$$W_{-k}W_{-(k-1)\ldots}W_{-2}W_{-1}AW_1W_{2\ldots}W_{(s-1)}W_s \tag{1}$$

where, the negative sign in subscript denotes the word in left context; $-k$ denotes that left context selects k words; s denotes that right context selects s words.

The sentences with polysemous word are classified by linguists, thus form t sets, each of which contains one sense. Here, t expresses that the word has t different senses: $A_1, A_2, \ldots, A_t$.

For every set $m(m = 1, 2, \ldots, t)$, we first align every sentence according to word A_m, then calculate the frequency of every word in position $i(-k \leq i \leq s)$ to word A_m, which is called local word frequency for this word at position i to A_m, denoted as $\mathrm{LocFrq}_{m,i}$(word)

In a very large corpus (named corpus bank), we count the frequency of every word occurred in the corpus, thus get word frequency for each word, called global word frequency, denoted as GlobFrq(word). Denote the RFR of this word at position i as $f_{m,i}$ (word) and define $f_{m,i}$ (word) as:

$$f_{m,i}(word) = LocFrq_{m,i}(word)/GlobFrq(word) \tag{2}$$

Hence we get RFR matrix as below:

$$F_{m,-k}F_{m,-(k-1)\ldots}F_{m,-2}F_{m,-1}A_mF_{m,1}F_{m,2\ldots}F_{m,(s-1)}F_{m,s} \tag{3}$$

where,

$$F_{m,i} = (f_{m,i}(word_1), f_{m,i}(word_2), \ldots, f_{m,i}(word_n))^T \tag{4}$$

n denotes that there are n occurrence words at position i for sense A_m.

RFR reflects the extent of attraction between the word and word A_m at position i. It can be used to evaluate collocation strength.

For simplicity, we take the left k words as left window and the right s words as right window. Then the RFR matrix is simplified as:

$$F_{m,left}A_mF_{m,right} \tag{5}$$

where,

$$F_{m,i} = (f_{m,i}(word_1), f_{m,i}(word_2), \ldots, f_{m,i}(word_n))^T, (i = left, right) \tag{6}$$

and

$$f_{m,left}(word_j) = \sum_{i=-1}^{-k} f_{m,i}(word_j), for\ left - window \tag{7}$$

$$f_{m,right}(word_j) = \sum_{i=1}^{s} f_{m,i}(word_j), for\ right - window \tag{8}$$

By means of above mentioned method, we get two RFR lists for each sense of polysemous word in left and right window. This is in fact the training process of WSD.

For word "黄色", Table 1 and Table 2 show the top 10 words with high RFR value for both senses in left window and right window respectively after we prune 95% lower frequency words from RFR lists (here,$k = s = 2$). We can see that the words with high RFR value are almost the collocations for their corresponding sense. In fact, RFR value can be used for collocation extraction[12].

Table 1. Top 10 words with high RFR value for yellow sense

Left window			right window		
word	RFR	Frq	word	RFR	Frq
橘(orange)	0.10714	24	葡萄球菌(Staphylococcus)	0.48000	36
褐(brown)	0.06061	32	袈裟(cassock)	0.08209	22
淡(light)	0.05051	267	油菜花(rape flower)	0.05641	11
乳(milky)	0.01687	38	麦浪 (wheat field)	0.04734	24
鹅(soft)	0.01553	49	棕色 (brown)	0.04000	18
呈(show)	0.01363	116	琉璃瓦 (glazed tile)	0.03583	11
浅(light)	0.01268	121	五角星 (pentacle star)	0.03217	12
身穿(wear)	0.00824	21	斑点(spot)	0.03040	10
金(gold)	0.00823	892	军服(uniform)	0.01852	19
片片(piece)	0.00788	18	粉末(powder)	0.01678	18

Table 2. Top 10 words with high RFR value for pornographic sense

Left window			right window		
word	RFR	Frq	word	RFR	Frq
查禁(ban)	0.01494	13	书刊(books)	0.02735	151
收缴(capture)	0.00664	17	录像(video)	0.02503	70
淫秽(bawdy)	0.00555	12	录像带(videotape)	0.02230	31
贩卖(vend)	0.00454	24	淫秽(bawdy)	0.02220	48
播放(play)	0.00415	13	出版物(publication)	0.00956	42
书刊(books)	0.00326	18	刊(periodical)	0.00706	40
取缔(ban)	0.00262	13	歌曲(song)	0.00520	92
抵制(reject)	0.00108	17	小说(novel)	0.00298	60
传播(spread)	0.00100	17	书籍(book)	0.00242	38
出售(sale)	0.00049	12	音乐(music)	0.00170	69

2.2 The RFR-SUM Model

After the training process, we can make use of the RFR matrix to disambiguate the word sense.

Given a certain sentence as (1), for every sense $A_m(m = 1, 2, \ldots, t)$, search for the RFR of W_i $(-k \leq i \leq s)$ from column i of RFR matrix and get $f_{m,i}(W_i)$.

If the word W_i is not in column i, then $f_{m,i}(W_i) = 0$. Thus we get:

$$\mathrm{SUM}_m = \sum_{i=-k}^{s} f_{m,i}(W_i) \tag{9}$$

In the simplified model,

$$\mathrm{SUM}_m = \sum_{i=-1}^{-k} f_{m,left}(W_i) + \sum_{i=1}^{s} f_{m,right}(W_i) \tag{10}$$

Among $m(m = 1, 2, \ldots, t)$, the sense that maximizes the SUM_m will be assigned as the word sense.

From the RFR-SUM model, we can see that the model takes the positional information in context and their RFR value into consideration, then sums up all the RFR values in context. This is similar to what human integrates all his knowledge he has ever learnt to make the decision.

Table 3 gives some examples for the sum of RFR values in sentences. The three sentences are very similar, but the RFR-SUM Model can discriminate them easily. Especially in the last sentence, where the context words but "的" are not occurred in training data, the functional words "的" can give a strong hint to make the true decision at a very high probability. This property is very useful in open test.

Table 3. Sentences and their RFR sum value

充斥|fill	黄色	的|of	内容|content	sum
0.00070	**bawdy**	0.00001	0.00012	0.00083
0.00000	yellow	0.00006	0.00000	0.00006
身穿|wear	黄色	的|of	军服|costume	
0.00000	bawdy	0.00001	0.00000	0.00001
0.00824	**yellow**	0.00006	0.01852	0.02682
眺望|watch	黄色	的|of	山峦|mountain	
0.00000	bawdy	0.00001	0.00000	0.00001
0.00000	**yellow**	0.00006	0.00000	0.00006

3 Experimental Results

We select frequently used polysemous Chinese words " 高度", "出发", "保守", "黄色", "合计", "地方", "黄金", which have two senses, and "分子", "材料", which have three senses, as WSD examples.

We employ 54 years' PDN corpus from 1946 to 1999 as corpus bank to count global word frequency, thus the global word frequency is more stable. The training data is selected from PDN corpus range from year 1991 to 1996. The testing data is from 1997 PDN corpus.

3.1 WSD Algorithm

We use the RFR-SUM Model to disambiguate polysemous words. Training process is described below:

Step.1 construct global word frequency list using 54 years' PDN corpus.

Step.2 select PDN corpus from year 1991 to 1996, processed by word segmentation and POS tagging without human proofreading. Here, we use ICTCLAS, available at http://www.nlp.org.cn.

Step.3 pick up sentences with polysemous word to get training data. Linguist classifies the sentences according to different word senses to form high frequency sense data, which occurs more in corpus, and low frequency sense data, which occurs less in corpus.

Step.4 for the high frequency sense data and low frequency sense data, calculate their word frequency in left window and right window respectively, thus formed 4 lists of local word frequency from different sense and different window.

Step.5 for each word w in the above-mentioned lists, calculate the RFR to form RFR lists. Thus four lists are formed for every sense at left and right window. For word W_i, the RFR value are denoted as:

$f_{HF,left}(W_i), f_{HF,right}(W_i), f_{LF,left}(W_i)$ *and* $f_{LF,right}(W_i)$ respectively.

The WSD process is very simple after the four lists are formed. Sum up the RFR value of all the words in the context for each word sense separately and make simple decision.

The process is described as follows:

begin
  sumHF=0, sumLF=0;
  for $(i = -1; i \geq L; i--)$ //L is left window size
  {
    sumHF+ = $f_{HF,left}(Wi)$;
    sumLF+ = $f_{LF,left}(Wi)$;
  }
  for$(i = 1; i \leq R; i++)$//R is right window size
  {
    sumHF+ = $f_{HF,right}(Wi)$;
    sumLF+ = $f_{LF,right}(Wi)$;
  }
if sumHF $* \alpha \geq$ sumLF then sense=HF;
  else sense=LF.
end

In order to eliminate the effect caused by the amount difference of examples for high frequency sense and low frequency sense, here we introduce a coefficient α to balance the difference, $0 < \alpha \leq 1$. The value of α can be determined by maximizing the accuracy of close test data. Precision is introduced to evaluate the WSD performance, which is defined as:

$$\text{precision} = \frac{\text{Number of words assigned a sense correctly}}{\text{Number of polysemous words in data set}} \tag{11}$$

We set the baseline as the precision when we assign all the word senses with the high frequency sense. Table 4 lists the example words, their senses, the numbers of test data, and baselines.

Table 4. Experimental words, their example numbers, and baselines

		close test		open test	
word	sense	Num. of examples	baseline%	Num. of examples	Baseline%
高度	altitude/ high degree	100/430	81.1	63/207	76.7
出发	depart/focus of attention	80/555	87.4	30/183	85.9
保守	keep/ conservative	102/1158	91.9	20/76	79.2
黄色	pornographic/ yellow	893/2136	70.5	50/143	74.1
合计	Think of/ add up to	83/187	69.3	13/32	71.1
地方	local/ place	387/591	60.4	83/115	58.1
黄金	Precious/ gold	648/2822	81.3	96/343	78.1
分子	Numerator/molecule /person belong to a class	7/454/502	52.1	5/14/192	91.0
材料	Stuff/facts,information /substance	44/1975/ 2526	55.6	3/106/ 136	55.5

In order to show the RFR-SUM performance, we compare the accuracy with Naïve Bayesian Model and Maximum Entropy Model, which are very common in WSD. More details about these two models are described in [13]. We select the same features with RFR-SUM model. The results are listed in Table 5. It shows that the precision by RFR-SUM Model is 5.95% and 4.48% higher than that of Naïve Bayesian Model and Maximum Entropy Model respectively.

Table 5. Experimental Results

	Naïve Bayes		Maximum Entropy		RFR-SUM	
	close%	open%	close%	open%	close%	open%
高度	100	88.5	100	90.15	99.81	**93.00**
出发	100	85.5	100	89.00	99.84	**90.00**
保守	100	93.7	100	95.80	99.92	**96.87**
黄色	99.69	90.15	99.94	95.33	99.18	**96.37**
合计	100	86.67	100	**91.11**	100	**91.11**
地方	99.29	75.25	99.90	75.25	98.88	**89.39**
黄金	99.60	89.40	100	91.24	98.07	**95.89**
分子	100	**91.00**	100	80.09	98.52	90.50
材料	99.40	78.74	98.73	84.25	99.56	**89.37**
avg	99.78	86.55	99.84	88.02	98.73	**92.50**

3.2 The Pruning of RFR List

Zipf's law tells us that most of the words in corpus are sparsely occurred and only a small amount of words happen at high frequency. In RFR lists, there are more than 50% words occurring only once. These words contribute less to WSD especially when in open test. We try to optimize the RFR lists, and prune words with less frequency. We remove words with less frequency from 10% to 90% step by 10%, the precision is unchangeable. Figure 2 shows that of from 91% to 100% step by 1%. The figures reveal that we can get almost the same precision by using only 5% important collocation information. At the same time, the speed is 20 times higher. The algorithm's running time is $O(n)$, where n is the number of words in RFR lists.

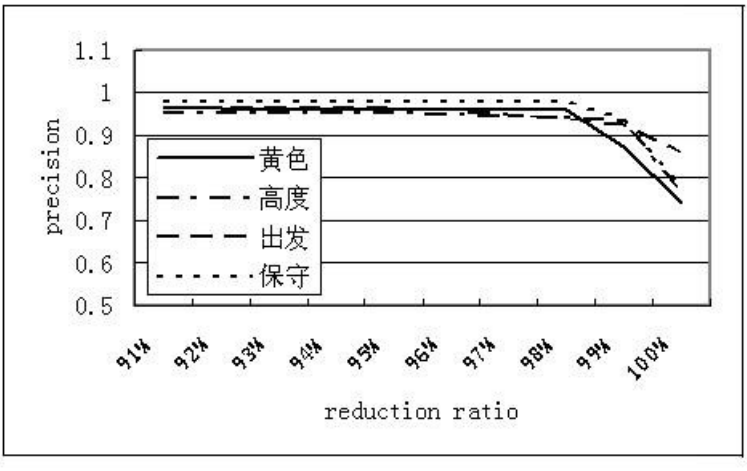

Fig. 2. Relation between reduction ratio and accuracy (91%-100% step 1%)

The result is very important. It guarantees that the speed is 20 times higher with less precision loss, thus makes the RFR-SUM model more valuable in practice.

4 Conclusions and Future Work

This paper presents a collocation-based WSD model: RFR-SUM, which introduces RFR to measure the collocation strength and sums up the RFR values of contextual words to make decision. The experimental results are inspiring. We also prune RFR lists. Experiment shows that we can get almost the same precision by using only 5% important collocation information. At the same item, the speed is 20 times higher.

In this paper, we only use the model in WSD task. We believe that the model can also tackle other lexical level ambiguity such as covering ambiguity resolution and overlapping ambiguity resolution in Chinese word segmentation,

named entity recognition, and so on. We also believe that the model is language independent. We will try to use the model in English WSD soon.

Acknowledgments. This paper is supported by 973 Natural Basic Research Program of China (Grant No. 2004CB318102), the National Natural Science Foundation of China (Grant No. 60503071, 60675035), China Postdoctoral Science Foundation(Grant No.20060400027), and Jiangsu Province Social Science Foundation (Grant No.06JSBYY001). My thanks go to the anonymous reviewers for their suggestive comments.

References

1. Zhang, Y., Gong, L., Wang, Y.: Chinese Word Sense Disambiguation Using HowNet. In: Wang, L., Chen, K., Ong, Y.S. (eds.) ICNC 2005. LNCS, vol. 3610, pp. 925–932. Springer, Heidelberg (2005)
2. Ide, N., Veronis, J.: Introduction to the Special Issue on Word Sense Disambiguation: The State of the Art. Computational Linguistics 24(1), 1–40 (1998)
3. Ng, H.T., Wang, B., Chan, Y.S.: Exploiting Parallel Texts for Word Sense Disambiguation: An Empirical Study. In: Dignum, F.P.M. (ed.) ACL 2003. LNCS (LNAI), vol. 2922, pp. 455–462. Springer, Heidelberg (2004)
4. Li, H., Li, C.: Word Translation Disambiguation Using Bilingual Bootstrapping. Computational Linguistics 30(1), 1–22 (2004)
5. Changqin, Q., Tingting, H., et al.: Chinese WSD based on Selecting the Best Seeds from Collocations. Journal of Chinese Information Processing (in Chinese) 19(1), 30–35 (2005)
6. Dang, H.T., Chia, C.-y., et al.: Simple Features for Chinese Word Sense Disambiguation. In: Proc. Of COLING-2002, Philadelphia, USA, pp. 769–772 (2002)
7. Li, W., Lu, Q., Li, W.: Integrating Collocation Features in Chinese Word Sense Disambiguation. In: Proceedings of the Fourth Sighan Workshop on Chinese Language Processing, pp. 87–94, Jeju, Korea (2005)
8. Smadja, F.: Retrieving Collocations from Text: Xtract. Computational Linguistics 19(1), 143–177 (1993)
9. Lin, D.: Extracting Collocations from Text Corpora. In: Proceedings of COLLING/ACL-98 Workshop on Computational Terminology, Montreal, Canada. pp. 57–63 (1998)
10. Manning, C.D., Schutze, H.: Foundations of Statistical Natural Language Processing. MIT Press, Cambridge (1999)
11. Qu, W.: Generalized Collocation and Context-based Computational Model, Ph. D Dissertation, Nanjing Normal University (2005)
12. Qu, W.: A Frame-based Approach to Chinese Collocation Automatic Extracting. Computer Engineering (in Chinese) 30(23), 22–24, 195 (2004)
13. Wang, Z., Wang, H., Duan, H., Han, S., Yu, S.: Chinese Noun Phrase Metaphor Recognition with Maximum Entropy Approach. In: Proceedings of the Seventh International Conference on Intelligent Text Processing and Computational Linguistics. pp. 235–244, Mexico (2006)

A Simple Probability Based Term Weighting Scheme for Automated Text Classification

Ying Liu[1] and Han Tong Loh[2]

[1] Department of Industrial and Systems Engineering
The Hong Kong Polytechnic University, Hung Hom, Kowloon, Hong Kong SAR, China
mfyliu@inet.polyu.edu.hk
[2] Department of Mechanical Engineering
National University of Singapore, 21 Lower Kent Ridge Road, Singapore 119077
mpelht@nus.edu.sg

Abstract. In the automated text classification, *tfidf* is often considered as the default term weighting scheme and has been widely reported in literature. However, *tfidf* does not directly reflect terms' category membership. Inspired by the analysis of various feature selection methods, we propose a simple probability based term weighting scheme which directly utilizes two critical information ratios, i.e. relevance indicators. These relevance indicators are nicely supported by probability estimates which embody the category membership. Our experimental study based on two data sets, including Reuters-21578, demonstrates that the proposed probability based term weighting scheme outperforms *tfidf* significantly using Bayesian classifier and Support Vector Machines (SVM).

1 Introduction

Text classification (TC) is such a task to categorize documents into predefined thematic categories. In particular, it aims to find the mapping ξ, from a set of documents D: $\{d_1, \ldots, d_i\}$ to a set of thematic categories C: $\{C_1, \ldots, C_j\}$, i.e. $\xi : D \rightarrow C$. In its current practice, which is dominated by supervised learning, the construction of a text classifier is often conducted in two main phases [2, 14]:

1. Document indexing – the creation of numeric representations of documents
   - Term selection – to select a subset of terms from all terms occurring in the collection to represent the documents in a better way, either to facilitate computing or to achieve best effectiveness in classification.
   - Term weighting – to assign a numeric value to each term in order to weight its contribution which helps a document stand out from others.
2. Classifier induction – the building of a classifier by learning from the numeric representations of documents

For term weighting, *tfidf* is often considered as the default scheme and hence has been widely reported in literature. However, *tfidf* does not really reflect terms' category membership which is what classification supposes to rely on. In this paper, we propose a novel term weighting scheme based on our inspiration from the existing feature selection methods. The classic *tfidf* scheme is briefly reviewed in Section 2.

H.G. Okuno and M. Ali (Eds.): IEA/AIE 2007, LNAI 4570, pp. 33–43, 2007.

Different feature selection methods are analyzed in Section 3. This is where we note four fundamental information elements. Our term weighting scheme is described in Section 4. Experimental results are reported in Section 5. Section 6 concludes.

2 Term Weighting Scheme

In information retrieval and machine learning, term weighting has long been formulated in a form as term frequency times inverse documents frequency, i.e. *tfidf* [1, 12, 13, 16]. The more popular "ltc" form [1, 12, 13] is given by,

$$tfidf(t_i, d_j) = tf(t_i, d_j) \times \log(\frac{N}{N(t_i)}) \tag{1}$$

and its normalized version is

$$w_{i,j} = \frac{tfidf(t_i, d_j)}{\sqrt{\sum_{k=1}^{|T|} tfidf(t_k, d_j)^2}} \tag{2}$$

where N and $|T|$ denote the total number of documents and unique terms contained in the collection respectively, and $N(t_i)$ represents the number of documents in the collection in which term t_i occurs at least once, and

$$tf(t_i, d_j) = \begin{cases} 1 + \log(n(t_i, d_j)), & \text{if } n(t_i, d_j) > 0 \\ 0, & \text{otherwise} \end{cases}$$

where $n(t_i,d_j)$ is the number of times that the term t_i occurs in document d_j. In practice, the summation in equation (2) is only concerned about the terms occurred in document d_j.

The significance of the classic term weighting schemes in equitation (1) and (2) is that they have embodied three fundamental assumptions of term frequency distribution in a collection of documents [2, 14]. These assumptions are:

- Rare terms are no less important than frequent terms – *idf* assumption
- Multiple appearance of a term in a document are no less important than single appearance – *tf* assumption
- For the same quantity of term matching, long documents are no more important than short documents – normalization assumption

Because of these, the "ltc" and its normalized form have been extensively studied by many researchers and show its good performance over a number of different data sets [14]. Therefore, they have become the default choice in TC.

3 Inspiration from Feature Selection

Feature selection serves as a key procedure to reduce the dimensionality of input space in order to save computation cost. It has been integrated as a default step for many learning algorithms, like artificial neuron network, *k*-nearest neighbors, decision Tree,

etc. In the research community of machine learning, the computation constraints imposed by the high dimensions of input data space and the richness of information available to maximally identify each individual object is a well known tradeoff. The ability of feature selection to capture the salient information by selecting the most important attributes, and thus making the computing tasks tractable has been shown in information retrieval and machine learning research [4, 9, 11, 20]. Furthermore, feature selection is also beneficial since it tends to reduce the over-fitting problem, in which the trained objects are tuned to fit very well the data upon which they have been built, but performs poorly when applied to unseen data [14].

In TC, several feature selection methods have been intensively studied to distill the important terms while still keeping the dimensions small. Table 1 shows the main functions of several popular feature selection methods. These methods are evolved either from the information theory or from the linear algebra literature [14, 20].

Table 1. Several feature selection methods, and their functions, where t_k denotes a term; c_i stands for a category; $P(t_k,c_i)$ denotes the probability of documents from category c_i where term t_k occurs at least once; $P(t_k,\overline{c}_i)$ denotes the probability of documents not from category c_i where term t_k occurs at least once; $P(\overline{t}_k,c_i)$ denotes the probability of documents from category c_i where term t_k does not occur; $P(\overline{t}_k,\overline{c}_i)$ denotes the probability of documents not from category c_i where term t_k does not occur

Feature Selection Method	Mathematical Form
Information Gain	$P(t_k,c_i)\log\frac{P(t_k,c_i)}{P(t_k)\cdot P(c_i)}+P(\overline{t}_k,c_i)\log\frac{P(\overline{t}_k,c_i)}{P(\overline{t}_k)\cdot P(c_i)}$
Mutual Information	$\log\frac{P(t_k,c_i)}{P(t_k)P(c_i)}$
Chi-square	$\frac{N\cdot\left[P(t_k,c_i)\cdot P(\overline{t}_k,\overline{c}_i)-P(t_k,\overline{c}_i)\cdot P(\overline{t}_k,c_i)\right]^2}{P(t_k)\cdot P(\overline{t}_k)\cdot P(c_i)\cdot P(\overline{c}_i)}$
Odds Ratio	$\log\frac{P(t_k\mid c_i)\cdot(1-P(t_k\mid\overline{c}_i))}{(1-P(t_k\mid c_i))\cdot P(t_k\mid\overline{c}_i)}$

Basically, there are two distinct ways to rank and assess the features, i.e. globally and locally. Global feature selection aims to select features which are good across all categories. Local feature selection aims to differentiate those terms that are more distinguishable for certain categories only. The sense of either 'global' or 'local' does not have much impact on the selection of method itself, but it does affect the performance of classifiers built upon different categories. In TC, the main purpose is to address whether this document belongs to a specific category. Obviously, we prefer the salient features which are unique from one category to another, i.e. a 'local' approach. Ideally, the salient feature set from one category does not have any items overlapping with those from other categories. If this cannot be avoided, then how to better present them comes into the picture.

While many previous works have shown the relative strengths and merits of these methods [4, 9, 11, 14, 20], our experience with feature selection over a number of standard or ad-hoc data sets shows the performance of such methods can be highly dependant on the data. This is partly due to the lack of understanding of different data sets in a quantitative way, and it needs further research. From our previous study of all feature selection methods and what has been reported in the literature [20], we noted when these methods are applied to text classification for term selection purpose, they are basically utilizing four fundamental information elements shown in Table 2, i.e. A denotes the number of documents belonging to category c_i where the term t_k occurs at least once; B denotes the number of documents not belonging to category c_i where the term t_k occurs at least once; C denotes the number of documents belonging to category c_i where the term t_k does not occur; D denotes the number of documents not belonging to category c_i where the term t_k does not occur.

Table 2. Fundamental information elements used for feature selection in text classification

	c_i	$\overline{c}_i$
t_k	A	B
$\overline{t}_k$	C	D

These four information elements have been used to estimate the probability listed in Table 1. Table 3 shows the functions in Table 1 as presented by these four information elements A, B, C and D.

Table 3. Feature selection methods and their formations as represented by information elements in Table 2

Method	Mathematical Form Represented by Information Elements
Information Gain	$-\frac{A+C}{N}\log\frac{A+C}{N}+\frac{A}{N}\log(\frac{A}{A+B})+\frac{C}{N}\log(\frac{C}{C+D})$
Mutual Information	$\log(AN/(A+B)(A+C))$
Chi-square	$N(AD-BC)^2/(A+C)(B+D)(A+B)(C+D)$
Odds Ratio	$\log(AD/BC)$

4 A Probability Based Term Weighting Scheme

4.1 Revisit of *tfidf*

As stated before, while many researchers believe that the term weighting schemes in the form as *tfidf* representing those three aforementioned assumptions, we understand *tfidf* in a much simpler manner, i.e.

1. Local weight - the *tf* term, either normalized or not, specifies the weight of t_k within a specific document, which is basically estimated based on the frequency or relative frequency of t_k within this document.

2. Global weight - the *idf* term, either normalized or not, defines the contribution of t_k to a specific document in a global sense.

If we temporarily ignore how *tfidf* is defined, and focus on the core problem, i.e. whether this document is from this category, we realize that a set of terms is needed to represent the documents effectively and a reference framework is required to make the comparison possible. As previous research shows that *tf* is very important [7, 12, 14] and using *tf* alone can already achieve good performance, we retain the *tf* term. Now, let us consider *idf*, i.e. the global weighting of t_k.

The conjecture is that if the term selection can effectively differentiate a set of terms T_k out from all terms T to represent category c_i, then it is desirable to transform that difference into some sort of numeric values for further processing. Our approach is to replace the *idf* term with the value that reflects the term's strength of representing a specific category. Since this procedure is performed jointly with the category membership, this basically implies that the weights of T_k are category specific. Therefore, the only problem left is how to compute such values.

4.2 Probability Based Term Weighting

We decide to compute those term values using the most direct information, e.g. *A*, *B* and *C*, and combine them in a sensible way which is different from existing feature selection measures. From Table 2, two important ratios which directly indicate terms' relevance with respect to a specific category are noted, i.e. *A*/*B* and *A*/*C*,

- *A*/*B*: it is easy to understand that if term t_k is highly relevant to category c_i only, which basically says that t_k is a good feature to represent category c_i, then the value of *A*/*B* tends to be higher.
- *A*/*C*: given two terms t_k, t_l and a category c_i, the term with a higher value of *A*/*C*, will be the better feature to represent c_i, since a larger portion of it occurs with category c_i.

In the following of this paper, we name *A*/*B* and *A*/*C* relevance indicator since these two ratios immediately indicate the term's strength in representing a category. In fact, these two indicators are nicely supported by probability estimates. For instance, *A*/*B* can be extended as (*A*/*N*)/(*B*/*N*), where *N* is the total number of documents, *A*/*N* is the probability estimate of documents from category c_i where term t_k occurs at least once and *B*/*N* is the probability estimate of documents not from category c_i where term t_k occurs at least once. In this manner, *A*/*B* can be interpreted as a relevance indicator of term t_k with respect to category c_i. Surely, the higher the ratio, the more important the term t_k is related to category c_i. A similar analysis can be made with respect to *A*/*C*. The ratio reflects the expectation that a term is deemed as more relevant if it occurs in the larger portion of documents from category c_i than other terms.

Since the computing of both *A*/*B* and *A*/C has its intrinsic connection with the probability estimates of category membership, we propose a new term weighting factor which utilizes the aforementioned two relevance indicators to replace *idf* in the classic

tfidf weighting scheme. Considering the probability foundation of *A*/*B* and *A*/*C*, the most immediate choice is to take the product of these two ratios. Finally, the proposed weighting scheme is formulated as $tf \cdot \log(1+\frac{A}{B}\frac{A}{C})$.

5 Experimental Study

Two data sets were tested in our experiment, i.e. MCV1 and Reuters-21578. MCV1 is an archive of 1434 English language manufacturing related engineering papers which we gathered by the courtesy of the Society of Manufacturing Engineers (SME). It combines all engineering technical papers published by SME from year 1998 to year 2000. All documents were manually classified [8]. There are a total of 18 major categories in MCV1. Figure 1 gives the class distribution in MCV1. Reuters-21578 is a widely used benchmarking collection [14]. We followed Sun's approach [15] in generating the category information. Figure 2 gives the class distribution of the Reuters dataset used in our experiment. Unlike Sun [15], we did not randomly sample negative examples from categories not belonging to any of the categories in our data set, instead we treated examples not from the target category in our dataset as negatives.

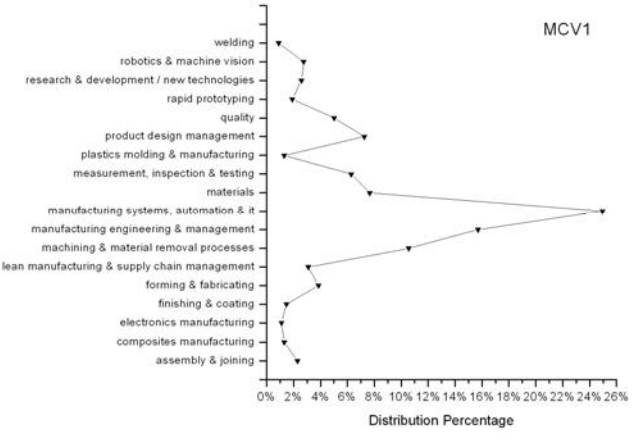

Fig. 1. Class distribution in MCV1

We compared our probability based term weighting scheme with the classic *tfidf* on MCV1 and Reuters-21578 using Bayesian classifier, i.e. Complement Naïve Bayes (CompNB) [10], and Support Vector Machine (SVM) [17] as the classification algorithms. The CompNB has been recently reported that it can significantly improve the performance of Naïve Bayes over a number of well known datasets, including Reuters-21578 and 20 Newsgroups. Various correction steps are adopted in CompNB, e.g. data transformation, better handling of word occurrence dependencies and so on. In our experiments, we borrowed the package implemented in Weka 3.5.3 Developer version [18]. For SVM, we chose the well known implementation SVM^{Light} [5, 6].

Linear function has been adopted as its kernel function, since previous work has shown that the linear function can deliver even better performance without tedious parameter tuning in TC [3, 5]. As for the performance measurement, *precision*, *recall* and their harmonic combination, i.e. the F_1 value, were calculated [1, 16]. Performance was assessed based on five-fold cross validation. Since we are very concerned about the performance of every category, we report the overall performance in macro-averaged manner, i.e. macro-average F_1, to avoid the bias for minor categories in imbalanced data associated with micro-averaged scores [14, 19].

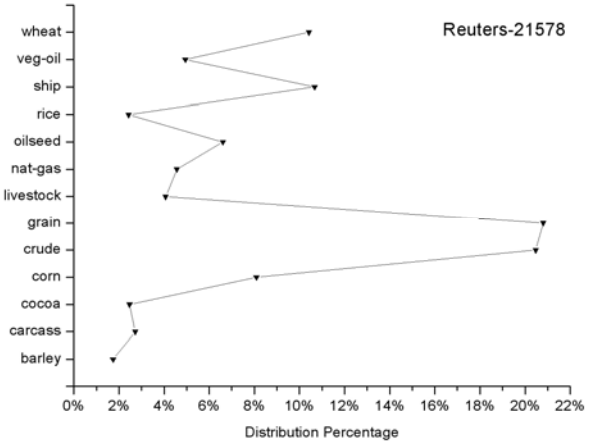

Fig. 2. Class distribution in Reuters-21578

Major standard text preprocessing steps were applied in our experiments, including tokenization, stop word and punctuation removal, and stemming. However, feature selection was skipped for SVM experiments and all terms left after stop word and punctuation removal and stemming were kept as features.

Figure 3 and 4 show the overall performance of *tfdif* and the probability based term weights on different categories in MCV1 and Reuters-21578 respectively. They are reported in terms of macro-averaged F_1 values. Our first observation is that the proposed scheme of probability based term weights is able to outperform *tfidf* over both data sets using SVM and Bayesian classifier. The results of *tfidf* based on Reuters-21578 is in line with the literature [15]. Table 4 presents the macro-averaged F_1 values of both term weighting schemes tested over two data sets. We note that using our proposed weighting scheme can improve the overall performance from 6% to more than 12%. Surprisingly, we also observe that when the probability based term weights are adopted, CompNB has delivered the result which is very close to the best one that SVM can achieve using classic *tfidf* scheme in Reuters-21578. This has demonstrated the great potential of using CompNB as a state-of-the-art classifier.

As shown in Figure 1 and Figure 2, both MCV1 and Reuters-21578 are actually skewed data sets. In MCV1, there are six categories that own only around 1% of text population each and 11 categories falling below the average. The same case also happens to the Reuters-21578 data set. While it has 13 categories, grain and crude, the

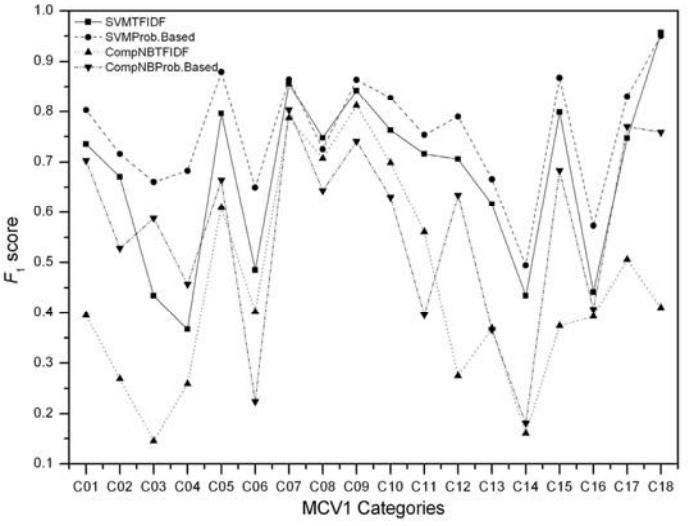

Fig. 3. F_1 scores of both *tfidf* and the probability based term weights using CompNB and SVM tested over MCV1

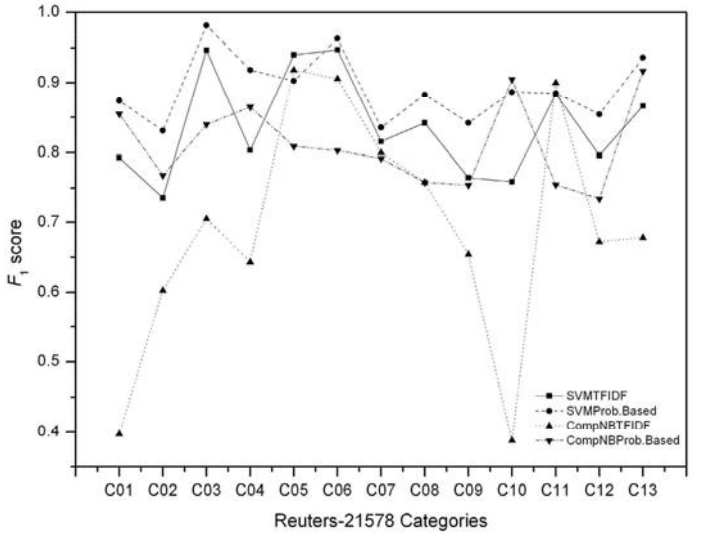

Fig. 4. F_1 scores of both *tfidf* and the probability based term weights using CompNB and SVM tested over Reuters-21578

two major categories, share around half of the text population. There are eight categories in total falling below the average. Previous literature did not report successful stories over these minor categories [15, 19].

Since our study shows that the probability based term weighting scheme works better than *tfidf* approach, we examine why this is the case. A close analysis shows that

the probability based scheme displays much better results over minor categories in both MCV1 and Reuters-21578, regardless of classifiers used. For all minor categories shown in both figures, we observed a sharp increase of performance occurs when the system's weighting method switches from *tfidf* to the probability one. Table 5 reveals more insights with respect to the system performance. In general, we observe that using the probability based term weighting scheme can greatly enhance the systems' recalls. Although it falls slightly below *tfidf* in terms of precision using SVM, it still improves the systems' precisions in CompNB, far superior to those *tfidf* can deliver. For SVM, while the averaged precision of *tfidf* in MCV1 is 0.8355 which is about 5% higher than the probability's, the averaged recall of *tfidf* is 0.6006 only, far less than the probability based's 0.7443. The case with Reuters-21578 is even more impressive. While the averaged precision of *tfidf* is 0.8982 which is only 1.8% higher than another, the averaged recall of probability based scheme reaches 0.9080, compared to *tfidf*'s 0.7935. Overall, the probability based weighting scheme surpasses *tfidf* in terms of F_1 values over both data sets.

Table 4. Macro-averaged F_1 values of *tfidf* and probability based term weights on MCV1 and Reuters-21578

	MCV1		21578	
Classifier	*tfidf*	Prob.Based	*tfidf*	Prob.Based
SVM	0.6729	0.7553	0.8381	0.8918
CompNB	0.4517	0.5653	0.6940	0.8120

Table 5. Macro-averaged *precision* and *recall* of *tfidf* and probability based term weights on MCV1 and Reuters-21578

		Precision		*Recall*	
Data	Classifier	*tfidf*	Prob.Based	*tfidf*	Prob.Based
MCV1	SVM	0.8355	0.7857	0.6006	0.7443
	CompNB	0.4342	0.6765	0.4788	0.5739
21578	SVM	0.8982	0.8803	0.7935	0.9080
	CompNB	0.5671	0.7418	0.9678	0.9128

6 Conclusion

In this paper, we have introduced a novel term weighting scheme which is generally formulated as *tf* times terms' relevance with respect to different categories. This scheme directly makes use of two critical information ratios as a new way to compute the terms' strengths in representing a category. These two ratios are nicely supported by the probability estimates which are deemed to embody the most salient information regarding terms' category membership. The experimental study using CompNB and SVM over two data sets, i.e. MCV1 and Reuters-21578,

demonstrates the merits of this new weighting scheme. Its combination with CompNB in delivering the state-of-the-art performance and the remarkable performance improvement over minor categories are noted. Its joint application with other algorithms in TC needs further exploration.

References

1. Baeza-Yates, R., Ribeiro-Neto, B.: Modern information retrieval. Addison-Wesley Longman Publishing Co, Boston (1999)
2. Debole, F., Sebastiani, F.: Supervised term weighting for automated text categorization. In: Proceedings of the 2003 ACM symposium on Applied computing (2003)
3. Dumais, S., Chen, H.: Hierarchical classification of Web content. In: Proceedings of the 23rd annual international ACM SIGIR conference on Research and development in information retrieval (SIGIR2000) (2000)
4. Forman, G.: An extensive empirical study of feature selection metrics for text classification. The Journal of Machine Learning Research, Special Issue on Variable and Feature Selection 3, 1289–1305 (2003)
5. Joachims, T.: Text categorization with Support Vector Machines: Learning with many relevant features. In: Nédellec, C., Rouveirol, C. (eds.) Machine Learning: ECML-98. LNCS, vol. 1398, Springer, Heidelberg (1998)
6. Joachims, T.: A Statistical Learning Model of Text Classification with Support Vector Machines. In: Proceedings of the 24th annual international ACM SIGIR conference on Research and development in information retrieval (2001)
7. Leopold, E., Kindermann, J.: Text Categorization with Support Vector Machines - How to Represent Texts in Input Space. Machine Learning 46, 423–444 (2002)
8. Liu, Y., Loh, H.T., Tor, S.B.: Building a Document Corpus for Manufacturing Knowledge Retrieval. In: Proceedings of the Singapore MIT Alliance Symposium (2004)
9. Ng, H.T., Goh, W.B., Low, K.L.: Feature selection, perception learning, and a usability case study for text categorization. ACM SIGIR Forum. In: Proceedings of the 20th annual international ACM SIGIR conference on Research and development in information retrieval (1997)
10. Rennie, J.D.M., Shih, L., Teevan, J., Karger, D.R.: Tackling the Poor Assumptions of Naive Bayes Text Classifiers. In: Proceedings of the Twentieth International Conference on Machine Learning (2003)
11. Ruiz, M.E., Srinivasan, P.: Hierarchical Text Categorization Using Neural Networks. Information Retrieval 5, 87–118 (2002)
12. Salton, G., Buckley, C.: Term Weighting Approaches in Automatic Text Retrieval. Information Processing and Management 24, 513–523 (1988)
13. Salton, G., McGill, M.J.: Introduction to Modern Information Retrieval. McGraw-Hill, New York (1983)
14. Sebastiani, F.: Machine Learning in Automated Text Categorization. ACM Computing Surveys (CSUR) 34, 1–47 (2002)
15. Sun, A., Lim, E.-P., Ng, W.-K., Srivastava, J.: Blocking Reduction Strategies in Hierarchical Text Classification. IEEE Transactions on Knowledge and Data Engineering (TKDE) 16, 1305–1308 (2004)
16. van_Rijsbergen, C.J.: Information Retrieval. 2nd edn. Butterworths, London, UK (1979)
17. Vapnik, V.N.: The Nature of Statistical Learning Theory, 2nd edn. Springer, New York (1999)

18. Witten, I.H., Frank, E.: Data Mining: Practical machine learning tools and techniques, 2nd edn. Morgan Kaufmann, San Francisco (2005)
19. Yang, Y., Liu, X.: A re-examination of text categorization methods. In: Proceedings of the 22nd annual international ACM SIGIR conference on Research and development in information retrieval (1999)
20. Yang, Y., Pedersen, J.O.: A Comparative Study on Feature Selection in Text Categorization. In: Proceedings of ICML-97, 14th International Conference on Machine Learning (1997)

Text Classification for Healthcare Information Support

Rey-Long Liu

Department of Medical Informatics
Tzu Chi University
Hualien, Taiwan, R.O.C.
rlliutcu@mail.tcu.edu.tw

Abstract. Healthcare information support (HIS) is essential in managing, gathering, and disseminating information for healthcare decision support through the Internet. To support HIS, text classification (TC) is a key kernel. Upon receiving a text of healthcare need (e.g. symptom description from patients) or healthcare information (e.g. information from medical literature and news), a text classifier may determine its corresponding categories (e.g. diseases), and hence subsequent HIS tasks (e.g. online healthcare consultancy and information recommendation) may be conducted. The key challenge lies on *high-quality* TC, which aims to classify most texts into suitable categories (i.e. recall is very high), while at the same time, avoid misclassifications of most texts (precision is very high). High-quality TC is particularly essential, since healthcare is a domain where an error may incur higher cost and/or serious problems. Unfortunately, high-quality TC was seldom achieved in previous studies. In the paper, we present a case study in which a high-quality classifier is built to support HIS in Chinese disease-related information, including the cause, symptom, curing, side-effect, and prevention of cancer. The results show that, without relying on domain knowledge and complicated processing, cancer information may be classified into suitable categories, with a controlled amount of confirmations.

1 Introduction

The Word-Wide Web (WWW) has been a main source of healthcare information for both health consumers and professionals. Healthcare information support (HIS) is thus essential. It aims to manage, gather, and disseminate information for healthcare decision support through the Internet. The challenging requirements of HIS lie on (1) medical information on the Internet may not be scientifically-based [10], while patients require validated healthcare information [5], (2) healthcare information should be rich in several essential aspects (e.g. cause, symptom, curing, side-effect, and prevention of a disease, e.g. [2]), (3) healthcare professionals only have a limited amount of time and effort to gather information and/or make validation, and (4) even those users that receive higher education are often unable to construct proper queries (i.e. keywords linked with conjunction and disjunction operators [3]).

1.1 Problem Definition and Motivation

In this paper, we present a case study in which HIS is approached by *high-quality* text classification (TC), which aims to classify most texts into suitable categories (i.e.

H.G. Okuno and M. Ali (Eds.): IEA/AIE 2007, LNAI 4570, pp. 44–53, 2007.

recall is very high), and avoid misclassifications of most texts (precision is very high). More specifically, we explore the extent to which a high-quality classifier may help to manage, gather and disseminate Chinese disease-related information, including the cause, symptom, curing, side-effect, and prevention of cancers.

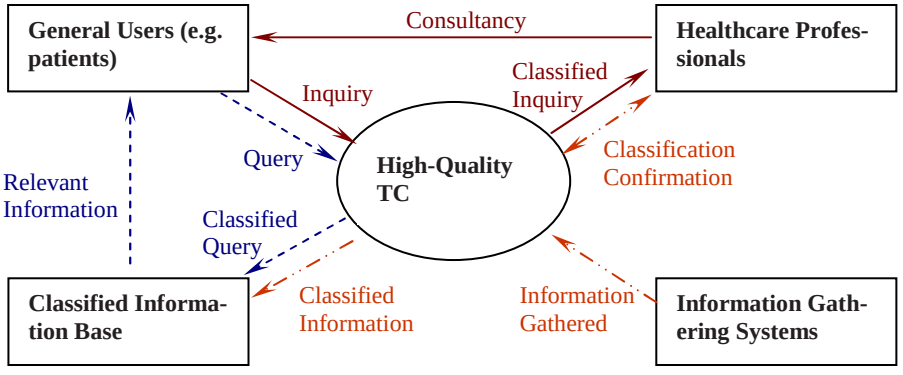

Fig. 1. High-quality TC for healthcare information support

High-quality TC is particularly essential since healthcare is a domain in which any processing error may incur higher cost and/or serious problems. Figure 1 illustrates the contributions of a high-quality classifier to HIS: (1) patients may employ natural language to express their interests (e.g. symptoms of diseases), which are classified to retrieve relevant information or send consultancy inquiries more precisely and completely, and (2) healthcare professionals may be consulted only when necessary to validate the classifier's decision (e.g. classifying the information gathered using various techniques, e.g. [10]) or respond to a patient's inquiries (e.g. online health consultancy services provided by many web sites). High-quality TC is thus essential for both patients and healthcare professionals in health promotion.

1.2 Main Challenges

Main challenges of the study lie on high-quality TC. Previous TC techniques often delegate a classifier to each category. The classifier is associated with a threshold, and upon receiving a document, it autonomously makes a yes-no decision for the corresponding category. Conceptually, a document is "accepted" by the classifier if its degree of acceptance (DOA) with respect to the category (e.g. similarity with the category or probability of belonging to the category) is higher than or equal to the corresponding threshold; otherwise it is "rejected." With the help of the thresholds, each document may be classified into zero, one, or several categories. Unfortunately, in practice, most classifiers may not be perfectly built and tuned [1] [6] [14], due to several common problems: (1) imperfect selection of training documents (e.g. noises, over-fitting and content ambiguities) and (2) imperfect system setting (e.g. parameter setting and feature selection). These problems are often inevitable and may incur improper DOA estimations. A document that belongs to (does not belong to) a category

could not always get a higher (lower) DOA value with respect to the category. Improper DOA estimations may heavily deteriorate the performance of TC.

Therefore, it is difficult to have a classifier that may achieve very high performances in both precision and recall. Low precision incurs the problem of false information recommendation, while low recall incurs the problem of incomplete information recommendation. Both problems are essential for HIS, especially when the information is critical for health promotion.

1.3 Contributions and Organization of the Paper

Section 2 explores the feasibility of employing interactive confirmations to approach high-quality TC. The main idea is to consult healthcare professionals to make confirmations to *some* of the TC decisions made by the classifier. Its challenge lies on the tradeoff between TC performance and cognitive load of the professionals in making confirmations: higher TC performance often incurs heavier cognitive load. Accordingly, in section 3 we present a confirmation strategy to achieve high-quality TC. To empirically evaluate the strategy, section 4 reports a case study in which real-world Chinese healthcare information about several categories of cancer are tested. The result shows that the strategy significantly performs better than baseline techniques. Moreover, without relying on any domain knowledge and complicated text processing, those diseases corresponding to Chinese descriptions of symptoms may be identified, making subsequent HIS tasks more targeted.

2 Interactive Confirmations for High-Quality TC

When classifiers have been built and tuned to their best extent, system-user interaction should be a final approach to confirm the classifier's decision to achieve high-quality TC. Therefore, the goal of employing interactive confirmation for high-quality TC differs from many previous attempts, which often aimed at improving the classifier building process (e.g. iterative classifier refinement [11]), the threshold tuning process (e.g. [6]), and the document selection process (e.g. boosting [8], adaptive resampling [4], and query zoning [9]).

The challenge of the confirmation lies on the tradeoff between the performance of TC and the cognitive load incurred to health professionals. To achieve higher-quality TC, the system often needs to consult the professionals more often, and hence increase the cognitive load in reading and validation. Conversely, to reduce the cognitive load of the professionals, the system should make decisions on its own, and hence deteriorate the performance of TC. To simultaneously achieve high-quality TC and control the cognitive load, the system should be intelligent enough to consult the professionals only when necessary. The intelligent behavior is a key challenge that did not get much attention in previous TC studies.

2.1 Evaluation Criteria

Since the ideal case is to achieve high-quality TC with a limited amount of interactive confirmations, there should be two criteria: *Confirmation Precision* (CP) and *Confirmation Recall* (CR). CP is measured by [number of necessary confirmations conducted) / [number of confirmations conducted]. Since a confirmation for a decision is

necessary if and only if the decision is wrong, CP may also be defined by [number of wrong decisions identified] / [number of decisions identified as potentially wrong]. On the other hand, CR is measured by [number of necessary confirmations conducted] / [number of confirmations that should be conducted]. Similarly, it may also be defined by [number of wrong decisions identified] / [number of wrong decisions that should be identified].

It is interesting to note that, CR is related to the quality of TC, while CP is related to the cognitive load incurred to the professional. To help the classifier to achieve perfect performance (both precision and recall of TC are 100%), CR should be 100%, indicating that all wrong decisions are identified for the professional to confirm (and hence be corrected by the professional). On the other hand, an extremely low CP may incur a very heavy cognitive load to the professional (e.g. when all decisions call for confirmations, CP will approach 0 and hence the classifier becomes nearly useless). Therefore, interactive high-quality TC aims to achieve nearly 100% in CR, under the requirement that CP should be as high as possible.

2.2 Straightforward Confirmation Strategies

Based on the criteria, there are two straightforward confirmation strategies to pursue interactive high-quality TC: *Uniform Confirmation* (UC) and *Probabilistic Confirmation* (PC). For each category *c*, both strategies are based on threshold tuning documents (i.e. validation documents [12]), which are either positive (belonging to *c*) or negative (not belong to *c*). UC sets a confirmation range. Once a document's DOA value falls in the range, a confirmation is conducted. Since the goal is to achieve high CR, UC sets a range that is large enough to cover the DOA values of those documents for which the classifier might make mistakes. The lower limit of the range may be set to the maximum DOA value below which no DOA values of positive documents lie. On the other hand, the upper limit may be set to the minimum DOA value beyond which no DOA values of negative documents lie. Obviously, UC may incur lower CP, and hence incur heavier cognitive load.

On the other hand, PC works for those classifiers that tune a threshold to optimize performance in some criterion, such as the popular F_1 measure, which integrates precision and recall by [2×precision×recall / (precision+recall)]. PC is based on the observation that those documents whose DOA values are closer to the threshold tend to have a higher probability of leading the classifier to make erroneous decisions. Suppose DOA values fall in the range of [*Min*, *Max*]. The probability of conducting a confirmation for a document with respect to a category is:

$$\begin{aligned} \text{Prob(confirmation)} &= (D - Max) / (T - Max), \text{ if } D \geq T; \\ &= (D - Min) / (T - Min), \text{ otherwise,} \end{aligned}$$

where D is the DOA value of the document with respect to the category, and T is the threshold tuned for the category. Obviously, PC hopes to promote CP, but may incur lower CR, and hence has difficulties in guaranteeing the classifier's performance.

Therefore, both UC and PC are not good enough to achieve interactive high-quality TC, which aims to achieve very high CR, under the requirement that CP should be as high as possible. To develop a more effective confirmation strategy, the main technical

issue lies on, among the decisions made by the classifier, intelligently identifying those decisions that deserve confirmations.

3 Intelligent Confirmation by Content Overlap Measurement

We present an intelligent confirmation technique for interactive high-quality TC. The technique is named ICCOM (Intelligent Confirmation by Content Overlap Measurement). The basic idea is to associate each category's classifier with ICCOM. Once a document is entered, the classifier is invoked to make its decision (either acceptance or rejection). Based on the decision, ICCOM is invoked to determine whether a confirmation is required. Therefore, the integrated system makes three kinds of decisions: acceptance, rejection, and confirmation. The expert is consulted only when the decision is confirmation.

Content overlap measurement (COM) is a key basis on which ICCOM makes decisions. It aims to measure the *degree of content overlap* (DCO) between a document and a category [7]. The basic idea is that if DCO between *c* and *d* is not high enough, *d* should not be classified into *c*, even though *d* mentions some content of *c*. COM is particularly helpful for previous TC techniques in which whether a feature may be selected mainly depends on content relatedness among the categories, without paying much attention to how the contents of a category *c* and a document *d* overlap with each other (i.e. DCO).

Table 1 presents the algorithm for COM. Given a category *c* and a document *d*, the algorithm considers two kinds of terms: those terms that are *positively correlated* with *c* but do not appear in *d* (ref. Step 2), and those terms that are *negatively correlated* with *c* but appear in *d* (ref. Step 3). Both kinds of terms lead to the reduction of DCO (ref. Step 2.1 and 3.1). Therefore, a smaller DCO indicates that *d* talks more information not in *c*, and vice versa. In that case, it is less proper to classify *d* into *c*.

Table 1. Content Overlap Measurement

Procedure *COM*(*c*, *d*), where
(1) *c* is a category,
(2) *d* is a document for thresholding or testing
Return: Degree of content overlap (DCO) between *d* and *c*
Begin
(1) DCO = 0;
(2) For each term *t* that is positively correlated with *c* but does not appear in *d*, do
(2.1) DCO = DCO - $\chi^2(t,c)$;
(3) For each term *t* that is negatively correlated with *c* but appears in *d*, do
(3.1) DCO = DCO - (number of occurrences of *t* in *d*) $\times \chi^2(t,c)$;
(4) Return DCO;
End.

The correlation strengths is estimated by χ^2 (chi-square). For a term *t* and a category *c*, $\chi^2(t,c) = [N \times (A \times D - B \times C)^2] / [(A+B) \times (A+C) \times (B+D) \times (C+D)]$, where N is the total number of documents, A is the number of documents that are in *c* and contain *t*, B

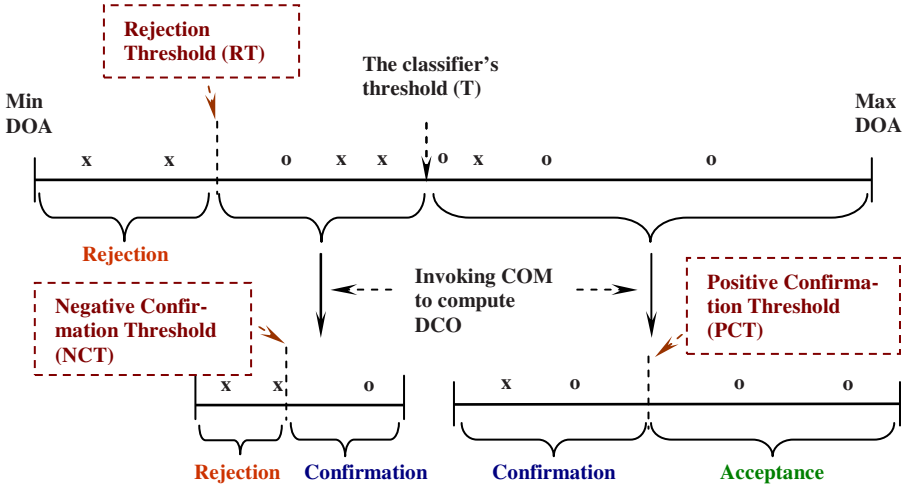

Fig. 2. Threshold tuning to identify confirmation zones (o: positive validation document; x: negative validation document)

is the number of documents that are not in *c* but contain *t*, C is the number of documents that are in *c* but do not contain *t*, and D is the number of documents that are not in *c* and do not contain *t*. Therefore, $\chi^2(t,c)$ indicates the strength of correlation between *t* and *c*. We say that *c* and *t* are *positively correlated* if A×D > B×C; otherwise they are *negatively correlated*. Note that, a term *t* may even appear in *d* but not in any training document. It needs to be considered when measuring DCO between *d* and *c* (ref. Step 3). However, its χ^2 value is incomputable (since both A and B are zero). ICCOM tackles the problem by treating *d* as a training document, and hence incrementing N and B by 1.

For each category, ICCOM collaborates with the classifier by tuning three thresholds: *rejection threshold* (RT), *positive confirmation threshold* (PCT) and *negative confirmation threshold* (NCT). As illustrated in Figure 2, the three thresholds work together to help the system to make decisions: rejection, acceptance, or confirmation. RT is used to identify those documents whose DOA values are too low, and hence may be rejected without any confirmation (i.e. rejection). PCT is used to check whether a document is accepted by both the classifier (i.e. DOA value ≥ the classifier's threshold T) and COM (i.e. DCO value ≥ PCT). If so, the document is accepted without confirmation (i.e. acceptance); otherwise a confirmation is required (i.e. confirmation). Similarly, NCT is used to check whether a document is rejected by both the classifier (i.e. DOA value < the classifier's threshold T) and COM (i.e. DCO value ≤ NCT). If so, the document is rejected without confirmation (i.e. rejection); otherwise a confirmation is required (i.e. confirmation).

4 A Case Study on Chinese HIS for Cancer

We present a case study to illustrate the contributions of ICCOM. In the case study, the targeted users include patients and healthcare professionals that use Chinese as

their native language. The disease domain is cancer. As noted in Section 1.1, with the support of the classifier, (1) patients may employ natural language to express their interests (e.g. symptoms), which are classified to retrieve relevant information or send consultancy inquiries, and (2) healthcare professionals are consulted only when necessary to validate the classifier's decision or respond to patients' inquiries.

4.1 Experimental Data

Experimental data is collected from Yahoo! at Taiwan (http://tw.yahoo.com/). We focus on 16 types of cancers (e.g. liver cancer, lung cancer, …, etc.), which are top-ranked by the department of health in Taiwan. For each type of cancer, documents are collected by sending its Chinese name as a query to the "知識+" (knowledge+) area. The documents are then selected and separated into 5 categories: cause, symptom, curing, side-effect, and prevention of the type of cancer. Therefore, there are totally 80 (=16×5) categories. They contain 2850 documents. We randomly select 1/10 of the documents as test documents, and the others as training documents.

As suggested by previous studies (e.g. [12]), the set of training documents is split into two subsets: the *classifier building* subset and the *threshold tuning* (or validation) subset. The former was used to build the classifier, while the latter was used to tune a threshold for each category. Both sets have the same number of documents. A 2-fold cross validation is conducted so that each training document is used for both classifier building and threshold tuning only once.

4.2 Evaluation Criteria

To measure the systems' performances, we employ two groups of criteria: (1) criteria to evaluate the effectiveness of confirmation, and (2) criteria to evaluate the quality of TC. For the former, we employ the criteria defined in Section 2: CP and CR. For the latter, we employ the popular criteria: *precision* (P), *recall* (R), and F_1. P is equal to [total number of correct classifications / total number of classifications made], R is equal to [total number of correct classifications / total number of correct classifications that should be made], and F_1 is equal to 2PR/(P+R).

Note that when measuring F_1, we assume that each confirmation request issued by the systems may get a correct answer (rejection or acceptance). With the assumption, CR is directly related to the system's performances in F_1 (and hence both P and R), since a higher CR means that more errors are identified and hence corrected (if necessary) by confirmations.

4.3 The Underlying Classifier and Confirmation Strategies

We employ the Rocchio's classifier (RO) as the underlying classifier. RO was commonly employed in text classification (e.g. [11]) and filtering (e.g. [8] [9]). Some studies even showed that its performances were more promising in several ways (e.g. [5] [6]). RO constructs a vector for each category, and the similarity between a document *d* and a category *c* is estimated using the cosine similarity between the vector of *d* and the vector of *c*. More specifically, the vector for a category *c* is constructed by considering both

relevant documents and non-relevant documents of c: $\eta_{1*}\sum_{Doc\in P}Doc/|P| - \eta_{2*}\sum_{Doc\in N}Doc/|N|$, where P is the set of vectors for relevant documents (i.e. the documents in c), while N is the set of vectors for non-relevant documents (i.e. the documents not in c). We set η_1=16 and η_2=4, since the setting was shown to be promising in previous studies (e.g. [11]).

RO requires a fixed (predefined) feature set, which is built using the documents for classifier building. After removing stop words, all Chinese characters may be candidate features. No domain knowledge and lexical processing are employed. The features are selected according to their weights estimated by the χ^2 (chi-square) weighting technique. The technique was shown to be more promising than others [13]. To conduct more thorough investigation, we try various feature set sizes.

To make TC decisions, RO also requires a thresholding strategy to set a threshold for each category. As in many previous studies (e.g. [8] [12] [14]), RO tunes a relative threshold for each category by analyzing document-category similarities. The threshold tuning documents are used to tune each relative threshold. As suggested by many studies (e.g. [12]), the thresholds are tuned in the hope to optimize the system's performance with respect to F_1.

To measure the contribution of ICCOM with respect to other confirmation strategies, we implement the two baseline confirmation strategies presented in Section 2: UC and PC. Therefore, we have three versions: RO+ICCOM, RO+UC, and RO+PC, which enhance RO with ICCOM, UC, and PC, respectively.

4.4 Results

Table 2 summarizes the experimental results in classifying all test documents into the 80 categories. We focus on the best version of RO under different sizes of feature set (FS). The results show that only UC and ICCOM may help RO to achieve very high F_1 (> 0.94). However, CP of ICCOM is significantly better than UC (31.8% improvement in the 1st fold and 60.8% improvement in the 2nd fold), indicating that ICCOM enhances RO to achieve high-quality TC with fewer confirmations.

Table 2. Classification of cancer information

	Best F_1 by RO	**F_1 by RO+PC**	**CP of RO+PC**	**F_1 by RO+UC**	**CP of RO+UC**	**F_1 by RO+ICCOM**	**CP of RO+ICCOM**
1st fold	0.3485 (FS=1500)	0.8413	0.0969	0.9610	0.0848	0.9607	0.1117
2nd fold	0.3270 (FS=1500)	0.7823	0.1037	0.9656	0.0725	0.9433	0.1166

We are also interested in symptom categories for the 16 cancer types. Experiments on the categories may measure the performance of the system in classifying patients' natural language symptom descriptions for cancer type identification. In testing, we remove cancer names in the test documents, since in practice patients often do not know cancer types for their symptoms. Table 3 summarizes the results. Although all the confirmation strategies may help RO to achieve very high F_1, ICCOM achieves the best CP again. The improvement ranges from 40.5% to 170.5%. For the 40 test

symptom documents, RO+ICCOM conducts 35 and 51 confirmations in the 1st and 2nd folds, respectively. Therefore, to achieve high-performance cancer type identification, only about 1 confirmation is required for a symptom description. The confirmation (i.e. possible cancer types) may provide the patients with additional reference to reduce possible identification errors.

Table 3. Classification of symptom description without cancer names

	Best F_1 by RO	F_1 by RO+PC	CP of RO+PC	F_1 by RO+UC	CP of RO+UC	F_1 by RO+ICCOM	CP of RO+ICCOM
1st fold	0.8919 (FS=300)	0.9610	0.0676	0.9744	0.1017	0.9610	0.1429
2nd fold	0.8718 (FS=300)	0.9620	0.1000	0.9750	0.0580	0.9744	0.1569

5 Conclusion and Future Work

Text classification is a key kernel to provide healthcare information support through the Internet. It helps to manage, gather, and disseminate healthcare information for decision support. Since healthcare is a domain where a classification error may incur high cost and/or serious problems, the classifier should be "conservative" in the sense that, when it is possible to make an error, a confirmation request should be issued to healthcare professionals or patients. For healthcare professionals, the confirmation request suggests the professionals to make validation only when necessary. For patients, the confirmation request provides an additional reference for patients to consider. The key challenge lies on the identification of possible errors for confirmation. In this paper, we present an intelligent conformation strategy, and explore its contributions in a case study on Chinese cancer information. The results are of practical significance to healthcare information support through the Internet. Future research directions lie on the development of an intelligent interface, which employs system-user interaction to elicit more detailed descriptions (e.g. symptoms) from users when users' original descriptions are not precise enough for classification.

Acknowledgments. This research was supported by the National Science Council of the Republic of China under the grants NSC 95-2221-E-320-002.

References

1. Arampatzis, A., Beney, J., Koster, C.H.A., van der Weide, T.P.: Incrementality, Half-life, and Threshold Optimization for Adaptive Document Filtering. In: Proceedings of the 9th Text Retrieval Conference (2000), pp. 589–600. Gaithersburg, Maryland (2000)
2. Fahey, D.K., Weinberg, J.: LASIK Complications and the Internet: Is the Public being Mislead? Journal of Medical Internet Research 5(1) (2003)
3. Ivanitskaya, L., O'Boyle, I., Casey, A.M.: Health Information Literacy and Competencies of Information Age Students: Results From the Interactive Online Research Readiness Self-Assessment (RRSA). Journal of Medical Internet Research 8(2), e6 (2006)

4. Iyengar, V.S., Apte, C., Zhang, T.: Active Learning using Adaptive Resampling. In: Proceedings of the 6th ACM SIGKDD International Conference on Knowledge Discovery and Data Mining, pp. 91–98. Boston, Massachusetts (2000)
5. Kittler, A.F., Hobbs, J., Volk, L.A., Kreps, G.L., Bates, D.W.: The Internet as a Vehicle to Communicate Health Information During a Public Health Emergency: A Survey Analysis Involving the Anthrax Scare of 2001, Journal of Medical Internet Research 6(1) (2004)
6. Liu, R.-L., Lin, W.-J.: Adaptive Sampling for Thresholding in Document Filtering and Classification. Information Processing and Management 41(4), 745–758 (2005)
7. Liu, R.-L.: Dynamic Category Profiling for Text Filtering and Classification. Information Processing and Management 43(1), 154–168 (2007)
8. Schapire, R.E., Singer, Y., Singhal, A.: Boosting and Rocchio Applied to Text Filtering. In: Proceedings of the 21st annual international ACM SIGIR conference on research and development in information retrieval, pp. 215–223. Melbourne, Australia (1998)
9. Singhal, A., Mitra, M., Buckley, C.: Learning Routing Queries in a Query Zone. In: Proceedings of the 20th annual international ACM SIGIR conference on research and development in information retrieval, pp. 25–32. Philadelphia, Pennsylvania (1997)
10. Tang, T.T., Hawking, D., Craswell, N., Griffiths, K.: Focused Crawling for both Topical Relevance and Quality of Medical Information. In: Proceedings of the ACM 14th Conference on Information and Knowledge Management, pp. 147–154. Bremen, Germany (2005)
11. Wu, H., Phang, T.H., Liu, B., Li, X.: A Refinement Approach to Handling Model Misfit in Text Categorization. In: Proceedings of the 8th ACM SIGKDD International Conference on Knowledge Discovery and Data Mining, pp. 207–216. Edmonton, Alberta, Canada (2002)
12. Yang, Y.: A Study of Thresholding Strategies for Text Categorization. In: Proceedings of the 24th annual international ACM SIGIR conference on research and development in information retrieval, pp. 137–145. New Orleans, Louisiana (2001)
13. Yang, Y., Pedersen, J.O.: A Comparative Study on Feature Selection in Text Categorization. In: Proceedings of the 14th International Conference on Machine Learning, pp. 412–420. Nashville, Tennessee (1997)
14. Zhang, Y., Callan, J.: Maximum Likelihood Estimation for Filtering Thresholds. In: Proceedings of the 24th annual international ACM SIGIR conference on research and development in information retrieval, pp. 294–302. New Orleans, Louisiana (2001)

Nurse Scheduling Using Fuzzy Multiple Objective Programming

Seyda Topaloglu and Hasan Selim

Dokuz Eylul University, Department of Industrial Engineering, 35100, Izmir, Turkey
seyda.topaloglu@deu.edu.tr, hasan.selim@deu.edu.tr

Abstract. Nurse scheduling is a complex scheduling problem and involves generating a schedule for each nurse that consists of shift duties and days off within a short-term planning period. The problem involves multiple conflicting objectives such as satisfying demand coverage requirements and maximizing nurses' preferences subject to a variety of constraints imposed by legal regulations, personnel policies and many other hospital-specific requirements. The inherent nature of the nurse scheduling problem (NSP) bears vagueness of information on target values of hospital objectives and on personal preferences. Also, the ambiguity of the constraints is some source of uncertainty that needs to be treated in providing a high quality schedule. Taking these facts into account, this paper presents the application of Fuzzy Set Theory (FST) within the context of NSP and proposes a fuzzy goal programming model. To explore the viability of the proposed model, computational experiments are presented on a real world case problem.

Keywords: Fuzzy system applications, Planning and scheduling.

1 Introduction

Nurse scheduling problem (NSP) consists of generating a configuration of individual schedules which are patterns of days off and on for each nurse, over a given planning horizon. The scheduling of nurses is particularly challenging because hospitals work around the clock and face fluctuating service demand on different days and shifts. Besides, there are conflicting viewpoints of the hospital and the nursing staff. Hospitals are required to fulfill minimum demand coverage during each shift, while nurses want individualized schedules that take into account their preferences.

Nurses make preference concerning total work hours to be assigned for the planning period, requested days off, shift types and work patterns. A critical measure for the quality of a nurse schedule is the perceived fairness or balance for nurses. If some nurses feel that their preferences are continually being ignored, bickering, absenteeism, low morale, poor job performance and high turnover rates will start to be seen. For these reasons, it is important to satisfy nurses' preferences evenly.

The NSP is subject to a variety of constraints which can be divided into two classes generally: hard constraints and soft constraints. Hard constraints usually include demand coverage requirements, while soft constraints include all the restrictions on personal schedules and are generally referred to as time related constraints such as

H.G. Okuno and M. Ali (Eds.): IEA/AIE 2007, LNAI 4570, pp. 54–63, 2007.

consecutive shift type restrictions, minimum and maximum consecutive working days, complete weekend off, nurses' preferences or requirements.

Traditional methods such as linear programming, integer programming and networks have been employed to solve the NSP [1,2]. When these methods are unable to cope with the complex nature of the NSP, artificial intelligence methods, heuristics, and metaheuristics have been developed for its solution [3,4].

As pointed in Burke et al. [5], nurse scheduling in hospital environments presents a range of objectives and requirements. For example, maximizing staff preferences may conflict with an objective that requires a certain number of staff to work a certain shift. Actually, the characteristic of this problem is that it is often over-constrained by personnel preferences and priorities. In case where there are multiple goals with priorities, goal programming (GP) and other tools have been used [6,7]. Much of the decision making in the real world takes place in an environment in which the goals, the constraints, and the consequences of the possible actions are not known precisely. In such cases, Fuzzy Set Theory (FST) [8] provides the appropriate framework.

In the real world applications of NSP, vagueness of information on target values of management objectives and on personal preferences, and ambiguity of the constraints are some source of uncertainty that need to be treated in providing a higher quality schedule. As emphasized by Burke et al. [5], there is a certain amount of promise in investigating fuzzy methodologies as an attempt to address the dynamic nature of the NSP problem in practice and to deal with the inherent uncertainty. To the best of our knowledge, no work has been carried out by now on addressing and dealing with the uncertainty that is inherent in the NSP using fuzzy modeling approach.

Considering the aforementioned needs, and the gap in the existing literature, this paper presents the application of FST within the context of NSP. More specifically, a fuzzy multi-objective goal programming model is developed to consider uncertainty in the target values of the hospital management and nurses' preferences. To confirm the viability of the proposed model, a real world application is provided. To provide the decision maker for a more confident solution set for policy decision making, a sensitivity analysis is presented.

2 The Proposed Model

The following indices, parameters and decision variables are considered for the formulation of the model.

Indices

n	number of nurses
m	number of days within the scheduling horizon (m = 14)
i	index for nurses; i = 1,…,n
j	index for the day of the week; j = 1,…,m
k	shift type; k = 0,1,2, and 3 (off day, day, evening and night shifts, respectively)
p	scheduling period; p = 1, 2, and 3 (day: 7 am-15 pm, evening: 15 pm-23 pm and night: 23 pm-7 am periods of a work day, respectively)
w	index for weeks, w=1, 2
D_w	set of weekend days in week w

Parameters

a_{pk} 1 if shift type k contains period p, 0 otherwise
dur_k duration of shift type k
lwh, uwh lower and upper bounds on total working hours of nurses for the scheduling period
whn_i the most preferred total working hour of nurse i
ld_{jp}, ud_{jp} lower and upper bounds on demand for nurses on day j in period p
st_{ik} preference score of nurse i for shift type k to be assigned
do_{ij} preference score of nurse i for day j to be off; j = 1,.., m-2 (weekend is considered as a single day, e.g., do_{i6} stands for the preference score of nurse i for the first weekend off over the two-week planning horizon)
max_st maximum preference score a nurse can achieve if assigned to all preferred shift types
min_st minimum preference score a nurse receives if assigned to the most undesirable shift types
max_do maximum preference score a nurse can achieve if all her/his requested days off are scheduled
min_do minimum preference score a nurse receives if all her/his requested days off are ignored
max_off maximum number of off-on-off patterns that a schedule can acquire
min_off minimum number of off-on-off patterns that a schedule can acquire
max_on maximum number of on-off-on patterns that a schedule can acquire
min_on minimum number of on-off-on patterns that a schedule can acquire

Decision variables

X_{ijk} 1 if nurse i is assigned to shift type k on day j, 0 otherwise
Y_{iw} 1 if nurse i takes the weekend off in week w, 0 otherwise
off_p_{ij} the amount of positive deviation from the undesirable isolated day/evening/night shifts on pattern for nurse i on day j
on_p_{ij} the amount of positive deviation from the undesirable isolated days off pattern for nurse i on day j
μ_{Hjp} membership function for demand coverage hospital objective in period p on day j
μ_{N1i} membership function for total working hour preference of nurse i
μ_{N2i} membership function for shift type preference of nurse i
μ_{N3i} membership function for requested days off preference of nurse i
μ_{N4i} membership function for the number of off-on-off patterns in the schedule of nurse i
μ_{N5i} membership function for the number of on-off-on patterns in the schedule of nurse i

Constraints

A nurse should either take a day off or be assigned to an available shift on each work day.

$$\sum_{k=0}^{3} X_{ijk} = 1 \quad \text{for all } i = 1,..,n \text{ and } j = 1,\ldots,m \tag{1}$$

Total work hours of a nurse should be greater that the specified lower bound.

$$\sum_{j=1}^{m}\sum_{k=1}^{3} dur_k X_{ijk} \geq lwh \quad \text{for all } i = 1,..,n \tag{2}$$

Total working hours of a nurse should not exceed the specified upper bound.

$$\sum_{j=1}^{m}\sum_{k=1}^{3} dur_k X_{ijk} \le uwh \quad \text{for all } i = 1,..,n \tag{3}$$

The minimum staff level for each period of a work day should be met.

$$\sum_{i=1}^{n}\sum_{k=1}^{3} a_{pk} X_{ijk} \ge ld_{jp} \qquad \text{for all } j = 1,\ldots,m \text{ and } p = 1,2,3 \tag{4}$$

A nurse should not work more than five consecutive days.

$$\sum_{k=1}^{3}(X_{ijk} + X_{i(j+1)k} + X_{i(j+2)k} + X_{i(j+3)k} + X_{i(j+4)k} + X_{i(j+5)k}) \le 5$$
$$\text{for all } i = 1,..,n \text{ and } j = 1,\ldots,m\text{-}5 \tag{5}$$

A nurse should take at least 12 hours off between consecutive shifts. For this reason, the following constraint sets (6), (7), (8) and (9) are required. For example, constraint set (6) ensures that no nurse is assigned to a day shift immediately after a night shift.

$$X_{ij3} + X_{i(j+1)1} \le 1 \qquad \text{for all } i = 1,..,n \text{ and } j = 1,\ldots,m\text{-}1 \tag{6}$$

$$X_{ij3} + X_{i(j+1)2} \le 1 \qquad \text{for all } i = 1,..,n \text{ and } j = 1,\ldots,m\text{-}1 \tag{7}$$

$$X_{ij2} + X_{i(j+1)1} \le 1 \qquad \text{for all } i = 1,..,n \text{ and } j = 1,\ldots,m\text{-}1 \tag{8}$$

$$X_{ij1} + X_{i(j+1)3} \le 1 \qquad \text{for all } i = 1,..,n \text{ and } j = 1,\ldots,m\text{-}1 \tag{9}$$

Constraint sets (10) and (11) ensure that a nurse is assigned at least two consecutive days in a particular shift.

$$X_{i2k} \ge X_{i1k} \qquad \text{for all } i = 1,..,n \text{ and } k = 1,2,3 \tag{10}$$

$$X_{i(j-1)k} + X_{i(j+1)k} \ge X_{ijk} \qquad \text{for all } i = 1,..,n \; j = 2,\ldots,m\text{-}1 \text{ and } k = 1,2,3 \tag{11}$$

Constraint sets (12) and (13) are required to indicate whether a nurse takes the weekend off in the assumed work week.

$$\sum_{j \in D_w} X_{ij0} - 2Y_{iw} \ge 0 \qquad \text{for all } i = 1,..,n \text{ and } w \in W \tag{12}$$

$$\sum_{j \in D_w} X_{ij0} - Y_{iw} \le 1 \qquad \text{for all } i = 1,..,n \text{ and } w \in W \tag{13}$$

It is attempted to avoid off-on-off and on-off-on patterns in each nurse's schedule. The occurrence of this pattern is indicated by the off_p_{ij} and on_p_{ij} variables in constraints (14) and (15), respectively.

$$X_{ij0} + \sum_{k=1}^{3} X_{i(j+1)k} + X_{i(j+2)0} - off\_p_{ij} \le 2 \qquad \text{for all } i = 1,..,n \text{ and } j = 1,\ldots,m\text{-}2 \tag{14}$$

$$\sum_{k=1}^{3} X_{i(j+1)k} + X_{i(j+1)0} + \sum_{k=1}^{3} X_{i(j+1)k} - on\_p_{ij} \le 2 \quad \text{for all } i = 1,..,n \text{ and } j = 1,\ldots,m\text{-}2 \tag{15}$$

As mentioned previously, we consider uncertainty in hospital's objective of fulfilling demand coverage and in nurses' objectives which are the satisfaction of their preferences concerning total work load, desired shift types, requested days off and work patterns. The trapezoidal type membership function is used for the hospital objective, while trapezoidal and triangular types are used for nurses' objectives. Graphical illustrations of some of these membership functions and their corresponding formulations are presented below:

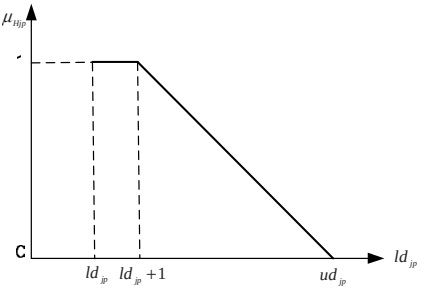

Fig. 1. Membership function for hospital's objective of fulfilling demand coverage

$$\mu_{Hjp} = \begin{cases} 1 & \text{if } ld_{jp} \le \sum_{i=1}^{n}\sum_{k=1}^{3} a_{pk} X_{ijk} \le (ld_{jp}+1) \\ \dfrac{ud_{jp} - \sum_{i=1}^{n}\sum_{k=1}^{3} a_{pk} X_{ijk}}{ud_{jp} - (ld_{jp}+1)} & \text{if } (ld_{jp}+1) \le \sum_{i=1}^{n}\sum_{k=1}^{3} a_{pk} X_{ijk} \le ud_{jp} \\ 0 & \text{if } \sum_{i=1}^{n}\sum_{k=1}^{3} a_{pk} X_{ijk} \ge ud_{jp} \end{cases} \tag{16}$$

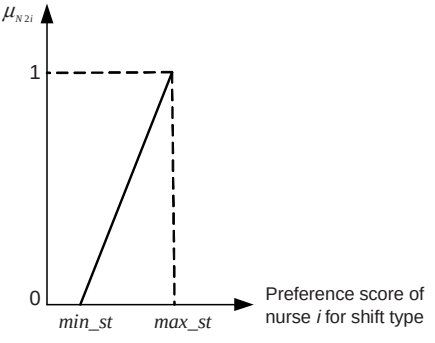

Fig. 2. Membership function for shift type preference

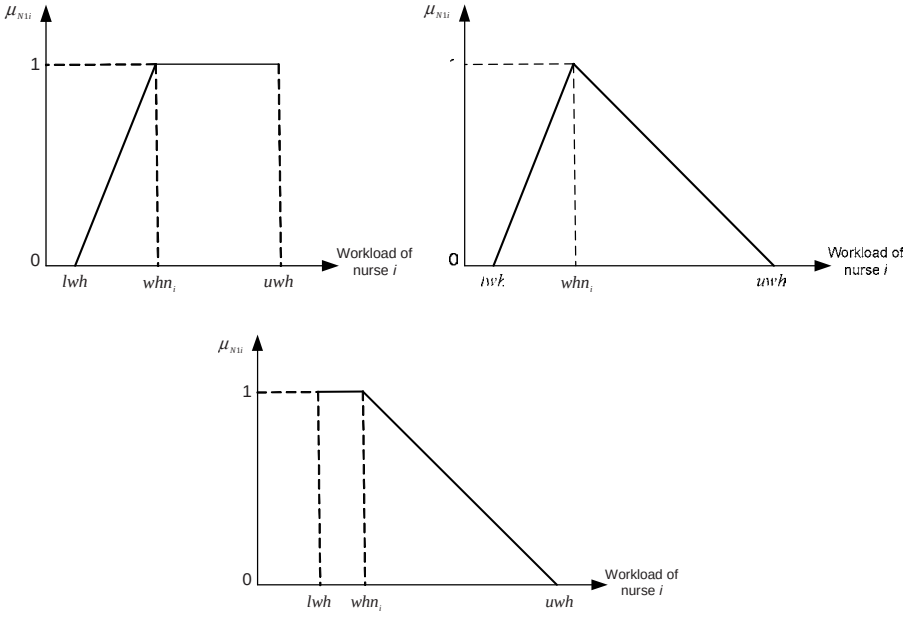

Fig. 3. Some examples for the membership functions defined for nurses' total working hour preference

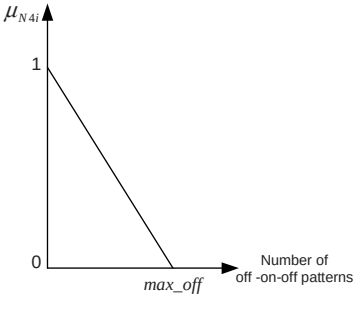

Fig. 4. Membership functions for the number of off-on-off patterns

Membership functions for the number of on-off-on patterns (μ_{N5i}) are defined as in the same manner for the number of off-on-off patterns.

3 The Fuzzy Solution Approach

Using Belman and Zadeh's [9] *min operator*, the feasible fuzzy solution set is obtained by the intersection of all membership functions representing the fuzzy goals and constraints. The m*in operator* focuses only on the maximization of the minimum membership grade. It is not a compensatory operator. That is, goals with a high

degree of membership are not traded off against goals with a low degree of membership. Therefore, some computationally efficient compensatory operators [see, 10] can be used to investigate better results. Among the compensatory operators which are well suited in solving multi-objective programming problems, Werners' [11] *fuzzy and* operator is easy to handle, and has generated reasonable consistent results in applications. For this reason, we use this approach in this paper. Werners [11] formulates the *fuzzy and* operator as follows.

$$\left.\begin{array}{ll} \text{maximize} & \gamma\lambda + (1-\gamma)(1/K)\sum_k \lambda_k \\ \text{subject to} & \mu_k(x) \geq \lambda + \lambda_k \ , \quad \forall k \in K, \ \forall x \in X \\ & \lambda, \ \lambda_k, \ \gamma \in [0, 1] \end{array}\right\} \tag{17}$$

and other system constraints.

Where λ is the overall satisfaction level, K is the total number of fuzzy objectives and parameters, $\mu_k(x)$ is the membership function of fuzzy goal k, and γ is the coefficient of compensation defined within the interval [0, 1].

4 Application of the Model to the Case Problem

In the case problem, 28 nurses working in a ward are scheduled for a two-week planning period. First 11 nurses prefer the day shift, next 11 nurses prefer the evening shift and the last 6 nurses prefer the night shift the most. Due to the hospital working hour regulations, minimum and maximum working hours (*lwh, uwh*) for a nurse within the planning period are specified as 64 and 96 hours, respectively. The work day is split into three shifts which are: day shift (D: 7 am-15 pm), evening shift (E: 15 pm-23 pm) and night shift (N: 23 pm-7 am). In order to specify the individual preferences of nurses as to the requested days off and shift types to work, Table 1 lists the degree or importance of a preference in qualitative terms, the corresponding value of v and the preference score p_{ij} (v). This pointing system has been adapted from Bard and Purnomo [12] and the only thing required is that each preference be assigned to one of the enumerated categories. The demand data for the day, evening and night shifts is taken from Ozkarahan [13]. Accordingly on weekdays, the minimum requested number of nurses (ld_{jp},) for the day and evening shifts is 6, whereas it is 4 for the night shift. On weekend days, the minimum requested number changes to 6, 5 and 3 for the day, evening and night shifts, respectively. The maximum requested number of nurses (ud_{jp}) has been specified as ld_{jp}+3. The minimum and maximum preference scores a nurse can achieve if assigned to all preferred shift types (*min_st* and *max_st*) are taken as 8 and 40 in order. The minimum and maximum preference score for the requested days off (*min_do* and *max_do*) are 0 and 16. The minimum and maximum number of off-on-off patterns (*min_off* and *max_off*) and on-off-on patterns (*min_on* and *max_on*) that a schedule can acquire are 0 and 6.

The model includes 5499 constraints and 2956 variables. It has been solved for different coefficients of compensation using CPLEX 9.0 software. The comparative results are presented in Table 2.

Table 1. Quantification of preferences

Degree of preference	Equivalent no. of preference points, v	Preference score, $p_{ij}(v)=2^{v-1}$
Simple	1	1
Serious	2	2
Severe	3	4
Extreme	4	8

Table 2. The solutions of the model

	γ	1 (min operator)	0.9	0.8	0.7	0.6	0.5	0.4	0.3	0.2	0.1	0 (ad. appr.
μ_{Hjp}	Min	0.50	0.50	0.50	0.50	0.50	0.50	0.50	0.50	0.50	0.50	1
	Max	1	1	1	1	1	1	1	1	1	1	1
	aver.	0.83	0.94	0.98	0.96	0.98	0.96	0.99	0.99	0.95	0.98	1
μ_{N1i}	Min	0.50	0.50	0.50	0.67	0.50	0.50	0.50	0.50	0.50	0.50	0
	Max	1	1	1	1	1	1	1	1	1	1	1
	aver.	0.63	0.89	0.89	0.90	0.88	0.89	0.85	0.87	0.89	0.87	0.83
μ_{N2i}	Min	0.50	0.50	0.50	0.56	0.50	0.56	0.56	0.50	0.63	0.53	0.50
	Max	1	1	1	1	1	1	1	1	1	1	1
	aver.	0.69	0.9	0.87	0.88	0.88	0.87	0.85	0.86	0.90	0.86	0.87
μ_{N3i}	Min	0.50	0.50	0.50	0.50	0.50	0.50	0.50	0.50	0.50	0.50	0.38
	Max	1	1	1	1	1	1	1	1	1	1	1
	aver.	0.6	0.75	0.77	0.77	0.78	0.79	0.80	0.78	0.78	0.79	0.79
μ_{N4i}	Min	1	1	1	1	1	1	1	1	1	1	1
	Max	1	1	1	1	1	1	1	1	1	1	1
	aver.	1	1	1	1	1	1	1	1	1	1	1
μ_{N5i}	Min	0.50	0.67	0.67	0.67	0.83	0.67	0.67	0.67	0.67	0.67	0.83
	Max	0.83	1	1	1	1	1	1	1	1	1	1
	aver.	0.74	0.93	0.95	0.96	0.95	0.94	0.95	0.96	0.95	0.94	0.96

As seen from Table 2, none of the solution alternatives are definitely superior over one another, and one of these alternatives can be selected as the best one concerning the priorities of the decision maker. It should be emphasized here that, the decision maker considers the tradeoffs among all of the solution alternatives. For example, if the satisfaction of nurses' working hour preference is more important than the other objectives, the fourth alternative (γ=0.7) can be treated as the best one. More specifically, we have the greatest value for the minimum μ_{N1i} and average μ_{N1i}, which means that among the 28 nurses the minimum achievement level for the total working hour preference is 0.67, whereas it is at most 0.50 in other solutions. Since, there is no significant difference between the membership functions of the other objectives, the alternative seems reasonable. In a similar way, if the shift type preference is more important, the ninth alternative (γ=0.2) is selected.

The solutions for γ values 0 and 1 correspond to the *min operator* and *simple additive approach*, respectively. If the average membership function values are taken into consideration, it can be seen that *min operator* approach performs worse relative

to the other alternatives. On the other hand, the s*imple additive approach* is also unsuitable for the NSP due to the uneven solution values. As seen in Table 2, the differences between the maximum and minimum membership function values for the first and third objectives of nurses are too big for a fair schedule. The schedule for γ=0.7 is presented in Table 3 as an example.

Table 3. The nurse schedule

	Week 1							Week 2						
Nurses	M	T	W	Th	F	Sa	Su	M	T	W	Th	F	Sa	Su
1	D	D	D	D	D			D	D	D	D	D		
2	D	D	D		D	D	D	D	D		D	D		
3				D	D	D	D			D	D	D	D	D
4	D	D	D	D	D			D	D			D	D	D
5	D	D	D			D	D	D	E	E			D	D
6	D	D	D	D				D	D				D	D
7			D	D	D	D	D			D	D	D	D	D
8					D	D	D			D	D	D	D	D
9	D	D				D	D	D	D	D		D	D	D
10			D	D	D	D	D		D	D	D	D		
11	D	D	D	D				D	D	D	D			
12			E	E	E	E	E			E	E	E	E	E
13	E	E	E	E	E			E	E	E	E	E		
14				E	E	E	E	E			E	E	E	E
15	E	E	E			E	E	E	E	E			E	E
16	E	E	E	E	E			E	E	E			E	E
17		E	E	E				E	E	N	N			E
18	E	E			E	E	E	E			E	E	E	N
19	E	E	E			E	E	N	N	N				
20	E	E	E	E	E			E	E	E	E	E		
21			N	N	N	N	N		E	E	E	E		
22				E	E	E	E				E	E	E	E
23	N	N	N	N	N				N	N	N	N	N	
24	N	N	N	N	N			N	N	N	N	N		
25	N	N	N	N						N	N	N	N	N
26	N	N			N	N	N	N	N			N	N	N
27	E	E			N	N	N	N			E	E	E	E
28	N	N	N	N		N	N	N	N					

For instance, nurse 1 prefers working a day shift severely. Her working hour preference is stated using trapezoidal membership function that increases between 64 and 80 hours. She requests both the weekends off. As seen from Table 3, nurse 1 has been assigned to the day shift on her working days. She works a total of 80 hours during the planning period and takes both of the weekends off as requested. Additionally, the off-on-off and on-off-on patterns in her schedule have been prevented completely. As a result, the values of all membership functions which reflect the degree of satisfaction of nurse 1's objectives are 1.

5 Conclusion

In this paper, a fuzzy multi-objective model has been developed for the NSP. Fuzzy goal programming approach is employed to consider uncertainty in the target values

of the hospital management, nurses' preferences and constraints. To confirm the viability of the proposed model, a real world application is provided. The individual preferences of nurses which differ from one another are treated effectively using fuzzy modeling approach, which otherwise is not possible by conventional mathematical programming methods. This work contributes to scheduling nurses more personalized and more equitably.

References

1. Miller, H.E., Pierskalla, W., Rath, G.: Nurse Scheduling Using Mathematical Programming. Operations Research 24, 857–870 (1976)
2. Millar, H.H., Kiragu, M.: Cyclic and Non-Cyclic Scheduling of 12 h Shift Nurses by Network Programming. European Journal of Operational Research 104, 582–592 (1998)
3. Meyer auf'm Hofe, H.: ConPlan/SIEDAplan: Personnel Assignment as a Problem of Hierarchical Constraint Satisfaction. In: Proceedings of the Third International Conference on the Practical Application of Constraint Technology. London, pp. 257–271 (1997)
4. Aickelin, U., White, P.: Building Better Nurse Scheduling Algorithms. Annals of Operations Research 128, 159–177 (2004)
5. Burke, E.K., De Causmaecker, P., Vanden Berghe, G., Van Landeghem, H.: The State of the Art of Nurse Rostering. Journal of Scheduling. 7, 441–499 (2004)
6. Ozkarahan, I., Bailey, J.E.: Goal Programming Model Subsystem of a Flexible Nurse Scheduling Support System. IIE Transactions 16, 306–316 (1998)
7. Azaiez, M.N., Al Sharif, S.S.: A 0-1 Goal Programming Model for Nurse Scheduling. Computers & Operations Research 32, 491–507 (2005)
8. Zadeh, LA.: Fuzzy Sets. Information and Control. 8, 338–353 (1965)
9. Bellman, R.E., Zadeh, L.A.: Decision Making in a Fuzzy Environment. Management Science 17, 141–164 (1970)
10. Lai, Y-J., Hwang, C-L.: Fuzzy Multiple Objective Decision Making Methods and Applications. Springer, New York (1994)
11. Werners, B.: Aggregation Models in Mathematical Programming. In: Mitra, G., Greenberg, H.J., Lootsma, F.A., Rijckaert, M.J., Zimmerman, H.-J. (eds.) Mathematical Models for Decision Support, pp. 295–305. Springer, Heidelberg (1988)
12. Bard, J.F., Purnomo, H.W.: Preference Scheduling Using Column Generation. European Journal of Operational Research 164, 510–534 (2005)
13. Ozkarahan, I.: A Flexible Nurse Scheduling Support System. Ph.D. Dissertation. Arizona State University (1987)

Fuzzy Adaptive Threshold Determining in the Key Inheritance Based Sensor Networks*

Hae Young Lee and Tae Ho Cho

School of Information and Communication Engineering, Sungkyunkwan University
300 Cheoncheon-dong, Jangan-gu, Suwon 440-746, Korea
{sofware, taecho}@ece.skku.ac.kr

Abstract. Sensor networks are often deployed in unattended environments, thus leaving these networks vulnerable to false data injection attacks. False data injection attacks will not only cause false alarms that waste real world response efforts, but also drain the finite amount of energy in a battery powered network. The key inheritance based filtering scheme can detect a false report at the very next node of the compromised node that injected the false report before it consumes a significant amount of energy. The choice of a security threshold value in this scheme represents a trade off between security and overhead. In this paper, we propose a fuzzy adaptive threshold determining method for the key inheritance based filtering scheme. The fuzzy rule based system is exploited to determine the security threshold value by considering the average energy level of all the nodes along the path from the base station to a cluster, the number of nodes in that cluster, and the number of compromised nodes. We also introduce a modified version of this scheme to reduce the overhead for changing the threshold value. The proposed method can conserve energy, while it provides sufficient resilience.

1 Introduction

Sensor networks have attracted a lot of attention recently due to their broad applications in both military and civilian operations [1]. In many applications sensor nodes are deployed in open environments, and hence are vulnerable to physical attacks, potentially compromising the nodes cryptographic keys [2]. An adversary may use compromised nodes to inject false report into the network [3]. [illegible] will not only cause false alarms that waste real world response efforts, but also drain the finite amount of energy in a battery powered network [4]. To minimize the grave damage, false reports should be dropped en-route as early as possible, and the few eluded ones should be further rejected at the base station [5]. The early dropping of false reports leads to significant savings of energy [4]. Several security solutions [1,3,4,5,6,7,8,9] have recently been proposed to detect false reports.

* This research was supported by the MIC (Ministry of Information and Communication), Korea, under the ITRC (Information Technology Research Center) support program supervised by the IITA (Institute of Information Technology Advancement). (IITA-2006-C1090-0603-0028).

H.G. Okuno and M. Ali (Eds.): IEA/AIE 2007, LNAI 4570, pp. 64–73, 2007.

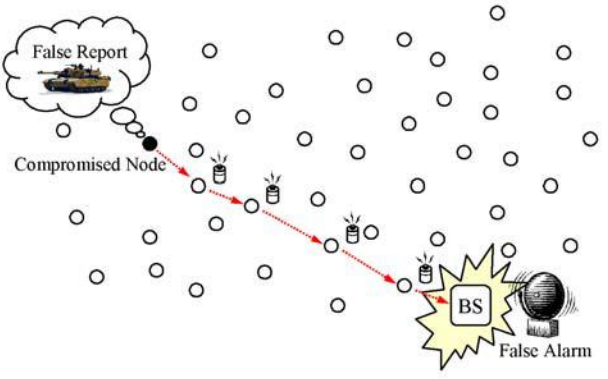

Fig. 1. False sensing report can be injected through compromised node (filled circle), which can lead to not only false alarms but also the depletion of limited energy resource

Especially, the [9] can detect a false report at the very next node of the compromised node that injected the false report before it consumes a significant amount of energy. Similar to [3,6], the choice of a security threshold value in this scheme is important since it represents a trade off between security and overhead. A large threshold value makes forging reports more difficult, but it consumes more energy in forwarding [6]. A small threshold value may make this scheme inefficient or even useless if the number of compromised node exceeds it [7]. Therefore, we should choose a threshold value such that it provides sufficient resilience, while still small enough to conserve energy [6].

In this paper, we propose a fuzzy adaptive threshold determining method for the key inheritance based filtering scheme. The fuzzy rule based system is exploited to determine a threshold value by considering the average energy level of all the nodes along the path from the base station to a cluster, the number of nodes in that cluster, and the number of compromised nodes. We also introduce a modified version of the key inheritance based filtering scheme to reduce the overhead for changing the threshold value. The proposed method can conserve energy, while it provides sufficient resilience. The effectiveness of the proposed method is shown with the simulation result at the end of the paper.

The remainder of the paper is organized as follows: Section 2 briefly describes the key inheritance based filtering scheme and motivation of this work. Section 3 introduces the proposed scheme in detail. Section 4 reviews the simulation result. Finally, conclusion is discussed in Section 5.

2 Background

In this section, we briefly describe the key inheritance based filtering scheme (KIF) [9] and motivation of this work.

2.1 The Key Inheritance Based Filtering Scheme (KIF) Overview

In [9], the key inheritance based filtering scheme (KIF) that can prevent forwarding of false reports is proposed. The keys of each node used in the message authentication consist of its own key and the keys [illegible] (shared with) its [illegible] (toward the base station) nodes. Every authenticated report contains the combination of MACs generated by using the keys possessed by the consecutive nodes along the path from the base station to a terminal node. If no more than a certain number T nodes are compromised, KIF can detect a false report at the very next hop node of the compromised node that injected the false report before it consumes a significant amount of energy. Here T is a [illegible] determined based on the security requirements of the application.

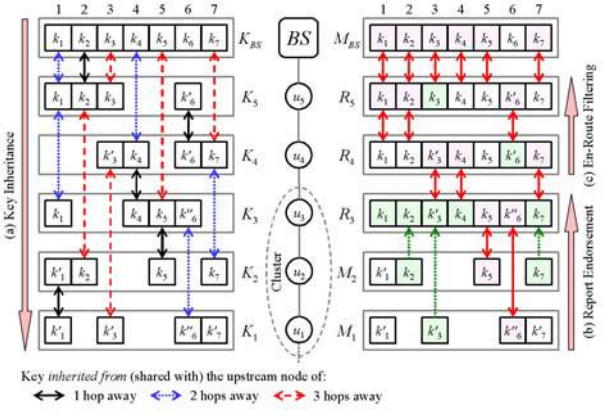

Fig. 2. KIF involves the three phases: *key inheritance*, *report endorsement*, and *en-route filtering*. In the key inheritance phase (a), every node along a path inherits the keys from its upstream nodes. In the report endorsement phase (b), multiple nodes generate a report collaboratively. In the en-route phase (c), every forwarding node authenticates the report and replaces the un-matching MAC in the report with the MAC generated by itself.

KIF involves the following three phases:

1. In the [illegible] phase, the base station prepares the $(T^2 + 3T + 4)/2$ keys for the path to a terminal node. For example, the base station in Fig. 2 prepares the seven keys, $k_1, \cdots, k_7$, for the path to node u_1 when $T = 2$. Every node along the path inherits the $T + 1$ keys from its $T + 1$ upstream nodes and a new key is assigned to the node as its own key. It thus has $T + 2$ keys. For example, node u_2 in Fig. 2 has the four keys, $K_2 = \{k'_1, k_2, k_5, k_7\}$. k_2, k_5, and k_7 are inherited from u_5, u_3, and u_4, respectively. k'_1 is its own key.

2. In the [illegible] phase, $T + 1$ nodes generate a report collaboratively when they sensed an event. More specifically, every participating node generates $T + 2$ MACs over the event then sends these MACs to its cluster head. The cluster head collects the MACs from all the participating nodes then put them into a report. Finally, it forwards the report toward the base station. Every report contains $(T^2 + 3T + 4)/2$ MACs. For example, the cluster head u_4 in Fig. 2 collects the four MACs for the same event from each cluster node and generates a report R_3 that contains the seven MACs, $\{m_{k_1}, m_{k_2}, m_{k'_3}, m_{k_4}, m_{k_5}, m_{k''_6}, m_{k_7}\}$, where m_k is the MAC generated by using key k.
3. In the [illegible] phase, every forwarding node verifies the MACs in a report based on its keys. Upon success, it replaces the one different MAC in the report to the one generated by itself. Finally, it forwards the report toward the base station. For example, when node u_4 receives the report R_3, it verifies the four MACs, $\{m_{k'_3}, m_{k_4}, m_{k''_6}, m_{k_7}\}$, in R_3 by using its four keys, $\{k'_3, k_4, k'_6, k_7\}$. Since $m_{k''_6} \neq m_{k'_6}$ and the other MACs match exactly, R_3 is authenticated. The node replaces $m_{k''_6}$ with $m_{k'_6}$ then forwards the report that contains $\{m_{k_1}, m_{k_2}, m_{k'_3}, m_{k_4}, m_{k_5}, m_{k'_6}, m_{k_7}\}$.

2.2 Motivation

Similar to [3,6], the choice of T in KIF is important since it represents a trade off between security and overhead. A large T makes forging reports more difficult, but it consumes more energy in forwarding [6]. A small T may make the filtering capability useless if the number of compromised node exceeds T [7]. Therefore, we should choose T adaptively such that it achieves sufficient resilience, while still small enough to conserve energy [6].

3 Fuzzy Adaptive Threshold Determining

In this section, we describe the proposed method in detail. To change T efficiently, a modified KIF for the proposed method is also introduced.

3.1 Assumptions

We assume that the base station can know or estimate the average energy level of all the nodes along the path from the base station to a cluster, the number of nodes in that cluster, and the number of compromised nodes. We also assumes that the base station has a mechanism to authenticate broadcast messages (e.g., based on μTESLA [10]), and every node can verify the broadcast messages.

3.2 Overview

In the proposed method, the base station periodically determines T for the path to each cluster with a fuzzy rule based system (Fig. 3 (a)). The average energy

level of the nodes along the path from the base station to a cluster, the number of nodes in that cluster, and the number of compromised nodes are used to determine T. If the new T differs from the current, the base station broadcasts the new T to all the nodes along the path (Fig. 3 (b)).

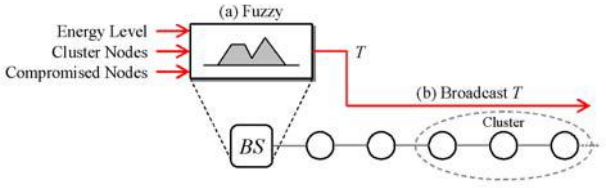

Fig. 3. The base station periodically determines T with a fuzzy rule based system (a). If the new T differs from the current, the base station broadcasts the new T (b).

3.3 Factors That Determine the Security Threshold Value

The energy is the most important resource that should be considered in sensor networks. Generally, sensor nodes are limited in power and irreplaceable since these nodes have limited capacity and are unattended [11]. Therefore, we have to determine T based on the energy level of nodes. In KIF, T should be smaller than the number of cluster nodes because a report is collaboratively generated by $T + 1$ cluster nodes. For example, if a cluster consists of four nodes, T can be 0 (disable filtering), 1, 2, or 3. KIF can be resilient to up to T colluding compromised nodes. Thus, if a certain number C nodes are compromised, we should set T to C or larger (but smaller than the number of cluster nodes). If C exceeds the number of cluster nodes, KIF may be useless [7]. For example, KIF cannot detect false reports injected by five colluding compromised nodes when T is smaller than 5. Under this situation, we may as well disable filtering, i.e., set T to 0. So, we have to determine T based on the number of cluster nodes and the number of compromised nodes.

3.4 Fuzzy Membership Functions

The membership functions of three input parameters - (a) Energy Level, (b) Cluster Nodes, and (c) Compromised Nodes - of the fuzzy logic are illustrated in Fig. 4. The labels in the fuzzy variables are presented as follows.

- Energy Level = {Very Low, Low, Above Half}
- Cluster Nodes = {Very Small, Small, Large, Very Large}
- Compromised Nodes = {Very Small, Small, Large, Very Large}

The output parameter of the fuzzy logic is Threshold = Very Small, Small, Large, Very Large, which is represented by the membership functions as shown in Fig. 4(d). Note that we can use additional fuzzy variables (e.g., Medium) if more detailed determining is required.

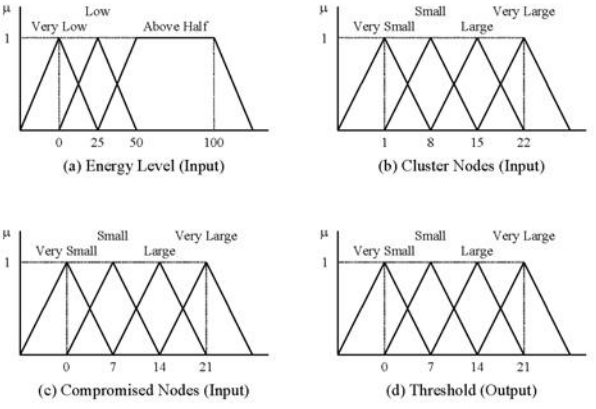

Fig. 4. The membership functions of three input parameters and of one output parameter are shown

3.5 Fuzzy Rules

If it is reported or estimated that no node has been compromised, T can be very small (e.g., 0).

R04: if **Energy Level** is **Above Half**
and **Cluster Nodes** is **Very Large**
and **Compromised Nodes** is **Very Small**
then **Threshold** is **Very Small**

If a few nodes are compromised and the number of compromised nodes does not exceed the number of cluster nodes, T should be equal to or greater than the number of compromised nodes.

R07: if **Energy Level** is **Above Half**
and **Cluster Nodes** is **Large**
and **Compromised Nodes** is **Small**
then **Threshold** is **Small**

If the number of compromised nodes exceeds the number of cluster nodes, KIF may be useless. Thus, we may as well disable filtering, i.e., set T to 0.

R11: if **Energy Level** is **Above Half**
and **Cluster Nodes** is **Small**
and **Compromised Nodes** is **Large**
then **Threshold** is **Very Small**

If non-compromised nodes have not enough energy, although the number of compromised nodes is smaller than the number of cluster nodes, T can be either the number of compromised or 0 (if the overhead for filtering consumes too much energy).

R34: if **Energy Level** is **Very Low**
and **Cluster Nodes** is **Very Large**
and **Compromised Nodes** is **Large**
then **Threshold** is **Very Small**

R35: if **Energy Level** is **Very Low**
and **Cluster Nodes** is **Very Large**
and **Compromised Nodes** is **Small**
Then **Threshold** is **Small**

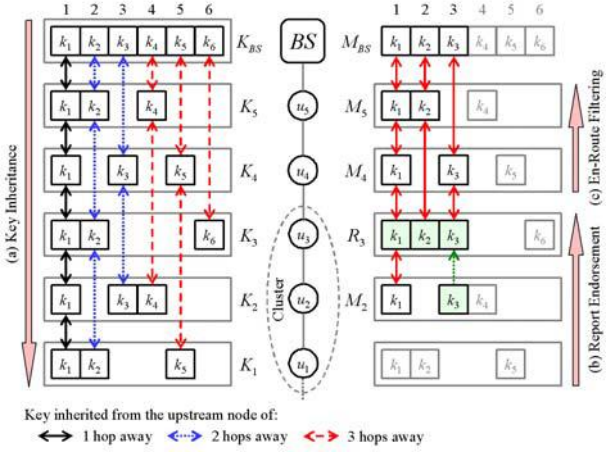

Fig. 5. This figure shows an example of the three phases of MKIF. Every node in MKIF inherits the keys at the deterministic indices from its upstream nodes. In MKIF, we can easily change T without key re-inheritance within the initial security threshold value.

3.6 A Modified KIF (MKIF)

In KIF, changing T may consume a significant amount of energy since all nodes have to re-inherit keys from (reestablish pairwise keys with) their upstream nodes. The proposed method may be inefficient if T is frequently changed. Thus, we introduce a modified KIF (MKIF) that does not need to re-inherit keys. In MKIF, every node inherits keys from its upstream nodes as shown in Fig. 5(a) ($T = 2$). The node has not its own key and the indices of its inherited keys are deterministic (similar to the concept of [illegible] in the [illegible] [3]). For example, node u_3 inherits k_1, k_2, and k_6 from its upstream nodes of one, two, and three hops away (i.e., u_4, u_5, and the base station), respectively. On the other hand, in KIF, these indices are randomly selected. As shown in Fig. 5(b) and (c), we can easily change T without key re-inheritance within the initial T_{init}. If T has been changed to 1, the cluster head, u_3, collects $M_3 = \{m_{k_1}, m_{k_2}\}$ and $M_2 = \{m_{k_1}, m_{k_3}\}$ from itself and u_2. It then generates a report R_3 that contains $\{m_{k_1}, m_{k_2}, m_{k_3}\}$ and forwards the report.

4 Simulation Result

To show the effectiveness of the proposed method, we have compared the proposed method with the fixed threshold based MKIF through the simulation. Note that KIF consumes more energy than MKIF. Each node takes 16.25, 12.5μJ to transmit/receive a byte and each MAC generation consumes 15μJ [6]. The size of an original report is 24 bytes. The size of a MAC is 1 byte.

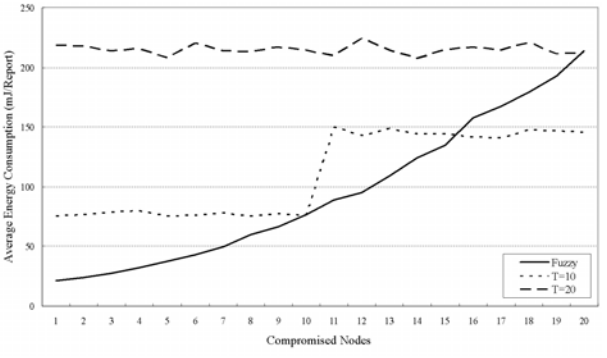

Fig. 6. This figure shows the average energy consumption caused by a report when the number of cluster nodes = 21 and the number of compromised nodes is between 1 and 20

Fig. 6 shows the average energy consumption caused by a report (authenticated or false) when the number of cluster nodes is 21 and the number of compromised nodes is between 1 and 20. As shown in the figure, the proposed method (solid line) consumes less energy than the fixed threshold based MKIF ($T = 10$ and 20) up to fifteen compromised nodes since the proposed method determines T adaptively according to the number of compromised nodes. MKIF with $T = 10$ consumes less energy than the proposed method if more than fifteen node have been compromised (it consumes about 150μJ/report). However, it cannot detect false reports when an adversary has compromised more than then nodes. That is, activating MKIF just drains the finite energy resource of the network. MKIF with $T = 20$ can detect forged reports up to twenty compromised nodes but consumes too much energy in energy forwarding. If no node has been compromised, it just decreases the lifetime of the network. On the other hand, the proposed method provides sufficient resilience, while still small enough to conserve energy.

Fig. 7 shows the average energy consumption caused by a report when the number of cluster nodes is 11 and the number of compromised nodes is between 1 and 20. Up to ten compromised nodes, energy consumption in the proposed method is increased as the number of compromised nodes is increased. But the energy consumption is reduced when more than ten nodes have been compromised since the method disables filtering if the number of capture nodes exceeds the number of cluster nodes. Thus, the proposed method can save energy.

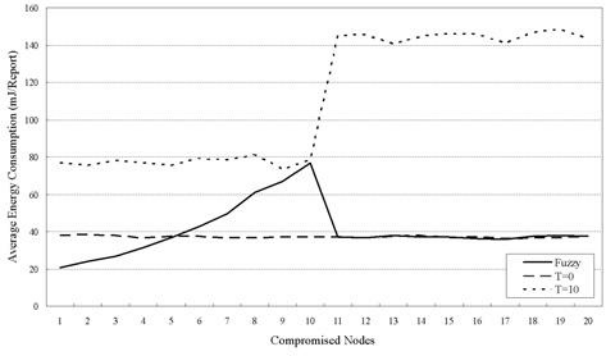

Fig. 7. This figure shows the average energy consumption caused by a report when the number of cluster nodes = 11 and the number of compromised nodes is between 1 and 20

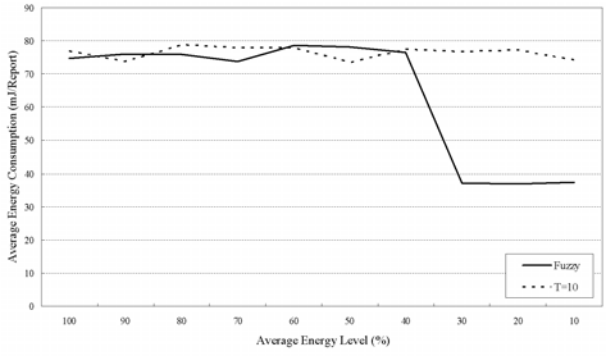

Fig. 8. This figure shows the average energy consumption per report when the number of cluster nodes = 11, the number of compromised nodes is 10, and the average energy level is between 100 and 10%

Fig. 8 shows the average energy consumption caused by a report when the number of cluster nodes is 11, the number of compromised nodes is 10, and the average energy level is between 100 and 10%. The proposed method disables filtering if the energy level is less than 40% (not enough energy to activate filtering). Thus, the proposed method can prolong network lifetime.

5 Conclusion

In this paper, we proposed a fuzzy based adaptive threshold determining method for the key inheritance based filtering scheme. The fuzzy rule based system is exploited to determine T by considering the average energy level of all the nodes along the path from the base station to a cluster, the number of nodes in that cluster, and the number of compromised nodes. We also introduced a modified

KIF to reduce the overhead for changing T. The proposed method can conserve energy, while it provides sufficient resilience. The effectiveness of the proposed method was shown with the simulation result.

References

1. Zhang, Y., Liu, W., Lou, W., Fang, Y.: Location-Based Compromise-Tolerant Security Mechanisms for Wireless Sensor Networks. IEEE J. Sel. Area Comm. 24(2), 247–260 (2006)
2. Przydatek, B., Song, D., Perrig, A.: SIA: Secure Information Aggregation in Sensor Networks. In: Proc. of SenSys, pp. 255–265 (2003)
3. Zhu, S., Setia, S., Jajodia, S., Ning, P.: An Interleaved Hop-by-Hop Authentication Scheme for Filtering of Injected False Data in Sensor Networks. In: Proc. of S&P, pp. 259–271 (2004)
4. Li, F., Wu, J.: A Probabilistic Voting-based Filtering Scheme in Wireless Sensor Networks. In: Proc. of IWCMC, pp. 27–32 (2006)
5. Yang, H., Lu, S.: Commutative Cipher Based En-Route Filtering in Wireless Sensor Networks. In: Proc. of VTC 2003, pp. 1223–1227 (2003)
6. Ye, F., Luo, H., Lu, S.: Statistical En-Route Filtering of Injected False Data in Sensor Networks. IEEE J. Sel. Area Comm 23(4), 839–850 (2005)
7. Zhang, W., Cao, G.: Group Rekeying for Filtering False Data in Sensor Networks: A Predistribution and Local Collaboration-based Approach. In: Proc. of INFOCOM 2005, pp. 503–514 (2005)
8. Zhang, Y., Yang, J., Vu, H.T.: The Interleaved Authentication for Filtering False Reports in Multipath Routing based Sensor Networks. In: Proc. of IPDPS (2006)
9. Lee, H., Cho, T.: Key Inheritance-Based False Data Filtering Scheme in Wireless Sensor Networks. Lect. Notes Comput. Sc. 4371, 116–127 (2006)
10. Perrig, A., Szewczyk, R., Tygar, J.D., Wen, V., Culler, D.E.: SPINS: Security Protocols for Sensor Networks. Wirel. Netw. 8(5), 521–534 (2002)
11. Chi, S., Cho, T.: Fuzzy Logic based Propagation Limiting Method for Message Routing in Wireless Sensor Networks. Lect. Notes Comput. Sc. 3983, 58–67 (2006)

A New Approach for Evaluating Students' Answerscripts Based on Interval-Valued Fuzzy Sets

Hui-Yu Wang[1] and Shyi-Ming Chen[2]

[1] Department of Education, National Chengchi University, Taipei, Taiwan, R.O.C.
94152514@nccu.edu.tw
[2] Department of Computer Science and Information Engineering, National Taiwan University of Science and Technology, Taipei, Taiwan, R.O.C.
smchen@mail.ntust.edu.tw

Abstract. In this paper, we present a new approach for evaluating students' answerscripts based on the similarity measure between interval-valued fuzzy sets. The marks awarded to the answers in the students' answerscripts are represented by interval-valued fuzzy sets, where each element in the universe of discourse belonging to an interval-valued fuzzy set is represented by an interval between zero and one. An index of optimism λ determined by the evaluator is used to indicate the degree of optimism of the evaluator, where $\lambda \in [0, 1]$. The proposed approach using interval-valued fuzzy sets for evaluating students' answerscripts can evaluate students' answerscripts in a more flexible and more intelligent manner.

Keywords: Similarity functions, students' answerscripts, interval-valued fuzzy grade sheets, interval-valued fuzzy sets, index of optimism.

1 Introduction

To provide students with evaluation reports regarding their examination as sufficient as possible and with the unavoidable error as small as possible is a chief goal of educational institutions [1]. In recent years, some methods [1], [2], [4]-[17] have been presented for students' evaluation based on the fuzzy set theory [18]. Biswas presented a fuzzy evaluation method (fem) for applying fuzzy sets in students' answerscripts evaluation. He also generalized the fuzzy evaluation method to propose a generalized fuzzy evaluation method (gfem) for students' answerscripts evaluation. In [1], the fuzzy marks awarded to answers in the students' answerscripts are represented by fuzzy sets. In a fuzzy set, the grade of membership of an element ui in the universe of discourse U belonging to a fuzzy set is represented by a real value between zero and one, However, if we can allow the marks awarded to the questions of the students' answerscripts to be represented by interval-valued fuzzy sets [8], [9], then there is room for more flexibility, where the grade of membership of an element in the universe of discourse belonging to an interval-valued fuzzy set is represented by an interval in [0, 1].

In this paper, we present a new approach for students' answerscripts evaluation based on interval-valued fuzzy sets. The marks awarded to the answers in the

H.G. Okuno and M. Ali (Eds.): IEA/AIE 2007, LNAI 4570, pp. 74–83, 2007.

students' answerscripts are represented by interval-valued fuzzy sets. An index of optimism λ determined by the evaluator is used to indicate the degree of optimism of the evaluator, where $\lambda \in [0, 1]$. If $0 \le \lambda < 0.5$, then the evaluator is a pessimistic evaluator. If $\lambda = 0.5$, then the evaluator is a normal evaluator. If $0.5 < \lambda \le 1.0$, then the evaluator is an optimistic evaluator. The proposed methods can evaluate students' answerscripts in a more flexible and more intelligent manner.

In Section 2, we briefly review similarity measures between interval-valued fuzzy sets from [3]. In Section 3, we present a new method for students' answerscripts evaluation using interval-valued fuzzy sets. The conclusions are discussed in Section 4.

2 Similarity Measures Between Interval-Valued Fuzzy Sets

In [19], Zwick et al. presented a method for measuring the distance between two real intervals. Let X and Y be two intervals in $[\beta_1, \beta_2]$, where $X = [x_1, x_2]$ and $Y = [y_1, y_2]$. Then, the distance $D(X, Y)$ between the intervals X and Y can be calculated as follows:

$$D(X, Y) = \frac{|x_1 - y_1| + |x_2 - y_2|}{2(\beta_2 - \beta_1)}. \tag{1}$$

Therefore, the degree of similarity $S(X, Y)$ between the intervals X and Y can be calculated as follows [3]:

$$S(X, Y) = 1 - D(X, Y). \tag{2}$$

Let X and Y be two intervals in $[0, 1]$, where $X = [x_1, x_2]$ and $Y = [y_1, y_2]$. Based on Eqs. (1) and (2), the degree of similarity $S(X, Y)$ between the intervals X and Y can be calculated as follows [3]:

$$S(X, Y) = \begin{cases} 1, & \text{if } y_1 \le x_1 \le x_2 \le y_2 \\ 1 - \dfrac{|x_1 - y_1| + |x_2 - y_2|}{2}, & \text{otherwise} \end{cases} \tag{3}$$

where $S(X, Y) \in [0, 1]$. It is obvious that if X and Y are identical intervals, then $D(A, B) = 0$ and $S(X, Y) = 1$. The larger the value of $S(X, Y)$, the higher the similarity between the intervals X and Y.

Assume that x and y are two real values between zero and one, where $x = [x, x]$ and $y = [y, y]$, then based on Eq. (3), we can see that

$$\begin{aligned} S(x, y) &= S([x, x], [y, y]) \\ &= 1 - \frac{|x - y| + |x - y|}{2} \\ &= 1 - |x - y|. \end{aligned} \tag{4}$$

Let $\tilde{A}$ and $\tilde{B}$ be two interval-valued fuzzy sets in the universe of discourse X, where

$$\begin{aligned} X &= \{x_1, x_2, \ldots, x_n\}, \\ \tilde{A} &= [a_{11}, a_{12}]/x_1 + [a_{21}, a_{22}]/x_2 + \ldots + [a_{n1}, a_{n2}]/x_n, \\ \tilde{B} &= [b_{11}, b_{12}]/x_1 + [b_{21}, b_{22}]/x_2 + \ldots + [b_{n1}, b_{n2}]/x_n, \end{aligned}$$

$[a_{i1}, a_{i2}]$ denotes the grade of membership of x_i belonging to the interval-valued fuzzy set $\tilde{A}$, $[b_{i1}, b_{i2}]$ denotes the grade of membership of x_i belonging to the interval-valued fuzzy set $\tilde{B}$, $0 \le a_{i1} \le a_{i2} \le 1$, $0 \le b_{i1} \le b_{i2} \le 1$, and $1 \le i \le n$. Based on the matrix representation method, the interval-valued fuzzy sets $\tilde{A}$ and $\tilde{B}$ can be represented by the matrices $\overline{A}$ and $\overline{B}$, respectively, where

$$\overline{A} = \langle [a_{11}, a_{12}], [a_{21}, a_{22}], \ldots, [a_{n1}, a_{n2}] \rangle,$$
$$\overline{B} = \langle [b_{11}, b_{12}]), [b_{21}, b_{22}]), \ldots, [b_{n1}, b_{n2}] \rangle.$$

If $\tilde{A}$ and $\tilde{B}$ are identical interval-valued fuzzy sets (i.e., $\tilde{A} = \tilde{B}$), then $a_{ij} = b_{ij}$, $1 \le i \le n$ and $1 \le j \le 2$. In this situation, we can see that $\overline{A} = \overline{B}$.

By applying Eq. (3), the degree of similarity $T(\overline{A}, \overline{B})$ between the interval-valued fuzzy sets $\tilde{A}$ and $\tilde{B}$ can be measured by the similarity function T [3],

$$T(\overline{A}, \overline{B}) = \frac{\sum_{i=1}^{n} S([a_{i1}, a_{i2}], [b_{i1}, b_{i2}])}{n},$$
$$= \frac{\sum_{i=1}^{n} 1 - \frac{|a_{i1} - b_{i1}| + |a_{i2} - b_{i2}|}{2}}{n}, \quad (5)$$

where $T(\overline{A}, \overline{B}) \in [0, 1]$. The larger the value of $T(\overline{A}, \overline{B})$, the higher the similarity between the interval-valued fuzzy sets $\tilde{A}$ and $\tilde{B}$. It is obvious that if $\tilde{A}$ and $\tilde{B}$ are identical interval-valued fuzzy sets (i.e., $\tilde{A} = \tilde{B}$), then $T(\overline{A}, \overline{B}) = 1$.

3 A New Method for Evaluating Students' Answerscripts Based on Interval-Valued Fuzzy Sets

In this section, we present a new method for evaluating students' answerscripts based on interval-valued fuzzy sets. Let X be the universe of discourse, where X = {0%, 20%, 40%, 60%, 80%, 100%}. In [1], Biswas used the five fuzzy linguistic hedges ***E*** (excellent), ***V*** (very good), ***G*** (good), ***S*** (satisfactory) and ***U*** (unsatisfactory) of the universe of discourse X, called the Standard Fuzzy Sets, for students' answerscripts evaluation, defined as follows:

E = 0/0% + 0/20% + 0.8/40% + 0.9/60% + 1/80% + 1/100%,
V = 0/0% + 0/20% + 0.8/40% + 0.9/60% + 0.9/80% + 0.8/100%,
G = 0/0% + 0.1/20% + 0.8/40% + 0.9/60% + 0.4/80% + 0.2/100%,
S = 0.4/0% + 0.4/20% + 0.9/40% + 0.6/60% + 0.2/80% + 0/100%,
U = 1/0% + 1/20% + 0.4/40% + 0.2/60% + 0/80% + 0/100%.

It is obvious that these five standard fuzzy sets ***E*** (excellent), ***V*** (very good), ***G*** (good), ***S*** (satisfactory) and ***U*** (unsatisfactory) also can equivalently be represented by interval-valued fuzzy sets $\tilde{E}$, $\tilde{V}$, $\tilde{G}$, $\tilde{S}$ and $\tilde{U}$, respectively, where

$\tilde{E}$ = [0, 0]/0% + [0, 0]/20% + [0.8, 0.8]/40% + [0.9, 0.9]/60% + [1, 1]/80% + [1, 1]/100%,

$\tilde{V}$ = [0, 0]/0% + [0, 0]/20% + [0.8, 0.8]/40% + [0.9, 0.9]/60% + [0.9, 0.9]/80% + [0.8, 0.8]/100%,

$\tilde{G}$ = [0, 0]/0% + [0.1, 0.1]/20% + [0.8, 0.8]/40% + [0.9, 0.9]/60% + [0.4, 0.4]/80% + [0.2, 0.2]/100%,

$\tilde{S}$ = [0.4, 0.4]/0% + [0.4, 0.4]/20% + [0.9, 0.9]/40% + [0.6, 0.6]/60% + [0.2, 0.2]/80% + [0, 0]/100%,

$\tilde{U}$ = [1, 1]/0% + [1, 1]/20% + [0.4, 0.4]/40% + [0.2, 0.2]/60% + [0, 0]/80% + [0, 0]/100%.

The standard interval-valued fuzzy sets $\tilde{E}$, $\tilde{V}$, $\tilde{G}$, $\tilde{S}$ and $\tilde{U}$ can be represented by matrices $\overline{E}$, $\overline{V}$, $\overline{G}$, $\overline{S}$ and $\overline{U}$, respectively, where

$\overline{E}$ = <[0, 0], [0, 0], [0.8, 0.8], [0.9, 0.9], [1, 1], [1, 1]>,

$\overline{V}$ = <[0, 0], [0, 0], [0.8, 0.8], [0.9, 0.9], [0.9, 0.9], [0.8, 0.8]>,

$\overline{G}$ = <[0, 0], [0.1, 0.1], [0.8, 0.8], [0.9, 0.9], [0.4, 0.4], [0.2, 0.2]>,

$\overline{S}$ = <[0.4, 0.4], [0.4, 0.4], [0.9, 0.9], [0.6, 0.6], [0.2, 0.2], [0, 0]>,

$\overline{U}$ = <[1, 1], [1, 1], [0.4, 0.4], [0.2, 0.2], [0, 0], [0, 0]>.

Assume that "***A***", "***B***", "***C***", "***D***" and "***E***" are letter grades, where $90 \le \boldsymbol{A} \le 100$, $70 \le \boldsymbol{B} < 90$, $50 \le \boldsymbol{C} < 70$, $30 \le \boldsymbol{D} < 50$ and $0 \le \boldsymbol{E} < 30$. Assume that an evaluator evaluates the *i*th question (i.e., *Q.i*) of a student's answerscript using an interval-valued fuzzy grade sheet as shown in Table 1.

Table 1. An interval-valued fuzzy grade sheet

Question No.	Interval-valued fuzzy mark						Derived fuzzy letter grade
Q.1	[0, 0]	[0.2, 0.3]	[0.4, 0.5]	[0.6, 0.7]	[0.8, 0.9]	[1, 1]	
Q.2							
Q.3							
⋮	⋮	⋮	⋮	⋮	⋮	⋮	⋮
Q.n							
							Total mark =

In the second row of the interval-valued fuzzy grade sheet shown in Table 1, the interval-valued fuzzy marks [0, 0], [0.2, 0.3], [0.4, 0.5], [0.6, 0.7], [0.8, 0.9] and [1, 1], awarded to the answer of question *Q.1*, indicate that the degrees of the evaluator's satisfaction for that answer are 0%, 20%, 40%, 60%, 80% and 100%, respectively. Let this interval-valued fuzzy mark of the answer of question *Q.1* be denoted by $\tilde{F}_1$. Then, we can see that $\tilde{F}_1$ is an interval-valued fuzzy set of the universe of discourse *X*, where

X = {0%, 20%, 40%, 60%, 80%, 100%},

$\tilde{F}_1$ = [0, 0]/0% + [0.2, 0.3]/20% + [0.3, 0.4]/40% + [0.6, 0.7]/60% + [0.8, 0.9]/80% + [1, 1]/100%.

In this case, $\tilde{F}_1$ can be represented by a matrix $\overline{F}_1$, shown as follows:

$\overline{F}_1$ = <[0, 0], [0.2, 0.3], [0.3, 0.4], [0.6, 0.7], [0.8, 0.9], [1, 1]>.

The proposed interval-valued fuzzy evaluation method (*IVFEM*) for students' answerscripts evaluation is presented as follows:

Step 1: For each question in the answerscript repeatedly perform the following tasks: The evaluator awards an interval-valued fuzzy mark $\tilde{F}_i$ represented by an interval-valued fuzzy set to each question *Q.i* by his/her judgment and fills up each cell of the *i*th row for the first seven columns, where $1 \le i \le n$. Let $\overline{F}_i$ be the matrix representation of the interval-valued fuzzy mark $\tilde{F}_i$ of question *Q.i*, where $1 \le i \le n$. Based on Eq. (5), calculate the degrees of similarity $H(\overline{E}, \overline{F}_i)$, $H(\overline{V}, \overline{F}_i)$, $H(\overline{G}, \overline{F}_i)$, $H(\overline{S}, \overline{F}_i)$ and $H(\overline{U}, \overline{F}_i)$, respectively, where $\overline{E}$, $\overline{V}$, $\overline{G}$, $\overline{S}$ and $\overline{U}$ are matrix representations of the standard fuzzy sets $\tilde{E}$ (excellent), $\tilde{V}$ (very good), $\tilde{G}$ (good), $\tilde{S}$ (satisfactory) and $\tilde{U}$ (unsatisfactory), respectively. Assume that $H(\overline{E}, \overline{F}_i) = \beta_{i1}$, $H(\overline{V}, \overline{F}_i) = \beta_{i2}$, $H(\overline{G}, \overline{F}_i) = \beta_{i3}$, $H(\overline{S}, \overline{F}_i) = \beta_{i4}$ and $H(\overline{U}, \overline{F}_i) = \beta_{i5}$, where $\beta_{ij} \in [0, 1]$, $1 \le i \le n$, and $1 \le j \le 5$. Because the standard fuzzy sets $\tilde{E}$, $\tilde{V}$, $\tilde{G}$, $\tilde{S}$ and $\tilde{U}$ correspond to the letter grades "***A***", "***B***", "***C***", "***D***" and "***E***", respectively, the derived fuzzy letter grade $\tilde{g}_i$ of question *Q.i* is represented by a fuzzy set, shown as follows:

$$\tilde{g}_i = \beta_{i1}/\boldsymbol{A} + \beta_{i2}/\boldsymbol{B} + \beta_{i3}/\boldsymbol{C} + \beta_{i4}/\boldsymbol{D} + \beta_{i5}/\boldsymbol{E}, \tag{6}$$

where ***A***, ***B***, ***C***, ***D*** and ***E*** are letter grades, $H(\overline{E}, \overline{F}_i) = \beta_{i1}$, $H(\overline{V}, \overline{F}_i) = \beta_{i2}$, $H(\overline{G}, \overline{F}_i) = \beta_{i3}$, $H(\overline{S}, \overline{F}_i) = \beta_{i4}$ and $H(\overline{U}, \overline{F}_i) = \beta_{i5}$, $\beta_{ij} \in [0, 1]$, $1 \le i \le n$, and $1 \le j \le 5$.

Step 2: Calculate the total mark of the student as follows:

$$\textit{Total Mark} = \frac{1}{100} \times \sum_{i=1}^{n} [T(Q.i) \times K(\tilde{g}_i)], \tag{7}$$

where $T(Q.i)$ denotes the mark allotted to the question *Q.i* in the question paper, $\tilde{g}_i$ denotes the fuzzy letter grade awarded to *Q.i* by Step 1, and $K(\tilde{g}_i)$ denotes the derived grade-point of the derived fuzzy letter grade $\tilde{g}_i$ based on the index of optimism λ determined by the evaluator, where $\lambda \in [0, 1]$. If $0 \le \lambda < 0.5$, then the evaluator is a pessimistic evaluator. If $\lambda = 0.5$, then the evaluator is a normal evaluator. If $0.5 < \lambda \le 1.0$, then the evaluator is an optimistic evaluator. Because $90 \le \boldsymbol{A} \le 100$, $70 \le \boldsymbol{B} < 90$, $50 \le \boldsymbol{C} < 70$, $30 \le \boldsymbol{D} < 50$ and $0 \le \boldsymbol{E} < 30$, the derived grade-point $K(g_i)$ shown in Eq. (7) is calculated as follows:

$$K(\tilde{g}_i) = \{\beta_{i1} \times [(1-\lambda) \times 90 + \lambda \times 100] + \beta_{i2} \times [(1-\lambda) \times 70 + \lambda \times 90] + \beta_{i3} \times [(1-\lambda) \times 50 + \lambda \times 70] + \beta_{i4} \times [(1-\lambda) \times 30 + \lambda \times 50] + \beta_{i5} \times [(1-\lambda) \times 0 + \lambda \times 30]\} / (\beta_{i1} + \beta_{i2} + \beta_{i3} + \beta_{i4} + \beta_{i5}), \quad (8)$$

where λ is the index of optimism determined by the evaluator, $\lambda \in [0, 1]$, $H(\overline{E}, \overline{F}_i) = \beta_{i1}$, $H(\overline{V}, \overline{F}_i) = \beta_{i2}$, $H(\overline{G}, \overline{F}_i) = \beta_{i3}$, $H(\overline{S}, \overline{F}_i) = \beta_{i4}$ and $H(\overline{U}, \overline{F}_i) = \beta_{i5}$, $\beta_{ij} \in [0, 1]$, $1 \le i \le n$, and $1 \le j \le 5$. Put the derived total mark in the appropriate box at the bottom of the interval-valued fuzzy grade sheet.

Example 3.1: Consider a student's answerscript to an examination of 100 marks. Assume that in total there are four questions to be answered:

TOTAL MARKS = 100,
Q.1 carries 30 marks,
Q.2 carries 20 marks,
Q.3 carries 30 marks,
Q.4 carries 20 marks.

Assume that an evaluator awards the student's answerscript using the interval-valued fuzzy grade sheet shown in Table 2, where the index of optimism λ determined by the evaluator is 0.60 (i.e., $\lambda = 0.60$). Assume that "***A***", "***B***", "***C***", "***D***" and "***E***" are letter grades, where $90 \le \boldsymbol{A} \le 100$, $70 \le \boldsymbol{B} < 90$, $50 \le \boldsymbol{C} < 70$, $30 \le \boldsymbol{D} < 50$ and $0 \le \boldsymbol{E} < 30$. Assume that the five standard fuzzy sets are $\tilde{E}$ (excellent), $\tilde{V}$ (very good), $\tilde{G}$ (good), $\tilde{S}$ (satisfactory) and $\tilde{U}$ (unsatisfactory) represented by interval-valued membership values, shown as follows:

$\tilde{E}$ = [0, 0]/0% + [0, 0]/20% + [0.8, 0.8]/40% + [0.9, 0.9]/60% + [1, 1]/80% + [1, 1]/100%,
$\tilde{V}$ = [0, 0]/0% + [0, 0]/20% + [0.8, 0.8]/40% + [0.9, 0.9]/60% + [0.9, 0.9]/80% + [0.8, 0.8]/100%,
$\tilde{G}$ = [0, 0]/0% + [0.1, 0.1]/20% + [0.8, 0.8]/40% + [0.9, 0.9]/60% + [0.4, 0.4]/80% + [0.2, 0.2]/100%,
$\tilde{S}$ = [0.4, 0.4]/0% + [0.4, 0.4]/20% + [0.9, 0.9]/40% + [0.6, 0.6]/60% + [0.2, 0.2]/80% + [0, 0]/100%,
$\tilde{U}$ = [1, 1]/0% + [1, 1]/20% + [0.4, 0.4]/40% + [0.2, 0.2]/60% + [0, 0]/80% + [0, 0]/100%.

Table 2. Interval-valued fuzzy grade sheet of Example 3.1

Question No.	Interval-valued fuzzy mark						Derived fuzzy letter grade
Q.1	[0, 0]	[0, 0]	[0, 0]	[0.5, 0.6]	[1, 1]	[0.7, 0.8]	
Q.2	[0, 0]	[0, 0]	[0, 0]	[0.7, 0.8]	[0.8, 0.9]	[1, 1]	
Q.3	[0, 0]	[0.5, 0.6]	[1, 1]	[0.7, 0.8]	[0.4, 0.5]	[0, 0]	
Q.4	[1, 1]	[0.7, 0.8]	[0.5, 0.6]	[0, 0]	[0, 0]	[0, 0]	
							Total mark =

From Table 2, we can see that the interval-valued fuzzy marks of the questions *Q.1*, *Q.2*, *Q.3* and *Q.4* represented by interval-valued fuzzy sets are $\tilde{\tilde{F}}_1$, $\tilde{\tilde{F}}_2$, $\tilde{\tilde{F}}_3$ and $\tilde{\tilde{F}}_4$, respectively, where

$\tilde{\tilde{F}}_1$ = [0, 0]/0% + [0, 0]/20% + [0, 0]/40% + [0.5, 0.6]/60% + [1, 1]/80% + [0.7, 0.8]/100%,
$\tilde{\tilde{F}}_2$ = [0, 0]/0% + [0, 0]/20% + [0, 0]/40% + [0.7, 0.8]/60% + [0.8, 0.9]/80% + [1, 1]/100%,
$\tilde{\tilde{F}}_3$ = [0, 0]/0% + [0.5, 0.6]/20% + [1, 1]/40% + [0.7, 0.8]/60% + [0.4, 0.5]/80% + [0, 0]/100%,
$\tilde{\tilde{F}}_4$ = [1, 1]/0% + [0.7, 0.8]/20% + [0.5, 0.6]/40% + [0, 0]/60% + [0, 0]/80% + [0, 0]/100%.

[Step 1] The standard interval-valued fuzzy sets $\tilde{\tilde{E}}$, $\tilde{\tilde{V}}$, $\tilde{\tilde{G}}$, $\tilde{\tilde{S}}$ and $\tilde{\tilde{U}}$ can be represented by the matrices $\overline{E}$, $\overline{V}$, $\overline{G}$, $\overline{S}$ and $\overline{U}$, respectively, where

$\overline{E}$ = <[0, 0], [0, 0], [0.8, 0.8], [0.9, 0.9], [1, 1], [1, 1]>,
$\overline{V}$ = <[0, 0], [0, 0], [0.8, 0.8], [0.9, 0.9], [0.9, 0.9], [0.8, 0.8]>,
$\overline{G}$ = <[0, 0], [0.1, 0.1], [0.8, 0.8], [0.9, 0.9], [0.4, 0.4], [0.2, 0.2]>,
$\overline{S}$ = <[0.4, 0.4], [0.4, 0.4], [0.9, 0.9], [0.6, 0.6], [0.2, 0.2], [0, 0]>,
$\overline{U}$ = <[1, 1], [1, 1], [0.4, 0.4], [0.2, 0.2], [0, 0], [0, 0]>.

The interval-valued fuzzy marks $\tilde{\tilde{F}}_1$, $\tilde{\tilde{F}}_2$, $\tilde{\tilde{F}}_3$, $\tilde{\tilde{F}}_4$ also can be represented by matrices $\overline{F}_1$, $\overline{F}_2$, $\overline{F}_3$ and $\overline{F}_4$, respectively, where

$\overline{F}_1$ = <[0, 0], [0, 0], [0, 0], [0.5, 0.6], [1, 1], [0.7, 0.8]>,
$\overline{F}_2$ = <[0, 0], [0, 0], [0, 0], [0.7, 0.8], [0.8, 0.9], [1, 1]>,
$\overline{F}_3$ = <[0, 0], [0.5, 0.6], [1, 1], [0.7, 0.8], [0.4, 0.5], [0, 0]>,
$\overline{F}_4$ = <[1, 1], [0.7, 0.8], [0.5, 0.6], [0, 0], [0, 0], [0, 0]>.

By applying Eq. (5), we can get

$$H(\overline{E}, \overline{F}_1) = \frac{1}{6}\left[\left(1-\frac{|0-0|+|0-0|}{2}\right)+\left(1-\frac{|0-0|+|0-0|}{2}\right)+\left(1-\frac{|0.8-0|+|0.8-0|}{2}\right)+\left(1-\frac{|0.9-0.5|+|0.9-0.6|}{2}\right)+\left(1-\frac{|1-1|+|1-1|}{2}\right)+\left(1-\frac{|1-0.7|+|1-0.8|}{2}\right)\right]$$

$$= \frac{1}{6}(1+1+0.2+0.65+1+0.75)$$

$$= 0.767,$$

$$H(\overline{V}, \overline{F}_1) = \frac{1}{6}\left[\left(1-\frac{|0-0|+|0-0|}{2}\right)+\left(1-\frac{|0-0|+|0-0|}{2}\right)+\left(1-\frac{|0.8-0|+|0.8-0|}{2}\right)+\left(1-\frac{|0.9-0.5|+|0.9-0.6|}{2}\right)+\left(1-\frac{|0.9-1|+|0.9-1|}{2}\right)+\left(1-\frac{|0.8-0.7|+|0.8-0.8|}{2}\right)\right]$$

$$= \frac{1}{6}(1+1+0.2+0.65+0.9+0.95)$$

$$= 0.783,$$

$$H(\overline{G}, \overline{F}_1) = \frac{1}{6}\left[\left(1-\frac{|0-0|+|0-0|}{2}\right)+\left(1-\frac{|0.1-0|+|0.1-0|}{2}\right)+\left(1-\frac{|0.8-0|+|0.8-0|}{2}\right)+\left(1-\frac{|0.9-0.5|+|0.9-0.6|}{2}\right)+\left(1-\frac{|0.4-1|+|0.4-1|}{2}\right)+\left(1-\frac{|0.2-0.7|+|0.2-0.8|}{2}\right)\right]$$

$$= \frac{1}{6}(1+0.9+0.2+0.65+0.4+0.45)$$

$$= 0.600,$$

$$H(\overline{S}, \overline{F}_1) = \frac{1}{6}\left[\left(1-\frac{|0.4-0|+|0.4-0|}{2}\right)+\left(1-\frac{|0.4-0|+|0.4-0|}{2}\right)+\left(1-\frac{|0.9-0|+|0.9-0|}{2}\right)+\left(1-\frac{|0.6-0.5|+|0.6-0.6|}{2}\right)+\left(1-\frac{|0.2-1|+|0.2-1|}{2}\right)+\left(1-\frac{|0-0.7|+|0-0.8|}{2}\right)\right]$$

$$= \frac{1}{6}(0.6+0.6+0.1+0.95+0.2+0.25)$$

$$= 0.450,$$

$$H(\overline{U}, \overline{F}_1) = \frac{1}{6}\left[\left(1-\frac{|1-0|+|1-0|}{2}\right)+\left(1-\frac{|1-0|+|1-0|}{2}\right)+\left(1-\frac{|0.4-0|+|0.4-0|}{2}\right)+\left(1-\frac{|0.2-0.5|+|0.2-0.6|}{2}\right)+\left(1-\frac{|0-1|+|0-1|}{2}\right)+\left(1-\frac{|0-0.7|+|0-0.8|}{2}\right)\right]$$

$$= \frac{1}{6}(0+0+0.6+0.65+0+0.25)$$

$$= 0.250.$$

Because the standard fuzzy sets are $\tilde{E}$, $\tilde{V}$, $\tilde{G}$, $\tilde{S}$ and $\tilde{U}$ corresponding to the letter grades "***A***", "***B***", "***C***", "***D***" and "***E***", respectively, the derived fuzzy letter grade $\tilde{g}_1$ of question *Q.1* is represented by a fuzzy set, shown as follows:

$\tilde{g}_1 = 0.767/\mathbf{A} + 0.783/\mathbf{B} + 0.600/\mathbf{C} + 0.450/\mathbf{D} + 0.250/\mathbf{E}$.

Because the value of the index of optimism λ given by the evaluator is 0.60 (i.e., λ = 0.60), by applying Eq. (8), we can get

$$K(\tilde{g}_1) = \{0.767\times[(1-0.60)\times 90 + 0.60\times 100] + 0.783\times[(1-0.60)\times 70 + 0.60\times 90] + 0.600\times[(1-0.60)\times 50 + 0.60\times 70] + 0.450\times[(1-0.60)\times 30 + 0.60\times 50] + 0.250\times[(1-0.60)\times 0 + 0.60\times 30]\} / (0.767+0.783+0.600+0.450+0.250)$$

$$= (0.767\times 96 + 0.783\times 82 + 0.600\times 62 + 0.450\times 42 + 0.250\times 18) / 2.85$$

$$= (73.632 + 64.206 + 37.2 + 18.9 + 4.5)/2.85$$

$$= 69.627.$$

In the same way, we can get $K(\tilde{g}_2)$ = 71.343, $K(\tilde{g}_3)$ = 60.466 and $K(\tilde{g}_4)$ = 44.575.

[Step 2] Because the questions *Q.1*, *Q.2*, *Q.3* and *Q.4* carry 30 marks, 20 marks, 30 marks and 20 marks, respectively (i.e., *T(Q.1)* = 30, *T(Q.2)* = 20, *T(Q.3)* = 30 and *T(Q.4)* = 20), based on Eq. (7), we can get

$$\begin{aligned} \textit{Total Mark} &= \frac{T(Q.1)\times K(\tilde{g}_1)+T(Q.2)\times K(\tilde{g}_2)+T(Q.3)\times K(\tilde{g}_3)+T(Q.4)\times K(\tilde{g}_4)}{100} \\ &= \frac{30\times 69.627+20\times 71.343+30\times 60.466+20\times 44.575}{100} \\ &= \frac{2088.81+1426.86+1813.98+891.50}{100} \\ &= 62.211 \\ &= 62 \text{ (assuming that no half mark is given in the total mark).} \end{aligned}$$

4 Conclusions

In this paper, we have presented a new method for evaluating students' answerscripts based on interval-valued fuzzy sets, where the marks awarded to the answers in the students' answerscripts are represented by interval-valued fuzzy sets. An index of optimism λ determined by the evaluator is used to indicate the degree of optimism of the evaluator, where $\lambda \in [0, 1]$. The proposed method can evaluate students' answerscripts in a more flexible and more intelligent manner.

Acknowledgements

The authors would like to thank Professor Jason Chiyu Chan, Department of Education, National Chengchi University, Taipei, Taiwan, Republic of China, for providing very helpful comments and suggestions. This work was supported in part by the National Science Council, Republic of China, under Grant NSC 95-2221-E-011-116-MY2.

References

1. Biswas, R.: An Application of Fuzzy Sets in Students' Evaluation. Fuzzy Sets and Systems 74, 187–194 (1995)
2. Chang, D.F., Sum, C.M.: Fuzzy Assessment of Learning Performance of Junior High School Students. In: Proceedings of the, First National Symposium on Fuzzy Theory and Applications, Hsinchu, Taiwan, Republic of China, pp. 10–15 (1993)
3. Chen, S.M.: A New Method for Handling Multicriteria Fuzzy Decision-Making Problems. Cybernetics and Systems 25, 409–420 (1994)
4. Chen, S.M.: Evaluating the Rate of Aggregative Risk in Software Development Using Fuzzy Set Theory. Cybernetics and Systems 30, 57–75 (1999)
5. Chen, S.M., Lee, C.H.: New Methods for Students Evaluating Using Fuzzy Sets. Fuzzy Sets and Systems 104, 209–218 (1999)
6. Cheng, C.H., Yang, K.L.: Using Fuzzy Sets in Education Grading System. Journal of Chinese Fuzzy Systems Association 4, 81–89 (1998)

7. Chiang, T.T., Lin, C.M.: Application of Fuzzy Theory to Teaching Assessment. In: Proceedings of the, Second National Conference on Fuzzy Theory and Applications, Taipei, Taiwan, Republic of China, pp. 92–97 (1994)
8. Gorzalczany, M.B.: A Method of Inference in Approximate Reasoning Based on Interval-Valued Fuzzy Sets. Fuzzy Sets and Systems s 21, 1–17 (1987)
9. Gorzalczany, M.B.: An Interval-Valued Fuzzy Inference Method – Some Basic Properties. Fuzzy Sets and Systems 31, 243–251 (1989)
10. Echauz, J.R., Vachtsevanos, G.J.: Fuzzy Grading System. IEEE Transactions on Education 38, 158–165 (1995)
11. Law, C.K.: Using Fuzzy Numbers in Education Grading System. Fuzzy Sets and Systems 83, 311–323 (1996)
12. Ma, J., Ma Zhou, D.: Fuzzy Set Approach to the Assessment of Student-Centered Learning. IEEE Transactions on Education 43, 237–241 (2000)
13. Wang, H.Y., Chen, S.M.: New Methods for Evaluating the Answerscripts of Students Using Fuzzy Sets. In: Proceedings of the 19th International Conference on Industrial, Engineering & Other Applications of Applied Intelligent Systems, Annecy, France, pp. 442–451 (2006)
14. Wang, H.Y., Chen, S.M.: New Methods for Evaluating Students' Answerscripts Using Fuzzy Numbers Associated with Degrees of Confidence. In: Proceedings of the, IEEE International Conference on Fuzzy Systems, Vancouver, BC, Canada, pp. 5492–5497 (2006)
15. Wang, H.Y., Chen, S.M.: New Methods for Evaluating Students Answerscripts Using Vague Values. In: Proceedings of the 9th Joint Conference on Information Sciences, Kaohsiung, Taiwan, Republic of China, pp. 1184–1187 (2006)
16. Wang, H.Y., Chen, S.M.: Evaluating Students Answerscripts Based on the Similarity Measure between Vague Sets. In: Proceedings of the 11th Conference on Artificial Intelligence and Applications, Kaohsiung, Taiwan, Republic of China, pp. 1539–1545 (2006)
17. Weon, S., Kim, J.: Learning Achievement Evaluation Strategy Using Fuzzy Membership Function. In: Proceedings of the 31st ASEE/IEEE Frontier in Education Conference, Reno, NV, T3A-19–T3A-24 (2001)
18. Zadeh, L.A.: Fuzzy Sets. Information and Control 8, 338–353 (1965)
19. Zwick, R., Carlstein, E., Budescu, D.V.: Measures of Similarity Among Fuzzy Concepts: A Comparative Analysis. International Journal of Approximate Reasoning 1, 221–242 (1987)

An Intelligent Multimedia E-Learning System for Pronunciations

Wen-Chen Huang[1], Tsai-Lu Chang-Chien[1], and Hsiu-Pi Lin[2,3]

[1] National Kaohsiung First University of Science and Technology, Kaohsiung, Taiwan
[2] Chia-Nan University of Pharmacy and Science, Tainan, Taiwan
[3] National Yunlin University of Science and Technology, Yunlin, Taiwan

Abstract. The proposed system relates to an interactive scoring system for learning a language, in which a means such as a web camera is used to capture the learners lip movements and then a score is given by making a comparison with images stored in the database. The images stored in the database are those previously recorded by a teacher. By means of the scoring system, the learner can identify and rectify pronunciation problems concerning the lips and tongue. The system also records sounds as well as images from the student. The proposed system processes this data with multimedia processing techniques. With regard to the interactive perspective, a user-friendly visual interface was constructed to help learners use the system. The learners can choose the words they want to practice by capturing their lip image sequences and speech. The lip region image sequences are extracted automatically as visual feature parameters. Combining the visual and voice parameters, the proposed system calculates the similarity between a learners and a teachers pronunciation. An evaluation score is suggested by the proposed system through the previous similarity computation. By this learning process, learners can see the corresponding lip movement of both themselves and a teacher, and correct their pronunciation accordingly. The learners can use the proposed system to practice their pronunciation as many times as they like, without troubling the human teacher, and thus they are able to take more control of improving their pronunciation.

Keywords: Multimedia E-Learning System, Speech evaluation, Automatic pronunciation scoring mechanism.

1 Introduction

An object of the proposed system is to provide an interactive scoring system for learning a language, which can evaluate a learners speech according to lip and tongue movements. To achieve this, the system basically comprises of a means for capturing images of a teacher and learners mouth movements; a database for storing the teacher movements and corresponding words; and a scoring mechanism for determining the learners score by comparing the learners mouth movements with those of the same words stored in the database. The image capturing means used in the system can be a web camera or other suitable equipment. To

H.G. Okuno and M. Ali (Eds.): IEA/AIE 2007, LNAI 4570, pp. 84–93, 2007.

facilitate comparison, the images can be previously unified in size and/or number before comparison, for example, by deleting one of the images having the least difference. The learners score can be a sum of differences between the learners images and the images of the same words stored in the database; alternatively, it can be determined according to a dynamic time warping (DTW) process. The interactive scoring system can also further include a mechanism for judging whether the words to be inputted exist in the database. Accordingly, the scoring system can provide the language learner a tool to understand differences between their lip movements and the teachers when speaking the same words, and thus improve the learners pronunciation. The proposed system exhibits the following advantages:

1. The interactive system allows learners to practice alone, which can aid both learners who wish to study more outside of class as well as those who are to shy to talk in group work.
2. The lip images can help the deaf to speak more accurately, as it is obviously impractical for them to learn a language by purely audio means .
3. A novel scoring mechanism for learning languages is developed by comparing images of mouth movements between learners and teachers, since these are key to correct pronunciation.
4. The use of voice recognition also works to enhance the judging performance of the proposed system.

Figure 1 shows main components of a scoring system and their relationships in operation. As shown in Figure 1 , a learner, teacher, database and scoring mechanism are involved in the proposed system.

Prior to being used by the learner, the teacher can input words (hereinafter this will also include a letter or sentence) into the database as both text and mouth images, as captured by the web camera. These data will be stored in the database for comparison, and this procedure can be updated at any time. The words and lip images stored in the database are accessible, the learner can first select a word for practicing, and a web camera provided with the system captures consecutive images of the learners mouth while saying the word. The appropriate area covering the learners mouth will be determined by moving a frame shown on the computer screen. The scoring mechanism is to determine a score or grade for the learners pronunciation by comparing the learners lip movements with those stored in the database. The accuracy of the learners pronunciation can be evaluated according to a difference process or a dynamic time warping process. The onscreen process is shown in Figure 2 . Notice that the blue ellipse lines are the detected lip regions operated by the proposed system.

The images will be further processed for comparison. The consecutive images in color mode are then presented on the screen for the user to determine an area covering the mouth by moving a selection frame. The frame can be scaled by inputting a width and a height or by directly dragging the frame.

Figure 3 shows the corresponding images for both teachers and learners lip images after dynamic time warping (DTW) operation. The top line of images is for the teacher and the bottom line of corresponding images is for the learner.

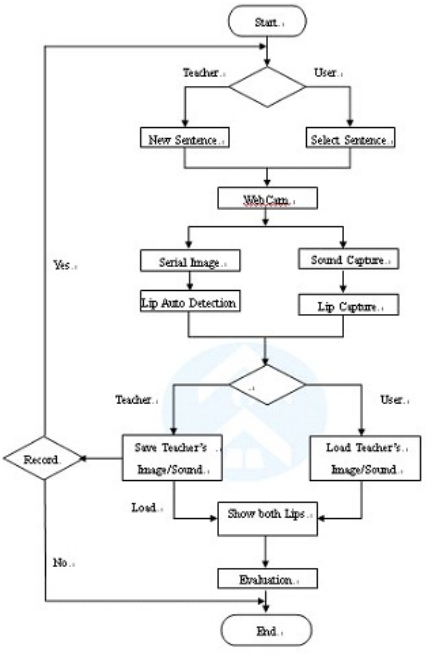

Fig. 1. System Framework

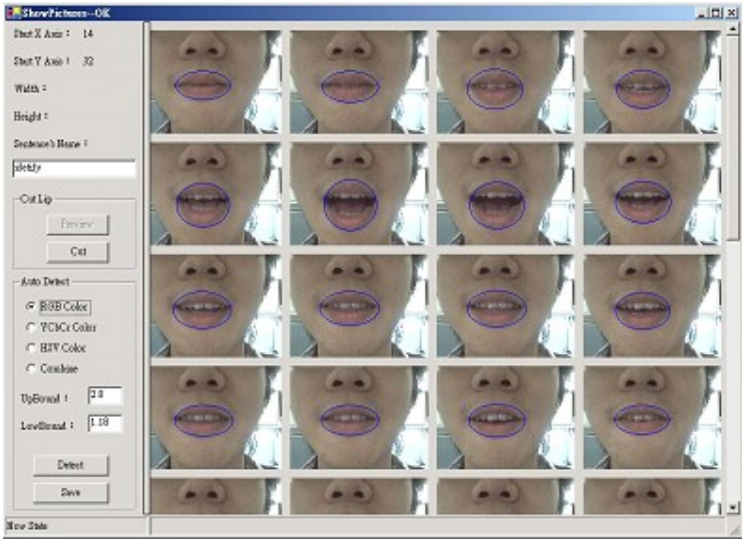

Fig. 2. The consecutive lip images captured by web camera

Through these corresponding images, the learner can compare the noticeable differences between these two images and correct their movements accordingly. Moreover, the recorded sound of the teacher and student can be listened to by

Fig. 3. The corresponding lip images between teacher and student

clicking the voice button. In the preferred embodiment of the proposed system, two processes, difference and dynamic time warping (DTW), are provided for comparison. This paper is organized as follows. In the next section, the current interactive scoring system and its place in operations are described. Section 3 illustrates the characteristics and methods used in the proposed system as well as its scoring mechanism. Section 4 demonstrates the experimental results by different algorithms. At the end of this paper, a conclusion is made in section 5.

2 Background

Currently, digital tools for learning languages are very popular with learners. Some of the tools even provide figured interfaces for users to conveniently operate and practice listening, speaking, reading and writing, for example, a multimedia storytelling website for foreign language learning [11]. However, most of the tools for practicing speaking are not efficient, as only real voice or demonstration films are provided, without any feedback of the learners practicing. Moreover, learning languages by listening is unfeasible for the deaf. Similar problems occur in asynchronous on-line courses, in which audio-visual information is sent to learners for practicing. It is difficult for the learners to find errors in pronunciation and syllables by distinguishing differences between their mouth movements and the teachers, and such tools are useless for the deaf. Therefore, it is difficult to evaluate the learners competency in speaking a language. The following techniques have been developed by some researchers to address this problem. In Deng et al.s speech evaluation [1], three types of speech characteristics, i.e., magnitude, pitch contour and Mel-Frequency Cepstral coefficients, are evaluated by dynamic time warping (DTW) and Hidden Markov Model (HMM). As a result, Mel-Frequency Cepstral coefficients show the highest relationship, pitch contour shows less, and magnitude shows the least. In Liangs research about speech practicing [5] , the main activities should include syllables associated with Pin-Yin and accent, rhythm, students speech and recognition in pronunciation types. In the investigations about recognition of lip shapes [6] [3], [4] [9], [2], lip contours for different vowels pronounced by different people are statistically analyzed. According to the results of statistics, several recognizable parameters are selected to establish a classification tree for a single vowel. The modified one-dimension

fast Hartley transform provides a structural analysis of lip contours, and the test results indicate that recognition ratios of single vowel with this classification tree are 95% for trained users and 85% for those that are untrained. Taking another approach, a bimodal audio-visual system has been developed. Mattews, etc [7] provide a recognition method for reading lips according to visual features. Three parameters representing consecutive lip contours are adapted and analyzed with Hidden Markov Model (HMM). Silsbee [10] provide other solutions in researching lip-reading with lip features, which, for example, are contour-based and image-based. In the contour-based process, edge information, deformable templates or active contours are used to find the features which can be preserved after translation, rotation, scaling and different illumination. However, much useful information may be omitted in this method, for example, features of teeth and tongue. The image-based process includes principal component analysis, wavelet and fast Fourier transform (FFT), which describe the consecutive lip images with less information. The automatic speech recognizer (ASR) provides is able to distinguish end users speech. However, the ASR system is usually disrupted by ambient noises, and thus its accuracy is lower. Leung [4] provide another solution, in which an area covering the mouth is selected according to Elliptic Shape Function and FUZZY C-MEANS. They also apply this technique to determine the lip contours on consecutive RGB images by dividing the lips into several parts, then finding the lip features and recognizing with Hidden Markov Model.

3 Methods

The technological basis of the proposed system is based on the hybrid of image and signal processing. For a sequence of lip movement images, automatic lip detection is executed. At the same time, the users sound is recorded and the voice parameters are extracted. The Pronunciation Evaluation Mechanisms will be introduced in the last subsection.

3.1 Automatic Lip Detection

Figure 4 shows the framework of automatic lip detection. First, we need to detect the location of the human face by using YCbCr color segmentation technique. Then we use the RGB and HSV color segmentation to extract the rough part of the lip image. The noise removal method is implemented by morphology operation and median filter. Finally, the refined lip detection is obtained by the connected component.

3.2 Voice Parameter Extraction

Voice is a time-varying signal. In signal processing, under the short time stationary assumption, a frame is extracted by fixed sampling windows size. There are three common characteristic parameters used in voice processing: Linear

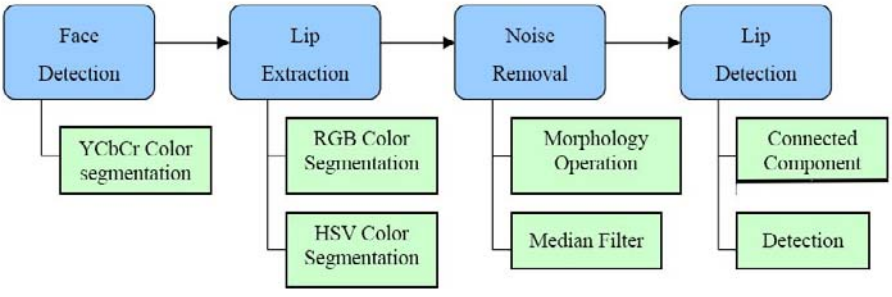

Fig. 4. Automatic lip detection framework

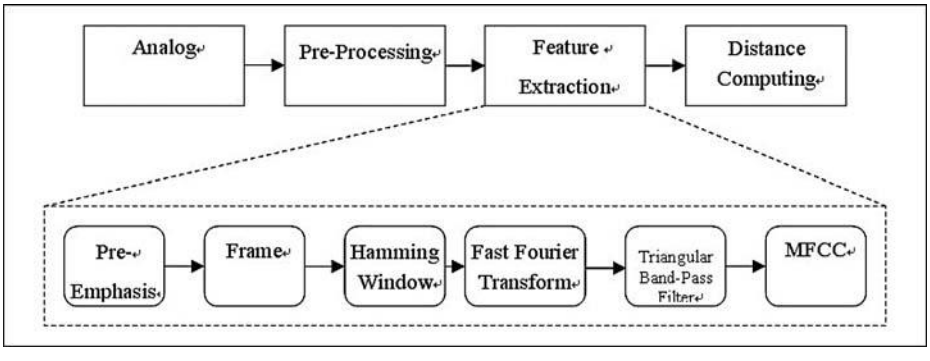

Fig. 5. Voice Parameter Extraction

Predictive Coding, Cepstrum Coefficient, Mel-scale Frequency Cepstral Coefficients [1,5] We adopt the Mel-scale Frequency Cepstral Coefficients as our voice parameter. Figure 5 shows the procedure of voice parameter extraction.

3.3 Pronunciation Evaluation Mechanisms

In the pronunciation evaluation mechanisms, we propose a hybrid method which includes information of sequences of lip images and their corresponding voice parameters. Currently, the voice recognition rate becomes acceptable in a relatively quiet environment. However, the voice recognition rate decreases dramatically with noisier surroundings. Therefore, through the use of sequences of lip images and voice recognition techniques, the evaluation of pronunciation should be significantly enhanced. Figure 6 shows the process of the proposed pronunciation evaluation mechanisms. There are three different evaluation techniques used in the proposed system. They are spatial-temporal difference, visual lip parameters evaluation, and voice parameter evaluation.

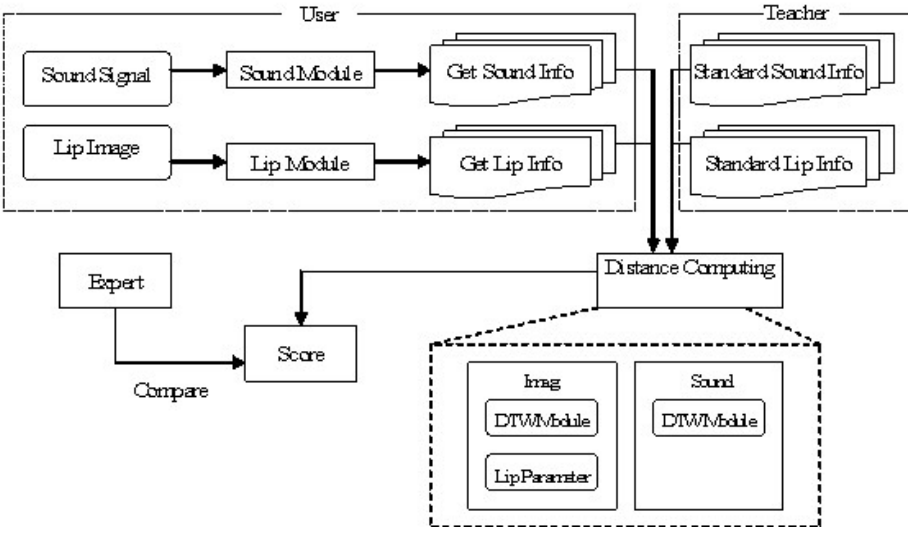

Fig. 6. The process of pronunciation evaluation

4 Experimental Results

After extracting lip image and voice parameters, real data experiments are implemented. The quantitative measurements of automatic lip detection and the pronunciation evaluation are performed.

4.1 Automatic Lip Detection

There were 15 people involved in testing the recognition rate of automatic lip detection and each person spoke 3 $\tilde{4}$ sentences. We used a web camera to capture lip images, and each image size was 320x240. The sampling rate was about 20 frames per second. The experimental platform was Pentium 4 CPU 2.4GHz, 256M RAM. Since every sentence had a different length, each person has about 90 120 frames. For each lip image, there are four parts of the lip to be evaluated, the top, bottom, left and right. Table 1 shows the correct detection rate for automatic lip detection. The overall correct detection rate is about 92%. [!t]

4.2 The Pronunciation Evaluation

In our experimental environment, there were nine people using the proposed system. Every one speak eleven different sentences. Each sentence was recorded three times. Therefore, there were a total of 297 sample sentences. From all these sample sentences, the maximal error between learner and teacher is obtained and is set to be the lowest score. The evaluation result from the proposed system was divided into five groups, very good, good, normal, not good, and

Table 1. The correct detection rate for automatic lip detection

Range	Correct	Error	Total	Percentage
Lip (top)	1570	104	1674	93.78%
Lip (bottom)	1637	37	1674	97.78%
Lip (left)	1625	49	1674	97.07%
Lip (right)	1628	46	1674	97.25%
Total	1543	131	1674	92.17%

Table 2. The evaluation level and its corresponding score range

Level	Range
Very good	$90 \leqq$ score $\leqq 100$
Good	$80 \leqq$ score < 90
Normal	$75 \leqq$ score < 80
Not good	$70 \leqq$ score < 75
Bad	score < 70

bad. The quantitative range and level representations are listed in Table 2. A human language expert was asked to grade the learners pronunciation as a benchmark to evaluate the proposed systems performan Table 3 shows the evaluation results from the human expert and the proposed system. Each row is scored by a human expert and each column is scored by the proposed system. The diagonal indicates the same level from both the human expert and the proposed system. From this confusion matrix, it shows that the correct rate is (10+80+50+9+4)/297=52%. From the evaluation level, the precision rate of very good is 10/19=53%; good is 80/121=67%; normal is 50/85=59%; not good is 9/51=18%; and bad is 4/21=19%.

Table 3. The confusion matrix between the human expert and the proposed system

System	Very good	Good	Normal	Not good	Bad	Total
Very good	10	1	2	1	1	15
Good	4	80	23	15	5	127
Normal	4	22	50	24	11	111
Not good	1	14	8	9	0	32
Bad	0	4	2	2	4	12
Total	19	121	85	51	21	297

5 Conclusions

This paper aims to develop an interactive scoring and training system for speech pronunciation by means of sequential lip images and their corresponding sounds.

These two parameters, sequences of images and recorded voices, are used to be a criterion of judging the similarity between learners and teachers. In the lip region extraction from image sequences, the current recognition rate is 92.17% successful for being able to locate the correct lip region. From the lip region extraction, the visual feature parameters can be defined. To compare the evaluation difference between the human expert and the proposed system, five levels V very good, good, normal, nor good, bad V were classified as a grading scale. The human experts grade was used as a benchmark. The proposed systems judgement was compared to the benchmark to evaluate the correctness of the system. A confusion matrix was constructed between the human expert and the proposed system. The overall correct rate was 52%. The proposed system performance was superior at the very good, good and ormal levels, with an average score of 60%, and inferior at the not good and bad levels, with average score of 18.5%. With regard to the interactive perspective, a user-friendly visual interface was constructed to help learners use the system. The learners can choose the words they want to practice by capturing their lip image sequences and speech. The lip region image sequences are extracted automatically as visual feature parameters. Combining the visual and voice parameters, the proposed system calculates the similarity between a learners and a teachers pronunciation. An evaluation score is suggested by the proposed system through the previous similarity computation. By this learning process, learners can see the corresponding lip movement of both themselves and a teacher, and correct their pronunciation accordingly. The learners can use the proposed system to practice their pronunciation as many times as they like, without troubling the human teacher, and thus they are able to take more control of improving their pronunciation. Future research includes finding an intelligent way to improve the correctness of the evaluation rate from the proposed system. Furthermore, by exporting the system to a handheld device and/or web-based application, the proposed system would be able to serve more learners, at any time, any place, and any where.

References

1. Deng, L., Yu, D., Li, X., Acero, A.: A Long-Contextual-Span Model of Resonance Dynamics for Speech Recognition: Parameter Learning and Recognizer Evaluation. In: IEEE workshop on Automatic Speech Recognition and Understanding, 384–389 (2005)
2. Kaynak, M.N.: Analysis of lip geometric features for audio-visual speech recognition. IEEE Transactions Systems, Man and Cybernetics, Part A, 564–570 (2004)
3. Lee, K.D., Lee, M.J., Lee, S.Y.: Extraction of frame-difference features based on PCA and ICA for lip-reading. In: IEEE International Joint Conference on Neural Networks, pp. 232–237 (2005)
4. Leung, S.H., Wang, S.L., Lau, W.H.: Lip Image Segmentation Using Fuzzy Clustering Incorporating an Elliptic Shape Function. In: IEEE Transactions on Image Processing, pp. 51–62 (2004)
5. Liang, W., Liu, J., Liu, R.: Automatic Spoken English Test for @Chinese Learners. In: International Conference on Communications, Circuits and Systems, vol. 2, pp. 27–30 (2005)

6. Littlefield, K., Hashemi-Sakhtsari, J.A.: Performance evaluation of an automatic speech recognizer incorporating a fast adaptive speech separation algorithm. In: IEEE International Conference on acoustic, speech and signal processings, vol. 6, pp. 6–10 (2003)
7. Mattews, I., Cootes, T.F., Bangham, J.A., Cox, S., Harvey, R.: Extraction of visual features for lipreading. IEEE Trans on Pattern Analysis and Machine Intelligence 24(2), 198–213 (2002)
8. Mok, L.L.: Visual speech features representation for automatic lip-reading. In: IEEE International Conference on Acoustics, Speech, and Signal Processing, pp. 397–400 (2004)
9. Ou, G.B., Li, X.: Speaker identification using speech and lip features. In: IEEE International Joint Conference on Neural Network 2565–2570 (2005)
10. Silsbee, P.L., Bovik, A.C.: Computer lipreading for improved accuracy in automatic speech recognition, IEEE Trans. Speech Audio Processing, 4(2), 337–351 (1996). Tamburini, F.: A multimedia framework for second language teaching in self-access environments. Computers and Education 32, 137–149 (1999)
11. Tsou, W., Wang, W., Tzeng, Y.: Applying a multimedia storytelling website in foreign language learning. Computers and Education 47, 17–28 (2006)

Phase-Based Feature Matching Under Illumination Variances

Masaaki Nishino, Atsuto Maki, and Takashi Matsuyama

Graduate School of Informatics, Kyoto University
nishino@mbox.kudpc.kyoto-u.ac.jp

Abstract. The problem of matching feature points in multiple images is difficult to solve when their appearance changes due to illumination variance, either by lighting or object motion. In this paper we tackle this ill-posed problem by using the difference of local phase which is known to be stable to a certain extent even under illumination variances. In order to realize a precise matching, we basically compute the local phase by convolutions with Gabor filters which we design in multi scales. We then evaluate the stability of local phase against lighting changes. Through experiments using both CG and real images that are with illumination variance, we show the relevancy of our theoretical investigations.

Keywords: computer vision, feature matching, local phase, Gabor filters, illumination.

1 Introduction

The problem of matching feature points in multiple images is important as a prerequisite for structure-from-motion or 3D reconstruction from multi-view images. Feature points are usually defined where high image gradients are observed in various directions so that they can be differentiated from their neighboring image points, and typically detected by operators [1,2,3] including Harris corner detectors. The task of feature matching is then to determine the set of corresponding points between input images by comparing the local intensity distributions. Given an image sequence, $I^{(k)}$ $(k = 1, 2, \cdots)$, that is due to relatively small motion from frame to frame, template matching is often employed by referring the intensities in small region around a feature point in k-th image, $I^{(k)}$, to find the corresponding point in the subsequent image, $I^{(k+1)}$.

One of the difficulties in finding the correspondence is to deal with illumination variance which tends to occur on the surface of a target object, in particular when it is in motion relative to the light sources. Namely, when the appearance of an object changes, in principle it is nearly impossible to accurately match a feature point in one image to another only by the direct comparison of intensity distributions. Some matches that are obviously wrong can be excluded as outliers by RANSAC [4], by investigating the consistency of matches as a group. However, the remaining matches would still suffer from drifts of feature points induced by the changes in their appearance.

H.G. Okuno and M. Ali (Eds.): IEA/AIE 2007, LNAI 4570, pp. 94–104, 2007.

The principal aim of this paper is to introduce a phase-based method for feature matching in order to cope with the issue of the drift under illumination variance. This is motivated for example by previous work of Fleet and Jepson [5] which shows that phase is amplitude invariant and robust with respect to smooth shading and lighting variation. Because of the characteristics, phase has been successfully applied to estimate optical flow [6], or stereo disparity in sub-pixel accuracy [7,8]. Also, Carneiro and Jepson [9] have recently proposed a phase-based local feature. They have empirically shown its improved performance over differential invariants when dealing with common illumination changes.

In the remainder of this paper, we propose to carry out feature matching by using local phase of input image which we compute by convolutions with Gabor filters. We design the filters in various forms both in terms of scales and directions, and realize a precise matching by effectively combine the outputs. We also investigate the relevancy of using local phase for feature matching theoretically on the basis of a shading model of image intensities. In the experiments we evaluate our propositions in comparison with conventional template matching, using both CG and real images with illumination variance.

2 Preliminary

Local Phase. This section provides an overview of the phase-based matching method using 1D signal. The discussion is extended to the case of 2D images in the next section.

For matching feature points we use local phase which we compute by convolutions of Gabor filters with the input signal. Gabor filter is a complex-valued function and has a form at point x,

$$g(x;\sigma,\omega_0) = \frac{1}{\sqrt{2\pi}\sigma} e^{\frac{-x^2}{2\sigma^2}} (e^{i\omega_0 x} - e^{\frac{-(\sigma\omega_0)^2}{2}}) \ , \tag{1}$$

where σ is a parameter which determines the width of the filter and ω_0 the central frequency of the power spectrum, respectively.[1] The term $e^{-(\sigma\omega_0)^2/2}$ is added to remove the DC component of the filter. Let $c(x_0,\omega_0)$ be a convolution of real-function, $f(x)$, and Gabor filter, $g(x;\omega_0)$, at point x_0, i.e. $c(x_0,\omega_0) = (f * g)(x_0,\omega_0)$. Since $c(x_0,\omega_0)$ is a complex function, we can formulate it as

$$c(x_0,\omega_0) = \rho(x_0,\omega_0) e^{i\phi(x_0,\omega_0)} \ , \tag{2}$$

by using two real functions, $\rho(x_0,\omega_0)$ and $\phi(x_0,\omega_0)$, which represent local amplitude and phase, respectively.

The Principle of Phase-Based Matching. Matching feature points in two images, $I^{(1)}$ and $I^{(2)}$, by using local phase is basically to find such points that have equivalent distributions of local phase. The spatial shift of the signal, d, is related to the phase difference, $\Delta\phi(\omega_0)$, by

[1] In below, σ is varied together with ω_0 so as to maintain the relation, $\sigma\omega_0 = \pi$.

$$d = \frac{\Delta\phi(\omega_0)}{\omega_0} \quad . \tag{3}$$

Since $\Delta\phi$ is limited to the range $-\pi \leq \Delta\phi(\omega_0) \leq \pi$, d is also limited to

$$\frac{-\pi}{\omega_0} \leq d \leq \frac{\pi}{\omega_0} \quad . \tag{4}$$

Our strategy is to first compute the phase at a feature point $z^{(1)}$ in image $I^{(1)}$ and then at a point $z^{(2)\prime}$ in $I^{(2)}$, which is a candidate to match $z^{(1)}$. Taking the phase difference, $\Delta\phi(\omega_0)$, we can directly derive d by (3), which is the residual distance between $z^{(2)\prime}$ and the point $z^{(2)}$ that precisely corresponds to $z^{(1)}$. Hence, we can match feature points by the local phase.

Although the discussion above assumes that local phase does not change between two images, we revisit the relevancy of the assumption in Sect. 4.

3 Phase-Based Feature Matching in 2D Images

3.1 Convolutions with 2D Gabor Filters

To detect local phase in 2D images, we use 2D Gabor filters, $g(x, y)$, which are

$$g(x, y; \omega_0, \theta_0) = \frac{1}{2\pi\sigma^2} e^{\frac{-1}{2}\frac{}{2}(\dot{x}^2+\dot{y}^2)} (e^{i\omega_0\dot{x}} - e^{\frac{-(\ \omega_0)^2}{2}}) \quad , \tag{5}$$

where $\dot{x}, \dot{y}$ are defined as

$$\begin{pmatrix} \dot{x} \\ \dot{y} \end{pmatrix} = \begin{pmatrix} \cos\theta_0 & \sin\theta_0 \\ -\sin\theta_0 & \cos\theta_0 \end{pmatrix} \begin{pmatrix} x \\ y \end{pmatrix} \quad , \tag{6}$$

and θ_0 and ω_0 denote the direction and the central frequency of the filter, respectively.

Here, we give a theoretical interpretation to the convolution of a 2D function and a 2D Gabor filter. Equation (5) can be expressed as a product of two components, $g_{\dot{x}}(\dot{x}; \omega_0, \theta_0)$ and $g_{\dot{y}}(\dot{y}; \omega_0, \theta_0)$, which are defined to be

$$g_{\dot{x}}(\dot{x}; \omega_0, \theta_0) = \frac{1}{\sqrt{2\pi}\sigma} e^{\frac{-\cdot^2}{2}\frac{}{2}} (e^{i\omega_0\dot{x}} - e^{\frac{-(\omega_0\ )^2}{2}}) \quad \text{, and} \tag{7}$$

$$g_{\dot{y}}(\dot{y}; \omega_0, \theta_0) = \frac{1}{\sqrt{2\pi}\sigma} e^{\frac{-\cdot^2}{2}\frac{}{2}} \quad , \tag{8}$$

respectively. Using them, we can represent $(f * g)(x_0, y_0)$, the convolution of a 2D signal $f(x, y)$ and a 2D Gabor filter $g(x, y)$ at point (x_0, y_0), as

$$\begin{aligned} (f * g)(x_0, y_0) &= \int_{-\infty}^{\infty}\int_{-\infty}^{\infty} f(x, y) g(x_0 - x, y_0 - y) dx dy \\ &= \int_{-\infty}^{\infty}\int_{-\infty}^{\infty} \dot{f}(\dot{x}, \dot{y}) g_{\dot{x}}(\dot{x}_0 - \dot{x}) g_{\dot{y}}(\dot{y}_0 - \dot{y}) d\dot{x} d\dot{y} \\ &= \int_{-\infty}^{\infty} g_{\dot{x}}(\dot{x}_0 - \dot{x}) \left\{ \int_{-\infty}^{\infty} \dot{f}(\dot{x}, \dot{y}) g_{\dot{y}}(\dot{y}_0 - \dot{y}) d\dot{y} \right\} d\dot{x} \quad , \end{aligned} \tag{9}$$

where $(\dot{x}_0, \dot{y}_0)$ corresponds to point (x_0, y_0) on $\dot{x}$-$\dot{y}$ coordinate system such that $\dot{x}_0 = x_0 \cos\theta_0 + y_0 \sin\theta_0$, and $\dot{y}_0 = -x_0 \sin\theta_0 + y_0 \cos\theta_0$, respectively. $\dot{f}(\dot{x}, \dot{y})$ also corresponds to the signal $f(x, y)$ in this coordinate system, i.e. $\dot{f}(\dot{x}, \dot{y}) = f(x, y)$. Now, defining the following function of $\dot{x}$,

$$\dot{f}_{\theta_0}(\dot{x}) = \int_{-\infty}^{\infty} \dot{f}(\dot{x}, \dot{y}) g_{\dot{y}}(\dot{y}_0 - \dot{y}) d\dot{y} \ , \tag{10}$$

we can interpret (9) as the convolution of the 1D function $\dot{f}_{\theta_0}(\dot{x})$ and a 1D Gabor filter, $g_{\dot{x}}$. We call $\dot{f}_{\theta_0}(\dot{x})$ the *directional function* for direction θ_0. $\dot{f}_{\theta_0}(\dot{x})$ turns out to be a 1D function obtained by convolving a 2D function $\dot{f}(\dot{x}, \dot{y})$ with the Gauss function, $g_{\dot{y}}$, at each point on line $\dot{y} = \dot{y}_0$ for the direction of $\dot{y}$.

3.2 Issues in 2D Phase-Based Matching

In 2D images, the relation between the difference of local phase and the distance of two points is formulated as

$$\boldsymbol{d} \cdot \boldsymbol{\omega}_0 = \Delta\phi(\boldsymbol{\omega}_0) \ , \tag{11}$$

where $\boldsymbol{d} = (d_x, d_y)$ and $\boldsymbol{\omega}_0 = (\omega_0 \cos\theta_0, \omega_0 \sin\theta_0)$ are both 2-vector and $\boldsymbol{d}$ represents the distance, while $\boldsymbol{\omega}_0$ the central frequency of the Gabor filters. However, different from the case in 1D signal, we cannot determine $\boldsymbol{d}$ directly from $\boldsymbol{\omega}_0$ and $\Delta\phi(\boldsymbol{\omega}_0)$ since $\Delta\phi(\boldsymbol{\omega}_0)$ is a scalar. Therefore we first assume that $\boldsymbol{d}'(\theta_0)$ is the projection of $\boldsymbol{d}$ to the direction θ_0, and substitute $\boldsymbol{d}'$ for $\boldsymbol{d}$ in (11). With this, we can determine $\boldsymbol{d}'(\theta_0)$ directly, and then calculate $\boldsymbol{d}$ using two estimates of $\boldsymbol{d}'(\theta_0)$ for different directions. This is valid when the 2D signal has simple form, but not always in real images. Moreover, the local phase may become unstable when the real component of the Fourier transform of the signal is small.

3.3 Integration of Filters by Using Evaluation Function

For the reasons stated above, we employ multiple Gabor filters to compute the distance, $\boldsymbol{d}$, and integrate the outputs of these filters. We then apply an evaluation function, $J_{\boldsymbol{x},\boldsymbol{x}'}(\boldsymbol{d})$, of the distance between two points $\boldsymbol{x}$ and $\boldsymbol{x}'$ that Wiskott et al. proposed [10] for solving a graph matching problem. When we use N different Gabor filters that have different combination of parameters ω_0 and θ_0, we have

$$J_{\boldsymbol{x},\boldsymbol{x}'}(\boldsymbol{d}) = \sum_{j=1}^{N} \rho_j(\boldsymbol{x}) \rho_j(\boldsymbol{x}') \{\Delta\phi_j(\boldsymbol{x}, \boldsymbol{x}') - \boldsymbol{d} \cdot \boldsymbol{\omega}_j\}^2 \ , \tag{12}$$

where $\Delta\phi_j(\boldsymbol{x}, \boldsymbol{x}') = \phi_j(\boldsymbol{x}) - \phi_j(\boldsymbol{x}')$, and $\boldsymbol{\omega}_j = (\omega_{jx}, \omega_{jy}) = (\omega_j \cos\theta_j, \omega_j \sin\theta_j)$. Since the term $\Delta\phi_j(\boldsymbol{x}, \boldsymbol{x}') - \boldsymbol{d} \cdot \boldsymbol{\omega}_j$ is a transformation of (11) and should be zero for proper $\boldsymbol{d}$ in an ideal case, we can obtain $\boldsymbol{d}$ as minimizing $J_{\boldsymbol{x},\boldsymbol{x}'}(\boldsymbol{d})$, and calculate it directly by solving equations $\partial J/\partial d_x = 0$ and $\partial J/\partial d_y = 0$ for $\boldsymbol{d}$. See Appendix for the details.

By this method we can integrate the outputs of arbitrary designs of Gabor filters. Moreover, since $J_{\boldsymbol{x},\boldsymbol{x}'}(\boldsymbol{d})$ uses amplitude ρ for weighting, the influence of unstable phase is attenuated.

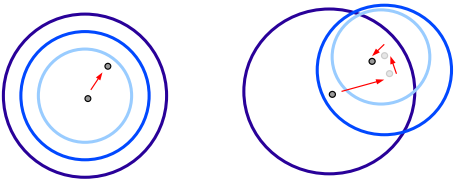

Fig. 1. Schematics of the use of multiple filters. Each circle represents the coverage of a filter. Left one is a sketch of matching in one shot. Right one shows the iterative matching. The iterative use of filters allows a coverage for wider disparities and a more reliable matching with filters of higher frequencies.

3.4 The Choice of Filters

Now that we have the method for integrating multiple filters, we need also consider the choice of filters and how to utilize them in practice. We set the parameters of Gabor filters as a combination of $\omega_\nu = 2^{-(\nu+1)}\pi$ $(\nu = 0, \ldots, 3)$ and $\theta_\mu = \mu\pi/8$ $(\mu = 0, \ldots, 7)$, and thereby we use $4 \times 8 = 32$ sorts of Gabor filters. In integrating these filters, we take a coarse-to-fine strategy. Equation (4) tells that $\boldsymbol{d}$ obtained from multiple filters is limited to the range $|\boldsymbol{d}| \leq \pi/\omega_{\max}$, where $\omega_{\max}$ is the greatest central frequency in the group of Gabor filters.

Thus, we group the filters into several sets by their central frequencies, ω_ν, and first use only those with the lowest central frequency. For the obtained matching points, we compute the residual of the distance using the set of filters with the second lowest frequency, and iteratively continue this procedure using filter groups with higher frequencies. In this way, we can use many filters and obtain more reliable matching even when $\boldsymbol{d}$ has a large value. Figure 1 is a sketch of this method. In the experiments in Sect. 5, we group 32 filters into four sets and use all of them for matching.

3.5 Matching Algorithm

We describe the matching algorithm. $I^{(k)}$ $(k = 1, 2, \ldots)$ denotes each frame in a sequence of images.

1. Apply a feature point detector to $I^{(1)}$, obtaining feature points $\boldsymbol{z}^{(1)} = (z_1^{(1)}, \ldots, z_m^{(1)})$. Set $k = 1$.
2. Set points $\boldsymbol{z}^{(k+1)\prime} = (z_1^{(k+1)\prime}, \ldots, z_m^{(k+1)\prime})$ in $I^{(k+1)}$. These points are candidates which is to match $\boldsymbol{z}^{(k)}$ or close to $\boldsymbol{z}^{(k)}$. When the difference between $I^{(k)}$ and $I^{(k+1)}$ is small, set $\boldsymbol{z}^{(k+1)\prime}$ at the same coordinate as $\boldsymbol{z}^{(k)}$ as the initial guess.
3. Match feature points by using (12), obtaining the feature points in $I^{(k+1)}$, i.e. $\boldsymbol{z}^{(k+1)}$. By the coarse-to-fine strategy, repeat matching for several times. Set $k = k + 1$, and return to step 2.

4 Analysis of Phase Under Illumination Variances

In this section, we analyze the local phase under illumination variances. We employ the Lambertian reflection model and represent the pixel intensity, $L(p)$, of a point p under incident light by a light source at infinity as

$$L(p) = \boldsymbol{b}(p) \cdot \boldsymbol{l}_0 \ . \tag{13}$$

The 3-vector $\boldsymbol{l}_0$ is the product of the strength of the light source with the unit vector for its direction whereas the 3-vector $\boldsymbol{b}(p)$ is defined to be the product of the albedo, $\eta(p)$, with the inward facing unit normal, $\hat{\boldsymbol{b}}(p)$, for point p. Hence, $\boldsymbol{b}(p) = \eta(p)\hat{\boldsymbol{b}}(p)$, and $\hat{\boldsymbol{b}}(p)$ can then be considered to encode the 3D shape of the surface around p, and $\eta(p)$ to represent the texture of the object.

The positions of detected feature points are according to η and $\hat{\boldsymbol{b}}$ since many of feature points detectors, such as Harris corner detector, extract feature points at the position where the image gradients are steep in two dimensions. We can thereby classify feature points into two categories by the parameters which give rise to high gradient. For these two types of feature points, we analyze the phase under illumination variances. We first assume 1D signal $f(x)$, which we define as the pixel intensity at position x as

$$f(x) = \eta(x)\hat{\boldsymbol{b}}(x) \cdot \boldsymbol{l}_0 \ . \tag{14}$$

We then extend the discussions to the case with a 2D signal.

Feature Points Due to Texture. First, we analyze the group of feature points that are detected due to steep gradient of the texture. We assume that these feature points are only due to texture and $\hat{\boldsymbol{b}}(x)$ is constant, i.e. $\hat{\boldsymbol{b}}(x) = \hat{\boldsymbol{b}}_0$, in the neighborhood of x. Let $f'(x)$ be the pixel intensity caused by the incident light $\boldsymbol{l}'_0$. Since the surface normal is constant, the effect of the change from $\boldsymbol{l}_0$ to $\boldsymbol{l}'_0$ is uniform and the relation between $f(x)$ and $f'(x)$ can be written as

$$f'(x) = \alpha f(x) \ , \tag{15}$$

where α is a coefficient. Let $\rho(\omega)$ and $\phi(\omega)$ be the amplitude and the phase of $f(x)$ at frequency ω, respectively. Analogously, let $\rho'(\omega)$ and $\phi'(\omega)$ be those of $f'(x)$. In frequency domain the relation of (15) corresponds to the change of the amplitude, and thus we have

$$\rho'(\omega) = \alpha\rho(\omega) \tag{16}$$

$$\phi'(\omega) = \phi(\omega) \ . \tag{17}$$

Hence, for 1D signals the local phase of a feature point due to its texture is stable even if the incident light changes. This is also true for 2D signals because the relation in (15) is not limited to the case with 1D signals.

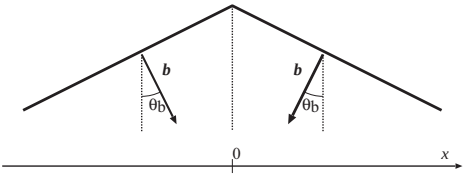

Fig. 2. The area where surface normal changes discontinuously

Feature Points Due to Shape. Next, we analyze the group of feature points due to the shape of an object. In particular we analyze an surface that is composed of two parts of different normal vector, see Fig. 2. We assume the texture of the parts is constant, i.e. $\eta(x) = \eta_0$. Let the coordinate where two different parts are connected be $x = 0$, then the normal $\hat{\boldsymbol{b}}$ can be expressed as

$$\arg \hat{\boldsymbol{b}}(x) = \begin{cases} -\theta_b & (x \geq 0) \\ +\theta_b & (x < 0) \end{cases} , \tag{18}$$

where θ_b denotes the angle between angle bisector of the corner made by the two different parts and the normal vector of each part. Then the pixel intensity is

$$f(x) = \begin{cases} \eta_0 |\boldsymbol{l}_0| \cos(\theta_l + \theta_b) & (x \geq 0) \\ \eta_0 |\boldsymbol{l}_0| \cos(\theta_l - \theta_b) & (x < 0) \end{cases} , \tag{19}$$

where θ_l is the angle of $\boldsymbol{l}_0$ defined relative to the angle bisector. Equation (19) implies that $f(x)$ under illumination variance is not uniform. However, $f(x)$ can be expressed as

$$f(x) = au(x) + b \ , \tag{20}$$

by using a step function, $u(x)$, and coefficients a and b. Using this expression, the pixel intensity caused by varying incident light can also be expressed as $f'(x) = a'u(x) + b'$ with coefficients a' and b'.

In the frequency domain the counterpart of (20) gives

$$F(\omega) = aU(\omega) + 2\pi b\delta(\omega) \ , \tag{21}$$

where $F(\omega)$ and $U(\omega)$ are the Fourier transforms of $f(x)$ and $u(x)$, respectively. As we have explained in Sect. 2, the DC component is excluded from the Gabor filter. Thus, $F(\omega) = aU(\omega)$. The amplitude and the phase change due to the variance of incident light as

$$\rho'(\omega) = \left| \frac{a'}{a} \right| \rho(\omega) \tag{22}$$

$$\phi'(\omega) = \begin{cases} \phi(\omega) & (a'/a \geq 0) \\ -\phi(\omega) & (a'/a < 0) \end{cases} . \tag{23}$$

This implies that the phase is stable under illumination change as long as $a'/a \geq 0$, i.e., as long as the sign of θ_l is unchanged.

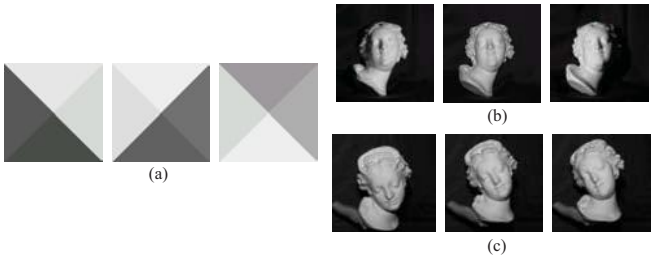

Fig. 3. Examples of images used in the experiments. (a) CG images. (b) Real images of a statue captured under different lighting positions. (c) Real images of the statue captured in different poses.

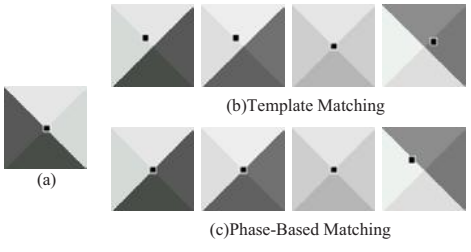

Fig. 4. Matching for CG images. (a) Reference image. (b) Results by template matching. (c) Results by phase-based matching.

For 2D signals, we have seen in Sect. 3.1 that the convolution with a 2D Gabor filter is attributed to that of directional function $\dot{f}_{\theta_0}(\dot{x})$ for direction θ_0 with 1D Gabor filter. Hence the phase is stable under illumination change as long as $\dot{f}_{\theta_0}(\dot{x})$ for certain directions satisfy the above described condition and the effect of them are dominant after integrating those functions in (12). In the next section we use CG simulated images to examine the stability of local phases experimentally.

5 Experiments

We use three classes of image sequences, including CG images and real images, for evaluating our method. We compare the results with those obtained by conventional template matching – SAD (Sum of Absolute Difference) of mean subtracted pixel intensities between a template and an input image,[2] which reduces the influence of uniform brightness change.

CG Images. Images in Fig. 3(a) are generated by viewing a pyramid shaped object with diffuse surface from the top, while changing the position of the light

[2] The template size is 9 × 9 pixels and the search area 21 × 21 pixels.

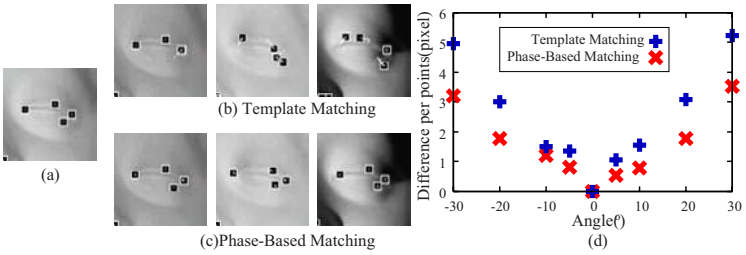

Fig. 5. Matching for real images of an object captured under different lighting positions. (a) Reference image. (b) Results by template matching. (c) Results by phase-based matching. (d) Average displacements of feature points (in pixels) for different lighting positions that are defined (in angle) relative to the reference image.

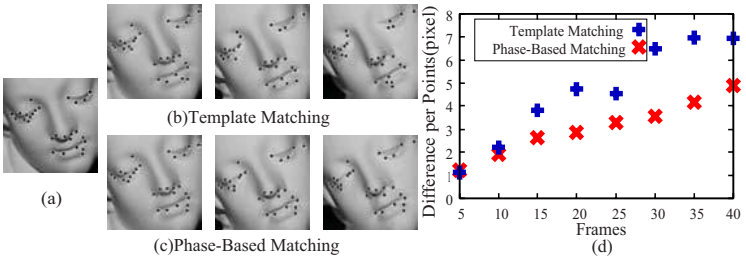

Fig. 6. Matching for a sequence of real images of an object in different poses. (a) First frame. (b) Results by template matching. (c) Results by phase-based matching. (d) Average distances (in pixels) between matched points and the epipolar line in the first frame.

source. Since image gradients are steep in two dimensions at the top of the pyramid, we define a feature point there in the reference image and match it in other images.

Figure 4(a) shows the reference image while (b) and (c) show the results by template matching and phase-based matching, respectively. These results show that the phase-based matching succeeded in some cases where template matching failed. In particular, for the leftmost image of Fig. 4(c), the matching succeeded even though the brightnesses in both side areas have been reversed. As a whole, in this experiment the phase-based matching turned out to be valid when the brightest area is common between two images. This result supports the argument in Sect. 4 that local phase stays constant as long as the change of the light position is limited to a certain range.

Real Images Under a Moving Light Source. We search for matching of feature points in real images as shown in Fig. 3(b). These images are captured by viewing a statue from its front, with a light source at 0°, 5°, 10°, 20°, 30° away from the optic axis of the camera to both left and right sides. We use the image with the light source at 0° as the reference image and detect feature points

by Harris corner detector. We then find matching of these points in the other images. Note that we preclude some of them that are shadowed in some images, and those on the boundary of the foreground.

Figure 5 shows the results of matching. Figure 5(d) plots the average displacements of the coordinates of the feature points measured from the reference image for different lighting positions. We can observe that the phase-based matching gives results with less displacements in all cases.

Real Images of an Object in Motion. We search for feature points in time series images of a statue which are captured while changing the pose of it as shown in Fig. 3(c). These images are taken at a rate of 30 frames per second and we examine a sequence of 40 images. We extract feature points in the first frame by applying Harris corner detector. Again, we remove those on the boundary of the foreground and those which are occluded in some frames.

For matching feature points between consecutive images, it is natural to refer image $I^{(k-1)}$ to obtain a corresponding feature point in image $I^{(k)}$. In this experiment, however, we choose to determine corresponding feature points in image $I^{(k)}$ by comparing their local phases or pixel intensities to those in the first frame, $I^{(1)}$, so that we can deal with the case that illumination variance under postural change is nontrivial. On the other hand, in order to narrow the search area, we utilize the coordinates of the feature points in $I^{(k-1)}$ as the initial estimates of those in $I^{(k)}$.

To evaluate the performance of the feature matching we use epipolar line. First, we compute the fundamental matrices by using the coordinates of the feature points in the first frame and those of corresponding feature points in each of 5, 10, 15, 20, 25, 30 and 35 frames. Then we use them to draw epipolar lines in the first frame image and check the average distance between matched points and the epipolar line in each case. Since the distance should become zero when the matching is ideally computed, we can employ this value as a measure of accuracy of the feature matching. We assumed affine camera model.

Figure 6 shows the results of matching. Figure 6(d) plots the average distances between matched points and the computed epipolar line. We can observe that the phase-based method realizes smaller average distance in all frames.

6 Conclusion

In this paper, we have proposed a phase-based method for feature matching and analyzed its stability under illumination variances. The method turned out to show improved results compared to conventional template matching in situations where illumination changes. In order to discuss the efficiency of our method more generally, we need further theoretical analysis of local phase under lighting changes. Analyses on signals which encode continuous changes in the orientation of objects surfaces would be typical ones. It will also be worth seeking further efficient ways to select and integrate multiple filters.

Acknowledgements. We wish to thank Prof. Akihiro Yamamoto for approving the research, and Dr.Takatsugu Hirayama for helpful comments. This work is supported by MEXT, Japan, under a Grant-in-Aid for Scientific Research (No.16680010) and in part by national project on "Development of high fidelity digitization software for large-scale and intangible cultural assets".

References

1. Harris, C., Stephens, M.: A combined corner and edge detector. In: Proc. the Fourth Alvey Vision Conference, pp. 147–152 (1988)
2. Shi, J., Tomasi, C.: Good features to track. In: Proc. of CVPR'94, IEEE Computer Society, pp. 593–600 (1994)
3. Smith, S.M., Brady, J.M.: SUSAN – A new approach to low level image processing (TR95SMS1c) (1995)
4. Hartley, R.I., Zisserman, A.: Multiple View Geometry in Computer Vision, 2nd edn. Cambridge University Press, Cambridge (2004)
5. Fleet, D.J., Jepson, A.D.: Stability of phase information. IEEE Trans. PAMI 15(12), 1253–1268 (1993)
6. Barron, J., Fleet, D.J., Beauchemin, S.: Performance of optical flow techniques. IJCV 12, 43–77 (1994)
7. Sanger, T.D.: Stereo disparity computation using Gabor filters. Biological Cybernetics 59, 405–418 (1988)
8. Maki, A., Bretzner, L., Eklundh, J.O.: Local Fourier phase and disparity estimates: an analytical study. In: Proc. 6th International Conference on Computer Analysis of Images and Patterns, pp. 868–873 (1995)
9. Carneiro, G., Jepson, A.D.: Phase-based local features. In: Proc. ECCV 2002, pp. 282–296. Springer, Heidelberg (2002)
10. Wiskott, L., Fellous, J.M., Krüger, N., von der Malsburg, C.: Face recognition by elastic bunch graph matching. In: Intelligent Biometric Techniques in Fingerprint and Face Recognition, pp. 355–396. CRC Press, Boca Raton (1999)

A Calculation of Distance from Evaluation Function

From (11), we can calculate $\boldsymbol{d}$ directly by solving equations $\partial J/\partial d_x = 0$ and $\partial J/\partial d_y = 0$ for $\boldsymbol{d}$, as

$$\begin{pmatrix} d_x \\ d_y \end{pmatrix} = \frac{1}{\Gamma_{xx}\Gamma_{yy} - \Gamma_{xy}\Gamma_{yx}} \times \begin{pmatrix} \Gamma_{yy} & -\Gamma_{yx} \\ -\Gamma_{xy} & \Gamma_{xx} \end{pmatrix} \begin{pmatrix} \Phi_x \\ \Phi_y \end{pmatrix} \quad , \tag{24}$$

where $\Gamma_{xx}\Gamma_{yy} - \Gamma_{xy}\Gamma_{yx}$ must be nonzero, and Γ_{xy}, Φ_x are

$$\Gamma_{xy} = \sum_{j=1}^{N} \rho_j(\boldsymbol{x})\rho_j(\boldsymbol{x}')\omega_{jx}\omega_{jy} \tag{25}$$

$$\Phi_x = \sum_{j=1}^{N} \rho_j(\boldsymbol{x})\rho_j(\boldsymbol{x}')\omega_{jx}\Delta\phi_j(\boldsymbol{x},\boldsymbol{x}') \quad , \tag{26}$$

respectively. Γ_{xx}, Γ_{yx}, Γ_{yy} and Φ_y are analogously defined by substituting ω_{jx} and ω_{jy} in (25) and (26).

Text Extraction for Spam-Mail Image Filtering Using a Text Color Estimation Technique

Ji-Soo Kim, S.H. Kim, H.J. Yang, H.J. Son, and W.P. Kim

Computer Science Dept., Chonnam National University, Korea
kimjisoo@iip.chonnam.ac.kr, {shkim, hjyang}@chonnam.ac.kr,
{sonhj, kwp2095}@iip.chonnam.ac.kr

Abstract. In this paper, we propose an algorithm for extracting text regions from images in spam-mails. The Color Layer-Based Text Extraction(CLTE) algorithm divides the input image into eight planes as color layers. It extracts connected components on the eight planes, and then classifies them into either text regions or non-text. We also propose an algorithm to recover damaged text strokes in Korean text images. There are two types of damaged strokes: (1) middle strokes such as ‘ㅣ’ or ‘ㅡ’ are deleted, and (2) the first and last strokes such as ‘ㅇ’ or ‘ㅁ’ are filled with black pixels. An experiment with 200 spam-mail images shows that the proposed approach is more accurate than conventional methods by over 10%.

Keywords: Text Extraction, Color Layer, Spam-mail Filtering, Character Segmentation.

1 Introduction

Images in spam-mails have many texts which are well-separated from the background regions. Texts in spam-mail images contain very important information to classify spam or non-spam emails. If we could recognize these texts accurately in real time, we can filter spam-mails. In this paper, we propose two algorithms to extract text regions from images in spam-mails using color layers and to recover damaged text strokes from the extracted text image by using color information.

Previous works on recognizing text in images can be briefly classified into a text extraction research[1,2,5,6] and a text recognition research[3,4]. [1] presented two methods for the localization of text in complex color images. The first one is based on a color segmentation step performed by searching for prototype colors as local maxima on the color histogram. The second considers the local spatial variance on a gray-level image computed over horizontal lines. [2] proposed two methods using a differential top-hats morphological operator and a direction filter. These methods show robustness to the light changes in images.

The binarization is the essential preprocessing for recognizing texts. One of the older methods in image binarization is Niblack's [3], based on local mean and standard. It uses a recognition engine in a commercial OCR software. [4] used topological features, weight-Euclidean distance and modified coarse-fine fuzzy c-means clustering. It also uses a commercial recognition software.

H.G. Okuno and M. Ali (Eds.): IEA/AIE 2007, LNAI 4570, pp. 105–114, 2007.

We propose two algorithms for extracting text regions from spam-mail images using color layers and recovering damaged text strokes from the extracted text image. The proposed approach has two advantages than conventional methods. First, the proposed approach with simple algorithm shows more accurate results than conventional methods. Second, the text extraction results produce the binary images while conventional methods do not display it.

2 Proposed System

As illustrated in Fig. 1, the proposed system consists of two steps: text extraction and text recovering. First, the proposed system extracts text region with word unit through color reduction, creating layer images, deleting noise and non-text regions and analyzing connected components. Second, it extracts the binary images through acquiring color of the text region, determining text color, recovering damaged text strokes.

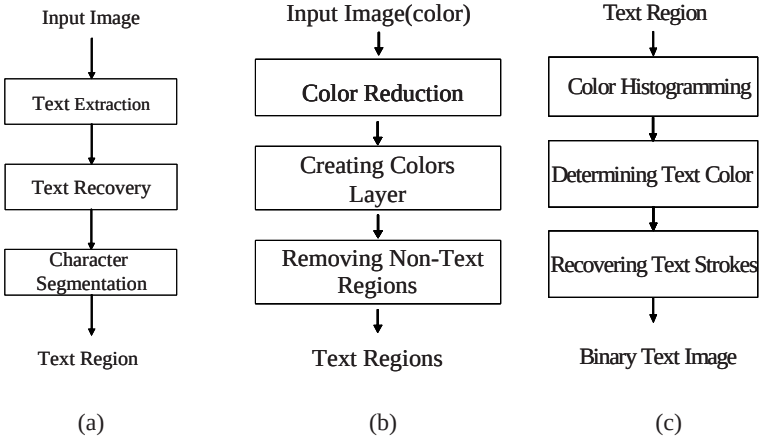

Fig. 1. Proposed system: (a) system architecture, (b) text extraction, (c) text recovery

Fig. 2 shows some spam-mail images. In this paper, we used 200 spam-mail images collected from the e-mail server of Chonnam National University and the one of Web-based. Table 1 summarizes the size of input images and resolution.

Table 1. Result of analyzing spam-mail images

Width of images(pixel)	300 - 900
Height of image(pixel)	250 - 700
Value of color	24 bit Color
Resolution of image(dpi)	72 - 96

Fig. 2. Examples of spam-mail images

2.1 Color Layer-Based Text Extraction(CLTE)

The proposed CLTE algorithm is quite simple but produces better results than conventional methods.

2.1.1 Color Reduction and Layer Images

The spam-mail images have well-separated text and background regions, for the purpose of advertisement. Color reduction is performed to reduce the number of colors and processing time. Even if colors in the spam-mail images are reduced, the text and background regions are retained. With a simple bit-dropping method, lower seven bits of each R, G, B component of each pixel are removed. The result image is expressed by 8 colors; (red=0, green=0, blue=0), (0,0,128), (0,128,0), (0,128,128), (128,0,0), (128,0,128), (128,128,0), (128,128,128). Fig. 3(a) shows an example of input images. Fig. 3(b) shows a result of color reduction.

(a) (b)

Fig. 3. Example of color reduction: (a) input image, (b) reduced image

We create eight layer images using an algorithm in Table 2.

Table 2. Algorithm for creating layer images

```
For all pixels in a reduced image
   If C(R,G,B)y,x = (0,0,0) then L1(y,x) = 1  //layer 1 image
   Else If C(R,G,B) y,x = (0,0,128) then L2(y,x) = 1  //layer 2 image
                …
   Else If C(R,G,B) y,x = (128,128,0) then L7(y,x) = 1  //layer 7 image
   Else If C(R,G,B) y,x = (128,128,128) then L8(y,x) = 1  //layer 8 image
End for
```

Here, $C(R,G,B)_{y,x}$ denotes the reduced image as in Fig. 3(b), $L_i(y,x)$ is a layer image of binary type. Fig. 4 shows 8 layer images generated by the algorithm in Table 2.

Fig. 4. Layer images for Fig. 3(b)

2.1.2 Deleting Noise and Non-text Region

We apply Blob Coloring[7] to each layer image and segment connected components. After measuring the size of bounding box on connected components, we removed noise and non-text regions if they satisfy Eq. (1), (2) and (3). Fig. 5 shows an image after deleting noise and non-text regions from a layer image.

$$CC\_H\_L_i < T_1 \text{ OR } CC\_W\_L_i < T_2. \tag{1}$$

$$CC\_H\_L_i > T_3 \text{ OR } CC\_W\_L_i > T_4. \tag{2}$$

$$CC\_W\_H\_R_i < T_5. \tag{3}$$

Here, $CC\_H\_L_i$ is the height of i-th CC(Connected Component), $CC\_W\_L_i$ is the width of i-th CC, $CC\_W\_H\_R_i$ is a ratio of width to height of i-th CC. $CC\_W\_H\_R_i$ is computed by dividing the larger by the smaller among $CC\_H\_L_i$ and $CC\_W\_L_i$. In this paper, we set T_1 and T_2 values to two pixels, T_3 and T_4 to half of the width and height of image, T_5 to five.

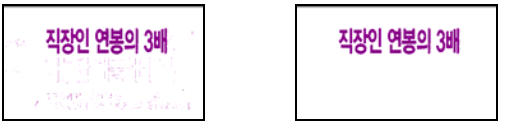

(a) (b)

Fig. 5. After deleting noise and non-text: (a) layer 8 image, (b) image after applying Eq. (1), (2) and (3)

After applying equation (1), (2) and (3) to each of the eight images, we combined eight images into one using an OR operation as in Fig. 6(a). Fig. 6(b) shows a binary image after applying Eq. (4).

$$L(y,x) = \begin{cases} 1, \text{ if } L_i(y,x) = 1 \ \exists\, i = 1,2,\cdots,8. \\ 0, \text{ otherwise.} \end{cases} \tag{4}$$

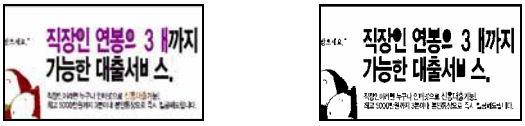

(a) (b)

Fig. 6. Deleting noise and non-text: (a) union of 8 layer images, (b) binarized image by Eq. (4)

2.1.3 Extraction of Text Region

Text regions can be extracted either character unit or word unit. In this paper, we select the latter one because we are interested in recognizing word unit. The processing of extraction is composed of two steps. First, after we have a horizontal projection profile in Fig. 7, we search for a dividing point of horizontal line, that is, to be zero point. Second, we use Blob Coloring[7] in the binarized image to segment connected components, after measuring the size of bounding box on the binarized image. We combine bounding boxes when either the distance between two bounding boxes is closer than the height of horizontal projection profile or a bounding box is overlapped to the other box. Fig. 8 shows the extracted words with bounding boxes for the image in Fig. 6(b).

Fig. 7. Image of horizontal projection

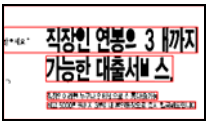

Fig. 8. Result of text extraction

The CLTE algorithm has two problems, First, middle strokes such as ‘ㅣ’ or ‘ㅡ’ are deleted when we remove noise and non-text areas using equation (1), (2), and (3). Second, the first or last strokes such as ‘ㅇ’ or ‘ㅁ’ are filled with black pixels of OR operation which combines eight images to one.

These problems do not matter in finding text location but they are important in recognizing and spotting the keywords. We explain the solution to it in the following section.

2.2 Recovering Damaged Text Strokes

In this paper, we propose an algorithm for solving the problem of damaged strokes by using a color information.

2.2.1 Estimating Text Color

Fig. 8 shows three text regions along with their bounding boxes. We can see some characters with deleted strokes and strokes filled with black pixels. Fig. 9 is a text region in Fig. 8.

Fig. 9. Text region in Fig. 8

The algorithm in Table 3 acquires color information and determines text colors.

Table 3. Algorithm for acquiring color information and determining text color

```
For i = 1 ⋯ n : number of bounding boxes extracted by CLTE algorithm
   Initialize C_1i ⋯ C_8i to zero
   For all pixels in i-th bounding box  //Acquiring color information
     If L(y,x) = 1 AND C(R,G,B)y,x = (0,0,0) then C_1i += 1
     Else if L(y,x) = 1 AND C(R,G,B)y,x = (0,0,128) then C_2i += 1
                          ⋯
     Else if L(y,x) = 1 AND C(R,G,B)y,x = (128,128,0) then C_7i += 1
     Else if L(y,x) = 1 AND C(R,G,B)y,x = (128,128,128) then C_8i += 1
   End for
   Set the text color TCi to the color of maximum frequency
End for
```

Here, $C(R,G,B)_{y,x}$ is a reduced image, L(x,y) is an output image of CLTE. The pixel value 1 in L(x,y) is black pixel. C_1_i to C_8_i in i-th bounding box is an accumulated value of C_1_i to C_8_i. TC_i is a text color in i-th bounding box. As an example, we graph accumulated values of C_1_i to C_8_i in Fig. 10. We know that the text color is color 7.

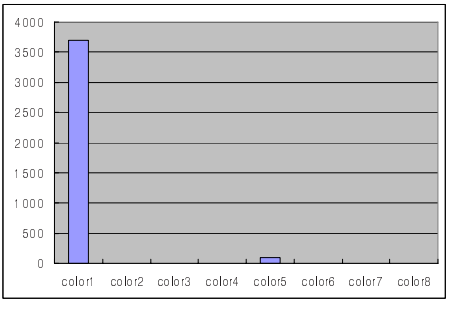

Fig. 10. Color distribution for the text pixels in Fig. 9

2.2.2 Recovering Damaged Text Strokes

Table 3 is an algorithm for recovering damaged text strokes. In addition, text and noise colors are deleted by an algorithm of Table 3. It compensates weak points of CLTE algorithm.

Table 4. Algorithm for recovering damaged text strokes

```
For i = 1 ⋯ n : number of bounding boxes extracted by CLTE algorithm
   For all pixels in i-th bounding box
     If C(R,G,B)y,x = TCi then L(y,x) = 1  //Recovering text strokes
     If C(R,G,B)y,x ≠ TCi then L(y,x) = 0  //Removing noise and non-text
   End for
End for
```

Here, TC_i is a text color for i-th bounding box. Fig. 11 shows a recovered image by the algorithm in Table 3.

Fig. 11. Recovering of text strokes: (a) before recovering, (b) after recovering

Fig. 11(a) is the image before recovering, (b) is the one after recovering. The final result of the system is a text region image of binary type.

2.3 Character Segmentation

In previous paper [8], we proposed a character segmentation algorithm for document images, based on small gaps between neighborhood characters. This method is composed of the four stages. Table 5 is an algorithm for character segmentation. The algorithm is adopted from [8].

Table 5. Algorithm for character segmentation

(1) guess the number of characters in the word
(2) search the split points to segment the word image using estimated length
(3) choose the best segmentation result
(4) perform a post-processing

Fig. 12 shows a segmentation example with the algorithm in Table 5. Fig 12(a) is the image before segmentation, (b) is the one after segmentation. Rectangles in Fig. 12(b) show the segmentation results. The final output of the system is a set of character images of binary type.

Fig. 12. Character segmentation: (a) before segmentation, (b) after segmentation

3 Experiments and Results

To evaluate the performance of the proposed system, we collected 1,369 spam-mails from the e-mail server of Chonnam National University and the one of Web-based. The number of spam-mails which include images is 1,226. It shows we have more spam-mails with images than the ones without images.

3.1 Text Extraction

We selected 200 images from the 1,226 spam-mails. We compared the performance to Kim[5] and Choi[6]. The proposed algorithm was implemented on Pentium Ⅳ 1.7GHz and RAM 512M with Visual C++ 6.0.

The performance of the text extraction is measured by precision and recall. Table 6 summarizes the performance. *Sum* represents the number of total words in images. *True* represents the number of text regions correctly identified. *Part* represents the number of partial text regions. *Error* represents the number of texts failed to detect. *False* counts the number of incorrectly identified texts. Precision represents *True*/(*True*+*Part*+*False*). Recall represents *True/Sum(True*+*Part*+*Error*).

Table 6. Comparison of text extraction algorithms(unit: no. of words)

System	*Sum*	*True*	*Part*	*Error*	*False*	Precision(%)	Recall(%)
Proposed system	1,241	984	133	124	89	81.6	79.3
Kim[5]	1,241	800	263	178	283	59.4	64.5
Choi[6]	1,241	769	12	460	130	84.4	62.0

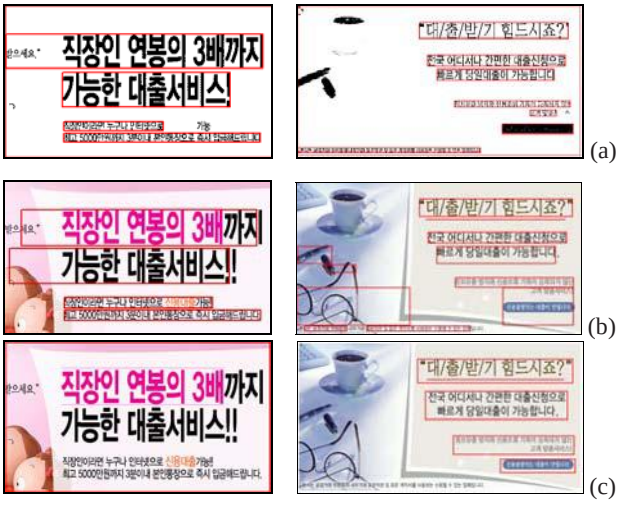

Fig. 13. Final results of text extraction: (a) proposed system, (b) Kim[5], (c) Choi[6]

Our experimental results show that the proposed approach is superior to the conventional methods. Fig. 13 shows a comparison of results by proposed system to Kim[5], and Choi[6] systems. The proposed system has a merit extracting text images in binary type which is quite different from conventional methods.

3.2 Character Segmentation

A total of 876 characters extracted, from the 200 spam-images, have been used for evaluating the performance of character segmenting. Fig. 14 shows another example of character segmentation. The performance of the character segmentation is measured by True and Error. Table 7 summarizes the performance. *Sum* represents the number of total characters in images. *True* represents the number of characters correctly segmented. *Error* represents the number of characters failed to split. Almost all errors occur in characters with italic and bold attributes.

Table 7. Result of character segmentation

Sum	876
True	717(81.8%)
Error	159(18.2%)

Fig. 14. Final results of character segmentation

4 Conclusions

In this paper, we propose two algorithms for extracting text regions from spam-mail images using color layer and for recovering the strokes from the extracted text image. Our experiment result shows that the proposed approach is more accurate than conventional methods by over 10%. Although the proposed algorithm is simple, it is more stable than conventional methods. Future work is to design the recognizer of text to be combined with the proposed system.

References

1. Zhong, Y., Zhang, H., Jain, A.K.: Automatic Caption Localization in Compressed Video. IEEE Transactions on Pattern Analysis and Machine Intelligence 22(4), 385–392 (2000)
2. Zhong, Y., Karu, K., Jain, A.K.: Locating Text in Complex Color Images. Pattern Recognition 28(10), 1523–1535 (1995)

3. Wolf, C., Jolion, J.M.: Extraction and Recognition of Artificial Text in Multimedia Documents. Pattern Analysis and Applications 6(4), 306–326 (2003)
4. Wang, X., Ding, X., Liu, C.: Character Extraction and Recognition in Natural Scene Images. In: Proc. Sixth ICDAR, pp. 1084–1088 (2001)
5. Kim, J.S., Park, S.C., Kim, S.H.: Text locating from Natural Scene Images Using Image Intensities. In: Proc. 8th ICDAR, pp. 655–659, Seoul, Korea (August 2005)
6. Choi, Y.U.: Scene Text Extraction in Natural Images Using Hierarchical Feature Combining and Verification. In: The 2nd KAIST-Tsinghua JWPR, pp. 76–102, Daejeon, Korea (2003)
7. Ballard, D.H., Brown, C.M.: Computer Vision. Prentice-Hall, Englewood Cliffs (1982)
8. Kim, S.H., Park, S.C., Jeong, C.B., Kim, J.S., Park, H.R., Lee, G.S.: Keyword Spotting on Korean Document Images by Matching the Keyword Image. In: Fox, E.A., Neuhold, E.J., Premsmit, P., Wuwongse, V. (eds.) ICADL 2005. LNCS, vol. 3815, pp. 158–166. Springer, Heidelberg (2005)

Intention Through Interaction: Toward Mutual Intention in Real World Interactions

Yasser F.O. Mohammad and Toyoaki Nishida

Nishida-Sumi Laboratory, Department of Intelligence Science and Technology,
Graduate School of Informatics, Kyoto University, Japan
yasser@ii.ist.i.kyoto-u.ac.jp, nishida@i.kyoto-u.ac.jp

Abstract. Human-Artifact interaction in real world situations is currently an active area of research due to the importance foreseen of the social capabilities of near future robots and other intelligent artifacts in integrating them into the human society. In this paper a new paradigm for mutual intention in human-artifact interactions based on the embodied computing paradigm called *Intention through Interaction* is introduced with theoretical analysis of its relation to the embodiment framework. As examples of the practical use of the framework to replace traditional symbolic based intention understanding systems, the authors' preliminary work in a real-world agent architecture (IECA) and a natural drawing environment (NaturalDraw) is briefed.

Keywords: Embodiment, Real World Agents, Interactive Perception, Mutual Intention.

1 Introduction

Classical approaches to intelligence under the symbolic computational paradigm are subject to heavy criticism that started in the last two decades of the twentieth century. The main problem with classical approaches is the detachment from the real world [1], [2].

In the same period of the last century research in human-robot interaction and human-artifact interactions attracted many researchers due to the increased use of robots and supposedly-intelligent artifacts in real life [3], [5]. To make the shift from the design-stance to the intentional-stance the artifact should be able to understand human intention and communicate its own intention to the human. The literature in human intention understanding is wide, but the approach used in most of this research is still based on the symbolic formalism, and so is still de-attached from the world [3].

In this paper we outline a new research direction toward mutual intention that is based on the embodied computation paradigm [2]. The proposed approach is not only a theoretical framework, but is a robust signal-processing/synthesis based approach to replace the traditional symbolic based approaches. To show the practical applicability of the proposed architecture, sections 5, and 6 highlights briefly two applications of the framework in the areas of Human-Agent Interaction (EICA) and Intelligent Human-Computer Interface (NauralDraw).

H.G. Okuno and M. Ali (Eds.): IEA/AIE 2007, LNAI 4570, pp. 115–125, 2007.

2 Embodied Intelligence

One of the main problems with GOFAI ("Good Old-Fashioned Artificial Intelligence") is the detachment from the real world which caused the famous grounding problem. The root of this problem can be tracked to the assumption that cognition or intelligence is a functional algorithm that operates in a central (or may be distributed) mind that is related to the world only through a set of inputs (sensors) and outputs (actuators) [1].

This view of intelligence as some transcendental phenomena is challenged by many authors on both philosophical and practical bases [1], [2]. The need of an alternative encouraged many authors to challenge the basic assumptions of GOFAI, leading to many interrelated hypotheses [2] including the dynamical hypothesis in cognitive science, and the behavioral approach in robotics [10]. There is something common in all of those alternatives; all of them are enactive approaches [2] that rely on some form of embodiment to overcome the grounding problem.

Five different notions of embodiment can be identified as suggested by Ziemke [2]. The first two of them are:

1. *Structural Coupling* which means that the agent is dynamically related to its environment forming a single combined dynamical system.
2. *Historical Embodiment* through a history of structural coupling with the environment that affects the agent's internal dynamical system.

We propose that the precondition level of embodiment for achieving intelligent autonomous real world agents is the *historical embodiment* level. What this level of embodiment emphasizes is the role of the extended interaction between the agent and the environment. This extended interaction is usually overlooked as a detail that is not important for implementing intelligent agents, but this interaction is the only way around the grounding problem as the history of the interaction can associate an *internal meaning* to the perceived signals, allowing the agent to act in the environment in a rooted and situated way, that is not possible using only externally coded algorithms.

The point to emphasize here is that the embodied intelligence that is needed is an interactive embodiment that is not only based on having a body, even one that is structurally coupled with the environment at all moments, but also having an *experience* that is evolving with the environment.

Although many researchers in the robotics and AI domains agree in general that some form of embodiment is needed [3], [5], [6], the importance of interactive or historical embodiment is not always appreciated. This situation can be seen clearly in the work done in the area of intention understanding in the Human-Robot Interaction domain. As will be seen in the next section, just naming the problem "intention understanding" [3], [5] reflects a passive attitude that ignores the need of co-evolution of intention and ignores the embodiment paradigm. For example the social embodiment paradigm of Dautenhahn [4], although mentioning the notion of interaction, is still in the structural coupling level (in accordance to his definition of embodiment as structural coupling).

3 Mutual Intention

To be able to interact naturally with humans, the real world agent (e.g. robot, ECA, etc) needs to have several faculties:

1. The ability to perceive human generated signals.
2. The ability to understand human behavior in a goal directed manner.
3. The ability to show its own intentions to the human in a natural way.

Usually those are treated as three separate problems (in accordance to the normal vertical decomposition of problems in GOFAI), but in natural interactions between humans this separation is not normally existing. In natural interaction situations the intentions of the two agents co-evolve rather than being communicated. Of course communication situations in which information is transferred in only one direction (as suggested by the points above) do exist, but this communication framework cannot be assumed to cover all possible interactions in the real world especially those involving nonverbal behavior.

Let's look at a very simple situation during which one person is giving another person directions to a specific location. This situation appears to be a one way transfer of information that should conform to the separate three steps formulation outlined above.

1. The listener *perceives* the signals given by the speaker (Passive Perception).
2. The listener *analyzes* the perceived signals (Intention Understanding).
3. The listener gives a *final feedback* (Intention Communication).

In reality the interaction will not go this way. The listener will not be passive during the instructions but will actively align his body and gives feedback to the speaker, and those actions by the listener will change the cognitive state of the speaker and indirectly changes the signals perceived by the listener. So perception will be in fact interactive not passive. The second step is also not realistic because during the interaction the listener will continuously shape her understanding (internal representation) of the speaker's intention, so no final analysis step separated from the perception will occur. The third step is again not realistic because the feedback given is continuous in the form of mutual alignment and not just a confirmation as suggested by the scenario decomposition above.

This analysis suggests recasting the problem in real world interaction from three separate problems to a single problem we call *Mutual Intention* formation and maintenance.

Mutual Intention is defined in this work as a dynamically coherent first and second order view toward the interaction focus.

First order view of the interaction focus, is the agent's own cognitive state toward the interaction focus.

Second order view of the interaction focus, is the agent's view of the other agent's first order view.

Two cognitive states are said to be in *dynamical coherence* if the two states co-evolve according to a fixed dynamical low.

Researchers in social robotics have introduced many ideas from developmental psychology like the use of imitation in learning. One problem of such work is that the task is usually the interaction itself and although the robot can actually learn new behaviors (like simple object manipulation) [7] and interacts better (joint attention) [8], the applications of those insights are still very limited because of the simplified environments/tasks and the low autonomy level (which translates to low embodiment degree).

The hypothesis we support here is that the ability to form and maintain mutual intention is a precondition to achieve acceptably intelligent real-world agents. Moreover, that this formation and maintenance process is only possible through an interactive operation of composite perception, analysis, and communication of the interacting agents' cognitive states.

4 Mutual Interaction and Embodiment

The relation between mutual intention as defined in the last section and embodiment as illustrated in the section before is very important to understand both of them. As mentioned in section 2, the level of embodiment required to achieve any nontrivial level of intelligent behavior in the real world is the interactive historical embodiment (as hypothesized by the authors), and, as shown in section 3, the precondition of natural interaction between intelligent agents is the ability to interactively form and maintain mutual intention.

The common concept here is the concept of interaction as a co-evolution between the agent and his environment (historical embodiment) and between the agent and the other agents (mutual intention formation and maintenance).

The whole vision of the Intention through Interaction framework can be stated as the following hypothesis: *Intention can be best modeled not as a fixed unknown value, but as a dynamically evolving function. Interaction between two agents couples their intention functions creating a single system that co-evolves as the interaction goes toward a mutual intention state*

5 Embodied Interactive Control Architecture (EICA)

In this section a general framework for the design of a real world agent architecture that is based on the Intention through Interaction paradigm is outlined. This design is still an ongoing work and is not completely realized into an actual agent although the Interactive Perception part (see Fig. 1) is already implemented and gave some promising results [9].

Fig. 1 gives the building blocks of the proposed architecture. The architecture consists of two major subsystems:

1. The sensorimotor control subsystem which is a reflexive control subsystem creating short loop between the sensed signals and the actions. This subsystem is essential for implementing embodiment.

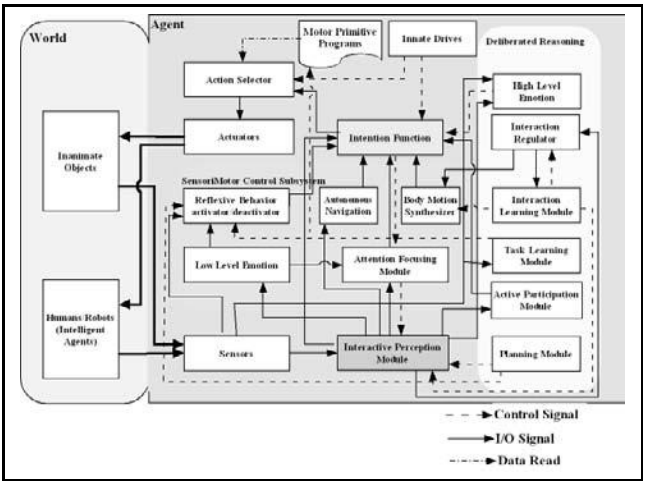

Fig. 1. Embodied Interactive Control Architecture (EICA)

2. The deliberative reasoning subsystem which is a deliberating non-symbolic subsystem that implements long term loose control loop between the sensed signals and the actions. The main responsibility of the modules of this subsystem is to control the modules of the lower sensorimotor system. This subsystem is essential for implementing historical embodiment.

The input to the agent in this framework is divided into two signal components.

1. The signal from the inanimate objects in the environment.
2. The signal from the intelligent agents (e.g. humans, animals, and robots).

This separation is essential to the design of the system as the two signals are treated differently.

The inanimate originated signals are processed through a feedback system that contains two loops, a short loop through the sensorimotor subsystem that implements reflexive behavior, and a long loop through the deliberative reasoning system that implements learning and behavior adaptation (historical embodiment).

The signals originating from intelligent agents are processed using another two control loops both passing through the Interactive Perception module, the first is a short interactive loop and the other is a long adaptation and learning loop (historical embodiment).

This separation is not compatible with the traditional passive sense-analyze-act architectures that process those two signals without using the possibility of behavior adaptation offered by the intelligent agents.

Measuring the performance of EICA can only be based on building actual systems and measuring both the performance in the real world and the ease to build those systems. This is one of the future research directions of the authors.

The most important subsystems of EICA will be illustrated in the following subsections.

5.1 Interactive Perception

This module is responsible of creating an interactive control loop around the intelligent agent generated signals in order to stabilize its perception.

Interactive Perception is defined as *allowing the perception module to intentionally affect the environment in order to align its actions with the feedback of the human*, which should also be aligned with the system's feedback. Fig. 2 gives the main building blocks of the Interactive Perception module. For implementation details refer to [9].

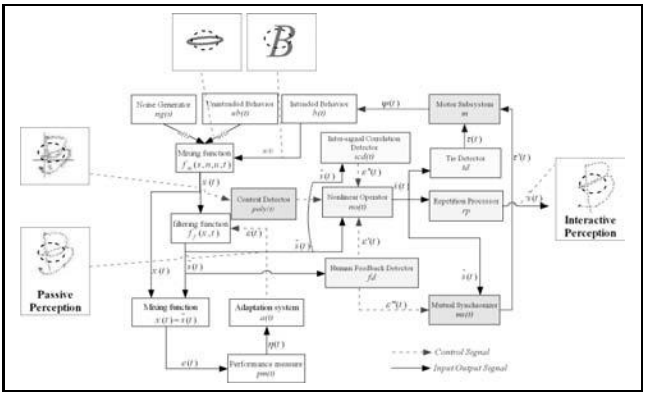

Fig. 2. The Interactive Perception Module. Example signals perceived at the key points of the system are shown when the human is showing the agent how to draw the B character.

To illustrate the operation of the module let's take an example where a human is trying to teach the agent how to draw the character "B" by illustration [9]. Fig. 2 shows the block diagram of the system and the signals perceived at the key points during this interaction. The intended behavior signal here is the character "B" and it should be clear that the intention in this case is not fixed (there is no pre-specified "B" inside the head of the human), but it evolves with the interaction, and this evolution of the intention is what is actually utilized by the module to robustly create a low level mutual intention with the human. As an example of an unintended behavior signal let's consider the third (middle) semi-circle added to the middle of the "B" character unintentionally. As usual in real world interaction there is some noise added to the signal. This is the input to the system signal x(t) in Fig. 2.

The processing is done as follows: first an adaptive filter is used to reduce the noise component creating the signal $\tilde{s}(t)$. This is what we call Passive Perception and at this point most systems stop. The result of passive perception

$\tilde{s}(t)$ is shown in Fig. 2 and it is clear that the unintended behavior is not attenuated. After that the signal $\tilde{s}(t)$ is processed by the Interactive part of the module which utilizes the temporal interaction pattern with the human to generate some form of low level mutual intention that allows the system to extract the intended behavior of the human. The implementation of this part is based on the correlation between multiple signal channels and the change in the acceleration of the human movement as related to his/her satisfaction level with the agent's perception which is given to the human online using projection on a screen (as done in [9]). The result of the Interactive Perception module is given in Fig. 2 $\hat{s}(t)$. It is clear that the unintended semi-circle is effectively eliminated by utilizing the interaction.

The main difference between interactive perception and the classical passive perception based on digital signal processing lies in two points:

1. The signal to be perceived is not assumed to be captured then analyzed offline, but the perception operation is taking part in the signal formation by the feedback that affects the human behavior [9].
2. The signal received by the sensors is assumed to be the result of nonlinear superposition of three signals, namely, the intended behavior signal, the unintended behavior signal, and noise, rather than only two components signal and noise.

5.2 Intention Function

The Intention Function module is the heart of EICA. This module is the computational realization of the view of intention that characterizes the Intention through Interaction approach. Together with the Interactive Perception module this module implements the paradigm. Together with the adaptable sensorimotor subsystem, and the task and interaction learning modules, this module implements embodiment by assigning internal meaning in the form of intention function change heuristics that grounds the agent's experiment on its perception. The intention function module is realized as an active memory module (a dynamical system) in which the required behavior plans of all the other active modules in the architecture are registered and then the module automatically updates the intentional degree (which is a measure of the probability of selection as the next action) of all those behavior tokens based on the outputs of the emotional module (that summarizes the information from the short past history), and the innate drives module (that implements a rough subjective coherence in the agent in the Uexkullian sense).

5.3 Action Selector/Attention Focusing

The action selection module is responsible of driving the actuators of the agent based on the motion primitives stored in the motion repertoire of the agent and the intention function. This module implements a judgment between various actions that are suggested by the weighted behaviors in the intention function in

the low action primitive level. The main objectives of this module are to ensure coherence in the agent actions by avoiding jumping between different behaviors and avoiding behavior conflicts. Those objectives can be shown to be conflicting and the heuristic used to bias the decision toward one of them is still an area of research.

The Attention Focusing module implements a low level weighting over the sensor generated signals to reduce the effect of irrelevant inputs based on the current state of the Intention Function and the Low Level Emotional state.

5.4 Low Level Emotion

This module continuously summarizes the inputs to the system forming a continuous representation of the internal emotional state in a multidimensional space that affects the action selector and may affect other low level behaviors like the navigation module which will go slower if the *confusion* dimension for example goes higher . The emotion dimensions of this module need not correspond to the the normal human emotions but should be based on the experience of the robot itself.

5.5 The Deliberative Subsystem

The deliberative part implements the extended experience embodiment of the agent by adjusting various parameters of the low level sensorimotor subsystem based on learning from the interaction between the agent and the environment and other intelligent agents.

Some extended time behaviors like interaction regulation can be implemented in the deliberative subsystem even though those behaviors do not represent experimental learning if there natural time scale is much longer than other sensorimotor behaviors, or if simple dynamical system implementation is not possible. Those behaviors should be implemented as control behaviors that affect the outputs of existing sensorimotor behaviors at runtime and should never update the Intention Function directly.

5.6 Relation to Other Robotic Architectures

Some other behavioral robotic control architectures can be related to EICA.

The subsumption architecture [10] is implementing a special case of EICA that disables all deliberative reasoning modules (no historical embodiment), and the Interactive Perception module (no mutual intention), and replaces the intention function, the drives, and the action selector with hard wired subsumption channels, and this is the reason that this architecture is very difficult to adopt in communicative robots.

The work of Iba [11] in Interactive Multimodal Robot Programming can be considered as another special case that do not use the intention function/action selection mechanism (no mutual intention), assumes a predefined set of programming gestures, and separates programming mode from operational mode.

A main difference between EICA and traditional robotic architecture is that it do not only specify the relation between the various processes and behaviors inside the agent but it also specifies the organization of those behaviors and the needed processes to achieve both autonomy and natural interaction with humans in the real world.

5.7 Example Robotic Implementations

Although a complete implementation of EICA in a mobile robot is not currently available, the authors have made a partial implementation that focuses on the Interactive Perception subsystem. This implementation and other suggested examples will be introduced briefly in the following subsections

Learning Paths by Demonstration. In [9] the authors gave the details of an implementation of the Interactive Perception module in the area of learning paths by demonstration using a virtual robot in the real environment. In this system the user faces the virtual robot and shows it how to draw any 2D drawing using a motion sensor attached to her finger, and the virtual robot projects the perceived signal on a monitor and uses the implicit feedback from the human to adjust its perception. Quantitative analysis revealed that the virtual robot was able to actually reduce the effects of the noise and unintended behavior better than using a passive perception system.

Path Following in a Partially Observable Environment. As a step toward implementing the EICA architecture in a robot targeting Human-Robot Team situations, the authors are building a miniature robot (using an e-puck robot) that can understand human gestures and communicates its own internal state. The robot will be used under the control of a human operator to follow a prespecified path in an environment that is partially observable to the human and partially observable to the robot. The robot will only use LEDs and motion cues to communicate its internal state as well as the environmental features it encounters to the operator. The system will implement the sensorimotor part of the architecture.

Sweeping Robot. Although not implemented yet, the EICA architecture can be used to build a sweeping robot that can be controlled by natural gesture. The interactive perception module will actively analyze the inputs from the human (sensed using motion capture devices, cameras or both) and produces a representation of the human body movements, this representation is processed by the module to interactively attenuate the signals that are not related to the current focus of the robot (decided by the attention focusing module), this operation affects the intention function by registering feedback behavior primitives to it. The same signal is also passed to the higher level interaction regularization module (and interaction learning module) for implementing body alignment, and other nonverbal natural feedback operations. The inanimate signals from the environment are processed through the reflexive subsystem to implement

low level behaviors like wandering, waste detection, following, avoidance, etc. Those behaviors also are registered to the intention function module. The inanimate signals are also passed to the deliberative subsystem to implement task learning, and planning. The robot also has a set of innate drives that manages its autonomous behavior like self charging, waste following, asking for help, etc. The only way for a behavior to affect the motor subsystem is through the intention function/action selection modules and both are adapted through the experience of the robot.

6 NaturalDraw

Real world agents are not only hardware agents. Software agents can be considered as real world agents as long as they are embodied in their information environment and interacting with humans in realtime. As an application of the *Intention Through Interaction* framework (that do not use the EICA architecture) in the software domain, the authors designed and implemented a natural drawing environment for both experienced and novice users [12] called NaturalDraw.

The feature of NaturalDraw most related to current discussion is Correction by Repetition. In natural interactions humans tend to repeat whatever they believe was not correctly perceived by the interacting partner, but most artifacts and computer systems cannot effectively use this feature of human behavior because of the inherent passivity in the dominating sensing modules. NaturalDraw overcame this limitation by using two features.

1. *Automatic Repetition Detection*, which enables the system to interactively detect the existence of repetition in the drawing. The detection operation is done using real-time tracking of the distance measure between the current stroke and the existing drawing and detecting the existence of repetition based on that history [12].
2. *Repetition Processing*, which is done using two algorithms (PFP and SA) based on the context of the interaction [12]. The result of this processing is to create a drawing that better resembles the intended one.

Preliminary experimentation with the system showed that NaturalDraw is more effective and easier to use than traditional drawing environment, and also showed that the system is equally easy to use for professional and novice users. For details about the algorithms used and statistical analysis of the results refer to [12].

7 Conclusion

The preliminary experimentation with systems designed under the guidelines of the Intention through Interaction paradigm suggests that this paradigm can be more effective in creating mutual intention between artifacts and humans than

the traditional passive intention understanding methods because it is based on an embodied signal processing and synthesis scheme, and provided two brief illustrations of it designed by the authors: *EICA* a general agent control architecture in the field of Human-Agent Interaction, and *NaturalDraw* as a free-hand drawing system in the field of HCI.

The main direction of future research is the complete realization of EICA into a real world robot to study the effectiveness of the proposed paradigm.

References

1. Vogt, P.: The Physical Symbol Grounding Problem. Cognitive Systems Research 3, 429–457 (2002)
2. Ziemke, T.: Rethinking Grounding. In: Riegler, Peschl, von Stein (eds.) Understanding Representations in the Cognitive Sciences, pp. 87–100. Plenum Press, New York (1999)
3. Tahboub, K.A.: Intelligent Human-Machine Interaction Based on Dynamic Bayesian Networks Probabilistic Intention Recognition. Journal of Intelligent and Robotic Systems 45, 31–52 (2006)
4. Dautenhahn, K., Ogden, B., Quick, T.: F rom embodied to socially embedded agents – Implications for interaction-aware robots. Cognitive Systems Research 3, 397–428 (2002)
5. Alqasemi, W.Y., Dubey, R., Pernalete, N.R.: Telemanipulation Assistance Based on Motion Intention Recognition. In: Proceedings of the 2005 IEEE International Conference on Robotics and Automation (ICRA 2005), pp. 1121–1126 (2005)
6. Dayan, P., Balleine, B.W.: Reward, Motivation, and Reinforcement Learning. Neuron 36, 285–298 (2002)
7. Lieberman, J.: Teaching a Robot Manipulation Skills through Demonstration. Msc. Thesis in Mechanical Engineering, MIT (2004)
8. Breazeal, C.: Towards sociable robots. Robotics and Autonumous Systems 42, 167–175 (2003)
9. Mohammad, Y.F.O., Nishida, T.: Interactive Perception for amplification of intended behavior in complex noisy environments. In: Proceedings of the International Workshop of Social Intelligence Design (SID2006), March 24–26, Osaka, Japan, pp. 173–187 (2006)
10. Brooks, R.A.: Challenges for Complete Creature Architectures. In: Meyer, J-A and S.W. Wilson: From Animals to Animats. In: Proceedings of the First International Conference on Simulation of Adaptive Behavior, pp. 434–443. MIT Press/Bradford Books (1991)
11. Iba, S., Paredis, C.J.J., Khosla, P.K.: Interactive Mulitmodal Robot Programming. The International Journal of Robotics Research 24, 83–104 (2005)
12. Mohammad, Y.F.O., Nishida, T.: NaturalDraw: Interactive Perception based Drawing for everyone. In: Proceedings of the 12th conference on Intelligent User Interfaces (IUI 2007), January 27–31, Honolulu, Hawaii, USA, pp. 251–260 (2007)

An Interactive Framework for Document Retrieval and Presentation with Question-Answering Function in Restricted Domain

Teruhisa Misu and Tatsuya Kawahara

School of Informatics, Kyoto University
Kyoto 606-8501, Japan
misu@ar.media.kyoto-u.ac.jp

Abstract. We propose a speech-based interactive guidance system based on document retrieval and presentation. In conventional audio guidance systems, such as those deployed in museums, the information flow is one-way and the content is fixed. To make the guidance interactive, we prepare two modes, a user-initiative retrieval/QA mode (pull-mode) and a system-initiative recommendation mode (push-mode), and switch between them according to the user's state. In the user-initiative retrieval/QA mode, the user can ask questions about specific facts in the documents in addition to general queries. In the system-initiative recommendation mode, the system actively provides the information the user would be interested in. We implemented a navigation system containing Kyoto city information. The effectiveness of the proposed techniques was confirmed through a field trial by a number of real novice users.

1 Introduction

Most of the conventional information retrieval systems assume that a display is available as an output device, and thus a list of relevant documents can be presented. However, this is not always the case when only speech interface is available, for example, audio guidance systems. Considering user's easiness of comprehension, we need to limit the amount of content presented. However, simply summarizing the retrieved document may cause the loss of an important portion of information that the user wanted to know or may have been interested in. Actually, in the conventional audio guidance systems deployed in museums and at sightseeing spots, users cannot ask questions concerning missed portions. Therefore, we propose a more interactive scheme that incorporates a question-answering (QA) technique to follow up the initial query, enabling random access to any part of the document.

Now, there are some problems with QA in such situations. One important issue is contextual analysis. During a dialogue session, users tend to make questions that include anaphoric expressions. In these cases, it is impossible to extract

H.G. Okuno and M. Ali (Eds.): IEA/AIE 2007, LNAI 4570, pp. 126–134, 2007.

the correct answer using only the current question. For example, "When was it built?" makes no sense being used by itself. In many conventional database query tasks, this problem is solved by using the task domain knowledge, such as the semantic slots of the backend database [1,2]. Whereas the majority of conventional QA tasks, such as TREC QA Track [3], have dealt with independent questions that have respective answers for each, there have been only a few works that have addressed successive questions [4]. However, they have basically hand-crafted questions rather than collecting real dialogues. In this work, we address the QA task in a real interactive guidance system using a topic tracking mechanism.

In addition, we introduce our system-initiative information recommendation function. In spoken dialogue systems, users often have difficulty making queries because they are unsure of what information the system possesses. Moreover, the system-initiative guidance is also useful in navigating users in the tasks without definite goals, such as sightseeing guidance. In order to make the guidance interactive, we propose the application of a QA technique to generate system-initiative recommendations.

Based on the above concepts, we have designed and implemented an interactive guidance system of "Dialogue Navigator for Kyoto City", and conducted a field trial for about three months. The key evaluation results of the QA function are presented in this paper.

2 System Framework

The proposed guidance system has two modes, a user-initiative retrieval/QA mode (pull-mode) and a system-initiative recommendation mode (push-mode), and switches between them according to the user's state. When a query or a question is posed by a user, the system switches to the retrieval/QA mode and generates a respective response. When the system detects the silence of the user, it switches to the system-initiative recommendation mode and presents information related to the current topic. The flow of this process is shown in Figure 1.

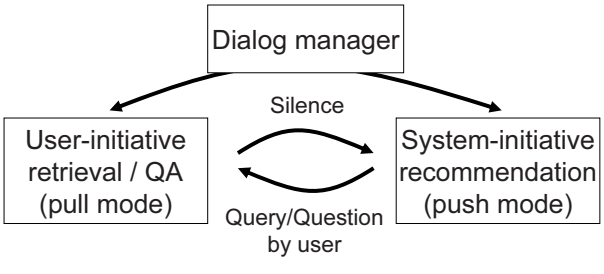

Fig. 1. System overview

Table 1. Knowledge base (KB) specifications

	# documents	# sections	# words
Wikipedia	269	678	150K
Tourist information	541	541	70K
Total	810	1,219	220K

We adopted a sightseeing guidance of Kyoto city for our target domain. The knowledge bases (KB) of this domain are Wikipedia[1] documents concerning Kyoto and the official tourist information of Kyoto city. Table 1 lists the size of these KBs.

3 User-Initiative Information Retrieval and Question-Answering

The user utterances are classified into two categories. One is an information query, such as "Please explain about the Golden Pavilion". For such queries, the system retrieves the appropriate information from the KB by section unit, and the section of the document with the highest matching score is presented to the user. The other is a question, such as "When was it built?". The system extracts the sentence from the KB that includes the answer to the question and presents it to the user. This procedure is shown in Figure 2.

3.1 Contextaul Analysis Based on Topic Detection

In dialogue systems, the incorporation of contextual information is important for generating meaningful queries for retrieval. As the deterministic anaphora resolution [5] is not easy and always error-prone, and stochastic matching is used in information retrieval, we adopt a strategy that concatenates the contextual information or keywords from the user's previous utterances to generate a query. The simplest way is to use all the utterances from the current user. However, this might also add inappropriate context because the topic might have been changed in the session. Therefore, we determine the context length (number of previous utterances) used for the retrieval by tracking the topic of the dialogue.

We use metadata of the KB or a title of the document as a topic. Thus, the topic can be tracked using the current focused documents, which usually correspond to sightseeing spots or Wikipedia entries.

3.2 Document Retrieval

We adopt an orthodox vector space model to calculate the matching score (degree of similarity) between a user query and the document in the KB. That is, the

[1] http://wikipedia.org/

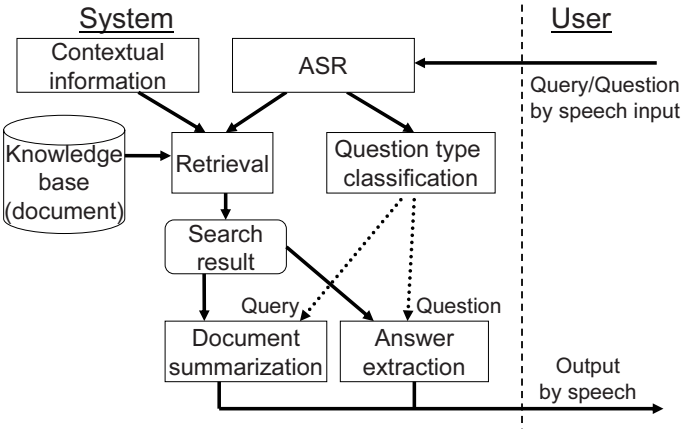

Fig. 2. Overview of document retrieval and QA

vector of the document is made based on the occurrence counts of nouns in the document by section unit. The vector for the user query is also made by merging the N-best hypotheses of the automatic speech recognition (ASR) result for the current utterance and previous utterances concerning the current topic as the context. We also use the ASR confidence measure (CM) as a weight for the occurrence count. The matching score is calculated by the product of these two vectors.

To deliver a concise presentation of the retrieved document, a summary is generated by extracting important sentences.

3.3 Answer Extraction

We have implemented the system with a general answer extraction module. A score is calculated using the following features for each named entity (NE) in the retrieved document that matches the question type (who, when, ...).

- Degree of similarity between the user utterance and the document (3.2).
- Number of matched content words in the sentence that includes the NE.
- Number of matched content words included in the clause that depend on/ depended by the clause that includes the NE.

The system then selects the NE with the highest score as an answer to the question.

4 System-Initiative Recommendation

For interactive information recommendation, we propose the generation of system-initiative questions. They are semi-automatically made from the current document using the QA technique. This is complemented by conventional

information recommendation techniques based on the document structure and similarity.

4.1 Generation of System-Initiative Questions (Method 1)

This method is intended to successively present more details on the target topic, after the initial summary presentation, because a user may be interested in some information that was not included in the summary. Although it is possible to prompt a user, such as "Would you like more details?", we propose a more interactive method by generating system-initiative questions in order to attract the interest of the user.

A set of possible questions is prepared using the following procedure. It is almost the reverse of the process to find an answer to the user's question.

1. Pick up the NE that may attract the user's interest based on $tf*idf$ criterion.
2. Substitute the NE with the corresponding interrogative.
3. Delete the subordinate clause using a syntactic parser.
4. Transform the sentence into an interrogative form.

Figure 3 shows an example of the transformation of a sentence in the KB into a question using the above-mentioned procedure.

Original: By the way, **Queen Elizabeth** praised this stone garden a lot, when ...

⇓ (Substitute target NE into the corresponding interrogative)

- By the way, **who** praised this stone garden a lot, when ...

⇓ (Delete subordinate clause)

- Who praised this stone garden a lot?

⇓ (Transform into interrogative)

Question: Do you know who praised this stone garden a lot?

Fig. 3. Example of system-initiative question generation

4.2 Recommendation Based on Document Structure and Similarity

We have also implemented following two conventional recommendation techniques based on the document structure and similarity.

– **Recommendation based on document structure (Method 2)**
Wikipedia documents are hierarchically described using the section structure. Thus, another section of the current document can be picked for presentation.

U1: Please explain about the Golden Pavilion.
S1: The Golden Pavilion is one of the buildings at the Rokuon-ji in Kyoto, and is the main attraction of the temple sites. The entire pavilion except the basement is covered with pure gold leaf.
U2: When was it built?
S2: It was originally built in 1397 to serve as a retirement villa for Shogun Ashikaga Yoshimitsu.
(Silence)
S3: Well then, do you know what was awarded to this temple in 1994?
U3: No, please tell me.
S4: It was awarded as listing on the UNESCO World Heritage in 1994.
U4: How can I get there?
.....

Fig. 4. Example dialogue 1

– **Recommendation based on document similarity (Method 3)**
We can select a document that has a large similarity with the current document. This technique is often adopted in the information recommendation of Web sites.

5 System Evaluation

We implemented the guidance system "Dialog Navigator for Kyoto City". An example dialogue of the system using the QA technique is shown in Figs. 4 and 5. We carried out a field trial at our university museum. Users range in age from children to seniors and apparently have little experience in using spoken dialogue systems. No instructions on the system were given. We collected a total of 2,500 dialogue sessions (20,000 utterances).

5.1 Analysis of User Utterances

We have transcribed 465 dialogue sessions chosen from a particular time period. There were in-domain sessions in 52.7% of these sessions, and 23.4% of these sessions included users' questions. For the ASR system, a trigram language model was trained using the KB, a dialogue corpus of a different domain, and Web texts that were automatically selected considering topics and styles [6]. The average word accuracy was 70.6%.

We then evaluated the content of the user utterances. There were 2,930 user utterances in the above dialogue sessions. Table 2 lists these their classification. In this table, "Query" denotes the search queries about sightseeing of Kyoto

U1: Tell me about Ryoan-ji.
S1: Ryoan-ji is a Zen temple located in northwest Kyoto. Belonging to the Myoshinji school of the Rinzai branch of Zen Buddhism, the temple is a UNESCO World Heritage Site.
(Silence)
S2: Do you want to know about the stone garden?
U2: Yes, please.
S3: This garden is a famous karesansui rock garden. It consists of raked gravel and fifteen moss-covered boulders, which are placed so that, when looking at the garden from any angle, only fourteen of the boulders are visible at one time.
(Silence)
S4: Well then, do you know who praised this stone garden a lot?
U3: No, I don't.
S5: Queen Elizabeth praised this stone garden a lot on her visit here.
U4: Who made this temple?
.....

Fig. 5. Example dialogue 2

(excludes questions). "Question" denotes specific questions about Kyoto, such as "When was the Golden Pavilion built?". "Acceptance/Rejection" is the user's reply for confirmation or recommendation by the system. "Greeting" denotes a greeting to the agent, such as "hello". "Out-of-domain" does not belong to any of the above categories. Most of them are non-sensical phrases. "Non-speech" denotes a false detection caused by background noise, which is supposed to be rejected.

5.2 Evaluation of Question-Answering Performance

First, we evaluated the performance of QA in terms of the success rate using 510 questions. Although the QA performance is usually evaluated using the mean reciprocal rank (MRR), we adopted the simple success rate, because it is not possible to audibly present alternative candidates. We regarded QA as successful when the system made an appropriate response to the question. That is, if an answer to the question exists in the KB, we regarded QA as successful when the system presented the answer. On the other hand, if there is no answer in the KB, we regarded QA as successful when the system said so. The QA success rate was 61.4% (64.0% for correct answers existed in the KB, and 46.8% for when they did not).

We then evaluated the effect of the context length (= number of previous utterances) used for the retrieval. This result is shown in Table 3. Without context, the success rate is significantly degraded. However, using all the previous utterances has an adverse effect. The incorporation of appropriate context information by topic tracking effectively improved the performance.

Table 2. Classification of user utterances

Content	Percentage (%)
Query	17.5
Question	8.0
Acceptance/Rejection	23.0
Greeting	23.3
Out-of-domain	15.2
Non-speech	13.1

Table 3. Contextual effect for QA

Use of context	Success rates (%) (correct answer exists, does not exist)
Current topic (proposed)	61.4 (64.0, 46.8)
No context	39.2 (33.3, 72.7)
Previous single utterance	55.9 (56.1, 54.5)
Previous three utterances	57.5 (58.7, 50.6)
All utterances	50.0 (50.3, 48.1)

Table 4. Comparison of recommendation method

Recommendation method	Acceptance rate (%)
Question (Proposed method 1)	74.7
Document structure (Method 2)	51.1
Document similarity (Method 3)	30.8

5.3 Evaluation of System-Initiative Recommendation

In order to confirm the effect of the proposed system-initiative question, the system was set to randomly make possible recommendations. The number of recommendations presented by the system during the 427 (hand-annotated subset of the 465 sessions) dialogue sessions was 319 in total. We regarded a recommendation as accepted when the user positively responded[2] to the proposal given by the system. The acceptance rate of each presentation technique is shown in Table 4. The acceptance rate by the system-initiative question (method 1) was much higher than that of other methods. This result suggests that the recommendations using the question form are more interactive and attractive.

Finally, we evalutated the number of mode shifts between the user-initiative retrieval/QA mode (pull-mode) and the system-initiative recommendation mode (push-mode) (Fig. 1). Among the 427 dialogue sessions, there were 420 mode shifts from the pull-mode to the push-mode, in 185 dialogues, and 297 from the push-mode to pull-mode, in 122 dialogues. This result suggests that many of the

[2] By human judgment.

users' interests in the target topic were initiated by the recommendations, and continued the dialogue.

6 Conclusion

We have proposed an interactive scheme for information guidance using question-answering techniques. Specifically, we incorporated question-answering techniques into both the user-initiative information retrieval and system-initiative information presentation. We have implemented a sightseeing guidance system and evaluated it with respect to the QA-related techniques. We confirmed that the proposed techniques worked well in improving the system performance.

References

1. Bohus, D., Rudnicky, A.I.: RavenClaw: Dialog management using hierarchical task decomposition and an expectation agenda. In: Proc. Eurospeech (2003)
2. Komatani, K., Kanda, N., Ogata, T., Okuno, H.G.: Contextual constraints based on dialogue models in database search task for spoken dialogue systems. In: Proc. Interspeech (2005)
3. NIST, DARPA: The twelfth Text REtrieval Conference (TREC 2003). In: NIST Special Publication SP 500–255 (2003)
4. Kato, T., Fukumoto, J., Masui, F., a.N.K.: Are open-domain question answering technologies useful for information access dialogues? – an empirical study and a proposal of a novel challenge. ACM Trans. of Asian Language Information Processing 4(3), 243–262 (2005)
5. Matsuda, M., Fukumoto, J.: Answering question of iad task using reference resolution of follow-up questions. In: Proc. the Fifth NTCIR Workshop Meeting on Evaluation of Information Access Technologies, pp. 414–421 (2006)
6. Misu, T., Kawahara, T.: A bootstrapping approach for developing language model of new spoken dialogue systems by selecting Web texts. In: Proc. Interspeech, pp. 9–12 (2006)

Generating Cartoon-Style Summary of Daily Life with Multimedia Mobile Devices*

Sung-Bae Cho, Kyung-Joong Kim, and Keum-Sung Hwang

Dept. of Computer Science, Yonsei University
134 Shinchon-dong, Sudaemoon-ku, Seoul 120-749, South Korea
{kjkim, sbcho}@cs.yonsei.ac.kr

Abstract. Mobile devices are treasure boxes of personal information containing user's context, personal schedule, diary, short messages, photos, and videos. Also, user's usage information on Smartphone can be recorded on the device and they can be used as useful sources of high-level inference. Furthermore, stored multimedia contents can be also regarded as relevant evidences for inferring user's daily life. Without user's consciousness, the device continuously collects information and it can be used as an extended memory of human users. However, the amount of information collected is extremely huge and it is difficult to extract useful information manually from the raw data. In this paper, AniDiary (Anywhere Diary) is proposed to summarize user's daily life in a form of cartoon-style diary. Because it is not efficient to show all events in a day, selected landmark events (memorable events) are automatically converted to the cartoon images. The identification of landmark events is done by modeling causal-effect relationships among various events with a number of Bayesian networks. Experimental results on synthetic data showed that the proposed system provides an efficient and user-friendly way to summarize user's daily life.

1 Introduction

Many people used to write a diary in order to memorize their daily life and it can help them recall what they did. When they write a diary, they attempt to remember daily events. Because it is not easy to remember all the events in the day, he needs to check other information sources such as pictures taken, call logs, SMS (short message service), scheduler and memos. Recent advances in mobile phone technologies allow the device not only to log user's daily activity (location, call log, SMS, and proximity information (Bluetooth)) but also to store personal multimedia information (photo, video and documents). The information is very private and contains relevant information to reveal user's daily events.

Our research aims to summarize user's daily life in a form of cartoons based on the information collected from mobile devices such as Smartphone. Cartoon-style representation has been used to summarize user's conference visit experience on PDA from user's explicit input without much exploitation of user's logs [1]. Although their

* This research was supported in part by MIC, Korea under ITRC IITA-2006-(C1090-0603-0046).

H.G. Okuno and M. Ali (Eds.): IEA/AIE 2007, LNAI 4570, pp. 135–144, 2007.

works showed that cartoon-style representation was useful compared to plain text representation, the scope of comic diary was limited to the conference visit scenario. In this work, the scope is extended to the daily life and all the available information sources in the Smartphone are used to derive cartoon-style diary automatically. The procedure of the diary generation is composed of information logging, preprocessing, landmark detection and selection, and cartoon generation. Landmark means very relevant or novel events that are useful to recall a sequence of events. Its organization is similar to the human memory structure and researchers try to adopt such concept in real-world systems [4].

In logging stage, GPS, call log, SMS, MP3 play lists, battery level and photo viewer usage information are recorded. Because extracting high-level information from the raw information directly is not efficient, statistical analysis on them is first done before the inference. Min, max and impact analysis are used to extract relevant trends or patterns of user's daily life. In landmark detection module, a number of Bayesian networks designed by experts are used to find memorable events. Bayesian networks are one of efficient tools to infer the situation given uncertain and partial information. Given memorable events selected, the most probable candidates are selected based on the relevance. Finally, they are converted to the cartoons by composing pre-stored cartoon image components. Figure 1 shows the procedure.

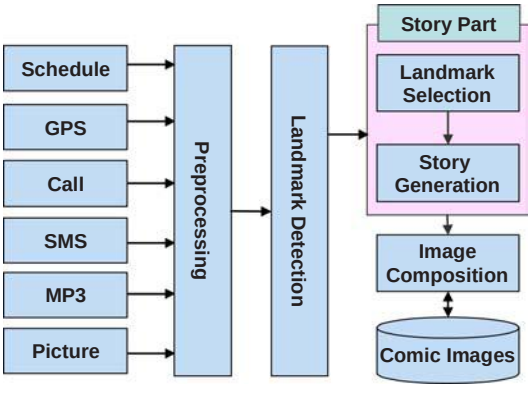

Fig. 1. The procedure of Anidiary generation

2 Related Works

Automatic diary generation from user's log (explicit or implicit) is one of hot research topics. Sumi *et al.* designed comic diary to summarize the user's conference tour in a cartoon-style form [1]. Their system is based on the explicit user input and user's schedule information. Eagle tried to develop a diary system based on the log information collected from cellular phone [2]. Because they show the raw information directly through GUI, it is difficult to understand the whole picture of the day in an intuitive way. A large amount of information is continuously stored from cellular phone and it is required to learn high-level context-information from the raw data but they do not focus much about the point. Nokia's Lifeblog provides a way to store and

manage user's photo, multimedia and SMS in a chronological manner [3]. It does not utilize any abstraction and summarization methods.

ContextPhone is a context logging software for Nokia 60 series Smartphone [5] and its source is available to public. It collects information including photo, sound, battery level, location, SMS, MMS, call logs, Bluetooth, and active applications. However, it is not easy to use such software in general because Nokia 60 series Smartphone is not available in some places. Because of this, we have developed a new context logging software and applied to Samsung Smartphone M4300.

Eric Horvitz *et al*. attempt to re-organize personal information storage in desk top PC into an episodic style memory [4]. Previous research on human memory revealed that the organizational principle is episodic storage and retrieval. Related events are grouped as an episode and landmark event is used to recall them from the storage. By finding landmark, he can also recall the related items. He learns Bayesian networks to detect landmark event from the data stored in outlook scheduler. His work called Bayesphone uses client-server communication for Bayesian network whose inference is done on server-side and the results are transmitted to device through network [6]. We expand the scope of his works to the personal storage in mobile devices.

MIT reality mining group develops serendipity service using the ContextPhone software [7]. The group collaborates with MIT common sense reasoning group to generate diary automatically. Because the research is at early stage, there is no concrete result about that. Only visualization tool for collected log is available in their paper. However, their work shows a new way to generate more interpretable high-level diary using common sense. Basic details about the common sense knowledge can be found in [8]. Our work is based on the ontology and it can be expanded to the more general model using such a common sense corpus.

Although there are many initial-stage papers about personal information management on mobile device, visualization of daily life, and detection of memory landmark, they are not integrated into one system for useful applications. In this paper, we will design an integrated system of logging, preprocessing, landmark detection, and visualization.

3 Cartoon Generation for Summary of Daily Life

In logging stage, basic user's log from system, sensors and web is collected and stored to file system. In preprocessing stage, the raw information is analyzed using statistical methods such as average, min, max, and more sophisticated tools. Impact factor is proposed to reflect the importance of event's density over time. In landmark detection stage, modular structure is adopted to minimize computational cost for inference and the expert's effort to design the knowledge-base. A number of Bayesian networks are designed at this stage to infer the probability of landmark given evidences. At story generation stage, the most probable landmarks among them are selected and their order for visualization is determined based on pre-stored knowledge (causal relationships). Finally, cartoon generation module generates a diary by converting the landmarks to cartoons.

3.1 Logging , Preprocessing and Memory Landmark Detection

We have implemented a logging system on Samsung Smartphone M4300 with small GPS receiver attached to the device. Weather information is retrieved from

http://www.kma.go.kr (Korea Meteorological Administration). GPS and battery level are sampled per 1 sec. Photo viewer and MP3 player are modified based on free source code to log usage information. User's current position is inferred from the GPS value that is a pair of (longitude, latitude). The raw information is transformed into semantic label using pre-stored information about the relationships between GPS value and semantic labeling information (building name and street name). The impact factor reflects the density of events. When the event occurs, the impact factor is increased and it decreases after pre-defined time. However, some events continuously occur after the event, the impact factor also continuously increases. Many events with less density (sparse distribution) will show low impact factor.

Various mobile log data are preprocessed in advance, and then the landmark reasoning module detects the landmarks. The BN (Bayesian Network) reasoning module performs complicated and probabilistic inference.

There are two general differences between the proposed Bayesian networks and the conventional Bayesian networks for landmark detection. Firstly, we modularize the Bayesian inference models according to their separated sub-domains (Figure 2) [10]. Secondly, in order to consider the co-causality of modularized BN, the proposed method operates 2-pass inference stages. The output of one module can be inputted to the other module for the 2nd inference.

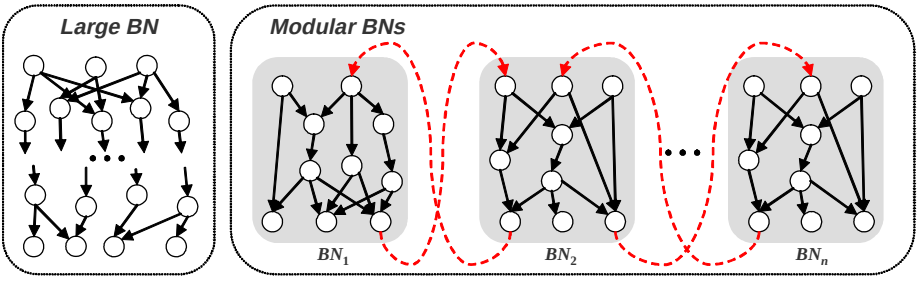

Fig. 2. The 2-pass inference process for the cooperation of modular Bayesian networks. The dotted line indicates the stream of the 2nd stage of inference processing.

There are four kinds of BNs, and totally 39 BNs are used. The BNs are as follows: Place-activity BNs={house, religion, shopping, photo, hospital, nature, meeting, workplace, sports, movement, food, call, music, school, traffic, watch, rest}, Emotion/condition BNs={joy, hungriness, hot, nonsense, surprise, busy, tiredness, drunken, anger, cold, fret, amusement, gloom, sick, bored}, Circumstance situation BNs={space, climate, time, device, group}, and event BNs={anniversary, event}.

3.2 Story and Cartoon Generation

Single cartoon cut is composed of 5 different types of images: text, sub character, main character, sub background, and main background (Figure 3) [9]. Designers prepare a set of images for each type. Cartoon generation module selects the character and background images that are the most appropriate given landmarks and user profiles. In the selection process, semantic similarity between images and landmark event is calculated based on the predefined annotations for the images. After selecting

the cartoon cuts for each landmark, they are organized into a story stream to make a plausible cartoon story using consistency constraints.

The semantic similarity between the cartoon images and landmark events are calculated using the equation (1). User profile is a set of values that reflect the user's preference about the cartoon image. From the images whose similarities are higher than certain threshold, the candidate list of cartoon cuts is generated. The threshold for image selection is defined in consideration of cartoon diversity and computational cost. Lower threshold composes more diverse cartoon expression, but requires more computational cost for the consistency constraint violation check.

$$Similarity\,(event_m, image_{kmh}) = \frac{|\,(p(event_m) \cup p(UP)) \cap p(image_{kmh})\,|}{|\,p(event_m) \cup p(UP) \cup p(image_{kmh})\,|} \quad (1)$$

$Similarity(event_m, image_{kmh})$ = similarities between $event_m$ and $image_{kmh}$
$event_m$ = the m^{th} landmark event
$image_{kmh}$ = cartoon image of type h in the k^{th} feasible cartoon cut composition for the m^{th} landmark event
# of feasible cartoon cut composition
= # of Main BG×# of Sub BG×#of Main CH×# of Sub CH×# of Text
UP = User profile
$p(X)$ = A set of attributes that object X has

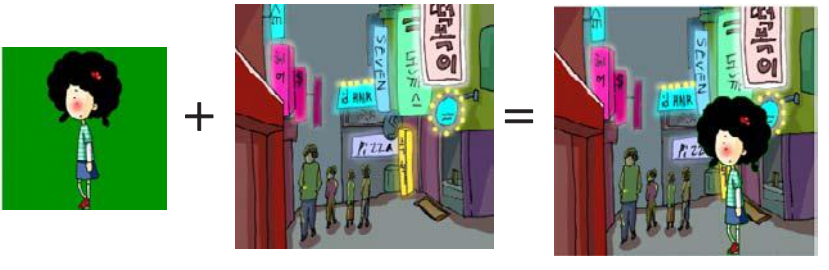

Fig. 3. Composition of image components for single cartoon cut

4 Experimental Results

At this stage, the performance of the system is tested using synthetic data because collecting real data requires much time. It takes more than one month to get useful statistics.

4.1 A Case Study and Performance Evaluation on Long-Term Data

We have tested the proposed landmark reasoning model with a scenario in order to confirm the performance. The left side of Figure 4 shows a scenario used. The BN set strongly related to the scenario is {food, photo, movement, nature, joy, home}. The probabilities are calculated when the related evidences are given.

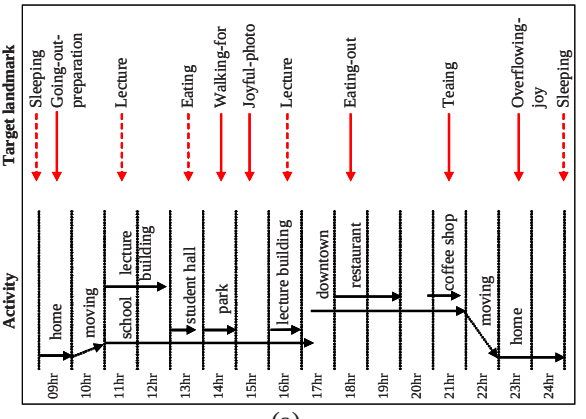

(a)

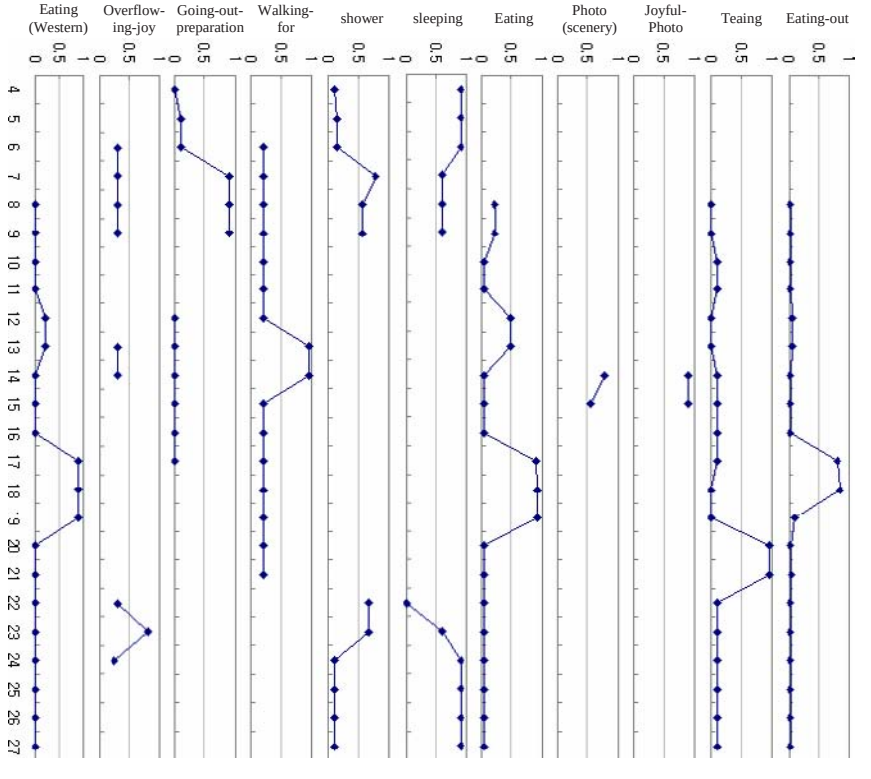

(b)

Fig. 4. (a) A scenario of an everyday life with mobile device of an undergraduate student for experiments. (b) The observation of the probability values of 11 target landmarks. The denoted time is from 4 o'clock to 27 o'clock (equal to 3 o'clock next day).

After generating the log contexts with quantity of a day, we have tested them. The right side of Figure 4 shows the inference results. We can see the increment of the probabilities of the related landmarks at the corresponding time. For example, there are ‘going-out-preparation’ and ‘shower’ landmarks at 7~9 o'clock, ‘eating’ at 12~13 and 17~19 o'clock, ‘walking-for’ at 13~14 and 20~21 o'clock, ‘joyful-photo’ at 14~15 o'clock, and ‘eating-out’ and ‘eating (western style)’ landmarks at 17~19 o'clock.

To evaluate the landmark reasoning performance, we grouped situations of everyday life on the two aspects: usual/unusual and idle/busy. We generated artificial high-level contexts for evidence because it was difficult to make raw data directly. For example, we made a context ‘a lot of phone calls’ instead of its phone call log data.

The target landmarks are categorized to three classes as shown in Table 1. There is no idle class because it is regarded as idle if it is not busy. The data set for a class was collected for 30 days and a day of data set contains two landmarks, which are selected randomly and one is before noon and the other is afternoon.

Table 1. The category of landmarks based on usual, unusual, and busy

Class (#)	**Related Landmarks**
busy (6)	busy, run with umbrella, joyful phone call, joyful SMS, annoying SMS, tired phone call
usual (82)	boarding airplane, …, boarding train, studying, meeting, …, walking for, showing, washing dish, caring for hair, washing face, shopping, sleeping, eating, painful, feel hot, overflowing-joy, …, sad, heavy traffic, joyful photo, …, self-photo, playing golf, …, playing basketball, mountain climbing, water skiing, swim, health-training
unusual (25)	Watch horse racing, …, watch performance, watching, anniversary, watching basket ball, very strange place, unusual place, watching baseball, trip, receiving celebration-SMS, …, make a celebration-phone-call, marriage, election, visiting the family graves, …, funeral ceremony, ancestor-memorial service of a festive day

Table 2 shows the statistics of experimental results and Table 3 shows some individual results. We have excluded the landmarks related to the default place 'home' and the low-weight landmarks from main landmarks set. The false-positive error of 'usual/idle' class is high and the precision is low, because 'usual' class includes many places and landmarks that have evidence duplication. For example, since the landmark 'boarding ship' of A-60302 in Table 3 is caused by the evidence 'sea' or 'river', a landmark 'swim (outdoor)' can be extracted. The false-positive error of 'usual/busy' class is low because the class includes relatively many landmarks that have distinct evidence. In the experiment, the overall recall rate was low as 75%. It results from the lack of tuning or the landmarks hard to detect.

Table 2. The experimental results with synthetic data. Two target objects (with few redundancies) are selected in each data set. 'unusual/busy' class data are composed of one 'unusual' landmark and one 'busy' landmark.

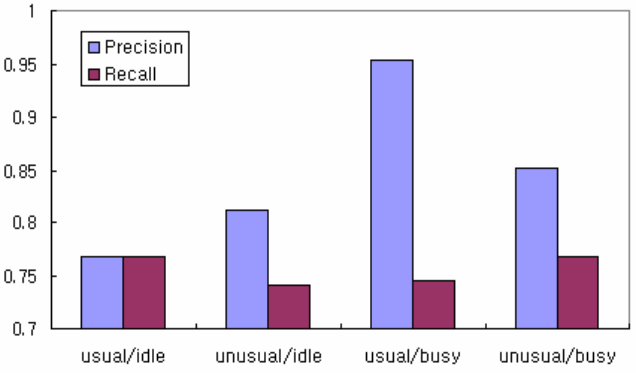

Table 3. A part of the obtained landmarks. We have excluded the landmarks related to the default place 'home' and the low-weight landmarks from main landmarks set. The target landmarks found are underlined. Abbreviations: OL (Number of Obtained Landmark), TP (True Positive), FP (False Positive). Data type: A (usual/idle), B (unusual/idle), C (usual/busy), D (unusual/busy).

Data	Target landmark	OL	TP	FP	Extracted main landmarks
A-60301	athletic meeting, boarding train	45	2	2	Athletic meeting, boarding subway train, boarding expressway bus, boarding train
A-60302	boarding ship, boarding train	47	1	3	Swimming (outdoor), boarding subway train, boarding expressway bus, boarding train
…	…	…	…	…	…
A-60330	boarding airplane, overflowing-joy	35	1	0	Swimming (outdoor), boarding airplane
Total	60 landmarks	866	46	14	78 landmarks

4.2 Image Generation Test

Because the fun of the composed cartoon story can be evaluated only in subjective measure, we evaluate the fun of the cartoon by evaluating the diversity and the consistency of the cartoon. To evaluate the generated cartoon story, we create sample scenario landmark events described in Table 4.

Figure 5 shows one of the composed cartoon story images. To evaluate the method, four composed cartoon story images were shown to participants. By composed cartoon stories, user evaluation tests for cartoon cuts and cartoon story were performed with five participants. For each question, 5-point scale measure is used to grade an item. At first, cartoon cuts generated by a landmark example are evaluated in the criteria of the diversity and the descriptiveness. Figure 6(a) shows the evaluation results. After cartoon cut evaluation, diversity and consistency of four cartoon stories

were asked to the participants. The diversity of cartoon stories results in 4.0 of average with 1.0 of standard deviation, and the consistency of cartoon stories is depicted in Figure 6(b). These data are not enough for the statistical significance, but the average score for each criterion shows affirmative tendencies.

Table 4. Landmark context examples

ID	Behavioral landmarks	Environmental landmarks
1	Movement, MP3, Stand	Bus, Indoor
2	Study, Take a class, Sit	University, Classroom, Indoor
3	Eat, Korean Food, Sit	University, Dinning Room, Indoor
4	Talk, Phone, Stand	University, Outdoor
5	Cheer, Watch, Stand	Stage, Outdoor
6	Drink, Beer, Sit, Cheer	Drinking House, Bar, Indoor

Fig. 5. A composed cartoon story from landmark examples in Table 4 to evaluate the diversity and the consistency

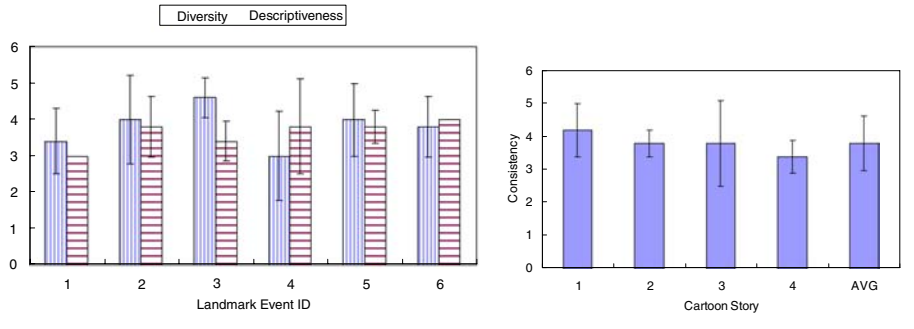

(a) (b)

Fig. 6. (a) Diversity and descriptiveness of cartoon cuts for each landmark event (n=5). (b) Consistency Scores of four generated cartoon stories (n=5).

5 Conclusions and Future Works

In this paper, we have proposed a cartoon diary generation system based on user's personal logs stored in mobile devices as a form of episodic memory. Modular Bayesian networks are used to infer the probability of landmark for each event. Some

selected landmarks are arranged using consistency ontology and converted to cartoon images. Experimental results on synthetic data show the possibility of the proposed methods for detecting landmarks and generating meaningful images. User's enormous logs are summarized into user friendly cartoon images and this gives a new way for managing his personal memories.

As a long-term goal, the system needs to be evaluated from real logs from subjects' real life. Also, learning algorithm for landmark detection is required for personalized detection models.

References

1. Sumi, Y., Sakamoto, R., Nakao, K., Mase, K.: ComicDiary: Representing individual experiences in a comic style. Ubicomp 2002, pp. 16–32 (2002)
2. Eagle, N.: Machine Perception and Learning of Complex Social Systems. Ph. D. Thesis. In: Program in Media Arts and Sciences, Massachusetts Institute of Technology (2005)
3. Nokia Lifeblog, http://www.nokia.com/lifeblog
4. Horvitz, E., Dumais, S., Koch, P.: Learning predictive models of memory landmarks. In: 26th Annual Meeting of the Cognitive Science Society (2004)
5. Raento, M., Oulasvirta, A., Petit, R., Toivonen, H.: ContextPhone-A prototype platform for context-aware mobile applications. IEEE Pervasive Computing 4(2), 51–59 (2005)
6. Horvitz, E., Koch, P., Sarin, R., Apacible, J., Subramani, M.: Bayesphone: Precomputation of context-sensitive policies for inquiry and action in mobile devices. User Modeling 2005, 251–260 (2005)
7. Kurlander, D., Skelly, T., Salesin, D.: Comic chat. In: Proceedings of the 23rd Annual Conference on Computer Graphics and Interactive Techniques, pp. 225–236 (1996)
8. Singh, P., Barry, B., Liu, H.: Teaching machines about everyday life. BT Technology Journal 22(4), 227–240 (2004)
9. Song, I.-J., Jung, M.-C., Cho, S.-B.: Automatic generation of funny cartoons diary for everyday mobile life. In: Sattar, A., Kang, B.-H. (eds.) AI 2006. LNCS (LNAI), vol. 4304, pp. 443–452. Springer, Heidelberg (2006)
10. Hwang, K.-S., Cho, S.-B.: Modular Bayesian networks for inferring landmarks on mobile daily life. In: Sattar, A., Kang, B.-H. (eds.) AI 2006. LNCS (LNAI), vol. 4304, pp. 929–933. Springer, Heidelberg (2006)

Economic Turning Point Forecasting Using Neural Network with Weighted Fuzzy Membership Functions

Soo H. Chai and Joon S. Lim

College of Software, Kyungwon University, Sungnam 461-701, Korea
soochai@hanmail.net, jslim@kyungwon.ac.kr

Abstract. This paper proposes a new forecasting model based on neural network with weighted fuzzy membership functions (NEWFM) concerning forecasting of turning points in business cycle by the composite index. NEWFM is a new model of neural networks to improve forecasting accuracy by using self adaptive weighted fuzzy membership functions. The locations and weights of the membership functions are adaptively trained, and then the fuzzy membership functions are combined by bounded sum. The implementation of the NEWFM demonstrates an excellent capability in the field of business cycle analysis.

Keywords: fuzzy neural network, rule extraction, business forecasting, turning point.

1 Introduction

A new forecasting model based on neural network with weighted fuzzy membership functions (NEWFM) [1] concerning forecasting of turning points in business cycle by the composite index is implemented in this paper. Fuzzy neural network (FNN) is the combination of neural network and the fuzzy set theory, and provides the interpretation capability of hidden layers using knowledge based the fuzzy set theory. Various FNN models with different algorithms such as learning, adaptation, rule extraction were proposed as a adaptive decision support tool in the field of pattern recognition, classification and forecasting [2], [3], [4].

The conventional econometrics approach has been widely used to analyze the business cycle [5]. However, many research works have recently been carried out and published based on the information technology including neural networks and wavelet [6], [7], [8], [9].

2 Neural Network with Weighted Fuzzy Membership Functions (NEWFM)

2.1 The Structure of NEWFM

The NEWFM [1] is a supervised fuzzy neural network that classifies using trained weighted fuzzy membership functions. The structure of NEWFM is illustrated in

H.G. Okuno and M. Ali (Eds.): IEA/AIE 2007, LNAI 4570, pp. 145–154, 2007.

Fig. 1. The NEWFM comprises three layers, namely input, hyperbox, and class layer. The input layer contains *n* input nodes for *n* featured input patterns. The hyperbox layer consists of *m* hyperbox nodes. Each hyperbox node B_l to be connected to a class node contains *n* fuzzy sets for *n* input nodes. The output layer is composed of *p* class nodes. Each class node is connected to one or more hyperbox nodes. An *h*th pattern can be recorded as $I_h = \{A_h=(a_1, a_2, \ldots, a_n), class\}$, where *class* is the result of classification and A_h is the pattern on *n* different features. The *i*th fuzzy set of B_l, denoted by B_l^i, has three weighted membership functions as shown in Fig.1. After learning, the weighted membership functions for classification are located in the hyperbox layer.

2.2 Learning Scheme

A hyperbox node B_l consists of n fuzzy sets. The i th fuzzy set of B_l, represented by B_l^i, has three weighted fuzzy membership functions (WFMs, grey triangles in Fig. 2) which randomly constructed before learning. The winner hyperbox node B_l that has the maximum value of output for an input I_h among the hyperbox nodes can be learned. Then, the selected winner hyperbox node B_l is learned by the Adjust(B_l) operation. This operation adjusts all WFMs in the B_l according to the input a_i, where i =1, 2, … , n.

The Adjust(B_l) operations are executed by a set of training data. If the classification rate for a set of test data is not reached to a target value, the learning scheme with Adjust(B_l) operation is repeated from the beginning by randomly reconstructing all WFMs in B_l s until the target value is reached.

2.3 Fuzzy Rule Extraction

The learned NEWFM can be used for fuzzy rule extraction in *if-then* form to classify input patterns. After learning, each of *n* fuzzy sets in hyperbox node B_l contains three WFMs where *n* is the number of input nodes.

The rules can be extracted directly from the WFMs. We suggest a rule extraction strategy as described below.

The *bounded sum*(one of fuzzy set operations) of WFMs (BSWFM) in the *i*th fuzzy set of $B_l^i(x)$, denoted as $\mu_b^i(x)$ (bold line in Fig. 2), is defined by

$$\mu_b^i(x) = \sum_{j=1}^{3} B_l^i(\mu_j(x)).$$

The BSWFM combines the fuzzy characteristics of three WFMs, which simplifies fuzzy rules and inference process. The rules for a class C_i is the fuzzy membership functions represented by BSWFMs in B_l. The visuality of the BSWFMs in B_l profers interpretability and finding significance of the rules.

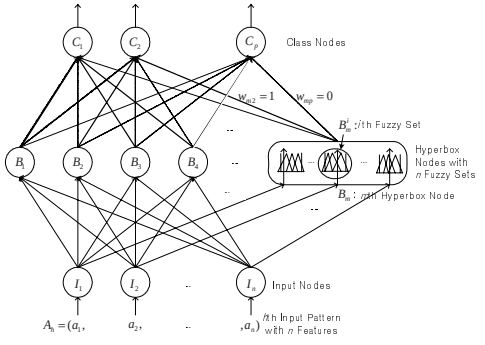

Fig. 1. Structure of NEWFM

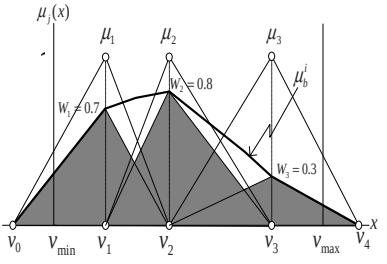

Fig. 2. Example of BSWFM (Bold Line)

3 Methodology of Business Forecasting

The business cycle, which was used to be a central part of economic theory before the Second World War, is a cyclic phenomenon of expansion and contraction phase of an aggregate economic activity in a country such as productions, prices, employment etc. This business cycle are normally divided into three types, i.e. Kitchin cycle, Juglar cycle and Kondratiev wave after J. Schumpeter [10], and much interest was concentrated on describing the Juglar cycle, the medium-term cycle which lasted 8 to 10 years. Although the opinions concerning the cause of business cycle was divided into various doctrines, it fell behind the mainstream of economics after Keynsians proved that financial and banking policy can overcome those phenomena [11].

However, the study of business cycle started to gain interest by the start of recession due to the oil crisis in the 70's after the unusual economic boom in the 60's. Recently much interest is focused on it because of the long recession in the world economy.

The study of business cycle has been based mainly on the conventional econometrics approach. However, new approach based on the information technology has been applied to it and much research work has been published recently. One of the conventional methodologies is the forecasting of the Reference Cycle Dates using the GDP (Gross Domestic Products) or other economic indicators which are closely related to the national economic activities, or economic situations. Composite indexes which closely reflect the economic situation are often used to distinguish economic turning points by analyzing coincident index or leading index. The sequential signaling method by Zarnowitz and Moore predicts the pattern of business cycle by analyzing 6 different signal patterns using both the changes of increase rates in leading index and coincident index [12].

There are various models such as Neftci model and state-space Markov switching model which can analyze the probability of occurrence of transfer in the phase of business cycle statistically and eliminate false signals. Neftci model predicts the trough of business cycle by analyzing the probability of economic turning point occurrence which is estimated from the theoretical probability density of the leading index both in the contraction and expansion phase [13]. Space-state Markov model is

the combination of the Hamilton model and Markov transfer model and quantize it assuming that phases of business cycle are the phenomena of the nonlinear transfer between two cycles with different characteristics [14].

With the help of recent development of information technology, the new research attempt using fuzzy theory, neural network, and wavelet is made in the wide range of economic field, such as money and banking, exchange rate, stock price, credit standing of companies etc. Among them are new models proposed in the field of business forecasting.

Hoptroff used the long-term and short-term leading indexes as main indicators to forecast economic turning points in the UK based on the backpropagation algorithm, and submitted the research results to the UK government [6]. Freisleben proved the superiority of the backpropagation algorithm compared to the ARIMA model by publishing the result of business forecasting in Germany using the data such as GDP, unemployment rate, and unemployees based on the backpropagation algorithm [7].

There are many other algorithms used for business forecasting application, and one of the examples is the business forecasting model in the US by Vishwakarm. Manufacturing products, unemployees and personal income data are used for the main indexes and they are processed using the Kalman filtering-based state space neural network [8].

In addition, new approaches to analyzing and predicting the business cycle based on the wavelet de-noising and multi-resolution analysis, which are one of the signal processing tools, are recently published. Mitra proposed a new approach to the business forecasting in India based on the wavelet filtering-based neural network using industrial production indexes [9]. Raihan analyzed the characteristics of business cycle in the US using the increase rates of the real GDP during 1960-1996 based on the wavelet-based time-frequency transform and published the result as a report for the Federal Reserve Bank of St. Louis [15].

4 Experimental Results

The data set of CI (Composite Index) components and GDP are used to generate the fuzzy rules (BSWFMs), thereby to forecast the business cycle. 10 BSWFMs are generated from the leading indexes and 8 BSWFMs from the coincident indexes, respectively. The forecasting results by the NEWFM are presented to evaluate the effectiveness of the overall business cycle analysis.

4.1 Used Indicators

The total number of 186 component samples of the composite index including leading indexes, coincident indexes, and lagging indexes published monthly by Korea National Statistical Office (KNSO) are used from Jan 1991 to May 2006. The target class is chosen to be the GDP which represents the aggregate activity of national economy and the monthly data of GDP is interpolated for classification. The GDP increase rates are used as a target class which is classified into two classes, i.e. class 0 and class 1. The class 0 and class 1 represent the lower (contraction) phase and upper (expansion) phase which are generally used in the business cycle classification. The summaries of input and test data are shown in Table 1.

Table 1. Used Indicators for the NEWFM Business Forecasting Model

Data set	Index (No)	Detail Index	Time Series
Training data	Leading Index (10)	employment1, manufacturing1, consumption1, investment3, money & banking3, trade1	180 (91.1~05.12)
Training data	Coincident Index (8)	employment1, manufacturing4, consumption2, trade1	180 (91.1~05.12)
Test data	Leading Index (10)	employment1, manufacturing1, consumption1, investment3, money & banking3, trade1	186 (91.1~06.5)
Test data	Coincident Index (8)	employment1, manufacturing4, consumption2, trade1	186 (91.1~06.5)
class 0: lower phase(less than 5.5% growth rate of GDP) class 1: upper phase(higher than 5.5% growth rate of GDP)			

4.2 Generation of Fuzzy Rule for Business Forecasting

10 leading indexes and 8 coincident indexes are used to generate the fuzzy rules for business forecasting. In case of leading index, 10 indexes including open-to-application ratio from Jan 1991 to Dec 2005 are used as input features for the training. The GDP average increase rate since 1970 is chosen to be the threshold value which decides the class 0 and the class 1. The threshold value is adjusted according to the declining tendency of potential growth rate [16]. In case of coincident index, 8 indexes including number of employed persons of non-farming household covering the same time series are used as input features for the training.

In this experiment, two hyperboxes are created for classification. While a hyperbox which contains a set of bold lines (BSWFMs) in Fig. 3 and Fig. 4 is a rule for class 0(lower phase), the other hyperbox which contains a set of light lines (BSWFMs) is another rule for class 1(upper phase). Each graph in Fig. 3 and Fig. 4 is obtained from the training process of the NEWFM program and shows the difference between lower phase and upper phase for each input feature graphically.

The classification result of NEWFM is shown in Table 2 and is compared with Fuzzy ARTMAP (Adaptive Resonance Theory MAP) [17] which is one of the similar supervised fuzzy neural networks. The comparison of classification performance between NEWFM and fuzzy ARTMAP is shown in Table 3. The final result of classification rate is 92.22% in case of the leading index and 93.88% in case of coincident index respectively. These classification capacity on the order of 92~94% are different from the experiment results of 99.56% from the medical data [1]. These are due to the irregularities and noisy nature of economic data. The BSWFMs for the business forecasting are shown in Fig. 3 and Fig. 4.

Table 2. Classification Rate of NEWFM

Composite Index	Total No of Time Series	Correct Classification	Classification Rate (%)	Error Rate (%)
Leading Index(10 indexes used)	180	166	92.22	7.78
Coincident Index(8 indexes used)	180	169	93.88	6.12

Table 3. Comparison of classification performance

Composite Index	Classification Rate (%)		Error Rate (%)	
	NEWFM	fuzzy ARTMAP	NEWFM	fuzzy ARTMAP
Leading Index(10 indexes used)	92.22	82.94	7.78	17.05
Coincident Index(8 indexes used)	93.88	88.23	6.12	11.76

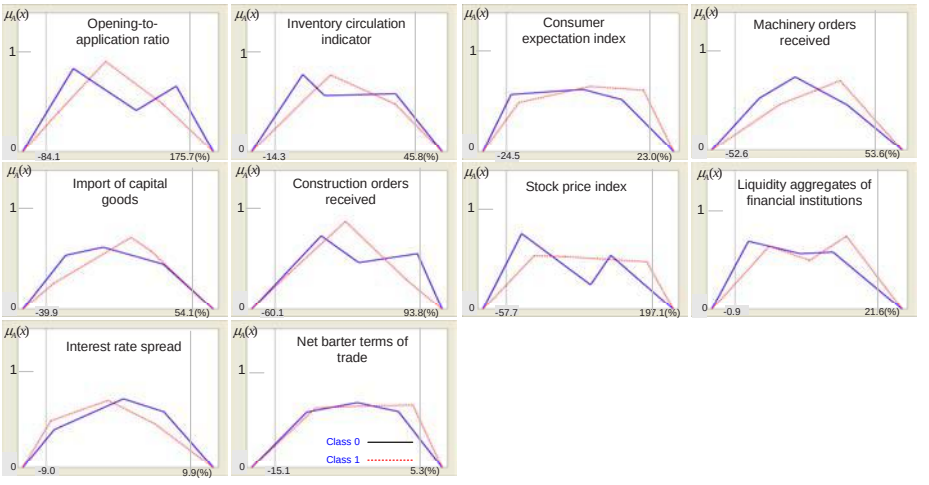

Fig. 3. BSWFMs generated by 10 Leading Indexes
(X axis: annual increase rate of each index, Y axis: fuzzy mapping value)

Fig. 4. BSWFMs generated by 8 Coincident Indexes
(X axis: annual increase rate of each index, Y axis: fuzzy mapping value)

4.3 Economic Turning Points Forecasting

The forecasting result of NEWFM can be represented by the trend lines using the defuzzyfication of center of gravity method (Mamdani). The forecasting results in Fig.5 during Jan 1991 and May 2006 demonstrate the similar fluctuations with GDP

and represent the expansion and the contraction phases of the economy. The time difference between the forecasting result of the NEWFM and cyclical component of coincident index is defined as the leading month, which varies in each cyclical period. The cyclical component of coincident index is a reference cycle and is published by the South Korean government.

The turning point forecasting capability of NEWFM model in detail is shown in Table 4. During the 5th to 8th cycle period, forecasting results lead over the Reference Cycle Date by 8 to 15 months in the peak points and by 5 to 8 months in the trough points respectively. The accuracy in the trough point is relatively higher than that in the peak points.

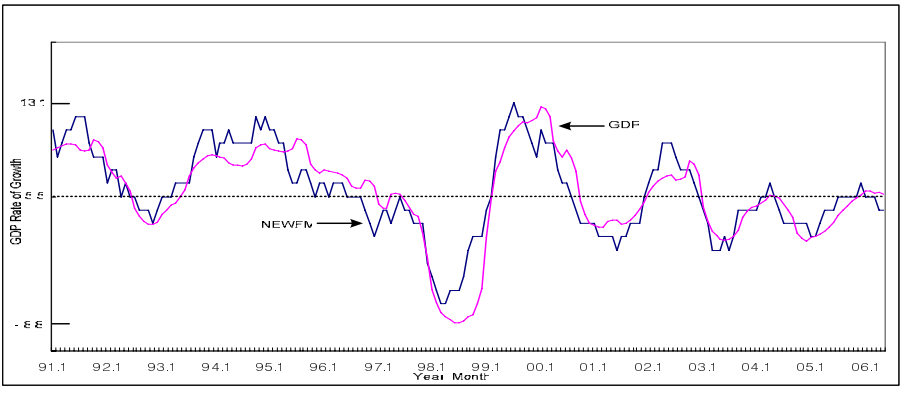

Fig. 5. The Forecasting Result of the Leading Indexes using the NEWFM Business Forecasting Model and GDP

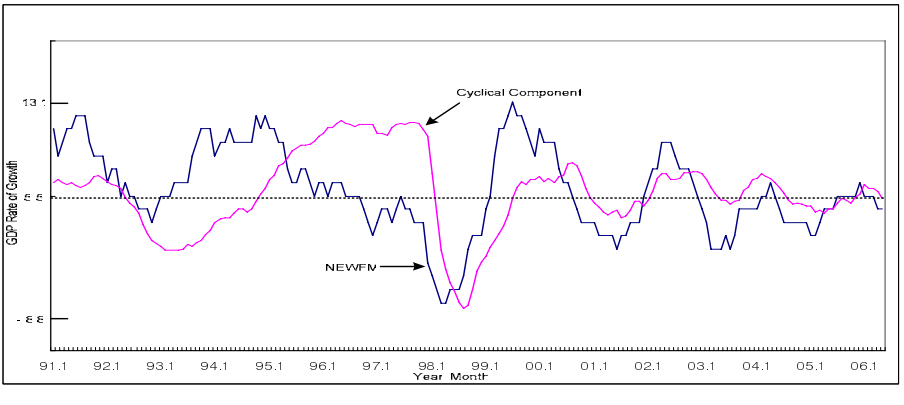

Fig. 6. The Forecasting Result of the Leading Indexes using the NEWFM Business Forecasting Model and the Cyclical Component of Coincident Indexes

Table 4. The Forecasting Results Using the NEWFM Business Forecasting Model and Reference Cycle Dates

Items	5th cycle		6th cycle		7th cycle		8th cycle	
	peak	trough	peak	trough	peak	trough	peak	trough
Reference Cycle Dates(y/m)	92/1	93/1	96/3	98/8	00/8	01/7[1)]	02/12[1)]	-
NEWFM forecasting results (y/m)	91/1	92/8	94/12	98/3	99/8	00/11	02/4	-
Leading months by NEWFM forecasting	-12	-5	-15	-5	-12	-8	-8	-
Leading months by KNSO forecasting	-15	-4	-15	-5	-12	-7	-8	-

1) Preliminary data

The trend line of the forecasting result from Jan. 1991 to May 2006 by the coincident indexes is shown in Fig.7. This result generally shows high correlation with the fluctuation of cyclical component of coincident composite index. However, it gives a little time difference between them during a certain period because GDP is used to train forecasting model.

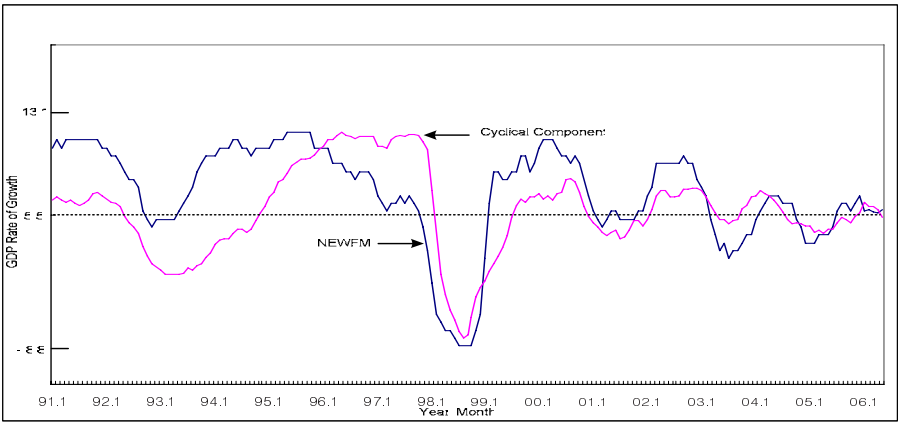

Fig. 7. The Forecasting Result of the Coincident Indexes using the NEWFM Business Forecasting Model and the Cyclical Component of Coincident Index

The irregularities and the noise of the trend lines can be removed and then smoothed using the wavelet transform to overview the economic phase more easily [18]. The wavelet transform at the level 3 of db4 is used to denoise the original forecasting result. Both the original trend lines and the denoised results of the leading indexes using NEWFM business forecasting model are shown in Fig. 8. Economic cycles are occupied in the lower region since the peak of the 8th cycle period. This is due to the use of single threshold value in data processing throughout the whole cycle periods even if the threshold value is adjusted according to the declining trend of the recent potential GDP growth rate. Therefore the more realistic forecasting result can be obtained by using the threshold values corresponding to the periodic changes of the potential GDP growth rate [16] estimated by the responsible authorities including the Bank of Korea.

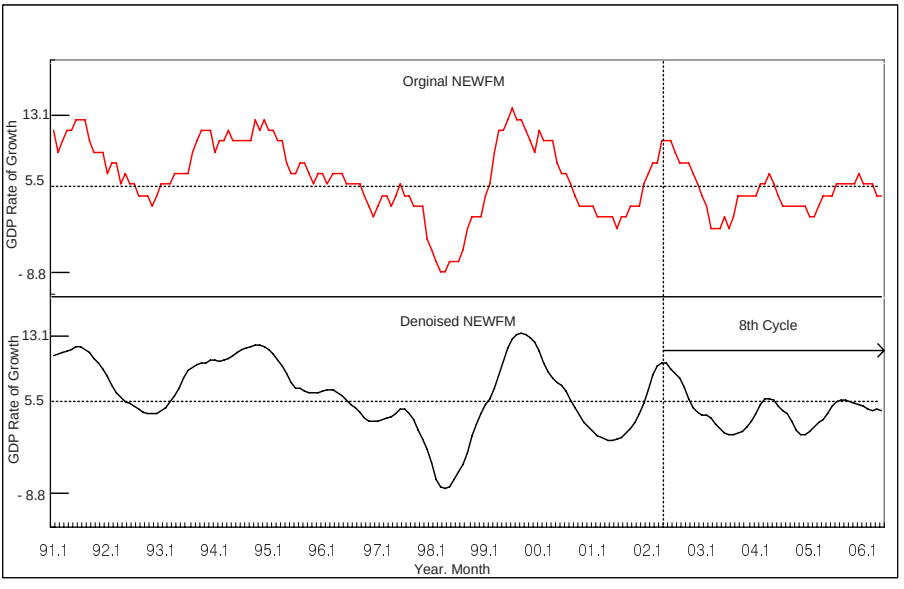

Fig. 8. The Wavelet Transform Result from the Forecasting Result of the Leading Indexes using NEWFM Business Forecasting Model

5 Conclusions

This paper proposes a new forecasting model based on neural network with weighted fuzzy membership functions (NEWFM). Although further study will be necessary to improve the accuracy of the economic forecasting capability, the automation of business cycle forecasting by business indicators can be used for policy making and establishing business plan by responsible authorities, CEOs of banking institutions, enterprises etc.

The accuracy of NEWFM business forecasting model can be improved if the careful selection of input economic data which reflects the real world economy is made and the recent trend of the potential economic growth rate to decide the upper and lower threshold values which result in the overall performance of the forecasting model is used.

References

1. Lim, J.S., Ryu, T.-W., Kim, H.-J., Gupta, S.: Feature Selection for Specific Antibody Deficiency Syndrome by Neural Network with Weighted Fuzzy Membership Functions. In: Wang, L., Jin, Y. (eds.) FSKD 2005. LNCS (LNAI), vol. 3614, pp. 811–820. Springer, Heidelberg (2005)
2. Ishibuchi, H., Nakashima, T.: Voting in Fuzzy Rule-Based Systems for Pattern Classification Problems. Fuzzy Sets and Systems 103, 223–238 (1999)
3. Nauk, D., Kruse, R.: A Neuro-Fuzzy Method to Learn Fuzzy Classification Rules from Data. Fuzzy Sets and Systems 89, 277–288 (1997)

4. Setnes, M., Roubos, H.: GA-Fuzzy Modeling and Classification: Complexity and Performance. IEEE Trans. Fuzzy Systems 8(5), 509–522 (2000)
5. The Bank of Korea, The Korean business cycle, Monthly bulletin, pp. 31–53 (January 2004)
6. Hoptroff, R.G., Bramson, M.N., Hall, T.J.: Forecasting Economic Turning Points With Neural Nets. IJCNN-91-Seattle 1, 347–352 (1991)
7. Freisleben, B., Ripper, K.: Economic Forecasting Using Neural Networks. In: Proceedings of the 1995 IEEE International Conference on Neural Networks, vol. 2, pp. 833–839. IEEE Press, New York (1995)
8. Vishwakarama, K.P.: Recognizing Business Cycle Turning Points by means of a Neural Network. Computational Economics 7, 175–185 (1994)
9. Mitra, A., Mitra, S.: Forecasting Business Cycle Movements Using Wavelet Filtering and Neural Networks. Finance India XVIII (4), 1605–1626 (2004)
10. Schumpeter, J.: Business Cycles: A Theoretical, Historical, and Statistical Analysis of the Capitalist Process. McGrow-Hill, New York (1939)
11. Cho, S., Chung, W.: Economics. Bummun co.Ltd, pp. 685–693 (1990)
12. Zarnowitz, V., Moore, G.H.: Sequential Signals of Recession and Recovery. Journal of Business 55, 55–85 (1982)
13. Neftci, S.N.: Optimal Prediction of Cyclical Downturns. Journal of Economics and Control 4, 225–241 (1982)
14. Hamilton, J.: A New Approach to the Economic Analysis of Non-Stationary Time Series and the Business Cycle. Econometrica 57, 357–384 (1989)
15. Raihan, S.M., Wen, Y., Zeng, B.: Wavelet: A New Tool for Business Cycle Analysis, FRB of ST. Louis Working Paper 2005 050A (2005)
16. The Bank of Korea, The causes of declining tendency of Korean potential economic growth rate, Monthly bulletin, pp. 23–58 (September 2005)
17. Carpenter, G.A., Grossberg, S., Markuzon, N., Reynolds, J.H., Rosen, D.B.: Fuzzy ARTMAP: A Neural Network Architecture for Incremental Supervised Learning of Analog Multidimensional Maps. IEEE Transactions on Neural Networks 3(5) (September 1992)
18. Walker, J.S.: A Primer on Wavelets and their Scientific Applications. CRC Press, Boca Raton (1999)

A New Approach for Automatically Constructing Concept Maps Based on Fuzzy Rules

Shih-Ming Bai and Shyi-Ming Chen

Department of Computer Science and Information Engineering, National Taiwan University of Science and Technology, Taipei, Taiwan , R.O.C.
smchen@mail.ntust.edu.tw

Abstract. In recent years, some methods have been presented for dealing with the concept map construction to provide adaptive learning guidance to students. In this paper, we present a new method to automatically construct concept maps based on fuzzy rules and students' testing records. We apply the fuzzy set theory and fuzzy reasoning techniques to automatically construct concept maps and evaluate the relevance degrees between concepts. The proposed method provides a useful way to automatically construct concept maps in adaptive learning systems.

Keywords: Adaptive learning, concept maps, question-relationship graphs, concepts-relationship graphs, testing records.

1 Introduction

In recent years, some researchers focused on the research topic of adaptive learning systems [1], [2], [3], [4], [5], [6], [7], [8], [9], [10]. In [1], Appleby et al. presented a method for dealing with knowledge-based diagnostic tests of basic mathematical skills. In [2], Carchiolo et al. presented a method for dealing with adaptive formative paths in a web-based learning environment. In [3], Gamboa presented a method for designing intelligent tutoring systems. In [4], Hwang presented a method for applying the conceptual map model for developing intelligent tutoring systems. In [5], Hwang et al. presented a computer-assisted approach for diagnosing students' learning problems in science courses. In [6], Hsu et al. presented a concept inheritance method for learning diagnosis of a networkbased testing and evaluation system. In [7], Novak presented a method for using concept maps as facilitative tools in schools and corporations. In [8], Popham pointed out what teachers need to know for classroom assessment. In [9], Tsai et al. presented a method for a two-phase fuzzy mining and learning algorithm for an adaptive learning environment. In [10], Su et al. presented a two-phase concept map construction (TP-CMC) algorithm to automatically construct a concept map of a course by students' historical testing records. They find the fuzzy association rules by students' historical testing records, then construct a concept map based on the fuzzy association rules and the question-concept mapping table. However, the drawbacks of the method presented in [10] are as follows:

H.G. Okuno and M. Ali (Eds.): IEA/AIE 2007, LNAI 4570, pp. 155–165, 2007.

(1) The influence weights between questions on the constructed concept map shown in [10] are too high.
(2) Because the two-phase concept construction algorithm presented in [10] uses fuzzy data mining techniques to obtain fuzzy association rules for constructing concept maps, it is not efficient enough.

In this paper, we present a new method to automatically construct concept maps based on fuzzy rules and students' testing records for adaptive learning systems. It constructs concept maps by using fuzzy reasoning based on fuzzy rules. The proposed method can overcome the drawbacks of [10]. It provides a useful way to construct concept maps in adaptive learning systems.

The rest of this paper is organized as follows. In Section 2, we present a new method to automatically construct concept maps based on fuzzy rules for adaptive learning systems. In Section 3, we use an example to illustrate the process of automatically construct concept maps based on fuzzy rules. The conclusions are discussed in Section 4.

2 A New Method for Automatically Constructing Concept Maps for Adaptive Learning Systems

In this section, we present a new method for automatically constructing concept maps for adaptive learning systems. Let S_i denote the *i*th student, where $1 \le i \le m$. Assume that there are *n* questions $Q_1, Q_2, \ldots,$ and Q_n in the students' answerscripts, then we can get a grade matrix *G*, shown as follows:

$$G = \begin{array}{c} \\ S_1 \\ S_2 \\ \vdots \\ S_m \end{array} \begin{array}{c} \begin{array}{cccc} Q_1 & Q_2 & \cdots & Q_n \end{array} \\ \begin{bmatrix} g_{11} & g_{12} & \cdots & g_{1n} \\ g_{21} & g_{22} & \cdots & g_{2n} \\ \vdots & \vdots & \ddots & \vdots \\ g_{m1} & g_{m2} & \cdots & g_{mn} \end{bmatrix} \end{array},$$

where g_{ij} denotes the grade of the *i*th student S_i with respect to the *j*th question Q_j, $g_{ij} \in [0, mark_j]$, $mark_j$ denotes the mark allotted to the *j*th question Q_j, $1 \le i \le m$, and $1 \le j \le n$. Furthermore, assume that we have a question-concept matrix *QC*, shown as follows:

$$QC = \begin{array}{c} \\ Q_1 \\ Q_2 \\ \vdots \\ Q_n \end{array} \begin{array}{c} \begin{array}{cccc} C_1 & C_2 & \cdots & C_p \end{array} \\ \begin{bmatrix} qc_{11} & qc_{12} & \cdots & qc_{1p} \\ qc_{21} & qc_{22} & \cdots & qc_{2p} \\ \vdots & \vdots & \ddots & \vdots \\ qc_{n1} & qc_{n2} & \cdots & g_{np} \end{bmatrix} \end{array},$$

where $qc_{ij} \in [0,1]$, $qc_{ij} = 1$ denotes the *i*th question Q_i including the *j*th concept C_j, $qc_{ij} = 0$ denotes the *i*th question Q_i not including the *j*th concept C_j, $1 \le i \le n$, and $1 \le j \le p$. The proposed method for constructing the concept map is now presented as follows:

Step 1: According to the students' testing records, calculate the average score $AvgQ_j$, the highest score $HighQ_j$ and the lowest score $LowQ_j$ of each question Q_j, respectively, where

$$AvgQ_j = \frac{\sum_{i=1}^{m} g_{ij}}{m}, \tag{1}$$

$$HighQ_j = \underset{i=1}{\overset{m}{\text{Max}}}\left(g_{ij}\right), \tag{2}$$

$$LowQ_j = \underset{i=1}{\overset{m}{\text{Min}}}\left(g_{ij}\right), \tag{3}$$

$g_{ij} \in [0, mark_j]$, $mark_j$ denotes the marks allotted to the *j*th question Q_j, *m* denotes the number of students, *n* denotes the number of questions, $1 \le i \le m$, and $1 \le j \le n$.

Step 2: Calculate the entropy of the students' scores of each question and delete the questions that have no discrimination from the students' testing records. We define the discrimination of a question as follows. Let the balance degree $= \frac{AvgQ_j - LowQ_j}{HighQ_j - LowQ_j}$ be in the range from 35% to 65%, i.e., most students do not get the score which is larger than the average score and most students do not get the score which is smaller than the average score either. In other word, the amount of students who gets the score which is larger than the average score and the amount of students who gets the score which is lower than the average score are nearly equal. Then, compute the entropy $E(Q_j)$ of the students' score of Question Q_j as follows:

$$E(Q_j) = \frac{\sum_{i=1}^{m}\left(\left|g_{ij} - AvgQ_j\right|\right)/m}{\left(HighQ_j - LowQ_j + 1\right)/2},$$

where the entropy should be over 40%, i.e., the students' score of this question does not around $AvgQ_j$, and $1 \le j \le n$.

If the balance degree and the entropy of a question are both in the range described above, we say the question has the discrimination capability. Otherwise we say the question does not have the discrimination capability.

Step 3: For each grade g_{ij}, calculate the relative percentage rp_{ij} as follows:

$$rp_{ij} = \begin{cases} \frac{g_{ij} - AvgQ_j}{HighQ_j - AvgQ_j} \times 100\%, & \text{if } g_{ij} - AvgQ_j \ge 0 \\ -\frac{g_{ij} - AvgQ_j}{LowQ_j - AvgQ_j} \times 100\%, & \text{if } g_{ij} - AvgQ_j < 0 \end{cases} \tag{4}$$

where $1 \le i \le m$ and $1 \le j \le n$. Then, we can get the relative percentage matrix *RP*, shown as follows:

$$RP = \begin{array}{c} \\ S_1 \\ S_2 \\ \vdots \\ S_m \end{array} \begin{array}{c} \begin{array}{cccc} Q_1 & Q_2 & \cdots & Q_n \end{array} \\ \begin{bmatrix} rp_{11} & rp_{12} & \cdots & rp_{1n} \\ rp_{21} & rp_{22} & \cdots & rp_{2n} \\ \vdots & \vdots & \ddots & \vdots \\ rp_{m1} & rp_{m2} & \cdots & rp_{mn} \end{bmatrix} \end{array},$$

where $g_{ij} \in [0, mark_j]$, $mark_j$ denotes the marks allotted to the jth question, $AvgQ_j$ denotes the average grade of the jth question Q_j, $1 \le i \le m$, and $1 \le j \le n$.

Step 4: Based on the relative percentages rp_{ij} obtained in Step 3, fuzzify each relative percentage rp_{ij} into a fuzzy set shown in Fig. 1, where $1 \le i \le m$, and $1 \le j \le n$.

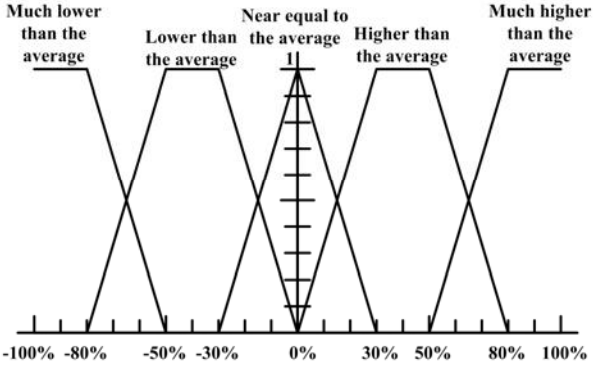

Fig. 1. Fuzzy sets of relative percentage

Then, we can get the fuzzy relative grade table, as shown in Table 1.

Table 1. Fuzzy relative grade table

Student ID	Q_1					…	Q_n				
	Much lower than the average	Lower than the average	Near equal to the average	Higher than the average	Much higher than the average	…	Much lower than the average	Lower than the average	Near equal to the average	Higher than the average	Much higher than the average
1						…					
2						…					
⋮						⋮					
m						…					

Step 5: Based on the fuzzy relative grade table shown in Table 1, perform fuzzy reasoning to get the membership degrees of the fuzzy sets "low" (L), "More or less low" (ML), "Medium" (M), "More or less high" (MH) and "High" (H) of the relationship degree between any two questions for the students' testing records, shown as follows:

IF the grade of the *i*th question is much lower than the average and the grade of the *j*th question is much lower than the average **THEN** the relationship degree between the *i*th question and the *j*th question is high,

IF the grade of the *i*th question is much lower than the average and the grade of the *j*th question is lower than the average **THEN** the relationship degree between the *i*th question and the *j*th question is more or less high,

IF the grade of the *i*th question is much lower than the average and the grade of the *j*th question is near equal to the average THEN the relationship degree between the *i*th question and the *j*th question is medium,

IF the grade of the *i*th question is much lower than the average and the grade of the *j*th question is higher than the average **THEN** the relationship degree between the *i*th question and the *j*th question is more or less low,

IF the grade of the *i*th question is much lower than the average and the grade of the *j*th question is much higher than the average **THEN** the relationship degree between the *i*th question and the *j*th question is low,
IF the grade of the *i*th question is lower than the average and the grade of the *j*th question is much lower than the average **THEN** the relationship degree between the *i*th question and the *j*th question is more or less high,
IF the grade of the *i*th question is lower than the average and the grade of the *j*th question is lower than the average **THEN** the relationship degree between the *i*th question and the *j*th question is high,
IF the grade of the *i*th question is lower than the average and the grade of the *j*th question is near equal to the average **THEN** the relationship degree between the *i*th question and the *j*th question is more or less high,
IF the grade of the *i*th question is lower than the average and the grade of the *j*th question is higher than the average **THEN** the relationship degree between the *i*th question and the *j*th question is medium,
IF the grade of the *i*th question is lower than the average and the grade of the *j*th question is much higher than the average **THEN** the relationship degree between the *i*th question and the *j*th question is more or less low,
IF the grade of the *i*th question is near equal to the average and the grade of the *j*th question is much lower than the average **THEN** the relationship degree between the *i*th question and the *j*th question is medium,
IF the grade of the *i*th question is near equal to the average and the grade of the *j*th question is lower than the average **THEN** the relationship degree between the *i*th question and the *j*th question is more or less high,
IF the grade of the *i*th question is near equal to the average and the grade of the *j*th question is near equal to the average **THEN** the relationship degree between the *i*th question and the *j*th question is high,
IF the grade of the *i*th question is near equal to the average and the grade of the *j*th question is higher than the average **THEN** the relationship degree between the *i*th question and the *j*th question is more or less high,
IF the grade of the *i*th question is near equal to the average and the grade of the *j*th question is much higher than the average **THEN** the relationship degree between the *i*th question and the *j*th question is medium,
IF the grade of the *i*th question is higher than the average and the grade of the *j*th question is much lower than the average **THEN** the relationship degree between the *i*th question and the *j*th question is more or less low,
IF the grade of the *i*th question is higher than the average and the grade of the *j*th question is lower than the average **THEN** the relationship degree between the *i*th question and the *j*th question is medium,
IF the grade of the *i*th question is higher than the average and the grade of the *j*th question is near equal to the average **THEN** the relationship degree between the *i*th question and the *j*th question is more or less high,
IF the grade of the *i*th question is higher than the average and the grade of the *j*th question is higher than the average **THEN** the relationship degree between the *i*th question and the *j*th question is high,
IF the grade of the *i*th question is higher than the average and the grade of the *j*th question is much higher than the average **THEN** the relationship degree between the *i*th question and the *j*th question is more or less high,
IF the grade of the *i*th question is much higher than the average and the grade of the *j*th question is much lower than the average **THEN** the relationship degree between the *i*th question and the *j*th question is low,
IF the grade of the *i*th question is much higher than the average and the grade of the *j*th question is lower than the average **THEN** the relationship degree between the *i*th question and the *j*th question is more or less low,
IF the grade of the *i*th question is much higher than the average and the grade of the *j*th question is near equal to the average **THEN** the relationship degree between the *i*th question and the *j*th question is medium,
IF the grade of the *i*th question is much higher than the average and the grade of the *j*th question is higher than the average **THEN** the relationship degree between the *i*th question and the *j*th question is more or less high,
IF the grade of the *i*th question is much higher than the average and the grade of the *j*th question is much higher than the average **THEN** the relationship degree between the *i*th question and the *j*th question is high,

where the membership functions “low” (L), “More or less low” (ML), “Medium” (M), “More or less high” (MH) and “High” (H) of each quiz’s grade are shown in Fig. 2. Then, we can get the fuzzy relationship degree table, as shown in Table 2, where L^{i}_{jk} denotes the membership degree belonging to the membership function “Low” between the *j*th question and the *k*th question of the *i*th student, ML^{i}_{jk} denotes the membership degree belonging to the membership function “More or less low” between the *j*th question and the *k*th question of the *i*th student, M^{i}_{jk} denotes the membership degree belonging to the membership function “Medium” between the *j*th question and the *k*th question of the *i*th student, MH^{i}_{jk} denotes the membership degree belonging to the membership function “More or less high” between the *j*th question and the *k*th question of the *i*th student, and H^{i}_{jk} denotes the membership degree belonging to the membership function “High” between the *j*th question and the *k*th question of the *i*th student.

Then, we combine the relative relationship degrees to calculate the relationship degree TRD_{jk} between any two adjacent questions Q_j and Q_k, shown as follows:

$$TRD_{jk} = \frac{\sum_{i=1}^{m}(L^{i}_{jk} \times 0 + ML^{i}_{jk} \times 0.2 + M^{i}_{jk} \times 0.5 + MH^{i}_{jk} \times 0.8 + H^{i}_{jk} \times 1)}{m}, \quad (5)$$

where $TRD_{jk} \in [0,1]$, $1 \le j \le n$, and $1 \le k \le n$.

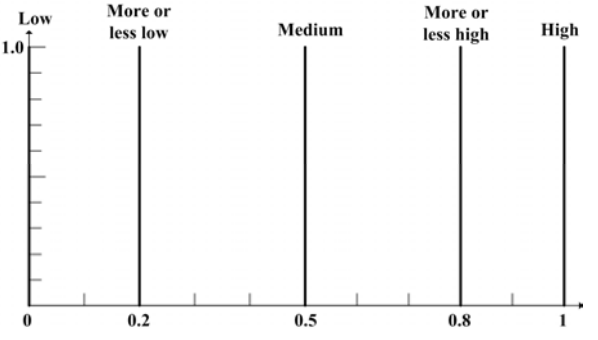

Fig. 2. Membership functions of each quiz's grade

Table 2. Relative relationship degree table

Student ID	Relative relationship degree between Q_1 and Q_2					…	Relative relationship degree between Q_{n-1} and Q_n				
	Low	More or Less Low	Medium	More or Less High	High	…	Low	More or Less Low	Medium	More or Less High	High
1	L^{1}_{12}	ML^{1}_{12}	M^{1}_{12}	MH^{1}_{12}	H^{1}_{12}	…	L^{1}_{n-1n}	ML^{1}_{n-1n}	M^{1}_{n-1n}	MH^{1}_{n-1n}	H^{1}_{n-1n}
2	L^{2}_{12}	ML^{2}_{12}	M^{2}_{12}	MH^{2}_{12}	H^{2}_{12}	…	L^{2}_{n-1n}	ML^{2}_{n-1n}	M^{2}_{n-1n}	MH^{2}_{n-1n}	H^{2}_{n-1n}
⋮	⋮	⋮	⋮	⋮	⋮	⋮	⋮	⋮	⋮	⋮	⋮
m	L^{m}_{12}	ML^{m}_{12}	M^{m}_{12}	MH^{m}_{12}	H^{m}_{12}	…	L^{m}_{n-1n}	ML^{m}_{n-1n}	M^{m}_{n-1n}	MH^{m}_{n-1n}	H^{m}_{n-1n}

Step 6: Construct the concept map by the following sub-steps:

Step 6.1: Calculate the summation of the percentage SP_j of each question Q_j, where $SP_j = \frac{\sum_{j=1}^{m}(g_{ij}/mark_j)}{m}$, m denotes the number of students, g_{ij} denotes the grade of the ith student for the jth question Q_j, $mark_j$ denotes the

marks allotted to the *j*th question Q_j, $1 \le i \le m$, and $1 \le j \le n$. If $SP_j > SP_k$, then add an arrow in the constructed graph from Q_j to Q_k associated with TRD_{jk}; If $SP_j < SP_k$, then add an arrow in the constructed graph from Q_k to Q_j associated with TRD_{jk}, where $1 \le j \le n$ and $1 \le k \le n$.

Step 6.2: Transform the graph of the relationships of questions obtained in Step 6.1 into the graph of the relationships of concepts based on the question-concepts matrix *QC*.

Step 6.3: If there are more than one arrow from a concept to another concept, calculate the average of the values associated with these arrows and merge these arrows into one arrow associated with the derived averaging value.

3 An Example

Assume that there are five questions Q_1, Q_2, Q_3, Q_4, Q_5 and five concepts *A*, *B*, *C*, *D*, *E*. Assume that there are ten students $S_1, S_2, \cdots, S_{10}$ to answer these questions. Assume that the grade matrix *G* and the question-concepts matrix *QC* are shown as follows:

$$G = \begin{array}{c} \\ S_1 \\ S_2 \\ S_3 \\ S_4 \\ S_5 \\ S_6 \\ S_7 \\ S_8 \\ S_9 \\ S_{10} \end{array} \begin{array}{c} \begin{array}{ccccc} Q_1 & Q_2 & Q_3 & Q_4 & Q_5 \end{array} \\ \begin{bmatrix} 12 & 18 & 20 & 20 & 7 \\ 12 & 14 & 18 & 3 & 7 \\ 12 & 16 & 14 & 4 & 7 \\ 2 & 8 & 12 & 6 & 20 \\ 2 & 8 & 12 & 2 & 12 \\ 2 & 10 & 8 & 2 & 20 \\ 20 & 5 & 5 & 4 & 1 \\ 10 & 6 & 6 & 1 & 5 \\ 10 & 5 & 5 & 1 & 5 \\ 10 & 3 & 4 & 0 & 5 \end{bmatrix} \end{array},$$

$$QC = \begin{array}{c} \\ Q_1 \\ Q_2 \\ Q_3 \\ Q_4 \\ Q_5 \end{array} \begin{array}{c} \begin{array}{ccccc} A & B & C & D & E \end{array} \\ \begin{bmatrix} 0 & 0 & 0 & 1 & 0 \\ 1 & 0 & 1 & 0 & 0 \\ 1 & 0 & 0 & 0 & 0 \\ 0 & 1 & 1 & 0 & 0 \\ 0 & 1 & 0 & 1 & 1 \end{bmatrix} \end{array}.$$

Based on Eq. (1), we can get $AvgQ_1 = 9.2$, $AvgQ_2 = 9.3$, $AvgQ_3 = 10.4$, $AvgQ_4 = 4.3$ and $AvgQ_5 = 8.9$. Based on Eq. (2), we can get $HighQ_1 = 20$, $HighQ_2 = 18$,

$HighQ_3 = 20,\ HighQ_4 = 20,$ and $HighQ_5 = 20.$ Based on Eq. (3), we can get $LowQ_1 = 2,$ $LowQ_2 = 3,\ LowQ_3 = 4,\ LowQ_4 = 0$ and $LowQ_5 = 1.$

Because the balance degree of Question Q_j is equal to $\frac{AvgQ_j - LowQ_j}{TopQ_j - LowQ_j}$ and the entropy of Question Q_j is equal to $\frac{\sum_{i=1}^{m}\left|g_{ij} - AvgQ_j\right|/m}{(HighQ_j - LowQ_j + 1)/2}$, where $1 \le j \le 5$, we can get the balance degree and the entropy of each question, as shown in Table 3.

Table 3. The balance degree and the entropy of each question

Questions	Q_1	Q_2	Q_3	Q_4	Q_5
Balance degree	40%	42%	40%	21.5%	41.58%
Entropy	45.47%	52%	56.47%	33.14%	50.6%

From Table 3, we can see that the balance degree of Q_4 does not fall in the range from 35% to 65% and the entropy of Q_4 does not go over 40%, so we remove Q_4 from the students' testing records.

Based on Eq. (4), we can get the relative percentage matrix *RP*, shown as follows:

$$RP = \begin{array}{c} \\ S_1 \\ S_2 \\ S_3 \\ S_4 \\ S_5 \\ S_6 \\ S_7 \\ S_8 \\ S_9 \\ S_{10} \end{array} \begin{array}{c} \begin{array}{cccc} Q_1 & Q_2 & Q_3 & Q_5 \end{array} \\ \begin{bmatrix} 25.93 & 100 & 100 & -24.05 \\ 25.93 & 54.02 & 79.17 & -24.05 \\ 25.93 & 77.01 & 37.50 & -24.05 \\ -100 & -20.63 & 16.67 & 100 \\ -100 & -20.63 & 16.67 & 27.93 \\ -100 & 8.05 & -37.50 & 100 \\ 100 & -68.25 & -84.38 & -100 \\ 7.41 & -52.38 & -68.75 & -49.37 \\ 7.41 & -68.25 & -84.38 & -49.37 \\ 7.41 & -100 & -100 & -49.37 \end{bmatrix} \end{array}$$

After fuzzifying each relative percentage rp_{ij} in the relative percentage matrix *RP* based on the membership functions of the fuzzy sets shown in Fig. 1, we can get the fuzzy relative grade table.

Based on the fuzzy relative grade table, after performing fuzzy reasoning to get the membership degrees of the fuzzy sets "low" (L), "More or less low" (ML), "Medium" (M), "More or less high" (MH) and "High" (H) between any two questions for students' testing records, we can get the relative relationship degree table. After combining the relative relationship degrees, we can get the relationship degree TRD_{jk} between any two questions Q_j and Q_k.

After calculating the summation of the percentage SP_j of each question Q_j, we can get the percentage SP_j of each question Q_j, where $j = 1, 2, 3, 5.$ Then, based on the following criteria:

If $SP_j > SP_k$, then we add an arrow from Q_j to Q_k associated with TRD_{jk} into the constructed graph,

If $SP_j < SP_k$, then we add an arrow from Q_k to Q_j associated with TRD_{jk} into the constructed graph,

we can get the questions-relationship graph, as shown in Fig. 3.

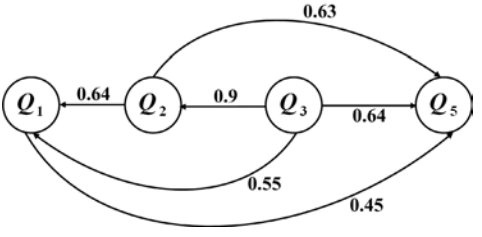

Fig. 3. The constructed questions-relationship graph

After transforming the derived questions-relationship graph into the relationships between concepts based on the mapping matrix QC, we can get the concepts-relationship graph, as shown in Fig. 4. If there are more than one arrow from a concept to the another concept in the constructed concepts-relationship graph shown in Fig. 4, we evaluate the average values associated with these arrows and merge these arrows into one arrow associated with the derived averaging value. Therefore, we can get the constructed concept map as shown in Fig. 5.

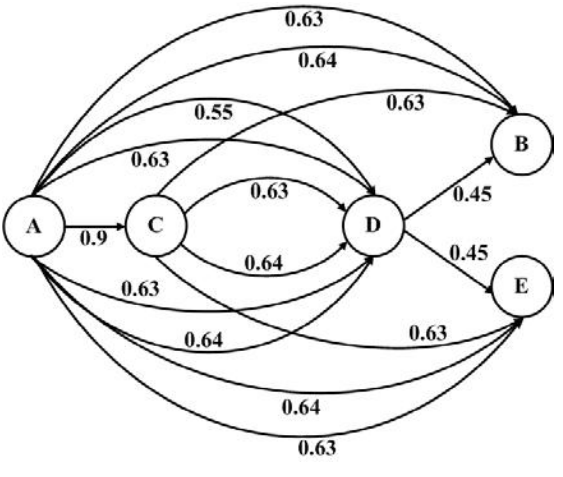

Fig. 4. The constructed concepts- relationship graph

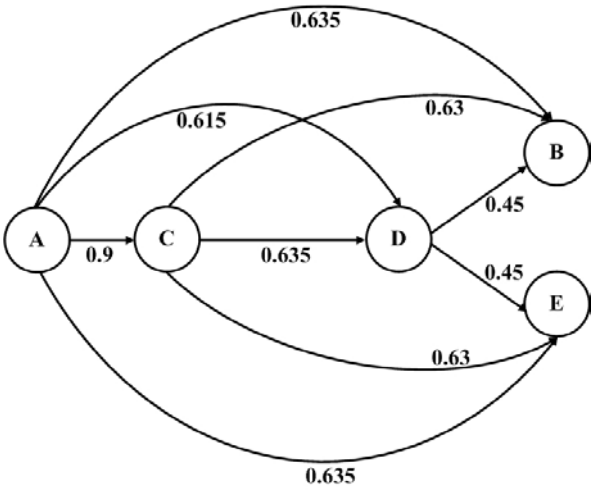

Fig. 5. The constructed concept map

4 Conclusions

In this paper, we have presented a new method based on fuzzy rules to automatically construct the concept map for students' testing records for adaptive learning. The proposed method can overcome the drawback of the method presented in [10]. It provides a useful way to construct concept maps in adaptive learning systems.

Acknowledgements

This work was supported in part by the National Science Council, Republic of China, under Grant NSC 95-2221-E-011-116-MY2.

References

1. Appleby, J., Samuels, P., Jones, T.T.: Diagnosis–A Knowledge-based Diagnostic Test of Basic Mathematical Skills. Computers & Education 28, 113–131 (1997)
2. Carchiolo, V., Longheu, A., Malgeri, M.: Adaptive Formative Paths in a Web-Based Learning Environment. Educational Technology & Society 5, 64–75 (2002)
3. Gamboa, H.: Designing Intelligent Tutoring Systems: A Bayesian Approach. In: Proceedings of the 3rd International Conference on Enterprise Information Systems, Setubal, Portugal, pp. 452–458 (2001)
4. Hwang, G.J.: A Conceptual Map Model For Developing Intelligent Tutoring System. Computers & Education 40, 217–235 (2003)
5. Hwang, G.J., Hsiao, C.L., Tseng, C.R.: A Computer-Assisted Approach to Diagnosing Student Learning Problem in Science Course. Journal of Information Science & Engineering 19, 229–248 (2003)

6. Hsu, C.S., Tu, S.F., Hwang, G.J.: A Concept Inheritance Method for Learning Diagnosis of a Networkbased Testing and Evaluation System. In: Proceeding of the 7th International Conference on Computer-Assisted Instructions, pp. 602–609 (1998)
7. Novak, J.D.: Learning, Creating, and Using Knowledge: Concept Maps As Facilitative Tools in Schools and Corporations. Lawrence Erlbaum Associates, Mahwah (1998)
8. Popham, W.J.: Classroom Assessment: What Teachers Need to Know. Pearson Allyn & Bacon, 222–227 (1999)
9. Tsai, C.J., Tseng, S.S., Lin, C.Y.: A Two-Phase Fuzzy Mining and Learning Algorithm for Adaptive Learning Environment. In: Alexandrov, V.N., Dongarra, J.J., Juliano, B.A., Renner, R.S., Tan, C.J.K. (eds.) Computational Science - ICCS 2001. LNCS, vol. 2074, pp. 429–438. Springer, Heidelberg (2001)
10. Sue, P.C., Weng, J.F., Su, J.M., Tseng, S.S.: A New Approach for Constructing the Concept Map. In: Proceedings of the, IEEE International Conference on Advanced Learning Technologies, pp. 76–80 (2004)
11. Zadeh, L.A.: Fuzzy sets. Information and Control 8, 338–353 (1965)

Application of Fuzzy Logic for Adaptive Interference Canceller in CDMA Systems

Yung-Fa Huang[1], Ping-Ho Ting[2], and Tan-Hsu Tan[3]

[1] Graduate Institute of Networking and Communication Engineering,
Chaoyang University of Technology
Taichung 41349, Taiwan, R.O.C
yfahuang@mail.cyut.edu.tw
[2] Dept.of Hospitality Management, Tunghei University
Taichung 407, Taiwan, R.O.C
ding@thu.edu.tw
[3] Dept.of Electrical Engineering, National Taipei University of Technology
Taipei, 105, Taiwan, R.O.C
thtan@ntut.edu.tw

Abstract. In this paper, the performance of the proposed fuzzy logic parallel interference cancellation (FLPIC) multiuser detector is evaluated for frequency-selective fading channels in wireless CDMA communication systems. A modified fuzzy logic system (FLS) with an adequate scaling factor (SF) is proposed to infer adequate partial factors (PFs) for the PIC scheme. Simulation results show that the proposed FLS can adapt to the large variations of users' fading effects. Therefore, the FLPIC outperforms the conventional PIC (CPIC) and constant weight PIC (CW-PIC) over two-path and three-path time-varying frequency-selective fading channels especially at heavy system load in DS-CDMA systems.

Keywords: DS-CDMA, multiuser detection, parallel interference cancellation (PIC), fuzzy logic system (FLS).

1 Introduction

The direct-sequence code-division multiple-access (DS-CDMA) cellular communication system, the most favorite candidate for the 3rd generation radio cellular communication systems, exhibits a highly potential capacity [1]. However, the two main shortcomings in a CDMA system, the multiple access interference (MAI) and the near-far problem, degrade the system performance [1-7]. The multiuser detector, an upcoming main-stream research for CDMA receivers, which attempts to eliminate MAIs and the near-far problem simultaneously, has become an approved capacity improving technique and received much significant attention recently [2-9]. The initial work on multiuser detection for CDMA is the optimal multiuser detector proposed by Verdu [2], which has a potential improvement in capacity and near-far resistance. However, the computational complexity of the optimal maximum likelihood (ML) detector grows exponentially with the number of users and the length of the bit sequence.

H.G. Okuno and M. Ali (Eds.): IEA/AIE 2007, LNAI 4570, pp. 166–175, 2007.

Several suboptimal multiuser detection schemes have been proposed [2–9]. Among the suboptimal multiuser detectors, the parallel interference cancellation(PIC) scheme for CDMA systems simultaneously subtracts the interference from each user's received signal. However, at high system load, the multistage conventional PIC approach, which attempts to completely cancel the interference caused by all other users, suffers performance degradations due to a poor cancellation, which is brought about by the relatively high error rate of bit decisions in the preceding stage. Thus, when the interference estimate is poor (as in the early stages of PIC), the partial cancellation proposed by Divsalar et al.[7], who prefer not to cancel the entire amount of estimated multiuser interference, contrarily is a better policy than the complete IC. The partial factor (PF) of the partial PIC scheme is a fraction smaller than one, which reflects the reliability of the tentative decision. However, when all the PFs are the same in one stage [7], its performance obviously suffers degradations in the near-far channels and fading channels. Moreover, the optimal weight of each interferer depends on their reliability, respectively. Consequently, to achieve the optimal performance of PIC, the PFs of the interferers should be adjusted according to the reliability of their estimate statistics. The fuzzy logic developed by Zadeh [10] has drawn a great deal of attention because of its universal approximation ability in the nonlinear problem [11]. Therefore, in this paper, we propose an adaptive fuzzy logic system (FLS) to infer adequate PFs to perform effective PIC over multipath frequency-selective fading channels.

2 System Models

2.1 System Model of DS-CDMA Systems

This paper considers a CDMA communication system in which K users are communicating simultaneously at the same rate over a common additive white Gaussian noise (AWGN) channel each with a binary phase-shift keying (BPSK) data modulation and its own PN code. The kth user transmits the binary data signal $b_k(t) = \sum_{i=-\infty}^{\infty} b_{k,i}(i)p_T(t-iT)$, where $b_{k,i} \in \{-1, +1\}$ is the ith data bit of the kth user and $p_T(t)$ is a rectangular pulse with amplitude 1 and duration T. During the ith bit, the kth user's signal is spread by the signature waveform $a_k(t) = \sum_{i\prime=-\infty}^{\infty} \sum_{j=1}^{N} a_{kj} P_T\,[t - i\prime T - (j-1)T_c]$, where $a_{kj} = \{-1, +1\}$ is the jth chip of the kth user, and $p_T\ (t)$ is a rectangular chip pulse with duration T_c. The ratio of the bit duration T to the chip duration T_c is the processing gain $N = T/T_c$. The signal $c_k(t)$ transmitted by the kth user is given by

$$c_k(t) = \sqrt{2P_k} b_k(t) a_k(t) \cos(\omega_c t + \theta_k), \tag{1}$$

where P_k and θ_k are the signal power and the phase of the kth user respectively, and wc is the common carrier frequency. Moreover, the multipath fading channel should be a reality for a wireless CDMA communication system. Therefore, the

equivalent complex baseband representation of the channel impulse response of the kth user's link, $h_k(t)$, $k = 1,\ldots,K$, can be modeled by

$$h_k(t) = \sum_{\lambda=1}^{L} g_{k,\lambda}(t)\delta(t - t_{k,\lambda})e^{j\varphi\ ,\ (t)}, \tag{2}$$

where $g_{k,\lambda}(t)$,t_k, λ and $\varphi_{k,\lambda}(t)$ is the path amplitude, the path delay and the path phase of the λth path of kth user, respectively. The maximum number of paths of the kth user is denoted by L_k. The path amplitude $g_{k,\lambda}$ has a Rayleigh fading distribution, and the path phase $\varphi_{k,\lambda}$ has a uniform distribution over $[0, 2\pi]$, for the λth path of the kth user.

For simplicity, the equivalent complex baseband representation for a synchronous CDMA system is considered in this paper. The received signal then becomes

$$r(t) = \sum_{\lambda=1}^{L}\sum_{k=1}^{K} A_{k,\lambda}(t) \cdot b_k(t - t_{k,\lambda}) \cdot a_k(t - t_{k,\lambda}) \cdot e^{j\phi\ ,\ (t)} + n(t), \tag{3}$$

where $A_{k,\lambda}(t)e^{j\phi\ ,\ (t)}$ is the complex-valued amplitude of the received baseband signal of the kth user and $n(t) = n_I(t) + jn_Q(t)$ is a complex-valued AWGN with independent real and imaginary components and the two-sided PSD equals to $N_o/2$.

Then, the complex form of the discrete-time received signal sampled with chip rate after normalized chip-matched filtering at the RAKE receiver is given by

$$r(m) = \sum_{\lambda=1}^{L}\sum_{k=1}^{K} A_{k,\lambda,i} \cdot b_k(m - \lambda + 1) \cdot a_k(m - \lambda + 1) \cdot e^{j\phi\ ,\ ,\ } + n(m), \tag{4}$$

where $a_k(m) = a_{k,j}$, $j = m \bmod N$, and $A_{k,\lambda,i}$ and $\phi_{k,\lambda,i}$ are the received signal amplitude and phase sampled in the ith bit for the lth path of kth user.

To take the advantage of frequency diversity, in the RAKE receiver the combining technique, referred to as the maximal ratio combining (MRC), can maximize the instantaneous signal to interference-and-noise-ratio (SINR) for frequency-selective fading channels [14]. Therefore, with MRC, the decision statistic for the ith bit of the kth user is obtained as

$$Z_{k,i} = \mathcal{R}\Big\{\frac{1}{L_k N}\sum_{\lambda=1}^{L}\sum_{m=iN+\lambda}^{(i+1)N+\lambda-1} r(m) \cdot \hat{A}_{k,\lambda,i} \cdot a_k(m - \lambda + 1) \cdot e^{-j\phi\ ,\ ,\ }\Big\}. \tag{5}$$

Then, the ith data bit can be estimated by hard decision using $\hat{b}_{k,i} = Z_{k,i}/|Z_{k,i}|$.

2.2 Multistage Parallel Interference Cancellation

The multistage PIC scheme is one of efficient ways to remove the MAIs. The tentative decision of the first stage of multistage PIC detector is a hard-decision

approach that is used in a conventional RAKE receiver. The decision statistic for the ith bit of the kth user at the first stage (i.e., before any interference cancellation) is obtained as (5). Then, the ith data bit can be estimated by hard decision as obtained by $\hat{b}_{k,i}^{(1)} = Z_{k,i}^{(1)}/|Z_{k,i}^{(1)}|$. The PIC is then performed by simutanously substracting the estimated signals of the interfering users from the received signal $r(m)$ to form a new received signal $r_{k,i,\lambda}^{(s)}(m)$ for the λth path of the kth user at stage s, given by

$$r_{k,i,\lambda}^{(s)}(m) = r(m) - \sum_{\gamma=1,\gamma\neq\lambda}^{L} \hat{A}_{k,i,\gamma}\hat{s}_{k,i,\gamma}^{(s)}(m) - \sum_{k\ =1,k\ \neq k}^{K}\sum_{\gamma=1}^{L} \hat{A}_{k\ ,i,\gamma}\hat{s}_{k\ ,i,\gamma}^{(s)}(m) - \sum_{\nu\neq i}\sum_{k\ =1}^{K}\sum_{\gamma=1}^{L} \hat{A}_{k\ ,\nu,\gamma}\hat{s}_{k\ ,\nu,\gamma}^{(s)}(m), \tag{6}$$

where $\hat{s}_{k,i,\gamma}^{(s)}(m) = \hat{b}_{k,i,\gamma}^{(s)} a_k(m-\gamma+1)e^{j\phi_{k,i}}$ is the estimated signal of the ith bit of the kth user at stage s. The signal amplitude can be estimated by transmitting a trainning sequence in the pilot-tone channel. By MRC, the decision statistic of the ith bit at stage s, $Z_{k,i}^{(s)}$, is then obtained by (5). Thus, the ith data bit of the kth user at stage s can be decided by $\hat{b}_{k,i}^{(s)} = Z_{k,i}^{(s)}/|Z_{k,i}^{(s)}|$. Using this procedure, an arbitrary number of stages of the PIC may be performed to obtain the data bits transmitted by each user.

Since the estimates of MAIs may not be completely correct, a partial factor (PF) can be added on the path of the interference cancellation, which is called partial PIC. With this modification, the new received signal $r_{k,i,\gamma}^{(s)}(m)$ for the lth path of the kth user after stage s for a partial PIC is given by

$$r_{k,i,\lambda}^{(s)}(m) = r(m) - \sum_{\gamma=1,\gamma\neq\lambda}^{L} w_{k,i,\gamma}^{(s)}(m)\hat{A}_{k,i,\gamma}\hat{s}_{k,i,\gamma}^{(s)}(m) - \sum_{k\ =1,k\ \neq k}^{K}\sum_{\gamma=1}^{L} w_{k\ ,i,\gamma}^{(s)}(m)\hat{A}_{k\ ,i,\gamma}\hat{s}_{k\ ,i,\gamma}^{(s)}(m) - \sum_{\nu\neq i}\sum_{k\ =1}^{K}\sum_{\gamma=1}^{L} w_{k\ ,\nu,\gamma}^{(s)}(m)\hat{A}_{k\ ,\nu,\gamma}\hat{s}_{k\ ,\nu,\gamma}^{(s)}(m), \tag{7}$$

where $w_{k,i,\gamma}^{(s)}(m)$ is the PF at the mth chip for the γth path of the ith bit of the kth user.

3 Adaptive Multistage Fuzzy Logic PIC Detection

The FLS is a decision-making logic which employs a set of fuzzy IF-THEN rules. It has drawn a great deal of attention because of its universal approximation ability in nonlinear problems [11]. Therefore, the optimal weights of the partial IC

scheme can be easily determined by an FLS with sufficient rules. We can establish these fuzzy rules by matching input-output pairs through an adaptation procedure. Here, for the practical implementations, we established both membership functions (MBFs) and rules by the heuristic basis and the knowledge about the input-output relations to find the optimal weight for each interferer.

It is easy to know that the optimal weight becomes larger as the number of user K decreases. Therefore, as the interference or noise increases the signal link becomes unreliable so that the PF should be set to a smaller value. On the other hand, if the interference decreases or the signal power becomes higher, the weight should be set to a larger value to reflect the reliability of the signal link. Moreover, with the benefits of frequency diversity, the MRC RAKE receivers improve the reliability of the conventional detector. Therefore, the optimal PFs inferred by the FLS in the FLPIC should be adapted to the benefits of the frequency diversity over the frequency-selective fading channels. Moreover, the scaling factor (SF) is used to adjust the scales of the input variables for the FLS. Then, we define the effective number of users for the lth path of the desired kth user as

$$K_{eff,k,\lambda} = \frac{\sum_{k\ =1}^{K} \sum_{\gamma=1}^{L} \hat{A}_{k\ ,\gamma}}{\hat{A}_{k,\gamma} \cdot SF} \tag{8}$$

and the other input, $SNR_{k,\lambda}$, by

$$SNR_{k,\lambda} = \hat{SNR}_{k,\lambda} \cdot SF \tag{9}$$

where $\hat{SNR}_{k,\lambda} \cdot SF$ is the estimated SNR for the lth path of the kth user and SF (scaling factor) is used to adjust the PFs to adapt to the reliability of bit-decisions.

We choose five and six Gaussian MBFs to cover the entire universe of discourse of two inputs, $K_{eff,k,\lambda}$ and $SNR_{k,\lambda}$, and one output $w_{k,l}$, respectively. The five linguistic terms, negative low (NL), zero (ZE), positive low (PL), positive medium (PM) and positive high (PH), are chosen to cover the universe of discourse for the SNR of the desired user. The five terms, very few (VF), few (F), medium (MED), many (M) and a great many (GM), are chosen to cover the universe of discourse for the effective number of users. As for the terms of the PF, the six terms, almost zero (AZ), small (S), medium (MED), large (L), very large (VL) and almost one (AO), are chosen to cover its universe of discourse. The Gaussian MBF of the fuzzy set F_i^l in each interval $[C_i^-\ ,C_i^+]$ of the universe of discourse U can be expressed by

$$\mu_{F}\ (x_i) = exp[-\frac{1}{2}(\frac{x_i - \bar{x}_i^l}{\sigma_i^l})^2], \tag{10}$$

where $l = 1, 2, \ldots, 5$, $i = 1, 2, 3$, $x_i \in [C_i^-, C_i^+]$, $\bar{x}_i^l$ and σ_i^l and are the mean and standard deviation of the Gaussian MBF, respectively. In this paper, we consider the fuzzy control rules of a two-input-single-output fuzzy system as

$$R^j : IF\ SNR_{k,i,\lambda}\ is\ F_1^{l_1}\ AND\ K_{eff,k,i,\lambda}\ is\ F_2^{l_2}\ ,\ THEN\ w_{k,i,\lambda}\ = F_3^{l_3}, \tag{11}$$

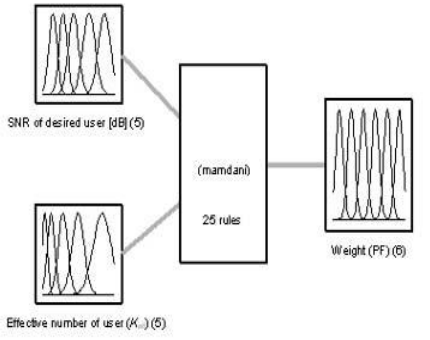

Fig. 1. The FLS for PIC multiuser detectors with 2 inputs, 1 output and 25 rules

Table 1. The rule base for the FLS in stage 2

$SNR \backslash K_{eff}$	VF	F	MED	M	GM
NL	MED	S	AZ	AZ	AZ
ZE	H	MED	S	S	AZ
PL	AO	H	MED	S	AZ
PM	AO	VH	H	MED	AZ
PH	AO	VH	H	MED	S

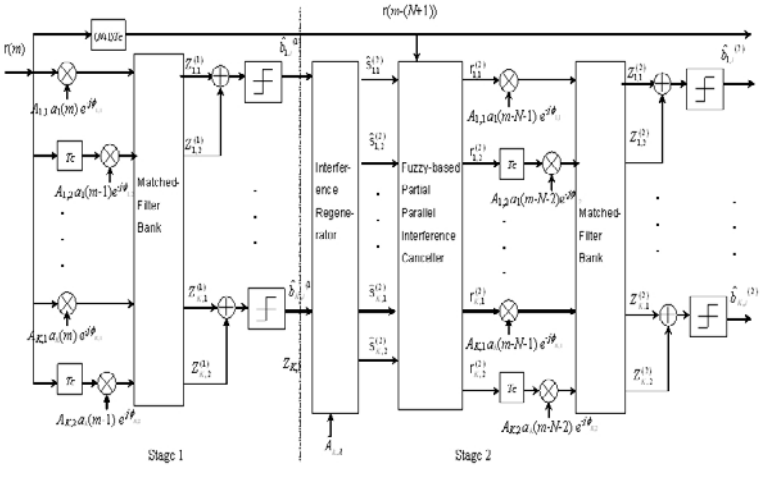

Fig. 2. Block diagram of two-stage FLPIC receiver with MRC for synchronous CDMA systems over a two-path frequency-selective fading channel

where $F_1^{l_1}$, $F_2^{l_2}$, and $F_3^{l_3}$ are the linguistic terms of the input variables $SNR_{k,i,\lambda}$, $K_{eff,k,i,\lambda}$ and the output variable $w_{k,i,l}$, respectively, and l_1, $l_2 = 1, 2, \ldots, 5$, $l_3 = 1, 2, \ldots, 6$, and the index of rule $j = 1, 2, \ldots, 25$. Then, the FLS for the

PPIC can be performed as shown in Fig. 1. The rule base, shown in Table 1, including 25 fuzzy IF-THEN rules for stage 2, can be established heuristically by the experimental results, which infer the relations between the adequate weights of interferers and their reliability.

There are many defuzzification methods [12] available and the following cetroid calculation, which returns the center of area under the aggregated MBFs curve, is being employed here:

$$w_k = \frac{\sum_{i=1}^{q} z_i \cdot \mu_{F_3^l}(z_i)}{\sum_{i=1}^{q} \mu_{F_3^l}(z_i)}, \tag{12}$$

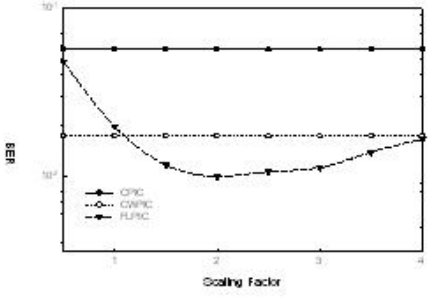

(a)

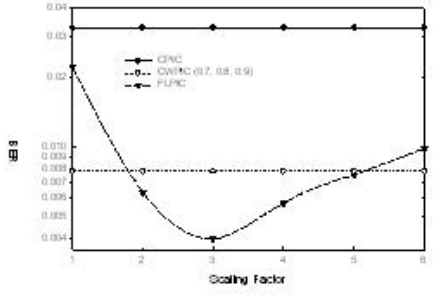

(b)

Fig. 3. BER vs. scaling factor for stage 4 of multistage FLPIC detection schemes over a frequency-selective fading channel: (a) two-path, (b) three-path (SNR=12 dB, K=30)

where q is the number of quantization levels of the output area under the aggregated MBFs, z_i is the amount of the inference output at the quantization level i and $\mu_{F_3^l}$ is its membership value in the output fuzzy set F_3^l. Similar to stage 2, the inference rule-base of stage 3 and the latter stages can also be set up by the further experimental results. The block diagram of a two-stage FLPIC multiuser detector over a two-path frequency-selective fading channel is shown in Fig. 2.

After performing the experiments of the FLPIC over the frequency-selective fading channels, we obtain the results shown in Fig. 3. From the cures of BER vs. SF at stage 4 of PIC schemes in Fig. 3(a), it is observed that the SF of optimal PFs equals 2 over two-path frequency-selective fading channels at heavy system load. Besides, it should be noted that if we adopt the FLS with SF=1, then the performance of the FLPIC is slightly inferior to the CWPIC scheme. Similarly, from Fig. 3(b), the SF equals 3 of the optimal PFs of the FLPIC over the three-path frequency-selective fading channels with SNR=12 dB, K=30. From Fig. 3(b), we know that when we select $2 \leq SF \leq 4$, the FLPIC outperforms the CWPIC, but not with $SF \leq 1$ or $4 \leq SF$.

4 Simulation Results and Discussions

In all simulations, the synchronous CDMA system model described in Section 2 is adopted. The Gold codes [13] are generated for each user and used to spread his or her random data bits with the processing gain 31. The results of these spreading operations are multiplied by the carrier phases following which Gaussian noise samples are added to the combined received signal with one sample per chip time. It is assumed that the time and phase synchronizations are perfect. The SNR and amplitudes of users in channel estimations are also assumed to be perfectly estimated. The terms CPIC (conventional PIC) and CWPIC are used to represent the PIC schemes mentioned in Section 2, while the FLPIC is used to denote the adaptive PIC detector based on FLS presented in Section 3. To compare the weight adaptation of FLPIC, we set the constant weight to 0.7, 0.8 and 0.9 on the stage 2, 3 and 4, respectively, in the CWPIC scheme [6]. Moreover, the PF is inferred by the FLS in the FLPIC described in Section 3, in which the PF inferred at the front stages should be less than that of the latter stages for the same interferer.

In this paper, we examined the performance of FLPIC scheme over both two-path and three-path frequency-selective fading channels. The BER vs. the capacity of the stage 4 of FLPIC, CPIC and CWPIC is shown in Fig.4 with MRC.

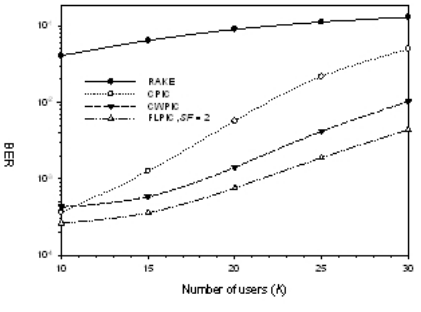

Fig. 4. BER vs. number of users for stage 4 of various multistage PIC detection schemes over a two-path frequency-selective fading channel based on MRC (SNR=18 dB)

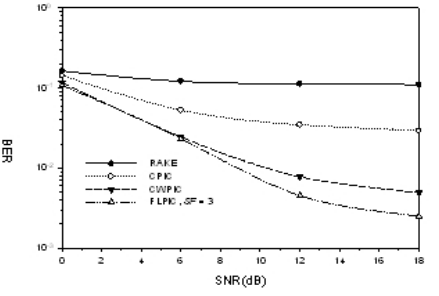

Fig. 5. BER vs. SNR for stage 4 of various multistage PIC detection schemes over a three-path frequency-selective fading channel based on MRC (K=30)

From Fig.4, it is shown that both CWPIC and FLPIC outperform the CPIC at the heavier system load is due to the higher MAI in a multipath frequency-selective fading channel. Besides, the FLPIC with $SF = 2$ outperforms the CWPIC due to its high adaptation to the time-varying fading over a two-path frequency-selective fading channel as shown in Fig.4.

Fig. 5 shows the comparisons on the BER vs. SNR of the stage 4 of CPIC, CWPIC and FLPIC schemes in the three-path frequency-selective fading channels with MRC. We can observe that FLPIC with SF=3 outperforms both CPIC and CWPIC over a three-path frequency-selective fading channel with MRC combining.

5 Conclusion

In this paper, an FLS is proposed to infer "adequate" PFs for the multistage PIC scheme. Simulation results show that with an adequate scaling factor, the proposed FLPIC is more robust than both the CPIC and the CWPIC over the frequency-selective fading channels, especially at heavy system load.

Acknowledgments

This work was funded in part by National Science Council, Taiwan, Republic of China, under Grant NSC 94-2213-E-324-029 for Y.-F. Huang.

References

1. Gilhousen, K.S., Jacobs, I.M., Padavani, R., Viterbi, A.J., Weaver, L.A., Wheatley, C.E.: On the capacity of a cellular CDMA system. IEEE Trans. Vehicular Tech. 40(2), 303–312 (1991)
2. Verdu, S.: Multiuser detection. Cambridge University Press, Cambridge (1998)
3. Duel-Hallen, A., Holtzman, J., Zvonar, Z.: Multiuser detection for CDMA systems. IEEE Pers. Commun. pp. 46–58 (April 1995)

4. Moshavi, S.: Multi-user detection for DS-CDMA communications. IEEE Commun. Mag. pp. 124–136 (October 1996)
5. Ojanpera, T.: Overview of multiuser detection/interference cancellation for DS-CDMA. In: Proc. of International Confer. Personal Wireless Commun. Mumbai, India, pp. 115–119 (December 1997)
6. Varanasi, M.K., Aazhang, B.: Multistage detection in asynchronous code division multiple-access communications. IEEE Trans. Commun. COM-38 (4), 509–519 (1990)
7. Divsalar, D., Simon, M.K., Raphaeli, D.: Improved parallel interference cancellation for CDMA. IEEE Trans. Commun. COM-46(2), 258–268 (1998)
8. Correal, N.S., Buehrer, R.M., Woerner, B.D.: A DSP-based DS-CDMA multiuser receiver employing partial parallel interference cancellation. IEEE J. Select. Areas Commun. 17(4), 613–630 (1999)
9. Huang, Y.-F.: Performance of adaptive multistage fuzzy-based partial parallel interference canceller for multi-carrier CDMA systems. IEICE Trans. Communications E88-B(1), 134–140 (2005)
10. Zadeh, L.A.: Fuzzy set. Inf. Control 8, 338–353 (1965)
11. Wang, L.-X., Mendel, J.M.: Fuzzy basis functions, universal approximation, and orthogonal least-square learning. IEEE Trans. Neural Network 3(5), 807–813 (1992)
12. Lin, C.-T., C.S.G., L.E.E.: Neural fuzzy systems: a neural-fuzzy synergism to intelligent systems. Prentice-Hall, Englewood Cliffs (1996)
13. Peterson, R.L., Ziemer, R.E., Borth, D.E.: Introduction to spread spectrum communications. Prentice-Hall, Englewood Cliffs (1995)
14. Proakis, J.G.: Digital communications, 4th edn. Prentice-Hall, Englewood Cliffs (2001)

Robust Multi-scale Full-Band Image Watermarking for Copyright Protection

Jung-Chun Liu, Chu-Hsing Lin, Li-Ching Kuo, and Jen-Chieh Chang

Department of Computer Science and Information Engineering
Tunghai University, 181 Section 3, Taichung-kang Road, Taichung, Taiwan
jcliu@thu.edu.tw, chlin@thu.edu.tw, ado@thu.edu.tw, g942817@thu.edu.tw

Abstract. With the exponential growth of digital materials in this age, the protection of Intellectual Property Right (IPR) becomes an important and urgent topic. In this paper, we propose a novel digital watermarking scheme based on the Singular Value Decomposition (SVD) method and the Distributed Discrete Wavelet Transformation (DDWT) method. Our scheme transforms original image data from the spatial domain into the frequency domain by using the multi-scale DDWT technique, and then applies the SVD technique by modifying singular values of two sub-bands with watermark data and the DDWT watermarking embedding process on the rest two sub-bands. Thus, watermark information is embedded into the four sub-bands of the last scale. We exploit both of the advantages of the DDWT method, which is robust against one kind of geometric attack, i.e. the cropping attack, and the SVD method, which is robust against other geometric attacks and non-geometric attacks. Experimental results show that the quality of the stego-image is superior and the embedded watermark has high resistance against a variety of common geometric and non-geometric attacks.

Keywords: Image processing, Singular value decomposition, Distributed discrete wavelet transformation, Digital watermark, Copyright protection, Image attack, Data hiding and recovery.

1 Introduction

With the exponential growth of digital materials in the information age, the protection of the Intellectual Property Right (IPR) becomes an important and urgent subject. We need some information technologies that could aid to digital incident investigation. In order to promote the protection of intellectual property right and the authentication of the legitimate owner, watermark information is embedded in digital multimedia materials.

Digital watermarking techniques have a wide range of applications, including copyright protection, tracking of illegal dissemination, copyright control and authentication, detection of tampering, and data hiding and recovery. In this paper, we propose a Multi-scale Full-Band Image Watermarking (FBIW) method which combines the Distributed Discrete Wavelet Transformation (DDWT) method [1]

H.G. Okuno and M. Ali (Eds.): IEA/AIE 2007, LNAI 4570, pp. 176–184, 2007.

with the Singular Value Decomposition (SVD) method [2]. We achieve the goals of data hiding and recovery, and robustness of the watermark against a variety of image attacks. We will demonstrate that our method is more robust than the DWT-SVD method [3]. Experimental results show that our multi-scale FBIW method has strong robustness against common geometric and non-geometric attacks.

This paper is organized as follows. In Section 2, the backgrounds of related technologies are described briefly. In Section 3, we will propose our multi-scale FBIW embedding and extraction schemes. Simulation results are shown in Section 4 and conclusions are made in Section 5.

2 Preliminaries

2.1 Distributed Discrete Wavelet Transformation

Due to the shortcoming of the Discrete Wavelet Transformation (DWT) method, which embeds watermark information in the LL sub-band and is very vulnerable to the cropping attack, Lin [1] proposed the Distributed Discrete Wavelet Transformation (DDWT) method to solve this problem. This method transforms image from spatial domain into frequency domain by using the multi-scale DDWT, and embeds watermark information in the frequency domain and then performs the inverse DDWT (IDDWT) to obtain the stego-image in the spatial domain.

The DDWT method distributes hidden watermark information in spatial coefficients. The purpose of distributing information is to handle malicious depredations of the center part of the image where the watermark information is located using the DWT method. Imperceptibility and distributed information are characteristics of DDWT watermarking so that it is very robust against the cropping attack. But the DDWT watermarking technology is not very robust against other geometric attacks such as rotation, scaling, transposition and non-geometric attacks such as sharpening, blurring, Gaussian noise.

The example of a 3-scale DDWT transform is shown in Fig. 1 and the example of an original image undergoing the 1-scale DDWT transform is illustrated in Fig. 2.

2.2 Singular Value Decomposition

Singular Value Decomposition (SVD) is based on the linear algebra technique and has various applications such as computing pseudo inverse of a matrix, multivariate analyses and solution of linear least-squares problems. It is also used in image compression [4]-[5], watermarking technologies [6], image-coding [7], noise estimation [8], etc.

A digital image $A \in R^{M \times N}$ of a size of $M \times N$, with $M \geq N$ and R is the real number, can be represented by A's SVD defined by

$$A = U \Sigma V^T \tag{1}$$

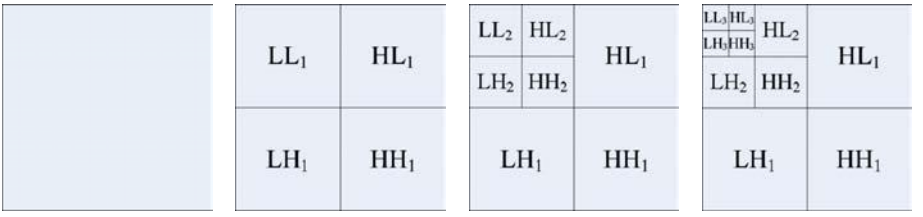

Fig. 1. (a) The original image (b) The result of 1-scale DDWT (c) The result of 2-scale DDWT (d) The result of 3-scale DDWT

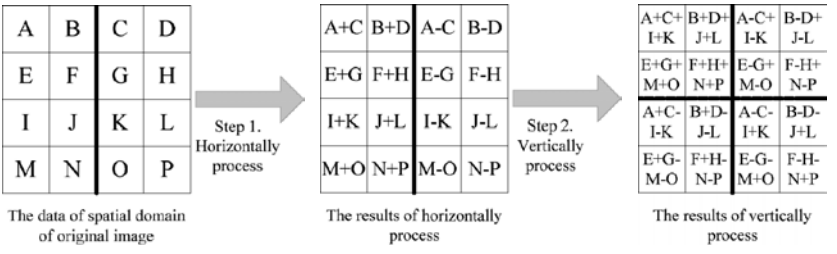

Fig. 2. Example of image performing 1-scale DDWT transform

Where $U_{M\times M}$ and $V_{N\times N}$ are orthogonal matrices and $\Sigma_{M\times N}$ is a matrix whose diagonal elements representing the singular values (σ_i) of A. The columns of the matrix U are called the *left singular vectors* (eigenvectors of AA^T) and the columns of matrix V are called the *right singular vectors* (eigenvectors of A^TA). The singular value decomposition operation is a useful tool that packs the maximum signal energy into as few coefficients as possible. In other words, SVD can use a few of information substituting for a large amount of data.

2.3 Ganic and Eskicioglus DWT-SVD Watermarking Scheme

Discrete Wavelet Transformation is commonly used in recent digital watermarking schemes. Ganic and Eskicioglu [3] proposed a DWT-SVD method to promote the function of the DWT method against image attacks. The DWT-SVD method transformed original image data from the spatial domain into the frequency domain by using the 1-scale DWT technique, and then applied the SVD method to embed watermark in four sub-bands of the 1-scale in the frequency domain. Four watermarks constructed from the four sub-bands were tabled and compared to evaluate robustness of their method against image attacks. Their experimental results showed that they had achieved the goal of watermarks robustness against many common attacks (except the cropping attack).

3 Proposed Scheme

The structure of our method includes the watermark embedding process and the watermark extracting process. For achieving protection of the legal owners rights and interests, we embed information by using a meaningful watermark. Our method belongs to invisible watermarking technique and will be described in detail in the following.

3.1 Watermark Embedding Process

Our digital watermark embedding process consists of 9 steps:

1) Input the original image $X(M \times M)$ and the watermark $W(N \times N)$;

2) Perform the K-scale DDWT (multi-scale DDWT) transform on X to obtain X', where K is the number of scale.
(Step **3** to Step **6** embedding the watermark in HL and LH sub-bands utilizing the SVD method)

3) Set initial values of the stego-image in the frequency domain Y' be the same as X', apply SVD to sub-bands HL and LH of the last scale:

$$(X')^{HL} = U_{X'}^{HL} \Sigma_{X'}^{HL} (V^T)_{X'}^{HL} \tag{2}$$

$$(X')^{LH} = U_{X'}^{LH} \Sigma_{X'}^{LH} (V^T)_{X'}^{LH} \tag{3}$$

Where $(X')^{HL}$ and $(X')^{LH}$ represent X' in sub-bands HL and LH, and the diagonal elements ($\sigma_{X'}^{HL}$ and $\sigma_{X'}^{LH}$) of $\Sigma_{X'}^{HL}$ and $\Sigma_{X'}^{LH}$ are the singular values on sub-bands HL and LH.

4) Apply SVD to the watermark: $W = U_W \Sigma_W (V^T)_W$, where the diagonal elements (σ_W) of Σ_W are the singular values of the watermark.

5) Process the singular values of X' in the frequency domain with the singular values of the watermark:

$$\sigma_{Y'}^{HL} = \sigma_{X'}^{HL} + \alpha \sigma_W \tag{4}$$

$$\sigma_{Y'}^{LH} = \sigma_{X'}^{LH} + \alpha \sigma_W \tag{5}$$

Where α is a scaling value, $\Sigma Y'$ is the singular matrix of Y' and $\sigma_{Y'}$is the singular values of $\Sigma Y'$.

6) Obtain $(Y')^{HL}$ and $(Y')^{LH}$ which has been embedded with watermarks on sub-bands HL and LH:

$$(Y')^{HL} = U_{X'}^{HL} \Sigma_{Y'}^{HL} (V^T)_{X'}^{HL} \tag{6}$$

$$(Y')^{LH} = U_{X'}^{LH} \Sigma_{Y'}^{LH} (V^T)_{X'}^{LH} \tag{7}$$

7) Take $(Y')^{HL}$ and $(Y')^{LH}$ of the last scale of Y' and perform inverse DDWT to obtain Y_{HLLH} in the spatial domain which has been embedded with watermarks in sub-bands HL and LH.
(Step **8** embedding the watermark in sub-bands LL and HH utilizing the DDWT method)

8) Take Y' data in the sub-bands LL and HH of the last scale and embed watermark information according to the following formula:

$$if\ W_{ij} = 0\ \ then\ (Y')_{ij}^{LL} = (Y')_{ij}^{LL} + \alpha(2^K)^2 \tag{8}$$

$$if\ W_{ij} = 1\ \ then\ (Y')_{ij}^{HH} = (Y')_{ij}^{HH} + \alpha(2^K)^2 \tag{9}$$

9) Apply inverse DDWT to Y' to produce the stego-image Y embedded with watermark information on the four sub-bands of the last scale. Subtract Y_{HLLH} from Y to obtain Y_{Diff}, which are the difference of pixel values in the spatial domain between Y_{HLLH} and Y.

3.2 Watermark Extracting Process

(Step **1** to Step **2** extracting the watermark from sub-bands LL and HH)

1) Input the stego-image Y, the original image X, the spatial domain data Y_{HLLH}, the spatial domain data Y_{Diff} and the watermark W.

2) Subtract Y_{HLLH} from Y to obtain Y_{LLHH}, and apply formula (10) on Y_{LLHH} to extract the embedded watermark W^{LLHH}:

$$W_{ij}^{LLHH} = \begin{cases} 0 & \text{if } Y_{LLHH} < 0, \\ 1 & \text{othrewise.} \end{cases} \tag{10}$$

(Step **3** to Step **6** extracting the watermark from sub-bands HL and LH)

3) Subtract Y_{Diff} from Y to obtain F, and then apply the multi-scale DDWT on F to obtain F'.

4) Apply SVD to F' on sub-bands HL and LH of the last scale:

$$(F')^{HL} = U_{F'}^{HL} \Sigma_{F'}^{HL} (V^T)_{F'}^{HL} \tag{11}$$

$$(F')^{LH} = U_{F'}^{LH} \Sigma_{F'}^{LH} (V^T)_{F'}^{LH} \tag{12}$$

Where $(F')^{HL}$ and $(F')^{LH}$ represent F' in the sub-bands HL and LH of the last scale, and the diagonal elements ($\sigma_{F'}^{HL}$ and $\sigma_{F'}^{LH}$) of $\Sigma_{F'}^{HL}$ and $\Sigma_{F'}^{LH}$ are the singular values of $(F')^{HL}$ and $(F')^{LH}$.

5) Extract the singular values of watermarks from $\Sigma_{F'}^{HL}$ and $\Sigma_{F'}^{LH}$:

$$\sigma_W^{HL} = \frac{\sigma_{F'}^{HL} - \sigma_{X'}^{HL}}{\alpha_i}, \quad \sigma_W^{LH} = \frac{\sigma_{F'}^{LH} - \sigma_{X'}^{LH}}{\alpha_i} \tag{13}$$

6) Obtain two watermarks embedded in sub-bands HL and LH:

$$W^{HL} = U_W^{HL} \Sigma_W^{HL} (V^T)_W \tag{14}$$

$$W^{LH} = U_W^{LH} \Sigma_W^{LH} (V^T)_W \tag{15}$$

4 Experimental Results

A variety of images have been tested in our experiment, but for the sake of space, we only show the results of the 512×512 full color image Lena (Figure 3(a)) and the 64×64 watermark "Tunghai University" (Figure 3(b)) under fifteen kinds of attacks: cropping (cropping on both sides, cropping 50%, cropping 75%, cropping 87%), contrast adjustment (adjustment −20, 40 and 80), rotation (rotate angle 20), Gamma correction, Gaussian noise, pixelate, sharpening, rescale, histogram equalization, and Gaussian blur. Table 1 shows parameters setting, attacked images and software used of all attacks on images embedded with watermarks using the FBIW and the DWT-SVD methods.

Table 1. Testing attacks, attacked images and software used

Attacks	Crop on both sides	Cropping 50%	Cropping 75%	Cropping 87%	Contrast −20
Parameters	Crop both sides 10% area	Crop 50% area	Crop 75% area	Crop 87% area	−20
Attacked Images					
Software	Photoshop	Photoshop	Photoshop	Photoshop	Photoshop
Attacks	Contrast 40	Contrast 80	Rotation	Gamma correction	Gaussian Noise
Parameters	40	80	Rotate 20°	0.6	0.3
Attacked Images					
Software	Photoshop	Photoshop	Photoshop	Xnview	Xnview
Attacks	Pixelate	Sharpen	Rescale	Histogram equalization	Gaussian Blur
Parameters	Mosaic 2	80	512 → 256 → 512	Auto-level	5 × 5
Attacked Images					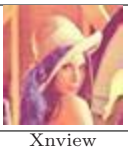
Software	Photoshop	Photoshop	Photoshop	Photoshop	Xnview

Figure 3(c) to Figure 3(f) shows the stego-image Lena and the extracted watermark from sub-bands LL and HH, HL and LH, respectively. In experiments with the DWT-SVD method, the original image has the same size as the one used in experiments with the FBIW method, but the size of the watermark is 256×256 since the size of the watermark used by the DWT-SVD method, which embeds watermark using the 1-scale DWT, is one half of the original image.

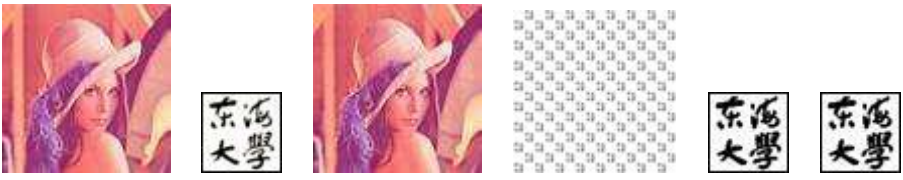

(a) (b) (c) (d) (e) (f)

Fig. 3. (a) The original image Lena (b) The watermark (c) The stego-image Lena (PSNR=45.459) (d) The extracted watermark from sub-bands LL and HH (e) The extracted watermark from the sub-band HL (f) The extracted watermark from the sub-band LH

Pearson's Correlation Coefficient is used for measurement of correlation between the original watermark (W) and the extracted watermark (W'). We use the formula defined below:

$$Corr(W, W') = \frac{\sum_{i=0}^{n-1}\sum_{j=0}^{n-1}(W_{(i,j)} - \overline{W})(W'_{(i,j)} - \overline{W}')}{\sqrt{\sum_{i=0}^{n-1}\sum_{j=0}^{n-1}(W_{(i,j)} - \overline{W})^2}\sqrt{\sum_{i=0}^{n-1}\sum_{j=0}^{n-1}(W'_{(i,j)} - \overline{W}')^2}} \tag{16}$$

Table 2 shows extracted watermarks of the DWT-SVD-based method and the FBIW-based method together with the value of the Pearson's correlation coefficient, which is the number under each extracted watermark. The FBIW method extracts three watermarks from sub-bands LL and HH, sub-band HL and sub-band LH. Considering that we can always choose the best one from all the extracted watermarks to claim ownership, we compare the FBIW method with the DWT-SVD method by using the best extracted watermark from both methods in this table.

Our experimental results show that the FBIW method is more robust than the DWT-SVD method against the following attacks: cropping (cropping on both sides, cropping 50%, cropping 75%, cropping 87%), contrast adjustment (adjustment -20, 40 and 80), rotation, and Gamma correction. Experimental results of Gaussian blur, Gaussian noise, pixelate, sharpen, rescale and histogram equalization show that the FBIW method is as robust as the DWT-SVD method, but for the sake of space they are not shown here.

Results of our experiment show that the FBIW method is as robust as or more robust than the DWT-SVD method against attacks. Under cropping attacks our scheme is robust by exploiting the advantage of the DDWT watermarking technique, which distributes watermark information in the spatial domain and is more robust against the cropping attack than the SVD method and DWT-SVD method. And by exploiting the advantage of the SVD watermark technique, under attacks of Gamma correction, Gaussian noise, pixelate, sharpen, rescaling and histogram equalization our method is as robust as or more robust than the

Table 2. Extracted watermarks with Pearson's correlation coefficient values

Attacks	FBIW	DWT-SVD	Attacks	FBIW	DWT-SVD	Attacks	FBIW	DWT-SVD
Crop on both sides			**Cropping 50%**			**Cropping 75%**		
$Corr(W, W')$	0.996	0.893	$Corr(W, W')$	0.996	−0.024	$Corr(W, W')$	0.996	−0.499
Sub-band	LL&HH	HH	Sub-band	LL&HH	HL	Sub-band	LL&HH	LH
Cropping 87%	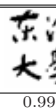	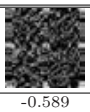	**Contrast −20**			**Contrast 40**		
$Corr(W, W')$	0.996	-0.589	$Corr(W, W')$	0.967	0.834	$Corr(W, W')$	0.988	0.970
Sub-band	LL&HH	HL	Sub-band	HL	HH	Sub-band	HL	HH
Contrast 80		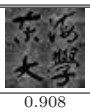	**Rotate** 20°			**Gamma correction**		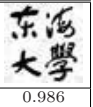
$Corr(W, W')$	0.985	0.908	$Corr(W, W')$	0.992	0.905	$Corr(W, W')$	0.991	0.986
Sub-band	LH	HH	Sub-band	HL	LH	Sub-band	LH	HH

DWT-SVD method. Therefore, our proposed scheme shows robustness against both geometric attacks and non-geometric attacks.

5 Conclusions

The DWT-SVD method, which combines the SVD technique with the DWT method, is more robust than the DWT-based method. But the DWT-SVD method also retains the drawback of the SVD method so that it is not robust against cropping attacks. In order to satisfy the security requirement for copyright protection, we propose a multi-scale Full-Band Image Watermarking scheme by combining both of the DDWT-based and the SVD-based techniques. We exploit both of the advantages of the DDWT method, which is robust against cropping attacks, and the SVD method, which is robust against geometric attacks such as rotation and scaling and non-geometric attacks such as Gaussian noise, sharpening, and contrast adjustment. Our experimental results show that the multi-scale Full-Band Image Watermarking scheme is more robust than the DWT-SVD method.

Acknowledgments. This research is partially supported by the National Science Council, Taiwan, Contract Number: NSC95-2221-E029-019, NSC95-2221-E029-020-MY3.

References

1. Lin, C.H., Jen, J.S., Kuo, L.C.: Distributed discrete wavelet transformation for copyright protection. In: The 7th International Workshop on Image Analysis for Multimedia Interactive Services, Incheon, Korea, April 19-21, pp. 53–56 (2006)

2. Chandra, D.V.S.: Digital image watermarking using singular value decomposition. In: The 45th Midwest Symposium on Circuits and Systems (MWSCAS 2002), vol. 3, pp. III-264–III-267. Tulsa, Oklahoma, USA (August 2002)
3. Ganic, E., Eskicioglu, A.M.: Robust DWT-SVD domain image watermarking: embedding data in all frequencies. In: The ACM Multimedia and Security Workshop, Magdeburg, Germany, September 20-21, pp. 166–174 (2004)
4. Inoue, K., Urahama, K.: DSVD: A tensor-based image compression and recognition method. In: The IEEE International Symposium on Circuits and Systems (ISCAS 2005), vol. 6, pp. 6308–6311. Kobe, Japan (May 23-26, 2005)
5. Tian, M.S., Luo, W., Liao, L.Z.: An investigation into using singular value decomposition as a method of image compression. In: Yeung, D.S., Liu, Z.-Q., Wang, X.-Z., Yan, H. (eds.) ICMLC 2005. LNCS (LNAI), vol. 3930, pp. 5200–5204. Springer, Heidelberg (2006)
6. Ma, L., Li, C., Song, S.: Digital watermarking of spectral images using SVD in PCA-transform domain. In: The IEEE International Symposium on Communications and Information Technology (ISCIT 2005), vol. 2, pp. 1489–1492. Beijing, China (October 12-14, 2005)
7. Ochoa, H., Rao, K.: A hybird DWT-SVD image-coding system (HDWTSVD) for monochromatic images. In: The IS&T/SPIE, Vol. 5022, pp. 1056–1066. Santa Clara, California USA (January 20-24, 2003)
8. Konstantinides, K., Yovanof, G.S.: Application of SVD based spatial filtering to video sequences. In: The IEEE International Conference on Acoustics, Speech and Signal Processing, Vol. 4, pp. 2193–2196. Detroit, MI (May 9-12, 1995)

Perimeter Intercepted Length and Color t-Value as Features for Nature-Image Retrieval

Yung-Fu Chen[1], Meng-Hsiun Tsai[2], Chung-Chuan Cheng[3], Po-Chou Chan[4,⋆], and Yuan-Heng Zhong[5]

[1] Department of Health Services Management, China Medical University, 404 Taichung, Taiwan
yungfu@mail.cmu.edu.tw
[2] Department of Management of Information Systems and
[3] Department of Electrical Engineering, National Chung Hsing University, 402 Taichung, Taiwan
{mht,d956411}@nchu.edu.tw
[4] Department of Management of Information Systems, Central Taiwan University of Science and Technology, 406 Taichung, Taiwan
Tel.: 886-4-22391647 ext 7703; Fax: 886-4-22397919
bjjem@ctust.edu.tw
[5] Department of CSIE, Dayeh University, 515 Changhua, Taiwan
f9106313@mail.dyu.edu.tw

Abstract. This paper proposes a context-based image retrieval system based on color, area, and perimeter intercepted lengths of segmented objects in an image. It characterizes the shape of an object by its area and the intercepted lengths obtained by intercepting the object perimeter by eight lines with different orientations passing through the object center, and the object color by its mean and standard deviation (STD). Recently, we reported that the color-shape based method (CSBM) is better than conventional color histogram (CCH) and fuzzy color histogram (FCH) in retrieving computer-generated images. However, its performance is only fair in the retrieval of natural images. For CSBM, object color is treated as uniform by reducing the number of colors in an image to only 27 colors. In this paper, we improve the performance by representing the color features of an object with its mean and STD. During the image retrieval stage, t-value is calculated based on the color features of two images, one in the query and the other in the database. The result shows that the proposed method achieves better performance in retrieving natural images compared to CCH, FCH, and CSBM. In the future, the proposed technique will be applied for the retrieval of digitized museum artifacts.

1 Introduction

Context-based image retrieval has been studied for more than two decades, which generally works with features including color, texture, and shape [1]. Color

⋆ Corresponding author. This work was supported in part by Council for Culture Affair of Executive Yuan and Taichung City Cultural Affair under the grant of Local Folklore Museums from 2005 to 2006.

H.G. Okuno and M. Ali (Eds.): IEA/AIE 2007, LNAI 4570, pp. 185–194, 2007.

histogram is one of the most commonly adopted features for designing image retrieval systems [2]. The advantages of color histogram are simple in operation and easy for calculation. In order to improve the efficiency of the conventional color histogram (CCH), a fuzzy-based technique, namely fuzzy color histogram (FCH) [3], is proposed for color histogram construction. It considers the degree of color similarity for each pixel to be associated with all the histogram bins using fuzzy memberships calculated based on the fuzzy c-means (FCM) algorithm [4]. It is demonstrated to be more robust than the CCH in dealing with quantization errors and changes in light intensity. However, CCH and FCH can delineate only the global properties of an image. To overcome this drawback, a color-shape based method (CSBM) based on the colors, areas, and the perimeter intercepted lengths (PILs) has been proposed and demonstrated to be effective in discriminating shapes of the objects and are immune to translation and rotation variations [5]. However, CSBM only works well for computer generated images such as cartoons, trade mark, flags, traffic sign, and synthesized images, etc. Its retrieval performance is only fair for true color natural images. In this paper, we improve the performance for natural image retrieval by introducing a feature based on means and standard deviations (STDs) of two images, one in the query and the other in the database.

2 Related Works

Color histogram has been widely used as a feature for image retrieval [2]. It first classifies colors of the database images as K clusters, known as color bins, using k-mean algorithm [6], in which the representative of each cluster is obtained by calculating its centroid. Then, the color histogram of an image can be obtained by assigning each pixel to a color bin with smallest distance. By observing distribution of the color histograms, one can distinguish the similarity between two images. The measure of similarity between two images is defined as:

$$s = \sum_{j=1}^{K} \min(H_j(I), H_j(I')) \Big/ \sum_{j=1}^{K} H_j(I') \tag{1}$$

where $H_j(I)$ and $H_j(I')$ indicate the $j-$th bin of K color histograms for image I and I'. The advantages for using color histogram as a feature are that it is very simple in operation and easy in calculation. Additionally, it is immune to shift, rotation, and scaling operations [7-11]. Unfortunately, it has several accompanied drawbacks: (1) the feature can be determined only by the number of pixels in each color bin; (2) the number of color bins should be large enough to have better retrieval efficiency, which in turn needs more memory space and computation time; and (3) the feature only accounts for global rather than local characteristics in an image, hence it cannot be used for local image retrieval.

Since CCH considers neither color similarity across different bins nor color dissimilarity in the same bin, it is sensitive to noisy interference coming from illumination changes and quantization errors. This motivated Han and Ma [3] to develop a system based on the FCH which associates the color similarity of

each pixel to all the color bins through a fuzzy-set membership function. Given a color space containing n color bins, the FCH, $F(I) = [f_1, f_2, \ldots, f_n]$, of an image I can be defined as:

$$f_i = \sum_{j=1}^{N} \mu_{ij} P_j = \frac{1}{N} \sum_{j=1}^{N} \mu_{ij} \tag{2}$$

where N is the number of pixels in the image, P_j represents the probability of a pixel j selected from image I, and μ_{ij} $(0 \leqq \mu_{ij} \leqq 1)$ indicates the membership degree of the j-th pixel to the i-th color bin.

To speed up the computation, fine uniform quantization is performed in the RGB color space by mapping all the pixel colors into n' histogram bins that n' must be large enough to make the color difference between two adjacent bins significantly small. Then, the n' colors are transformed from RGB to CIELAB color space. Finally, it classifies the n' colors in the CIELAB space into n clusters using the FCM algorithm [4] with each represents an FCH bin.

During image retrieval, the FCH of a query image is extracted using the above approach, and then the system compares the FCH with the FCHs of all the database images. Dissimilarity between two images with FCHs represented as F_Q (query) and F_D (database), respectively, can be measured as:

$$d^2(F_Q, F_D) = [F_Q - F_D]^T [F_Q - F_D] \tag{3}$$

FCM classifies the n' fine colors into n coarse colors and calculates the membership matrix at the same time. The optimal solution is obtained by minimizing an objective function J_m, which is the weighted sum of squared errors within each group:

$$J_m(U, V; X) = \sum_{k=1}^{n} \sum_{i=1}^{c} \mu_{ik}^m \left\| x_k - v_i \right\|^2 \tag{4}$$

The algorithm stops when J_m is less then a given threshold ε. Here, $V=[v_1, v_1, \ldots, v_1,]^T$ represents a vector of unknown cluster prototypes, and the weighting exponent m controls the degree of membership shared by c clusters. The value of μ_{ik} indicates the degree of membership for a data point x_k in set $X = \{x_1, x_2, \ldots, x_n\}$ related to i-th cluster. The membership for a data point to any cluster can be delineated by a matrix $U = [\mu_{ik}]$, $\mu_{ik} \in [0, 1]$, satisfying the following constraints:

$$\sum_{k=1}^{n} \mu_{ik} = 1, \quad 1 \leq k \leq n \text{ and } x_i \in X \tag{5}$$

The drawbacks of FCH are that the features can only be used for accounting the global characteristics and it needs a lot of time for calculating the memberships. Recently, Color-Shape Based Method (CSBM)[5] was proposed to improve these shortcomings.

If the possible pixel colors in a color image, such as trademark, cartoon, flag, traffic sign, and synthesized images, are reduced to fewer colors, it usually turns into an image consisting of only several large regions that each one is made up of a set of pixels having the same color. Since it is very difficult to segment the objects contained in an image, this paper regards a region consisting pixels with identical color as an object. Two similar images generally contain several bigger

objects having similar colors and shapes. Figure 1(a) shows an image containing five objects, in which A and B are treated as different objects because of different shapes even with identical color. Objects A and C are also different because of distinctive colors although having the same shapes and sizes.

CSBM first classifies the pixels of images into K clusters using the k-mean clustering algorithm [6]. The mean value of each cluster is regarded as a representative color in a color palette, namely common color palette (CCP), for all images including the database and query images. For an image I, its color-reduced image I' containing only K colors is generated by replacing each pixel in I with a closest color found in CCP. Each object has its distinctive color, area, and shape. For an object O with an area greater than a threshold value Th_A, its features including color (mean and standard deviation), area, and shape are recorded; otherwise, it is treated as noise and is simply ignored. The PILs obtained by intercepting the perimeter of each object in an image by eight lines having different orientations passing through the object center was proposed as a shape feature, which has been demonstrated to be effective in discriminating shapes of objects and are immune to translation and rotation variation [5]. Although the CSBM outperforms CCH and FCH, it only works well for computer generated images [5]. The retrieval performance is degraded for true-color natural images. In this paper, we improve the CSBM performance by introducing the t-value as a distance measure between corresponding objects in a query image and a database image based on their color means and STDs.

3 Object Color t-Value Method (OCTM)

3.1 Feature Extraction and Image Matching

The PILs proposed by CSBM are adopted to delineate the shape of an object, while t-value used in statistical t-test is calculated based on the means and standard deviations of the colors of two related objects, as shown in Eq. (6):

$$t - value = \frac{\mu_1 - \mu_2}{\sqrt{\sigma_1^2/n_1 + \sigma_2^2/n_2}} \tag{6}$$

where (μ_1, σ_1) and (μ_2, σ_2) represent the color means and STDs of two related objects, respectively; n_1 and n_2 indicate the numbers of pixels for both objects. Smaller t-value indicates two objects are less different and, therefore, smaller distance in color. As shown in Fig. 1(b), a minimal bounding rectangle (MBR) with its sides parallel to X and Y axes is applied to enclose the object. The area is featured as the number of pixels within O, whereas the shape as a set of 8 PILs obtained by 8 lines passing through the central pixel of the MBR with different orientations intersecting the perimeter of object O. The orientations of these eight lines are separated by 22.5^o from 0 to 180^o. For object O, OCTM records its color, area, and PILs into a database. The difference between the PILs of two objects has been demonstrated to be a good indicator of shape variation [5]. As shown in Fig. 2, although the areas of all three objects are the same,

their shapes are greatly different. To achieve rotation invariance, two objects are compared in 8 different orientations and the smallest Euclidean distance is used as an indicator for shape differentiation.

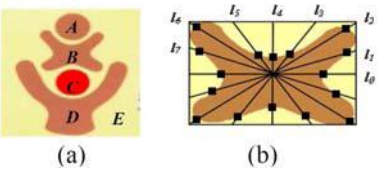

Fig. 1. (a) An image and (b) the 8 perimeter intercepts of object ***B*** bounded by an MBR

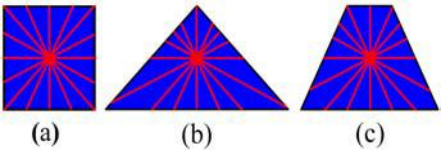

Fig. 2. Objects that have the same area but different shapes (PILs)

Let I be an image with the size of $H \times W$ pixels. To remedy the problem caused by scale variation, this paper normalizes the features by dividing each value of PILs by $(H + W)$ and the object area by $(H \times W)$, respectively. Let $O^q_{hi}(1 \leqq \ i \leqq n^q_h)$ and $O^d_{hj}(1 \leqq \ j \leqq n^d_h)$ be the objects with the $h-$th color in CCP obtained from I'_q and I'_d, color-reduced images of the query image I_q and database imageI_d, respectively. Also, n^q_h and n^d_h denote the total numbers of objects in I'_q and I'_d with h-th color in CCP. OCTM calculates the distance d_{ij} between objects O^q_{hi} and O^d_{hj} according to Eq. (7):

$$d_{ij} = d^L_{ij} + w \times d^T_{ij} \tag{7}$$

in which w is a weighted constant, whereas d^L_{ij} and d^T_{ij} are the distances for the PIL and t-value, respectively, between O^q_{hi} and O^d_{hj}. With PILs denoted as L^q=**{**l^q_0, l^q_1, **. . .** , l^q_7**}** and L^d=**{** l^d_0,l^d_1, **. . .** , l^d_7**}** for O^q_{hi} and O^d_{hj}, d^L_{ij} and d^T_{ij} in Eq. (7) can be calculated from the following equations with z as a given constant.

$$d^L_{ij} = \sqrt{\min_{r=0}^{7} \left(\sum\nolimits_{s=0}^{7} \left| l^q_s - l^d_{(r+s) \bmod 8} \right|^z \right)} \tag{8}$$

$$d^T_{ij} = \sqrt{\left(\frac{\quad}{\sqrt{(\quad)^2 \quad +(\quad)^2}}\right)^2 + \left(\frac{\quad}{\sqrt{(\quad)^2 \quad +(\quad)^2}}\right)^2 + \left(\frac{\quad}{\sqrt{(\quad)^2 \quad +(\quad)^2}}\right)^2} \tag{9}$$

The dynamic programming method, as described in **Algorithm OBJ_ Match( )**, was used to calculate the minimal matching distance between two sets of objects O^q_h and O^d_h, in which the objects were sorted by area in descending order**.** In the algorithm, a two-dimensional $n^q_h \times n^d_h$ matrix MMD^h is used to record the minimal matching distance between O^q_h and O^d_h. An element in the matrix is represented as $MMD^h(i, j)$ which indicates the minimal matching distance between any one object in $\{O^q_{h1}, O^q_{h2}, \ldots, O^q_{hi}\}$ and any one in $\{O^d_{h1}, O^d_{h2}, \ldots, O^d_{hj}\}$; therefore, the element $MMD^h(n^q_h, n^d_h)$denotes the final minimal matching distance between O^q_h andO^d_h.

Algorithm OBJ_Match( )

Input: O^q_{h1},O^q_{h2},..,O^q_{hn} and O^d_{h1},O^d_{h2},..,O^d_{hn}
Output:MMD^h

$MMD^h_{0,0}$ =0
for $i = 0$ to n^q_h
  $MMD^h_{i,0} = Penalty(O^q_{hi}) + MMD^h_{i-1,0}$
for $j = 0$ to n^d_h
  $MMD^h_{0,j} = Penalty(O^d_{hj}) + MMD^h_{0,j-1}$
for $i = 1$ to n^q_h
  for $j = 1$ to n^d_h
    $MMD^h_{i,j}$ =$min(MMD^h_{i-1,j}$+ $Penalty(O^q_{hi})$, $MMD^h_{i,j-1}$
      +$Penalty(O^d_{hj}), MMD^h_{i-1,j-1} + d_{i,j})$

For an object O_{hm} in either a query with $1 \le m \le n^q_h$ or a database image with $1 \le m \le n^d_h$ which does not have a corresponding matched object in its counterpart, a penalty is given according to the equation defined in Eq. (10).

$$Penalty(O) = \sqrt{\sum_{=0}^{7} (l\ )} + w \times \sqrt{(\frac{}{\sqrt{(\ \ )^2}})^2 + (\frac{}{\sqrt{(\ \ )^2}})^2 + (\frac{}{\sqrt{(\ \ )^2}})^2} \qquad (10)$$

Finally, the image matching distance $Dist$ between I_q and I_d is defined as:

$$Dist = \sum_{h=1}^{K} MMD^h(n^q_h, n^d_h) \qquad (11)$$

3.2 Experimental Images and System Evaluation

Two image sets, each consists of 429 true-color natural images, were used as the query and database, respectively. The database contains corresponding images with variations in rotation, distortion, noise, scaling, hue, luminance, and contrast from the query images. Table 1 demonstrates examples of query images and their corresponding images with geometry (rotation, scaling, spreading, distorsion, and translation), color (luminance, contrast, and hue), and noise variations.

In order to evaluate the system performance, average normalized modified retrieval rank ($ANMRR$), as shown in Eq. (12), proposed by MPEG-7 [12-13] was used as a benchmark. It not only reflects the recall rate and precision information of the retrieved images, but also shows the ranks of all the retrieved images.

$$ANMRR = \sum_{q=1}^{Q} (\frac{MRR(q)}{T + 0.5 - 0.5 \times I(q)})/Q \qquad (12)$$

where

$$MRR(q) = AVR(q) - 0.5 - NG(q)/2 \qquad (13a)$$

$$AVR(q) = \sum_{t=1}^{I(q)} R'(t)/I(q) \qquad (13b)$$

Table 1. Examples of query images and their corresponding ground truth images with different variations

	Trans. & Rot.	Lumin.	Contrast	Distort. & Scaling	Spreading	Hue	Noise
Query					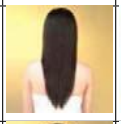		
Database							

In Eq. (13), T is Min$\{4\times I(q), 2\times GTM\}$ with GTM defined as Max$\{I(q)\}$ representing the maximum number of individual ground truth images among all the query images; $I(q)$ indicates the number of returned images which are most similar to the query image$q$; Q indicates the total number of queries under evaluation; $R'(t)$ represents the rank of a returned image and is defined as:

$$R'(t) = \begin{cases} R(t), & \text{if } R(t) \leq T \\ T+1, & \text{if } R(t) > T \end{cases} \tag{14}$$

Notice that smaller $ANMRR$ value indicates better retrieval performance.

Additionally, average match percentile (AMP) which is a standard measure used in the color indexing literature [2], as defined in Eq. (15), was also applied for evaluation of retrieval performance.

$$AMP = \frac{I(q) - R(t)}{I(q) - 1} \tag{15}$$

4 Experimental Results and Discussions

Table 2 lists the retrieval performance of the OCTM for different values of w with z, K, and Th_A are fixed to 0.4, 27, and 5, respectively. As shown in this table, w=1 achieves the best retrieval performance ($ANMRR$=0.17715). For larger w, the performance is degraded indicating that the color is over emphasized and the shape is depreciated. On the other hand, if w is too small, the retrieval performance is decreased as well. According to the examples shown in Table 3, for larger w (e.g. w=3) the ground truth images are ranked outside No. 2, that is R'(t)=3, which indicates the images been retrieved are mostly similar in color and less in shape.

Table 4 demonstrates the influence of z for the OCTM. The larger the z value, the greater the shape feature (PIL) will be emphasized. In this case, the system will retrieve the images with great similarity in shape while color

Table 2. Effect of $\boldsymbol{w}$ on retrieval performance for OCTM with z=0.4, K=27, and Th_A=5

w	$R'(t)=1$	$R'(t)=2$	$AMP(\%)$	$ANMRR$
0.5	247	310	98.99	0.35081
0.8	247	316	99.03	0.34382
1	**327**	**379**	**99.60**	**0.17715**
2	327	378	99.61	0.17832
3	323	377	99.61	0.18414

Table 3. Larger value of w (e.g. w=3) causes the retrieved images to have great similarity in color rather than in shape. Notice that the ground true images are ranked outside No. 2 with $R'(t)$=3 in these examples.

Query No.	*Query*	*R'(t)=1*	*R'(t)=2*	*R'(t)=3*
No. 147				
No. 384				

Table 4. Effect of z on retrieval performance of OCTM with w has been fixed to 1

z	$R'(t)=1$	$R'(t)=2$	$AMP(\%)$	$ANMRR$
0.1	319	380	99.68	0.18532
0.3	324	379	99.67	0.18065
0.4	**327**	**378**	**99.61**	**0.17832**
0.6	308	364	99.58	0.21678
0.8	297	356	99.51	0.23892

Table 5. Larger value of z (z=0.6) causes the retrieved images to have great similarity in shape while color is depreciated. The ground true images are ranked outside No. 2 in these examples.

Query No.	*Query*	*R'(t)=1*	*R'(t)=2*	*R'(t)=3*
No. 189				
No. 372				

feature is depreciated, as shown in Table 5. On the other hand, smaller z tends to depreciate the shape feature which has the same effect as larger w, as the retrieval results shown in Table 3.

The performances among OCTM, CSBM, FCH, and CCH, are compared in Table 6, in which AMP indicates average matching percentile. For best performance, the parameters, w, z, K and Th_A, were set to 1, 0.4, 27 and 5, respectively, for both OCTM and CSBM. In this study, since there is only one ground truth for each query image, hence the value of T used for calculating $ANMRR$, as shown in Eq. (7), has been set to 2. By comparing the performance between OCTM and CSBM, it can be found that OCTM ($ANMRR$=0.17715) outperforms the CSBM ($ANMRR$=0.18765) under the parameters setting. The number of retrieved images with rank $R'(t)$=1 and $R'(t)$=2 are 327 and 379 for OCTM and 322 and 375 for CSBM, respectively. Notice that both OCTM and CSBM are better than FCH and CCH, except the case with Th_A=20. The results show that the performance of OCTM is better than CSBM, which indicates that the color feature compared using t-value has great improvement in retrieval performance.

Table 6. Comparisons of retrieval performances among 4 methods

Method	***K***	***Th_A***	***R'(t)=1***	***R'(t)=2***	***AMP(%)***	***ANMRR***
OCTM	16	5	296	358	99.54	0.23776
		10	273	347	99.45	0.27739
		20	253	316	99.22	0.33683
	27	**5**	**327**	**379**	**99.60**	**0.17715**
		10	310	360	99.53	0.21911
		20	284	333	99.22	0.28089
CSBM	16	5	284	355	99.43	0.25525
		10	269	336	99.34	0.29487
		20	240	296	98.82	0.37529
	27	**5**	**322**	**375**	**99.59**	**0.18765**
		10	298	349	99.39	0.24592
		20	265	312	98.97	0.32751
FCH	N/A		268	330	97.45	0.30303
CCH	N/A		145	197	96.55	0.60140

5 Conclusion

In CSBM, the color is treated as uniform by reducing the number of colors of an image to only 27 colors while OCTM characterize the color of an object as mean and STD. The PILs of an object can be used to effectively characterize the shape of the object, while the color mean and STD of an object in an image are good indicators for representing the color feature of an object. As shown in the previous investigation [5], although CSBM is more robust in resisting geometric, luminance, distortion, and hue variations than the FCH and CCH in computer generated images, it is not very suitable for the retrieval of the true-color natural images. In this paper, we improve the performance of CSBM by representing

the color feature with means and STD of the color in an object. During the image retrieval stage, t-value is calculated based on the color means and STDs of two images, one in the query and the other in the database. In conclusion, the experimental results show that the proposed method (OCTM) achieves better performance than FCH, CCH, and CSBM in retrieving natural images.

Since the color patterns of the digitized artifacts are generally more complicated than the computer-generated images while they are less complicated than the nature images, the proposed technique will be expected to have great efficiency in the retrieval of digitized museum and folklore artifacts [14,15].

References

1. Smeulders, A.W.M., Worring, M., Santini, S., Gupta, A., Jain, R.: Content-Based Image Retrieval at the End of the Early Years. IEEE Trans. Pattern Anal. Mach. Intell. 22, 1349–1380 (2000)
2. Swain, M.J., Ballard, D.H.: Color Indexing. Int. J. Comp. Vis. 7, 11–32 (1991)
3. Han, J., Ma, K.K.: Fuzzy Color Histogram and Its Use in Color Image Retrieval. IEEE Trans. Image Proc. 11, 944–952 (2002)
4. Sintas, A.F., Cadenas, J.M., Martin, F.: Membership Functions in the Fuzzy C-Means Algorithm. Fuzzy Sets and Systems 101, 49–58 (1999)
5. Hong, K.L., Chen, Y.F., Chan, Y.K., Cheng, C.C.: An Image Retrieval System Based on Colors and Shapes of Objects. In: Yang, Q., Webb, G. (eds.) PRICAI 2006. LNCS (LNAI), vol. 4099, pp. 1094–1098. Springer, Heidelberg (2006)
6. Su, M.C., Chou, C.H.: A Modified Version of the K-means Algorithm with a Distance Based on Cluster Symmetry. IEEE Trans. Pattern Anal. Mach. Intell. 23, 674–680 (2001)
7. Brunelli, R., Mich, O.: Histograms Analysis for Image Retrieval. Pattern Recognition 34, 1625–1637 (2001)
8. Chan, T., Chen, L.H.: Fast Mapping Algorithm for Histogram to Binary Set Conversion. Pat. Recog. Let. 21, 899–906 (2000)
9. Gevers, T.: Robust Histogram Construction from Color Invariants. In: The 8th IEEE International Conference on Computer Vision, vol. 1, pp. 615–620 (2001)
10. Guillamet, D., Vitria, J.: A Comparison of Global Versus Local Color Histograms for Object Recognition. In: The 15th International Conference on Pattern Recognition, vol. 2, pp. 422–425 (2000)
11. Hafner, J.: Efficient Color Histogram Indexing for Quadratic Form Distance Functions. IEEE Trans. Pattern Anal. Mach. Intell. 17, 729–736 (1996)
12. Manjunath, B.S., Ohm, J.R., Vasudevan, V.V., Yamada, A.: Color and Texture Descriptors. IEEE Trans. Cir. and Sys. for Video Technology 11, 703–715 (2001)
13. Vasudevan, V.V., Manjunath, B.S.: Report on AHG of Color and Texture. ISO/IEC/JTC1/SC29/WG11, Doc. M5560, Maui, p. 332 (December 1999)
14. Chan, P.C., Chen, Y.F., Huang, K.H., Lin, H.H.: Digital Content Development of Taiwanese Folklore Artifacts. In: Fox, E.A., Neuhold, E.J., Premsmit, P., Wuwongse, V. (eds.) ICADL 2005. LNCS, vol. 3815, pp. 90–99. Springer, Heidelberg (2005)
15. Chen, Y.F., Chan, P.C., Huang, K.H., Lin, H.H.: A Digital Library for Preservation of Folklore Crafts, Skills, and Rituals and Its Role in Folklore Education. In: Sugimoto, S., Hunter, J., Rauber, A., Morishima, A. (eds.) ICADL 2006. LNCS, vol. 4312, pp. 32–41. Springer, Heidelberg (2006)

Selecting an Appropriate Segmentation Method Automatically Using ANN Classifier

Yih-Chih Chiou and Meng-Ru Tsai

Institute of Mechanical and Aerospace Engineering, Chung Hua University, Hsinchu, Taiwan, 30012, R.O.C.
chiou@chu.edu.tw

Abstract. In general, we can easily determine the manufacturing step that does not function properly by referring to the flaw type. However, a successful segmentation of flaws is the prerequisite for the success of the subsequent flaw classification. It is worth noticing that, different segmentation methods are needed for different types of images. In the study, a mechanism that is capable of choosing a proper segmentation method automatically has been proposed. The mechanism employed artificial neural networks to select a suitable segmentation method from three methods, i.e., Otsu, HV standard deviation, and Gradient Otsu. The selection is based on the four features extracted from an image including standard deviation of background image, variance coefficient, the ratio of the width to height of both foreground and background histograms. The results show the success of the proposed mechanism. The high segmentation rate reflects the fact that the four carefully selected features are adequate.

Keywords: Segmentation, Feature Extraction, Flaw Detection, Flaw Classification, BPN Network.

1 Introduction

Flaw detection is an important procedure in the quality assurance of products. In general, by referring to the defect type, we can easily determine the manufacturing step that does not function properly. Hence, the ultimate goal of flaw classification is to identify each flaw type such that the sources of flaws can be identified and the manufacturing parameters can be adjusted accordingly. However, a successful segmentation is the prerequisite for the success of the subsequent flaw detection and classification. Segmentation is a process to separate desired flaws from background. Thresholding is the most commonly used flaw detection method [1], [2], [3], [4], [5]. Several researchers [3], [6], [7], [8], [9] have suggested the use of image gradient to detect flaws. On the other hand, a number of authors have applied standard deviation [9], [10], [11] to discover flaws. It is worth noting that most segmentation methods are sensitive to noise, illumination variance, object shape and size, grayscale variance of foreground and background, etc. In addition, different types of flaws need different segmentation methods.

H.G. Okuno and M. Ali (Eds.): IEA/AIE 2007, LNAI 4570, pp. 195–206, 2007.

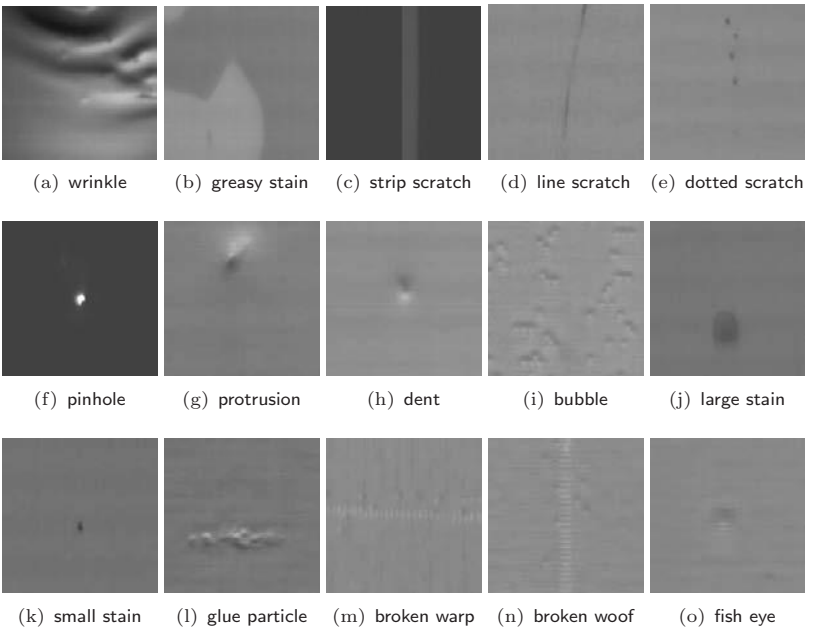

Fig. 1. Sample images of the fifteen types of flaws

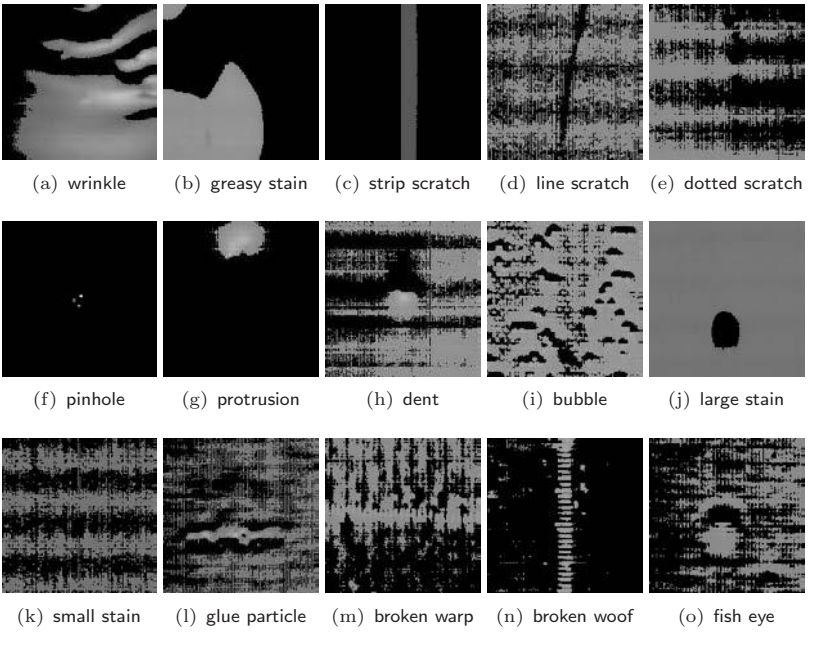

Fig. 2. Segmentation results of the fifteen types of flaws as shown in Fig. 1 using Otsu's method. It is evident that Otsu method is good for wrinkles, greasy stains, strip scratches, and large stain, but it is not suitable for segmenting other flaw types.

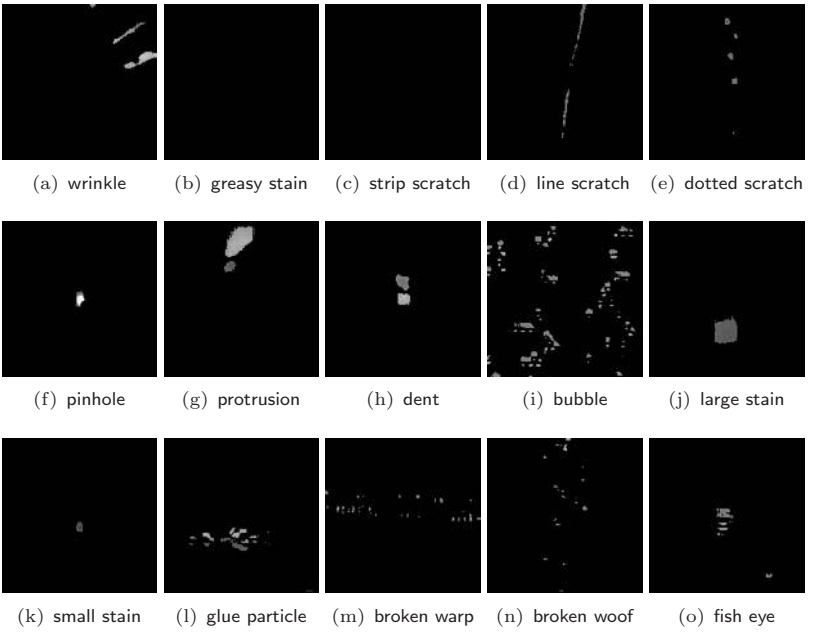

Fig. 3. Segmentation results of the fifteen types of flaws as shown in Fig. 1 using HVStd method. It is evident that HVStd is good for some flaw types, but quite bad for others.

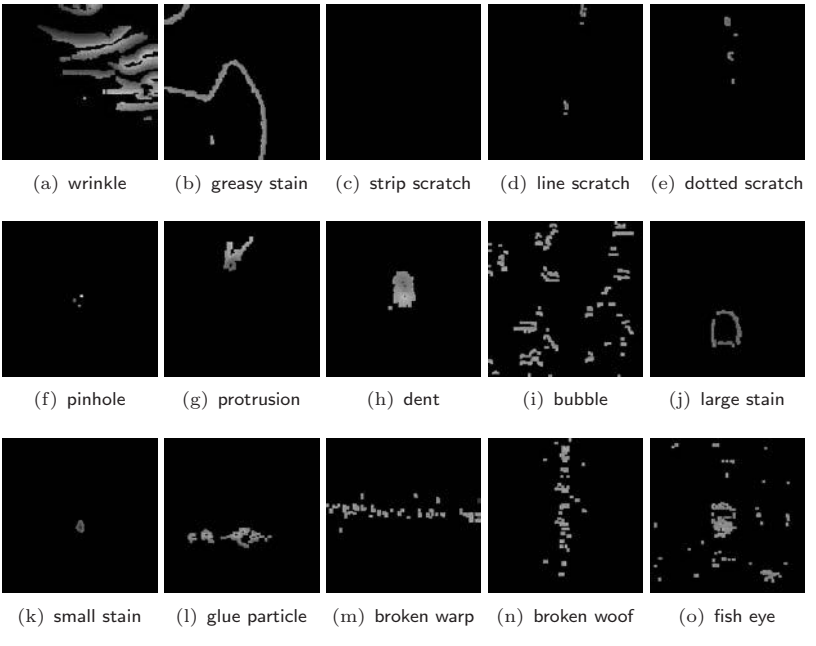

Fig. 4. Segmentation results using GradOtsu method. It is clear the method is suitable for segmenting wrinkle and small defects. For large defects, only their profiles are shown.

Figure 1 shows 15 types of flaws to be segmented and classified. As shown since these images were collected at different time and from different production lines of paper and plastics manufacturing industries, they differ greatly; some are brighter, some are darker, and some have textured background. Besides, flaws differ greatly in size, shape, and quantity. Strictly speaking, satisfactory results are unobtainable if one segmentation method is applied to all types of images. For example, Fig. 2 shows the segmentation results using Otsu's method [12]. It is apparent that some results are good while others are unacceptable. Similar results (Figs. 3 and 4) were observed when Horizontal and Vertical Standard Deviation (HVStd) method or Gradient Otsu method (GradOtsu) were applied. The two segmentation methods developed in the research will be described in detail in Sect. 2.2. The results suggest that if an inadequate method is applied, the desired flaws might not even present in the result image. As a result, misclassification of flaws occurs. In other words, attempting to use one single segmentation method to process all types of flaws is impractical. In view of that, the object of the study was to develop a mechanism that is capable of selecting a suitable segmentation method automatically.

2 Methodology Overview

It is evident that it is not possible to obtain acceptable results for all types of images by using one particular segmentation method. A better approach would be to select an appropriate segmentation method for each image type. Nevertheless, the selection should be automatic. Thus, it is desirable to develop a mechanism that is capable of selecting an appropriate segmentation method automatically. In the study, 1697 sample images of size 152×152 were used. All samples contain at least one flaw. To achieve the aforementioned objective, each sample was segmented using Otsu, HVStd, and GradOtsu sequentially. Then, by visual inspection of the three segmentation results, each sample was assigned to one of the three groups according to which method derived the best segmentation result. It is worth noting that for some samples two methods derived equally well segmentation results. If this is the case, we randomly assigned them to either group. Nevertheless, the random assignment might affect the final segmentation rate.

The proposed mechanism starts with the segmentation of the input image using HVStd method. The segmentation results in two images, i.e., flaw image and background image. A flaw image is referred to as the image containing only pixels that are regarded as abnormal while a background image is referred to as the image containing pixels other than abnormal pixels. The next step is to extract features from the images. As to which feature is useful in discriminating one group from another, we used the extracted features to construct scatter diagrams. By examining the distributions of the three groups, whether a feature is suitable for classification was learned. After that, an artificial neural network using backpropagation learning algorithm [13] (hereafter we called the kind of network BPN network) was established. Finally, a segmentation method chosen by the BPN network was used to segment the input image so as to discover flaws.

2.1 Segmentation Methods

In this study, three segmentation methods, including Otsu, HVStd, and GradOtsu, were used to segment images. Aside from Otsu method, the other two methods are described in detail as follows:

(1) HVStd: The method first calculates grayscale means and standard deviations for each row and column and then uses the derived information to generate a threshold value for segmentation. Let I_O be an original image, $I_O(i,j)$ be the grayscale value of the pixel located at column i and row j. The grayscale mean for each column and row are given by

$$\mu_{col}(i) = \frac{1}{H}\sum_{j=0}^{H} I_O(i,j);\ for\ i = 1, W \tag{1}$$

$$\mu_{row}(j) = \frac{1}{W}\sum_{i=0}^{W} I_O(i,j);\ for\ j = 1, H \tag{2}$$

where W and H are the width and height of the image. After that, (3) and (4) are used to calculate standard deviations for each column $\sigma_{col}(i)$ and each row $\sigma_{row}(j)$.

$$\sigma_{col}(i) = \sqrt{\frac{1}{H}\sum_{j=0}^{H}(I_O(i,j) - \mu_{col}(i))}\ \ ;\ for\ i = 1, W \tag{3}$$

$$\sigma_{row}(j) = \sqrt{\frac{1}{W}\sum_{i=0}^{W}(I_O(i,j) - \mu_{row}(j))};\ for\ j = 1, H \tag{4}$$

Let δ_{row} and δ_{col} be deviations of rows and columns, respectively. We have

$$\delta_{col}(i,j) = |I_o(i,j) - \mu_{col}(i)|\ ;\ for\ i = 1, W \tag{5}$$

$$\delta_{row}(i,j) = |I_o(i,j) - \mu_{row}(j)|\ ;\ for\ j = 1, H. \tag{6}$$

Finally, we can use the following equation to derive the resulting image, I_R.

$$I_R(i,j) = \begin{cases} I_O(i,j),\ if\ |\delta_{col}(i,j) - \sigma_{col}(i)| > T_{std}\ and \\ \qquad |\delta_{row}(i,j) - \sigma_{row}(j)| > T_{std} \\ 0,\ otherwise \end{cases}. \tag{7}$$

The pre-selected value T_{std}, is determined to be 5.0 after a rigorous test of images at hand.

(2) GradOtsu: Different from Otsu's method, which segment an image directly, the method first calculate the image's gradient and then uses Otsu's method to segment the gradient image in order to reveal flaws. The method was developed specifically for extracting defects from wrinkles corrugated type surfaces. First of all, we use Sobel's edge detector to derive each point's gradient and generate

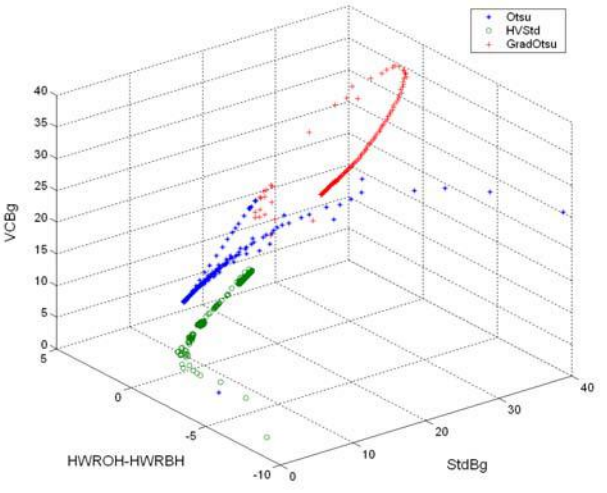

Fig. 5. Scatter diagram of the three segmentation methods. It is clear that the three groups of images are well separated.

a gradient image I_G. In general, pixels with high gradient can be regarded as defects. Therefore, gradient image, I_G, is segmented subsequently using Otsu's method to obtain a binary image, I_B. After segmented using Otsu, the resulting binary image, I_B, denotes a defect map of the input image.

2.2 Features for Network Training

To enable the proposed mechanism to select a suitable segmentation method automatically, we need to realize that why one segmentation method produces better result than that produced by others. Hence, we extracted several features from images. After a rigorously check, we decided to use the following four features, i.e., standard deviation of background (StdBg), variance coefficient of background (VCBg), the ratio of height to width of the histogram of the original image (HWROH), and the ratio of height to width of the histogram of the background image (HWRBH). The reasons for choosing the four features are due to their ability to distinguish one image group from another. Referring to the scatter diagram shown in Fig. 5, the three groups are well separated if the four features are used to construct the plot. Definitions of the four features are depicted as follows.

(1) StdBg: StdBg is the abbreviation of Standard Deviation of Background image. Standard deviation is commonly used in statistics to measure how spread out the values in a data set is. *StdBg* is defined as

$$StdBg = \sqrt{\frac{\sum\sum (f_{bg}(i,j) - \mu_{bg})^2}{N_{bg}}}, \tag{8}$$

where $f_{bg}(i,j)$ denotes the grey level of the pixel located at column i and row j of the background image, μ_{bg} is the grayscale mean of the background image, $N_{bg}$is the count of background pixels. Here, *StdBg* was used primarily to check the uniformity of the background image. If grayscale values of the background pixels are all close to their grayscale mean, then the standard deviation is low.

(2) VCBg: In a statistical sense, variance coefficient is defined as the ratio of standard deviation to grayscale mean. Since background image was used to calculate grayscale mean, μ_{bg}, and standard deviation, σ_{bg}, we called the ratio of σ_{bg} to μ_{bg} variance coefficient of background ($VCBg$), i.e.

$$VCBg = \sigma_{bg}/\mu_{bg}. \tag{9}$$

Statistically speaking $VCBg$ can be used to evaluate the degree of dispersion of background pixels' grayscales, too. The larger the number is, the more dispersed the grayscale values are.

(3) HWROH: The ratio of height to width of the histogram of the original image ($HWROH$) is another useful feature. We defined HWROH as

$$HWROH = \frac{H_{raw}/N_{raw}}{W_{raw}/256}, \tag{10}$$

where H_{raw} and W_{raw} are the height and width of the histogram of the original image, respectively, N_{raw} is the count of the pixels in the image. The height of a histogram is defined as the count of the bin with the maximum count of pixels. As to the width of a histogram, it is defined as the difference between the largest bin number and the smallest bin number with non-zero count. This feature is useful in measuring how complex an image is. In general, the larger the number is; the narrower the grayscale spreads. A small value of HWROH usually implies that there are several objects in the image.

(4) HWRBH: The ratio of height to width of the histogram of the background image ($HWRBH$) is a useful feature, too. We defined HWRBH as

$$HWRBH = \frac{H_{bg}/N_{bg}}{W_{bg}/256}, \tag{11}$$

where H_{bg} and W_{bg} are the height and width of the background histogram, respectively, N_{bg} is the count of the background pixels. We can obtain H_{bg} and W_{bg} in a similar manner. $HWRBH$ is useful in knowing the grayscale distribution of background pixels. The higher the value is, the narrower the grayscale spreads.

2.3 Flaw Segmentation Using BPN Networks

Unlike classification tree or other statistical methods, neural network approaches do not require exact knowledge of the statistical distribution of input items. A BPN network is the most popular among all the known ANNs. Hence, we employ

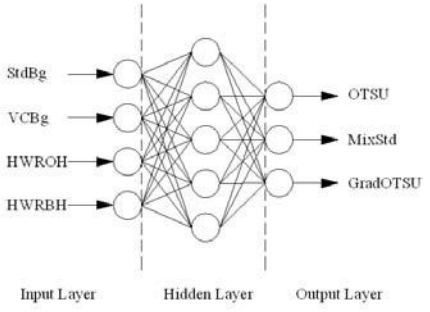

Fig. 6. The 4×5×3 network structure for selecting a segmentation method

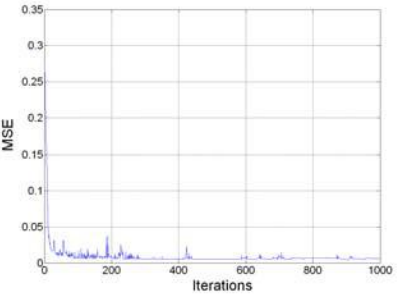

Fig. 7. The plot of mean squared errors vs. iterations (η=0.25; MSE=0.01)

a BPN network to select an appropriate segmentation method. Let T_i and O_i be the i^{th} desired and actual outputs, respectively, then the Mean Squared Error (MSE) between them can be determined by

$$MSE = \frac{1}{2}\sum_{i=1}^{n}(O_i - T_i)^2. \tag{12}$$

The back-propagation network uses the gradient steepest decent method to iteratively adjust the connection weights between two consecutive layers so as to minimize MSE between the actual output and the desired output. For example, the adjustment of the weights connecting the last hidden layer j and the output layer k is done as follow:

$$W_{jk}^{o} = W_{jk}^{o} + \eta\delta_k^o H_j, \tag{13}$$

where η is known as the learning rate, δ_k^orefers to the error signal at each node of the output layer k, and H_j refers to the output signal at each node of the hidden layer j. The adjustment is repeated until the MSE drops below a prespecified value. In general, if the samples contained in the training set are the representatives of the objects to be recognized later the classification results should be satisfactory.

As can be seen from Fig. 5, the three groups of images clustered at different locations. In view of that, a simple network structure can be expected. Figure 6 shows the ANN network for selecting a proper segmentation method. The input layer consists of four units, i.e., the four features extracted from the image to be classified, including *StdBg*, *VCBg*, *HWROH*, and *HWRBH*. The output layer consists of three units, i.e., the three segmentation methods to choose from, i.e., Otsu, HVStd, and GradOtsu. Before a BPN network can be effectively used to classify, it must be trained with sufficient number of samples. The samples are randomly divided into two sets. The training and testing sets consist of 929 and 768 samples, respectively. We first used the images in the training set to train the network. As shown in Fig. 7, the training using back-propagation algorithm

converges quickly. The recall process shows that only 4 samples were misclassified, i.e., the recall rate is 99.57%. To explore the ability of the trained network, we presented each sample in the testing set to the network one-by-one. At the recognition stage, the network is fed with the four features extracted from the inputted image and a proper method is chosen. The recognition rate is 99.61%. The high recall and recognition rates strongly imply that the selected features are extremely appropriate for discriminating one class of image from another.

3 Results and Discussions

For comparison, the same 15 images, as shown in Fig. 1, were segmented using the proposed mechanism and the results were shown in Fig. 8. In contrast with the segmentation results shown in Figs. 2-4, the results are satisfactory. The outcomes suggest that the proposed method perform well in selecting a suitable segmentation method automatically. In addition, the results indicate that the four carefully selected features, i.e. StdBg, VCBg, HWROH, and HWRBH, proved to be well suited for discriminate one group from another. To explore the capability of the proposed mechanism further, the images in the testing set were segmented and classified. The experimental results are listed in Table 1. With regard to the classification of the 15 types of flaws, we made use of BPN

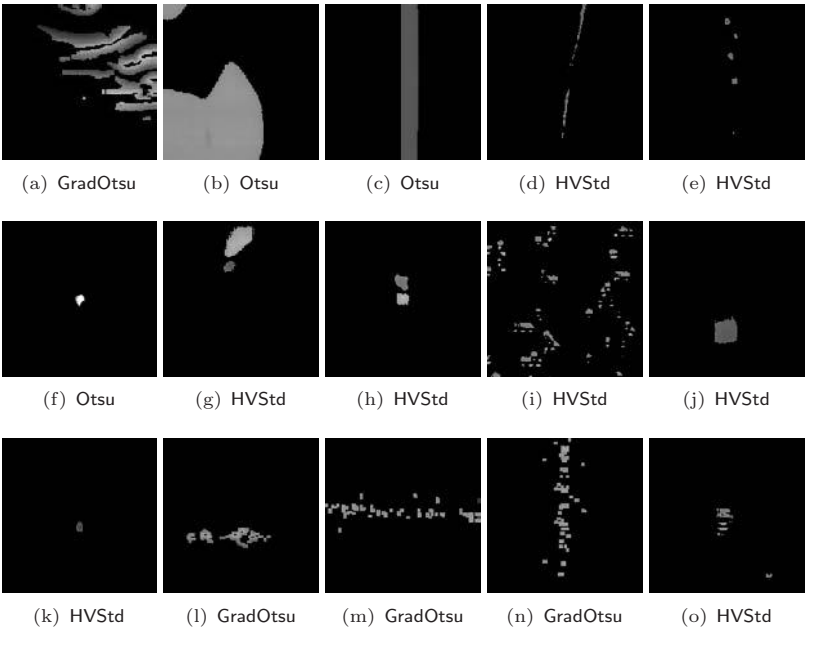

Fig. 8. Segmentation results of the 15 images shown in Fig. 1 using the proposed methodology. The method below each image indicates the method automatically selected.

network, too. The five-layer 10×10×15×10×15 network for flaw classification is composed of an input layer, three hidden layers, and one output layer. The input layer consists of 10 units, i.e., the 10 features extracted from the image to be classified. The output layer consists of 15 units, i.e., the 15 types of flaws to be categorized. The classification rate is 97.66%. Detailed classification results are listed in Table 1.

In the course of the experiment, we found that the sample images could be classified into three categories, i.e., images with point/line flaws, images with smooth surface, and images with corrugated surfaces, according to the types of flaws. The finding is important because the decision of which segmentation method should be used is closely related to this. In other words, although the selection of segmentation methods is done automatically, some facts can be observed as followings:

- HVStd is the most frequently selected method. It is suitable for segmenting images with point/line flaws, such as small stains and dotted scratches.
- GradOtsu is suitable for segmenting images with corrugated surfaces, such as wrinkles.
- Otsu method is most suitable for segmenting images with smooth surfaces, such as greasy stains, strip scratches, and large stains.
- For some types of flaws, different segmentation methods might derive similar well results. For examples, either HVStd or GradOtsu can be used to segment bubbles and small stains.

Table 1. Flaw detection and classification results of the samples in test set

Flaw Type	Samples	Misclass. samples	Classification Rate (%)	Method Chosen	Run-Time (ms)
Wrinkle	77	0	100.00	GradOtsu	34.1
Strip Scratch	12	1	91.67	Otsu	29.2
Greasy Stain	17	1	94.12	Otsu	45.5
Line Scratch	4	1	85.71	HVStd	24.6
Protrusion	7	1	85.71	HVStd	40.1
Dent	91	0	100.00	HVStd	17.3
Pinhole	5	0	100.00	Otsu	26.0
Large Stain	52	0	100.00	HVStd	18.9
Small Stain	160	3	98.12	HVStd	17.2
Dotted Scratch	16	3	81.25	HVStd	22.7
Bubbles	102	2	98.04	HVStd	18.3
Glue Particles	137	2	98.54	GradOtsu	31.9
Fish Eye	34	0	100.00	HVStd	31.1
Broken Warp	12	2	83.33	GradOtsu	29.9
Broken Woof	42	3	92.86	GradOtsu	31.3
Total	768	18	97.66		

Execution time is an important issue, too. HVStd is the default method for segmenting an incoming image; therefore, if it is selected for the subsequence segmentation, the image has no need to be segmented again. On the other hand, if other methods are chosen, the image will be re-segmented. Therefore, the run time depends on the segmentation method chosen. Besides, the run time is related to the flaw types. The average run time evaluated by a 1200MHz personal computer can be seen in Table 1.

4 Conclusion

In this paper, we have proposed a novel methodology for segmenting a variety of images. The main advantage of the proposed thresholding scheme is its ability to choose an appropriate method from the three segmentation methods automatically. The proposed method does not require establishing complicated classification tree; we use ANN classifiers for both image segmentation and flaw classification, instead. The automatic selection is according to the features extracted from the image to be segmented. The overall segmentation and classification rates of the 768 images in the test set are 99.69% and 97.66%, respectively. The experimental results show the effectiveness of the selected features for classification and the power of BPN networks.

Acknowledgements. This work was supported by National Science Council (NSC), Taiwan, R.O.C., under Grant No. 95-2622-E-216-009-CC3.

References

1. Ng, H.F.: Automatic Thresholding for Defect Detection. In: Proc. 3rd Int. Conf. Image and Graphics, pp. 532–535 (2004)
2. Yeh, C., Perng, D.B.: A Reference Standard of Defect Compensation for Leather Transactions. The Int. J. of Advanced Manufacturing Technology 25(11-12), 1197–1204 (2005)
3. Mery, D., Carrasco, M.: Automated Multiple View Inspection Based on Uncalibrated Image Sequences. In: Kalviainen, H., Parkkinen, J., Kaarna, A. (eds.) SCIA 2005. LNCS, vol. 3540, pp. 1238–1247. Springer, Heidelberg (2005)
4. Cheriet, M., Said, J.N., Suen, C.Y.: A Recursive Thresholding Technique for Image Segmentation. IEEE Trans. Image Processing 7(6), 918–921 (1998)
5. Chan, F.H.Y., Lam, F.K., Hui, Z.: Adaptive Thresholding by Variational Method. IEEE Trans. Image Processing 7(3), 468–473 (1998)
6. Mery, D.: Crossing Line Profile: A New Approach to Detecting Defects in Aluminum Die Castings. In: Bigun, J., Gustavsson, T. (eds.) SCIA 2003. LNCS, vol. 2749, pp. 725–732. Springer, Heidelberg (2003)
7. Gao, H., Siu, W.C., Hou, C.H.: Improved Techniques for Automatic Image Segmentation. IEEE Trans. Circuits Syst. Video Technol. 11(12), 1273–1280 (2001)
8. Tancharoen, D., Jitapunkul, S., Chompun, S.: Spatial Segmentation based on Modified Morphological Tools. In: Proc. Int. Conf. Information Technology: Coding and Computing, pp. 478–482 (2001)

9. Bellon, O.R.P., Silva, L.: New Improvements to Range Image Segmentation by Edge Detection. IEEE Signal Processing Lett. 9(2), 43–45 (2002)
10. Stojanovic, R., Mitropulos, P., Koulamas, C., Karayiannis, Y., Koubias, S., Papadopoulos, G.: Real-time Vision-based System for Textile Fabric Inspection. Real-Time Imaging. 7(6), 507–518 (2001)
11. Sauvola, J., Pietikainen, M.: Adaptive Document Image Binarization. Pattern Recognition 33, 225–236 (1999)
12. Otsu, N.: Threshold Selection Method from Gray-Level Histograms. IEEE Trans. Syst. Man, Cybern. SMC-9(1), 62–66 (1979)
13. Freeman, J.A., Skapura, D.M.: Neural Networks Algorithms, Applications and Programming Techniques, 1st edn. pp. 89–128. Addison-Wesley, London (1991)

Efficient Reinforcement Hybrid Evolutionary Learning for Recurrent Wavelet-Based Neuro-fuzzy Systems

Cheng-Hung Chen[1], Cheng-Jian Lin[2,⋆], and Chi-Yung Lee[3]

[1] Dept. of Electrical and Control Engineering
National Chiao-Tung University
Hsinchu 300, Taiwan, R.O.C.
[2] Dept. of Computer Science and Information Engineering
Chaoyang University of Technology
168 Gifeng E. Rd., Wufeng
Taichung County 413, Taiwan, R.O.C.
Tel.: +886-4-23323000 Ext. 4408
Fax: +886-4-23742375
cjlin@mail.cyut.edu.tw
[3] Dept. of Computer Science and Information Engineering
Nankai Institute of Technology
Nantou County 542, Taiwan, R.O.C.

Abstract. This paper proposes a recurrent wavelet-based neuro-fuzzy system (RWNFS) with the reinforcement hybrid evolutionary learning algorithm (R-HELA) for solving various control problems. The proposed R-HELA combines the compact genetic algorithm (CGA) and the modified variable-length genetic algorithm (MVGA), performs the structure/ parameter learning for dynamically constructing the RWNFS. That is, both the number of rules and the adjustment of parameters in the RWNFS are designed concurrently by the R-HELA. In the R-HELA, individuals of the same length constitute the same group. There are multiple groups in a population. The evolution of a population consists of three major operations: group reproduction using the compact genetic algorithm, variable two-part crossover, and variable two-part mutation. An illustrative example was conducted to show the performance and applicability of the proposed R-HELA method.

1 Introduction

In recent years, a fuzzy system used for control problems has become a popular research topic [1]. The reason is that classical control theory usually requires a mathematical model for designing controllers. Inaccurate mathematical modeling of plants usually degrades the performance of the controllers, especially for nonlinear and complex problems [3]. A fuzzy system consists of a set of fuzzy

⋆ Corresponding author.

H.G. Okuno and M. Ali (Eds.): IEA/AIE 2007, LNAI 4570, pp. 207–216, 2007.

if-then rules. By convention, the selection of fuzzy if-then rules often relies on a substantial amount of heuristic observations to express knowledge of proper strategies. Obviously, it is difficult for human experts to examine all the input-output data from a complex system to find the proper rules for a fuzzy system.

In this paper we proposed a new hybrid evolutionary learning algorithm to enhance the VGA [8]. The performance of the number of fuzzy rules in the VGA has not been evaluated, so that the best group that has the same length of chromosomes can not be reproduced many times for each generation. In this study, we use the elite-based reproduction strategy to keep the best group that has chromosomes of the same length. Therefore, the best group can be reproduced many times for each generation. The elite-based reproduction strategy is similar to the maturing phenomenon in society, where individuals become more suited to the environment as they acquire more knowledge of their surroundings.

In this paper, we present a recurrent wavelet-based neuro-fuzzy system (RW NFS) with the reinforcement hybrid evolutionary learning algorithm (R-HELA). The proposed R-HELA automatically determines the number of fuzzy rules and processes the variable-length chromosomes. The length of each individual denotes the total number of genes in that individual. The initial length of one individual may be different from another individual, depending on the total number of rules encoded in it. Individuals with an equal number of rules constitute the same group. Thus, initially there are several groups in a population. We use the elite-based reproduction strategy to keep the best group. Therefore, the best group can be reproduced many times for each generation. The reinforcement signal from the environment is used as a fitness function for the R-HELA. That is, we formulate the number of time steps before failure occurs as the fitness function. In this way, the R-HELA can evaluate the candidate solutions for the parameters of the RWNFS model.

The advantages of the proposed R-HELA method are summarized as follows: 1) it determines the number of fuzzy rules and tunes the free parameters of the RWNFS model in a highly autonomous way. Thus, users need not give it any a priori knowledge or even any initial information on these parameters. 2) It is applicable to chromosomes of different lengths. 3) It does not require precise training data for setting the parameters of the RWNFS model. 4) It performs better and converges more quickly than some traditional genetic methods.

2 Structure of a Recurrent Wavelet-Based Neuro-fuzzy System

This section introduces the structure of a RWNFS model. For traditional TSK-type fuzzy systems [2], the consequence of each rule is a function of the input linguistic variable. A widely adopted function is a linear combination of input variables plus a constant term. This study adopts a nonlinear combination of input variables (i.e., wavelet neural network (WNN)). Each fuzzy rule corresponds to a sub-WNN consisting of single-scaling wavelets [19]. We adopt the non-orthogonal and compact wavelet functions as the node function (wavelet bases).

The structure of the RWNFS model is shown in Fig. 1. For TSK-type fuzzy networks [2], the consequence of each rule is a linear function of input linguistic variables. A widely adopted function is a linear combination of input variables plus a constant term. This study adopts a nonlinear combination of input variables (i.e., WNN). Each fuzzy rule corresponds to a sub-WNN consisting of single-scaling wavelets. A novel RWNFS model is composed of fuzzy rules that can be presented in the following general form:

$$\begin{array}{c} R^j: \text{ IF } I_{1j} \text{ is } A_{1j} \text{ and } \cdots I_{ij} \text{ is } A_{ij} \text{ and } \cdots I_{nj} \text{ is } A_{nj} \\ \text{THEN } \widehat{y}_j^1 = \sum_{k=1}^{M} w_{jk}^1 \varphi_{a.b} = w_{j1}^1 \varphi_{0.0} + w_{j2}^1 \varphi_{1.0} + w_{j3}^1 \varphi_{1.1} + \cdots \\ \text{and } \widehat{y}_j^2 = \sum_{k=1}^{M} w_{jk}^2 \varphi_{a.b} = w_{j1}^2 \varphi_{0.0} + w_{j2}^2 \varphi_{1.0} + w_{j3}^2 \varphi_{1.1} + \cdots \end{array} \quad (1)$$

where R^j denotes the jth rule; $\{I_{1j}, \ldots, I_{ij}, \ldots, I_{nj}\}$ is the network input pattern $\{x_1, \ldots, x_i, \ldots, x_n\}$ plus the temporal term for the linguistic term of the precondition part A^j=$\{A_{1j}, \ldots, A_{ij}, \ldots, A_{nj}\}$; the local WNN model outputs $\widehat{y}_j^1$ and $\widehat{y}_j^2$ are calculated for outputs Y_1 and Y_2, and rule R_j. Details of the structure of the recurrent wavelet-based neuro-fuzzy system (RWNFS) can be found in [3].

3 A Hybrid Evolutionary Learning Algorithm (HELA)

This section introduces the proposed hybrid evolutionary learning algorithm (HELA). Recently, many efforts to enhance the traditional GAs have been made [10]. Among them, one category focuses on modifying the structure of a population or the role an individual plays in it [11]-[13], such as the distributed GA [11], the cellular GA[12], and the symbiotic GA [13]. In a traditional evolution algorithm, the number of rules in a model must be predefined. Our proposed HELA combines the compact genetic algorithm (CGA) and the modified variable-length genetic algorithm (MVGA). In the MVGA, the initial length of each individual may be different from each other, depending on the total number of rules encoded in it. Thus, we do not need to predefine the number of rules. In this paper, individuals with an equal number of rules constitute the same group. Initially, there are several groups in a population. Not following the traditional variable-length genetic algorithm (VGA) notation, Bandyopadhyay et. al. [8] used "♯" to mean "does not care". In this study, we adopt the variable two-part crossover (VTC) and the variable two-part mutation (VTM) to make the traditional crossover and mutation operators applicable to different lengths of chromosomes. Therefore, we do not use "♯" to mean "does not care" in the VTC and the VTM. In this study, we divide a chromosome into two parts. The first part of the chromosome gives the antecedent parameters of a RWNFS model while the second part of the chromosome gives the consequent parameters of a RWNFS model. Each part of a chromosome can be performed using the VTC on the overlapping genes of two chromosomes. In the traditional VGA, Bandyopadhyay et. al. [8] only evaluated the performance of each chromosome in a population. The performance of the number of rules was not evaluated in [8]. In this study, we use the elite-based reproduction strategy to keep the best group that has chromosomes of the

same length. Therefore, the best group can be reproduced many times for each generation. The elite-based reproduction strategy is similar to the maturing phenomenon in society, in which individuals become more suited to the environment as they acquire more knowledge of their surroundings. In the proposed HELA method, we adopt the compact genetic algorithm (CGA) [14] to carry out the elite-based reproduction strategy. The CGA represents a population as a probability distribution over the set of solutions and is operationally equivalent to the order-one behavior of the simple GA [15]. The advantage of the CGA is that it processes each gene independently and requires less memory than the normal GA. The building blocks (BBs) in the CGA represent the suitable lengths of the chromosomes, and the CGA reproduces the chromosomes according to the BBs. The coding scheme consists of the coding done by the MVGA and the CGA. The MVGA codes the adjustable parameters of a RWNFS model into a chromosome, as shown in Fig. 2, where MS_j represents the parameters of the antecedent of the jth rule in the RENFN and C_j represents the parameters of the consequent of the jth rule. In Fig. 3, the CGA codes the probability vector into the building blocks (BBs), where each probability vector represents the suitability of the rules of a RWNFS model. In the CGA, we must predefine the maximum number of rules (M_{max}) and the minimum number of rules (M_{min}) to prevent generating the number of fuzzy rules beyond a certain bound (i.e., [M_{max}, M_{min}]).

The learning process of the HELA involves six major operators: initializing, evaluating, sorting, elite-based reproduction strategy, variable two-part crossover, and variable two-part mutation. The whole learning process is described step-by-step as follows:

a. **Initializing:** The initializing step sets the initial values in the MVGA and the CGA. In the MVGA, individuals are initially randomly generated to construct a population. In order to keep the same number of rules in a RWNFS model, the number of rules for each chromosome needs to be generated η chromosomes. That is, we predefine the number of chromosomes generated for each group (η). Therefore, the population size is set to $\eta^*(M_{max}\text{-}M_{min}+1)$. In the CGA, the probability vectors of the BBs are initially set to 0.5.

b. **Evaluating:** The evaluating step evaluates each chromosome in a population. The goal of the R-HELA method is to maximize the fitness value. The higher a fitness value, the better the fitness. The fitness function is used by a reinforcement signal that we will introduce in the next section.

c. **Sorting:** After the evaluating step, we sort the chromosomes in the population. After the whole population is sorted, we sort the chromosomes in each group in the top half of population. The sorting step can help us to perform the reproduction step because we can keep the best chromosome in each group. After the chromosomes in the population are sorted, the algorithm goes to the next step.

d. **Elite-Based Reproduction Strategy (ERS):** Reproduction is a process in which individual strings are copied according to their fitness value. A fitness

value is assigned to each individual. The goal of the R-HELA method is to maximize the fitness value. The higher a fitness value, the better the fitness. In this study, we use an elite-based reproduction strategy (ERS) to mimic the maturation phenomenon in society, in which individuals become more suited to the environment as they acquire more knowledge of their surroundings.

The CGA is used here to carry out the ERS. The CGA represents the population as a probability distribution over the set of solutions and is operationally equivalent to the order-one behavior of the simple GA. The CGA uses the BBs to represent the suitable lengths of the chromosomes and reproduces the chromosomes according to the probability vector in the BBs. The best performing individuals in the top half of each population are used to perform the ERS. According to the results of the ERS, using the crossover and the mutation operations generates the other half of the individuals. The ERS, the suitable length of chromosomes will be preserved and the unsuitable length of chromosomes will be removed. Details of the ERS are shown below.

Step 1. Update the probability vectors of the BBs according to the following equations:

$$\begin{cases} V_k = V_k + (Upt\_value_k * \lambda) \text{ if } Avg \leq Max\_fit_k \\ V_k = V_k - (Upt\_value_k * \lambda) \text{ otherwise} \end{cases} \tag{2}$$

where k=[R_{max}, R_{min}].

$$Avg = \frac{\sum_{p=1}^{Nc} fit_p}{Nc} \tag{3}$$

$$Upt\_value_k = \frac{Total\_fit_k}{\sum_{p=1}^{Nc} fit_p} \tag{4}$$

$$Total\_fit_k = \sum_{p=1}^{Nk} fit_{kp} \tag{5}$$

Step 2. Determine the reproduction number according to the probability vectors of the BBs as follows:

$$Rep_k = \frac{P_{size}}{2} * \frac{V_k}{Total\_Velocy} \tag{6}$$

where k=[R_{max}, R_{min}].

$$Total\_Velocy = \sum_{k=R}^{R} V_k \tag{7}$$

where P_{size} represents the population size and Rep_k is the recorder, and a chromosome has k rules for constructing a RWNFS.

Step 3. After step 2, the reproduction number of each group in the top half of a population is obtained. Then we generate Rep_k chromosomes in each group using the roulette-wheel selection method [16].

Step 4. If any probability vector in the BBs reaches 1, then stop the ERS and set the probability vector to 1 for all groups with the same number of rules, according to step 2. The lack of the chromosomes are generated randomly. To replace the ERS step, we use the roulette-wheel selection method [16] - a simulated roulette is spun - for this reproduction process.

e. **Variable two-part crossover:** Although the ERS operation can search for the best existing individuals, it does not create any new individuals. In nature, an offspring has two parents and inherits genes from both. The main operator working on the parents is the crossover operator, the operation of which occurs for a selected pair with a crossover rate.

In this paper, we propose using the variable two-part crossover (VTC) to perform the crossover operation. In the VTC, the parents are selected from the enhanced elites using the roulette-wheel selection method [16]. The two parents may be selected from the same or different groups. Performing crossover on the selected parents creates the offspring. Since the parents may be of different lengths, we must avoid misalignment of individuals in the crossover operation. Therefore, a variable two-part crossover is proposed to solve this problem. The first part of the chromosome gives the antecedent parameters of a RWNFS model while the second part of the chromosome gives the consequent parameters of a RWNFS model. The two-point crossover is adopted in each part of the chromosome. Thus, new individuals are created by exchanging the site's values between the selected sites of the parents' individuals. To avoid misalignment of individuals in the crossover operation, in the VTC, the selection of the crossover points in each part will not exceed the length of the shorter chromosome of the two parents. Two individuals of different lengths resulting from the use of the variable two-part crossover operation are shown in Fig. 4. MSj represents the parameters of the antecedent part of the jth rule in the RENFN; W_j represents the parameters of the consequent of the jth rule in the RENFN; and M_k is the number of fuzzy rules in the kth chromosome. After the VTC operation, the individuals with poor performances are replaced by the new offspring.

f. **Variable two-part mutation:** Although the ERS and the VTC produce many new strings, these strings do not provide any new information to every population at the site of an individual. Mutation can randomly alter the allele of a gene.

In this paper, we propose using the variable two-part mutation (VTM) to perform the mutation operation. The proposed VTM is different from the traditional mutation and is applicable to chromosomes of different lengths. The first and second parts of the chromosome are the same as the crossover operation. In each part of a chromosome, uniform mutation is adopted, and the mutated gene is drawn randomly from the domain of the corresponding variable. The VTM operation for each individual is shown in Fig. 5.

After the above-mentioned operations are carried out, the problem of how groups are to be constituted by the most suitable number of rules will be solved. The number of elites in other groups will decrease and most of them will become

zero (in most cases, there will be no elites). That is, our method indeed can eliminate unsuitable groups and rules.

4 Control of a Cart-Pole Balancing System

In this section, we compare the performance of the RWNFS model using the R-HELA method with some existing models for a cart-pole balancing system application [17]. The initial parameters for the two simulations are set as population size=54, crossover rate=0.5,mutation rate=0.3, $[\sigma_{min}, \sigma_{max}]$=[0,2], $[m_{min}, m_{max}]$=[0,2], $[w_{min}, w_{max}]$=[-20,20], M_{max}=12, M_{min}=3, λ=0.01, and η=6. The initial parameters were determined by practical experimentation or trial-and-error tests.

In this example, we apply the R-HELA method to the classic control problem of a cart-pole balancing. This problem is often used as an example of inherently unstable and dynamic systems to demonstrate both modern and classic control techniques [17], or the reinforcement learning schemes [6]-[7] and is now used as a control benchmark. As shown in Fig. 6, the cart-pole balancing problem is the problem of learning how to balance an upright pole. The bottom of the pole is hinged to a cart that travels along a finite-length track to its right or left. Both the cart and the pole can move only in the vertical plane; that is, each has only one degree of freedom.

There are four state variables in the system: θ, the angle of the pole from an upright position (in degrees); $\dot{\theta}$, the angular velocity of the pole (in degrees/seconds); x, the horizontal position of the cart's center (in meters); and $\dot{x}$, the velocity of the cart (in meters/seconds). The only control action is f, which is the amount of force (in *Newtons*) applied to the cart to move it toward left or right. The system fails when the pole falls past a certain angle (± 12 is used here) or the cart runs into the bounds of its track (the distance is 2.4 m from the center to each bound of the track). The goal of this control problem is to determine a sequence of forces that is applied to the cart to balance the pole upright.

In this experiment, the initial values were set to (0, 0, 0, 0). A total of thirty runs were performed. Each run started in the same initial state. Figure 7(a) shows that the RWNFS model learned on average to balance the pole at the $54th$ generation. In this figure, each run represents that largest fitness value in the current generation being selected before the cart-pole balancing system fails. When the R-HELA method was stopped, we chose the best strings in the population in the final generation and tested them on the cart-pole balancing system. Figure 8 shows the results of the probability vectors in CGA. In this figure, the final average optima number of rules is 4.

Figure 9(a) shows the angular deviation of the pole when the cart-pole balancing system was controlled by a well-trained RWNFS model starting in the initial state: $x(0)$=0, $\dot{x}(0)$=0, $\theta(0)$=0, $\dot{\theta}(0)$=0 . The average angular deviation was 0.01^o. The results show that the trained RWNFS model had good control in the cart-pole balancing system.

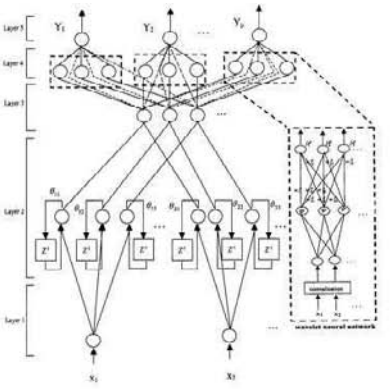

Fig. 1. Schematic diagram of RWNFS model.

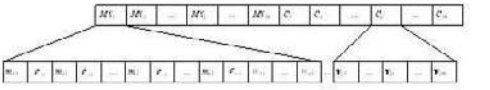

Fig. 2. Coding the adjustable parameters of a RWNFS into a chromosome in the MVGA.

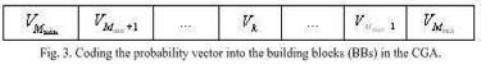

Fig. 3. Coding the probability vector into the building blocks (BBs) in the CGA.

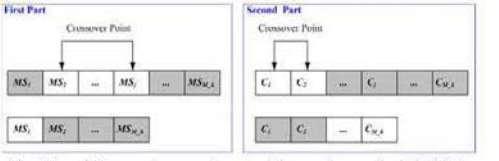

Fig. 4. The variable two-part crossover two-partmutation operation operation in the HELA.

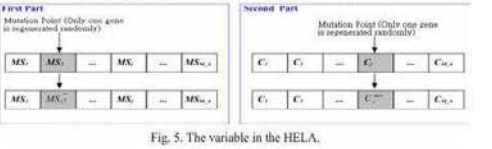

Fig. 5. The variable in the HELA.

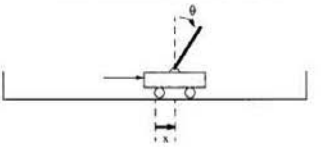

Fig. 6. The cart-pole balancing system.

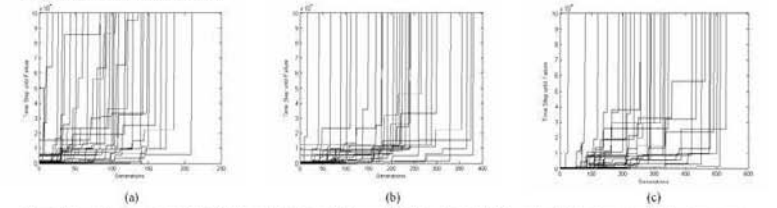

(a) (b) (c)

Fig. 7. The performance of (a) the R-HELA method, (b) the R-SE method [98], and (c) the R-GA method [7] on the cart-pole balancing system.

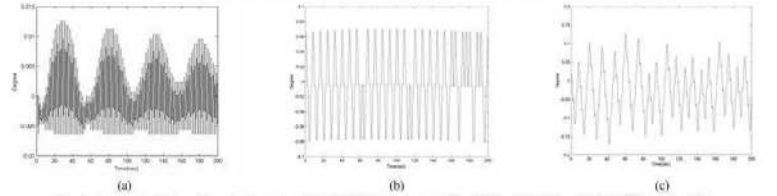

(a) (b) (c)

Fig. 9. Angular deviation of the pole by a trained (a) the R-HELA method, (b) the R-SE method [9], and (c) the R-GA method [7].

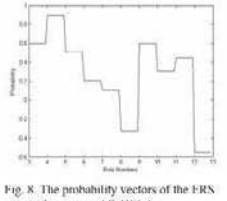

Fig. 8. The probability vectors of the ERS step in the proposed R-HELA.

Table I: The comparison of CPU time for various existing models.

Method	Mean	Dest	Worst
GENITOR	70.95	33.34	246.36
SANE	43.56	16.54	136.84
R-GA	47.59	11.85	102.63
R-SE	38.85	8.53	90.78
TDGAR	30.23	7.97	76.25
CQGAF	28.15	6.39	61.57
R-HELA	**23.12**	**5.42**	**50.71**

Table II: Performance comparison of various existing models.

Method	Mean	Dest	Worst
GENITOR	3268	415	18743
SANE	1984	46	5865
R-GA	324	26	550
R-SE	214	15	380
TDGAR	186	18	310
CQGAF	133	12	288
R-HELA	**104**	**10**	**210**

Table III: Performance comparison of three different methods

Method	Mean	Best	Worst
Type I method (the proposed R-HELA method)	**104**	**10**	**210**
Type II method (the proposed R-HELA method without ERS)	115	15	229
Type III method (the fixed length genetic algorithm)	210	21	380

We also compared the performance of our system with the reinforcement symbiotic evolution (R-SE) [7] and the reinforcement genetic algorithm (R-GA) [5] when they were applied to the same problem. In the R-GA and the R-SE, the population size was set to 200 and the crossover and mutation probabilities were set to 0.5 and 0.3, respectively. Figures 7(b)-(c) show that the R-SE and the R-GA methods learned to balance the pole on average at the $80th$ and $149th$ generations. Figures 9(b)-(c) show the angular deviation of the pole when the cart-pole balancing system was controlled by [7] and [5]. The average angular deviations of [7] and [18] models were 0.06^o and 0.1^o. As shown in Figs. 7 and 9, the control capabilities of the trained RWNFS model using the R-HELA are better than [5] and [7] in the cart-pole balancing system.

The GENITOR [17], the SANE (Symbiotic Adaptive Neuro-Evolution) [13], the TDGAR [6], and the CQGAF [9] have been applied to the same control problem. Their simulation results are listed in Table II. Table II shows the number of pole-balancing trials (which reflects the number of training episodes required). The CQGAF [9] fulfills the GA-based fuzzy system design in a reinforcement learning environment where only weak reinforcement signals, such as "success" and "failure" are available. As shown in Table II, the proposed R-HELA is feasible and effective. We also compared the CPU times with those of other existing methods ([4], [5], [6], [7], [9], [13], and [17]). The results are shown in Table I. In this experiment, we used a Pentium 4 chip with a 1.5GHz CPU, a 512MB memory, and the visual C++ 6.0 simulation software. Table I shows that our proposed HELA method obtains smaller CPU times than those of other existing models. Table III shows the performance comparison of the three methods. As shown in Table III, our proposed HELA with the ERS method performs better than the other methods.

5 Conclusion

In this paper, a recurrent wavelet-based neuro-fuzzy system (RWNFS) with the reinforcement hybrid evolutionary learning algorithm (R-HELA) was proposed for dynamic control problems. The proposed R-HELA has structure-and-parameter learning ability. That is, it can determine the average optimal number of fuzzy rules and tune the free parameters in the RWNFS model. The proposed learning method also processes variable lengths of chromosomes in a population. Computer simulations have shown that the proposed R-HELA performs better than the other methods. In addition to being used to solve the problems given in this paper, the proposed R-HELA method was also used in our laboratory to solve practical control problems in magnetic levitation systems.

Acknowledgement

This research is supported by the National Science Council of the R.O.C. under grant NSC 95-2221-E-324-028-MY2.

References

1. Lin, C.T., Lee, C.S.G.: Neural Fuzzy Systems: A Neuro-Fuzzy Synergism to Intelligent System. Prentice-Hall, Englewood Cliffs (1996)
2. Takagi, T., Sugeno, M.: Fuzzy identification of systems and its applications to modeling and control. IEEE Trans. Syst. Man, Cybern. 15, 116–132 (1985)
3. Lin, C.J., Chin, C.C.: Prediction and identification using wavelet-based recurrent fuzzy neural networks. IEEE Trans. on Systems, Man, and Cybernetics (Part:B) 34, 2144–2154 (2004)
4. Fogel, L.J.: Evolutionary programming in perspective: The top-down view. In: Zurada, J.M., Marks II, R.J., Goldberg, C. (eds.) Computational Intelligence: Imitating Life, IEEE Press, Piscataway, NJ (1994)
5. Karr, C.L.: Design of an adaptive fuzzy logic controller using a genetic algorithm. In: Proc. The Fourth Int. Conf. Genetic Algorithms, pp. 450–457 (1991)
6. Lin, C.T., Jou, C.P.: GA-based fuzzy reinforcement learning for control of a magnetic bearing system. IEEE Trans. Syst. Man, Cybern. Part B 30, 276–289 (2000)
7. Juang, C.F., Lin, J.Y., Lin, C.T.: Genetic reinforcement learning through symbiotic evolution for fuzzy controller design. IEEE Trans. Syst. Man, Cybern. Part B 30, 290–302 (2000)
8. Bandyopadhyay, S., Murthy, C.A., Pal, S.K.: VGA-classfifer: design and applications. IEEE Trans s. Syst. Man, and Cyber. Part B 30, 890–895 (2000)
9. Juang, C.F.: Combination of online clustering and Q-value based GA for reinforcement fuzzy system design. IEEE Trans. Fuzzy Systems 13, 289–302 (2005)
10. Michalewicz, Z.: Genetic Algorithms+Data Structures=Evolution Programs. Springer, New York (1999)
11. Tanese, R.: Distributed genetic algorithm. In: Proc. Int. Conf. Genetic Algorithms, pp. 434–439 (1989)
12. Arabas, J., Michalewicz, Z., Mulawka, J.: GAVaPS-A genetic algorithm with varying population size. In: Proc. IEEE Int. Conf. on Evolutionary Computation, pp. 73–78 (1994)
13. Moriarty, D.E., Miikkulainen, R.: Efficient reinforcement learning through symbiotic evolution. Mach. Learn. 22, 11–32 (1996)
14. Harik, G.R., Lobo, F.G., Goldberg, D.E.: The compact genetic algorithm. IEEE Trans. Evolutionary Computation, 450–457 (1991)
15. Lee, K.Y., Bai, X., Park, Y.-M.: Optimization method for reactive power planning by using a modified simple genetic algorithm. IEEE Trans. Power Systems 10, 1843–1850 (1995)
16. Cordon, O., Herrera, F., Hoffmann, F., Magdalena, L.: Advances in Fuzzy Systems-Applications and Theory. World Scientific Publishing, NJ (2001)
17. Whitley, D., Dominic, S., Das, R., Anderson, C.W.: Genetic reinforcement learning for neuro control problems. Mach. Learn. 13, 259–284 (1993)
18. Wang, H., Kwong, S., Jin, Y., Wei, W., Man, K.F.: Multi-objective hierarchical genetic algorithm for interpretable fuzzy rule-based knowledge extraction. Fuzzy Sets and Systems 149, 149–186 (2005)
19. Ho, D.W.C., Zhang, P.A., Xu, J.: Fuzzy wavelet networks for function learning. IEEE Trans. Fuzzy Systs. 9, 200–211 (2001)

A Relation-Based Genetic Algorithm for Partitioning Problems with Applications

Jiah-Shing Chen, Yao-Tang Lin, and Liang-Yu Chen

Department of Information Management
National Central University
Jhongli, Taiwan 320
{jschen,s0443003,93423015}@cc.ncu.edu.tw

Abstract. This paper proposes a new relation-based genetic algorithm named relational genetic algorithm (RGA) for solving partitioning problems. In our RGA, a relation-oriented representation (or relational encoding) is adopted and corresponding genetic operators are redesigned. The relational encoding is represented by the equivalence relation matrix which has a 1-1 and onto correspondence with the class of all possible partitions. It eliminates the redundancy of previous GA representations and improves the performance of genetic search. The generalized problem-independent operators we redesigned manipulate the genes without requiring specific heuristics in the process of evolution. In addition, our RGA also supports a variable number of subsets. It works without requiring a fixed number of subsets in advance. Experiments for solving some well-known classic partitioning problems by RGA and GGA with and without heuristics are performed. Experimental results show that our RGA is significantly better than GGA in all cases with larger problem sizes.

Keywords: relational genetic algorithm (RGA), grouping genetic algorithm (GGA), relational encoding, partitioning problems, grouping problems.

1 Introduction

The set partitioning problem belongs to the class of NP-hard optimization problems. Lots of such well-known classic problems and extended applications have been proposed, discussed and solved in the past [1, 3, 7, 9]. Among these methodologies for solving partitioning problems, genetic algorithms (GA) are very popular and suitable due to their comprehensive capability to search a large solution space. However, previous works of applying GA to solving the partitioning problems, such as group genetic algorithm (GGA), have non-unique encoding, rely heavily on some problem-specific heuristics, and require a fixed number of subsets [3, 6]. Non-unique encoding results in poor performance of genetic search due to its redundancy. Genetic operators involve specific heuristics can't be generalized and some partitioning problems have no natural heuristics [3]. Requiring a fixed number of subsets in advance prohibits its applicability to problems without such prior information. For these reasons, GA needs some new structures and generalized problem-independent operators to address these drawbacks.

H.G. Okuno and M. Ali (Eds.): IEA/AIE 2007, LNAI 4570, pp. 217–226, 2007.

To create a generalized GA-based framework for solving partitioning problems efficiently, this paper proposes a new relation-based genetic algorithm named relational genetic algorithm (RGA). In our RGA, a relation-oriented representation (or relational encoding) is adopted and corresponding genetic operators are redesigned. The relational encoding is represented by equivalence relation matrix which has a 1-1 and onto correspondence with the class of all possible partitions. It eliminates the redundancy of previous GA representations and improves the performance of genetic search. The generalized problem-independent operators we redesigned manipulate the genes without requiring specific heuristics in the process of evolution. In addition, our RGA also supports a variable number of subsets. It works without requiring a fixed number of subsets in advance [3].

Experiments for equal/similar piles problems and map/graph coloring problems are designed and performed. Each of them is solved by RGA and GGA respectively. We also design some similar heuristics for RGA and GGA in the last set of experiments. Experimental results show that our RGA is significantly better than GGA in all cases with larger problem sizes.

The rest of this paper is organized as follows. Section 2 reviews the partitioning problems and previous GAs for solving them. Section 3 describes our relational genetic algorithm. Some qualitative comparisons between RGA and previous GAs are also made in this section. Section 4 presents some experimental results which demonstrate our RGA is significantly better than GGA. Finally, conclusions and future works are summarized in section 5.

2 Background

2.1 Partitioning Problems

The partitioning (or set-partitioning) problem, also known as the grouping problem [6], is defined as partitioning a set into a collection of mutually disjoint subsets. In addition, some hard constraints and cost functions are pre-defined for individual partitioning problem. A solution to the problem must comply with various hard constraints, and the objective of partitioning is to optimize the cost function defined over the set of all valid partitions [6].

Well-known classic partitioning problems include bin packing [7], equal piles [9], graph/map coloring [1, 5], line balancing, and workshop layout [4]. They have been solved by using various approaches, such as greedy algorithms, tabu search [4], simulated annealing [8], and genetic algorithms [2, 5, 6, 9, 10]. Two of these classic partitioning problems, the equal/similar piles problem and the map/graph coloring problem, are solved for empirical study in this paper. They are detailed as follows.

Equal Piles/Similar Piles Problem

Equal piles problem is proposed originally by Jones and Beltramo in 1991 [9]. It partitions a given set of integers into a predetermined number of piles such that all piles have the same sum.

To make the equal piles problem more difficult and without obvious heuristics, we generalize it to the similar piles problem by relaxing the requirement of equal sum. The objective of the similar piles problem is to partition a given set of integers into a predetermined number of piles such that the differences between their sums are minimal.

Map/Graph Coloring Problem
The objective of graph coloring problem is to color all vertices in a given undirected graph with as few colors as possible so that no two adjacent vertices have the same color.

The objective of map coloring problem is to coloring regions of a map with as few colors as possible so that no regions sharing a common border are colored the same color. A map coloring problem can be transformed into a special type of graph coloring problem, i.e., the planar graph coloring problem. It has been shown that any planar graph can be colored within 4 colors. A well-known American Map Coloring problem originally proposed by Appel (1997) [1] is adopted for experimentation in this paper.

2.2 Previous GAs for Solving Partitioning Problems

Genetic algorithms are suitable for solving partitioning problems due to their capability to search a large solution space. Previous works of applying GA on partitioning problems can be divided into two categories. One is based on object-oriented representations (also known as traditional representation), which include permutation encoding and membership encoding [9]. Another is based on a group-oriented representation proposed by Falkenauer (1992) [6]. The object-oriented representations lead to a large degree of redundancy, high schema disruption, and context insensitivity [6]. The group-oriented representation partially improves the drawbacks of object-oriented representations, but still results in some degree of redundancy and schema disruption. In addition, it requires some additional problem-specific heuristics [2]. Neither category of previous GA approaches can be used to solve the partitioning problem effectively. Therefore, a new relation-based genetic algorithm named relational genetic algorithm (RGA) is proposed for solving partitioning problems and is described in the next section.

3 Relational Genetic Algorithm

Our relational genetic algorithm consists of a relation-based representation named relational encoding and a set of generalized problem-independent operators. They are described as follows. In addition, some qualitative comparisons between RGA and previous GAs are also made at the end of this section.

3.1 Relational Encoding

It is well-known that an equivalence relation can be induced by a partition and vice versa. Thus, a partition can be uniquely represented by its induced equivalence relation matrix.

In this relational encoding, each chromosome is an equivalence relation matrix $M_R = \left[m_{ij} \right]$ which represents an equivalence relation R such that $m_{ij} = 1$ if objects i and j are in the same subset, and $m_{ij} = 0$ otherwise. An example is shown in figure 1(a).

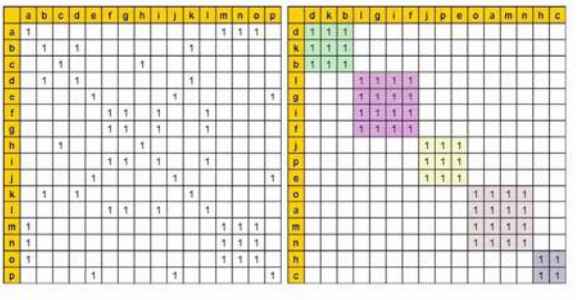

Fig. 1. (a) A partition encoded by an equivalence relation matrix. **(b)** Reordered matrix according to clusters.

Each equivalence relation matrix must be reflexive, symmetric, and transitive. These three properties must also be maintained in the process of evolution. Furthermore, relationships in same subset can be clustered together by reordering objects so that the groups can be identified more easily as shown in figure 1(b).

3.2 Genetic Operators

The two genetic operators of RGA, crossover and mutation, are redesigned to maintain the properties of equivalence relation matrix.

Crossover

Crossover operator for RGA consists of three traditional procedures and one additional repairing procedure. They are explained as follows, and an example for one-point crossover is demonstrated.

1. **Select crossing points:** Randomly select crossing points on diagonal in each parent matrix. One-point, two-point, and uniform crossovers are supported. Figure 2 gives an example of one-point crossover.

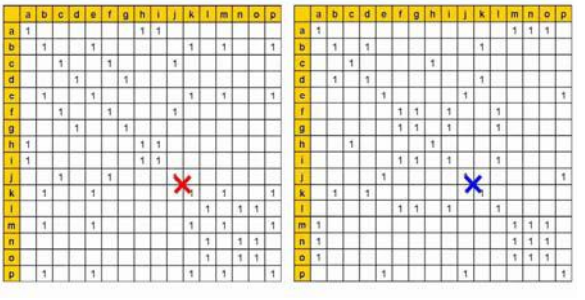

Fig. 2. Crossing points on diagonal are selected for one-point crossover

2. **Determine crossing and repairing areas:** Further divide each matrix into several areas according to the selected crossing points. The genes in crossing areas will be

reserved until next generation and the genes in repairing areas will be disrupted. The disrupted genes are replaced by question marks temporarily and are then rebuilt by repairing later as shown in figure 3.

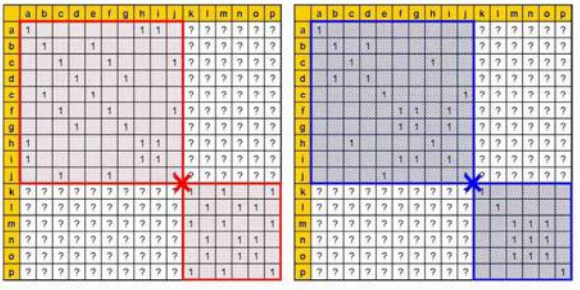

Fig. 3. Two crossing areas (colored) and two repairing areas (uncolored) are determined in each parent for one-point crossover. The genes in repairing areas are replaced by question marks.

3. **Swap crossing areas:** Swap crossing areas to generate descendants as shown in figure 4.

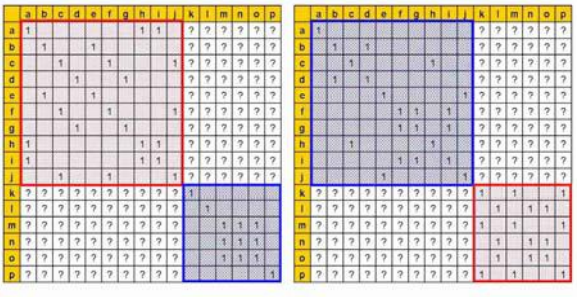

Fig. 4. Descendants inherit genes form parents by swapping crossing areas

4. **Repairing:** There are three objectives for repairing. They are controlling the number of subsets, maintaining symmetry, and maintaining transitivity. A simple recursive naïve (non-heuristic) repairing algorithm is illustrated as follows. Figure 5 shows the resulting matrices after repairing.

```
Target = random (LowerBound, UpperBound)
// decide the new number of subsets

while (Subset > Target)
  calculate weights of each cell in repairing areas
  insert an 1 into repairing areas by roulette method
  determine symmetric and transitive closure
  determine new repairing areas
  recalculate the number of subset
end while
```

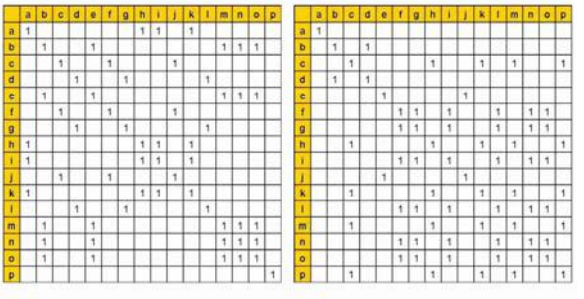

Fig. 5. Two complete descendants are generated after repairing

Mutation

The swap mutation operator in classic genetic algorithms is generalized to work on the equivalence relation matrix as follows: two randomly selected columns are swapped and their corresponding rows are also swapped to maintain the properties of the equivalence relation matrix.

3.3 Qualitative Comparisons

To analyze and understand the factors which influence the performance of genetic search, a set of qualitative comparisons between RGA and previous GAs are summarized in table 1. The object-oriented representations lead to the highest redundancy, highest schema disruption, and serious context insensitivity problem [6]. The poorest performance is consequently expected and induced for them. The group-oriented representation partially improves the drawbacks of object-oriented representations, but still results in some degree of redundancy and schema disruption. In addition, it requires some additional problem-specific heuristics [2].

Furthermore, some related literatures have showed that GGA outperforms GAs with object-oriented encodings [6]. Thus, our experiments in section 4 are designed to compare RGA and GGA only.

Table 1. Qualitative comparisons between RGA and previous GAs

	Representation	Redundancy	Heuristics	Schema Disruption	Context Insensitivity
RGA	Relation-oriented	None	Optional	Low	No
GGA	Group-oriented	Low	Required	Middle*	No
SGA_{PE}	Object-oriented	High	N/A	High	Yes
SGA_{ME}	Object-oriented	High	N/A	High	Yes

SGA_{PE} : Standard GA with permutation encoding

SGA_{ME} : Standard GA with membership encoding

* : Fewer subsets result in higher schema disruption

4 Experiments

Three sets of experiments for equal/similar piles problems and map/graph coloring problems are designed and performed to compare the performances of RGA and GGA. Each of them includes a well-known instance with smaller problem size and an extended application with larger problem sizes. All individual problems are solved by RGA and GGA respectively. We also design some similar heuristics for RGA and GGA in the last set of experiments. In addition, the performance of RGA is compared with that of GGA in each experiment.

For RGA and GGA, two-point crossover is adopted because it outperforms other crossover methods (one-point and uniform crossovers) in our pretests. The population size of RGA and GGA is set to 50, generation is 3500, selection method is stochastic remainder with replacement and elitism, crossover rate is 1, mutation rate is 0.01, and the fitness functions are dependent on specific problems.

In experiment 1, we solve the equal piles problem proposed originally by Jones and Beltramo (1991) and the similar piles problem extended form the equal piles problem. Generalized naïve (non-heuristic) repairing schemes are adopted by RGA and GGA respectively instead of problem-specific heuristics.

For the original equal piles problem (experiment 1-1), the only specific case, i.e., to partition a set of 34 integers into 10 piles, is solved by 30 iterations for statistical paired-samples t-test. The cost function $Diff_E$ is the error sum of all piles and is defined as $Diff_E = \sum_{k=1}^{K} |S_k - S|$, where S is the average of piles, S_k is the sum of kth pile, and K is the total number of piles.

For the similar piles problem (experiment 1-2), 30 cases are generated randomly with larger problem sizes to make the problems difficult for GAs. Six classes are designed to partition 50 and 90 integers into 10, 15, and 20 piles respectively and each class includes 5 different cases. The cost function $Diff_S$ is the same as in the equal piles problem.

Averages of error sums that result from RGA and GGA are shown in table 2. Furthermore, statistical significances of Paired-samples t-tests are also determined and are shown in table 3.

Table 2. Averages of error sums result form RGA and GGA in experiment 1

	RGA	GGA
Average of $Diff_E$	4668.40	9606.87
Average of $Diff_S$	24954.73	99946.33

Table 3. Statistical significances of paired-samples t-tests in experiment 1

	Statistical Significance
$Diff_E(GGA) - Diff_E(RGA)$	2.55428E-09
$Diff_S(GGA) - Diff_S(RGA)$	3.55387E-07

In experiment 2, we solve the American map coloring problem proposed originally by Appel (1997) and the general graph coloring problem. The naïve (non-heuristic) repairing schemes are also adopted instead of problem-specific heuristics here.

For the American map coloring problem (experiment 2-1), the only specific case is also solved by 30 iterations. The cost function Vio_M is defined as the number of common borders shared by regions that have the same color.

For the graph coloring problem (experiment 2-2), 30 cases are generated randomly with larger problem sizes to make the problems difficult for GAs, too. Each case consists of 100 vertices and about 200 edges, and is colored by 6 colors. The cost function Vio_G is defined as the number of edges which connect two adjacent vertices that have the same color.

The results of Experiment 2 are shown in table 4 and table 5.

Table 4. Average of errors result form RGA and GGA in experiment 2

	RGA	GGA
Average of Vio_M	3.83	4.13
Average of Vio_G	0.47	8.87

Table 5. Statistical significances of paired-samples t-tests in experiment 2

	Statistical Significance
$Vio_M(GGA) - Vio_M(RGA)$	0.246216
$Vio_G(GGA) - Vio_G(RGA)$	5.11E-20

In experiment 3, we solve the equal piles problem and the similar piles problem again but adopt similar greedy heuristics for RGA and GGA repairing. Besides, all case and configuration designs are the same as experiment 1. The results of Experiment 3 are shown in table 6 and table 7.

Table 6. Average of error sums result form RGA and GGA in experiment 3

	RGA	GGA
Average of $Diff_E$	23.40	20.93
Average of $Diff_S$	550.10	980.40

Table 7. Statistical significances of paired-samples t-tests in experiment 3

	Statistical Significance
$Diff_E(GGA) - Diff_E(RGA)$	0.380656595
$Diff_S(GGA) - Diff_S(RGA)$	1.871373E-03

To analyze and conclude the experimental results, we further brief the summaries of statistics shown in table 2 to table 7. The summaries of experimental results are shown in table 8.

Table 8. Summaries of experimental results

Experiment Description			Experimental Result	
No.	Problem	Repairing Scheme	Best Performing	Statistically Significant
1-1	Original Equal Piles *	Naïve	RGA	Yes
1-2	Similar Piles **	Naïve	RGA	Yes
2-1	American Map Coloring *	Naïve	RGA	No
2-2	Graph Coloring **	Naïve	RGA	Yes
3-1	Original Equal Piles *	Heuristics	GGA	No
3-2	Similar Piles **	Heuristics	RGA	Yes

* : single specialized problem instance solved by 30 iterations.
** : 30 enlarged cases generalized from original one.

According to the summarized results in table 8, we have:

1. Our RGA does not significantly outperform GGA in only two special smaller cases (experiment 2-1 and 3-1).
2. For all generalized larger cases (experiment 1-2, 2-2, and 3-2), our RGA significantly outperforms GGA, whether heuristics are involved or not.
3. For all cases without using heuristics (experiment 1-1, 1-2, 2-1, and 2-2), our RGA outperforms GGA, and all cases except one special smaller case are significant.

Finally, we further conclude that our RGA almost dominates over GGA significantly, whether heuristics are involved or not. In addition, we also find that, for some specific problems, additional heuristics can guide local search to refine the optimization effectively.

5 Conclusion

This paper proposed a new relation-based genetic algorithm named relational genetic algorithm which improves major drawbacks of previous GAs and contributes as a general problem-independent GA framework for solving partitioning problems. We adopted a relational encoding which is represented by equivalence relation matrix and has a 1-1 and onto correspondence with the class of all possible partitions. The encoding effectively enhances the performance of genetic search by completely eliminating the redundancy in previous GA representations. We also redesigned a set of generalized problem-independent operators which manipulate the genes without requiring specific heuristics in the process of evolution. Thus, partitioning problems that do not have natural heuristics can also be solved by using this general framework. In addition, it has been demonstrated that our RGA supports a variable number of subsets [3]. It works without requiring a fixed number of subsets in advance if

necessary. As a result, the genetic search becomes more flexible and the search space of RGA becomes more complete.

Experimental results and statistical tests show that our RGA almost dominates over GGA significantly, whether heuristics are involved or not. In addition, we also found that some additional heuristics can guide local search to refine the optimization effectively. However, operators that involve such heuristics can not be generalized, because the heuristics are heavily problem-dependent.

Our future works include applying our RGA to other classic partitioning problems, designing specific heuristics for other partitioning problems, and extending our RGA to solving other types of relation-based problems.

References

[1] Appel, K., Haaken, W.: Every map is four-colourable I: discharging. Illinois J. Math 21, 429–490 (1997)
[2] Brown, E.C., Sumichrast, R.T.: Evaluating performance advantages of grouping genetic algorithms. Engineering Applications of Artificial Intelligence 18, 1–12 (2005)
[3] Chen, J.S., Lin, Y.T.: A Partitioned Portfolio Insurance Strategy by Relational Genetic Algorithm. In: Sattar, A., Kang, B.-H. (eds.) AI 2006. LNCS (LNAI), vol. 4304, pp. 857–866. Springer, Heidelberg (2006)
[4] Chiang, W-C., Kouvelis, P.: An improved tabu search heuristic for solving facility layout design problem. International Journal of Production Research 34(9), 2565–2585 (1996)
[5] Eiben, A.E., van der Hauw, J.K., van Hemert, J.I.: Graph coloring with adaptive evolutionary algorithms. J. Heuristics 4(1), 25–46 (1998)
[6] Falkenauer, E.: The Grouping Genetic Algorithms – Widening The Scope of The GAs. JORBEL?Belgian Journal of Operations Research, Statistics and Computer Science 33(1,2), 79–102 (1992)
[7] Garey, M. R., Johnson, D.S.: Computers and Intractability – A Guide to the Theory of NP-completeness, W.H. Freeman, San Francisco, USA (1979)
[8] Johnson, D., Aragon, C., McGeoch, L., Schevon, C.: Optimization by Simulated Annealing: An Experimental Evaluation; Part II, Graph Coloring and Number Partitioning. Operations Research 39(3), 378–406 (1991)
[9] Jones, D.R., Beltramo, M.A.: Solving partitioning problems with genetic algorithms. In: Belew, K.R., Booker, L.B. (eds.) Proc. 4th Intnl. Conf. on Genetic Algorithms, pp. 442–449. Morgan Kaufmann, San Francisco (1991)
[10] Smith, D.: Bin Packing with Adaptive Search. In: Proceeding of an International Conference on Genetic Algorithms and Their Application, pp. 202–206 (1985)

Constrained Optimization of a Newsboy Problem with Return Policy Using KKT Conditions and GA

P.C. Yang[1], H.M. Wee[2], S.L. Chung[3], and S.H. Kang[1]

[1] Industrial Engineering and Management Department, St. John's University, Tamsui, Taipei 25135, ROC
pcyang@mail.sju.edu.tw
[2] Industrial Engineering Department, Chung Yuan Christian University, Chungli, Taiwan, 32023, ROC
[3] Information Management Department, St. John's University, Tamsui, Taipei, 25135, ROC

Abstract. A newsboy problem model in which a vendor has limited resource is developed. It is assumed that the supplier will either sell the items to the vendor outright or offer the items to the vendor with return policy. In the latter case, the supplier buys back at certain percentage of original cost from the vendor the unsold items at the end of the selling season. The purpose of this study is to investigate how the vendor should replenish the items with return policy, constrained resources and changing procured price. Three numerical examples are provided. In one example with two constrained variables, an optimal solution is derived by using KKT (Karush-Kuhn-Tucker) conditions. The other two multiple variables examples with a minimum service level or a limited budget are solved using GA (genetic algorithm).

1 Introduction

This study investigates a problem with a single purchase opportunity. The vendor has the option of purchasing the item outright and/or obtaining the item with a return-policy agreement. A return policy allows a vendor to return the unsold products for a full or partial refund. This will entice the vendor to order a larger quantity, resulting in an increase in the joint profit. Style goods like dress and catalogue product are examples where return policies are used (Emmons and Gilbert [1]; Mantrala and Raman [2]).

Pasternack [3] modeled a return policy and derived a global optimal single period model with uncertain demand. He demonstrated that a return policy where a manufacturer offers the vendors partial credits for all unsold products could achieve channel coordination. Emmons and Gilbert [1] studied the effect of return policy on both the manufacturer and the vendor. Such policy maximizes the manufacturer's profit by inducing the vendor to place larger order.

The importance of the single period problem increases due to the shorten product life cycle in recent years. Many extensions of the single period problem have been studied [4]. Two major extensions are the unconstrained, single-item single-period problem, and the constrained, multi-item single-period problem. Khouja [5] developed a newsboy model in which multiple discounts are used to sell excess inventory. Khouja

H.G. Okuno and M. Ali (Eds.): IEA/AIE 2007, LNAI 4570, pp. 227–237, 2007.

and Mehrez [6] extended Khouja's model [5] to the multi-item case. This model considers a newsboy problem with multiple items under budget constraint. Lau and Lau [7] derived a capacitated multiple-product single period inventory model. Pasternack [8] developed a capacitated single-item newsboy model with revenue sharing.

GA (genetic algorithm) is a powerful tool to solve the complex-structure problem with many variables. John Holland and his team applied their understanding of the adaptive processes of natural systems to design a software for creating artificial systems that retained the robustness of natural systems (Holland [9]). During the last decade, GA, which is a search technique based on the mechanics of natural selection and natural genetics, has been commonly used to solve global optimization problems. Jinxing and Jiefang [10] studied the application of GA for solving lot-sizing problems. Li et al. [11] demonstrated that GA is effective for dealing with production planning and scheduling problems.

This study considers one item with constrained resources. The vendor has the option of purchasing the goods outright, obtaining the goods with return policy, or a combination of both. Our analysis proposes an optimal inventory policy theorem. We discuss the conditions for obtaining goods through outright purchase, return-policy purchase, and a combination of both. In Section 2, we present a general model for three cases. In Section 3, a numerical example with constrained two variables is given to illustrate the theorem. In Section 4, GA solution procedure is presented. Two numerical examples with multiple variables and constrained resources are followed in Section 5. The concluding remark is given in the last section.

2 Mathematical Modeling and Analysis

The mathematical model is developed based on the following assumptions:

(a) The demand is uncertain with known probability density function.
(b) An item with single order period, short selling season and long production lead-time is considered (an example of this type of product is the catalogue or style product).
(c) A vendor has the option of purchasing the item outright and/or obtaining the item through a return-policy agreement with the supplier.
(d) The products purchased through return policy begin selling only after the outright purchase items are sold out.

The decision variables are:

Q_1 number of units the vendor obtained from the manufacturer through outright purchase
Q_2 number of units the vendor obtained from the manufacturer through return policy
The known parameters are:
$f(x)$ probability density function of uncertain demand x
$F(x)$ cumulative distribution function of the probability density function f(x)
C_1 purchase price through outright purchase
C_2 purchase price through return policy
P unit retail price
S shortage cost per unit if the item is out of stock

R return price per unit if the item is unsold
T total amount of funds the vendor has for obtaining the item through outright purchase, return policy, or both.
SL service level
EP expected profit

The model with outright purchase and return policy is illustrated in Figure 1.

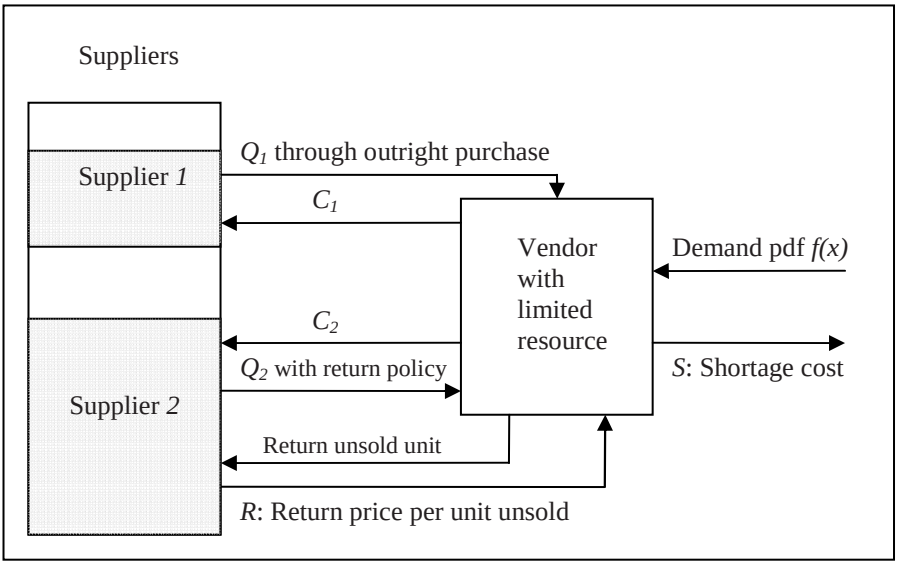

Fig. 1. Representation of this model with outright purchase and return policy

The vendor's expected profit can be expressed as:

$$EP = P[\int_0^{\sum_{i=1}^{2} Q_i} xf(x)dx + \int_{\sum_{i=1}^{2} Q_i}^{\infty} (\sum_{i=1}^{2} Q_i) f(x)dx] + R[\int_0^{Q_1} Q_2 f(x)dx$$

$$+ \int_{Q_1}^{\sum_{i=1}^{2} Q_i} (\sum_{i=1}^{2} Q_i - x) f(x)dx] - S\int_{\sum_{i=1}^{2} Q_i}^{\infty} (x - \sum_{i=1}^{2} Q_i) f(x)dx - \sum_{i=1}^{2} C_i Q_i \qquad (1)$$

The first term in (1) is the expected sales revenue. The second term is the return revenue for the unsold units. The third term is the expected shortage cost and the last term is the purchase costs. The problem is a nonlinear programming with constraints as follows:
Maximize EP

$$\textit{Subject to:} \sum_{i=1}^{2} C_i Q_i \le T\,,\ Q_1 \ge 0 \text{ and } Q_2 \ge 0$$

Taking at the partial second derivatives of *EP*, one has:

$$\frac{\partial^2 EP}{\partial Q_1^2} = -f(Q_1+Q_2)(P+S-R) - Rf(Q_1) \tag{2}$$

$$\frac{\partial^2 EP}{\partial Q_2^2} = -f(Q_1+Q_2)(P+S-R) \tag{3}$$

$$\frac{\partial^2 EP}{\partial Q_1 \partial Q_2} = -f(Q_1+Q_2)(P+S-R) \tag{4}$$

Hence, EP is concave if $P+S-R \geq 0$.

The following KKT conditions are required for optimality:

(a) $u_1(T - C_1Q_1 - C_2Q_2) = 0$
(b) $u_3 Q_2 = 0$
(c) $u_2 Q_1 = 0$
(d) $P+S-C_1(1+u_1)+u_2 - F(Q_1+Q_2)(P+S-R) - F(Q_1)R = 0$
(e) $P+S-C_2(1+u_1)+u_3 - F(Q_1+Q_2)(P+S-R) = 0$
(f) $u_1 \geq 0, u_2 \geq 0, u_3 \geq 0, Q_1 \geq 0, Q_2 \geq 0$

Three cases of solution are discussed. The first case is ($Q_1 > 0$ and Q_2=0). The second case is (Q_1=0 and Q_2>0). The last case is (Q_1>0 and Q_2>0).

Case 1: Q_1>0 and Q_2=0 (i.e., u_2=0, Q_1=T/C_1)

From KKT conditions (d) and (e), one has

$$P+S-C_1(1+u_1) - F(Q_1)(P+S) = 0 \tag{5}$$

and $$P+S-C_2(1+u_1)+u_3 - F(Q_1)(P+S-R) = 0 \tag{6}$$

From (5), one has

$$1+u_1 = \frac{1}{C_1}[P+S-F(Q_1)(P+S)] \geq 1 \tag{7}$$

Then, $$F(T/C_1) \leq (P+S-C_1)/(P+S) \tag{8}$$

Substituting (7) into (6), one has

$$C_1 u_3 = -F(Q_1)[(P+S)(C_2-C_1)+C_1R] + (P+S)(C_2-C_1) \geq 0 \tag{9}$$

If $C_2 < C_1$ and $(P+S)(C_2-C_1)+C_1R < 0$, then

$$F\left(\frac{T}{C_1}\right) \geq \frac{(P+S)(C_2-C_1)}{(P+S)(C_2-C_1)+C_1R} > 1 \text{ (Contradiction)} \tag{10}$$

If $C_2 < C_1$ and $(P+S)(C_2 - C_1) + C_1 R > 0$, then

$$F(\frac{T}{C_1}) \geq \frac{(P+S)(C_2 - C_1)}{(P+S)(C_2 - C_1) + C_1 R} < 0 \text{ (Contradiction)} \tag{11}$$

If $C_2 = C_1$, then

$$C_1 u_3 = -F(Q_1) C_1 R \geq 0 \text{ (Contradiction)} \tag{12}$$

If $C_2 > C_1$, then

$$F(\frac{T}{C_1}) \leq \frac{(P+S)(C_2 - C_1)}{(P+S)(C_2 - C_1) + C_1 R} \tag{13}$$

One can see that conditions (8) and (13) must be satisfied simultaneously for the case of (Q_1>0, Q_2=0).

Case 2: Q_1=0 and Q_2>0 (i.e., u_3=0, Q_2=T/C_2)
Derived from KKT conditions (d) and (e), one has

$$C_2 u_1 = P + S - C_2 - F(Q_2)(P + S - R) \geq 0 \tag{14}$$

and $$C_2 u_2 = (P+S)(C_1 - C_2) - F(Q_2)(C_1 - C_2)(P + S - R) \geq 0 \tag{15}$$

From (14), one has

$$F(\frac{T}{C_2}) \leq \frac{P + S - C_2}{P + S - R}, \text{ where } R < C_2 \tag{16}$$

From (15), if $C_1 \leq C_2$, one has

$$F(\frac{T}{C_2}) \geq \frac{P+S}{P+S-R} > 1 \text{ (Contradiction)} \tag{17}$$

From (15), if $C_1 \geq C_2$, one has

$$F(\frac{T}{C_2}) \leq \frac{P+S}{P+S-R} \tag{18}$$

From (16) and (18), one can see that conditions $C_1 \geq C_2$ and $F(\frac{T}{C_2}) \leq \frac{P+S-C_2}{P+S-R}$ must be satisfied simultaneously for the case of Q_1=0 and Q_2>0.

Case 3: Q_1>0 and Q_2>0 (i.e., $u_2 = 0$, $u_3 = 0$, $C_1 Q_1 + C_2 Q_2 = T$)
From KKT conditions (d) and (e), one has

$$P + S - C_1(1 + u_1) - F(Q_1 + Q_2)(P + S - R) - F(Q_1) R = 0 \tag{19}$$

and $$P + S - C_2(1 + u_1) - F(Q_1 + Q_2)(P + S - R) = 0 \tag{20}$$

The optimal solution of Q_1 and Q_2 must satisfy (19), (20) and $C_1 Q_1 + C_2 Q_2 = T$ simultaneously. If the solution Q_1 is positive, after substituting $(T - C_1 Q_1)/C_2$ into Q_2, the first derivatives of *EP* with respect to Q_1 is greater than zero when Q_1 =0, that is

$$(C_1 - C_2)[F(\frac{T}{C_2})(P + S - R) - (P + S)] > 0 \tag{21}$$

If $C_1 > C_2$, one has

$$F(\frac{T}{C_2}) > \frac{P+S}{P+S-R} > 1 \text{ (Contradiction)} \tag{22}$$

If $C_2 > C_1$, one has

$$F(\frac{T}{C_2}) < \frac{P+S}{P+S-R} \tag{23}$$

If the solution Q_2 is positive, then, after substituting $(T - C_2Q_2)/C_1$ into Q_1, the first derivatives of *EP* with respect to Q_2 is greater than zero when Q_2 =0, that is

$$F(\frac{T}{C_1})[(P+S)(C_2-C_1)+RC_1] - (P+S)(C_2-C_1) > 0 \tag{24}$$

If $C_2 > C_1$, one has

$$F(\frac{T}{C_1}) > \frac{(P+S)((C_2-C_1)}{(P+S)(C_2-C_1)+RC_1} \tag{25}$$

If $C_2 < C_1$ and $(P+S)(C_2-C_1)+RC_1 < 0$, one has

$$F(\frac{T}{C_1}) < \frac{(P+S)(C_2-C_1)}{(P+S)(C_2-C_1)+RC_1} \text{ (Contradiction)} \tag{26}$$

If $C_2 < C_1$ and $(P+S)(C_2-C_1)+RC_1 > 0$, one has

$$F(\frac{T}{C_1}) > \frac{(P+S)(C_2-C_1)}{(P+S)(C_2-C_1)+RC_1} \tag{27}$$

Solution for Q_1>0 and Q_2>0 is located at the intersection of (23) and {(25) or (27)}. One can find that the two conditions $C_2 > C_1$ and $F(\frac{T}{C_1}) > \frac{(P+S)((C_2-C_1)}{(P+S)(C_2-C_1)+RC_1}$ must be satisfied for the case ($Q_1 > 0, Q_2 > 0$).

The theorem resulted from the above discussion can be stated as follows:

THEOREM

For $T = C_1Q_1 + C_2Q_2$ and $P+S-R \geq 0$, one has

(i) $Q_1 > 0$ and $Q_2 = 0$,

if $C_2 > C_1$, $F(\frac{T}{C_1}) \leq \frac{(P+S)(C_2-C_1)}{(P+S)(C_2-C_1)+RC_1}$ and $F(\frac{T}{C_1}) \leq \frac{P+S-C_1}{P+S}$

(ii) $Q_1 = 0$ and $Q_2 > 0$,

if $C_2 \leq C_1$ and $F(\frac{T}{C_2}) \leq \frac{P+S-C_2}{P+S-R}$

(iii) Q_1>0 and Q_2>0,

if $C_2 > C_1$ and $F(\frac{T}{C_1}) > \frac{(P+S)(C_2-C_1)}{(P+S)(C_2-C_1)+RC_1}$

3 Example with Two Variables Subject to a Limited Budget

The preceding theorems are illustrated by the following example.

Example 1

This example illustrates the sensitivity analysis of the purchase price through return policy when the available limited fund is fixed at $T = 4000$. For demand's probability density function $f(x)=U(0,600)$, P= 20, S= 10, R= 6 and C_1= 12, the result of the sensitivity analysis is given in Table 1 and Figure 2. When $C_2 < 6.938$, the inventory fund needed is less than \$4000. Therefore, when C_2 is not greater than C_1 (i.e., $6.938 \le C_2 \le 12$), the optimal strategy is to buy Q_2 only; when C_2 increases slightly (i.e., $12 < C_2 < 15$), the optimal strategy is to buy both Q_1 and Q_2. However, when C_2 increases significantly ($C_2 \ge 15$), it is more economical to buy Q_1 only.

Table 1. Sensitivity analysis of the purchase price subject to $T \le 4000$

C_2	Q_1	Q_2	Remark	THEOREM
<6.94	0	>576	Unlimited budget	THEOREM (ii)
7	0	571	$C_2 \le C_1$, $F(\frac{T}{C_2}) \le \frac{P+S-C_2}{P+S-R}$ (i.e., $6.938 \le C_2 \le 23$)	
9	0	444		
12	0	333		
12.1	14	317	$C_2 > C_1$, $F(\frac{T}{C_1}) > \frac{(P+S)(C_2-C_1)}{(P+S)(C_2-C_1)+RC_1}$ (i.e., $C_2 < 15$)	THEOREM (iii)
13	132	185		
14	245	75		
15	333	0	$C_2 > C_1$, $F(\frac{T}{C_1}) \le \frac{P+S-C_1}{P+S}$ (i.e., $10 \le C_1 \le 20$), $F(\frac{T}{C_1}) \le \frac{(P+S)(C_2-C_1)}{(P+S)(C_2-C_1)+RC_1}$ (i.e., $C_2 \ge 15$)	THEOREM (i)
16	333	0		
17	333	0		
18	333	0		

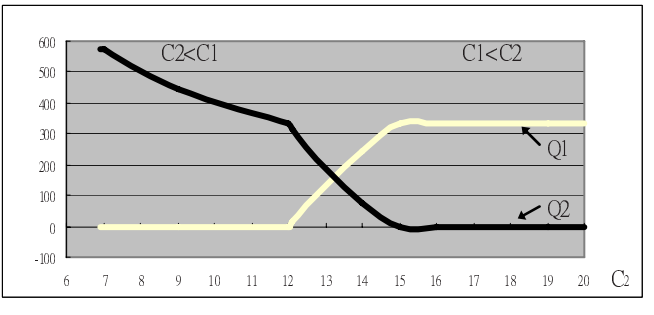

Fig. 2. The relationship between Q_1, Q_2 and C_2 for T=4000, C_1=12

4 GA Solution Procedure

Using a direct analogy to this natural evolution, Genetic algorithm (GA) presumes a potential solution in the form of an individual that can be represented by strings of genes. Throughout the genetic evolution, some fitter chromosomes tend to yield good quality offspring inherit from their parents via reproduction.

This study derives the economic order quantity to maximize the expected profit. The objective function is $EP(Q_1, Q_2 ... Q_n)$ with n decision variables Q_1, Q_2…and Q_n. GA deals with a chromosome of the problem instead of decision variables. The values of Q_1, Q_2…and Q_n can be determined by the following GA procedure:

(a) Representation: Chromosome encoding is the first problem that must be considered in applying GA to solve an optimization problem. Phenotype chromosome could represent a real numbers and an integer numbers here. For each chromosome, real numbers and integer numbers representation are used as follows: $y = (Q_1, Q_2 ... Q_n)$

(b) Initialization: Generate a random population of chromosomes (which are suitable solutions for the problem)

(c) Evaluation: Assess the fitness g(y) of each chromosome y in the population. The fitness value $g_k = g(y_k) = EP(Q_k)$ where $k= 1, 2…n$

(d) Selection schemes: Select two parent chromosomes from a population based on their fitness using a roulette wheel selection technique, thus ensuring high quality individuals which have a higher chance of becoming parents than low quality individuals.

(e) Crossover: Approximately 50%-75% crossover probability exists, indicating the probability that the parents will cross over to form new offspring. If no crossover occurs, the offspring are an exact copy of the parents.

(f) Mutation: About 0.5%-1.0% of population mutation rate mutate new offspring at each locus (position in the chromosome). Accordingly, the offspring might have genetic material information not inherited from either parent, thus avoiding falling into the local optimum.

(g) Replacement: An elitist strategy and a steady-state evolution are used to generate a new population, which can be used for an additional algorithm run.

(h) Termination: If the number of generations exceeds 300, then stop.

5 Examples with Multiple Variables Subject to a Limited Budget or a Minimum Service Level

Example 2

There are four suppliers which offer the same item with different prices. Supplier 1 offers outright price, supplier 2 through 4 offers prices with different return policy. With the same parameters as Example 1 except purchase price C_i and return price R_i (see Table 2), derive Q_i to optimize the expected profit subject to a limited budget $T \leq 4000$.

The expected profit function with multiple variables is shown in Appendix A. Using GA, the evolutionary result is given in Table 2. When the purchase price with return policy is greater than the outright purchase over a certain threshold value, purchase Q_1

only. When the purchase price with return policy is less than the outright purchase, purchase Q_2 or/and Q_3, or/and Q_4. When the purchase price with return policy is greater than outright purchase below a certain threshold value, Q_1 through Q_4 may be purchased simultaneously.

Example 3

Supplier 1 offers outright price, supplier 2 through 4 offers prices with different return policy. With the same parameters as Example 1 except purchase price C_i and return price R_i (see Table 3), derive Q_i to optimize expected profit subject to a minimum service level 0.6. The service level is defined as the percentage units demanded that will be satisfied.

The expected profit function with multiple variables is shown in Appendix A. Using GA, the evolutionary result is given in Table 3. When the purchase price with return policy is greater than the outright purchase over a certain threshold value, purchase Q_1 only, a budget of $4,320 is needed and the service level is 0.600. When the purchase price with return policy is less than the outright purchase, purchase Q_2 or/and Q_3, or/and Q_4 except Q_1, a budget of $4,397 is needed and the optimal service level is 0.830. When

Table 2. Optimization with multiple variables subject to budget $T \leq 4000$

Various purchases	Purchase with outright	Purchase with various return policies		
i	*i*= 1	*i*= 2	*i*= 3	*i*= 4
Supplier *i*	Supplier *1*	Supplier *2*	Supplier *3*	Supplier *4*
Known C_i	12	15	16	17
Known R_i	0	2	4	6
Variable Q_i	333	0	0	0
Known C_i	12	8	9	10
Known R_i	0	2	4	6
Variable Q_i	0	338	0	129
Known C_i	12	12.1	12.4	12.8
Known R_i	0	2	4	6
Variable Q_i	40	80	40	160

Table 3. Optimization with multiple variables subject to service level ≥ 0.6

Various purchase	Purchase with outright	Purchase with various return policies			Budget T needed; Service Level
i	*i*= 1	*i*= 2	*i*= 3	*i*= 4	
Supplier *i*	Supplier *1*	Supplier *2*	Supplier *3*	Supplier *4*	
Known C_i	12	15	16	17	*T*= 4320
Known R_i	0	2	4	6	*SL*= 0.600
Variable Q_i	360	0	0	0	
Known C_i	12	8	9	10	*T*= 4400
Known R_i	0	2	4	6	*SL*= 0.833
Variable Q_i	0	300	0	200	
Known C_i	12	12.1	12.4	12.8	*T*= 5426
Known R_i	0	2	4	6	*SL*= 0.717
Variable Q_i	30	60	30	310	

the purchase price with return policy is greater than outright purchase below a certain threshold value, Q_1 through Q_4 may be purchased simultaneously, a budget of $4,730 is needed and the optimal service level is 0.625.

6 Concluding Remark

This study analyzes the vendor's replenishment strategy using a newsboy problem model with constraints. We show that there exists a set of conditions under which the vendor's optimal strategy will change based on the amount of available resources for product procurement. If the purchase price with return policy is greater than the price of outright purchase and the vendor has a small amount of available budget, only outright purchase will be optimal. However, if the resource reaches a certain threshold amount, mixed strategies where items are obtained by outright purchase and return policy are used. We also show that when the purchase price with return policy is not greater than the outright purchase, the vendor will only obtain the items with return policy.

When the available resource is fixed, three conditions to obtain the optimal strategies are derived. The first condition is when the purchase price with return policy is not greater than the price with outright purchase; it is better to buy the items with return policy only. The second condition is when the purchase price with return policy is greater than the price of outright purchase over a certain threshold value; it is better to choose outright purchase only. The last condition is when the purchase price with return policy is between the two conditions, it is better to choose a mixture of items with outright purchase and return policy.

When the number of variables is less, it is easy to derive the constrained newsboy problem by Lagrange multipliers, KKT conditions and other mathematical methods. When the number of variables increases with the degree of complexity in a real business environment, GA can be used to solve these problems.

References

1. Emmons, H., Gilbert, S.M.: The role of returns policies in pricing and inventory decisions for catalogue goods. Management Science 44(2), 277–283 (1998)
2. Mantrala, M.K., Raman, K.: Demand uncertainty and supplier's returns policies for a multi-store style-good retailer. European Journal of Operational Research 115, 270–284 (1999)
3. Pasternack, B.A.: Optimal pricing and return policies for perishable commodities. Marketing Science 4(2), 166–176 (1985)
4. Khouja, M.: The single-period (news-vendor) problem: literature review and suggestions for future research. The International Journal of Management Science 27, 537–553 (1999)
5. Khouja, M.: The newsboy problem under progressive multiple discounts. European Journal of Operational Research 84, 458–466 (1995)
6. Khouja, M., Mehrez, A.: A multi-product constrained newsboy problem with progressive multiple discounts. Computers & Industrial Engineering 30, 95–101 (1996)
7. Lau, H.-S., Lau, A.H.-L.: The newsstand problem: A capacitated multi-product single-period inventory problem. European Journal of Operational Research 94, 29–42 (1996)

8. Pasternack, B.A.: The capacitated newsboy problem with revenue sharing. Journal of Applied Mathematics and Decision Sciences 5(10), 21–33 (2001)
9. Holland, J.H.: Adaptation in Natural and Artificial Systems. University of Michigan Press, Ann Arbor (1975)
10. Jinxing, X., Jiefang, D.: Heuristic genetic algorithm for general capacitated lot-sizing problems. Computers and Mathematics with Applications 44, 263–276 (2002)
11. Li, Y., Man, K.F., Tang, K.S.: Genetic algorithm to production planning and scheduling problems for manufacturing systems. Production Planning & Control 11(5), 443–458 (2000)

Appendix A. Expected profit function for Example 3 and 4

$$
\begin{aligned}
EP = P[&\int_0^{\sum_{i=0}^{4} Q_i} xf(x)dx + \int_{\sum_{i=0}^{4} Q_i}^{\infty} (\sum_{i=0}^{4} Q_i) f(x)dx] + \int_0^{Q_1} (\sum_{i=2}^{4} Q_i R_i) f(x)dx \\
&+ \int_{Q_1}^{\sum_{i=1}^{2} Q_i} [R_2(\sum_{i=1}^{2} Q_i - x) + \sum_{i=3}^{4} Q_i R_i] f(x)dx + \int_{\sum_{i=1}^{2} Q_i}^{\sum_{i=1}^{3} Q_i} [R_3(\sum_{i=1}^{3} Q_i - x) + R_4 Q_4] f(x)dx \\
&+ \int_{\sum_{i=1}^{3} Q_i}^{\sum_{i=1}^{4} Q_i} R_4(\sum_{i=1}^{4} Q_i - x) f(x)dx - S\int_{\sum_{i=1}^{4} Q_i}^{\infty} (x - \sum_{i=1}^{4} Q_i) f(x)dx - \sum_{i=1}^{4} C_i Q_i
\end{aligned}
\tag{A1}
$$

Fuzzy Interpolative Reasoning Via Cutting and Transformations Techniques

Yaun-Kai Ko and Shyi-Ming Chen

Department of Computer Science and Information Engineering
National Taiwan University of Science and Technology
Taipei, Taiwan, R.O.C.
smchen@mail.ntust.edu.tw

Abstract. Fuzzy interpolative reasoning techniques can reduce the complexity of a sparse fuzzy rule-based system. In this paper, we present a new fuzzy interpolative reasoning method via cutting and transformations techniques for sparse fuzzy rule-based systems. It produces more reasonable reasoning consequences than the ones presented in [1] and [3]. The proposed method provides a useful way to deal with fuzzy interpolative reasoning in sparse fuzzy rule-based systems.

Keywords: Fuzzy interpolative reasoning, cutting and transformation techniques, increment and ratio transformations, sparse fuzzy rule-based systems.

1 Introduction

In sparse fuzzy rule-based systems, their fuzzy rule bases are usually incomplete. In this situation, the systems may not properly perform fuzzy reasoning to get reasonable conclusions. In order to overcome the drawback of sparse fuzzy rule-based systems, Koczy and Hirota presented linear interpolative reasoning techniques [3] and [4]. However, in [9] and [11], Yan et al. pointed out that Koczy-and-Hirota's method has the drawback that sometimes it gets non-convex fuzzy interpolative reasoning consequences.

In recent years, some methods [1], [2], [7], [10] have been presented to overcome the drawback of Koczy-and-Hirota's method. In [1], Hsiao presented a fuzzy interpolative reasoning method for sparse fuzzy rule-based systems based on the slope of the fuzzy sets. In [7], Huang and Shen presented a fuzzy interpolative reasoning method via scale and move transformation techniques. It can deal with complex fuzzy sets, such as trapezoidal, hexagon, polygonal and Gaussian fuzzy sets.

In this paper, we present a new fuzzy interpolative reasoning method for sparse fuzzy rule-based systems via cutting and transformations techniques. The proposed method uses the cutting of geometric membership functions and incremental and ratio transformations for dealing with fuzzy interpolative reasoning. It produces more reasonable reasoning consequences than the methods presented in [1] and [3]. The proposed method provides a useful way to deal with fuzzy interpolative reasoning in sparse fuzzy rule-based systems.

H.G. Okuno and M. Ali (Eds.): IEA/AIE 2007, LNAI 4570, pp. 238–249, 2007.

The rest of this paper is organized as follows. In Section 2, we present a new fuzzy interpolative reasoning method for sparse fuzzy rule-based systems. In Section 3, we make a comparison of the experimental results of the proposed method with the ones of the existing methods. The conclusions are discussed in Section 4.

2 A New Fuzzy Interpolative Reasoning Method for Sparse Fuzzy Rule-Based Systems

In this section, we present a new fuzzy interpolative reasoning method for sparse fuzzy rule-based systems via cutting and transformations techniques. First, we present the definitions of normal fuzzy sets.

***Definition 2.1*:** Let A be a normal fuzzy set in the universe of discourse X. The collection of highest points of the fuzzy set A, denoted as $hst\{A\}$, is defined as follows:

$$hst\{A\} = \{x \mid \mu_A(x) = 1, x \in X\}. \tag{1}$$

***Definition 2.2*:** Let the minimal element in $hst\{A\}$ be denoted as $ihst\{A\}$ and the maximum element in $hst\{A\}$ be denoted as $shst\{A\}$, where

$$ihst\{A\} = inf\{hst\{A\}\}, \tag{2}$$

$$shst\{A\} = sup\{hst\{A\}\}. \tag{3}$$

2.1 Single Antecedent Variable with Trapezoidal Fuzzy Sets

In the following, we present the new fuzzy interpolative reasoning techniques with normal trapezoidal fuzzy sets. For a normal trapezoidal fuzzy set A, we let its four points be defined as $inf\{A\}$, $ihst\{A\}$, $shst\{A\}$ and $sup\{A\}$, i.e., $A = (inf\{A\}, ihst\{A\}, shst\{A\}, sup\{A\})$. Fig. 1 shows a trapezoidal fuzzy set A, $A = (a_0, a_1, a_2, a_3)$, where a_1 and a_2 are called the "top points", a_0 is called the "minimum-bottom-point", and a_3 is called the "maximum-bottom-point".

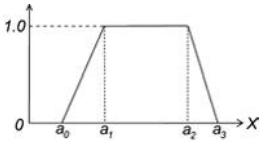

Fig. 1. A trapezoidal fuzzy set

The "*representative value*" of a trapezoidal membership function is defined as the average of its four points. That is, the representative value *Rep(A)* of the fuzzy set A shown in Fig. 1 is calculated as follows [2]:

$$Rep(A) = (a_0 + a_1 + a_2 + a_3)/4. \tag{4}$$

Assume that there are two adjacent fuzzy rules $A_1 => B_1$ and $A_2 => B_2$ and assume that the observation A^* which is located between the fuzzy sets A_1 and A_2 is given. The

following fuzzy interpolative reasoning scheme concerning two linguistic variables X and Y can be described through the modus ponens interpretation, as illustrated in Fig. 2:

Observation: X is A^*
Rules: If X is A_1, then Y is B_1
If X is A_2, then Y is B_2
Conclusion: Y is B^*

where $A_i = (a_{i0}, a_{i1}, a_{i2}, a_{i3})$, $B_i = (b_{i0}, b_{i1}, b_{i2}, b_{i3})$, $1 \le i \le 2$, $A^* = (a_0, a_1, a_2, a_3)$, and $B^* = (b_0, b_1, b_2, b_3)$.

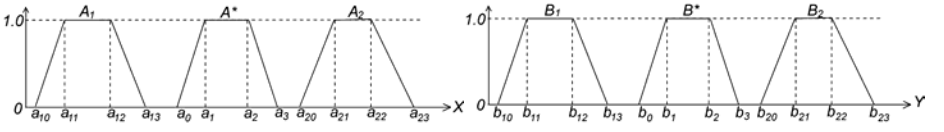

Fig. 2. Fuzzy interpolation with trapezoidal membership functions

The first step of the proposed fuzzy interpolative reasoning method is to find the two top points b_1 and b_2 shown in Fig. 2, respectively. According to the proportion of the positions of representative values, we can get the positions of the points b_1 and b_2 of the fuzzy set B^* shown in Fig. 2, respectively, where $b_1 = ihst\{B^*\}$ and $b_2 = shst\{B^*\}$. The definitions of λ_{a_1} and λ_{a_2} are defined as follows:

$$\lambda_{a_1} = d(A_1, a_1) / d(A_1, A_2) = d(Rep(A_1), a_1) / d(Rep(A_1), Rep(A_2)), \tag{5}$$

$$\lambda_{a_2} = d(A, a_2) / d(A_1, A_2) = d(Rep(A_1), a_2) / d(Rep(A_1), Rep(A_2)), \tag{6}$$

where $d(X, Y) = d(Rep(X), Rep(Y))$ represents the distance between the fuzzy sets X and Y. Therefore, b_1 and b_2 of B^* shown in Fig. 2 are calculated as follows:

$$b_1 = ihst\{B^*\} = (1 - \lambda_{a_1}) \times Rep(B_1) + Rep(B_2) \times \lambda_{a_1}, \tag{7}$$

$$b_2 = shst\{B^*\} = (1 - \lambda_{a_2}) \times Rep(B_1) + Rep(B_2) \times \lambda_{a_2}, \tag{8}$$

where $Rep(B_i) = (b_{i0}+b_{i1}+b_{i2}+b_{i3})/4$ and $1 \le i \le 2$.

The next step of the proposed fuzzy interpolative reasoning method is to find the points b_0 and b_3 of the fuzzy set B^* shown in Fig. 2, respectively, by comparing the two right-angled triangles of every fuzzy set, as shown in Fig. 3.

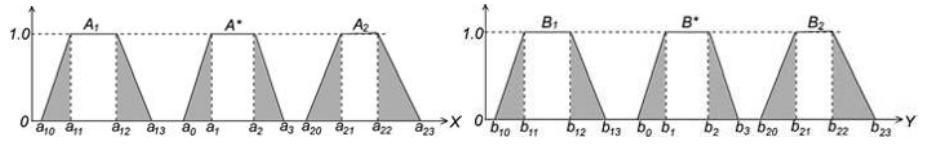

Fig. 3. Right-angled triangles of trapezoidal fuzzy sets

Because the height of the right-angled triangle of each fuzzy set is the same, we only use its leg's length for comparison. Every fuzzy set has two right-angled triangles, so we only focus on the left right-angled triangles. Let

$$\lambda_{rep} = d(A_1, A^*) / d(A_1, A_2) = d(Rep(A_1), Rep(A^*)) / d(Rep(A_1), Rep(A_2)). \quad (9)$$

Let l_{a_i} denote the length between a_{i0} and a_{i1} shown in Fig. 3, where $1 \le i \le 2$. Let l_a denote the length between a_0 and a_1 shown in Fig. 3. Then, l_a' is calculated as follows:

$$l_a' = (1 - \lambda_{rep}) \times l_{a_1} + \lambda_{rep} \times l_{a_2}. \quad (10)$$

Let

$$a_0' = a_1 - l_a'. \quad (11)$$

By computing l_a', we can get an average fuzzy set A' from A_1 and A_2, as shown in Fig. 4. By considering the degree of similarity between A^* and A', it is intuitive that we can infer the consequence B^* by the same degree of similarity between B^* and B'. Finally, we transform B' into B^*. In this paper, two transformations are proposed, i.e., the increment transformations and the ratio transformations, described as follows.

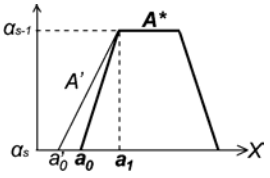

Fig. 4. A comparison of the fuzzy set A' obtained from A_1 and A_2 with the fuzzy set A^*

(1) ***Increment transformations:*** When l_a is greater than or equal to l_a', we use this kind of transformation, as shown in Fig. 5(a). Let L be the increment length, where

$$L = l_a - l_a'. \quad (12)$$

The next step is to compute the average fuzzy set B' from the fuzzy sets B_1 and B_2. Let l_{b_i} denote the length between b_{i0} and b_{i1}, where $1 \le i \le 2$. Let l_b' denote the length between b_0' and b_1'. Then, we can calculate the length l_b', which forms the new fuzzy set B', where

$$l_b' = (1 - \lambda_{rep}) \times l_{b_1} + \lambda_{rep} \times l_{b_2}, \quad (13)$$

$$b_0' = b_1 - l_b'. \quad (14)$$

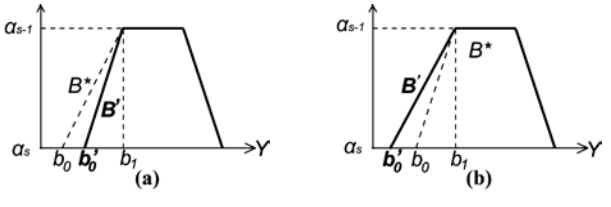

Fig. 5. New average fuzzy set B' obtained from B_1 and B_2 is used to infer the fuzzy set B^* by increment transformations (left figure) and ratio transformations (right figure)

Finally, we can get l_b by using L and l_b'. From l_b, we can calculate the point b_0 and get the fuzzy set B*, where

$$l_b = L + l_{b_1}', \tag{15}$$

$$inf\{B^*\} = b_0 = b_1 - l_b. \tag{16}$$

(2) ***Ratio transformations:*** When l_a is smaller than l_a', we use this kind of transformation, as shown in Fig. 5(b). Let γ be the ratio rate, where

$$\gamma = l_a / l_a'. \tag{17}$$

The next step is to compute the average fuzzy set B' from the fuzzy sets B_1 and B_2. Let l_{b_i} denote the length between b_{i0} and b_i, where $1 \le i \le 2$. Let l_b' to represent the length between b_0' and b_1'. Then, we can calculate the length l_b', which forms the new fuzzy set B', where

$$l_b' = (1 - \lambda_{rep}) \times l_{b_1} + \lambda_{rep} \times l_{b_2}, \tag{18}$$

$$b_0' = b_1 - l_b'. \tag{19}$$

Finally, we get l_b by using γ and l_b'. From l_b, we can calculate the point b_0 and get the fuzzy set B*, where

$$l_b = \gamma \times l_b', \tag{20}$$

$$inf\{B^*\} = b_0 = b_1 - l_b. \tag{21}$$

In the same way, the right right-angled triangle of the fuzzy set B* is calculated by the same method. Finally, we can get the completed trapezoidal fuzzy set.

***Theorem 2.1*:** The consequence fuzzy set of the proposed method is always convex.

***Proof*:** The fuzzy set that is convex means that $l_b \ge 0$.

(1) When $l_a \ge l_a'$, we can see that $L = (l_a - l_a') \ge 0$. Because B_1 and B_2 are convex (i.e. $l_{b_1} \ge 0$, $l_{b_2} \ge 0$) and $1 \ge \lambda_{rep} \ge 0$, we can see that $l_b' = (1 - \lambda_{rep}) \times l_{b_1} + \lambda_{rep} \times l_{b_2} \ge 0$. Thus, we can see that $l_b = L + l_{b_1}' \ge 0$.

(2) When $l_a < l_a'$, we can see that $0 \le \gamma = (l_a / l_a') < 1$. Because B_1 and B_2 are convex (i.e. $l_{b_1} \ge 0$, $l_{b_2} \ge 0$) and $1 \ge \lambda_{rep} \ge 0$, we can see that $l_b' = (1 - \lambda_{rep}) \times l_{b_1} + \lambda_{rep} \times l_{b_2} \ge 0$. Thus, we can see that $l_b = \gamma \times l_b' \ge 0$.

Therefore, the consequence fuzzy set of the proposed method is always convex.

(Q. E. D.)

2.2 Single Antecedent Variable with Triangular Fuzzy Sets

A triangular fuzzy set is a special case of trapezoidal fuzzy sets. Fig. 6 shows the membership functions of the fuzzy interpolative reasoning scheme.

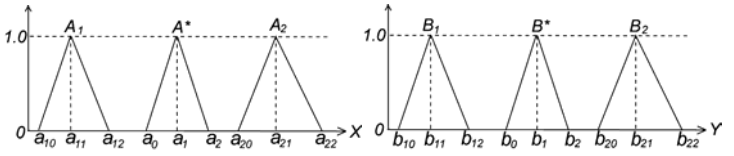

Fig. 6. Fuzzy interpolation with triangular membership functions

The representative value *Rep(A)* of the triangular fuzzy set *A* is shown as follows [2]:

$$Rep(A) = (a_0 + a_1 + a_2)/3 . \tag{22}$$

The first step of the proposed fuzzy interpolative reasoning method is to find the top point *hst*{*B**} of the triangular fuzzy set *B** (i.e., b_1 shown in Fig. 6). According to the proportion of the positions of the representative values, we can get the top point b_1 of the fuzzy set *B**. Let

$$\lambda_{a_1} = d(A_1, a_1)/d(A_1, A_2) = d(Rep(A_1), a_1)/d(Rep(A_1), Rep(A_2)), \tag{23}$$

where $d(A_1, A_2) = d(Rep(A_1), Rep(A_2))$ represents the distance between the fuzzy sets A_1 and A_2. By using the value of λ_{a_1}, we can see that b_1 of *B** is calculated as follows:

$$b_1 = hst\{B^*\} = (1 - \lambda_{a_1}) \times Rep(B_1) + Rep(B_2) \times \lambda_{a_1} , \tag{24}$$

where $Rep(B_i) = (b_{i0} + b_{i1} + b_{i2})/3$.

The next step of the proposed method is to find the bottom points $b_0 = inf\{B^*\}$ and $b_2 = sup\{B^*\}$ of the fuzzy set *B**, respectively, by comparing the two right-angled triangles of every fuzzy set. This step is the same as the situation of trapezoidal fuzzy sets, described in Section 2.1.

2.3 Single Antecedent Variable with Polygon Fuzzy Sets

The complex polygon fuzzy sets shown in Fig. 7 can be dealt with by doing α-cuts at all the turning points. The step divides the polygon into many trapezoids or triangles. Fig. 7 shows the α_1-cuts, the α_2-cuts, …, and the α_m-cuts of the fuzzy sets A_1, *A**, A_2, B_1, *B** and B_2, respectively.

The *"representative value"* of a polygon membership function is defined as the average of the coordinates of its *n* points. Assume that *A* is a polygon fuzzy set, where $A = (a_0, a_1, \cdots, a_{n-2}, a_{n-1})$. The representative value *Rep(A)* of the fuzzy set *A* is defined as follows [2]:

$$Rep(A) = (a_0 + a_1 + \cdots + a_{n-2} + a_{n-1})/n . \tag{25}$$

The first step of the proposed method is to find the two points b_{p-1} and b_p of the polygon fuzzy set *B** shown in Fig. 7, respectively. According to the proportion of the position of the representative value, we can get the points b_{p-1} and b_p of the α_1-cut of the fuzzy set *B**, respectively. Let

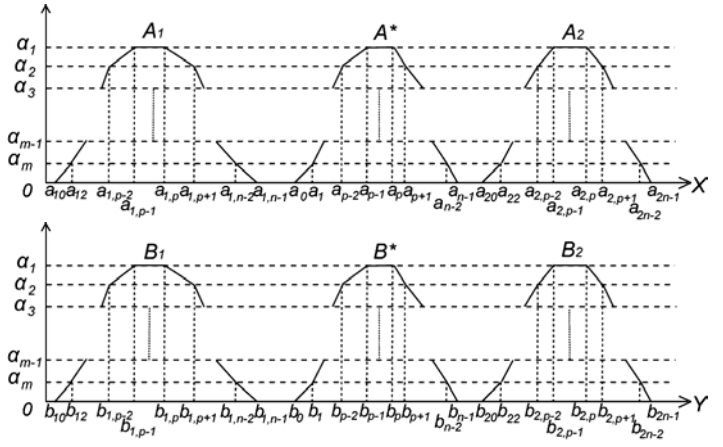

Fig. 7. Fuzzy interpolating reasoning with polygon membership functions

$$\lambda_{ihst} = d(A_1, ihst\{A^*\}) / d(A_1, A_2)$$
$$= d(Rep(A_1), ihst\{A^*\}) / d(Rep(A_1), Rep(A_2)), \tag{26}$$

$$\lambda_{shst} = d(A_1, shst\{A^*\}) / d(A_1, A_2)$$
$$= d(Rep(A_1), shst\{A^*\}) / d(Rep(A_1), Rep(A_2)), \tag{27}$$

where $d(X, Y) = d(Rep(X), Rep(Y))$ represents the distance between two fuzzy sets X and Y. Then, b_{p-1} and b_p of the α_1-cut of B^* are calculated as follows:

$$b_{p-1} = ihst\{B^*\} = (1 - \lambda_{ihst}) \times Rep(B_1) + Rep(B_2) \times \lambda_{ihst}, \tag{28}$$

$$b_p = shst\{B^*\} = (1 - \lambda_{shst}) \times Rep(B_1) + Rep(B_2) \times \lambda_{hst}. \tag{29}$$

where $Rep(B_i) = (b_{i,0}, b_{i,1}, \cdots, b_{i,n-2}, b_{i,n-1})$ and $1 \le i \le 2$.

After finding the points b_{p-1} and b_p of the α_1-cut of B^*, we can calculate the α_2-cut of B^*, where $B^*_{\alpha_2} = \{y \mid \mu_{B^*}(y) \ge \alpha_2, y \in Y\} = [b_{p-2}, b_{p+1}]$ and $0 < p < n - 1$. Let (a_0, a_1, a_2, a_3), $(a_{i0}, a_{i1}, a_{i2}, a_{i3})$, (b_0, b_1, b_2, b_3) and $(b_{i0}, b_{i1}, b_{i2}, b_{i3})$ denote $(a_{p-2}, a_{p-1}, a_p, a_{p+1})$, $(a_{i,p-2}, a_{i,p-1}, a_{i,p}, a_{i,p+1})$,$(b_{p-2}, b_{p-1}, b_p, b_{p+1})$ and $(b_{i,p-2}, b_{i,p-1}, b_{i,p}, b_{i,p+1})$ shown in Fig. 3, respectively, where $1 \le i \le 2$. According to the ratio and increment transformations described in Section 2.1, we can get the points b_{p-2} and b_{p+1}, respectively. In the same way, we can get the α_3-cut, …, the α_m-cut and the 0-cut of B^*, respectively, where $B^*_{\alpha_3} = \{y \mid \mu_{B^*}(y) \ge \alpha_3, y \in Y\} = [b_{p-3}, b_{p+2}]$, …, $B^*_{\alpha_m} = \{y \mid \mu_{B^*}(y) \ge \alpha_m, y \in Y\} = [b_{12}, b_{n-2}]$ and $B^*_0 = \{y \mid \mu_{B^*}(y) \ge 0, y \in Y\} = [b_0, b_{n-1}]$.

Consider the situation that two fuzzy rules $A_1 \Rightarrow B_1$, $A_2 \Rightarrow B_2$ and the observation are represented by Gaussian fuzzy sets, as shown in Fig. 8, where $P(x) = e^{-(x-c)^2/2\sigma^2}$ and $\boldsymbol{c}$ and σ are the mean and the standard deviation, respectively.

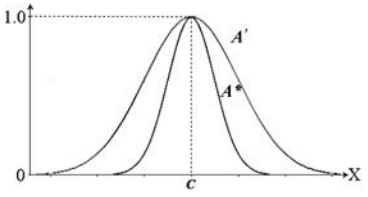

Fig. 8. Fuzzy interpolation with Gaussian membership functions

The construction of the intermediate rule is slightly different from the situation of using polygonal fuzzy membership functions in the sense that the standard deviations are used to deal with the interpolation. Since the Gaussian membership function is symmetrical, ***c*** is chosen to be the representative value of such a fuzzy set. Thus, $Rep(A_i) = c_{A_i}$, $Rep(B_i) = c_{B_i}$, $Rep(A^*) = c_{A^*}$, $Rep(B^*) = c_{B^*}$, and $1 \le i \le 2$. Let

$$\lambda_{rep} = \frac{d(A_1, A^*)}{d(A_1, A_2)} = \frac{d(Rep(A_1), Rep(A^*))}{d(Rep(A_1), Rep(A_2))} = \frac{c_{A^*} - c_{A_1}}{c_{A_2} - c_{A_1}}, \tag{30}$$

$$c_{B^*} = (1 - \lambda_{rep}) \times Rep(B_1) + d(Rep(B_2)) \times \lambda_{rep} = (1 - \lambda_{rep}) \times c_{B_1} + \lambda_{rep} \times c_{B_2}. \tag{31}$$

The leg length of the right-angled triangle is replaced with the standard deviation, where

$$\sigma_{A'} = (1 - \lambda_{rep}) \times \sigma_{A_1} + \lambda_{rep} \times \sigma_{A_2}, \tag{32}$$

$$\sigma_{B'} = (1 - \lambda_{rep}) \times \sigma_{B_1} + \lambda_{rep} \times \sigma_{B_2}. \tag{33}$$

(1) ***Increment Transformations****:* When σ_{A^*} is greater than or equal to $\sigma_{A'}$, we use this kind of transformation. Let *L* be the increment quantity, where

$$L = \sigma_{A^*} - \sigma_{A'}. \tag{34}$$

Then, we let

$$\sigma_{B^*} = L + \sigma_{B'}. \tag{35}$$

(2) ***Ratio* T*ransformations****:* When σ_{A^*} is smaller than $\sigma_{A'}$, we use this kind of transformation. Let γ be the ratio rate, where

$$\gamma = \sigma_{A^*} / \sigma_{A'}. \tag{36}$$

Then, we let

$$\sigma_{B^*} = \gamma * \sigma_{B'}. \tag{37}$$

3 Experimental Results

In this section, we use the examples shown in [1], [3] and [7] to compare the fuzzy interpolative reasoning result of the proposed method with the existing methods.

***Example* 3.1 [7]:** This example only considers triangular fuzzy sets, where $A^* = (7, 8, 9)$ and all the conditions and the fuzzy interpolative reasoning results are shown in Table 1 and Fig. 9. Let $B^* = (b_0, b_1, b_2)$. First, according to Eqs. (23) and (24), b_1 is calculated by the interpolation of A_1, A_2, B_1 and B_2, where $b_1 = hst\{B^*\} = 6.31$. According to Eqs. (9) and (10), we can see that l_a is smaller than l_a' at the left right-angled triangle. Thus, the proposed method uses the ratio transformations to get $b_0 = inf\{B^*\} = 5.81$. By the same method, we can see that l_a is larger than l_a' at the right right-angled triangle. Thus, the proposed method uses increment transformations to get $b_2 = sup\{B^*\} = 8.31$. Therefore, the proposed method gets the fuzzy interpolative reasoning consequence $B^* = (5.81, 6.31, 8.31)$. From Fig. 9, we can see that the KH method [3] gets a nonconvex conclusion. We also can see that the proposed method, the HCL method [1] and the HS method [7] get normal and convex fuzzy sets.

Table 1. Fuzzy interpolative reasoning results for Example 3.1 with $A^* = (7, 8, 9)$

Attribute Values	Results	
$A_1 = (0, 5, 6)$	Methods	B^*
$A_2 = (11, 13, 14)$	KH Method [3]	(6.36, 5.38, 7.38)
$B_1 = (0, 2, 4)$	HCL Method [1]	(6.36, 6.58, 7.38)
$B_2 = (10, 11, 13)$	HS Method [7]	(5.83, 6.26, 7.38)
	The Proposed Method	(5.81, 6.31, 8.31)

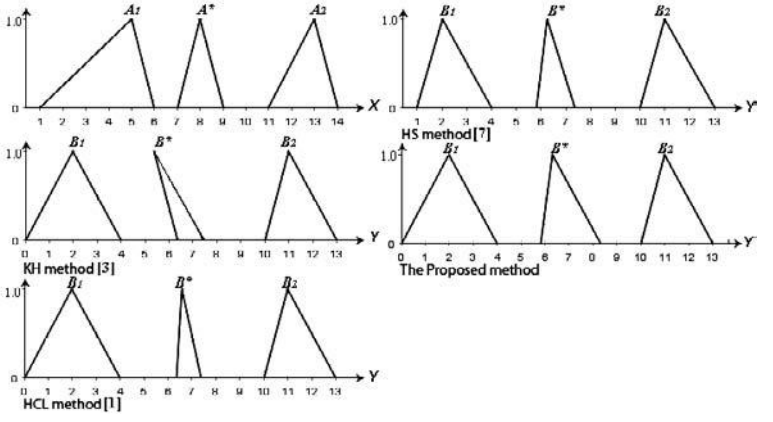

Fig. 9. A comparison of the fuzzy interpolative reasoning results of Example 3.1 for different methods

***Example* 3.2 [7]:** This example considers the situation that the antecedents are crisp sets, where the given observation is a triangular fuzzy set (5, 6, 8). Table 2 and Fig. 10 show the antecedents and the interpolated fuzzy sets, where $A^* = (5, 6, 8)$. Let $B^* = (b_0, b_1, b_2)$. Based on Eqs. (23) and (24), b_1 is calculated by the fuzzy interpolation of A_1 , A_2, B_1 and B_2 where $b_1 = hst\{B^*\} = 6.44$. Based on Eqs. (9) and (10), we can see that l_a is larger than l_a' at the left right-angled triangle. The proposed method uses the increment transformations and gets $b_0 = inf\{B^*\} = 5.07$. In the same way, we can see that l_a is larger than l_a' at the right right-angled triangle. The proposed method uses the

ratio transformations and gets $b_2 = sup\{B^*\} = 9.18$. Finally, the method gets the consequence $B^* = (5.07, 6.44, 9.18)$. From Table 2, we also can see that the HCL method [1] can not deal with this situation due to the fact that the slopes of the antecedent fuzzy sets do not exist.

Table 2. Fuzzy interpolative reasoning results for Example 3.2 with $A^* = (5, 6, 8)$

Attribute Values	Results	
$A_1 = (3, 3, 3)$	Methods	B^*
$A_2 = (12, 12, 12)$	KH Method [3]	(5.33, 6.33, 9.00)
$B_1 = (4, 4, 4)$	HCL Method [1]	-
$B_2 = (10, 11, 13)$	HS Method [7]	(5.71, 6.28, 8.16)
	The Proposed Method	(5.07, 6.44, 9.18)

Note:"-" denotes that the method can not deal with this situation.

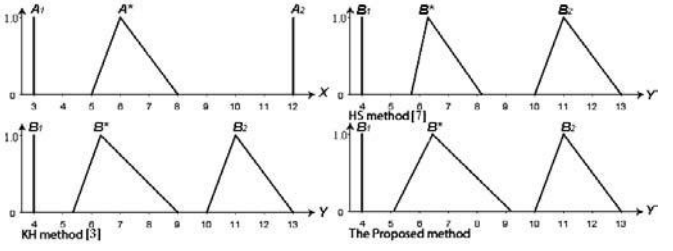

Fig. 10. A comparison of the fuzzy interpolative reasoning results of Example 3.2 for different methods

Example* 3.3 [7]*: This example considers the fuzzy interpolative reasoning using trapezoidal fuzzy sets, where all the conditions and the fuzzy interpolative reasoning results for the different methods are shown in Table 3 and Fig. 11, where $A^* = (6, 6, 9, 10)$. Let $B^* = (b_0, b_1, b_2, b_3)$. According to (5)-(8), b_1 and b_2 are calculated by the interpolation of A_1, A_2, B_1 and B_2. Then, we can get $b_1 = ihst\{B^*\} = 4.68$ and $b_2 = shst\{B^*\} = 7.83$. According to Eqs. (9) and (10), we can see that l_a is smaller than l_a' at the left right-angled triangle. The proposed method uses the ratio transformations and gets $b_0 = inf\{B^*\} = 4.68$. In the same way, we can see that l_a is equal to l_a' at the right right-angled triangle. The proposed method uses the increment transformations and gets $b_4 = sup\{B^*\} = 8.83$. Therefore, the proposed method gets the fuzzy interpolative reasoning result $B^* = (4.68, 4.68, 7.83, 8.83)$. From Table 3, we also see that the HCL method [1] can not deal with this situation.

Table 3. Fuzzy interpolative reasoning results for Example 3.3 with $A^* = (6, 6, 9, 10)$

Attribute Values	Results	
$A_1 = (0, 4, 5, 6)$	Methods	B^*
$A_2 = (11, 12, 13, 14)$	KH Method [3]	(5.45, 4.25, 7.5, 8.5)
$B_1 = (0, 2, 3, 4)$	HCL Method [1]	-
$B_2 = (10, 11, 12, 13)$	HS Method [7]	(5.23, 5.23, 7.61, 8.32)
	The Proposed Method	(4.68, 4.68, 7.83, 8.83)

Note:"-" denotes that the method can not deal with this situation.

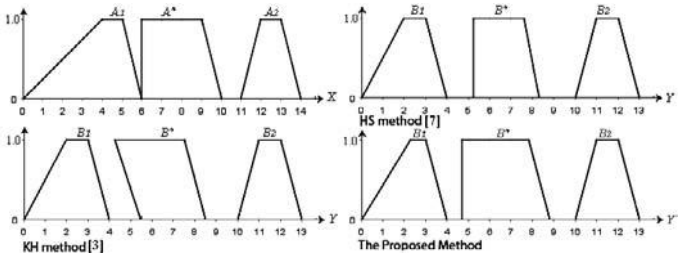

Fig. 11. A comparison of the fuzzy interpolative reasoning results of Example 3.3 for different methods

4 Conclusions

In this paper, we have presented a new fuzzy interpolative reasoning method for sparse fuzzy rule-based systems via cutting and transformation techniques. The proposed method can handle the interpolation of complex fuzzy sets. It produces more reasonable fuzzy interpolative reasoning results than the ones presented in [1] and [3]. Moreover, the fuzzy interpolative reasoning result of the proposed method coincides with the ones presented in [7]. The proposed method provides a useful way to deal with fuzzy interpolative reasoning in sparse fuzzy rule-based systems.

Acknowledgments. This work was supported in part by the National Science Council, Republic of China, under Grant NSC 95-2221-E-011-116-MY2.

References

1. Hsiao, W.H., Chen, S.M., Lee, C.H.: A new interpolative reasoning method in sparse rule-based systems. Fuzzy Sets and Systems 93, 17–22 (1998)
2. Huang, Z.H., Shen, Q.: A new fuzzy interpolative reasoning method based on center of gravity. In: Proceedings of the 2003, IEEE International Conference on Fuzzy Systems, vol. 1, pp. 25–30 (2003)
3. Koczy, L.T., Hirota, K.: Approximate reasoning by linear rule interpolation and general approximation. International Journal of Approximate Reasoning 9, 197–225 (1993)
4. Koczy, L.T., Hirota, K.: Interpolative reasoning with insufficient evidence in sparse fuzzy rule bases. Information Sciences 71, 169–201 (1993)
5. Koczy, L.T., Hirota, K.: Size reduction by interpolation in fuzzy rule bases. IEEE Transactions Systems, Man and Cybernetics 27, 14–25 (1997)
6. Yan, S., Mizumoto, M., Qiao, W.Z.: Reasoning conditions on Koczy's interpolative reasoning method in sparse fuzzy rule bases. Fuzzy Sets and Systems 75, 63–71 (1995)
7. Huang, Z.H., Shen, Q.: Fuzzy Interpolative Reasoning via scale and move Transformations. IEEE Transactions on Fuzzy Systems 14, 340–359 (2006)
8. Mizumoto, M., Zimmermann, H.-J.: Comparison of fuzzy reasoning methods. Fuzzy Sets and Systems 15, 253–283 (1982)
9. Zadeh, L.A.: Interpolative reasoning in fuzzy logic and neural network theory. In: Proceedings of the First International Conference on Fuzzy Systems (1992)

10. Qiao, W.Z., Mizumoto, M., Yan, S.Y.: An improvement to Koczy and Hirotas interpolative reasoning in sparse fuzzy rule bases. International Journal of Approximate Reasoning 15, 185–201 (1996)
11. Shi, Y., Mizumoto, M.: Some considerations on Koczy's interpolative reasoning method. In: Proceedings of the 1995 IEEE International Conference on Fuzzy Systems, pp. 2117–2122 (1995)
12. Tikk, D., Baranyi, P.: Comprehensive analysis of a new fuzzy rule interpolation method. IEEE Transactions on Fuzzy Systems 8, 281–296 (2000)
13. Yam, Y., Koczy, L.T.: Cartesian representation for fuzzy interpolation. In: Proceedings of the 37th Conference on Decision and Control, pp. 2936–2937 (1998)

Using Fuzzy Theory for Packaging Attribute Deployment for New Notebook Computer Introduction

Hsin Rau, Chien-Ping Liao, Wei-Jung Shiang, and Chiu-Hsiang Lin

Department of Industrial Engineering, Chung Yuan Christian University
Chungli, Taiwan 320, R.O.C
hsinrau@cycu.edu.tw

Abstract. The purpose of this study is to focus on the packaging issues at the new product introduction (NPI) stage of notebook computer that enterprises encounter when practicing global logistics. It acquires the weight of product design by quality function deployment in two phases: package design and product design. This study uses product's attributes and their weights as the measurement index for TOPSIS to evaluate the risk priority number of FMEA. Design suggestions generated from reverse feedback can increase logistics efficiency and enable designers to design-out logistics inefficiency caused by product design at the early stage. With effective cooperation, we can learn the critical attributes in NPI when considering logistics factors and assist designers to dissolve design inefficiency. As a result, we can achieve the mechanism of prevention inefficiency in advance, decrease engineering changes, lower costs to speed up the NPI and increase enterprises' competitiveness.

Keywords: new product introduction, packaging, QFD, TOPIS, FMEA.

1 Introduction

The operation of the notebook computer industry faces a lot of unprecedented awkward situations in recent years, such as development of globalization, innovation of new technology, shortening of product life cycle, increase of operation cost, variation of market demands, etc. All these factors make the industry encounter more harsh challenges. Speeding up NPI and lowering logistic costs have become the critical key elements for enterprises to fight in the global market. How to develop products that meet customers' demand within the shortest time, and to send products to customers at the lowest logistics cost have become a trial for enterprises' R&D and logistic capability.

"Packaging" is part of logistics management and its main function is to guarantee products well protected in the logistics process, and more than that, the packaging system also influences shipping, storing, piling and loading/unloading, etc. Therefore, packaging is one of the most important factors that influence logistics efficiency. In accordance with the six steps in "Packaging Development Process" defined by packaging design manual MIL-HDBK-304C [10], it indicates clearly that besides the consideration of the shock/drop in the logistics environment and the materials used for cushioning, the most influential factor in determining packaging design is product

H.G. Okuno and M. Ali (Eds.): IEA/AIE 2007, LNAI 4570, pp. 250–259, 2007.

itself. The cushioning design in packaging is mainly to remedy the differences between the shock/drop in logistics environment and the external force intensity that products itself can really bear. If packaging design can not provide appropriate cushioning for products or the design itself causes over-packaging, it will end up in wasting logistics resources or changing product design again.

In view of this, this research proposes to solve these issues from the logistics department by promoting the related design regulation in NPI to the R&D department and thus the packaging inefficiency will be designed-out. As a result, it will not only speed up the NPI, but also enhance the logistics efficiency.

The purposes of this research are stated as below:

(1) Probe into the fuzzy weight of product design attributes under consideration of packaging design requirements;
(2) Combine fuzzy TOPSIS (Technique for Order Preference by Similarity to Ideal Solution Method) to evaluate the RPN (risk priority number) order in FMEA (failure mode and effects analysis) according to the fuzzy weights of product design attributes;
(3) Combine fuzzy QFD (quality function deployment) and fuzzy TOPSIS in the application of FMEA.

2 Literature Review

2.1 DFX

DFX can be translated as “Design for Excellence.” Its development can be traced back to 1960’s and the most famous example was that the “Manufacturing Productivity Handbook” from General Electric Corp. mentioned that with a large number of manufacturing information [5], engineers can complete design efficiently and effectively. Nevertheless, DFX at that time emphasized productivity only and did not emphasize much on the improvement of manufacturing and assembling procedures. From late 1970’s, Boothroyd and Dewhurst started to carry out researches on DFA (Design for Assembly) organizationally and systematically. Their research focused on the impacts generated from the limited conditions of assembling systems (such as assembling method and cost limitations) in each design stage [1]. This method had proved that by changing design concepts, the assembly time could be reduced and accordingly, the final cost could be lowered as well.

2.2 DFL

The topics that Lee [7] discussed about introducing design for logistics (DFL) in NPI include three important elements: (1) economical packaging and transportation, (2) concurrent and parallel processing, (3) postponement/delayed differentiation. In DFL, the most significant concept is to consider the efficient packaging and storage in the product design stage. Usually, the logistics cost of the product is calculated based on

the product volume, instead of weight. Therefore, if shipment can be packaged tightly, it can save shipping cost. Besides saving freight, if decreasing the product dimension can reduce storage space and make it easy to pile, it can also reduce stock costs. To assist designer to consider related logistics operation in initial design stage, Dowlatshahi [3, 4] divided the dimension of DFL into four areas: (1) logistics engineering; (2) manufacturing engineering; (3) design for packaging; (4) design for transportability. In item 3, the packaging process covered material costs, types, disposability or non-disposability, thickness and tightness to prevent damage, etc. Finally, he utilized clustering algorithm to figure out the critical logistics factors and types for R&D's reference. Melanie [9] pointed out that to meet each goals in logistics, it needed to consider the integration of operation, repair, shipping and supply while designing products, then to use the minimum product life cycle cost and maximum efficiency as objective function, product design requirement as constrains, and finally to get the best parameter by dynamic planning. According to Lin & Chen [8], for product development, product management, and logistics management, it should include the variance of regional demands, product trademarks, rapid product volume change, average spoilage, delivery, trust for distribution, flexibility to meet customers' requirements and shipping costs, etc.

From the above researches, we can learn that initial product development has great impacts on logistics activities, such as packaging, storing and shipping, etc. However, the previous researches only provide a general concept of logistics design and do not focus on the discussion of NPI process. Therefore, this research undertakes the packaging issues in logistics via reverse design concept to lead the innovation in NPI, to establish the design regulation, and to implement DFL. As a result, it enhances the design and logistics efficiency.

3 Research Approaches

This section is to introduce the theoretical basis and the related resolution for building our model. Hereunder, it introduces more about QFD, FMEA, fuzzy theory and TOPSIS and finally the multi-criteria decision analysis for FMEA will discuss in this research. Fig. 1 describes the research process.

This research utilizes the QFD analysis for the conversion of packaging attributes. First of all, it evaluates the relation between the packaging design requirement and the package design attributes. With this, we can establish the initial fuzzy relation matrix (QFD-1) to get the packaging design attribute weights under the consideration of packaging design requirements. Then, according to the weights, we can get the input of the second fuzzy relation matrix (QFD-2) and get the product design attributes by listing out the attributes that affect packaging design decisions. Then this study generates the improvements for design inefficiency by using the fuzzy TOPSIS. In

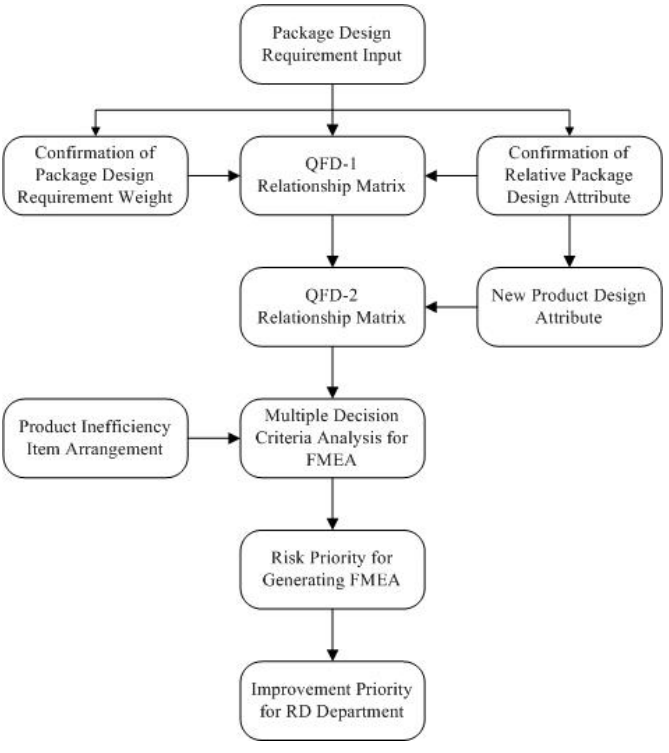

Fig. 1. Process of research approaches

consequent, designer can consider packaging requirement in logistics while designing products. This will not only decrease inefficiency of negligent package, but also enhance the logistics efficiency.

3.1 QFD Theory

QFD is a kind of systematized method. With the participation of the staff in every department, it utilizes binary matrix to deploy the product design process and to ensure that the activities of product development and manufacturing are based on customer requirements. QFD follows the analysis stated above and its execution is mainly carried out through “House of Quality,” as shown in Fig.2. In each deployment process, it uses a matrix to establish the relationship between goals and means, namely the connection between “What” and “How.” In the bottom, it indicates the target value and the relationship strength is expressed by symbols or figures. Then the result of “How” and “How Much” at every stage can be expanded to “What” of the next stage. With such duplicated analysis, it can ensure that every stage meets customer requirements [11, 13].

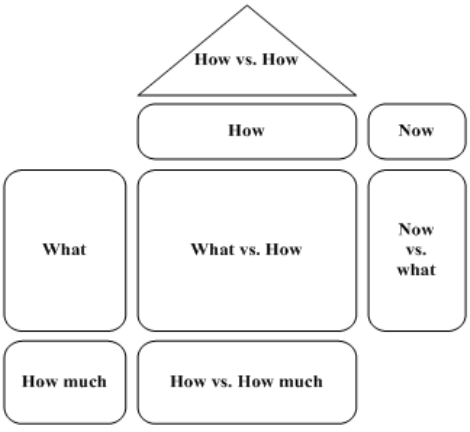

Fig. 2. House of quality

3.2 FMEA Theory

The so-called "FMEA" is a kind of systematized engineering design auxiliary tool as well as a kind of prevention technology. It is used to discuss the cause-effect relation before design and manufacturing are confirmed. It mainly uses forms to assist engineers to find the potential defects and their influence degree in early engineering design and to seek the solutions earlier. It can avoid inefficiency or reduce its effects while it occurs [2].

The first step to implement FMEA is to arrange a list of potential inefficiencies for product or process and the results they may cause. Then, the group members need to assess the probability that these inefficiencies may happen and find a way to prevent them before handing over the products to customers. Certainly, how inefficiencies affect quality depends on the combination of severity rating, occurrence rating, and detection rating. The information obtained from FMEA procedure can be used to arrange priority, adopt necessary actions, and reduce or dispel the problem with supreme risks.

Nevertheless, the traditional FMEA mostly only evaluates the failure mode risk value with utility function and in accordance to carry out the improvement. The traditional evaluation assessment of RPN is to take occurrence, detection, and severity as determinate or indeterminate description criterion and give a rating of 1 to 10 to them separately, and multiply these three numbers to get the result. However, sometimes there might be a dispute that people consider it not objective enough. In view of this, this research proposes the methodology according to Chien [2] and considers FMEA as a multiple criteria decision issue. It forsakes the traditional FMEA concept that uses utility function to calculate failure mode risk and tries to combine the fuzzy theory and TOPSIS. Moreover, it uses the product design attributes and weights derived from QFD as a multiple criteria decision factor and apply it as the consideration of multiple packaging and the RPN order strategy for designing FMEA.

3.3 Fuzzy Theory

The fuzzy theory was proposed by Zadeh [14], a science to discuss how to realize the fuzzy situation in the world with the help of mathematics. It allows "belong completely", "belong partially" and "not belong at all" in the same field, which is the concept of belonging relatively [12, 13] and quantifies "belong concept". In Fuzzy Set, the level of belonging is a random value between 0 and 1 and the fuzzy set can have many membership functions. By using the advantages of fuzzy, it can have more promotion ability, endurance ability and more suitable for the non-linear system in the real world. As fuzzy numbers includes triangular, trapezoidal, and such kinds as normal distribution, for simplicity this research is to analyze the process of using triangular to solve the fuzzy evaluation problems for professionals. Hereunder, we use triangular fuzzy as an example to introduce the basic fuzzy operation formula.

3.4 TOPSIS Theory

TOPSIS is an assessment method and proposed by Yoon and Hwang in 1981 [6]. The basic concept for TOPSIS is to define the positive ideal and passive ideal solution. The positive ideal solution (PIS) is the greatest common value for all substitutions and the lowest common value for the cost evaluation. The negative ideal solution (NIS) is the lowest common value for all substitutions and the greatest common value for the cost evaluation. The best choice of a proposal is based on the nearest value to PIS and farthest value to NIS. TOPSIS is a method that adopts "the relative value for PIS" to process the proposal orders and it can prevent the situation that the value is the closest to PIS and NIS or the farthest to PIS and NIS and thus does not know how to compare the disadvantages.

3.5 Multiple Criteria Decision for FMEA Analysis

This research integrates the methodologies proposed by the above methods and under the consideration of multiple design requirements to define the methodology of deciding the RPN order of FMEA. The below shows the fuzzy TOPSIS steps:

Step 1: Set up the membership function for fuzzy evaluation - Convert linguistic assessment obtained from experts into fuzzy membership function.

Step 2: Set up fuzzy attribute deployment matrix - Set up the attribute deployment matrix according to the design requirement and ask professionals to follow the membership function in Step 1 to evaluate the matrix relationship. And after integrating the fuzzy relationship matrix, it must calculate the total points of evaluation.

Step 3: Standardize fuzzy attribute weight - After operating the total points of fuzzy assessment weight, all the fuzzy values need to be standardized.

Step 4: Set up fuzzy TOPSIS decision matrix - Ask experts to evaluate the decision factors and their relative FMEA items to set up the initial fuzzy TOPSIS decision matrix. The decision factors are not only the attributes derived from QFD but also considered as the deployment for severity in RPN. Moreover, occurrence and detection are used in decision factors so that the decision model can be more practical.

Step 5: Calculate standardized decision matrix.
Step 6: Calculate standardized decision matrix after weighting.
Step 7: Calculate PIS and NIS - In this step, it needs to judge the value of fuzzy numbers and figure out which proposal is PIS and which is NIS. It uses the center of gravity method to solve and define the fuzzy value. If all substitute proposals become fuzzy and have the same value, it can be randomly chosen.
Step 8: Calculate the distance between the proposals and fuzzy PIS/NIS - This research adopts the extreme point method.
Step 9: Calculate the similarity with fuzzy PIS.
Step 10: Prioritize the advantages and disadvantages of proposals - After fuzzy TOPSIS decision evaluation, it is apparently that $0 \le C_i^* \le 1$, $i = 1,2,\ldots,m$。 When the similarity C_i^* is closer to 1 and case i is closer to NPI, the priority of the case is higher.

4 Case Discussions

This section is to use the failure modes data provided by one of Taiwan notebook companies and the questionnaire is surveyed by the RD experts in that company to verify the FEMA analysis for packaging design in this research. The analysis process is as follows:

Step 1: We set up the evaluation matrix relationship for fuzzy levels. This research sets the evaluation description as “very low,” “low,” “medium low,” “medium,” “medium high,” “high,” “very high” and integrates the differences among experts to provide the fuzzy description transfer in matrix foundation. The description variation after integration is shown in Table 1.
Step 2: This research refers to the literature and uses the questionnaires to get the package design requirements, package design attributes and product design attributes, as shown in Table 2, under the consideration of package design system in logistics. The initial QFD-1 matrix is based on the first house of quality design requirement (What) and resolution for design requirement (How) according to the input of the package design requirement and package design attribute. This research needs to evaluate the package requirement and package design attribute so that the deployment can get the most critical factors needed. We can get the total weights of package design attributes through QFD-1 matrix and then introduce the attributes and their weights to QFD-2 matrix as the requirement input (What). The engineering analysis (How) in the matrix provides the design attributes.
Step 3: Calculate the total value of product design attribute fuzzy relationship and then standardize the total value so that all values are between 0 and 1.
Step 4: We use product design attribute, occurrence, detection, and so on to form 12 fuzzy TOPSIS decision items. Table 3 shows the notebook mechanical design inefficiency model. The multiple criteria fuzzy relationship matrix of FMEA is the integration fuzzy value after integrating different opinions of experts.

Step 5: Calculate standardized decision matrix. As the fuzzy evaluation values defined by decision factors in the decision matrix are between [0, 1], the matrix does not need to be standardized.

Table 1. Linguistic variance and its relative fuzzy value

Linguistic Variance	Variance Symbol	Relative Fuzzy Value
Very Low	VL	(0,0. 08, 0.2)
Low	L	(0.1, 0.25, 0.5)
Medium Low	ML	(0.2, 0.39, 0.6)
Medium	M	(0.4, 0.54, 0.7)
Medium High	MH	(0.55, 0.7, 0.8)
High	H	(0.7, 0.82, 0.9)
Very High	VL	(0.8, 0.93, 1)

Table 2. Relationship among package design requirement, package design attribute, and product design

Package Design Requirement	Package Design Attribute	Product Design Attribute
Easy to pile	Package size	Package cost
Easy to load/unload	Package weight	Package size
Easy to move	Package cost	Package weight
Easy to inspect	Package efficiency	Product appearance
Easy to withdraw	Operation cost	Product function
……	……	……
Consideration of piling space		
Protection for content	Moisture	Drop
Total cost	Vibration	Vibration
Consideration of reducing package	Shock	Pressure
Consideration of package recycling	Compression	Failure Rate

Step 6: Multiplying the decision factor weight in Step 3 and the decision matrix in Step 5, we obtain the multiple fuzzy relationship matrix of FMEA.

Step 7: Calculate fuzzy PIS and NIS from (6).

Step 8: Obtain the distance between each proposal and PIS or NIS, S_i^* or S_i^-.

Step 9: After getting measurement of S_i^* and S_i^- for every proposal, we can calculate the relative similarity for each failure mode.

Step 10: According to the process of fuzzy TOPSIS decision evaluation, we can get the risk priority of each failure mode under the consideration of package design requirement as shown in Table 4.

With the improved FMEA developed in this research, we can get more objective and clearer RPN order and thus, the R&D department can improve the inefficiency at the design stage according to the suggestion. This will not only speed up the NPI, but also reduce problems of package or logistics cost increase due to the bad design of product itself.

Table 3. Design inefficiency model

Failure Mode Number	Failure Mode	Failure Impact	Possible Reason for Failure Mode
FM1	Hook is loose	Top and bottom covers can not be locked	Distance between upper/lower hooks is too long
FM2	Screw hole is broken	Motherboard can not be assembled tightly	Screw hole is frail.
…	…	…	…
FM11	Case is too thick	Case size too big	Material for outer chase is not appropriate
FM12	Case is too heavy	Affect total weight	Material for outer chase is not appropriate

Table 4. Result of multiple citeria decision from the modified FMEA analysis

Order	Failure Mode Number	Failure Mode	Failure Impact
1	FM10	Gap between components is too big	CASE size is too big
2	FM9	Components on motherboard are damaged	Not stable
3	FM5	LCD hinge is broken	LCD monitor can not be open
4	FM1	Hook is loose	Top and bottom covers can not be locked
5	FM12	CASE is too heavy	Affect total weight
6	FM8	CASE top cover deforms	Poor appearance
……	……	……	……
11	FM4	Motherboard is broken	Bad connection
12	FM6	CASE is broken	Poor appearance

5 Conclusions

In the past, the NPI is led by marketing and R&D departments, but neglects the product design requirement from other departments. As a result, much inefficiency occurs. This research adopted the concurrent engineering concept to provide the recommendation from promoting design regulations to the R&D department from the point of view of logistics package design. This enabled the initial product development to consider the requirements from the logistics operation, reduce rework and re-design, and implement DFL thoroughly. This research used QFD to find the product design attributes and their weights under the package design consideration. Then, it combines TOPSIS and RPN order of FMEA so that the R&D department can dissolve inefficiency decidedly. This will not only speed up the NPI but also increase the logistics efficiency.

Although this research can induce DFL regulations, there might be conflicts if there are many DFX at the same time and then the RPN order in FMEA might become complicated. Therefore, it is suggested that the future research can use other

statistic methods to get the resolutions for design conflicts and use a program to set up an automatic decision system to simplify the evaluation process for experts.

Acknowledgments. This work is supported in part by National Science Council of Republic of China under the grant NSC 95-2221-E-033-048-MY3.

References

[1] Boothroyd, G., Dewhurst, P.: Design for assembly - a designers handbook. Technique Report, Department of Mechanical Engineering, University of Massachusetts (1983)
[2] Chien, C.L.: Application of fuzzy set theory & TOPSIS for failure mode & effects analysis. Master thesis of department of Industrial Engineering & Systems Management of Feng Chia university (2002)
[3] Dowlatshahi, S.: The role of logistics in concurrent engineering. International Journal of Production Economics 44, 189–199 (1996)
[4] Dowlatshahi, S.: A modeling approach to logistics in concurrent engineering. European Journal of Operational Research 115, 59–76 (1999)
[5] General Electric Co.: Manufacturing Producibility Handbook(MPH). Manufacturing Services Schenectady, NY (1960)
[6] Hwang, C.L., Yoon, K.: Multiple attributes decision making methods & applications. Springer, Heidelberg (1981)
[7] Lee, H.: Design for supply chain management: Concepts & Examples. Working paper, Department of Industrial Engineering & Engineering Management, Stanford University (1992)
[8] Lin, C.W., Chen, H.Y.: A fuzzy strategic alliance selection framework for supply chain partnering under limited evaluation resources. Computer in Industry 55, 159–179 (2004)
[9] Melanie, L.H., Badinelli, R.D.: Concurrent optimization in designing for logistics support. European Journal of Operational Research 115, 77–97 (1999)
[10] MIL-HDBK-304C: Package cushioning design. U.S. Department of Defense, Washington (1997)
[11] Myint, S.: A framework of an intelligent quality function deployment (IQFD) for discrete assembly environment. Computers & Industrial Engineering 45, 269–283 (2003)
[12] Negi, D.S.: Fuzzy analysis & optimization. Ph. D. Thesis, Department of Industrial Engineering, Kansas State University (1989)
[13] Sohn, S.Y., Choi, I.S.: Fuzzy QFD for supply chain management with reliability consideration. Reliability Engineering & System Safety 72, 327–334 (2001)
[14] Zadeh, L.A.: Fuzzy sets. Information & Control 8, 84–85 (1965)

Fuzzy System Model to Assist with Real Estate Appraisals

Dariusz Król[1], Tadeusz Lasota[2], Wojciech Nalepa, and Bogdan Trawiński[1]

[1] Wrocław University of Technology, Institute of Applied Informatics, Wybrzeże S. Wyspiańskiego 27, 50-370 Wrocław, Poland
{dariusz.krol, trawinski}@pwr.wroc.pl
[2] Agricultural University of Wrocław, Faculty of Environmental Engineering and Geodesy, C.K. Norwida 25/27, 50-375 Wroclaw, Poland
tadeusz.lasota@wp.pl

Abstract. Real estate appraisal requires expert knowledge and should be performed by licensed professionals. Prior to the evaluation the appraiser must conduct a thorough study of the appraised property i.e. a land parcel and/or a building. Despite the fact that he sometimes uses the expertise of the surveyor, the builder, the economist or the mortgage lender, his estimations are usually subjective and are based on his experience and intuition. The primary goal of the paper is to present the concept of a fuzzy rule-based system to assist with real estate appraisals. The input variables of the system comprise seven attributes of a property and as the output the system proposes the property's value. For the appraisal area, so called representative property is determined and in fact the deviations of property attribute values from the representative ones are the input into the fuzzy system. The proportion of the representative property price to the value of the property being assessed is produced as the output of the system. The experts have built the Mamdani model of the system, however they have not been able to construct the rule base. Therefore an evolutionary algorithm has been employed to generate the rule base. The Pittsburgh approach has been applied. The learning process has been conducted using training and testing sets prepared on the basis of 150 sales transactions from one city.

1 Introduction

There are three most common approaches to determining the market value of a property: a cost approach, a sales comparison approach, and an income approach. The appraiser chooses an appropriate approach, methods and techniques taking into account such criteria as the goal of the evaluation, the type of a property, its location, its purpose, transaction prices, etc. The most popular is sales comparison approach. Applying this approach it is necessary to have transaction prices of the properties sold which have attributes similar to the one being appraised. If good comparable transactions are available, then it is possible to obtain reliable estimates. Prior to the evaluation the appraiser must conduct a thorough study of the appraised property using available sources of

H.G. Okuno and M. Ali (Eds.): IEA/AIE 2007, LNAI 4570, pp. 260–269, 2007.

information such as cadastral systems, transaction registers, market analyses, and on-site inspection. Despite the fact that he sometimes uses the expertise of the surveyor, the builder, the economist or the mortgage lender, his estimations are usually subjective and are based on his experience and intuition. Automated valuation models (AVMs) are being more and more accepted. These are based on statistical models such as multiple regression analysis, soft computing methods and geographic information systems (GIS) [2]. A series of methods based on artificial intelligence have been developed to support appraisers' works. Among them are artificial neural networks [4], [5], [13], data mining [12], neurofuzzy networks [11], case-based reasoning [6], and hybrid soft computing methods [1].

The primary goal of the paper is to present the concept of a fuzzy rule-based system assisting the real estate appraisal. The input variables of the system comprise seven attributes of a property and as the output the system proposes the property's value. For the appraisal area, so called representative properties are determined and in fact the deviations of property attribute values from the representative ones are the input into the fuzzy system. The proportion of the representative property price to the value of the property being assessed is produced as the output of the system. The experts have built the Mamdani model of the system. However they have not been able to construct the rule base. Therefore an evolutionary algorithm has been employed to generate the rule base. The Pittsburgh approach has been applied [8]. The overall structure of the evolutionary algorithm used in the experiments conformed to the structure of a classic genetic algorithm, but a different way of coding chromosomes and a modified crossover and mutation operations were applied. The extensive overview of genetic fuzzy systems can be found in [3], [7].

2 Information Systems Aiding Real Estate Appraisal

The fuzzy system assisting real estate appraisal is devoted to an information centres maintaining cadastral systems and property sales transaction registries. Due to the substantial dispersion in Poland, these systems are located in district local self-governments as well as in the municipalities of bigger towns, and there are above 400 such centres all over the country. All three systems together could create a complex data source for real estate appraisers accessible through internet (see Fig. 1). At present the information centres are the place which appraisers contact when they start evaluating properties. Moreover the appraisers are obliged to deliver the results of their estimates to the governmental registry of real estate transactions. Therefore the actual values and prices of properties are available in the registry. On the basis of data taken from the registry and the cadastral system the initial parameters of the fuzzy system aiding real estate appraisal can be determined such as the sections of comparable characteristics and the representative properties for each land section.

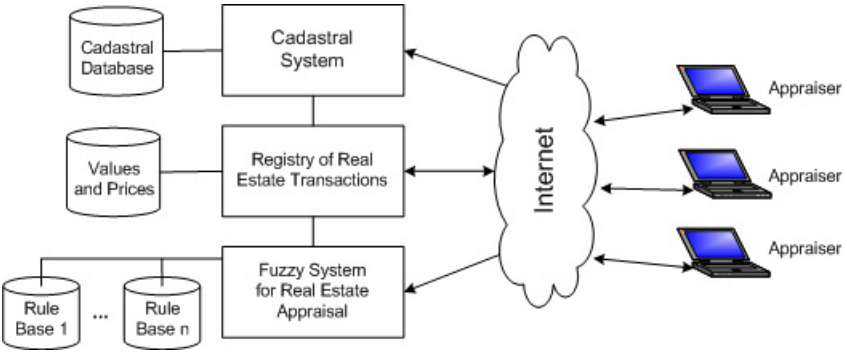

Fig. 1. Information systems aiding real estate appraisal

3 Fuzzy Model for Real Estate Appraisal

The fuzzy system for real estate appraisal has been based on sales comparison method. It has been assumed that whole appraisal area, that means the area of a city or a district, has been divided into sections of comparable property attributes. As the most important attributes location and land use characteristics were regarded. An adequate representative property as well as the parameters of fuzzy sets and rule bases have been determined for each section.

The architecture of the fuzzy system aiding real estate appraisal has been shown in Fig. 2. The appraiser accesses the system through internet and chooses an appropriate section and input the values of the attributes of the property being evaluated.

Then the system using the parameters of the representative property for the section indicated, calculates the input values to the fuzzy model. The classic fuzzy inference mechanisms, applying a proper rule base, calculates the output. Then on the basis of the parameters of the representative property the final result is determined and as a suggested value of the property is sent to the appraiser.

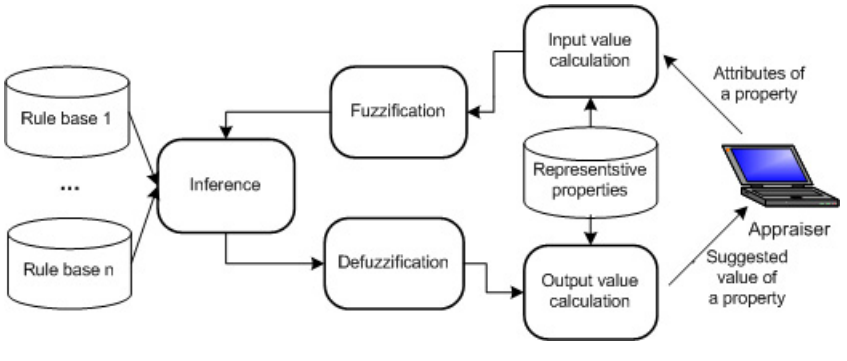

Fig. 2. Architecture of the fuzzy system for real estate appraisal

The Mamdani model for real estate appraisal has been built with the aid of experts. It has comprised 7 input variables and each of them referred to the difference or proportion of attribute values between a property being appraised and the representative one. The representative properties have been determined for each section, having similar characteristics, by means of calculating average values of attributes of all properties in the training set of data used in the experiment. For each input variable five triangular and trapezoidal membership functions have been defined and for output - nine (see Fig. 3.). Therefore the input of the fuzzy system is defined by the vector of seven following variables:

- *Distance* - it is the difference in the distance from a local centre expressed in meters. The domain of this variable is the interval form -1000 to 1000 meters. Negative values denote that the representative property is located closer to the local centre than the appraised one.
- *Front* - it is the difference in the length of fronts of parcels expressed in meters. The domain of this variable is the interval form -50 to 50 meters. Positive values mean that the examined parcel has longer front than the representative one what is considered as a better result.
- *Area* - it is the ratio of the area of the examined parcel to the area of the representative one. The domain of this variable is the interval form 0 to 10. Values greater than 1 indicate that the examined property has the bigger area.
- *Infrastructure, arrangement neighborhood and communication* - values of these four attributes are appraiser's judgments of what is the difference in a given attribute between the appraised and the representative parcels. The values are taken from the range 0-200 where 100 means that both parcels are equal in this respect, values greater than 100 - that the examined parcel is better and the ones lower than 100 - the opposite.
- *Infrastructure* - refers to what extent the technical infrastructure of a given property is better than the representative one.
- *Arrangement* - pertains to the assessment of how better a given property was arranged than the representative one.
- *Neighborhood* - concerns the difference in the quality of properties' neighborhood.
- *Communication* - deals with the evaluation of the means of public transportation available to the residents.

The output of the system is the ratio of the property value being appraised to the value of the representative one. The linguistic values are as follows: very much lower than (VMLT), much lower than (MLT), lower than (LT), slightly lower than (SLT), equal (EQ), slightly greater than (SGT), greater than (GT), much greater than (MGT) and very much greater than (VMGT).

4 Learning Fuzzy Rules by an Evolutionary Algorithm

Constructing the fuzzy model with 7 input variables, the experts have not been able to construct the rule base. Therefore the evolutionary algorithm has been

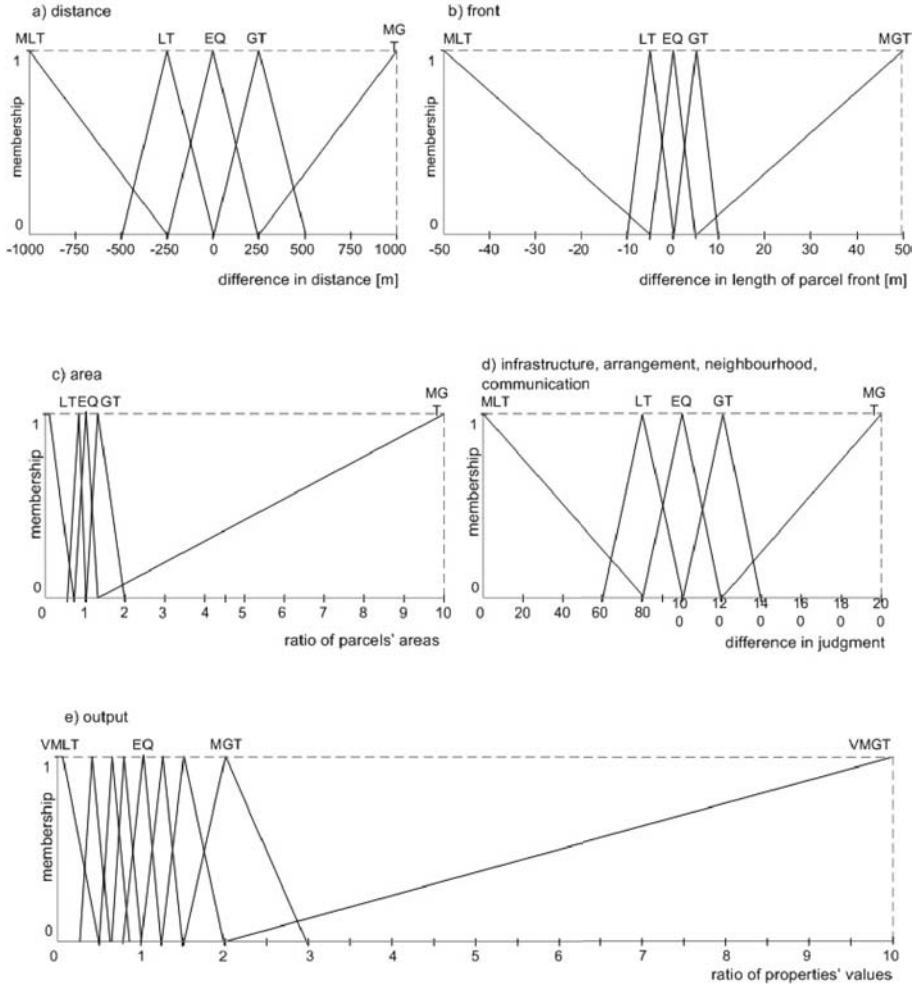

Fig. 3. Membership functions of input and output variables

employed to generate the rule base and the Pittsburgh approach has been applied. The learning process has been carried out employing the MATLAB software tools. Some preliminary tests revealed that it was very hard to carry out experiments employing a classic genetic algorithm to assure acceptable execution time using available hardware, therefore a modified evolutionary method has been used. The structure of an evolutionary algorithm is the same as the structure of a classic genetic algorithm [11] (see Fig. 4), but the algorithm applied differs in the way of chromosome coding and crossover and mutation operations.

Training and testing sets. The set of data used in the process of generating rules comprised 150 sales transactions made in one of Polish cities and located in residential sections what assured comparable attributes of properties. The data

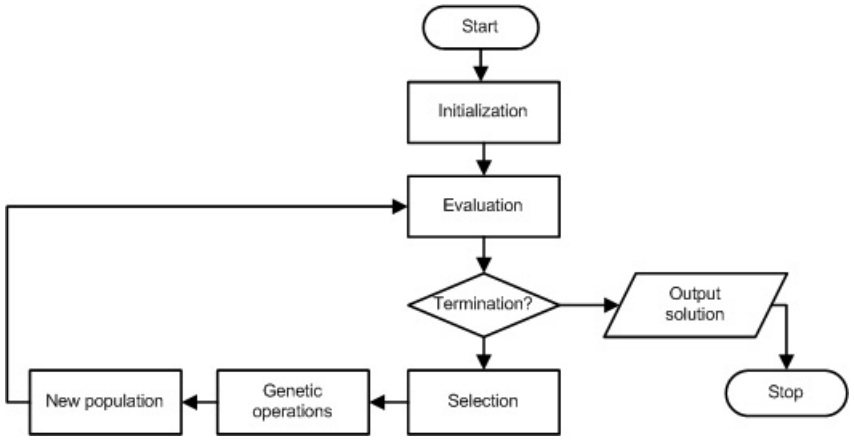

Fig. 4. Structure of the evolutionary algorithm

were taken from the governmental registry of real estate sales transactions. The attributes of the properties embraced by those transactions were determined by an expert, who had visited and studied personally all of them. The set of data was bisected into learning and verifying sets by clustering the property descriptions including their prices using the k-means method and then by splitting randomly each cluster into two parts. Finally the training data set counted 77 properties and the verifying one 73 properties.

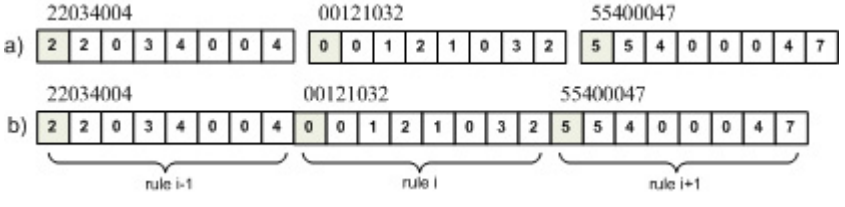

Fig. 5. Coding scheme: a) three rules encoded by natural numbers and b) the fragment of a resulting chromosome

Coding chromosomes. The rule base was coded using the Pittsburgh method, where one chromosome comprised whole rule base. We assumed constant length of the chromosome composed of n rules. Each i-th rule was represented by 8 bytes: $b_i^1, b_i^2, \ldots, b_i^8$, where first seven bytes contained natural numbers from 1 to 5 corresponding to linguistic values of seven input variables (see Fig. 5), e.g. MLT (much less than), LT (less than), EQ (equal), GT (greater than), MGT (much greater than) respectively. Zero value on the position of a given input meant that this attribute did not occur in the rule. The 8-th byte represented the output and could contain natural number randomly taken out of the range from 1 to 9 referring to linguistic value of the output: VMLT (very much less than), MLT

(much less than), LT (less than), SLT (slightly less than), EQ (equal), SGT (slightly greater than), GT (greater than), MGT (much greater than), VMGT (very much greater than) respectively.

Initialization. At the beginning the space of all possible rules was confined to that comprising only those rules which could be activated by the set of training data. Let us call this set as activated rules. Then each chromosome was composed of rules taken randomly out of the activated rules and so the initial population of randomly generated chromosomes was obtained.

Fitness function was calculated as an average error between values of properties included in the training set and the values of corresponding properties determined by the fuzzy system using a rule base produced by a subsequent generation of the evolutionary algorithm.

Crossover. Uniform crossover operation was employed, where the pattern of the position of rules to be exchanged was determined randomly for each pair of parents separately with the probability of 0.5. According to this pattern whole rules were exchanged between the parents of a given pair instead of individual genes. In Fig. 6 it is shown that i-1-th and i+1-th rules are exchanged between parent chromosomes.

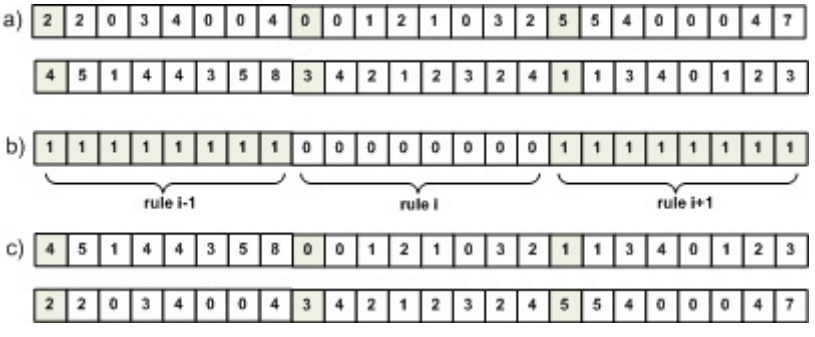

Fig. 6. Crossover operation a) parents, b) crossover pattern, c) offspring

Mutation. During the experiment we noticed that our algorithm converged faster when operator of mutation was modified. Instead of altering individual alleles in a randomly selected chromosome with the probability of 0.07, we removed it entirely from the population and replaced it by a completely new chromosome composed of the rules taken randomly from the set of activated rules.

Results. Preliminary experiments were conducted with different number of rules in one chromosome i.e. 5, 20, 50, 100 and 250 and different size of population counting 100, 250 and 1000 chromosomes. In Table 1 the values of the fitness function for the best combinations of chromosome length and population size, which resulted in the lowest values, are presented. The table header indicates the combination of the number of rules in a chromosome (100 or 250) and the

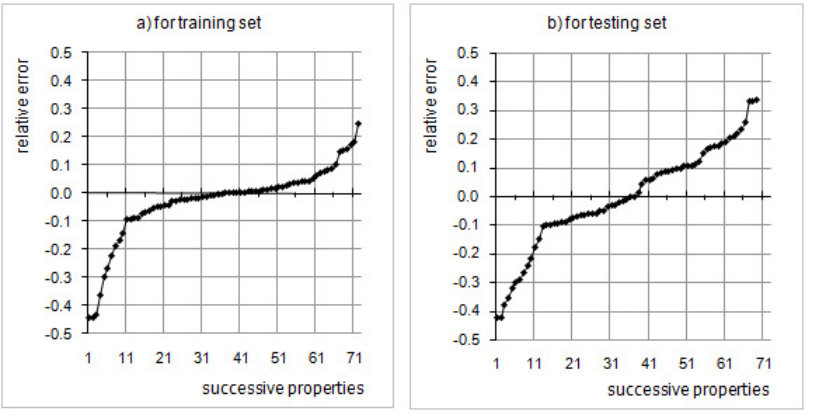

Fig. 7. Relative error distribution for training and testing sets

size of a population (250 or 1000). For each combination test run was repeated 3 times and stopped after 40 generations of the evolutionary algorithm.

Table 1. Values of fitness function for different parameters of an evolutionary algorithm

Test no.	100/1000	250/250	250/1000
1	25,59	30,87	31,90
2	39,72	36,78	27,52
3	18,45*	17,68	15,42

Table 2. Mean absolute and relative errors for selected rule base

Set of data	Mean absolute error	Std dev. of absolute error	Mean relative error	No. of outliers
training	18,46	27,71	8%	0
training and testing	26,46	36,29	11%	4
testing	34,56	43,48	14%	4

For the rule base obtained in test number 3 for 100 rules in a chromosome and the population of 1000 (one marked with an asterisk in Table 1) the suggested prices for all properties constituting training and testing sets were determined by means of the fuzzy model defined in the MATLAB software tool. Then absolute and relative errors with reference to real prices were calculated for each property. Properties, for which an absolute error was above 50%, were regarded as outliers and discarded from further calculations. In Fig. 7 the distribution of relative errors for training and testing sets is shown. In Table 2 the resulting mean absolute and relative errors are presented. The results obtained are promising

because the mean relative errors were rather low and for the testing set it was equal to 14%. Nevertheless further investigations are needed for greater number of generations of an evolutionary algorithm as well as for different parameters of fuzzy model and evolutionary algorithm.

5 Conclusions and Future Work

The Mamdani fuzzy model for assisting the property appraisers' work was proposed in the paper. The model comprises 7 input variables referring to the attributes of a property being evaluated. As an output it produces the suggested price for a given property. Rule base of the model was generated and optimized using an evolutionary algorithm based on Pittsburgh approach. The results of learning rule base are promising, despite they were achieved for a relatively small number of generations performed by an evolutionary algorithm. This encouraged us to plan further investigations with different parameters of fuzzy model and evolutionary algorithm. It will be worth to investigate how simplifying the model by means of removing the least important input variables will influence the accuracy of the fuzzy model and what degree of accuracy will be required to be acceptable to users. Training and testing sets could be revised in order to detect and exclude possible outliers. We intend to construct the equivalent TSK fuzzy model and carry out experiment to compare the results with those obtained using Mamdani one. It is also planned to implement the model and to deploy it in one information centre.

References

1. Bonissone, P.P., Chen, Y.-T., Goebel, K., Khedkar, P.S.: Hybrid soft computing systems: industrial and commercial applications. In: Proceedings of the IEEE, vol. 87(9), pp. 1641–1667 (1999)
2. Castle, G.H.: GIS: Meeting the Information Demand. Valuation Insights and Real Estate Investor 42(1), 66–71 (1998)
3. Cordón, O., Gomide, F., Herrera, F., Hoffmann, F., Magdalena, L.: Ten years of genetic fuzzy systems: current framework and new trends. Fuzzy Sets and Systems 141, 5–31 (2004)
4. Do, Q., Grudnitski, G.: A Neural Network Approach to Residential Property Appraisal. Real Estate Appraiser, pp. 38–45 (December 1992)
5. Evans, A., James, H., Collins, A.: Artificial Neural Networks: An Application to Residential Valuation in the UK. Journal of Property Valuation and Investment 11(2), 195–204 (1991)
6. Gonzalez, A.J.: A case-based reasoning approach to real estate property appraisal. Expert Systems with Applications 4(2), 229–246 (1992)
7. Herrera, F.: Genetic Fuzzy Systems: Status, Critical Considerations and Future Directions. International Journal of Computational Intelligence Research 1(1), 59–67 (2005)
8. Hoffmann, F., Pfister, G.: Evolutionary design of a fuzzy knowledge base for a mobile robot. International Journal of Approximate Reasoning 17(4), 447–469 (1997)

9. McCluskey, W.J., Anand, S.: The application of intelligent hybrid techniques for the mass appraisal of residential properties. Journal of Property Investment and Finance 17(3), 218–239 (1999)
10. Nalepa, W.: Fuzzy Expert System for Real Estate Appraisal. M.Sc. Thesis (in Polish). Wrocław University of Technology (2006)
11. Rutkowski, L.: Methods and techniques of artificial intelligence (in Polish). PWN Warsaw (2005)
12. Soibelman, L., González, M.A.S.: A Knowledge Discovery in Databases Framework for Property Valuation. Journal of Property Tax Assessment and Administration 7(2), 77–106 (2002)
13. Worzala, E., Lenk, M., Silva, A.: An Exploration of Neural Networks and Its Application to Real Estate Valuation. The Journal of Real Estate Research 10(2), 185–201 (1995)

Application of Fuzzy System on a Server-Dependent Queue Modeled with Empirical Bayesian Estimation

Pei-Chun Lin[1] and Jenhung Wang[2]

[1] Department of Transportation and Communication Management Science,
National Cheng Kung University,
No. 1, University Road, Tainan 701, Taiwan
peichunl@mail.ncku.edu.tw
[2] Department of Logistics Management,
National Kaohsiung First University of Science and Technology,
No. 2, Juoyue Road, Nantz District, Kaohsiung, Taiwan
jenhung@ccms.nkfust.edu.tw

Abstract. This study presents a fuzzy system by collecting membership function and rules based on a decision model that uses empirical Bayesian estimation to construct a server-dependent $M/M/2/L$ queue. A Markovian queue of finite capacity in which the number of servers depends upon queue length is considered. First, data on the interarrival times and service times are collected by observing a queuing system, and the empirical Bayesian method is adopted to estimate its server utilization. Second, the costs are associated with the operation of the second server and the waiting of customers, to establish a cost minimization model to determine the optimal number of customers in the system to activate the second server (N), and the optimal number of customers in system to deactivate the second server (Q). The decision model provides knowledge to construct rules used in a fuzzy inference system. The MATLAB Fuzzy Inference Toolbox is used to construct a fuzzy system to aid management in determining when to initiate the second server and when to turn it off, according to specific parameters.

1 Introduction

One way to shorten the job waiting time for flexible manufacturing system (FMS) is to increase the number of machines (servers), increasing the cost of facilities. Operational managers require domain knowledge or assistance to decide how to allocate servers or resources efficiently to balance the cost of unnecessary facilities, the cost of idleness, the cost of losing orders, and to meet the variation in demand. The optimal decision is usually derived based upon known parameters which sometimes are not deterministic and the decision process often involves gray areas. The decision process becomes necessary to incorporate fuzzy logic, developed by Zadeh [4] to deal with uncertainties by simulating the process of human reasoning, allowing the computer to behave less precisely and logically than conventional computers.

H.G. Okuno and M. Ali (Eds.): IEA/AIE 2007, LNAI 4570, pp. 270–279, 2007.

The main objective of this study was to establish a fuzzy system that can resolve when to initiate the second server and when to turn it off for an $M/M/2/L$ queue. The difference between an $M/M/2/L$ server-dependent queue with single waiting line and a general queuing system is that in the former the number of servers depends on the queue length. Firstly, the empirical Bayesian approach proposed by Thiruvaiyaru and Basawa [2] is adopted to estimate the service requirement, based on the actual arrival of orders. The controllable queuing system initiates another server whenever the number of jobs in system reaches a certain length and turns off the second server whenever the number of jobs in system falls to a certain length. Utilization rate is used as the indicator of the amount of service required. The accuracy of estimation strongly influences the subsequently constructed model of cost analysis. The analytical results of the decision model by Lin [1] provide an understanding of the optimal control strategy for the server-dependent queue, and the acquirable knowledge is used to construct a fuzzy system. By replicating the procedures, a nonexpert can get the benefit of expert advice in a specific application area of server-dependent queue.

2 Analytical Solution

This investigation applied an empirical Bayesian approach to estimate the demand for service. A server-dependent queuing system which utilizes the queue length to activate and deactivate the second server was constructed to minimize the expected cost for a decision maker. The utilization rate was first estimated using numerical data from simulation or empirical observation with the empirical Bayesian approach proposed by Thiruvaiyaru and Basawa [2]. The probability for each state was then calculated for an $M/M/2/L$ server-dependent queuing system. Next, the cost parameters were incorporated to solve the optimal queue lengths N for starting a second server, and Q for switching it off.

Thiruvaiyaru and Basawa [2] considered there are H independent $M/M/1$ queues in which the interarrival times $\{u_{ik},\ i = 1 \ldots n\}$ of the first n jobs, and the service times $\{v_{jk},\ j = 1 \ldots m\}$ of the first m jobs are observed for $k = 1 \ldots H$. Given the arrival rate λ_k, the probability density function $f_{\mathbf{U}}\ (\mathbf{u}_k|\lambda_k) = \lambda_k^n \exp\{-\lambda_k \sum_{i=1}^{n} u_{ik}\}$, where the arrival rates $\{\lambda_1, \ldots, \lambda_k\}$ are independently identical distributed as $Gamma(\alpha_1, \beta_1)$ (prior distribution). Given the service rate μ_k, the probability density function $f_{\mathbf{V}}\ (\mathbf{v}_k|\mu_k) = \mu_k^m \exp\{-\mu_k \sum_{j=1}^{m} \nu_{jk}\}$, where the service rates $\{\mu_1, \ldots, \mu_k\}$ are independently identical distributed as $Gamma$ (α_2, β_2). The empirical Bayesian estimator is derived as

$$\hat{\rho} = \frac{(n + \hat{\alpha_1})(\sum_{j=1}^{m} v_j + \hat{\beta}_2)}{(m + \hat{\alpha_2} - 1)(\sum_{i=1}^{n} u_i + \hat{\beta}_1)} \tag{1}$$

where $\hat{\alpha_1}$, $\hat{\alpha_2}$, $\hat{\beta}_1$, and $\hat{\beta}_2$ denote the one-step maximum likelihood estimators of α_1, α_2, β_1, and β_2 respectively. Next, a server-dependent $M/M/2/L$ queuing

system with finite capacity L must be established. This system is set up so that the first server is always on. When the number of unprocessed jobs reaches N, the second sever is activated to release the congestion in the system; when the number of unprocessed jobs in systems falls to Q, then the system is no longer congested, and the second server can be switched off to cut cost. The next step is to establish a server-dependent $M/M/2/L$ queuing system with finite capacity L. The parameters and variables adopted in the model are defined as follows.

λ: arrival rate of transfer requests;
μ: service rate of server;
ρ: utilization rate $= \lambda/\mu$;
i: number of servers in service, $i = 1, 2$;
j: number of transfer requests in system, $j = 0, \ldots, L$;
$P(1, j)$: the steady-state probability that only one server is in service when the number of transfer requests in system is j, where $j = 0, 1, 2, \ldots, Q, Q+1, \ldots, N-1$;
$P(2, j)$: the steady-state probability that only one server is in service when the number of transfer requests in system is j, where $j = Q+1, Q+2, \ldots, N, N+1, \ldots, L-1, L$.

This study builds a server-dependent $M/M/2/L$ system based on the above assumptions and symbols. To solve the birth-death flow balance equations, this study begins with expressing each $P(1, j)$ and $P(2, j)$ in terms of $P(1, 0)$. The steady-state probability of no job in the system, given by $P(1, 0)$, is derived by Lin [1] as follows:

$$P(1,0) = \left\{ \frac{1}{1-\rho} - \frac{\rho^N \{(2-\rho)(N-Q) + \rho(1-\rho)(\frac{\rho}{2})^{L-N}[1-(\frac{\rho}{2})^{N-Q}]\}}{(2-\rho)^2(1-\rho^{N-Q})} \right\}^{-1} \tag{2}$$

Then (2) can then be utilized to determine $P(1, j)$, $P(2, j)$. Each term of $P(1, j)$, $P(2, j)$ is a function of the traffic intensity ρ, and the decision variables N, Q. The cost parameters can now be adopted to formulate an NLP to minimize the expected cost of waiting for unprocessed jobs and the machine operation. An objective function is then established to minimize the expected cost of the $M/M/2/L$ controllable queuing system. Let

C_s: fulltime operating cost for second server per day;
C_i: fulltime idle cost for second server per day;
C_e: cost for system being empty per day;
C_{on-off}: start up cost for turning the second server on and off;
C_w: the average waiting cost for each transfer request per day,

The expected cost function is then given by

$$\begin{aligned} Ec(N, Q \,|\, \hat{\rho}^{EB}) &= C_s \sum_{Q+1}^{L} P(2, j) \\ &+ C_w \sum_{j=0}^{N-1} Max[0, (j-1)] P(1, j) + C_w \sum_{j=Q+1}^{L} Max[0, (j-2)] P(2, j) \\ &+ C_i \sum_{j=0}^{N-1} P(1, j) + C_{on-off}[P(2, N) + P(1, Q)] + C_e P(1, 0) \end{aligned} \tag{3}$$

Equation (3) is written as a function of the traffic intensity ρ and decision variables N and Q. *rho* is estimated by substituting an empirical Bayesian estimator $\hat{\rho}^{EB}$ and substituting $\hat{\rho}^{EB}$ into (3) to yield $\hat{P}(1,0)$:

$$\hat{P}(1,0) = \left\{ \frac{1}{1-\hat{\rho}} - \frac{(\hat{\rho}\quad)\left((2-\hat{\rho}\quad)(N-Q)+\hat{\rho}\quad(1-\hat{\rho}\quad)(\frac{\hat{}}{2})^{-}\left(1-(\frac{\hat{}}{2})^{-}\right)\right)}{(2-\hat{\rho}\quad)^2(1-(\hat{\rho}\quad)^{-})} \right\}^{-1} \tag{4}$$

The expected cost minimization model derived by Lin [1] is as follows:

$$\begin{aligned}
&Minimize \qquad Ec(N,Q\,|\hat{\rho}^{EB}) \\
&= C_s \sum_{j=Q+1}^{N} \frac{(\hat{\rho}\quad)(1-\hat{\rho}\quad)[1-(\frac{\hat{}}{2})^{-}]}{(2-\hat{\rho}\quad)[1-(\hat{\rho}\quad)^{-}]}\hat{P}(1,0) \\
&+C_s \sum_{j=N+1}^{L} \frac{(\hat{\rho}\quad)(1-\hat{\rho}\quad)[1-(\frac{\hat{}}{2})^{-}](\frac{\hat{}}{2})^{-}}{(2-\hat{\rho}\quad)[1-(\hat{\rho}\quad)^{-}]}\hat{P}(1,0) \\
&+C_w \sum_{j=0}^{Q} Max[0,(j-1)](\hat{\rho}^{EB})^j\hat{P}(1,0) \\
&+C_w \sum_{j=Q+1}^{N-1} Max[0,(j-1)]\frac{\hat{\rho}\quad[(\hat{\rho}\quad)^{-1}-(\hat{\rho}\quad)^{-1}]}{[1-(\hat{\rho}\quad)]^{-}}\hat{P}(1,0) \\
&+C_w \sum_{j=Q+1}^{N} Max[0,(j-2)]\frac{(\hat{\rho}\quad)(1-\hat{\rho}\quad)[1-(\hat{\rho}\quad/2)^{-}]}{(2-\hat{\rho}\quad)(1-(\hat{\rho}\quad)^{-})}\hat{P}(1,0) \\
&+C_w \sum_{j=N+1}^{L} Max[0,(j-2)]\frac{(\hat{\rho}\quad)(1-\hat{\rho}\quad)[1-(\hat{\rho}\quad/2)^{-}]}{(2-\hat{\rho}\quad)(1-(\hat{\rho}\quad)^{-})}(\frac{\hat{\rho}}{2})^{j-N}\hat{P}(1,0) \\
&+C_i\left[\sum_{j=1}^{Q}(\hat{\rho}^{EB})^j\hat{P}(1,0) + \sum_{j=Q+1}^{N-1}\frac{\hat{\rho}\quad[(\hat{\rho}\quad)^{-1}-(\hat{\rho}\quad)^{-1}]}{[1-(\hat{\rho}\quad)]^{-}}\hat{P}(1,0)\right] \\
&+C_{on-off}\left[\frac{(\hat{\rho}\quad)(1-\hat{\rho}\quad)[1-(\hat{\rho}\quad/2)^{-}]}{(2-\hat{\rho}\quad)(1-(\hat{\rho}\quad)^{-})}\hat{P}(1,0) + (\hat{\rho}^{EB})^Q\hat{P}(1,0)\right] \\
&+C_e\hat{P}(1,0)
\end{aligned} \tag{5}$$

The above NLP is hard to prove that its feasible region is a convex set possessing the optimal N^* and Q^* and to solve analytically. Accordingly, a numerical method is required to examine how changes in the NLP's parameters change the optimal solution. The optimal solution for the NLP is derived from the known parameters. In practice, some of those parameters are not deterministic or unable to be obtained with certainty. Next, this study demonstrates the knowledge acquisition process using an example and expects by replicating the procedures, a non-expert can get the benefit of expert advice in a specific application area of server-dependent queue.

3 Construction of the Rule Base

In this section, the knowledge acquisition process utilizing the numerical results and the method proposed by Turksen et al. [3] is presented to generate the rule base for the expert system that was described in section 2.

3.1 Knowledge Acquisition

In the expert system considered here, six inputs that relate to the cost and two output variables are considered. These are ρ; C_s; C_i; C_e; C_{on-off}; C_w and N; Q, respectively. Based on the numerical analysis, the values of ρ vary in the interval $(0, 2)$, and Figure 1 reveals that 1.1 and 1.4 are the values on the utilization rate axis that divides the low, medium and high linguistic subintervals. By checking into individual figure for the rest of the variables, we come up with the following linguistic terms for each variable. Three linguistic terms for variable ρ = {low, medium, high}; C_w = {low, medium, high}; C_{on-off} = {low, medium, high}; C_i = {low, medium, high}; C_e = {low, medium, high}; two linguistic terms for variable C_s = {low, medium} are used. The code, notation and interval for each linguistic term are defined in Table 1. Six linguistic terms for variables N; Q, respectively: N = {very short, short, medium, rather long, long, very long} and Q = {very short, short, medium, rather long, long, very long} are used. The code, notation and interval for each linguistic term are defined in Table 2.

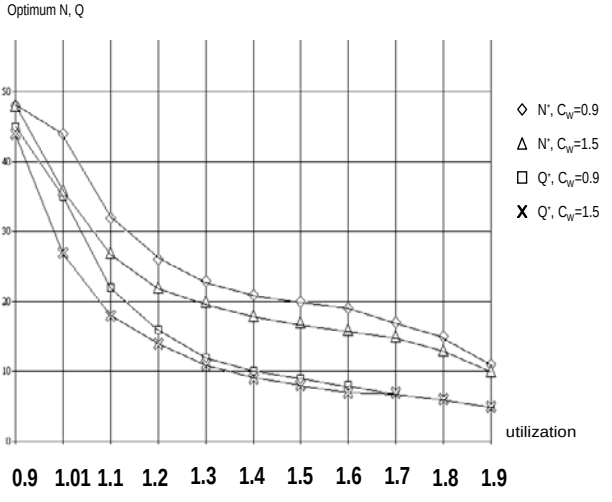

Fig. 1. Relationship between variables C_w, ρ and optimum N, Q

3.2 Membership Function

Three linguistic terms subintervals for ρ; C_i; C_e; C_{on-off}; C_w, two for C_s, six for N and Q, are uses, respectively. The membership functions of the linguistic terms are set by the numerical results of decision model and the built-in triangle and trapezoid functions of Fuzzy Logic Toolbox, providing the advantage of simplicity and adequate representation for membership function. Figure 2 shows the fuzzy sets associated with all linguistic variables used in this problem. The Fuzzy Logic Toolbox is a collection of functions that are built in the

Table 1. The code, linguistic term, notation, interval value, and normalized interval values for the input variables

Code	Linguistic Term	Notation	Interval Value	Normalized Interval Value
$\rho 1$	Low	L	[0.9, 1.1]	[0, 2]
$\rho 2$	Medium	M	(1.1, 1.4]	(2, 5]
$\rho 3$	High	H	(1.4, 2.0)	(5, 10)
C_{w1}	Low	L	[0.1, 0.3]	[1, 2.5]
C_{w2}	Medium	M	(0.3, 0.7]	(2.5, 5]
C_{w3}	High	H	(0.7, 1.5]	(5, 10]
$C_{on-off1}$	Low	L	[0, 12.5]	[0, 1.25]
$C_{on-off2}$	Medium	M	(12.5, 62.5]	(1.25, 6.25]
$C_{on-off3}$	High	H	(62.5, 100]	(6.25, 10]
C_{s1}	Low	L	[0, 200]	[0, 5]
C_{s2}	Medium	M	(200, 400]	(5, 10]
C_{i1}	Low	L	[0, 150]	[0, 3.75]
C_{i2}	Medium	M	(150, 300]	(3.75, 7.5]
C_{i3}	High	H	(300, 400]	(7.5, 10]
C_{e1}	Low	L	[0, 250]	[0, 1.25]
C_{e2}	Medium	M	(250, 750]	(1.25, 3.75]
C_{e3}	High	H	(750, 2000]	(3.75, 10]

Table 2. The code, linguistic term, notation, and interval values for the output variables

Code	Linguistic Term	Notation	Interval Value
N_1	Very Short	VS	[2, 9]
N_2	Short	S	(9, 17]
N_3	Medium	M	(17, 25]
N_4	Rather Long	RL	(25, 33]
N_5	Long	L	(33, 41]
N_6	Very Long	VL	(41, 49]
Q_1	Very Short	VS	[0, 7]
Q_2	Short	S	(7, 15]
Q_3	Medium	M	(15, 23]
Q_4	Rather Long	RL	(23, 31]
Q_5	Long	L	(31, 39]
Q_6	Very Long	VL	(39, 47]

MATLAB numerical computing environment. It offers tools to generate and edit fuzzy inference systems within the framework of MATLAB. Experts may modify these figures to elucidate various problems.

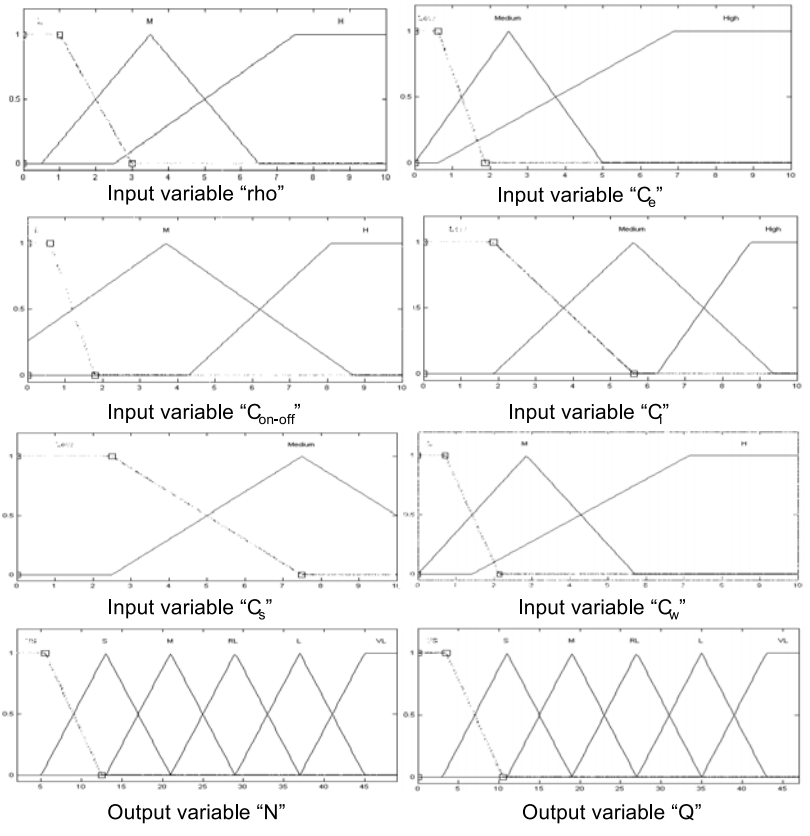

Fig. 2. Membership function plots

3.3 Rule Construction

If-then rule statements are used to formulate conditional statements that comprise fuzzy logic. A form of such a rule is: "If A=(ρ, C_i, C_e, C_{on-off}, C_w, C_s) THEN B=(N, Q)". The numerical solutions of decision model (5) with all the possible combinations of cost parameters determine the linguistic term of the decision variables N, Q. Recall that there are three linguistic terms for ρ, C_i, C_e, C_{on-off}, and C_w, and two are associated with C_s, Accordingly, there are $3 \times 3 \times 3 \times 3 \times 3 \times 2 = 486$ potential rules to be constructed. For instance, if $\rho = L$, and $C_w = M$, and $C_{on-off} = M$, and $C_s = M$, and $C_i = L$, and $C_e = H$, the determination procedure of decision variables is as described below.

1. Determine the midpoint of the respective subinterval of the linguistic term using the values given in section 3.1. If A=(L, M, M, M, L, H), then $\rho = L = (0.9 + 1.1)/2 = 1$; $C_w = M = (0.3 + 0.7)/2 = 0.5$; $C_{on-off} = M = (12.5 + 62.5)/2 = 37.5$; $C_s = M = (200 + 400)/2 = 300$; $C_i = L = (0 + 150)/2 = 75$; $C_e = H = (75 + 2000)/2 = 1037.5$.

2. The numerical results of equation (5) yield $N = 47$ and $Q = 43$.
3. From section 3.1, $N = 47$ falls in the subinterval $(41, 49]$ (VL) and $Q = 43$ falls in the subinterval $(39, 47]$ (VL). Therefore, the following rule is obtained. $(L, M, M, M, L, H) \rightarrow (VL, VL)$

3.4 Inference Engine

Mamdani-type of fuzzy inference systems in the Fuzzy Logic Toolbox are implemented. They represent the most commonly seen fuzzy methodology. The built-in function "evalfis" is applied to evaluate the output of a fuzzy system for a given multiple collections of inputs and determine a single output value from the set.

3.5 System and Simulation Experiment

The MATLAB Fuzzy Login Toolbox was primarily adopted to build this fuzzy expert system. Figure 3 presents the systematic framework. The system performance can be improved by increasing number of sets for inputs, and extending the rule base. Various test situations are considered to determine whether the fuzzy expert system fulfills the requirements that were specified initially. This system has six inputs and two outputs and displaying the results of all inputs-outputs in a three-dimensional plot is difficult. Figure 4 demonstrates some combinations of inputs and resulting outputs.

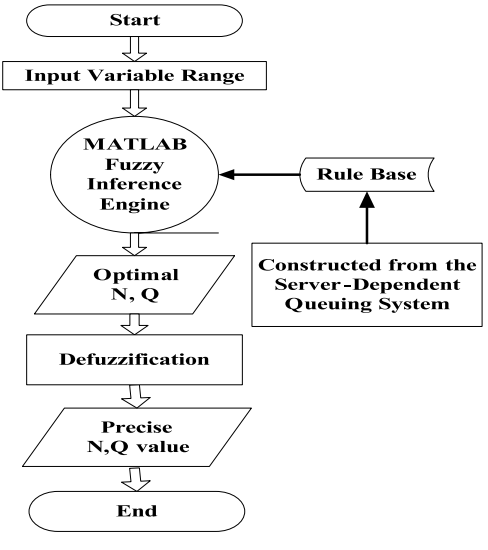

Fig. 3. System flow diagram

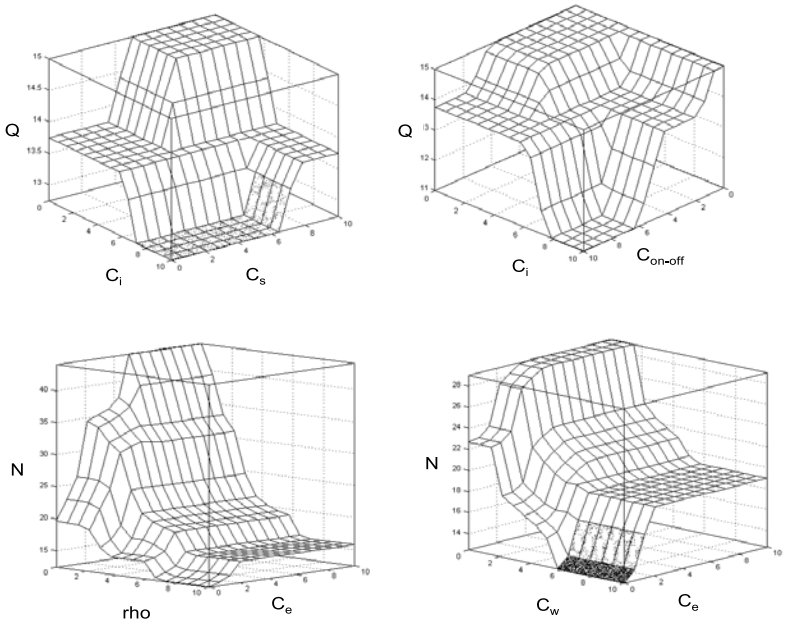

Fig. 4. Three-dimensional plots for input and output variables

4 Conclusions

This study applied the empirical Bayesian approach to estimate the demand for machining in FMS and constructed a server-dependent queuing system. Then, employed the queue length was adopted to activate and deactivate the second server, and was used as decision variables to construct a model of minimum expected cost. A fuzzy expert system was then set up according to the knowledge provided by the decision model of minimization cost. The utilization rate was first estimated using numerical data from simulation or empirical observation with the empirical Bayesian approach to indicate the required amount of machining. Next, the probabilities of each state for an M/M/2/L server-dependent queuing system were derived. Then, the parameters of cost were added to determine the optimal queue length N for starting a second server, and to determine the optimal queue length Q for turning off the second server. Finally, knowledge obtained from the queuing model was exploited to construct the rules and the MATLAB Fuzzy Inference Toolbox was employed to build the fuzzy expert system and assist decision-making.

Future study will examine performance of the system and the design of various membership function and inference engine.

Acknowledgements

This study was supported in part by the Global Logistics Research Center at National Cheng Kung University in Taiwan under the "Promoting Academic Excellence of Universities" program.

References

1. Lin, P.: Application of empirical Bayesian estimation to the optimal decision of a server-dependent queuing system. Yugoslav Journal of Operations Research 15(2), 191–207 (2005)
2. Thiruvaiyaru, D., Basawa, I.: Empirical Bayes estimation for queueing systems and networks. Queueing Systems 11, 179–202 (1992)
3. Turksen, I., Tian, Y., Berg, M.: A Fuzzy expert system for a service centre of spare parts. Expert Systems with Applications 5, 447–464 (1992)
4. Zadeh, L.: Fuzzy logic, neural networks, and soft computing. Communication of the ACM 37(3), 77–84 (1994)

Real-Time Auditory and Visual Talker Tracking Through Integrating EM Algorithm and Particle Filter

Hyun-Don Kim, Kazunori Komatani, Tetsuya Ogata, and Hiroshi G. Okuno

Speech Media Processing Group, Department of Intelligence Science and Technology,
Graduate School of Informatics, Kyoto University,
Yoshida-honmachi, Sakyo-ku, Kyoto, 606-8501, Japan
{hyundon,komatani,ogata,okuno}@kuis.kyoto-u.ac.jp

Abstract. This paper presents techniques that enable a talker tracking for effective human-robot interaction. We propose new way of integrating an EM algorithm and a particle filter to select an appropriate path for tracking the talker. It can easily adapt to new kinds of information for tracking the talker with our system. This is because our system estimates the position of the desired talker through means, variances, and weights calculated from EM training regardless of the numbers or kinds of information. In addition, to enhance a robot's ability to track a talker in real-world environments, we applied the particle filter to talker tracking after executing the EM algorithm. We also integrated a variety of auditory and visual information regarding sound localization, face localization, and the detection of lip movement. Moreover, we applied a sound classification function that allows our system to distinguish between voice, music, or noise. We also developed a vision module that can locate moving objects.

Keywords: Human-Robot Interaction, Talker Tracking, EM, Particle Filter, Sound source localization, Lip movement detection.

1 Introduction

In the near future, we expect the participation of intelligent robots in human society to grow rapidly. Therefore, since effective interaction between robots and the average person will be essential, robots should identify people in social and domestic environments, pay attention to the voices of people and look at speakers to identify them visually and associate voice and visual images so as to robustly realize interaction between the robot and the desired person [1-3].

The objective of this research has been to develop techniques that enable a talker tracking for effective human-robot interaction. Recently, Nakadai et al. developed real-time auditory and visual multiple-talker tracking technology [1, 2]. However, the program for this system has many conditional statements that enable multiple-talker tracking. Specifically, this system has auditory, vision, and motor modules and generates a stream through events extracted by each module. Streams can be associated in a pair of auditory and visual streams to create a higher level stream called an associated stream. Unfortunately, this algorithm needs many conditional

H.G. Okuno and M. Ali (Eds.): IEA/AIE 2007, LNAI 4570, pp. 280–290, 2007.

statements to create associated streams because the system has to compare every stream that differs from the others. Moreover, if the entirely new kind of an event is applied to the system, the program structure has to modify all parts of the algorithm related to streams and associations. For these reasons, the program is complex and difficult to modify for changing conditions. We propose a way of selecting an appropriate path to track a talker from various events through expectation maximization (EM) algorithm [4]. Our method is simple because many conditional statements are not needed to create associated streams and it is flexible because newly added streams can be easily applied to the system without modifying the entire algorithm. Moreover, to obtain a reliable tracking path, we added a particle filter [5] to the tracking process after executing the EM algorithm. That can help the robot to continuously track a designated talker.

Our auditory system also has a sound classification module that can distinguish between voice, music, and noise to enable reliable talker tracking in real environments. To achieve this, we used a Gaussian mixture model (GMM). To make up for the fact that a face detection module cannot detect a face that is turned away or tilted, we also developed a module to locate moving objects. The vision system can also detect lip movement to identify the talker.

2 Design of System

As a test of real-time talker tracking, we use a humanoid robot called SIG2 (left of Fig. 1). SIG2 has two omni-directional microphones inside humanoid ears at the left and right ear positions, and its head has three degrees of freedom (DOF) and the body has one DOF, each of which is enabled by a DC motor controlled by an encoder sensor. SIG2 is equipped with a pair of CCD cameras, but the current vision module only uses one camera.

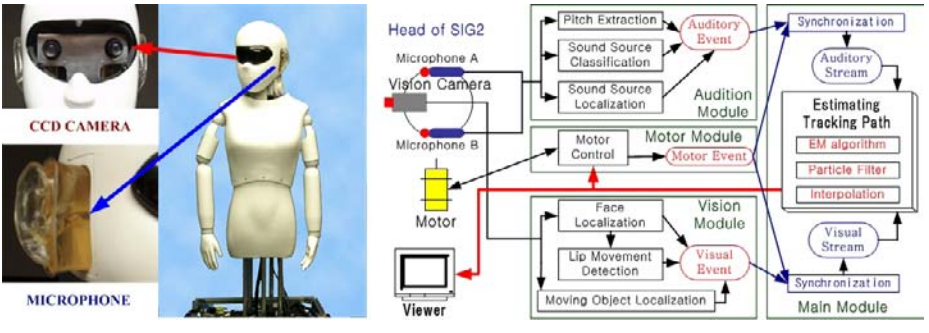

Fig. 1. SIG2 and System Overview

The right part of Figure 1 shows the structure of the system based on a client/server model. Our system consists of four client modules (audition, vision, motor, and viewer) and a server module (main). Each module has the following functions:

1) Audition: Generates auditory events through pitch extraction, sound source localization, and sound source classification. In particular, an audition module can discriminate between three classes (voice, music, or noise). The sampling frequency is 16 kHz, the processing time for each event generation is 32 ms, and 4.5 frames (one frame consists of 1024 samples) must be calculated to classify sound sources.

2) Vision: Generates vision events through face localization, the detection of lip movement, and the localization of moving objects. The processing time for the generation of each event is up to 250 ms.

3) Motor: Generates motor events and controls the motors for tracking a talker. The time needed to generate each event is 100 ms.

4) Viewer: Displays various streams, result data, and the tracking status.

5) Main: The main (server) module can currently create four streams (sound, face, moving objects, and motor) using events extracted by the subsystems. Beyond that, the main module estimates an appropriate tracking path through the EM and particle filter to track the desired talker from a group of people in a noisy environment.

3 Audition System

Our system can classify three types of sounds (voice, music, and noise) to track a talker in a real environment. It uses four auditory features (pitch, SF, MFCC, and sound source localization), and needs to calculate a period of 4.5 frames to classify sounds.

1) Sound Source Localization: We used a CSP method for sound source localization [6]. The CSP method can usually estimate one delay of arrival (DOA) between signals entering from two microphones at a frame. Therefore, for the purpose of localizing multiple sound sources, we estimate multiple direction of sound after we have gathered the results of CSP every 0.5 frame (one frame consists of 1024 samples) for 4.5 frames.

2) Pitch Extraction: We used a cepstrum method to extract a pitch signal [7]. One of the most important features of the cepstrum is that if a signal is periodic, it will present peaks at intervals for each period. Therefore, the cepstrum can reliably extract the pitch of a speech signal.

3) Spectrum Flux: Spectrum flux (SF) is the average variation in the spectrum between two adjacent frames [8]. In our experiments, we found that, in general, the SF values for voice were higher than those for music or noise. Therefore, SF is a good feature for classifying speech signals. This is used to discriminate between speech and non-speech.

4) Mel Frequency Cepstral Coefficients: There are two dominant types of acoustic measurements of speech signals for the feature extraction of speech. One is the parametric approach, which was developed to match closely the resonant structure of the human vocal tract that produces the corresponding speech sound. It is mainly derived from linear predictive analysis, such as LPC-based cepstrum (LPCC). The other is the non-parametric method which models the human auditory perception system. Mel frequency cepstral coefficients (MFCCs) are used for this purpose [9]. Here, we used the 0 to 12^{th} MFCCs. MFCC provides useful information for

discriminating between speech and non-speech. Usually, the 0 to 12th MFCCs of speech signals have different patterns for speech, music, or noise.

3.1 Sound Source Classification Using GMM

For the purpose of classifying sound signals base on auditory features, we first applied each feature data extracted from the cepstrum, MFCC, SF, or CSP to mean and covariance. Then, for the cepstrum, SF, and CSP, if the values calculated from the mean and the covariance are within the boundary of those of speech signals, final feature values, $f_t^{2\sim4}$, will have the resulting value as a speech signal.

When using MFCCs, we applied the 0 to 12th MFCCs to Gaussian Mixture Model (GMM) defined by (1). The GMM is a powerful statistical method widely used for speech classification [10].

$$P_{mixture}\left(X_{0\sim12}|\theta_{0\sim12}\right)=\sum_{L=0}^{12}P_L\left(X_L|\theta_L\right)w(L)\quad\sum_{L=1}^{L+1}w(L)=1,\quad 0\le w(L)\le 1 \tag{1}$$

where P is the component density function, L is the number of the MFCC order, X is the 0 to 12th MFCC data, and θ is the parameter vector concerning MFCCs. Moreover, to classify speech signals robustly, we designed two GMM models for speech and noise derived as

$$f_t^1=\log\left(P_s\left(x_s(t)|\Theta_s\right)\right)-\log\left(P_n\left(x_n(t)|\Theta_n\right)\right) \tag{2}$$

where P_s is the GMM related to speech, and $X_s(t)$ is the speech feature data set in the t-*th* frame belonging to the speech parameters, Θ_s. On the other hand, P_n is the GMM related to noise and $X_n(t)$ is the noise feature data set in the t-*th* frame belonging to the noise parameters, Θ_n. Finally, all final feature values, $f_t^{1\sim4}$, are combined to judge whether the frame is voice, music, or noise. To train the GMM parameter, we used 30 speech data (15 male and 15 female), 15 noise data (white, brown, pink, and clapping), and 15 music data (instrumental pop music).

4 Vision System

For the purpose of detecting human faces, we used open computer vision (OpenCV), the open source vision library created by the Intel Company. This library supplies functions for detecting human faces. Therefore, we can obtain the numbers and coordinates of detected faces through OpenCV [3]. Our system used 320 x 240 images and can calculate about four images per second.

We detect lip movement using an OpticalFlow function in OpenCV. This function can detect variations between the former and present image. Therefore, our system can accurately distinguish when a speaker is talking. The left of Fig. 2 shows feature masks applied to the area of detected faces to detect lip movement and the top-right of Fig. 2 presents the results for face and lip movement detection among three people. In this picture, blue boxes indicate detected faces and the person at left, whose box has turned red, is selected as the talker because lip movement is detected among the detected faces. The left side shows the applied feature masks. However, OpenCV has

some limitations. First, it cannot determine a face over 2m away by using 320 x 240 images. Second, it cannot detect a face which is turned away or tilted. Consequently, a person must be looking straight at the camera. To overcome these shortcomings, we developed a function for localizing moving objects by using OpticalFlow. It can infer a moving object's position from a position where the value calculated by OpticalFlow is high. Therefore, although faces are not detected even if people are in front of the camera, it can obtain the positions of people when they are moving. The bottom-right of Fig. 2 shows an image captured by SIG's camera, and the red lines indicate how different objects are moved between a former and a present image.

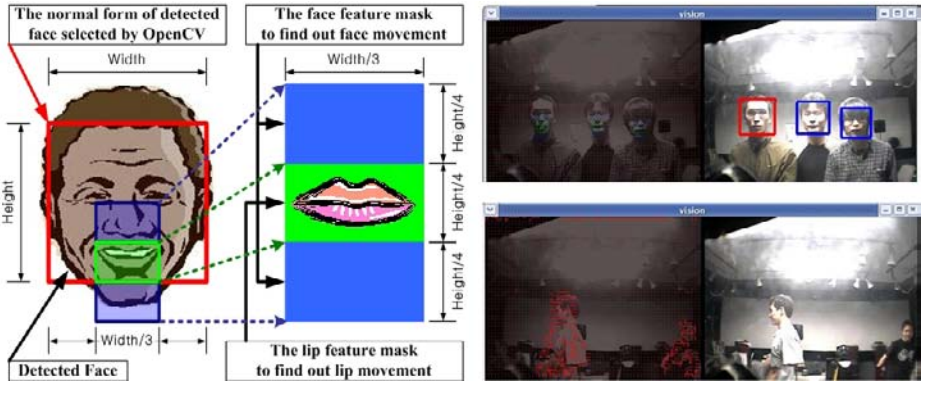

Fig. 2. Feature mask for detecting lip movement and resulting images

5 Talker Tracking System

Figure 3 shows the process for selecting an appropriate tracking path using the EM algorithm and particle filter. In Fig. 3, for simplicity, there are just two kinds of streams (sound and vision stream) and four Gaussian mixture components for EM

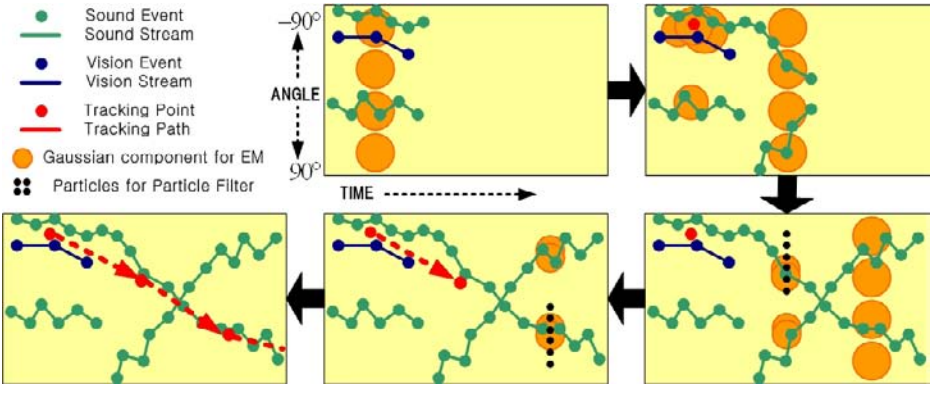

Fig. 3. Process to select the path for talker tracking

training. However, our system actually has three kinds of streams (sound, face, and moving object localization) and uses eight Gaussian mixture components for training. Sub-section 5.1 to 5.3 describe this processing in detail.

5.1 Arranging Gaussian Mixture Components

Since our system determines a tracking path according to the distribution of events, the system increases the number of specific events in order to raise the density of the specific events in the first step. For example, in case of sound events extracted from voice or face events when lip movement, it increases the actual number of events three to four times so that the Gaussian components for EM training are located near the area of the events that has the highest priority. After that, the set of increased data, X_m, are substituted for a one-dimensional Gaussian mixture that is denoted as

$$P\left(X_m|\mu_k,\sigma_k\right)=P\left(X_m|\theta_k\right)=\frac{1}{\sqrt{2\pi\sigma_k^2}}e^{-\frac{(X_m-\mu_k)^2}{2\sigma_k^2}} \tag{3}$$

where μ_k is the mean, σ_k^2 is the variance, θ_k is a parameter vector, and k is the number of mixture components. The objective is to find the parameter vector, θ_k, describing each component density, $P(X_m|\theta_k)$.

Then, for EM training (iteration), eight Gaussian components are located between -90° and 90° at 500ms intervals and the interval to run the EM algorithm also shifts every 100 ms. This step is at the top center of Fig. 3.

5.2 Executing the EM Algorithm

We should apply an EM algorithm in this process [4], which allows us to easily obtain the range of directions for tracking from various streams. Therefore, after locating the Gaussian components, the system runs the E-step and M-step for less than 10 iterations. This EM step is detailed as follows.

1) E-step: The expectation step essentially computes the expected values of the indicators, $P(\theta_k|X_m)$, that each data point X_m is generated by component k, given N is the number of mixture component, the current parameter estimates θ_k and weight w_k, using Bayes' Rule derived as

$$P\left(\theta_k|X_m\right)=\frac{P\left(X_m|\theta_k\right)\cdot w_k}{\sum_{k=1}^{N}P\left(X_m|\theta_k\right)\cdot w_k} \tag{4}$$

2) M-step: At the maximization step, we can compute the cluster parameters that maximize the likelihood of the data assuming that the current data distribution is correct. As a result, we can obtain the recomputed mean using (5), the recomputed variance using (6), and the recomputed mixture proportions (weight) using (7). M is the total number of data.

$$\mu_k = \frac{\sum_{m=1}^{M} P(\theta_k | X_m) \cdot X_m}{\sum_{m=1}^{M} P(\theta_k | X_m)} \tag{5}$$

$$\sigma_k^2 = \frac{\sum_{m=1}^{M} P(\theta_k | X_m) \cdot (X_m - \mu_k)^2}{\sum_{m=1}^{M} P(\theta_k | X_m)} \tag{6}$$

$$w_k = \frac{1}{N} \sum_{m=1}^{M} P(\theta_k | X_m) \tag{7}$$

After the E and M steps are iterated an adequate number of times, we can obtain the estimated mean, variance, and weight corresponding to the current data distribution.

Consequently, Gaussian mixture components are relocated around the streams and these are mainly concentrated where the density of streams is high. In addition, the mean, variance, and weight of components are respectively decided according to, the location value, the distributional range, and the priority of events. Also, the starting point for talker tracking will be determined where the weight calculated by EM is the highest if the means and variances for 3 or 4 shift intervals are similar. This step is at the top right of Fig. 3.

5.3 Particle Filter Implementation

If there are several streams that have the same kind or weight, it will be difficult to determine the tracking path because the EM results for classified areas may have the same conditions. Therefore, we also proposed a way of adding a particle filter [5] to the tracking process after executing the EM algorithm. The particle filter can help a robot to maintain the designated tracking path that it has tracked. The details on the process of applying particle filter are as follows. First, we can estimate the present tracking position by using some past tracking positions using this model:

$$x_{t+1}^i = x_t^i + \dot{x}_t^i \cdot T_s + \ddot{x}_t^i \frac{T_s^2}{2} \tag{8}$$

where i is the number of particle, T_s is a sample period, x^i_{t+1} is a estimated tracking position, x^i_t is the former tracking position, $\dot{x}^i_t$ is the differential value between x^i_t and x^i_{t-1}, and the differential value between $\dot{x}^i_t$ and $\dot{x}^i_{t-1}$ is $\ddot{x}^i_t$. Then, the particle filter spreads particles within a range of $\pm 15°$ of the estimated position. This step is at the bottom right of Fig. 3.

Second, it should calculate the weight of particles that is defined as in (9) by using resulting values (mean, variance, and weight) calculated with the EM algorithm. It should then iterate the update routine until the re-sampling condition is satisfied. It is defined in (10). Then, tracking points can be determined at the bottom center of Fig. 3. The iteration routine for the particle filter is detailed as follows.

1) Measurement update: Update the weights by the likelihood:

$$\omega_t^i = \omega_{t-1}^i P\left(\theta_t^i \middle| x_t^i\right) = \omega_{t-1}^i \frac{P\left(x_t^i \middle| \theta_t^i\right) \cdot w_t^i}{\sum_{i=1}^{N} P\left(x_t^i \middle| \theta_t^i\right) \cdot w_t^i} \tag{9}$$

$i = 1, 2, \ldots, N$ and normalize to $\omega_t^j := \omega_t^j \left[\sum_{i=1}^{N} \omega_t^j\right]^{-1}$

As an approximation to, take $x_t \approx \sum_{i=1}^{N} \omega_t^i x_t^i$

2) Re-sampling:

(a) Bayesian bootstrap: Take *N* samples with replacement from the set $\{x_t^i\}_{i=0}^N$ where the probability to take sample i is ω_t^j. Let $\omega_t^j = 1/N$. This step is also called Sampling Importance Re-sampling (SIR).

(b) Importance sampling: Only resample as above when the effective number of samples is less than a threshold, N_{th},

$$N_{eff} = \frac{1}{\sum_{i=0}^{N} \left(\omega_t^i\right)^2} < N_{th} \tag{10}$$

Here, $1 \le N_{eff} \le N$, where the upper bound is attained when all particles have the same weight, and the lower bound when all probability mass is at one particle. The threshold can be chosen as $N_{th} = 2N/3$. Let $t := t+1$ and iterate to measurement update.

Finally, the appropriate path for tracking a talker can be continuously determined by iterating EM and particle filter. The interval for executing the particle filter is 0.5 s and it shifts every 100 ms. Consequently, as you see the bottom left of Fig. 3, although the classified areas of streams have the same conditions or the paths of streams even cross one another, we are able to estimate a reliable tracking path.

6 Experiments

As you see Fig. 4, a viewer module displays various streams, the current position of a motor, and the results and status of a talker tracking received from the main module. The red rings indicate the path selected for talker tracking by the EM algorithm and the particle filter. To achieve the reliable talker tracking in a real environment, the proposed system was designed with the following points in mind.

1) The sound stream created from noise is rejected for tracking. Besides, when there are only moving object streams, they are also rejected for tracking. However, the sound stream created from voice and the face stream create from a face localization are accepted.
2) If two sound streams created from voice occur at the same time, the system will select the sound stream where vision information (face and moving object) exists nearby. Also, when a sound stream created from music or noise occurs with a face stream, the system selects the face stream.

Fig. 4 shows that the robot is actually turning its head towards the direction of a path selected by the EM and particle filter algorithm. The pink area indicates the visibility range of the vision camera and the center of the area indicates the position of the rotation motor of a head. From (A) in Fig. 4, we can see that a designated tracking path, that was first started compared to another path, is continuously selected by our proposed method even if several sound streams exist at the same time. However, if a vision stream appears in another area that did not belong to the tracking path, the tracking path will be changed. This is because visual information is usually more reliable than audio information. From (B) in Fig. 4, we can see that although the paths of streams cross one another, it is able to maintain the initial tracking path. (C) in Fig. 4 shows the talker tracking with all kinds of streams. Needless to say, the area including all kinds of streams has top priority when tracking the talker. Therefore, this is always determined as the tracking path.

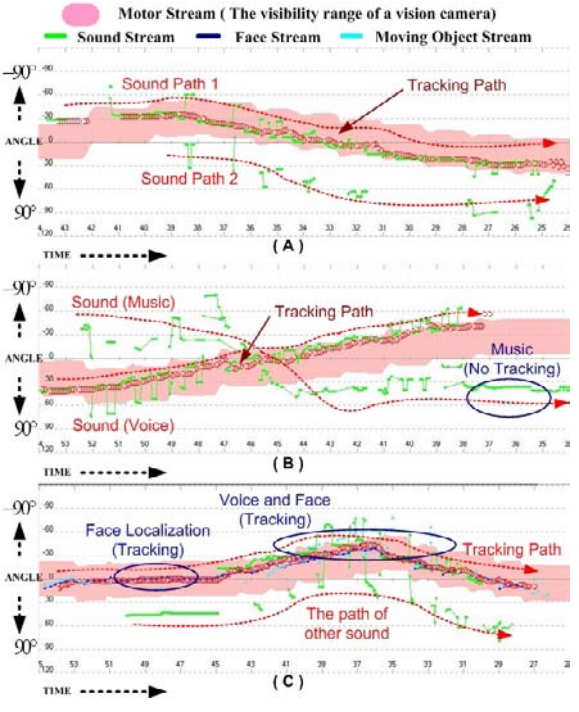

Fig. 4. Results for talker-tracking experiments

7 Conclusion and Future Work

We described new way of using an EM algorithm and particle filter to select an appropriate tracking path for the purpose of tracking a talker. Our system based on this approach has some principal merits. First, the proposed algorithm is simple because it contains relatively few conditional statements. It is also not necessary to

associate streams, unlike the conventional system, because our system can easily infer the distributional range of streams from the variance calculated by EM. Second, although developers do not need to modify the entire algorithm, the proposed system can easily adapt new kinds of events or streams to the tracking system. Since this system estimates the position of a desired talker through means, variances, and weights calculated from EM training regardless of the number and kinds of events and streams, they only determine the initial conditions according to the priorities of the new events or streams. Finally, to produce a reliable tracking path, we added the particle filter to the tracking process after executing the EM algorithm. The particle filter can help it to maintain the designated tracking path that the robot has tracked regardless of the changing conditions of streams or the position of the tracking path.

However, we need to refine our system to achieve real-time auditory and visual talker tracking in practical environments. First, we plan to develop a system that can track a group of talkers in practical environments. Therefore, sound identification and face recognition will be necessary. Reliable multiple sound source localization will be also necessary. In this respect, we are considering a way of integrating the best features of several methods for sound source localization. Second, to realize a practical active auditory system, we need to add speech recognition and a voice synthesis function to our system so that it will be able to talk with humans. In addition, we intend to add sound source separation to our system so that it can deal with various sound signals.

Acknowledgments. This research was partially supported by MEXT, Grant-in-Aid for Scientific Research, and COE program of MEXT, Japan.

References

1. Nakadai, K., Hidai, K.-i., Mizoguchi, H., Okuno, H.G., Kitano, H.: Real-Time Auditory and Visual Multiple-Object Tracking for Humanoids. In: Proc. of 17th Int. Conf. on Artificial Intelligence (IJCAI-01), Seattle, August 2001. pp. 1425–1432 (2001)
2. Okuno, H.G., Nakadai, K., Hidai, K.-i., Mizoguchi, H., Kitano, H.: Human-Robot Interaction Through Real-Time Auditory and Visual Multiple-Talker Tracking. In: Proc. of IEEE/RSJ Int. Conf. on Intelligent Robots and Systems (IROS-2001), October 2001, pp. 1402–1409 (2001)
3. Kim, H.D., Choi, J.S., Kim, M.S.: Speaker localization among multi-faces in noisy environment by audio-visual integration. In: Proc. of IEEE Int. Conf. on Robotics and Automation (ICRA2006), May 2006, pp. 1305–1310 (2006)
4. Moon, T.K.: The Expectation-Maximization algorithm. IEEE Signal Processing Magazine 13(6), 47–60 (1996)
5. Gustafsson, F., Gunnarsson, F., Bergman, N., Forssell, U., Jansson, J., Karlsson, R., Nordlund, P.: Particle Filters for Positioning, Navigation and Tracking. IEEE Trans. on Acoustics, Speech, and Signal Processing 50(2), 425–437 (2002)
6. Nishiura, T., Yamada, T., Nakamura, S., Shikano, K.: Localization of multiple sound sources based on a CSP analysis with a microphone array. In: IEEE/ICASSP Int. Conf. Acoustics, Speech, and Signal Processing, June 2000, pp. 1053–1056 (2000)
7. Kobayashi, H., Shimamura, T.: A Modified Cepstrum Method for Pitch Extraction. In: IEEE/APCCAS Int. Conf. Circuits and Systems, pp. 299–302 (November 1988)

8. Lu, L., Zhang, H.J., Jiang, H.: Content Analysis for Audio Classification and Segmentation. IEEE Trans. on Speech and Audio Processing 10(7), 504–516 (2002)
9. Shah, J.K., Iyer, A.N., Smolenski, B.Y., Yantormo, R.E.: Robust Voiced/Unvoiced classification using novel feature and Gaussian Mixture Model. In: IEEE/ICASSP Int. Conf. Acoustics, Speech, and Signal Processing, Montreal, Canada (May 2004)
10. Bahoura, M., Pelletier, C.: Respiratory Sound Classification using Cepstral Analysis and Gaussian Mixture Models. In: IEEE/EMBS Int. Conf. San Francisco, USA (September 1-5, 2004)

Self-organizing Multiple Models for Imitation: Teaching a Robot to Dance the YMCA

Axel Tidemann and Pinar Öztürk

IDI, Norwegian University of Science and Technology
tidemann@idi.ntnu.no

Abstract. The traditional approach to implement motor behaviour in a robot required a programmer to carefully decide the joint velocities at each timestep. By using the principle of learning by imitation, the robot can instead be taught simply by *showing* it what to do. This paper investigates the self-organization of a connectionist modular architecture for motor learning and control that is used to imitate human dancing. We have observed that the internal representation of a motion behaviour tends to be captured by more than one module. This supports the hypothesis that a modular architecture for motor learning is capable of self-organizing the decomposition of a movement.

Keywords: Human Robot Interaction, Machine Learning, Neural Networks.

1 Introduction

Learning by imitation is an important part of human cognitive behaviour, and this approach has gained considerable interest in the artificial intelligence community [1]. Dancing is an area where imitation learning is easily observable. When learning to dance, students imitate the movement of the teacher with only visual input to guide their own motor system.

This paper presents a humanoid robot simulation that mimics this phenomenon. Our model is based on an on-line imitation learning algorithm for acquisition of dance movements. As our research agenda includes the study of the mechanisms for composing complex movements from simpler motor primitives we have a special focus on how motor primitives are acquired. Towards this end we implemented a modular architecture where a module learns and represents such a primitive. A module may be envisioned as an expert that specializes on one or several such primitives. We investigate whether an architecture with several such expert modules can self-organize learning and execution of motor primitives. The underlying architecture uses multiple paired inverse/forward models, implemented using recurrent neural networks. The research question of this paper reads: *How and to what extent will multiple paired inverse and forward models self-organize when used as controllers for a humanoid robot?*

H.G. Okuno and M. Ali (Eds.): IEA/AIE 2007, LNAI 4570, pp. 291–302, 2007.

2 Imitation in Psychology, Neuroscience and AI

Developmental psychologists have long focused on how infants learn by imitating their parents and the people in their surroundings. Piaget [2] describes imitation as the continuation of *accommodation* (i.e. adjustment or adaptation) of sensory-motor schemas (i.e. motor and perception stimuli) to the external world, an important part of intelligent human behaviour. Meltzoff and Moore suggest that imitation in newborns is due to a process they call *active intermodal mapping* (AIM) [3]. The intermodal mapping relies on a representational system capable of uniting perception and production of human acts, which can be used to correct the child's behaviour so that it will match that of the demonstrator.

The discovery of mirror neurons [4] has caught the interest of researchers in several disciplines. Mirror neurons, which are observed to activate both when observing and performing a certain action, are suggested to play an important role in imitation [1], language [5] and mind reading [6].

Research in the field of imitation learning in computer science is coarsely divided in two groups: those focusing on transforming visual information to a meaningful representation for the agent (also called the *correspondence problem*) or the motor part (all perceptual information is already present, ready to be input to a perception-action system) [1]. Schaal believes that the most interesting approach to imitation learning is *model-based learning* (note that this brief review focuses on *multiple model* approaches to imitation learning), where an inverse model will output a motor command to achieve a desired state, given the current state and the desired state. The output of the inverse model is given as input to a forward model that will predict the outcome of the motor commands acting on the environment. It is because of the predictive aspect that he favors this approach. Schaal also thinks the modular approach fits nicely with the simulation theory of mind-reading, as well as a possible way to implement the AIM framework of Meltzoff and Moore.

Demiris [7,8] and Wolpert [9] have worked on multiple inverse/forward models for imitation learning (note that this is in principle similar to Jacobs' mixtures of experts, [10]). Wolpert argues that the cerebellum has several forward and inverse models [11], and that they correspond to different motor primitives. Wolpert believes the inverse/forward models should be implemented as neural networks, whereas Demiris uses different techniques such as PID controllers and Bayesian belief networks to represent the models.

Matarić has a holistic modular approach to imitation; her architecture also addresses the visual processing of imitation [12] (it is one of the modules, along with attention, motor primitives and learning modules). She uses different techniques for implementation of the modules, and has tested the architecture on several robots testbeds.

3 A Multiple Paired Model for Dance Imitation

We have implemented a multiple paired models architecture (abbreviated MPMA) inspired from Demiris' HAMMER [8] and Wolpert's MOSAIC [9,13]

architectures. Both MOSAIC and HAMMER use multiple paired inverse and forward models. Why use multiple paired models as a control architecture? The modularity of the brain serves as a good inspiration for modeling artificial intelligence. Even though multiple paired inverse/forward models may not be the actual organization of the brain, it is a computational approach that is well understood in the control literature [14]. In addition, multiple models can be seen as a solution to the problem of trying to compress too much information into one network and when learning of new concepts destroys what has previously been learnt, i.e. *catastrophic forgetting* [15]. Furthermore, modular architectures can implement redundancy which is an important feature of intelligent systems [16], and hence ensure robustness. Modular architectures can also expand their capabilities by adding new modules (although this is not done in our implementation). Such a modular system enables the exploration of whether and how a movement is decomposed into smaller submovements and how and why these can be represented by different modules.

The MPMA can also exploit the advantages of both a localist and distributed representation, a localist representation (i.e. a module[1]) makes it easy to tell where a certain concept is stored, whereas a distributed representation (i.e. the neural networks in the models) is noise-tolerant and can still function even if some of the nodes of the network become destroyed.

Figure 1 illustrates the architecture. The forward model and responsibility predictor are *predictors* of the next state and the suitability of the module, respectively. The inverse model can be thought of as a *controller* or *behaviour*. The different models will now be explained in more detail.

3.1 The Models

The forward model learns to predict the next state $\hat{x}^i_{t+1}$ based on the motor command u^i_t applied to the current state x_t. The error signal (i.e. dashed arrow) used for training[2] the forward model is the difference between the predicted and the actual next state.

The inverse model learns how to produce the motor commands u^i_t to achieve the target state $x^{'}_t$ given the current state x_t. The error signal of the inverse model is the *feedback motor error command*, u_{feedback}. The feedback controller [17] computes the difference between the target state at time t with the actual state at time $t+1$. The difference is multiplied with a constant K, and used as motor commands to pull the system in the right direction, i.e. the error in joint *angles* is used to compute joint angle *velocities*. Training an inverse model is a hard problem, since there are many ways to achieve a certain desired state [14]. The feedback error motor signal represents a simple way to find a trajectory since it will coarsely pull the system in the right direction when the system issues bad motor commands, with decreasing influence as the system performs better.

[1] The term *module* is used in this paper to group three components together: an inverse and forward model, and a responsibility predictor, which will be explained shortly.

[2] All the recurrent neural networks are trained using the backpropagation through time algorithm.

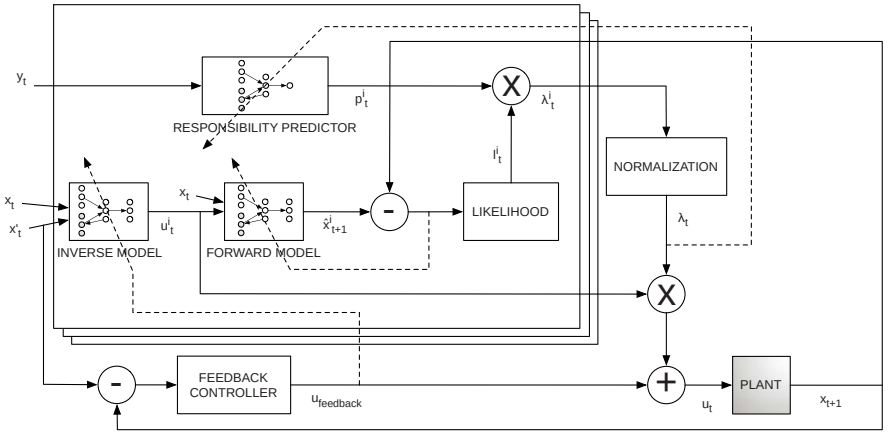

Fig. 1. The multiple paired models architecture. See the text for explanation of the different variables. Inspired from [13] and [8].

The responsibility predictor learns to predict the suitability p_t^i of a module *prior* to movement, based on the context signal y_t. Its error signal is λ_t^i. The λ_t^i value is calculated based on two factors: 1) the likelihood l_t^i calculates how well the forward model predicts the next state, based on the difference between the predicted next state and the actual next state, assuming it is influenced by gaussian noise with a standard deviation σ, and 2) the predicted responsibility p_t^i. The λ_t^i values are normalized across the modules, resulting in the final λ_t vector. The λ_t vector corresponds to which of the modules is most suitable to control the motor commands sent to the plant (i.e. robot). The output of the inverse models u_t^i is multiplied with the normalized λ_t vector. Modules with a high λ value will then achieve more influence over the total motor command u_t sent to the plant than modules with a low λ value. This is how switching between modules is realized. In addition, the λ value is used to gate the learning of the inverse and forward models, by multiplication with the error signal. If a module makes bad predictions and receives a low λ value, it will not influence the final motor command, nor will it receive much of its error signal. Modules that make good predictions will gain more control over the total motor command, and also receive more of its error signal to further fine-tune its predictions.

The difference between λ_t^i and p_t^i was used as a performance measure during training. When the difference was below a certain threshold the training would stop, since the system then correctly predicts which module is more suitable to control different parts of the movement.

3.2 Input/Output of the MPMA

The input to the MPMA was the joint angles of the demonstrator. This was done to overcome the correspondence problem, i.e. the transformation from an

extrinsic to an intrinsic frame of reference [18]. Demiris and Hayes [7] take the same approach. It is questionable whether this is a biologically plausible approach, however studies in neuroscience anticipate the existence of a geometric stage where sensory input is transformed to postural trajectories which in turn can be used by the motor system, as argued by Torres and Zipser [19]. Furthermore, experiments done by Desmurget and Prablanc [20] show that humans actually use estimation of joint angles when imitating.

The other input to the system is the context signal. As an example of a context signal, Wolpert uses whether a cup is empty or full [9] in order to select between two inverse models that both will generate motor commands to lift the cup. We let the context signal correspond to the music playing while dancing, i.e. it can be thought of as a representation of the melody the imitator hears while it is dancing.

The output of the system are motor commands to be applied on the plant. In this case, the robot is the plant, and the motor commands are the *joint angle velocities* of the robot. Joint angle velocities are not directly equal to motor commands, since motor commands are expressed in *forces* of the actuators. We define that the inverse models output joint angle velocities because the simulator (see section 4) takes joint angle velocities as input, *not* forces. The simulator will calculate the forces that will yield the desired joint angle velocity. This approach is similar to [21], which calculates desired trajectories and relies on an inverse dynamics controller for the motor commands. Still, issuing joint angle velocities is closer to motor commands than a desired trajectory, and it is a simpler problem to solve for the inverse dynamics controller. To resume the argument above by Torres and Zipser; there is some indication that this is how the brain plans. After application of the motor commands, the plant returns the actual next state.

3.3 Details of the MPMA

In MOSAIC [9] there is a difference between action production and observation; when *producing* an action, each forward model is fed the *sum* of all the inverse motor commands. When *observing* an action for imitation, the output of *each* inverse model is fed into the paired forward model, this is similar to the HAMMER architecture. The MPMA does not have two modus operandi, the architecture design is the same as MOSAIC in *action observation mode*, since we consider this best models the action/prediction-relationship of having multiple paired inverse/forward models. This design choice is also related to the fact that there is no "observation phase" with inhibition of the motor commands as the imitator is watching the teacher, with a subsequent selection of appropriate modules that will imitate the action (as is the case in both MOSAIC and HAMMER). The imitator tries to imitate the perceived movement as it is being demonstrated. Children often imitate what they are observing without being aware that they are imitating (Piaget defines this as the sixth level of imitation [2]). The MPMA uses a divide-and-conquer technique to learn a movement. A movement is divided

into meaningful pieces (which may also be called motor primitives), each of which is learned by a module. The modules can split movements amongst themselves as they see fit.

Our implementation seeks to combine the best of both HAMMER and MOSAIC, i.e. the inverse/forward pairing of the former (note that MOSAIC also has inverse/forward pairing, but this was only in *action observation mode*), and the responsibility predictor and the focus on self-organization from the latter.

4 Experimental Setup

The breve simulator[3] (an open-source graphical simulator, using the Open Dynamics Engine[4]) was used to implement the humanoid robot. The MPMA was implemented in MatLab, and the communication between MatLab and breve was done via sockets. MatLab sent the motor commands to the breve simulator, and breve returned the state of the simulator after the application of the motor commands for 13 timesteps. This required the forward models to predict the state of the robot for 13 timesteps into the future.

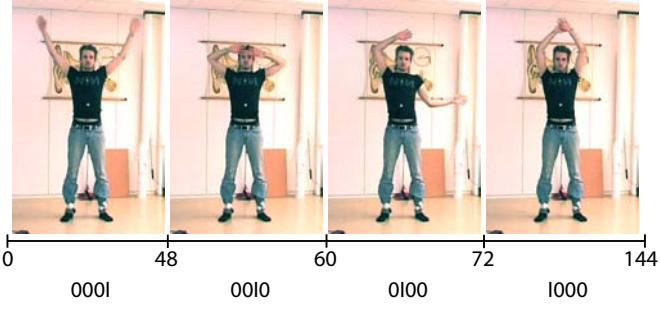

Fig. 2. The YMCA movement. The letters *Y M C A* are spelled out using arm movements. The numbers directly below the figure show how many timesteps are spent forming each letter. The context signal is shown below the time scale.

Two conditions were examined for the experiment: 1) the system was allowed to completely self-organize, and 2) the responsibility predictors were trained on the context signals *before* the training of the system as a whole, i.e. biasing the system to learn specific parts of the movement in each of the modules. This was done to see whether the system would self-organize differently, and how it would affect the performance of the system. Note that the responsibility predictors would still be trained during the training of the entire system in the second condition, retaining its self-organizing capabilities. It is the perspective of the designer that one module should be allocated to each of the context signals, since they represent different parts of the melody and also different movements.

[3] http://www.spiderland.org/breve/
[4] http://ode.org/

The experiment consisted of imitating the dance from a song called YMCA by the Village People, a 70s disco group from New York, see figure 2. Training data was collected by using the Pro Reflex tracking system at the Developmental Neuropsychology lab at the Institute of Psychology, NTNU. The system is able to track the position of fluorescent balls within a certain volume by using five infrared cameras. The tracking of the balls yields Cartesian coordinates of the balls, which can be used to calculate the joint angles of the demonstrator, which were scaled to the range $[0, 1]$. No averaging or smoothing of the data was done. The noisy data was added small amounts of Gaussian noise with mean 0 and standard deviation 0.01 at each training epoch, to render it slightly different for each training epoch. Only the arm movements are imitated, so the robot has four degrees of freedom (one at each shoulder and elbow joints). The learning rate of the inverse, forward and responsibility predictor networks were $\delta_{inv} = \delta_{forw} = 0.1$, $\delta_{rp} = 0.3$ (the learning rate of the responsibility predictor is higher than the other networks to make it adapt quickly to λ_i^t), $\sigma = 0.25$ (of the likelihood function), the feedback error motor constant was $K = 3$, and the error proportion $ep = 1.1$ was used to bias the learning of the winning module (as is done in [22]). The biasing was done as follows: after normalization of the λ_t vector, the highest λ value is multiplied with ep, and then the λ_t vector is normalized again. The stopping criterion was the following: the mean difference between p_i^t and λ_i^t throughout an epoch had to be lower than 0.0045 for all modules.

5 Results

Each of the conditions was run 20 times. The results are presented in table 1. The robot imitating the human dancer can be seen in figure 3. Figure 4 shows how the MPMA switches between different modules for both the conditions after training by plotting λ_t^i. p_t^i is also plotted in the same figure. Note that they overlap. This is an indication of stability in the system, and was used as a stopping criterion, as discussed above. Figure 5 shows the performance of the system regarding the target trajectory versus the actual trajectory. The background color correspond to λ_t^i, making it easy to see which module controls which part of the movement.

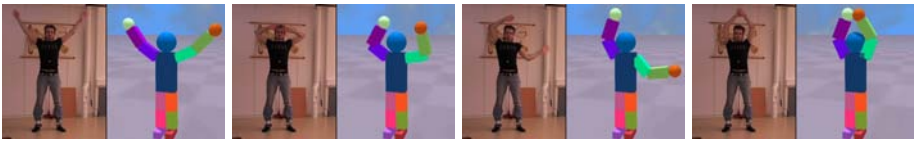

Fig. 3. Imitation of the YMCA, demonstrator on the left, imitator on the right

Table 1. Results of the experiments. Transitions mean the changing between modules for controlling the robot. If there are 0 transitions, only one module controlled the robot through the entire last epoch. If there is one transition, two modules controlled the robot, and so on. However, multiple transitions does not ensure different modules were in control for each transition, therefore the number of unique modules that controlled the robot are also listed. u_{feedback}/u_t says how strong the feedback error motor signal was relative to the total motor command at the last epoch. The performance error p_e is the accumulated difference between the desired state and the actual state of the system at the last epoch.

	min/max/avg epochs	min/max/avg p_e	min/max/avg u_{feedback}/u_t	Transitions				Unique modules			
				0	1	2	3	1	2	3	4
Cond. 1	667/1864/1121	10.4/19.0/12.6	0.05/0.11/0.07	7	12	0	1	7	13	0	0
Cond. 2	491/1857/1013	9.8/21.6/14.7	0.05/0.12/0.08	1	5	7	7	1	12	1	6

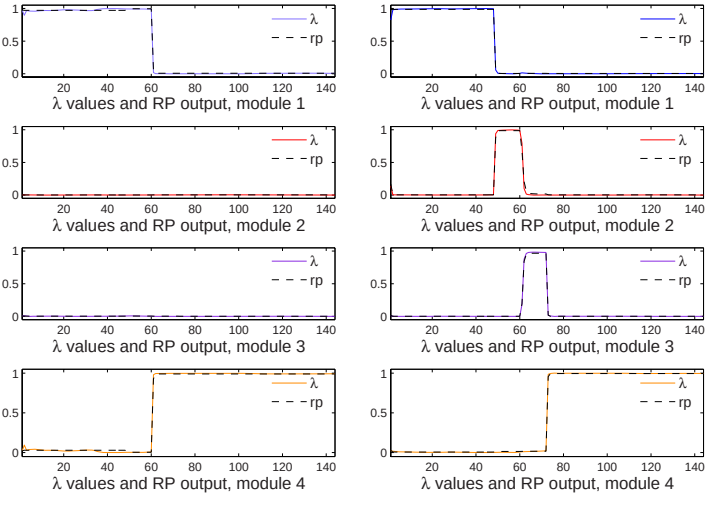

Fig. 4. The switching of control between the modules. The graph on the left shows one run in the first condition, with two different modules (1 and 4) in control. The graph on the right shows one run in the second condition, with all four modules in control at different timesteps through the imitation.

6 Discussion

From the results, the system more often than not makes use of more than one module indicating that a movement is divided into smaller submovements. In cases where the responsibility predictor is not trained beforehand, usually two modules are involved in the representation of the movement. In the second condition, the system uses more than two modules for capturing the movement.

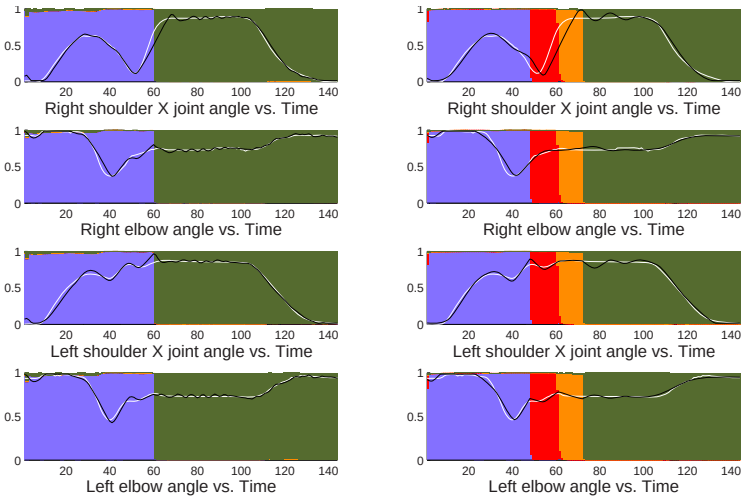

Fig. 5. How well the trajectory of the system (white line) matched the target trajectory (black line). The background color shows which module was in control, condition 1 on the left and condition 2 to the right. The graphs are from the same experiment as in figure 5.

These results indicate that the system promotes self-organized decomposition of movement when learning motion behaviours.

Representation of small and reusable motions, under different names such as 'motion segments', 'motor primitives' or 'symbols', has attracted researchers interest across different disciplines. Some of these researchers predefine the motor primitives and make the robot learn these [12]. Others, similar to us, adopts the idea of self-decomposition and aims at determining the global, invariant structures and criteria underlying motor primitives. For example, [23] illustrates that a humanoid robot can successfully learn such global structures through self-exploration. The learned structures are represented as attractors in a neural network. In our case we have several neural networks each representing different primitives. It is in our future work agenda to investigate how the modules of the MPMA may possibly be capturing attractors.

One interesting question is what qualifies as a motor primitive. Matarić also points out this is hard to define [12]. From figure 5, it seems like the modules learn some motor primitives, but instead of learning the motor primitives according to the context signal (which is how the designer of the system would define a motor primitive), the modules find distinctions in the sensory flow to define them separately. The hypothetical (i.e. designer's) switch points in the YMCA movement at timesteps 48, 60 and 72 are not always obeyed. The system's own motor primitives are usually bigger than what the designer had thought as a meaningful motor primitive. In fact, the system has a lower average performance error when the responsibility predictors are *not* trained beforehand, indicating that only a few modules are necessary to control the movement to be imitated.

On the other hand, the differences in p_e and the number of epochs spent to train the system are quite small, so performance-wise a clear preference cannot be made.

The main point of the MPMA is the decomposition of a movement into segments and simultaneously learning these segments in different modules. Our goal is to explore the possible criteria the system might be using for the decomposition. For this purpose, the coordinate system of the movement is first transformed into an internal referential frame. The idea of such a conversion is adopted by researchers in both neuroscience and robotics [19,21], where planning of a movement is done in form of postural trajectories, independent of motor commands. Our research has not been focused on *how* this geometrical transformation is done, but these ideas and solutions can be integrated into the MPMA.

One drawback of the YMCA movement is the symmetry of the Y, M and A movements, only the C movement breaks this symmetry. Closer examination reveals that for all the experiments (for both conditions) that have one or more transition, a switch between modules occurs at around the 60th timestep, which is exactly when the C movement begins, see figure 2. This may imply that not having symmetrical movements would help the separation of the modules, probably because it is more difficult to imitate and therefore needs to be stored in a separate module. Research in neuroscience supports this claim maintaining that nonsymmetric action in bimanual movements leads to interference and takes longer time compared to symmetrical ones [24]. It is interesting to see that the system agrees on the switch point around the 60th timestep in both conditions. This suggests that the human guesses of what makes up a motor primitive somehow aligns with what the system decides to be a motor primitive as well. The architecture and the experiments presented in this paper are the early and promising results of our work on motor imitation learning.

7 Future Work

We are currently examining how differences in speed and direction might affect the self-organization of the system. Research related to human motor learning suggests the changes in direction and velocity as determining factors in learning motion behaviour. It has also been suggested that specific muscle synergies are shared across different motor behaviours [25] and by various animals. We are also investigating how repetition of the target movement will affect the self-organization. Preliminary results indicate that repetition affects the way the modules will self-organize, in the way that more modules are being used. In addition, we are looking at making the movements to be imitated more complex, both in term of having longer patterns to imitate and more degrees of freedom. This will hopefully reveal if we can find a level of complexity where the system will be saturated, i.e. all the neural resources are used and new modules must be added in order to achieve the desired imitative behaviour. As mentioned above, we are also interested in how the MPMA captures attractors, for example it will

be interesting to see how the attractor landscape would be for a module that seems to represent several primitives.

References

1. Schaal, S.: Is imitation learning the route to humanoid robots? Trends in Cognitive Sciences 3(6), 233–242 (1999)
2. Piaget, J.: Play, dreams and imitation in childhood. W. W. Norton, New York (1962)
3. Meltzoff, A.N., Moore, M.K.: Explaining facial imitation: A theoretical model. Early Development and Parenting 6, 179–192 (1997)
4. Rizzolatti, G., Fadiga, L., Gallese, V., Fogassi, L.: Premotor cortex and the recognition of motor actions. Cognitive Brain Research 3, 131–141 (1996)
5. Arbib, M.: The Mirror System, Imitation, and the Evolution of Language. In: Imitation in animals and artifacts, pp. 229–280. MIT Press, Cambridge (2002)
6. Gallese, V., Goldman, A.: Mirror neurons and the simulation theory of mind-reading. Trends in Cognitive Sciences 2(12) (1998)
7. Demiris, Y., Hayes, G.: Imitation as a dual-route process featuring predictive and learning components: a biologically-plausible computational model. In: Imitation in animals and artifacts, pp. 327–361. MIT Press, Cambridge (2002)
8. Demiris, Y., Khadhouri, B.: Hierarchical attentive multiple models for execution and recognition of actions. Robotics and Autonomous Systems 54, 361–369 (2006)
9. Wolpert, D.M., Doya, K., Kawato, M.: A unifying computational framework for motor control and social interaction. Philosophical Transactions: Biological Sciences 358(1431), 593–602 (2003)
10. Jacobs, R.A., Jordan, M.I., Nowlan, S.J., Hinton, G.E.: Adaptive mixtures of local experts. Neural Computation 3, 79–87 (1991)
11. Wolpert, D.M., Miall, R.C., Kawato, M.: Internal models in the cerebellum. Trends in Cognitive Sciences 2(9) (1998)
12. Matarić, M.J.: Sensory-Motor Primitives as a Basis for Learning by Imitation: Linking Perception to Action and Biology to Robotics. In: Imitation in animals and artifacts, pp. 392–422. MIT Press, Cambridge (2002)
13. Wolpert, D.M., Kawato, M.: Multiple paired forward and inverse models for motor control. Neural Networks 11, 1317–1329 (1998)
14. Jordan, M.I., Rumelhart, D.E.: Forward models: Supervised learning with a distal teacher. Cognitive Science 16, 307–354 (1992)
15. Ans, B., Rousset, S., French, R.M., Musca, S.: Self-refreshing memory in artificial neural networks: learning temporal structures without catastrophic forgetting. Connection Science 16(2), 71–99 (2004)
16. Pfeifer, R., Scheier, C.: Understanding Intelligence (Illustrator-Isabelle Follath). MIT Press, Cambridge (2001)
17. Kawato, M.: Feedback-error-learning neural network for supervised motor learning. In: Eckmiller, R. (ed.) Advanced neural computers, pp. 365–372 (1990)
18. Nehaniv, C.L., Dautenhahn, K.: The Correspondence Problem. In: Imitation in Animals and Artifacts, pp. 41–63. MIT Press, Cambridge (2002)
19. Torres, E.B., Zipser, D.: Simultaneous control of hand displacements and rotations in orientation-matching experiments. J Appl Physiol 96(5), 1978–1987 (2004)
20. Desmurget, M., Prablanc, C.: Postural Control of Three-Dimensional Prehension Movements. J Neurophysiol 77(1), 452–464 (1997)

21. Ijspeert, A., Nakanishi, J., Schaal, S.: Trajectory formation for imitation with nonlinear dynamical systems. In: Proceedings of the IEEE/RSJ Int. Conference on Intelligent Robots and Systems (IROS2001), pp. 752–757 (2001)
22. Haruno, M., Wolpert, D.M., Kawato, M.: MOSAIC model for sensorimotor learning and control. Neural Comp. 13(10), 2201–2220 (2001)
23. Kuniyoshi, Y., Yorozu, Y., Ohmura, Y., Terada, K., Otani, T., Nagakubo, A., Yamamoto, T.: From humanoid embodiment to theory of mind. In: Pierre, S., Barbeau, M., Kranakis, E. (eds.) ADHOC-NOW 2003. LNCS, vol. 2865, pp. 202–218. Springer, Heidelberg (2003)
24. Diedrichsen, J., Hazeltine, E., Kennerley, S., Ivry, R.B.: Moving to directly cued locations abolishes spatial interference during bimanual actions. Psychological Science 12(6), 493–498 (2001)
25. d'Avella, A., Bizzi, E.: Shared and specific muscle synergies in natural motor behaviors. PNAS 102(8), 3076–3081 (2005)

An Efficient Flow-Shop Scheduling Algorithm Based on a Hybrid Particle Swarm Optimization Model*

I-Hong Kuo[2], Shi-Jinn Horng[1,2,3,4], Tzong-Wann Kao[5], Tsung-Lieh Lin[2], and Pingzhi Fan[1]

[1] Institute of Mobile Communications, Southwest Jiaotong University, 610031, Chengdu
[2] Department of Electrical Engineering, National Taiwan University of Science and Technology, 106, Taipei
horng@mouse.ee.ntust.edu.tw or horngsj@yahoo.com.tw
[3] Department of Computer Science and Information Engineering, National Taiwan University of Science and Technology, 106, Taipei
[4] Department of Electronic Engineering, National United University, 36003, Miao-Li
[5] Department of Electronic Engineering, Technology and Science Institute of Northern Taiwan, Taipei

Abstract. In this paper, a new hybrid particle swarm optimization model named HPSO that combines random-key (RK) encoding scheme, individual enhancement (IE) scheme, and particle swarm optimization (PSO) is presented and used to solve the flow-shop scheduling problem (FSSP). The objective of FSSP is to find an appropriate sequence of jobs in order to minimize makespan. Makespan means the maximum completion time of a sequence of jobs running on the same machines in flow-shops. By the RK encoding scheme, we can exploit the global search ability of PSO thoroughly. By the IE scheme, we can enhance the local search ability of particles. The experimental results show that the solution quality of FSSP based on the proposed HPSO is far better than those based on GA [1] and NPSO [1], respectively.

Keywords: Flow-Shop Scheduling Problem, Particle Swarm Optimization, Random-Key Encoding Scheme, Individual Enhancement Scheme.

1 Introduction

Flow-shop scheduling problem (FSSP) is a combinatorial optimization problem and it is an NP-Complete Problem [2]. The objective of FSSP is to find a permutation schedule that minimizes the maximum completion time of a sequence

* This work was supported in part by the Southwest Jiaotong University Visiting Professor Fellowship and the University Doctorial Research Foundation under grant No.20020613020, Ministry of Education. It was also partially supported by the National Science Council under contract number NSC 92-2213-E-011-084.

H.G. Okuno and M. Ali (Eds.): IEA/AIE 2007, LNAI 4570, pp. 303–312, 2007.

of jobs in a flow-shop. FSSP has interested many researchers during the past decades, and many heuristic methods have been developed, such as Johnson's rule [3], Palmer's slope index [4], CDS [5], and NEH [6]. The heuristic methods get the solutions by the pre-defined rules, but the rules are not suitable for every environment. So some researchers made use of evolution algorithms to get the solutions, such as Taillard's tabu search method [7], Ogbu and Smith's simulated annealing algorithm [8], Reeves's genetic algorithm [9], and Lian et al.'s particle swarm optimization algorithm [1].

In this paper, we propose a new hybrid particle swarm optimization algorithm named HPSO in order to solve FSSP. We use the continuous version of PSO to be the main component of HPSO because of its excellent searching ability in the continuous space. PSO's global searching ability is better in comparison with the local searching ability; for the sake of improving the PSO's local searching ability, an individual enhancement scheme is also proposed as the other component of HPSO. In addition to the schemes described above, we consider the influence of time-varying coefficients of PSO. The experimental results show that HPSO outperforms GA [1], and NPSO [1] in solution quality for FSSP, respectively.

The paper is organized as follows: A brief overview of FSSP and PSO are described in Section 2 and Section 3, respectively. Section 4 discusses the details of the HPSO algorithm. Section 5 discusses the experimental results obtained by the HPSO algorithm. Finally, Section 6 summarizes the contribution of this paper and conclusions.

2 Flow-Shop Scheduling Problem

The objective of the flow-shop scheduling problem (FSSP) is to find an appropriate permutation schedule for jobs that minimizes the maximum completion time. Every job has m operations. The flow-shop has m machines. Every operation of any job must follow the same machine sequence M_1, M_2, ..., M_m. That is, the rth operation of job i is performed by machine M_r with fixed processing time $T(r,i)$, $1 \leq r \leq m$, and $1 \leq i \leq k$. Every machine can execute only an operation at the same time. The operations of a job cannot be preemption. All machines execute jobs in the order of the pre-defined permutation schedule. The equation of computing the maximum completion time of the permutation schedule is given as follows:

$$\begin{aligned} C(1,1) &= T(1,1) \\ C(1,i) &= C(1,i-1) + T(1,i) \\ C(r,1) &= C(r-1,1) + T(r,1) \\ C(r,i) &= max(C(r,i-1), C(r-1,i)) + T(r,i) \end{aligned} \tag{1}$$

In Equation (1), $T(r,i)$ means the execution time of the rth operation of the ith job on machine M_r, $C(r,i)$ means the maximum completion time of the ith job on machine M_r, $1 \leq r \leq m$, and $1 \leq i \leq k$. If m is equal to the total number of machines, and k is equal to the total number of jobs, then $C(m,k)$ means

Table 1. The execution time for every operation of every job on every machine

	job_1	job_2	job_3	job_4	job_5
M_1	3	4	7	8	10
M_2	12	15	6	10	8

Table 2. *Makespan* of the example shown in Table 1

	job_1	job_2	job_3	job_4	job_5
M_1	3	7	14	22	32
M_2	15	30	36	46	54

makespan. We give an example of FSSP in Table 1, where the total number of jobs is 5, and the total number of machines is 2. The *makespan* of the example is listed in Table 2, that is, $C(2,5)$=54.

3 Particle Swarm Optimization

Particle Swarm Optimization (PSO) is a computational evolution model developed by Kennedy and Eberhart [10] that can search solution of input problem in the virtual space. PSO is composed by a number of particles in a swarm. Every particle can move its position in the virtual search space, just like a bird flying in the sky. Every particle always remembers its best position in the experience. When a particle moves to another position, it must refer to its best experience and the best experience of all particles in the swarm. A particle's movement is based on Equations (2) and (3):

$$V_{id} = \omega \times V_{id} + C_1 \times Rand() \times (P_{id}^{best} - P_{id}) + C_2 \times Rand() \times (P_{gid}^{best} - P_{id}) \quad (2)$$

$$P_{id} = P_{id} + V_{id} \quad (3)$$

In Equation (2), V_{id} means a particle's one-step movement distance, and it is limited to $[-VMAX, VMAX]$ in which $VMAX$ is the max movement distance in one step. The variable ω is named inertial weight which can increase or decrease a particle's one step movement distance. C_1 is the self confidence coefficient which means how much this particle believes in its self experience. $Rand()$ is a function which can generate a random number between 0 and 1. C_2 is the neighbor confidence coefficient which means how much this particle believes in its neighbor's experience. P_{id} means the position of the idth particle. P_{id}^{best} means P_{id}'s best experience. P_{gid}^{best} means the gidth particle's best experience, which is the best experience of all particles in the swarm. A particle's next position in virtual search space is given by adding the one-step distance in V_{id} to its current position P_{id}, according to Equation (3).

4 The HPSO Algorithm

In this paper, we present a new hybrid swarm optimization algorithm named HPSO to solve FSSP. The HPSO algorithm is composed by the following parts: random-key (RK) encoding scheme, individual enhancement (IE) scheme, and the particle swarm optimization (PSO) component.

4.1 RK Encoding Scheme

The RK encoding scheme can transform a position in the RK virtual space and the FSSP solution space. Every position in the RK virtual space is a vector of real numbers. Every position in the FSSP solution space is a vector of integers. Suppose there is a position A in the RK virtual space that is (λ_1, λ_2, ..., λ_k), where λ_i, 1≤i≤k, is the corresponding weight of job i. We then sort these weights in ascending order with the job indexes. The sorted job indexes correspond to a position in the FSSP solution space. For example, if there is a position A in the RK virtual space that is (0.3, 0.5, 0.2, 0.4), the RK encoding scheme can encode it to (3, 1, 4, 2) which is a position in the FSSP solution space corresponding to a job sequence 3, 1, 4, 2. In this example, a real number of position A corresponds to a job's weight. That is, job 1's weight = 0.3, job 2's weight = 0.5, job 3's weight = 0.2, job 4's weight = 0.4. When we sort these weights in ascending order with the job indexes, we get (3, 1, 4, 2), which is a position in the FSSP solution space.

The individual is called particle in the PSO component. We represent a particle as a vector of real numbers. The real numbers of a particle mean a position in the RK virtual space. A position in the RK virtual space can be transformed to a position in the FSSP solution space by the RK encoding scheme.

4.2 Individual Enhancement Scheme

The individual enhancement (IE) scheme searches an individual's neighborhood of Hamming distance of length 2 in the FSSP solution space thoroughly in order to find a better solution. The example of Hamming distance is given as follows: If there are two individuals in the FSSP solution space which are (3,1,2,4,5) and (3,4,2,1,5), we compare every item of two individuals and record the number of the items whose job indexes are not equal. Hence, the Hamming distance of the given example is shown to be 2.

The idea of IE scheme is to exchange the job order of two jobs of an individual, and to compare the *makespan* before being exchanged and after being exchanged. If the *makespan* after being exchanged is better, keep this change and update the permutation of this individual. Suppose there are k jobs corresponding to the k positions of an individual. Then we will exchange the job of position i to that of position j, 1≤i≤k and i<j≤k and evaluate the *makespan* for a possibility of updating the job sequence.

An example is given in Fig. 1. In this example, we want to enhance an individual P=(2, 1, 3, 4, 5), which represents a permutation schedule of a 2-machine

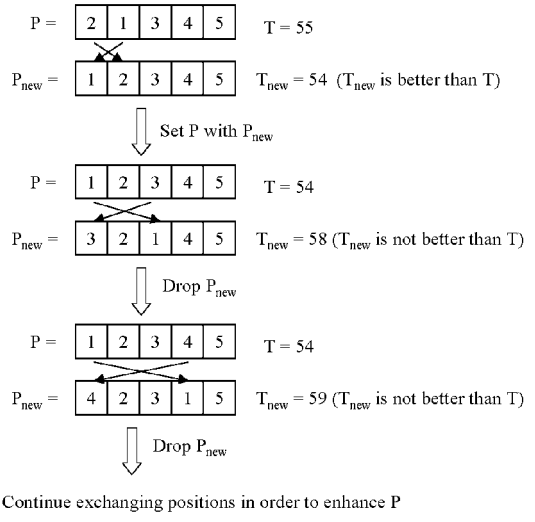

Fig. 1. An Example of IE Scheme

flow-shop, and the execution time of every operation of every job on every machine is listed in Table 1. P will be enhanced by the IE scheme through the following steps. First, we set T with 55, which is the *makespan* of P according to Table 1. Then we set P_{new} with P, and exchange the job of position 1 to that of position 2 in the job order of P_{new}, currently P_{new} = (1, 2, 3, 4, 5). Based on P_{new} and Table 1, now we set T_{new} with 54, which is the *makespan* of P_{new}. From T_{new} and T, we can see that T_{new} is better than T, so we set P with P_{new}, and T with T_{new}. Therefore, we get a better P now. Next, we try to exchange the pair of jobs on position_1 and position_3 in P, and again check whether it can get a better P or not. After the exchange of all pairs of jobs, we have already searched the individual P's neighborhood of Hamming distance of length 2 in the FSSP solution space thoroughly. Therefore, we can get a better P by the IE scheme.

We list the pseudo code of the IE scheme in Algorithm 1. In Algorithm 1, P means the individual that we want to enhance it, T means the *makespan* of P, and $TotalJobs$ means the total number of jobs.

4.3 PSO Component

The PSO component is the main component of the HPSO algorithm. In the PSO component, every particle moves its position in the RK virtual space based on Equations (2) and (3), and PSO evaluates every particle's solution in the FSSP solution by the transformation of the RK encoding scheme. Because of the diversity between positions in the RK virtual space, we need a neighborhood search technique to search every particle's neighborhood in the FSSP solution space in order to get better solutions. We use the IE scheme to search a particle's neighborhood in the FSSP solution space, which is described in the section above.

Algorithm 1. IE Scheme

Require: An individual P that we want to enhance it.
  $T \leftarrow P$'s makespan
  $i \leftarrow 0$
  repeat
    $i \leftarrow i + 1$
    $j \leftarrow 0$
    repeat
      $j \leftarrow j + 1$
      $P_{new} \leftarrow P$
      exchange the pair of jobs on $position_i$ and $position_j$ in P_{new}
      $T_{new} \leftarrow$ the makespan of changed P_{new}
      if $T_{new} < T$ **then**
        $P \leftarrow P_{new}$
        $T \leftarrow T_{new}$
      end if
    until $j = TotalJobs$
  until $i = TotalJobs$

We also add the mutation scheme into PSO component. When a particle satisfies the condition of mutation scheme, it will be moved to the global best particle's neighborhood according to Equation (4):

$$P_{id} = P_{gid}^{best} + ((Rand() - 0.5) \times VMAX \times 2) \tag{4}$$

In this paper, we also consider the influence of time-varying coefficients in Equation (2). We consider that if the coefficients ω, C_1, and C_2 in Equation (2) are varying nonlinearly with evolution generations, maybe we can improve the solution quality for FSSP. Differing from the linearly increasing (or decreasing) coefficients in [11][12], our coefficients are varying nonlinearly during the evolution generations. We propose a new nonlinear adjusting scheme for the new time-varying coefficients ω, C_1, and C_2 used in the HPSO algorithm. First, we consider the coefficient ω, and we think the value of ω should be nonlinearly decreased during the evolution process. The reason is that we initialize the swarm randomly, and the solutions found by particles are not good at the beginning stage of the evolution. In this situation, every particle should believe more in its own trajectory rather than other particles' trajectories in order to keep the diversity of the swarm. Second, we consider the coefficient C_1, and we think the value of C_1 should be nonlinearly decreased during the evolution process. The reason is that every particle should explore the search space more independently at the beginning stage of the evolution. At last, we consider the coefficient C_2, and we think that the value of C_2 should be nonlinearly increased during the evolution process. The reason is that every particle should refer to other particles' experiences at the latter stage of the evolution. We compute the values of ω, C_1, and C_2 based on Equations (5), (6), and (7):

$$\omega = (\omega^{default} - \omega^{base}) \times \frac{1}{1 + e^{-\alpha \times \left(\frac{\quad}{\quad}\right)}} + \omega^{base} \tag{5}$$

$$C_1 = (C_1^{default} - C_1^{base}) \times \frac{1}{1 + e^{-\alpha \times \left(\frac{\quad}{\quad} - \frac{\quad}{\quad}\right)}} + C_1^{base} \tag{6}$$

$$C_2 = (C_2^{default} - C_2^{base}) \times \frac{1}{1 + e^{-\alpha \times \frac{\quad}{\quad}}} + C_2^{base} \tag{7}$$

In Equations (5), (6), and (7), where ω^{base} means the minimum value of ω, C_1^{base} means the minimum value of C_1, C_2^{base} means the minimum value of C_2, $\omega^{default}$ means the default value of ω, $C_1^{default}$ means the default value of C_1, $C_2^{default}$ means the default value of C_2, $MaxIter$ means the total number of generations, $IterNow$ means the running generation number, and α means the nonlinear increasing (or decreasing) speed of the time-varying coefficients.

By the use of the mutation scheme and the time-varying coefficients, we can lower down the convergence speed of the swarm and keep the diversity of the swarm during the evolution process.

We list the pseudo code of the PSO component in Algorithm 2. In Algorithm 2, $MaxIter$ means the generation number of the PSO component; $Prob_{IE}$ means the probability of the IE scheme switch on; $Prob_{Muta}$ means the mutation probability of the particle; $SwarmSize$ means the swarm size of the PSO component.

Algorithm 2. HPSO Algorithm

Require: $MaxIter \geq 1$
  $IterNow \leftarrow 0$
  repeat
    $IterNow \leftarrow IterNow + 1$
    $i \leftarrow 0$
    repeat
      $i \leftarrow i + 1$
      evaluate $Particle_i$'s solution
      if $Rand() < Prob_{IE}$ **then**
        enhance $Particle_i$ by IE scheme
      end if
      update $Particle_i$'s local best
      update the global best
      calculate the values of the time-varying coefficients in the equation (2) according to equations (5), (6), and (7)
      move $Particle_i$ to next position according to equations (2) and (3)
      if $Rand() < Prob_{Muta}$ **then**
        move $Particle_i$ to the global best particle's neighborhood according to equation (4)
      end if
    until $i = SwarmSize$
  until $IterNow = MaxIter$

5 Experimental Results

We use 7 problems of Taillard's benchmark [13] to be the test input of the HPSO algorithm. We coded the HPSO algorithm in ANSI C language with the environment of Microsoft Visual C++ 6.0, and simulated it with a 1.73 GHz Intel Pentium M PC. In the HPSO, we set the coefficients $\alpha = 10$, $\omega^{default} = 1.0$, $\omega^{base} = 0.4$, $C_1^{default} = 2$, $C_1^{base} = 0.4$, $C_2^{default} = 2$, and $C_2^{base} = 0.4$. The population size is 50 in the HPSO algorithm, which means we use only 50 particles to search solutions for every problem. We simulated the HPSO algorithm with 10 runs for every problem. In order to compare the convergence rate of HPSO with NPSO [1], we evolved 400, 400, 400, 500, 2000, 2000, and 800 generations for the 7 problems ta001, ta011, ta021, ta031, ta041, ta051, and ta061 in each run, respectively. We listed the convergence rate of HPSO for the 7 problems in Fig. 2. The simulated experimental results are listed in Table 3. In Table 3, PS means the problem's size: the number of jobs multiplies the number of machines, WK means the well-known optimal solutions in the benchmark, $Time$ means the average seconds of total runs, Min means the best solution found by HPSO, Max means the worst solution found by HPSO, Avg means the average value of total run solutions, and Std means the standard deviation. We list the experimental results of NPSO [1] for the same 7 problems in Table 4. According to the values of Min, Max and Avg in Table 3 and those in Table 4, we can see that HPSO outperforms NPSO in the total solution quality thoroughly. According to the convergence rate listed in Fig. 2, we can see that the convergence rate of HPSO is very large at the beginning stage, and becomes slow down during the later stage of the evolution.

Summing up the experimental results described above, we can find that HPSO can find the optimal area in the search space quickly with smaller population size, and can make use of its better local searching ability to get the final optimal solution at the end of evolution. In [1], the researchers showed when the genetic algorithm (GA) made use of the same type of crossover and mutation operators as NPSO did, the experimental results of the GA were weaker than the results of the NPSO. Therefore, HPSO outperforms GA in solution quality, too.

Table 3. The experimental results of this paper

PS			HPSO				
(Js×Ms)	FSSP	WK	Min	Max	Avg	Std	Time
20×5	ta001	1278	1278	1278	1278.0	0	1.9
20×10	ta011	1582	1582	1596	1587.3	4.1	3.7
20×20	ta021	2297	2297	2315	2307.0	5.1	7.5
50×5	ta031	2724	2724	2724	2724.0	0	29.8
50×10	ta041	2991	3034	3063	3053.6	9.2	249.9
50×20	ta051	3771-3850	3923	3963	3944.6	12.2	560.6
100×5	ta061	5493	5493	5493	5493.0	0	353.4

Table 4. The experimental results of Lian et al. [1]

		NPSO[1]			
FSSP	WK	Min	Max	Avg	Operators
ta001	1278	1278	1297	1279.9	C1, M6
ta011	1582	1582	1639	1605.8	C1, M2
ta021	2297	2297	2376	2334.9	C1, M3
ta031	2724	2724	2729	2725.0	C1, M3, M8, M9
ta041	2991	3034	3129	3086.9	C1, M9
ta051	3771-3850	3938	3989	3964.3	C1, M2
ta061	5493	5493	5495	5493.2	C1, M9

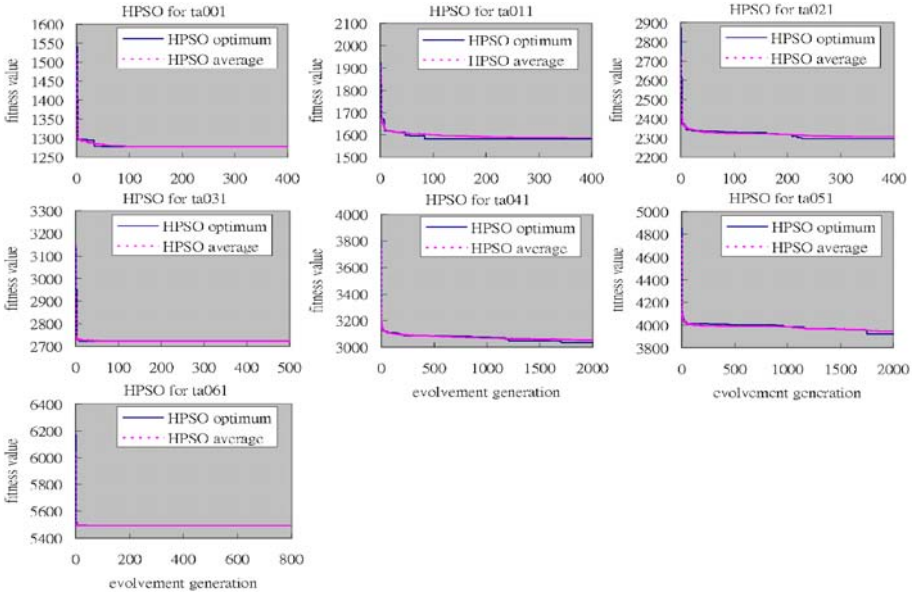

Fig. 2. HPSO for ta001, t011, ta021, ta031, ta041, ta051,and ta061

6 Conclusions

In this paper, we present a new hybrid swarm optimization algorithm named HPSO to solve FSSP. The HPSO algorithm is composed by the RK encoding scheme, the IE scheme, and the PSO algorithm with time-varying coefficients. Our HPSO algorithm differs greatly from NPSO [1] in the search space. The NPSO searches a solution in the discrete multi-dimensional FSSP space directly. Every point in the FSSP space is a sequence of jobs. Our HPSO algorithm searches a solution in the multi-dimensional real space. We call it the RK space, and every point in the RK space is a sequence of real numbers. We transform the point in the RK space to the point in the FSSP space in order to get a solution.

One of our main contributions is to prove that HPSO can reach the optimal area in the search space quickly with smaller population size than NPSO [1] and GA [1] did, because of its high convergence rate. Our another contribution is to prove that the quality of solution for FSSP found by the HPSO algorithm is better than those found by NPSO [1] and GA [1] algorithms, respectively. The last contribution is to prove that we can enhance the local searching ability of the PSO algorithm by our IE scheme and our new time-varying coefficients which can influence the size of the next step of the PSO algorithm.

Although the HPSO algorithm proposed in this paper outperforms other evolution algorithms like GA [1] and NPSO [1] in solution quality, respectively, we still suffer from the local optimal trap problem like the experiments of ta041 and ta051 in the Taillard's benchmark. Thus, the objective of further research is to improve the ability of escaping the local optimal area in the search space of the HPSO algorithm.

References

1. Lian, Z., Gu, X., Jiao, B.: A novel particle swarm optimization algorithm for permutation flow-shop scheduling to minimize makespan. Chaos, Solitons and Fractals (In Press, Corrected Proof)
2. Garey, M., Johnson, D., Sethi, R.: The complexity of flowshop and jobshop scheduling. Mathematics of Operations Research, 117–129 (1976)
3. Johnson, S.M.: Optimal two- and three-stage production schedules with setup times included. Naval Research Logistics Quarterly, 61–68 (1954)
4. Palmer, D.: Sequencing jobs through a multi-stage procrss in the minimun total time- a quick method of obtaining a near optimun. Operational Research Quarterly, 101–107 (1965)
5. Campbell, H.G., Dudek, R.A., Smith, M.L.: A heuristic algorithm for the n-job, m-machine sequencing problem. Management Science, 630–637 (1970)
6. Nawaz, M., Enscore, E.E., Ham, I.: A heuristic algorithm for the m-machine, n-job flow shop sequencing problem. OMEGA, 91–95 (1983)
7. Taillard, E.: Some efficient heuristic methods for the flow shop scheduling problem. European Journal of Operational Research, 65–74 (1990)
8. Ogbu, F.A., Smith, D.K.: The application of the simulated annealing algorithm to the solution of the n/m/cmax flow shop problem. Computers and Operations Research, 243–253 (1990)
9. Reeves, C.R.: A genetic algorithm for flow shop sequencing. Computer Operational Research, 5–13 (1995)
10. Kennedy, J., Eberhart, R.: Particle swarm optimization. In: Proceedings of IEEE international Conference on Neural Network, pp. 1942–1948 (1995)
11. Shi, Y., Eberhart, R.C.: Empirical study of particle swarm optimization. In: Proceedings of the Congress on Evolutionary Computation, pp. 1945–1950 (1999)
12. Ratnaweera, A., Halgamuge, S.K., Watson, H.C.: Self-organizing hierarchical particle swarm optimizer with time-varying acceleration coefficients. IEEE Transactions on Evolutionary Computation, 240–255 (2004)
13. Taillard, E.: Benchmarks for basic scheduling problems. European Journal of Operational Research, 278–285 (1993)

Towards the Automated Design of Phased Array Ultrasonic Transducers – Using Particle Swarms to Find "Smart" Start Points

Stephen Chen[1], Sarah Razzaqi[2], and Vincent Lupien[3]

[1] School of Information Technology, York University
4700 Keele Street, Toronto, Ontario M3J 1P3
sychen@yorku.ca
[2] Centre for Hypersonics, Division of Mechanical Engineering
University of Queensland, Brisbane, Australia 4072
s.razzaqi@uq.edu.au
[3] Acoustic Ideas Inc.
27 Eaton Street, Wakefield, MA 01880
vincent.lupien@acousticideas.com

Abstract. Continuum Probe Designer^{TM} by Acoustic Ideas Inc. is a tool that can help design the "best" phased array ultrasonic transducer for a given inspection task. Given a specific surface geometry for the ultrasonic transducer, one component of Continuum Probe Designer^{TM} can determine the number of elements, and the required size and shape of each element to meet a list of ultrasonic inspection goals. Using the number of elements as a cost function, an optimization problem to find the best surface geometry for the transducer is created. Previous work has demonstrated that a $(1+\lambda)$-evolution strategy (ES) can be a very effective search technique for this problem. The performance of this ES was improved by starting it from "smart" (i.e. better than random) start points. Particle swarm optimization (PSO) can be used to improve the "smart" start points, and the overall PSO-ES hybrid is capable of finding feasible transducer designs from all of the start points in a benchmark test suite. This level of performance is an important step towards the use of Continuum Probe Designer^{TM} as a fully automated tool for the design of phased array ultrasonic transducers.

1 Introduction

An evolution strategy (ES) [1] has been developed for use with Continuum Probe Designer^{TM} – a tool developed by Acoustic Ideas Inc. that uses exclusive patent pending technology to design the best possible ultrasonic transducer (or probe) for a specified task [6,10]. In the developed ES, a high correlation was observed between the quality of the initial start point and the quality of the final solution. The performance of this ES was improved by using "smart" start points – start points that are better than random start points. Since the use of random search to find the "smart" start points was so successful [4], it is expected that the use

H.G. Okuno and M. Ali (Eds.): IEA/AIE 2007, LNAI 4570, pp. 313–323, 2007.

of particle swarm optimization (PSO) [5] to find the "smart" start points will lead to an even better performance in the evolution strategy.

The selection of PSO was inspired by WoSP (Waves of Swarm Particles) – a particle swam optimization technique that has been modified to find and explore multiple optima [7]. In a traditional PSO implementation, all of the particles will eventually converge and fully explore the region around a single optimum. In WoSP, as particles begin to converge, a short-range force can lead to the "ejection" of particles away from the neighbourhood of the current optimum into new waves of particles that will explore for additional optima.

Compared to a traditional PSO, an implementation of WoSP will explore several optima coarsely rather than a single optimum exhaustively. Subsequently, WoSP benefits from being paired with a local optimizer that can find the exact minimum or maximum after the general neighbourhood of the optimum has been found. A local optimizer can also receive unique benefits from WoSP – WoSP can provide a small number of highly diverse and highly promising "smart" start points. The current implementation does not need WoSP to find multiple start points since random search is used to find the four initial start points. Therefore, four independent PSOs are used instead to improve upon these start points before applying a greedier local search technique (i.e. the evolution strategy).

The use of WoSP with a local optimizer [7] appears to be quite different from other coarse search and local optimizer combinations. For example, simulated annealing [9] can be viewed as having a coarse search performed at higher temperatures for the start point that will eventually be optimized at lower temperatures [3]. However, simulated annealing (like a traditional PSO) eventually explores only a single optimum exhaustively. At the other end of the spectrum, memetic algorithms [11] perform a special kind of "search over the subspace of local optima" [12] – every search point is locally optimized.

In the current application, a single local optimum can take over an hour to find with an evolution strategy. Therefore, it is only practical to explore a small number of optima neighbourhoods exhaustively. This small number (four in the current experiments) makes it impractical to maintain a population of local optima for a memetic algorithm to operate on. Conversely, significant benefits are still possible from exploring multiple optima. These two features of the current problem domain make it an ideal candidate for a coarse search-greedy search hybrid approach.

The PSO-ES hybrid approach has been tested on a benchmark probe design problem. The experiments involve 30 initial probe geometries – one selected by an expert and 29 selected randomly. In the previous results, the ES was able to find feasible solutions for at most 25 of the 29 random start points. To have confidence in the ability of Continuum Probe Designer^{TM} to find acceptable solutions for any given real-world design problem when it is used by a non-expert designer, it is important to have an optimization technique that is robust enough to find feasible solutions for all 29 random start points on the benchmark design problem. The developed PSO-ES hybrid has been able to achieve this level of performance.

Before presenting these recent developments towards the automated design of phased array ultrasonic transducers, an overview of Continuum Probe Designer™ is presented in section 2 and previous work on its optimization solver is reviewed in section 3. A new analysis of "smart" start points in section 4 provides a foundation and justification for the current research with PSO that is introduced in section 5. Section 6 has the results for the new PSO-ES hybrid, and these results lead to a discussion of coarse search-greedy search hybrids in section 7. Conclusions and acknowledgements follow.

2 Background

Ultrasound can be used to perform nondestructive evaluation (NDE) of structures for many industrial applications. For example, the benchmark design problem used in this paper represents an inspection challenge posed by the Federal Aviation Administration (FAA) for the inspection of titanium disks in aircraft engines. The beam requirements in this inspection challenge can be difficult to achieve with the existing instrumentation which can only control 32 independent channels at a time. The purpose of Continuum Probe Designer™ is to help scientists and engineers develop feasible and even optimal (e.g. least cost) probes for any inspection task.

Continuum Probe Designer™ consists of two key components: a cost function generator and an optimization solver (see Fig. 1). For a given input (which represents an ultrasonic transducer's surface geometry), the cost function generator can determine the fewest number of elements that a probe having the input shape will require to perform the specified inspection task. The role of the optimization solver is to find the optimal probe geometry – i.e. the surface geometry for the ultrasonic transducer that minimizes the cost function. The heuristic search techniques discussed in this paper are part of the optimization solver.

For the purposes of this paper, the cost function generator of Continuum Probe Designer™ is treated like a black box. The input into the cost function is a vector of rational numbers that represents the probe's shape, and the output

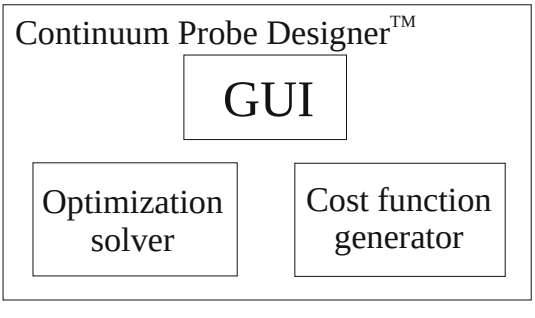

Fig. 1. The components of Continuum Probe Designer™

that needs to be optimized is a rational value which varies with the number of elements. The number of elements required can be calculated by `ceil`(raw output / (π/3)) – the floating point output is provided mainly to help optimization methods search for the solution.

3 Evolution Strategy

Evolution strategies [1] are a heuristic search technique within the broad category of evolutionary computation. In evolutionary computation, heuristic search is performed by simulating the effects of Darwinian evolution on a population of solutions. Each of these solutions has a fitness value – e.g. the objective value of a function that is being minimized or maximized. Using this fitness value, natural/artificial selection allows the fitter solutions to survive and reproduce, whereas the less fit solutions will be removed from the population. In an evolution strategy that has a population of one (e.g. a (1+λ)-ES), all of the offspring solutions are created from the best found solution.

A (1+λ)-ES has been developed for the optimization solver in Continuum Probe Designer™ [4]. This ES uses $\lambda = 3$, runs for 100 generations, and has a mutation strength of $\sigma = 0.01$. Specifically, the `randn` function in MATLAB® (which creates a random number with a Gaussian distribution) is called and multiplied by 0.01.

The performance of the ES was evaluated from 30 start points – the origin (which is deemed by expert knowledge to be a reasonably good start point) and 29 additional start points which were generated by making each term a uniform random number from [-0.2, 0.2] (using the `rand` function in MATLAB®). The

Table 1. Number of elements in the phased array ultrasonic transducers designed by Continuum Probe Designer™ for the FAA inspection challenge. The origin and 29 random points were used as the initial probe geometries. Designs with 32 or fewer elements are considered "feasible". A "better" design was recorded for one of the methods if it found a solution with fewer elements for a given start point. A paired, one-tailed t-test was used to test for significance since the experiments used the same 30 start points. A value of less than 5% shows that the result is significant to at least the 1 in 20 level.

	(1+λ)-ES	Four independent ES runs
average	32.5	31.3
std. dev.	3.9	2.9
maximum	45	39
minimum	27	27
feasible	18	22
better	8	15
t-test	2.1%	

high variation in the results for the (1+λ)-ES (see Table 1) suggested that its performance could be easily improved by using several independent runs and returning the best overall solution. For all of the previous 30 start points, three additional start points were created by adding a uniform random mutation of [-1, 1]/6 to each term. In each set, the same ES as before was run from all four start points.

The use of the three additional independent runs achieved a less than expected reduction in the average number of elements used. A quick analysis suggested that there was a high correlation between the quality of start and end points – the high variation in results might be directly related to the high variation in the quality of the initial start points. Using 49 random start points (rather than just three), a follow-up experiment had the ES runs started from the four best of the 50 candidate start points – the initial geometry (e.g. the origin) was not necessarily used. These "smart" start points led to an even larger reduction in the average number of elements used (see Table 2).

Table 2. Results comparing the use of "smart" start points with four independent ES runs. See Table 1 for explanations of the data.

	Four independent ES runs	"Smart" Start Points
average	31.3	30.1
std. dev.	2.9	3.2
maximum	39	42
minimum	27	27
feasible	22	25
better	8	18
t-test	2.2%	

4 An Analysis of "Smart" Start Points

To verify the observation that the quality of the start and end points is indeed correlated, 90 addition runs of the (1+λ)-ES have been performed starting from random start points with a [-0.2,0.2] range. (Note: data from the original parallel runs are not useful since the grouped start points are clustered around the 30 random start points.) Using the 90 new and 30 original ES runs, Table 3 shows that there is a significant improvement in the performance of the (1+λ)-ES when it is started from better (i.e. "smart") start points.

The verification that the current problem domain can benefit from "smart" start points is not a trivial addition – all problem domains and/or local optimization techniques will not necessarily have this high correlation between the quality of a random solution and the quality of its local optimum. To demonstrate, "smart" start points have been used on the LIN318 instance of the travelling salesman problem (TSP) using two-opt as the local optimizer. Generating

Table 3. Results comparing the quality of the 30 best and 30 worst of 120 random start points, and the subsequent quality of their ES solutions on the benchmark probe design problem. A two-tailed, homoscedastic t-test shows that the difference in the quality of the ES solutions is significant at the 1 in 20 level.

	30 worst	30 best
average start	770.5	121.5
std. dev.	87.1	66.3
t-test	0.0%	
average end	34.1	31.7
std. dev.	5.7	3.1
feasible	22	25
t-test	4.2%	

Table 4. Results comparing the quality of the 30 best and 30 worst of 120 random initial tours, and the subsequent quality of their two-opt solutions for the TSP. A two-tailed, homoscedastic t-test shows no significant difference in the quality of the two-opt solutions.

	30 worst	30 best
average start	559138	516242
std. dev.	7443	6683
t-test	0.0%	
average end	46651	46795
std. dev.	560	988
t-test	48.8%	

Table 5. Results comparing the performance of using "smart" start points and using four random initial tours on the TSP. A two-tailed, homoscedastic t-test shows no significant difference in the quality of the best two-opt solution found in each set.

	Four independent two-opt runs	"Smart" Start Points
average	45876	45747
std. dev.	485	577
t-test	35.4%	

120 random initial tours and two-opt minima, it can be seen that the (inverse) correlation between the quality of the final solutions for the 30 best and 30 worst initial tours is not significant (see Table 4).

Without a correlation between the quality of the start and end solutions, there is no expected benefit of using "smart" start points for independent parallel runs. This expectation is confirmed by grouping the 120 previous TSP runs into 30 sets of four (e.g. set 1 is runs 1, 31, 61, and 91) and comparing them against

runs using "smart" start points – 50 random TSP solutions are generated, and the four best are optimized with two-opt. The results in Table 5 show that no significant improvement was achieved by using "smart" start points on the TSP.

5 Using PSO to Find "Smart" Start Points

The above analysis of "smart" start points suggests that the performance of the ES on the probe design problem can be improved by pairing it with a coarse search strategy. Specifically, the role of the coarse search strategy is to find better initial start points. Building upon the success of random search (the coarsest of coarse search strategies) and inspired by the coarse search-greedy search combination presented with WoSP [7], particle swarm optimization is hereby tried as the coarse search technique.

```
Finding "Smart" Start Points with PSO                          line
Begin                                                            1
  start with one initial point (e.g. the origin)                 2
  create a pool of 50 points by generating 49 random points      3
  choose the 4 best points from this pool of points              4
  For each of the four best points                               5
    choose 4 random points from the pool (no replacement)        6
    give all 5 points/particles a random initial velocity        7
    For i = 1 to n (number of iterations for each particle)      8
      For each particle                                          9
        calculate and announce fitness                          10
      End For                                                   11
      update best particle for each wave                        12
      For each particle                                         13
        calculate new velocity                                  14
        calculate new location                                  15
      End For                                                   16
    End For                                                     17
  End For                                                       18
  return the best solution from each of the four PSOs           19
End                                                             20
```

Fig. 2. Pseudocode for the coarse search strategy to find "smart" start points

The pseudocode for the coarse search strategy is presented in Fig. 2. In line 3, the 49 additional start points are created by adding a uniform random mutation of [-1, 1]/12 to each term of the initial start point. After line 10, the best particle location B of each PSO is updated. The calculation of particle velocities on line 14 is performed with the following equation:

$$\bar{\mathbf{V}}_{t+1} = \left(M\bar{\mathbf{V}}_t + G\bar{\mathbf{U}}_B\right) \tag{1}$$

In (1), the new velocity of a particle is a weighted average of its previous velocity and a velocity towards the best particle location. $\bar{\mathbf{U}}_B$ is the unit vector from the current particle to the best particle location. The terms $M = 0.5$ and $G = 0.9$ were chosen such that the average influence of the momentum term (M) is slightly larger than the influence of the gravity term (G). This weighting promotes exploration over convergence.

6 PSO-ES Results

Similar to the previous experiments with four random start points and four "smart" start points found by random search, the four "smart" start points found by PSO are used as the initial start points for four independent, parallel (1+λ)-evolution strategies. Each ES has $\lambda = 3$, runs for 100 generations, and has a mutation strength of $\sigma = 0.01$. Thus, the results shown in Table 6 isolate the benefits of the improved start points found by using PSO. The key features of these results are a 3.1% reduction in the average number of elements required and an increase by two in the number of feasible solutions found.

Table 6. Results comparing the use of "smart" start points found randomly and by PSO. See Table 1 for explanations of the data.

	Random "Smart" Start Points	PSO "Smart" Start Points
average	30.1	29.2
std. dev.	3.2	1.9
maximum	42	34
minimum	27	27
feasible	25	27
better	7	15
t-test	3.1%	

The search space of probe geometries is known to be globally convex [4]. Thus, better solutions can often be found by searching between other (locally optimal) solutions. If two solutions are on opposite sides of the "big valley", a point in between these two solutions may be closer to the centre of the "big valley" where better solutions (and the global optimum) are found. Crossover (which generates an offspring that is the arithmetic mean of two solutions) has been added to the parallel ES runs – two random parents are mated after each generation, and the worst of the four original solutions is replaced if the offspring produced by crossover is fitter.

The results with the addition of crossover finally achieve the desired result (see Table 7) – feasible solutions are found for all 30 start points. This achievement is critical for the future use of Continuum Probe Designer^{TM} by non-expert users. In addition to the 2.6% reduction in the average number of elements used,

Table 7. Results comparing independent parallel ES runs and ES runs coordinated by using crossover. See Table 1 for explanations of the data.

	PSO "Smart" Start Points	PSO-ES with crossover
average	29.2	28.5
std. dev.	1.9	1.3
maximum	34	32
minimum	27	27
feasible	27	30
better	6	13
t-test	1.1%	

the large reduction in the standard deviation of the results also provides an important level of confidence in the performance of the optimization solver.

7 Discussion

The idea from WoSP of combining coarse global search and greedy local search techniques is quite different from the ideas behind metaheuristics like memetic algorithms [11]. In memetic algorithms and other restart techniques, the local search technique is applied to every start point that is generated. These search strategies subsequently perform a special kind of "search over the subspace of local optima" [12]. If this subspace of local optima is significantly smaller than the overall search space (as it is in globally convex search spaces [2]), then these search strategies can be very efficient.

Conversely, the use of coarse search makes the assumption that there is a correlation between the quality of a random and/or intermediate start point and the final quality of its local optimum. This correlation is independent of a search spaces global convexity – it exists for probe geometries, and it does not exist for the travelling salesman problem (even though both search spaces are globally convex [2,4]). In a non-globally convex search space, this correlation could be particularly useful since memetic algorithms and other restart techniques should receive little benefit from exploring in the neighbourhood of other local optima. Coarse search also has advantages over memetic algorithms in problem domains (like the one currently studied) where the local optimization technique is too expensive to run a large number of times.

Since the most commonly used benchmark optimization problem (i.e. the TSP) does not show the required correlation between the quality of a random start point and the quality of its local optimum, it is understandable why coarse search and "smart" start points have not previously received extensive analysis. It is hypothesized that the correlation required to make "smart" start points effective is more likely to occur in continuous rather than discrete search spaces. This hypothesis is a promising topic for future research.

8 Conclusions

Particle swarm optimization has been used to find "smart" start points for a greedier local optimization technique (e.g. an evolution strategy). These "smart" start points have led to an important objective in the development of Continuum Probe Designer^{TM} as an industry-leading commercial application. The ability to find feasible solutions from all of the random starting points in a benchmark test suite represents the minimum level of robustness required to have confidence that Continuum Probe Designer^{TM} is ready for use by non-expert designers. The results also demonstrate the potential benefits of coarse search-greedy search hybrids in search spaces that have a correlation between the quality of a random start point and the quality of its local optimum.

Acknowledgements

This work has received funding support from the Natural Sciences and Engineering Research Council of Canada and the Atkinson Faculty of Liberal and Professional Studies, York University

References

1. Beyer, H.-G., Schwefel, H.-P.: Evolution Strategies: A comprehensive introduction. Natural Computing 1, 3–52 (2002)
2. Boese, K.D.: Models for Iterative Global Optimization. Ph.D. diss. Computer Science Department, University of California at Los Angeles (1996)
3. Brünger, A.T., Krukowski, A., Erickson, J.W.: Slow-cooling protocols for crystallographic refinement by simulated annealing. Acta Crystallographica A46, 585–593 (1990)
4. Chen, S., Razzaqi, S., Lupien, V.: An Evolution Strategy for Improving the Design of Phased Array Transducers. In: Proceedings of the 2006 IEEE Congress on Evolutionary Computation, pp. 2859–2863. IEEE Press, New York (2006)
5. Kennedy, J., Eberhart, R.C.: Particle Swarm Optimization. In: Proceedings of the IEEE International Conference on Neural Networks, vol. 4, pp. 1942–1948. IEEE Computer Society Press, New York (1995)
6. Hassan, W., Vensel, F., Knowles, B., Lupien, V.: Improved Titanium Billet Inspection Sensitivity through Optimized Phased Array Design, Part II: Experimental Validation and Comparative Study with Multizone. In: AIP Conference Proceedings, Quantitative Nondestructive Evaluation, vol. 820, pp. 861–868. AIP (2006)
7. Hendtlass, T.: WoSP: A Multi-Optima Particle Swarm Algorithm. In: Proceedings of the 2005 IEEE Congress on Evolutionary Computation, vol. 1, pp. 727–734. IEEE Press, New York (2005)
8. Hendtlass, T., Rodgers, T.: Discrete Evaluation and the Particle Swarm Algorithm. In: Proceedings of the 7th Asia-Pacific Conference on Complex Systems, pp. 14–22. Central Queensland University Press (2004)
9. Kirkpatrick, S., Gelatt Jr., C.D., Vecchi, M.P.: Optimization by Simulated Annealing. Science 220, 671–680 (1983)

10. Lupien, V., Hassan, W., Dumas, P.: Improved Titanium Billet Inspection Sensitivity through Optimized Phased Array Design, Part I: Design Technique, Modelling and Simulation. In: AIP Conference Proceedings, Quantitative Nondestructive Evaluation, vol. 820, pp. 853–860. AIP (2006)
11. Norman, M.G., Moscato, P.: A Competitive and Cooperative Approach to Complex Combinatorial Search. In: Proceedings of the 20th Informatics and Operations Research Meeting, pp. 3.15–3.29 (1991)
12. Radcliffe, N.J., Surry, P.D.: Formal memetic algorithms. In: Fogarty, T.C. (ed.) Evolutionary Computing. LNCS, vol. 865, pp. 1–16. Springer, Heidelberg (1994)

Solution of the Perspective-Three-Point Problem

Calculation from Video Image by Using Inclinometers Attached to the Camera

Loic Merckel[1,2] and Toyoaki Nishida[1]

[1] Dept. of Intelligence Science and Technology, Graduate School of Informatics, Kyoto University, Yoshida-Honmachi, Sakyo-ku, Kyoto 606-8501 Japan
loic@ii.ist.i.kyoto-u.ac.jp
nishida@i.kyoto-u.ac.jp
[2] Dept. of Scientific Systems R&D, Horiba Ltd., Kyoto 601-8510 Japan

Abstract. In this paper, we describe a method for finding the pose of an object from a single image. We assume that we can detect and match in the image three feature points of the object, and that we know their relative geometry on the object. At first we present the exact pose calculation with an existing method and emphasize the limitation. Then we introduce a new method which consists of adding to the camera an inclinometer so that we reduce the number of unknown parameters and thus are able to compute the pose efficiently by using a classical iterative optimization method.

1 Introduction

The pose calculation of a 3D object from a single video image is a well known problem in many fields such as photogrammetry, robotics, computer vision, real world interaction, etc and many researchers have elaborated methods or algorithms in order to find a solution [1][2][3][4][5][6][7][8].

The problem of finding the position and orientation of an object from the images of n points at known locations on the object is known as the Perspective-n-Point problem [9].

Our interest is to develop a knowledge management agent for scientific instruments aiming to guide the user through the correct operation procedure of subject instruments. The level and needs of users cover a large range. Indeed, some users, with a scientific background, want to use all the capacity of the instrument. Usually, a user belonging to this category knows very well about the meaning of each parameter or action he needs to set and he is not afraid by complex software or mechanical architecture. On the opposite side, some users want to use the same instruments as an easy to operate tool and does not have any will to study an inaccessible and imposing manual. The agent should support the users to share the experience and knowledge of specialists with the others.

Thus we aim to develop a system which interact with the user in the real world. The system displays and manages knowledge associated to a given scientific instrument. The user takes a video of the unit via the system, and the

H.G. Okuno and M. Ali (Eds.): IEA/AIE 2007, LNAI 4570, pp. 324–333, 2007.

system displays some arrows showing the position of each important part of the instrument on the live video image. The unit is static, it means that only the camera is moving, and we can add some markers on the unit in order to indicate the feature points and make it easier to detect.

Our motivation to solve the Perspective-*Three*-Point problem lies in the fact that a difficult part in the pose estimation in real time from a live video image is to match the observed image points with the feature points of the object [10]. However, this problem is easily solvable with three points and becomes more difficult from four points.

The existing methods are unadapted in order to solve the Perspective-*Three*-Point problem. Indeed, Fischler, Bolles [9] Daniel DeMenthon and Larry S. Davis [2] described a solution permitting to calculate the exact pose of a triangle and consisting of solving a four degree polynomial equation. Most of the other methods to solve the Perspective-n-Point problem have relied on iterative optimization methods which require at least four points [4][3].

In the rest of this paper we will introduce an existing method in order to calculate the pose of the object from three feature points and we will show the limitation of such method. Then we will introduce a new method by using the information provided by inclinometers attached to the camera. This method permits to compute a solution only with three feature points and uses an iterative optimization method based on the Lavenberg-Marquardt algorithm. Since the performance of the Lavenberg-Marquardt algorithm to converge very quickly to the correct solution depends on the initial guess needed to start the optimization, we will describe a method in order to approximate the initial pose by using very few and constant number of mathematics operations.

2 Problem Formulation

The Perspective-*Three*-Point problem consists of compute the rotation matrix and the translation vector between the camera coordinate system and the object one from three feature points of the object detected and matched in the image.

In our study, we suppose that the object is static and only the camera is moving.

3 Existing Method and Limitation

Fischler, Bolles [9] Daniel DeMenthon and Larry S. Davis [2] described a solution which consists of solving a four degree polynomial equation.

However the solution is usually not unique and sometime we get two or four possible triangle pose solutions. Fischler and Bolles [9] described that in some specific geometric configurations several triangles with the same shape project to a same single image triangle. Therefore we cannot, a priori, calculate the pose of the object with only three feature points in a general situation. In other words, we cannot solve the Perspective-3-Point problem with, in addition to the feature

points of the object, only the information picked up from the image. In addition, this method is very sensitive to the video image noise.

4 Using Inclinometers to the Camera

4.1 Principle

The rotation matrix between the two coordinate systems is defined by three angles (Fig. 1) . By placing inclinometers [1] to the camera we can get two of them. Thus there is only one unknown angle to compute the rotation matrix.

The rotation matrix is $R = R_x(\alpha) \times R_y(\beta) \times R_z(\gamma)$ with:

$$R_x(\alpha) = \begin{pmatrix} 1 & 0 & 0 \\ 0 & \cos\alpha & -\sin\alpha \\ 0 & \sin\alpha & \cos\alpha \end{pmatrix}, R_y(\beta) = \begin{pmatrix} \cos\beta & 0 & \sin\beta \\ 0 & 1 & 0 \\ -\sin\beta & 0 & \cos\beta \end{pmatrix}$$

$$\text{and } R_z(\gamma) = \begin{pmatrix} \cos\gamma & -\sin\gamma & 0 \\ \sin\gamma & \cos\gamma & 0 \\ 0 & 0 & 1 \end{pmatrix} \quad . \tag{1}$$

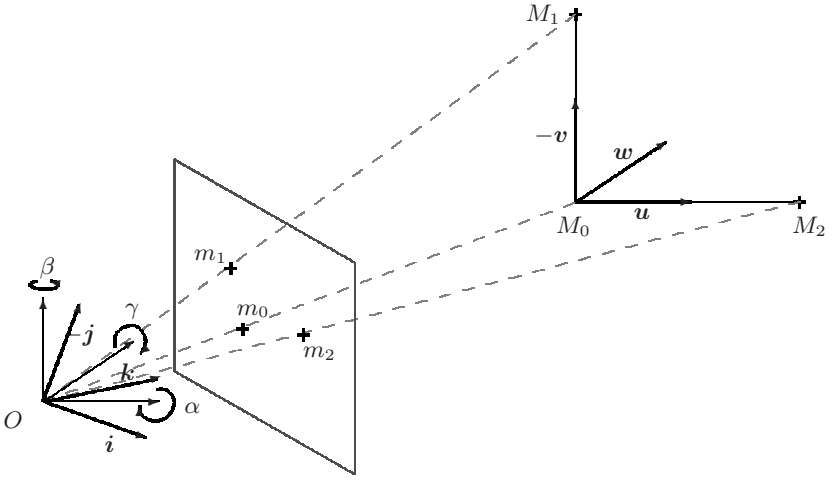

Fig. 1. Object and image space

The inclinometers will provide the α and γ angles. We need to calculate β in order to compute the rotation matrix R.

[1] Inclinometer is an instrument for measuring angles of slope and inclination of an object. It is also known as a tilt sensor, tilt indicator, slope meter, slope gauge, gradient meter, gradiometer, level gauge and level meter.

Concerning the angles calculated by the inclinometers, obviously the response time as well as the precision depends on the quality of the device. However many devices will provide a real time measurement with a precision range going from $\pm 0.001^\circ$ to $\pm 0.1^\circ$.

Let $M_i = (U_i, V_i, W_i)^T$ be expressed in the object space coordinate system $(M_0, \boldsymbol{u}, \boldsymbol{v}, \boldsymbol{w})$. The corresponding point $(X_i, Y_i, Z_i)^T$ in the camera space coordinate system $(O, \boldsymbol{i}, \boldsymbol{j}, \boldsymbol{k})$ are related by the transformation:

$$\begin{pmatrix} X_i \\ Y_i \\ Z_i \end{pmatrix} = R \begin{pmatrix} U_i \\ V_i \\ W_i \end{pmatrix} + T \text{ where } T = \overrightarrow{OM_0} = \begin{pmatrix} X_0 \\ Y_0 \\ Z_0 \end{pmatrix} \in \mathbb{R}^3 \ . \tag{2}$$

In the video image (the camera has been calibrated), considering the coordinate system $(C, \boldsymbol{i}, \boldsymbol{j})$ we know $m_i\,(x_i, y_i)$. We assume (idealized pinhole imaging model) :

$$x_i = \frac{fXi}{Z_i}, y_i = \frac{fYi}{Z_i} \text{ and } z_i = f \tag{3}$$

where f is the focal of the camera ($f = OC$).

4.2 Optimization Method Via the Levenberg-Marquardt Algorithm

A common approach in order to estimate the pose is to formulate the problem as a nonlinear least-squares problem and solve it by using optimization algorithms such as the Gauss-Newton method or the Levenberg-Marquardt algorithm [11][4]. However these methods need at least four points in order to be used. The approach using inclinometers permits to get over this limit and solves the problem with only three points (even two points could be enough). Indeed (3) yields:

$$X_0 = \frac{x_0 Z_0}{f} \text{ and } Y_0 = \frac{y_0 Z_0}{f} \ . \tag{4}$$

Therefore we need to compute only Z_0 and β. Let $\psi_i : \mathbb{R}^2 \to \mathbb{R}$ be defined by:

$$\psi_i(Z_0, \beta) = \sqrt{\left(x_i - \frac{fX_i(Z_0,\beta)}{Z_i(Z_0,\beta)}\right)^2 + \left(y_i - \frac{fY_i(Z_0,\beta)}{Z_i(Z_0,\beta)}\right)^2} \ . \tag{5}$$

A solution to the pose estimation problem is given by optimizing the following cost function:

$$\sigma(Z_0, \beta) = \sum_{k=0}^{2} \left(\psi_k(Z_0, \beta)\right)^2 \ . \tag{6}$$

In order to optimize this function, we prefer the Levenberg-Marquardt method because it is more robust than the Gauss-Newton algorithm.

Another approach is presented in [3]. The cost function is defined by considering the *object space* collinearity.

4.3 Initial Guess Estimation

We aim to calculate the pose of an object from a live video image *i.e.* in real time. The Levenberg-Marquardt method should converge very quickly to the correct solution if the initial guess is good enough.

Since two successive frames of the video should be very similar we can use the previous calculated pose as the initial approximate solution of the current calculation.

However we must think about the first frame as well as the case of the object went out of the field of view of the camera. In this part we will give a method to calculate an approximation of the pose.

Choice of the feature points. Since the object is static and we can choose the feature points M_0, M_1, M_2, we make them define a right triangle which the adjacent side (M_0M_2) is horizontal and the opposite side (M_0M_1) is vertical (fig. 2). We justify this choice by the fact that with such configuration we can estimate the pose easily from the data provided by the inclinometer.

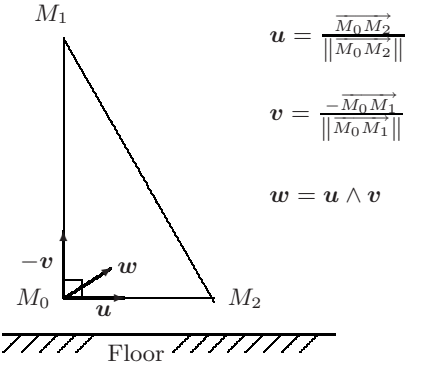

Fig. 2. Three feature points defining a right triangle

Translation vector. We will estimate the translation vector T by a geometry approach of the scene. Let H be the point defined by $(M_0M_1) /\!\!/ (Hm_0)$ and $H \in (OM_1)$ (Fig. 3). The Thales' theorem and (3) yield:

$$Z_0 = \frac{\left\|\overrightarrow{M_0M_1}\right\| \sqrt{f^2 + \left\|\overrightarrow{Cm_0}\right\|^2}}{\left\|\overrightarrow{Hm_0}\right\| \sqrt{1 + \left(\frac{x_0}{f}\right)^2 + \left(\frac{y_0}{f}\right)^2}} \ . \tag{7}$$

Therefore in order to estimate Z_0, which is enough to estimate the translation vector T, see (3), we can estimate $\| \overrightarrow{Hm_0} \|$. For instance if $\theta < 0$ (i.e. $\alpha < 0$) and $y_1 \leq y_c \leq y_0$ (Fig. 4), we have, with $s = 1$ and $\delta = |\theta| - \varphi$:

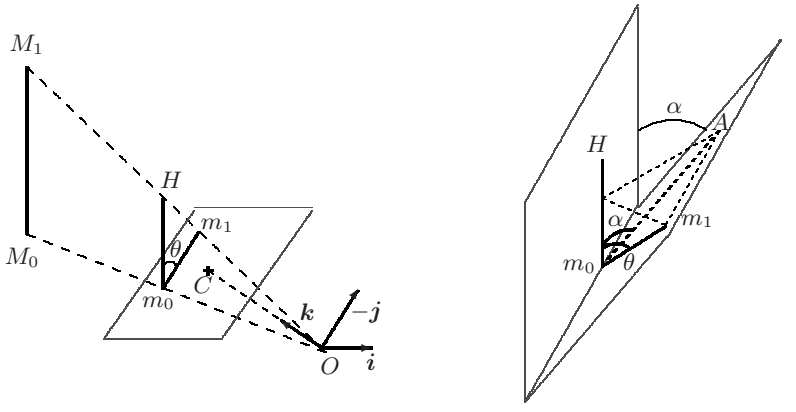

Fig. 3. Definition of the point H: $(M_0M_1) /\!\!/ (Hm_0)$ and $H \in (OM_1)$. The right sketch shows the difference between α (given by the inclinometer) and θ.

$$\left\|\overrightarrow{Hm_0}\right\| = \|\overrightarrow{m_0m_1}\| \left(\cos\theta - s\frac{\sin|\theta|}{\tan(\delta)}\right) \text{ with } \begin{cases} \sin\varphi = \frac{\sqrt{d^2+f^2}}{\left\|\overrightarrow{Om_1}\right\|} \\ d = d\,(C, [m_0m_1]) \end{cases} . \quad (8)$$

The Table (1) gives the values of δ and s depending on the sign of α and the relative position of y_0, y_1 and y_c.

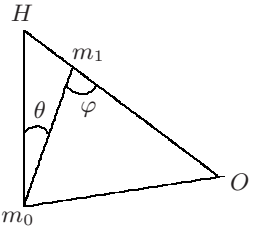

Fig. 4. $\theta < 0$ and $y_1 \leq y_c \leq y_0$

Table 1. δ and s values to calculate Hm_0

	$y_c < y_1$	$y_1 \leq y_c \leq y_0$	$y_0 < y_c$
$\alpha \geq 0$	$\delta = \alpha - \varphi$, $s = 1$	$\delta = \alpha + \varphi$, $s = 1$	$\delta = -\alpha - \varphi$, $s = -1$
$\alpha < 0$	$\delta = -\lvert\alpha\rvert - \varphi$, $s = -1$	$\delta = \lvert\alpha\rvert - \varphi$, $s = 1$	$\delta = \lvert\alpha\rvert - \varphi$, $s = 1$

The difference between α (given by the inclinometer) and $\theta = \widehat{Hm_0m_1}$ (Fig. 3) is negligible, thus in order to approximate Z_0 we can consider that $\alpha \approx \theta$.

Rotation matrix. We must approximate the rotation matrix R. The equations (2) and (3) yield the following system ($i = 1$ or $i = 2$):

$$A_i.X = B_i \tag{9}$$

with

$$A_i = \begin{pmatrix} a_{11} & a_{12} \\ a_{21} & a_{22} \end{pmatrix}, \; B_i = \begin{pmatrix} b_1 \\ b_2 \end{pmatrix} \text{ and } X = \begin{pmatrix} \cos\beta \\ \sin\beta \end{pmatrix} \quad .$$

These coefficients are defined with:

$$\begin{aligned} a_{11} &= -x_i W_i \cos\alpha + f\,(V_i \sin\gamma - U_i \cos\gamma) \\ a_{12} &= x_i\,(V_i \sin\gamma - U_i \cos\gamma)\cos\alpha - f W_i \\ a_{21} &= W_i\,(y_i \cos\alpha + f \sin\alpha) \\ a_{22} &= (y_i \cos\alpha + f \sin\alpha)\,(V_i \sin\gamma - U_i \cos\gamma) \end{aligned}$$

and

$$\begin{aligned} b_1 &= f X_0 - x_i\,[Z_0 + \sin\alpha\,(V_i \cos\gamma + U_i \sin\gamma)] \\ b_2 &= V_i \cos\gamma\,(f\cos\alpha - y_i \sin\alpha) - y_i Z_0 + f Y_0 + U_i \sin\gamma\,(f\cos\alpha - y_i \sin\alpha) \quad . \end{aligned}$$

This system is linear with two equations and two unknowns $\cos\beta$ and $\sin\beta$. We can solve it by using either the point M_1 or M_2.

5 Implementation and Simulations

The method and model. A set of 3D reference points defining an isosceles right triangle which the two legs length is 10 cm is chosen as the model. The model is rotated randomly and projected onto the image plane [2]. This is equivalent to a static object viewed by a moving camera. All simulations are repeated for 500 times. We use a pinhole camera model with focal length of 550 pixels and principal point of $(305, 225)$. Gaussian noise of mean zero and standard deviations $\sigma = 0.01$ is added to both angles calculated by the inclinometers independently. Throughout the simulation, we measure the angle error with the Euclidean distance $d : \mathbb{R} \times \mathbb{R} \to \mathbb{R}^+, (x, y) \mapsto |x - y|$ and the translation vector error with the distance $d_\infty : \mathbb{R}^3 \times \mathbb{R}^3 \to \mathbb{R}^+, (X, Y) \mapsto \|X - Y\|_\infty$. The error is the distance between the theoretic value and the calculated value. For each simulation we conduct two tests:

1. Distance to camera / object size: The translation vector is generated by fixing $T_x = -9\,cm$ and $T_y = -1\,cm$, and varies $T_z/10$ from 15 to 50 by a step of 1.
2. Distance to optical axis / object size: The translation vector is generated by fixing $T_z = 30\,cm$, and varies $T_x/10$ from 2 to 20 by step of 1. For each step T_y is defined so that the angle $\widehat{(\boldsymbol{T}, \boldsymbol{i})}$ varies from 0 to 2π by step of $\pi/4$.

[2] We have developed implementation of our method in C++.

Simulation 1: Pose error. Gaussian noise of mean zero and varying standard deviations σ is added to both image plane coordinates independently. We vary the noise level between 0 to 2 pixels. The Figures (5) and (6) show the result. If the object is near enough to the camera, the result is satisfactory even in noisy environment. Indeed the angular error (β) is lower than 4°, considering the fact that the precision of α and γ is high, the rotation matrix is well approximated. Concerning the translation vector the approximation is excellent.

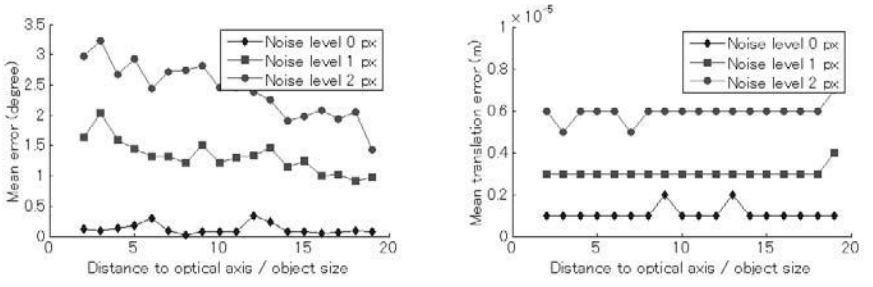

Fig. 5. Angle and translation error depending on the distance to the optical axis and noise level

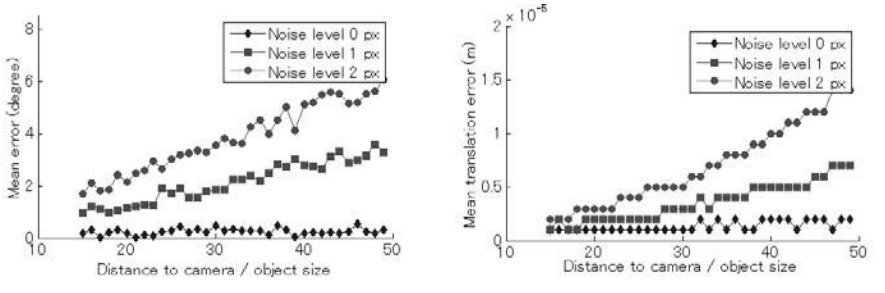

Fig. 6. Angle and translation error depending on the distance to the camera and noise level

Simulation 2: Number of iterations. Figure (7) shows that the number of iterations required is high. It is due to the fact we are using only three points.

Comparison with other methods. We compare our approach against two existing methods: POSIT [1] and a classical optimization method (based on Levenberg-Marquardt). The previous model is rotated and translated randomly in the field of view of the camera. All simulations are repeated 1000 times. Gaussian noise level is set at 1 pixel. We define the relative pose error as $E = 2\,\|A_{theoretic} - A_{calculated}\|_\infty / (\|A_{theoretic}\|_\infty + \|A_{calculated}\|_\infty)$. From 4 feature points, In order to initialize the iterative algorithms we use the result of the POSIT method. Table (2) shows that for 4 and 5 feature points our method

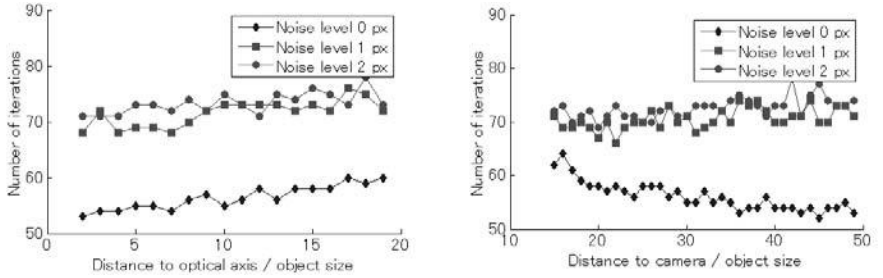

Fig. 7. Number of iterations

gives better pose estimation. We noticed that, considering 4 or 5 points, both methods based on the Levenberg-Marquardt algorithm have a convergence rate of 99.9 % while for 3 points the convergence rate is about 93 % and becomes approximatively 60 % with only two points. Concerning the number of iteration, for 4 and 5 points, a classical method needs more than 120 iterations whereas the method using inclinometers converges in less than 60 iterations.

Table 2. Comparison with other methods. r_e and t_e are respectively the mean rotation error and the mean translation error.

	POSIT	Opt. Algo.	Inclinometer
2 points	Failed	Failed	$r_e = 0.13$, $t_e = 7.10^{-6}$
3 points	Failed	Failed	$r_e = 0.016$, $t_e = 4.10^{-6}$
4 points	$r_e = 0.014$, $t_e = 0.005$	$r_e = 0.010$, $t_e = 8.10^{-6}$	$r_e = 0.005$, $t_e = 9.10^{-6}$
5 points	$r_e = 0.011$, $t_e = 0.004$	$r_e = 0.008$, $t_e = 9.10^{-6}$	$r_e = 0.004$, $t_e = 9.10^{-6}$

6 Conclusion

In this paper, we have presented a new method to solve the Perspective-*Three*-Point problem for a static object viewed via a moving camera. This method is based on the usage of inclinometers attached to the camera and uses common optimization algorithm. Although we are using only three features points, this method gives a good result and is robust to additive noise. We have also shown that this method can be used to solve the Perspective-*Two*-Point problem and offers better pose estimation for the Perspective-*Four,Five*-Point problem than a classical method using Levenberg-Marquardt minimization.

References

1. DeMenthon, D., Davis, L.S.: Model-based object pose in 25 lines of code. In: European Conference on Computer Vision, pp. 335–343 (1992)
2. DeMenthon, D., Davis, L.S.: Exact and approximate solutions of the perspective-three-point problem. IEEE Trans. Pattern Anal. Mach. Intell. 14(11), 1100–1105 (1992)
3. Lu, C.P., Hager, G.D., Mjolsness, E.: Fast and globally convergent pose estimation from video images. IEEE Trans. Pattern Anal. Mach. Intell. 22(6), 610–622 (2000)
4. Lee, P.Y., Moore, J.B.: Pose estimation via gauss-newton-on-manifold. In: Proceedings of the Sixth International Symposium on Mathematical Theory of Networks and Systems, Pacific Grove, California, USA, pp. 131–135 (2004)
5. Or, S.H., Luk, W.S., Wong, K.H., King, I.: An efficient iterative pose estimation algorithm. ACCV (2), 559–566 (1998)
6. Lowe, D.G.: Fitting parameterized three-dimensional models to images. IEEE Transactions on Pattern Analysis and Machine Intelligence PAMI-13(5), 441–450 (1991)
7. Quan, L., Lan, Z.D.: Linear n-point camera pose determination. IEEE Transactions on Pattern Analysis and Machine Intelligence 21(8), 774–780 (1999)
8. Fabrizio, J., Devars, J.: The perspective-n-point problem for catadioptric sensors: An analytical approach. In: International Conference on Computer Vision and Graphics (ICCVG'04), Warsaw, Poland (2004)
9. Fischler, M.A., Bolles, R.C.: Random sample consensus: a paradigm for model fitting with applications to image analysis and automated cartography. Commun. ACM 24(6), 381–395 (1981)
10. Breuel, T.M.: An efficient correspondence based algorithm for 2D and 3D model based recognition. Technical Report AIM-1259 (1990)
11. Lowe, D.G.: Three-dimensional object recognition from single two-dimensional images. Artificial Intelligence 31(3), 355–395 (1987)

A Decision Support System for Underground Mining Method Selection

Serafettin Alpay[1] and Mahmut Yavuz[2]

[1] Eskisehir Osmangazi University, Industrial Engineering Department,
[2] Eskisehir Osmangazi University, Mining Engineering Department, Eskisehir, Turkey
{salpay, myavuz}@ogu.edu.tr

Abstract. Underground mining method selection (UMMS) is one of the most important decisions that should be made by mining engineers. Choosing a suitable underground mining method to carry out extraction from a mineral deposit is very important in terms of the economics, safety and the productivity of mining operations. In reality, UMMS is one of the Multiple Criteria Decision Making (MCDM) problems and decision makers have some difficulties in making the right decision in the multiple criteria environment. In this paper, a decision support system for underground mining method selection (UMMS-DSS) has been designed and developed in order to take into account the whole related problem criteria, research the entire effects of different scenarios of all available criteria and carry out sensitive analysis when needed. UMMS-DSS was designed as to use Analytic Hierarchy Process (AHP), one of the MCDM methods, to manage those tasks and to produce acceptable solution alternatives.

Keywords: Underground Mining Method Selection, Decision Support System, Multiple Criteria Decision Making, Analytic Hierarchy Process.

1 Introduction

Mineral exploitation in which all extractions are carried out beneath the earth's surface is termed as underground mining. Underground methods are employed when the depth of the deposit, the stripping ratio of overburden to ore (or coal or stone), or both become excessive for surface exploitation. Once economic analysis points to underground methods, the choice of a proper mining procedure hinges mainly on determining the appropriate form of ground support, if necessary, or its absence; and designing the openings and their sequence of extraction to conform to the spatial characteristics of the mineral deposit [5].

Underground mining method should be primarily selected to make use of underground resources optimally [4]. Working safely in the underground, increasing the productivity and eliminating the production costs and losses are the basic priorities. Underground mining method selection (UMMS) is often closely related to the geology of the deposit [5]. Besides, the ground control on the mining areas, planning the ventilation system, decreasing the maintenance costs of gallery, developing new mining panels and preparing the underground production schedule

H.G. Okuno and M. Ali (Eds.): IEA/AIE 2007, LNAI 4570, pp. 334–343, 2007.

are also directly related to the selection of underground mining method. Because of these reasons, UMMS process is extremely important in mine designs.

To make a right decision on UMMS, all known criteria related to the problem should be analyzed. Although an increasing in the number of related criteria makes the problem more complex and more difficult to reach a solution, this may also increase the rightness of the decision made in consideration of those criteria. Because of the arising complexity in the decision process, many conventional methods are able to consider limited criteria and may be generally deficient. So, it is obviously seen that evaluating the all of the known criteria related to the mining method selection by incorporating the decision making process is very important.

Because it is nearly impossible to change the mining method once selected by the reasons of rising costs and mining losses, it is very important to reanalyze the decision made before carry out it. Therefore, decision makers frequently require going back to any stage of the decision process and need to change some settings of the criteria to analyze the sensitivity of the decision.

A Decision Support System (DSS) can be used to manage all of the related problem criteria and make a correct decision. At this point, a decision support system having good decision support models for UMMS will provide not only a simple way to reach a solution quickly but also make the decision makers to reanalyze the decision process and carry out the required sensitivity analyzes.

In this paper, a decision support system is developed to help the decision makers to analyze an UMMS problem and make a decision on the right and suitable mining method. To produce solution alternatives, the developed a decision support system for underground mining method selection (UMMS-DSS) uses two Analytic Hierarchy Process (AHP) models. The AHP, since its invention, has been a tool at the hands of decision makers and researchers; and it is one of the most widely used the Multiple Criteria Decision Making (MCDM) tools. Although many outstanding works have been published based on the AHP in the literature, the only works related with mining operations [1], [2], [3], [7], [13].

This paper is organized as follows; DSS is basically described in Section 2. Section 3 introduces the developed decision support system and illustrates its AHP based decision support models. The AHP method is also described in Section 3. A real example using the developed UMMS-DSS through a real case study about Karaburun-Eskisehir chromite ore deposit is presented in Section 4. Conclusions are offered in Section 5.

2 Decision Support Systems

In recent years, DSS' have been widely applied in the decision-making activities of managers and other knowledge workers in organizations. The concepts involved in DSS were first articulated in the early 1970s and since then many viewpoints appeared in defining and formalizing DSS [8].

A survey of the literature indicates that there is no universal definition of DSS [8]. A DSS is, however, defined to be software which allows the user to make a decision based on information supplied by the software program [14]. Nof et al. [9] define a

DSS to be an information system that provides control capability by searching for an appropriate response by exploring models and data that combine for a reasonable decision. Some authors have extended the definition of DSS to include any system that supports a decision or makes some contribution to decision making [8]. The basic function of the DSS in a general sense is to facilitate judgment by organizing data and relating pertinent information to the decision maker [10].

The key ideas are that the DSS should support and enhance, but not replace management's judgment, synergize models and different techniques using data access and retrieval functions, be easy for non computer literate users, use interactive problem solving and emphasize flexibility and adaptability to changes in the environment [10].

3 A Decision Support System for Underground Mining Method Selection (UMMS-DSS)

In this paper, UMMS-DSS has been designed and developed. One of the important goal is to be able to take into account the all criteria in the decision making process of a mining method selection problem. Other important goals are to research the effects of different scenarios of all available criteria and carry out a sensitivity analysis when needed.

The developed UMMS-DSS includes three modules: Database Management Module, Model Management Module and Dialog Module. The details of these modules will be given in the following sections.

3.1 Database Management Module

Database management module consists of a database for storing all data and knowledge related to the mining methods and criteria to be used for selection of underground mining method. This module is also responsible for managing (means querying, updating, adding and deleting actions) the database. The database contains two tables, titled by Criteria and Methods, saving descriptive data and the data of known issues concerning with criteria and methods. The data and knowledge pertaining to six main group criteria and their subcriteria which have been classified by Hartman and Mutmansky [5] are stored in the table of criteria. Those criteria and their subcriteria stored in the table of criteria are C_1: Spatial characteristics of the deposit (Subcriteria are S_{11}: Size, S_{12}: Attitude, S_{13}: Depth, S_{14}: Regularity of the ore boundaries, S_{15}: Existence of previous mining), C_2: Geologic and hydrologic conditions (Subcriteria are S_{21}: Mineralogy and petrography, S_{22}: Chemical composition, S_{23}: Deposit structure, S_{24}: Planes of weakness, S_{25}: Uniformity of grade, S_{26}: Alteration and weathered zones, S_{27}: Existence of strata gases), C_3: Geotechnical (soil and rock mechanics) properties (Subcriteria are S_{31}: Elastic properties, S_{32}: Plastic or viscoelastic behavior, S_{33}: State of stress, S_{34}: Rock mass rating, S_{35}: Other physical properties affecting competence), C_4: Economic considerations (Subcriteria are S_{41}: Reserves, S_{42}: Production rate, S_{43}: Mine life, S_{44}: Productivity, S_{45}: Comparative mining costs, S_{46}: Comparative capital costs), C_5: Technological factors

(Subcriteria are S_{51}: Recovery, S_{52}: Dilution, S_{53}: Flexibility of the method to changing conditions, S_{54}: Selectivity of the method, S_{55}: Concentration or dispersion of workings, S_{56}: Ability to mechanize and automate, S_{57}: Capital and labor intensities) and C_6: Environmental concerns (Subcriteria are S_{61}: Ground control to maintain integrity of openings, S_{62}: Subsidence or caving effects at the surface, S_{63}: Atmospheric control, S_{64}: Availability of suitable waste disposal areas, S_{65}: Workforce, S_{66}: Comparative safety conditions of the suitable mining methods).

The data and knowledge related to the underground mining methods are stored in the table of methods. Those methods are Unsupported methods (Room-and-pillar mining, Stope-and-pillar mining, Shrinkage stoping, Sublevel stoping, Underhand open stoping), Supported methods (Cut-and-fill stoping, Stull stoping and Square-set stoping) and Caving methods (Longwall mining, Sublevel caving, Block caving, Block mining with square-sets, Pillar caving and Top slicing) [5], [15].

The decision maker can reach the database by using dialog module and get all information about the mining methods and the criteria. Moreover, the decision maker can manipulate the tables whenever he/she wants.

3.2 Model Management Module

The UMMS-DSS uses the AHP to produce solution alternatives and two AHP models which are included in the model management module. The AHP method developed by Saaty [11], [12] gives an opportunity to represent the interaction of multiple factors in complex unstructured situations. The method is based on the pair-wise comparison of components with respect to attributes and alternatives. A pair-wise comparison matrix $n \times n$ is constructed, where "n" is the number of elements to be compared. The method is applied for the hierarchy problem structuring. The problem is divided in to three levels [12]: problem statement, object identification to solve the problem, and selection of evaluation criteria for each object.

The hierarchy structures of the AHP models of the developed UMMS-DSS are shown in Fig. 1. The first level of the both models is the general object. In the first model, six main group criteria are placed in the second level and their subcriteria are placed in the third level. If a decision maker intends to increase the rightness of his/her decision, he/she should use the first model. On the other hand, when the first model is used, the number of pair-wise comparison matrices increases quite and this also makes the needed time much longer to reach a solution. If the time is restricted and/or the six main group criteria without their subcriteria are enough to make a decision, the second model can be used as an alternative. In the second model, only main group criteria are considered in the decision-making process and are placed in the second level of the structure of the model. The last level of either of models is the alternatives. These alternatives are the underground mining methods and they may vary according to the shape of deposit and ore strength. To determine the valid alternatives, the UMMS-DSS uses a structure which is given by Hartman and Mutmansky [5] in Fig. 2. By using this structure, the decision maker will decide on which alternatives will be valid in the solution process according to the problem type.

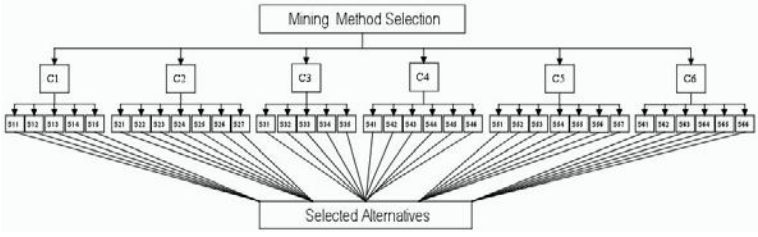

Fig. 1. The AHP model including all criteria and their subcriteria

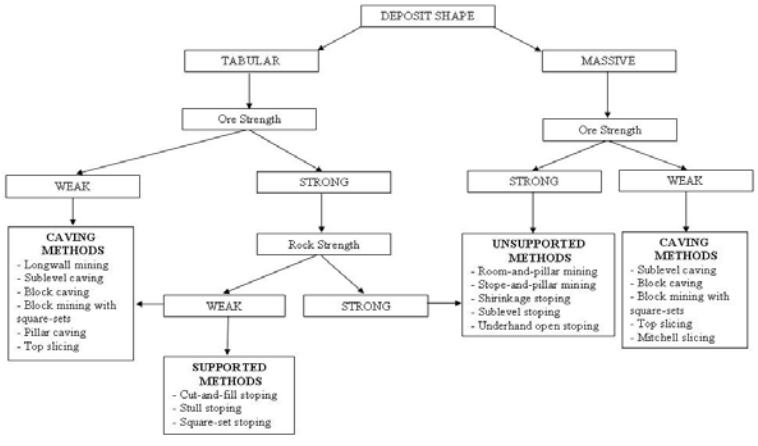

Fig. 2. Selection structure of alternatives by the developed UMMS-DSS

After the hierarchy structuring the pair-wise comparison matrix is constructed for each level, where a nominal discrete scale from 1 to 9 is used for the evaluation (Table 1) [11], [12].

Table 1. Scale for pair-wise comparisons

Relative Intensity	Definition
1	Of equal value
3	Slightly more value
5	Essential or strong value
7	Very strong value
9	Extreme value
2,4,6,8	Intermediate values

The next step is to find the relative priorities of criteria or alternatives implied by this comparison. The relative priorities are worked out using the theory of eigenvector. For example, if the pair comparison matrix is "*A*", then,

$$(A - \lambda_{max} \times I) \times w = 0 \tag{1}$$

where "λ_{max}" is maximal or principal eigenvalue and "*I*" is unit matrix. To calculate the eigenvalue λ_{max} and eigenvector $w=(w_1, w_2,..., w_n)$, weights can be estimated as relative priorities of criteria or alternatives [12].

Since the comparison is based on the subjective evaluation, a Consistency Ratio (*CR*) is required to ensure the selection accuracy. The Consistency Index (*CI*) and *CR* of the comparison matrix is computed as follows:

$$CI = \frac{\lambda_{max} - n}{n - 1} \tag{2}$$

$$CR = \frac{CI}{RI} \tag{3}$$

where "*RI*" Random Consistency Index. *RI* values are given in Table 2 [12].

Table 2. The consistency indices of randomly generated reciprocal matrices

	Order of the matrix												
RI	1, 2	3	4	5	6	7	8	9	10	11	12	13	14
value	0.00	0.58	0.90	1.12	1.24	1.32	1.41	1.45	1.49	1.51	1.48	1.56	1.57

As a general rule, a consistency ratio of 0.10 or less is considered acceptable. In practice, however, consistency ratios exceeding 0.10 occur frequently.

In brief, the UMMS-DSS with model management module provides a decision maker two AHP models to form the underground mining method selection problem and provides a way to find the best alternative.

3.3 Dialog Module

Dialog module provides an interaction between the decision makers and the AHP models, the decision makers and database module. Dialog module contains a user interface with which a decision maker is able to control all stages of the decision making process and make the UMMS-DSS produce the best underground mining method to the problem by using AHP models.

4 Case Study

The selection of mining method has been considered for Eskisehir-Karaburun chromite ore. The Karaburun chromite mine is located 120 kilometers east of Eskisehir which is located in the northwest part of Turkey. The total ore reserve of the Karaburun chromite mine is calculated as 230 000 tons. The physical and mechanical characteristics of the deposit are shown in Table 3 [6].

Table 3. Technical parameters of the Karaburun Chromite Mine

Parameter	Quality
Inclination	Average 65° NE
Thickness	1.5-3.5 m, average 2.7 m
Dip	N 80° W
Type	Massive
Grade distribution	Uniform
Depth	Shallow
Gravity for hanging wall, footwall and ore	2.630, 2.586 and 3.244 gr/cm^3
Uniaxial strength of ore, hanging wall and footwall	40 MPa, 49 MPa, 53 MPa
RQD for walls and ore	72 and 40 %
RMR for hanging wall, footwall and ore	47, 53 and 34

The first stage of the UMMS is to determine the deposit shape, and strengths of ore and rock. As shown in Table 3, the deposit type is massive and uniaxial strength of ore is 40 MPa. The ore strength is defined as "Weak" according to Table 4 proposed by Hartman and Mutmansky [5]. So, the Caving Methods (Sublevel Caving, Block Caving, Block Mining with square-sets, Top slicing and Mitchell slicing) can be applied for this type of deposit according to the structure in Fig. 2. The required settings are chosen by selecting the corresponding values of the deposit shape and ore strength in the main screen of UMMS-DSS as shown in Fig. 3.

Table 4. Classification of ore and rock strengths

Mineral or Rock	Relative Strength	Compressive Strength (MPa)
Coal, decomposed and badly altered rock	Very weak	<40
Friable sandstone, mudstone, weathered rock, soft shale	Weak	40-100
Shale, limestone, sandstone, shistosite rock	Moderate	100-140
Most igneous rock, strong metamorphic rock, hard limestone and dolomite	Strong	140-200
Quartzite, basalt, diabase	Very strong	>200

To make a decision by using an AHP model, the criteria to be used for the decision process should be determined. For our problem, the second AHP model was selected for determining the best underground mining method quickly. The current alternatives of the model are A_1: Sublevel caving, A_2: Block Caving, A_3: Block Mining with square-sets, A_4: Top slicing and A_5: Michell slicing. According to the model, the pair-wise comparison of the criteria should be performed first. The pair-wise comparison of the main criteria performed by the UMMS-DSS is given Fig. 4. It is apparent that Spatial characteristics of the deposit is the most important criterion (priority of C_1 0.429), then Economic considerations follows (priority of C_4 0.265).

On the other hand, the pair-wise comparison of the alternatives based on the each criterion should also be performed. Thus, six matrices are formed. As there are five alternatives, the matrix order will be 5×5. It is readily observed from the tables that

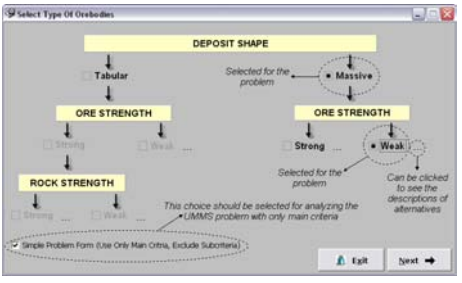

Fig. 3. The settings of the problem in the main screen of the UMMS-DSS

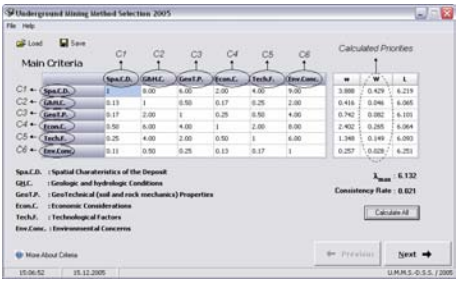

Fig. 4. The pair-wise comparison matrix of the main criteria

the most suitable alternatives are A_3, A_3, A_1, A_2, A_3 and A_2 when judged by the criteria of C_1, C_2, C_3, C_4, C_5 and C_6, respectively. The overall rating of each method (alternative) is calculated by summing the product of the relative priority of each criterion and the relative priority of the method considering the corresponding criteria. For example, the overall rating of alternative A_1= (0.429×0.260) + (0.046×0.269) + (0.082×0.469) + (0.265×0.143) + (0.149×0.118) + (0.028×0.270) = 0.226.

The overall ratings calculated by the UMMS-DSS are presented in Fig. 5. From the Fig. 5, it is obvious that A_3 (Block Mining with Square-Sets) with a rating of 0.321 is the most preferred mining method. In Table 5, all calculated priorities and final ratings are summarized.

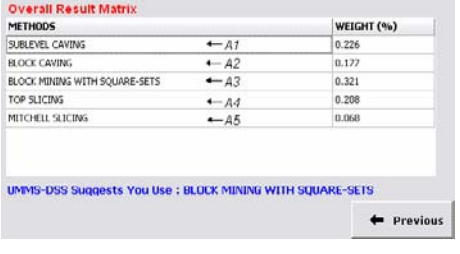

Fig. 5. The final solution screen of the UMMS-DSS

Table 5. Overall result/final matrix

	A_1	A_2	A_3	A_4	A_5	Priority
C_1	0.260	0.042	0.480	0.158	0.060	0.429
C_2	0.269	0.043	0.469	0.076	0.143	0.046
C_3	0.469	0.043	0.143	0.269	0.076	0.082
C_4	0.143	0.469	0.043	0.269	0.076	0.265
C_5	0.118	0.103	0.446	0.271	0.062	0.149
C_6	0.270	0.471	0.143	0.066	0.050	0.028
Overall	0.226	0.177	0.321	0.207	0.069	

As the comparisons are based on the subjective evaluation, the *CR* should be calculated using Equation (3) to ensure the selection accuracy. Table 6 presents λ_{max}, and *CR* of the corresponding matrices. Thus, for all the matrices the *CR* is less than 0.10. So, the logically substantiated decision of constructing the pair-wise comparison of the criteria or alternatives has been made.

Table 6. λmax, *CI*, *RI*, and *CR* of different matrices

	Goal	C_1	C_2	C_3	C_4	C_5	C_6
λ_{max}	6.132	5.110	5.046	5.046	5.046	5.068	5.164
CR	0.021	0.025	0.010	0.010	0.010	0.015	0.037

After reaching the optimal solution, a decision maker can go back to any pair-wise comparison stage and change any value of pair-wise comparisons so as to analyze the sensitivity of the solution.

5 Conclusions

In this paper, a decision support system for underground mining method selection has been designed and developed to eliminate the difficulties in taking into consideration many decision criteria simultaneously in the underground mining method selection process and to guide the decision makers to select the optimal underground mining method.

Two AHP models are proposed by the UMMS-DSS. Using the first AHP model, it is possible to analyze an UMMS problem with respect to the total of thirty six criteria clustered in six main groups. This also makes possible to increase the consistency of decisions made for selection of optimal mining method. Moreover, there is no work, which has been done in the literature, proposes a way or method which is able to manage as many criteria as the AHP model can use in decision process of selecting most suitable underground mining method. On the other hand, if the time is restricted and/or the six main group criteria without their subcriteria are enough to make a decision, the second model can be used as an alternative.

With the UMMS-DSS, it is now possible to evaluate many different underground mining methods depending on the deposit shapes and the strengths of ore and rock. Another important support of the UMMS-DSS to decision-making process is the

decision makers can go back to any previous step of the decision process after reaching a solution. In this way, they can analyze the sensitivity of the proposed solution by the UMMS-DSS by making some changes in the previous pair-wise comparisons if they want.

With the UMMS-DSS, a decision maker can analyze the underground mining method selection problem and derive the solution alternatives quickly even if the experienced person is not available.

References

1. Acaroglu, O., Ergin, H., Eskikaya, S.: Analytical hierarchy process for selection of roadheaders. The Journal of The South African Institute of Mining and Metallurgy 106(8), 569–575 (2006)
2. Ataei, M.: Multicriteria selection for alumina-cement plant location in East-Azerbaijan province of Iran. The Journal of The South African Institute of Mining and Metallurgy 105(7), 507–514 (2005)
3. Bascetin, A.: An application of the analytic hierarchy process in equipment selection at Orhaneli open pit coal mine, Mining Technology. Trans. Inst. Min. Metall. A 113, A192–A199 (2004)
4. Guray, C., Celebi, N., Atalay, V., Pasamehmetoglu, A.G.: Ore-age: a hybrid system for assisting and teaching mining method selection. Expert Systems with Applications 24, 261–271 (2003)
5. Hartman, H.L., Mutmansky, J.M.: Introductory Mining Engineering. John Wiley & Sons, New Jersey (2002)
6. Kahriman, A., Ceylanoğlu, A., Demirci, A., Arpaz, E., Görgülü, K.: Selection of Optimum Underground Mining Method for Eskisehir-Karaburun Chromite Ore. In: 3rd National Rock Mechanics Symposium (In Turkish), January 15-16, 1996, Ankara, pp. 47–60 (1996)
7. Kazakidis, V., Mayer, N., Scoble, M.J.: Decision making using the analytic hierarchy process in mining engineering, Mining Technology. Trans. Inst. Min. Metall. A 113, A30–A42 (2004)
8. Mukherjee, K., Chattopathyay, U.: A DSS for Project Investment Decisions, Computers in Mineral Industry, pp. 41–49, India (1994)
9. Nof, S.Y., Whinston, A.B., Bullers, W.I.: Control and decision support in automatic manufacturing systems. AIIE Transactions 12(2), 156–167 (1980)
10. Parker, S., Malstrom, E.M., Irwin, L.M., DuCote, G.: A decision support system for personal scheduling in a manufacturing environment. Computers Ind. Eng. 27, 185–188 (1994)
11. Saaty, T.L.: The Analytic Hierarchy Process. McGraw-Hill Publications, New York (1980)
12. Saaty, T.L.: Fundamentals of Decision Making and Priority Theory with the Analytic Hierarchy Process 2000, RWS Publications (2000)
13. Samanta, B., Sarkar, B., Murherjee, S.K.: Selection of opencast mining equipment by a multi-criteria decision-making process, Mining Technology. Trans. Inst. Min. Metall. A 111, A136–A142 (2002)
14. Turban, E.: Decision Support and Expert System, 2nd edn. Macmillan Publishing Company, NY (1990)
15. Yavuz, M., Alpay, S.: A Guideline for DSS System for Underground Mining Method Selection. In: 18 International Mining Congress and Exhibition of Turkey, pp. 347–349 (2003)

Efficient Modified Bidirectional A^* Algorithm for Optimal Route-Finding*

Taeg-Keun Whangbo

Dept. of Computer Science, Kyungwon University
Seongnam-Si, Gyeonggi-Do, Korea
tkwhangbo@kyungwon.ac.kr

Abstract. A* algorithm, a kind of informed search, is widely used for finding an optimal car route, because the location of starting and ending point are known beforehand. Unidirectional A* algorithm guarantees an optimal route but requires considerable search time. On the other hand, bidirectional A* algorithm, usually known faster than unidirectional A*, does not guarantee the route found to be optimal, if the search ends when the forward and backward search meet in the middle. It may even take longer than unidirectional search to find an optimal route. In this paper, a new modified bidirectional A* algorithm which takes less search time and guarantees an optimal route is proposed. To evaluate the efficiency of the proposed algorithm, several experiments are conducted in real urban road environment and the results show that the algorithm is very effective in terms of finding an optimal route and search time.

Keywords: Heuristic search, Car Navigation System, Optimal route, A* search.

1 Introduction

Another change brought by current digital technology in our everyday life is that the printed road map for drivers is getting obsolete. The digital equipment, known as CNS (Car Navigation System), is rapidly replacing the printed maps. In CNS, one of the fundamental functions required is to present an optimal route minimizing the necessary time to the destination.

Finding an optimal route requires considering many factors such as travel distance, traffic condition, etc., and those factors can be represented as some cost function which affects the optimal route. Then the subject is generalized as the search problem for finding a path with minimal cost between source and destination.

Because this kind of problem has been occurred in many different application areas for long time, many appropriate search solutions are developed. Dijkstra method, for example, is a traditional one, and A* algorithm is well-known as an efficient method in finding an optimal route with minimal cost [1].

* This research was supported by the Ministry of Education, Seoul, Korea, under the BK21 project.

H.G. Okuno and M. Ali (Eds.): IEA/AIE 2007, LNAI 4570, pp. 344–353, 2007.

A* algorithm, which combines the advantage of uniform-cost search and greedy search, can expand the next node in either unidirectional manner or bidirectional manner. Unidirectional A* algorithm searches forward until the goal state is reached. It guarantees an optimal route, although considerable searching time is required. Bidirectional A* algorithm is to simultaneously proceed both forward from the initial state and backward from the goal, and stop searching when the two searches meet in the middle [2]. In such a condition, bidirectional A* is usually faster than unidirectional A* in finding a route, but does not guarantee the route found optimal. Although the route found in *bidirectional* may not be optimal, it is still appropriate for some application due to the reduction of time complexity. When the optimality is a critical factor, the above stop condition for bidirectional is not enough, but needs more extra steps. These extra steps make bidirectional A* take longer search time and take twice more time than unidirectional in worst case.

In this paper, we proposed a very efficient modified bidirectional A* which always guarantees the optimality and takes much less search time comparing the other modified A* algorithm. To evaluate the time complexity of the algorithm proposed, several experiments using the real urban road data are conducted and it shows the proposed algorithm in this paper is very efficient and reliable.

2 Related Research

Finding an optimal route given source (s) and destination (t) in a directed graph is a traditional graph searching problem, and many various solutions have been suggested. Dijkstra's algorithm is the classical one, with a worst-case running time of O(m+nlogn) using Fibonacci heaps. It is common practice to improve the running time of Dijkstra's algorithm heuristically while maintaining the correctness of the solution. Recent algorithms, with better running time that solve variants and special case of the shortest-path problem with better running time, are surveyed in [2], [3]. Each solution differs more or less in terms of time complexity, memory usage, etc.

If the search is guided by heuristics, it is called a heuristic search. Heuristic search normally deals with unidirectional approaches, which start from source(s) heading towards goal/destination(t). When there is one goal explicitly given, then bidirectional search is possible, which proceeds both in the forward direction from s to t and in the backward direction from t to s simultaneously. In backward searching, the node expands to the next node when there is an inward link. For example, assume there is a directed link from x_1 to x_2, but no link from x_2 to x_1, which is one-way street. In that case, if x_1- x_2 is a part of link in the optimal route, then x_2 can expand to x_1 in backward search. But in reverse case, which is no link from x_1 to x_2 but a link from x_2 to x_1. Then x_2 can not expand to x_1, although there is a link from x_2 to x_1.

A* algorithm, a traditional BFS (Best First Search), is widely used for an optimal route finding [4]. The cost function used in A* is:

$$f(n) = c(n) + h(n)$$

where *c(n)* is gives the cost from the start node to node *n*, and *h(n)* is the estimated cost of the cheapest path from *n* to the destination. A* maintains the set OPEN of nodes that have been generated but not yet expanded, i.e., the frontier nodes. It selects a node from OPEN with minimum estimated cost, which is considered "best". This node is then expanded and move from OPEN to CLOSED.

Under certain condition, unidirectional A* is optimal over any admissible unidirectional heuristic search algorithms using same information, in a sense that it never expands more nodes than any of these. There are a large number of minor and major variations of A*. The major limitation of A* is its memory requirement, and IDA* and SMA*, which both are optimal and memory-bound algorithms, were suggested in [5] and [6] respectively.

Due to the optimality of unidirectional A* algorithm, a bidirectional approach is reasonable to improve its performance. The first bidirectional heuristic search, BHPA, was proposed in [2]. In BHPA, whenever the forward and backward frontiers meet at some node *n*, a solution is found. Its cost is $g_1(n) + g_2(n)$, i.e., the cost of the path found by the forward search from *s* to *n*, plus the cost of the path found by the backward search from n to t. Even when each part of the solution is optimal, however, the concatenated solution is not necessarily optimal. Thus a special termination condition is required to guarantee optimal solutions, and it in BHPA is as follows:

$$L_{min} \leq \max\left(\min_{x \in OPEN_1} f_1(x), \min_{x \in OPEN_2} f_2(x)\right) \tag{1}$$

where $OPEN_1$ is a set of frontier nodes in forward search, and $OPEN_2$ is a set of frontier nodes in backward search. This condition essentially means that the cost L_{min} of a solution from s to t so far is not larger than an estimate computed from the $f_x(x)$ in both search frontiers. Although this condition guarantees the solution optimal, it decreases its performance, which even takes twice more search time compare to unidirectional A* in worst case.

There was a consensus that the problem in BHPA was caused by the fact that the two search frontiers would pass each other in many case, and this generated a large number of unnecessary frontier nodes. To prevent this problem, the algorithms, which perform front-to-front evaluations, were suggested [7], [8]. Although these algorithms were efficient in terms of the number of nodes generated, the overall performance was not much improved due to the increase of an amount of computation.

Perimeter Search is also efficient in terms of the number of nodes generated, but requires a large amount of computation [9], [10]. Holzer [11] proposed the combined speed-up techniques for shortest-path computations. He used edge weights for both the forward and the backward search to overcome the deficiency of optimality, but still does not guarantee the optimality. Ikeda [12] proposed a fast bidirectional A* algorithm, but not guaranteeing the optimality.

3 Suggested Algorithm

Traditionally, bidirectional A* algorithm proceeds both in the forward direction from start (s) to destination (t) and in the backward direction from t to s simultaneously, and it stops the search when its two searches meet at some node. The stop condition for the search is defined in two cases. One is when two searches' frontiers meet at a certain node, p, as in Fig. 1 (a), and the other is when a search moves to the node, p, which is already a part of the route of the other search, as in Fig. 1 (b). In this paper, both cases are considered as two searches meet, and if those cases are the stop condition for bidirectional A* algorithm, it does not guarantee the optimal route.

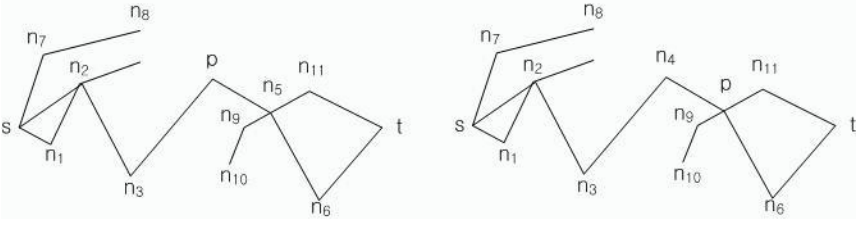

Fig. 1. Two cases when bidirectional search stops (a) forward search s-n_1-n_2-n_3-p, backward search moved to node p from n_5 in t-n_6-n_5 (b) backward search t-n_{11}-p-n_9, forward search moved to node p from n_4 in s-n_1-n_2-n_3-n_4

It is well-known that, in bidirectional A* algorithm, if the search stops when the forward search and the backward search meet at some node, it never guarantees the path found optimal. Thus, to guarantee the optimality, bidirectional A* algorithm needs to continue the searching until equation (2) is satisfied. This causes the complexity of bidirectional A* increased. Although the path found in bidirectional A* may not be optimal, it could be used as a quasi-optimal path, since its average cost does not much differ from the optimal average cost and it reduces the complexity of search space.

The algorithm suggested in this paper improves the previous bidirectional A* algorithm in two aspects: one is rather a simple improvement, a method avoiding repetitive searching. The algorithm and its proof are described in Lemma 1. Second and major improvement is a method reducing the complexity of bidirectional A*. A new mathematical condition for guarantee the optimality is derived and its completeness is proved in Theorem 1.

Lemma 1. *A path(*t*) or route(*t*) is a list of edges connected from start node to node t. In bidirectional A*, the cost of optimal path(*t*) is always smaller than or equal to the cost of all other paths(*t*), which pass through the edge included in the optimal path(*t*). Thus when selecting a next move at node t, all paths(*t*), except an optimal path(*t*), which pass through the edge included in the optimal path(*t*) can be ignored.*

Proof 1. *Assume that nodes* n_2, n_9, n_6 *are in* $OPEN_1$ *list, and the path*(n_7), s-n_3-n_5-n_7, *is found and optimal so far in the forward A* search, as shown is Fig 2. Then the following relationships are possible:*

$$f(n_7) \leq f(n_2), f(n_7) \leq f(n_4)$$

Which means that the cost of other paths(n_7) which pass through edge n_5-n_7, s-n_1-n_2-n_5-n_7 and s-n_4-n_6-n_5-n_7, is larger than or equal to the cost of the optimal path(n_7), s-n_3-n_5-n_7. Thus all other paths(n_7), except the optimal path(n_7), which pass through the edge included in the optimal path(n_7) can be ignored in the entire search.

This theory can be used effectively when manipulating the P-TURN in the car navigation application.

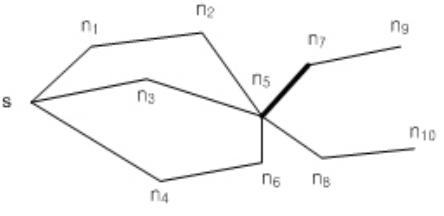

Fig. 2. There are three different paths(n_7) passing through the edge n_5-n_7

When searches in both directions meet at some node p, we draw a line which passes through node p and is perpendicular to the line connecting the source node and the destination node, which is the dotted line labeled D in Fig 3. This dotted line is called separating line. In case that source and destination are in the opposite side each other of separating line, nodes in list $OPEN_1$ and $OPEN_2$ are in the side of either source or destination. The normal distance from nodes in $OPEN_1$ and $OPEN_2$ to separating line is denoted as

$$l_1(x) = \frac{(s-p)\cdot(x-p)}{|(s-p)|}, x \in OPEN_1$$
$$l_2(x) = \frac{(t-p)\cdot(x-p)}{|(t-p)|}, x \in OPEN_2$$

Theorem 1. *To guarantee the optimality in bidirectional A*, it should satisfy the following condition:*

$$L^1_{min} \leq \min(c_1(x) + l_1(x)), x \in OPEN_1$$
$$L^2_{min} \leq \min(c_2(x) + l_2(x)), x \in OPEN_2 \quad (2)$$

where L^1_{min} *and* L^2_{min} *are the minimum cost of the path so far,* L^1_{min} *is the minimum cost from source to the node where two searches meet, and* L^2_{min} *is the minimum cost from destination to the node. The total cost of the path from source to destination is the sum of two costs;* $L_{min} = L^1_{min} + L^2_{min}$.

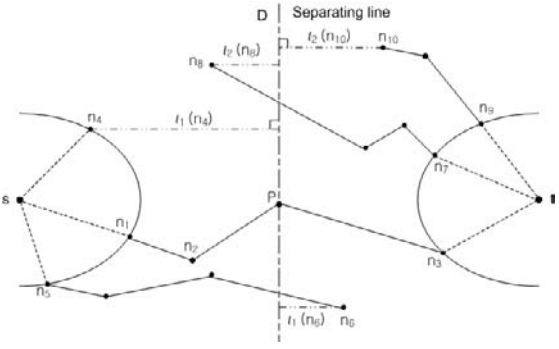

Fig. 3. Distance from the frontier nodes to separating line when both searches meet

Proof 2. *The theorem is proved by contradiction. Let both searches meet at some node* p*, and the path found, $path_f$, satisfy the above relation (2). Now assume that there exists another path, $path_a$, whose overall cost is less than the path found, $path_f$, but not satisfying the condition (2).*

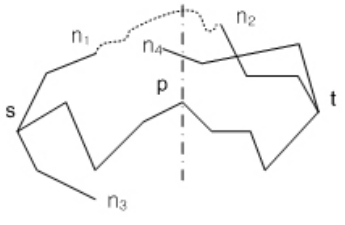

Fig. 4. Both searches meet at p, and there exists another optimal path

To clarify the assumption, in Fig. 4 both searches meet at node p, nodes n_1, n_3 are in list $OPEN_1$, n_2 and n_4 are in list $OPEN_2$. Without loss of generality, let the assumed optimal path, $path_a$, is made by expanding n_1 and n_2, then n_1 and n_2 belong to one of the following four cases.

a. n_1 is in source side of separating line, n_2 is in destination side. Then normal distances become $l_1(n_1)>0$, $l_2(n_2)>0$

b. n_1 and n_2 both are in the side of destination of separating line. Then normal distances are $l_1(n_1)<0$, $l_2(n_2)>0$

c.Opposite case of b. Then normal distances are $l_1(n_1)>0$, $l_2(n_2)<0$

d.n_1 is in destination side of separating line, n_2 is in source side. Then normal distances become $l_1(n_1)<0$, $l_2(n_2)<0$

Now consider case **a**. Since the path found, $path_f$, satisfies the condition (2), the cost for the forward search, L^1_{min}, $L^1_{min} \leq (c_1(n_1) + l_1(n_1))$, and the cost for the backward search, L^2_{min}, $L^2_{min} \leq (c_2(n_2) + l_2(n_2))$. The distance between n_1

and n_2 is larger than or equal to $l_1(n_1)+l_2(n_2)$, thus the lowest possible cost for the path made by expanding n_1 and n_2 is $(c_1(n_1)+l_1(n_1))+(c_2(n_2)+l_2(n_2))$, which is $\geq L^1_{min}+L^2_{min}$, Thus it contradicts the assumption.

Case **d** is similar to the case of **a**, except that its normal distances are negative. Since $(c_1(n_1)-l_1(n_1))+(c_2(n_2)-l_2(n_2)) \geq L^1_{min}+L^2_{min}$, thus the sum of the cost of n_1 and n_2, $c_1(n_1)+c_2(n_2)$, is already larger than the cost of $path_f$. It contradicts the assumption.

Case **b** is the case shown in Fig. 5, the shortest distance between n_1 and n_2 is larger than or equal to $|l_2(n_2)+l_1(n_1)|$, where $l_1(n_1)<0$. If the path made by n_1 and n_2, $path_a$, is optimal, then its cost, L, is

$$L \geq c_1(n_1)+c_2(n_2)+|l_1(n_1)+l_2(n_2)| \geq c_1(n_1)+c_2(n_2)+l_1(n_1)+l_2(n_2)$$

Since the path found, $path_f$, satisfies the condition (2),

$$c_1(n_1)+l_1(n_1) \geq L^1_{min}, \text{ and } c_2(n_2)+l_2(n_2) \geq L^2_{min}.$$

Thus

$$L \geq L^1_{min}+L^2_{min} = L_{min}$$

Therefore the path made by n_1 and n_2, $path_a$, is not optimal.

Case **c** is proved similarly as case **b**.

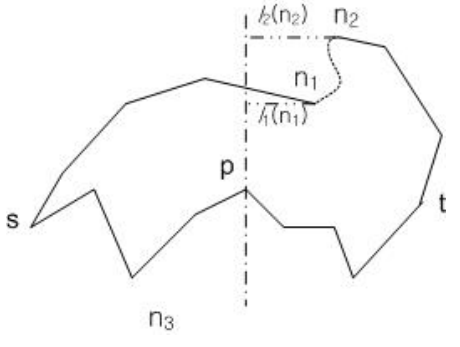

Fig. 5. When n_1 and n_2 are in the side of destination, (case b)

In order to guarantee that the cost of the path found is the lowest, the equation (1) used in BHPA examines all the possibilities of frontier nodes in $OPEN_1$ and $OPEN_2$. Since it uses the estimated cost, which is usually very different from the actual cost, it makes many frontier nodes expand further to satisfy the equation (1). That is the reason that bidirectional A* does not outperform unidirectional A*, in worst case bidirectional A* takes twice more search time than unidirectional A*.

As the equation (2) suggested in this paper, however, does not use the entire path from source to destination, and also consider forward and backward

searches separate, it reduce the search space drastically and make bidirectional A* efficient and fast in searching an optimal path.

In the following section, some experimental results are presented to verify the efficiency of the algorithm suggested in this paper.

4 Experiments

In order to evaluate the performance of the algorithm suggested in this paper, several experiments for finding an optimal path are conducted using a real urban road data of Seoul, Korea. Fig 6 shows a result of finding an optimal path, which is denoted as a thick line, given source and destination.

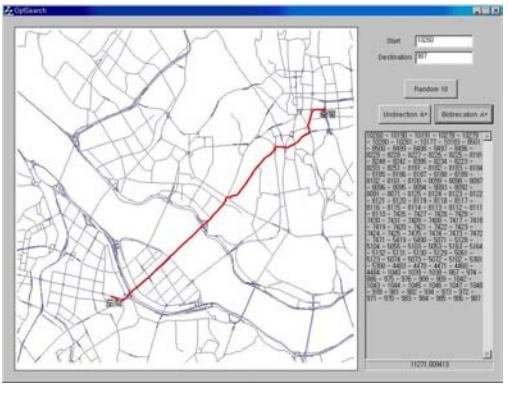

Fig. 6. Experimental result of an optimal path found

The road data used in this experiment has 10,590 nodes and 22,874 links.

Experiments compare unidirectional A*, BHPA, and the method suggested in this paper, by conducting an optimal path finding 30 times given different sources and destinations, as shown in Fig. 7. Since all three methods guarantee the optimality, comparison is only performed in the context of the number of nodes expanded and the time taken for finding an optimal path.

Experimental results show that the method suggested in this paper is far better than unidirectional A* and BHPA. In the number of nodes expanded, our method is almost 1/2 of unidirectional A*, and 1/3 of BHPA as shown in Fig. 8. The running time is also reduced almost the same rate as the number of nodes expanded is decreased.

The reason that there is some difference in the reduction rate of the running time and the number of nodes expanded is possibly that our method needs a little more calculation than unidirectional A* and BHPA.

Start	Destnation	Route Cost	Generated node			Running Time		
			Uni	BHPA	New	Uni	BHPA	New
5696	7706	6475,4	758	1544	537	6	14	5
3706	6277	1066,6	64	84	43	0	1	1
1293	818	5239,2	797	857	220	7	7	2
7885	2555	11076,3	1363	2068	180	12	17	2
2212	171	9570,0	1865	2602	1454	15	21	12
1684	7883	12690,4	3905	3783	1216	33	32	10
1928	8335	8693,0	2041	2929	1738	17	25	15
1822	5083	3720,3	421	591	216	4	5	2
3959	5148	4163,3	484	669	198	4	6	2
7085	9872	7271,5	1273	1994	783	11	17	6
3085	6967	3855,9	746	713	216	6	6	2
10094	4853	6525,8	1221	1874	1007	11	16	9
8836	6476	1640,9	50	55	26	0	1	1
7917	7502	8713,1	1493	2124	748	13	18	6
491	1709	6503,6	1413	1853	816	12	16	7
441	3222	1634,3	107	222	83	1	2	1
10507	4196	11650,0	2037	3949	2026	18	34	18
7794	4256	8822,2	1564	3059	781	14	27	7
5248	3875	6138,6	1209	1757	672	10	15	6
2664	6090	10880,6	2579	3094	1388	21	26	12
1884	5303	4437,1	590	730	264	5	6	2
2975	6608	13407,5	3281	4070	1391	27	34	12
2217	8300	5731,8	689	1407	323	6	12	3
4983	929	6787,8	1309	1836	616	11	15	5
3292	586	2396,3	328	399	220	3	3	2
6852	2886	12176,0	3631	4082	1196	31	33	10
2204	7207	9945,7	2510	3736	1563	21	32	13
8355	3646	12827,1	3820	4203	2550	33	35	22
9610	1330	9177,0	2280	3738	1629	19	32	14
8012	8594	2294,2	75	99	12	1	1	0
Total		215511,7	43903	60121	24112	372	509	209

Fig. 7. Data used for the experiment and its results (Uni means unidirectional A*, New means our method suggested in this paper)

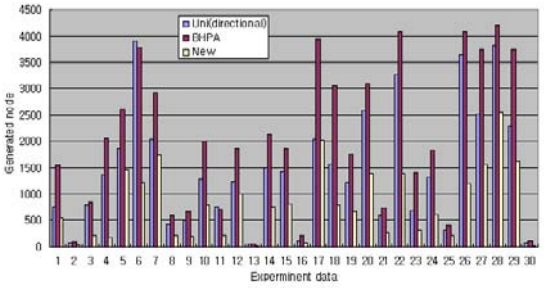

Fig. 8. Comparison of the number of nodes generated in unidirectional A*, BHPA, our method

5 Conclusion

Although finding an optimal route problem has been studied in many different application areas, recently due to the proliferation of ITS(Intelligent Traffic System) and CNS(Car Navigation System), the necessity for more efficient and fast optimal route finding algorithm has increased.

In this paper, we proposed a new robust bidirectional A* algorithm, which improves the conventional bidirectional A* algorithm drastically, is suggested.

The performance of the suggested algorithm is evaluated with various experiments, and the experimental result shows that the algorithm suggested is very efficient and powerful in terms of the number of nodes expanded and the running time.

The suggested algorithm is derived in the conventional connected graph. To be used in real application, such as CNS, it needs to be extended to include traffic condition, road status, weather, etc., and that extension does not seem to be a hard challenge.

References

1. Dijkstra, E.W.: A note on two problems in connecxion with graphs. Numerische Mathematik 1, 269–271 (1959)
2. Kaindl, H., Kainz, G.: Bidirectional Heuristic Search Reconsidered. J. of Artificial Intelligence Research 7, 283–317 (1979)
3. Pettie, S., Ramachandran, V., Sridhar, S.: Experimental evaluation of a new shortest path algorithm. In: Mount, D.M., Stein, C. (eds.) ALENEX 2002. LNCS, vol. 2409, pp. 126–142. Springer, Heidelberg (2002)
4. Russel, S., Norvig, P.: Artificial Intelligence: A Modern Approach. Prentice Hall, Englewood Cliffs (1995)
5. Korf, R.: Depth-first Iterative Deepening: An optimal admissible tree search. Artificial Intelligence 27(1), 97–109 (1985)
6. Russell, S.: Efficient memory-bounded search methods. In: Proc. Tenth European Conf. on AI (ECAI-92), pp. 1–5 (1992)
7. Politowski, G., Pohl, I.: D-node retargeting in bidirectional heuristic search. In: National Conf. on A.I (AAAI-91), pp. 434–440. MIT Press, Cambridge (1984)
8. Davis, H., Pollack, R., Sudkamp, T.: Towards a better understanding of bidirectional search. In: Proc. Fourth National Conf. on A.I (AAAI-84), pp. 68–72. MIT Press, Cambridge (1984)
9. Dillenburg, J., Nelson, P.: Perimeter Search. Artificial Intelligence 65(1), 165–178 (1994)
10. Manzini, G.: BIDA*: an important perimeter search algorithm. Artificial Intelligence 75(2), 347–360 (1995)
11. Holzer, M., Schulz, F., Willhalm, T.: Combining Speed-up Techniques for Shortest-path Computations. In: Ribeiro, C.C., Martins, S.L. (eds.) WEA 2004. LNCS, vol. 3059, pp. 269–284. Springer, Heidelberg (2004)
12. Ikeda, T., Hsu, M.Y., et al.: A Fast Algorithm for Finding Better Routes By AI Search Techniques. IEEE VNIS94 (1994)

Toward a Large Scale E-Market: A Greedy and Local Search Based Winner Determination

Naoki Fukuta[1] and Takayuki Ito[2]

[1] Faculty of Informatics, Shizuoka University, 3 5 1 Johoku, Hamamatsu, Shizuoka 432-8011 Japan
fukuta@cs.inf.shizuoka.ac.jp
[2] Graduate School of Engineering, Nagoya Institute of Technology, Gokiso, Showa-ku, Nagoya, 466-8555, Japan
ito.takayuki@nitech.ac.jp

Abstract. Combinatorial auction is one of the most popular market mechanisms and it has a huge effect on electronic markets and political strategies. On large scale e-markets, we need a good approximation algorithm for winner determination that is robust for changing the distribution and the number of bids in an auction. We proposed approximate algorithms for combinatorial auctions with massively large number of (more than 100,000) bids. In this paper, we show the robustness of our winner determination algorithms for combinatorial auctions with large number of bids. Experimental results demonstrate that our proposed algorithms are robust on changing the distribution and the number of bids in an auction. Finally, we shortly describe a theoretical limitation about our algorithms that concerns with giving truthfulness of the auction mechanism.

Keywords: E-Commerce and Multi-agent systems.

1 Introduction

Combinatorial auction is one of the most popular market mechanisms and it has a huge effect on electronic markets and political strategies. For example, Sandholm et al.[1] created a large market by using their innovative combinatorial auction algorithms. It is a well-known fact that FCC tried to employ a combinatorial auction for assigning spectrums to companies[2]. Also, there is a report[3] that shows Chile succeeded feeding nation-wide children by using a combinatorial auction mechanism for the nation wide school meal delivery network.

Increasingly, the huge markets become important. For example, the long tail concept makes us envision a huge online market in which the huge number of potential participants can exchange their goods via combinatorial auctions. The large number of sellers can provide their goods on the market, then the large number of buyers can make the numerous number of combinatorial bids on the goods. An electronic ad-market is one example. In it, a seller can provide a set of places (goods) on the web for advertisements and many buyers (advertisers) bid on their preferred places (ad places). A seller can add new sets of places (ad places) anytime and buyers can make bids anytime. The mechanism has to clear the market very frequently. So, there is no time to compute an exact

H.G. Okuno and M. Ali (Eds.): IEA/AIE 2007, LNAI 4570, pp. 354–363, 2007.

optimal solution. If a seller computes the optimal solution then he will lose his customers (buyers) and may lose revenue. Furthermore, e-market is dynamically changing, the distribution and the number of bids are varied and changing all the time.

Since we assume the number of agents is large and the market is dynamic, the computational cost must be considered. In general, the winner determination problem is NP-hard[4]. Thus, there are a lot of works that are focused on tackling the computational costs for winner determination[4][5]. These works basically try to achieve the optimal solution in winner determination. Even so, the computational complexity is very high and remains a key problem.

There are some works[6][7] that try to achieve *approximate* solutions in winner determination. The most recent well-known theoretical work is Lehmann et al. [6]. In this work, Lehmann et al. proposed a greedy approximation algorithm that relaxes the (economic) efficiency and prove the lower bound in terms of the efficiency. The paper [6] rather focuses on more elegant theoretical aspects, i.e., the lower bounds of efficiency and truthfulness. We argue that it is still important to solve winner determination problem more efficiently even if truthfulness is not guaranteed. We understand giving truthfulness is important on auction mechanisms. However, there are some cases that the auction mechanisms are used for the purpose that are not considered by the designer of mechanisms. Therefore, we need a good approximation algorithm for winner determination that is robust for changing the distribution and the number of bids in an auction.

This paper consists of the following parts. In section 2, we describe the basic terms in combinatorial auctions In section 3, we show our local search-based algorithms focused on efficiency of combinatorial aucitons. In section 4, we show our experimental results. In section 5, we show some related works and clarify the differences from them. In section 6, we show our algorithms cannot satisfy monotonicy that is required for truthful mechanisms. Section 7 includes our concluding remarks and shows our future work.

2 Preliminaries

2.1 Combinatorial Auction

A combinatorial auction is a popular e-market mechanism[4]. The combinatorial auction is an auction mechanism that allows bidders to locate bids for a bundle of items rather than single item[4]. The winner determination problem is defined as follows[4]: The set of bidders is denoted by $N = 1, \ldots, n$, and the set of items by $M = \{1, \ldots, m\}$. $|M| = k$. A bundle S is a set of items : $S \subseteq M$. We denote by $v_i(S)$ the combinatorial bid that bidder i makes for bundle S. In other words, $v_i(S)$ means the maximum price that bidder i is willing to pay for S. An allocation of the items is described by variables $x_i(S) \in \{0, 1\}$, where $x_i(S) = 1$ if bidder i wins the bundle S. An allocation, $x_i(S)$, is feasible if it allocates no item more than once, $\sum_{i \in N} \sum_{S \ni j} x_i(S) \leq 1$ for all $j \in M$. The winner determination problem is the problem to maximize total revenue $\max_X \sum_{i \in N, S \subseteq M} v_i(S) x_i(S)$ for feasible allocations $X \ni x_i(S)$.

2.2 Lehmann's Greedy Winner Determination

The combinatorial auction is an auction mechanism that allows bidders to locate bids for a bundle of items rather than single item[4]. To overcome the computational complexity of the winner determination problem, some studies focus on approximated algorithms. One of well-known approximated algorithm is Lehmann's greedy algorithm[6].

Lehmann's greedy algorithm is a very simple linear algorithm. Here, a single-minded bidder declaring $< a, s >$, with $s \subseteq M$ and $a \in \mathcal{R}_+$ will be said to put out a bid $b =< a, s >$. Two bids $b =< a, s >$ and $b' =< a', s' >$ conflict if $s \cap s' \neq \emptyset$. The greedy algorithm can be described as follows: (1)The bids are sorted by some criterion. The paper[6] proposed sorting the list L by descending average amount per good. More generally, they proposed sorting L by a criterion of the form $a/|s|^c$ for some number c, $c \geq 0$, possibly depends on the number of goods, k. (2) A greedy algorithm generates an allocation. L is the sorted list in the first phase. Walk down the list L, accepting bids if the goods demanded are still unallocated and not conflicted.

In the paper[6],they argue that $c = 1/2$ seems a best heuristic parameter for the approximation. In this paper, we use $c = 1/2$ as the initial parameter for using Lehmann's algorithm. For our local searches, it is a good strategy to use $c = 1/2$ as the initial state.

Example. Assume there are three goods a, b, and c, and three bidders $Alice$, Bob, and $Charles$. $Alice$ bids 10 for a. Bob bids 20 for $\{b, c\}$. $Charles$ bids 18 for $\{a, b\}$. We sort the bids by the criterion of the form $a/\sqrt{|s|}$. $Alice$'s bid is calculated as $10/\sqrt{1} = 10$. Bob's bid is calculated as $20/\sqrt{2} = 14$(approximately). $Charles$'s bid is calculated as $18/\sqrt{2} = 13$(approximately). The sorted list is now Bob's bid $< 20, \{b, c\} >$, $Charles$'s bid $< 18, \{a, b\} >$, and $Alice$'s bid $< 10, \{a\} >$. The algorithm walks down the list. At first, Bob wins $\{b, c\}$ for 20. Then, $Charles$ cannot get the good because his bid conflicts with Bob's bid. Finally, $Alice$ gets $\{a\}$ for 10.

3 Enhanced Algorithms with Greedy Winner Determination

3.1 Hill-Climbing Search

Lehmann's greedy winner determination could succeed specifying the lower bound of the efficiency. The straightforward extension of the greedy algorithm is to construct a local search algorithm that continuously updates the allocation so that the efficiency is increased. Intuitively, one allocation corresponds to one state of a local search.

An initial idea of this approach is shown in [8]. In this section, we summarize the algorithm in which we update the Lehmann's initial allocation with the remaining bundles that could produce higher revenue. Our local search is the hill-climbing search, in which we explore new neighbor allocations until the point where there are no more allocations that have a higher revenue. In general, the definition of neighbors of a state for a local search is a key point. Here, we define *single bid distance* for neighbors of a state. Intuitively, the *single bid distance* is the distance when a state (bid allocation) can be transformed to another state (bid allocation) with inserting single bids, excluding bids that are conflicted with the inserted bids, and inserting other bids by greedy allocation while it is possible. The following algorithm describes the detailed behavior

of our Hill-climbing search with *single bid distance*. We consider the main aim of this algorithm is "allocating the goods as much as possible to each buyers". This means that in this algorithm we do not aim to sell all goods.

The inputs are L and $Allocation$. L is the bid list of an auction. $Allocation$ is the initial greedy allocation of items for the bid list.

```
1:  function LocalSearch(Alloc, L)
2:    currentPrice:= price(Alloc); remainBids:= L - Alloc;
3:    for each b ∈ remainBids as sorted order
4:      if b conflicts B ∈ Alloc ( B is a set of bids ) then
5:        newAlloc:= Alloc-B+b; consBids:= consistentBids(newAlloc, remainBids);
6:        newAlloc:=newAlloc+consBids;
7:    newPrice := price(newAlloc);
8:    if currentPrice < newPrice then return LocalSearch(newAlloc,L);
9:    end for each
10:   return Alloc
```

The function "consistentBids" finds consistent bids for the set "newAllocation" by walking down the list "remainBids". Here, a new inserted bid will wipe out some bids that are conflicted with the inserted bid. So there will be free items to allocate after the insertion. The function "consistentBids" tries to insert the other bids for selling the higher value goods as much as possible.

Example. Assume there are three goods a, b, and c, and there are six bids, $\{a, b, c\} = 30, \{a\} = 15, \{c\} = 13, \{d, e\} = 15, \{a, c\} = 14, \{b\} = 8$. Further we assume the values of Lehmann's criterion $a/\sqrt{|s|}$ are $17.6, 15, 13, 10.7, 10$, and 8, respectively. In this case, the initial allocation is Lehmann's greedy allocation $\{a, b, c\}, \{d, e\}$ and the total revenue is 45. Here, the remaining list is $\{a\}, \{c\}, \{a, c\}, \{b\}$. In this algorithm, we pick $\{a\}$ since it is the top of the remaining list. Then we insert $\{a\}$ to the allocation and remove $\{a, b, c\}$. The allocation is now $\{a\}, \{d, e\}$. We then try to insert the other bids that do not conflict with the allocation. Then, the allocation becomes $\{a\}, \{b\}, \{c\}, \{d, e\}$. The total revenue is 51. The total revenue is increased. Thus, the allocation is updated to $\{a\}, \{b\}, \{c\}, \{d, e\}$. Our local algorithm continues to update the allocation until there is no allocation that has a greater revenue. This could improve and reinforce the revenue that Lehmann's greedy allocation can achieve.

3.2 Local Search for Multiple Values of the Sorting Factor 'c'

Lehmann's greedy winner determination could succeed specifying the lower bound of the efficiency. The straightforward extension of the greedy algorithm is to construct a local search algorithm that continuously updates the allocation so that the efficiency is increased. Intuitively, one allocation corresponds to one state of a local search.

The efficiency of revenues got by Lehmann's algorithm (and its enhancements) deeply depend on which value was set to the bid sorting factor c. Lehmann et al. reported $c = 1/2$ is the approximately best value. But the optimal values for each auction are varied from 0 to 1 even if the number of items is constant. Here, we propose an

enhancement for proposed local search algorithms with multiple values parallel search for the sorting factor c. In the algorithm, the value of factor c for Lehmann's algorithm is selected from a pre-defined list. It is reasonable to select c from neighbors of $1/2$, namely, $C = \{0.0, 0.1, \ldots, 1.0\}$. The results are aggregated and the best one (that has highest revenue) is selected as the final result.

The outline of the algorithm is described as follows. Essentially, we selected some values for c, and for each c we conducted a local search. This part can be done sequentially and further can be done in parallel manner. The outline is very simple.
The inputs are L and C. L is the bid list, namely, a set of bundles. C is a candidate c's value list.

1: **Function** LSForMultiCValues(L,C)
2: $maxAlloc := \emptyset$
3: **while** $|C| > 0$
4: c is selected from C; $C := C - c$; $Allocation$:=LocalSearch(L,c);
5: **if** $price(maxAlloc) < price(Alloc)$ **then** $maxAlloc := Alloc$;
6: **return** $maxAlloc$

Function $LocalSearch(L, c)$ finds a value when the value of sorting factor c is c for initial allocation with Lehmann's algorithm and the bid set is L. For this function, we can use both the hill-climbing search and Lehmann's greedy search for the demanding revenue/speed balances.

3.3 Simulated Annealing Search

We also prepared a small extension of the proposed algorithm to the simulated annealing local search. The algorithm is a combination of the presented hill-climbing approach and a random search based on the standard simulated annealing algorithm. We use a parameter that represents the temperature. The temperature is set high value at beginning and continuously decreased during the temperature is larger than 0. For each cycle, a neighbor is randomly selected and its value may be less than the current value in some cases. Even such a case, if a probability value based on the temperature is larger than 0, the state is moved to the new allocation that has less value. This could make us to get off from local minimum.

Also, we prepared a soft restart mechanism for SA. In the restart mechanism, c is just randomly chosen each time and continue loops until the revenue will not be updated in last k times of search. Here, we used $k = 5$ for our experiments.
The inputs are L and $Alloc$. L is Bid List. $Alloc$ is the initial allocation.

1: $temp = constant$;
2: **function** SASearch($Alloc$, L)
3: $currentPrice$:= price($Alloc$); $remainBids$:= L - $Allocation$;
4: **while**$temp > 0$
5: b:= randomlySelectedFrom($remainBids$).
6: **if** b conflicts $B \in Alloc$ (B is a set of bids)**then**
7: $newAlloc$:= $Alloc$-B+b;

8: $consBids$:= consistentBids($newAlloc, remainBids$);
9: $newAlloc$:=$newAlloc$+$consBids$;
10: **if** $newAlloc == \emptyset$ **then break**;
11: $newPrice$:= price($newAlloc$);
12: **if** $currentPrice < newPrice$ **then return** SASearch($newAlloc$,L);
13: **else if** $currentPrice >= newPrice$ and $SomeProbability(temp) > 0$ **then**
14: $temp := temp - 1$;
15: **return** SASearch($newAlloc$,L);
16: **return** $currentPrice$

Since SA is a random search algorithm that will produce different results at each time with same parameter sets, it is reasonable to choose c just randomly and continue loops until the revenue will not be updated in last k times of search. Here, we used $k = 5$ for our experiments.

4 Experimental Results

4.1 Experimental Settings

The following are the common settings of the experiments conducted in this paper.

We implemented our algorithms in a C program for the following experiments. The experiments have been done with C-based implementations for examining the performance differences among algorithms. A prolog-based distributed and parallel execution environment is used for examining the effects of parallelism in our algorithms. The program was employed on Mac OS X 10.4.6, CPU: CoreDuo 2.0GHz, and 2GBytes memory. Thus, the actual computation time will be much smaller if we employ a massively parallel and distributed execution environment. We leave this for the future work.

On each experiment, we compared the following four search algorithms. "greedy-(C=0.5)" uses Lehmann's greedy allocation algorithm with parameter ($c = 0.5$). "greedy-all" uses the best results of Lehmann's greedy allocation algorithm with parameter ($0 \leq c \leq 1$). This is a simple algorithm but Lehmann's et,al. did not mention about this algorithm. "HC(c=0.5)" uses a local search in which the initial allocation is Lehmann's allocation with $c = 0.5$ and conduct the hill-climbing search shown in the previous section. "HC-all" is the aggregated best result of the hill-climbing search with parameter ($0 \leq c \leq 1$). "SA" uses the simulated annealing algorithm shown in the last section.

4.2 Robustness of Bid Size Changes

In [8], we have shown the basic performance of each algorithm in the context of revenue maximization for middle size numbers of bids(from 100 to 1000 bids) in an auction. We showed that "HC-all" and "SA" perform best, and their performance is increasing when the number of bids in an auction increases. On the situation of 1000 bids in an auction, both algorithms got approximately 0.997 of optimal revenues in average. We also showed that it takes approximately 600 seconds to handle 100,000 bids in an auction when we use HC-all, and it takes less than 60 seconds when we use HC(C=0.5).

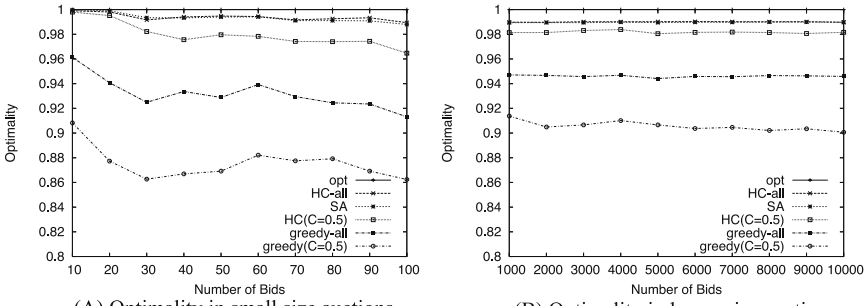

Fig. 1. The optimality of our hill-climbing algorithm in small-size bids and larger-size bids

In this section, we analyze the effects of bid size in an auction. Here, the items and the price for a bid (bundle) were set by the following. The number of items per one bundle is sampled from distribution $Uniform(1, 10)$. The basic value (Y) of an item is sampled from distribution $Uniform(100, 10100)$. The actual value (X) of a bundle is defined by $X = Z + (Z \times j) \times R$. Where Z is the sum of each basic item value Y in the bundle, j is a constant parameter, and R is a random number sampled from a Gaussian distribution with mean 0 and standard deviation 1.0. We use $j = 0.1$ in the following experiments. Here, complementarity of items is not assumed.

To cover whole phenomena in the experiments, we set the number of items to 30. We conducted 100 trials for each experimental settings and the average results of them are shown. The optimality of each determined winners for a auction is normalized to the range of the optimal solutions for value 1, and the worst solution (no items are allocated) for value 0. Here, we used CASS[5] to get the optimum solutions.

Figure 1(A) shows the result of the experiment for smaller number of bids in a auction (less than 100 bids for each). Here, we can see the performance of "SA" is best if the bids are less than 30 in a auction. The performance of "HC-all" is stable and almost best, its the optimality value is constantly closer to 99.05 %. The performance of "SA" is nearly equal to "HC-all" if the bids are more than 30 in a auction. Figure 1(B) shows the result of the experiment for larger number of bids in a auction (up to 10000 for each). Since it is difficult to get optimal allocations when bid size exceeds 1000, we estimated the optimal value as 101 % of best allocations obtained by all algorithms we proposed.[1] We can see the performance of "HC-all" and "SA" is best. The relationship among algorithms is stable.

4.3 Comparison to Zurel's Algorithm with Standard Datasets

Zurel and Nisan[7] proposed a very competitive approximate winner determination algorithm for combinatorial auctions. In [7], they evaluated the performance of their presented algorithm with the data set presented in [9]. Since the data set in [9] is relatively

[1] The purpose of showing this figure is to compare performance of each algorithm. Therefore, it is not serious problem when we use estimated optimal values here.

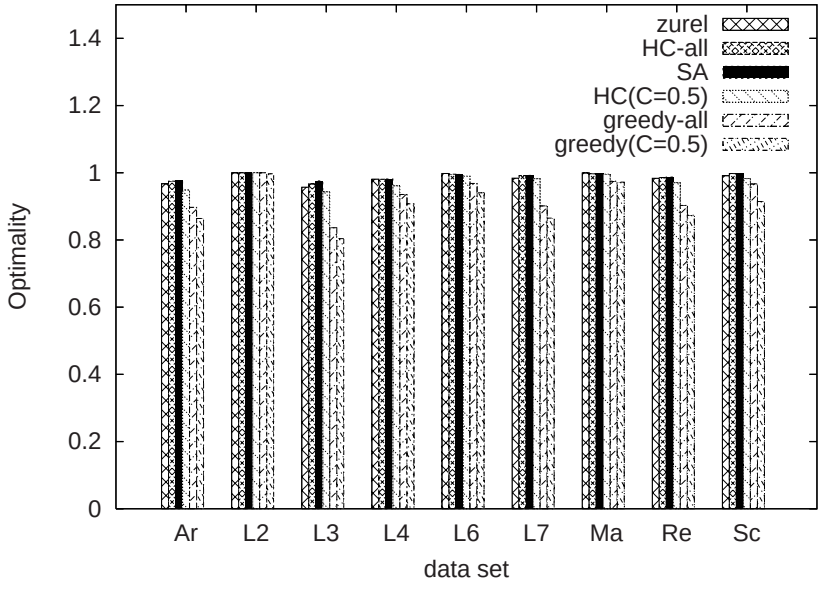

Fig. 2. The comparison between Zurel's and ours

small size, we conducted detailed comparisons to the Zurel's approach with common datasets from CATS benchmark[10]. Here, we used varsize dataset that supports most type of bid distributions, and it has over 800 trials for each distribution. According to Figure 2, our approach (especially, SA) is slightly better in optimality for each test set.

5 Concerns on Truthfulness

For a truthful greedy protocol, Lehmann[6] pointed out the following 4 requirements: Exactness, Monotonicity, Critical, and Participation. Exactness requires that the allocation must be exact, that is, a single-minded bidder either gets exactly the set of goods he desires or he gets nothing. Monotonicity requires that if j's bid is granted if he declares $< s, v >$, it is also granted if he declares $< s', v' >$ for any $s' \subseteq s, v' \geq v$. Critical says that the payment for a bid that is granted does not depend on the amount of the bid, it depends only on the other bids. Then, it says that it is exactly equal to the critical value below which the bid would have lost. Participation ensures that bidders do not lose by participating in the auction. At least the above 4 requirements need to be satisfied. However, unfortunately, we found that the protocol that uses our proposed winner determination algorithm does not satisfy Monotonicity. Here, we show that our protocol does not satisfy Monotonicity.

The following is one of our counter examples that show the cases that do not satisfy Monotonicity.

Suppose player i's bid as follows:

$$bid\ s = \{a, b, c, x1\}, v = 10000, v/|s|^c = 2500$$
$$bid\ s' = \{a, b, c\}, v = 10001, v/|s|^c = 3334$$

v is the value for a bid. $v/|s|^c$ is the criterion for sorting. We assume $c = 1$ in this counter example. From the definition of Monotonicity, if s is granted, it is also granted if i declares s'.

Suppose the other bids are declared as follows:

$$bid\ A = \{x1, x2\}, v = 10000, v/|s|^c = 5000$$
$$bid\ B = \{x2, x3, x4, x5\}, v = 12000, v/|s|^c = 3000$$
$$bid\ C = \{x3, x10, x11, x12, x13\}, v = 11000, v/|s|^c = 2200$$
$$bid\ D = \{x10, x11, x12, x13, x14, x15, x16\}, v = 13000, v/|s|^c = 1857$$
$$bid\ E = \{a, x2\}, v = 12002, v/|s|^c = 6001$$
$$bid\ F = \{b, x11\}, v = 11020, v/|s|^c = 5510$$
$$bid\ G = \{c, x10\}, v = 11010, v/|s|^c = 5505$$

Here, if the bid set is $\{A, B, C, D, E, F, G, s\}$, then the winner set is $\{B, D, s\}$. However, if the bid set is $\{A, B, C, D, E, F, G, s'\}$, then the winner set is $\{E, F, G\}$. Because of the interest on the space, we omit the trace of both case. Essentially, our algorithm often enters into local optimal points in the sense of search space. Thus, Monotonicity is not satisfied.

6 Related Work

There have been a lot of works on the optimal algorithm for winner determination in combinatorial auctions[9]. For example, CABOB[1] and CASS[5] have been proposed by aiming to get the optimal allocations. On the other hand, approximated algorithms have been proposed by using the techniques in the combinatorial optimization field. Lehmann[6] proposed the greedy allocation algorithm which inspired us to propose the reinforcement method proposed in this paper. Recently, Dobzinski et,al. proposed improved approximation algorithms for auctions with submodular bidders[11]. Lavi et,al, reported an LP based algorithm that can be extended to support the classic VCG[12]. Those researches are mainly focused on theoretical aspects. In the contrast to those papers, we rather focus on experimental and implementation aspects. Those papers did not present experimental analysis about the settings with large number of bids we presented in this paper. Also, Hoos[13] and Guo[14] proposed local-search based winner determination algorithms for combinatorial auction problems. We provided an analysis about effects of bid size in auction they did not provide. Furthermore, we showed the performance on standard dataset with comparison of the sophisticated algorithm proposed by Zurel.

7 Conclusions

This paper showed the robustness of our winner determination algorithms for combinatorial auctions with large number of bids. The proposed algorithms are based on the Lehmann's greedy allocation with local improvement for multiple c values. Experimental results demonstrated that our proposed algorithms are robust on changing the distribution and the number of bids in an auction. Also, we showed that some of our algorithms perform well compared with an existing sophisticated algorithm proposed by Zurel et,al. Finally, we shortly described a theoretical limitation about our algorithms that concerns with giving truthfulness of the auction mechanism. Currently, our implementation can handle (at least) more than 1,000,000 bids. To apply our algorithms for real e-markets is one of our future work.

References

1. Sandholm, T., Suri, S., Gilpin, A., Levine, D.: Cabob: A fast optimal algorithm for winner determination in combinatorial auctions. Management Science 51(3), 374–390 (2005)
2. McMillan, J.: Selling spectrum rights. The Journal of Economic Perspectives (1994)
3. Epstein, R., Henriquez, L., Catalan, J., Weintraub, G.Y., Martinez, C., Espejo, F.: A combinatorial auction improves school meals in chile: A case of or in developing counteries. International Transactions in Operational Research 11, 593–612 (2004)
4. Cramton, P., Shoham, Y., Steinberg, R.: Combinatorial Auctions. MIT Press, Cambridge (2005)
5. Fujishima, Y., Leyton-Brown, K., Shoham, Y.: Taming the computational complexity of combinatorial auctions: Optimal and approximate approarches. In: Proc. of the 16th International Joint Conference on Artificial Intelligence (IJCAI99), pp. 548–553 (1999)
6. Lehmann, D., O'Callaghan, L.I., Shoham, Y.: Truth revelation in rapid, approximately efficient combinatorial auctions. Journal of the ACM 49, 577–602 (2002)
7. Zurel, E., Nisan, N.: An efficient approximate allocation algorithm for combinatorial auctions. In: Proc. of the Third ACM Conference on Electronic Commerce (EC 2001), pp. 125–136 (2001)
8. Fukuta, N., Ito, T.: Towards better approximation of winner determination for combinatorial auctions with large number of bids. In: Proc. of The 2006, WIC/IEEE/ACM International Conference on Intelligent Agent Technology(IAT2006), pp. 618–621 (2006)
9. de Vries, S., Vohra, R.V.: Combinatorial auctions: A survey. International Transactions in Operational Research 15(3), 284–309 (2003)
10. Leyton-Brown, K., Pearson, M., Shoham, Y.: Towards a universal test suite for combinatorial auction algorithms. In: Proc. of EC 2000 (2000)
11. Dobzinski, S., Schapira, M.: An improved approximation algorithm for combinatorial auctions with submodular bidders. In: SODA '06: Proceedings of the seventeenth annual ACM-SIAM symposium on Discrete algorithm, pp. 1064–1073. ACM Press, New York (2006)
12. Lavi, R., Swamy, C.: Truthful and near-optimal mechanism design via linear programming. In: 46th Annual IEEE Symposium on Foundations of Computer Science (FOCS'05), pp. 595–604 (2005)
13. Hoos, H.H., Boutilier, C.: Solving combinatorial auctions using stochastic local search. In: Proc. of the AAAI2000 (2000)
14. Guo, Y., Lim, A., Rodrigues, B., Zhu, Y.: A non-exact approach and experiment studies on the combinatorial auction problem. In: Proc. of HICSS2005 (2005)

Agent Based Dynamic Job Shop Simulation System

Şerafettin Alpay

Eskişehir Osmangazi University, Bademlik, 26030, Eskişehir, Turkey
salpay@ogu.edu.tr

Abstract. Although most real manufacturing systems have dynamic job shop structures, there is no general analytic method that has been found for analyzing them yet and computer simulation is still an outstanding tool. One of the most difficult problems in a dynamic job shop environments is to assign the optimal due dates. Due date assignment is an important task in shop-floor control, affecting both timely delivery and customer satisfaction. The ability to meet the due dates, however, is dependent not only on reasonableness of the due dates but also on the scheduling or dispatching procedures. In this paper, an agent based dynamic job shop simulation system is designed and developed to help the decision makers who have to mainly solve the problems of selecting correct due date assignment models and dispatching rules depending on selected performance criteria in their multi machine dynamic stochastic job shop environment.

Keywords: Multi-Agent Systems, Dynamic Job Shop Scheduling, Simulation, Due Date Assignment, Dispatching.

1 Introduction

One of the most popular models in scheduling theory is that the job shop, as it is considered to be a good representation of general domain and has earned for being notoriously difficult to solve [1]. The job shop scheduling problem may be characterized as one in which a number of jobs, each comprising one or more operations to be performed in a specified sequence on specified machines and requiring certain amounts of time, are to be processed. The objective usually is to find a processing order or a scheduling rule on each machine for which a chosen measure of performance is optimal. In the common industrial setting, the scheduling problem is dynamic one in that jobs arrive at random over time and the processing times are not, in general deterministic. The analytical approach to dynamic problem has proved to extremely difficult, even with several limiting assumptions. In the face of the difficulties associated with analytic techniques, researchers in this area have relied on computer simulation of real representative of job shops to make a decision in the dynamic scheduling environments [2].

Because there is an important relationship between due dates and dispatching procedures that was found in the first studies on scheduling [3], to determine the optimal due date assignment models and dispatching rules to be used for selected

H.G. Okuno and M. Ali (Eds.): IEA/AIE 2007, LNAI 4570, pp. 364–373, 2007.

performance criteria in a dynamic stochastic job shop environment is an important task that has to be performed by the decision makers.

In this paper, an agent based dynamic job shop simulation system (AB-DJSS) is designed and developed to help the decision makers who have to mainly solve the problems of selecting optimal due date assignment models and dispatching rules depending on selected performance criteria in their multi machine dynamic stochastic job shop environment.

2 Dynamic Stochastic Job Shops

The job shop scheduling literature can be categorized into *static* problems with a fixed set of jobs and *dynamic* problems that allow jobs to arrive to shop in as ongoing, and usually random, fashion. If all problem parameters are known with certainty, the dynamic scheduling problem called *deterministic*. However, it is sometimes assumed that scheduler can not observe the parameters in advance, but only has knowledge of a probability distribution for the various problem parameters, in which case the dynamic scheduling problem referred to as *stochastic* [4]. In this paper, we are concerned with dynamic stochastic job shop scheduling.

In a dynamic stochastic job shop, the number of jobs available for processing varies over time. Jobs continually enter and leave the production system in a random manner governed by some probabilistic laws [5]. The release times, routings and processing times of the jobs are stochastic parameters and not known in advance [6]. Incorporation this dynamic and stochastic behavior of job arrival in the theoretical model renders the results that obtained more applicable in realistic situations [5]. Analysis of dynamic job shops is usually so complicated and difficult that a feasible analytical solution procedure can hardly be found and computer simulation becomes the only feasible solution [2, 5, 7, 10].

2.1 Due Date Assignment

The consideration of due date assignments is an important element in production control, affecting both timely delivery and reduced finished goods inventory [8]. Because product and service delivery systems are not capable of successfully achieving an arbitrary set of due dates, the reasonableness of assigned due dates directly affects due date performance. Due date performance can be quantitatively measured by the conformity of a schedule to assigned due dates. Particular measures are functions of job flow time and assigned due date, such as job lateness, job tardiness and job earliness [9].

The due date management problem is of great practical significance to an organization for many vital planning functions, such as planned order release and resource requirements planning. Completion of jobs ahead of due dates would result in storage costs; on the other hand, if the jobs are completed after the due dates there will be tangible costs (e.g. clerical work, plant overtime) as well as intangible costs (e.g. loss of goodwill, dwindled customer satisfaction etc.). Management therefore desires both predictability (i.e. to set due dates correctly) and controllability (i.e. to meet the set due dates) [5]

Due date based scheduling of manufacturing systems has been widely examined in the related literature [8,9,10,17,18,19]. Generally, the models of assigning due dates are divided into two categories: *static* models based on long-term shop experience, and *dynamic* models based on the continuously changing shop conditions such as resource availability. The availability of resources may vary over time as customer's demands change. Under static models, arriving jobs are classified into a few groups and each job within a group is assigned the same fixed due date. Since static models do not consider continuously changing shop conditions, they do not produce realistic results. Nonetheless, they are simple and easy to implement. Under dynamic models, the job's manufacturing interval dynamically changes according to processing and resource requirements, and to current shop conditions. Dynamic models are more complex to implement, but produce more realistic results [11].

2.2 Dispatching Rules

Dispatching is a procedure that uses logical decision rules to select a job for processing on a machine that has just become available. These decision rules, also called dispatching or priority rules, determine the value of priority attribute that is assigned to each job. Once the priorities for all candidate jobs are determined, the jobs are sorted and the job with the highest priority is chosen [12].

Researchers and practitioners have used dispatching rules which essentially sub-optimal, though nevertheless effective and simple in their application even to job shop problems of fairly large size [13]. One classification of the rules is based on the detail of information they use. A *local rule* ignores all information except that which is locally available. In contrast, a *global rule* is not confined to the local details and may use information gathered from other machines, such as that pertaining to the queue at the next machine in the job route. Another classification of dispatching rules is based on the influence of the timing on their decisions. A *static rule* makes decisions that only depend on the status quo of the jobs and machines, i.e., the decisions made by the rule are not affected by when they are made, and assigned job priorities do not change over time. A *dynamic rule*, on the other hand, incorporates time-dependent information based on the current state of the scheduling environment or even the anticipated status of the environment at some time in the future. Consequently, job priorities assigned by dynamic rules do change over time [12]. For a detailed list of such rules and classifications, please see Panwalker and Iskander study [14].

2.3 Performance Criteria

Several performance criteria have been used to evaluate shop scheduling performance. The classification of the more commonly used criteria may be given as: time based measures (e.g. mean waiting time, machine idle time), work in process measures (e.g. average number of jobs in queue), due date related measures (e.g. mean tardiness, mean earliness, mean absolute lateness) and cost based measures (e.g. cost of idle machines, cost of carrying work in process inventory). Among those criteria, due date related measures are well known and they suggest several objectives that one can use to formulate scheduling problems. Two of them that have become

classics are minimizing the summarized tardiness and minimizing the maximum lateness [10].

3 Agent Based Dynamic Job Shop Simulation System (AB-DJSS)

Job shop type manufacturing systems consist of different machines with unique capabilities. Depending on job routing there are two types of job shops: classic job shop and job shop with recirculation. In the latter case, a job may visit a machine more than once, whereas in the former it does not. Depending on how many machines the job shop consists of, the number of machines in a job route is limited, but combinatorially increasing by the number of machines. In case of dynamic scheduling problem, the arrival of jobs is continuous, the time interval between the arrivals is mainly set by statistical analysis of the modeled real manufacturing system. Decreasing or increasing the time interval causes higher or lower demand and shop load ratio.

AB-DJSS has been developed to meet the requirements of high flexibility and compatibility. Multi-agent architecture has been found to be the most suitable for the purpose of simulating the different job shop environments and collecting required output information of the system. AB-DJSS provides the decision makers an opportunity to construct the different multi machine dynamic stochastic job shop models including classic job shops or job shop with recirculation. AB-DJSS presents many due date assignment models and dispatching rules that decision makers can select to analyze. AB-DJSS is also capable of gathering the information related to many performance criteria. That information may be very explanatory in analyzing the due date performance of a real system and be very useful to make a decision if necessary.

Three types of agents have been built: shop agent, machine agent and job agent.

Shop agent creates machines. The number of machines (m) is defined by the decision maker according to the real manufacturing environments. Each machine is then assigned to one machine agent. Due to multi machine architecture, the number of machines can be extended or reduced easily. After creating the machines, shop agent creates jobs by given time interval of job arrivals which has been set by using negative exponential distribution with λ parameter. Shop agent sets λ parameter value according to the expected shop utilization rate (shop load ratio). The expected shop utilization rate can be determined by:

$$\rho = \lambda \mu_o \mu_g / m \tag{1}$$

where ρ is the expected shop utilization rate, μ_o is the mean operation time and μ_g is the mean number of operations per job. Whenever a job is created, one job agent is assigned to the job. The shop agent also creates an operation list for newly generated job. The operation list defines the job route as well and it is randomly generated by using uniform distribution between minimum and maximum number of operations. For classic job shops, a machine can appear only once in the operation list whereas for the job shops with recirculation, a machine can appear more than once. For each operation in the list, an operation time is assigned by using exponential distribution considering the defined mean operation time (μ_o). Total processing time of the job is the sum of all its operation times. After the operation list and operation times are

generated, the due date of the job can be determined. Shop agent assigns the due date of the job by using the selected due date assignment model. Available due date assignment models classified as dynamic and static models provided by AB-DJSS are given below**:**

- Static models
  - Slack time (SLK),
  - Total work content (TWK),
  - Number of operations (NOP),
  - TWK + NOP,
  - Processing time + Wait (PPW),
- Dynamic models
  - Job in Queue (JIQ),
  - Job in System (JIS),
  - Operation Flow time Sampling (OPF)
  - Dynamic TWK, Dynamic PPW

Some of the models like JIQ and JIS require an allowance value and they have to be determined before using. When decision maker can not supply a value and/or no historical data is available for estimation, this determination process may need special pre-simulation runs to generate the historical data and statistical analysis of them for estimation. AB-DJSS is also capable of doing pre-simulation studies and generating all required information for further analysis.

All information about the operation list, operation times, and the due date are then sent to the related job agent through the communication and then the processing of the job starts.

Each job agent carries all necessary information about its job. That information may vary depending on the selected due date assignment models and dispatching rules. The job agent manages the job through the machines in its operation list. When a job enters the queue of a machine, job agent provides all required information to the machine agent for dispatching operation when the machine is in idle. This information consists of expected operation time on the machine, due date and remaining processing time of the job. The job agent continuously monitors the job in the system and refreshes remaining processing time information when required by the machine agent. When all operations on the job are completed, the job agent finalizes the process related to the job. This finalization process includes all calculation operations related to the selected performance criteria and collecting the statistical data. This information is then sent to the shop agent so that it gathers and produces the final performance results for the simulation run and the life cycle of a job agent ends. The number of job agents at a time depends only on the number of jobs in the shop and there is no limitation for it. Some of the selectable performance criteria provided by AB-DJSS are given below:

- Performance criteria
  - Flow time related measures,
  - Tardiness related measures,
  - Earliness related measures,
  - Lateness related measures, and also
  - Mean absolute lateness (MAL),
  - Mean squared lateness (MSL).

When the job agent sends the job to the next machine’s queue in its operation list, it informs the machine agent related with the machine that a new job enters its queue.

When the machine is in idle, the machine agent queries the required information from the shop agent and the job agents related to the jobs in its queue and determines the priorities of the jobs according to the selected dispatching rule. Available rules provided by AB-DJSS are classified as static and dynamic rules and given below:

- Static rules
  - First in first out (FIFO),
  - Last in first out (LIFO),
  - Shortest processing time (SPT),
  - Longest processing time (LPT),
  - Earliest due date (EDD),
  - First in system first served (FISFS),
- Dynamic rules
  - Slack time (SLK)
  - Slack time per operation (SLK/OPN)
  - Modified operation due date (MOD),
  - Critical ratio (CR),
  - Critical ratio + shortest processing time (CR+SPT),
  - Allowance + Critical ratio + Shortest processing time (ALL+CR+SPT).

After determination of the job priorities, the machine agent sequences the jobs according to their priorities and selects the job with the highest priority as the next job to be processed in the machine. When the job leaves the machine, the job agent reads the next operation from the operation list of the job and sends the job to the next machine's queue.

The shop agent is also responsible for managing the simulation runs and requires some simulation parameters be determined by decision makers to start the simulation. These parameters are given below:

- Simulation parameters
  - Simulation period or total number of jobs to be simulated,
  - Replication number, and
  - Number of jobs to be ignored to reach the steady state: AB-DJSS helps decision makers to determine the number of jobs to be ignored by providing "*Welch's graphical procedure*" [15].

While a simulation run is in progress, the shop agent collects much information about the process like flow time, waiting time, due dates, jobs in route, time in route and jobs in system. After the simulation is completed, the shop agent summarizes and presents the results related to the selected performance criteria. All the results and collected information can also be saved into a data file for further analysis.

4 Analysis of Performance of AB-DJSS

One of the important advantages of AB-DJSS is that AB-DJSS is very flexible and provides the decision makers an opportunity to construct the simulation models for the different dynamic job shop environments quickly. Extendable structure of

AB-DJSS and no more needing any programming knowledge for the simulation process are other important advantages.

Although there is no general analytic method for analyzing dynamic job shops, Cheng [16] made an analysis of job flow time in a dynamic job shop. Cheng, in his study, generated the mean and standard deviation of job flow time analytically in a dynamic job shop in which First In First Out (FIFO) dispatching rule was used. Cheng also made a simulation study for the same shop conditions and compared the simulation results with analytically obtained results to test.

As it will be true to test the results of AB-DJSS with the results of Cheng's analytic model instead of comparing with the results of different simulation studies, a simulation study in a dynamic stochastic job shop which has the same specifications and assumptions, was designed and performed by AB-DJSS. For 10 replications by AB-DJSS, the obtained mean and standard deviation values of flow-time (F) are given in Table 1. In the Table, m denotes the number of machines and ρ denotes shop load ratio.

Table 1. Mean and standart deviation values of Flow-time for 10 replications by AB-DJSS

			m=5, ρ=0.90		m=9, ρ=0.50		m=9, ρ=0.90	
No	Mean	Std.	Mean	Std.	Mean	Std	Mean	Std.
1	13,184	9,31	53,891	40,91	24,407	16,79	116,150	75,01
2	12,954	10,06	56,816	40,26	25,108	16,38	105,940	58,08
3	13,575	9,14	59,602	42,03	22,832	14,48	94,508	68,01
4	13,178	9,50	57,580	41,53	24,796	16,67	125,802	80,01
5	13,483	10,58	56,829	36,80	23,740	15,79	106,247	67,40
6	13,119	9,27	52,323	36,04	24,282	15,94	119,514	77,06
7	13,196	9,45	51,909	36,31	22,920	15,33	83,807	54,73
8	13,208	9,83	44,361	30,64	24,085	15,39	107,879	68,33
9	12,725	9,55	63,383	42,96	25,764	17,97	129,276	97,24
10	13,367	9,41	57,475	39,15	23,637	15,96	127,303	83,58
Av	**13,198**	**9,61**	**55,417**	**38,66**	**24,157**	**16,07**	**111,642**	**72,95**

Final results of AB-DJSS and Cheng's analytic and simulation results are summarized in Table 2.

Table 2. Final results of AB-DJSS and Cheng (1985)

	F mean			F Std. Dev.		
	Cheng's simulation results	Cheng's analytic results	AB-DJSS results	Cheng's simulation results	Cheng's analytic results	AB-DJSS results
m=5, ρ=0.50	13,17	13,32	13,20	8,88	8,28	9,61
m=5, ρ=0.90	55,29	56,59	55,42	41,84	37,82	38,66
m=9 ρ=0.50	24,38	23,97	24,16	15,50	14,45	16,07
m=9 ρ=0.90	109,44	112,69	111,64	100,32	71,03	72,95

The final results of AB-DJSS are closer to the analytically obtained results than Cheng's simulation results and Table 2 confirms that AB-DJSS is more capable of producing the valid simulation results.

AB-DJSS is superior to a non-agent based simulation architecture from many different viewpoints: flexibility, extendibility, construction speed of new and different dynamic job shop simulation models and ease of use.

5 Case Study

Dispatching Rules: Four commonly used dispatching rules were selected [17]:
1. FIFO, 2. SPT, 3. CR+SPT, 4. All+CR+SPT

Due Date Assignment Models: The following due date assignment models were used [17]: 1. TWK, 2. PPW, 3. DTWK, 4. DPPW

Performance Measures : Two shop performance measures, Mean Absolute Lateness (MAL) and Mean Squared Lateness (MSL) [17] were considered.

Shop Utilization: Two shop utilization rates were considered in the study: 90% and 80% [17].

The shop model: General job shop scheduling assumptions were applied for the purpose of model standardization [17]. The parameters of the model are as follows:

1. The shop is composed of 5 non-identical machines.
2. Job arrivals at the shop form a Poisson process. The shop arrival rate is determined by the shop utilization setting.
3. The number of operations per job varies uniformly between 1 and 9.
4. To determine a job's routing, each machine is equally likely to perform the job's next operation. A machine can perform more than one operation of a job under the constraint that no two successive operations require the same machines.
5. Operation processing times are exponentially distributed with a mean of 1 unit of time.
6. Number of jobs to be ignored is first 1.000 jobs (determined by using Welch's graphical procedure).
7. To minimize the variation of the results, 6 replications were made.

Results and discussions

For each of 32 experiments (i.e. 4×4×2), 6 independent runs were made and 10.000 jobs were completed after the completion of the first 1.000 jobs in each run. The data were then gathered and averaged over the 6 runs. All MAL and MSL results are summarized in Table 3.

The results in Table 3 indicate a great variation among the combinations of the three decision factors. Performance deteriorates as shop utilization increases. In particular, there is a drastic deterioration in the mean squared lateness (MSL). This is because the more congested the shop is, the less stable the scheduling system becomes, thus, causing increases in job flow time as well as in its variability. For the performance of dispatching rules, the results in Table 3 demonstrate that due date dependent rules, CR+SPT and ALL+CR+SPT, outperforms due date independent rules, FIFO and SPT. They also shows that due date information is very helpful in

controlling and coordinating the scheduling process that renders the performance more robust to the variations on the shop load.

Dynamic due date assignment models exhibit a performance superior to that of their static counterparts. Under almost all combinations of dispatching rules, both MAL and MSL performances are improved when dynamic due date assignment models are employed. This case is more evident in higher shop loads with CR+SPT and ALL+CR+SPT rules. Thus, dynamic due date assignment models, especially DTWK model, in conjunction with due date related dispatching rules provide the greatest improvement in heavily loaded shop in respect of MAL and MSL performances.

Table 3. Experimental results for MAL and MSL (MSL results are given in parenthesis)

UTIL.	D.D.A. Mod.	FIFO	SPT	CR+SPT	ALL+CR+SPT
%90	TWK	23.37 (1004.3)	13.30 (1216.6)	14.56 (457.1)	14.46 (454.9)
	PPW	19.73 (766.7)	14.44 (1401.3)	14.64 (458.2)	14.48 (446.9)
	DTWK	20.68 (891.9)	13.03 (1191.6)	7.62 (131.3)	7.54 (126.6)
	DPPW	14.77 (413.9)	18.09 (1442.0)	9.81 (184.1)	9.76 (182.1)
%80	TWK	11.12 (232.7)	5.99 (165.6)	7.32 (121.5)	7.14 (113.2)
	PPW	9.65 (186.6)	13.15 (310.2)	7.26 (121.2)	7.14 (114.5)
	DTWK	10.23 (231.3)	6.65 (166.2)	4.59 (50.2)	4.58 (49.7)
	DPPW	9.20 (160.1)	10.22 (247.7)	7.22 (99.9)	7.22 (99.8)

6 Conclusions

In this paper, an agent based dynamic job shop simulation system is designed and developed to help the decision makers who have to mainly solve the problems of selecting correct due date assignment models and dispatching rules depending on selected performance criteria in their multi machine dynamic stochastic job shop environment.

To reduce the complexity of analyzing the dynamic job shops and increase the flexibility in the decision making process, the system is designed and developed as multi agent system. Using the developed system, it is possible to simulate many dynamic manufacturing processes with different job structures under various operating conditions and monitor the system behaviors.

The system provides 10 due date assignment models (5 of them are static and other 5 are dynamic), 12 dispatching rules (6 of them are static and other 6 are dynamic) and many performance criteria for analyzing the dynamic job shops. By determining many other shop parameters, it is also possible to generate and collect the large number of simulation data for further analysis. All generated and collected data can also be saved into disk files in mostly known statistical formats.

As the system is in multi agent architecture, new due date assignment models and new dispatching rules as well as new performance criteria can be easily added to the system and the system can be easily extended.

References

1. Jain, A.S., Meeron, S.: A state-of-the-art-review of job shop scheduling tecniques (1998) http://citeseer.nj.nec.com/jain98stateart.htm
2. Ramasesh, R.: Dynamic job shop scheduling: a survey of simulation research. OMEGA 18, 43–57 (1990)
3. Roman, D.B., del Valle, A.G.: Dynamic assignation of due dates in an assembly shop based simulation. International Journal of Production Research 34(6), 1539–1554 (1996)
4. Wein, L.W., Ou, J.: The impact of processing time knowledge on dynamic job shop scheduling. Management Science 37(8), 1003–1014 (1991)
5. Cheng, T.C.E, Gupta, M.C.: Survey of scheduling research involving due date determination decisions. European. Journal of Operations Research 38, 156–166 (1989)
6. Jones, A., Rabelo, L.C.: Survey of job shop scheduling (1999) http://www.nist.gov/msidlibrary/doc/jobshop1.pdf
7. Cheng, T.C.E: Optimal common due date with limited completion time deviation. Comput. Opns. Res. 15(2), 185–188 (1988)
8. Tsai, C.H, Chang, G.T., LI, R.K.: Integrating order release control with due date assignment rules. International Journal of Production Research 35(12), 3379–3392 (1997)
9. Vig, M.M., Dooley, K.J.: Dynamic rules for due date assignment. International Journal of Production Research 29(7), 1361–1377 (1991)
10. Lengyel, A., Hatono, I., Ueda, K.: Scheduling for on-time completion in job shops using feasibility function. Computers & Industrial Engineering 45, 215–229 (2003)
11. Rajasekera, J.R, Murr, M.R., So, K.C.: A due date assignment model for a flow shop with application in a lightguide cable shop. Journal of Manufacturing Systems 10(1), 1–7 (1991)
12. Bhaskaran, K., Pinedo, M.: Dispatching. In: Salvendy, G. (ed.) Handbook of Industrial Engineering. ch. 83, John Wiley and Sons, New York (1992)
13. Blackstone, J.H., Phillips, D.T., Hogg, G.L.: A state-of-the-art survey of dispatching rules for manufacturing job shop operations. International Journal of Production Research 20, 27–45 (1982)
14. Panwalker, S.S., Iskander, W.: A survey of dispatching rules. Operations Research 25, 45–61 (1977)
15. Law, A.M., Kelton, W.D.: Simulation modeling and analysis. McGraw-Hall, New York (1991)
16. Cheng, T.C.E: Analysis of job flow time in a job shop. Journal of Operations Research Society 36(3), 225–230 (1985)
17. Cheng, T.C.E, Jiang, J.: Job shop scheduling for missed due dates performance. Computers and Industrial Engineering 34(2), 297–307 (1998)
18. Chang, F.C.R.: A study of factors affecting due date predictibility in a simulated dynamic job shop. Journal of Manufacturing Systems 13(6), 393–400 (1997)
19. Sha, D.Y., Liu, C.-H.: Using data mining for due date assignment in a dynamic job shop environment. Int. Adv. Manuf. Technol. 25, 1164–1174 (2005)

A Manufacturing-Environmental Model Using Bayesian Belief Networks for Assembly Design Decision Support*

Wooi Ping Cheah[1], Kyoung-Yun Kim[2], Hyung-Jeong Yang[1,**], Sook-Young Choi[3], and Hyung-Jae Lee[1]

[1] Dept. of Computer Science, Chonnam National University, Gwangju 500-757, South Korea
cheahwooiping@gmail.com, hjyang@chonnam.ac.kr, hjgumsin@hanmail.net
[2] Dept. of Indust. and Manuf. Eng., Wayne State University, Detroit, MI 48202, USA
kykim@eng.wayne.edu
[3] Dept. of Computer Education, Woosuk University, Samruy, Chonbuk, South Korea
sychoi@mail.woosuk.ac.kr

Abstract. Assembly design decision making is to provide a solution of currently violating design by evaluating assembly design alternatives with the consideration of the assembly design decision (ADD) criteria and of the causal interactions with manufacturing-environmental factors. Even though existing assembly design support systems have a systematic mechanism for determining the decision-criterion weight, the system still has a limitation to capture the interactions between manufacturing-environmental factors and ADD criteria. Thus, we introduce in this paper, Bayesian belief networks (BBN) for the representation and reasoning of the manufacturing-environmental knowledge. BBN has a sound mathematical foundation and reasoning capability. It also has an efficient evidence propagation mechanism and a proven track record in industry-scale applications. However, it is less friendly and flexible, when used for knowledge acquisition. In this paper, we propose a methodology for the indirect knowledge acquisition, using fuzzy cognitive maps, and for the conversion of the representation into BBN.

Keywords: Applications to manufacturing, assembly design, decision support, Bayesian belief networks, fuzzy cognitive maps.

1 Introduction

An assembly design decision (ADD) problem occurs when the current assembly design violates assembly specifications, such as maximum allowance in surface straightness or maximum stress. An example is that of the corner joint in which a designer specifies a sharp edge of a corner joint as a weld seam; and a low weld penetration and high stress level around the weld seam is indicated by an assembly analysis. When a problem is indicated on the current assembly design, the designer

* This work was supported by the Korea Research Foundation Grant funded by the Korean Government (MOEHRD, Basic Research Promotion Fund) (KRF-2006-003-D00511).
** Corresponding author.

H.G. Okuno and M. Ali (Eds.): IEA/AIE 2007, LNAI 4570, pp. 374–383, 2007.

must make a decision whether to accept the current joint or modify it, and whether the current joining method should be controlled or another joining method considered, if the joint must be modified. Assembly design decision making is to provide a solution for such a dilemma by evaluating the weights of various ADD criteria, such as assembly cost, assembly quality, and assembly design.

Typically, assembly design decision making is a multi-disciplinary task. It requires negotiations between diverse stakeholders: manufacturing engineers, financial and marketing analysts, quality experts, design specialists; all must resolve trade-offs while maintaining performance goals. It involves consideration of interdependent behavior among different disciplines (i.e., causal interactions between various manufacturing-environmental factors, such as competitiveness and market demand). The task is complicated due to the complex nature of such interactions. The results are often subjective, causing biases on the final decision. Assembly design decision support provides an efficient methodology for capturing causal interactions between manufacturing-environmental factors and ADD criteria. It also provides an automated mechanism for determining ADD criterion weights based on the interactions [1].

In this paper, we introduce Bayesian belief network (BBN) for the representation and reasoning of the manufacturing-environmental knowledge. It has a sound mathematical foundation based on probability theory and a powerful reasoning capability. It supports predictive, diagnostic, and mixed modes of reasoning, and its results are consistent and unambiguous. It has an efficient evidence propagation mechanism based on conditional independence, with high scalability. It also has a proven track record in industry-scale applications as shown in the next section. However, when BBN is used as a front-end tool for knowledge acquisition, it is less friendly and flexible. Elicitation of root and conditional probability distributions is often a challenge with a BBN. Domain experts find it unnatural and difficult to specify causal relationships in terms of conditional probabilities, especially when the number becomes large. Therefore, in this paper, we propose a methodology for the indirect acquisition of domain knowledge using cognitive map (CM) with causal weights, called fuzzy cognitive map (FCM), as a front-end tool, and for the conversion of the representation into a BBN.

2 Related Work

There has been much research on decision supporting in manufacturing domain. Subru et al. used genetic algorithms for a design-manufacturing-supplier decision problem for an agile manufacturing environment [2]. Rekiek et al. proposed a method to treat the resource planning for the assembly line problem [3]. In their work, designer's preferences were captured by adjusting the weight of the different objectives. Zha proposed a neuro-fuzzy approach for assemblability and assembly sequence evaluation [4] and also introduced knowledge intensive Petri net models to integrate design and assembly planning and utilized knowledge-based agents acting as decision supporting tools [5]. LeBacq et al. presented a methodology for the joining selection [6]. Their method was based on a questionnaire and a database including the characteristics of joining and the material. A Hierarchical Semantic Net model was presented by Kim [1] to allow design alternatives to be systematically evaluated. However, this model has a limitation to capture the interactions between manufacturing-environmental factors and assembly design decision criteria.

BBN is a well established method for reasoning under uncertainty, using a graphical structure to represent causal relationships and probability calculus to quantify these relationships and update beliefs given new information. BBN has had considerable industry-scale applications: Microsoft's Lumiere project [7] for inferring the goals and needs of software users; MIT's HDP project [8] for differential therapy of cardiovascular disorders; and HP's SACSO project [9] for printer trouble shooting. Even though there are many applications of BBN in various decision support systems, to the best of our knowledge, there is no existing research ever applied BBN to assembly design decision support. So far the closest to our work is the application of BBN in change impact analysis in the domain of architecture design [10].

A CM [11] is a collection of nodes connected by some causal links or edges. The nodes represent variables of a domain. The links represent the direction of influence. Links have a sign, which can be positive (a promoting effect) or negative (an inhibitory effect). An FCM [12] is a "fuzzified" version of cognitive map, which allows causal links to have a value in [–1, 1]. It also allows feedback, which adds a temporal aspect to its operation.

3 Capturing Causal Knowledge with FCM

Causal knowledge is important in decision making because decision problems are described and understood through causal connections. Cognitive mapping is an efficient methodology for capturing causal knowledge of domain experts. It represents knowledge visually and more descriptively, hence, it is more comprehensible, less time-consuming and causes lesser inconvenience to experts during knowledge elicitation.

Nadkarni et al. proposed a systematic approach for capturing causal knowledge from domain experts [13]. It includes a method for the elicitation of unstructured knowledge, with a set of open ended interview questions. It also includes a procedure for the subsequent derivation of environmental factors and initial causal structure. Figure 1 shows an initial CM for the assembly design environment, elicited from the domain experts based on this approach.

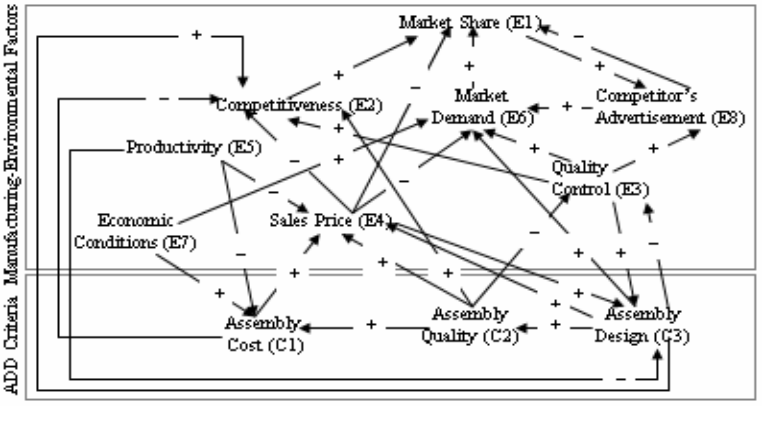

Fig. 1. Causal structure for the manufacturing-environmental factors and ADD criteria

However, Nadkarni et al. did not propose a method for capturing causal strengths. Instead, they used conditional probability distributions to quantify the causal relationships between a node and the parents. This approach is less friendly and less natural to the domain experts. In our methodology, causal weights or values are elicited from the experts and represented using an FCM. Conditional probability distributions can be derived directly from the causal values in the FCM.

In general, an FCM with n nodes can be described by an $n \times n$ adjacency matrix, M_{ij}, whose elements, e_{ij}, are the causal value (representing causal strength) of the link directed out of V_i into V_j. Table 1 shows an adjacency matrix for the FCM. In the table, the causal value for the link from C2 to E2 is 0.8, which indicates a strong positive causality from C2 to E2.

Table 1. Adjacency matrix for FCM.

	E1	E2	E3	E4	E5	E6	E7	E8	C1	C2	C3	Notations:
E1	0	0	0	0	0	0	0	0.3	0	0	0	E1: Market Share
E2	0.7	0	0	0	0	0	0	0	0	0	0	E2: Competitiveness
E3	0	0.6	0	0	0	0.1	0	0.4	0	0	0.7	E3: Quality Control
E4	-0.5	-0.2	0	0	0	-0.2	0	0	0	0	0.3	E4: Sales Price
E5	0	0	0	-0.8	0	0	0	0	-0.3	0	-0.8	E5: Productivity
E6	0.4	0	0	0	0	0	0	0	0	0	0	E6: Market Demand
E7	0	0	0	0	0	0.6	0	0	0.4	0	0	E7: Economic Conditions
E8	-1	0	0	0	0	0.2	0	0	0	0	0	E8: Competitor's Advertisements
C1	0	-0.9	0	1	0	0	0	0	0	0	0	C1: Assembly Cost
C2	0	0.8	-1	0.5	0	0	0	0	0.6	0	0	C2: Assembly Quality
C3	0	0.8	-0.3	0.4	0	0.9	0	0	0	0.7	0	C3: Assembly Design

4 Constructing BBN from FCM

The migration involves two stages, qualitative and quantitative. Qualitative migration involves the transformation of the qualitative structure of FCM (i.e., the original "un-fuzzified" or un-weighted CM into a BBN compatible qualitative causal structure). Quantitative migration involves the transformation of "fuzzified" causal weights or causal values into the conditional probability distributions in BBN. For each variable or node in the BBN compatible qualitative causal structure, there will be a conditional probability table (CPT) associated with it.

4.1 Building BBN Compatible Causal Structure from CM

The initial CM is less structured due to the way knowledge is elicited from the experts. Conducting interviews using open ended questions often produces incomplete or redundant representation. Therefore, a more structured interview with guided questions is required to ensure the completeness and to eliminate redundancy in the representation. The initial CM requires modification to make it compatible with BBN by performing four operations: 1) ensuring conditional independency; 2) removing indirect relationships; 3) converting abductive links to deductive; and 4) eliminating circular relations [13]. The operations are elaborated below and the result is shown in Figure 2.

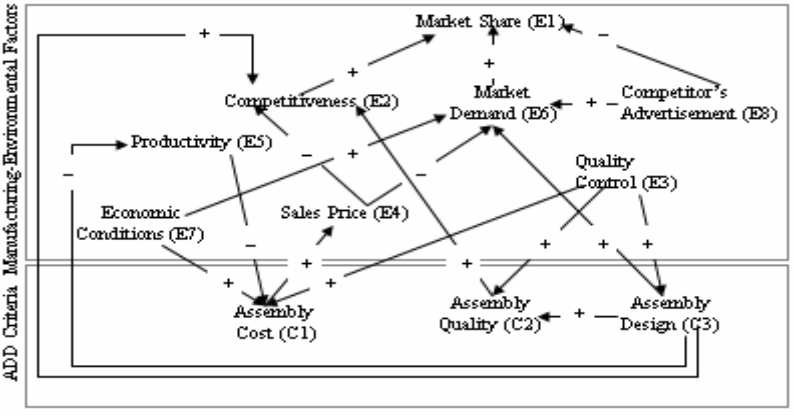

Fig. 2. BBN compatible causal structure

In BBN, all the dependent nodes are to be linked with an arrow, so that when there is no link between two nodes, we can conclude that the nodes are conditionally independent. A systematic analysis of the CM yielded an additional positive link, from quality control to assembly quality. This is intuitive as increased quality control naturally improves the assembly quality. Another positive link, from quality control to assembly cost, is also added. It is logical to believe that the resources and effort spent in practicing quality control increases the assembly cost. Quality control was, somehow, not perceived as a direct factor to assembly cost. Instead, assembly quality was perceived as a direct factor. Hence, the direct causal link from quality control to assembly cost will replace the indirect link from assembly quality to assembly cost.

In BBN, only variables with direct causal relationships are linked with an arrow directly. Hence, the links between variables which are indirectly related are to be removed. The indirectly related variables are to be separated as conditionally independent variables. The direct links between the following pairs of variables were removed: (E3, E2), (E3, E6), (E3, E8), (E4, E1), (E5, E4), (C1, E2), (C2, C1), (C2, E4), (C3, E4). Each of them is substituted by one or more indirect links which indicate the propagation of causal effects. For example, the positive link from quality control to competitiveness was removed. After the removal, quality control affects competitiveness positively through assembly design. It also affects competitiveness positively through assembly quality via (or without via) assembly design. It affects competitiveness negatively through sales price via assembly cost.

Causal statements involving abductive reasoning are often represented by a link from effect to cause in CM. These causal links are to be converted as links from cause to effect (i.e., in the direction of causation). The reverse, effects to cause, relationships will be inferred by using the probabilistic inference mechanism of BBN. In Figure 1, there is a negative link from productivity to assembly design. The link is abductive and it is removed. Instead, a negative deductive link from assembly design to productivity is added in Figure 2. The rationale is that a better (often more complex) assembly design usually requires more time and effort, hence lower productivity.

In CM, circular relations violate the acyclic graphical structure required in BBN, hence, they are to be removed. Figure 1 shows a two-way relation between assembly design and sales price. The link from assembly design to sales price represents the

correct cause to effect relationship between the two variables. The positive abductive link, from sales price to assembly design is a redundant reciprocal relationship, which is removed. The positive abductive link, from assembly design to quality control is redundant and also removed. The two-way relation between competitor's advertisement and market share can be resolved by separating the linkages into two different time frames. In the current time frame the concern is the negative effect of the competitor's advertisement to the market share. In the future time frame the concern is the positive effect of the market share to the competitor's advertisement. It is important to clearly separate events for future time frame from the current time frame to avoid ambiguity in the interpretation of the reasoning results. In this work, we confine our model to the current time frame of the decision being modeled, and we remove the link from market share to competitor's advertisement. There is a loop between the three variables: quality control, assembly design, and assembly quality. The negative link from assembly quality to quality control represents the fact that high quality assembly will require less control and managing in the future; though, currently, the high quality assembly is the result of the high quality control. Since the link pertains to the future time frame, it is removed.

4.2 Constructing CPTs of BBN from Causal Weights of FCM

The above four operations have modified the qualitative structure of the FCM making it compatible with BBN. The conversion has also changed the adjacency matrix and the result is shown in Table 2. This updated matrix is useful for constructing CPTs for the BBN. There are three steps involved in the construction of CPTs from causal weights: 1) summing the causal effects; 2) normalizing the tables; and 3) assigning probability to the opposite state.

Table 2. BBN compatible adjacency matrix

	E1	E2	E3	E4	E5	E6	E7	E8	C1	C2	C3	Notations:
E1	0	0	0	0	0	0	0	0	0	0	0	E1: Market Share
E2	0.7	0	0	0	0	0	0	0	0	0	0	E2: Competitiveness
E3	0	0	0	0	0	0	0	0	0.6	1	0.7	E3: Quality Control
E4	0	-0.2	0	0	0	-0.2	0	0	0	0	0	E4: Sales Price
E5	0	0	0	0	0	0	0	0	-0.3	0	0	E5: Productivity
E6	0.4	0	0	0	0	0	0	0	0	0	0	E6: Market Demand
E7	0	0	0	0	0	0.6	0	0	0.4	0	0	E7: Economic Conditions
E8	-1	0	0	0	0	0.2	0	0	0	0	0	E8: Competitor's Advertisements
C1	0	0	0	1	0	0	0	0	0	0	0	C1: Assembly Cost
C2	0	0.8	0	0	0	0	0	0	0	0	0	C2: Assembly Quality
C3	0	0.8	0	0	-0.8	0.9	0	0	0	0.7	0	C3: Assembly Design

Table 3(a) shows a result of summing the causal effects from three sources: E3, E5, and E7. It shows the probability distributions for C1, one for each configuration of states of its parents. For example, what is the probability C1 increases (or the probability it decreases) given E3, E5, and E7 all increase. From the updated adjacency matrix, in C1 column there is a positive effect of 0.6 from E3, a negative effect of 0.3 from E5, and a positive effect of 0.4 from E7. When E3, E5 and E7 all increase the resultant causal effect is the algebraic sum of the individual effects, i.e., (+0.6)+(–0.3)+(+0.4) = +0.7. When all decrease, the resultant causal effect is

Table 3. Three-step construction of CPT for assembly cost (C1)

CPT for C1				
E3	E5	E7	C1	
			+	-
+	+	+	0.70	
+	+	-		0.10
+	-	+	1.30	
+	-	-	0.50	
-	+	+		0.50
-	+	-		1.30
-	-	+	0.10	
-	-	-		0.70

(a)

CPT for C1				
E3	E5	E7	C1	
			+	-
+	+	+	0.54	
+	+	-		0.08
+	-	+	1.00	
+	-	-	0.38	
-	+	+		0.38
-	+	-		1.00
-	-	+	0.08	
-	-	-		0.54

(b)

CPT for C1				
E3	E5	E7	C1	
			+	-
+	+	+	0.77	0.23
+	+	-	0.46	0.54
+	-	+	1.00	0.00
+	-	-	0.69	0.31
-	+	+	0.31	0.69
-	+	-	0.00	1.00
-	-	+	0.54	0.46
-	-	-	0.23	0.77

(c)

(–0.6)+(+0.3)+(–0.4) = –0.7 and so fourth. When the resultant causal effect is positive, it represents an effect to the '+' state of C1, and a negative resultant causal effect represents an effect to the negative state of C1.

After summing the causal effects, the value for the '+' state of C1 is greater than 1 (i.e., 1.3), when both E3 and E7 increase but E5 decreases. The value for the '–' state of C1 is also 1.3, when both E3 and E7 decrease but E5 increases. A probability value greater than 1 is not acceptable in probability theory. Therefore, a normalization process is necessary. Since we only want the relative strength, it is fine to modify the values, as long as their ratios remain unchanged. We normalize the probabilistic values by dividing each of them using the maximum value, which is greater than 1. In our example, we divide all the values by 1.3, and the result is shown in Table 3(b).

In Table 3(b), when both E3 and E5 increase, E7 decreases. The three factors, collectively, produce a causal effect of 0.08, to the '–' state of C1, which is the state of interest. We have no knowledge about the causal effect to the counterpart (i.e., the '+' state of C1). However, in BBN, the '+' state has to be assigned 0.92 (1 – 0.08). This causes a semantic problem because it implies that the collective effect from the three factors is more likely to cause an increase to C1 (0.92) than a decrease (0.08). This is commonly recognized as a limitation of the classical probability theory. We propose a simple and practical method which ensures the assigned probability is always smaller than the probability of the state of interest, though it does not eliminate the assignment of probability to the counterpart state.

Without any knowledge, we assume a prior probability of 0.5 for both '+' and '–' states of a variable. The value of 0.5 indicates absolute uncertainty of their likelihood (i.e., the variable has the same chance for increase and decrease (fifty-fifty)). Once concrete evidence (complete certainty) is acquired for a particular state of interest, its probability immediately increases to 1, and the counterpart state immediately decreases to 0. Hence, the *probability range* of the state of interest is 0.5. The *minimum probability* is 0.5 and the *maximum probability* is 1. The counterpart state, on the other hand, stays within 0 and 0.5; hence, it is always less than the state of interest. Suppose we are 50% sure (0.5 *initial probability*) that a variable will increase (i.e., in between absolute uncertainty and absolute certainty). Based on our proposed method, the *moderated probability* should fall exactly in between 0.5 and 1, which is 0.75. It can be computed using a simple proportionality formula, as follow: *Moderated Probability = (Initial Probability × Probability Range) + Minimum Probability*.

In the example related to the CPT of C1, the initial probability for the state of interest (i.e., the '–' state) is 0.08. Applying the formula, we do the following moderation: (0.08 × 0.5) + 0.5 = 0.54. The probability for the counterpart (i.e., the '+' state) is therefore 1 – 0.54 = 0.46. We perform the same moderation for all the other combinations, and the result is shown in Table 3(c).

5 Experimental Results

A simulation is implemented using BBN software, Hugin Lite 6.7 [14], and the experimental results are discussed below. Initially, when no evidence has been added (i.e., no change of any manufacturing-environmental factors or no emphasis on any ADD criteria), the original marginal probability, for all the states is 0.5 (50%). It indicates that there is a 50% chance for all the states in the network.

As manufacturing-environmental changes are introduced to the system, we want to predict their effect to the ADD criteria. Alternatively, as one or more ADD criteria are emphasized, we want to predict the effect to the manufacturing-environmental variables. Let us assume that there is an increase of 0.8 (initial probability) in the emphasis for assembly quality. This change is inserted as evidence to set the '+' state of the node to 90% [(0.8 × 0.5) + 0.5 = 0.9]. Given this evidence, we can do a what-if analysis and predict that there is an 80% chance that the competitiveness will increase (see Figure 3). The impact flows further up to the market share but with a lesser effect, there is a 62.4% chance that it will increase. As such, the market share changes come from its indirect dependency on assembly quality.

Another application is to diagnose possible causes and influences for a change or emphasis in assembly design. Given a domain variable, we want to reason about the factors which influence it. For instance, if we increase market share by 0.8 (i.e., to set

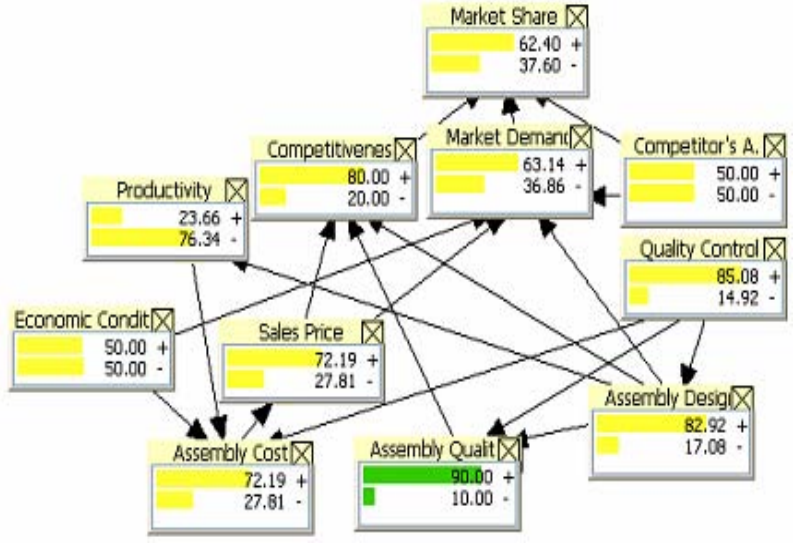

Fig. 3. Predictive BBN model

its '+' state to 90%), as in Figure 4, we observe that there is a 65.53% chance that competitiveness will increase, 59.66% chance that market demand will increase, and 68.41% chance that competitor's advertisement will decrease. These three variables are regarded as direct factors or causes to market share. We can continue the analysis to all the ancestor nodes by tracing "downwards" as far as to assembly cost with the '+' state probability of 56.52%, assembly quality 62.4%, and assembly design 63.15%. If increasing market share is our main concern, it is obvious that the competitor's advertisements have the greatest negative effect (–68.41%), and competitiveness the greatest positive effect (65.53%). Assembly design, in turn, has the greatest positive effect (63.15%) to the competitiveness.

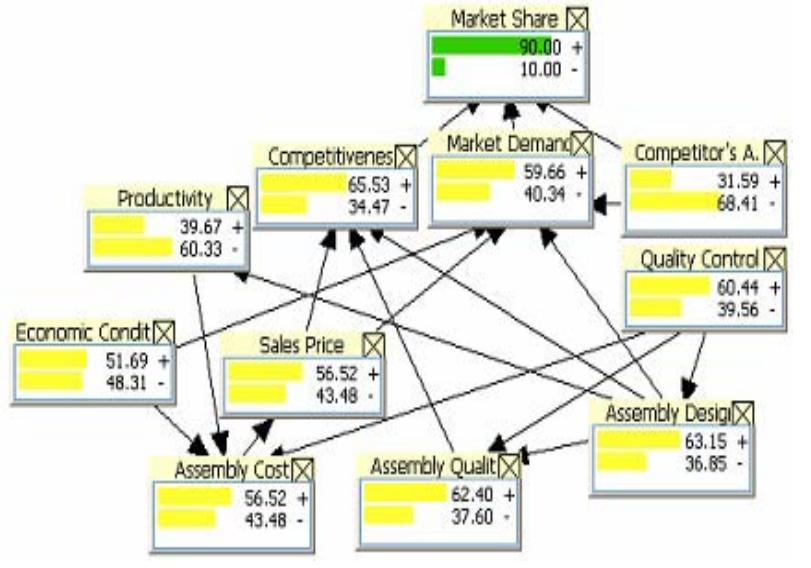

Fig. 4. Diagnostic BBN model

In practice, a domain variable is rarely only a source or a target of a change. Instead, it is often a probable source causes a change to other variables, and at the same time a probable target affected by their changes. As an example, competitiveness has been identified as a probable (65.53%) cause to the increase of market share, as shown in Figure 4. It has, however, become a probable (80%) target affected by an increase in assembly quality, as shown in Figure 3. If both market share and assembly quality increase at the same time, the combining effect is cumulative. In other words, the combination of both the predictive and diagnostic inference will push up the probability of the increase in competitiveness to 87.99%. It will also change the posterior probability for the increase of both market share and assembly quality to 93.72%, higher than what was entered initially (i.e., 90%).

Due to space limit, only a small system is discussed in this paper. A more realistic system can be implemented by extending the model with additional domain variables.

6 Concluding Remarks

When used as a front-end tool for knowledge acquisition, BBN is less friendly and flexible as compared to FCM. Elicitation of root and conditional CPTs from domain experts is often a challenge with BBN. Several methods have been established to facilitate the indirect acquisition of such knowledge from experts. One way is to use FCM as a front-end tool and then convert the representation to BBN as was discussed in this paper. Another way is to apply machine learning techniques to acquire the graph structure and the conditional probability distributions from data. Cycles are not permitted in the BBN formalism. The acyclic prohibition limits exact modeling of systems to those without feedback or bidirectional causality. Dynamic BBN is an ongoing area of research which seeks to model systems that change over time.

References

1. Kim, K.: Assembly Operation Tools for e-Product Design and Realization. Ph.D. Dissertation, University of Pittsburgh (2003)
2. Subru, R., Sanderson, A., Hocauğlu, C., Graves, R.: Evolutionary Decision Support for Distributed Virtual Design in Modular Product Manufacturing. Production Planning and Control 7, 627–642 (1999)
3. Rekiek, B., De Lit, P., Delchambre, A.: Hybrid Assembly Line Design and User's Preferences. Int. J. of Production Research 5, 1095–1111 (2002)
4. Zha, X.: Neuro-Fuzzy Comprehensive Assemblability and Assembly Sequence Evaluation. Artificial Intelligence for Eng. Design, Analysis, and Manufacturing 5, 367–384 (2001)
5. Zha, X.: A Knowledge Intensive Multi-Agent Framework for Cooperative/Collaborative Design Modeling and Decision Support of Assemblies. Knowledge-Based Systems 8, 493–506 (2002)
6. LeBacq, C., Brechet, Y., Shercliff, H., Jeggy, T., Salvo, L.: Selection of Joining Methods in Mechanical Design. Materials and Design 23, 405–416 (2002)
7. Horvitz, E., Breese, J., Heckerman, D., Hovel, D., Rommelse, K.: The Lumiere Project - Bayesian User Modeling for Inferring the Goals and Needs of Software Users. In: Proc. 14th Conf. Uncertainty in Artificial Intelligence, pp. 256–265 (1998)
8. Long, W.: Medical Diagnosis Using a Probabilistic Causal Network. Applied Artificial Intelligence 2(3), 367–383 (1989)
9. Skaanning, C., Jensen, F., Kjaerulff, U.: Printer Troubleshooting Using Bayesian Networks. In: Logananthara, R., Palm, G., Ali, M. (eds.) IEA/AIE 2000. LNCS (LNAI), vol. 1821, pp. 367–379. Springer, Heidelberg (2000)
10. Tang, A., Nicholson, A., Jin, Y., Han, J.: Using Bayesian Belief Networks for Change Impact Analysis in Architecture Design. To appear in J. Systems and Software, DOI: 10.1016/j.jss.2006.04.004
11. Axelrod, R.: Structure of Decision - The Cognitive Maps of Political Elites. Princeton Univ. Press, Princeton (1976)
12. Kosko, B.: Fuzzy Cognitive Maps. Int. J. Man-Machine Studies 1, 65–75 (1986)
13. Nadkarni, S., Shenoy, P.: A Causal Mapping Approach to Constructing Bayesian Networks. Decision Support Systems 2, 259–281 (2004)
14. Hugin Expert A/S: How to Get Started with Hugin Software (2006) URL: http://www.hugin.com/Products_Services/Products/Demo/Lite/

Evaluation of Two Simultaneous Continuous Speech Recognition with ICA BSS and MFT-Based ASR

Ryu Takeda, Shun'ichi Yamamoto, Kazunori Komatani, Tetsuya Ogata, and Hiroshi G. Okuno

Graduate School of Informatics, Kyoto University, Japan
{rtakeda, shunichi, komatani, ogata, okuno}@kuis.kyoto-u.ac.jp

Abstract. An adaptation of independent component analysis (ICA) and missing feature theory (MFT)-based ASR for two simultaneous continuous speech recognition is described. We have reported on the utility of a system with isolated word recognition, but the performance of the MFT-based ASR is affected by the configuration, such as an acoustic model. The system needs to be evaluated under a more general condition. It first separates the sound sources using ICA. Then, spectral distortion in the separated sounds is estimated to generate missing feature masks (MFMs). Finally, the separated sounds are recognized by MFT-based ASR. We estimate spectral distortion in the temporal-frequency domain in terms of feature vectors, and we generate MFMs. We tested an isolated word and the continuous speech recognition with a cepstral and spectral feature. The resulting system outperformed the baseline robot audition system by 13 and 6 points respectively on the spectral features.

1 Introduction

Robot audition systems need to be able to separate speech and recognize the separated speech signals because they "hear" a mixture of sounds in the real world. We proposed integrating independent component analysis (ICA) and missing feature theory (MFT)-based automatic speech recognition (ASR) [1], to achive a robot audition system that does not assume any constraints on the surrounding environment.

ICA only assumes mutual independence of component sound signals and does not need *a priori* information about such things as head-related transfer functions of robots. Because the mixture of sounds can never be completely separated by ICA or other technologies, post-processing of imperfectly separated or distorted signals is necessary. MFT-based ASRs only need an acoustic model to cope with the distortion of separated signals unlike multi-condition training methods, and they recognize the signal based on its reliability. We estimated the distortion by focusing on the amount of change in the features with noise by using separated signals.

Some researchers have previously integrated speech separation and missing data techniques. Kolossa et al. integrated ICA and time-frequency masking and

H.G. Okuno and M. Ali (Eds.): IEA/AIE 2007, LNAI 4570, pp. 384–394, 2007.

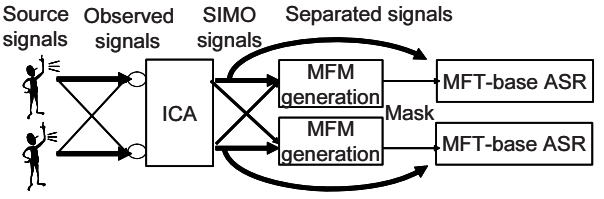

Fig. 1. Outline of our system

missing data techniques using a Mel-frequency cepastral coefficient (MFCC) feature [2]. Yamamoto et al. generated a time-frequency mask by using estimated noises from a post filter [3]. Kalle et al. reported that combining the MFCC and spectrum features is effective for reverberant speech [4]. Because missing data techniques are affected by the method used for signal separation, feature, the acoustic model, and the method for implementing MFT with ASR, we needed to validate our method under various conditions. Therefore, we tested our method with isolated word and continuous speech recognition and with spectral and cepstral features.

The rest of this paper is organized as follows: Section 2 explains the ICA and the MFT-based ASR. Section 3 presents how missing feature masks (MFMs) can be automatically generated. Section 4 describes the experiments, Section 5 shows the results, and Section 6 concludes the paper.

2 Speech Separation and Speech Recognition

The overview of our system is shown in Fig. 1. We selected ICA for speech separation because it offers blind source separation and is useful in various environments with MFT-based ASR.

2.1 Speech Separation: ICA

ICA needs no information other than the independence of sound. We used the frequency domain representation instead of the temporal domain one because ICA converges faster in the frequency domain.

Mixing Process for Speech Signals. We assumed that the signals would be observed by linearly mixing sound sources. This mixing process is expressed as

$$\boldsymbol{x}(t) = \sum_{n=0}^{N-1} \boldsymbol{a}(n)\boldsymbol{s}(t-n), \tag{1}$$

where $\boldsymbol{x}(t) = [x_1(t), \ldots, x_J(t)]^T$ is the observed signal vector, and $\boldsymbol{s}(t) = [s_1(t), ..., s_I(t)]^T$ is the source signal vector. In addition, $\boldsymbol{a}(n) = [a_{ji}(n)]_{ji}$ is the mixing filter matrix of length N, where $[X]_{ji}$ denotes a matrix that includes the element X in the i-th row and the j-th column. We assume both the number of microphones, J, and the number of sound sources, I, are 2.

Frequency-Domain ICA. We used frequency-domain (FD)-ICA. First, a short-time analysis of the signal we observed was conducted with a frame-by-frame discrete Fourier transform (DFT) to obtain the observed vector, $\boldsymbol{X}(\omega, f) = [X_1(\omega, f), \ldots, X_J(\omega, f)]$ in each frequency bin, ω, and at each frame, f. The unmixing process can be formulated in a frequency bin as

$$\boldsymbol{Y}(\omega, f) = \boldsymbol{W}(\omega)\boldsymbol{X}(\omega, f), \tag{2}$$

where $\boldsymbol{Y}(\omega, f) = [Y_1(\omega, f), \ldots, Y_I(\omega, f)]$ is the estimated source signal vector, and $\boldsymbol{W}$ represents a (2 by 2) unmixing matrix in a frequency bin.

An algorithm based on the minimization of Kullback-Leibler divergence is often used on speech signals for estimating the unmixing matrix, $\boldsymbol{W}(\omega)$, in Eq. (2). Therefore, we used the following iterative equation with non-holonomic constraints [5].

$$\boldsymbol{W}^{j+1}(\omega) = \boldsymbol{W}^{j}(\omega) - \alpha\{\text{off-diag}\langle\boldsymbol{\phi}(\boldsymbol{Y})\boldsymbol{Y}^{h}\rangle\}\boldsymbol{W}^{j}(\omega), \tag{3}$$

where α is a step-size parameter that controls the speed of convergence, j expresses the value of the j th step in the iteration, and $\langle\cdot\rangle$ denotes the time-averaging operator. The operation, off-diag($\boldsymbol{X}$), replaces each diagonal element of matrix X with zero. The nonlinear function, $\boldsymbol{\phi}(\boldsymbol{y})$, is defined as $\phi(y_i) = \tanh(|y_i|)e^{j\theta(y)}$ [6].

The problems of FD-ICA are ambiguities with scaling and permutation. We solved these with Murata's method, i.e., by using the envelope of a power spectrum [7].

2.2 Speech Recognition Based on Missing Feature Theory

The following two points are very important when we use MFT-based ASR because they are part of the main processing of speech recognition.

1. Features of speech recognition
2. Calculation of likelihood with reliability

Features of MFT-Based ASR. The spectral feature, Mel scale log spectrum (MSLS), is used as the main feature in MFT-based speech recognition because the MFCC is unsuitable for identifying distorted features. We used MSLS (24 + Δ24) by applying an inverse discrete cosine transform (DCT) to the MFCC features.

Calculation of Likelihood with Reliability. MFT-based ASR is a hidden Markov model (HMM)-based recognizer that assumes input consists of reliable and unreliable spectral features. We used the multi-band approach [8] which is a the marginalization approach that takes into account the reliability of the feature in calculating the likelihood.

Let $M(i)$ be an MFM vector, which represents the reliability of the i-th acoustic feature. The output probability, $b_j(x)$, is given by

$$b_j(x) = \sum_{l=1}^{L} P(l|S_j) \exp\left(\sum_{i=1}^{N} M(i) \log f(x(i)|l, S_j)\right), \tag{4}$$

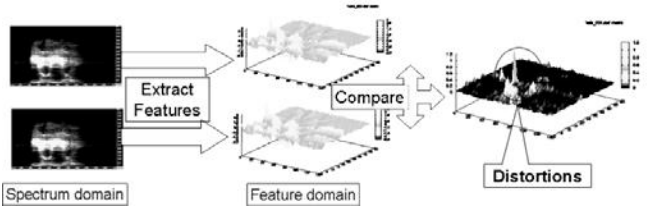

Fig. 2. Detection of distortion in MSLS

where $P(\cdot)$ is a probability operator, $x(i)$ is an acoustic feature vector, N is the size of the acoustic feature vector, S_j is the j th state, and $f(x_j|S_j)$ is a mixture of L multivariate Gaussians in the j th state. In the marginalization approach [9], the output probability is calculated based on using knowledge about unreliable features. If knowledge about unreliable features is unavailable, the output probability equation is equivalent to Eq. (4).

3 Automatic Generation of Missing Feature Mask

The following three steps are needed to generate the missing feature mask.

1. Detection of the distortion in the feature domain
2. Setting of the reliability in accordance with the distortion
3. Generation of the MFM from the separated signals

3.1 Detection of Distortion

Distortion in the Feature Domain. Features for speech recognition should be irrelevant to scaling because they are affected by the volume of the speakers without it. First, we define the mapping of the vector feature-extraction function, $\boldsymbol{F}$, from the time-frequency spectrum for the time-dimension feature. Here, we assume $\boldsymbol{F}$ is continuous and continuously differentiable.

A feature with the scaling-free property satisfies the equation

$$\boldsymbol{F}(\boldsymbol{x}) = \boldsymbol{F}(\boldsymbol{\alpha} .* \boldsymbol{x}), \tag{5}$$

where $.*$ denotes the product of the corresponding element of the vectors, $\boldsymbol{x} \cdot \boldsymbol{y} = (x_0 y_0,$
$x_1 y_1, \ldots, x_n y_n)$. We now focus on the target signal, $\boldsymbol{s}$, in the mixture signal, $\boldsymbol{\alpha x} + \boldsymbol{\beta y}$, and express its feature as

$$\boldsymbol{F}(\boldsymbol{\alpha x} + \boldsymbol{\beta y}) = \boldsymbol{F}(\boldsymbol{x} + (\boldsymbol{\beta} ./ \boldsymbol{\alpha})\boldsymbol{y}) = \boldsymbol{F}(\boldsymbol{x} + \boldsymbol{\theta} .* \boldsymbol{y}). \tag{6}$$

We define the distortion of the feature of the signal and noise together, $\boldsymbol{s} + \boldsymbol{n}$, as

$$\boldsymbol{D} = \boldsymbol{F}(\boldsymbol{s} + \boldsymbol{n}) - \boldsymbol{F}(\boldsymbol{s}) \tag{7}$$

Detection of the Distortion. We suppose the feature changes almost completely monotonically with the noise. In particular, the feature has linearity, and the distortions in the feature are proportional to the difference in the distortions represented by the following equation.

$$\boldsymbol{D} = \boldsymbol{F}(\boldsymbol{s} + \theta\boldsymbol{n}) - \boldsymbol{F}(\boldsymbol{s}) \simeq \theta\frac{\partial \boldsymbol{F}}{\partial \boldsymbol{s}}(\boldsymbol{s})\boldsymbol{n}. \tag{8}$$

Then, if we have two features, $\boldsymbol{F}(\boldsymbol{s} + \boldsymbol{\alpha} .* \boldsymbol{n})$ and $\boldsymbol{F}(\boldsymbol{s} + \boldsymbol{\beta} .* \boldsymbol{n})$, and the ratio between $\boldsymbol{\alpha}$ and $\boldsymbol{\beta}$ is a constant, γ, we can detect the distortions by predictinging the ambiguity of the scaling based on the following approximation.

$$\begin{aligned}\boldsymbol{D} &\simeq \boldsymbol{F}(\boldsymbol{s} + \boldsymbol{\alpha} .* \boldsymbol{n}) - \boldsymbol{F}(\boldsymbol{s} + \boldsymbol{\beta} .* \boldsymbol{n}) \\ &\simeq \boldsymbol{F}(\boldsymbol{s} + \boldsymbol{\alpha} .* \boldsymbol{n}) - \boldsymbol{F}(\boldsymbol{s} + \gamma\boldsymbol{\alpha} .* \boldsymbol{n}) \simeq \gamma\frac{\partial \boldsymbol{F}}{\partial \boldsymbol{s}}(\boldsymbol{s})\boldsymbol{\alpha} .* \boldsymbol{n}.\end{aligned} \tag{9}$$

3.2 Setting the Reliability

The mask to the distortion, $\boldsymbol{D}$, is generated from the following approximation,

$$\boldsymbol{D} \simeq \left|\boldsymbol{F}(\boldsymbol{s} + \boldsymbol{\alpha} .* \boldsymbol{n}) - \boldsymbol{F}(\boldsymbol{s} + \boldsymbol{\beta} .* \boldsymbol{n})\right|. \tag{10}$$

For this distortion, we generate an MFM, M, with a threshold, T_n, as follows:

$$\boldsymbol{M} = \begin{cases} 1 \ |\boldsymbol{F}(\boldsymbol{s} + \boldsymbol{\alpha} .* \boldsymbol{n}) - \boldsymbol{F}(\boldsymbol{s} + \boldsymbol{\beta} .* \boldsymbol{n})| < T_n \\ 0 \ otherwise \end{cases}, \tag{11}$$

where T_n is the threshold for the n-delta feature.

MFM Generation from Signals Separated by ICA. ICA gives the following separated signals.

$$\boldsymbol{Y}(\omega, t) = \boldsymbol{S}(\omega, t) + \boldsymbol{W}(\omega)\boldsymbol{E}(\omega)\boldsymbol{S}(\omega, t). \tag{12}$$

Here, $\boldsymbol{W}$ is the estimated unmixing matrix, $\boldsymbol{E}$ is an error matrix derived from $\boldsymbol{E} = \boldsymbol{H} - \boldsymbol{W}^{-1}$, and $\boldsymbol{H}$ is a true mixing matrix. Because the estimation of the unmixing matrix is not perfect, error terms invariably exist. We use signals that are scaled to solve the problem of ambiguity in scaling. The scaled signal, $y_1(\omega, t)$, with g_1 is expressed as

$$g_1 y_1(\omega, t) = g_1\left((1 - w_{11}e_{11} - w_{12}e_{21})s_1(\omega, t) - (w_{11}e_{12} + w_{12}e_{22})s_2(\omega, t)\right) \tag{13}$$

$$= g_1\left(1 + e_1\right)s_1(\omega, t) - \hat{e}_1 g_1 s_2(\omega, t), \tag{14}$$

where e_1 and $\hat{e}_1$ are error coefficients. We obtain $y_2(\omega, t)$ the same way. By calculating the following equation, we can get two signal and detect distortions from Eq. (9).

$$\hat{y}_1(\omega, t) = g_1 y_1(\omega, t) - \gamma g_2 y_2(\omega, t). \tag{15}$$

Fig. 3. Humanoid SIG2 and its ear

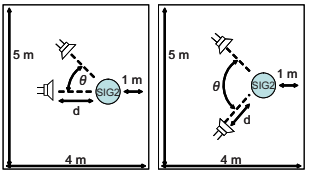

Fig. 4. Configurations: symmetric and asymmetric positions

Table 1. Experimental conditions

@	Experiment 1	Experiment 2
Test Set	Male and Female (200 words)	Male and Female (100 sent.)
Training Set	10 Males, 12 Females, 216 words	100 Males, 100 Females, 150 sent.
Acoustic Model	Triphone: 3-state 4-mix. HMM	Triphone: 3-state 8-mix. HMM
Language Model	Finite Grammar: 200 words	Statistical Language: 20,000 words

4 Experiments

We used two omni-directional microphones installed as ears in the SIG2 humanoid robot (Fig. 3). We evaluated our method by getting the robot to recognize two simultaneous speech signals based on the following criteria.

1. Experiment 1: Isolated word recognition
   (a) The relation between parameters γ and T_0
   (b) The effect of ICA and MFM on Word Correct (WC)
   (c) The difference between MSLS and MFCC
2. Experiment 2: Continuous speech recognition
   (a) The effect of ICA and MFM on WC and Word Accuracy (WA)
   (b) The difference between MSLS and MFCC

Isolated word recognition is an evaluation for practical use, and continuous speech recognition is an evaluation under a general condition. In these experiments, we determined (1) the relation between the two parameters, (2) the effect of ICA and MFM on WC and WA, and (3) the difference between MSLS and MFCC.

4.1 Recording Conditions

Two voices, one male and one female, were recorded simultaneously from loudspeakers placed 1.0 m from the robot, as shown in Fig. 4. Asymmetric and symmetric configurations were used because ICA-based separation is affected by the positions of the speakers. The angle, θ, between the two loudspeakers was 30, 60, or 90°. The female speaker was to the left of the robot, and the male was to the right. The room we used is 4×5 m, and has a reverberation time of 0.2–0.3 sec.

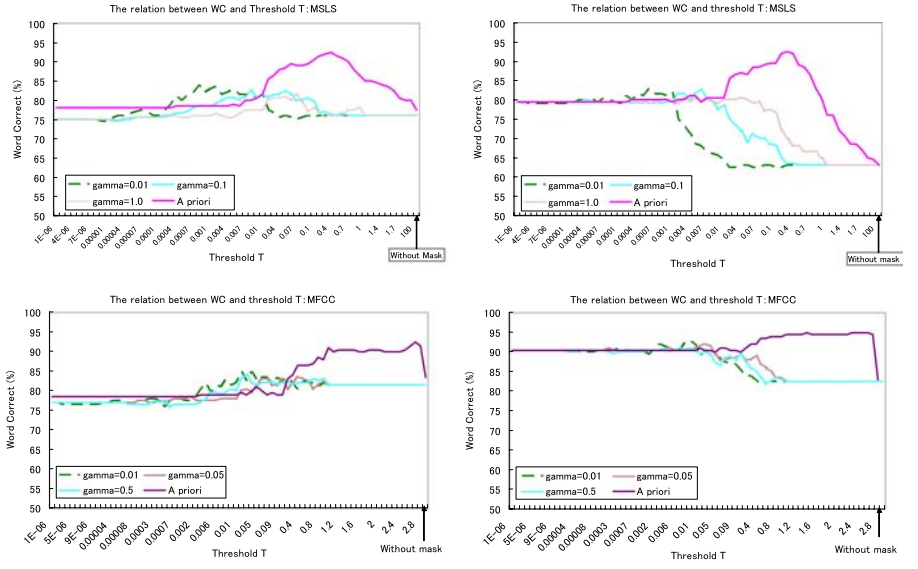

Fig. 5. Change in WC with TFasymmetric position at 60 degrees, left: male, right: female, up: MSLS, down: MFCC

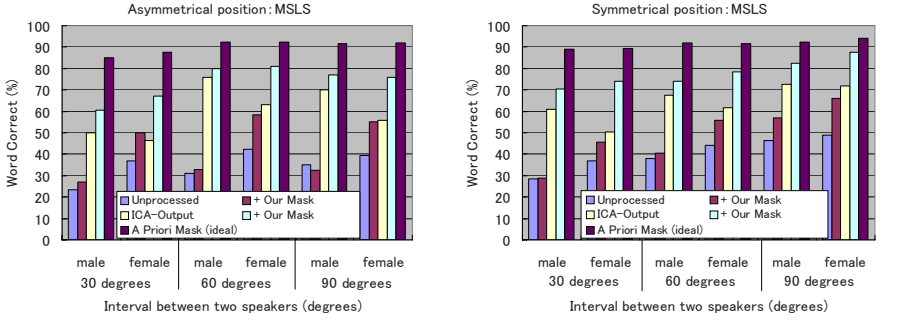

Fig. 6. WC of isolated word recognition: MSLS

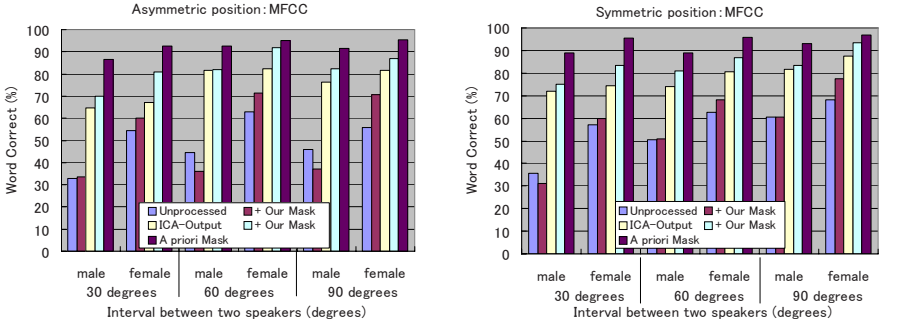

Fig. 7. WC of isolated word recognition: MFCC

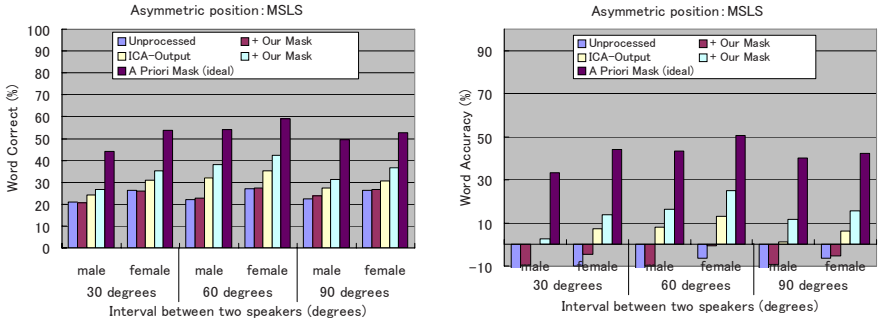

Fig. 8. WA and WC at asymmetric position: MSLS

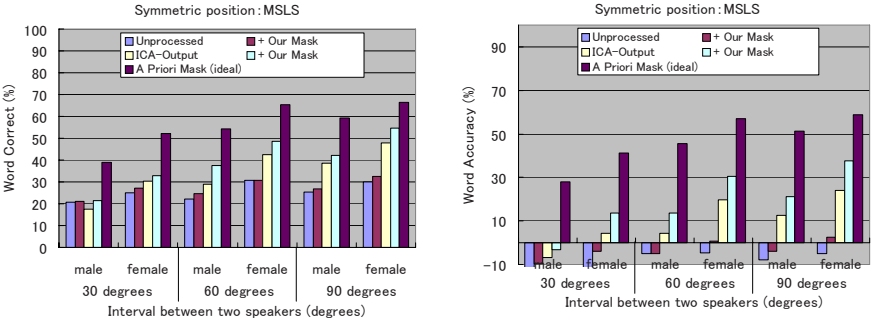

Fig. 9. WA and WC at symmetric position: MSLS

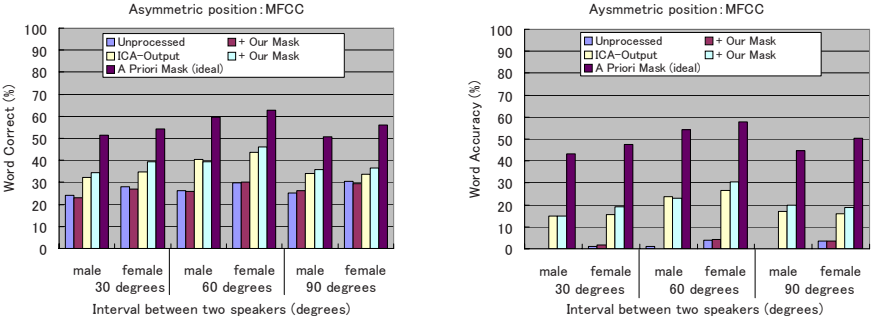

Fig. 10. WA and WC at asymmetric position: MFCC

We used combinations of two different words selected from a set of 200 phonemically balanced Japanese words for Exp. 1, and we used two different sentences selected from a set of 100 newspaper articles and 50 phonemically balanced Japanese sentences for Exp. 2.

4.2 Experimental Conditions

We used a multi-band Julian [8] as the MFT-based ASR. It uses a triphone-based acoustic model (3-state, 4-mixture) trained with 216 words of clean speech uttered by 22 male and female speakers for Exp. 1, and a triphone (3-state, 8-mixture) trained with 150 sentences clean speech uttered by 200 male and female speakers for Exp. 2. These training data sets do not include the data for the evaluation (open test). The number of HMM mixtures is different for Exp. 1 and Exp. 2, but this is not important for the purpose of these experiments. The statistical language model was used for Exp. 2, and it consists of 20,000 words, which were extracted from newspapers. Table 1 lists these conditions.

The main conditions for ICA are a data-sampling rate of 16 kHz, a frame length of 2,048 points, and a frame shift of 512 points. After separating the signals in the frequency domain, we converted them to those in the time domain with the overlap-add method and extract the features because the best frame length is different for separation and feature extraction. The initial values for the unmixing matrix, $\boldsymbol{W}(\omega)$, were given at random. We used 0.005 for Exp. 1 and 0.02 for Exp. 2 with MSLS and 0.01 for Exp. 1 and 0.2 for Exp. 2 with MFCC. We did not mask the delta parameters.

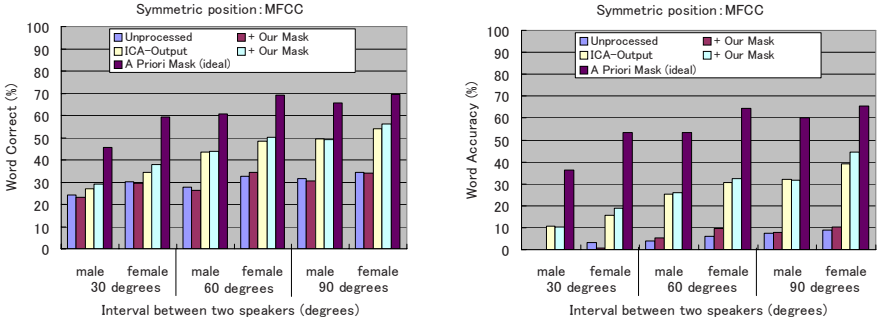

Fig. 11. WA and WC at symmetric position: MFCC

5 Results

5.1 Isolated Word Recognition

Figure 5 shows the relation between the threshold, T, and the scaling factor, γ. The curve of an *a priori* mask is a convex function because if the threshold is too low, few of the features are used for recognition, and if the threshold is too high, the features include distorted ones.

Figures 6 and 7 show the average improvement in the recognition, 24 points for the ICA and 13.3 points for the MFM with the MSLS, and with the MFCC, 24 points for the ICA and 6.2 points for the MFM. Clearly, We can see the MFM is effective when used after ICA by 8.2 points on average. If an *a priori*

mask is adapted, the WC was improved by over 90%. With the MFM, the MSLS performs as well as the MFCC. In terms of absolute WC, MFCC + MFM is the best combination in Exp. 1.

5.2 Continuous Speech Recognition

Figures 8, 9, 10, and 11 show the results of each feature. ICA improved 11.0 point with the MSLS and 17.23 point with the MFCC, and the MFM improved 8.68 points and 1.89 points with the MSLS and the MFCC on average.

In this experiment, the MFCC mask was not effective, unlike in the experimentt on isolated-word recognition. An *a priori* mask works well, but it is not sufficient compared with an limit of 80% WA. The difference in WC and WA between the auto-generated and *a priori* masks is very large. Therefore, generating an effective MFM under general conditions is difficult.

6 Conclusion

We integrated ICA and MFT-based ASR and generated an automatic MFM. The average word accuracy achieved with MFT-based ASR improved about 13 points for isolated word recognition and 5 points for continuous speech recognition.

In the isolated word recognition, the automatically generated MFM for both the MSLS and the MFCC worked well, but even *a priori* mask did not work well in the continuous speech recognition. Because the large size of vocabulary means that the number of classes that should be recognized is very large, the possibility of false recognition caused by erros in the mask increases. In addition, since continuous speech recognition uses language constraints, we should also take into account this information in MFM generation. A more robust estimation of MFM and an improved MFT-based ASR are required for further investigation of the feature for speech recognition.

In future work, we will generate generate more effective MFMs by adapting the distortion to the target speaker, and determining the best features for speech recognition.

References

1. Takeda, R., Yamamoto, S., Komatani, K., Ogata, T., Okuno, H.G.: Improving speech recognition of two simultaneous speech signals by integrating ica bss and automatic missing feature mask generation. In: Proceedings of International Conference on Spoken Language Processing (2006)
2. Kolossa, D., Klimas, A., Orglmeister, R.: Separation and robust recognition of noisy, convolutive speech mixtures using time-frequency masking and missing data techniques. In: IEEE Workshop on Applications of Signal Processing to Audio and Acoustics, pp. 82–85 (2005)
3. Yamamoto, S., Valin, J.-M., Nakadai, K., Rouat, J., Michaud, F., Ogata, T., Okuno, H.G.: Enhanced robot speech recognition based on microphone array source separation and missing feature theory. In: Proceedings of IEEE International Conference on Intelligent Robots and Systems (2005)

4. Palomaki, K.J., Brown, G.J., Barker, J.P.: Recognition of reverberant speech using full cepstral features and spectral missing data. In: Proceedings of International Conference on Acoustics, Speech and Signal Processing, pp. 289–292 (2006)
5. Choi, S., Amari, S., Cichocki, A., Liu, R.: Natural gradient learning with a nonholonomic constraint for blind deconvolution of multiple channels. In: Proceeding of International Workshop on ICA and BBS, pp. 371–376 (1999)
6. Sawada, H., Mukai, R., Araki, S., Makino, S.: Polar coordinate based nonlinear function for frequency-domain blind source separation. IEICE Trans. Fundamentals E86-A (3), 505–510 (2003)
7. Murata, N., Ikeda, S., Ziehe, A.: An approach to blind source separation based on temporal structure of speech signals. Neurocomputing 1–24 (2001)
8. Nishimura, Y., Shinozaki, T., Iwano, K., Furui, S.: Noise-robust speech recognition using multi-band spectral features. In: Proc. of 148th Acoustical Society of America Meetings (2004)
9. Cooke, M., Green, P., Josifovski, L., Vizinho, A.: Robust automatic speech recognition with missing and unreliable acoustic data. In: Speech Communication, vol. 34(3)

Knowledge Based Discovery in Systems Biology Using CF-Induction

Andrei Doncescu[1,3], Katsumi Inoue[1,2], and Yoshitaka Yamamoto[2]

[1] National Institute of Informatics
2-1-2 Hitotsubashi, Chiyoda-ku, Tokyo 101-8430, Japan
adoncesc@nii.ac.jp
[2] Department of Informatics, Graduate University for Advanced Studies
2-1-2 Hitotsubashi, Chiyoda-ku, Tokyo 101-8430, Japan
ki@nii.ac.jp
[3] LAAS-CNRS 31007 Toulouse, France
yy@grad.nii.ac.jp

Abstract. The cell is an entity composed of several thousand types of interacting proteins. Our goal is to comprehend the biological system using only the revelent information which means that we will be able to reduce or to indicate the main metabolites necessary to measure. In this paper, it is shown how the Artificial Intelligence description method functioning on the basis of Inductive Logic Programming can be used successfully to describe essential aspects of cellular regulation. The results obtained shows that the ILP tool CF-induction discovers the activities of enzymes on glycolyse metabolic pathway when only partial information about it has been used. This procedure is based on the filtering of the high processes to reduce the space search.

1 Introduction

Since the days of Norbert Wiener, the understanding of the systems at different levels has been a recurrent theme in biological science. The main interest to restart this kind of approach is due to the progress in molecular biology, particularly in genome sequencing. That was not possible in the days of Wiener when the molecular biology was an emerging field of research. Today's advances in measurement, data acquisition and handling technologies provide a wealth of new data which can be used to improve existing models. Four properties give an insight into the understanding of a biological system:

1. System structure: network of gene expression and biochemical pathway
2. System dynamics: the behavior of the system over the time
3. The control method: minimize the one of desired function of the cells
4. The design method: strategy to modify and construct biological systems having desired properties by finding the optimum conditions of cells development

H.G. Okuno and M. Ali (Eds.): IEA/AIE 2007, LNAI 4570, pp. 395–404, 2007.

The biological system studies in this article is the yeast *Saccharomyces Cerevisiae*. Yeast is one of the smallest eukaryotic systems sequenced that is unparallel for the level of molecular investigations accumulated and range of possible manipulations. It is an ideal target for comprehensive study at system-level.

2 Metabolic Pathways

Neuberg and his proposed scheme was the first researcher which introduced the notion of biochemical pathway [12]. But, it was far to be perfect. The boom of the fermentation is due to the discover of penicillin in the early 1940. With the application of continuous culture techniques, it became possible to study metabolism at defined physiological states. The cellular metabolism is defined as the huge set of biochemical reactions that occurs inside the living cell for growth and reproduction.

In aerobic glucose-limited continuous cultures of *S. cerevisiae*, two distinct metabolic regimes are observed. At low dilution rate, which at steady state is equal to the specific growth rate, purely respiratory growth is observed. At a certain dilution rate, the critical dilution rate, aerobic fermentation sets in, and the metabolism is respiro-fermentative above this dilution rate. During respiratory growth the specific rate of CO2 production (rCO2) and O2 consumption (rO2) increase linearly with dilution rate and the respiratory quotient (RQ) is close to unity. Above the critical dilution rate, where the metabolism is respiro-fermentative, rCO2 increases sharply, whereas rO2 is constant or decreases and RQ is greater than one [12]. In this paper we investigate the metabolic pathway corresponding to the metabolism respiro-fermentative.

In yeast fed-batch production is very important to recognize the physiological state of the micro-organism since reflects the activity of growth and ethanol production. The physiological states which could be identified on-line are :

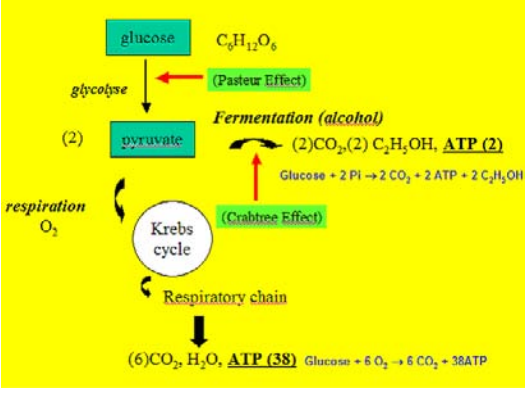

Fig. 1. Metabolic Pathways

oxidation, fermentation and the growth on two carbonate substrates glucose and ethanol.

In the same time it is possible to trig the conditions unknown by the biologists which product a metabolite. This is possible in fed-batch productions due to the grate number of PID regulators involves in the control of: pH, temperature, oxygen.

The main regulatory effects present inside the yeast are:

1. The Pasteur Effect: suppression of fermentative activity by respiration
2. The Crabtree effect: saturation of the respiratory system under excess of oxygen and sugar
3. The Glucose Effect: repression of uptake system at high concentration of glucose, which could be considered a particular case of Crabtree Effect.

The Glucose Effect is studied in this paper using a logic description of the Metabolic Pathway Activity. In literature are different approaches for example Metabolic Flux Balancing. Metabolic Flux Balancing is one of the first approaches to determine the intracellular fluxes based on the measures of the extracellular fluxes. In fact it is necessary to measure the consummation of the substrate, the new products obtained like biomass and gas exchanges. However, this technique is not sufficient to determine all the intracellular fluxes of central metabolism without adding assumptions about the enzymatic activity and energetically yields which limit the validity of the results.

The emerging field of data mining has recently attracted significant attention in metabolic analysis. This approach is interesting to determinate the metabolites tendencies but for the optimization of the system it is not suitable.

3 Inductive Logic Programming: Background

An ILP system aims to output a rule that covers (entails) a set of positive observation or examples and does not cover a set of negative examples. In essence, ILP tries to synthesize a logic program, given background knowledge and examples which are described using logical clauses.

A *clause* is a disjunction of literals, and is often denoted by the set of its disjuncts. A clause $\{A_1, \ldots, A_m, \neg B_1, \ldots, \neg B_n\}$, where each A_i, B_j is an atom, is also written as $B_1 \wedge \cdots \wedge B_n \supset A_1 \vee \cdots \vee A_m$. Any variable in a clause is assumed to be universally quantified at the front. A *definite clause* is a clause which contains only one positive literal. A *positive* (*negative*) *clause* is a clause whose disjuncts are all positive (negative) literals. A negative clause is often called an *integrity constraint*. A *Horn clause* is a definite clause or negative clause; otherwise it is *non-Horn*. The *length* of a clause is the number of literals it contains. A *unit clause* is a clause with the length 1. A *clausal theory* is a finite set of clauses. A clausal theory is *full* if it contains non-Horn clauses. On the other hand, a *Horn program* is a clausal theory containing Horn clauses only.

Let B, E, and H be clausal theories, representing a *background theory*, *(positive) examples*, and a *hypothesis*, respectively. The most popular formalization

of ILP is *learning from entailment* (or *explanatory induction*), in which the task is: given B and E, find H such that $B \wedge H \models E$ and $B \wedge H$ is consistent. On the other hand, in the case of *abduction*, E and H are usually called *observations* and an *explanation*, respectively, for the same task as induction.

4 Integrating Induction and Abduction in CF-Induction

Both *induction* and *abduction* are ampliative reasoning, and agree with the logic to seek hypotheses which account for given observations or examples. That is, given a background theory B and observations (or positive examples) E, the task of induction and abduction is common in finding a hypothesis H such that

$$B \wedge H \models E, \tag{1}$$

where $B \wedge H$ is consistent. There are several discussions on the difference between abduction and induction in the philosophical and pragmatic levels. On the computational side, induction usually involves *generalization*, while abduction gives *minimal explanations* for individual observation.

Inverse entailment (IE) is a logically principled way to compute abductive and inductive hypotheses H in (1) based on the logically equivalent transformation of the equation (1) to

$$B \wedge \neg E \models \neg H. \tag{2}$$

The equation (2) says that, given B and E, any hypothesis H *deductively* follows from $B \wedge \neg E$ in its negated form. The equation (2) is seen in literature, e.g., [4] for abduction and [8] for induction. The equation (2) is useful for computing abductive explanations of observations in abduction. This is because, without loss of generality, in abduction E is written as a ground atom, and each H is usually assumed to be a conjunction of literals. These conditions make abductive computation relatively easy, and *consequence-finding* algorithms [4] can be directly applied.

In induction, however, E can be clauses and H is usually a general rule. Universally quantified rules for H cannot be easily obtained from the negation of consequences of $B \wedge \neg E$. Then, Muggleton [8] introduced a *bridge formula* U between $B \wedge \neg E$ and $\neg H$:

$$B \wedge \neg E \models U, \quad U \models \neg H.$$

As such a bridge formula U, Muggleton considers the conjunction of all unit clauses that are entailed by $B \wedge \neg E$. In this case, $\neg U$ is a clause called the *bottom clause* $\bot(B, E)$. A hypothesis H is then constructed by generalizing a sub-clause of $\bot(B, E)$, i.e., $H \models \bot(B, E)$. This method with $\bot(B, E)$ is adopted in Progol, but it has turned out that it is incomplete for finding hypotheses satisfying (1).

In [5], Inoue proposed a simple, yet powerful method to handle inverse entailment (2) for computing inductive hypotheses. The resulting method called *CF-induction* does not restrict the bridge formula U as the set of literals entailed

by $B \wedge \neg E$, but consider the *characteristic clauses* [4] of $B \wedge \neg E$, which obviously generalizes the method of the bottom clause. CF-induction then realizes sound and complete hypothesis finding from *full clausal theories*, and not only definite clauses but also non-Horn clauses and integrity constraints can be constructed as H.

In most previous inductive methods including Progol [8], there are syntactical restrictions such that: (i) each constructed hypothesis in H is usually assumed to be a single Horn clause, (ii) an example E is given as a single Horn clause, and (iii) a background theory B is a set of Horn or definite clauses. From the viewpoint of applications, these restrictions are due to the easiness for handling such formulas. An extension to multiple non-Horn clauses in B, E, and H is, however, useful in many applications.

First, an extension allowing *multiple clauses* in either a hypothesis H or an observation E is essential in applications of abduction. In fact, recent work on abductive inference in metabolic pathways [13] uses an independent abductive procedure to obtain a set of literals that explain an observation. In general, there are multiple missing data to account for an observation. This abductive inference is independently computed in [13] not by Progol, and the inductive process for generalization takes place by Progol only after abductive hypotheses have been obtained. On the other hand, CF-induction can be used to compute abductive explanations simply by taking the bridge formula U as a deduced clause. CF-induction thus integrates induction and abduction from the viewpoint of inverse entailment through consequence-finding [5].

Second, an extension to *non-Horn clauses* in representation of B, E, H is also useful in many applications. For example, indefinite statements can be represented by disjunctions with more than one positive literals, and integrity constraints are usually represented as negative clauses. The clausal form is also useful to represent causality. For example, when we want to represent *inhibition* of reaction in a causal pathway network, positive and negative literals with the predicate like `inhibited` can be used in the premise of each causal rule, which results in a non-Horn clause (we will see an example afterwards). Again, the inductive machinery of CF-induction can handle all such extended classes.

Third, introducing *multiple, non-Horn clauses* in a hypothesis H is an unifying extension that combines the first and second extensions. In this case, a hypothesis H forms a *theory*, which can also account for multiple observed data at once. In our application to metabolic pathways, given the background theory of network structures of a pathway and observations, we need a hypothesis H that explains the behavior of the metabolic system. In principle, such a hypothesis consists of multiple non-Horn clauses each of which represents a causal relation. CF-induction is thus particularly useful for this type of applications.

Here the structure of representation is based on the specification of CF-induction program, which is compatible with the consequence-finding program SOLAR [10] and the TPTP format for theorem proving. SOLAR is a Java implementation of the tableaux variant of SOL resolution [4].

For example, the input clauses can be described as

```
input_clause(axiom1,    bg, [-p(X), -q(X), r(X)]).
input_clause(example1, obs, [r(a)]).
production_field([predicates(pos_all), length < 3]).
```

Here, `axiom1` and `example1` are ID names of clauses, and `bg` and `obs` represent background knowledge and observation, respectively. The axiom1 means $\rceil p(x) \vee \rceil q(x) \vee r(x)$. Each clause is represented as a list of literals. The predicate `production_field` indicates the *production field* of SOLAR, and this example allows it to generate consequences consisting of less than 2 positive literals. In this way, a production field can be used to specify an *inductive bias* in CF-induction. There is other meta information to control deduction in SOLAR such as the search strategy and the depth limit.In this case, CF-induction produces the abductive hypothesis:

```
Hypotheses: [ [p(a)], [q(a)] ]
```

The current CF-induction program has several *generalizers*, which, given a set T of clauses, produce a set S of clauses such that $S \models T$. These basic generalizers include *anti-instantiation*, *reverse Skolemization*, *Plotkin's least generalization*, and *dropping literals* (see [5]).

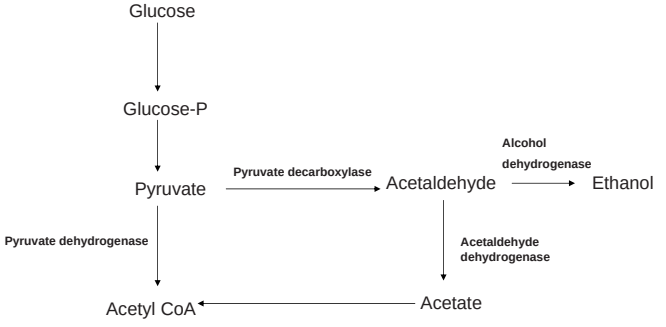

Fig. 2. Metabolic Pathways of Pyruvate

5 CF-Induction Reasoning About Metabolic Pathways

Cell activity is usually represented by an intrinsic network connecting involved biochemical species called metabolites. Pathways of the network are called metabolic pathways. We shall limit ourselves to simple metabolic pathways which are made up of sequences of mono-molecular enzyme-catalyzed reactions of the form $X_s \rightarrow X_p$, where X_s is the concentration of the substrate and X_p is the product. Those reactions can be inhibited by the presence of other metabolites in the networks.

Glycolysis is a metabolic pathway found universally in biological systems. It is the metabolic pathway which converts glucose via a series of reactions to 2

molecules of pyruvate. As a result of these reactions, a small amount of ATP and NADH are produced. Most of the metabolic energy derived from glucose comes from the entry of pyruvate into the citric acid cycle and oxidative phosphorylation. These pathways occur under aerobic conditions. Under anaerobic conditions, pyruvate can be converted to lactate in muscle or ethanol in yeast. We first explain the metabolic pathway of Pyruvate represented by Fig. 2 using logical clauses. We notice that the branch point on the level of Acetaldehyde where respiration and fermentation are in competition using the same substrate is very important.

The data from bioreactor allows us to consider that we are in a fermentation state, therefore an increasing of the ethanol concentration. In this case the input of our system is glucose and the concentrations are described by the next clauses:

```
input_clause(e1,bg,[concentration(glucose,up)]).
input_clause(e2,obs,[concentration(ethanol,up)]).
input_clause(e3,obs,[concentration(pyruvate,up)]).
```

The reactions associated with the metabolic pathway presented in the Fig. 2 are described by the next clauses :

```
input_clause(reaction1,bg,[reaction(glucose,glucosep)]).
input_clause(reaction2,bg,[reaction(glucosep,pyruvate)]).
input_clause(reaction3,bg,[reaction(pyruvate,acetaldehide)]).
input_clause(reaction4,bg,[reaction(acetaldehide,ethanol)]).
input_clause(reaction5,bg,[reaction(acetaldehide,acetate)]).
input_clause(reaction6,bg,[reaction(acetate,acetylcoa)]).
input_clause(reaction7,bg,[reaction(pyruvate,acetylcoa)]).
```

Based on biological knowledge and on our goal to discover the inhibitions in the case of ethanol production we have considered the next non-inhibition :

```
input_clause(b2,bg,[-inhibited(pyruvate,ethanol)]).
```

The clause above means that the only active pathway is from Pyruvate to Ethanol passing by the Acetaldehyde knot The causal rules that we have introduced contain the two clauses:

```
input_clause(be0,bg,[-reaction(Y,X),-reaction(X,Z),inhibited(Y,X),
-inhibited(X,Z),concentration(X,up)]).
input_clause(be0,bg,[-reaction(Y,X),-reaction(X,Z),-inhibited(Y,X),
-inhibited(X,Z),concentration(X,down)]).
```

which described from a very simpler manner the evolution of one metabolite when the reaction are inhibited or not.

Using CF-induction with the generalizer dropping we have obtained the next result.

```
B & H is consistent

Hypotheses: [
[concentration(pyruvate, up), inhibited(pyruvate,
acetylcoa), inhibited(pyruvate, acetaldehide),
-concentration(glucose, up)]

[concentration(pyruvate, up), -concentration(glucose, up)]

[concentration(pyruvate, up), -concentration(glucosep, up),
inhibited(glucose, glucosep), -concentration(glucose, up)]

[concentration(pyruvate, up), -concentration(glucosep, up),
-concentration(glucose, up)]

[concentration(pyruvate, up), inhibited(pyruvate, acetylcoa),
inhibited(pyruvate, acetaldehide), inhibited(acetaldehide, acetate),
inhibited(acetaldehide, ethanol), -concentration(glucose, up)]

[concentration(pyruvate, up), inhibited(pyruvate, acetylcoa),
inhibited(pyruvate, acetaldehide), -concentration(acetaldehide, up),
-concentration(glucose, up)]

[concentration(ethanol, up), -concentration(glucose, up)]
]
```

the time for constructing CC = 3000 ms the time for generating Hypotheses = 150125 ms (the time for operating Dropping =150109 ms) (the time for consistency-checking =16 ms) Running time(ms) = 153125 ms.

The most important result is that both reaction pyruvate-acetaldehyde and pyruvate-acetylCoA are not inhibited (activated) which confirms the biologists knowledge concerning this important knot: pyruvate. The only action which is not discover by CF-induction is between Acetyl CoA and Acetate. But, from the results concerning concentrations (Glucose-P, Pyruvate, Acetaldehyde, Ethanol) and from the experimental data concerning the production of Acetate we deduce that the pathway from Acetate to Acetyl CoA is inhibited. The last hypothesis is exactly the Crabtree effect presented in the introduction of this paper, which means that a strong concentration of pyruvate will increase the capacity of the microorganism to produce ethanol.

From a general view point these results have indicated that CF-induction discovers the qualitative level of concentrations of metabolites and the inhibitions of the pyruvate metabolic pathway.

6 Conclusion

The challenge now is to transfer and adapt the developed methodology from technical to more complex biological systems. The logical models are the most

precise representation of knowledge because they have a unique and objective interpretation and they do not permit any vague statement. In this paper, we have studied an architecture based on CF-induction for explanation of metabolic mechanisms. Given the background theory of the network structure of a pathway and observations, a set of non-Horn clauses constructed by CF-induction as a hypothesis can explain the behavior of the metabolic system. This approach is interesting to determinate not only the apparition of the inhibitions but also the prediction of the tendencies of different metabolites. The most important result is related to the pathway Pyruvate-Ethanol where the variation of the metabolite Acetaldehyde and the non-inhibitions Pyruvate-Acetaldehyde and Acetaldehyde-Pyruvate are discovered by CF-induction. At our knowledge is for the first time that an Intelligent System based on Inductive Logic Programming is able to explain the evolution of a metabolic pathway from an incomplete level of description related to essential aspects of cellular regulation.

Acknowledgement

The authors want to thank to JSPS for financing of this work and particulary to Oliver Ray for his remarks and encouragements.

References

1. Breiman, L.: Bagging predictors. Machine Learning 26, 123–140 (1996)
2. Chassagnole, C., Rodrigues, J.C., Doncescu, A., Yang, L.T.: Differential evolutionary algorithms for in vivo dynamic analysis of glycolysis and pentose phosphate pathway in Escherichia Coli. In: Zomaya, A. (ed.) Parallel Computing in Bioinformatics and Computational Biology, Jossey-Bass an imprint of Wiley Book. ISBN 0-471-71848, -3
3. Doncescu, A., Yamamoto, Y., Inoue, K.: Biological Systems Analysis using Inductive Logic Programming. In: The 2007 IEEE International Symposium on Bioinformatics and Life Science Computing BLSC07, Niagara Fall, Ontario, Canada (2007)
4. Inoue, K.: Linear resolution for consequence finding. Artificial Intelligence 56, 301–353 (1992)
5. Inoue, K.: Induction as consequence finding. Machine Learning 55, 109–135 (2004)
6. Juvan, P., Demsar, J., Shaulsky, G., Zupan, B.: GenePath: from mutation to genetic networks and back. Nucleic Acids Research 33, 749–752 (2005)
7. King, R., Whelan, K., Jones, F., Reiser, P., Bryant, C., Muggleton, S., Kell, D., Oliver, S.: Functional genomic hypothesis generation and experimentation by a robot scientist. Nature 427, 247–252 (2004)
8. Muggleton, S.: Inverse entailment and Progol. New Gen. Comput. 13, 245–862 (1995)
9. Muggleton, S., Firth, J.: CProgol4.4: a tutorial introduction. Report of Department of Computer Science, University of York
10. Nabeshima, H., Iwanuma, K., Inoue, K.: SOLAR: a consequence finding system for advanced reasoning. In: Mayer, M.C., Pirri, F. (eds.) TABLEAUX 2003. LNCS, vol. 2796, pp. 257–263. Springer, Heidelberg (2003)

11. Schugerl, K., Bellgardt, K.H. (eds.): Bioreaction Engineering: Modeling and Control. Springer, Heidelberg (2000)
12. Stephanopoulos, G., Aristidou, A., Nielsen, J.: Metabolic engineering. Academic Press, London (1998)
13. Tamaddoni-Nezhad, A., Chaleil, R., Kakas, A., Muggleton, S.: Application of abductive ILP to learning metabolic network inhibition from temporal data. Machine Learning 64, 209–230 (2006)

Environment Recognition System for Biped Walking Robot Using Vision Based Sensor Fusion

Tae-Koo Kang[1], Heejun Song[2], Dongwon Kim[3], and Gwi-Tae Park[4]

Department of Electrical Engineering, Korea University, 1, 5-ka, Anam-dong, Seongbuk-ku, Seoul 136-701, Korea
{tkkang,nyaong7,upground,gtpark}@korea.ac.kr

Abstract. This paper addresses the method of environment recognition specialized for biped walking robot. Biped walking robot should have the ability to autonomously recognize its surrounding environment and make right decisions in corresponding to its situation. In the realization of the vision system for biped walking robot, two algorithms have been largely suggested, they are; object detection system with unknown objects, and obstacle recognition system. By using the techniques mentioned above, a biped walking robot becomes to be available to autonomously move and execute various user-assigned tasks in an unknown environment. From the results of experiments, the proposed environment recognition system can be said highly available to be applied to biped walking robot walking and operated in the real world.

1 Introduction

With the aid of development in biped walking robot technologies, it is expected that humanoid robots which are more human friendly and operated in real human living environments will appear in the near future. They will exist in various forms such as servant robots, cleaning robots or entertaining robots, etc. However, there are still remaining problems which keep biped walking robot technologies to be familiarized to human. First of all, most of the previous researches on biped walking robot have only focused on theoretical walking algorithm itself. Obviously, the ability of walking is the most fundamental function. However, humanoid robots which are able to walk only in previously known (programmed) environments could not possibly be utilized in real world situations. Therefore, algorithms enabling biped walking robot to autonomously determine its actions and paths in unknown environments should be developed in advance that humanoids serve human beings in real lives. So many researches are ongoing in moving object detection and obstacle recognition area. The most common method for detecting a moving object in an image is background subtraction in the literatures of vision systems[1]. In recent years, color-based object detection methods which use the characteristics of objects represented by color histograms have been widely used in wheeled and biped walking robot researches[2]. However, those are not appropriate methods for biped walking robots since the whole

H.G. Okuno and M. Ali (Eds.): IEA/AIE 2007, LNAI 4570, pp. 405–414, 2007.

background moves with the target object when a robot walks unlike the cases of using fixed cameras. Moreover, it is needed to have the predetermined color information of target object to use color-based methods. Optical flow method is a commonly used technique for the motion area extraction in the mobile robot or vehicle[3]. It groups the optical flow vectors that are associated with the same motion or structure. So it can be used to detect independently moving object even in the presence of camera motion.

The purpose of this paper is building a system for recognizing environments of robot and making appropriate decisions against the change of environments. In this paper, a method for moving object detection using clustering based optical flow is proposed. The obstacle recognition method is also developed to make a robot to be provided proper information to climb up and down or avoid obstacles. Unlike the detection process of moving object, those obstacles do not move. Consequently it is not possible to detect them by the method for moving object detection. To overcome the problem, hierarchical SVM(Support Vector Machines) is proposed to classify the obstacles such as walls, stairs or slopes. SVM tends to perform well when applied to data outside the training set[4]. Indeed, it has been reported that SVM-based approaches are able to significantly outperform competing methods in many applications.

This paper is organized as follows. In Chapter 2, the proposed environment recognition system is introduced. More specifically, the concepts of moving object detection system and obstacle recognition system for a biped walking robot are illustrated. In Chapter 3, the results of experiments focusing on verifying the performances of the proposed system are presented. They are object detection tests and obstacle avoiding/climbing tests using the whole proposed system. Also, this chapter gives the ways of utilizing the proposed environment recognition system in biped walking robot. They are distance measuring to a moving object and adaptive walking trajectory planning for walking in unknown environments. Chapter 4 concludes the paper by presenting the contributions.

2 Environment Recognition System

The overall system is constructed as illustrated in Fig. 1. The system largely consists of two parts, a biped walking robot and a Host PC. Those are connected with a Bluetooth wireless communication module using RS-232C. Since the realization of a biped walking robot which autonomously moves in an unknown environment as well as executes assigned tasks by a user is the main purpose of the system, the robot is equipped with several kinds of sensors which gather the information of the surrounding environments. Consequently, the robot is basically designed to move autonomously without any control from the user by recognizing the environment using sensors. For instance, the robot can control its posture stability by itself, by using gyro sensors and actuators in the waist joints.

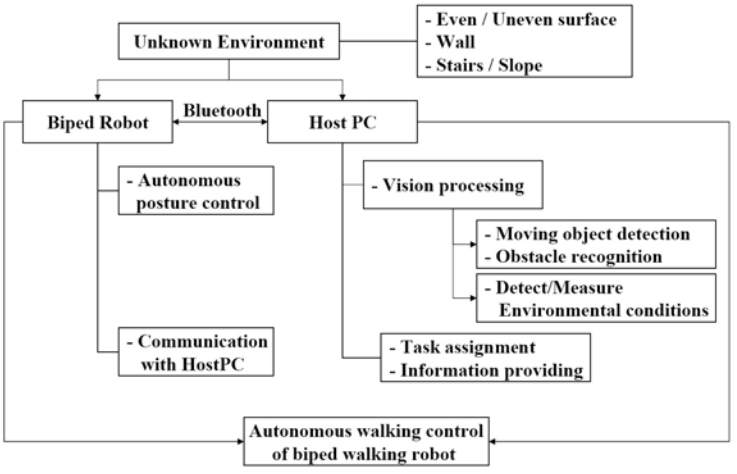

Fig. 1. Overall system architecture

2.1 Vision System for Environment Recognition

In environment recognition system, environment conditions for a biped walking robot are classified into three categories: even or uneven surface, moving object and obstacles in a broad sense. Fig. 2 shows the image processing methods in the environment recognition system built for the biped walking robot. As shown in Fig. 2, this system is composed of two parts: moving object detection and obstacle recognition.

In the moving object detection part, the clustering based optical flow method is proposed due to the always non-stationary background so that the background subtraction method detects the whole region of input image as foreground. Roughly speaking as shown in Fig. 2, the moving object detection part is composed of Optical flow, Feature mapping, FCM(Fuzzy C-Means). The proposed moving object detection method is illustrated more detail in Chapter 2.2.

In the obstacle detection part, the environment recognition system provides not only the information of existence of objects and obstacles, but also the details of them. For instance, when the system detects a stairs in front of the robot, it estimates the distance to the stairs, the height and width of a stair so that the robot can calculate the corresponding motion trajectory to go up the stairs. The obstacle recognition process is composed of Adaboost[5], PCA(Principal Component Analysis)[6], and hierarchical SVM(Support Vector Machines). The proposed obstacle recognition method is illustrated in Chapter 2.3.

2.2 Moving Object Detection System

Optical Flow for Non-stationary Background. The optical flow is an efficient algorithm for extracting moving components or detection of moving objects in images. However, the original optical flow method is not applicable in case of

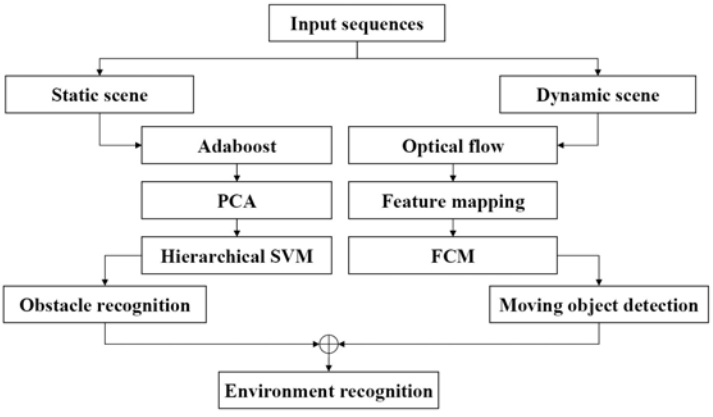

Fig. 2. Vision system for environment recognitiion

biped walking robot, because the whole image varies so that all the points in an image have the optical flow components of velocities and directions.

Therefore, moving objects as well as background are considered that they are moving in such case. To resolve this problem, a clustering based the optical flow method is proposed to eliminate background components by using fuzzy clustering method to the optical flow components. Even in case of a fixed camera, there are some extracted features to be detected. However, it can be empirically known that the components of a moving object and ones of background are possibly classified into different groups. Therefore, in case that an object is moving in an image, the whole set of extracted motion features from the optical flow field can be classified into two groups. However, a problem still remains, that is, how to determine which group consists of the object. To overcome this problem, it is assumed that the features in a moving object have a larger distribution than ones in the background. To divide the features of each group, FCM algorithm is applied to the set in the feature space[7]. In addition, it would not be necessary to divide the object and the background in case of non-moving object. Therefore, the distance between the centers belonging to each group is calculated by mahalanobis norm[8] and it is considered as one group when the distance is small enough. The detailed description of the procedure is given in Fig 3. By using the proposed method, moving objects in images can be detected in most cases.

2.3 Obstacle Recognition System

The whole procedure of obstacle recognition system is illustrated in the left column of Fig. 2. The obstacle recognition system classifies an obstacle which a robot faces while walking and determines the details of the obstacle so that the robot is enabled to autonomously determine its behavior and generate the appropriate trajectory. This must be a mandatory system to realize humanoid robots since the current walking robots are only possible to walk in pre-programmed known environments.

```
while(Calculate_optical_flow){
   feature = Get_optical_flow_feature(pre_img, curr_img);
   // get velx, vely
   [intensity, direction] = Calculate_element(feature);
   // get optical flow elements
}
FCM(intensity, direction);
sd = Calculate_standard_deviation(group.position);
for(num_groups){
    if(sd = largest) then eliminate(group.feature);
}
// eliminate group of largest standard deviation
Conneted_componet_labeling( remaining_feature_points );
for(num_blobs){
     if(blob.count < threshold) then eliminate(group.feature);
}
// eliminate the minor features
Center_of_gravity( remaining_feature_points );
// finds center of moving object
```

Fig. 3. Procedure of the moving object detection

Obstacle Region Extraction. In the obstacle recognition system, boosted classifier used a set of Haar filters as features is used as an obstacle region extractor[9]. A weak classifier is not capable of detecting a rotated or translated input image. However, once a boosted classifier is generated, it is able to adaptively detect the obstacles even when they are rotated or translated.

Feature Extraction in Obstacle Region. PCA is known as a useful technique to extract dominant features or reduce the dimensionality of large data sets in image processing and data mining and can also be used to find signals in noisy data in signal processing. In some cases, the dimension of the input is too large, but the components in the input are highly correlated (redundant), PCA is useful to reduce the dimension of the input. We extracted the PCs from the original image(320X240). Hence, the finally resulting arrays contain 50 or 25 dimensional data containing the principal information of the original input image. These arrays are split into training and test dataset and used to train and test using SVM.

Obstacle Recognition. To recognize and classify the obstacles which a biped walking robot faces while walking, a hierarchical SVM is implemented to construct an efficient classifier. In this paper, we categorized obstacle into two groups, obstacles which a biped walking robot can climb up and ones which should be avoided. In addition, the former group can be classified into two groups again, slope and stairs, since the walking characteristics of them are quite different. Consequently, there exist at least four kinds of obstacles including an even surface. The use of the original SVM is not appropriate in this case. Therefore, a hierarchical SVM is proposed to classify a variety of obstacles, more than two kinds.

The structure of the proposed hierarchical SVM is depicted in Fig. 4.When an obstacle is detected by the vision and ultrasonic sensors installed in the

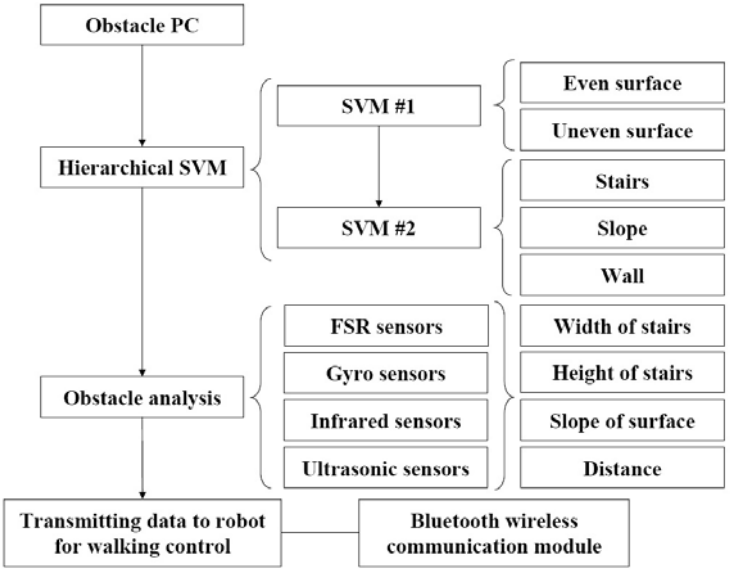

Fig. 4. Procedure of the obstacle recognition

robot, the input image is processed by the procedures represented in Fig. 4 in advance to being applied to SVM classifier. In the classification process, a SVM classifier trained to classify even surfaces and walls is applied to the extracted features of the input image at the first stage. It determines whether the robot can climb up the obstacle or not, and returns the possibility of climbing up to the robot by using the Bluetooth communication. Then the robot modifies its motion trajectory in a way of avoiding in case of walls or other unclimbable obstacles. If the obstacle is classified as climbable by the first SVM classifier, the features are applied to the SVM second classifier. It classifies the object into the categories of stairs or a slope. Then the recognition system determines the more detailed information such as the height and width of a stair and the inclining degree of a slope, according to the information obtained from infrared sensors. Also, the determined result is transmitted to the robot and the robot generates a corresponding trajectory to the obstacle.

3 Experimental Results

We evaluate the performances of the proposed moving object detection and obstacle recognition. The detailed results of the experiment are given as follows.

3.1 Moving Object Detection Experiment

The proposed moving object detection algorithm is evaluated with real-time video streams. There are 100 video streams with human moving used for the

Fig. 5. Object detection results - Fixed camera(left), Camera in a biped robot(right)

test and each video stream consists of 600 frames. Final results of processing the clustering based optical flow method are presented in Fig. 5. The centers of moving human are marked with circles. From Fig. 5, it can be known that the proposed method effectively detects moving objects in both cases of fixed camera and moving camera. The evaluation of detection accuracy is given in Table 1.

Table 1. Accuracy test results of the moving object detection

Camera	Num_features	Processing time (ms)	Accuracy
Fixed	200	18.2	91.78
	300	21.2	93.14
	400	23.3	92.52
Moving	200	17.8	85.38
	300	21.4	88.43
	400	23.2	87.59
Average		20.9	89.81

Considering the proposed algorithm is performed in every frame so that there is no possibility of being affected by occlusions or losing objects while detecting. In addition, the average processing time is 20.9 ms and the camera carries out to send images at the speed of 30 frames per second. Therefore, the proposed algorithm can be concluded to be effective for moving object detection system in biped robot walking.

3.2 Obstacle Recognition Experiment

The proposed obstacle recognition system is evaluated by applying 100 of 10 second video streams at the speed of 30 frames per second in each test category. (30000 frames in total) Table 2 gives the experimental result of the proposed system. The classification accuracy is measured by calculating the ratio of correct classification for the 30000 input images.

From the evaluation in Table 2, the proposed obstacle recognition algorithm shows appropriate processing time, approximately 22 ms and it is enough to be

Table 2. Performance test results of the obstacle recognition

Adaboost	PCA	SVM	Accuracy			Processing Time
Ada_win_size	Num_PC	SVM_kernel	Wall	Slope	Stairs	(ms)
25x25	25	linear	80.1	83.1	92.9	22.38
		polynomial	85.2	83.4	95.5	22.76
		RBF	88.1	87.2	97.6	23.21
	50	linear	85.1	84.2	93.4	23.35
		polynomial	86.2	85.9	95.7	24.12
		RBF	87.3	86.2	97.8	24.06
30x30	25	linear	84.1	84.1	93.1	23.78
		polynomial	86.1	85.9	95.5	24.35
		RBF	87.6	86.6	97.8	24.89
	50	linear	84.9	84.6	94.1	24.43
		polynomial	86.8	87.2	95.9	25.32
		RBF	88.4	86.7	98.1	25.47
Average			85.8	85.4	95.6	22.16

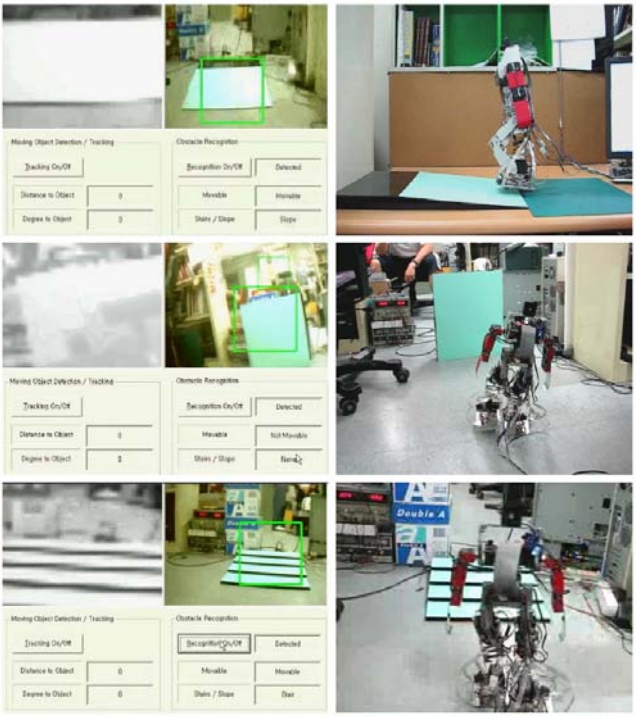

Fig. 6. Environment recognition results and the corresponding robot walkings

carried out in real time with camera at the transmission speed of 30 frames per second. The results of accuracy tests show differences by the types of obstacles. In case of wall and slope, the region detection accuracy by Adaboost is relatively

high. However, they also have high false alarm rate so that the total accuracies of both cases are about 85 percent, which is not satisfactory. On the contrary, the classification accuracy of stairs is approximately 10 percent higher than the ones of other obstacles. In addition, cases with larger window size, larger number of principle components and RBF kernel show little better results for the cases of all types of obstacles. Fig. 6 shows the obstacle recognition for a wall, a slope, stairs and corresponding actual robot walking respectively. The left of each figure shows the region detected by Adaboost algorithm and it is marked with a rectangle. The right of each figure shows the actual robot walking respectively.

4 Conclusion

We present the systems of environment recognition for biped walking robot. For the realization of humanoid robot, they are the mandatory conditions to make a robot autonomously recognize its surrounding environment and adaptively walk by generating its motion trajectories. Therefore, this paper has the meaning of developing aid technologies for biped robot walking control. The environment recognition system is realized by combining sensory data obtained from a walking robot including image data taken by a single camera. The problems in developing vision system in biped walking robot operated in a real world are derived from the fact that the condition for the vision system of a biped walking robot quite differs from the one of a fixed camera or a camera mounted on a wheeled robot. Moving object detection system by using modified optical flow method and obstacle recognition system by using a hierarchical Support Vector Machines are proposed in this paper. Those systems are realized and verified their effectiveness with a number of experiments by implementing them into a biped walking robot. Moreover, there is a need of developing a stand alone vision system which works in a biped walking robot system itself, because the proposed system totally depends on the Host PC.

References

1. Li, L., Huang, W., Yu-Hua Gu, I., Tian, Q.: Statistical Modeling of Complex Backgrounds for Foreground Object Detection. IEEE Transactions on Image Processing. 13, 1459–1472 (2004)
2. Fieguth, P., Terzopoulos, D.: Color-based Tracking of Heads and Other Mobile Objects at Video Frame Rates. In: Proceeding of IEEE Computer Vision and Pattern Recognition, pp. 21–27 (1997)
3. Lee, D.: The Optic Flow Field: The Foundation of Vision. Philosophical Transactions of the Royal Society of London. Series B. Biological Sciences 290, 169–178 (1980)
4. Muller, K., Mika, R., Ratsch, S., Tsuda, G., Scholkopf, K.: An Introduction to Kernel-Based Learning Algorithms. IEEE Transactions on Neural Networks 12, 181–201 (2001)
5. Viola, P., Jones, M.: Rapid object detection using a boosted cascade of simple features. In: Proceedings of IEEE Conference on Computer Vision and Pattern Recognition, vol. 1, pp. 511–518 (2001)

6. Jolliffe, I.T.: Principal Component Analysis. Springer, New-York (1986)
7. Cannon, R., Dave, L., Bezdek, J.V.: Efficient implementation of the fuzzy c-means clustering algorithms. IEEE Transactions on Pattern Analysis and Machine Intelligence 8, 248–255 (1986)
8. Deer, P.J., Eklund, P.W.: A study of parameter values for a Mahalanobis Distance fuzzy classifier. Fuzzy Sets and Systems 137, 191–213 (2003)
9. Lienhart, R., Maydt, J.: An Extended Set of Haar-like Features for Rapid Object Detec-tion. In: Proceedings of IEEE International Conference on Image Processing, vol. 137, pp. 900–903 (2002)

Design of a SOA-Oriented E-Diagnostics System for Hydroelectric Generating Sets*

Liangliang Zhan[1], Yongchuan Zhang[1], Jianzhong Zhou[1], Yucheng Peng[2], and Zheng Li[3]

[1] School of Hydropower and Information Engineering, Huazhong University of Science and Technology, Wuhan 430074, P.R. China
fluidstar@smail.hust.edu.cn
[2] School of Energy and Power Engineering, Huazhong University of Science and Technology
[3] Harbin Electric Machinery Co., Ltd.

Abstract. In order to resolve existing problems such as low efficiency, high cost and lack of technical resource in current maintenance, it is necessary to realize remote diagnosis for hydroelectric generating sets (HGSs). In this work, basing on the Service-Oriented Architecture (SOA) and Web Services technology, a SOA-oriented E-diagnostics system for HGSs (HGS-SES) is proposed, the framework of HGS-SES is constructed, a layout of the system's hardware settings is described, the key modules of the system and a specific diagnostic procedure are given. HGS-SES makes rapid and convenient information transmission for services function and diagnosis decision-making, develops a dynamic network diagnostic platform for HGSs, and has broad prospects for farther research.

Keywords: SOA, Web Services, E-diagnostics system, Hydroelectric generating sets.

1 Introduction

Along with continuous progress of Chinese hydropower technology,the development trend of hydroelectric generating sets is increasingly towards high head, high speed, high efficiency and big capacity. With improved accuracy, increased crew size and structure complexity in building HGS, the running of HGS is easy to cause more problems[1]. Once faults occur, because of advanced technology, complex construction, great overhaul workload, and more technology fields involved in HGS, the on-site diagnostic system and technical staffs in a hydropower plant can hardly resolved them independently. Experts of relevant fields are often to be resorted. In China, most experts of HGS are in universities, research institutes and hydro-generator manufactories. Because of geographical and trade

* This work is supported by the Important Project of National Natural Science Foundation of China (NSFC) (No.: 50539140), the Project of National Natural Science Foundation of China (NSFC) (No.:50579022), and the research funds of University and college PhD discipline of China (No.:20050487062).

H.G. Okuno and M. Ali (Eds.): IEA/AIE 2007, LNAI 4570, pp. 415–423, 2007.

limitation, contact among them is very loose, which makes actual technical resource seriously short. At the same time, there is considerable potential resource which can't be fully exploited. When more than one HGS fault occur, experts are weighed down with them. Considerably increasing financial expense on various aspects of hydropower plants, faults still can not be ruled out in time[2]. Thus, it is necessary to establish an internet-based remote fault diagnosis system.

Up to now, many plants have their own HGS monitoring systems or fault diagnostic systems. In order to maximize using existing resources, improve diagnostic accuracy and reliability, and decrease HGS-SES developing costs, it is necessary to integrate the exiting systems of all hydropower plants. Since developers of those systems are different, development languages, deployed platforms and communication protocols are likely to be significant differences, which made most systems heterogeneous[3]. How to exchange and integrate information in a heterogeneous environment has become a key issue of integration.

To fulfill the requirements of e-diagnostics system and remedy the shortcomings of existing diagnostic systems,an SOA-oriented E-diagnostics system for hydroelectric generating sets (HGS-SES)has been proposed in this paper.It is a new way to provide remote diagnostic services for HGS faults.

2 Targets of HGS-SES Basing on SOA

Service-oriented architecture (SOA) is a way of designing a software system to provide services to either end-user applications or other services through published and discoverable interfaces. SOA is not a new notion; it is important at this time because of the emerging Web services technology. Web services can be seen as a new network distributed computing model for the Web[4].Its related technologies mainly include the Extensible Markup Language (XML), Simple Object Access Protocol (SOAP), Web Services Description Language (WSDL), Universal Description, Discovery and Integration (UDDI). Web services aim to provide efficient and seamless applications for all kinds of internet communication [5,6]. They are adaptive, self-describing, modular application procedures,

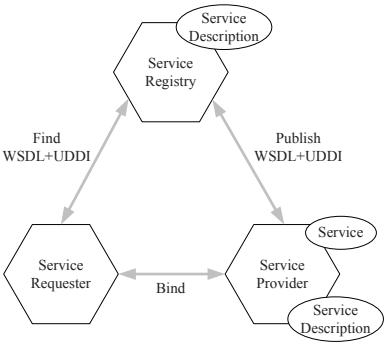

Fig. 1. Architecture of Web Services

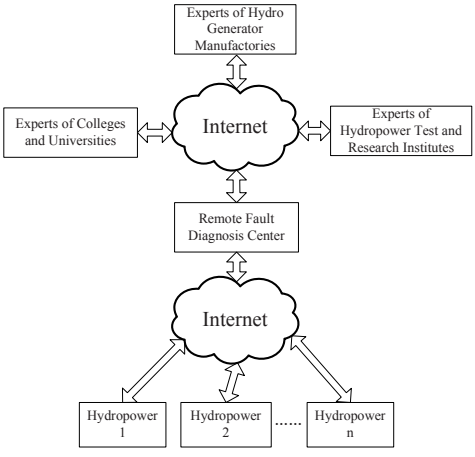

Fig. 2. Sketch map of HGS-SES

which can be published, located, and dynamically invoked across Web[7]. As shown in Fig.1, the Web services framework describes the relation-ship between the three roles (service provider, service requester, and service agent) and the three operations (deploy, find out, and bind)[8].

Basing on SOA, the HGS-SES should provide an open architecture, allowing both the existing legacy applications and the new leading-edge applications to be rapidly and seamlessly integrated into the system. Consolidating the function of the participating, the system should be capable of providing integrated business services to various types of utility users, ranging from technical staffs in hydropower plants to experts on remote places. The relationship among different objects in HGS-SES is shown in Fig.2.

3 Framework of HGS-SES

According to the targets of HGS-SES and combining running situation of hydropower plants, the framework of HGS-SES is shown in Fig.3, which consists of four main components, such as the internet UDDI registry node, the specialist or technical staff visit module, the on-site fault diagnosis subsystem (OFDS) of a hydropower plant and the remote fault diagnosis subsystem (RFDS) of remote diagnosis center. HGS-SES publishes its service on the internet UDDI registry node, which may facilitate users, such as hydropower plants and experts, to search and visit. Experts and technical staffs can use Web browser or client model to visit HGS-SES,which can increase visit flexibility.

OFDS of hydropower plants is made up of the on-site data acquisition module (ODAM), the on-site diagnostic module (ODM), the local diagnostic databases (LDD) and the client module. ODAM and ODM are divided basing on different

service objects. Through ODAM, ODM can activate corresponding application procedure and acquire HGS running data.

RFDS of the remote diagnosis center is made up of the remote diagnosis integrated management module (RDIMM), the remote diagnostic database (RDD), the diagnosis center UDDI and the client module. The main function of RFDS is to provide the interface of HGS-SES, manage services registry of subsystems, and respond to users' request.

In HGS-SES, the relationship between the service requester and the service provider is often relative. For example,hydropower plant and remote diagnostic center can serve not only as service requesters, but also as service providers.

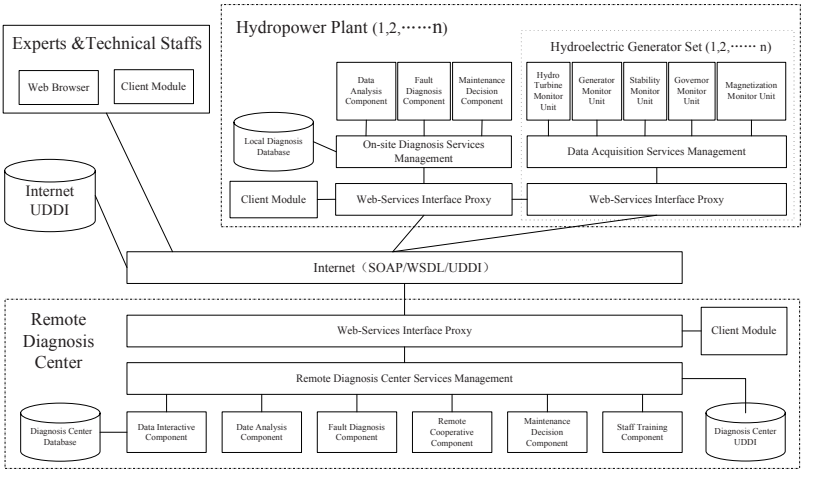

Fig. 3. Framework of HGS-SES

4 Hardware Layout of HGS-SES

According to the framework of HGS-SES, the actual targets of fault diagnosis and the objective system condition, the system hardware layout is shown in Fig.4. Because the layout of hydropower plant is representative, only a generic model is given. In the hardware layout, the Web services interface proxies are placed in Web server, and services management modules are placed in corresponding application servers, such as local diagnostic services management in on-site diagnostic server (ODS), data acquisition management in on-site data acquisition server (ODAS), and remote fault diagnosis center services management in remote diagnosis server (RDS). The workstations in and out of subsystems access HGS-SES through Web services interface proxies, who can realize sharing Web services between the structure of browser/server (B/S) and client/server (C/S), and avoid repeated business logic development of the traditional functions of browser/client/server (B/C/S) structure. Firewalls isolated subsystems out of the world outside to protect system information and data security. In order to

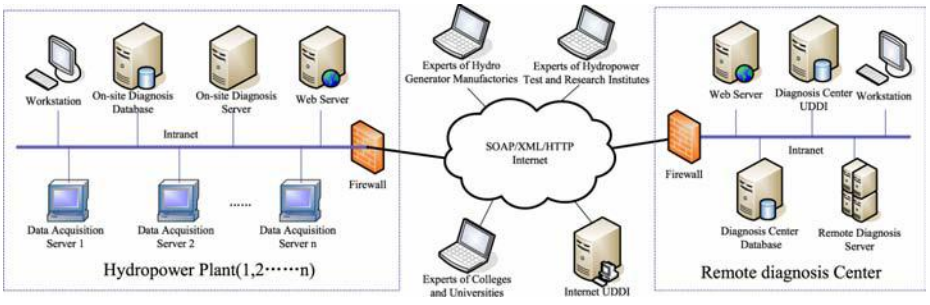

Fig. 4. Hardware layout of HGS-SES

facilitate managing the Web services registry of subsystems, a private UDDI server is placed in the RFDS. Through it, Web services registry, categorization and use can be achieved.

5 Key Modules and Technology of HGS-SES

5.1 Services Management Module

Shown in Fig.6, services management module is designed as a common module which could be adopted by the remote diagnosis center services management, on-site diagnosis services management and on-site data acquisition services management. The main function of service management is to wrap application programs, integrate Web services according to users' requests, and response them. The sub-module functions are described below:

1. SOAP interface is designed to communicate information with Web server;
2. Workflow engine automatically distributes the information from the soap interface to the corresponding Web service adapter according to business rules;
3. Transaction management engine acts as the coordinator of distributed transaction;
4. Web service adapter mainly provides an interface to different component technology, such as CORBA, RMI and DCOM, and so on;
5. Application integration console implements the configuration and management, and accomplishes the dynamic configuration of users, including workflow management, business management, application resource management and current interface management;
6. Monitor console manages and monitors Web services, including dynamic monitoring and management;
7. Information console provides data and module service for the transaction service console and monitor console, and accomplishes management and maintenance of information security lifecycle, including shared information management, shared module management and data operation management.

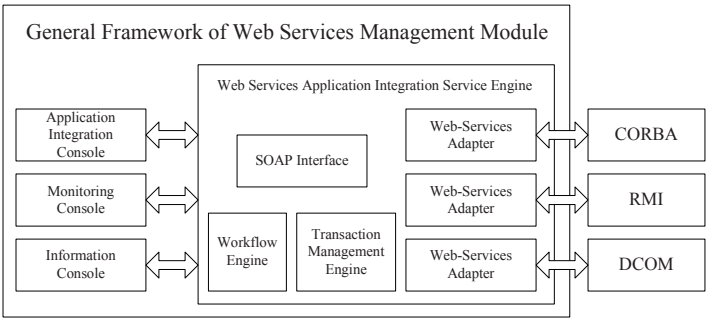

Fig. 5. General framework of Web Services management

5.2 Diagnosis Center UDDI

The structure of diagnosis center UDDI service is shown in Fig.7. Relative to the Internet UDDI, the diagnosis center UDDI is a private UDDI of HGS-SES.

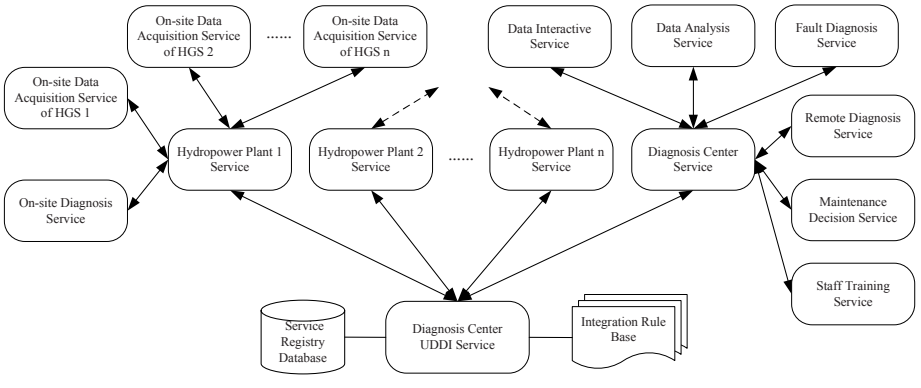

Fig. 6. Structure of the diagnostic center UDDI

Orchestration engine is the core module of the Diagnosis center UDDI service [9], which can manage registry, modification and deletion of Web services, and also can search and call Web services according to users' request and need. It connects to a service registry database and an integration rule base, shown in Fig.8. The service registry is a private UDDI registry designed to store the information of participating business services. The integration rule base is built to store the integration business logic, which specifies how to respond to each type of request. By separating such integration meta-data from the integration process, a generic orchestration engine can be built to drive the process. In response to each received request, the orchestration engine searches the integration rule base for the matched integration rule and then executes its specified integration steps.

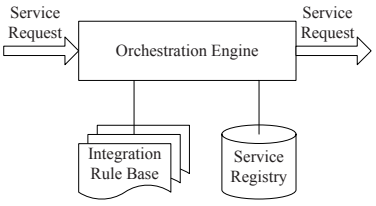

Fig. 7. Implementation of the orchestration engine

6 Faults Diagnosis Workflow

When a HGS fault occurs, first, the hydropower plant technical staffs adopt OFDS for diagnosis; then, set a request to the RFDS if OFDS can not solve the problem, with the assistance of RFDS to handle the fault. Fig.8 indicates an information interactive process among different parts of the system in a fault diagnosis. The specific steps are as follows:

1. When a fault occurs, ODAS acquires the error message from HGS;
2. ODAS passes the error message to ODS;
3. ODS searches LDD for the diagnostic solution based on the error message;
4. The local technical staffs provide the diagnostic result and maintenance decision combining with ODS;
5. If no diagnostic solution of the occurring fault is found locally, or the fault cannot be remedied, ODAS delivers the error message to RDS.
6. The local technical staffs search LDD for the diagnostic solution based on the error message for "self-diagnosis";
7. If there is an explicit solution, then deliver it to ODS.
8. The local technical staffs maintain HGS basing on the solution from ODS;
9. If the solution is correct, ODS saves it to LDD as a new case;
10. If still no diagnostic solution is found, then request the RDS to notify experts and technical stuffs to make a date for the remote cooperative fault diagnosis;
11. RDS requests experts and HGS maintenance staffs to attend the remote cooperative diagnosis;
12. According to ideas of the remote cooperative diagnosis, RDS gives the diagnostic conclusion and maintenance decision, and returns them to ODS;
13. The local technical staffs maintain the HGS according to the diagnostic conclusion and maintenance decision;
14. If success, ODS saves it to LDD as a new case;
15. ODS returns the main-tenancy information to RDS;
16. According to the feedback information of ODS, RDS decides whether to save the diagnosis information to RDD as a new case.

If there are still problems in the HGS, according to the feedback information, the whole system will repeat step 11 to step 15 until a reasonable diagnostic result is given.

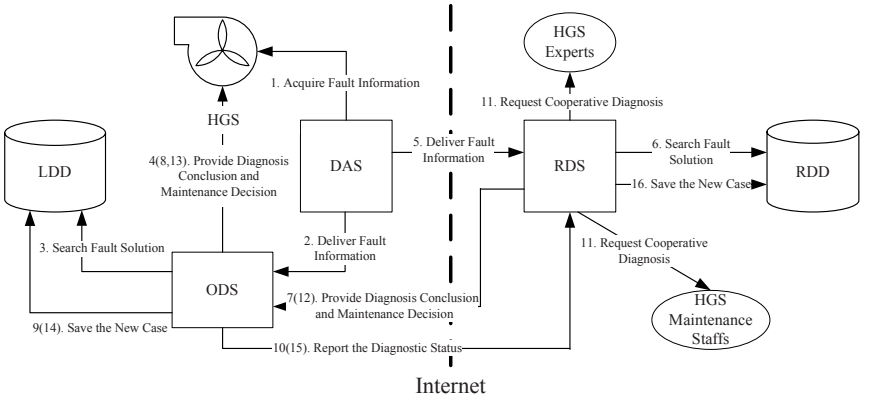

Fig. 8. Example of a fault diagnosis process

7 Summary and Conclusion

Aiming at problems existing in the fault diagnosis process of HGSs, this paper presents a Web services based SOA-oriented E-diagnostics system, discusses how to design and implement it in system architecture, hardware layout,key functional modules,fault diagnosis process and other aspects. In HGS-SES, SOAP is used as the basic messaging protocol, the remote diagnosis center serves as the institution of management and coordination, devices of hydropower plants, maintenance staffs and experts of HGS will be put together to provide a full range of services for fault diagnosis and decision making. With the constant improvement of Web services known as the 3rd revolution in the information technology, HGS-SES will have broad application prospects.

References

1. He, Y., Ren, J., Chen, W.: Remote condition monitoring, tracking analysis and fault diagnosis system for hydropower sets. JTsinghua Univ(Sci and Tech) 46(5), 629–632 (2006)
2. Zhu, J., Lai, X.: Design and implementation of an internet based remote monitoring and diagnosis system for hydroelectric generating set. Power System Technology 28(24), 5–9 (2004)
3. Yu, R., Ye, L., Zhang, Y.: Intelligent control-maintenance-technical management system(ICMMS) and its application in power system, Part One Ideology, Constitution and Characteristic. Automation of Electric Power Systems 23(23), 50–54 (1999)
4. World Wide Web Consortium, WSDL Web-service Description Language [Online]. Available: `http://www.w3.org/TR/wsdl`
5. Sham, P., Jenngs, M.: Protocol Engineering for Web Services Conversations. Engineering Applications of Atificial Intelligence 18(2), 237–254 (2005)
6. Lu, J., He, Y.: A web product data management system based on simple object access protocol. Journal of Chongqing University-Eng.Ed. 2(1), 57–62 (2003)

7. Dustdar, S., Gall, H.: Software configuration, distribution, and deployment of Web-Services. SEKE'02, July 15-19, 2002. Ischia, Italy, pp. 649–656 (2002)
8. Gottschalk, K., Graham, S., et al.: Introduction to Web services architecture. IBM Systems Journal 41(2), 12–18 (2002)
9. Zhu, J.: Web Services Provide the Power to Integrate. IEEE Power and Energy Magazine, 40–49 (November/December 2003)

A Systematic Layout Planning of Visualizing Devices on a Non-rectangular Plane by Genetic Heuristics

Chir-Ho Chang[1] and Jin-Ling Lin[2]

[1] Department of Industrial Engineering Management,
LungHwa University of Science and Technology, Taipei, Taiwan, 333, R.O.C
chchang@mail.lhu.edu.tw
[2] Department of Information Management
Shih Hsin University , Taipei, Taiwan, 116, R.O.C
jllin@cc.shu.edu.tw

Abstract. As the new era of RFID (Radio Frequency Identification) has come, it makes the visualizing of a plane possible. The proposed research focuses on how to plan the locations of RFID readers in a non-rectangular plane such that regions with or without forbidden blocks can be fully monitored by using a well developed RFID system under the spending of a minimum cost. An algorithm constitutes of three phases is used to obtain the optimal devices' layout planning. In the beginning, we scrutinize a non-rectangular plane and its forbidden blocks so that a general grid-scheme can be applied. Secondly, the linear programming (LP) approach is applied to decide the number of RFID readers needed. At last, a hybrid genetic algorithm (GA) is used to find the appropriate locations for these designated number of RFID readers. The overall cost of deploying RFID readers and the total monitored region of the proposed RFID system are recorded. They are two key performance indexes to evaluate the efficiency of the proposed method. Simulation results show the proposed method has high efficiency on dealing RFID readers' planning problems in visualizing a non-rectangular plane.

Keywords: RFID, Layout Planning, Genetic Algorithm, Heuristic Rules.

1 Introduction

As the radio frequency identification (RFID) technology has recalled its second wind, most people realize the RFID era has finally arrived [1,5]. For warehouses, supermarkets, shopping malls, and a lot of planar spaces, users care not only about whether objects are inside or outside, but also where the exact locations of specific objects under monitored. Therefore, a fully visualized plane with the help of a systematic layout planning (SLP) RFID system becomes important in real world applications. A planar space to be monitored is not necessarily with a rectangular shape. Tracing the locations of interested objects more efficiently in a non-rectangular plane has practicable values.

H.G. Okuno and M. Ali (Eds.): IEA/AIE 2007, LNAI 4570, pp. 424–433, 2007.

The proposed research focuses on how to allocate RFID readers on a non-rectangular plane such that all selected regions of a plane can be monitored by the proposed SLP-RFID system with the spending of a minimum cost. The number of RFID readers and the monitored region of RFID readers are the major issues in the planning of such a plane to be visualized. As we know, linear programming (LP) in operations research has some advantages in solving optimal problems with linear constraints and linear objectives. And, many of us believe genetic algorithm (GA) work well in finding quasi-optimal solutions for non-linear and non-polynomial problems. Therefore, LP technology is used to find the optimal number of RFID readers, and then GA is applied to decide the locations of these RFID readers on a non-rectangular plane.

2 Problem Definition

How to determine the locations of RFID readers in a non-rectangular plane such that some interested regions with or without the forbidden blocks of a planar space can be fully monitored was considered in this paper. A cost-saving SLP-RFID system was developed to achieve this goal. We deal with a non-rectangular shaped plane with some forbidden blocks scattered inside. In order to reduce the cost of building such an RFID system, we expect the number of required RFID readers the less the better. In the mean time, the total feasible region under surveillance by the SLP-RFID system can be as wide as possible. A mathematical model was built and two objectives were used in this study. More details are described as follows.

2.1 Assumptions and Inputs

In order to describe our work clearly and present the proposed method concisely, several assumptions (reasonable enough) on the non-rectangular working plane, scattered forbidden blocks, and a SLP-RFID system are used.

a) General plane with/without forbidden blocks
   - o A forbidden block can occupy its area inside or outside a plane, but they are all required to remain inside a minimum rectangle which specifies the plane.
   - o When a forbidden block stay inside a plane, it means the block is an intrinsically unfeasible region which is not necessary to be monitored by any means.
   - o Overlapped forbidden blocks will be treated as a contiguous forbidden block. Theoretically, overlapping is not allowed for any two forbidden blocks.

b) RFID system
   - o The cost of building the proposed SLP-RFID system consists of purchasing RFID readers which are used to monitor the plane only.
   - o For simplicity, only one single type of RFID reader is used in each run of the proposed system. The cost and the scanning region of a RFID reader remain the same throughout cases studied. Combinatorial tags, mixed

brands, crossover bandwidths, and multiple detection frequency are not allowed in the proposed SLP-RFID system.

Before using the proposed method to optimally allocate RFID readers, the following information is necessary

a) Plane and forbidden blocks
   - The information of a plane
   - The information of forbidden blocks inside the specified plane

b) RFID readers
   - The cost of a single RFID reader
   - The radius of the detecting range of a RFID reader

2.2 Problem Model

The objectives of solving the proposed problem are of two-aspects. One of them is to minimize the total cost of this SLP-RFID system. And the other is to maximize the monitoring region of the SLP-RFID system for a number of given non-forbidden blocks inside the specified plane. The multiple objectives problem can be split into two single objective problems. And the result comes from the first problem, which minimizes cost of the SLP-RFID system, is used to solve the second problem. A corresponding mathematical model with the proposed method is shown in Table 1 and notations used are listed as followings,

RR_k: the i^{th} RFID reader
cRR_i: the center of i^{th} RFID reader
dRR: the detecting diameter of the specified RFID reader
rRR: the radius of a specified RFID reader's detecting range
lRR: the list of locations for RFID readers
nRR: the number of RFID readers
FA_i: the i^{th} forbidden block
FA_iLen: the length of the i^{th} forbidden block
FA_iWid: the width of the i^{th} forbidden block
RFA_i: the minimum rectangle which can contain a forbidden block *i* (FA_i)
nFA: the number of contiguous forbidden blocks
aFA_i: the area of a forbidden block *i*
RP: the minimum rectangle which can contain the specified plane
RPLen: the length of RP
RPWid: the width of RP
RP[i,j]: the basic element of RP in location (i,j)
MR(listRR,Rect): a function to compute the area under surveillance. (The area was monitored by the proposed SLP-RFID system and only feasible region inside a rectangle plane *Rect* was counted.)
FR(Rect): a function to compute the feasible region inside a rectangle plane *Rect*

Table 1. Mathematic model of the proposed problem

Frist objective: minimize the cost of an RFID system Minimize: *Cost* = *nRR* Subject to: $nRR * \pi * (rRR)^2 \geq RPLen * RPWid - \sum_{i=1}^{nFA} aFA_i$
Second objective: maximize monitoring region of RFID system Maximize: $\text{Monitoring Region} = \frac{MR(lRR, RP)}{FR(RP)} * 100$ Subject to: $RP \geq 1$

The function *MR* can be done by the procedure shown in Table 2. Table 3 shows the procedure of function *FR*.

Table 2. The procedure of function *MR*

Step 1 *monitoringRegion* = 0; Step 2 for (*i*=0; *i*<*RPLen*; *i*++) Step 2.1 for (*j*=0; *j*<*PLWid*; *j*++) Step 2.1.1 if (*RP[i,j]* does not belong to forbidden block) Step 2.1.1.1 for (*k*=0; *k*<*nRR*; *k*++) Step 2.1.1.1.1 if (*RP[i,j]* inside the scanning region of RR_k) Step 2.1.1.1.1.1 monitoringRegion++; Step 2.1.1.1.1.2 goto Step 2.1;

Table 3. The procedure of function *FR*

Step 1 *feasibleRegion* = 0; Step 2 for (*i*=0; *i*<*RPLen*; *i*++) Step 2.1 for (j=0; *j*<*PLWid*; *j*++) Step 2.1.1 if (*RP[i,j]* is not in a forbidden block) *feasibleRegion*++;

3 Algorithm Analysis

Our algorithm includes three phases, which are applied to implement an SLP-RFID system for visualizing a plane. At the first stage, the non-rectangular plane was under a so called normalization treatment. Where non-rectangular plane will be padding with pseudo forbidden block units, and pillars, beams, and pre-occupied spaces inside a plane were also marked as forbidden block units via a grid-scheme. Then, a linear programming (LP) model is used to decide the minimal number of RFID readers in the second stage. Last but not the least, a hybrid genetic algorithm (GA) is used to find the appropriate locations for each RFID reader. These procedures of SLP-RFID are shown in Figure 1.

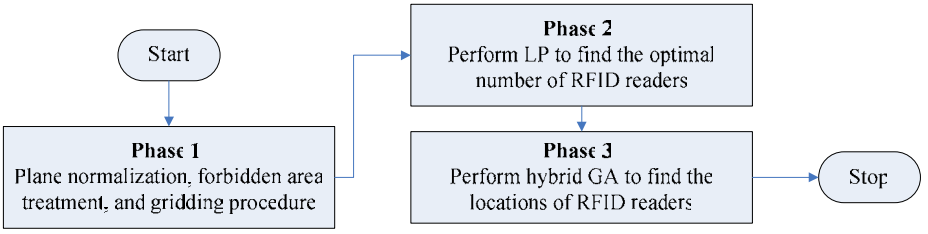

Fig. 1. Three phases for developing an SLP-RFID system to visualize a non-rectangular plane

3.1 Scale-Adjusting

The use of grid-representation of a non-rectangular shape makes the problem easy to solve. Therefore before building a SLP-RFID system, some fundamentals for model representation should be done. Properly scaling the related planar regions and the scanning range of a RFID reader can help to reduce the overheads when allocating RFID readers. Consequently, we compute a minimum rectangular space which can contain the specified plane (*RP*) and this minimum rectangle can contain all forbidden blocks inside the specified plane (FA_i, i = 1 to *nFA*, *nFA* denotes the number of forbidden blocks). Then, we calculate the GCD (Greatest Common Divisor) of the diameter of a RFID reader, the length of *RP* (*RPLen*), the width of *RP* (*RPWid*), the length of each forbidden block (FA_iLen, i = 1 to *nFA*), and the width of each forbidden block (FA_iWid, i = 1 to *nFA*). Finally, we use the greatest common divisor as the basic scaling unit for ticking the length of RP, the width of RP, the length of each forbidden block, the width of each forbidden block, and the diameter of RFID readers. By this way, we can successfully characterize a planar space. These scale-adjusting steps are summarized in Figure 2.

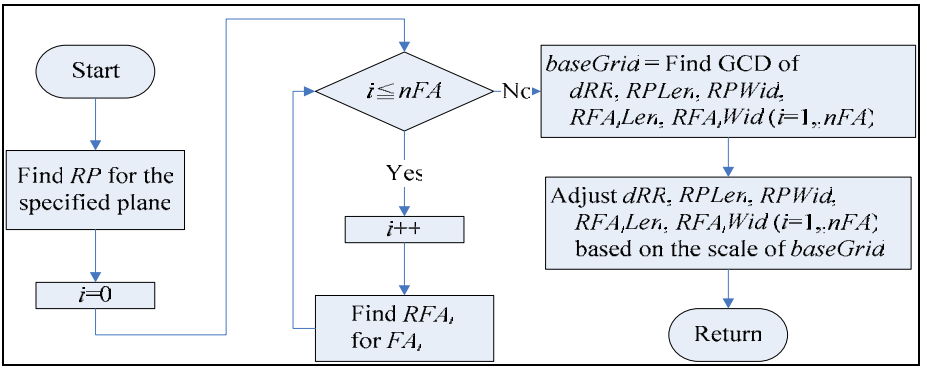

Fig. 2. The procedures of scale adjusting algorithm

3.2 Minimum Cost

One of our goals is to find the optimal number of RFID readers such that all of feasible regions inside the specified plane can be monitored. The problem model is described

in Section 2.2. Since there is only one type of RFID readers can be used for each run of the proposed SLP-RFID system, the cost and the radius for all of RFID readers will be the same. We also assume the cost of purchasing RFID readers is the only cost for building the SLP-RFID system. Finding minimum cost of this SLP-FRID system is equivalent to find the minimum number of RFID readers. Linear programming is the best way to solve the minimum cost of the proposed problem with linear constraints, so the solution can be found by the standard operations of LP easily.

3.3 Maximum Monitoring Region

The last phase is to find the maximum feasible region under surveillance inside the specified plane. Genetic algorithm (GA) combined with adequate heuristics is used to solve this problem. The procedures of finding maximum monitoring region are shown in Figure 3.

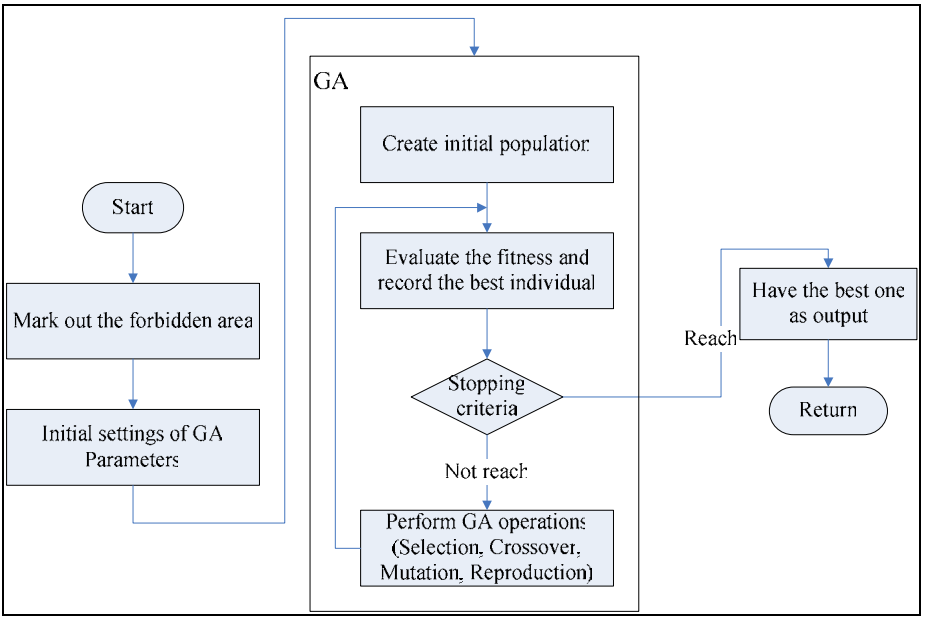

Fig. 3. The procedures of maximum monitoring region algorithm

The operations in the third phase are counted on a grid matrix which was obtained from stage #1. First of all, we mark the forbidden block in the working planar space (*RP*, the minimum rectangle which can contain the working plane). The minus one (-1) denotes forbidden blocks outside the working plane but inside *RP* (minimum rectangle which can contain the plane). The zero (0) denotes a feasible region, which is the region expected to be monitored by the proposed SLP-RFID system. The numeric number 1, 2, …, *n* (*n* is equal to *nFA*, the number of forbidden block inside the working plane) denotes different forbidden blocks, respectively. The corresponding algorithm is shown in Table 4.

Table 4. The algorithm of mark out forbidden blocks

Step 1	for (i=0; i<*RPLen*; i++)
Step 1.1	for (j=0; j<*RPWid*; j++)
Step 1.1.1	k = 1; // check inside forbidden blocks in the working plane
Step 1.1.2	do
Step 1.1.2.1	if (*RP*[i,j] in FA_k)
Step 1.1.2.1.1	*RP*[i,j] = k;
Step 1.1.2.1.2	goto Step 1.1;
Step 1.1.2.2	k++;
Step 1.1.3	while (k<= *nFA*);
Step 1.1.3	if (*RP*[i,j] not in the working plane)
Step 1.1.3.1	*RP*[i,j] = -1;
Step 1.1.4	else
Step 1.1.4.1	*RP*[i,j] = 0;

For finding a better solution, the initial population is created by an experienced "locating curve" heuristics. First, we construct a set of locating curves then allocate RFID readers according to a zigzag-generated locating curve. The procedure of creating initial population is shown in Figure 4. Notation *PS* denotes the population size and *nLC* denotes the number of locating curves which is set to 24 by default in this paper.

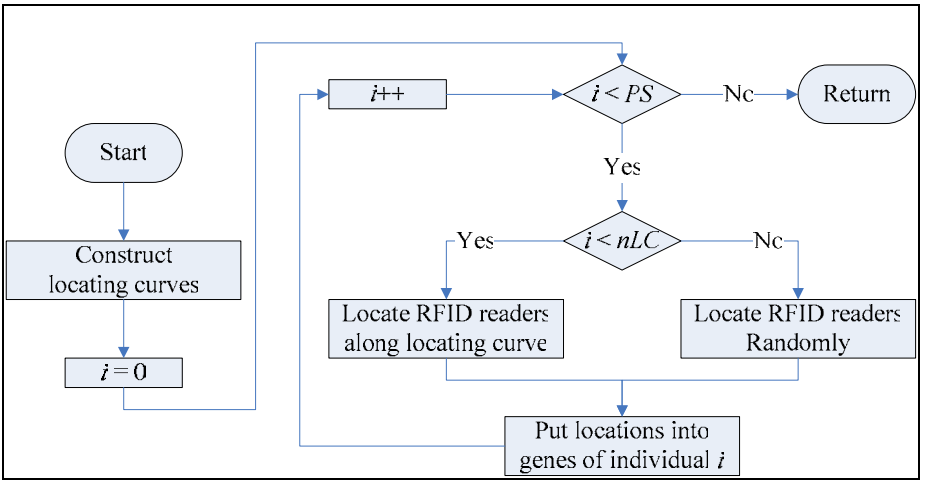

Fig. 4. The procedures of creating initial population

Each individual accompanied with a different locating curve, we assign varied locating curves with different moving directions for different starting locations. In fact, there are five starting locations: upper left, upper right, bottom left, bottom right

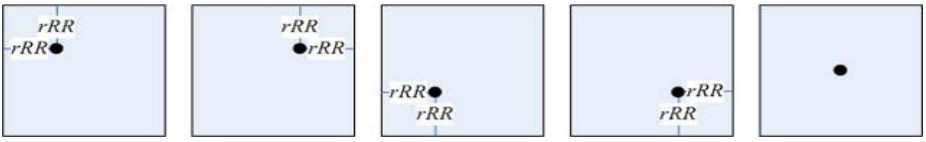

Fig. 5. The starting points of a locating curve

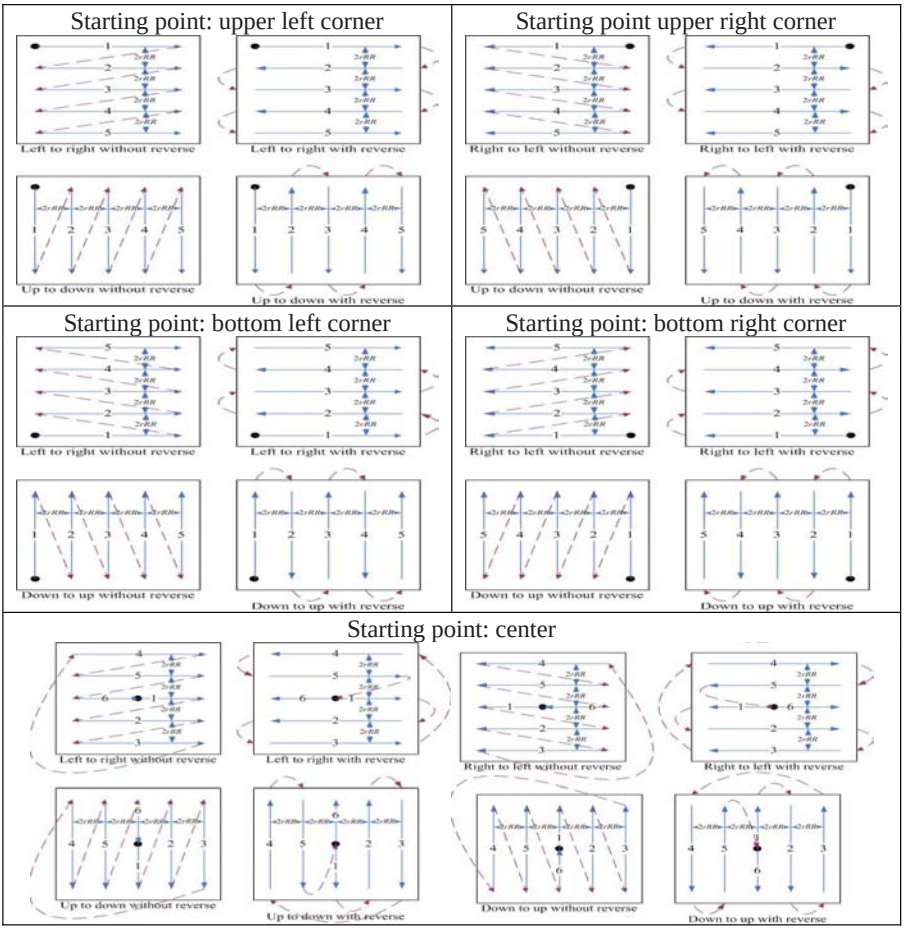

Fig. 6. Locating curves for locating RFID readers

corner of *RP*, and the center of *RP*, as a whole, they are shown in Figure 5. The moving directions can be arranged as up to down, down to up, left to right, and right to left. These directions are also dependent on the locations of their starting points. Reversed directions are also taken into account when the movement reaches the boundary of an *RP*. The possible locating curves are shown in Figure 6. Solid black circles are the starting points, solid arrows are the locating curves, the number on the

lines are the sequences of each independent locating curve set, and dashed arrows are auxiliary descriptions for illustrating a moving direction of location curves.

The stopping criterion is set to a predefined generation number. The common roulette wheel is the selection method, PMX (Partially Matching Crossover) is the crossover method, and the mutation is straight-forwardly done by randomly exchange two locations inside an individual during GA operations. Elitist policy is adopted in order to keep the best solution during the improving phases.

4 Simulation and Discussion

In order to evaluate the performance of the proposed method, a computer program that coded with the proposed algorithm was developed. Thousands of testing cases, which were randomly generated first, were simulated and analyzed. The number of contiguous forbidden blocks scattered in the plane for these testing cases is of six different discrete levels denoted as 0~5. The locations of them have 2 types of scattering patterns, i.e. uniform and random distributions. The total area of forbidden blocks has 5 different variations, they are 10%, 15%, 20%, 25%, and 30% of the total area of a plane under surveillance). Eight types of non-rectangular planes (rectangular shaped, + shaped, I-shaped, L-shaped, O-shaped, S-shaped, T-shaped, U-shaped) are simulated in the testing cases and each type of non-rectangular plane has 5 different sizes (10, 20, 30, 40, and 50 times of the scanning range of the specified RFID reader).

From the simulation results, we found the percentage of feasible monitoring region of SLP-RFID system in testing plane is around 85% for 90% of these testing cases. The performance has around 20% improvement after performing the hybrid GA approach. The improvement of the key performance indices is more obvious when the number of contiguous forbidden blocks is increasing. The larger number of contiguous forbidden blocks in the specified plane, the worse monitoring rate of this SLP-RFID system has. Contiguous forbidden blocks with uniform distribution, in general, have better performance than those generated via random distributions.

Rectangular shaped planes have better performance than those of the other shaped planes can have. Via statistic hypothesis test, there exist no substantial evidence to state that the size of non-rectangular plane has effects on the feasible monitoring rate in the SLP-RFID system when the number of forbidden blocks scattered in the plane is less than 2. The larger the number of RFID readers need to be used, the more acceptable monitoring rate can be obtained. The higher ratio of the feasible region (plane without forbidden block) to the scanning range of a RFID reader of a testing case, the better performance the proposed SLP-RFID system can provide.

The time complexity for proposed method is strongly dependents on the dimensions of *RP* (the minimum rectangle which can contain the specified plane). It takes O(*nFA*RPLen*RPWid*) for adjusting algorithm. The proposed minimum cost algorithm only needs constant computational time, O(1). It takes O(*nFA*RPLen*RPWid*) to mark out forbidden blocks. And, creating initial population takes O(*PS*RPLen*RPWid*), where *PS* denotes the population size. The procedure of GA improvement is determined by the number of generation, fitness function, and

population size. Therefore, it is obvious that the time complexity for the proposed research is linearly dependent on the dimension of *RP* and parameters of GA.

5 Conclusion

This research proposed an algorithm to systematically deploy minimal number of RFID detecting devices in a general plane. By adequately and smartly planning these devices' layout, we can actually visualize RFID tagged items in a general-shaped plane. We consider not only the number of RFID readers needed, but also exclude non-feasible regions for monitoring in an RFID system. The outputs of the planning system suggest the minimum cost and the maximum monitoring region for different attributed scanning devices. And the most important of all, it finds the proper locations of each RFID reader within a reasonable computational time.

Besides proposing the algorithm, a computer program was developed to realize the SLP-RFID system. The system is not only a simulation tool for performance analysis, but also provide practical solutions for realize a customer-designated visualizing plane. Thousands of cases were simulated and analyzed to evaluate the performance of the proposed approach. We have proved the applicability of this system from simulations results. The efficient computational time also makes the proposed method more practicable and useful in applications.

The proposed method provides users with multiple solutions for varied combinations of cost and even more complicated monitoring regions in a reasonable computational time. Such complicated cases are multi-purposed plane that each may have both partially transparent departments and partially visualizing interiors. Because the parameters of GA can be adjusted by users, they make the proposed method applicable and efficient for real planning.

References

[1] Maier, K.: A COTS developer's point of view on Radio Frequency Identification. Technology Feature: Homeland Security, CompactPCI and AdvancedTCA Systems (2005)
[2] Sangni, K.: RFID SEES ALL. IEE Review, April 2004 (2004)
[3] Murphy-Hoye, M., Lee, H.L., Rice, J.B.: A Real-World Look at, Supply Chain Management Review, July-August 2005 (2005) http://www.scmr.com
[4] Morley, G.: Radio Frequency ID Tags - What They Are, How They Can Be Used and How Production Costs Can Be Reduced, Technique Report, Automation Research Centre, Univ. of Limerick, August 2003 (2003)
[5] Weinstein, R.: RFID: A Technical Overview and Its Application to the Enterprise. IEEE Computer Society, Los Alamitos (2005)

Promising Search Regions of Crossover Operators for Function Optimization

Hiroshi Someya

The Institute of Statistical Mathematics,
4-6-7 Minami-Azabu, Minato-ku, Tokyo, Japan
some@ism.ac.jp
http://www.ism.ac.jp/~some/

Abstract. Performance of a genetic algorithm for function optimization, often appeared in real-world applications, depends on its crossover operator strongly. Existing crossover operators are designed for intensive search in certain promising regions. This paper, first, discusses where the promising search regions are on the basis of some assumptions about the fitness landscapes of objective functions and those about a state of a population, and this discussion reveals that existing crossover operators intensively search some of the promising regions but not all of them. Then, this paper designs a new crossover operator for searching all of the promising regions. For utilizing the advantageous features of this crossover operator, a new selection model considering characteristic preservation is also introduced. Several experiments have shown the proposed method has worked effectively on various test functions.

Keywords: Genetic Algorithms, Crossover Operators, Function Optimization.

1 Introduction

Function optimization often appears in real-world applications, such as designing lens systems, designing aircrafts and protein structure prediction. For such applications, various Real-Coded Genetic Algorithms (RCGAs), which use real number vector representation of chromosomes, have been proposed. Generally, crossover operators for RCGAs are designed for searching certain regions near a parent population intensively. The regions are determined on the basis of some assumptions about the fitness landscapes of objective functions and those about a state of an individual population. First, we discuss where the promising search regions are. Then, this paper designs a new crossover operator in consideration of this discussion. In the remainder of this paper, the terms "solution candidate", "search point", and "individual" are used without distinction because our discussion covers various stochastic optimization methods. Objective functions are treated as minimization problems.

RCGA is one of stochastic optimization methods. The most primitive stochastic optimization method must be Random Search method (RS). The performance

H.G. Okuno and M. Ali (Eds.): IEA/AIE 2007, LNAI 4570, pp. 434–443, 2007.

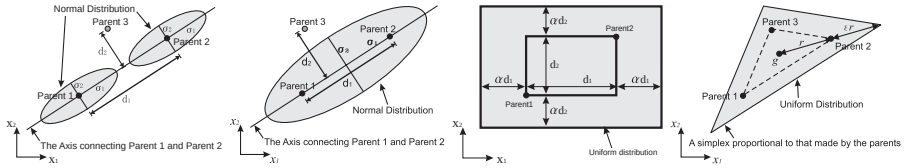

(a) BNDX (b) UNDX (c) BLX-α (d) SPX

Fig. 1. Examples of representative crossover operators

of RS is often unsatisfactory because it disregards any features of the landscapes of objective functions. Other stochastic optimization methods such as Hill-Climbing method (HC) and Simulated Annealing (SA) using a local search operator are designed on the basis of an assumption, *global smoothness of the landscape*. Such methods expect that a rough shape of the landscape of an objective function is smooth even though a microscopic shape could be ragged, and they estimate the evaluation value of a solution candidate to be approximate equivalent to those of its nearby solution candidates. Since they show better performance than RS in general, the first promising search region must be

Promising Search Region 1: *near a promising solution candidate.*

The behavior of a local search operator is controlled by its probability density function (p.d.f.) normally expressed in a multi-dimensional normal distribution. This distribution has two kinds of parameters: the mean and the standard deviations. Usually, the peak of the distribution, indicated by the former parameter, is set to be the current search point, and the latter parameters are determined by the user's empirical knowledge or pilot studies. In contrast, crossover operators of RCGAs determine the search direction on the basis of the relative position of parents and adjust the search step width according to the distance between parents, adaptively. An example of such crossover operator BNDX [1] is shown in Fig.1a.

RCGAs are generally designed to realize an ideal search behavior of an individual population as shown in Fig.2. First, the initial population is randomly distributed in the search space. Then, the population members globally explore in early search stages because the user has no clue to find the optimum. As the search goes on, the individuals converge into around the optimum and exploit there. Therefore, after middle search stages, we expect that the individuals are surrounding the optimum. When the parents are randomly chosen from the population, we can apply this assumption of the population to the parents. UNDX [2, 3] is an example designed for this ideal search process (see Fig.1b). Its p.d.f. is expressed in a multi-dimensional normal distribution, and the peak of the p.d.f is located at the middle point of parent1 and parent2. The search region can be summarized in *around a parent population* rather than *around a parent*. It has been reported that the performance of UNDX is greater than that of BNDX on high-dimensional multimodal functions because UNDX urges parents to escape from local minima [2]. Thus, this paper proposes that the second promising search region should be

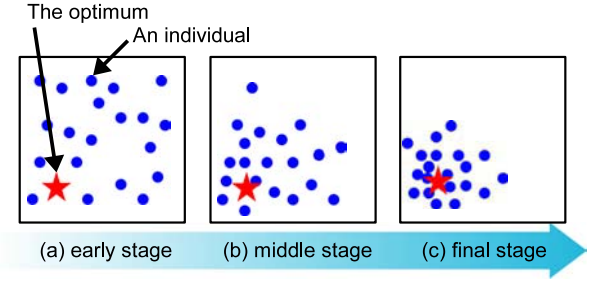

Fig. 2. An example of an ideal process of population distribution

Promising Search Region 2: *the inner region of a parent distribution.*

Other examples that can mainly search the second promising search region include BLX-α [4] and SPX [5] (see Fig.1c and Fig.1d). The comparison of their search regions explains that search regions of crossover operators should be independent of coordinate axes. The search region of BLX-α is in a hyper rectangular region where each side is parallel to the corresponding coordinate axis. Let consider in the case that the ups and downs of the landscape of an objective function are not parallel to the coordinate axes. Although crossover operators should focus on the diagonal connecting the parents, BLX-α does not behave in such a manner (demonstrated by Ono *et.al* [1,3]). In contrast, SPX intensively searches near the line, and its performance is independent of coordinate systems. Thus, the promising search region must be

Promising Search Region 3: *independent of coordinate systems.*

Kita *et al.* have discussed guidelines for designing crossover operators [6, 7]. A guideline recommended is *preservation of statistics*. It requires that "distribution of the children generated by crossover operators should preserve the statistics such as the mean vector and the covariance matrix of the distribution of parents well". If the children distributed narrower or wider than their parents, it may let the optimum escape or wastes computation time in searching hopeless region. Therefore, sampling new solutions in the region that the parents reside will be an appropriate choice. The authors have also reported that a crossover operator with its tuned parameters to satisfy the guideline showed higher performance than that with other parameters. Thus, the fourth promising search region should be

Promising Search Region 4: *a region satisfying "preservation of statistics"*

Table 1 summarizes the main search regions of the representative search operators mentioned above, where PCX [8] and UNDX-m [7] are multi-parental extensions of BNDX and UNDX respectively. We can observe that no existing search operators satisfy to search all the promising search regions.

Table 1. The main search regions of representative search operators and the proposed crossover. The PSR is the abbreviation for "promising search region".

	around a parent	around a parent population		
	PSR1	PSR2	PSR3	PSR4
Local Search, SA	◯	-	-	-
BNDX, PCX	◯	-	◯	-
UNDX, UNDX-m	-	◯	◯	◯
BLX-α	-	◯	-	◯
SPX	-	◯	◯	◯
ANDX (proposed)	◯	◯	◯	◯

2 Proposed Crossover Operator

This section designs a new crossover operator, Asymmetrical Normal Distribution Crossover (ANDX), for searching all the promising search regions.

ANDX produces children near each parent. Let $\boldsymbol{g}$ be the center of mass of m parents, $\boldsymbol{p}^{(1)}, \ldots, \boldsymbol{p}^{(m)}$, and let $\boldsymbol{d}^{(j)} = \boldsymbol{p}^{(j)} - \boldsymbol{g}$. A child $\boldsymbol{c}^{(s)}$ is produced near $\boldsymbol{p}^{(s)}$, chosen from the parents randomly, in the following equation:

$$\boldsymbol{c}^{(s)} = \boldsymbol{p}^{(s)} - \sum_{j \neq s}^{m} \boldsymbol{d}^{(j)} \omega^{(j)} + \boldsymbol{q} \ . \tag{1}$$

The symbol $\sum_{j \neq s}^{m}$ expresses the notation for summation of index $j = 1, \ldots, m$ except for $j = s$. Each ω is an asymmetrical normal random variable defined as:

$$\omega \sim \begin{cases} 2\zeta_o N(0, \sigma_o^2) & (x \geq 0) \\ 2\zeta_i N(0, \sigma_i^2) & (x < 0) \end{cases} \tag{2}$$

where $\zeta_o + \zeta_i = 1, \sigma_o = \zeta_o \sigma$, and $\sigma_i = \zeta_i \sigma$. The ζ_o and σ are the parameters of ANDX. Let W be the subspace spanned by $\boldsymbol{d}^{(1)}, \ldots, \boldsymbol{d}^{(m)}$, and let $W^{\perp}$ be the orthogonal complement. The $\boldsymbol{q}$ is a vector defined in $W^{\perp}$. For example, if $\boldsymbol{q}$ would be defined as the same manner of UNDX and UNDX-m:

$$\boldsymbol{q} = D \sum_{k=1}^{n-m+1} \boldsymbol{e}^{(k)} v^{(k)} \tag{3}$$

where D is the length of the component of $\boldsymbol{d}^{(m+1)}$, the vector drawn from $\boldsymbol{g}$ to an additional parent $\boldsymbol{p}^{(m+1)}$, orthogonal to $\boldsymbol{d}^{(1)}, \ldots, \boldsymbol{d}^{(m)}$, and each $\boldsymbol{e}^{(k)}$ is an orthonormal basis of $W^{\perp}$. Each normal random variable $v^{(k)}$ is defined as $N(0, \sigma_\eta^2)$.

ANDX intensively searches all the promising regions. The correspondence between the peak of the probability density distribution of each $\boldsymbol{c}^{(j)}$ and the position of $\boldsymbol{p}^{(j)}$ as shown in Fig.3 explains that ANDX searches the promising search region 1. To realize searches that prefer the promising search region 2,

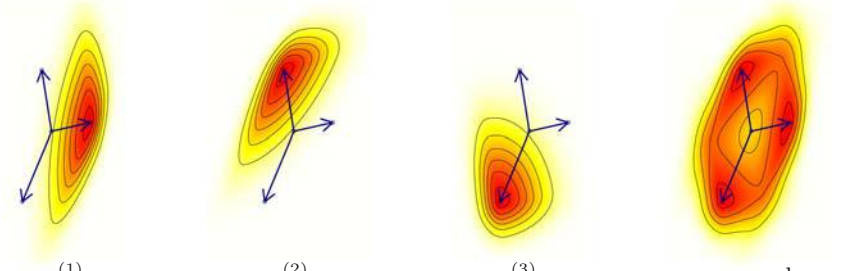

Fig. 3. Examples of probability density distribution of ANDX on a 2-dimensional search space. The parameter values are $\zeta_o = 0.3$ and $\sigma \fallingdotseq 1.0$. The parent vectors are $\boldsymbol{p}^{(1)} = (4, 1), \boldsymbol{p}^{(2)} = (-1, 7)$ and $\boldsymbol{p}^{(3)} = (-3, -8)$.

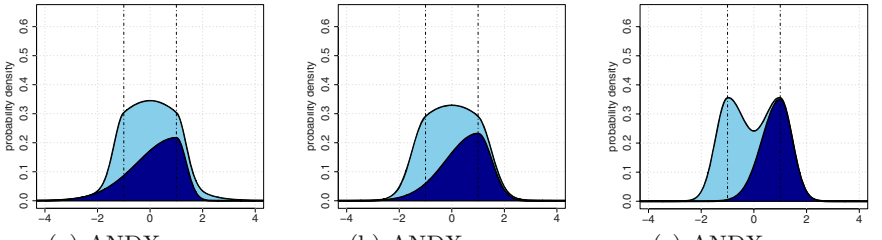

(a) ANDX$_{\zeta=0.2}$ (b) ANDX$_{\zeta=0.3}$ (c) ANDX$_{\zeta=0.4}$

Fig. 4. Examples of p.d.f.s on a 1-dimensional search space. Each parent is located at $\boldsymbol{p}^{(1)} = -1$ and $\boldsymbol{p}^{(2)} = 1$, respectively. The parameters are set to satisfy (4). The dark filled curves indicate p.d.f.s of $\boldsymbol{c}^{(2)}$ only.

the parameter ζ_o is set to satisfy $\zeta_o < \zeta_i$. As for the promising search region 3, ANDX is independent of coordinate systems. When the parameters are set after

$$\sigma = \frac{2\sqrt{2\pi}(2\zeta_o - 1)}{2(m-2)(2\zeta_o - 1)^2 - \pi(m-1)(3\zeta_o^2 - 3\zeta_o + 1)} \ , \tag{4}$$

the children are placed in the promising search region 4. The derivation of this equation is summarized in Appendix. Examples of p.d.f.s introduced by such parameters are demonstrated in Fig.4. As for the $W^{\perp}$ component, when (3) is adopted, the following parameter value, recommended in [7], preserves the statistics:

$$\sigma_\eta = \frac{1}{\sqrt{n-m+1}} \frac{\sqrt{m}}{\sqrt{m+1}} \frac{\sqrt{3}}{\sqrt{2}} \beta, \quad \beta = 0.35 \ . \tag{5}$$

3 Selection Model

To avoid premature convergence of the population in the early stages improves performance of RCGAs [4,9]. For appropriate maintenance of the diversity of the

population, the population should contain a variety of characteristics of genes. For this, only one individual should survive the competition in a family, a group that consists of parents and their children, because each individual that belongs to the family has similar characteristics of genes. This paper calls this survival strategy *exclusive replacement strategy*. We apply this strategy to MGG model [9] by dividing the family into subfamilies. Each subfamily consists of a parent and especially similar children to the parent. In this selection model, eXclusive-MGG (X-MGG), only one individual is allowed to survive from a subfamily. Procedure of a generation of this model using ANDX is described as follows:

Step 1 Choose $m+1$ parents, $P = \{\boldsymbol{p}^{(1)}, \ldots, \boldsymbol{p}^{(m)}\}$ and $\boldsymbol{p}^{(m+1)}$, randomly from the population.
Step 2 Produce children, $C = \{C^{(1)}, \ldots, C^{(m)}\}$ where $C^{(j)}$ is a group including $\boldsymbol{c}^{(j)}$ produced near $\boldsymbol{p}^{(j)}$, using ANDX. Let $S = \{S^{(1)}, \ldots, S^{(m)}\}$ where $S^{(j)}$ is a subfamily that consists of $\boldsymbol{p}^{(j)}$ and $C^{(j)}$.
Step 3 Select the best individual $\boldsymbol{I}_{best}$ in S. Let $S^{(best)}$ be the $S^{(j)}$ that includes $\boldsymbol{I}_{best}$, and let $\boldsymbol{p}^{(best)}$ be the parent that belongs to $S^{(best)}$.
Step 4 Select one individual $\boldsymbol{I}_{roulette}$ by fitness-based or rank-based roulette-wheel selection from the group derived from S by removing $S^{(best)}$. Let $\boldsymbol{p}^{(roulette)}$ be the parent that belongs to the $S^{(j)}$ including $\boldsymbol{I}_{roulette}$.
Step 5 replace $\boldsymbol{p}^{(best)}$ with $\boldsymbol{I}_{best}$.
Step 6 replace $\boldsymbol{p}^{(roulette)}$ with $\boldsymbol{I}_{roulette}$.

4 Empirical Studies

4.1 Conditions

This section performs several computer experiments to measure the performance and to study appropriate parameter values of the proposed method, ANDX with X-MGG. In real-world applications, the landscapes of objective functions are characterized by several different structures. Therefore optimization methods for them are required to deal with not only a specific structure but also various kinds of structures. This paper covers the following structures:

(A) discreteness
(B) big valley / punch bowl The landscapes have one big valley in which the optimum is located near the center. Multimodal and unimodal landscapes are called big valley and punch bowl, respectively.
(C) the optimum exists near a boundary rather than in the center of the search space
(D) ridge structure The optimum exists in a very narrow valley like a ridge.
(E) epistasis Ups and downs of the landscapes are not parallel to the coordinate axes.
(F) UV structure The landscapes have two different types of valleys: *U valley* and *V valley*. The former has subotima in itself, and the latter has the optimum in itself. On such landscapes the population members often converge into a U valley because the shape or the position of V valley is hard to be searched for RCGAs.

Table 2. Test functions. Each d_i is set to be $0.0, 1.5, 3.0$ or 4.5. The "max." indicates the maximal number of evaluations. The (A)∼(F) in this table correspond to those in Section 4.1.

	experimental conditions			landscape					
	domain	dimension	max.	(A)	(B)	(C)	(D)	(E)	(F)
F_{step}	$(-5.12 + d_i, 5.12 + d_i)$	50	1e6	√	√	√	-	-	-
$F_{rastrigin}$	$(-5.12 + d_i, 5.12 + d_i)$	10	3e6	-	√	√	-	-	-
$F_{rosenbrock}$	$(-2.048, 2.048)$	40	3e7	-	√	√	√	√	-
F_{ikeda}	$(0, 3)$	2	2e8	-	-	√	-	-	√

This paper adopted the following four test functions:

$$
\begin{aligned}
F_{step} &= \textstyle\sum_{i=1}^{n} \lfloor x_i + 0.5 \rfloor^2 \ , \\
F_{rastrigin} &= 10n + \textstyle\sum_{i=1}^{n} \left\{ x_i^2 - 10\cos(2\pi x_i) \right\} \ , \\
F_{rosenbrock} &= \textstyle\sum_{i=2}^{n} \left\{ 100(x_1 - x_i^2)^2 + (x_i - 1)^2 \right\} \ , \\
F_{ikeda} &= \textstyle\sum_{i=1}^{2} \left\{ 4(x_i - \lfloor x_i \rfloor - 0.5)^2 + bB(x_i) \right\} + A \ , \\
B(x_i) &:= 1 - \left\{ \tfrac{1+\cos(2\pi C x\ )}{2} \right\}^D \ , \\
(A, C, D) &:= \begin{cases} (0{,}c \quad ,d \quad), & \text{if } \lfloor x_1 \rfloor = r_1 \text{ and } \lfloor x_2 \rfloor = r_2 \\ (a{,}c \quad ,d \quad), & \text{otherwise} \end{cases} \ .
\end{aligned}
$$

The experimental conditions and the characteristic structures of the landscapes of the test functions are summarized in Table 2. Although each the optimum of F_{step} and $F_{rastrigin}$ exists at the origin, its relative position in the domain is moved by the value of d_i. For example, the relative position of the optimum is set to be at the center or near a corner when d_i is 0.0 or 4.5, respectively. The optimum of $F_{rosenbrock}$ is located at $1, \ldots, 1$. F_{ikeda} is formed into five different UV structures by its parameter settings. Our experiments adopted the same parameter settings except for $a = 0.05$ as those in [10, 11] for $f_{9c}, f_{9e}, f_{9s}, f_{9s+}$ and f_{9s*}. The f_{9c} consists one V valley centered in the search space and eight U valleys surrounding this V valley. The landscapes of f_{9s} and f_{9e} differ from that of f_{9c} in the position of the V valley. Their V valleys exist near a side and near a corner of the search space respectively. The f_{9s+} and f_{9s*} are similar to f_{9s} except that the V valley of f_{9s+} is narrower and deeper than that of f_{9s} and the U valleys of f_{9s*} have smoother surface than those of f_{9s}.

The parameter ζ_o of ANDX was set to be $0.2, 0.3$, or 0.4, and the value of σ was determined under (4) (see Fig.4). The vector $\boldsymbol{q}$ in (3) was defined as (5). The proposed method was compared to UNDX with MGG because it has frequently shown higher performance than other existing methods. Both methods used two parents and one additional parent in each crossover operation. No mutation was performed in either method. The population size was fixed at 100 for multimodal functions, but 30 for unimodal ones. The number of children produced in each generation was set to be 50. The performance measure adopted was rate of finding the optimum.

Table 3. The percentages, rounded off to the first decimal place, of runs in which each method succeeded in finding the global optimum in 300 runs

F_{step}		d_i			
		0.0	1.5	3.0	4.5
MGG	UNDX	98	63	39	34
	ANDX$_{\zeta\ =0.2}$	98	78	53	47
	ANDX$_{\zeta\ =0.3}$	**100**	98	94	91
	ANDX$_{\zeta\ =0.4}$	**100**	**100**	**100**	**100**
X-MGG	ANDX$_{\zeta\ =0.2}$	99	80	64	61
	ANDX$_{\zeta\ =0.3}$	**100**	**100**	99	99
	ANDX$_{\zeta\ =0.4}$	**100**	**100**	**100**	**100**

$F_{rastrigin}$		d_i			
		0.0	1.5	3.0	4.5
MGG	UNDX	**61**	8	1	0
	ANDX$_{\zeta\ =0.2}$	60	11	3	1
	ANDX$_{\zeta\ =0.3}$	59	17	5	3
	ANDX$_{\zeta\ =0.4}$	51	**21**	**9**	**6**
X-MGG	ANDX$_{\zeta\ =0.2}$	68	17	3	2
	ANDX$_{\zeta\ =0.3}$	79	28	12	9
	ANDX$_{\zeta\ =0.4}$	**99**	**97**	**97**	**97**

$F_{rosenbrock}$		
MGG	UNDX	62
	ANDX$_{\zeta\ =0.2}$	63
	ANDX$_{\zeta\ =0.3}$	62
	ANDX$_{\zeta\ =0.4}$	**65**
X-MGG	ANDX$_{\zeta\ =0.2}$	72
	ANDX$_{\zeta\ =0.3}$	74
	ANDX$_{\zeta\ =0.4}$	**96**

F_{ikeda}		UV type			
		f_{9e}	f_{9s}	f_{9s+}	f_{9s*}
MGG	UNDX	36	77	25	55
	ANDX$_{\zeta\ =0.2}$	47	83	23	63
	ANDX$_{\zeta\ =0.3}$	46	85	26	59
	ANDX$_{\zeta\ =0.4}$	**58**	**87**	**33**	**70**
X-MGG	ANDX$_{\zeta\ =0.2}$	44	85	25	62
	ANDX$_{\zeta\ =0.3}$	49	90	32	64
	ANDX$_{\zeta\ =0.4}$	**67**	**93**	**40**	**83**

4.2 Experimental Results and Discussions

All the methods perfectly succeeded on f_{9c}. The other results, shown in Table 3, report that the proposed method performed well in all the cases. The results on F_{step} and $F_{rastrigin}$ show the effectiveness of ANDX on landscapes featuring discrete punch bowl or big-valley structure. We observe that every method decreases its performance as d_i increases. This is explained by a sampling bias of the crossover operators toward points near the center of the parents. The sampling bias urges the population members to converge on the center of the search space. Therefore it works advantageously in the case that the optimum exists in this region. In contrast this bias becomes disadvantage in the other cases. The inferior performance of ANDX$_{\zeta\ =0.4}$ with MGG on $F_{rastrigin}$ with $d_i = 0.0$ is also explained by the sampling bias, because the optimum of this function exists at the center of the search space and the sampling bias of ANDX$_{\zeta\ =0.4}$ is weaker than that of UNDX. With regard to this inferior performance, this paper claims that the robustness should be given priority over the performance in a specific case because no one knows where the optimum exists before a trial in real-world applications.

On $F_{rosenbrock}$ ANDX performed well with X-MGG. These experimental results present importance of diversity maintaining for ridge structure. In the case that a landscape contains this structure, a population of RCGAs tends to be converged into a certain point (often far from the optimum) on a ridge. X-MGG assists in avoiding this situation. ANDX$_{\zeta\ =0.4}$ with X-MGG outperformed the

others on F_{ikeda}. Although enough parallel searches with individuals distributed in each valley in the landscape are necessary for a function featuring UV structure, this behavior also leads to slow and unstable convergence. In fact, the convergence curves of the best method were such curves. To deal with this trade-off property, adaptive tuning of the parameter values should be useful.

5 Conclusions and Future Works

This paper presented several promising search regions for crossover operators and designed a new crossover operator ANDX for searching all these regions. In some experiments, ANDX with a new selection model introduced worked effectively. These experiments were performed under a condition where only two parents and one additional parent are used in each crossover operation. We should investigate behaviors of ANDX with more parents toward real-world applications. Adaptive parameter tuning mentioned in the previous section is also a future work.

Acknowledgements. I thanks Prof. H. Kita (Kyoto Univ.) for helpful advice on the covariance matrix of UNDX-m. This work was supported in part by the "Function and Induction research project" by ROIS of Japan.

References

1. Ono, I., Yamamura, M., Kobayashi, S.: A genetic algorithm with characteristic preservation for function optimization. In: Proc. of the IIZUKA'96, pp. 511–514 (1996)
2. Ono, I.: Genetic algorithms for optimization taking account of characteristics preservation (in Japanese). PhD thesis, Tokyo Institute of Technology (1997)
3. Ono, I., Kobayashi, S.: A real-coded genetic algorithm for function optimization using unimodal normal distribution crossover. In: Proc. of the 7th International Conference on Genetic Algorithms, pp. 246–253 (1997)
4. Eshelman, L.J., Schaffer, J.D.: Real-Coded Genetic Algorithms and Interval-Schemata. In: Foundations of Genetic Algorithms, vol. 2, pp. 187–202. Morgan Kaufman, Washington (1993)
5. Tsutsui, S., Yamamura, M., Higuchi, T.: Multi-parent recombination with simplex crossover in real coded genetic algorithms. In: Proc. of the Genetic and Evolutionary Computation Conference 1999, pp. 657–664 (1999)
6. Kita, H., Yamamura, M.: A functional specialization hypothesis for designing genetic algorithms. In: Proc. of 1999, IEEE International Conference on Systems, Man and Cybernetics, pp. 579–584 (1999)
7. Kita, H., Ono, I., Kobayashi, S.: Multi parental extension of the unimodal normal distribution crossover for real-coded genetic algorithms. In: Proc. of the 1999 Congress on Evolutionary Computation, pp. 1581–1587 (1999)
8. Deb, K., Anand, A., Joshi, D.: A computationally efficient evolutionary algorithm for real-parameter optimization. Evolutionary Computation 10(4), 371–395 (2002)
9. Satoh, H., Yamamura, M., Kobayashi, S.: Minimal generation gap model for GAs considering both exploration and exploitation. In: Proc. of the IIZUKA'96, pp. 494–497 (1996)

10. Ikeda, K., Kobayashi, S.: UV phenomenon on genetic algorithms, and UV structure hypothesis (in Japanese). Transactions of the Japanese Society for Artificial Intelligence 17(3), 239–246 (2002)
11. Ikeda, K., Kobayashi, S.: GA based on the UV-structure hypothesis and its application to JSP. In: Proc. of the Sixth International Conference on Parallel Problem Solving from Nature, pp. 273–282 (2000)

Appendix: Parameter Setting for Preservation of Statistics

First, we discuss the statistics of the children produced by ANDX without the $W^{\perp}$ component. As for the mean vector of $\boldsymbol{c}^{(s)}$, we obtain

$$\langle \boldsymbol{c}^{(s)} \rangle = \boldsymbol{p}^{(s)} - \langle \sum_{j \neq s}^{m} \boldsymbol{d}^{(j)} \omega^{(j)} \rangle = \boldsymbol{p}^{(s)} + \boldsymbol{d}^{(s)} \langle \omega \rangle \ .$$

Therefore, the mean vector of the whole children $\langle \boldsymbol{c} \rangle$ coincides with that of the parents $\boldsymbol{g}$ as shown in the following equation:

$$\langle \boldsymbol{c} \rangle = \langle \boldsymbol{p}^{(s)} \rangle + \langle \boldsymbol{d}^{(s)} \rangle \langle \omega \rangle = \boldsymbol{g} \ . \tag{6}$$

Let $\mathit{\Gamma}_p$, $\mathit{\Gamma}_c^{(s)}$ and $\mathit{\Gamma}_c$ be the covariance matrixes of the parents, the children $\boldsymbol{c}^{(s)}$, and the whole children, respectively. $\mathit{\Gamma}_c^{(s)}$ is calculated as follows:

$$\begin{aligned}
\mathit{\Gamma}_c^{(s)} =& \langle (\boldsymbol{c}^{(s)} - \langle \boldsymbol{c} \rangle)(\boldsymbol{c}^{(s)} - \langle \boldsymbol{c} \rangle)^T \rangle \\
=& (\boldsymbol{p}^{(s)} - \boldsymbol{g})(\boldsymbol{p}^{(s)} - \boldsymbol{g})^T \\
&+ 2\langle \omega \rangle (\boldsymbol{p}^{(s)} - \boldsymbol{g})(\boldsymbol{p}^{(s)} - \boldsymbol{g})^T \\
&+ \langle \omega^2 \rangle \textstyle\sum_{j \neq s}^{m} (\boldsymbol{p}^{(j)} - \boldsymbol{g})(\boldsymbol{p}^{(j)} - \boldsymbol{g})^T \\
&- \langle \omega \rangle^2 \textstyle\sum_{j \neq s}^{m} (\boldsymbol{p}^{(j)} - \boldsymbol{g})(\boldsymbol{p}^{(j)} - \boldsymbol{g})^T \\
&+ \langle \omega \rangle^2 (\boldsymbol{p}^{(s)} - \boldsymbol{g})(\boldsymbol{p}^{(s)} - \boldsymbol{g})^T \ .
\end{aligned} \tag{7}$$

Hence we obtain

$$\mathit{\Gamma}_c = \langle \mathit{\Gamma}_c^{(s)} \rangle = \{1 + 2\langle \omega \rangle + (m-1)\langle \omega^2 \rangle - (m-2)\langle \omega \rangle^2\} \mathit{\Gamma}_p \ . \tag{8}$$

The constraint for $\mathit{\Gamma}_c = \mathit{\Gamma}_p$ must be

$$2\langle \omega \rangle + (m-1)\langle \omega^2 \rangle - (m-2)\langle \omega \rangle^2 = 0 \ . \tag{9}$$

Substituting the following equations into (9) gives (4).

$$\begin{aligned}
\langle \omega \rangle &= \int_{-\infty}^{0} 2\zeta_i N(0, \sigma_i^2) x dx + \int_{0}^{\infty} 2\zeta_o N(0, \sigma_o^2) x dx \\
&= \frac{2(\zeta_o \sigma_o - \zeta_i \sigma_i)}{\sqrt{2\pi}} = \frac{2(\zeta_o - \zeta_i)\sigma}{\sqrt{2\pi}} = \frac{2(2\zeta_o - 1)\sigma}{\sqrt{2\pi}},
\end{aligned} \tag{10}$$

$$\begin{aligned}
\langle \omega^2 \rangle &= \int_{-\infty}^{0} 2\zeta_i N(0, \sigma_i^2) x^2 dx + \int_{0}^{\infty} 2\zeta_o N(0, \sigma_o^2) x^2 dx \\
&= \zeta_o \sigma_o^2 + \zeta_i \sigma_i^2 = (\zeta_o^2 - \zeta_o \zeta_i + \zeta_i^2)\sigma^2 = (3\zeta_o^2 - 3\zeta_o + 1)\sigma^2 \ .
\end{aligned} \tag{11}$$

Automatic Fingerprints Image Generation Using Evolutionary Algorithm

Ung-Keun Cho, Jin-Hyuk Hong, and Sung-Bae Cho

Dept. of Computer Science, Yonsei University
Biometrics Engineering Research Center
134 Sinchon-dong, Seodaemun-ku
Seoul 120-749, Korea
{bearoot,hjinh}@sclab.yonsei.ac.kr, sbcho@cs.yonsei.ac.kr

Abstract. Constructing a fingerprint database is important to evaluate the performance of automatic fingerprint recognition systems. Because of the difficulty in collecting fingerprint samples, there are only few benchmark databases available. Moreover, various types of fingerprints are required to measure how robust the system is in various environments. This paper presents a novel method that generates various fingerprint images automatically from only a few training samples by using the genetic algorithm. Fingerprint images generated by the proposed method include similar characteristics of those collected from a corresponding real environment. Experiments with real fingerprints verify the usefulness of the proposed method.

Keywords: fingerprint identification performance evaluation, genetic algorithm, image filtering, image generation.

1 Introduction

Due to the persistence and individuality of fingerprints, fingerprint recognition has become a popular personal identification technique [1]. Recently, people consider it important to evaluate its robustness for practical application [2]. Performance evaluation, mostly dependent on benchmark databases, is a difficult process, because of the lack of public fingerprint databases involving large samples. Except for some popular fingerprint databases such as NIST database [3] and FVC databases [2], researchers usually rely on their own small-scale database to evaluate their system. The construction of fingerprint databases requires an enormous effort so that, in practice, it is often too costly or the resulting database is incomplete or unrealistic [4]. Moreover, the database should include samples collected in various environments in order to estimate the robustness under realistic applications [5].

In order to measure the performance of fingerprint recognition systems from various points of view, researchers proposed several performance evaluation protocols and databases. Jain, *et al.* developed a twin-test by measuring the similarity of identical twins' fingerprints [6], while Pankanti, *et al.* theoretically estimated the individuality of fingerprints [1]. Hong, *et al.* reviewed performance evaluation for

H.G. Okuno and M. Ali (Eds.): IEA/AIE 2007, LNAI 4570, pp. 444–453, 2007.

biometrics systems including fingerprint verification systems [7]. Khanna and Weicheng presented benchmarking results using NIST special database 4 [3], and Maio, *et al.* initiated several competitions of fingerprint verification such as FVC [2]. Simon-Zorita, *et al.* collected MCYT Fingerprint Database in consideration of position variability control and image quality [5].

There were some works on the generation of synthetic images for constructing databases with little cost and effort. FaceGen [9] is a modeler for generating and manipulating human faces. It manages shape, texture, expression, phones, and accessories (hair, glasses), and reconstructs 3D face from single images to test face recognition techniques [10]. Cappelli, *et al.* developed a software (SFinGE) [4] that heuristically generated fingerprint images according to some parameters, where the synthetic databases were used as one of benchmark databases in FVC [2].

In this paper, we propose a novel method that generates fingerprint images from only a few initial samples, in which the images get similar characteristics to ones manually collected from a real environment. When a target environment is given, the proposed method constructs a set of filters that modifies an original image so as to become similar to that collected in the environment. A proper set of filters is found by the genetic algorithm [8,11], where fitness evaluation is conducted using various statistics of fingerprints to measure the similarity.

2 Proposed Method

2.1 Overview

The proposed method works based on a simple genetic algorithm as shown in Fig. 1, and fitness evaluation optimizes a filter set that can produce fingerprint images corresponding to a given environment. In the initialization step, it sets basic parameters including the population size, the maximum number of generations, the length of chromosomes, selection strategy, selection rate, crossover rate and mutation rate. The length of chromosomes means the size of a filter composed, where each gene in the chromosome represents the corresponding filter in the pool of filters. A target environment should be also determined in initialization so that the proposed method can generate images having the similar characteristics of fingerprints collected by that environment. Only a few samples are required to calculate several statistics for the target environment to evaluate a chromosome.

After initializing population, the proposed method iteratively conducts fitness evaluation, selection, crossover and mutation until satisfying a terminal condition, in which the last 3 steps work the same as the genetic algorithm. Especially, the fitness of a chromosome is obtained from the similarity between a few real images from the target environment and images generated after filtering. The value of each gene means a filter to apply for images of the training database. If we collect some samples from an environment which we target, the proposed method automatically analyzes the environment and finds out a set of proper filters without any expert knowledge.

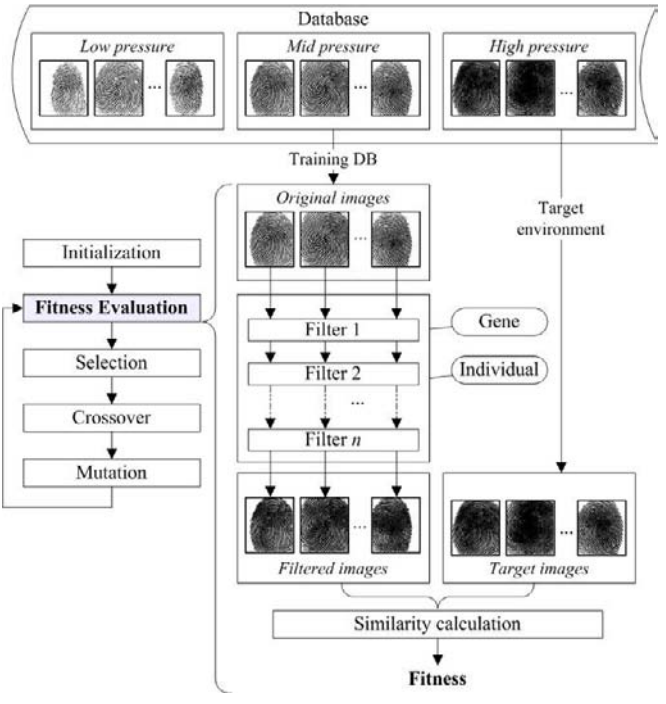

Fig. 1. Overview of the proposed method

2.2 Image Filter Pool

Popular image filters are used to produce similar effects in real environments. Even though each filter has a simple effect as shown in Table 1, they are able to produce various results when appropriately compounding with each other. The order and type of filters used in the filter set are determined by the genetic algorithm, because it is practically impossible to test all the cases of composition.

Table 1. Image filters used in this paper

Group	Filter	Index
Histogram	Brightness (3 values), Contrast (3 values), Stretch, Equalize, Logarithm	1~9
Mask	Blur (6 masks), Sharper (4 masks), Median (10 masks)	10~29
Morphology(10 masks)	Erosion, Dilation, Opening, Closing	30~69
	None	0

Table 1 shows the description of image filters used in this paper. They are widely used to reduce noises, smooth images, or stress the focus of images [12]. Typically, there are several categories of image filters such as histogram-based filters, mask

filters and morphological filters. Various parameters like mask types make the effect of filtering more diverse. Total 70 filters construct the pool of filters.

2.3 Fitness Evaluation

The fitness of a filter set is estimated by measuring the similarity between fingerprints collected from the target environment and images generated by the composite filter. Several representative features of fingerprints, such as the mean and variance of images, directional contrasts [13], average ridge thickness and interval [14], singularities [13] and minutiae [1], are used to design the fitness evaluation function. As mentioned before, fingerprints are easily affected by an input environment, where the statistics of fingerprints obtained might manifest the environment. Table 2 shows the features of fingerprint images used in this paper with some explanation.

Table 2. Features of fingerprint images for fitness evaluation

Feature	Description	Purpose
Mean	The mean of gray values	Measurement of whole gray level
Variance	The variance of gray values	Uniformity of gray values
Directional contrast	The mean of block directional difference	Distinctness between ridges and valleys
Thickness	The mean of ridge thickness	Measurement of ridge thickness
Interval	The mean of valley thickness	Measurement of valley thickness
Singularity	The region of discontinuous directional field	Major features of fingerprints
Minutiae	Ending and bifurcation point of ridges	Major features of fingerprint recognition

There are 4 directional contrasts obtained by estimating the block directional difference in 8 cardinal directions without regard for the opposite direction.

Singularity is detected by the Poincare index [13], which is a popular method to compute core and delta points based on the orientation field. According to results by the algorithm and human experts, 3 types of singularities are defined as follows:

- Missing singularity: A set of real singularities which the algorithm cannot detect.
- Spurious singularity: A set of points which the algorithm detects but are not real.
- Paired singularity: A set of real singularities which the algorithm detects well.

Minutiae points are extracted through the process of Gabor filtering, binarization and thinning the ridges [1]. Minutiae including ending and bifurcation and nothing can be detected by the algorithm and identified by human experts, respectively, so as to define 8 types of combinations as follows: ending-ending, ending-bifurcation, ending-nothing, bifurcation-ending, bifurcation-bifurcation, bifurcation-nothing, nothing-ending, and nothing-bifurcation.

With these various statistics for fingerprints, the fitness evaluation function, in which weights are heuristically determined, is defined as follows. The statistics of the target environment is calculated from the environment database. All the values are normalized from 0 to 1.

$$\begin{aligned} fitness(i) = {} & w_1 \times (mean_i - mean_{\text{target}}) \\ & + w_2 \times (variance_i - variance_{\text{target}}) \\ & + w_3 \times \sum_{j=1}^{4} (contrast_i^j - contrast_{\text{target}}^j) \\ & + w_4 \times (thickness_i - thickness_{\text{target}}) \\ & + w_5 \times (interval_i - interval_{\text{target}}) \\ & + w_6 \times \sum_{c \in singularityType} (singularity_i(c) - singularity_{\text{target}}(c)) \\ & + w_7 \times \sum_{c \in minutiaeType} (minutiae_i(c) - minutiae_{\text{target}}(c)) \end{aligned} \tag{1}$$

3 Experimental Results

3.1 Experimental Environment

The usability of the proposed method is verified by comparing the fingerprints collected from real environments with those generated. A fingerprint database, used in this work, is constructed by Computer Vision Laboratory in Inha University, in which three fingerprints images were captured from each finger according to the input pressure (high (H), middle (M) and low (L)) [15]. Forty two fingerprint images of fourteen fingers are used for training, while forty five fingerprint images of fifteen fingers are for test. In the experiment, we aim to generate the fingerprints of high and low pressures from those of middle pressure. With the training data, two filter sets (M→H, M→L) are evolved by the proposed method for each environment. Real fingerprints of high and low pressures in the training data are used to calculate the statistics of target environments as shown in Fig. 1. After evolution, we apply the filter obtained to the test data and measure the similarity between the real fingerprints of high and low pressures and fingerprints generated from middle pressure.

Fig. 2 shows the distribution of features for the training data. The input pressure affects the value of fingerprint features, which might also influence fingerprint recognition. The ridges of highly pressed fingerprints are easily connected and spurious bifurcation points are generated, while fingerprints of low pressure are apt to generate spurious ending points. It is natural that the thickness and interval of ridges are divided to the input pressure. On the other side, singularity is less affected by the input pressure since it is calculated by the global feature like orientation. The fingerprints, collected in the environment of middle input pressure, show good performance in extracting minutiae points rather than the others. Especially, ‘real ending-extracted bifur’ and ‘real bifur-extracted ending’ of minutiae strongly show the trend of effects of the input pressure.

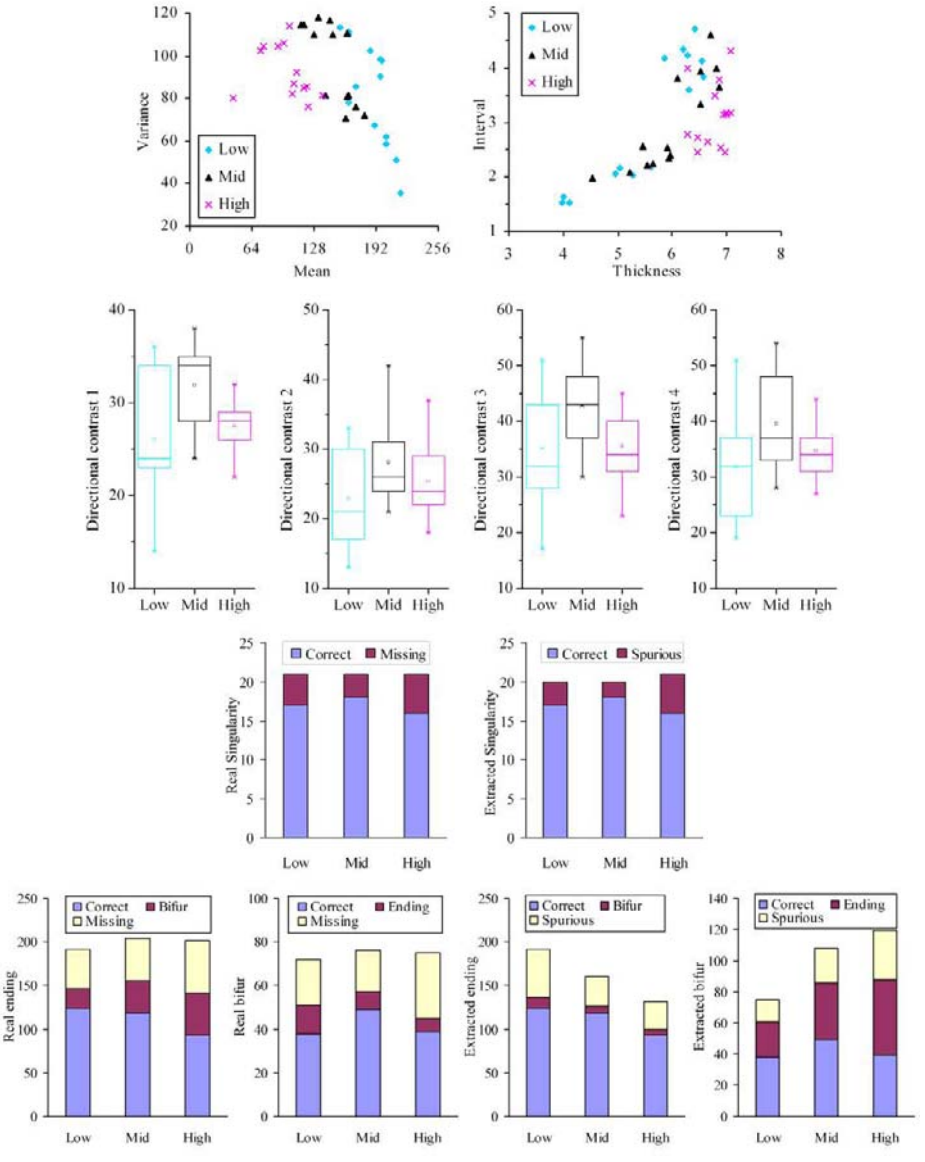

Fig. 2. Minutiae analysis of the training data

3.2 Analysis of the Process of Evolution

Parameters of the genetic algorithm in the experiment are set as follows: 100 generations, 50 populations, 5 gene lengths, 0.7 selection rate, 0.7 crossover rate and 0.05 mutation rate. At most five filters are used to compose a filter set because the

size of chromosomes is set as five. Roulette-wheel selection is used as a basic selection mechanism. Weights used in the fitness function are set as (1, 1, 1, 2, 2, 1, 3), since the ridge information is highly affected by the input pressure.

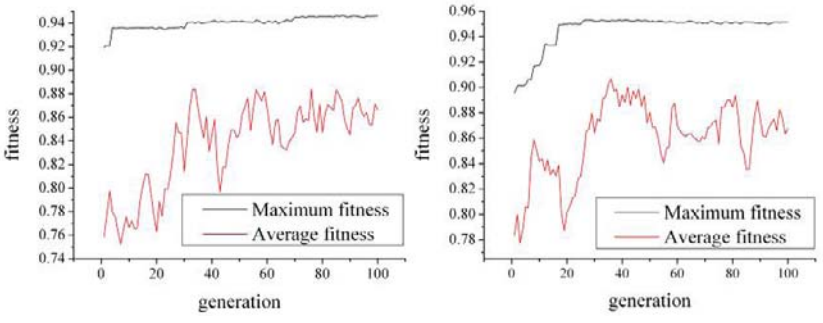

Fig. 3. Fitness through evolution (left: high pressure, right: low pressure)

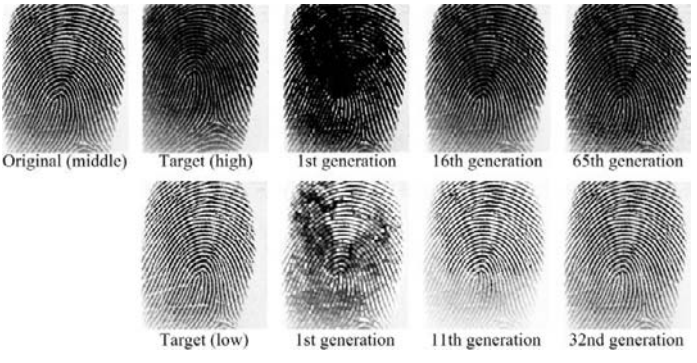

Fig. 4. Fingerprints produced by the proposed method

Table 3. Filter sets obtained through evolution

Environment	Filter type				
High	Highpass 3×3 #2	Erosion 1×3	Closing 3×1	Closing Rectangle 3×3	None
Low	None	None	Stretch	Dilation Diamond 3×3	None

Better filter sets are obtained by the proposed method through evolution as shown in Fig. 3. The maximum and average fitness increase as the generation grows for both target environments. Fig. 4 shows the resulting fingerprints that show similar figures to those collected from the target environments, while Table 3 presents the best filter sets obtained in the last generation.

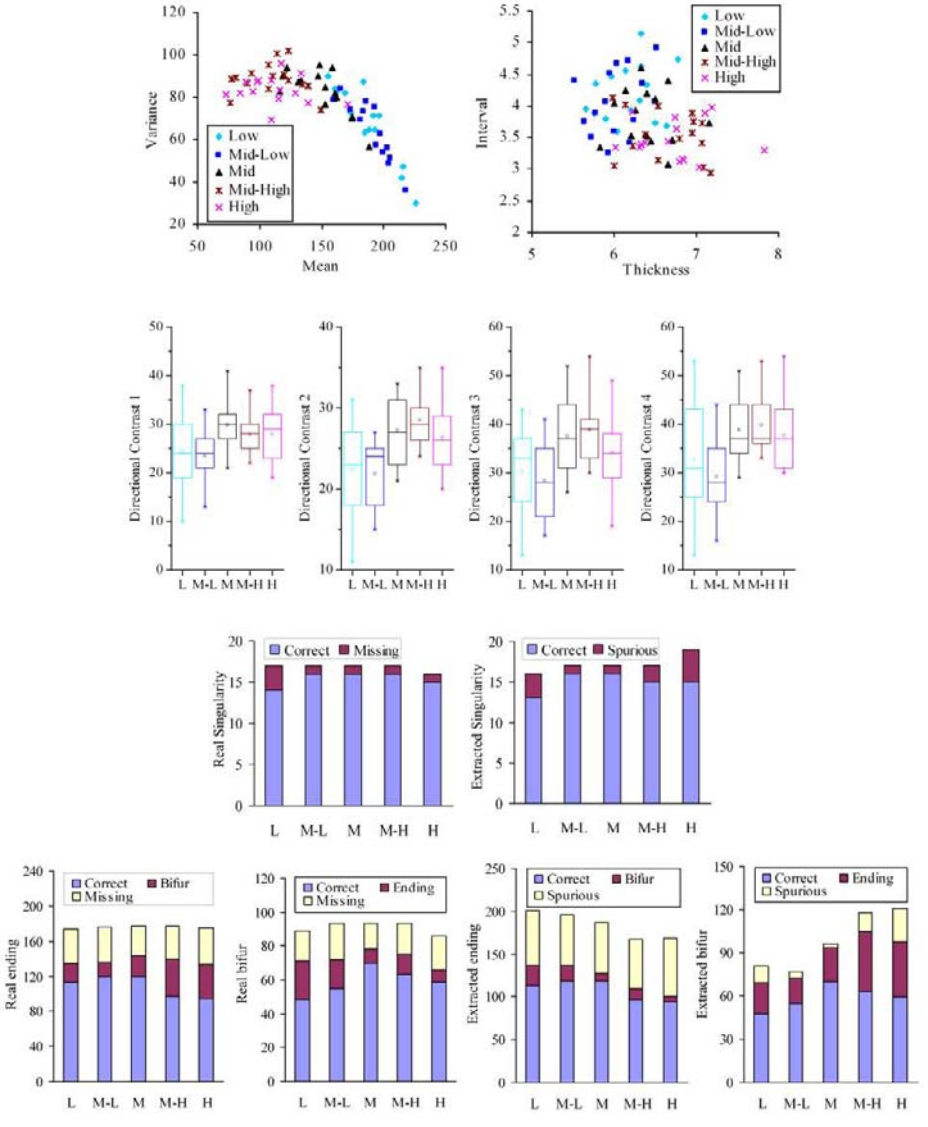

Fig. 5. Minutiae analysis of the test data

3.3 Analysis of Generated Fingerprints

We have analyzed the resulting fingerprints by comparing with fingerprints collected from the target environment. As shown in Fig. 5, the statistics of the fingerprints of middle pressure has been closer to those calculated from the target environments, especially for mean, directional contrasts, ridge thickness and interval. Since singularity is hardly dependent on the orientation of original images, however, it is not able to correctly model the target environment. Fig. 5 shows that the proposed

method is very useful in the distribution of minutiae extracted, where the generated fingerprints show similar aspect to those of the target environments in most cases of extracting minutiae points. Generated-high and generated-low signify the results of the proposed method.

Fig. 6 shows the impostor/genuine distribution and FMR/FNMR curves [4] on collected and generated fingerprint databases using VeriFinger 4.2 SDK. Although they are the same source fingerprints, generated images have lower performance than originals and little difference from those in the target environment.

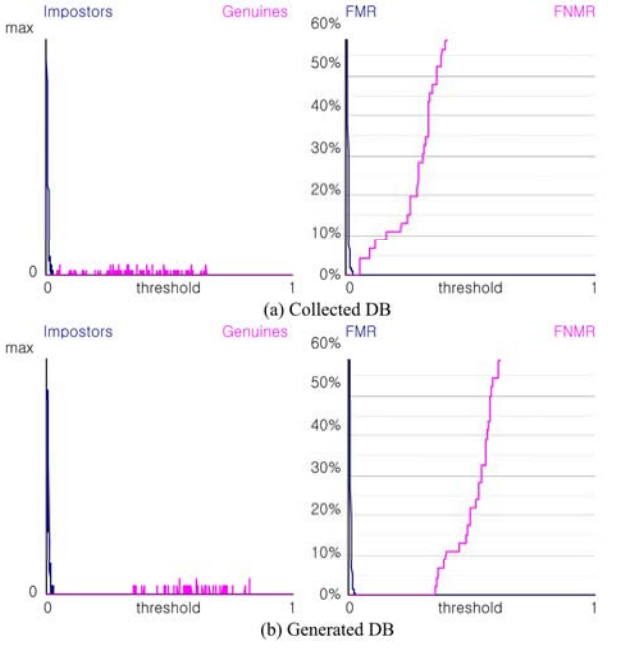

Fig. 6. Impostor/genuine distribution and FMR/FNMR curves

4 Concluding Remarks

In this paper, we have proposed a novel method that automatically generates fingerprint images by using the genetic algorithm. Various simple image filters are used to construct a composite filter where the genetic algorithm searches their proper types and order. We have conducted experiments on the real database collected according to input pressure, where fingerprints generated by the proposed method showed the similar characteristics to those collected from real environments in terms of various statistics of fingerprint images. The generated images might be used to evaluate the performance of fingerprint recognition systems. Moreover, the proposed method has the applicability to the fingerprint image enhancement by modifying the fitness evaluation module.

As the future work, in order to generate realistic fingerprints more precisely, we will develop a fingerprint model that characterizes them with various measures. Heuristic filters that deform fingerprints might be used to include various effects into them.

Acknowledgments. This work was supported by the Korea Science and Engineering Foundation (KOSEF) through the Biometrics Engineering Research Center (BERC) at Yonsei University.

References

[1] Pankanti, S., Prabhakar, S., Jain, A.: On the individuality of fingerprints. IEEE Trans. Pattern Analysis and Machine Intelligence 24(8), 1010–1025 (2002)
[2] Cappelli, R., Maio, D., Maltoni, D., Wayman, J.L., Jain, A.K.: Performance evaluation of fingerprint verification systems. IEEE Trans. Pattern Analysis and Machine Intelligence 28(1), 3–18 (2006)
[3] Khanna, R., Weicheng, S.: Automated fingerprint identification system (AFIS) benchmarking using the National Institute of Standards and Technology (NIST) Special Database 4. In: Proc. 28th Int. Carnahan Conf. on Security Technology, pp. 188–194 (1994)
[4] Maltoni, D.: Generation of Synthetic Fingerprint Image Databases. In: Ratha, N., Bolle, R. (eds.) Automatic Fingerprint Recognition Systems, Springer, Heidelberg (2004)
[5] Simon-Zorita, D., Ortega-Garcia, J., Fierrez-Aguilar, J., Gonzalez-Rodriguez, J.: Image quality and position variability assessment in minutiae-based fingerprint verification. IEEE Proc. Vision, Image Signal Process 150(6), 402–408 (2003)
[6] Jain, A., Prabhakar, S., Pankanti, S.: On the similarity of identical twin fingerprints. Pattern Recognition 35(11), 2653–2663 (2002)
[7] Hong, J.-H., Yun, E.-K., Cho, S.-B.: A review of performance evaluation for biometrics systems. Int. J. Image and Graphics 5(2), 501–536 (2005)
[8] Goldberg, D.: Genetic Algorithm in Search, Optimization and Machine Learning. Addison Wesley, London (1989)
[9] Blanz, V., Vetter, T.: A Morphable Model for the Synthesis of 3D Faces. In: Proc. Computer Graphics SIGGRAPH, pp. 187–194 (1999)
[10] Orlans, N., Piszcz, A., Chavez, R.: Parametrically controlled synthetic imagery experiment for face recognition testing. In: Proc. ACM SIGMM workshop on Biometrics Methods and Applications, pp. 58–64 (2003)
[11] Cho, U.-K., Hong, J.-H., Cho, S.-B.: Evolutionary singularity filter bank optimization for fingerprint image enhancement. In: Rothlauf, F., Branke, J., Cagnoni, S., Costa, E., Cotta, C., Drechsler, R., Lutton, E., Machado, P., Moore, J.H., Romero, J., Smith, G.D., Squillero, G., Takagi, H. (eds.) EvoWorkshops 2006. LNCS, vol. 3907, pp. 380–390. Springer, Heidelberg (2006)
[12] Gonzalez, R., Woods, R.: Digital Image Processing. Addison-Wesley, London (1992)
[13] Karu, K., Jain, A.: Fingerprint Classification. Pattern Recognition 29(3), 389–404 (1996)
[14] Lim, E., Jiang, X., Yau, W.: Fingerprint quality and validity analysis. IEEE Int. Conf. on Image Processing 1, 22–25 (2002)
[15] Kang, H., Lee, B., Kim, H., Shin, D., Kim, J.: A study on performance evaluation of fingerprint sensors. In: Proc. 4th Int. Conf. Audio-and Video-based Biometric Person Authentication, pp. 574–583 (2003)

A Hybrid Genetic Algorithm for the Cut Order Planning Problem

Ahlem Bouziri[1] and Rym M'hallah[2]

[1] Institut Supérieur des Arts Multimédia, Manouba University, 13 rue des Entrepreneurs, Charguia II, Tunisia
ahlem.bouziri@wanadoo.tn
[2] Department of Statistics and Operations Research, Kuwait University, P.O. Box 5969, Safat 13060, Kuwait
mhallah@kuc01.kuniv.edu.kw

Abstract. This paper proposes a new hybrid heuristic to a difficult but frequently occurring problem in the apparel industry: the cut order planning (COP). This problem consists of finding the combination of ordered sizes on the material layers that minimizes total material utilization. The current practice in industry solves COP independently from the two-dimensional layout (TDL) problem; i.e., COP estimates the length of the layout required to cut a particular combination of sizes instead of packing the pieces on the fabric and determining the actual length used. Evidently, this results in a build up of estimation errors; thus increased waste. Herein, COP and TDL are combined into a single problem CT. The resulting problem is modeled and solved using a hybrid heuristic which combines the advantages of population based approaches (genetic algorithms) with those of local search (simulated annealing). The experimental results show the validity of the proposed model, and the sizeable savings it induces when solved using the proposed hybrid heuristic.

Keywords: hybrid heuristics, simulated annealing, genetic algorithms.

1 Introduction

Cut order planning (COP) is a frequent problem in the apparel industry. It consists of finding the best combination of the layout of the patterns of the sizes ordered by the clients on a rectangular fabric of fixed width W. The best combination optimizes material utilization; that is, minimizes L, the total length of fabric used to generate all the pieces of the patterns included in the order. An apparel manufacturing order undergoes four stages. First, a COP problem is solved. Second, Two-Dimensional Layouts (TDL) are generated. Third, the layouts are cut and divided into lots. Fourth and last, the lots are sewn, assembled and packaged. Currently, stages 1 and 2 are undertaken independently. In stage 1, human experts or dedicated software solve COP using an *estimated* length of the layout of a combination of sizes. The estimate is generally a coarse approximation that is read from catalogs prescribing material usage of basic models.

H.G. Okuno and M. Ali (Eds.): IEA/AIE 2007, LNAI 4570, pp. 454–463, 2007.

The COP solution is then transferred to the TDL room where it is packed on rectangles of fixed width, and maximal length $\overline{l}$ where $\overline{l}$ is the length of the cutting table.

An order, in the apparel manufacturing process, consists of one or more garments (eg., a pair of pants, a shirt, a suit, etc.) in varying colors, sizes and quantities per size per color. The order is split according to garment type and color into suborders. Since different colored clothes are layered separately and different garments are treated separately (to minimize the risk of errors during assembly), hereafter, an order denotes a suborder. An order is characterized by its set S of sizes, their number n, and the order quantity q_s for size $s \in S$.

A garment is a finite set G of pieces which when assembled according to a preset procedure yield the garment. The dimensions of each piece depend on its size s. Let G_s denote the set of pieces of a garment in size $s \in S$. Each set $G_s, s \in S$, is duplicated q_s times. The duplicated sets are positioned on a fabric of known fixed width W as to minimize the total length L. The positioned pieces are cut using a computer guided cutter. Since the length of the cutting table is finite, and the set up for the cutting stage is high, producers choose to layer the cloth and to position sets of pieces on layered cloth. The automatic guided cutter works best when the number of layers or *ply height* is in the interval $[\underline{h}, \overline{h}]$, where $\underline{h}$ and $\overline{h}$ are respectively minimal and maximal ply height.

The ply height is an additional variable of the problem. For instance, if the order requires producing 20 blouses of size XP, then G_{XP} can be positioned 20 times on a fabric of a single layer, or 4 times on a fabric that has 5 plies, or only once on a fabric having 20 plies, depending on $\overline{l}, \underline{h}, \overline{h}$, and on the overall efficiency of the layout. The layered cloth is called a *section*. An order may be split into one or more sections; each having a different number of plies and different sets.

Formally, the problem can be stated as follows. Given a set S of sizes, the sets $G_s, s \in S$ of pieces composing the garment, the fabric width W, the minimum and maximum ply height $\underline{h}$ and $\overline{h}$, and the maximum length of the cutting table $\overline{l}$, find the configuration that minimizes the *total* length L of used fabric. A configuration is completely specified by the number of sections p required to position all the pieces, where the sections need not be identical. Each section $i,\ i = 1, \ldots, p$ is characterized by its ply height h_i, the number of occurrences O_{is} of each size $s \in S$, and the shortest length layout l_i of the pieces it contains when set on a rectangle of fixed width W. The configuration is feasible if $l_i \leq \overline{l}$, and $\underline{h} \leq h_i \leq \overline{h},\ i = 1, \ldots, p$. The total length of the layout $L = \sum_{i=1}^{p} h_i l_i$.

In industry, markers solve COP using cataloged l_i values. Herein, $l_i,\ i = 1, \ldots, p$ is determined by solving a two dimensional layout problem for section i. That is, stages 1 and 2 of the apparel manufacturing process are combined into a single COP-TDL problem. The resulting problem, denoted CT, yields an overall total length that is more accurate than that estimated by markers. Fig. 1 provides an example of the input and output of CT for an order consisting of $n = 6$ different sizes: XP, P, M, T, XT, XXT with $q_{XP} = 20, q_P = 25, q_M = 35, q_T = 30, q_{XT} = 20$, and $q_{XXT} = 10$.

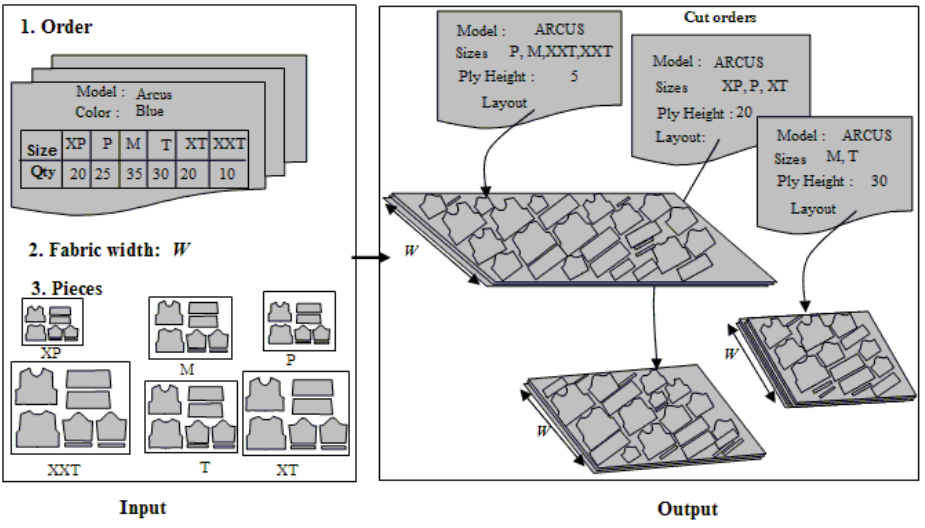

Fig. 1. Input and Output for COP

CT, which is a complex combinatorial problem, is NP-complete. It is an extension of COP, which is in turn NP-complete [7]. Herein, CT is approximately solved using genetic annealing (GAn), a hybrid heuristic that combines the advantages of local and global optimization procedures.

This paper is organized as follows. Section 2 gives a brief review of the COP and TDL literature. Section 3 describes the solution configuration. Section 4 details GAn. Section 5 assesses the performance of GAn and evaluates the potential savings induced by combining COP and TDL. Finally, Section 6 summarizes this research and indicates possible extensions.

2 Literature Review

TDL, which is a Cutting and Packing Problem, consists of finding the minimal length layout of a set of (ir)regular two-dimensional pieces on a stock sheet of finite width but infinite length. The layout must not contain any overlap. Even though NP-hard, TDL has been widely studied in the literature [1] - [4], [6], [8]. Proposed methods fit into one of two classes. In the first class, prior to being packed, irregular items are nested into regular shapes. In the second class, irregular pieces are packed using complex geometric computations [6].

COP has been addressed by ElOmri [5] and Jacobs-Blecha et al. [7] who focused on the cut order planning stage of the manufacturing process. They both assumed that the length of the layouts are catalogued. Jacobs-Blecha et al. [7] concluded that the cut order cost is the most dominant component of the cutting process. M'Hallah et al. [9] provided the example of a local industry which sells its value added for a $1/ garment, making a net profit of $.4/ garment while

its estimated cost for cloth is \$17.5/ garment. Reducing waste by 6% multiplies the original net profit by a factor of 3.5. Any saving on cloth represents a large percentage of the gross gain and a further larger percentage of the net gain. Herein, it is assumed that the cost of fabric is the dominant cost of COP and that minimizing the total COP cost minimizes the total length of the layout.

3 Solution Configuration

A solution to CT is represented by a $(p \times n + 2)$ matrix. The first n columns contain $O_{is}, i = 1, \ldots, p, s \in S$. Columns $n + 1$ and $n + 2$ contain respectively h_i and $l_i, i = 1, \ldots, p$. The number of columns of the matrix is constant but the number of sections is not necessarily identical for all feasible solutions. A solution to CT is feasible if it satisfies the demand constraints; i.e., if $\sum_{i=1}^{p} h_i O_{is} = q_s,\ s \in S$. The fitness of a feasible solution is the total length of fabric needed to cut all its sections: $fitness = \sum_{i=1}^{p} h_i l_i$. The solution corresponding to the output of Fig. 1 is given by the 3×8 matrix

$$\begin{pmatrix} 0\,0\,1\,1\,0\,0\,30\,l_1 \\ 1\,1\,0\,0\,1\,0\,20\,l_2 \\ 0\,1\,1\,0\,0\,2\ \ 5\,l_3 \end{pmatrix}.$$

The first row of the matrix represents section 1, which includes two sizes, and has a ply height equal to 30 and a length l_1. The third column shows that size M occurs once on section 1 (i.e., $O_{1M} = 1$) but does not appear on section 2 (i.e., $O_{2M} = 0$) and appears once on section 3 (i.e., $O_{3M} = 1$). The sets of pieces assigned to any section $i, i = 1, \ldots, p$, are packed using the sequential best local position (BLP) layout procedure of [6].

4 The Hybrid Approach

CT is solved using a hybrid heuristic: genetic annealing, which combines the advantages of global and local optimization. It guides the diversification / intensification of the search of the solution space. During the first generations, it favors diversification, but gradually increases intensification by imposing stricter criteria for the inclusion of offsprings into the population as time evolves.

GAn is implemented using a low-level teamwork hybridization [10]. It explores several regions of the solution space using a population based meta heuristic, which in this case is GA. An offspring is immediately admitted into the population if its fitness is lower than that of its parent. However, a non-improving offspring is allowed into the population if and only if its fitness is less than its parent's threshold level. Initially, the threshold level of an individual is its fitness. As it proliferates, an individual is either replaced by its offspring -if it produces a fitter offspring- or has its threshold decreased; that is, its endurance is increased allowing it to further proliferate. At each iteration, a set composed of the fittest chromosomes is subject to intensification around its immediate neighborhood using SA. Formally, the adopted GAn proceeds as follows.

Initialization.

1. Create an initial population that has $popsize$ random chromosomes.
2. Compute the fitness L_j of each chromosome j and set its threshold level $\theta_j = L_j,\ j = 1, \ldots, popsize$.

Iterative Step.

For $generation = 1, n_g$,

1. For $j = 1, popsize$,
   (a) Let chromosome j be Parent1 and let Child be the offspring obtained by mutation or crossover of Parent1.
   (b) Compute L_c, the fitness of Child.
   (c) If $L_c < L_j$, then replace chromosome j by Child, set $\theta_j = L_c$,
   (d) Else,
   - Set $\tau_0 = 0.6$, and $\theta_j = \theta_j * \alpha$, where $\alpha \in [.95, .99]$.
   - If $\exp(-\theta_j)$ > Rand[0,1], replace chromosome j by Child, and set $\theta_j = L_c$.
2. Select the $n_{SA}/2$ fittest chromosomes of the current population
3. Set $\tau_0 = 0.2$.
4. For $j = 1, n_{SA}/2$,
   -- Apply SA with chromosome j being the initial solution and T_0 such that $\tau_0 = e^{-\frac{|\overline{\Delta}|}{T_0}}$, where $\overline{\Delta}$ is the average variation of the fitness of the chromosomes of the current population from their threshold levels.
5. Randomly pick $n_{SA}/2$ chromosomes from the current population
6. Set $\tau_0 = 0.6$.
7. For $j = 1, n_{SA}/2$,
   -- Apply SA with chromosome j being the initial solution and T_0 such that $\tau_0 = e^{-\frac{|\overline{\Delta}|}{T_0}}$, where $\overline{\Delta}$ is the average variation of the fitness of the chromosomes of the current population from their threshold levels.

Crossover produces a new chromosome (offspring or Child) from two parents: Parent1 and Parent2. The Child inherits part of its genes from the p_1 genes of Parent1 and is completed according to the p_2 genes of Parent2, as explained below.

1. Pick two integer random numbers i_1 and i_2 from the discrete uniform $[1, p_1]$.
2. Copy sections i_1 through i_2 from Parent1 to the first $i_2 - i_1 + 1$ genes of Child.
3. Set the current number of sections of Child $p^{\text{Child}} = i_2 - i_1 + 1$, and set $i = 1$.
4. Calculate the residual demand for Child: $r_s = q_s - \sum_{i=1}^{p^{\text{Child}}} O_{is} h_i, s \in S$.
5. If $\max_{s \in S}\{r_s\} = 0$, stop.
6. Generate for Child a new gene $i' = p^{\text{Child}} + i$, whose $h_{i'} = \min\{h_i^{\text{Parent2}}, LCD(r_s : r_s > 0, O_{is}^{\text{Parent2}} > 0, s \in S)\}$, with $O_{i's} = \frac{r_s}{h_{i'}},\ s \in S$, where h_i^{Parent2} is the ply height of section i of Parent2, and O_{is}^{Parent2} is the number of occurrences of size s in section i of Parent2.
7. Increment i by 1. Goto step 4.

To illustrate how crossover proceeds, consider the example of crossing `Parent1`

$$\begin{pmatrix} 1\,0\,0\,0\,0\,1\;10\;l_1 \\ 0\,1\,0\,0\,1\,0\;20\;l_2 \\ 0\,0\,1\,1\,0\,0\;30\;l_3 \\ 2\,1\,1\,0\,0\,0\;\;5\;l_4 \end{pmatrix}$$

and `Parent2`

$$\begin{pmatrix} 2\,2\,3\,3\,2\,1\;10\;l_1 \\ 0\,0\,1\,1\,0\,0\;\;5\;\;l_2 \end{pmatrix}.$$

Let i_1 and i_2, generated from the discrete Uniform $[1, 4]$, be 2 and 3, respectively. `Child` inherits genes 2 and 3 of `Parent1`:

$$\begin{pmatrix} 0\,1\,0\,0\,1\,0\;20\;l_2 \\ 0\,0\,1\,1\,0\,0\;30\;l_3 \end{pmatrix}.$$

Computing the residual demand yields: $r_{XP} = 20,\ r_P = 25 - 20 = 5,\ r_M = 35 - 30 = 5,\ r_T = 30 - 30 = 0,\ r_{XT} = 20 - 20 = 0$, and $r_{XXT} = 10 - 0 = 10$. Since $\max_{s \in S}\{r_s\} = 20 > 0$, then `Child` is completed using the genes of `Parent2`. The third section of `Child` has $h_3 = \min\{20, 5\}$, where 20 is the ply height of section 1 of `Parent2`, and $5 = LCD(r_s : r_s > 0, O_{is} > 0, s \in S) = LCD(r_{XP}, r_P, r_M, r_{XXT}) = LCD(20, 5, 5, 10)$.

Computing $O_{3s} = \frac{r_s}{h_3}$ yields $O_{3XP} = 4, O_{3P} = 1, O_{3M} = 1,\ O_{3XXT} = 2$, and $r_s = 0, s \in S$. Therefore, `Child` has only 3 sections:

$$\begin{pmatrix} 0\,1\,0\,0\,1\,0\;20\;l_2 \\ 0\,0\,1\,1\,0\,0\;30\;l_3 \\ 4\,1\,1\,0\,0\,2\;\;5\;\;l_3' \end{pmatrix}.$$

Mutation is applied to some of the offspring population to make them better adapted to their new environment. It is not intended to greatly disturb the current structure of an offspring. As such, mutation moves a size from its original section to another section. A formal statement of the mutation operator follows.

1. Randomly choose a section i of the p sections of Parent.
2. Randomly choose a size s from set $S' = \{s \in S : O_{is} > 0\}$.
3. Compute the residual demand resulting from moving s from section i, i.e., $r_s = h_i O_{is}$.
4. Find a section $j,\ j = 1, \ldots, p, j \neq i$, whose h_j is a divider of r_s.
   - If only one such section exists, set $O_{js} = O_{js} + \frac{r_s}{h_j}$.
   - Else if more than one section exist say j and j', then add size s to the section whose total length will be smallest when s is added.
   - Else if no such section exists, set $J = \{j = 1, \ldots, p,\ j \neq i : h_j \leq r_s\}$.
     * If $J \neq \emptyset$, dispatch r_s among the sections of J such that $\sum_{j \in J} \Delta O_{js} h_j = r_s$, where ΔO_{js} is the additional number of occurrences of size s in section j.
     * If $J = \emptyset$, create a new section $p + 1$ whose $h_{p+1} = h_i, O_{p+1s} = O_{is}$, and $O_{p+1s'} = 0, s' \in S, s' \neq s$.

The **Genetic parameters** are the population size *popsize*, the number of generations n_g, and the probability of mutation P_m. A large population size insures the diversification of the population while a large number of generations gives chromosomes a higher chance of strengthening their better genes. However, the increase of these two parameters increases runtime. A good tradeoff between diversification and intensification is therefore needed. We opted for a moderately large population size and a relatively small number of generations; thus, opting for diversification of the search in the solution space. Intensification is achieved by allowing the best chromosomes to proliferate at least once and to be mutated more frequently than lower quality chromosomes. Indeed, P_m is set inversely proportional to the rank of the chromosome in the population.

Simulated Annealing (SA) is a meta strategy for optimization by local improvements. It is a local search heuristic that allows occasional uphill moves. It allows moves from a current solution to a not necessarily improving one in hope that it leads to a minimal cost one. The process becomes more selective and accepts fewer non-improving solutions as it ages or gains experience. A description of SA follows.

1. Let Sol be the initial solution and f_{Sol}. its fitness
2. Let T_0 be the initial temperature
3. Set $Sol^* = Sol$, and $f* = f_{Sol}$.
4. Fix the size of the neighborhood M (i.e., M is the length of the plateau).
5. Set $k = 0$.
6. Repeat M times.
   - Obtain a neighboring solution N_{Sol}, and evaluate its fitness $f_{N_{Sol}}$.
   - If $\Delta = f_{N_{Sol}} - f_{Sol} \leq 0$ then
     -- $Sol = N_{Sol}$, and $f_{Sol} = f_{N_{Sol}}$;
     -- if $f_{N_{Sol}} < f^*$, then $Sol^* = N_{Sol}$, and $f^* = f_{N_{Sol}}$;
   - else if $\exp(\frac{-\Delta}{T_k}) > Uniform[0,1]$, then
     -- $Sol = N_{Sol}$, and $f_{Sol} = f_{N_{Sol}}$.
7. Increment$k$ by 1, and compute T_k, the temperature at plateau k.
8. If the stopping criterion is not satisfied, go to Step 5.

In Step 5, the acceptance of an uphill move is controlled by the probability $\exp(\frac{-\Delta}{T_k})$. The probability that an uphill move of size Δ is accepted diminishes as the temperature declines. For a fixed T_k, small uphill moves have higher probabilities of acceptance than large ones. In this implementation of SA, the **temperature** of the annealing process is decreased geometrically; that is, at plateau k, $T_k = 0.9T_{k-1}$.

The **initial temperature** T_0 is a function of the probability of acceptance $\tau_0 = e^{-\frac{|\overline{\Delta}|}{T_0}}$, where $\overline{\Delta}$ is the average variation of the fitness of 100 randomly generated solutions. τ_0 is, in turn, a function of the quality of the initial solution. $\tau_0 = 0.2$ when the initial solution is "good", and $\tau_0 = 0.6$ otherwise. The initial solution is "good"if its percent deviation from a computed lower bound is less than 25%. Setting $\tau_0 = 0.2$ makes the algorithm very selective starting its first

Table 1. First problem set

Instance	S	$\|G\|$	W (m)	q_s	L^*
a_1	$\{P, M, T, XT\}$	7	1.0	$q_P = 2, q_M = 5, q_T = 2, q_{XT} = 1$	1.40
a_2	$\{P, M, T, XT\}$	7	1.0	$q_P = 10, q_M = 25, q_T = 10, q_{XT} = 5$	7.00
a_3	$\{P, M, T, XT\}$	7	1.0	$q_P = 20, q_M = 50, q_T = 20, q_{XT} = 30$	22.00
a_4	$\{P, M, T, XT\}$	7	1.0	$q_P = 10, q_M = 25, q_T = 10, q_{XT} = 15$	11.00
b_1	$\{P, M, T, XT\}$	11	1.6	$q_P = 6, q_M = 6, q_T = 2, q_{XT} = 2$	4.00
b_2	$\{P, M, T, XT\}$	11	1.2	$q_P = 20, q_M = 30, q_T = 20, q_{XT} = 5$	26.67
b_3	$\{P, M, T, XT\}$	11	1.6	$q_P = 12, q_M = 12, q_T = 18, q_{XT} = 18$	25.5
b_4	$\{P, M, T, XT\}$	11	1.2	$q_P = 20, q_M = 30, q_T = 20, q_{XT} = 15$	37.34
c_1	$\{XP, P, M, T, XT, XXT\}$	20	2.0	$q_{XP} = 18, q_P = 30, q_M = 12, q_T = 18, q_{XT} = 6, q_{XXT} = 6$	99.00
c_2	$\{XP, P, M, T, XT\}$	20	2.5	$q_{XP} = 24, q_P = 24, q_M = 42, q_T = 24, q_{XT} = 6$	90.00
c_3	$\{XP, P, M, T, XT, XXT\}$	20	2.0	$q_{XP} = 18, q_P = 30, q_M = 12, q_T = 18, q_{XT} = 12, q_{XXT} = 12$	136.5
c_4	$\{XP, P, M, T, XT\}$	20	2.5	$q_{XP} = 24, q_P = 24, q_M = 42, q_T = 24, q_{XT} = 12$	100.8

Table 2. Computational Results for first problem set

Instance	$L*$	Δ_{SA}	Δ_{GA}	Δ_{GAn}
a_1	1.40	3.57	3.57	3.57
a_2	7.00	1.07	1.07	1.07
a_3	22.00	0.68	0.45	0.11
a_4	11.00	0.91	0.68	0.45
b_1	4.00	1.88	2.50	1.87
b_2	26.66	0.50	0.87	0.50
b_3	25.50	6.18	2.05	0.29
b_4	37.33	1.92	1.72	1.58
c_1	99.00	4.95	3.03	2.42
c_2	90.00	5.81	2.66	0.69
c_3	136.50	4.29	2.96	2.96
c_4	100.80	6.67	2.77	2.38

iterations whereas setting $\tau_0 = 0.6$ makes the algorithm accept uphill moves more often during the first iterations.

A **neighbor** is obtained by randomly moving a size $s \in S$ from a random section $i,\ i = 1, \ldots, p$ in the current solution Sol to a different existing section $j,\ j = 1, \ldots, p,\ i \neq j$ while maintaining demand feasibility. Removing a size s from its section i creates a residual demand $r_s = h_i * O_{is}$. Restoring demand feasibility without creating an additional section requires moving size s to a section j whose h_j is a divider of r_s. When such a section j is identified, its corresponding O_{js} is updated; i.e., $O_{js} = O_{js} + \frac{r_s}{h_j}$. If no such section exists, a different size from a different section is considered for a move. The **size** M of the **plateau** or of the **neighborhood** is set to 12 accepted solutions. The algorithm is **stopped** if the best current solution is not improved for 3 consecutive plateaus.

5 Computational Results

The purpose of the computational results is twofold. First, we evaluate the performance of GAn. Second, we assess the need for combining the COP and TDL problems into a single CT problem. GAn and the sequential TDL algorithm are coded in `Fortran` and run on a `Pentium IV,` 1.7 GHz and 256 Mb of RAM.

The computational results for the instances of Table 1 are displayed in Table 2. Columns 1 and 2 display the instance and its corresponding optimal length. Columns 3 - 5 report the deviation from L^* of the SA, GA and GAn solutions. Δ_{SA} is computed based on the best solution obtained when replicating SA six times with each replication initiated with a randomly generated solution.

Table 3. Industrial problems

Instance	S	$\|G\|$	W (m)	q_s	$L*$	$\underline{h}$	$\overline{h}$	$\overline{l}$
I_1	4	21	1.5	10-20-20-10	144.00	5	30	12.00
I_2	3	21	1.5	6-12-12	78.00	5	30	12.00
I_3	4	18	1.1	6-24-24-12	87.8	5	20	8.00

Table 4. Computational results for the industrial problems

Instance	$L*$	Δ_{SA}	Δ_{GA}	Δ_{GAn}
I_1	144.00	0	0	5
I_2	78.00	5	7	11
I_3	87.00	0	1	4

Our experimentation shows that SA's solution is not very sensitive to the initial solution. Yet, starting SA from a very bad solution will not lead to a global optimum. Furthermore, increasing GA's population size does not necessarily improve the quality of GA's solution. GA's local optimum is generally obtained randomly during the initial population or is the result of crossover; i.e., it is the result of diversification rather than of intensification. Starting GA with a population whose individuals are of high quality leads to premature stagnation; hindering the escape from local optima. These conclusions highlight the need for diversification and intensification of the search as in GAn.

The results of Column 4 are consistently better than those reported in Column 3, demonstrating the need for the intensification search. (Note that both GA and GAn were run with an identical population size and number of generations.)

Second, we assess the performance of the proposed approach on real life industrial problems where the garments are a collection of non-convex irregular pieces. Problems $I1-I3$, summarized in Table 3, were obtained from a medium-sized local apparel manufacturer along with the "adopted" cut order plan and the corresponding layout for each of its sections. Column 1 of Table 3 displays the instance number. Columns 2-4 indicate the number of ordered sizes n, the number of pieces per garment $|G|$, and the width of the fabric W. Columns 5 and 6 display respectively the ordered quantity per size $q_s, s \in S$, and the best known solution L^*. Finally, columns 7-9 display respectively $\underline{h}, \overline{h}$, and $\overline{l}$ the minimum and maximum ply height and the maximum length of a section.

The computational results for the industrial instances are reported in Table 4. Column 2 indicates the best known length L^*. Column 3 tallies Δ_{SA}, the minimum percent improvement of total length when SA is replicated six times starting each replication with a random initial solution. Column 4 gives Δ_{GA}, the percent improvement of total length when GA is applied without any intensification strategy. Finally, Column 5 displays Δ_{GAn}, the percent improvement of the total length when GAn is applied. The results show that the solutions

obtained by human experts/specialized software can be improved. They further demonstrate the need to combine COP and TDL into a single problem. Finally, they emphasize the role of hybridization in refining the search.

6 Conclusion

This paper tackles a real life problem that is of sizeable importance to the apparel manufacturing industries. This problem consists of finding the optimal cut order plan for a given order subject to the industrial set of constraints such as maximum and minimum ply height, maximum length of a section, etc. The problem is solved using a hybrid heuristic which diversifies the search by undertaking a global search via genetic algorithms and intensifies the search using local search via simulated annealing. The computational results highlight the need for hybridization, and assesses the percent improvements that industry can incur by adopting the proposed approach.

References

1. Blazewicz, J., Hawryluk, P., Walkowiak, R.: Using a tabu search approach for solving the two dimensional irregular cutting problem, Annals of Operations Research 41, 313–325 (1994)
2. Dowsland, K.A., Dowsland, W.: Solution approaches to irregular nesting problems. European Journal of Operational Research 84, 506–521 (1995)
3. Li, Z., Milenkovic, V.: Compaction and separation algorithms for non-convex polygons and their applications. European Journal of Operational Research 84, 539–561 (1995)
4. Dighe, R., Jakiela, M.J.: Solving pattern nesting problems with GA employing task decomposition and contact detection. Evolutionary Computation 3, 239–266 (1996)
5. ElOmri, Méthode d'optimisation dans un contexte productique, Ph.D. Dissertation, Université de Bordeaux1 (1992)
6. Hifi, M., M'Hallah, R.: A best-local position procedure-based heuristic for the two-dimensional layout problem. Studia Informatica Universalis. International Journal on Informatics (Special Issue on Cutting, Packing and Knapsacking) 2(1), 33–56 (2002)
7. Jacobs-Blecha, C., Ammons, J.C., Schutte, A., Smith, T.: Cut order planning for apparel manufacturing. IIE Transactions 30, 79–90 (1996)
8. Jakobs, S.: On the genetic algorithms for the packing of polygons. European Journal of Operational Research 88, 165–181 (1996)
9. M'Hallah, R., Bouziri, A., Jilani, W.A.: Layout of Two Dimensional Shapes Using Genetic Algorithms. In: Del Pobil, A.P., Mira, J., Ali, M. (eds.) Lecture Notes in Artificial Intelligence, subseries of Lecture Notes in Computer Science, pp. 403–411 (2001)
10. Talbi, E.G.: A Taxonomy of Hybrid Metaheuristics. Journal of Heuristics 8, 541–564 (2002)

Supervised Adaptive Control of Unknown Nonlinear Systems Using Fuzzily Blended Time-Varying Canonical Model

Yau-Zen Chang[1] and Zhi-Ren Tsai[2]

[1] Department of Mechanical Engineering,
Chang Gung University, Tao-Yuan 33302, Taiwan
zen@mail.cgu.edu.tw
[2] Department of Electrical Engineering,
Chang Gung University, Tao-Yuan 33302, Taiwan
d9021001@stmail.cgu.edu.tw

Abstract. In spite of the prosperous literature in adaptive control, application of this promising control strategy has been restricted by the lack of assurance in closed-loop stability. This paper proposes an adaptive control architecture, which is augmented by a supervising controller, to enhance the robustness of an adaptive PID control system in the face of exaggerated variation in system parameters, disturbances, or parameter drift in the adaptation law. Importantly, the supervising controller is designed based on an on-line identified model in a fuzzily blended time-varying canonical form. This model largely simplified the identification process, and the design of both the supervising controller and the adaptation law. Numerical studies of the tracking control of an uncertain Duffing–Holmes system demonstrate the effectiveness of the proposed control strategy.

Keywords: Supervised Control, Fuzzily Blended Time-Varying Canonical Model, On-line Identification.

1 Introduction

The techniques of adaptive control and robust control have been under intensive investigation to account for plant variation and uncertainty in nonlinear systems. In the approach of adaptive control, the idea of combining system identification, either directly or indirectly, and modifying control parameters during on-line control course has been successfully applied to many nonlinear and time-varying plants. However, installation of practical adaptive control systems is rare due to the lack of guarantee in long-term closed-loop stability in the face of exaggerated variation in system parameters, disturbances, or parameter drift in the adaptation law.

[1],[2] proposed a supervising controller to enhance the robustness of an adaptive controller. However, the controller is designed based on the assumption of complete knowledge in plant dynamics. Clearly, this assumption violates practical situations of

H.G. Okuno and M. Ali (Eds.): IEA/AIE 2007, LNAI 4570, pp. 464–472, 2007.

most nonlinear systems. In this paper, a supervising controller is designed based on an on-line identified fuzzy model of the plants under control, which are either unknown in system parameters or partially uncertain in system dynamics.

The model used to identify the nonlinear and time-varying plants is in a fuzzily blended time-varying canonical form. As will be seen in the following derivation, this model largely simplified the identification process and the design of both the supervising controller and a PID adaptation law. Parameters in the model are identified on-line by the Simplex method [4]. The method is an efficient optimization strategy but strongly depends on initial conditions. This shortage can be alleviated by initializing the identified parameters with results of accurate off-line identification, specifically, the parallel genetic algorithms [3].

Furthermore, the adaptation law of the PID adaptive controller is designed using the modified projection method.

2 Problem Formulation

The plants under investigation are unknown SISO nonlinear systems, which are disturbed and can be described in the following canonical form, S :

$$S: \begin{cases} \dot{x}_1 = x_2 \\ \dot{x}_2 = x_3 \\ \vdots \\ \dot{x}_{n-1} = x_n \\ \dot{x}_n = f(x) + \Delta f(t) + g(x) \cdot u(t) + w(t) \\ y = x_1, \end{cases} \tag{1}$$

where $x = [x_1 \quad x_2 \quad \ldots \quad x_n]^T$, the parameters of $f(x)$ and $g(x)$ are not exactly known, and $w(t)$ is external disturbance. Besides, $\Delta f(t)$ denote unknown dynamic terms, which is bounded such that $|\Delta f(t)| \le \Delta f_U \in R^+$ with Δf_U being a known constant.

The task is to design a robust adaptive controller that can drive the system output, y, to follow the output, r, of a reference model:

$$\dot{y}_d = A_r \cdot y_d + r(t) \cdot \tag{2}$$

In the face of parameter variation, model uncertainty, and disturbances, we propose the following time-vary fuzzy canonical model, F, to identify the unknown plant.

$$F: \ \dot{x}_n = \sum_{i=1}^{L} h_i \cdot \left\{ [a_i \quad 1] \cdot \begin{bmatrix} x \\ \delta(t) \end{bmatrix} + b_i \cdot u + v_i \right\} + e_{\mathrm{mod}}(t), \tag{3}$$

where $\delta(t) = \sum_{j=0}^{I} c_j \cos(t)^j$,

$$e_{\mathrm{mod}}(t) = f(x) + \Delta f(t) + g(x) \cdot u + w - \sum_{i=1}^{L} h_i \cdot \left\{ [a_i \quad 1] \cdot \begin{bmatrix} x \\ \delta(t) \end{bmatrix} + b_i \cdot u + v_i \right\},$$

$E=[e \quad \dot{e} \quad ... \quad e^{(n-1)}]^T=[(y_d-y) \quad (\dot{y}_d-\dot{y}) \quad ... \quad ({y_d}^{(n-1)}-y^{(n-1)})]^T$, and $Y_d=[y_d \quad \dot{y}_d \quad ... \quad {y_d}^{(n-1)}]^T$.

The parameters of F, h_i, a_i, b_i, v_i, and c_j, to be identified on-line were initialized by accurate off-line identification using the parallel genetic algorithm, a kind of evolutionary global optimization techniques. Started with accurate initial values, the parameters are constantly updated by the simplex algorithm [4].

Firstly, we define an ideal feedback control law, u^*, as

$$u^*=(\sum_{i=1}^{L} h_i \cdot b_i)^{-1} \cdot [-\sum_{i=1}^{L} h_i \cdot a_i \cdot x-\delta-\sum_{i=1}^{L} h_i \cdot v_i-e_{\text{mod}}+{y_d}^{(n)}+K^T \cdot E], \tag{5}$$

where the vector,

$$K=[k_0 \quad k_1 \quad ... \quad k_{n-1}]^T, \tag{4}$$

is designed such that all roots of $s^n+k_{n-1} \cdot s^{n-1}+...+k_0=0$, are in the open left-half complex plane. We have the following inequality:

$$|u^*| \le \left|(\sum_{i=1}^{L} h_i \cdot b_i)^{-1}\right| \cdot \left[\left|\sum_{i=1}^{L} h_i \cdot (a_i \cdot x+v_i)\right|+|\delta|+e_U+\left|{y_d}^{(n)}\right|+\left|K^T \cdot E\right|\right], \tag{6}$$

where $|e_{\text{mod}}| \le e_U$.

3 Supervisory Controller Design

Next, let the control input be given by

$$u=u_{PID}+u_S, \tag{7}$$

where $$u_{PID}(t)=K_P \cdot e(t)+K_I \cdot \int_0^{t_f} e(t) \cdot dt+K_D \cdot \frac{de(t)}{dt}=\theta^T \cdot \xi(e), \tag{8}$$

$\theta=[K_P, K_I, K_D]^T$, and $\xi(e)=[e(t), \int_0^{t_f} e(t) \cdot dt, \frac{de(t)}{dt}]^T$. u_S is the extra supervisory controller that is fired only when magnitude of the state vector exceeds some predefined bound. The approach guarantees stability of the system.

Based on the concept of sliding mode control, an adaptation law using the simplex method is proposed below to minimize a sliding condition for updating the PID control gains.

By substituting (7) into (3), we have, in view of (5),

$$\dot{x}_n=\sum_{i=1}^{L} h_i \cdot a_i \cdot x+\sum_{i=1}^{L} h_i \cdot b_i \cdot (u_{PID}+u_S)+\delta+\sum_{i=1}^{L} h_i \cdot v_i+\sum_{i=1}^{L} h_i \cdot b_i \cdot u^*-\sum_{i=1}^{L} h_i \cdot b_i \cdot u^*+e_{\text{mod}}$$

$$={y_d}^{(n)}+K^T \cdot E-\sum_{i=1}^{L} h_i \cdot b_i \cdot (u^*-u_{PID}-u_S) \cdot \tag{9}$$

This implies that

$$e^{(n)} = -K^T \cdot E + \sum_{i=1}^{L} h_i \cdot b_i \cdot (u^* - u_{PID} - u_S) \cdot \tag{10}$$

Let

$$A_c = \begin{bmatrix} 0 & 1 & 0 & ... & 0 & 0 \\ 0 & 0 & 1 & ... & 0 & 0 \\ 0 & 0 & 0 & ... & 0 & 0 \\ \vdots & \vdots & \vdots & ... & \vdots & \vdots \\ 0 & 0 & 0 & ... & 0 & 1 \\ -k_0 & -k_1 & -k_2 & ... & -k_{n-2} & -k_{n-1} \end{bmatrix}, \quad B_c = [0 \quad 0 \quad ... \quad \sum_{i=1}^{L} h_i \cdot b_i]^T, \tag{11}$$

which is in companion form. From (10) and (11), we have

$$\dot{E} = A_c \cdot E + B_c \cdot (u^* - u_{PID} - u_S) \cdot \tag{12}$$

Next, we define the Lyapunov function candidate

$$V_E = 2^{-1} \cdot (E^T \cdot P \cdot E), \tag{13}$$

where P is a positive and definite symmetric matrix which satisfies the Lyapunov equation

$$A_c^T \cdot P + P \cdot A_c = -Q, \tag{14}$$

where Q is also a positive definite symmetric matrix. In the following, we choose Q such that $\lambda_{\min}(Q) > 0$, where $\lambda_{\min}(Q)$ denotes the minimum Eigen-value of Q. Furthermore, we define

$$V_M = 2^{-1} \cdot \lambda_{\min}(P) \cdot (M_x - \|Y_d(t)\|_\infty)^2 \cdot \tag{15}$$

Note that, if $\|x\| \geq M_x \geq \|Y_d(t)\|_\infty = \sup_{t \geq 0} \|Y_d(t)\|$, we have, from (13),

$$V_E \geq 2^{-1} \cdot \lambda_{\min}(P) \cdot \|E\|^2 \geq 2^{-1} \cdot \lambda_{\min}(P) \cdot (\|x\| - \|Y_d(t)\|)^2 \geq 2^{-1} \cdot \lambda_{\min}(P) \cdot (M_x - \|Y_d(t)\|_\infty)^2 = V_M. \tag{16}$$

Hence, if $V_E < V_M$, we have that $\|x\| < M_x$. Moreover, the derivative of V_E along the trajectories of the closed-loop system (12) satisfies

$$\dot{V}_E = 2^{-1} \cdot [E^T \cdot (A_c^T \cdot P + P \cdot A_c) \cdot E + 2 \cdot E^T \cdot P \cdot B_c \cdot (u^* - u_{PID} - u_S)] \cdot \tag{17}$$

By (14), we have

$$\begin{aligned} \dot{V}_E &= 2^{-1} \cdot [-E^T \cdot Q \cdot E + 2 \cdot E^T \cdot P \cdot B_c \cdot (u^* - u_{PID} - u_S)] \\ &\leq 2^{-1} \cdot [-E^T \cdot Q \cdot E + 2 \cdot |E^T \cdot P \cdot B_c| \cdot (|u^*| + |u_{PID}|) - 2 \cdot |E^T \cdot P \cdot B_c| \cdot u_S]. \end{aligned} \tag{18}$$

The supervisory controller is then designed, inferring (18) and (6), as

$$u_S = I^* \cdot \text{sgn}(E^T \cdot P \cdot B_c) \cdot \left\{ |u_{PID}| + \left| (\sum_{i=1}^{L} h_i \cdot b_i)^{-1} \right| \cdot \left[\left| \sum_{i=1}^{L} h_i \cdot (a_i \cdot x + v_i) \right| + |\delta| + e_U + \left| y_d^{(n)} \right| + |K^T \cdot E| \right] \right\}, \tag{19}$$

where the indicator function, I^*, is defined as: $I^* = \begin{cases} 1 & \text{if } V_E \geq V_M \\ 0 & \text{if } V_E < V_M \end{cases}$. From (6) and (19), it is guaranteed, referring to [1] and [2], that $\dot{V}_E < 0$ if $V_E \geq V_M$.

4 Adaptation Law with Projection for the PID Controller

In order to derive the adaptation law for θ, we define the optimal parameter vector, θ^*, by

$$u_{PID}^* = \theta^{*T} \cdot \xi, \tag{20}$$

such that the approximation error

$$\delta u = u_{PID}^* - u^*, \tag{21}$$

is minimized, where $|\delta u| \leq \delta\tilde{u}$.

Next, let us consider another Lyapunov function candidate, which contains tracking error and the deviation between θ^* and θ:

$$V_\theta = 2V_E + \gamma^{-1} \cdot (\theta^* - \theta)^T \cdot (\theta^* - \theta) = E^T \cdot P \cdot E + \gamma^{-1} \cdot (\theta^* - \theta)^T \cdot (\theta^* - \theta), \tag{22}$$

where $\gamma > 0$ is the tuning rate which determines the convergence speed.

By (17) and (22), we have

$$\begin{aligned}
\dot{V}_\theta &= \dot{E}^T \cdot P \cdot E + E^T \cdot P \cdot \dot{E} - 2\gamma^{-1} \cdot (\theta^* - \theta)^T \cdot \dot{\theta} \\
&= -E^T \cdot Q \cdot E - 2E^T \cdot P \cdot B_c \cdot (u_{PID} + u_S - u_{PID}^* + \delta u) - 2\gamma^{-1} \cdot (\theta^* - \theta)^T \cdot \dot{\theta} \\
&\leq -E^T \cdot Q \cdot E - 2E^T \cdot P \cdot B_c \cdot (u_{PID} - u_{PID}^* + \delta u) - 2\gamma^{-1} \cdot (\theta^* - \theta)^T \cdot \dot{\theta} \\
&= -E^T \cdot Q \cdot E - 2E^T \cdot P \cdot B_c \cdot [(\theta - \theta^*)^T \cdot \xi + \delta u] - 2\gamma^{-1} \cdot (\theta^* - \theta)^T \cdot \dot{\theta} \\
&= -E^T \cdot Q \cdot E - 2E^T \cdot P \cdot B_c \cdot (\theta - \theta^*)^T \cdot \xi - 2\gamma^{-1} \cdot (\theta^* - \theta)^T \cdot \dot{\theta} - 2E^T \cdot P \cdot B_c \cdot \delta u \\
&= -E^T \cdot Q \cdot E + 2(\theta^* - \theta)^T \cdot \xi \cdot E^T \cdot P \cdot B_c - 2\gamma^{-1} \cdot (\theta^* - \theta)^T \cdot \dot{\theta} - 2E^T \cdot P \cdot B_c \cdot \delta u \\
&= -E^T \cdot Q \cdot E - 2\gamma^{-1} \cdot (\theta^* - \theta)^T \cdot (\dot{\theta} - \gamma \cdot E^T \cdot P \cdot B_c \cdot \xi) - 2E^T \cdot P \cdot B_c \cdot \delta u.
\end{aligned} \tag{23}$$

Hence, if the adaptation law is defined as

$$\begin{cases} \dot{\theta} = \gamma \cdot E^T \cdot P \cdot B_c \cdot \xi, & \text{if } (\|\theta\| < M_\theta) \text{ or } (\|\theta\| = M_\theta \text{ and } \dot{\theta}^T \cdot \theta \leq 0), \\ \dot{\theta} = \gamma \cdot E^T \cdot P \cdot B_c \cdot \xi - \gamma \cdot E^T \cdot P \cdot B_c \cdot \dfrac{\theta}{M_\theta^2} \cdot \theta^T \cdot \xi, & \text{otherwise,} \end{cases} \tag{24}$$

we have

$$\dot{V}_\theta \leq -E^T \cdot Q \cdot E - 2E^T \cdot P \cdot B_c \cdot \delta u. \tag{25}$$

Furthermore, by (25) and assuming $|E^T \cdot P \cdot B_c| \leq \tilde{e}$, we have:

$$\dot{V}_\theta \leq -E^T \cdot Q \cdot E + 2|E^T \cdot P \cdot B_c| \cdot |\delta u| \leq -\lambda_{\min}(Q) \cdot \|E\|^2 + 2\delta\tilde{u} \cdot \tilde{e}. \tag{26}$$

This guarantees that $\dot{V}_\theta < 0$ if $\|E\| > \frac{\sqrt{2\delta\tilde{u}\cdot\tilde{e}}}{\sqrt{\lambda_{\min}(Q)}}$. It is clear that if (14) and (26) are satisfied, the system is UUB stable.

Note that, if the initial PID control gains, θ, are not selected adequately, the resultant closed-loop system will exhibit overshooting transient behavior. In these circumstances, the supervisory controller, defined in (19), will play an important role that provides an extra input to pull the states back to the pre-specified state region and guarantees system stability.

The overall block diagram of the augmented adaptive PID control system is depicted in Fig. 1.

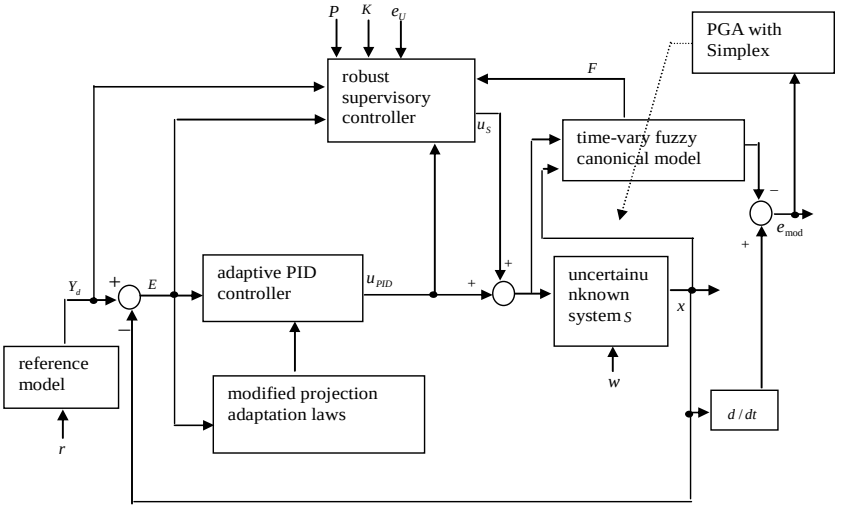

Fig. 1. The augmented adaptive PID control system

5 Case Study

The system demonstrated is an uncertain Duffing–Holmes system with external disturbance, $w(t)$, which can be described as follows:

$$\begin{cases} \dot{x}_1(t) = x_2(t), \\ \dot{x}_2(t) = x_1(t) - 0.25x_2(t) - x_1^{\,3}(t) + \Delta f(t) + w(t) + u(t), \\ y = x_1, \\ \dot{y}_d = A_r \cdot y_d + r(t), \end{cases} \tag{27}$$

where $\Delta f(t) = 0.3\cos(t) + 0.2\varsigma(t)\cdot\|x\| \le 0.3 + 0.2\|x\| \equiv \Delta f_U$; $\varsigma = [-1,1]$; $w \in [-1.2,1.2]$; $r(t) = [0, 2\cos(t)]^T$; and $A_r = \begin{bmatrix} 0 & 1 \\ -1 & -2 \end{bmatrix}$.

During the preparation of data for off-line identification, the system is driven by white noise with magnitudes between [-15, 15]. Using the parallel genetic algorithms, we obtain the following time-varying fuzzy model of (27):

Rule 1: IF x_1 is about -1.5, THEN $\dot{x}_2 = a_1 \cdot x + b_1 \cdot u + \delta + v_1$,
Rule 2: IF x_1 is about 0, THEN $\dot{x}_2 = a_2 \cdot x + b_2 \cdot u + \delta + v_2$,
Rule 3: IF x_1 is about 1.5, THEN $\dot{x}_2 = a_3 \cdot x + b_3 \cdot u + \delta + v_3$,

where $a_1 = [-16.2688 \quad -0.2500]$, $a_2 = [9.8556 \quad -0.2500]$, $a_3 = [-16.2690 \quad -0.2500]$,

$b_1 = b_2 = b_3 = 1$, $v_1 = 2.9257$, $v_2 = 0$, $v_3 = -2.9257$, and $\delta = 0.298\cos(t)$.

Fig. 2 shows the three Gaussian membership functions used in the fuzzy model.

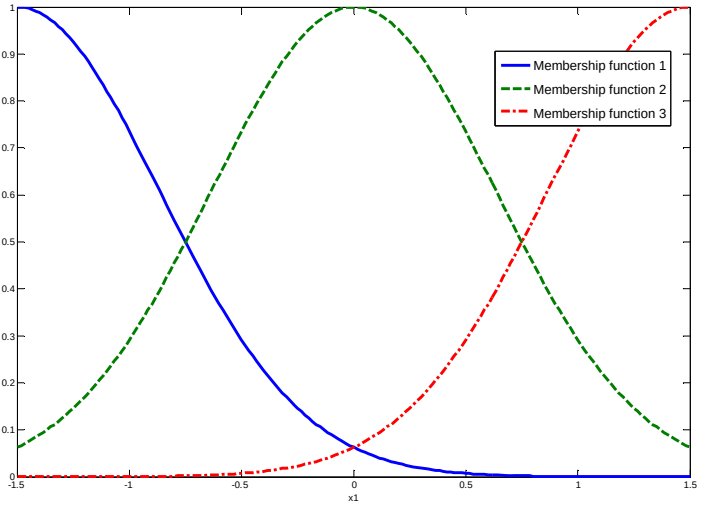

Fig. 2. The Gaussian membership functions used in the fuzzy model, where Membership function 1 is for the antecedent part of Rule 1, Membership function 2 for Rule 2, and Membership function 3 for Rule 3

For the following study, we further define the constraint parameter, $M_x = 5$, and upper bounds of $|e_{\text{mod}}|$, $e_U = 0.02$. The initial control gains are selected as $K_P = 35$, $K_I = 45$, and $K_D = 35$. Fig. 3 shows the time history of the system output, y, when the control gains are fixed at these initial values. The simulation is based on initial states $x_1(0) = 0.2$ and $x_2(0) = 0.2$ with the disturbance, $w(t)$, being applied at t = 20 sec.

Next, we choose $K = [1 \quad 20]^T$, $Q = \begin{bmatrix} 2 & 0 \\ 0 & 2 \end{bmatrix}$, and find the solution $P = \begin{bmatrix} 20.1 & 1 \\ 1 & 0.1 \end{bmatrix}$ to construct the supervisory controller, u_S. Fig. 4 shows the state trajectories of the plant,

y, when both the adaptive law and the supervisory controller are applied. Fig. 5 shows the time history of the PID gains, demonstrating internal adaptation for the disturbance. Comparing Fig. 3 and Fig. 4, it is clear that the tracking performance of the augmented adaptive controller significantly outperform that of a constant gain PID controller. Also, the transient behavior during start and unexpected application of disturbance is bounded and acceptable.

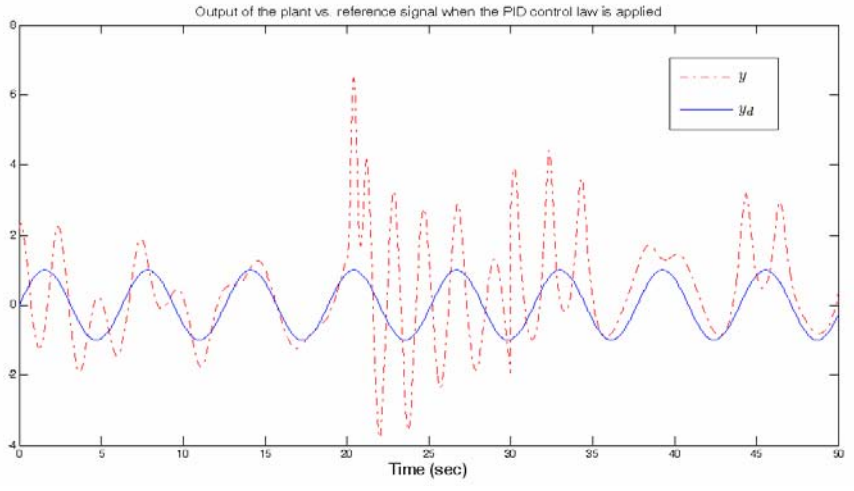

Fig. 3. Comparison of the trajectories between the plant output, y (-.-), and the reference signal, y_d (—), when a fixed-gain PID control law, $K_P = 35$, $K_I = 45$, and $K_D = 35$, is applied

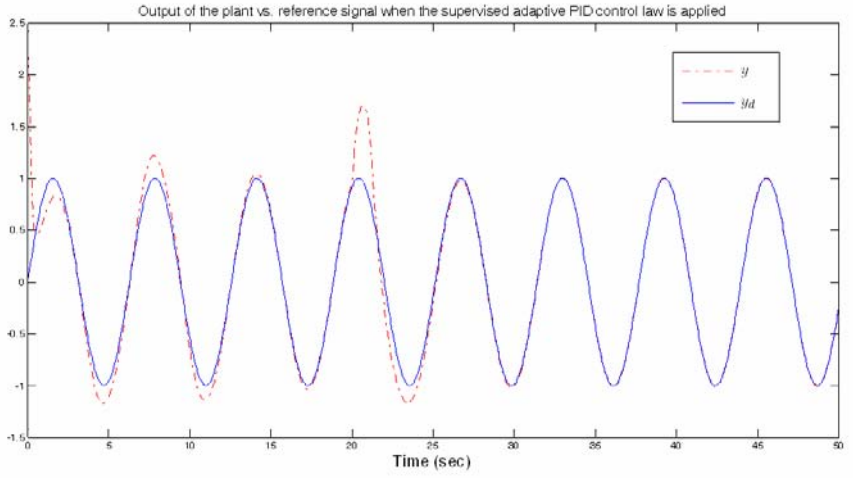

Fig. 4. Comparison of the trajectories between the plant output, y (-.-), and the reference signal, y_d (—), when both the adaptive law and the supervisory controller are applied

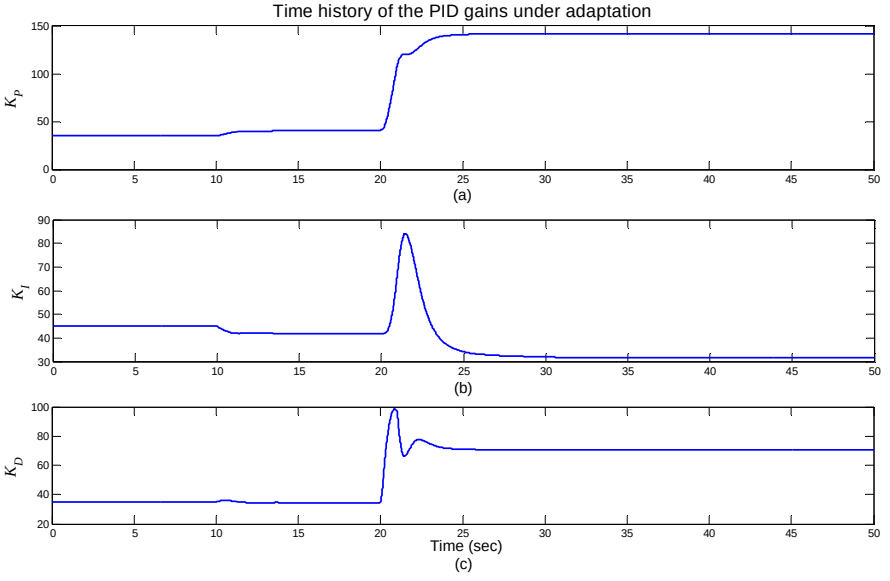

Fig. 5. Time history of the PID gains, K_P, K_I, and K_D, in the proposed scheme

6 Conclusion

We propose new adaptive control architecture in this paper. The architecture is augmented by a supervising controller to enhance its robustness in the face of exaggerated variation in system parameters, disturbances, or parameter drift in the adaptation law. The supervising controller is designed based on an on-line identified model in a fuzzily blended time-varying canonical form. The identification strategy is the Simplex method initialized with other global optimization techniques, specifically, the parallel genetic algorithms.

Numerical studies of the tracking control of an uncertain Duffing–Holmes system demonstrate the superior tracking performance of the proposed control strategy in the face of plant uncertainties and unexpected disturbances.

Acknowledgments. The authors would like to thank the support of the National Science Council of Taiwan under contract NSC-95-2221-E-182-074 and Professor B.S. Chen for his valuable encouragement.

References

1. Wang, L.X.: Adaptive Fuzzy Systems and Control: Design and Stability Analysis. Prentice-Hall, New Jersey (1994)
2. Wang, L.X.: A Course in Fuzzy Systems and Control. Prentice-Hall, New Jersey (1997)
3. Chang, Y.Z., Chang, J., Huang, C.K.: Parallel Genetic Algorithms for a Neuro-control Problem. In: Int. Joint Conference on Neural Networks, pp. 10–16 (1999)
4. Bixby, R.E.: Implementing the Simplex Method: The Initial Basis. ORSA Journal on Computing 4(3), 267–284 (1992)

Multi-agent System with Hybrid Intelligence Using Neural Network and Fuzzy Inference Techniques

Kevin I-Kai Wang, Waleed H. Abdulla, and Zoran Salcic

Department of Electrical and Computer Engineering, University of Auckland. Private Bag 92019, Auckland, New Zealand
{kevin.wang,w.abdulla,z.salcic}@auckland.ac.nz

Abstract. In this paper, a novel multi-agent control system incorporating hybrid intelligence and its physical testbed are presented. The physical testbed is equipped with a large number of embedded devices interconnected by three types of physical networks. It mimics a ubiquitous intelligent environment and allows real-time data collection and online system evaluation. Human control behaviours for different physical devices are analysed and classified into three categories. Physical devices are grouped based on their relevance and each group is assigned to a particular behaviour category. Each device group is independently modelled by either fuzzy inference or neural network agents according to the behaviour category. Comparative analysis shows that the proposed multi-agent control system with hybrid intelligence achieves significant improvement in control accuracy compared to other offline control systems.

1 Introduction

With advanced embedded technology, computational devices ubiquitously merge with individuals' daily activities. The demand for devices, applications, and processes to become more intelligent has increased dramatically due to insufficient availability of human supervisions and abundance of computational resources. Thus, intelligent systems are developed and are expected to be able to adapt, to predict and to have high level of autonomy [1]. More specifically, intelligent systems should be aware of the environment context, be able to model and adapt to user's behaviour and respond on user's behalf [2].

The MIT AI Lab started Intelligent Environment (IE) researches around mid 90s [3]. At that time, their research focus was to introduce intelligence via smart sensors and camera networks and can be considered as Human-Computer Interaction (HCI) and sensor network research. In 1999, a Multi-Agent System (MAS) called Metaglue which had no built-in intelligence, was developed to control the IE [4]. However, in the past few years, intelligent knowledge-based resource management [5] and reactive behaviour systems [6] had been developed and integrated into the MAS to introduce intelligence.

The Adaptive Building Intelligence (ABI) project collaborated by several Swiss universities uses MAS approach to provide general building services rather than

H.G. Okuno and M. Ali (Eds.): IEA/AIE 2007, LNAI 4570, pp. 473–482, 2007.

personal space services [7]. The University of Essex focuses on online learning of personalised behaviour using Fuzzy Inference System (FIS) [8]. In University of Colorado, Artificial Neural Networks (ANNs) are used to control the lighting and heating services of a normal residential environment involving different types of living spaces such dining room, living room and bathroom [9].

There are also many other research efforts such as the Microsoft Smart House [10], IBM BlueSpace [11] and MASSIHN project [12]. However, most of them focus on integrating working behaviour and device automation into the control system. These control systems neither capture or model the human behaviour nor adapt to human needs, and do not reveal the true meaning of intelligence.

In this paper, user control behaviours occurred on different physical devices are analysed. Based on the analysis, two soft computing techniques, neural network and Multi-Agent Fuzzy Inference System (MAFIS) are used to model different control behaviours. A novel Multi-Agent Neural Net Fuzzy Inference System (MANNFIS) is developed to merge the two techniques into one multi-agent control system. In addition to the high level software control system, a complete system architecture including middleware layer and underlying hardware infrastructure, has been proposed. A physical testbed named Distributed Embedded Intelligence Room (DEIR) has been constructed according to the system architecture to enable real-time system evaluation and data collection.

The paper is laid out as follows. Section 2 introduces the physical infrastructure and system architecture of the testbed. Section 3 explains the soft computing techniques used and the rationales of using those techniques. Section 4 compares the performances of the proposed control system with other contemporary control systems. Section 5 gives ongoing research directions for the project and section 6 concludes the paper.

2 Distributed Embedded Intelligence Room (DEIR)

Distributed Embedded Intelligence Room (DEIR) is the physical testbed designed by the Embedded Systems Research Group of the University of Auckland [13]. As shown in Fig. 1, DEIR resembles the target environment such as personal office, single studio accommodation, and convalescent nursing room. DEIR is equipped with

Fig. 1. Distributed Embedded Intelligence Room (DEIR)

a number of embedded sensors including light intensity, temperature, pressure, smoke, and motion sensors to monitor the environment states. It also contains a number of actuators for automating windows, blinds, dimmable lights and house appliances. The underlying physical infrastructure is comprised of three different device networks for connecting various types of sensors and devices. Middleware is incorporated in the software counterpart of the devices, the device agents, to integrate hybrid physical networks and to improve system flexibility on future extensions. High level multi-agent control system communicates with the device agents through middleware channels to exchange context information and to issue control commands.

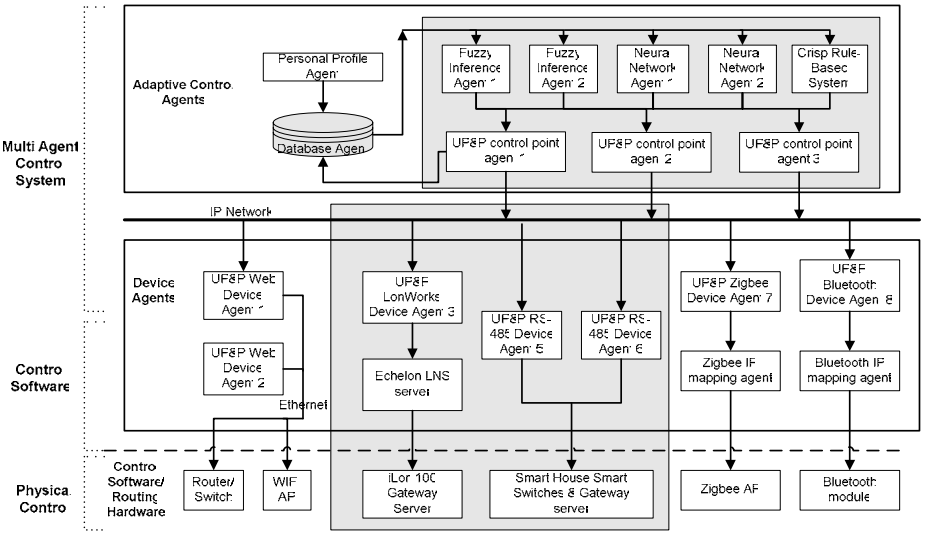

Fig. 2. DEIR system architecture

2.1 DEIR Physical Infrastructure

Refer to Fig. 2, three physical networks namely IP network, LonWorks network [14] and RS-485 network are used to interconnect all the devices implemented in DEIR. Each network has its own protocol, control software and control hardware. In LonWorks network, all devices are connected to the iLon100 gateway server which communicates with the control software, the LNS server. In RS-485 network, devices are separately grouped and controlled by smart hardware switches. Each smart switch has a M16C microcontroller, a infra-red receiver, and a RS-485 network connection. The devices can be controlled through traditional switch interface, infra-red remote control and RS-485 network commands. All the smart switches are connected to another RS-485 gateway server to exchange RS-485 messages with the software device agents. Different to LonWorks and RS-485 networks, IP network is not solely used as a device network, but it is also used by the middleware to integrate other physical networks. The middleware layer allows new device networks to be added into the system architecture easily. Wireless device networks such as Zigbee and Bluetooth are possible extensions for the system.

2.2 Middleware and Multi-agent Platform

In DEIR, Universal Plug and Play (UPnP) is used as the middleware. The implementation of UPnP protocol can be considered in two parts: the control point and device agents. Control point agent is the server component which keeps all the information of registered device agents and acts as a software interface between high level control and device agents. Device agent is the client component which links the control point agent with corresponding network control software such as LNS server or sends out commands directly as in RS-485 network. The UPnP protocol is implemented using CyberGarage UPnP Java API [15]. In order to integrate all the software entities smoothly, a widely used and tested agent platform, JADE (Java Agent DEvelopment Framework), was selected [16]. Agents of JADE are developed using the provided Java API which enables UPnP components to be implemented as JADE agents directly. JADE also provide extensive plug-ins such as J2ME support, which helps in developing mobile agent applications.

3 Hybrid Learning Techniques

The ultimate goal of the proposed multi-agent control system is to capture user habits and to provide autonomous monitoring and controlling services in ubiquitous intelligent spaces. In the previous multi-agent control system, Multi-Agent Fuzzy Inference System (MAFIS) was the only technique used to capture and to model user control behaviours [13]. It was found that MAFIS can not satisfactorily model all kinds of control behaviours. To improve control accuracy, another modelling technique, neural network, is introduced in the system to model part of the user behaviours. The control behaviours are analysed to justify the use of MAFIS and neural network and to assign each device with the most suitable modelling technique. The proposed multi-agent control system incorporating hybrid intelligence is referred as the Multi-Agent Neural Net Fuzzy Inference System (MANNFIS).

3.1 Device Behaviour Categorisation

In order to select the optimal modelling technique, user control behaviours need to be categorised based on realistic data analysis. Based on the analysis, three behaviour categories are defined in MANNFIS. The first category involves common reactive control behaviours which rarely change among different users. This type of behaviour can easily be modelled using a traditional rule-based system. Security control such as autonomous door lock in absence of occupants is a good example. Due to the fact that this type of behaviour contains minimum uncertainties and the corresponding modelling technique requires no learning, they will not be included in the discussions.

The second category involves daily routine behaviours that constantly follow certain environment context(s). This type of behaviour is typically user dependent but contains low uncertainties. In the past experiments, curtain devices show the exact characteristics of this category. Fig. 3 shows the curtain control behaviour collected

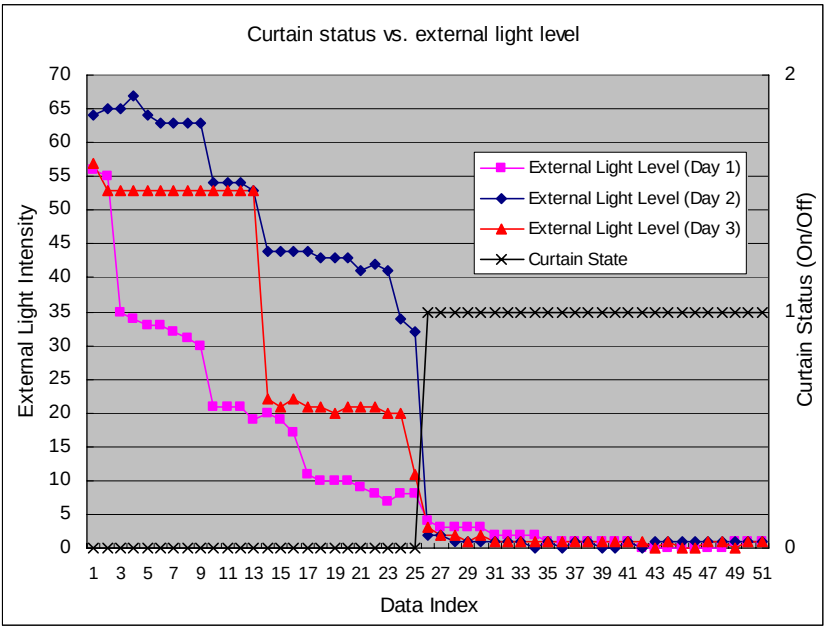

Fig. 3. Curtain status vs. external light intensity

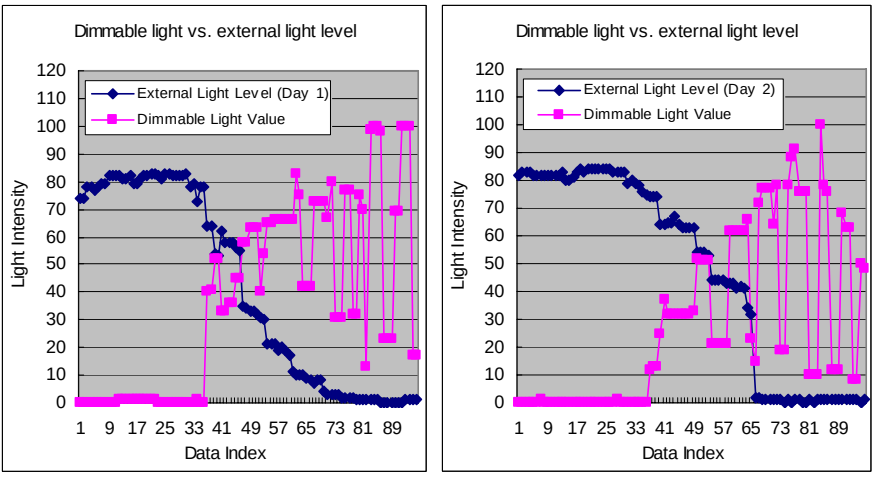

Fig. 4. Dimmable light level vs. external light intensity

over 3 consecutive days. It can be depicted that the curtain is turned on (i.e. it is closed) when external light intensity drops below five. Despite the fact that different users might control the curtain with different environmental parameters or parameter values, such personal preferences should not vary very often. Thus, a feed-forward

neural network is a suitable tool to classify (or model) the device status according the relevant environmental parameters.

The last category consists of behaviours that follow certain trend roughly but could be highly non-deterministic. Typical device that characterises this type of behaviour is the dimmable light as shown in Fig. 4. There is a rough trend to increase the light level when external light intensity drops such that the ambient light level is maintained. With great tolerance of uncertainties, MAFIS has been proved to handle this type of devices with great accuracy in the previous multi-agent control system [13].

In MANNFIS, devices are grouped with relevant environmental parameters to enhance the quality of model. Each device group is pre-assigned to a particular behaviour category according to the analysis. Based on the category, different modelling techniques are applied to different device groups. Detailed device groupings are shown in Fig. 5. The same groupings are used to execute the performance evaluation, which is discussed in Section 4.

Group 1 (9 features)		**Group 2 (9 features)**		**Group 3 (7 features)**	
Input set	Output set	Input set	Output set	Input set	Output set
Int. Light Sensor	Dimmable Light 1	Int. Light Sensor	MS Word	Int. Light Sensor	Bed Light
Ext. Light Sensor	Dimmable Light 2	Ext. Light Sensor	MS Media	Ext. Light Sensor	Desk Light
Chair Pressure	Dimmable Light 3	Int. Temp. Sensor		Chair Pressure	
Bed Pressure	Dimmable Light 4	Ext. Temp. Sensor		Bed Pressure	
Time		Chair Pressure		Time	
		Bed Pressure			
		Time			

Group 4 (5 features)		**Group 5 (2 features)**	
Input set	Output set	Input set	Output set
Int. Light Sensor	Heater	Ext. Light Sensor	Blind
Ext. Light Sensor			
Int. Temp. Sensor			
Ext. Temp. Sensor			

Fig. 5. Device Grouping in MANNFIS

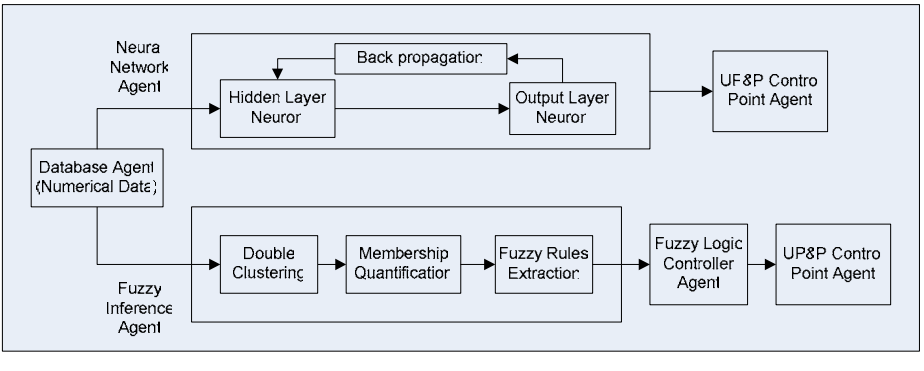

Fig. 6. MANNFIS architecture

3.2 Multi-Agent Neural Net Fuzzy Inference System (MANNFIS)

As shown in Fig. 6, MANNFIS is a combination of neural network and MAFIS. The neural network implemented in MANNFIS is the most common feed-forward Multi-Layer Perceptron (MLP) [17]. Numerical data that represents user control behaviours is used to train the neural network with back propagation algorithm. Detailed implementation can be found in [17]. MAFIS, on the other hand, was the first soft computing technique selected in DEIR project due to its great tolerance of uncertainties. The learning technique used in MAFIS is adopted from the Adaptive Online Fuzzy Inference System (AOFIS) developed at the University of Essex [8]. The numerical data are first processed by double clustering algorithm which generates fuzzy granules [18]. Fuzzy granules are then quantified using Gaussian membership functions. Eventually, fuzzy rules are extracted based on the input data and Gaussian membership functions, using the extended Mendel Wang's method [19]. The implementation of MAFIS was provided in our previous publication [15].

4 Performance Analysis

To examine the control accuracy of MANNFIS, a comparative analysis with other offline control systems has been performed. In order to conduct a fair comparison, the dataset provided by our colleagues at the University of Essex is used to evaluate all the control systems. The dataset used for the analysis contains seven input features, namely internal light sensor, external light sensor, internal temperature sensor, external temperature sensor, chair pressure sensor, bed pressure sensor and time; and ten output features including 4 dimmable lights, blinds, desk light, bed light, heater and two PC applications: MS Word and MS Media Player. This particular dataset contains 408 data instances collected over three consecutive days monitoring real user activities. The data instances are split into 272 data instances in the training set and 136 data instances in the testing set. Before evaluating the system performance, the main difference between MANNFIS and other control systems should be addressed. MANNFIS is a multi-agent based system rather than a centralised system as the others. Refer to Fig. 5, output devices are grouped with their relevant input devices where each device group can be modelled and controlled independently in parallel.

The Scaled Root Mean Square Error (SRMSE) is used to measure the control accuracy. The traditional RMSE is scaled by the dynamic range of the output to take into consideration the different dynamic ranges of output devices. As shown in Fig. 7, both MLP and MAFIS perform well in modelling their assigned device groups. On the other hand, the computational efficiency (i.e. the execution time) for MLP is much higher compare to MAFIS due to two reasons. First, MAFIS is used to model control behaviours with high uncertainties, and usually works on a multi-dimensional feature space. Second, MAFIS requires fair amount of fuzzy sets to achieve good control accuracy. Nevertheless, by taking advantages of the multi-agent architecture, device groups can be further divided to make MAFIS more suitable for embedded applications. Fig. 8 shows the performance comparison with other control systems including AOFIS, Genetic Programming (GP), Adaptive Network-based Fuzzy Inference System (ANFIS), MLP and MAFIS. By introducing neural network into the

control system, MANNFIS achieves up to 94% control accuracy, which is 15% improvements in control accuracy compared to its predecessor, MAFIS. It is also clear that MANNFIS outperforms other control systems by generating around 50% less control errors.

	Group 1	Group 2	Group 3	Group 4	Group 5	Average
Techniques	MAFIS	MAFIS	MAFIS	MAFIS	MLP	-
No. of fuzzy sets/neurons	13	15	20	15	1	-
SRMSE	0.0716	0.0976	0.0488	0.0368	0.0572	0.0624
Execution time (s)	17.32	16.20	19.07	6.38	3.87	12.57

Fig. 7. Performance evaluation of MANNFIS

	MANNFIS (Average)	MAFIS (Average)	AOFIS	GP	ANFIS	MLP
SRMSE	0.0624	0.0729	0.1261	0.1106	0.1115	0.1555

Fig. 8. Offline system performance comparison

5 Future Works

So far, the algorithms implemented in and the evaluation performed on MANNFIS and its predecessor MAFIS are all offline. The next step is to incorporate online adaptation ability in the algorithms and perform real-time data collection and system performance evaluation. With sufficient real-time data, a more thorough user control behaviour analysis could be carried out. Eventually, an algorithm should be developed to autonomously classify behaviours into different categories and to assign the most suitable modelling and controlling techniques.

6 Conclusions

In this paper, a physical intelligent environment testbed, DEIR, and a multi-agent control system with hybrid intelligence, MANNFIS, are presented. DEIR consists of a large number of embedded devices, which are interconnected by hybrid physical networks. Extra layer of middleware is introduced in the system architecture to integrate hybrid physical networks and to improve system flexibility for future extension. DEIR resembles a true ubiquitous intelligent environment which allows real-time data collection and online system evaluation. MANNFIS is the top level control in DEIR system architecture, implemented using JADE agent platform. It employs two types of learning techniques, namely MAFIS and MLP, to model different types of human control behaviours. Devices to be controlled are grouped in terms of their relevance and modelled by either MAFIS or MLP at the same time. Performance analysis shows that both MAFIS and MLP achieve excellent accuracy in controlling the assigned device groups. The analysis also shows that MANNFIS outperforms other offline control systems by generating about 50% less control errors.

Acknowledgement. This research is supported by UARC research grant 3604552 and top achiever doctoral scholarship. The authors would like to thank Dr. Faiyaz Doctor, Prof. Victor Callaghan and Prof. Hani Hagras for their kind contribution of providing the dataset for comparative analysis and various helps regarding to the use of their AOFIS learning technique.

References

1. Augusto, J.C., Nugent, C.D. (eds.): Designing Smart Homes. LNCS (LNAI), vol. 4008. Springer, Heidelberg (2006)
2. Ducatel, K., Bogdanowicz, M., Scapolo, F., Burgelman, J.-C.: Scenarios for Ambient Intelligence in 2010. Information Soc. Technol., Advisory Group (ISTAG), Inst. Prospective Technol. Studies (IPTS), Seville (2001)
3. Brooks, R.A.: The Intelligent Room Project. In: Second International Conference on Cognitive Technology, pp. 271–278 (1997)
4. Philips, B.A.: Metaglue: A Programming Language for Multi-Agent Systems. M.Eng. thesis, Massachusetts Institute of Technology, Cambridge, MA, USA (1999)
5. Gajos, K.: A Knowledge-Based Resource Management System For The Intelligent Room. M.Eng. thesis, Massachusetts Institute of Technology, Cambridge, MA, USA (2000)
6. Kulkarni, A.A.: A Reactive Behavioral System for the Intelligent Room. M.Eng. thesis, Massachusetts Institute of Technology, Cambridge, MA, USA (2002)
7. Rutishauser, U., Schaefer, A.: Adaptive Building Intelligence: A multi-Agent approach. Diploma thesis, University of Applied Science Rapperswil, Switzerland and Institute of Neuroinformatics, Swiss Federal Institute of Technology and University of Zurich, Switzerland (2002)
8. Doctor, F., Hagras, H., Callaghan, V.: A Fuzzy Embedded Agent-Based Approach for Realizing Ambient Intelligence in Intelligent Inhabited Environment. IEEE Trans. Sys. Man Cybern. 35(1), 55–65 (2005)
9. Mozer, M.: The neural network house: An environment that adapts to its inhabitants. In: Proc. Amer. Assoc. Artif. Intell. Spring Symp. Intell. Environ. pp. 110–114 (1998)
10. Brumitt, B., Cadiz, J.J.: Let There Be Light! Comparing Interfaces for Homes of the Future. Microsoft Research, Redmond, WA 98052, MSR-TR-2000-92 (2000)
11. Yoshihama, S., Chou, P., Wong, D.: Managing Behavior of Intelligent Environments. In: Proc. of the First IEEE Int. Conf. on Pervasive Comp. and Communications, pp. 330–337 (2003)
12. Tsai, C.F., Wu, H.C.: MASSIHN: A Multi-Agent Architecture for Intelligent Home Network Service. IEEE Trans. on Consumer Electronics 46, 505–514 (2002)
13. Wang, K.I., Abdulla, W.H., Salcic, Z.: Distributed Embedded Intelligence Room with Multi-agent Cooperative Learning. In: Ma, J., Jin, H., Yang, L.T., Tsai, J.J.-P. (eds.) UIC 2006. LNCS, vol. 4159, pp. 147–156. Springer, Heidelberg (2006)
14. Echelon Corporation, LonWorks Overview (February 2006) http://www.echelon.com/solutions/overview/default.htm
15. Wang, K.I., Abdulla, W.H., Salcic, Z.: Multi-agent fuzzy inference control system for intelligent environments using JADE. In: Proc. of 2nd IET Int. Conf. on Intel. Environ. pp. 285–294 (2006)
16. Wang, K.I., Abdulla, W.H., Salcic, Z.: A Multi-Agent System for Intelligent Environments using JADE. In: IEE Int. Workshop on Intell. Environ. pp. 86–91 (2005)

17. Kecman, V.: Learning and Soft Computing: Support Vector Machines. In: Neural Networks, and Fuzzy Logic Models, MIT Press, Cambridge (2001)
18. Castellano, G., Fanelli, A.M., Mencar, C.: Generation of interpretable fuzzy granules by a double clustering technique. Arch. Contr. Sci. 12(4), 397–410 (2002)
19. Wang, L.X.: The MW method completed: A flexible system approach to data minig. IEEE Trans. Fuzzy Syst. 11(6), 678–782 (2003)

Analysis of Log Files Applying Mining Techniques and Fuzzy Logic

Víctor H. Escobar-Jeria[1], María J. Martín-Bautista[2,⋆], Daniel Sánchez[2], and María-Amparo Vila[2]

[1] Department of Informatics and Computer Science, Metropolitan Technological University of Santiago de Chile, Chile
[2] Department of Computer Science and Artificial Intelligence, University of Granada, Periodista Daniel Saucedo Aranda s/n, 18071, Granada, Spain
mbautis@decsai.ugr.es

Abstract. With the explosive growth of data available on the Internet, a recent area of investigation called Web Mining has arise. In this paper, we will study general aspects of this area, principally the process of Web Usage Mining where log files are analyzed. These files register the activity of the user when interact with the Web. In the Web Usage Mining, different techniques of mining to discover usage patterns from web data can be applied. We will also study applications of Fuzzy Logic in this area. Specially, we analyze fuzzy techniques such as fuzzy association rules or fuzzy clustering, featuring their functionality and advantages when examining a data set of logs from a web server. Finally, we give initial traces about the application of Fuzzy Logic to personalization and user profile construction.

Keywords: Web Mining, Web Usage Mining, Fuzzy Logic, Fuzzy Association Rules, User Profiles.

1 Introduction

Today, the information is very important for companies, organizations and users, but it is more important that the information is precise, opportune and good-quality. With the development of technology, the growth of the information increases exponentially every day due to different factors; one of the most relevant is the Web.

With the need to be able to manage huge quantities of data and discover new knowledge, a new area of study rises, the Knowledge Discovery in Databases or KDD. The main stage of KDD is the Data Mining process. Through mining techniques, non explicit knowledge can be found in data, usually stored in relational databases in a structured form [Agrawal et al., 1993]. Other research areas have raised with the coming of the Web and the explosion of documental information in companies and organizations. These areas are based on Data Mining, although the particularities of the data, specially the lack of structure, have

⋆ Corresponding author.

H.G. Okuno and M. Ali (Eds.): IEA/AIE 2007, LNAI 4570, pp. 483–492, 2007.

implied specific features of the processes and techniques. These areas are called Text Mining and Web Mining, applied to documents and Web data, respectively.

The investigation of the World Wide Web Web has been converted in one of the research fields further interesting in the latter time. As Kleinberg comments in [Kleinberg et al., 1999], few events of story of computing Web has had so much influence in the society like the arrival and growth of the World Wide Web.

The Web grows and changes very rapidly, and its use has been extended not only to the information searching and retrieval but also to make commercial transactions. The competition in the e-commerce makes necessary the application of intelligent methods to store and to examine the information of sessions of Web users or potential customers. For this reason the user's behavior and the user's objectives are elements to obtain. The knowledge about the user is used not only to characterize to the user but also to discover generic tendencies for marketing purposes and for the web site improvement. These data about the users are collected from the activity of the user in the web site through log files.

The objective is to mine web server logs to find relations among users about navigational aspects. The nature of the data in the log files and the information to predict such as time, user age, cultural level, etc. makes Fuzzy Logic a perfect tool to model this information. From all the techniques with Fuzzy Logic, we will extend our study in fuzzy association rules [Delgado et al., 2003]. Concretely, we present an application of fuzzy association rules in the area of Web Usage Mining.

In this paper, we review some of the main applications of Fuzzy Logic to Web Mining. For this purpose, we first explain the three types of Web Mining: Web Content Mining, Web Structure Mining and Web Usage Mining. Then, we focus on Web Usage Mining including a study the personalization process and user profiles construction in Web. We overview the main applications of Fuzzy Logic found in the literature and present some preliminary experiments with Fuzzy Association Rules.

2 Web Mining

Nowadays, Internet and the Web play a very important role in the diffusion of information. Technological tools like the e-mail, the FTP, the e-business or simply reading the newspaper in the Web have meant a very important social change. However, there exist many challenges with respect to the obtaining of information from the Web.

There are different situations that make difficult to get the needed information: the huge amount the data, the diversity of language, the quality of information, the distribution of data at different platforms and finally, one of the most important, the lack of structure in the data.

These points, specially the unstructured data and the great heterogeneity, are also the main inconveniences of mining processes in the web. In these processes, data mining techniques are used to automatically discover and extract information from web documents and services [Etzioni, 1996].

Cooley distinguishes three forms to understand Web Mining: from the point of view of the content, the structure and the use [Cooley et al., 1997]. Web Content Mining is the automatic discovery of patterns from the content in Web documents [Mitra and Pal., 2002],[Chakrabati, 2000] ; Web Structure Mining consists on studying the structures of link enter or intra documents to discover useful patterns of link structures [Chakrabati, 2000], [Delgado et al., 2002]; and finally, Web Usage Mining, that we will study in this article more detailed. We can define the Web Usage Mining as the process of automatic discovery of access patterns or use of web services, based on the user's behavior when interact with the Web [Delgado et al., 2003]. At the following section we will focus on the study of the Web Usage Mining.

2.1 Web Usage Mining

At the present time, there is a lot of the sites dedicated to the e-commerce or to supply information. These sites need to learn every day about the clients or users that navigate through their pages so the services of the site can be improved.

When the users interact with the Web, they leave digital tracks (IP, agents, cookies, etc) that the servers store automatically in a journal of accesses. This activity is principally stored in the log files of the web server, and it is usually completed with other sources of information such as the proxy server and the user's machine.

The log files contain information about the connection server or the user's identity and authentication. This information collects the on-line user's activities and reflects several kinds of behavioral different patterns. These navigational patterns can evidence user's preferences, the on-line client's behavior and the future directions of improvement of the web site.

This information is used by the companies from the point of view of marketing, principally, where the assignment of a general profile to a user surfing in the web site based on his/her navigational behavior can be utilized to apply diverse measures, and to identify users with social groups. For the exploitation of different kinds of data, different techniques of pattern discovery can be used. The extracted knowledge can be used to execute tasks like prediction, personalization and improvement of the web site infrastructure.

2.2 Personalization and User Profiles in the Web

The ability of a web site to process the visits in a detailed level and to guide his/her clients or users through useful and pertinent information successfully, is becoming one of the crucial goals for any website nowadays. One of the forms to get this goal is through the personalization of Web.

The personalization of Web can be seen from two points of view: the company and the user. The company's point of view is related to the marketing and identification of demographic classes. The user's point of view is related to navigational recommendations and obtaining of information. This process can be described as a group of actions done by the user in the navigation so that these

actions can be processed to improve the web site according to user preferences [Mobasher, 2005]. Part of this information can be stored in what is called user profiles. User profiles can be defined as a representation of the knowledge about the user's interesting information [Martín-Bautista et al, 2002].

In [Martín-Bautista et al, 2002] the authors propose two different types of profiles: the simple profiles, which are represented by data extracted from documents supposedly interesting for the user; and the extended profiles containing additional knowledge about the user such as the age, the language level, the country, among others.

The extended profiles can be described then as a tuple of four variables. One of them is the demographic variable, that is related to social aspects like the user's age range or the education level, among others. Other variable is the identification one, that is related to the information stored in the log files from the user server. Then, the clickstream variables which are related to the page weights, where if one page has a zero value, this implies that the page has not been visited. The last variable is related to the session simple profiles described previously [Martín-Bautista et al, 2002].

For the obtaining of these profiles, clustering and association rules are applicable usually. Through clustering processes, an grouping of clients or data with similar characteristics is initially obtained automatically without having a previous classification. User profiles derived from these groups can be utilized to guide strategies of marketing according to the groups [Nasraoui et al., 1997]. The association rules discover associations and correlations among items where the presence of an item or a group of them in a transaction implies (with a confidence grade) the presence of other items [Carbonell et al., 1998]. One of the most direct applications of association rules to Web Usage Mining comes from the relations among visits of users with a certain navigational pattern to the web site.

The principal inconvenience of handling of profiles in the Web is the lack of knowledge about the identity of the user. Two different situations can rise: first, the unregistered users where users' profile can provide evidence of identity or associating with a social group. A general profile is then assigned to the user. Preferences stored in the profile can be applied to the web site for the user while she/he navigates.

The second situation refers to the registered users. If a user is identified in some way, then the web site can change according to the user's preferences. The system keeps the track of the user in her/his previous visits in the web site together with the users' profile. This information is utilized to personalize the site. To characterize user groups with similar behavior a clustering method can be performed [Martín-Bautista et al, 2002]. In order to have a more ample vision of Web Usage Mining and personalization, we will see some previous works in this area.

2.3 Related Work

In [Mobasher, 2005], an overview of the process of personalization based in Web Usage Mining is shown. Techniques of data mining such as clustering

to discover groups of users are utilized. Furthermore, association rules can be used to find important relations among the articles the users are interested in, based on navigational site patterns. Other different proposal is found in [Martín-Bautista et al, 2002], where the authors propose a scalable clustering methodology, inspired in the natural immunologic system with the facility to learn continuously and to adapt to coming new patterns.

One of the most well-know system developed for personalization can be found in [Cooley et al., 1997]. The system called WebMiner is based on a behavior model of user's navigation. By the grouping of web pages references, the system generate transactions, from which association rules are discovered. Other system related to personalization is presented in [Cernuzzi and Molas, 2004], where a study of Ridier's Web site (http://www.rieder.net.py) is carried out. The log files of the web server are stored and analyzed. From the transactions, behavioral patterns are extracted to describe the users' way of surfing using clustering and association rules. In [Wong et al., 2001] the authors propose a structure for a guided personalization and adaptation in the Web by means of user profiles and the accesses collected through the web log files.

At the following section we will comment some proposals realized in this area connected with the Fuzzy Logic.

3 Different Aspects of Web Mining with Fuzzy Logic

In all these types of Web Mining as well as in traditional Data Mining, both from the data or from the technique point of view, optimization tools coming from Soft Computing have been applied such as Fuzzy Logic, Genetic Algorithms, Neural Networks and Rough Sets [Arotaritei and Mitra., 2004][Hüllermeier, 2005]. Fuzzy Logic helps to represent an user-oriented selection of data, giving flexibility to the system and producing more interpretable solutions [Mitra and Pal., 2002].

Recently, these techniques have been applied to other data areas such as document collections[Justicia et al., 2004] and the Web. In Web Mining, the main techniques utilized in the literature are Fuzzy Clustering and Fuzzy Association Rules. These are the techniques that we will use too to obtain generic navigational tendencies of the user and the construction user profiles.

Fuzzy clustering algorithms such as the fuzzy c-means (FCM), with the fuzzy-c trimmed medoids (FCTM), and fuzzy-c medians (FCLMedS) are used in [Mitra and Pal., 2002] for Web Content and Web Usage Mining. Another application with fuzzy clustering can be looked up in [Nasraoui et al., 1997] for Web Usage and Web Structure Mining. The authors apply an algorithm called CARD (Competitive Agglomeration of Relational Data) to group different sessions of users. For this purpose, not only the entries in log files are considered, but also the structure of the site and the URLs to calculate the similarity between two users' sessions. The objective of this application is to identify users' sessions from the users' accesses to the Web site and its structure.

Along with the fuzzy clustering, one of the techniques more utilized in Web Mining is fuzzy association rules. An application of this technique can be found

in [Garofalakis et al, 1999], where a refinement of queries from an initial group of documents retrieved from Web is carried out. The textual transactions are constructed also with fuzzy values. The purpose of this work is to provide the system with an ability of reformulation of queries using mining technologies.

Other approach using fuzzy association rules can be found in [Wong et al., 2001], where a proposal with a description of a system architecture to predict Web accesses is presented. The fuzzy association rules and the generation of a fuzzy index tree are utilized to improve the accuracy and the efficiency of predictions of access Web paths.

3.1 Fuzzy Logic and User Profiles

Fuzzy Logic [Zadeh, 1975] permits the manipulation and exploitation of incomplete data or with a grade of uncertainty, situation that is very frequent in the data to mine [Delgado et al., 2003].

Sometimes, we do not have explicit information of the users in log files besides the information got from the server. We can complete the user's identity and authentication through another sources or inferring the information through techniques of mining. For example, we can infer in the education level of the user according to her/his navigation or may be according to the information that the users proportionate explicitly.

Therefore, when the extended user profiles are constructed, there is information to manage related to different concepts about the user. Some of these concepts such as the age of the user are imprecise, since the system must approximate the data if the user does not proportionate it, or the patience of the user surfing through the site. These characteristics can be modeled by means of linguistic labels, for example {very low, low, regular, high, very high} [Martín-Bautista et al, 2002].

We have seen different aspects and proposals realized in the area of Web Usage Mining, principally association rules and clustering techniques. Our investigation is based in these techniques with fuzzy logic and thus obtaining results more meaningful. So, fuzzy association rules permit to us to discover rules related with the navigational behavior of the user. At the following section, we will comment the Fuzzy Association Rules and experiments related with this technique.

3.2 Fuzzy Association Rules

The Association Rules look for relations or affinities among of groups of items or fields, generally in a relational database. Let I be a set of elements called "items" and let T be a set of elements called "transactions", each transaction being a set of items. Let us consider two itemsets (sets of items) $I_1, I_2 \subseteq I$, where $I_1 \cap I_2 = \emptyset$. An association rule [Agrawal et al., 1993] $I_1 \Rightarrow I_2$ is an implication rule meaning that the apparition of itemset I_1 in a transaction implies the apparition of itemset I_2 in the same transaction. The reciprocal does not have to happen necessarily [Kraft et al., 2003]. I_1 and I_2 are called antecedent and

consequent of the rule, respectively. The measures more utilized to describe the relations among antecedent and consequent of the association rules are the Support, and the Confidence. Support is the percentage of transactions where the rule holds, while confidence measures the strength of the rule as the percentage of transactions containing I_1, that contain I_2.

Several authors have proposed *fuzzy association rules* as a generalization of association rules when data is fuzzy or has been previously fuzzyfied
[Lee and Kwang, 1997],[Au and Chan, 1998],[Kuok et al., 1998],
[Hong et al., 1999],[Delgado et al., 2003].

Fuzzy association rules can be extracted from a group of fuzzy transactions by means of an algorithm of extraction such as the algorithm APrioriTID [Agrawal et al., 1993].

A fuzzy transaction can be defined as a nonempty subset where $\tilde{\tau} \subseteq I$. For every $i \in I$ we note $\tau(\tilde{i})$ the membership degree of i in a fuzzy transaction $\tilde{\tau}$ [Etzioni, 1996]. We note$\tau(\tilde{I}_0)$ the degree of inclusion of an itemset $I_0 \subseteq I$ in a fuzzy transaction $\tilde{\tau}$, defined in (1):

$$\tilde{\tau}(I_0) = \min_{i \in I} \tilde{\tau}(i) \tag{1}$$

Therefore, fuzzy transactions manage imprecision and give more flexibility because they allow us to deal with intermediate values between 0 and 1 to represent the membership degree of the items to the transaction.

For the evaluation of the performance of the association rules, we employ a semantic approach based on the evaluation of quantified sentenced [Zadeh, 1975]. A quantified sentence is an expression of the form "Q of F are G" where F and G two fuzzy subsets of a finite set X, and Q is a relative fuzzy quantifier. Relative quantifiers are linguistic labels that can be represented by means or fuzzy sets on [0,1], such as "most", "almost", or "many". This way we can define the estimated measures of goodness of rules. Let us remark that families of support and confidence measures can be obtained depending on the evaluation method and the quantifier of our choice. We evaluate the sentences by means of the method GD [Delgado et al., 2000], which has been shown to verify good properties with better performance than others. The evaluation of "Q of F are G" by means of GD is defined in (4),

$$\mathrm{GD}_Q(\frac{G}{F}) = \sum_{\alpha_i \Delta(\frac{G}{F})} (\alpha_i - \alpha_{i+1}) Q(\frac{\mid (G \cup F)_{\alpha_i} \mid}{F_{\alpha_i}}) \tag{2}$$

Another interesting measure is the certainty factor of a fuzzy association rule [Delgado et al., 2000]. Given a $A \rightarrow C$, the certainty factor takes values in [1, 1]. It is positive when the dependence between A and C is positive, 0 when there is independence and a negative value when the dependence is negative. We say that a fuzzy association rule is strong when its certainty factor and support are greater than two user-defined thresholds minCF and minSupp, respectively.

3.3 Implementation and Experimentation

Once examined all the related issues with the web usage mining, which is the principal base for our implementation, we will explain briefly our application for the search of patterns through fuzzy association rules.

The data to analyze is a subset of log files available for the ECML/PKDD Conference 2005 [ECML/PKDD 2005]. These files are in a CSV (Comma Separated Value) format. Table 1 shows a line of one of these log files, which is composed by 6 fields (identifier of shopping, date, IP, session, visited page, referenced page).

Table 1. Entry line in a log file sample

Id shop	**Date**	**IP**
11	Tue Jan 20 19:00:132004	213.235.141.105
Session	**Visited Page**	**Referenced Page**
1f75ccd2afbf87dc9abccde23f3	/dt/?c=11670	http://www.shop2.cz/ls/index.php

Once we have the data set for the analysis in a transactional form, we can decide which type of information can be obtained, based on the fields chosen to take part of the rule. For example, if the user chooses the fields of date and visited pages, the extracted knowledge can give us an idea about which pages have been more visited at certain hours. Also, if the user selects the fields of IP and visited pages, we could somehow identify the users that visit those pages.

In order to be able to obtain all this information from the Web log files, we extract the association rules with the algorithm APrioriTID [Agrawal et al., 1993]. Any other Apriori like algorithm can be used, although we have chosen the AprioriTID for its capability of reducing the number of groups considered.

We present an example of results that we can obtain to know the page that the users visit starting from an initial visited page. The form of the rules to extract would be:

Initial visited page ⟶ Referenced page

1. dt/?c=11670 ⟶ http://www.shop2.cz/ls/index.php
   - Support = 0.6
   - Confidence = 1.0
   - FC = 1.0
2. dt/?c=12397 ⟶ http://www.shop7.cz/akce/kat=239
   - Support = 0.2
   - Confidence = 1.0
   - FC = 1.0

These two rules have been extracted from a small set of transactions where rule 1 appears with a percentage of 60% and rule 2 appears with a percentage of 20%. In both cases, the confidence and the certainty factor are 1, which means

that the users visiting the page in the antecedent also visit the page in the consequent. The results coming from these processes must be easy to interpret, since generally, the marketing purpose of this kind of applications implies that the final user is not very related to computing.

4 Conclusions and Future Work

In this article we have reviewed the main aspect of the Web Mining focusing in the Web Usage Mining area, including a short state of the art. We have also shown an application of fuzzy logic, where we analyze the information of the log files of Web server applying fuzzy association rules.

Other aspect important in the article is the personalization, where the user behavior is modeled by means of a profile, where most of the elements are imprecise by nature. The future work will be go further in this area principally, continuing with the development of a tool that allows us to integrate other techniques of mining such as clustering and/or fuzzy clustering.

References

Agrawal et al., 1993. Agrawal, R., Imielinski, T., Swami, A.: Mining association rules between sets of items in large databases. In: Proceedings of the 1993, ACM SIGMOD Conference, pp. 207–216 (1993)

Arotaritei and Mitra., 2004. Arotaritei, D., Mitra, S.: Web Mining: a survey in the fuzzy framework. Fuzzy Sets and Systems (2000)

Au and Chan, 1998. Au, W.H., Chan, K.C.C.: An effective algorithm for discovering fuzzy rules in relational databases. In: Proc. Of IEEE International Conference on Fuzzy Systems, vol. II, pp. 1314–1319 (1998)

Carbonell et al., 1998. Carbonell, J., Carven, M., Fienberg, S., Mitchell, T., Yang, Y.: Report on the conald workshop on learning from text and the web. In: CONALD Workshop on Learning from Text and The Web (June 1998)

Cernuzzi and Molas, 2004. Cernuzzi, L., Molas, M.L.: Integrando diferentes Técnicas de Data Mining en procesos de Web Usage Mining (2003)

Cooley et al., 1997. Cooley, R., Mobasher, B., Srivastava, J.: Web mining: Grouping Web Page References into Transactions for Mining World Wide Web Browsing Patterns, pp. 1–11 (2000)

Chakrabati, 2000. Chakrabati, S.: Data Mining for hypertext: A tutorial survey. ACM SIGKDD Explorations 1(2), 1–11 (2000)

Delgado et al., 2000. Delgado, M., Sánchez, D., Vila, M.A.: Fuzzy cardinality based evaluation of quantified sentences. Int. J. Aprox.Reasoning 3, 23 (2000)

Delgado et al., 2002. Delgado, M., Martín-Bautista, M.J., Sánchez, D., Vila, M.A.: Mining Text Data: Special Features and Patterns. Pattern Detection and Discovery. In: Hand, D.J., Adams, N., Bolton, R. (eds.) Proceedings ESF Exploratory Workshop. Lecture Notes in Artificial Intelligence Series, pp. 140–153 (2002)

Delgado et al., 2003. Delgado, M., Marín, N., Sánchez, D., Vila, M.A.: Fuzzy Association Rules: General Model and Applications. IEEE Transactions on Fuzzy Systems 11, 214–225 (2003)

ECML/PKDD 2005. ECML/PKDD Conference 2005, Web Site. Porto, Portugal (2005) http://ecmlpkdd05.liacc.up.pt/

Etzioni, 1996. Etzioni, O.: The World Wide Web: Quagmire or gold mine. Comunications of the ACM 39, 65–68 (1996)

Garofalakis et al, 1999. Garofalakis, M.N., Rastogi, R., Seshadri, S., Shim, K.: Data Mining and the web: Past, present nad future. In: WorkShop on Web Information and Data Managament, pp. 43–47 (1999)

Hong et al., 1999. Hong, T.P., Kuo, C.S., Chi, S.C.: Mining association rules from quantitative data. Intelligent Data Analysis 3, 363–376 (1999)

Hüllermeier, 2005. Hüllermeier, E.: Fuzzy methods in machine learning and data mining: Status and prospects. Fuzzy Sets and Systems 156(3), 387–406 (2005)

Justicia et al., 2004. Justicia, C., Martín-Bautista, M. J., Sánchez, D.: Minería de textos: Aplicaciones con lógica difusa. Actas del Congreso Español de Tecnologías con Lógica Difusa, Jaén (In Spanish) (2004)

Kleinberg et al., 1999. Kleinberg, J.M., Kumar, R., Raghavan, P.: The Web as a graph: measurements, models, and methods. In: Proceedings of the Fifth Annual International Computing and Combinatorics Conference (1999)

Kraft et al., 2003. Kraft, D.H., Martín-Bautista, M.J., Chen, J., Vila, M.A: Rules and fuzzy rules in text: concept, extraction and usage. International Journal of Approximate Reasoning 34, 145–161 (2003)

Kuok et al., 1998. Kuok, C.-M., Fu, A., Wong, M.H.: Mining fuzzy association rules in databases. SIGMOD Record 27(1), 41–46 (1998)

Lee and Kwang, 1997. Lee, J.H., Kwang, H.L.: An extension of association rules using fuzzy sets. In: Proc. of IFSA'97, Prague, Czech Republic (1997)

Martín-Bautista et al, 2002. Martín-Bautista, M.J., Kraft, D.H., Vila, M.A., Chen, J., Cruz, J.: User profiles and fuzzy logic for Web retrieval issues. Soft Computing Journal 6(5), 365–372 (2004)

Mitra and Pal., 2002. Mitra, S., Pal, S.K: Data Mining in Soft Computing Framework: A Survey. IEEE Transactions on Neural Networks, 3–14 (2002)

Mobasher, 2005. Mobasher, B.: Web Usage Mining and Personalization. In: Singh, M.P. (ed.) Practical Handbook of Internet Computing, CRC Press, Boca Raton (2005)

Nasraoui et al., 1997. Nasraoui, O., Frigui, H., Joshi, A., Krishnappuram, R.: Mining Web accses logs using relational competitive fuzzy clustering. In: Proceedings of springs Symposium On Natural Language Proccesing Form the www, Stanford, California. March 1997 (1997)

Wong et al., 2001. Wong, C.: Shiu, S. and Pal, S.: Mining Fuzzy Association Rules for Web Access Case Adaptation. In: Workshop Proceedings of Soft Computing in Case-Based Reasoning Workshop, in conjunction with the 4th International Conference in Case-Based Reasoning, Vancouver, Canada, pp. 213–220 (2001)

Zadeh, 1975. Zadeh, L.: The concept of linguistic variable and its application to approximate reasoning I. Information Sciences 8, 199–251 (1975)

Stability Analysis for Nonlinear Systems Subjected to External Force

Ken Yeh[1], Cheng-Wu Chen[2,⋆], Shu-Hao Lin[1],
Chen-Yuan Chen[3], Chung-Hung Tsai[4], and Jine-Lih Shen[1]

[1] Department of Civil Engineering, De-Lin Institute of Technology, Tucheng, Taipei, Taiwan, R.O.C.
[2] Department of Logistics Management, Shu-Te University, Yen Chau, Kaohsiung, Taiwan 82445, R.O.C
cwchen@mail.stu.edu.tw
[3] Department of Management Information System, Yung-Ta institute of Technology and Commerce, Ping-Tung 909, Taiwan, R.O.C.
[4] Center of Tour Geographical Information Systems, Taiwan Hospitality and Tourism College, Hualien, Taiwan, R.O.C.

Abstract. This paper considers a fuzzy Lyapunov method for stability analysis of nonlinear systems subjected to external forces. The nonlinear systems under external forces can be represented by Tagagi-Sugeno (T-S) fuzzy model. In order to design a nonlinear fuzzy controller to stabilize this nonlinear system, the parallel distributed compensation (PDC) scheme is used to construct a global fuzzy logic controller. We then propose the robustness design to ensure the modeling error is bounded and some stability conditions are derived based on the controlled systems. Based on the stability criterion, the nonlinear systems with external forces are guaranteed to be stable. This control problem can be reformulated into linear matrix inequalities (LMI) problem.

Keywords: Fuzzy Lyapunov method, fuzzy control.

1 Introduction

Since Zadeh (1965) proposed a linguistic approach to simulate the thought process and judgement of human beings, there has been rapidly growing interest in FLC (fuzzy logic control) and many successful works on industrial and academic fields had been seeking (see [1], [2], [3], [4]). However, FLC techniques suffer from one problem that the design of the FLC is difficult because few theoretical bases are available. Since then, some types of fuzzy models are developed such as Mamdani models, Takagi-Sugeno models, and neuro-fuzzy models etc. to increase accuracy and dimensionality and to simplify the structure of nonlinear systems. The advantage of fuzzy models over conventional mathematical models is the possibility of their being elaborated using much less information about a system. Takagi-Sugeno (T-S) model is first described in [5] which is

⋆ Corresponding author.

H.G. Okuno and M. Ali (Eds.): IEA/AIE 2007, LNAI 4570, pp. 493–500, 2007.

also calledTakagi-Sugeno-Kang model. This kind of fuzzy model can combine the flexibility of fuzzy logic theory and the rigorous mathematical analysis tools into a unified framework. For the reason that it employs linear models in the consequent parts, using conventional linear system theory for analysis becomes simple. Moreover, local dynamics in different state space regions are represented by a set of linear sub-models. The overall model of the system is then a fuzzy blending of these linear sub-models. Based on the T-S model, the parallel distributed compensation (PDC) concept was used to design the fuzzy controller of nonlinear systems [6]. In the PDC concept, the fuzzy controller shares the same fuzzy sets with the fuzzy model in the premise parts and each control rule is distributively designed for the corresponding rule of the fuzzy model. The overall nonlinear control system is not always stable even if all its subsystems are stable.

Since then, some significant research efforts have been presented for stability analysis of fuzzy system and fuzzy controller design based on T-S model (for example, see [7], [8], [9], [10], [11] and the references therein). However, there are two issues we have to emphasize in this paper. One of the issues is that most of the above reported results show that the stability analysis is based T-S fuzzy systems but not for nonlinear systems. That is, the T-S fuzzy model is used to represent practical nonlinear systems and controllers are designed only for fuzzy systems. However, the effect of modeling error between nonlinear system and T-S fuzzy model is not considered. The modeling error is a possible factor to influence the performance of the controlled systems. The other one of the issues is to extend the Lyapunov functions for stability issues of T-S type systems. Beside the above successful results in fuzzy control of T-S type fuzzy model, many papers considered single Lyapunov function for stability conditions of fuzzy control such as [12], [13], [14], [15], [16], [17]. These basically reduce the stability problem to linear matrix inequalities (LMIs) problems in terms of a common Lyapunov function. TheLMI theory is a new and rapidly growing field that provides a valuable alternative to the analytical method (for more details, see [18], [19]). A variety of problems that arise in system and control theory can be reduced to a few standard convex or quasiconvex optimization problems involving the LMI. These resulting optimization problems can be easily solved by numerical computation, so LMI techniques are very efficient and practical tools for solving complex control problems. In order to avoid conservatism of stability and stabilization problems, multiple Lyapunov functions have been paid increasing attention e.g., ([20], [21], [22]). Therefore, here we propose the fuzzy Lyapunov approaches on stability analysis of nonlinear systems subjected to external forces.

The organization of this paper is presented as follows: First, in order to model nonlinear systems with external forces, the T-S fuzzy modeling is briefly reviewed and the parallel distributed compensation (PDC) scheme is used to construct a global fuzzy logic controller. Then, the stability condition derived via fuzzy Lyapunov functions is proposed to guarantee the stability of the controlled system and the robustness is inspected by this condition.

2 Recalled Model and Control Methods

The representation of a plant and controller via T-S type fuzzy model makes it easier to prove the stability of control systems due to the formulation of a locally linear structure. Therefore, T-S fuzzy modeling is employed in this paper to simplify the controller design problem and stability conditions are derived in terms of Lyapunov direct methods in combination with LMI. First of all, the T-S fuzzy model can have the form of a set of rules as well as membership functions represented below.

R1: IF $\{z$ is $F_1\}$ THEN $\{\gamma = f_1(z)\}$
R2: IF $\{z$ is $F_2\}$ THEN $\{\gamma = f_2(z)\}$
$\vdots$
Rm: IF $\{z$ is $F_m\}$ THEN $\{\gamma = f_m(z)\}$

Then the output can be obtained on the basis of the grade of activation of the particular conclusions $f_i, i = 1, 2, \ldots, m$ which is determined by following formula:

$$\gamma = \frac{\sum_{i=1}^{m} \mu F_i(z) f_i(z)}{\sum_{i=1}^{m} \mu F_i(z)}$$

Where F_i is the fuzzy set; the function$f_i(z)$ can be nonlinear. Then, a nonlinear system can be approximated by this T-S fuzzy model technique. The T-S model consists of a set of If-Then rules and each rule represents the local linear input-output relation of the nonlinear system.

2.1 System Description

A nonlinear system with external forces can be approximated by a T-S fuzzy model. Consider nonlinear systems that are represented as follow:

$$\dot{x} = f(x(t), u(t) + \phi(t) \tag{1}$$

where f is a nonlinear vector-valued function, t denotes time, $x(t) \in R^n$ is the state vector, $\phi(t)$denotes the external force, $\dot{x}(t)$is derivative of $x(t)$, $u(t) \in R^m$ is the input vector.

Definition 1. *(Khalil, 1992[23]): The solution of a dynamic system are said to be uniformly ultimately bounded (UUB) if there exist positive constants β and κ, and for every $\delta \in (0, \kappa)$ there is a positive constant $T = T(\delta)$,*
such that$\|x(t_0)\| < \delta \Rightarrow \|x(t)\| \leq \beta, \forall t \geq t_0 + T$

The T-S model consists of a set of If-Then rules. Each rule represents the local linear input-output relation of the nonlinear system and has the following form:

A. T-S Fuzzy Model
Plant Rule i: IF $z_1(t)$ is M_{i1} and ... and $z_g(t)$ is M_{ig}

$$\text{THEN } \dot{x}(t) = A_i(t) + B_i u(t) + \phi(t), i = 1, 2, \ldots, r \tag{2}$$

where state vector$x^T(t) = [x_1(t), x_2(t), \ldots, x_n(t)] \in R^{1\times n}$
control input$u^T(t) = [u_1(t), u_2(t), \ldots, u_m(t)] \in R^{1\times m}$
and unknown disturbance$\phi^T(t) = [\phi_1(t), \phi_2(t), \ldots, \phi_z(t)] \in R^{1\times z}$ with a known upper bound $\phi_{upj}(t) \geq \| \phi_j(t) \|$, M_{ip} (p=1,2,..., g) is the fuzzy set; γ is the rule number; $z_1(t) \ldots z_g(t)$ are the premise variables; $A_i \in R^{n\times n}$,$B_i \in R^{n\times m}$

B. PDC Design
The fuzzy controller rules have the same premise parts as those of the T-S model. Linear control rule i is derived based on the state equation (2) in the consequent part of the ith model rule.
Control Rule i: IF $z_1(t)$ is M_{i1} and ... and $z_g(t)$ is M_{ig}

$$\text{THEN } u(t) = -F_i x(t), i = 1, 2, \ldots, r \tag{3}$$

where F_i is the local feedback gain matrix. The final control u is inferred using the Sum-Product reasoning method:

$$u(t) = -\frac{\sum_{i=1}^{r} \omega_i(t) F_i x(t)}{\sum_{i=1}^{r} \omega_i(t)} \tag{4}$$

where ω_i is the activation degree of the ith rule, calculated as:$\omega_i(t)$=$\Pi_{p=1}^{g} M_{ip}(z_p)$
By substituting Eq.(4) into Eq. (2), the models of closed-loop control system are obtained as

$$\dot{x}(t) = \sum_{i=1}^{r} \sum_{l=1}^{r} h_i(t) h_l(t) (A_i - B_i F_l) x(t) + \phi(t) \tag{5}$$

Definition 2. *(Lu et al., 1998 [24]): LMI Formulation of the Design Specifications*
The linear matrix inequality (LMI) is any constraint of the form

$$F(\nu) = F_0 + \sum_{i=1}^{m} \nu_i F_i \tag{6}$$

where $\nu = [\nu_1, \nu_2 \ldots, \nu_0] \in R^m$ is the variable vector, and the symmetric matrices $F_i = F_i^t \in R^{n\times n}, i = 0, 1, \ldots, m$ are given. It can be shown that the solution set $\{\nu \mid F(\nu) > 0\}$ may be empty, but it is always convex. Thus, although (6) has no analytic solution in general, it can be solved numerically by efficient numerical algorithms. Many control problems can be reformulated into LMIs and solved efficiently by recently developed interior-point methods [18].

3 Robustness Design of Controlled Systems Via Fuzzy Lyapunov Method

In this section, we will inspect the stability under the influence of modeling error between the T-S fuzzy model and the nonlinear system (1). In the beginning, the nonlinear system (1) can be described as follow:

$$\dot{x}(t) = f(x(t), u(t)) + \phi(t) + \sum_{i=1}^{r}\sum_{l=1}^{r} h_i(t)h_l(t)(A_i - B_iF_l)x(t)$$

$$= \sum_{i=1}^{r}\sum_{l=1}^{r} h_i(t)h_l(t)(A_i - B_iF_l)x(t) + e(t) + \phi(t) \tag{7}$$

where $e(t) \equiv f(x(t), u(t)) - \sum_{i=1}^{r}\sum_{l=1}^{r} h_i(t)h_l(t)(A_i - B_iF_l)x(t)$. Suppose that there exists a bounding matrix ΔH such that
$\| e(t) \| \leq \| \sum_{i=1}^{r}\sum_{l=1}^{r} h_i(t)h_l(t)\Delta H x(t) \|$ and $\Delta H = \delta H$ where $\| \delta \| \leq 1$. Then we can readily obtain

$$e^T(t)e(t) \leq [Hx(t)]^T[Hx(t)] \tag{8}$$

That means modeling error can be bounded by the matrix H. The proof of Eq. (8) and the procedures for determining δ and H can be referenced in [25].
Here we define a fuzzy Lyapunov function and consider the stability conditions for controlled system (7).

Definition 3. *Equation (9) is said to be a fuzzy Lyapunov function for the T-S fuzzy system if the time derivative of $V(x(t))$ is always negative at $x(t) \neq 0$.*

$$V(x(t)) = \sum_{i=1}^{r} h_i(t)x^T(t)P_ix(t) \tag{9}$$

where P_i is a positive definite matrix. In this paper, in order to consider the term of the time derivative $\dot{h}_\rho(t)$ can be solved numerically, an upper bound of time derivative, i.e.$\|\dot{h}_\rho(t)\| \leq \phi_\rho$, is used.

In the following, a stability criterion is proposed to guarantee the stability of the closed-loop nonlinear system with external forces. Before a stability condition is proposed, a useful concept is given below:

Lemma 1. *(Li and Souza, 1997[26] ; Chen et al., 2004[8]): For any A, $B \in R^n$ and for any symmetric positive definite matrix $G \in R^{n\times n}$ or R , we have*

$$-2A^TB \leq A^TGA + B^TG^{-1}B \tag{10}$$

Theorem 1. *The controlled system (7) is stable in the large if there exist common positive definite matrices such that the following inequality is satisfied:*

$$\sum_{\rho=1}^{r} \phi_\rho P_\rho + (A_j - B_jF_l)P_i + P_i(A_j - B_jF_l)$$
$$+\alpha^{-1}P_iP_i + \beta H^T(t)H(t) + \beta^{-1}P_iP_i < 0 \tag{11}$$

Proof. Consider the Lyapunov function candidate

$$V(x(t)) = \sum_{i=1}^{r} h_i(t)^T(t) P_i x(t)$$

The time derivative of V is

$$\begin{aligned}
\dot{V}(X(t)) &= \sum_{\rho=1}^{r} \dot{h}_\rho(t) x^T(t) P_\rho x(t) + \sum_{i=1}^{r} h_i(t)\{\dot{x}^T(t) P_i x(t) + x^T(t) P_i \dot{x}(t)\} \\
&= \sum_{\rho=1}^{r} \dot{h}_\rho(t) x^T(t) P_\rho x(t) \\
&\quad + \sum_{i=1}^{r} h_i(t)\{[\sum_{j=1}^{r}\sum_{l=1}^{r} h_j(t) h_l(t)(A_j - B_j F_l)x(t) + e(t) + \phi(t)]^T P_i x(t)\} \\
&\quad + \sum_{i=1}^{r} h_i(t)\{x^T(t) P_i [\sum_{j=1}^{r}\sum_{l=1}^{r} h_j(t) h_l(t)(A_j - B_j F_l)x(t) + e(t) + \phi(t)]\}
\end{aligned} \tag{12}$$

Based on Lemma 1 and (12), we get

$$\begin{aligned}
\dot{V}(X(t)) \le & \sum_{\rho=1}^{r} \dot{h}_\rho(t) x^T(t) P_\rho x(t) + x^T(t)[\alpha^{-1} P_i P_i + \beta^{-1} P_i P_i] x(t) \\
& + \alpha \phi^T(t)\phi(t) + \beta e^T(t) e(t) \\
& + \sum_{i=1}^{r}\sum_{j=1}^{r}\sum_{l=1}^{r} h_i(t) h_j(t) h_l(t) x^T(t) \\
& \{(A_j - B_j F_l) P_i + P_i (A_j - B_j F_l)\} x(t)
\end{aligned} \tag{13}$$

Based on Eq. (8) and note that $\phi_{upj}(t) \ge \| \phi_j(t) \|$, we would have

$$\begin{aligned}
\dot{V}(X(t)) \le & \\
& \sum_{i=1}^{r}\sum_{j=1}^{r}\sum_{l=1}^{r} h_i(t) h_j(t) h_l(t) x^T(t) \\
& \{\sum_{\rho=1}^{r} \phi_\rho P_\rho + (A_j - B_j F_l) P_i + P_i (A_j - B_j F_l) \\
& + \alpha^{-1} P_i P_i + \beta H^T(t) H(t) + \beta^{-1} P_i P_i\} x(t) + \alpha \parallel \phi_{up}(t) \parallel^2
\end{aligned} \tag{14}$$

The nonlinear system with external force is UUB stable if Theorem 1 is satisfied. Based on stability condition of Theorem 1, the proof is thereby completed.

4 Conclusions

This paper considered a fuzzy Lyapunov method to derive the stability condition for the nonlinear system with external force. The fuzzy Lyapunov function is defined by fuzzy blending quadratic Lyapunov functions. First, the nonlinear systems are represented by T-S fuzzy model. In order to ensure the system can be stabilized by proposed T-S fuzzy controller, the robustness design is proposed to overcome the modeling error. Then, Stability conditions of closed-loop controlled systems are derived based on fuzzy Lyapunov functions to avoid conservatism.

Acknowledgments

This work was supported by the National Science Council of Republic of China under Grant No. NSC 95-2221-E-366-001 and NSC 95-2221-E-237-011 The authors wish to appreciate the constructive suggestions from anonymous reviewers to this paper.

References

1. Chang, S.S.L., Zadeh, L.A.: On fuzzy mapping and control. IEEE Trans. Syst. Man Cybern. 2, 30–34 (1972)
2. Zadeh, L.A.: Outline of a new approach to the analysis of complex systems and decision processes. IEEE Trans. Syst. Man, Cybern. 3, 28–44 (1973)
3. Kickert, W.J.M., Mamdani, E.H.: Analysis of a fuzzy logic controller. Fuzzy Sets Syst. 1, 29–44 (1978)
4. Braae, M., Rutherford, D.A.: Theoretical and linguistic aspects of the fuzzy logic controller. Automatic 15, 553–577 (1979)
5. Takagi, T., Sugeno, M.: Fuzzy identification of systems and its applications to modeling and control. IEEE Trans. Syst. Man, Cybern. 15, 116–132 (1985)
6. Wang, H.O., Tanaka, K., Griffin, M.F.: Parallel distributed compensation of nonlinear systems by Takagi and Sugenos fuzzy model. In: Proceedings of 4th IEEE International Conference on Fuzzy Systems, Yokohama, Japan, pp. 531–538 (1995)
7. Chen, X.J., Sun, Z.Q., He, Y.Y.: Analysis and design of fuzzy controller and fuzzy observer. IEEE Trans. Fuzzy Syst. 6, 41–51 (1998)
8. Chen, C.W., Chiang, W.L., Hsiao, F.H.: Stability analysis of T-S fuzzy Models for nonlinear multiple time-delay interconnected systems. Mathematics and Computers in Simulation 66, 523–537 (2004)
9. Guerra, T.M., Vermeriren, L.: Control law for Takagi-Sugeno fuzzy models. Fuzzy Sets Syst. 120, 95–108 (2001)
10. Li, J., Wang, H.O., Niemann, D., Tanaka, K.: Dynamic parallel distributed compensation for Takagi-Sugeno fuzzy systems: an LMI approach. Information Sciences 123, 201–221 (2000)
11. Wang, H.O., Tanaka, K., Griffin, M.F.: An approach to fuzzy control of nonlinear systems: stability and design issues. IEEE Trans. Fuzzy Syst. 4, 14–23 (1996)
12. Tanaka, K., Sugeno, M.: Stability analysis and design of fuzzy control systems. Fuzzy Sets Syst. 45, 135–156 (1992)

13. Chen, C.VL., et al.: Analysis and design of fuzzy control systems. Fuzzy Sets Syst. 57, 125–140 (1993)
14. Wang, L.K., Leung, F.H.F., Tam, P.K.S.: Fuzzy model-based controller for inverted pendulum. Electron. Letters 32, 1683–1685 (1996)
15. Cao, S.G., Rees, N.W., Feng, G.: Stability analysis and @design for a class of continuous-time fuzzy control systems. Int. J. Control 64, 1069–1087 (1996)
16. Cuesta, F., Gordillo, F., Aracil, J., Ollero, A.: Stability analysis of nonlinear multivariable Takagi-Sugeno fuzzy control systems. IEEE Trans. Fuzzy Syst. 7, 508–520 (1999)
17. Chen, C.Y., Hsu, R.C., Chen, C.W.: Fuzzy logic derivation of neural network models with time delays in subsystems. Int. J. Artificial Intelligence Tools 14, 967–974 (2005)
18. Boyd, S., El Ghaoui, L., Feron, E., Balakrishnan, V.: Linear matrix inequalities in system and control theory. Philadelphia, PA: SIAM (1994)
19. Nesterov, Yu., Nemirovsky, A.: Interior-point polynomial methods in convex programming. SIAM, Philadelphia, PA (1994)
20. Tanaka, K., Hori, T., Wang, H.O.: A dual design problem via multiple Lyapunov functions. In: Proc. IEEE Int. Conf. Fuzzy Systems, pp. 388–391 (2001)
21. Tanaka, K., Hori, T., Wang, H.O.: A multiple Lyapunov function approach to stabilization of fuzzy control systems. IEEE Trans. Fuzzy Syst. 11, 582–589 (2003)
22. El-Farra, N.H., Mhaskar, P., Christofides, P.D.: Output feedback control of switched nonlinear systems using multiple Lyapunov functions. Systems and Control Letters 54, 1163–1182 (2005)
23. Khalil, H.K.: Nonlinear Systems. Macmilllan, London. U.K (1992)
24. Lu, L.T., Chiang, W.L., Tang, J.P.: Application of model reduction and LQG/LTR robust control methodology in active structure control. J. Eng. Mech. ASCE 124, 446–454 (1998)
25. Tseng, C.S., Chen, B.S.: Decentralized fuzzy model reference tracking control design for nonlinear interconnected systems. IEEE Trans. Fuzzy Syst. 9, 795–809 (2001)
26. Li, X., de Souza, C.E.: Criteria for robust stability and stabilization of uncertain linear systems with state delay. Automatica 33, 1657–1662 (1997)

Integrated Framework for Reverse Logistics

Heng-Li Yang and Chen-Shu Wang

Department of MIS, National Cheng-Chi University,
64, Sec. 2, Chihnan Rd., Mucha Dist, Taipei 116, Taiwan
{yanh, 93356506}@nccu.edu.tw

Abstract. Although reverse logistics has been disregarded for many years, pressures from both environmental awareness and business sustainability have risen. Reverse logistical activities include return, repair and recycle products. Traditionally, since the information transparency of the entire supply chain is restricted, business is difficult to predict, and prepare for these reverse activities. This study presents an agent-based framework to increase the degree of information transparency. The cooperation between sensor and disposal agents helps predict reverse activities, avoid return, speed up repair and prepare for recycling behaviors.

Keywords: Reverse Logistics, information transparency, agent-based system.

1 Introduction

A complete supply chain concept typically includes forward and reverse logistics [16,17]. However, reverse logistics has been much less examined than forward logistics. Reverse logistics has recently emerged as crucial issues in both practices and academic studies [13,15,17]. Reverse logistics encompasses planning, implementing and controlling the efficient and cost-effective flow of raw materials, in-process inventory, finished goods and related information from the point of consumption to the point of origin to recapture value or dispose properly [16]. In the European Union, the Waste Electrical and Electronic Equipment (WEEE) directive, this came into force in August 2005, and the Restriction of Hazardous Substances (RoHS) directive, which came into force in 2006; requires companies to take responsibility for product that they sell throughout the product entire lifecycle [8]. Reverse logistics has become imperative for business [4]. Many previous studies have attempted to formulate mathematical models of reverse logistics. Among these studies, Min et al. presented a genetic algorithm model to deploy centralized return centers [12]. Klausner and Hendrickson explored the relationship between product return ratio and reverse logistics strategy [9]. Kulshreshtha and Sarangi examined the link between recycling and price discrimination [10]. Although these optimization models provide partial reverse logistic solutions, they include many assumptions that would not hold in reality. Since reverse logistic activities are too uncertain to formulize [7], the information about them should ideally be combined. Additionally, some studies have investigated this issue from the perspective of the entire supply

H.G. Okuno and M. Ali (Eds.): IEA/AIE 2007, LNAI 4570, pp. 501–510, 2007.

chain. For instance, Beamon extended the forward supply chain, and proposed the green supply chain concept [2]. Tibben-Lembake and Rogers discussed the distinction between forward and reverse logistics in multiple dimensions [17]. Mollenkopf and Closs discussed the hidden value of reverse logistics from the entire supply chain [13]. Richey *et al.* surveyed reverse logistics programs, and claimed that information is a critical factor [15].

Companies are increasingly utilizing reverse logistics as a business strategy [9]. For instance, loose return policies might give customers the impression of high product quality [16]. Additionally, a business may earn goodwill from socially or environment responsible behavior [4,13]. However, these reverse logistics strategies might lead to a large amount of returned and recycled merchandise. Businesses require additional information to resolve this vicious circle. Otherwise, the opaque information might invoke a huge bullwhip effect. As business obtains more information, they can predict and prepare, or even prevent bad effects in reverse activities. If the returned products are fashion merchandise, such as 3C electronic product or seasonal clothes, then the product remaining value might fall when they are sent back by the consumer to the producer site [8]. Therefore, if sufficient information is available to enable businesses to predict returns early, then business could properly prepare and reduce process time to maintain their remaining values.

Additionally, due to the enforcement of WEEE or RoHS in European Union, manufacturers would become concerned with the recycle ratio at any time. This study considers these reverse logistic activities more actively. An agent-based model is presented to increase information transparency degree (ITD) of the entire supply chain management (SCM). A supply chain with a high ITD serves as an early warning system, and works very efficiently. A High ITD enhances information sharing within an entire supply chain management (SCM).

2 Problem Descriptions

Previous studies [2,3,6,11,12,13,18] have categorized reverse logistic activities into three groups, as shown in Table 1, namely return, repair and recycle. In the process of forward logistics, suppliers provide raw material to manufacturers, who make products, which are then sent to customers, generally through distributors. Conversely, a customer might send a product back for return, repair or recycling. Additionally, manufacturers and suppliers also need to deal with defective or non-working products. Recycling collectors need to dispose of these recycled products properly, and transfer reusable materials back to the supplier and manufacturer. This process is known as reverse logistics. These reverse activities have the following problems. (1) If a customer returns product to a distributor, then the distributor might stock returned products to a particular level, then send them back to manufacturer. However, this practice adversely affects the manufacturer, who has less time to process the returned products, thus the lowering their remaining value. (2) Recycling laws, such as WEEE and RoHS in the European Union, increase the importance of recycling activities. Businesses need to monitor recycle ratios, and raise them to comply with recycling laws. (3) Finally, in the repair aspect, repairing processing time should be reduced to maintain the image of a business.

Table 1. The definition of reverse logistic activities

Activity	Definition	Result
Return	Consumers return the products bought within certain period of time for any reason (rational or irrational).	Depending on policies, customer may receive another identical new product, an equivalent product exchange or full money back.
Repair	Consumers send broken product to repair center (or original producer).	Customer generally would receive workable product back.
Recycle	Consumers send unvalued or unwanted product to recycling collectors.	Customers might or might not receive rewards.

All these problems are customer-centric and difficult to predict. However, if the ITD of the entire supply chain could be improved, then the prediction accuracy could be enhanced to enable the upstream and downstream enterprises of supply chain to be prepared early.

3 Proposed Framework

This study assumes symbiosis in the entire supply chain system. The supply chain's participants are assumed to share three databases, namely customer, product and transaction. The access permissions are as follows. (1) In the customer DB, the distributor can insert and update and all other participants can only query. (2) In the product DB, the manufacturer can insert and update and all other participants can only query. (3) In the transaction DB, the distributor can insert and update; manufacturer can update, and all other participants can only query. The shared data are updated regularly. This symbiosis assumption is consistent with the concept of strategic partners, in which innovative enterprises share sales data, customer buying patterns and future plans with their partners [14].

Since most reverse activities are triggered by customers, and are hard to predict accurately by conventional analytic approaches, heuristics and AI techniques might help [14]. In the forward supply chain, Piramuthu [5] developed an agent-based framework to automate supply chain configuration, and to improve the performance of the supply chain with dynamic configuration. However, to our knowledge, no study has applied agents to reverse activities. This study presents an agent-based approach. As illustrated in Figure 1, two agents, the sensor agent and the disposal agent, are integrated within the proposed framework. Since an agent could autonomously monitor the changing environment and react automatically to complete a goal, they might helpfully manage this customer-centric problem.

3.1 The Sensor Agent

The sensor agent autonomously monitors the recent data, and transmits warning signals to the disposal agent at appropriate times. Additionally, it performs marketing

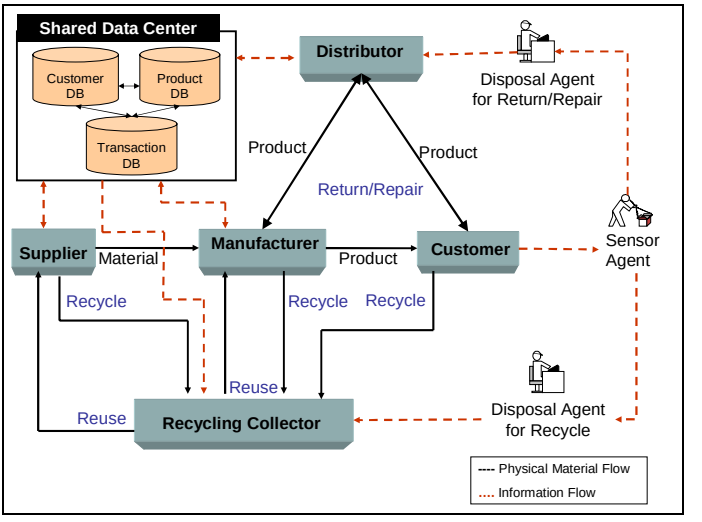

Fig. 1. The proposed agent-based framework

Table 2. Some rules for detecting reverse activities

Dimensions	Attributes	Return Ratio	Repair Ratio	Recycle Ratio
Customer	(recency, frequency, monetary)=(H,H,M)	H	-	M
	Gender= Female and Education= High	H	M	-
Product	Size= Huge	L	-	H
	Price= High	H	-	-
	Hard to Operating	-	H	-
Customer and Product	Customer_Location= Moist and Product=3C Electric Equipments	-	H	-
Customer and Marketing Strategic	Customer_Income=Low and Market_Strategy= "Buy 1 get 1 free"	L	-	-
Product and Marketing Strategic	Product_Size= Small and Market_Strategy= "Double Credit"	H	-	L

Note: H=High, M=Moderate, L=Low

surveys if required. Since product returns might result in serious supply chain problems, return data should be monitored at least weekly. Conversely, since monitoring repair data is likely to be less urgent than monitoring return data, a monthly monitoring period might be sufficient. The possible product recycle time

could be estimated from the product life cycle. Therefore, this study recommends enabling active database triggers in customer profile data to provide notice signals. The monitoring should follow rules to detect possible reverse activities. Table 2 lists some such rules.

These rules come from heuristics and data mining results. The sensor agent should periodically perform data mining on the historical data or data warehouse. Some data mining techniques (e.g., those in Table 3) could be considered. The cluster analysis considers some transaction level attributes, e.g., recency, frequency and monetary (RFM) attributes, to cluster customer and discover the reverse activity patterns of customer demographic information. Additionally, in the product dimension, product characteristics could be adopted to cluster products rather than original product types. Furthermore, since some patterns might be cross clusters, the association analysis would take at least two cluster results from cluster analysis as inputs to discover the reverse patterns between these two inputs. For instance, some clusters of customers, who bought products, might be found to have high return ratios. These discovered patterns would be reviewed by experts, and then fed into the rule base of the sensor agent. Therefore, the sensor agent would have a learning capability to improve its own monitoring correctness.

Table 3. Examples of data mining of sensor agent

Cluster Analysis
Adopting transaction level attributes (e.g., Recency, Frequency, Monetary) to segment the customers. Then, observing demographic level (e.g., gender, education, income, location) attributes to discover reverse activity patterns of customer clusters.
Adopting product properties (e.g., size, price, operation) to cluster product to discover reverse patterns of product properties.
Association Analysis
Finding reverse activity patterns between customer and product clusters.
Identifying reverse activity patterns between customer clusters and marketing strategies.
Detecting reverse activity patterns between product clusters and marketing strategies.
Discovering reverse activity patterns among customer clusters, product clusters and marketing strategies.

3.2 The Disposal Agent

After receiving signals from the sensor agent, the disposal agent recommends treatments by case-based reasoning (CBR) [1], and reference supplementary rules if necessary. The case base stores successful cases from previous experience. The rule base includes some supplementary heuristics from domain experts.

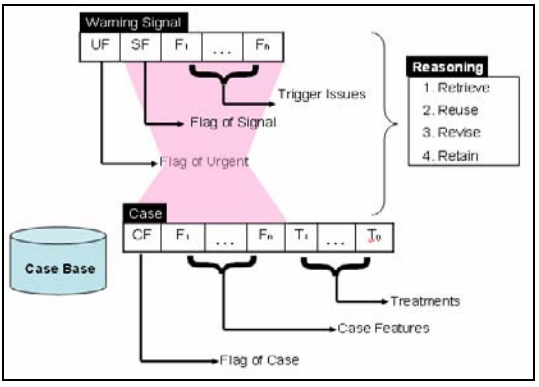

Fig. 2. The case-based reasoning of disposal agent

```
While (Warning Signal)
  {  Reasoning by cases and supplementary rules
     Switch (UF)
      Case: Moderate
          1.  Suggests some particular treatments
          2.  Disposal agent performs these treatments automatically
      Case: Influential
          1.  Suggests particular treatments to decision maker for
              preventing return and enhancing recycling ratio
          2.  Decision-maker refers these treatments and may revise.
      Case: Serious
          1.  Suggests treatments to decision-maker.
          2.  Schedule business processes to prepare for possible
              reverse activities.
     End Switch;
     Evaluate performance of suggestion;
     If the event performance is good, then retain to Case base}
```

Fig. 3. The disposal agent suggestion

As revealed in Figure 2, a warning signal consists of three parts {urgent degree (UF), signal flag (SF), trigger features}. SF could be “return”, “recycle”, or “repair”. UF indicates degrees of impact. In Figure 3, depending on the different UF, the system would have different actions. It compares {SF, trigger features} to those {CF, case features} of cases in case base, and retrieve the treatments of the fittest case to decision maker. It might refer to supplementary rules for detailed suggestions or other suggestions (if no suitable case could be found). Then, disposal agent might perform

treatments automatically or suggest to decision-makers. It would cooperate with other systems, e.g., programs of scheduling, inventory management or quality checking. If the response of this problem solving is good, then the experiences may be annotated by human experts, and then retained in the case base as further references. Therefore, the disposal agent could have learning capability to improve its performance next time.

3.3 The Integrated System Framework

As illustrated in Fig. 4, the framework has three stages. At stage I, the sensor agent monitors the data; predicts the possibilities of reverse activities, and transmits different warning signals to the disposal agent. The rule base comes from heuristics, and is periodically updated by data mining techniques (e.g., clustering and association analyses). At stage II, the disposal agent recommends feasible treatments from past cases and referencing rules. At stage III, for possible serious effects, disposal might further recommend or automatically initiate some related business process preparations (e.g., scheduling). Additionally, the disposal agent should notify the sensor agent of its treatment, and ask for a necessary follow-up. For instance, if a sensor agent discovers that the frequencies of customer complaint phones have risen, and predicts that the possible return rate is likely to increase, then the disposal agent recommends employing customer specialists to listen to customer concerns. After the treatment has been completed, the sensor agent performs a customer satisfaction survey to check whether the problems have been solved. The sensor agent also gives the disposal agent the evaluation feedback concerning the effectiveness of the treatment. Based on the feedback, the disposal agent adds annotations to the original case base, and recommends further treatment if needed.

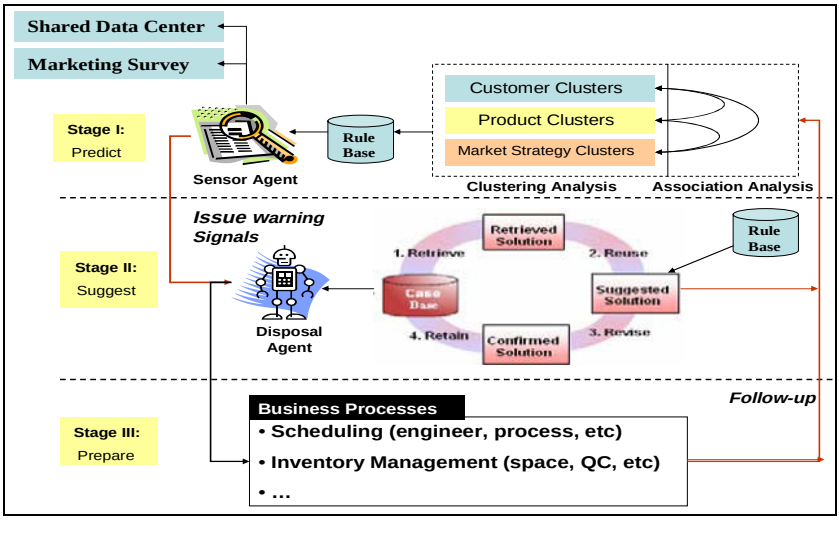

Fig. 4. The cooperation between sensor agent and disposal agent

4 Illustrative Scenarios

To understand the proposed framework clearly, the three classes of reverse logistic activity are described as follows.

4.1 Return Scenario

According to the proposed framework, the sensor agent monitors the data, which are gathered from the consumer site and shared data center; performs weekly cross-analyses to diagnose the return probability, and transmits alarm signals. For instance, assume customer is making an increasing number of complaints, and that her (his) profile (Gender, Education)=(Female, High) matches one return pattern in Table 3. The sensor agent verifies the warrant period of the related transaction. If the guarantee period has expired, then a "moderate" signal is sent. Conversely, if the product is still under guarantee, then an "influential" signal is sent, while if the original transaction amount was also large, then a "serious" signal is flagged. The disposal agent then recommends appropriate treatments. For moderate signals, the disposal agent automatically sends an e-mail to a customer acknowledging the customer's concerns. For "influential" signals, the disposal agent advises a customer specialist to contact the customer in order to prevent possible return. For serious signals, the disposal agent recommends performing related business processes such as preparing return stock-location. After the treatment is completed, the sensor agent should follow up the customer satisfaction and give feedback to the disposal agent. The proposed framework could provide an early warning to the manufacturer about possible returns, and additionally could summarize the top 10 return reasons for product re-design. The ITD would increase under this framework.

4.2 Repair Scenario

Based on the proposed framework, the sensor agent would analyze the complaints from consumers monthly, and calculate the repair possibilities. For instance, suppose that some customers of electronic products live in the moist area, matching a rule in Table 2. The sensor agent judges, according to the past data, that some parts of these products might malfunction later. If these parts are normal materials, then a "moderate" signal is transmitted. If these parts contain special materials, then an "influential" signal is sent. If the repairing behaviors would require particular engineer skills, then a "serious" signal is flagged. The disposal agent recommends appropriate treatments to the decision maker. For a "moderate" signal, the disposal agent verifies the material stocks, and automatically schedules these repair requirements. For "influential" signals, the disposal agent recommends material procurements to the decision maker. In this case, owing to the longer repair period, the disposal agent arranges a temporary replacement product for customers. For serious signals, the disposal agent schedules another engineer, or recommends further training for engineers. After the treatment is completed for certain period (say one month), the sensor agent follows up customer opinions, and gives feedback to the

disposal agent for further improvement. The ITD of the SCM is higher under the proposed framework than in other systems, enabling the repair center to prepare for possible repairs to accelerate the repair time.

4.3 Recycling Scenario

According to the proposed framework, database triggers notify the sensor agent the possibilities for recycling when the product approaches the end its life. The product size and materials is checked. If the product materials are normal, then the sensor agent sends a moderate signal. If the products contain toxic or harmful materials, then the senor agent sends a "serious" signal. The disposal agent then recommends treatments to the decision maker. For a "moderate" signal, distributors are recommended to conduct relationship marketing to their customers to express concerns about their product usage. Additionally, some notification messages could be transmitted automatically to the recycling collector to raise the ratio of recycled material. For serious signals, the disposal agent should report to the decision maker to comply with WEEE and RoHS requirements. The proposed framework raises the ITD of SCM. Moreover, the recycling ratio could be expected to increase if the recycling promotion becomes more active.

5 Conclusions

Reverse logistic activities have recently become a critical issue for both consumer and producer sites, but present some dilemmas. (1) Businesses are increasingly adopting loose return policy as strategy. However, in practice, the returned products are stocked by distributors, cannot be processed quickly by manufacturers to regain economic value quickly. (2) As new environmental laws are increasingly being enforced, recycling activities are additional burdens to the manufacturer, but are also social and environment responsibilities. Additionally, the recycling behaviors are not necessary for customer, for whom the reward is limited. Therefore, recycling is difficult to implement well in practice. (3) Repair is inconvenient for both customers and repair centers. Customers cannot use their products during the repair period. Thus, decreasing the repair time could improve customer's satisfaction. However, without proper information, repair centers cannot schedule the required resources to shorten the repair time.

This study presents an agent-based framework to improve information transparency degree of these reverse activities. A sensor agent operates like an early warning system to detect possible reverse activities actively. A disposal agent operates like a consultant, recommending treatments to decision maker, and even arouse related business processes automatically. The proposed framework is expected to increase the supply chain's information transparency degree, and improve the performance of reverse supply chain activities. Future research will concentrate on implementing this framework, and on verifying its performance and effectiveness using real-world data and field studies.

References

1. Aamodt, A., Plaza, E.: Case Based Reasoning: Foundational Issues, Methodological Variations, and System, Approaches. In: AI Communications, vol. 7(1), pp. 39–59. IOS Press, Amsterdam (1994)
2. Beamon, B.M.: Designing the Green Supply Chain. Logistics Information Management 12(4), 332–342 (1999)
3. Campbell, G.C.: Merchandise Returns: Retailer's Viewpoint. Quarterly Review of Commerce 8(2), 141–151 (1941)
4. Carter, C.R.: Purchasing and Social Responsibility: A Replication and Extension. Journal of Supply Chain Management 40(4), 4–16 (2004)
5. Emerson, D., Piramuthu, S.: Agent Based Framework for Dynamic Supply Chain Configuration. In: Procedings of the 37th Hawaii International Conference on System Sciences, pp. 1–9 (2004)
6. Guide, D.R., Jayaraman, V., Srivastava, R., Beton, W.C.: Supply Chain Management for Recoverable Manufacturing Systems. Interface 30(3), 125–142 (2002)
7. Inderfurth, K.: Impact of Uncertainties on Recovery Behavior in a Remanufacturing Environment. International Journal of Physical Distribution & Logistics Management 35(5), 318–336 (2005)
8. Kempfer, L.M.: New Ideas for Handling Electronic Product Returns. Material Handling Management 60(5), 35–36 (2005)
9. Klausner, M., Hendrickson, C.T.: Reverse Logistics Strategy for Product Take Back. Interfaces 30(3), 156–165 (2000)
10. Kulshreshtha, P., Sarangi, S.: No Return, No Refund: An Analysis of Deposit Refund Systems. Journal of Economic Behavior & Organization 46, 379–394 (2001)
11. Lambert, A.J.D., Boelaarts, H.M., Splinter, M.A.M.: Optimal Recycling System Design: With an Application to Sophisticated Packaging Tools. Environmental and Resource Economics 28(3), 273–299 (2004)
12. Min, H., Ko, H.J., Ko, C.S.: A Genetic Algorithm Approach to Developing the Multi-Echelon Reverse Logistics Network for Product Returns. Omega 34, 56–69 (2006)
13. Mollenkopf, D.A.: The Hidden Value in Reverse Logistics. Supply Chain Management Review 9(5), 34–43 (2005)
14. Papazoglou, M.P.: Agent-Oriented Technology in Support of E-Business. Communications of the ACM 44(4), 71–77 (2001)
15. Richey, R.G., Chen, H., Genchev, S.E., Daugherty, P.J.: Developing Effective Reverse Logistics Programs. Industrial Marketing Management 34, 830–840 (2005)
16. Rogers, D.S., Tibben-Lembke, R.S.: An Examination of Reverse Logistics Practices. Journal of Business Logistics 22(2), 129–148 (2001)
17. Tibben-Lembke, R.S., Rogers, D.S.: Differences Between Forward and Reverse Logistics in a Retail Environment. Supply Chain Management 7(5), 271–282 (2002)
18. Walton, S.V., Handfield, R.B., Melnyk, S.A.: The Green Supply Chain: Integrating Suppliers into Environmental Management Processes. International Journal of Purchasing and Materials Management 34(2), 2–11 (1998)

Screening Paper Formation Variations on Production Line

Marcus Ejnarsson[1], Carl Magnus Nilsson[1], and Antanas Verikas[1,2]

[1] Intelligent Systems Laboratory, Halmstad University, Box 823, SE-301 18 Halmstad, Sweden
Marcus.Ejnarsson@ide.hh.se, Carl-Magnus.Nilsson@ide.hh.se
[2] Department of Applied Electronics, Kaunas University of Technology, Studentu 50, LT-513 68, Kaunas, Lithuania
Antanas.Verikas@ide.hh.se

Abstract. This paper is concerned with a multi–resolution tool for screening paper formation variations in various frequency regions on production line. A paper web is illuminated by two red diode lasers and the reflected light recorded as two time series of high resolution measurements constitute the input signal to the papermaking process monitoring system. The time series are divided into blocks and each block is analyzed separately. The task is treated as kernel based novelty detection applied to a multi–resolution time series representation obtained from the band-pass filtering of the Fourier power spectrum of the series. The frequency content of each frequency region is characterized by a feature vector, which is transformed using the canonical correlation analysis and then categorized into the *inlier* or *outlier* class by the novelty detector. The ratio of outlying data points, significantly exceeding the predetermined value, indicates abnormalities in the paper formation. The tools developed are used for online paper formation monitoring in a paper mill.

1 Introduction

To stand the high competition in the market related to the papermaking industry, companies are striving to get the best possible return from their equipment. Therefore, ensuring manufacturing of products of a desired constant quality that meets customer's specifications offers a significant advantage for the companies. To assure the high constant quality of the end-products, a producer must have a possibility to objectively measure and monitor the quality of the products.

Various defects can be encountered in paper. The most common ones are holes, impurities, too big variation of the paper formation, uneven paper shrinkage profile, etcetera. Tools utilized for paper production monitoring depend on a task. The paper shrinkage profile is usually assessed off-line. One of such techniques can be found in [1]. Image analysis based commercial systems exist for detecting holes and relatively large-size-impurities. The degree of small-size-impurities is usually assessed at a pulp level by analyzing images taken from pulp samples [2,3]. The mass distribution on the sheet—formation—is commonly assessed

H.G. Okuno and M. Ali (Eds.): IEA/AIE 2007, LNAI 4570, pp. 511–520, 2007.

off-line by using the β-radiography [4]. However, the technique is rather time consuming. Therefore, various image analysis based techniques are often used instead [5,6,7,8,9]. Too big variation of the paper formation is one of the most common paper deficiencies encountered. This study is also concerned with monitoring this type of paper deficiencies.

In a modern paper machine, the paper production process runs at about 30 m/s speed. The high production speed entails snapshot or coarse grid measurements. The sensors are typically mounted on a head traversing the web. The typical transverse time for the head is about 30 seconds. Approximately 700 meters of paper would have passed through the paper machine during that time. Variability of the paper structure has been studied by a number of researchers [8,9,10] and it was found that such a course sampling strategy works well for assuring the stability of the paper machine itself. However, it is not always adequate for assuring low variations in the paper structure.

Most paper produced is used for printing. Printed colour pictures are made of small halftone dots of primary colours. Fig. 1 presents an example of an enlarged view of a small part of a colour picture printed using cyan, magenta, yellow and black primary inks.

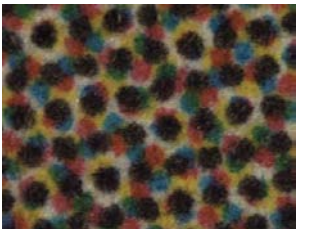

Fig. 1. An enlarged view of a small part of a colour picture

The quality of such halftone printed colour pictures depends to a great extent on the quality of printed dots, which in turn is dependent on the paper formation. The size of the printed dots is only a fraction of a millimeter. Thus, to assess the printability of the sheet of paper the very local paper properties ought to be monitored on-line. This requires a high measurement capacity. A large amount of data must be continuously acquired and processed. Obviously, the interpretation of the data measured becomes more complex and time-critical. On the other hand, it is also important to detect low frequency variations of paper formation. Thus, a paper formation on-line monitoring system used should cover a broad range of formation variation frequencies.

Creation and investigation of such a system is the main objective of this study. The system aims detecting abnormalities in various frequency regions ranging from millimeters to several meters. The abnormalities detected in different frequency regions give an indication to the paper maker about specific disturbances in the paper production process. To obtain an on-line fine characterization of the

paper structure at a paper mill, a paper web running at about 30 m/s speed is illuminated by a red diode laser, the reflected light is collected by a photo-detector and recorded as a time series of high resolution measurements. Two such sensors mounted at about 50 mm distance from each other are utilized. The two time series constitute the input signal to the papermaking process monitoring system.

2 The Approach

The time series obtained from each detector is first divided into consequent blocks of a predetermined length and the fast Fourier transform (FFT) is applied to each block. Let us assume that $F(u)$ is the Fourier transform of the time series $f(x)$ and $P(u)$ is the Fourier power spectrum:

$$P(u) = \|F(u)\|^2 = R^2(u) + I^2(u) \tag{1}$$

where $R(u)$ and $I(u)$ are the real and imaginary parts of $F(u)$, respectively.

To enable monitoring in various frequency regions, the frequency axis is divided into several frequency regions R_i of different average frequency. The following way of partitioning has been applied:

$$u \in R_i \quad \texttt{if} \quad iW \leq \log^2(u) < (i+1)W \tag{2}$$

where

$$W = \frac{\log^2[N/(2\sqrt{2})]}{N_r - 1} \tag{3}$$

with N_r being the number of regions of different average frequency and N is the number of data points in the signal. The partitioning can be viewed as band selection in the frequency domain. Other way of partitioning can be utilized.

The frequency content of the region a is characterized by a set of k features—a feature vector $\mathbf{x}^a \in \Re^k$. The features used will be presented shortly.

Having such representations for all the frequency regions, the task of screening paper formation variations in various frequency regions is treated as a novelty detection problem using the obtained representations. A separate novelty detector is trained for each frequency region. The novelty detector is trained so that $\mathbf{x}^a$ calculated using a time series block exhibiting too high formation variations in the frequency region a is classified by the detector as a novel data point. Time series obtained from the two sensors are analyzed by separate detectors and decisions obtained from the detectors are aggregated.

A kernel based novelty detector was adopted in this work. The optimal values of the parameter vector $\boldsymbol{\alpha}^*$ of the detector are found by maximizing the following objective function [11]

$$W(\boldsymbol{\alpha}) = \sum_{i=1}^{N} \alpha_i \kappa(\mathbf{x}_i^a, \mathbf{x}_i^a) - \sum_{i=1}^{N}\sum_{j=1}^{N} \alpha_i \alpha_j \kappa(\mathbf{x}_i^a, \mathbf{x}_j^a) \tag{4}$$

subject to $\sum_{i=1}^{N} \alpha_i = 1$ and $0 \leq \alpha_i \leq 1/\nu N$, $i = 1, ..., N$, with $\kappa(\mathbf{x}^a, \mathbf{x}^a)$ being a kernel and N is the number of data points used to train the detector. The optimal

parameter $0 < \nu < 1$ value is usually found by cross-validation. In this study, the parameter has been assigned the value equal to the expected fraction of outlying—novel—data points, known from the apriori process knowledge. Then, in the operating phase, the ratio of outlying data points, significantly exceeding the value of ν, indicates abnormalities in the paper formation.

The function $f(\mathbf{x}^a)$ used to categorize the data point $\mathbf{x}^a$ into the *novel* or *non-novel* class is given by:

$$f(\mathbf{x}^a) = \mathcal{H}\big[\kappa(\mathbf{x}^a, \mathbf{x}^a) - 2\sum_{i=1}^{N} \alpha_i^* \kappa(\mathbf{x}_i^a, \mathbf{x}^a) + T\big] \tag{5}$$

where the parameters α_i^* and T are found by maximizing Eq. 4 and the Heaviside function $\mathcal{H}[y(\mathbf{x}^a)] = 1$ if $y(\mathbf{x}^a) \geq 0$ and -1 otherwise. The data point $\mathbf{x}^a$ is assigned to the *novel* class if $\mathcal{H}[y(\mathbf{x}^a)] = 1$ while $\mathcal{H}[y(\mathbf{x}^a)] = -1$ means that the data point comes from the *non-novel* class. A comprehensive description of the detector can be found in [12].

2.1 Features

Four measures characterizing the region frequency content are extracted. The measures utilized are: the average region energy $\overline{E}_i$, the normalized maximum region energy E_{mi}, the Chi-square χ_i, and the entropy M_i of the Fourier power. The average region energy is given by

$$\overline{E}_i = \frac{1}{N_i} \sum_{u \in R_i} P(u) \tag{6}$$

where $P(u)$ is the Fourier power at frequency u and N_i is the number of distinct frequencies in the region R_i. The normalized maximum region energy E_{mi} is computed according to the following equation:

$$E_{mi} = \frac{1}{\overline{E}_i} \max_{u \in R_i} P(u) \tag{7}$$

The Chi-square value χ_i in the ith frequency region is computed as

$$\chi_i = N_i^2 \sum_{u \in R_i} \Big[\frac{P_i(u)}{\sum_{u \in R_i} P_i(u)} - \frac{1}{N_i}\Big]^2 \tag{8}$$

The Chi-square measures the difference between the power spectrum of the region R_i and the "white noise spectrum". The entropy measure M_i we use is given by

$$M_i = -\frac{1}{\log N_i} \sum_{u \in R_i} P_i^n(u) \log P_i^n(u) \tag{9}$$

The $\overline{E}_i$, E_{mi}, χ_i, and M_i values computed for the R_i region constitute the measurement vector $\mathbf{z}^i$.

2.2 Transforming the Features

In this study, we are interested in paper formation variations occurring in the web in "machine direction" (MD). The sensor used monitors a very narrow track of paper in MD. To increase the robustness of the analysis, two sensors monitoring two parallel tracks are used. Nonetheless our interest in paper formation variations occurring in the machine direction only, formation variations in the cross-web direction (CD) are always present. Thus, signals obtained from the two sensors depend on the measuring positions chosen in CD. To mitigate the influence of the measuring positions chosen and the disparity in parameters of the two sensors on the analysis results, the data vectors $\mathbf{z}^{1i}$ and $\mathbf{z}^{2i}$, where the indices 1 and 2 refer to the two sensors, are transformed into a new coordinate system. Components of the corresponding data vectors $\mathbf{x}^{1i}$ and $\mathbf{x}^{2i}$ in the new coordinate system are given by the linear or nonlinear combination of the components $z_1^1, ..., z_4^1$ and $z_1^2, ..., z_4^2$, respectively. The linear/nonlinear transformation applied is found by employing the canonical correlation analysis (CCA) or kernel canonical correlation analysis (KCCA), respectively.

The classical CCA describes linear relations between variables. If we have two data sets Z^1 and Z^2 containing the same number of data points N, the transformation implemented by the CCA is such that correlation between the new variables x_1^1 and x_1^2 given by the linear combination $x_1^1 = \mathbf{w}^{1T}\mathbf{z}^1$and $x_1^2 = \mathbf{w}^{2T}\mathbf{z}^2$, where T stands for the transpose, is maximized. The new directions $\mathbf{w}^1$ and $\mathbf{w}^2$ (canonical vectors) are found as a solution to the following eigenvector problems:

$$\mathbf{C}_{Z11}^{-1}\mathbf{C}_{Z12}\mathbf{C}_{Z22}^{-1}\mathbf{C}_{Z12}^{T}\mathbf{w}^1 - \lambda^2\mathbf{w}^1 = 0 \tag{10}$$

$$\mathbf{C}_{Z22}^{-1}\mathbf{C}_{Z12}^{T}\mathbf{C}_{Z11}^{-1}\mathbf{C}_{Z12}\mathbf{w}^2 - \lambda^2\mathbf{w}^2 = 0 \tag{11}$$

where $\mathbf{C}_{Z11}$, $\mathbf{C}_{Z12}$, and $\mathbf{C}_{Z22}$ are covariance matrices of the corresponding variables. If the rank of $\mathbf{C}_{Z12}$ is p, then p solution triples $(\lambda_j, \mathbf{w}_j^1, \mathbf{w}_j^2)$ can be obtained.

In the case of KCCA, the data are first projected into a high-dimensional feature space $\phi : \mathbf{z} = (z_1, ..., z_4) \rightarrow \phi(\mathbf{z})$ using the kernel trick $\kappa(\mathbf{z}, \mathbf{y}) = \langle\phi(\mathbf{z}), \phi(\mathbf{y})\rangle$, where $\langle\rangle$ stands for the inner product and CCA is then performed in the new feature space. In this work, we use the regularized KCCA. In the regularized KCCA case, the jth canonical vectors can be found as a solution to the following eigenvalue problems [13]:

$$(\mathbf{C}_1^T\mathbf{C}_1 + \gamma_1\mathbf{I})^{-1}\mathbf{C}_1^T\mathbf{C}_2(\mathbf{C}_2^T\mathbf{C}_2 + \gamma_2\mathbf{I})^{-1}\mathbf{C}_2^T\mathbf{C}_1\boldsymbol{\psi}_j = \lambda^2\boldsymbol{\psi}_j \tag{12}$$

$$(\mathbf{C}_2^T\mathbf{C}_2 + \gamma_2\mathbf{I})^{-1}\mathbf{C}_2^T\mathbf{C}_1(\mathbf{C}_1^T\mathbf{C}_1 + \gamma_1\mathbf{I})^{-1}\mathbf{C}_1^T\mathbf{C}_2\boldsymbol{\xi}_j = \lambda^2\boldsymbol{\xi}_j \tag{13}$$

where $\gamma_1, \gamma_2 > 0$ are the ridge parameters chosen experimentally, $\mathbf{I}$ is the identity matrix, and $\mathbf{C}_1 = \mathbf{K}(\mathbf{z}^1, \mathbf{z}^1)\mathbf{A}_1$, with $\mathbf{K}$ being the kernel matrix. The matrix $\mathbf{A}_1$ is found using the eigendecomposition $\mathbf{K}(\mathbf{z}^1, \mathbf{z}^1) = \mathbf{V}\boldsymbol{\Lambda}\mathbf{V}^T$ and is given by the first d columns of $\mathbf{V}\boldsymbol{\Lambda}^{-1/2}$. The matrix $\mathbf{C}_2$ is found likewise. The kernel canonical variates $\mathbf{x}_j^1$ and $\mathbf{x}_j^2$ are then given by $\mathbf{x}_j^1 = \mathbf{K}(\mathbf{z}^1, \mathbf{z}^1)\mathbf{A}_1\boldsymbol{\psi}_j$ and $\mathbf{x}_j^2 = \mathbf{K}(\mathbf{z}^2, \mathbf{z}^2)\mathbf{A}_2\boldsymbol{\xi}_j$.

3 Experimental Setup

The data acquisition system consists of a commercial PC with a National Instruments Data Acquisition Card (DAQ) and the LabVIEW 7 software. Two assembled optical surface reflection sensors are mounted between the calendering part and the winder, see Fig. 2.

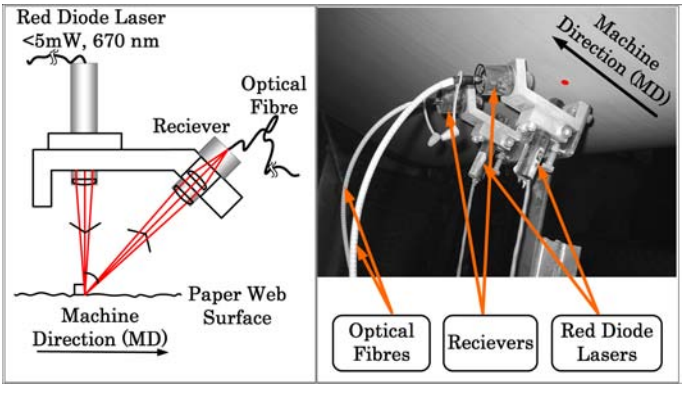

Fig. 2. Reflection sensor design (left) and arrangement (right)

The external encoder signal from the paper machine is used to keep the spatial distance $\delta = 0.1\ mm$ between adjacent samples, independent of the paper production speed.

The sensors, both identically constructed, consist of a red diode laser with a wavelength of 670 nm and an output power less than 5 mW. The light from the laser is directed, at a right angle, to the paper web surface and the reflected light is recorded at an angle of 60^o from the angle of incidence. The reflected light is guided by a pair of lenses into an optical fibre and the other end of the fibre connects the sensor to the DAQ, through a high speed photodiode amplifier.

4 The Data Set

The data set used in the experimental investigations has been acquired at a Swedish paper mill and corresponds to 9200 km of newsprint divided into $M = 9200$ blocks. In this study, we subdivided each block into $N_r = 14$ frequency regions. The data set available has been randomly divided into the training (50%), validation (25%), and the test (25%) sets. The abnormalities screened were located in the wavelength region of $0.2 - 0.4\ mm$ and $1.6 - 3.2\ m$.

5 Parameters

The Gaussian kernel $\kappa(\mathbf{x}_i, \mathbf{x}_j) = \exp\{-||\mathbf{x}_i - \mathbf{x}_j||/\sigma\}$, governed by the Gaussian width parameter σ, has been utilized in the kernel novelty detector. The width

parameter σ was selected from the interval given by 0.1 and 0.9 quintile of the $||\mathbf{x}_i - \mathbf{x}_j||$ statistic. To perform the KCCA, the polynomial kernel has been employed. The polynomial degree d of the kernel has been chosen experimentally and was found to be $d = 2$.

The data modelling approach adopted in this work aims at building a model that categorizes ν percent of the training data points as outliers. Then, in the operating phase, the fact of observing the percentage of outlying data points, significantly exceeding the value of ν, indicates abnormalities in paper formation. Both the apriori process knowledge and cross-validation tests have been used to find a suitable value of ν. The choice of the appropriate value of σ has been based on cross-validation aiming to obtain approximately the same percentage of outliers in both the learning and validation data sets. The polynomial degree and the ridge parameters γ_1 and γ_2 were found by cross-validation aiming to retain the determined ratio ν of outliers in the validation set and to maximize the correlation between the outputs of detectors processing signals of the two sensors. All the parameters have been determined separately for each frequency region.

6 Results

First, a test has been run to asses the correlation in different frequency regions between the feature values as well as the values of the detector outputs computed using signals from the two sensors. Three cases were explored, namely, without preprocessing (original), preprocessing by CCA, and preprocessing by KCCA. The usefulness of four different feature sets: $\{\overline{E}_i, E_{mi}\}$, $\{\overline{E}_i, E_{mi}, \chi_i\}$, $\{\overline{E}_i, E_{mi}, M_i\}$, and $\{\overline{E}_i, E_{mi}, \chi_i, M_i\}$ has been investigated. Table 1 presents the values of correlation between the detector outputs computed for the three feature types in the highest frequency region.

Table 1. Correlation between the detector outputs in the highest frequency region

Features	Feature set	N# features	Correlation
Original	$\overline{E}_i$, E_{mi}, χ_i, M_i	4	0.15
CCA	$\overline{E}_i$, E_{mi}, χ_i, M_i	2	0.30
KCCA	$\overline{E}_i$, E_{mi}, χ_i, M_i	2	0.70

In Table 1, the column "Feature set" presents the set of original features providing the highest correlation. The column "N# features" gives the number of original, CCA, or KCCA components providing the highest correlation presented in Table 1. The results of the test computed using data from the lowest frequency region are summarized in Table 2.

As it can be seen from Table 1 and Table 2, in both the low and the high frequency regions, the KCCA-based preprocessing of sensor signals results into

Table 2. Correlation between the detector outputs in the lowest frequency region

Features	Feature set	N# features	Correlation
Original	$\overline{E}_i$, E_{mi}, χ_i, M_i	4	0.10
CCA	$\overline{E}_i$, E_{mi}, χ_i, M_i	2	0.25
KCCA	$\overline{E}_i$, E_{mi}, χ_i, M_i	2	0.45

the most similar behaviour of detectors analyzing signals coming from the two sensors. Therefore, the KCCA-based preprocessing was utilized in further tests.

In the next experiment the behaviour of the detectors in paper formation variation monitoring has been studied. The outputs of detectors analyzing signals coming from the two sensors were aggregated into a committee output via averaging. The usefulness of two- and four-member committees has been explored. In a four-member committee, in addition to the two detectors, the short term moving average of the detector outputs is also utilized. Given the data point $\mathbf{x}_t^a$, the detector operating in the ath frequency region outputs the real valued signal $y(\mathbf{x}_t^a)$ and the binary decision $f(\mathbf{x}_t^a)$. The short term moving average τ_t^a is then given by

$$\tau_t^a = \frac{1}{P}\left[\tau_{t-1}^a(P-1) + y(\mathbf{x}_t^a)\right] \tag{14}$$

with P being the size of the averaging window.

In this test, the value of ν has been set $\nu = 0.05$; it is assumed that there are about 5% of outliers in the training data. Since data from the learning, validation and test sets come from the same distribution, it is expected that approximately the same percentage of outliers is also present in the validation and test sets. Table 3 presents the data categorization results obtained from the committees for the learning, validation, and test set data representing the highest (the upper part of the table) and the lowest (the lower part of the table) frequency region. In the table, Committee 2 and Committee 4 stand for a committee made of two and four members, respectively.

As it can be seen from Table 3, the committee made of four members provides the lower discrepancy between the data categorization results obtained for the three sets of data. Similar results were obtained for the data recorded from other frequency regions. It is obvious that assessing the data categorization

Table 3. The percentage of the highest and lowest frequency region data categorized as outliers

Detector	Learning set	Validation set	Test set
Committee 2	3.7	5.5	3.0
Committee 4	4.3	5.0	3.5
Committee 2	4.5	4.0	3.5
Committee 4	3.8	4.1	3.6

results is not an easy task, since the "ground truth" is not known. Therefore, an experiment was conducted using data, where it was apriori known that at some point process disturbances, resulting into more pronounced paper formation variations in some frequency regions, took place. The result of the test, given by the Committee 4 output, is shown in the main window of the software developed. The disturbances manifest themselves in the detector output values steadily exceeding the categorization threshold. The wavelength of the paper formation variations monitored in this experiment ranges from 0.2 to 0.4 mm.

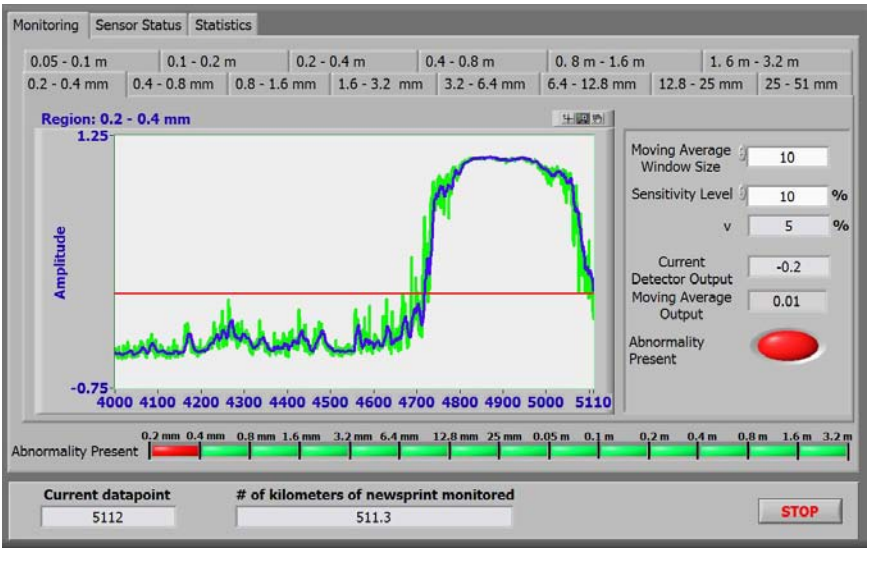

Fig. 3. Committee 4 output in the highest frequency region

Fig. 3 illustrates the user interface of the software developed. The value of ν, the sensitivity level, and the frequency regions to be visualized are the parameters that can be chosen by a user. The sensitivity level defines the degree to which the moving average of the percentage of outliers found is to exceed the ν value for the warning message to be generated.

7 Conclusions

A method and a tool for detecting and monitoring paper formation variations online in various frequency regions has been developed. To increase the robustness of the analysis, two optical sensors recording the reflected light from a paper web have been used to generate the input data. To characterize the region frequency content, four Fourier power spectrum based features are extracted in each frequency region. Having the representation, the task is treated as a kernel based novelty detection. Two detectors (one for each sensor), the outputs of which

are aggregated into a committee output, are used in each frequency region. The experimental investigations performed have shown that all the four features are useful for obtaining a concise and informative representation of the frequency content. It has been found that the use of a new feature space obtained based on the canonical correlation analysis significantly improves the agreement between the analysis results obtained from two detectors operating in each frequency region. A software implementing the method was developed and used for online paper formation monitoring at a Swedish paper mill.

References

1. Kaestner, A., Nilsson, C.M.: Estimating the relative shrinkage profile of newsprint. Optical Engineering 42(5), 1467–1475 (2003)
2. Verikas, A., Malmqvist, K., Bergman, L., Engstrand, P.: Colour speck counter for assessing the dirt level in secondary fibre pulps. Journal of Pulp and Paper Science 29(7), 220–224 (2003)
3. Bacauskiene, M., Verikas, A.: The evidence theory based post-processing of colour images. Informatica 15(3), 315–328 (2004)
4. Norman, B., Wahren, D.: The measurement of mass distribution in paper sheet using a beta radiographic method. Svensk Papperstidning 77(11), 397–406 (1974)
5. Trepanier, R.J., Jordan, B.D., Nguyen, N.G.: Specific perimeter: a statistic for assessing formation and print quality by image analysis. TAPPI Journal 81, 191–196 (1998)
6. Bouydain, M., Colom, J.F., Navarro, R., Pladellorens, J.: Determination of paper formation by Fourier analysis of light transmission images. Appita Journal 54(2), 103–105 (2001)
7. Turtinen, M., Pietikainen, M., Silven, O., Maenpaa, T., Niskanen, M.: Paper characterisation by texture using visualisation-based training. International Journal of Advanced Manufacturing Technology 22(11-12), 890–898 (2003)
8. Keller, D.S., Lewalle, J., Luner, P.: Wavelet Analysis of Simulated Paper Formation. Paperi ja Puu 81(7), 499–505 (1999)
9. Nesic, Z., Davies, M., Dumont, G.: Paper Machine Data Analysis and Compression using Wavelets. Tappi Journal 80(10), 191–204 (1997)
10. Timberlake, A., Strom, E.: Do You Know What Causes the Variability in the Paper You Produce? In: 2004 Paper Summit, Spring Technical & International Environmental Conference, TAPPI Proceedings (2004)
11. Shawe-Taylor, J., Cristianini, N.: Kernel Methods for Pattern Analysis. Cambridge University Press, Cambridge (2004)
12. Ejnarsson, M., Nilsson, C.M., Verikas, A.: A kernel based multi-resolution time series analysis for screening deficiencies in paper production. In: Wang, J., Yi, Z., Zurada, J.M., Lu, B.-L., Yin, H. (eds.) ISNN 2006. LNCS, vol. 3973, pp. 1111–1116. Springer, Heidelberg (2006)
13. Kuss, M., Graepel, T.: The geometry of kernel canonical correlation analysis. Technical Report 108, Max Planck Institute for Biological Cybernetics (2003)

Multi-modal Data Integration Using Graph for Collaborative Assembly Design Information Sharing and Reuse*

Hyung-Jae Lee[1], Kyoung-Yun Kim[2], Hyung-Jeong Yang[1,**], Soo-Hyung Kim[1], and Sook-Young Choi[3]

[1] Dept. of Computer Science, Chonnam University, 300 Young-Bong, Gwangju, Korea
hjgumsin@hanmail.net,{hjyang,shkim}@chonnam.ac.kr
[2] Dept. of Industry and Manufacturing Engineering, Wayne State University, Detroit, MI 48202, USA
kykim@eng.wayne.edu
[3] Dept. of Computer Education, Woosuk University, Samruy, Chonbuk, Korea
sychoi@mail.woosuk.ac.kr

Abstract. Collaborative design has been recognized an alternative environment for product design in which multidisciplinary participants are naturally involving. Reuse of product design information has long been recognized as one of core requirements for efficient collaborative product design. This paper addresses integration of multi-modal data using a graph for an assembly design information sharing and reuse in the collaborative environment. In the system, assembly product images obtained from multi-modal devices are utilized to share and to reuse design information. The proposed system conducts the segmentation of an assembly product image by using a labeling method and generates an attribute relation graph (ARG) that represents properties of segmented regions and their relationships. The generated ARG is extended by integrating corresponding part/assembly information. In this manner, the integration of multi-modal data has been realized to retrieve assembly design information using a product image.

Keywords: ARG, Design Information, CAD/CAM, Image segmentation, Image Retrieval.

1 Introduction

Recently, many manufacturing companies have paid attention to collaborative environment to reduce total product development time and to increase efficiency of the product development process [1]. In a collaborative environment, multidisciplinary (e.g., design, marketing, and distribution) stakeholders participate locally and remotely in overall product development processes; therefore, to realize smooth

* This research is partially supported by the Korea Research Foundation Grant funded by the Korean Government (MOEHRD, Basic Research Promotion Fund) (KRF-2006-003-D00511) and by KOCCA as the result of the research project for 2007 C.N.U culture technology development.
** Corresponding author.

H.G. Okuno and M. Ali (Eds.): IEA/AIE 2007, LNAI 4570, pp. 521–530, 2007.

communication in the collaborative environment, an efficient communication protocol should be established. Since a product image is an intuitive data type, it can be used by various stakeholders as a front-end medium.

More than 75% of product design activities have been conducted repeatedly due to the lack of product design information/knowledge reuse. Therefore, it has been long recognized as a critical problem in product design [2]. Previous research on design information reuse has been focused on search by matching keyword and file name or search by specific indexes (e.g., part number, relationship among parts, etc.). However, these methods indicate various drawbacks [3]. First, product model information is often incomplete or is not defined detailed enough. Second, it is often not true knowing proper keywords (e.g., project name or part name) before an actual search. Third, search by product relationships may generate too detailed search results or too broad results. Additionally, the previous works use 3D models that are generated by specific CAD systems and it is often difficult for general users who do not know how to use the specific CAD systems.

This paper presents an integration of multi-modal data to allow assembly design sharing and reuse while utilizing intuitive and user-friendly 2D image (that is independent to specific CAD tools) and assembly information. For the multi-modal integration between visual properties of images and assembly information, we propose to use a graph as a uniform framework. An image is segmented by a labeling method, and the segmented regions are matched with corresponding part information. The visual properties of region and associated design information are represented in an Attributed Relational Graph (ARG). When a designer wants to reuse certain assembly design, an image of the design (ad-hoc image) is provided to the system as a query, the system conducts a similarity test between the ad-hoc image and images in database. Once a similar image is determined by the similarity test, the design information that is represented in the ARG of the similar image is utilized for assembly design information reuse.

The main advantages of this reuse system are following: 1) the system is not dependent to specific CAD systems, because it utilizes multimedia images that can be obtained easily from peripheral devices; 2) the system has shown outstanding search performance, because ARG represents various information of segmented regions and their relationships; 3) Since multi-modal data is represented by using graph, seamless integration is performed for the efficient design information sharing.

2 Related Work

Related to product design information sharing, [4][5][6] conduct search by using harmonics-based functions consisted by 3D shapes and signals. They decompose 3D model using spherical function or Fourier function that represents 3D signals. The harmonics-based approaches are efficient computationally; however, these methods cannot differentiate different shapes and show low searching performance. [7][8][9] use 3D object recognition techniques for design reuse and aspect graphs[7], spin images[8], and geometric hashing[9] are applied respectively. These methods require significantly large data storage and high computational cost.

Existing research related to image segmentation can be classified into area-based, histogram-based, and boundary-based segmentation. As an area-based segmentation

method, Blobworld[10] applies smoothing technique to an image and maximizes the difference of pixel values by translating the image to L*a*b color system for image segmentation. This method shows limitations when the difference of pixel values is very small. Normalized-cut[11] uses eigenvalues and eigenvectors, and segment pixel repetitively into two groups. The segmentation results are typically generating very small areas and this method is not adequate for product image segmentation that this paper is targeting.

[12] presented method that uses a histogram obtained from an input image and conduct color quantization for the image by using two gray values that have the highest frequency. [13] translates an image into HSV color system and applies smoothing process for image similarity tests. Histogram-based method is often difficult to determine thresholds when the distribution of a histogram is complex. Some researchers presented boundary-based segmentation methods [14, 15]. The method of Jiamp et al. [14] is based on preprocessing that separate the color of an image into each channel (e.g., Y. U. V) and it often take long time.

3 Integration Ad-Hoc Images and Assembly Design Information

In this paper, for the assembly information reuse by multi-modal data integration, there are three parts; image segmentation, multi-modal data integration and image retrieval. After an image is segmented by edge-based labeling method, it is represented by Attributed-Relational Graph which represents visual properties of image regions as nodes and relations such as angles and distance as links. ARG is further extended by adding product design information. A query image is also represented a query ARG to be computed similarities against ARG in a database. To reuse design information a user browses the product design information from the retrieved images.

3.1 Part Segmentation

Conventional image segmentation approaches group pixels if they are similar in terms of colors, motions, and brightness. In this paper, we perform image segmentation to distinguish parts in an assembly. We applied edge-based labeling which does not require preprocessing as much as the conventional approaches do. Edge-based labeling recognizes parts after extracting edges from an image [16]. Over segmented regions are integrated to be reformed as a part which should be matched to user's intuition. As shown in Figure 1, AND operation is applied on a given image and an edge image from step 1 to enhance the edges. In the second step, edge-based labeling is applied to segment parts.

Edges are pixels whose values are much different from adjacent pixels. In this paper, we employ Sobel mask[17] which is known robust for noses. We modify Sobel mask to reduce time complexity producing binary images while edges are extracted. In other words, after derivations are applied on each pixel, it is distinguished into two groups by a threshold value α which is set as a significant point in the distribution of derivation values. Edges are enhanced by AND operation between a given image and

the edge-extracted image. Edge enhanced images must be binarized to distinguish a product and background in an image to be applied by labeling. We applied one cluster method which divides pixels into two clusters according to one average value. Since the image we are targeting show large differences between a region of an assembly and background, one cluster method shows simple and less time complexity than k-means[18].

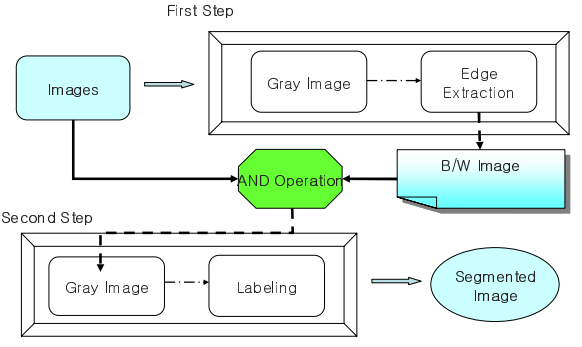

Fig. 1. Part Segmentation

Labeling methods recognize regions by tagging same numbers on pixels within an edge. Therefore, pixels in one part have same numbers and each part has a different number. In this paper, we exclude parts whose size is smaller than 1% of an image considering they are not meaningful parts which designers want to reuse. Labeled parts are integrated to be a significant part in terms of slope of a line from a left hand side point to a right hand side point as shown in formula (1). The slope means the ratio of a part. Therefore, two parts in similar slopes tend to be one part which maybe over segmented. We ignore a part if Δx =0 since it is not a useful part.

$$Slope(o_i) = \frac{\Delta y}{\Delta x} = \frac{y_{right} - y_{left}}{x_{right} - x_{left}} \tag{1}$$

When the slopes of two segmented regions o_i, o_j hold one condition as follows, they are merged as one part.

Condition 1: $-1<Slope(o_i)$ *and* $Slope\ (o_j)<0$
Condition 2: $0<Slope\ (o_i)$ *and* $Slope\ (o_j)<1$
Condition 3: $1< Slope\ (o_i)$ *and* $Slope\ (o_j)$
Condition 4: $Slope\ (o_i)$ *and* $Slope\ (o_j)<-1$.

Figure 2 shows integration of over segmented parts. In Figure 2(b) since the slopes of parts *a* and *b* satisfy condition 2, parts *a* and *b* are integrated. Parts *c* and *d* also integrated holding condition 4.

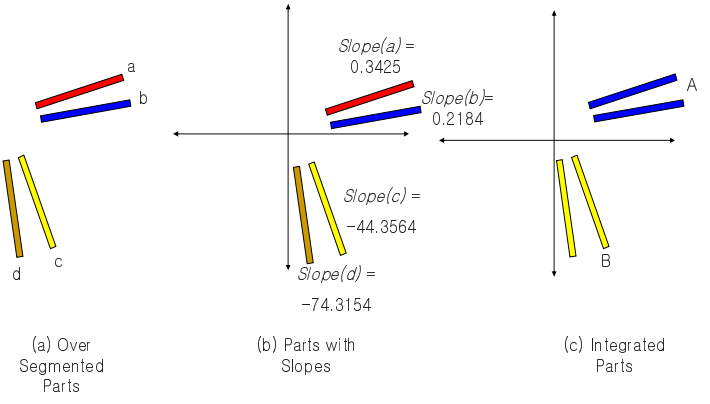

Fig. 2. Parts Integration

3.2 Attributed Relational Graph (ARG)

In this section, we introduce Attributed Relational Graph (ARG) to integrate visual features of image regions and design information simultaneous. ARG is first constructed with segmented images and it is extended with design information to be reused. Therefore, multi-modal data such as visual properties of image data and design data are expressed in a uniform framework.

Segmented parts as shown in the section 3.1 are considered as nodes in ARG. Image features such as ratio, area, and average of RGB extracted from each part are added to nodes as attributes. Between nodes are linked with relations such as |distances and angles between parts. Figure 3 (b) shows ARG of the segmented image in (a)

To generate ARG, segmented regions in an image and corresponding product design information are mapped according to the positions. However, since the coordinates of images and product design information are different, we extract relative positions and match them as follows;

(1) Center gravities are extracted from each region in the segmented image.
(2) Regions are arranged according to x coordinates in ascending order.
(3) If x coordinates of two regions are in the same position, y coordinates are compared to be arranged.
(4) Center gravities in world coordinate are extracted from each part in design information for a corresponding product to the segmented image.
(5) Design information of parts are arranged according to horizontal coordinate.
(6) If horizontal coordinates of two parts are in the same position, vertical coordinates are compared to be arranged.
(7) Arranged regions in an image and arranged design information are mapped.

For example, if *x, y* coordinates of regions in an image and *h, v* coordinates of part design information in world coordinate are given as in Figure 4, a region whose *x=211* and a part whose *h= -571.50* are mapped in terms of the relative position. Therefore, ARG is extended

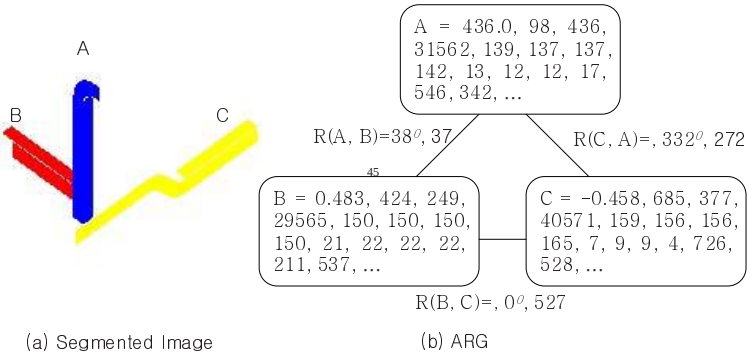

Fig. 3. An Example of ARG

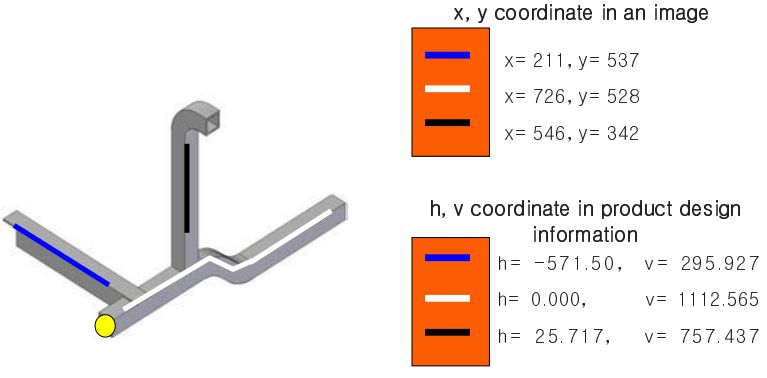

Fig. 4. Coordinates of a Product

with design information so that image data and design information are integrated in ARG to be reused by designers in collaborative environment.

Design information of a part is browsed once a designer selects a region from an image as shown in Figure 5 since multi-modal data such as image features and design information are integrated in a graph.

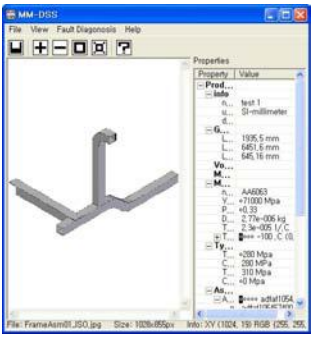

Fig. 5. Product Design Information

3.3 Image Retrieval

When a designer provides an image acquired from peripheral devices, a query ARG is generated from this ad-hoc image. Images in database are retrieved by computing the similarities between the query ARG and ARGs of images in database. The similarities are computed according to the image features such as node attributes and relations for each node. After similarities for each product unit are computed, the most similar products are retrieved. In this paper, we use Euclidian distance to compute similarities/dissimilarities. In Figure 6, retrieved images for a given query image are showed.

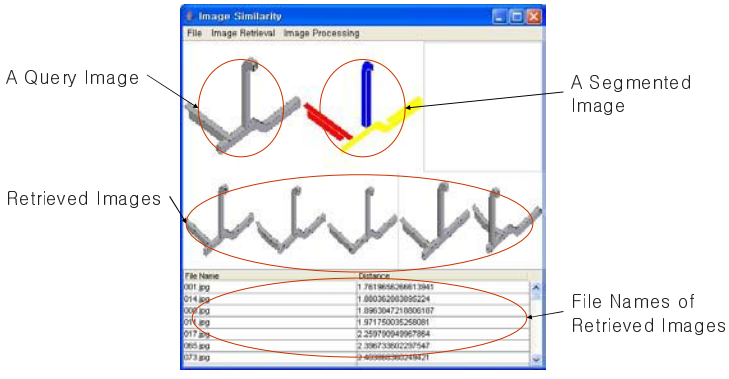

Fig. 6. Retrieved Images for a Given Query Image

4 Experiments

In this work, three experiments are conducted. The first experiment is to compare the performance of three search algorithms (i.e., ARG, gray histogram, and ARG with background removal). For image retrieval, precision (p), recall (r), and F1 measure are computed. In the first experiment, we are able to identify the difference of the three algorithms' performance for colored query images and gray query images, as shown in Table 1. The tests are conducted with 4 color query images and 10 gray images, and 474 images that include resized images. This resizing operation is included to increase the complexity of the test. As shown in Table 1, when color images are queried, ARG with background removal shows higher F1 value, while histogram method shows higher F1 for gray query images. However, the more number of tests is required to state this trend statistically. In future research, additional tests will be conducted to study this issue.

We also conducted the second experiment to understand the difference when images generated by CAD tools are used as a query image and when real images for querying are obtained from a digital camera. The 27 images generated by CAD tools are used as query images and 503 images in a database are searched. The average F1 measure is 23.65%. When 24 real images are queried individually for the 503 images,

Table 1. Precision and Recall for Colored Image Search and Gray Image Search

Search algorithm	Query image	Images in database	p	r	F1
ARG	4 color image (more than 2 colors)	474 images (including resized images)	21.74%	29.20%	24.92%
Gray histogram			16.30%	22.95%	19.07%
ARG with background removal			25.00%	37.61%	**30.04%**
ARG	10 gray image	474 images (including resized images)	34.39%	45.58%	39.20%
Gray histogram			38.74%	60.77%	**47.31%**
ARG with background removal			33.60%	41.04%	36.95%

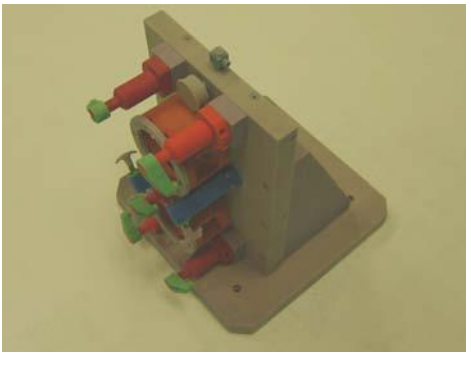

Fig. 7. Real Image Example

the average F1 measure is 10.58%. It turns out that the current system should be enhanced further to be used to incorporate real images. Figure 7 illustrates an example of the real images that used for the experiment.

The third experiment is for segmentation considering reasonable parts. In this paper, we count the number of parts after integration of over segmented regions. We compare the segmented regions by the proposed system and the number of parts which are recognized by 5 users. If three of five users agree with the number of parts in an image, this is considered the ground truth part numbers of the assembly. The proposed system segments 252 parts correctly from 111 images while the number of ground truth parts is 281. It shows 89.68% of accuracy on part segmentation.

5 Conclusion and Future Work

We proposed to use ARG for the integration of multi-modal data such as image features and design information to support image-based design information reuse system in collaborative design environment. While previous design information reuse systems target 3D model in specific CAD systems, the proposed method uses 2D ad-hoc images acquired from peripheral devices so that the proposed method is independent from specific CAD tools.

In this paper, image retrieval is performed taking various features for each region into account so that the retrieval performance is improved while conventional image retrieval approaches consider features from a whole image. Since the image retrieval in the proposed method is performed using features of each resign and relationships on ARG, F1 is 10.97% higher than histogram method for color query images. However, histogram method showed a higher F1 value when gray images are queried.

The proposed method will be further investigated to improve performance for multiple conditions, especially for real image query. Also, we are interested in improving the performance of segmentation using fuzzy logic. In other words, when over-segmented regions are integrated to be a part corresponding to the users' intuition, fuzzy logic will help to reduce the semantic gap between regions the proposed system identifies and actual parts. In addition to this, an adaptive multimedia decision support system in collaborative product development environment integrating multimedia data and decision making model will be our next step.

References

1. Florida-James, B., Rossiter, N., Chao, K.M.: An Agent System for Collaborative Version Control in Engineering. Integrated Manufacturing Systems 11, 258–266 (2000)
2. Ullman, D.G.: The mechanical design process, 2nd edn. McGraw-Hill, New York (1997)
3. Iyer, N., Jayanti, S., Lou, K., Kalyanaraman, Y., Ramani, K.: Shape-based searching for product lifecycle applications. Computer-Aided Design 37, 1435–1446 (2005)
4. Cyr, C.M., Kimia, B.: 3D Object Recognition using Shape Similarity-Based Aspect Graph. In: Proceedings of ICCV, pp. 254–261 (2001)
5. Ruiz-Correa, S., Shapiro, L., Meila M.: A New Signature Based Method for Efficient 3D Object Recognition. In: Proceedings of CVPR (2000)
6. Landom, Y., Wolfson, H.J.: Geometric hashing: A General and Efficient Model-Based Recognition Scheme. In: Proceedings of ICCV (1998)
7. Bajcsy, R., Lee, S.W.: Color Image Segmentation with Detection of Highlights and Local Illumination Induced by Inter-Reflection. In: Proceedings of International Conference on Pattern Recognition, pp. 785–790 (1990)
8. Wang, D., Hakghton, P., Wang, L., Vincent, A.: Motion Estimation using Segmentation and Consistency Constrint. In: Proceedings of SPIE Conf. Visual Common Image Processing, vol. 3024, pp. 667–708 (1997)
9. Fan, J., Yau, D.K.Y.: Automatic Image Segmentation by Integrating Color-Edge Extraction and Seeded Region Growing. IEEE Transactions on Image Processing 10, 1454–1466 (2001)
10. Zhou, X., Thomas, S.S.: Edge-Based Structural Features for Content-Based Image Retrieval. Pattern Recognition Letters 22, 457–468 (2001)
11. Bock, J.D., Bock, P.D., Philips, W.: Watershed and Normalized Cuts as Basic Tools for Perceptual Grouping. In: ProRISC, pp. 238–245 (2004)
12. Wang, D.: hakghton, P., Wang, l., vincent, A.: Motion Etimation using Segmentation and Consistency Constrint. In: Proceedings of SPIE Conf. Visual Common Image processing, vol. 3024, pp. 667–708 (1997)
13. Shamik, S., Gang, Q., Sakti, P.: A Histogram with Perceptually Smooth Color Transition for Image Retrieval. CVPRIP (2002)

14. Fan, J., Yau, D.K.Y.: Automatic Image Segmentation by Integrating Color-Edge Extraction and Seeded Region Growing. IEEE Transactions on Image Processing 10, 1454–1466 (2001)
15. Zhou, X., Thomas, S.S.: Edge-Based Structural Features for Content-Based Image Retrieval. Pattern Recognition Letters 22, 457–468 (2001)
16. Lee, H.J., Kim, Y.I., Yang, H.J.: Image Segmentation by Edge-based Labeling for Integrating Product Design Information and Image Data. In: Proceedings of the 24th Kips Fall Conference (2005)
17. Maar, D., Hildreth, E.: Theory of Edge Detection. In: Proceedings Royal Society, vol. 207, pp. 187–217. London (1980)
18. Dhillon, I., Guan, Y., Kulis, B.: Kernel K-means, Spectral Clustering and Normalized Cuts. In: KDD, pp. 551–556 (2004)

Enhanced Probabilistic Filtering for Improving the Efficiency of Local Searches*

Byoungho Kang and Kwang Ryel Ryu

Department of Computer Engineering, Pusan National University,
Jangjeon-Dong San 30, Kumjeong-Ku 609-735, Busan, Korea
{bhokang, krryu}@pusan.ac.kr

Abstract. The probabilistic filtering method filters out an unpromising candidate solution by conducting a simple preliminary evaluation before a complete evaluation in order to improve the efficiency of a local search. In this paper, we improve probabilistic filtering so that it can be applied in general to large-scaled optimization problems. As compared to the previous probabilistic filtering method, our enhanced version includes a scaling and truncation function to increase the discriminating power of probabilistic filtering and repair some defects of the previous bias function in adjusting the level of greediness. Experiments have shown that our method is more effective in improving the performance of a local search than the previous method. It has also been shown that the probabilistic filtering can be effective even when the preliminary evaluation heuristic is somewhat inaccurate, and the lesser the cost of preliminary evaluation, the greater is its effectiveness.

1 Introduction

Probabilistic filtering is a method for improving the efficiency of a local search by saving the time expended for completely evaluating candidate solutions that will eventually be discarded. The time thus saved can be used to investigate other candidate solutions that appear more promising. The probabilistic filtering technique was originally proposed by Kang and Ryu [1] to efficiently solve a load balancing problem in production scheduling. In this paper, we improve this technique so that it can be applied in general to large-scaled optimization problems.

A local search starts from a certain candidate solution and continues iteratively from point to point in the search space until a satisfactory solution is found. Therefore, the search cost of these algorithms is proportional to the total number of candidates evaluated throughout the iterations. However, resources are wasted if the evaluated candidates are eventually discarded, and the severity

* This paper is a part of the result of the project "Development of Intelligent Port and Logistics System for Super-Large Container Ships", which was sponsored by Ministry of Maritime Affairs and Fishery in Korea. This study was financially supported by Pusan National University in the program, Post-Doc. 2006.

H.G. Okuno and M. Ali (Eds.): IEA/AIE 2007, LNAI 4570, pp. 531–540, 2007.

of the resource waste increases as the evaluation becomes more expensive. Probabilistic filtering filters out a seemingly bad candidate based on a simple preliminary evaluation heuristic, thus saving time for the evaluation with a complete objective function. A cheap pre-evaluation heuristic is usually obtained by relaxing the objective function by using domain knowledge. Since the pre-evaluation heuristic thus obtained yields only rough estimates of the quality of a candidate, the selection or filtering out of a candidate is decided probabilistically.

In Kang and Ryu [1], the pre-evaluation heuristic yields values in [0, 1], which are directly used as the probability for filtering. However, when the distribution of the pre-evaluation heuristic values is skewed, the ability to discriminate candidates is impaired significantly. Therefore, in this paper, we introduce a scaling function to flatten the distribution based on the standard deviation of the pre-evaluation values. It has also been found out that it is often advantageous to deliberately bias this distribution so that the filtering strength and consequently, the level of greediness of search can be adjusted. Although this notion was already implemented by Kang and Ryu [1], their bias function had a drawback that too much discriminating power is lost when the bias is directed toward weaker filtering. In this paper, we propose a new bias function that eliminates this problem.

It should be noted that an important precondition for the probabilistic filtering to be useful is that the cost of the pre-evaluation should be negligible as compared to that of evaluating the original objective function. At the same time, the pre-evaluation heuristic must be as accurate as possible. Therefore, in this paper, we have conducted an empirical study using an artificially generated problem to observe the extent to which the cost and accuracy of the pre-evaluation heuristic affects the effectiveness of the probabilistic filtering. It is observed that the cost must be literally negligible. However, a somewhat inaccurate pre-evaluation still helps in improving search efficiency.

In previous studies, probabilistic decision had been mostly used as a means of diversifying searches in order to improve search performance. Stochastic hill climbing and simulated annealing employ probabilistic decision making for determining a neighborhood to which they will move. However, in both the algorithms, probability is derived from the evaluation value obtained by using the original objective function of the given problem. As shown in the experiments in this paper and [1], probabilistic filtering can be applied effectively to local search algorithms as a preprocessing in order to select (or discard) a neighbor before the candidate solution is completely evaluated. Selman and Kautz [2] proposed a mixed random walk strategy to improve the method known as GSAT [3]. This strategy basically performs a greedy local search, but moves randomly with a fixed probability p at each iteration. However, the concept of generating and filtering neighbor solutions does not exist. Heuristic-biased stochastic sampling (HBSS) [4][5] improved the iterative sampling method [6] by heuristically evaluating all the child nodes and applied a bias function in order to assign probabilities based on the child node being sampled. More recently, Binato et al. [7] proposed a notion of a probabilistic job selection, which is similar to HBSS,

in order to solve job-shop scheduling problems within the framework of GRASP [8]. Although our method is structurally similar to HBSS, the two methods have different objectives. Our method is focused on filtering unacceptable candidates that will eventually be discarded before they are completely evaluated to improve efficiency of a local search. In contrast, HBSS focuses on sampling a single child node among all the candidates in the constructive search tree, resulting in an increase in the time needed for the search.

We have tested a simulated annealing search equipped with probabilistic filtering by applying it to a large-scaled real world problem of load balancing in production scheduling. Experimental results have shown that the simulated annealing search with probabilistic filtering outperforms conventional simulated annealing searches in solution quality, given the same amount of CPU time. We have also confirmed that the bias function, if adjusted appropriately, plays an important role in improving the search efficiency by providing a good balance between exploration and exploitation. Further, additional experiments involving an artificial optimization problem have shown that although the pre-evaluation heuristic is inaccurate, probabilistic filtering can still be effective for improving the efficiency of a local search. Furthermore, the higher the relative cost of evaluation of the original objective function, the greater is the effectiveness of the probabilistic filtering.

The following section describes the probabilistic filtering algorithm generalized in this paper. Sections 3 and 4 present a scaling and truncation function and a newly formulated bias function in complete detail. Section 5 describes the application of the proposed method to target problems and reports the experimental results. Section 6 presents the conclusion.

2 Probabilistic Filtering Algorithm

Figure 1 shows the algorithm of selecting neighbors based on probabilistic filtering. The algorithm repeats until a predetermined number (n) of neighbors are collected. First, a candidate solution c is randomly generated and its goodness is pre-evaluated by using a simple preliminary evaluation function. Then, the pre-evaluation value h is mapped to a value p in the interval [0, 1] by using a scaling and truncation function, which is explained in detail in the next section. Although p might be directly used as the filtering probability, the distribution of its values is adjusted by applying a bias function to control the search toward either a more random or greedier direction. Again, a detailed explanation of the bias function is given in section 4. Finally, based on this p, it is determined whether the candidate solution should become a neighbor or be filtered out.

3 Scaling and Truncation

In Kang and Ryu [1], the pre-evaluation heuristic is devised to give values in [0, 1], and these values are directly used as the probability for filtering. However, the distribution of the pre-evaluation values is often skewed and it becomes difficult

in those cases to discriminate bad candidates from good ones. For example, when there are a very small number of exceptionally bad candidates, the pre-evaluation values of most other candidates will be mapped close to 1 and they will all look similarly good. Therefore, we map the pre-evaluation value h of a candidate to a value $p(h)$ in [0, 1] in such a way that $p(h)$ is distributed between 0 and 1 as uniformly as possible. For this purpose, we propose the following scaling function that can rescale and truncate the pre-evaluation values based on their average μ and standard deviation σ.

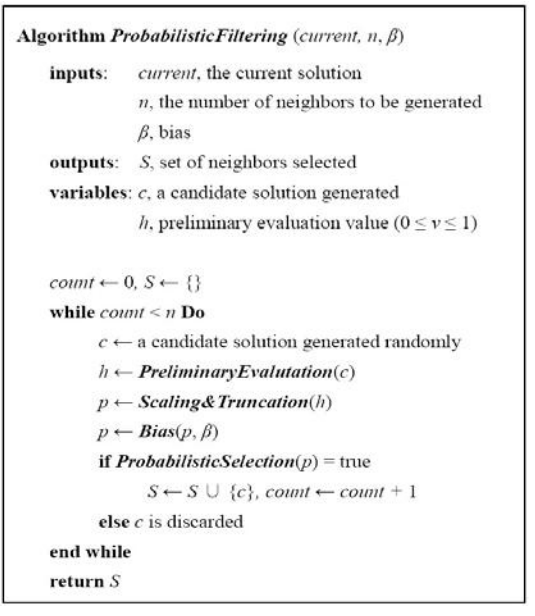

Algorithm ***ProbabilisticFiltering*** (*current*, n, β)

inputs: *current*, the current solution
n, the number of neighbors to be generated
β, bias

outputs: S, set of neighbors selected

variables: c, a candidate solution generated
h, preliminary evaluation value ($0 \leq v \leq 1$)

count ← 0, S ← {}
while *count* < n **Do**
  c ← a candidate solution generated randomly
  h ← ***PreliminaryEvalutation***(c)
  p ← ***Scaling&Truncation***(h)
  p ← ***Bias***(p, β)
  if ***ProbabilisticSelection***(p) = true
    $S \leftarrow S \cup \{c\}$, *count* ← *count* + 1
  else c is discarded
end while
return S

Fig. 1. Probabilistic filtering algorithm

$$p(h) = \begin{cases} 1 & (h \geq \mu + k\sigma) \\ \frac{h-(\mu-k\sigma)}{2k\sigma} & (\mu - k\sigma < h < \mu + k\sigma) \\ 0 & (h \leq \mu + k\sigma) \end{cases} \tag{1}$$

By using this function, the pre-evaluation values within $k\sigma$ from the average μ are mapped linearly to the values between 0 and 1, and the values above $\mu + k\sigma$ and below $\mu - k\sigma$ are all truncated and mapped to 1 and 0, respectively. As a last step to avoid an unconditional rejection (zero probability), we apply the Laplace estimator technique using a very small constant ε, and thus, the probability finally becomes as follows:

$$p(h) \leftarrow \frac{p(h) + \varepsilon}{1 + \varepsilon} \tag{2}$$

Notice that the goodness of a candidate solution generated at a certain point during the entire course of search cannot be absolute but relative. For example, near a local optimum, the quality of the candidate neighbors generated should be mostly good. Still, we would like to filter out the candidates that are relatively bad. Therefore, the average μ and the standard deviation σ are estimated at every iteration (i.e., whenever a new neighbor is accepted as the next current solution) by collecting an appropriately sized sample set of candidate neighbors. Although this estimation by sampling at each iteration is a nontrivial overhead, it has been confirmed empirically this procedure brings about better results. The number k, however, is not changed dynamically at every iteration. Its appropriate value can be empirically chosen by using a set of random candidate solutions sampled before the search starts.

4 A Generalized Bias Function

Recall that the distribution of the probability values obtained from the above scaling process is almost uniform between 0 and 1. If this probability is directly applied to the filtering of candidate solutions, about half of the candidates will be discarded on an average. It may be desirable to make the filtering stronger if the pre-evaluation heuristic is believed to be fairly accurate. This seems to make sense because the more we discard bad-looking candidates, the more we save time needed to completely evaluate them with the original objective function. However, a filtering that is too strong can cause the search to become too greedy, thereby resulting in a premature convergence to a suboptimal solution. On the contrary, when the pre-evaluation heuristic is not so accurate, the filtering should be done more conservatively, i.e., less greedily. As the filtering becomes weaker, the effect of saving time needed for complete evaluation diminishes. A filtering that is too weak merely slows down the search because the filtering process itself now acts only as an overhead without being able to provide any benefit.

Kang and Ryu [1] proposed the notion of adjusting the strength of filtering by using a bias function of the kind shown in Figure 2(a). As can be seen from the figure, their bias function has the defect of losing too much discriminating power when the bias is toward a weaker filtering. The bias function that we propose, which eliminates this problem, is given as follows:

$$F(p,\beta) = \begin{cases} (1-(1-p)^{\beta})^{1/\beta} & (\beta > 1) \\ p & (\beta = 1) \\ (1-(1-p)^{-\beta})^{-1/\beta} & (\beta < -1) \end{cases} \tag{3}$$

where $\beta(|\beta| = 1)$ is a control parameter called bias, which is used for adjusting the strength of the filtering, as shown in Figure 2(b). When $\beta = 1$, there is no bias. As β becomes smaller than -1, the number of filtered candidate solutions increases. However, as β becomes bigger than 1, the number of filtered candidate solutions decreases. Unlike the previous bias function, however, the candidate solutions with very low pre-evaluation values are still unlikely to survive. A good value of β is usually chosen empirically because we do not know *a priori* how accurate our pre-evaluation heuristic is.

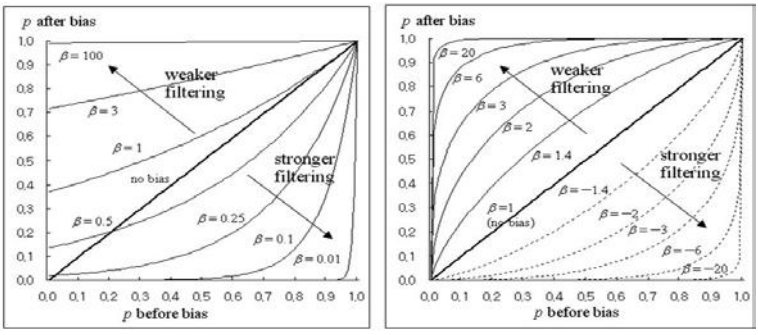

(a) The previous bias function ($e^{-(1-p)/\beta}$) (b) The proposed bias function

Fig. 2. The previous and new bias functions with various bias values

5 Experimental Results

We have conducted experiments with a real world problem of load balancing in production scheduling, which has objective function that is very expensive to evaluate. We have also conducted experiments with an artificial optimization problem to observe how the accuracy and cost of preliminary evaluation heuristic affects the search performance.

5.1 Load Balancing in Production Scheduling

Production scheduling involves the problem of allocating resources to multiple processes over time in order to achieve a target global behavior, while simultaneously satisfying various constraints among the processes and resources. Our target problem is a one year project that comprises many jobs to be carried out in different shops. The objective is to schedule jobs in a manner such that the weekly loads of the shops are balanced as much as possible without violating the given constraints. We have conducted experiments for the production scheduling problem introduced in [1]. In this problem, a candidate solution is a job schedule which satisfies the partial ordering constraints among jobs and the job duration[1] constraints. A candidate solution is generated in two stages: selecting a job and adjusting its start and end times. We applied the probabilistic filtering only to the first stage of selecting a job as in [1]. The criticality of a job can be easily pre-evaluated by dividing the peak load value within the duration of the job by the global peak load value over the entire year. We did not apply the probabilistic filtering to the second stage of candidate generation because it is very hard to find any reasonable pre-evaluation heuristic for the adjustment of job duration without actually calculating the original objective function.

[1] Each job has its own minimum and maximum possible durations.

Figure 3 shows different runs of simulated annealing with various filtering strategies given an initial schedule with the objective function value of 18.9. Overall, filtering with appropriate bias (no bias should also be considered as a certain bias) is better than no filtering. Filtering with too strong a bias ($\beta = -20$) shows much worse performance than no filtering due to the greediness. Strong filtering selects only those jobs which are very critical. However, the adjustment of the duration of such jobs often cannot be done by an enough amount due to the ordering constraints with other preceding or succeeding jobs. Once this schedule becomes the next candidate solution to move to anyway, it is likely that the search is caught in a local optimum hard to escape from. On the other hand, filtering with no or weak bias ($\beta = 1$ or 2) has more chances to select and adjust the schedules of less critical jobs. This sometimes provides enough room for other preceding or succeeding critical jobs to be adjusted into the right direction in subsequent iterations, thus giving opportunities for significant improvement.

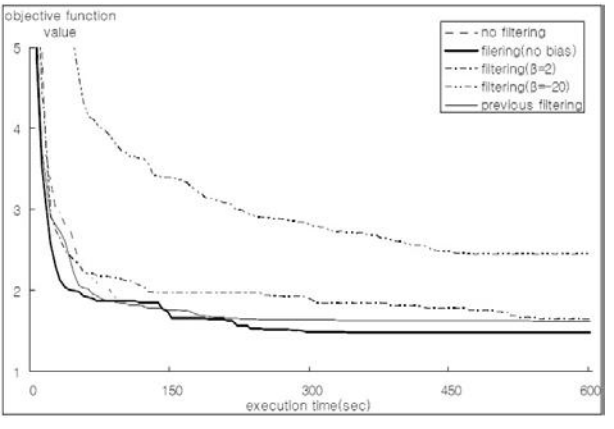

Fig. 3. Different runs of simulated annealing with various filtering strategies for the load balancing problem

Table 1 compares the quality of the solutions obtained by the simulated annealing using different probabilistic filtering strategies. The numbers in the table are the averages of the results of five runs with 30 minutes of CPU time allocated for each run. Further improvement has hardly been observed after 30 minutes. The evaluation has been performed by using the objective function in [1]. We can observe that filtering with no bias ($\beta = 1$) yields the best performance. As mentioned earlier, the previous filtering method [1] did not employ any scaling function, which implies that the performance improvement of 16.1% over 7.5% is mainly due to the newly introduced scaling and truncation process. A careful look at the numbers of evaluated and filtered candidates reveals that both numbers are severely reduced by employing the scaling process because of its heavy computational overhead. Nevertheless, the improvement in the quality of solution obtained by using our scaling function is significant.

Table 1. Performances of simulated annealing with different probabilistic filtering strategies for the load balancing problem

	no filtering	previous filtering	filtering		
			weaker bias ($\beta = 2$)	no bias ($\beta = 1$)	greedy bias ($\beta = -20$)
degree of load imbalance	1.74	1.61 (−7.5%)	1.62 (−6.9%)	1.46 (−16.1%)	2.27 (+30.5%)
# evaluated	567,359	730,000	425,832	447,369	275,990
# filtered	0	1.4×10^7	124,945	452,587	3.3×10^7

5.2 An Artificial Problem

We think that an appropriate pre-evaluation heuristic should be devised by using domain knowledge to enable probabilistic filtering to improve the efficiency of a local search. The suitability of a pre-evaluation heuristic can be considered with regard to two important aspects of the heuristic used—the accuracy and the cost. We have conducted additional experiments with an artificially generated optimization problem in order to determine the effects of the accuracy and cost on the improvement of search efficiency. The following equation shows the Rastrigin's function [9] that is used as the objective function of our optimization (minimization) problem.

$$f(x) = 500 + \sum_{i=1}^{50} x_i^2 - 10\cos(2\pi x_i) \quad (-5.12 \leq x_i \leq 5.12) \tag{4}$$

This is a multimodal function with many local optima obtained by using a sphere model with a cosine function. The global minimum of this function occurs at (0, 0, . . . , 0).

In our experiment, equation (4) with an additional noise term $G(0, \omega)$ is used as the pre-evaluation heuristic, where $G(0, \omega)$ is the normal distribution with a mean of 0 and a standard deviation of ω. As the main objective function of the problem, equation (4) is repeatedly evaluated m times to increase the evaluation cost Note that the average of $G(0, \omega)$ in absolute value is ????. We can increase the amount of noise by increasing ω, which results in a pre-evaluation heuristic with decreased accuracy.

Figure 4 and Table 2 compare different runs and performances of simulated annealing with no filtering, with filtering using a perfect pre-evaluation heuristic ($\omega = 0$), and with filtering using a noisy pre-evaluation heuristic ($\omega = 2$). The numbers in the table are the averages of the results of five runs with 60 minutes of CPU time allocated for each run. In these experiments, the cost ratio of the main evaluation to pre-evaluation is set as 3,000 (i.e., $m = 3,000$), and the bias function has been empirically tuned to a best-looking bias $\beta = 2$. The results show that even when the noise level of the pre-evaluation heuristic is increased

up to twice the standard deviation σ of the objective function values, filtering still improves the performance of simulated annealing search. In a separate experiment, we gradually decreased m and observed that probabilistic filtering is no longer able to improve the search efficiency when m becomes smaller than approximately 1,500.

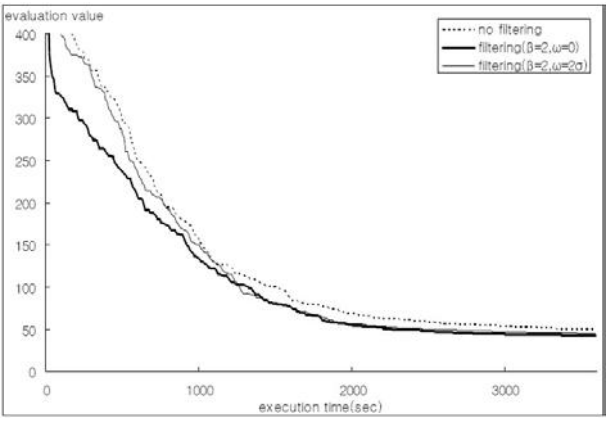

Fig. 4. Different Runs of simulated annealing with different filtering strategies for the artificial optimization problem

Table 2. Performances of simulated annealing without and with filtering and different noise levels of pre-evaluation for the artificial optimization problem ($\beta = 2$, $m = 3{,}000$)

	no filtering	filtering ($\omega = 0$)	filtering ($\omega = 2\sigma$)
best solution	49.77	42.62 (–14.4%)	44.99 (–9.5%)
# evaluated	266,980	246,727	244,595
# filtered	0	314,622	310,316

6 Conclusion

We have proposed an enhanced version of probabilistic filtering which incorporates a new scaling and truncation function as well as a more generalized bias function. We have tested the enhanced probabilistic filtering method with a large-scaled real world problem of load balancing in production scheduling which has a very expensive objective function to evaluate. The test results have shown that the new method can filter out unpromising candidate solutions more effectively than the previous method and thus discovers a better solution, given the same amount of CPU time. In separate experiments with an artificially generated optimization problem, we have observed that the probabilistic filtering

is fairly robust in that it can improve the search performance even when the preliminary evaluation heuristic used for filtering is not so accurate. It has also been shown that the lesser the relative cost of preliminary evaluation, the greater is the effectiveness of the probabilistic filtering.

References

1. Kang, B., Ryu, K.R.: Neighborhood Selection by Probabilistic Filtering for Load Balancing in Production Scheduling. In: Orchard, B., Yang, C., Ali, M. (eds.) IEA/AIE 2004. LNCS (LNAI), vol. 3029, pp. 533–542. Springer, Heidelberg (2004)
2. Selman, B., Kautz, H.A.: Domain-Independent Extensions to GSAT: Solving Large Structured Satisfiability Problems. In: Proceedings of IJCAI-93, Chambery, France, pp. 290–295 (1993)
3. Selman, B., Levesque, H.J., Mitchell, D.G.: A New Method for Solving Hard Satisfiability Problems. In: Proceedings of AAAI-92, San Jose, CA, pp. 440–446 (1992)
4. Bresina, J.L.: Heuristic-Biased Stochastic Sampling. In: Proceedings of AAAI-96, pp. 271–278 (1996)
5. Cicirello, V.A., Smith, S.F.: Amplification of search performance through randomization of heuristics. In: Van Hentenryck, P. (ed.) CP 2002. LNCS, vol. 2470, pp. 124–138. Springer, Heidelberg (2002)
6. Langley, P.: Systematic and Non-Systematic Search. In: Proceedings of AIPS-92, College Park, MD, Morgan Kaufmann, San Francisco (1992)
7. Binato, S., Hery, W.J., Loewenstern, D., Resende, M.G.C.: A GRASP for job shop scheduling. In: Ribeiro, C.C., Hansen, P. (eds.) Essays and surveys on metaheuristics, pp. 59–79. Kluwer Academic Publishers, Boston (2001)
8. Feo, T.A., Resende, M.G.C.: Greedy randomized adaptive search procedures. Journal of Global Optimization 6, 109–133 (1995)
9. Back, T., Hoffmeister, F., Schwefel, H.P.: Applications of Evolutionary Algorithms, Report of Systems Analysis Research Group SYS-2/92, University of Dortmund, Department of Computer science (1992)

A Weighted Feature C-Means Clustering Algorithm for Case Indexing and Retrieval in Cased-Based Reasoning

Chuang-Cheng Chiu and Chieh-Yuan Tsai

Industrial Engineering and Management Department, Yuan-Ze University, Taiwan, R.O.C.
cytsai@saturn.yzu.edu.tw

Abstract. A successful Case-Based Reasoning (CBR) system highly depends on how to design an accurate and efficient case retrieval mechanism. In this research we propose a Weighted Feature C-means clustering algorithm (WF-C-means) to group all prior cases in the case base into several clusters. In WF-C-means, the weight of each feature is automatically adjusted based on the importance of the feature to clustering quality. After executing WF-C-means, the dissimilarity definition adopted by K-Nearest Neighbor (KNN) search method to retrieve similar prior cases for a new case becomes refined and objective because the weights of all features adjusted by WF-C-means can be involved in the dissimilarity definition. On the other hand, based on the clustering result of WF-C-means, this research proposes a cluster-based case indexing scheme and its corresponding case retrieval strategy to help KNN retrieving the similar prior cases efficiently. Through our experiments, the efforts of this research are useful for real world CBR systems.

Keywords: Case-based reasoning, K-nearest neighbor search, Case indexing scheme, C-means clustering algorithm, Feature weighting.

1 Introduction

Case-based reasoning (CBR) is a problem-solving methodology commonly seen in artificial intelligence [1]. It has been successfully applied to various industrial applications such as sales operation, quality management, product development, health diagnosis, and so on [2], [3], [4], [5], [6]. Similar to human reasoning, a CBR system uses prior cases to find out suitable solutions for a new case. A CBR system stores prior cases in a data repository called a case-base. Each prior case in the case-base consists of the problem description part and solution part. For a new case, its problem description part is inputted into a CBR system. Prior cases similar to the new case are retrieved by evaluating the dissimilarity between the new case and each prior case in terms of their problem description parts. Then, the solution part of the new case is reasoned from the solution parts of these similar past cases.

A successful CBR system highly depends on how to design an effective and efficient case retrieval mechanism. K-Nearest Neighbor (KNN) search method has been extensively used in the case retrieval phase of CBR [7]. Traditional KNN method adopts an exhaustive search strategy to scan the overall case-base, and then

H.G. Okuno and M. Ali (Eds.): IEA/AIE 2007, LNAI 4570, pp. 541–551, 2007.

select *K* prior cases which have the minimum dissimilarities with the new case from the case-base. However, most previous studies related to the KNN method simply assumed all features in the problem description part of a case are equally important when evaluating the dissimilarity between two cases in terms of their problem description parts [7], [8]. This makes the case retrieval result tend to be biased and undesired, especially when the number of features is large. In addition, the number of prior cases stored in the case-base increases progressively as time goes by. How to incorporate a case indexing scheme to improve search efficiency, therefore, becomes a great challenge for the KNN method [9], [10], [11], [12].

The basic prerequisite of performing a CBR system is that two cases with similar problem description parts should reveal similar solution parts. Thus, it is meaningful and reasonable to use the solution parts of similar prior cases to reason the solution part of a new case. It implies that all prior cases in the case-base can be partitioned into several clusters based on their problem description parts. The prior cases in the same cluster are similar to each other and are different from cases in other clusters.

Based on this concept, this research proposes a Weighted Feature C-means clustering algorithm (WF-C-means) and a cluster-based case indexing scheme to conquer ineffective and inefficient problems occurred in KNN. In WF-C-means, the weight of each feature is automatically adjusted based on the importance of the feature to the clustering quality. Then, a clustering procedure similar to C-means [13], a classical clustering algorithm, is conducted using weighted features to partition all prior cases into several clusters. After executing WF-C-means, the dissimilarity definition adopted by KNN to retrieve similar prior cases for a new case becomes refined and objective because the weights of all features adjusted by WF-C-means can be involved in the dissimilarity definition. On the other hand, based on the clustering result of WF-C-means, this research proposes a cluster-based case indexing scheme and its corresponding case retrieval strategy to help KNN retrieving the similar prior cases efficiently.

2 A Weighted Feature C-Means Clustering Algorithm

The development of the proposed Weighted Feature C-means clustering algorithm (WF-C-means) is derived from the C-means clustering algorithm [13]. WF-C-means adopts three main procedures to partition all objects into *C* clusters based on the objective of minimizing the sum of dissimilarities between all objects and their corresponding cluster centers. The number of clusters, *C*, is generally pre-assigned by users. The first procedure is to assign each object to one of the *C* clusters properly. The second procedure is to update the *C* cluster centers based on the assignments in the first procedure. In the third procedure, the features that are important for the clustering result are given high weights by dimming the weights of trivial features. The three procedures are iterated until all *C* cluster centers remain the same without being changed.

Let a case-base $\mathbf{X} = \{\mathbf{x}_1, \cdots, \mathbf{x}_m, \cdots, \mathbf{x}_M\}$ include *M* prior cases and a feature set $\mathbf{F} = \{\mathbf{f}_1, \cdots, \mathbf{f}_n, \cdots, \mathbf{f}_N\}$ comprise *N* features in the problem description part of a case. A prior case $\mathbf{x}_m = (x_{m1}, \cdots, x_{mn}, \cdots, x_{mN})$ is composed of *N* feature values where x_{mn} is the

feature value of $\mathbf{f}_n$ in $\mathbf{x}_m$. Let $\mathbf{C} = \{\mathbf{C}_1, \cdots, \mathbf{C}_i, \cdots, \mathbf{C}_C\}$ be a set of the C clusters and $\mathbf{A} = \{\mathbf{a}_1, \cdots, \mathbf{a}_i, \cdots, \mathbf{a}_C\}$ be the set of the C cluster centers where $\mathbf{a}_i = (a_{i1}, \cdots, a_{in}, \cdots, a_{iN})$ is the cluster center of the ith cluster $\mathbf{C}_i$ and a_{in} is the feature value of $\mathbf{f}_n$ in $\mathbf{a}_i$. Accordingly, the dissimilarity between a prior case $\mathbf{x}_m$ and a cluster center $\mathbf{a}_i$, termed as $diss(\mathbf{x}_m, \mathbf{a}_i)$, can be defined as:

$$diss(\mathbf{x}_m, \mathbf{a}_i) = \sum_{n=1}^{N} w_n \times (x_{mn} - a_{in})^2 = \sum_{n=1}^{N} w_n \times d(x_{mn}, a_{in}) \tag{1}$$

where $w_n \in \mathbf{w}$ is the feature weight of the feature $\mathbf{f}_n$ and $\mathbf{w} = \{w_1, \cdots, w_n, \cdots, w_N\}$ is the set of the N feature weights, $\sum_{n=1}^{N} w_n = 1$, $0 \le w_n \le 1$. In addition, $d(x_{mn}, a_{in})$ is the difference between $\mathbf{x}_m$ and $\mathbf{a}_i$ in terms of feature $\mathbf{f}_n$. The smaller the value of $diss(\mathbf{x}_m, \mathbf{a}_i)$, the higher the probability that $\mathbf{x}_m$ belongs to cluster $\mathbf{C}_i$.

The objective of the WF-C-means algorithm, equivalent to C-means, is to minimize the sum of the dissimilarities between all prior cases to their corresponding cluster centers, which can be expressed as follows:

$$Minimize \;\; S(\mathbf{U}, \mathbf{A}, \mathbf{w}) = \sum_{m=1}^{M} \sum_{i=1}^{C} u_{mi} \times diss(\mathbf{x}_m, \mathbf{a}_i) = \sum_{m=1}^{M} \sum_{i=1}^{C} \sum_{n=1}^{N} u_{mi} \times w_n \times d(x_{mn}, a_{in}) \tag{2}$$

subject to

$$\begin{cases} \sum_{i=1}^{C} u_{mi} = 1 \\ u_{mi} \in \{1, 0\} \\ \sum_{n=1}^{N} w_n = 1 \\ w_n \ge 0 \end{cases} \quad \text{for} \; 1 \le m \le M, \; 1 \le i \le C, \; 1 \le n \le N \tag{3}$$

where $\mathbf{U}$ is a matrix of size $M \times C$ that records the case-cluster memberships and $u_{mi} \in \{1, 0\}$ is an element in $\mathbf{U}$ that represents the membership of $\mathbf{x}_m$ with the ith cluster $\mathbf{C}_i$. If $u_{mi} = 1$, $\mathbf{x}_m$ belongs to $\mathbf{C}_i$. If $u_{mi} = 0$, by contrast, $\mathbf{x}_m$ does not belong to $\mathbf{C}_i$. The WF-C-means algorithm solves the described optimization problem by iteratively solving the following three reduced problems:

1. Problem P_1: Fix $\mathbf{A} = \hat{\mathbf{A}}$ and $\mathbf{w} = \hat{\mathbf{w}}$ to solve the reduced problem $S(\mathbf{U}, \hat{\mathbf{A}}, \hat{\mathbf{w}})$.
2. Problem P_2: Fix $\mathbf{U} = \hat{\mathbf{U}}$ and $\mathbf{w} = \hat{\mathbf{w}}$ to solve the reduced problem $S(\hat{\mathbf{U}}, \mathbf{A}, \hat{\mathbf{w}})$.
3. Problem P_3: Fix $\mathbf{A} = \hat{\mathbf{A}}$ and $\mathbf{U} = \hat{\mathbf{U}}$ to solve the reduced problem $S(\hat{\mathbf{U}}, \hat{\mathbf{A}}, \mathbf{w})$.

The purpose of solving P_1 is to assign a prior case to a cluster whose cluster center is closest to the prior case, defined as Equation (4):

$$\begin{cases} u_{mi} = 1, \text{ if } \sum_{n=1}^{N} w_n \times d(x_{mn}, a_{in}) \le \sum_{n=1}^{N} w_n \times d(x_{mn}, a_{jn}) \\ u_{mi} = 0, \text{Otherwise} \end{cases} \quad \text{for} \; 1 \le i, j \le C, \; j \ne i \tag{4}$$

Accordingly, the procedure for solving P_2 is considered as a cluster-center updating procedure. Equation (5) can be used to calculate the solution of P_2.

$$a_{in} = \sum_{m=1}^{M} u_{mi} \times x_{mn} \Big/ \sum_{m=1}^{M} u_{mi} \quad \text{for} 1 \le i \le C,\ 1 \le n \le N \tag{5}$$

The difference between WF-C-Means and C-means is that WF-C-Means needs further solving the weight adjusting problem P_3 but C-means does not. The weight of a feature can be evaluated based on how the feature affects the quality of clustering result. In this research, the clustering quality is defined as the degree of minimizing the separations within clusters and maximizing the separations between clusters. Therefore, the problem P_3 is redefined as:

$$Maximize\ V(\hat{\mathbf{U}}, \hat{\mathbf{A}}, \mathbf{w}, \hat{g}) = \frac{S'(\hat{\mathbf{A}}, \mathbf{w}, \hat{g})}{S(\hat{\mathbf{U}}, \hat{\mathbf{A}}, \mathbf{w})} = \frac{\sum_{n=1}^{N}\left[w_n \times \left(\sum_{i=1}^{C} \| \mathbf{C}_i \| \times d(a_{in}, g_n) \right) \right]}{\sum_{n=1}^{N}\left[w_n \times \left(\sum_{m=1}^{M}\sum_{i=1}^{C} u_{mi} \times d(x_{mn}, a_{in}) \right) \right]} \tag{6}$$

subject to

$$\begin{cases} \sum_{n=1}^{N} w_n = 1 & \text{for} 1 \le n \le N \\ w_n \ge 0 \end{cases} \tag{7}$$

where $S(\hat{\mathbf{U}}, \hat{\mathbf{A}}, \mathbf{w})$ and $S'(\hat{\mathbf{A}}, \mathbf{w}, g)$ represent the sum of the separations within clusters and the sum of the separations between clusters, respectively. In addition, $g = (g_1, \cdots, g_n, \cdots, g_N)$ is the global center of all M prior cases in the case-base $\mathbf{X}$, and g_n is the feature value of g in terms of $\mathbf{f}_n$ which can be obtained using $g_n = \sum_{m=1}^{M} x_{mn} / M$. In addition, $\| \mathbf{C}_i \|$ represents the number of prior cases in the ith cluster $\mathbf{C}_i$ such that $\sum_{i=1}^{C} \| \mathbf{C}_i \| = M$.

Let $e_n = \sum_{m=1}^{M}\sum_{i=1}^{C} u_{mi} \times d(x_{mn}, a_{in})$ be the sum of separations within clusters in terms of $\mathbf{f}_n$ and $f_n = \sum_{i=1}^{C} \| \mathbf{C}_i \| \times d(a_{in}, g_n)$ be the sum of separations between clusters in terms of $\mathbf{f}_n$. Accordingly, Equation (6) can be simplified as:

$$Maximize\ V(\hat{\mathbf{U}}, \hat{\mathbf{A}}, \mathbf{w}, \hat{g}) = \frac{\sum_{n=1}^{N} w_n \times f_n}{\sum_{n=1}^{N} w_n \times e_n} \tag{8}$$

This research proposes a feature weight adjusting rule to derive $\mathbf{w}$ from Equation (8). Let $\mathbf{w}^{\text{new}} = \{w_1^{\text{new}}, \cdots, w_n^{\text{new}}, \cdots, w_N^{\text{new}}\}$ be the set of the new weights for original N feature weights in $\mathbf{w}$ after the adjustment. For each feature $\mathbf{f}_n$, its new weight w_n^{new} can be evaluated by adding an adjustment margin Δw_n to its origin weight w_n. By applying

a common decision optimization method in linear programming theory [14], Δw_n can be derived as: $\Delta w_n = (f_n / e_n) \big/ \sum_{n=1}^{N} (f_n / e_n)$. Therefore, the new weight w_n^{new} of $\mathbf{f}_n$ can be calculated using Equation (9).

$$w_n^{\text{new}} = w_n + \Delta w_n = w_n + \frac{f_n / e_n}{\sum_{n=1}^{N} (f_n / e_n)} \quad \text{for } 1 \le n \le N \tag{9}$$

Notes that the new weights derived by Equation (9) might violate the constraint of $\sum_{n=1}^{N} w_n^{\text{new}} = 1$. Therefore, Equation (9) is further modified as Equation (10) through the normalization process.

$$w_n^{\text{new}} = \frac{w_n + \dfrac{f_n / e_n}{\sum_{n=1}^{N} (f_n / e_n)}}{\sum_{n=1}^{N} w_n + \sum_{n=1}^{N} \left(\dfrac{f_n / e_n}{\sum_{n=1}^{N} (f_n / e_n)} \right)} \quad \text{for } 1 \le n \le N \tag{10}$$

In WF-C-means, the procedures of prior case assignment, cluster center update, and feature weight adjustment are executed iteratively until all C cluster centers remain the same without being changed. The pseudo-code of the WF-C-means algorithm is summarized in Fig. 1. After executing WF-C-means, the dissimilarity definition adopted by KNN for case retrieval, defined as Equation (1), becomes refined and objective because the weights of all features can be involved in the dissimilarity definition. Therefore, it prevents KNN from obtaining the unbiased and undesired retrieval results.

Input: a set of M prior cases in which each prior case has N features in its problem description part; the number of clusters, C
1: Select C cluster centers randomly for these C clusters.
2: Let the feature weight of each feature be $(1/N)$.
3: Repeat
4: Form C clusters by assigning each prior case to its closest cluster center using Equation (4).
5: Update the cluster center in each cluster using Equation (5).
6: Adjust the feature weight of each feature using Equation (10).
7: Until all C cluster centers are not changed.

Fig. 1. The pseudo-code of the WF-C-means algorithm

3 Case Indexing and Retrieval Based on WF-C-Means

As stated, prior cases in the same cluster have similar problem description part. In other words, in a certain cluster if one prior case is similar to the new case, other prior cases in the same cluster might be similar to the new case under certain degree. Based on this concept, this research proposes a cluster-based case indexing scheme from the clustering result generated by WF-C-means. With this proposed case indexing scheme, KNN can adopt a novel case retrieval strategy to search similar prior cases for a new case instead of its original exhaustive search strategy. Not only the efficiency of KNN can be improved, but also the final retrieval result is the same with

the one using the exhaustive search strategy. The proposed cluster-based case indexing scheme is introduced as follows:

1. For each cluster $\mathbf{C}_i$, its cluster center $\mathbf{a}_i$ is considered as a representative case for all prior cases in $\mathbf{C}_i$. Let $y_i = \| \mathbf{C}_i \|$ be that the number of prior cases belongs to $\mathbf{C}_i$ such that $\sum_{i=1}^{C} y_i = M$.
2. For each cluster $\mathbf{C}_i$, all y_i prior cases in $\mathbf{C}_i$ are assigned index numbers based on the ascending order of their dissimilarities with their cluster center $\mathbf{a}_i$. Therefore, $\mathbf{C}_i$ is reorganized as $\mathbf{C}_i = \{\mathbf{c}_1^i, \mathbf{c}_2^i, \cdots, \mathbf{c}_{t-1}^i, \mathbf{c}_t^i, \cdots, \mathbf{c}_{y_i}^i \mid diss(\mathbf{c}_{t-1}^i, \mathbf{a}_i) \le diss(\mathbf{c}_t^i, \mathbf{a}_i)\}$. Meanwhile, The radius of a cluster $\mathbf{C}_i$, termed as r_i, is defined as $r_i = Maximum\{diss(\mathbf{c}_t^i, \mathbf{a}_i) \mid \mathbf{c}_t^i \in \mathbf{C}_i\}$.

Based on the proposed cluster-based case indexing scheme, the corresponding case retrieval strategy adopted by KNN is introduced as follows, and its pseudo-code is illustrated in Fig. 2.

1. Let $\mathbf{Sim_Q}$ be the set stores the prior cases similar to the new case $\mathbf{Q}$ in terms of their problem description part. At the beginning of case retrieval, $\mathbf{Sim_Q}$ is an empty set. During the processing of case retrieval, if the dissimilarity between a prior case and $\mathbf{Q}$ is less than a user-defined dissimilarity threshold, termed as *r*, the prior case is added into $\mathbf{Sim_Q}$.
2. For each cluster $\mathbf{C}_i$, we first calculate the dissimilarity $diss(\mathbf{a}_i, \mathbf{Q})$ between its cluster center $\mathbf{a}_i$ and the new case $\mathbf{Q}$.
3. If $diss(\mathbf{a}_i, \mathbf{Q}) \ge r_i + r$, all prior cases in $\mathbf{C}_i$ are not similar enough to $\mathbf{Q}$. Therefore, no further dissimilarity calculation is required for any prior case in $\mathbf{C}_i$ with $\mathbf{Q}$. That is, no prior case in $\mathbf{C}_i$ can be added into $\mathbf{Sim_Q}$.
4. If $diss(\mathbf{a}_i, \mathbf{Q}) < r_i + r$, a further dissimilarity checking procedure is then conducted for all prior cases in $\mathbf{C}_i$. Any prior case $\mathbf{c}_t^i$ in $\mathbf{C}_i$ that satisfies the constraint: $diss(\mathbf{a}_i, \mathbf{Q}) - r < diss(\mathbf{a}_i, \mathbf{c}_t^i) < diss(\mathbf{a}_i, \mathbf{Q}) + r$ can be considered as a *candidate* for $\mathbf{Sim_Q}$. The candidates can be found easily using a binary search since all prior cases in $\mathbf{C}_i$ have been indexed based on their dissimilarities from their cluster center $\mathbf{a}_i$ in ascending order in the proposed case indexing scheme.
5. For each candidate case in $\mathbf{C}_i$, we calculate its dissimilarity with $\mathbf{Q}$. If the dissimilarity is less than *r*, it becomes a formal member of $\mathbf{Sim_Q}$.
6. After adding similar prior cases of all *C* clusters into $\mathbf{Sim_Q}$, if the number of cases in $\mathbf{Sim_Q}$ is larger than or equal to *K*, the first *K* prior cases with the minimum dissimilarities with $\mathbf{Q}$ are outputted as the retrieval result. By contrary, if the number of cases in $\mathbf{Sim_Q}$ is less than *K*, the dissimilarity threshold *r* is widened by adding a increasing margin Δr, i.e., $r = r + \Delta r$. With the new threshold, the retrieval proceeding goes back to execute step 3 until all *K* similar prior cases has been retrieved.

Instead of starting from scratch, the dissimilarity threshold r can be initialized using Equation (11). Equation (11) is formulated based on the following concept. For each cluster $\mathbf{C}_i$, if $y_i \geq K$, we can easily identify the Kth prior case $\mathbf{c}_K^i$ based on its index number. Therefore, the dissimilarity $diss(\mathbf{a}_i, \mathbf{c}_K^i)$ can be considered as a candidate dissimilarity threshold for $\mathbf{C}_i$. However, if $y_i < K$, the radius r_i of $\mathbf{C}_i$ is considered as the candidate dissimilarity threshold for $\mathbf{C}_i$. The maximum among these specific dissimilarity thresholds, defined as Equation (11), is therefore suggested as a reasonable value of r. In addition, the increasing margin Δr, as stated in step 6 of the case retrieval strategy, is also suggested as the value of r for convenient reason.

$$r = Maximum\{diss(\mathbf{a}_i, \mathbf{c}_K^i) \mid \mathbf{c}_K^i \in \mathbf{C}_i, 1 \leq i \leq C\} \tag{11}$$

Input: a new case **Q** given its problem description part; a user-defined dissimilarity threshold r
Output: The first K prior cases which have minimum dissimilarities with **Q** in a case set $\mathbf{Sim_Q}$
1: Let the set $\mathbf{Sim_Q}$ be an empty set.
2: Repeat
3: For each cluster $\mathbf{C}_i$ in the cluster-based case indexing scheme {
4: Calculate the dissimilarity $diss(\mathbf{a}_i,\mathbf{Q})$ between the cluster center $\mathbf{a}_i$ and the new case **Q**
5: If $diss(\mathbf{a}_i,\mathbf{Q}) < r_i + r$ { // r_i is the radius of the cluster $\mathbf{C}_i$
6: For each prior case $\mathbf{c}_i^t$ in $\mathbf{C}_i$ {
7: If $diss(\mathbf{a}_i,\mathbf{Q}) - r < diss(\mathbf{a}_i,\mathbf{c}_i^t) < diss(\mathbf{a}_i,\mathbf{Q}) + r$ {
8: Calculate the dissimilarity $diss(\mathbf{c}_i^t,\mathbf{Q})$ between $\mathbf{c}_i^t$ and the new case **Q**
9: If $diss(\mathbf{c}_i^t,\mathbf{Q}) < r$ {
10: Add $\mathbf{c}_i^t$ into $\mathbf{Sim_Q}$
11: }
12: }
13: }
14: }
15: }
16: If the number of cases in $\mathbf{Sim_Q} < K$ {
17: $r := r +$
18: }
19: Until the number of cases in $\mathbf{Sim_Q}$ is larger than or equal to K.
20: Return the first K prior cases which have minimum dissimilarities with **Q** in $\mathbf{Sim_Q}$

Fig. 2. The pseudo-code of retrieving K prior cases similar to a new case

4 Experiments

4.1 Clustering Performance of WF-C-Means

A series of experiments on three popular datasets [15] are made to demonstrate the performance of the proposed WF-C-means algorithm. The properties of the three datasets are shown in Table 1. Because the scales of all features in the wine dataset are different, all features in the wine dataset are standardized. This research adopts the

Sum of Square within-cluster Error (SSE), defined as Equation (2), as the measure to judge the clustering accuracy for the traditional C-means and proposed WF-C-means algorithms. The less the SSE value, the more the clustering accuracy is.

The experiments for the same dataset are conducted 100 replicates. In each replicate, the two algorithms use equivalent initial cluster centers that are generated randomly, while the weight values for all N features are initially assigned as $1/N$. The number of clusters, C, is specified as the default class number of each dataset. The clustering performances of the two algorithms using the three datasets are shown in Table 2. Notes that the results are generated through averaging the experimental results of the 100 replicates.

As shown in Table 2, the clustering accuracy of the proposed WF-C-means algorithm is obviously superior to the accuracy of C-means in terms of SSE measures. For the iris and wine datasets, the number of iterations in WF-C-means is nearly the same with the ones in C-means. When the number of cases increases such as the yeast dataset, WF-C-means needs more iterations to converge the optimal solution. The computational efficiency of WF-C-means, therefore, is slightly inferior to C-means. However, the tradeoff between them is worth based on our study.

Table 1. The properties of the three real world datasets

Dataset	Number of instances (cases)	Number of features	Number of classes
iris	150	4	3
wine	178	13	3
yeast	1484	8	10

Table 2. The clustering performances for the three datasets using the two algorithms

Algorithm	C-means			WF-C-means		
Dataset	iris	wine	yeast	Iris	wine	yeast
SSE	23.513	98.688	6.213	22.251	66.044	3.372
Number of iterations	7.370	7.367	31.077	7.223	8.943	38.562

Through WF-C-means, the final weights of the four features in the iris dataset are $\{w_1, w_2, w_3, w_4\} = \{0.09, 0.04, 0.53, 0.34\}$. It is clear that the third and fourth features are more important than other two features. When substituting these weights into Equation (1), an objective dissimilarity between two cases $\mathbf{x}_m$ and $\mathbf{x}_p$ is calculated by $0.09(x_{m1} - x_{p1})^2 + 0.04(x_{m2} - x_{p2})^2 + 0.53(x_{m3} - x_{p3})^2 + 0.34(x_{m4} - x_{p4})^2$. Similarly, the top four features with the highest weights in the wine datasets are w_{12}, w_{13}, w_7, and w_6. Their weights are $\{w_{12}, w_{13}, w_7, w_6\} = \{0.24, 0.19, 0.12, 0.10\}$. Similarly, the top four features with the highest weights in the yeast datasets are $\{w_1, w_4, w_2, w_8\}=\{0.60, 0.23, 0.08, 0.05\}$. The important features identified by WF-C-means are almost the same as the result discovered in the paper of [16]. This also verifies that the dissimilarity definition with weighted features is reliable and can contribute accurate case retrieval result.

4.2 Performance of Case Retrieval Based on Our Case Indexing Scheme

The traditional KNN method adopts an exhaustive search strategy to evaluate the dissimilarity between each prior case in the case-base and the new case. It requires huge computation time on dissimilarity calculations, especially the number of prior cases in the case-base is considerable. The computational complexity of the exhaustive search strategy is O(M) if the dissimilarity calculation time between two cases is constant.

In opposition, when KNN adopts the proposed case retrieval strategy with the proposed case indexing scheme, its computational complexity equals to O(C+pM) where p is the probability of the event that $diss(\mathbf{a}_i,\mathbf{Q}) < r_i + r$ in the case retrieval strategy and $0 \le p \le 1$. If C is close to 1 (all cases are located within a cluster), the radius of the cluster is large enough to cover all cases. As a result, p tends to be 1 for the cluster. It makes the computational complexity close to O(M). If C is close to M (each case is considered as an individual cluster), p tends to be 0 since the radius of each cluster is close to 0, so the computational complexity is also close to O(M). However, in practice, $C<<M$ so that the computational complexity of the proposed case retrieval strategy can be simplified as O(pM). It is much less than the computational complexity using the exhaustive search strategy.

Let us take the yeast dataset as an example to show the search efficiency using the proposed case retrieval strategy with the proposed case indexing scheme. In this experiment, the leave-one-out validation approach is adopted. That is, each case in the dataset sequentially serves as a new case, while other 1483 cases are considered as the prior cases in the case-base. For each new case, we count the number of dissimilarity calculations required to retrieve K similar prior cases where K is set as 5 in all experiments. Fig. 3 depicts the search efficiency of KNN using the proposed case retrieval strategy. In the figure, the number of required dissimilarity calculations

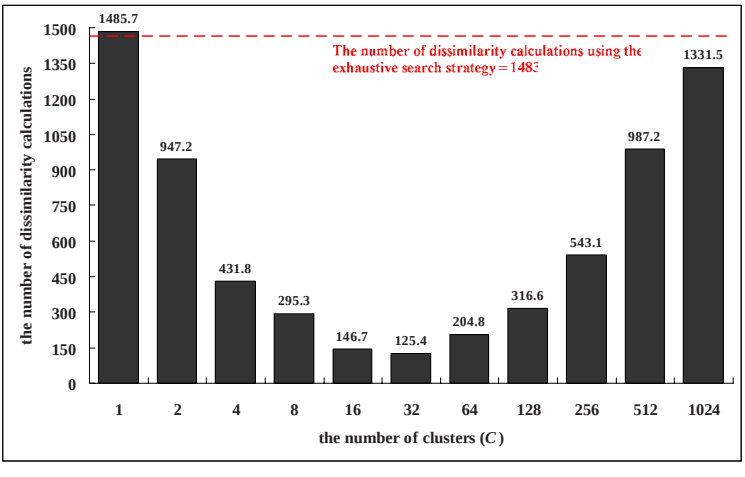

Fig. 3. The efficiency of KNN using the proposed case indexing and retrieval method for the yeast dataset (K=5)

through our method is significantly less than the number using the exhaustive search strategy. The calculation numbers form a concave quadratic shape. When C is between 8 and 128, our method can decrease at least 70% similarity calculations compared to the exhaustive search strategy. From the experiments, we can know that the search efficiency of KNN becomes obviously increased when using the proposed cluster-based case indexing scheme and corresponding case retrieval strategy instead of the exhaustive search strategy.

5 Conclusions

This research aims at improving the accuracy and efficiency of the case retrieval phase in a CBR system. A WF-C-means algorithm is proposed to group all prior cases in the case-base into several clusters. Based on the clustering result of WF-C-means, an objective dissimilarity definition can be obtained from the adjusted feature weights. KNN can use the dissimilarity definition to effectively retrieve similar prior cases for a new case. Based on the clustering result, furthermore, a cluster-based case indexing scheme and its corresponding case retrieval strategy are also proposed in order to increase the search efficiency of KNN in the case retrieval phase. Through our experiments, the efforts of this research are useful for real world CBR systems.

In our experiments, we observed that some settings for the cluster number in WF-C-means might increase search efficiency in the case retrieval phase. In the future, we will study how to determine an appropriate number of clusters before performing WF-C-Means so that the final accuracy and efficiency in the case retrieval phase can be further improved.

References

1. Aamodt, A., Plaza, E.: Case-Based Reasoning: Foundational Issues Methodological Variations, and System Approaches. Artificial Intelligence Communications 7, 39–59 (1994)
2. Gardingen, D., Watson, I.: A Web Based CBR System for Heating Ventilation and Air Conditioning System Sales Support. Knowledge Based System 12, 207–214 (1999)
3. Suh, M.S., Jhee, W.C., Ko, Y.K., Lee, A.: A Cased-Based Expert System Approach for Quality Design. Expert Systems with Applications 15, 181–190 (1998)
4. Belecheanu, R., Pawar, K.S., Barson, R.J., Bredehorst, B., Weber, F.: The Application of Case Based Reasoning to Decision Support in New Product Development. Integrated Manufacturing Systems 14, 36–45 (2003)
5. Li, L.L.X.: Knowledge-Based Problem Solving: An Approach to Health Assessment. Expert Systems with Applications 16, 33–42 (1999)
6. Tsai, C.Y., Chiu, C.C., Chen, J.S.: A Cased-Based Reasoning System for PCB Defect Prediction. Expert Systems with Applications 28, 813–822 (2005)
7. Watson, I., Marir, F.: Case-Based Reasoning: A Review. The Knowledge Engineering Review 9, 355–381 (1994)
8. Kolodner, J.L.: Case-Based Reasoning. Morgan Kaufmann, San Francisco (1993)
9. Guttman, A.: R-trees: A Dynamic Index Structure for Spatial Searching. In: Proceedings of the 1984, ACM SIGMOD International Conference on Management of Data, pp. 47–57 (1984)

10. Fukunaga, K., Narendra, P.M.: A Branch and Bound Algorithm for Computing K-Nearest Neighbors. IEEE Transaction on Computers 24, 750–753 (1975)
11. Gargantini, I.: An Effective Way to Represent Quadtrees. Communications of the ACM 25, 905–910 (1982)
12. Yianilos, P.N.: Data Structures and Algorithms for Nearest Neighbor Search in General Metric Spaces. In: Proceedings of the 4th annual ACM-SIAM symposium on Discrete algorithms, pp. 311–321 (1993)
13. McQueen, J.: Some Methods for Classification and Analysis of Multivariate Observations. In: Proceedings of the 5th Berkeley Symposium on Mathematical Statistics and Probability, pp. 281–297 (1967)
14. Hillier, F.S., Lieberman, G.J.: Introduction to Operation Research. McGraw-Hill, New York (2001)
15. Newman, D.J., Hettich, S., Blake, C.L., Merz, C.J.: UCI Repository of Machine Learning Databases (1998) http://www.ics.uci.edu/~mlearn/MLSummary.html
16. Ahmad, A., Dey, L.: A Feature Selection Technique for Classificatory Analysis. Pattern Recognition Letters 26, 43–56 (2005)

Neural Networks for Inflow Forecasting Using Precipitation Information

Karla Figueiredo, Carlos R. Hall Barbosa*, André V.A. Da Cruz**,
Marley Vellasco**, Marco Aurélio C. Pacheco**, and Roxana J. Conteras**

Electrical and Telecommunications Engineering Department, UERJ
Rua São Francisco Xavier, 524, Maracanã - CEP 20550-900, Rio de Janeiro RJ – Brazil
karlaf@uerj.br
ICA – Applied Computational Intelligence Laboratory
*Post-graduation Program in Metrology,
**Department of Electrical Engineering
Pontifícia Universidade Católica of Rio de Janeiro
Rua Marquês de São Vicente, 225, Rio de Janeiro – 22453-900 – RJ - Brazil
{hall, andrev, marley, marco, roxana}@ele.puc-rio.br

Abstract. This work presents forecast models for the natural inflow in the Basin of Iguaçu River, incorporating rainfall information, based on artificial neural networks. Two types of rainfall data are available: measurements taken from stations distributed along the basin and ten-day rainfall forecasts using the ETA model developed by CPTEC (Brazilian Weather Forecating Center). The neural nework model also employs observed inflows measured by stations along the Iguaçu River, as well as historical data of the natural inflows to be predicted. Initially, we applied preprocessing methods on the various series, filling missing data and correcting outliers. This was followed by methods for selecting the most relevant variables for the forecast model. The results obtained demonstrate the potential of using artificial neural networks in this problem, which is highly non-linear and very complex, providing forecasts with good accuracy that can be used in planning the hydroelectrical operation of the Basin.

Keywords: Artificial Neural Networks, Inflow Forecast, Time Series Forecating.

1 Introduction

The National Electrical System Operator (ONS) [1] is responsible for elaborating the daily, weekly and monthly forecast of the average natural inflow for every hydraulic utilization place of the National Integrated System (SIN). Considering the meaningful predominance of hydraulic generation in the Brazilian electrical system, the quality of this natural flow forecast is one of the main inputs to the planning of SIN operation.

Natural inflow is defined as the inflow that occurs in a river section, where there are no anthropic actions that are able to alter its regular pattern. In other words, it is the inflow that would happen in a river section if the upstream reservoir operation did not

H.G. Okuno and M. Ali (Eds.): IEA/AIE 2007, LNAI 4570, pp. 552–561, 2007.

happen, neither the inflow evaporation from artificial lakes, and neither from supplied water with an upstream reservoir and irrigation system. In short, it is all about natural inflow. Natural inflows are calculated based on the observed inflows, measured by fluviometric stations and a series of other information referring to the hydrographic basin (river basin), being a synthesized numerical series from experimental data. On the other hand, natural incremental inflow corresponds to the change of natural inflow that takes place between two specific points of hydroelectrical usage.

Nowadays, the forecast inflow models used by ONS are usually stochastic and do not consider information about precipitation. However, in the last decades, different technologies for modeling the natural phenomena have evolved, enhancing the knowledge about nature's physical and biological process. Advances in climate variability and weather forecast are on the spot due to forecasting quality evolution through the years. For hydrology, there is a high potential for making use of this climatic estimation of rain for inflow forecasting. As a result of these advances, ONS aims to develop new inflow forecast systems including precipitation information, either forecasted or observed. It is in this context that this work applies artificial neural networks for the creation of inflow forecast models.

The next section presents the hydraulic basin of River Iguaçu, which was used as the case study for this work. Section 3 describes the historical data available for training the neural network models. Sections 4 and 5, respectively, present data pre-processing methods and the selection of input variables.

Intelligent models for inflow forecasting and the results obtained are described in the sequence. Finally, the last section presents the conclusions and suggests future works.

2 River Iguaçu Basin

Figure 1 shows River Iguaçu basin together with various hydroelectrical plants (UHE) that exist through out of this river (pointed out by triangles in figure 1). The hydroelectrical plants are called Foz do Areia, Segredo, Salto Santiago, Salto Osório and Salto Caxias (from east to west). There are fluviometric stations available in these Hydroletrical Plants – UHE, which are responsible for inflow measurements. There are also many pluviometric stations in the basin that measure the precipitations. This basin can be divided in three big subbasins, defined by Foz do Areia and Salto Santiago UHE. Lastly, there is an upstream reservoir from Segredo, in Jordão river.

In order to meet ONS need for the Monthly Operation Program (PMO) [1], the goal of this work is to build forecasting models for three separate areas of Rio Iguaçu basin, that is:

- Natural inflow at UHE Foz do Areia
- Natural inflow at Jordão reservoir
- Incremental natural inflow between UHE Foz do Areia, Jordão reservoir and UHE Salto Osório

For each series, the PMO needs 12-days daily inflow forecast, always starting on Wednesdays. Also, it is needed an average weekly inflow forecast for the so-called "electrical week", from Saturday to Friday, from the 4^{th} to the 10^{th} days.

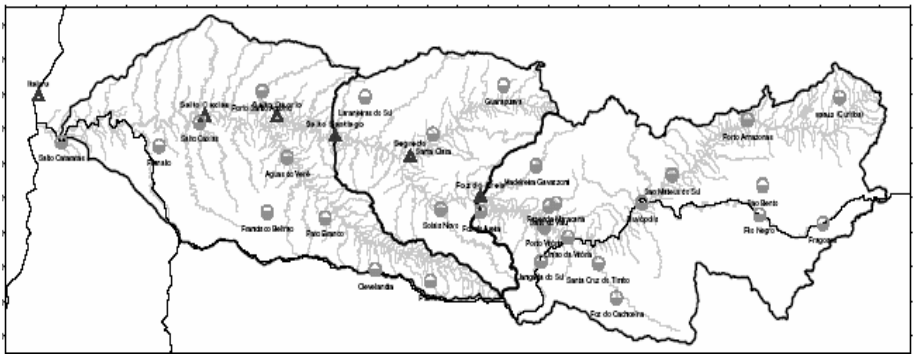

Fig. 1. Rio Iguaçu hydrographic basin. Hydroelectric plants are indicated by triangles and pluviometrical stations are indicated by circles. The biggest circle points out Curitiba.

3 Historical Data

The historical data available for the construction of the forecasting models can be divided in four big groups, as follows:

- Daily precipitation, observed and measured by 30 pluviometric stations, in mm, data from 1922 to 2001;
- Daily average inflow observed and measured by 14 fluviometric stations, in m3/s, with data from 1930 to 2001;
- Daily precipitation forecast, weekly generated by ETA model [2],[3] with 10 days forecast window, in a 40 km resolution grid, in mm, with the historical data from 1996 to 2001; and
- Natural daily average inflow (either incremental or not), corresponding to the series that is intended to be forecasted in m3/s, with the historical data from 1931 to 2001.

Considering that the precipitation forecast data (ETA) are only available from 1996 to 2001, all the other series are limited to the same period, excluding all the other data. Therefore, there is a six year old daily database, considering that the last year available (2001) was used for the forecast model test.

4 Preprocessing Data

Next, the preprocessing applied in the various historical data series available is described.

4.1 Observed Precipitation

In order to make the construction of forecasting models viable, the data related to 30 rain gauges were aggregated in a single series of observed precipitation for the whole hydrographic basin. For that, the Thiessen Method [4] was applied, commonly used in

hydrometeorology. This method generates polygons around the pluviometrical stations, defining the area that is convered by each pluviometric station. The characteristic of a Thiessen polygon is that the distance from any point within the region to the pluviometric station is smaller than the distance from this same point to any other station. Figure 2 below shows the Thiessen polygons acquired from the available measurement points. The series corresponding to various pluviometers are then weighted by the relative areas of the corresponding polygons. Figure 3 shows the Thiessen series obtained for the period from 1996 to 2001.

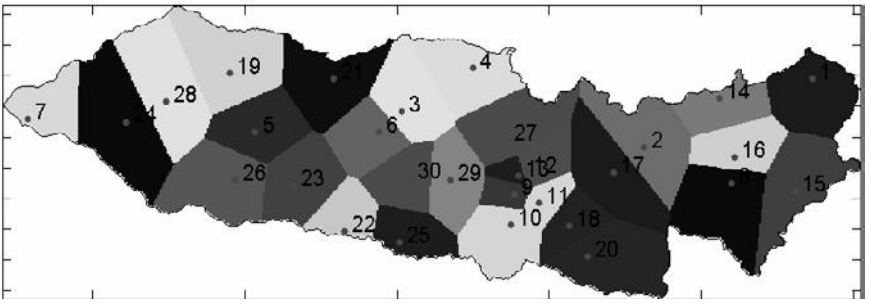

Fig. 2. Thiessen polygons for River Iguaçu basin

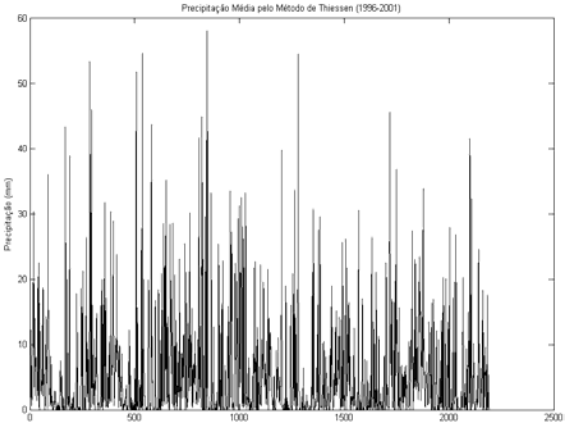

Fig. 3. Fixed series of observed precipitation, calculated by Thiessen Method

4.2 Precipitation Forecast

These series are processed in a similar way to the observed precipitation, as it is necessary to aggregate the forecast series, available in a grid with 40 Km resolution in a single series, representing the entire basin.

It was initially selected which point of the forecasting grid should be considered, located in the border line, or very close to it. Figure 4 below shows 68 selected points.

Next, since every point corresponds to eographic areas with the same dimensions, the aggregated series can be obtained by simply calculating the average of every individual series.

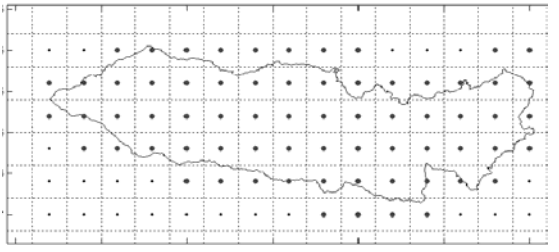

Fig. 4. ETA grid. The larger points indicate the ones selected as belonging to the Basin.

4.3 Observed Inflow and Natural Inflow

For the observed and natural inflows, it was simply applied the logarithmic transformation, followed by a linear data normalization, with the intent of normalizing the values of inflow series for the neural network model, reducing its variability.

5 Variables Selection

Even after the consolidation obtained by preprocessing, a great number of inflow observed series (measured by fluviometers) is still available for the construction of forecasting models. Consequently, the application of variable selection methods was needed to identify the fluviometric stations that have higher relation to the inflow series that are needed to be forecast.

First, the cross correlation [5] among each fluviometric series and the inflow series were calculated, in order to determinate and later on eliminate the lag among series.

Then, it was done a pre-selection of the stations that could have influence in each of the three areas of the River Iguaçu Basin, based on geographic and hydrometeorological criteria.

Finally, two methods of variable selection were applied to select the set of pluviometric stations, called Least Squares Estimator [6] and SIE - Single Input Effectiveness [7], combining both methods in a heuristic way.

So, 4 stations were selected out of the 14 fluviometric stations available, for UHE Foz do Areia area, 4 stations for Jordão reservoir area and 7 stations for the area between UHE Foz do Areia, Jordão reservoir and UHE Salto Osório.

6 Inflow Forecasting Models

After the more significant historical data were preprocessed and pluviometric stations were selected for obtaining forecasting models, the forecast models were built, based in the following techniques:

- Multi-layer Perceptron Artificial Neural Networks, Levenberg-Marquardt [8] – MLP-LM training; and
- Multi-layer Perceptron Artificial Neural Networks, Bayesian training [9] – MLP-BAY.

Various models were tested with different sets of input variables. Each model is specialized in one of the 12 days to be forecasted and in the average of the electrical week. Next, the structure of the models used for daily and weekly forecast are presented.

6.1 Models of Daily Inflow Forecast

6.1.1 Neural Networks MLP-LM

Data set from 1996 to 2000 was used for training (80% for training and 20% for validation) and data set from 2001 was used for testing. Cross-validation was used to stop the training of the networks, and 30 networks were trained for each topology.

The following input series were used:

- Average precipitation calculated by Thiessen method of the last 7 days (from Tuesday to Wednesday of the previous week);
- Average inflow observed in the last 7 days (from Tuesday to Wednesday of the previous week);
- Precipitation forecasted by ETA model for the next 10 days;
- Inflows measured on Tuesday by the selected fluviometric stations.

Various topologies were evaluated with the number of neurons in the hidden layer varying between an interval of 1 neuron and 2 times the number of inputs + 5 neurons, that is, for the network with 10 inputs topologies were evaluated from 1 neuron in the hidden layer up to 25 neurons.

6.1.2 Neural Networks MLP-BAY

Data set from 1996 to 2000 was used for training (since neural networks with bayesian training do not need to use cross-validation, every data was used for training) and data set related to 2001 was used for testing. This procedure is repeated 30 times for each topology. This enables the choice of the one that shows the best performance among the 30.

In this case, topologies were evaluated with a number of neurons in the hidden layer varying from 1 to 10.

Since this network is able to select the more relevant input series that are able to acquire better forecasting, it was used every fluviometric station for MLP with Bayesian training. So, in the same way as previous case, there are the following sets of input variables:

- Average precipitation calculated by Thiessen method of the last 7 days (from Tuesday to Wednesday of the previous week);
- Inflow of the last 7 days (from Tuesday to Wednesday of the previous week);
- Precipitation based on ETA model for the next 10 days; and
- Average inflows on Tuesday at all fluviometric stations.

6.2 Weekly Forecasting Inflow Models

6.2.1 Neural Networks MLP-LM

Various input sets were tested according to the description in table 1.

- M1: 8 inputs for the forecast of the Natural Inflow at UHE Foz do Areia: 1 to 21 neurons in the hidden layer
- M2: 5 inputs for the forecast of the Natural Inflow at Jordão reservoir: 1 to 15 neurons in the hidden layers.
- M3: 9 inputs for the forecast of the Incremental Natural Inflow between Foz do Areia UHE, Jordão Reservoir and Salto Osório UHE: 1 to 23 neurons in the hidden layer.

6.2.2 Neural Networks MLP-BAY

According to table 1, various input sets were tested.

- M4: 22 inputs for the forecast of the Natural inflow at UHE Foz do Areia:
- M5: 13 inputs for the forecast of the Natural Inflow of Jordão Reservoir:
- M6: 24 inputs for the forecast of the Incremental Natural Inflow among UHE Foz do Areia, Reservatório Jordão and UHE Salto Osório:

Since the Bayesian trained networks had an inferior performance, with higher errors for every sub-basin for the electrical week from Saturday to Friday, this model was not used for the weekdays of Sundays to Saturdays and Mondays to Sundays.

Table 1. Variables input configuration

Model	Neural Network Input Configuration								
		V_{3a}	Prev ETA_{10}	Sum ETA_{10}	VPF_{3a}	VM_1	VM_2	VM_3	VDP
MLP-LM	M1	x		x	x			x	
	M2	x		x	x			x	
	M3	x		x	x	x			x
MLP-Bay	M4	x	x		x	x			
	M5	x	x	x	x	x			
	M6	x	x		x	x	x	x	

In table 1 the columns are organized as following:

First column divides, horizontally, the table in MLP-LM and MLP-BAY models; second column enumerates different combinations of inputs for both neural network models.

The following columns are:

V_{3a} observed inflow on Tuesday;
Prev $ETA_{10:}$ forecast of 10 days of precipitations through ETA model;
Sum ETA_{10}: sum of 10 days of precipitations forecast by ETA;

VPF_{3a}: Inflow measured on Tuesday by fluviometric stations;

VM_1: Average inflow observed during the week previous to the electrical week to which the forecast is done;

VM_2: average inflow observed two weeks before the electrical week to which the forecast is done;

VM_3: average inflow observed three weeks before the electrical week to which the forecast is done;

VDP: Daily inflow from Wednesday to Friday (by using the results provided with the daily forecasting).

7 Results

In table 2 are the results provided by the topology that had the best performance for each single step forecasting day, up to 12 days ahead, among various evaluated topologies. First column presents the forecasting days; second, third and fourth columns present the performance of two Neural Network Models evaluated, for three sub-basins that are: Foz do Areia, Jordão and Salto Osório. The value presented is MAPE (Mean Absolute Percentage Error) error, calculated every day for 2001 test period. The criteria for choosing the topologies not only considered the MAPE errors, but also the topologies with less numbers of neurons.

Table 2. MAPE errors for daily forecasting

	Foz da Areia		Jordão		Salto Osório	
	MLP-LM	***Bayes***	MLP-LM	***Bayes***	MLP-LM	***Bayes***
1	3.96	4.00	7.60	8.48	10.46	10.34
2	8.55	7.77	11.90	13.03	17.19	19.64
3	11.34	12.12	14.96	14.07	23.68	26.38
4	17.18	16.97	16.99	14.68	24.29	27.94
5	20.77	21.45	25.43	19.24	30.59	33.30
6	23.51	24.73	26.86	24.17	33.25	42.09
7	25.86	26.78	28.02	26.62	36.22	49.28
8	27.40	28.45	28.38	29.63	38.36	48.63
9	27.56	28.77	28.22	30.03	38.16	46.42
10	29.53	28.68	26.77	26.84	39.60	42.60
11	29.49	31.47	25.04	25.16	34.33	40.01
12	34.54	35.08	27.94	31.24	37.87	42.86

Table 3. MAPE errors for weekly forecasting

Sub-basins	MLP-LM	MLP-BAY	Estatistic
Foz do Areia	20.39	24.68	32.80
Jordão	22.71	24.14	30.30
Salto Osório	30.35	37.92	47.10

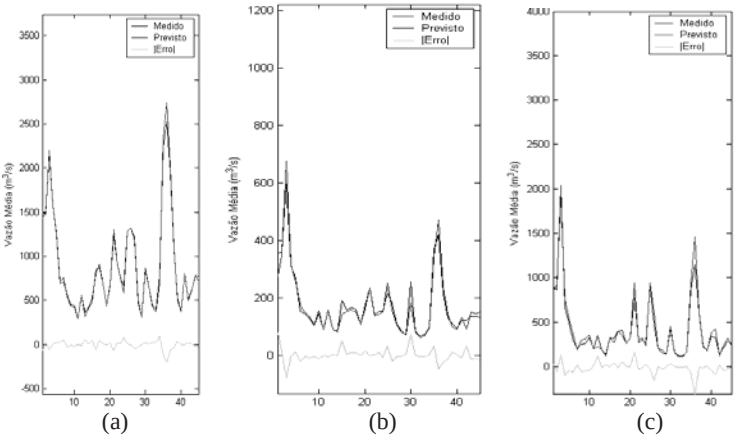

Fig. 5. Daily Forecasting (1st Day) (a) UHE Foz do Areia Natural Inflow using MLP (LM) network with 22 neurons; MAPE=3.9%6. (b) Jordão Reservoir Natural Inflow using MLP (LM) networks with 3 neurons; MAPE = 7.6%; (c) Incremental Natural Inflow among UHE Foz do Areia, Jordão Reservoir and UHE Salto Osório of Daily Inflow using MLP (LM) Neural Networks with 11 neurons; MAPE = 10.46%.

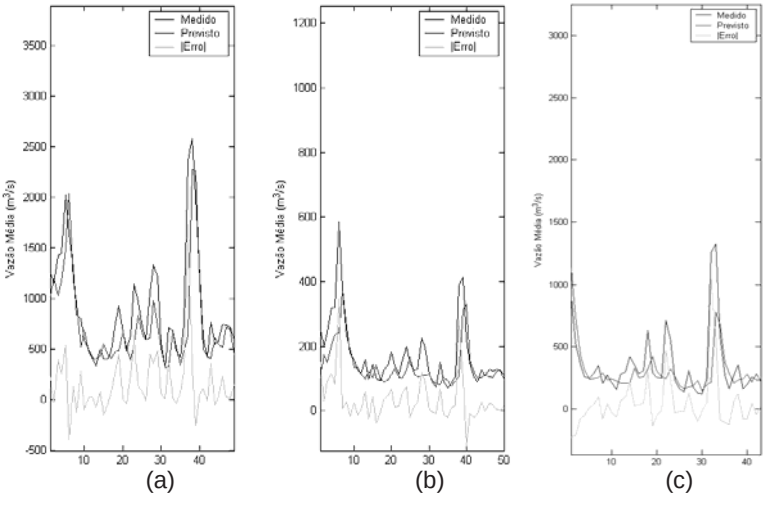

Fig. 6. (a)Weekly Forecast (Saturday to Friday) from UHE Foz do Areia Natural Inflow using MLP (LM) Neural Networks with 6 neurons; MAPE = 20.39%; (b) Weekly Forecasting (Saturday to Friday) from Jordão Reservoir Natural Inflow using MLP (LM) Neural Networks; MAPE = 22.71%; (c) Weekly forecasting (Saturday to Friday) from Incremental Natural Inflow among UHE Foz do Areia, Jordão Reservoir and UHE Salto Osório using MLP (LM) Networks with 12 neurons; MAPE = 30.35%

In the first column of table 3 the sub-basins are presented for weekly forecasting. In table 3 he the results exposed by Statistic model systematically present results with higher error for every sub-basins for the electrical week (Saturday to Friday). These results were compared to a statistic model based on dynamic regression.

The results acquired for daily forecasting through Bayesian training were, in many days, very close to the ones acquired through MLP-LM networks, as observed in Table 2. Therefore, in order to keep Computational methodology commonality (that is, not varying the methodology applied during the 12 days), the MLP-LM network was chosen, since it has yielded a model that offers a better daily forecast for most of the days in every sub-basins.

In figure 5 the graphs present the results for the first day of forecasting for the following sub-basins: Foz do Areia, Jordão and Salto Osório. In figures 6a, 6b and 6c, the graphs show the result for electrical week forecasting (Saturday to Friday) for the following sub-basins: Foz do Areia, Jordão and Salto Osório.

8 Conclusions

Generally speaking, it's well known that, as the forecasting window increases, the forecasting ability of any model deteriorates. Therefore, it is expected that in daily models, for each basin, the forecasting MAPE errors increases as the forecast window increases. Consequently, as expected, the performance was better than the one obtained by using a single neural network to forecast 12 steps ahead, in a multi-step procedure (MAPE of 12^{th} day in Foz do Areia = 38.84%; MAPE of 12^{th} day in Jordão = 34.36% and MAPE of 12^{th} day in Salto Osório = 51.00%).

For weekly forecast, the best performance was obtained by MLP (LM) model, except in the first day when both models had the same results.

Since this is a basin with complex behavior, the Intelligent Models (non linear models) have better results than the statistic methods applied [10].

References

1. ONS (2006) http://www.ons.org.br/home/
2. Previsões Numéricas CPTEC (2006) http:// www.cptec.inpe.br/prevnum/
3. Black, T.L.: NMC Notes: The New NMC mesoscale Eta model: Description and forecast examples. Weather and Forecasting 9, 256–278 (1994)
4. Pinto, N. L.S.: Hidrologia Básica (1976) ISBN: 85-212-0154-0
5. Manual de Estatística (2006) http:// www.bertolo.pro.br/AdminFin/StatFile/Manual_Estatistica.htm
6. Cao, Y., Rossiter, D.: An Input Pre-screening Technique for control Structure Selection. Computers Chem. Engng. 21(6), 5363–5369 (1997)
7. Chung, F.-L., Duan, J.-C.: On Multistage Fuzzy Neural Network Modeling. IEEE Transactions on Fuzzy Systems 8, 125–816 (2000)
8. Haykin, S.: Neural Networks – A Comprehensive Foundation. Macmillan College Publishing, Oxford (1998)
9. Mackay, David, J.C: Bayesian Non-Linear Modelling with Neural Networks. Cavendish Laboratory, Cambridge, UK (1995) http://wol.ra.phy.cam.ac.uk/is/papers/
10. Relatório Técnico Final de Metodologia, Projeto PreVIP: Modelo de Previsão de Vazões com Incorporação de Informações de Precipitação, ONS - PUC-Rio (2005)

A Gradational Reduction Approach for Mining Sequential Patterns

Jen-Peng Huang[1], Guo-Cheng Lan[1], and Huang-Cheng Kuo[2,⋆]

[1] Department of Information Management
Southern Taiwan University of Technology
jehuang@mail.stut.edu.tw
[2] Department of Computer Science and Information Engineering
National Chiayi University
hckuo@mail.ncyu.edu.tw

Abstract. The technology of data mining is more important in recent years, and it is generally applied to commercial forecast and decision supports. Sequential pattern mining algorithms in the field of data mining play one of the important roles. Many of sequential pattern mining algorithms were proposed to improve the efficiency of data mining or save the utility rate of memory. So, our major study tries to improve the efficiency of sequential pattern mining algorithms.

We propose a new algorithm - GRS (A Gradational Reduction Approach for Mining Sequential Patterns) which is an efficient algorithm of mining sequential patterns. GRS algorithm uses gradational reduction mechanism to reduce the length of transactions and uses GraDec function to avoid generating large number of infrequent sequential patterns; and it is very suitable to mine the transactions of databases whose record lengths are very long. The GRS algorithm only generates some sequences which are very possible to be frequent. So, the GRS algorithm can decrease a large number of infrequent sequences and increase the utility rate of memory.

Keywords: data mining, sequential patterns, algorithm.

1 Introduction

Recent developments in computing technologies have resulted in computerizing enterprises which were recorded by hand. For example, customers' records in enterprises, patients' records in hospitals, transaction records in sales ... etc., those data are transferred and stored in files or database format which make the maintenance easier, more convenient and more efficient than before by using sorting, indexing and relationship between tables.

As people use computer to deal with different kinds of affairs, the amount of data are stored and accumulated in surprising speed. Those large amounts of data need new technologies and tools to analyze and extract useful information

⋆ Corresponding author.

H.G. Okuno and M. Ali (Eds.): IEA/AIE 2007, LNAI 4570, pp. 562–571, 2007.

from them. The category of those new knowledge and technologies becomes a new domain, data mining, in computer science.

Data mining refers to extracting knowledge from large amounts of data by some technologies which include association rule mining, sequential pattern mining, clustering, and classification etc. Association rule mining which finds the relation between items or attributes is one of the most popular topics among these data mining technologies. For example, association rule mining can be applied to supermarkets. Managers of supermarkets can rearrange the positions between merchandises in supermarket and increase the profits.

The paper is organized as follow. The literature review will be introduced in section 2. We propose definitions, problems, and algorithms in section 3, and we also provide examples to explain our proposed algorithms in section 3. In section 4, we evaluate the performances of our algorithms with the past algorithms under different parameters. The conclusion and future development are given in section 5.

2 Background

In the past, we seldom consider mining the time sequence databases. However, the sequential pattern plays the important role in the transactions database, credit card databases, and so on. The reason is that there are usually the relationships of order for the implicit information in these databases. If we can discover the rules which often appears from these databases, the rules are great useful and valuable for us. For example, one person will buy the scanner after buying the laser printer. Later, he will buy the burning machine. Therefore, if we can discover such information from the various databases, we can really know the customers' behaviors or other information, and then let the enterprises obtain the greatest benefits.

Sequential pattern mining have been studied by some researchers [5][3][2][9]. Because they are extended from the Apriori[1] algorithm of association rule, they have the same defects as Apriori[1]. The defects are that the algorithms must generate a huge number of candidate sets and repeatedly scan the database to count the support of each candidate sequence. Therefore, the efficiency of the algorithms is bad.

In addition, some researchers propose the algorithms [8][9] which are different from Apriori-based algorithms. The algorithms use the divide-and-conquer and projected-based techniques to perform the mining task. The efficiency of the algorithms is better than Apriori-based algorithms, but the algorithms must spend a great deal of memory setting up the projection databases when the items of the database averagely appear in each sequence record. The algorithms easily cause the insufficient memory and inefficiency problems.

Srikant[6] et al. define the problems of discovering sequential patterns in database. Let $I = \{I_1, \ldots, I_m\}$ be a set of items, D be a set of sequences. An itemset is a non-empty set of items. A sequence is an ordered list of itemsets. We denote a sequence s by $< s_1 s_2 \ldots s_n >$, where s_j is an itemset. We also call s_j an

element of the sequence. We denote an element of a sequence by $(x_1, x_2, \ldots, x_m)$, where x_j is an item. An item can occur only once in an element of a sequence, but can occur multiple times in different elements. An itemset is considered to be a sequence with a single element.

A sequence $< a_1 a_2 \ldots a_n >$ is a sub-sequence of another sequence $b_1 b_2 \ldots b_m$ if there exist integers $i_1 < i_2 < \ldots < i_n$ such that $a_1 \subset b_{i1}, a_2 \subset b_{i2}, \ldots, a_n \subset b_{in}$. For example, the sequence $< (3), (4, 5), (8) >$ is a sub-sequence of <(7), (3, 8), (9), (4, 5, 6), (8)>, since (3) $\subset$ (3, 8), (4, 5) $\subset$ (4, 5, 6), and (8) $\subset$ (8). However, the sequence $< (3), (5) >$ is not a sub-sequence of $< (3, 5) >$. The problem of mining sequential patterns is to find all sequences whose support is greater than the user-specified minimum support. Each such sequence represents a sequential pattern, also called a frequent sequence.

The AprioriAll[2] algorithm is a level-wise technique. In the mining sequential patterns, AprioriAll must repeatedly scan the database and generate the candidate sets until there are no frequent sequences to be found.

The GSP[6] (Generalized Sequential Pattern) algorithm effectively reduces the number of candidate sets, and modifies the join phase of candidate generation in the mining sequential patterns. However, because the GSP algorithm will spend a great deal of time to perform the processes of candidate sets reducing, and GSP also needs to scan the database repeatedly, the performance of GSP is not good.

FreeSpan[8] (Frequent pattern-Projected Sequential Pattern Mining) uses the frequent items to project many small projected databases from original database. Next, FreeSpan only scans and decomposes the small projected databases, and then discover the sequential patterns. Because FreeSpan does not scan the original database repeatedly, the mining efficiency is better than the Apriori-based algorithms. However, FreeSpan may suffer from the following two nontrivial costs under some conditions: (a) FreeSpan will waste unnecessary memory to build these projected databases. (b) FreeSpan will generate many unnecessary candidate sets.

To improve the defects of FreeSpan[8], PrefixSpan[9] (Prefix-projected Sequential Pattern Mining) recursively uses divide-and-conquer and projected-based to discover the sequential patterns, the performance of PrefixSpan is better than the Apriori-based algorithms when patterns are long. However, PreficSpan must set up many large projected databases when the items are distributed equally in the database. Thus it easily causes insufficient memory problems.

3 Gradational Reduction Approach for Mining Sequential Patterns, GRS

When the lengths of sequence records are long or the minimum supports are low, the past algorithms [2][10][8][9] need to spend a great deal of time to discover the frequent sequences. Therefore, to improve the mining efficiency, we propose a new algorithm GRS (Gradational Reduction Approaches for Mining Sequential Patterns). GRS is a level-wise technique, and the algorithm uses the

mask technique to generate sequences quickly. GRS algorithm uses a mechanism called gradational reduction mechanism which uses the frequent sequences as the information of filtration mechanisms to delete the infrequent sequences of database in every phase. Besides, GRS uses the gradational reduction mechanism to reduce the length of transactions. In the beginning of every phase, GRS uses the frequent k-sequences which are obtained from previous phase to delete the items which are not in frequent k-sequences. To avoid decomposing the same sequence records repeatedly in each phase, the every shortened sequence record is saved into a new database and the same sequence records are accumulated in each phase. By above processes, the database is gradually becoming small. Thus the GRS algorithm can effectively reduce the number of infrequent sequences in every phase, and then increase the performance and the utility rate of memory.

3.1 Processes of Generating Possible Frequent Sequences

To decompose the transactions records gradually, we use a function GraDec to decompose the transactions records into possible frequent sequences of specified length.

We suppose two numbers n and k where n is greater than k. If a subset s which consists of the preceding *k-1* items of an n-sequence S is not a frequent sequence in L_{k-1}, then all k-sequences which contain the subset s are impossible to be frequent sequences in L_k. The set of frequent k-sequences is commonly denoted by L_k.

For example, let A(BC)BDE be the 6-sequence S, and A(BC)B is not a frequent sequence in L_4. We can discover that A(BC)BD and A(BC)BE are not possible to be frequent sequences in L_5.

We use the frequent sequences of preceding phase as the information of the filtration mechanism in every phase. We suppose the specified length of sequence is k. If a subset s which consists of the preceding *k-1* items of an n-sequence is not a frequent sequence in L_{k-1}, then all k-sequences which contain the subset s are impossible to be frequent in L_k. Then function GraDec stops generating k-sequences which contain the subset s. Otherwise, function GraDec generates all k-sequences which contain the subset s. This filtration mechanism can effectively reduce the number of infrequent sequences, and increases the performance and the utility rate of memory.

In generating candidate sequences, function GraDec only generates possible frequent sequences. For example, given a sequence record "A(BC)DE", and the specified length of sequences 4, there is only "A(BC)" in the frequent 3-sequences which is obtained in previous phase. Thus GRS passes "A(BC)DE", length 4, and the frequent 3-sequence "A(BC)" to function GraDec. GRS will continue to call the function GraDec until it generates all of the possible frequent 4-sequences of "A(BC)DE".

First, the function GraDec initiates the mask value to "11110". The subset which consists of the preceding 3 items of "A(BC)DE" with the mask value "11110" is "A(BC)". The function GraDec needs to determine whether the subset "A(BC)" is a frequent sequence in the frequent 3-sequences. Because the

subset "A(BC)" is a frequent sequence, the function GraDec generates all of the 4-sequences of "A(BC)DE" which contain "A(BC)". Thus the function GraDec returns "A(BC)D" and "A(BC)E". Fig. 1(a) shows the processes of infrequent sequences filtering.

Next, the function GraDec sets the mask value to "11011". The subset which consists of the preceding 3 items of "A(BC)DE" with the mask value "11011" is "ABD". In the same way, the function GraDec needs to determine whether "ABD" is a frequent 3-sequence in L_3. Because the subset "ABD" is not a frequent 3-sequence in L_3, the function GraDec directly sets the mask value to "10111". Fig. 1(b) shows the processes. The subset which consists of the preceding 3 items of "A(BC)DE" with the mask value "10111" is "ACD". The function GraDec needs to determine whether "ACD" is a frequent 3-sequence in L_3. Because the subset "ACD" is not a frequent 3-sequence in L_3, the function GraDec directly sets the mask value to "01111". Fig. 1(c) shows the processes. The subset which consists of the preceding 3 items of "A(BC)DE" with the mask value "01111" is "(BC)D". The function GraDec needs to determine whether "(BC)D" is a frequent 3-sequence in L_3. Because the subset "(BC)D" is not a frequent 3-sequence in L_3, we stop the processes of sequences generating. Fig. 1(d) shows the processes.

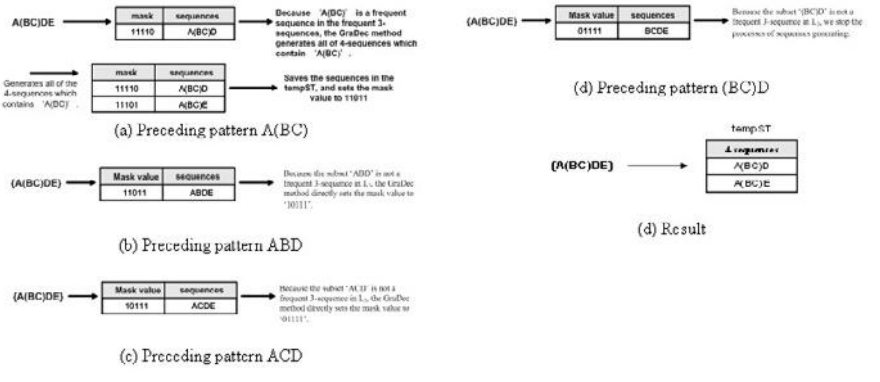

Fig. 1. GraDec function on A(BC)DE

In Fig 1(e) we can discover that GRS only generates sequences which are very possible to be frequent via the mechanism of infrequent sequences filtering in tempST. Thus GRS can effectively increase the efficiency and the utility rate of memory.

3.2 Process of Gradational Reduction Mechanism

Although the function GraDec can generate all of the possible frequent sequences of specified length, in order to reduce the lengths of transactions in every phase,

we add a gradational reduction mechanism in the GRS algorithm. In the beginning of every phase, GRS uses the frequent k-sequences which are obtained from previous phase to delete the items which are not in frequent k-sequences. After reducing transactions in every phase, we accumulate the number of the same transactions to save the unnecessary decomposition time in order to avoid decomposing the same transactions repeatedly. Besides, to save the access time of the support of every sequence, we will use the sequence table to increase the access efficiency. Because the sequence table is modified from the Hash Map of JAVA API, the sequence table is helpful to the access efficiency. By gradational reduction mechanism GRA can early filter out the infrequent items of next phase and avoid generating any infrequent sequences. And then increase the performance and the utility rate of memory.

If an element of sequences is not in L_{n-1}, then the element is impossible to be an element of sequences in L_n. Thus the element can be eliminated in next mining phases, and L_n is the set of frequent n-sequences.

We provide an example to explain whole processes. First, we compute the occurrence frequency of each item of database DB. Then we find the frequent 1-sequences which satisfy the user-specified minimum supports and save in FST[0]. Next, we apply a filtration mechanism which is a length shortening method to delete non-L_1 items of every transaction, and then save and accumulate the shortened transactions in temp_DB. The processes are shown in Fig. 2(a).

Next, we use function GraDec to generate all of the possible frequent 2-sequences and use user-specified minimum supports to find all of the frequent 2-sequences from temp_DB and save in FST[1]. After finding the frequent 2-sequences, we save all of the items of FST[1] into tempFST. The items which are saved in tempFST are possible elements of frequent sequences which will be found in next phase. Next, we delete the items of temp_DB which are not in tempFST, and then accumulate and save the rest in temp_DB. Fig. 2(b) shows the processes and result of FST[1] and temp_DB.

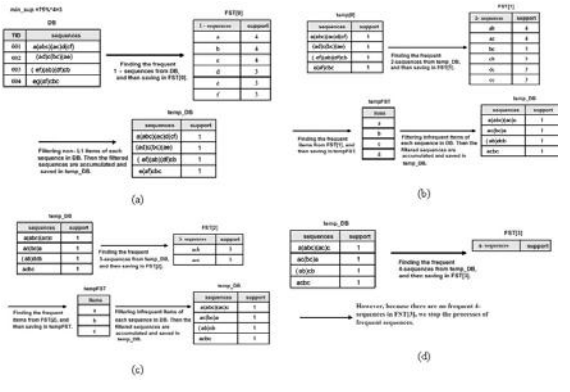

Fig. 2. The process of infrequent items filtering

The function GraDec continues to generate all of the possible frequent 3-sequences and use user-specified minimum supports to find all of the frequent 3-sequences from temp_DB and save in FST[2]. After finding the frequent 3-sequences, we save all of the items of FST[2] into tempFST. The items which are saved in tempFST are possible elements of frequent sequences which will be found in next phase. Next, we delete the items of temp_DB which are not in tempFST, and then accumulate and save the rest in temp_DB. Fig. 2(c) shows the processes and result.

We perform the above processes repeatedly. There are no frequent 4-sequences in FST[3], the process of finding frequent sequences stops. Fig. 2(d) shows the processes of the filtration mechanism.

4 Experimental Results

4.1 Experiment Environment

All the experiments are performed on the following environment: ¡br¿ Intel Pentium IV 2.8GHz CPU, 512MB DDR RAM, Windows 2000 Server, IBM Data Generator[6], J2SDK 1.4.2 Programming Language.

The experiments are pursued on synthetic data sets which are generated by IBM Data Generator[6] with the following factors. S: Average transactions per customer. T: Average items per transactions. I_I: Average length of maximal pattern. I_T: Average length of maximal pattern. N: Total number of different items. D: Total number of transactions.

4.2 Comparison Algorithms

Our proposed algorithms are to discover the sequential patterns, so our experiment includes the famous algorithms such as AprioriAll[2] and PrefixSpan[9]. In addition, we also consider the version based on pseudo-projection name PrefixSpan-2 in the experiment. The PrefixSpan-2 algorithm uses a structure to link all of the customer sequences in a projection database. This mechanism can reduce the costs on projecting databases when the projected database can be built in the main memory. Besides, to avoid external factors causing the difference of performances, each algorithm is written in Java2 SDK 1.4.2 and performed on the same environments.

To be the fairness of the performance, we need to show the performances of our implemented algorithm PrefixSpan is not worse than the original one. Because the AprioriAll algorithm is not our main competitive algorithm, we omit the performance figure comparison. We use the performance figure of study which is proposed by Pei[9] et al., to compare the performance with our implemented algorithms.

In Fig. 3 they use dataset S8T8I8N1KD10K and the different minimum supports to test the performance of PrefixSpan. Because we do not have original PrefixSpan[9], we try our best to implement PrefixSpan. The result of execution on dataset S8T8I8N1KD10K within min_sup range between 0.5% and 3% are

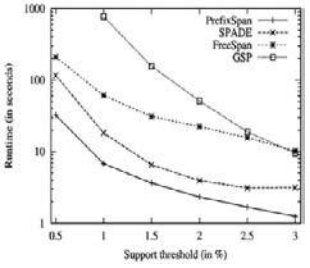

Fig. 3. Comparison of the algorithms in different min_sup. (Source: Pei[9]).

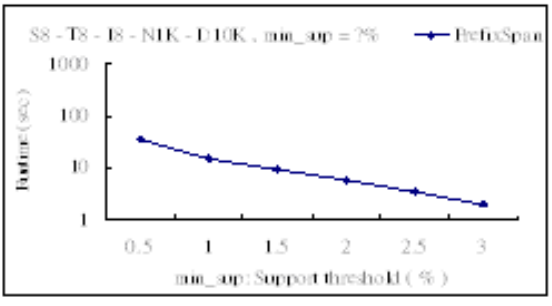

Fig. 4. Comparison of the algorithms in different min_sup

shown in Fig. 4. In Fig. 3 and Fig. 4 we can discover that the performance of our implemented algorithm is similar to the original one.

4.3 Experiment Evaluations

Comparison of the algorithms in different min_sup. First, we use dataset S3-N10K-D100K-T2.5-IS4-IT1.25 with min_sup range between 0.2% and 1% to evaluate the performance of algorithms in different minimum supports (min_sup). The result is shown in Table 2. Because the performance of AprioriAll is the worst one among algorithms, we remove AprioriAll from the algorithms and continue to compare the performances with others. In the advanced experiments, we use dataset S10-N10K-D100K-T2.5-IS4-IT1.25 with min_sup range between 0.5% and 3% to evaluate the performance of algorithms in different minimum supports (min_sup). We discover that the execution time is increasing when the minimum supports are decreasing. The reason is that the number of frequent items is increasing when minimum supports are decreasing. Thus the algorithms spend more time discovering frequent sequences. The performance of AprioriAll is very good when the minimum supports are between 0.8% and 1%. However, the execution time of the algorithm is rapidly increasing when min_sup is decreasing. The reason is that AprioriAll need to spend a great deal of time generating large number of candidate sets and count the supports of candidate sets from the

database. Thus the performance of AprioriAll is the worst algorithm among algorithms. The performance of GRS is better than others. Because it can effectively filter infrequent sequences via their own filtration mechanisms. In addition, because PrefixSpan-1 and PrefixSpan-2 use the projection techniques to discover the frequent sequences, the algorithms need to spend a great deal of memory building the projections. Therefore their performances are not good.

Comparison of utility rate of memory in different parameters S. In this experiment, we use dataset N10K-D100K-T2.5-IS4-IT1.25 and min_sup 0.5% within S range between S3 and S11 to evaluate the utility rate of memory of algorithms in different number of transactions per sequence (S). We observe that the memory usage is increasing when the S is increasing. Because both PrefixSpan-1 and PrefixSpan-2 use projection techniques to discover the frequent sequences, the algorithms spend more memory building these projection databases when S is increasing. Thus the utility rates of memory are not better than others. Because AprioriAll is a level-wise method, AprioriAll can release unnecessary memory space in each phase. Thus the utility rate of memory is very good. Because GRS can effectively reduce the number of infrequent sequences via the filtration mechanisms, the algorithm can save a good deal of memory to increase memory utility rates.

Comparison of the algorithms in different parameters D. In this experiment, we use dataset S10-N10K-T2.5-IS4-IT1.25 and min_sup 0.75% within D range between 100K and 500K to evaluate the performance of algorithms in different sizes of datasets (D). We discover that the execution time is increasing when D is increasing. The execution time of AprioriAll is rapidly increasing when D is increasing. The reason is that AprioriAll spends more time counting supports of candidate sets when D is increasing. Besides, when D is greater than 500K, the execution of AprioriAll is very long. Therefore, we remove AprioriAll from algorithms and continue to compare the performance with others.

5 Conclusion

One of the characters of GRS algorithm is the gradational reduction mechanisms. The main mining method of GRS algorithm is similar to Apriori-like algorithm which is level by level, but the GRS algorithm does not need to generate candidate sequential patterns during the mining processes. At the same time, it can shorten the length of sequences and compress the size of database in every phase so it can reduce a great number of infrequent sequences effectively, and then increase the efficiency and the utility rate of memory substantially.

The advantages of GRS algorithm are as follows:

1. Because the GRS algorithm will release the memory of storing infrequent sequences and the shortening length and the size compressing of database in every phase, it only generates the sequences that are the most possible to be frequent sequences. Therefore, the GRS algorithm can increase the utility rate of memory effectively.

2. The GRS algorithm can finish the mining task ahead of time when there are no frequent sequences at one phase
3. In the mining sequential patterns, GRS does not need to generate candidate sets; it uses the gradational reduction mechanisms to filter a huge number of infrequent sequences, and avoids wasting time on the infrequent sequences generation.
4. The framework of GRS is easy to be implemented.

Acknowledgment. This work was partially supported by grants NSC 93-2213-E-218 -012 and NSC 95-2221-E-415-013- from National Science Council, Taiwan.

References

1. Agrawal, R., Srikant, R.: Fast Algorithm for Mining Association Rules in Large Databases. In: Int'l Conf. VLDB, pp. 487–499 (1994)
2. Agrawal, R., Srikant, R.: Mining Sequential Patterns. In: Int'l Conference on Data Engineering, pp. 3–14 (1995)
3. Chen, M.S., Park, J.S., Yu, P.S.: Data Mining for Path Traversal Patterns in a Web Environment. In: Int'l Conf. Distributed Computing Systems, pp. 385–392
4. Lee, C.-H., Lin, C.-R., Chen, M.-S.: Sliding-Window Filtering: An Efficient Algorithm for Incremental Mining. In: ACM Int'l Conference on Information and Knowledge Management (2001)
5. Masseglia, F., Cathala, F., Poncelet, P.: The PSP Approach for Mining Sequential Patterns. European Symp. Principle of Data Mining and Knowledge Discovery, pp. 176–184 (1998)
6. IBM Almaden Research Center. Quest synthetic data generation code. `http://www.almaden.ibm.com/cs/quest/syndata.html`
7. Han, J., Pei, J., Yin, Y.: Mining Frequent Patterns without Candidate Generation. In: ACM Int'l Conference on Management of Data, pp. 1–12 (2000)
8. Han, J., Pei, J., Mortazavi-Asl, B., Chen, Q., Dayal, U., Hsu, M.C.: FreeSpan: Frequent Pattern-Projected Sequential Pattern Mining. In: Int'l Conf. on Knowledge Discovery and Data Mining, pp. 335–359 (2000)
9. Pei, J., Han, J., Mortazavi-Asl, B., Pinto, H., Chen, Q., Dayal, U., Hsu, M.C.: Mining Sequential Patterns by Pattern-growth: the PrefixSpan Aapproach. IEEE Transactions on Knowledge and Data Engineering 16, 1424–1440 (2004)
10. Srikant, R., Agrawal, R.: Mining Sequential Patterns: Generalizations and Performance Improvements. In: Int'l Conference on Extending Database Technology, pp. 3–17 (1996)

A Kernel Method for Measuring Structural Similarity Between XML Documents

Buhwan Jeong[1], Daewon Lee[1], Hyunbo Cho[1], and Boonserm Kulvatunyou[2]

[1] Department of Industrial and Management Engineering,
Pohang University of Science and Technology (POSTECH),
San 31, Hyoja, Pohang, 790-784, South Korea
{bjeong,woosuhan,hcho}@postech.ac.kr
[2] Manufacturing Engineering Laboratory,
National Institute of Standards and Technology (NIST),
100 Bureau Dr., Gaithersburg, MD, 20899
serm@nist.gov

Abstract. Measuring structural similarity between XML documents has become a key component in various applications, including XML data mining, schema matching, web service discovery, among others. The paper presents a novel structural similarity measure between XML documents using kernel methods. Results on preliminary simulations show that this outperforms conventional ones.

Keywords: Information compatibility analysis, kernel methods, schema matching, string kernel, structural similarity, XML mining.

1 Introduction

Nowadays, XML has been rooted as the standard means to express enterprise data and exchange the data among enterprise applications. Along with its explosive use, it has several bothersome obstacles including profusion, redundancy, and reproduction of similar information contents in differing way. Proper manipulation of XML content has become a main research issue both in academia and in industry. Two of the main issues of interest in this paper involve XML formalisms [1] [2] [3] and a variety of similarity measures [1] [3] [4] [5] [6]. Most of those measures focus primarily on the semantic/linguistic similarity between data items; in this paper, however, we focus on a novel measure of structural similarity.

This paper proposes a novel structural similarity measure for comparison of XML documents. We base this measure on well-known kernel methods for structured data. We first introduce an interface representation to capture the structure of an XML document, and then deploy the kernel methods to manipulate that representation. We use this approach to compute measures for two examples: OAGIS Core Components and ACMSIGMOD Records.

The rest of the paper is organized as follows: Section 2 illustrates a motivating example, in which software components are replaced based on the semantic similarity between information models. Section 3 describes our use of kernel methods to compute the structural similarity between XML documents. Section 4 includes preliminary simulation results, and Section 5 provides our concluding remarks.

H.G. Okuno and M. Ali (Eds.): IEA/AIE 2007, LNAI 4570, pp. 572–581, 2007.

2 Motivating Example: Component Replacement and Selection

Consider the following common example. A company decides to replace a software component that is integrated with other components in the enterprise. This decision may arise because the original component provider goes out of business, ceases to support that particular version of the software, or introduces a newer version that is deemed to be more powerful. It may also arise when another version has better or less expensive alternative. In either case, the principal problem is to determine if the new component is compatible with the functionality of and is easily integrated with the other existing component(s).

To find the answer to this problem, an IT manager must perform an information compatibility analysis. This analysis is complicated because, as noted above, this replacement must meet both functional and connectivity requirements. Fig. 1 illustrates this situation with some particular software components. Suppose that the company has an Inventory Visibility (IV) system that is already integrated with its ERP system. An IV system consists of a processing module and web client interfaces. The system allows for the customer to share inventory information with suppliers. They both can visualize and manage inventory levels based on a specific inventory policy from the web clients [7].

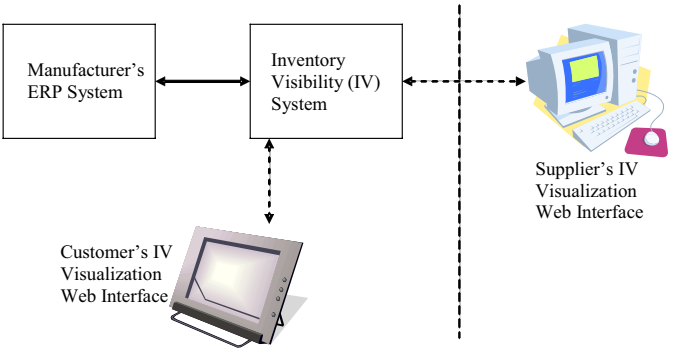

Fig. 1. A software component connectivity scenario

Since the ERP typically does not provide these capabilities, it is common for the ERP and the IV system to be separate software components provided by different software vendors. Therefore, an integration interface exists between the ERP and the IV systems as indicated by the bold-solid arrow connection in Fig. 1 This also implies that a mapping between the corresponding information models exists. Fig. 2 shows part of such a mapping. The most desirable software replacement should have an information model compatible with (or similar to) those in the IV system as well as in the ERP.

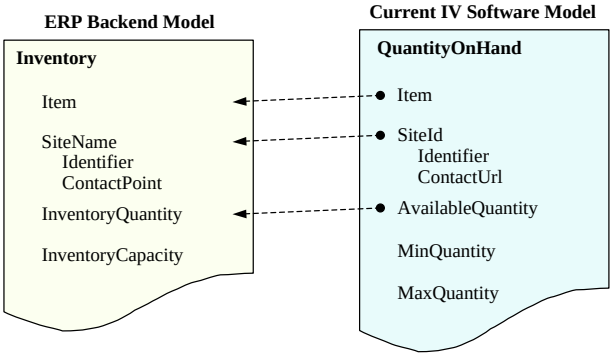

Fig. 2. An exemplary mapping of data between the ERP and the IV system

3 Kernel-Based Measurement of XML Structural Similarity

Our approach to computing structural similarity between XML documents using the kernel method has two steps. First, we transform the tree-structured XML documents into normalized plain documents. Then, we apply the word sequence kernel to the normalized documents to compute the structural similarity. We discuss these two steps in the following subsections after succinct introduction to string kernels.

3.1 String Kernel

Kernel methods, such as support vector machines, construct non-linear algorithms by mapping samples in original space $\mathcal{X}$ into those in a higher-dimensional Hilbert space $\mathcal{H}$. However, they have a computational explosion for large-scale problems [8]. Fortunately, the so-called *kernel trick* resolves it by getting the scalar product implicitly computed in $\mathcal{H}$ when an algorithm solely depends on the inner product between vectors. Recent kernel methods for structured data employ this kernel trick to incorporate types of data other than numerical and vector data. In particular, we introduce the string subsequence kernel dealing with string data. The following definition is critical to our application to computing structural similarity.

Definition 1 (String Subsequence Kernel [10]). *Let Σ be a finite alphabet. A string is a finite sequence of characters from Σ, including the empty sequence. For string s and t, we denote by $|s|$ the length of the string $s = s_1...s_{|s|}$, and by st the string obtained by concatenating them. The string $s[i:j]$ is the substring $s_i...s_j$ of s. We say that u is a subsequence of s, if there exist indices $\mathbf{i} = (i_1, ..., i_{|u|})$, with $1 \leq i_1 < ... < i_{|u|} \leq |s|$, such that $u_j = s_{i_j}$, for $j = 1, ..., |u|$, or $u = s[\mathbf{i}]$ for short. The length $l(\mathbf{i})$ of the subsequence in s is $i_{|u|} - i_1 + 1$. We denote by Σ^n the set of all finite strings of length n, and by Σ^* the set of all strings, i.e., $\Sigma^* = \bigcup_{n=0}^{\infty} \Sigma^n$. We now define feature spaces $F_n = \mathbb{R}^{\Sigma^n}$. The feature mapping ϕ for a string s is given by defining the u coordinate $\phi_u(s)$ for each $u \in \Sigma^n$. We define $\phi_u(s) = \sum_{\mathbf{i}:u=s[\mathbf{i}]} \lambda^{l(\mathbf{i})}$, for some $\lambda \leq 1$. These features measure the number of occurrences of subsequences in the string s weighting them according to their length. Hence, the inner product of the feature vectors for two*

string s and t gives a sum over all common subsequences weighted according to their frequency of occurrence and lengths

$$K_n(s,t) = \sum_{u \in \Sigma^n} \langle \phi_u(s) \cdot \phi_u(t) \rangle = \sum_{u \in \Sigma^n} \sum_{\mathbf{i}: u = s[\mathbf{i}]} \sum_{\mathbf{j}: u = t[\mathbf{j}]} \lambda^{l(\mathbf{i}) + l(\mathbf{j})}. \quad (1)$$

Since a direct computation of these features would involve $\mathcal{O}(|\Sigma|^n)$ time and space, a recursive computation in $\mathcal{O}(n|s||t|)$ is provided in [10]. The $K(s,t)$, i.e., the inner product of the feature vectors, is defined as the similarity between the strings s and t [11]. In addition, an extension to the basic string kernel is found in [12] [13], where the characters are replaced with words or syllables – **word sequence kernel** – as well as soft matching is allowed. This extension yields a significant improvement in computation efficiency for large documents.

Furthermore, one of the most critical factors to determine kernels' performance is the choice of the decay factor λ. Compared with the original string kernel, which uses the same λ for every character, [12] introduces a different λ-weighting strategy that assigns a different weight (λ_c) to each character ($c \in \Sigma$). The weighted string kernel K^w of two strings s and t is defined as

$$K_n^w(s,t) = \sum_{u \in \Sigma^n} \langle \phi_u^w(s) \cdot \phi_u^w(t) \rangle = \sum_{u \in \Sigma^n} \sum_{\mathbf{i}: u = s[\mathbf{i}]} \sum_{\mathbf{j}: u = t[\mathbf{j}]} \prod_{k=i_1}^{i_{|\mathbf{i}|}} \prod_{l=j_1}^{j_{|\mathbf{j}|}} \lambda_{s_k} \lambda_{t_l}. \quad (2)$$

The evaluation of K^w can be computed recursively using a technique similar to the one used in the original string kernel [12]. The use of different decay factors is one way of incorporating prior knowledge, such as synonymous relation between words, into the string kernel. We discuss the determination of weights for XML document structure later in the paper (in Section 3.3).

3.2 Transformation of XML Tree Structure into a Normalized Document

Recall that an XML document, both XML schema and XML instance, can be represented in a tree structure, which provides a computational representation to deal with intended semantics of an XML document. That is, an upper node represents a more general and contextual meaning than its descendant nodes; whereas, leaf nodes often capture the most specific atomic data that the XML document ultimately describes and are treated as semantically more important. Therefore, the normalized representation should explicitly retain node orders – parent-to-child and left-to-right order, for example. Here, we adopt the representation in a sequence of node labels ordered by a depth-first traversal. This representation satisfies the ordering requirement. The construction procedure is made up of abstraction, serialization, and normalization, as shown in Fig. 3.

The first step is the abstraction that makes a specific document structure of an XML schema (and pseudo XML instance). This step is necessary only when considering (comparing) XML schemas and not needed when considering XML instances. The step allows for the creation of a concrete/finite path structure for an XML schema (e.g., to deal with the indefinite max cardinality). The abstract tree is the most fundamental but expressive (labeled) tree capturing the common structural information among various

(A) XML Schema document

```
<xsd:element name="QuantityOnHand" type="QuantityOnHandType" />
<xsd:complexType name="QuantityOnHandType">
  <xsd:sequence>
    <xsd:element ref="Item" />
    <xsd:element ref="SiteId" minOccurs="0"/>
    <xsd:element ref="AvailableQuantity" />
    …
  </xsd:sequence>
</xsd:complexType>
<xsd:element name="SiteId" type="SiteIdType" />
…
```

(B) Abstraction

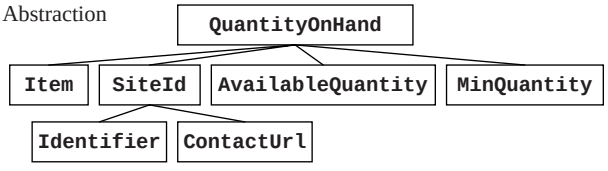

(C) Serialization

QuantityOnHand Item SiteId Identifier ContactUrl AvailableQuantity …

(D) Normalization

Quantity Hand Item Site Identifier Identifier Contact Universal …

Fig. 3. Transformation of an XML document into a normalized document

instances derived from the same schema. A fundamental property of the resulting tree is that it disallows inclusive/duplicate structures. This means that each path is exclusive, i.e., a sequence of element/attribute names from the root node to a leaf node[1] does not contain other paths. Another property is that the tree is expressive. That is any contents in an XML instance must be reachable by the resulting tree. This means that the abstract tree is a collection of the longest (or most general) paths between the root and the leaf nodes. For more on this process, see [14].

In the second step, the serialization transforms the abstract tree representation into a sequence of words. This serialization process is the key idea to manipulating the XML's tree structure because it enables us to apply the word sequence kernel without any modification. We visit every node by a depth-first traversal of the tree producing a long sentence, which is a sequence of node labels from the root node to the rightmost leaf node.

In the last step, the normalization process deals with the problems that each word is often a compound word comprised of several individual terms – for example, *QuantityOnHand* and *InventoryQuantity* in Fig. 2. The normalization process recursively consists of (1) tokenization, which separates a compound word into atomic dictionary words; (2) lemmatization, which analyzes these words morphologically in order to find all their possible basic forms; (3) elimination, which discards meaningless stop words such as article, preposition, and conjunction; and, (4) stemming, which finds a stem form of a given inflected word [14] [15].

Take the *QuantityOnHand* schema document in Fig. 2, for example, The serialization process yields {*QuantityOnHand*, *Item*, *SiteId*, *Identifier*, *ContactUrl*, *Available-*

[1] A leaf node can be either an element or an attribute, while intermediate nodes must be elements.

Quantity, *MinQuantity*, *MaxQuantity*}. The normalization process yields {*Quantity*, *Hand*, *Item*, *Site*, *Identifier*, *Identifier*, *Contact*, *Universal*, *Resource*, *Locator*, *Available*, *Quantity*, *Minimum*, *Quantity*, *Maximum*, *Quantity*}. Note, the elimination procedures removes the preposition *On* from *QuantityOnHand*; the lemmatization process changes *Id* into *Identifier* and *Url* into *Universal*, *Resource*, and *Locator*.

3.3 Applying Word Sequence Kernel to Measure Structural Similarity

We compute structural similarity measures only for normalized documents. For two XML documents d_1 and d_2 and a kernel function K, we define their structural similarity as $Sim(d_1, d_2) = K(s_1, s_2)$, where s_1 and s_2 are their respective normalized strings. We use a modified word-sequence kernel that reads a pair of strings, generates two feature vectors, and then calculates their inner product $\langle \cdot, \cdot \rangle$. The final inner product is the structural similarity.

As noted above, we use equation (2) with different weights assignments. That is, we assign different decay factor λ to different nodes. To make this assignment, we introduce a depth-dependent decay factor $\lambda_n = \lambda_0 / depth(n)^r$, where $depth(n)$ is the depth of the node n ($depth(root) = 1$) and $r \geq 1$ is a relevant factor. Since, as shown in the example below, the size of inputs, length of strings, is usually not a constant, the kernel value is sometimes normalized to [0, 1] by $\hat{K}(s,t) = K(s,t)/\sqrt{K(s,s) \cdot K(t,t)}$, $\hat{K}(s,t) = 1$ if and only if strings s and t are identical.

Take an illustrative example to compute the structural similarity between *Inventory* and *QuantityOnHand* (in Fig. 2 above). For simplicity, we use following symbols to each word in the normalized documents: A(vailable), C(ontact), H(and), I(dentifier), L(ocator), M(inimum), N(ame), P(oint), Q(uantity), R(esource), S(ite), T(Item), U(niversal), V(Inventory), X(Maximum), Y(Capacity). After normalized document transformation, we get the string 'VTSNICPVQVY' for the *Inventory* document and the string 'QHTSIICURLAQMQXQ' for the *QuantityOnHand* document. The common subsequences are {C, $I^{(2)}$, $Q^{(4)}$, S, T, $CQ^{(3)}$, $IC^{(2)}$, ..., $TSICQ^{(6)}$}. Note that numbers in parentheses indicate the number of possible occurrences. Accordingly, as detailed in Fig. 4, their similarity is easily computed via equation (2) as $K^w \simeq 2.1399$ and $K^w \simeq 0.6149$ with respect to $r = 1$ and $r = 2$, and $\lambda_0 = 1$, whereas computed via equation (1) with with $\lambda = 0.5$ yields $K = 2.3699$.

4 Preliminary Experiments

To evaluate the proposed method, we performed experiments with XML schema documents from OAGIS[2]. We designed two types of experiments. The first experiment is to show the correlation between the proposed method and the human's similarity scoring; the other is to verify that the proposed measures could discriminate relevant information from irrelevant information from the information retrieval perspective.

[2] The OAGIS BOD (Business Object Document) schemas are open and standard specifications for supporting interoperable data exchange by providing enterprise/domain-neutral data structures and definitions. http://www.openapplications.org

(A) Input strings s = 'VTSNICPVQVY', t = 'QHTSIICUAQMQXQ' and r = 1

Sequence	C	I	Q	S	T	CQ	…	TSICQ
s	1/3	1/3	1/2	1/2	1/2	1/36		…
t	1/3	1/2+1/3	1+3×1/2	1/2	1/2	1/36+1/144+1/576		…
Product	0.1111	0.2778	1.2500	0.25	0.25	0.001		0.0000
								$K^w(s, t) = 2.1399$

(B) Input strings s = 'VTSNICPVQVY', t = 'QHTSIICUAQMQXQ' and r = 2

Sequence	C	I	Q	S	T	CQ	…	TSICQ
s	1/9	1/9	1/4	1/4	1/4	1/1296		…
t	1/9	1/4+1/9	1+3×1/4	1/4	1/4	…		…
Product	0.0123	0.0401	0.4375	0.0625	0.0625	0.0000		0.0000
								$K^w(s, t) = 0.6149$

Fig. 4. Exemplary structural similarity computation using the proposed kernel method with relevant factor $r = 1$ and $r = 2$

For the first experiment, we randomly selected 200 pairs of CC's (Core Components) and let four human experts (based on their own domain and linguistic knowledge) score every pair to assign their degree of relatedness in [0, 1]. We implemented four algorithms – TED (Tree Edit Distance)[3]; VSM by means of cosine of the angle [9]; kernels both with a fixed penalty (i.e., $\lambda_n = c$) and with a variant penalty (i.e., $\lambda_n = f(\lambda_0, depth(n), r)$). The experimental result is depicted in Fig. 5 in terms of correlation with the operators' average score. 'Kern.1' and 'Kern.2' implemented a fixed weighting scheme with $\lambda = 1$ and $1/2$, respectively. 'Kern.3' and 'Kern.4' implemented a variable weighting scheme ($\lambda_0 = 1$) with relevant factors $r = 1$ and 2, respectively.

As shown in the figure, the kernel methods outperform the conventional measures, TED and VSM. Although VSM is a special type of the kernel method, the proposed ones give better performance because they preserve the parent-child relationship between elements in XML documents. In other words, the bag-of-words model, VSM, gives the same importance between, for example, the root node and a leaf node. It is also noted that the proposed depth-depedent λ-weighting gives a more accurate measure than the fixed one does.

The second experiment was a mapping test that evaluates whether mappings established by an algorithm are correct compared with true mappings. We configured four experiment sets, each of which consists of two data sets having 10 CC's and 20 CC's. Between the two data sets, an algorithm and human operators selected no more than 10 plausible mappings[4]. Then, we compared the selections using three widely used information retrieval performance metrics: Precision, Recall, and F-Meausre. Let $\mathbf{A}$ be a set of alignments mapped by an algorithm, and $\mathbf{T}$ be a set of true mappings by human

[3] A state-of-the-art similarity measure for tree structures [4] [16].

[4] The human selections are treated as true mapping; the algorithm selection are treated as test mappings.

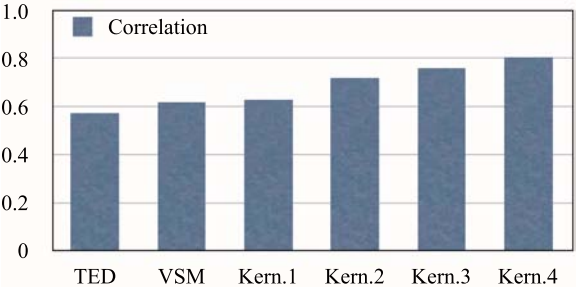

Fig. 5. Correlation between human judgment and various structural similarity measures – TED (Tree Edit Distance), VSM with cosine of the angle $\cos\theta$, and Kernel-based measures (i.e., $\lambda = 1$, $\lambda = 0.5$, $\lambda_0 = 1$ & $r = 1$, and $\lambda_0 = 1$ & $r = 2$, respectively)

experts. Then the metrics are defined as follows: $Precision = |\mathbf{A} \bigcap \mathbf{T}|/|\mathbf{A}|$, $Recall = |\mathbf{A} \bigcap \mathbf{T}|/|\mathbf{T}|$, and $F-Measure = 2 \times Precision \times Recall/(Precision + Recall)$. The experimental results are depicted in Fig. 6. Same as the first experiment, the kernel-based measures give better performance than TED- and VSM-based ones do.

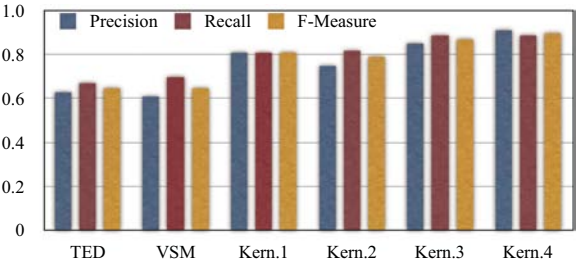

Fig. 6. Precision, Recall and F-measure

We conducted additional experiments with XML instance documents from ACM-SIGMOD Records[5]. We prepared two groups of XML instances. Each group had 50 documents randomly selected, but conforming to the same DTD (Document Type Definition). The two DTD's shared several common element definitions (e.g., *author*, *title*). Confirming to the same DTD apparently means its instances are structurally similar. We tried to discriminate the documents using the PAM (Partitioning Around Medoids) algorithm [17] with ten replications. The clustering results are depicted in Table 1, in which the low structural diversity among documents, particularly in the second group, makes them well-separated, except TED. Another implication from the result is the normalized document representation is a simple yet effective means to express XML's tree structure. It should be noted that the experiment does not care about contents of those

[5] http://www.sigmod.org/record/xml

Table 1. Clustering results for ACMSIGMOD Record: A comparison matrix

Methods		TED		VSM		Kern.1		Kern.2	
		C_1	C_2	C_1	C_2	C_1	C_2	C_1	C_2
Real	C_1	34	16	50	0	50	0	50	0
	C_2	1	49	0	50	0	50	0	50

documents, but their structure only. For all that, the proposed kernel-based measures require a significant modification to reduce computation time for large datasets.

5 Conclusion

The paper presented a novel approach to compute the structural similarity between XML documents by incorporating a modified string kernel. To apply the proposed kernel methods to XML documents, we proposed normalized document representation for XML document structure and a λ-weighted word sequence kernel for structural similarity computation. The experimental results showed that the proposed kernel-based measure outperforms state-of-the-art approaches (i.e., TED and VSM). In particular, the kernel-based measure can help web services to be properly discovered, selected, and composed when those activities are performed based on the message type. Moreover, we also expect that the result of this research will improve significantly the performance of XML-based applications such as XML document clustering and classification, schema matching, XML message mapping, ontology reconciliation.

Disclaimer
Certain commercial software products are identified in this paper. These products were used only for demonstration purposes. This use does not imply approval or endorsement by NIST, nor does it imply that these products are necessarily the best available for the purpose.

References

1. Flesca, S., Manco, G., Masciari, E., Pontieri, L., Pugliese, A.: Fast detection of XML structural similarity. IEEE Transactions on Knowledge and Data Engineering 17(2) (February 2005)
2. Yang, J., Cheung, W., Chen, X.: Learning the kernel matrix for XML document clustering. In: Proceedings of the 2005 IEEE International Conference on e-Technology, e-Commerce and e-Service (EEE'05), Washington, DC, pp. 353–358. IEEE Computer Society Press, Los Alamitos (2005)
3. Lee, J., Lee, K., Kim, W.: Preparations for semantics-based XML mining. In: Proceedings of IEEE International Conference on Data Mining (ICDM 2001), pp. 345–352 (2001)
4. Nierman, A., Jagadish, H.: Evaluating structural similarity in XML documents. In: Proceedings of the 5th International Workshop on the Web and Database (WebDB2002) (2002)

5. Shvaiko, P., Euzenat, J.: A survey of scham-based matching. Journal of Data Semantics IV 3730, 14–171 (2005)
6. Jeong, B., Kulvatunyou, B., Ivezic, N., Cho, H., Jones, A.: Enhance reuse of standard e-business XML schema documents. In: Proceedings of International Workshop on Contexts and Ontology: Theory, Practice and Application (C&O'05) in the 20th National Conference on Artificial Intelligence (AAAI'05) (2005)
7. Ivezic, N., Kulvatunyou, B., Frechette, S., Jones, A., Cho, H., Jeong, B.: An interoperability testing study: Automotive inventory visibility and interoperability. In: Proceedings of e-Challenges (2004)
8. Muller, K., Mika, S., Ratsch, G., Tsuda, K., Schölkopf, B.: An introduction to kernel-based learning algorithms. IEEE Transactions on Neural Networks 12(2), 181–201 (2001)
9. Kobayashi, M., Aono, M.: Vector Space Models for Search and Cluster Mining, pp. 103–122. Springer, New York (2003)
10. Lodhi, H., Saunders, C., Shawe-Taylor, J., Cristianini, N., Watkins, C.: Text classification using string kernels. Journal of Machine Learning Research 2, 419–444 (2002)
11. Vert, J., Tsuda, K., Schölkopf, B.: A Primer on Kernel Methods, pp. 35–70. MIT Press, Cambridge (2004)
12. Saunders, C., Tschach, H., Shawe-Taylor, J.: Syllables and other string kernel extensions. In: Proceedings of the 19th International Conference on Machine Learning (ICML'02) (2002)
13. Cancedda, N., Gaussier, E., Goutte, C., Renders, J.: Word-sequence kernels. Journal of Machine Learning Research 3, 1059–1082 (2003)
14. Jeong, B.: Machine Learning-based Semantic Similarity Measures to Assist Discovery and Reuse of Data Exchange XML Schemas. PhD thesis, Department of Industrial and Management Engineering, Pohang University of Science and Technology (2006)
15. Willett, P.: The porter stemming algorithm: Then and now. Electronic Library and Information Systems 40(3), 219–223 (2006)
16. Zhang, Z., Li, R., Cao, S., Zhu, Y.: Similarity metric for XML documents. In: Proceedings of Workshop on Knowledge and Experience Management (FGWM2003) (2003)
17. Reynolds, A., Richards, G., Rayward-Smith, V.: The application of k-medoids and PAM to the clustering of rules. In: Yang, Z.R., Yin, H., Everson, R.M. (eds.) IDEAL 2004. LNCS, vol. 3177, pp. 173–178. Springer, Heidelberg (2004)

A Neural Network Based Data Least Squares Algorithm for Channel Equalization

Jun-Seok Lim

Dept. of Electronics Eng., Sejong University,
Kunja, Kwangjin, 98,143-747, Seoul, Korea
jslim@sejong.ac.kr

Abstract. Using the neural network model for oriented principal component analysis (OPCA), we propose a solution to the data least squares (DLS) problem, in which the error is assumed to lie in the data matrix only. In this paper, We applied this neural network model to channel equalization. Simulations show that DLS outperforms ordinary least squares in channel equalization problems.

1 Introduction

Many different kinds of engineering problems can be modelled using least squares problems. In [1], least squares problems are well categorized. Linear least squares (LS) problems involve finding "good" approximate solutions to a set of independent, but inconsistent, linear equations

$$\mathbf{A}\ \mathbf{x} = \mathbf{b}, \tag{1}$$

where $\mathbf{A}$ is an $m \times n$ complex data matrix; $\mathbf{b}$ is a complex $m \times 1$ observation vector; and $\mathbf{x}$ is a complex $n \times 1$ prediction vector, which is optimally chosen to minimize some kind of squared error measure. It is usually assumed that the underlying noiseless data satisfy (1) with equality. Different classes of LS problems can be defined in terms of the type of perturbation necessary to achieve equality in the system of equations described by (1). For example, in the ordinary least squares (OLS) problem, the error (or perturbation) is assumed to lie in $\mathbf{b}$.

$$\mathbf{A}\mathbf{x}_{OLS} = (\mathbf{b} + \mathbf{r}), \tag{2}$$

where $\mathbf{r}$ is the residual error vector that corresponds to a perturbation in $\mathbf{b}$. The OLS solution vector $\mathbf{x}_{OLS}$ is chosen so that the Euclidean (or Frobenius) norm of $\mathbf{r}$ is minimized. It is implicitly assumed in the OLS problem that $\mathbf{A}$ is completely errorless, and therefore the columns of $\mathbf{A}$ are not perturbed in the solution [2]. On the other hand, the total least squares (TLS) problem assumes error in both $\mathbf{A}$ and $\mathbf{b}$.

$$(\mathbf{A} + \mathbf{E})\mathbf{x}_{TLS} = (\mathbf{b} + \mathbf{r}). \tag{3}$$

The TLS solution vector is chosen so that the Euclidean norm of $[\mathbf{E}\ \mathbf{r}]$ is minimal. Another interesting case described and solved in [1] assumes that errors occur in

H.G. Okuno and M. Ali (Eds.): IEA/AIE 2007, LNAI 4570, pp. 582–590, 2007.

A but not in **b.** We call this case the data least squares (DLS) problem because the error is assumed to lie in the data matrix **A** as indicated by

$$(\mathbf{A} + \mathbf{E})\mathbf{x}_{DLS} = \mathbf{b}. \tag{4}$$

DeGroat, et al. [1] developed a closed form solution to (4) and demonstrated that it outperformed OLS and TLS in the case of a noisy data matrix. However, the solution is a kind of batch type algorithm.

In this paper, we propose a neural network model for DLS solution with a neural network model for oriented principal component analysis (OPCA). We applied this neural network model to channel equalization. Simulations for the performance comparison show that the proposed DLS network outperforms ordinary least squares in symbol error rate (SER).

2 Generalized Total Least Square Problem

Given an unknown system with finite impulse response and assuming that both the input and output are corrupted by Gaussian white noise, the system should be estimated from the noisy observation of the input and output, as shown in Fig.1. The unknown system is described by

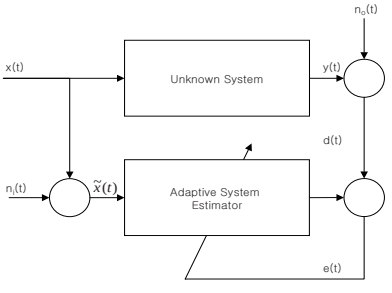

Fig. 1. Model of generalized total least squares

$$\mathbf{h} = [h_0, h_1, \cdots, h_{N-1}]^H \in \mathrm{C}^{N\times 1}, \tag{5}$$

where **h** may be time-varying or time-invariant. The output is given by

$$d(n) = \mathbf{x}^H(n)\mathbf{h} + n_o(n), \tag{6}$$

where the output noise $n_o(n)$ is Gaussian white noise with variance σ_o^2 and is independent of the input signal, and the noise-free input vector is represented as

$$\mathbf{x}(n) = [x(n), x(n-1), \cdots x(n-N+1)]^T. \tag{7}$$

The noisy input vector of the system is given by

$$\tilde{\mathbf{x}}(n) = \mathbf{x}(n) + \mathbf{n}_i(n) \in C^{N\times 1}, \tag{8}$$

where $\mathbf{n}_i(n) = [n_i(n), n_i(n-1), \cdots n_i(n-N+1)]^T$and the input noise $\mathrm{n}_i(n)$ is Gaussian white noise with variance σ_i^2. Notice that the input noise may originate from the measured error, interference, quantized noise and so on. Hence, we adopt a more general signal model than the least squares-based estimation. Moreover, the augmented data vector is defined as

$$\overline{\mathbf{x}}(n) = \left[\tilde{\mathbf{x}}^T(n), d(n)\right]^T \in \mathrm{C}^{(N+1)\times 1}. \tag{9}$$

The correlation matrix of the augmented data vector has the following structure

$$\overline{\mathbf{R}} = \begin{bmatrix} \tilde{\mathbf{R}} & \mathbf{p} \\ \mathbf{p}^H & c \end{bmatrix}, \tag{10}$$

where $\mathbf{p} = E\left\{\tilde{\mathbf{x}}(n)d^*(n)\right\}$, $c = E\left\{d(n)d^*(n)\right\}$, $\tilde{\mathbf{R}} = E\left\{\tilde{\mathbf{x}}(n)\tilde{\mathbf{x}}^H(n)\right\} = \mathbf{R} + \sigma_i^2\mathbf{I}$, and $\mathbf{R} = E\left\{\mathbf{x}(n)\mathbf{x}^H(n)\right\}$. We can further establish that $\mathbf{p} = \mathbf{R}^H\mathbf{h}$ and $c = \mathbf{h}^H\tilde{\mathbf{R}}\mathbf{h} + \sigma_o^2$. The constrained Rayleigh quotient is defined as

$$J(\mathbf{w}) = \frac{[\mathbf{w}^T, -1]\overline{\mathbf{R}}[\mathbf{w}^T, -1]^H}{[\mathbf{w}^T, -1]\overline{\mathbf{D}}[\mathbf{w}^T, -1]^H}, \tag{11}$$

where $\overline{\mathbf{D}} = \begin{bmatrix} \mathbf{I} & \mathbf{0} \\ \mathbf{0} & \gamma \end{bmatrix}$ with $\gamma = \frac{\sigma_o^2}{\sigma_i^2}$[3]. The generalized total least squares solution is obtained by solving

$$\min_{\mathbf{w}} J(\mathbf{w}). \tag{12}$$

DLS is a special case in (11) with γ=0 [3].

3 Oriented PCA

In this section, we extend the standard principal component analysis problem by introducing OPCA [4] which corresponds to the generalized eigenvalue problem of two random signals and bears the same relationship to generalized eigenvalue decomposition (GED) as PCA bears to ordinary eigenvalue decomposition (ED). More precisely, the goal is to find the direction vector w that maximizes the signal-to-signal ratio

$$J_{OPC} = \frac{E\{(\tilde{\mathbf{w}}^H\mathbf{x}_1)^2\}}{E\{(\tilde{\mathbf{w}}^H\mathbf{x}_2)^2\}} = \frac{\tilde{\mathbf{w}}^H\mathbf{R}_1\tilde{\mathbf{w}}}{\tilde{\mathbf{w}}^H\mathbf{R}_2\tilde{\mathbf{w}}} \tag{13}$$

where $\mathbf{R}_1 = E\{\mathbf{x}_1\mathbf{x}_1^H\}$ and $\mathbf{R}_2 = E\{\mathbf{x}_2\mathbf{x}_2^H\}$. We assume that $\mathbf{R}_2$ is strictly positive definite, hence nonsingular. Quite often, $\{\mathbf{x}_{1k}\}$ and $\{\ \mathbf{x}_{2k}\ \}$ are stationary stochastic processes, where $\mathbf{R}_1 = E\{\mathbf{x}_{1k}\mathbf{x}_{1k}^H\}$ and $\mathbf{R}_2 = E\{\mathbf{x}_{2k}\mathbf{x}_{2k}^H\}$ and OPCA is still defined by (13). As usual, there is little difference between random vectors

and stationary random processes, and hence the term OPCA is used for both cases interchangeably.

The optimal solution to (13) will be called the principal oriented component of the pair $(\mathbf{x}_1, \mathbf{x}_2)$. The adjective "oriented" is justified by the fact that the principal component of $\mathbf{x}_1$ is now steered by the distribution of $\mathbf{x}_2$. J_{opc} is nothing but the generalized Rayleigh quotient for the matrix pencil $(\mathbf{R}_1, \mathbf{R}_2)$, so the principal oriented component is the principal generalized eigenvector of the symmetric generalized eigenvalue problem [5].

$$\mathbf{R}_1\tilde{\mathbf{w}} = \lambda\mathbf{R}_2\tilde{\mathbf{w}}. \tag{14}$$

4 Network Models for OPC Extraction

We initially focus on the extraction of the first component as in [4]. The maximum value of J_{opc} in (13) is the principal generalized eigenvalue λ_1. Therefore, the function

$$V(\tilde{\mathbf{w}}) = \frac{1}{2}(\lambda_1 - J_{OPC}(\tilde{\mathbf{w}})) \tag{15}$$

is such that $V(\tilde{\mathbf{w}}) > 0$, and $V(\tilde{\mathbf{w}}) = 0$ only for $\tilde{\mathbf{w}} = \mathbf{e}_1$, so $V(\tilde{\mathbf{w}})$ may serve as a Lyapunov energy function for a system to be proposed. The proper gradient descent algorithm would be

$$\frac{d\tilde{\mathbf{w}}}{dt} = -\nabla V = \frac{1}{\tilde{\mathbf{w}}^H\mathbf{R}_2\tilde{\mathbf{w}}}\left(\mathbf{R}_1\tilde{\mathbf{w}} - \frac{\tilde{\mathbf{w}}^H\mathbf{R}_1\tilde{\mathbf{w}}}{\tilde{\mathbf{w}}^H\mathbf{R}_2\tilde{\mathbf{w}}}\mathbf{R}_2\tilde{\mathbf{w}}\right) \tag{16}$$

with the globally asymptotically stable fixed point $\tilde{\mathbf{w}} = \mathbf{e}_1$. In fact, even the simpler equation

$$\frac{d\tilde{\mathbf{w}}}{dt} = \left(\mathbf{R}_1\tilde{\mathbf{w}} - \frac{\tilde{\mathbf{w}}^H\mathbf{R}_1\tilde{\mathbf{w}}}{\tilde{\mathbf{w}}^H\mathbf{R}_2\tilde{\mathbf{w}}}\mathbf{R}_2\tilde{\mathbf{w}}\right) \tag{17}$$

is stable because

$$\frac{dV}{dt} = \frac{d\tilde{\mathbf{w}}^H}{dt}\nabla V = -\frac{1}{\tilde{\mathbf{w}}^H\mathbf{R}_2\tilde{\mathbf{w}}}\left\|\mathbf{R}_1\tilde{\mathbf{w}} - \frac{\tilde{\mathbf{w}}^H\mathbf{R}_1\tilde{\mathbf{w}}}{\tilde{\mathbf{w}}^H\mathbf{R}_2\tilde{\mathbf{w}}}\mathbf{R}_2\tilde{\mathbf{w}}\right\|^2 \leq 0 \tag{18}$$

and again the point $\tilde{\mathbf{w}} = \mathbf{e}_1$ is the globally asymptotically stable attractor.

5 Neural Network-Based Data Least Squares Algorithm

We can apply the neural network based method in section 4 to solve the DLS. If we modify (11) and (12), the object function for DLS becomes

$$\tilde{J}(\mathbf{w}) = \frac{\tilde{\mathbf{w}}^H\overline{\mathbf{D}}\tilde{\mathbf{w}}}{\tilde{\mathbf{w}}^H\overline{\mathbf{R}}\tilde{\mathbf{w}}} = \frac{[\mathbf{w}^H, -1]\overline{\mathbf{D}}[\mathbf{w}^T, -1]^T}{[\mathbf{w}^H, -1]\overline{\mathbf{R}}[\mathbf{w}^T, -1]^T}. \tag{19}$$

The DLS solution can be derived as (20). Applying the recursive algorithm in section III for the maximization of (19) yields,

$$\max_{\tilde{\mathbf{w}}} \tilde{J}(\tilde{\mathbf{w}}), \text{ and then } \mathbf{w} = \tilde{\mathbf{w}}(1:N)/(-\tilde{\mathbf{w}}(N+1)), \tag{20}$$

Table 1. OPCA based Data Least Squares (NN-DLS) Algorithm

1. Initialize λ_f,β,$\bar{\mathbf{x}}(0) = [\mathbf{x^T}(0),\ d(0)]$, $\tilde{\mathbf{w}}(0) = [\mathbf{w^T}(0),\ -1]$with the $\mathbf{w}(0) \in \mathrm{C}^{N\times 1}$ to a random vector
2. Fill the matrix $\mathbf{Q}(0) \in \mathrm{C}^{N\times N}$ with small random values
3. Initialize scalar variables $C(0)$ to zero
For j >0
4. Compute $z(j) = \tilde{\mathbf{w}}^H(j-1)\bar{\mathbf{x}}(j)$
5. Update $\mathbf{R_2}$ as
$\mathbf{R}_2(j) = \lambda_f \mathbf{R}_2(j-1) + \bar{\mathbf{x}}(j)\bar{\mathbf{x}}^H(j)$
6. Compute $\mathbf{z}_1(j) = \mathbf{R}_2(j)\tilde{\mathbf{w}}(j-1)$ and $z_2(j) = \tilde{\mathbf{w}}^H(j-1)\mathbf{z}_1(j)$
7.Update the weight vector as
$\tilde{\mathbf{w}}(j) = \tilde{\mathbf{w}}(j-1)+$
$\beta\left(z_2(j)\bar{\mathbf{D}}\tilde{\mathbf{w}}(j-1) - (\mathbf{w}^H(j-1)\mathbf{w}(j-1))\mathbf{z}_1(j)\bar{\mathbf{x}}(j)\right)$
8. Normalize the weight vector
9. $\mathbf{w}(j) = \tilde{\mathbf{w}}(1:n-1)/(-\tilde{\mathbf{w}}(n+1))$
loop

where $\tilde{\mathbf{w}}(1:N)$ is a vector with the elements from the *1-st* to the *N-th*, and $\tilde{\mathbf{w}}(N+1)$ is the *(N+1)-th* element in $\tilde{\mathbf{w}}$. When we apply the OPCA to (19), we have a update equation.

$$\Delta\tilde{\mathbf{w}} = \frac{1}{(\tilde{\mathbf{w}}^H\overline{\mathbf{R}}\tilde{\mathbf{w}})^2}\left((\tilde{\mathbf{w}}^H\overline{\mathbf{R}}\tilde{\mathbf{w}})\overline{\mathbf{D}}\tilde{\mathbf{w}} - (\tilde{\mathbf{w}}^H\overline{\mathbf{D}}\tilde{\mathbf{w}})\overline{\mathbf{R}}\tilde{\mathbf{w}}\right). \tag{21}$$

$$\tilde{\mathbf{w}}(n) = \tilde{\mathbf{w}}(n-1) + \tag{22}$$
$$\beta\left((\tilde{\mathbf{w}}^H(n-1)\overline{\mathbf{R}}(n)\tilde{\mathbf{w}}(n-1))\bar{\mathbf{D}}\tilde{\mathbf{w}}(n-1) - (\mathbf{w}^H(n-1)\mathbf{w}(n-1))\overline{\mathbf{R}}(n)\tilde{\mathbf{w}}(n-1)\right),$$

where $\overline{\mathbf{R}}(n) = \lambda_f\overline{\mathbf{D}}(n-1) + \bar{\mathbf{x}}(n)\bar{\mathbf{x}}^H(n)$ and λ_f is a forgetting factor. We summarize the algorithm in table 1.

If we cancel the estimation of the autocorrelation matrix, we can obtain a simpler update equation as follows.

$$\tilde{\mathbf{w}}(n) = \tilde{\mathbf{w}}(n-1)+\beta\left(z^2(n)\bar{\mathbf{D}}\tilde{\mathbf{w}}(n-1) - (\tilde{\mathbf{w}}^H(n-1)\tilde{\mathbf{w}}(n-1))z(n)\bar{\mathbf{x}}(n)\right), \tag{23}$$

where $z(n) = \tilde{\mathbf{w}}^H(n-1)\bar{\mathbf{x}}\,(n)$.

6 Analysis of Convergence

We will now investigate the convergence characteristics of the OPCA algorithm given by (22) using the stochastic approximation techniques developed by Rao [6], Ljung [7] and Kushner [8]. (22) is a special case of the generic stochastic approximation algorithm $\tilde{\mathbf{w}}(n+1) = \tilde{\mathbf{w}}(n) + \eta(n)h(\tilde{\mathbf{w}}(n), \bar{\mathbf{x}}(n))$. The asymptotical update function is given by

$$h(\tilde{\mathbf{w}}(n), \bar{\mathbf{x}}(n)) = \frac{\tilde{\mathbf{w}}(n+1) - \tilde{\mathbf{w}}(n)}{\eta}$$

$$= \frac{\tilde{\mathbf{w}}^H(n)\bar{\mathbf{R}}\tilde{\mathbf{w}}(n)}{\tilde{\mathbf{w}}^H(n)\bar{\mathbf{D}}\tilde{\mathbf{w}}(n)}\bar{\mathbf{R}}^{-1}\bar{\mathbf{D}}\tilde{\mathbf{w}}(n) - \tilde{\mathbf{w}}(n). \tag{24}$$

$$\rightarrow \frac{d\tilde{\mathbf{w}}(t)}{dt} = \frac{\tilde{\mathbf{w}}^H(t)\bar{\mathbf{R}}\tilde{\mathbf{w}}(t)}{\tilde{\mathbf{w}}^H(t)\bar{\mathbf{D}}\tilde{\mathbf{w}}(t)}\bar{\mathbf{R}}^{-1}\bar{\mathbf{D}}\tilde{\mathbf{w}}(t) - \tilde{\mathbf{w}}(t). \tag{25}$$

Let $\tilde{\mathbf{w}}(t)$ be expanded in terms of the complete set of m generalized eigenvectors of $(\bar{\mathbf{D}}, \bar{\mathbf{R}})$ as

$$\tilde{\mathbf{w}}(t) = \sum_{k=1}^{m} \theta_k(t)\mathbf{q}_k, \tag{26}$$

where $\theta_k(t)$ is a time-varying projection and $\mathbf{q}_k$ is the generalized eigenvector corresponding to the eignenvalue λ_k. Using this expansion, we can rewrite (25) as

$$\frac{d\theta_k(t)}{dt} = \frac{\sum_l^m \theta_l^2(t)}{\sum_l^m \lambda_l\theta_l^2(t)}\lambda_k\theta_k(t) - \theta_k(t). \tag{27}$$

With (27) and a new definition, $\alpha_k(t) = \theta_k(t)/\theta_1(t)$ for $1 < k \leq m$, we derive two more differential equations:

$$\alpha_k(t) = \frac{1}{\theta_1(t)}\frac{d\theta_k(t)}{dt} - \frac{\alpha_k(t)}{\theta_1(t)}\frac{d\theta_1(t)}{dt}. \tag{28}$$

$$\frac{d\alpha_k(t)}{dt} = -\alpha_k(t)\left[\frac{\sum_l^m \theta_l^2(t)}{\sum_l^m \lambda_l\theta_l^2(t)}\right]\{\lambda_1 - \lambda_k\}. \tag{29}$$

Note that $\sum_l^m \theta_l^2(t)/\sum_l^m \lambda_l\theta_l^2(t) > 0$ for all t. Therefore, it can be easily shown using Lyapunov stability theorems that, with $\lambda_1 > \lambda_2 > \cdots > \lambda_m > 0$, $\alpha_k(t) = 0$ as $t \rightarrow \infty$, $k > 1$ and hence $\tilde{\mathbf{w}}(t) = \pm c\mathbf{q}_1$, where c is an arbitrary constant. This means $\tilde{\mathbf{w}}(t)$ goes to the principal eigenvector asymptotically.

7 A Channel Equalization Application

In this section, we demonstrate the usefulness of the DLS-based neural network model by comparing it with the optimal and OLS methods in a channel equalization problem. The channel equalization problem is graphically described by the block diagram in Fig.2. Basically, the solution vector, $\mathbf{w} = [\mathrm{w}_1, \mathrm{w}_2, \ldots, \mathrm{w}_p]^T$ represents a finite impulse response (FIR) approximant inverse filter to the channel characteristic $H(z)$. The output of the inverse (equalization) filter can be written in matrix form using the output of the channel as input to the FIR equalization filter. The output of the equalized channel should be approximately equal to the original input

$$\begin{bmatrix} \tilde{s}_{p-1} \\ \tilde{s}_p \\ \vdots \\ \tilde{s}_{N-1} \end{bmatrix} = \begin{bmatrix} v_{p-1} & \cdots & v_1 & v_0 \\ v_p & \cdots & v_2 & v_1 \\ \vdots & \vdots & \vdots & \vdots \\ v_{N-1} & \cdots & v_{N-p+1} & v_{N-p} \end{bmatrix} \begin{bmatrix} w_1 \\ w_2 \\ \vdots \\ w_p \end{bmatrix} \approx \begin{bmatrix} s_{p-1} \\ s_p \\ \vdots \\ s_{N-1} \end{bmatrix}, \tag{30}$$

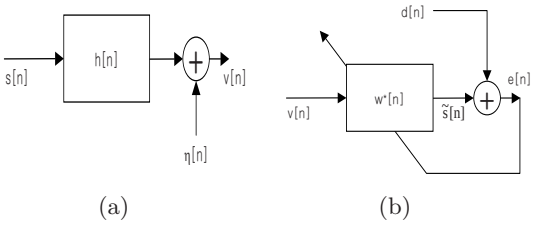

(a) (b)

Fig. 2. Transmission and equalization model: (a) received signal model, (b) equalizer model (s[n]:transmitted signal, h[n]: channel model, η[n]: additive noise, v[n]:received signal, d[n]:training signal)

where p is the FIR filter order and N is the total number of output samples. In this problem, we assume that the left side in (30) is known without error because the input training signal is assumed to be known without error. It is easy to see that (30) has the form of (4).

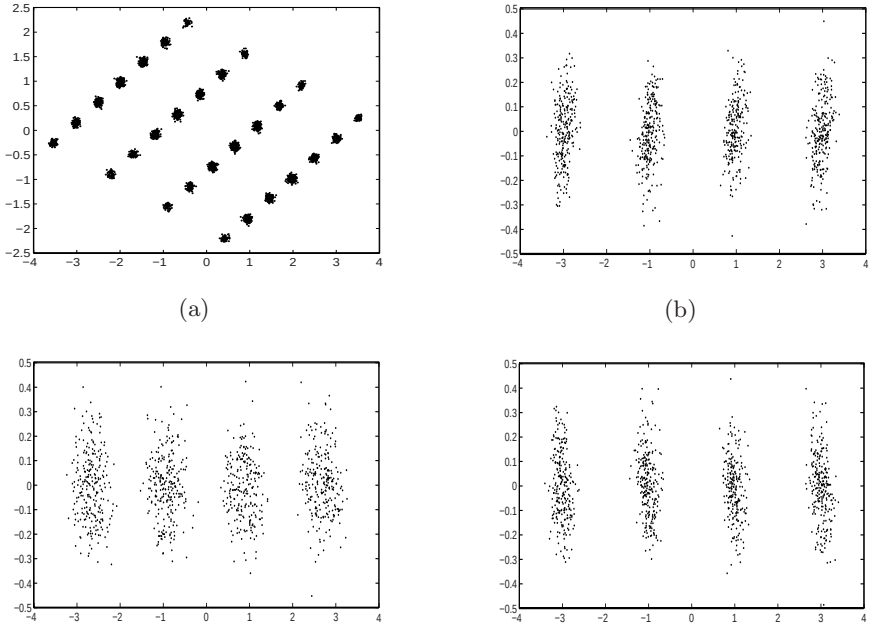

(a) (b)

(c) (d)

Fig. 3. Equalization results in 4-PAM signaling: (a) constellation of received signals (b) constellation of outputs of optimal equalizer (c) constellation of outputs of LMS equalizer (d) constellation of outputs of the proposed equalizer

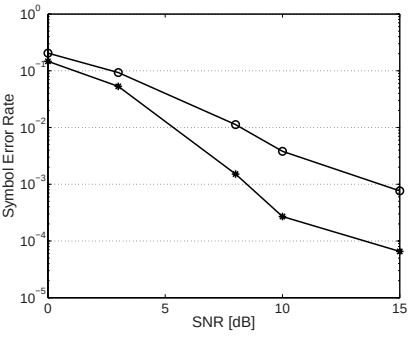

Fig. 4. SER comparison in 4-PAM signaling (-*-: the proposed algorithm, -o-: LMS algorithm

For the simulation, a well-known complex nonminimum-phase channel model introduced by Cha and Kassam [9] was used to evaluate the proposed neural network-based DLS equalizer performance for 4-PAM signaling. The channel output $v(n)$ (which is also the input of the equalizer) is given by

$$v(n) = (0.34 - j0.27)s(n) + (0.87 + j0.43)s(n-1) + (0.34 - j0.21)s(n-2) + \eta(n), \tag{31}$$

where $\eta(n)$ is white Gaussian noise. The 4-PAM symbol sequence $s(n)$ is passed through the channel, and the sequence $s(n)$ is valued from the set $\{\pm 1, \pm 3\}$. All the equalizers — the least mean square (LMS)-based equalizer and the proposed neural network-based equalizer — were trained with 1000 data symbols at 15 dB SNR. The LMS was adopted for an adaptive solution algorithm on the OLS problem. The order of equalizers was set to 7.

Fig. 3 (a) shows the distribution of the input data of the different equalizers. This figure shows received signals scattered severely due to transmission channel effects. Figures 3 (b), (c) and (d) show the scatter diagrams of the outputs of the three equalizers — optimal, LMS based, and the proposed, respectively. From these figures, we can see that the equalized signal from the proposed algorithm centers on $\{\pm 1, \pm 3\}$, and it is almost the same as the equalized signals by the optimal equalizer derived from the Wiener solution. On the contrary, the LMS-based equalizer produced more widely scattered outputs.

For the performance comparison, we show the symbol error rate (SER) for the proposed equalizer and an LMS-based equalizer. They were trained in several SNRs, from 0 dB to 20 dB. We set the step-size to 10^{-4} for both equalizers. Fig. 4 shows the SER in the above linear nonminmum phase channel with 4-PAM sequences. It shows that the proposed algorithm outperforms the LMS-based equalizer in the entire SNR range. Therefore, the proposed DLS algorithm outperforms the OLS algorithm.

8 Conclusion

In this paper, we proposed a neural network model for a data least squares (DLS) solution method. Channel equalization simulations were performed to compare the proposed algorithm with the algorithms in OLS, and we found the DLS performed better than OLS method.

References

1. DeGroat, R.D., Dowling, E.M.: The Data Least Squares and Channel Equalization. IEEE Trans. Signal Processing 41, 407–411 (1993)
2. Golub, G.H., Van Loan, C.F.: An analysis of the total least squares problem. SIAMJ. Numer. Anal. 17, 883–893 (1980)
3. Davila, C.E.: An Efficient Recursive Total Least Squares Algorithm for FIR Adaptive Filtering. IEEE Trans. Signal Processing. 42, 268–280 (1994)
4. Diamantaras, K.I., Kung, S.Y.: Principal Component Neural Networks: Theory and Applications. Wiley, New York (1996)
5. Deprettere, E.F. (ed.): SVD and Signal Processing, pp. 209–232. Elsevier, New York (1973)
6. Rao, Y.N., Principe, J.C.: Fast RLS-Like Algorithm for Generalized Eigendecomposition and its Applications. Journal of VLSI Signal Processing 37, 333–344 (2004)
7. Ljung, L.: Analysis of Recursive Stochastic Algorithms. IEEE Transactions on Automatic Control 22, 551–575 (1977)
8. Kushner, H.J., Clark, D.S.: Stochastic Approximation Methods for Constrained and Unconstrained Systems. Springer, New York (1978)
9. Cha, I., Kassam, S.A.: Channel equalization using adaptive complex radial basis function networks. IEEE J. Sel. Area. Comm. 13, 122–131 (1995)

Novelty Detection in Large-Vehicle Turbocharger Operation

David A. Clifton[1,2], Peter R. Bannister[1], and Lionel Tarassenko[1]

[1] Department of Engineering Science, University of Oxford,
Parks Road, Oxford OX1 3PJ, UK
{davidc, prb, lionel}@robots.ox.ac.uk
[2] Oxford BioSignals Ltd., Magdalen Centre, Oxford Science Park,
Oxford, OX4 4GA, UK

Abstract. We develop novelty detection techniques for the analysis of data from a large-vehicle engine turbocharger in order to illustrate how abnormal events of operational significance may be identified with respect to a model of normality. Results are validated using polynomial function modelling and reduced dimensionality visualisation techniques to show that system operation can be automatically classified into one of three distinct state spaces, each corresponding to a unique set of running conditions.

This classification is used to develop a regression algorithm that is able to predict the dynamical operating parameters of the turbocharger and allow the automatic detection of periods of abnormal operation. Visualisation of system trajectories in high-dimensional space are communicated to the user using parameterised projection techniques, allowing ease of interpretation of changes in system behaviour.

Keywords: Novelty Detection, Visualisation, Industrial Applications.

1 Introduction

Examples of abnormal behaviour in high-integrity systems are few in comparison to the quantity of examples of normal behaviour, due to the rarity of system failure. Knowledge of specific faults is often very limited, with their relationship to overall system state often ill-defined [14]. This is particularly true for highly complex industrial systems, in which "state" is defined in terms of large numbers of components. Such complexity may also result in significant system-to-system operational variability, further confounding understanding of fault conditions. Thus, conventional fault-detection, or "fingerprinting", techniques may only provide limited benefit [13,3] when applied to such systems [4].

Novelty detection, in which departures from a model of normality are identified, is particularly suited to the condition monitoring of complex high-integrity systems [17]. Previously unseen or incompletely-defined faults may be detected as being significant deviations from "normality". This paper presents results of an investigation of novelty detection in operational data from a large-vehicle

H.G. Okuno and M. Ali (Eds.): IEA/AIE 2007, LNAI 4570, pp. 591–600, 2007.

Table 1. Observed parameters

Parameter	Description
SAF	shaft angular frequency (s^{-1})
SBT	shaft bearing temperature (°C)
TT_{in}, TP_{in}	inlet turbine temperature (°C) and pressure (mbar)
TT_{out}, TP_{out}	outlet turbine temperature (°C) and pressure (mbar)
CT_{in}, CP_{in}	inlet compressor temperature (°C) and pressure (mbar)
CT_{out}, CP_{out}	outlet compressor temperature (°C) and pressure (mbar)
OT	oil temperature (°C)

turbocharger. The investigation was performed "blind", in that events occurring within the period of recording were not divulged by the system owners until project completion. This paper validates identifications of abnormality achieved through novelty detection with actual system events.

For reasons of commercial sensitivity, data have been anonymised where necessary by not divulging absolute values of some operational parameters; e.g., axes on plots have absolute values removed, or normalised.

2 Data Description

Data used in this study are recorded from a large-vehicle turbocharger over a period of 403 days. Samples of 11 parameters were taken at an interval $T_s = 30$s, provided the angular frequency of the turbine shaft (SAF) exceeded some minimal frequency, $SAF \geq SAF_{min}$. This angular frequency SAF can be considered to be the *operating point* of the system. Thus, an 11-D vector of observed parameters was formed at each valid sample point, as shown in Table 1.

A gap in recording of 25 days exists from day 175 to day 199. Throughout the operating period, inspection shows that the turbocharger is operated in approximately constant manner for prolonged periods (often weeks at a time). It was also noted by the system owners that the first 20 days of operation could be considered normal.

3 Identifying Abnormal Behaviour

In this section, novelty detection methods previously shown to provide benefit in jet-engine analysis [5,6] are adapted for use with turbocharger data, and compared to results from conventional function-fitting approaches. Visualisation of high-dimensional data is used to investigate evolution of system state, which provides the basis for a neural network solution described in Section 5, then compared to results from previous methods to draw conclusions on detected abnormalities in Section 6.

3.1 Signature-Based Models of Normality

Previous investigations [9,5] have shown that signatures of an observed parameter y constructed with respect to operating-point parameter x can be used to characterise normal behaviour in rotating-component systems. Speed-based signatures of engine vibration and performance data have been used to identify abnormality in gas-turbine engines used in commercial and military aircraft [8].

In such signatures, values of y are collected for each value of x, over the range $x : [x_{min}\ x_{max}]$. The conditional distributions $p(y|x), \forall x$ may be learned from normal data and used for subsequent identification of abnormality. Figure 1(a) shows an example in which the range of x is divided into $b = 400$ sub-ranges (or *bins*) of equal width. Values of y observed within each sub-range of x are used to set novelty thresholds, within which x is considered "normal", $y_{min,b} \leq x_b \leq y_{max,b}$.

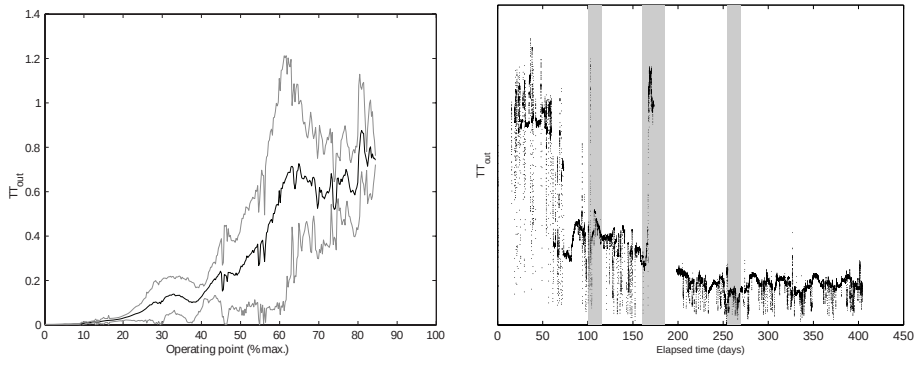

(a) **(b)**

Fig. 1. (a) Example signature of TT_{out} w.r.t. SAF. Mean μ_b, and novelty thresholds $(y_{min,b}, y_{max,b})$ within sub-ranges $b = 1 \ldots 400$ are shown in black and grey respectively. (b) TT_{out} values throughout recording period; periods determined as abnormal with respect to signature-based model of normality shown in grey.

Initial examination showed that most observed parameters are not normally distributed over the *whole range* of the operating-point ($x \equiv SAF$). However, they are approximately Gaussian in distribution when considered over a number of discrete sub-ranges of SAF (effectively quantising x), suggesting that a signature-based approach may be applicable [4]. Results presented were obtained when $b = 8$ sub-ranges of SAF were used, though similar results were found for values up to $b = 20$.

Within each sub-range b of SAF, values of observed parameter y were collected throughout a training period. Thresholds for each sub-range ($y_{min,b}$, $y_{max,b}$) have previously been set using density-modelling methods; this investigation uses $\mu_b \pm 3\sigma_b$ to determine thresholds, where σ_b is the standard deviation

of $\boldsymbol{y}_b$. A "sliding window" approach was taken, in which the training period used to construct signatures for each observed parameter was 30 days, then used for testing of values within the subsequent 10 days. Windows were advanced every 10 days.

Figure 1(b) shows periods of operation in which TT_{out} lies outside novelty thresholds $(y_{min,b}, y_{max,b})$, at 103 days, 167 days, and 260 days. It should be noted that while the identifications at 103 days and 167 days correspond to periods of high signal magnitude, it is the fact they are abnormal with respect to the operating point SAF that makes them abnormal: a conventional "trending" approach to signal analysis would result in many false-positive abnormality detections [18,19], a typical disadvantage of many generic industrial condition monitoring systems.

Similar periods of abnormality were noted for TT_{in} and TP_{out}. Examination of continuous novelty scores $z = (x - \mu_b)/\sigma_b$ throughout the recording period shows that a highly consistent region of operation begins at 82 days (during which $z \approx 0$), which corresponds to a period of uninterrupted turbocharger operation of more than 20 days. Later analyses show that this corresponds to the second of three distinct modes of turbocharger operation.

3.2 Polynomial Function Modelling

Observations noted with signature-based analysis may be compared with those obtained from more conventional methods. The correlation between SAF and other turbine parameters may be illustrated and explored by two-dimensional function-fitting: uncorrelated behaviour of a signal is then represented as deviations from previous loci of "normal" operation. Assuming that the initial period may be considered to be normal operation, a low-order polynomial function, $y = f(x)$, may be found that best fits a pair of signals (x, y) under consideration. Variations from that function of best fit (residuals) may illustrate deviations of a signal which are indicative of abnormal behaviour.

Figure 2(a) shows a low-order polynomial fit (minimising least squares distance) to the first 20 days of SBT and SAF data, exhibiting the dynamic relationship expected between the two parameters. Deviations of SBT between elapsed time 120 and 140 days from the functional fit provide a simple description of abnormality.

Functional fits between SAF and other signals allow operating-point correlation to be examined. Fits between sensors mounted at the same site (e.g. TT_{in} and TP_{in}) allow local correlations to be examined at one particular component interface. Fits between sensors of similar type mounted at different sites allow cross-component behaviour to be examined (e.g. CP_{in} and CP_{out}).

Examination of TT_{out} vs. SAF throughout the data set shows a downward TT_{out} trend in response with respect to the operating point. Figure 2(b) shows the relationship between the two parameters during the initial period of known "normal" operation, used to fit the function shown by the dashed line. The decrease in TT_{out} with respect to the operating point is shown by Figure 2(c), in which the original function fit is retained for comparison.

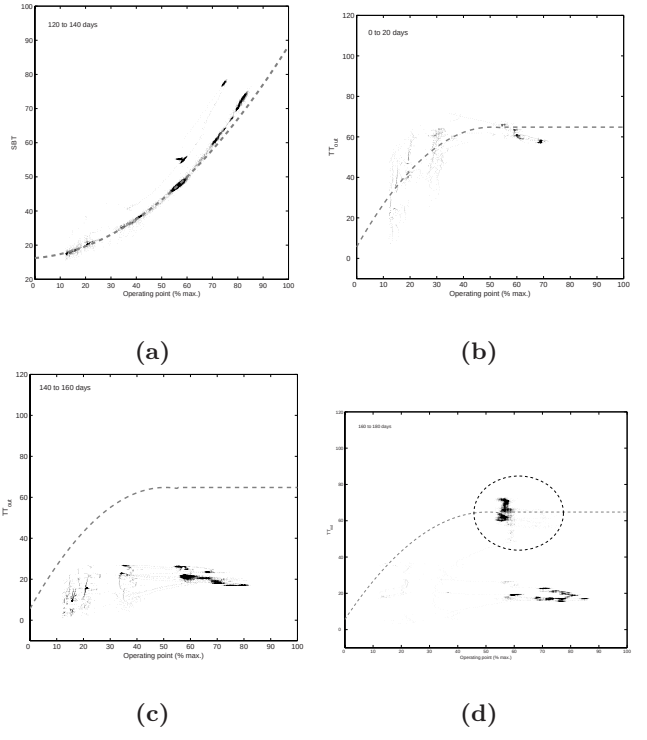

Fig. 2. (a) Functional fit for SBT vs. SAF shown in dashed grey. Deviations from normal functional relationship are evident as excursion far above the model. (b) TT_{out} vs. SAF shown in dashed grey, in "normal" conditions. (c) TT_{out} vs. SAF shown in dashed grey, showing decrease throughout the recording period. (d) TT_{out} vs. SAF shown in dashed grey, with abnormal excursion marked by an ellipse.

This decrease was also seen in similar plots of TT_{in}. Such decreases may be anticipated at the inlet and outlet of the turbine during the running life of a turbocharger as accumulation of exhaust residue takes place.

The overall downward trend is occasionally punctuated by step-changes in the TT_{out} vs. SAF relationship, as shown in Figure 2(d), which corresponds with unidentified periods of abnormality observed previously using signature-based analysis. Sudden parameter step-changes uncorrelated with operating points may often be indicative of a fault, and it is significant that this increase occurred immediately before the gap in the data, suggesting that the turbocharger may have been taken off-line to address a problem.

4 Visualisation of System State

In order to explore the evolution of system state throughout the period of recording, the data set was visualised by projecting the set of 11-dimensional feature

vectors into 2 dimensions. This allows a holistic approach to analysis, in which all parameters are considered in conjunction. Models of normality may be directly formed in high-dimensional space [7].

Topographic projection is a transformation that attempts to best preserve, in the projected space of lower-dimensionality (*latent space*, $\mathbb{R}^q$), distances between data in their original high-dimensional space (*data space*, $\mathbb{R}^d$). Typically $d > q$, $q = 2$ or 3. The *Sammon stress metric*[15] is based upon the distance d_{ij} between points (x_i, x_j) in $\mathbb{R}^d$, and the distance d^*_{ij} between projected points (y_i, y_j) in $\mathbb{R}^q$:

$$E_{\text{sam}} = \sum_{i=1}^{N} \sum_{j>i}^{N} (d_{ij} - d^*_{ij})^2 \tag{1}$$

in which the distance measure is typically Euclidean. The NeuroScale model [10,11] trains a radial basis function (*RBF*) neural network to perform the mapping from $\mathbb{R}^d$ to $\mathbb{R}^q$, in which E_{sam} is minimised; i.e. distances between points are best preserved after projection.

Component-wise normalisation [5] was applied to the 11-dimensional feature vector in order to ensure that projection is not dominated by the dimension with the largest dynamic range.

The projection network was trained using a summary of the data set obtained by placing kernels in 11-dimensional space using the batch k-means algorithm [16], in order to ensure tractable training time whilst still retaining projection accuracy.

Normalised 11-dimensional feature vectors were then projected through the resulting network. Note that this ability to project vectors not contained in the network's training set is an important tool for system exploration, and is supported by the ability of the network to interpolate and generalise to previously-unseen feature vectors.

Figure 3(a) shows data from 45 days to 50 days of operation projected into 2 dimensions in black. Projected data from previous days are shown in grey. Note that the axes after projection are unitless. The "V" shape of the projected data is stable during this period of initial operation, indicating that the initial period of normality (previously assumed to be 20 days) extends to around 50 days.

Figure 3(b) shows the system state at 105 days. Again, projected data from this period are plotted in black, with all previous days' projections shown in grey for comparison. Behaviour of the system has been stable up to this point (in the "V" formation noted previously), but a sudden step-change is observed, indicated by an ellipse in the figure. This corresponds to the first period of abnormality observed from signature-based analysis in Section 3.1.

Returning to stable system state, the next step-change in projected data is observed between 170 and 175 days, as shown in Figure 3(c), which corresponds with the second region identified by signature-based analysis. Figure 3(d) shows the final step-change in visualised system state, at 255 days, corresponding to the third region identified by signature-based analysis.

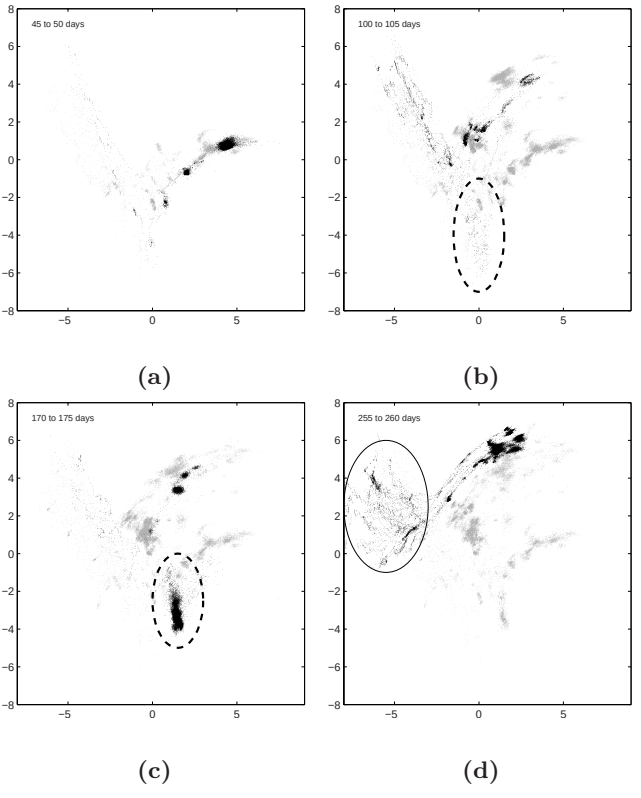

Fig. 3. Projections of 11-dimensional feature vectors: (a) initial period of "normal" operation; (b) consistent period of "abnormal" operation, marked by an ellipse; (c) later significant step-change in state, marked by an ellipse; (d) final period of "abnormality", marked by an ellipse

An individual "run" of the turbocharger may be defined to be a single operating session, in which the system is activated, operated, then deactivated. The recording period (400 days) contains 108 individual runs, varying in length from under 1 day to over 3 weeks. Data within each run are summarised by a small number of prototype kernels placed in high-dimensional space using the batch k-means algorithm. The projection of each single run is then performed, as shown in Figure 4(a), allowing the evolution of the system to be examined "by run", rather than by individual samples as was performed previously. As shown in the figure, three main modes of turbocharger operation are seen. Prior to the gap in recording at 175 days, the period of significantly abnormal behaviour forms a fourth region, as shown. This method is particularly useful for examining the long-term behaviour of a system.

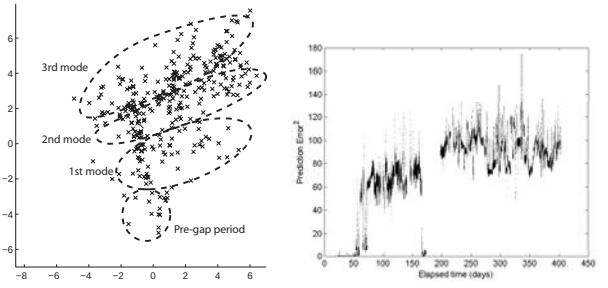

(a) **(b)**

Fig. 4. (a) Visualisation of system state, in which each separate operating run of the turbocharger is projected as a cross. Three modes of operation, and a significantly "abnormal" region are seen. (b) Squared error of MLP regression target, TT_{out}.

5 Learning Normal Behaviour

Neural networks can be used to perform prediction of a system's parameters, and are often used in practice for automated fault detection. Here, results from previous novelty-detection methods are compared to those from a multi-layer perceptron (MLP) neural network used to model the behaviour of the turbine outlet temperature, TT_{out}, selected for the purposes of illustration.

In this investigation, parameters used as input to the MLP predictor are the dynamical inputs of the turbocharger system (input temperature and pressure of the turbine and compressor: TP_{in}, TT_{in}, CP_{in}, CT_{in}) and those pertaining to the rotary mechanism that connects the turbine and compressor sub-systems (SAF, SBT). The selection of input parameters in a more complex model could contain those relating to the oil supply. Network architecture parameters were selected empirically.

5.1 Network Training

Previous visualisation showed that the period of "normal" operation extends to 50 days, which formed the basis for the MLP training set. In order to ensure balanced training, the number of feature vectors from each sub-range of SAF is kept constant. Without such balancing, the regression capacity of the network would be biased towards the sub-range of SAF with the highest representation in the training set [1,2]. This amounts to 8% of total data being used for (balanced) training.

5.2 Prediction of Expected Behaviour

Squared error between the predicted and observed values of TT_{out} are shown in Figure 4(b).

The training set (0 to 50 days) shows low prediction error, as expected. Previous analyses shown that after 50 days, the system entered a second mode of operation (as shown in Figure 4(a)); this corresponds to a rise in MLP prediction error over the same period. During this period, automatic detection of the largest transients could be achieved by setting a threshold on the squared-error at 100.0.

At 167 days, the prediction error decreases rapidly to zero. This corresponds to TT_{out} rapidly leaving the second mode of operation. This extreme change was previously noted in system state visualisations (Figure 3(c)). After the gap in recording, the prediction error rises yet further. From previous analyses, it was seen that the system enters a third mode of operation during this period, and stays within it with little variation.

In practice, rather than using the fixed window training set, re-training could occur at appropriate intervals or in a sliding window manner (as shown for signature-based analysis, in Section 3.1). Retraining the network using a balanced training set drawn from the first 20 days *after* the gap (approximately 200 to 220 days) gives prediction errors of approximately zero, emphasising the consistent nature of operation after the gap in recording.

This illustrates the potential need for retraining when system state enters a new region of "normal" operation different to the original, as may reasonably be expected to occur after significant system maintenance has occurred.

6 Conclusions

We have illustrated the novelty detection approach to detection of events within large-vehicle turbocharger operation. Signature-based analysis has been shown to identify three significant areas of abnormality within the provided data set, which coincided with events of system and sensor distress later confirmed by the system owners.

These observations were compared to conventional function-fitting techniques, and shown to result in little false-positive detection of abnormality, a critical consideration for practical industrial condition monitoring systems.

Visualisation techniques were shown to allow the tracking of system state evolution throughout the data set, graphically supporting observations made by signature-based analysis, and providing the means for communicating changes in system state to a user.

Comparison to MLP regression techniques showed that abnormality could be detected on-line, emphasising the need for intelligent estimation of "normal" periods of operation, here performed using the results of visualisation.

Acknowledgements. The authors gratefully acknowledge the support of Oxford BioSignals Ltd., and the HECToR project (a UK DTI-funded project).

References

1. Bishop, C.: Neural Networks for Pattern Recognition. Oxford University Press, Oxford (1995)
2. Bishop, C.: Pattern Recognition and Machine Learning. Springer, Berlin (2006)
3. Chen, H., Hakeem, I., Martinez-Botas, RF.: Modelling of a Turbocharger Turbine Under Pulsating Inlet Conditions. IMechE J. of Power and Energy 210(5), 397–408 (1996)
4. Clifton, D.A.: Condition Monitoring of Gas-Turbine Engines. Department of Engineering Science, University of Oxford, Transfer Report (2005)
5. Clifton, D.A., Bannister, P.R., Tarassenko, L.: Application of an Intuitive Novelty Metric for Jet Engine Condition Monitoring. In: Ali, M., Dapoigny, R. (eds.) IEA/AIE 2006. LNCS (LNAI), vol. 4031, pp. 1149–1158. Springer, Heidelberg (2006)
6. Clifton, D.A., Bannister, P.R., Tarassenko, L.: Learning Shape for Jet Engine Novelty Detection. In: Wang, J., Yi, Z., Zurada, J.M., Lu, B.-L., Yin, H. (eds.) ISNN 2006. LNCS, vol. 3973, pp. 828–835. Springer, Heidelberg (2006)
7. Clifton, L.A., Yin, H., Zhang, Y.: Support Vector Machine in Novelty Detection for Multi-channel Combustion Data. In: Wang, J., Yi, Z., Zurada, J.M., Lu, B.-L., Yin, H. (eds.) ISNN 2006. LNCS, vol. 3973, pp. 836–843. Springer, Heidelberg (2006)
8. Clifton, D.A., Bannister, P.R., Tarassenko, L.: A Framework for Novelty Detection in Jet Engine Vibration Data. In: Proc. 7th Int. Conf. on Damage Assessment of Structures, Torino, Italy (in press)
9. Hayton, P., Scholkopf, B., Tarassenko, L., Anuzis, P.: Support Vector Novelty Detection Applied to Jet Engine Vibration Spectra. In: Proc. NIPS (2000)
10. Lowe, D., Tipping, M.E.: Feed-Forward Neural Networks and Topographic Mappings for Exploratory Data Analysis. Neural Computing and Applications 4(2), 83–85 (1996)
11. Nabney, I.T.: NETLAB, Algorithms for Pattern Recognition. Springer, New York (2002)
12. Nairac, A., Corbett-Clark, T.A., Ripley, R.M., Townsend, N.W., Tarassenko, L.: Choosing an Appropriate Model for Novelty Detection. In: IEE 5th International Conference on Artificial Neural Networks (1997)
13. Nelles, O., Sinsel, S., Isermann, R.: Local Basis Function Networks for Identification of a Turbocharger. In: Proc. UKACC Int. Conf. on Control, pp. 7–12 (1996)
14. Pantelelis, N.G., Kanarachos, A.E., Gotzias, N.: Neural Networks and Simple Models for the Fault Diagnosis of Naval Turbochargers. Mathematics and Computers in Simulation 51(3), 387–397 (2000)
15. Sammon, JW.: A Non-linear Mapping for Data Structure Analysis. IEEE Transactions on Computers (1969)
16. Tarassenko, L.: A Guide to Neural Computing Applications. Arnold (1998)
17. Tarassenko, L., Nairac, A., Townsend, N., Buxton, I., Cowley, P.: Novelty Detection for the Identification of Abnormalities. Int. J. Systems Science 31(7), 1427–1439 (2000)
18. Tarassenko, L., Hann, A., Patterson, A., Braithwaite, E., Davidson, K., Barber, V., Young, D.: BioSign: Multi-parameter Monitoring for Early Warning of Patient Deterioration. In: 3rd IEE Int. Sem. on Medical Applications of Signal Processing (2005)
19. Tarassenko, L., Hann, A., Young, D.: Integrated Monitoring and Analysis for Early Warning of Patient Deterioration. British J. of Anaesthesia 97(1), 64–68 (2006)

Equalization of 16 QAM Signals with Reduced BiLinear Recurrent Neural Network

Dong-Chul Park[1] and Yunsik Lee[2]

[1] Center for Intelligent Image Processing Systems Research,
Myong Ji University, Korea
parkd@mju.ac.kr
[2] Digital Convergence R & D Center, Korea Electronics Tech. Inst.,Korea
leeys@keti.re.kr

Abstract. A novel equalization scheme for 16 QAM signals through a wireless ATM communication channel using Reduced-Complex Bilinear Recurrent Neural Network (R-CBLRNN) is proposed in this paper. The 16 QAM signals from a wireless ATM communication channel have severe nonlinearity and intersymbol interference due to multiple propagation paths in the channel. The R-CBLRNN equalizer is compared with the conventional equalizers including a Volterra filter equalizer, a decision feedback equalizer (DFE), and a multilayer perceptron type neural network (MLPNN) equalizer. The results show that the R-CBLRNN equalizer for 16 QAM signals gives very favorable results in both of the Mean Square Error(MSE) and the Symbol Error Rate (SER) criteria over conventional equalizers.

1 Introduction

The Asynchronous Transfer Mode (ATM) has been used as a high-speed backbone network that provides a common infrastructure network to a diverse set of mobile technologies. One of the major problems which occur in wireless ATM network is the intersymbol interference leading to degradation in performance and capacity of the system. The received signals tend to get elongated and smeared into each other by the intersymbol interference. Several techniques have been used to build wireless ATM equalizers which aim to correct the received signal. One of the simpler types of equalizers is a Linear Equalizer (LE). With the presence of channel nonlinearities, it appears that techniques based on linear signal processing such as a LE show limited performance. Others types of equalizers such as Decision Feedback Equalizers (DFE), Volterra filter based equalizers, and Viterbi equalizers are based on nonlinear signal processing techniques. The DFE is the most commonly used technique for equalization, some of its variants and applications can be found in the literature[1,2]. Volterra filter-based approaches[3] utilize the capability of nonlinear modeling in the Volterra filter and do improve the SNR at the output of the equalizer when compared with linear filter-based techniques such as a decision feeback equalizer (DFE). General problem with the Volterra filter-based approaches include computational

H.G. Okuno and M. Ali (Eds.): IEA/AIE 2007, LNAI 4570, pp. 601–610, 2007.

complexities involved in their implementation while their practical use has been hindered by computational limitations that confine them to low order nonlinearities, i.e., only estimations of low order kernels is practically feasible. In contrast to DFE and Volterra filters, Viterbi equalizers[4,5] recover the transmitted signals by sequence patterns instead of individual symbols. From the received sequence of symbol, the Viterbi algorithm finds the corresponding transmitted sequence which maximizes the likelihood function. Like Volterra filters, Viterbi equalizers require high computational complexity.

Another promising approach to designing equalizers are neural network (NN)-based approaches[6,7]. As shown in a wide range of computing applications, NN has been successfully used for modelling complex nonlinear systems. The most distinguishable feature of NNs over conventional techniques is the ability of learning[8,9]. When properly trained, NNs can produce rather good output even though the input data contains severe noises. In addition, recent researches have shown that a recurrent type NN is more suitable than a feedforward NN in predicting time series signals[10]. Recent researches on the use of recurrent type NN for designing nonlinear equalizer have shown promising results[6,10]. Among recurrent neuron networks, the Complex Bilinear Recurrent Neural network (CBLRNN) -based equalizer gives very favorable results in both the MSE and SER criteria over Volterra filter equalizers, DFEs, and Complex Multiplayered Perceptron type NN (CMLPNN) equalizers. However, the CBLRNN also suffers from slow convergence because of its rather complicated architecture. A reduced version of the CBLRNN for faster and stable convergence is first proposed and then applied to equalization of a wireless ATM channel for 8 PSK[11]. The results show that the reduced CBLRNN is an effective scheme for the equalization of 8 PSK signals. However, 16 QAM signals include a far severer nonlinear distortion than 8 PSK signals and the effectiveness of the reduced CBLRNN is about to be verified.

In this paper, a reduced structure of CBLRNN is applied to the equalization of wireless ATM channels for 16 QAM signals. The Reduced-CBLRNN (R-CBLRNN) uses only a part of the feedback components for bilinear component calculation. Section 2 gives a brief review of BLRNN and then introduces a reduced version of BLRNN with its training algorithm. The channel model to be used as the target model for experiments of R-CBLRNN applications is introduced in section 3. Section 4 presents experiments and results including performance comparisons of R-CBLRNN with some conventional equalizers. The experiments are performed on 16 QAM signals. Concluding remarks are given in Section 5.

2 Channel Model

Multi-path channels with time-varying transmission characteristics have been modelled with linear time-varying filters [1]. The modulated signal $s_m(t)$ with symbol duration $T = 12.8\ ns$ ($156 MBit/s$ signal) is transmitted over an ATM

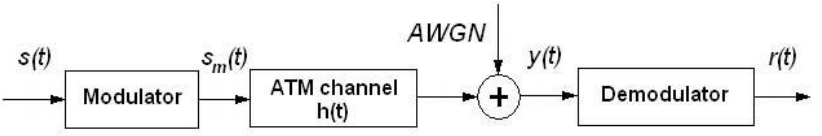

Fig. 1. The signal transmission over ATM channel

channel with P propagation paths modelled by the following time-varying impulse response:

$$h(t/T) = \sum_{i=1}^{P} a_i.\delta(t/T - \tau_i).e^{j\varphi_i(t/T)} \tag{1}$$

where δ(t) is the unit impulse and φ_i is a random phase. The signal is also assumed to be contaminated with AWGN, $n(t/T)$, which causes the signal distortion to be more severe. Received signal $y(t)$ is then represented as follows:

$$y(t/T) = \sum_{i=1}^{P} a_i.s_m(t/T - \tau_i).e^{-j(\omega_c+\varphi_i)(t/T)} + n(t/T) \tag{2}$$

where w_c is the carrier frequency.

From Eq. (2), we see that $y(t)$ is the sum of several multi-path components with the scale a_i and a phase shift $\omega_c + \varphi_i$. In this paper, a 40GHz broadband channel which is introduced in [1] is used for experiments and their channel impulse responses are given by Eq. (1). In our experiments, the channel model has 6 propagation paths. The gain and delay for each path is given in Table 1. Fig. 2 displays constellations of the transmitted and received 16 QAM signals through a wireless ATM channel.

Table 1. Channel gain and delay for each propagation path

path i	1	2	3	4	5	6
$\{a_i\}$	1	0.5	0.4	0.32	0.1	0.08
$\{\tau_i\}$	0	1/2	9/8	13/8	21/8	39/8

3 Complex Bilinear Recurrent Neural Network

3.1 Bilinear Recurrent Neural Network (BLRNN)

The BLRNN is a recurrent NN which has a robust ability in modelling nonlinear systems and was originally introduced in[12].

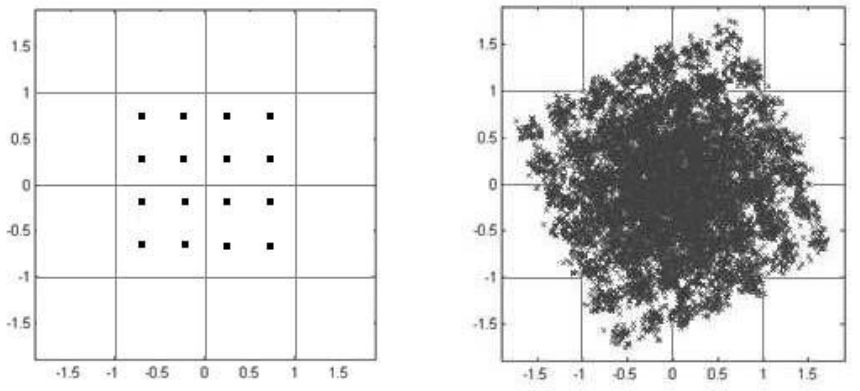

(a) (b)

Fig. 2. Constellation of 16QAM signals: (a) the transmitted (b) the received

The output value of a bilinear recurrent neuron is computed by the equation:

$$s_p[n] = d_p + \sum_{k_2=0}^{N_f-1} a_{pk_2} o_p[n-k_2] + \sum_{k_1=0}^{N_i-1} c_{pk_1} x[n-k_2] \tag{3}$$
$$+ \sum_{k_1=0}^{N_i-1} \sum_{k_2=0}^{N_f-1} b_{pk_1k_2} x[n-k_1] o_p[n-k_2]$$
$$= w_p + {A_p}^T {A_p}^T[n] + Z_p[n] {B_p}^T X[n] + {C_p}^T X[n]$$

where d_p is the weight of bias neuron for the $p{-}th$ hidden neuron, $p = 1, 2..., N_h$. N_h, N_i, and N_f are the number of hidden neurons, input neurons, and feedback lines, respectively. A_p is the weight vector for recurrent portion, B_p is the weight matrix for the bilinear recurrent portion, and C_p is the weight vector for the feed-forward portion. T represents the transpose of a matrix.

3.2 Complex Bilinear Recurrent Neural Network (CBLRNN)

CBLRNN is the complex version of BLRNN. CBLRNN has been designed to deal with the problems with complex number operations found in equalizer design. Fig. 3 shows the output of a neuron in CBLRNN. More detailed explanation on the CBLRNN can be found in [6].

3.3 Reduced-CBLRNN

Even though the CBLRNN shows very promising results when applied to equalizer problems, it still suffers from slow convergence in practical use. For CBLRNN, most of the computational loads are due to the number of multiplications between complex values. Consider a CBLRNN with structure N_i-N_h-N_o

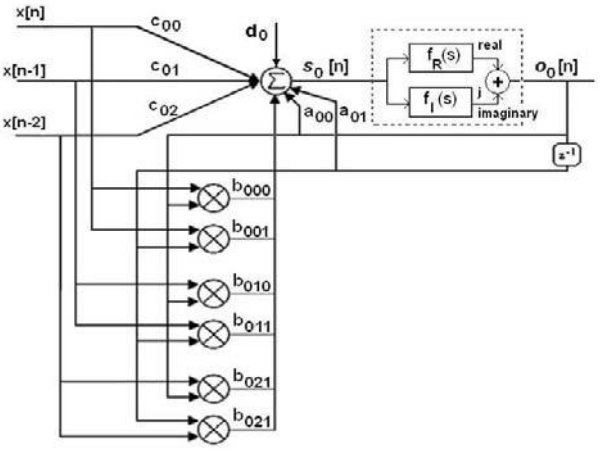

Fig. 3. A complex bilinear recurrent neuron

using N_f feedback taps where N_i, N_h, and N_o are the numbers of input neuron, hidden neuron, and output neuron respectively. When $N_o = 1$, a simple case, the total number of multiplications for CBLRNN:

$$N_C = (N_i + N_f + N_f \cdot N_i) \cdot N_h + N_h \tag{4}$$

From Eq. (4), we infer that the bilinear component (corresponding to $N_f \cdot N_i$ multiplications) contributes most to the total number of multiplications.

Choi *et.al* propose a simplified version of the bilinear DFE[13]. In this approach, only a part of feed-forward inputs are multiplied to the feedback portion for bilinear components without suffering from performance degradation. The results show that this simplified version gives an insight on the formation of bilinear components. By adopting this idea of reduced bilinear components to the CBLRNN, the output of the BLRNN is changed as follows:

$$\begin{aligned} s_p[n] = d_p + \sum_{k_1=0}^{N_f-1} a_p[k_1] o_p[n-k_1] + \sum_{k_2=0}^{N_i-1} c_p[k_2] x[n-k_2] \\ + \sum_{k_1=0}^{N_f-1} \sum_{k_2=S}^{E} b_p[k_1,k_2] o_p[n-k_1] x[n-k_2] \end{aligned} \tag{5}$$

where $E = \frac{N_i-1}{2} + p$ and $S = \frac{N_i-1}{2} - p$

The total number of multiplications after applying common feedback tabs to bilinear components in the R-CBLRNN becomes:

$$N_S = N_f \cdot N_i + (2N_i + N_f) \cdot N_h + N_h \tag{6}$$

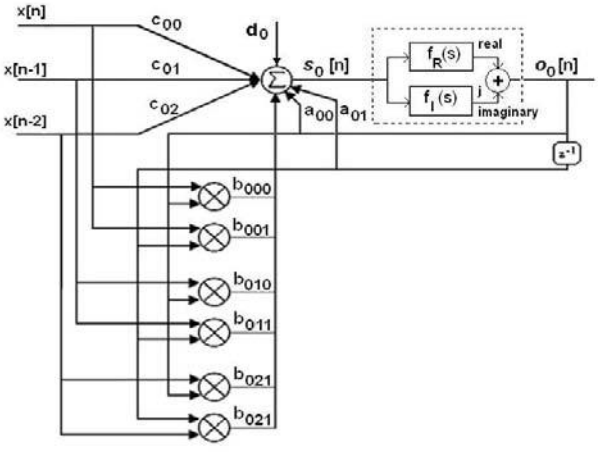

Fig. 4. A reduced bilinear recurrent neuron

When N_S in Eq. (6) is compared with N_C in Eq. (4), the number of reduced multiplications, $\triangle N$, is:

$$\triangle N = N_C - N_S = N_h \cdot N_f \cdot N_i - N_h \cdot N_i - N_f \cdot N_i \tag{7}$$

Fig. 5 shows the comparison of convergence for CBLRNN and R-CBLRNN. Fig. 5 confirms that the R-CBLRNN converges much faster than a CBLRNN

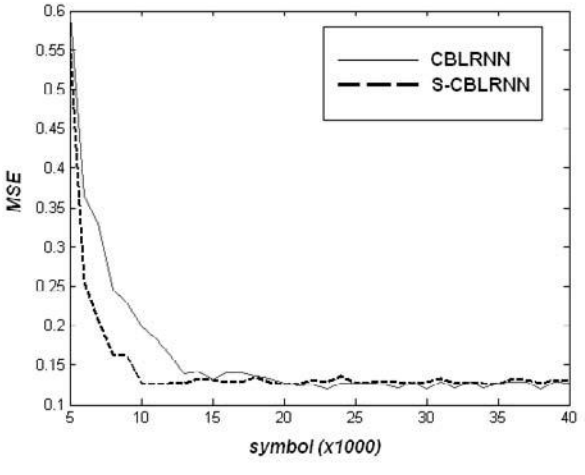

Fig. 5. Comparison of convergence for R-CBLRNN and CBLRNN (16QAM, SNR=15 dB)

and savings on the convergence speed of the R-CLRNN roughly matches with the savings on multiplication, $\triangle N$.

4 Experiments and Results

The ATM channel for experiments is modelled by the Eq. (2) with 6 propagation paths whose gains and delays are given in Table 1. The transmitted data symbols are randomly generated and transmitted signals over the ATM channel are corrupted with AWGN with various SNRs. Fig. 2 shows typical constellations for the original 16QAM symbols and the received symbols through the ATM channel with 20dB AWGN.

In experiments, randomly generated 30,000 data symbols are used for training the equalizers and another 100,000 data symbols are used for testing the performance of the equalizers. The proposed equalizer based on a R-CBLRNN is compared with a CDFE, a Volterra equalizer, a CMLPNN-based equalizer, and a CBLRNN-based equalizer. In order to acquire fair comparisons, a structure of

Table 2. Network structure and computational complexity

Algorithm	Network structure	Number of multiplication
CDFE	10 input taps 30 feedback taps	40
Volterra	10 input taps (1, 3 order combiners)	1010
CMLPNN	10-25-1	275
CBLRNN	10-4-1 5 feedback taps	264
Reduced CBLRNN	10-4-1 5 feedback taps	154

R-CBLRNN is selected to have the same or less number of inputs and feedback tabs when compared with other cases. Note that all equalizer models have 10 input tabs in our experiments. The total number of complex-valued multiplications per an iteration for each equalizer model is given in Table II. We can observe from Table II that the proposed R-CBLRNN requires much less computational effort when compared with Volterras, CMLPNNs, and CBLRNNs.

Fig. 6 and Fig. 7 show constellation after equalization and SER performance for 16QAM signal, correspondingly. When compared with the results on 8 PSK case in 8, the improvement of R-CBLRNN over CMLPNN is not significant in this case unlike the 8 PSK case. However, the improvement of the R-CBLRNN over the Volterra filter and the DFE is still noticeable. The slight improvement of R-CBLRNN over CMLPNN for the 16 QAM case implies a room for improvement in R-CBLRNN based equalizer.

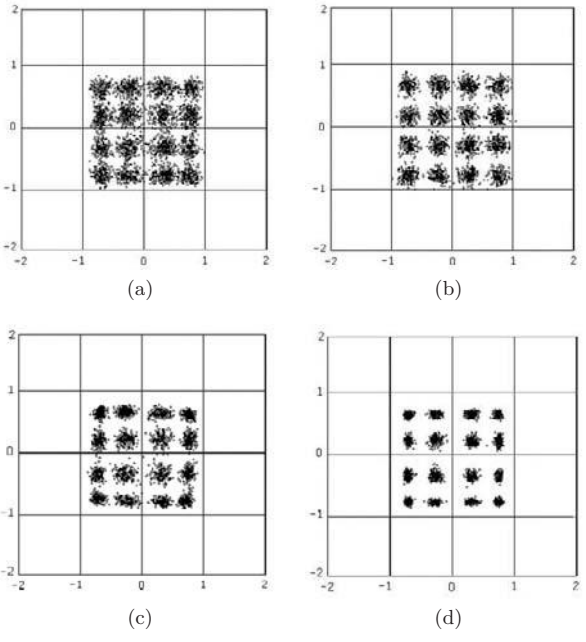

Fig. 6. Constellations after equalization for experiments, SNR=20 dB. (a) CDFE (MSE=0.12213), (b) Volterra (MSE=0.10671), (c) CMLPNN (MSE=0.09465),(d)R-CBLRNN (MSE=0.08821).

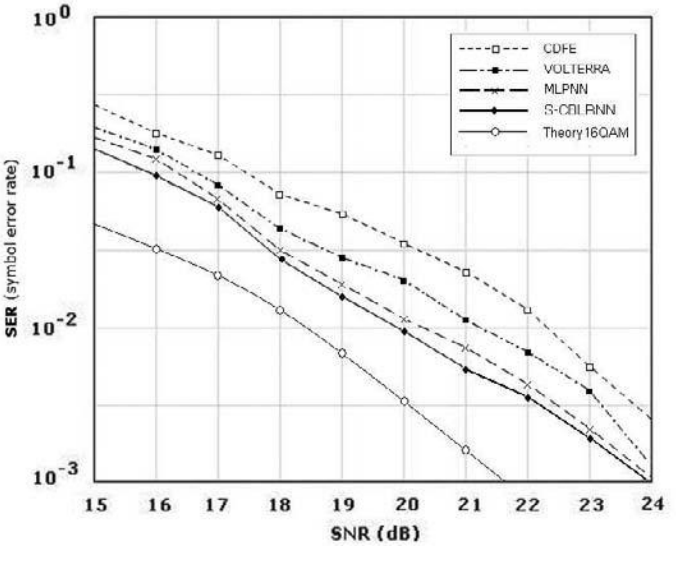

Fig. 7. SER performance for equalizers on 16QAM signals

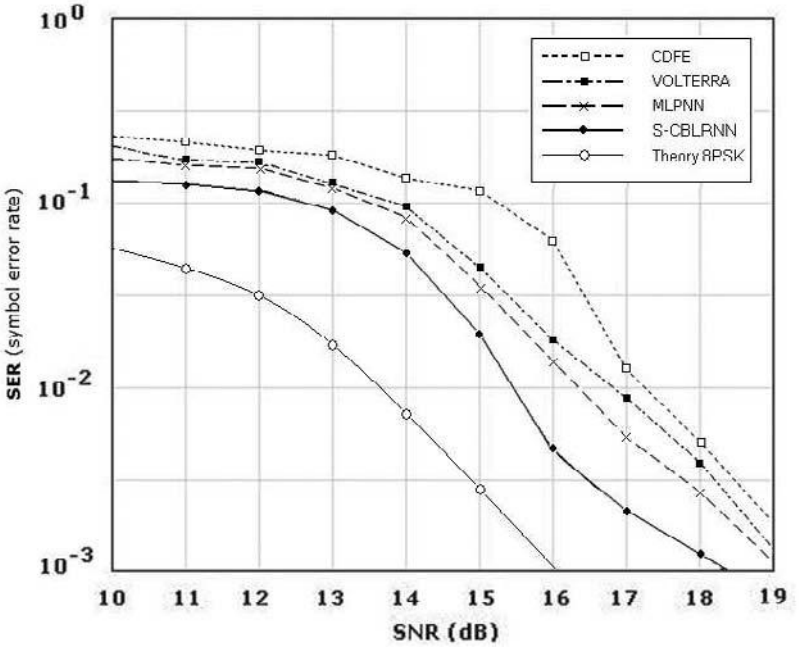

Fig. 8. SER performance for equalizers with 8PSK signal [11]

5 Conclusion

A reduced version of the Complex Bilinear Recurrent Neural Network (R-CBLRNN) is applied to the problem of 16 QAM signal equalization of wireless ATM channels in this paper. The R-CBLRNN reconfigures the bilinear components in the BLRNN and reduces a part of the bilinear components. By doing so, the resultant R-CBLRNN can reduce its convergence time about 40 % without suffering from any performance degradation. Experiments on the equalization of a wireless ATM channel for 16QAM signals, which have severe nonlinearity and inter-symbol interference due to multiple propagation paths show very favorable results in both of the MSE and SER criteria over the equalizers such as a Volterra filter equalizer, decision feedback equalizer (DFE), and a MLPNN equalizer.

References

1. Drewes, C., Hasholzner, R., Hammerschmidt, J.S.: Adaptive equalization for wireless ATM. In: 13th Int Conf. DSP' 97, Santorini, Greece, pp. 57–60 (1997)
2. Proakis, J.G., Salehi, M.: Communication system engineering, pp. 592–595. Prentice-Hall, Englewood Cliffs (1994)
3. Marmarelis, V., Zhao, X.: Volterra Models and Three-Layer Perceptions. IEEE Transaction on Neural Networks 8(6), 1421–1433 (1997)

4. Hagenauer, J., Hoener, P.: A viterbi algorithm with soft-decision outputs and its application. GLOBECOM'89, vol. 3, pp. 47.1.1–47.1.7 (1989)
5. Han, S.S, No, J.S., Jeung, Y.C, Kim, K.O, Shin, Y.B, Hahm, S.J., Lee, S.B.: New soft-output MLSE equalization algorithm for GSM digital cellular systems. In: Fourth IEEE International Conference on Universal Personal Communications, pp. 919–923 (1995)
6. Park, D.C., Jeong, T.K.: Complex Bilinear Recurrent Neural Network for fqualization of a satellite channel. IEEE Transactions on Neural Network 13(3), 711–725 (2002)
7. Gibson, G., Siu, S., Cowan, C.: Multilayer perceptron structures applied to adaptive equalizer for data communication. IEEE Transactions on Acoustics,Speech, and Signal Processing 39(9), 2101–2104 (1991)
8. Park, D.C., El-Sharkawi, M.A., Marks II, R.J.: Adaptively trained neural network. IEEE Transactions on Neural Networks 2, 334–345 (1991)
9. You, C., Hong, C.: Nonlinear blind equalization schemes using complex-valued multilayer feedforward neural networks. IEEE Transaction on Neural Networks 9, 1442–1445 (1998)
10. Zhang, X., Wang, H., Zhang, L., Zhang, X.: A blind equalization algorithm based on bilinear recurrent neural network. WCICA, Fifth World Congress on Intelligent Control and Automation 3, 198–1984 (2004)
11. Park, D.C., Min, B.J., Choi, H.S.: Equalization of 8PSK Signals with a Recurrent Neural Network. In: 2007 Int. Sym. on Neural Networks (2007) (submitted)
12. Park, D.C., Zhu, Y.: Bilinear Recurrent Neural Network. IEEE ICNN 3, 1459–1464 (1994)
13. Choi, J., Ko, K., Hong, I.: Equalization techniques using a simplified bilinear recursive polynomial perceptron with decision feedback. In: Proceedings. IJCNN '01. International Joint Conference on Neural Networks, vol. 4, pp. 2883–2888 (2001)

Enhanced Neural Filter Design and Its Application to the Active Control of Nonlinear Noise

Cheng-Yuan Chang[1], I-Ling Chung[2], Chang-Min Chou[3], and Fuh-Hsin Hwang[4]

[1,2,3] Department of Electronic Engineering, Ching Yun University,
Jhongli City, Taiwan 320, R.O.C.
[4] Department of Optoelectronics and Communication Engineering, National Kaohsiung Normal University, Kaohsiung County 824, Taiwan, R.O.C.
cychang@cyu.edu.tw, ling@cyu.edu.tw, changmin@cyu.edu.tw, fuhsin@nknucc.nknu.edu.tw

Abstract. A novel neural filter and its application to active control of nonlinear noise are proposed in this paper. This method helps to avoid the premature saturation of backpropagation algorithm; meanwhile, guarantees the system convergence by the proposed self-tuning method. The comparison between the conventional filtered-X least-mean-square (FXLMS) algorithm and proposed method for nonlinear broadband noise in active noise cancellation (ANC) system is also made in this paper. The proposed design method is very easy to be implemented and versatile to the other applications. Several simulation results show that the proposed method can effectively cancel the narrowband and nonlinear broadband noise in a duct.

Keywords: neural filter, convergence, active noise cancellation, broadband noise.

1 Introduction

Industrial noises, including the noises of fans, engines, machine tools, and automated manufacturing equipments etc., are always annoying to most people in many occasions. These industrial noises may generate acoustic levels up to 120 dB and often have the significant power in their low frequency range. However, the conventional passive control methods, suppressing acoustic noise using sound absorbing materials, generally do not work well at low frequency. This is because the thicknesses of the absorbers are not large enough, when compared to the acoustic wavelength at low frequency. Besides, reducing low frequency sound being transmitted from one space to another space is also difficult unless the intervening barrier is very heavy. For these reasons, passive schemes can not control low frequency noise well. Besides, the back pressure, arousing by using absorber, will also deteriorate the system performance. Hence, the ANC systems, which do not use any sound absorbing material, have received a lot of attentions in recent years because of the development of high-speed microprocessors and digital hardware [6].

H.G. Okuno and M. Ali (Eds.): IEA/AIE 2007, LNAI 4570, pp. 611–620, 2007.

The ANC, which was initially presented by Lueg [7], uses the principle of acoustic superposition and achieves the attenuation of the unwanted sound. It involves an electro acoustic system that cancels the unwanted noise; specifically, an anti-noise of equal amplitude and opposite phase is generated and combined with the primary noise, thus resulting in the cancellation of both noises. The ANC has to be adaptive because of changes in environment, degradation of system components and alteration of the noise source. Most of the conventional ANCs, employing the standard filtered-X least mean square (FXLMS) algorithm, are linear in nature [1],[9]. However, the FXLMS algorithm is not capable of training a nonlinear controller, since this algorithm exploits the linearity of the controller. So, active control of nonlinear noise is hard to achieve.

A normalized Gaussian radial basis function neural network is proposed to compensate the non-minimum phase secondary path transfer function and control the nonlinear noise process in [10]. Tan and Chiang introduced the adaptive Volterra filters for feedforward ANC based on multi-channels structure [11]. In [2],[8], fuzzy-neural and recurrent neural networks have also been used to control the nonlinear noises in the ANC system. Observing the various methods presented in past years, it reveals that the ANC structures for nonlinear control are complex or hard to realize [5].

Keeping these in view, the authors propose the neural based ANC algorithm to control the nonlinear noise. The proposed method also avoids the premature saturation of backpropagation; meanwhile, achieves minimum error by using the proposed self-tuning method.

2 Active Noise Control with Conventional FXLMS Algorithm

Utilizing FXLMS algorithm [12], the conventional ANC system is shown in the Fig. 1. The plant model $H_p(z)$ represents the primary speaker and the model $P(z)$ denotes the mathematical transfer function of the acoustic duct, the input signal $x(k)$ represents the k^{th} unwanted noise sample and the residual noise $e(k)$ is measured by an error microphone with plant model $M_e(z)$. The output signal of the FXLMS $u(k)$ drives an anti-noise speaker with the transfer function $H_s(z)$ to cancel the unwanted noise in the duct. The acoustic transfer function between the location of the anti-noise speaker and the error microphone is referred to as the error path which is represented by $H_e(z)$. The N^{th}-order ANC with weighting parameters $W(k)$ is updated by the FXLMS algorithm. Thus, the residual error noise $e(k)$ can be expressed as

$$e(k) = x(k)H_p(z)P(z)H_e(z)M_e(z) + y(k)H_s(z)H_e(z)M_e(z), \tag{1}$$

where $y(k) = W(k)^T X(k)$, the weighting parameter $W(k) = [w_0(k), w_1(k), ..., w_{N-1}(k)]^T$ and the input noise $X(k) = [x(k), x(k-1), ..., x(k-N+1)]^T$. The corresponding gradient estimation and adaptations of the weights are taken as:

$$\nabla_k = \frac{\partial e^2(k)}{\partial W(k)} = 2e(k)[X(k)H_s(z)H_e(z)M_e(z)] \tag{2}$$

$$W(k+1) = W(k) - 2\mu e(k)[X(k)H_s(z)H_e(z)M_e(z)], \tag{3}$$

where μ is the learning rate. Equation (3) is called FXLMS algorithm, which differs from the conventional LMS algorithm (4) at the correction term,

$$W(k+1) = W(k) - 2\mu e(k)X(k). \tag{4}$$

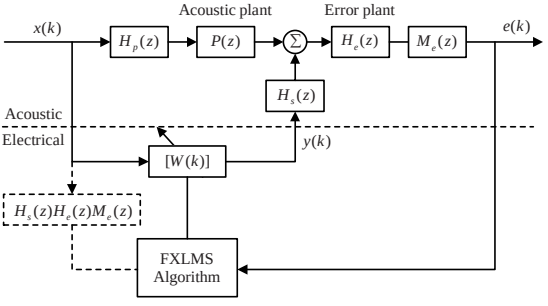

Fig. 1. Conventional ANC system with FXLMS algorithm

3 The Neural Based ANC Algorithm

The ANC system is designed on the basis of a mathematical description and its linearized model. It can be suitably tuned to its desired response using the well-known FXLMS algorithm. However, this method is only effective in canceling narrowband noise but can not provide adequate performance in broadband noise cancellation. The authors propose the neural based ANC system, shown in Fig. 2, to be an alternative. The architecture of the proposed neural filter is depicted in Fig. 3, where the parameters, $w_{ij}(k)$ is the weight between the input layer and hidden layer (i=1,2,…,n_1, j=1,2,…,n_2), $v_j(k)$ is the weight between the hidden layer and output layer. Thus, $h_j(k)$, the output of the hidden node will be:

$$h_j(k) = f_h(net_j) = f_h(\sum_{i=1}^{n_1} w_{ij}(k)x(k-i+1)), \tag{5}$$

where f_h is the activation function of the hidden node, and output of the output node $y(k) = f_o(net_o)$, with f_o is the activation function,

$$y(k) = f_o(net_o) = f_o(\sum_{j=1}^{n_2} h_j(k)v_j(k)) \tag{6}$$

The error function in ANC system to be minimized is defined as:

$$E(k) = \frac{1}{2}[x(k)H_pPH_eM_e + y(k)H_sH_eM_e]^2. \tag{7}$$

The backpropagation and the gradient descent methods are used to achieve the objective. The gradients of $v_j(k)$ and $w_{ij}(k)$ are shown in the following:

$$\frac{\partial E(k)}{\partial v_j(k)} = e(k)H_s H_e M_e f_o'(net_o)h_j'(k) \tag{8}$$

and

$$\frac{\partial E(k)}{\partial w_{ij}(k)} = e(k)H_s H_e M_e f_o'(net_o) f_h'(net_h)v_j'(k) \tag{9}$$

hence, with η is the learning rate, we have

$$v_j(k+1) = v_j(k) - \eta e(k)H_s H_e M_e f_o'(net_o)h_j'(k) \tag{10}$$

$$w_{ij}(k+1) = w_{ij}(k) - \eta e(k)H_s H_e M_e f_o'(net_o) f_h'(net_j)v_j'(k)\,. \tag{11}$$

In this paper, the activation functions $f_h(net_h) = net_h$ and $f_o(net_o) = net_o$ are used to prevent the processing units' saturation which might be induced by sigmoid or hyperbolic tangent functions. Those functions act as implicit constraints for the hidden-node activations may get driven to their limits, making the resultant derivatives of saturated nodes very small due to $f_*'(net_*)$. Hence, even with a sophisticated unconstrained optimization method, neural network learning might fail due to saturation. Therefore, (10) and (11) can be expressed as follows, respectively.

$$v_j(k+1) = v_j(k) - \eta e(k)H_s H_e M_e h_j'(k) \tag{12}$$

$$w_{ij}(k+1) = w_{ij}(k) - \eta e(k)H_s H_e M_e v_j'(k)\,. \tag{13}$$

One can find $h_j(k)$ is also the function of $x(k)$, shown in (5). The correction terms in (12) and (13) are different from the conventional FXLMS at the correction factors.

To achieve the optimal learning rate for the adaptive filter, the Taylor series of the error function is:

$$e(k+1) = e(k) + \sum_{j=1}^{n_2} \frac{\partial e(k)}{\partial v_j(k)} \Delta v_j(k) + \sum_{i=1}^{n_1} \frac{\partial e(k)}{\partial w_{ij}(k)} \Delta w_{ij}(k) + h.o.t. \tag{14}$$

The partial differential terms in (14) can be represented by:

$$\frac{\partial e(k)}{\partial v_j(k)} = H_s H_e M_e f_o'(net_o)h_j'(k) = H_s H_e M_e h_j'(k) \tag{15}$$

$$\frac{\partial e(k)}{\partial w_{ij}(k)} = H_s H_e M_e f_o'(net_o) f_h'(net_j)v_j'(k) = H_s H_e M_e v_j'(k). \tag{16}$$

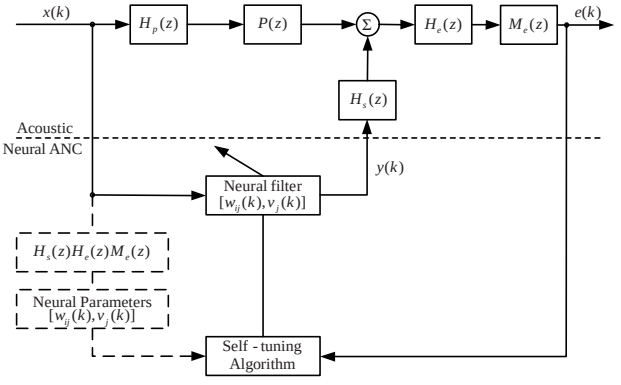

Fig. 2. Neural based ANC system

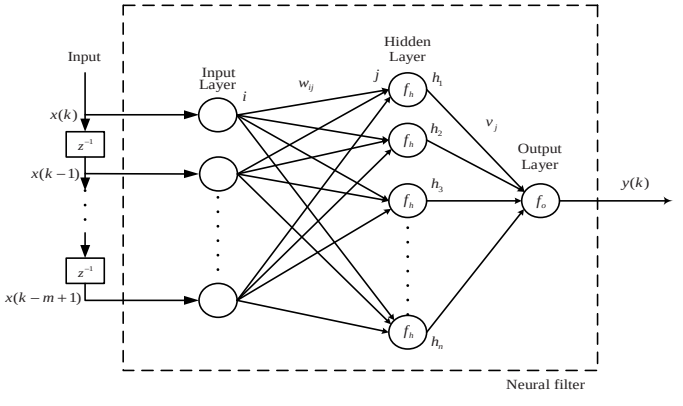

Fig. 3. Architecture of the neural filter

Thus, the correction term is:

$$\Delta e(k) = -\eta e(k)(H_s H_e M_e)^2 \left(\sum_{j=1}^{n_2} \left(h_j'(k) \right)^2 + \sum_{i=1}^{n_1} \left(v_j'(k) \right)^2 \right) \tag{17}$$

by excluding the *h.o.t*. of (14). So, one can minimize the residual noise $e(k)$ by choosing the optimal learning rate η_{opt} in (18).

$$\eta_{opt}(k) = \left[(H_s H_e M_e)^2 \left(\sum_{j=1}^{n_2} \left(h_j'(k) \right)^2 + \sum_{i=1}^{n_1} \left(v_j'(k) \right)^2 \right) \right]^{-1}. \tag{18}$$

4 Simulation Results

The ANC system in a duct is used to verify the proposed neural based method in this paper. The duct model [3],[4] is depicted as follows. The acoustic plant of duct $P(z)$

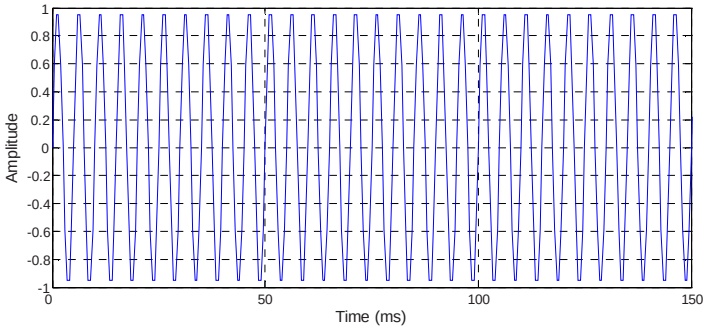

(a)

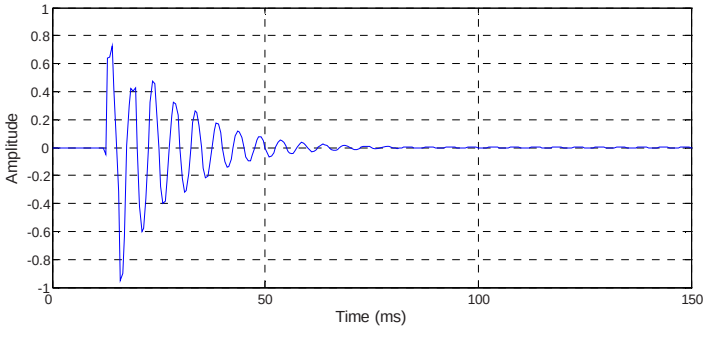

(b)

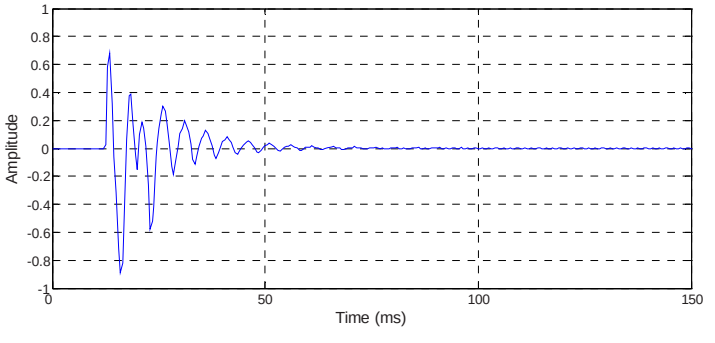

(c)

Fig. 4. Residual error of ANC with 200 Hz periodic noise, (a) Original periodic noise, (b) ANC with FXLMS, (c) proposed neural ANC

and the error path $H_e(z)$ are modeled by pure time delays of 25 samples and 5 samples, respectively. Both the speakers, $H_p(z)$, $H_s(z)$, and the error microphone $M_e(z)$ are represented by the second-order Butterworth high-pass filters with a cutoff frequency 80 Hz. Several different noise signals are used to verify the virtue of the proposed neural based ANC. All the initial weights, $w_{ij}(0)$ and $v_j(0)$, are randomly

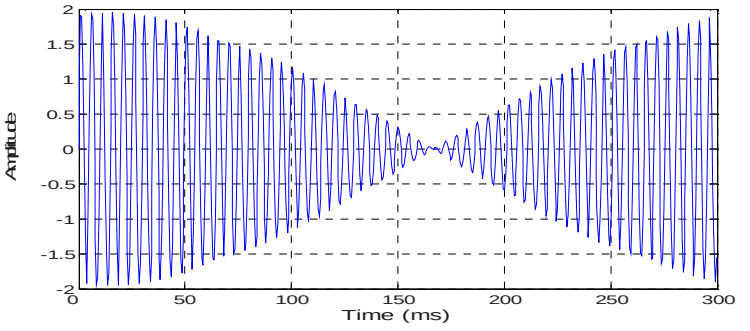

(a)

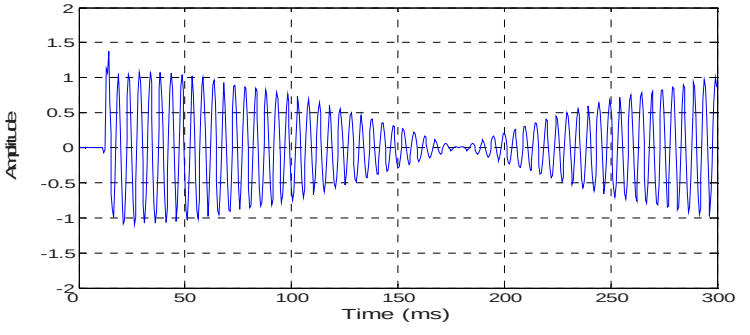

(b)

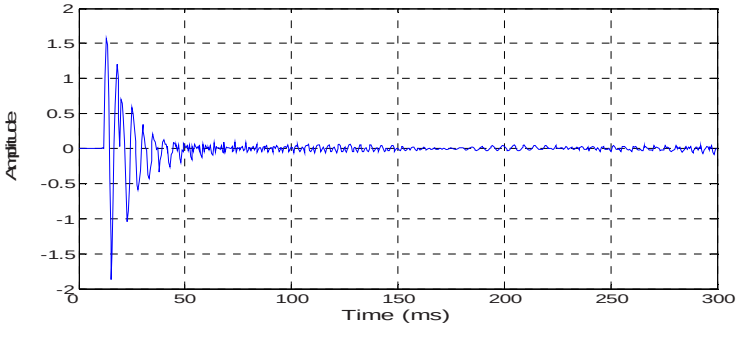

(c)

Fig. 5. Residual error of ANC with composition of 200 and 203 Hz periodic noise (a) Original composite periodic noise (b) ANC with FXLMS (c) proposed neural ANC

initialized between the range [-0.5, 0.5]. The neural ANC algorithm is a 4-input-node, 6-hidden-node and 1-output-node neural network. A 32^{nd}-order adaptive FIR filter with zero initial weighting parameters and constant learning rate $\eta = 0.2$ is used to perform the FXLMS algorithm to be a contrast.

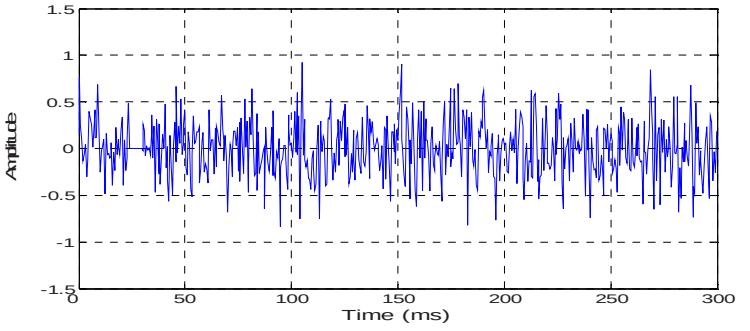

(a)

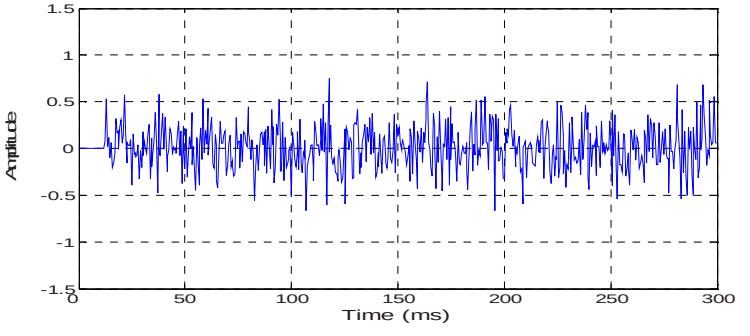

(b)

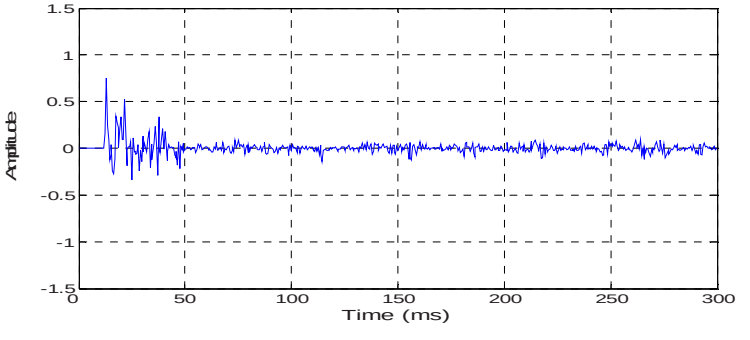

(c)

Fig. 6. Residual error of ANC with broadband noise, (a) Original broadband noise, (b) ANC with FXLMS, (c) proposed ANC

The first experiment uses a 200 Hz periodic signal as the undesired noise to illustrate the effectiveness of the proposed algorithm. Figure 4(a) is the original periodic noise. Figure 4(b) represents the result of the conventional FXLMS algorithm and Fig. 4(c) shows the proposed approach. One finds that both the conventional and the proposed schemes cancel the unwanted noise well.

The next experiment uses the combination of 200 and 203 Hz periodic signals to be the undesired noise signal. Figure 5(a) is the original composite periodic signals. Figures 5(b) and (c) are the noise canceling results by the FXLMS and proposed neural algorithms, respectively. It is clear that the proposed neural algorithm also performs excellently in canceling the composite periodic signals. Nevertheless, the conventional FXLMS algorithm cannot cancel the noise satisfactorily.

In the third experiment, we use the broadband noise to be the unwanted noise. Figure 6(a) shows the nonlinear broadband noise. Figure 6(b) shows the result of the noise cancellation by conventional FXLMS algorithm. From which one can see the ineffectiveness of the FXLMS in canceling broadband noise. However, one can see the effectiveness of the proposed method in canceling the broadband noise as shown in Fig. 6(c). In addition, all the initial zeros of the residual error signals in Figs. 4(c), 5(c) and 6(c) are caused by the pure time delays of $P(z)$ and $H_e(z)$.

These results illustrate that the conventional FXLMS algorithm can only control the narrowband noise yet the proposed algorithm can cancel both the periodic and broadband noises well. The optimal learning rate also helps to achieve faster convergence of the proposed algorithm.

5 Conclusions

In this paper, we develop the neural based method with error backpropagation learning algorithm for the ANC system in a duct. The nonlinear processing ability of the neural network helps to improve the performance of canceling random noise. By choosing $f_h(net_j) = net_j$ and $f_o(net_o) = net_o$ as the activation functions of the neural filter, the proposed neural ANC can also avoid the premature saturation of backpropagation algorithm. At the same time, the proposed way to have the optimum learning rate helps to accelerate the convergence. Computer simulations have been carried out to demonstrate the performance of the proposed method as a useful method for nonlinear ANC. The performance of residual error has been compared to that of FXLMS. It is obvious that the neural based algorithm outperforms FXLMS algorithm for the nonlinear ANC system.

Acknowledgement

This work was supported by the National Science Council under the Grant No. NSC-94-2213-E-231-020.

References

1. Bouchard, M.: Multichannel affine and fast affine projection algorithms for active noise control and acoustic equalization systems. IEEE Transactions on Speech and Audio Processing 11, 54–60 (2003)
2. Bouchard, M., Paillard, B., Dinh, C.T.L.: Improved training of neural networks for the nonlinear active noise control of sound and vibration. IEEE Transactions on Neural Networks 10, 391–401 (1999)

3. Chang, C.Y., Shyu, K.K.: A self-tuning fuzzy filtered-U algorithm for the application of active noise cancellation. IEEE Transactions on Circuits and Systems I: Fundamental Theory and Applications 49, 1325–1333 (2002)
4. Chang, C.Y., Shyu, K.K.: Active noise cancellation with a fuzzy adaptive filtered-X algorithm. IEE Proceedings-Circuits Devices and Systems 150, 416–422 (2003)
5. Das, D.P., Panda, G.: Active mitigation of nonlinear noise Processes using a novel filtered-s LMS algorithm. IEEE Transactions on Speech and Audio Processing 12, 313–322 (2004)
6. Kuo, S.M., Vijayan, D.: A secondary path modeling technique for active noise control systems. IEEE Transactions on Speech Audio Processing 5, 374–377 (1997)
7. Lueg, P.: Process of Silencing Sound Oscillation. U.S. Patent 2, 043, 416 (1936)
8. Mastorocostas, P.A., Theocharis, J.B.: A recurrent fuzzy-neural model for dynamic system identification. IEEE Transactions on Systems, Man and Cybernetics, Part B 32, 176–190 (2002)
9. Sicuranza, G.L., Carini, A.: Filtered-X affine projection algorithm for multichannel active noise control using second-order Volterra filters. IEEE Signal Processing Letters 11, 853–857 (2004)
10. Strauch, P., Mulgrew, B.: Active control of nonlinear noise processes in a linear duct. IEEE Transactions on Signal Processing 46, 2404–2412 (1998)
11. Tan, L., Jiang, J.: Adaptive Volterra filter for active control of nonlinear noise processes. IEEE Transactions on Signal Processing 49, 1667–1676 (2001)
12. Widrow, B., Stearns, S.D.: Adaptive signal processing. Prentice-Hall, Englewood Cliffs (1985)

Case Analysis of Criminal Behaviour

Tibor Bosse, Charlotte Gerritsen, and Jan Treur

Vrije Universiteit Amsterdam, Department of Artificial Intelligence
De Boelelaan 1081, NL-1081 HV, Amsterdam, The Netherlands
{tbosse,cg,treur}@few.vu.nl
http://www.few.vu.nl/~{tbosse, cg, treur}

Abstract. In this paper, it is shown how behavioural properties can be specified for three types of violent criminals. Moreover, it is shown how empirical material in the form of informal descriptions of traces of crime-related events can be formalised. Furthermore, it is shown how these formalised traces and behavioural properties can be used in automated analysis, for example in order to determine which type of criminal can have committed such a crime. Moreover, an underlying dynamical model is presented that shows causal mechanisms behind each of the behaviours, and their dependencies on the characteristics of the type of criminal and inputs in terms of stimuli from the environment.

1 Introduction

Criminology is a multi-disciplinary area focusing on the analysis of criminal behaviour; e.g., [1, 9, 10, 14, 20, 22, 23]. Some contributions to the literature addressing formalisation and computational modelling of criminal behaviour are found in [2, 8, 17, 18]. This paper first presents a modelling and analysis approach for certain types of violent criminal behaviour against data available from crime cases. The paper addresses the question: given information about a committed crime, and a number of suspects, what can be said about the person who committed the crime? It is shown how also automated tools can be used to address this type of question. In particular, it is shown how dynamic properties can be specified that characterise the behaviour of certain types of criminals and how they can be automatically checked on formalisations of partially given traces of crime-related events.

Dynamic properties that characterise the behaviour of a criminal can be specified from an external or from an internal perspective. From an external perspective more complex temporal relationships between inputs and outputs over time have been expressed using the Temporal Trace Language TTL [6]. Dynamic properties from an internal perspective involve direct temporal or causal relationships between internal state properties and have been specified using the language LEADSTO [7]. This is an executable language that also can be used for simulation: given some input in terms of characteristics of a particular type of criminal and stimuli from the environment, the behaviour of this type of criminal in that particular environment can be simulated.

H.G. Okuno and M. Ali (Eds.): IEA/AIE 2007, LNAI 4570, pp. 621–632, 2007.

In Section 2 a brief overview of the types of criminals addressed is given. Section 3 addresses formalisation of partially given traces of crime-related events. Section 4 discusses the behavioural properties from an external perspective, and formal analysis of these properties against formalised cases. Section 5 discusses dynamic properties formalising the mechanisms underlying the criminal behaviours as considered from an internal perspective. In Section 6 one of the generated simulation traces is shown. Section 7 is a discussion.

2 Three Types of Criminals

The case study made in this paper focuses on three types of violent offenders: the violent psychopath, the offender with an antisocial personality disorder (APD), and the offender who suffers from an intermittent explosive disorder (IED). Below, these types of criminals are briefly introduced and commonalities and differences between them are discussed, based on [11, 19, 20]:

- Violent psychopaths do not have feelings like the rest of us. They lack the normal mechanisms of anxiety arousal, which ring alarm bells of fear in most people. Their kind of violence is similar to predatory aggression, which is accompanied by minimal sympathetic arousal, and is purposeful and without emotion. Moreover, they like to exert power and have unrestricted dominance over others, ignoring their needs and justifying the use of whatever they feel compelling to achieve their goals. They do not have the slightest sense of regret.
- Persons with APD have characteristics that are similar to the psychopath. However, they may experience some emotions towards other persons, but these emotions are mainly negative: they are very hostile and intolerant.
- Persons with IED, in contrast, appear to function normally in their daily life. However, during some short periods (referred to as *episodes* from now on), their brain generates some form of miniature epileptic fit. Such episodes can be triggered by minor negative experiences. As a result, some very aggressive impulses are released and expressed in serious assault or destruction of property. After these episodes, IED persons have no recollection of their actions and show feelings of remorse.

Table 1. Overview of characteristics for the three types of violent criminals

	Anxiety threshold	Excitement threshold	Theory of mind	Positive emotional attitude to others	Negative emotional attitude to others	Aggressive-ness	Impulsive-ness	Sensitive to alcohol
Violent Psychopath	high	high	high	low	low	high	high	yes
Antisocial Personality Disorder	medium /high	high	low	low	medium	high	high	yes
Intermittent Explosive Disorder	normally: medium in episode: high	normally: medium in episode: high	normally: medium in episode: low	normally: medium in episode: low	normally: medium in episode: high	normally: medium in episode: high	normally: medium in episode: high	yes

These three types of criminals can be distinguished by taking a number of aspects into account (see also Table 1 for an overview); these are also the aspects incorporated in the model from an internal perspective.

Firstly, the *Anxiety Threshold* is a threshold that needs to be passed by certain stimuli, in order to make a person anxious. Thus, when a person's anxiety threshold is high, it is very difficult for this person to become anxious (and as a result, (s)he hardly knows any fear). This is the case for the violent psychopath and the person with APD: in these persons, a notion of fear is almost completely lacking. In contrast, persons with IED have a medium anxiety threshold. Nevertheless, under some special circumstances (i.e., during episodes) the anxiety threshold of a person with IED suddenly becomes much higher. Moreover, the *Excitement Threshold* needs to be passed by certain stimuli, in order to make a person excited. Thus, when a person's excitement threshold is high, it is very difficult for this person to become excited (and as a result, (s)he is often bored). This is the case for the violent psychopath and for persons with APD. Persons with IED have a medium excitement threshold, but under certain circumstances (during episodes) their excitement threshold becomes high, and they get bored very easily, which makes that they generate the desire to perform certain actions that provide strong stimuli (which are often criminal actions).

Theory of mind e.g., [3, 12, 15] refers to the understanding that others (also) have minds, which can be described by separate mental concepts, such as the other persons' own beliefs, desires, and intentions, and how they play a role in their behaviour. The violent psychopath has a theory of mind that is specialised in aspects that can contribute to his own goals, for example, to manipulate the other person. A person with APD has a less developed theory of mind. Persons who are diagnosed with IED normally have a medium theory of mind, but when they have an aggressive episode, their theory of mind decreases. *Emotional attitudes towards others* express the extent to which a person may have positive or negative feelings with respect to other persons' wellbeing. For the violent psychopath, both are low: these persons hardly show any emotion concerning other persons. For the criminal with APD, the situation is slightly different. Like the violent psychopaths, these persons do not have much positive feelings towards others, but they may have some negative feeling towards others. Finally, criminals with IED usually have a normal (medium) positive and negative emotional attitude towards others, but during the episodes of discontrol, all their positive feelings disappear, and substantial negative feelings arise.

Since this paper focuses on violent criminals, by definition all considered types of criminals are *aggressive*. However, the criminals with IED only become highly aggressive during a short period, whereas the other two types are always aggressive. *Impulsiveness* means that an action was not planned. All types of violent criminals mentioned in this paper are impulsive, but they differ in the type of impulsive action they perform. While the APD offender may lash out in disproportionate overreaction, the psychopath, with his emotional detachment, will impulsively take whatever course of action will supply him with the necessary gratification. Persons with IED normally have a medium impulsiveness, but when they have a seizure they become highly impulsive. For psychopaths and persons with APD, only a small amount of *alcohol or drugs* can become a compulsion and result in violent behaviour. Persons with IED can have episodes triggered by the smallest amount of alcohol.

3 Formalising Crime Cases

In this section, it is shown how partial information related to a crime case can be formalised, in order to characterise the type of person who committed this crime case. Below, two of such cases are shown, in the form of partially given traces (comparable to descriptions of real scenarios as reported by the police).

> ***Case 1*** *Person 1 is walking down the street. Person 2 approaches him and asks for a light for his cigarette. Person 1 answers that he does not have a lighter and continues his walk. After a couple of minutes, person 1 meets person 3 and assaults this person 3. He hits him over 10 times in his face and stomach. For the assault he uses a large stick that he found on the street. During the assault, person 1 constantly calls person 3 names.*

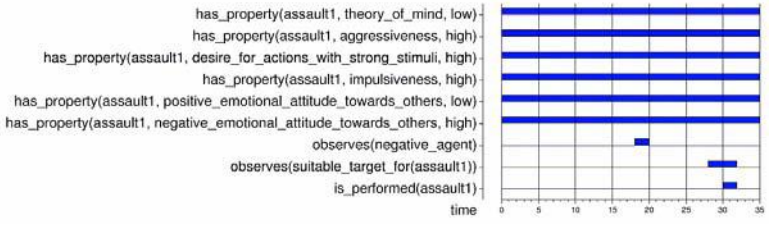

Fig. 1. Example partial trace for Case 1

Using a formal ontology, the dynamics as described by Case 1 can be formalised and visualised as shown in Figure 1. Here, assault1 stands for the assault as described in the story. Moreover, the encounter with person 2 is assumed to be a 'negative experience', which might be sufficient for persons with IED to cause an episode; this is formalised by state property observes(negative_agent). Moreover, observes(suitable_target_for(assault1)) formalises that the agent observes an opportunity for a crime of type assault1. In addition, some atoms of the form has_property(...) are shown. These atoms do not represent events in the scenario, but rather describe some useful common background knowledge (e.g. the fact that hitting someone in the face is a highly aggressive act). Similarly, the dynamics as described by Case 2 below are visualised in Figure 2.

> ***Case 2*** *Person 1 is walking down the street. He is on his way to the ATM because he needs some money for the groceries. However, an old lady is standing in front of the ATM. She is not very fast and it takes her some time to get the money. Person 1 sees a stick lying on the ground, picks it up and hits the old lady. She steps away for the machine because it really hurts. Person 1 walks past her and uses the ATM.*

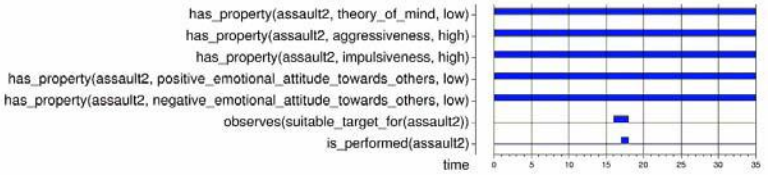

Fig. 2. Example partial trace for Case 2

4 Formalising Criminal Behaviour: External Perspective

In this section it is shown how dynamic properties can be specified to characterise the types of criminals discussed earlier from an external perspective. Moreover, it is discussed how these dynamic properties can be automatically checked against the example traces to find out which type of criminal performed the crime. To analyse traces as discussed in the previous section, the following dynamic properties have been specified in the Temporal Trace Language TTL [6] to characterise, from an external perspective, the different types of violent criminal behaviour considered. To characterise an assault by an IED criminal, two properties are used. The first property checks whether a negative person has been encountered just before the assault (which might have caused an episode); the second property checks whether the assault itself corresponds to some typical characteristics for crimes by persons with IED.

Intermittent Explosive Disorder

a) The assault was performed by a person that first met a negative agent, and later met a passer-by.

IED1(γ:TRACE, t:TIME, a:ACTION) ≡
∃t',t'' [t' < t''< t &
state(γ, t') |= observes(negative_agent) &
state(γ, t'') |= observes(suitable_target_for(a)) &
state(γ, t) |= is_performed(a)]

b) The performed assault is characterised by a high aggressiveness, a high impulsiveness, a low positive emotional attitude towards others, and a high negative emotional attitude towards others.

IED2(γ:TRACE, t:TIME, a:ACTION) ≡
state(γ, t) |= is_performed(a) ∧
has_property(a, aggressiveness, high) ∧ has_property(a, impulsiveness, high) ∧
has_property(a, positive_emotional_attitude_towards_others, low) ∧
has_property(a, positive_emotional_attitude_towards_others, high)

Here state(γ, t) |= X denotes that within the state state(γ, t) at time point t in trace γ state property X holds, with the infix predicate |= within the language denoting the formalised satisfaction relation. Similarly, state(γ, t) |≠ X denotes that X does not hold. See [6] for more details of TTL. Next, the following property characterises an assault by a violent psychopath:

Violent Psychopath

The performed assault is characterised by a high aggressiveness, a high impulsiveness, a low positive emotional attitude towards others, and a low negative emotional attitude towards others.

psychopath(γ:TRACE, t:TIME, a:ACTION) ≡
state(γ, t) |= is_performed(a) ∧
has_property(a, aggressiveness, high) ∧ has_property(a, impulsiveness, high) ∧
has_property(a, positive_emotional_attitude_towards_others, low) ∧
has_property(a, positive_emotional_attitude_towards_others, low)

These dynamic properties have been checked automatically for the cases 1 and 2 described above (see also Figure 1 and 2) using the TTL checker tool [6]. For case 1 it turns out that IED1 and IED2 hold and psychopath does not hold. For case 2 psychopath holds and IED1 and IED2 do not hold. This indicates that the first case the criminal may be of IED type and in the second case a violent psychopath. Thus, using these checks, it indeed turned out possible to assign certain types of criminals to certain (partial) traces.

5 Formalising Criminal Behaviour: Internal Perspective

In this section, it is shown how criminal behaviour is formalised from an internal perspective. A dynamical system model for the underlying mechanisms that has been developed is briefly described. This model was developed within the LEADSTO environment, see [7]. In LEADSTO, direct temporal dependencies between two state properties in successive states are modelled by *executable dynamic properties*, defined as follows. Let α and β be state properties of the form 'conjunction of ground atoms or negations of ground atoms'. In the LEADSTO language the notation $\alpha \rightarrow\!\!\!\!\rightarrow_{e, f, g, h} \beta$, means:

> *if state property* α *holds for a certain time interval with duration g,*
> *then after some delay (between e and f) state property* β *will hold*
> *for a certain time interval of length h.*

Here atomic state properties can have a qualitative, logical format, such as an expression desire(d), expressing that desire d occurs, or a quantitative, numerical format such as an expression has_value(x, v) which expresses that variable x has value v. For more details, see [7]. The dynamical system model has been built by composing three submodels:

1. a *BDI-model* to determine actions based on beliefs, desires and intentions
2. a submodel *to determine desires*, used as input by the BDI-model.
3. a submodel *to determine beliefs in an opportunity*, as input for the BDI-model.

The *BDI-model* bases the preparation and performing of actions on motivational states such as beliefs, desires and intentions e.g., [13, 16, 21]. It uses as input desires and beliefs in opportunities, generated by the other two submodels. In this model an action a is performed when the subject has the intention to do this action and it has the belief that the opportunity to do the action is there. Beliefs are created on the basis of stimuli that are sensed or observed. The intention to do a specific type of action a is created if there is a certain desire d, and there is the belief that in the given world state, performing this action will fulfil this desire.

$$\text{desire(d)} \wedge \text{belief(satisfies(a, d))} \rightarrow\!\!\!\!\rightarrow \text{intention(a)}$$
$$\text{intention(a)} \wedge \text{belief(opportunity\_for(a))} \rightarrow\!\!\!\!\rightarrow \text{to\_be\_performed(a)}$$

Assuming that beliefs in reason for intentions are internally available, what remains to be generated in this model are the desires and the beliefs in opportunities. Generation of desires often depends on domain-specific knowledge, which also seems

to be the case for criminal behaviour. Beliefs in opportunities are based on the Routine Activity Theory by [9].

The *submodel to determine desires* is a rather complex submodel, incorporating various aspects. To model these, both causal and logical relations (as in qualitative modelling) and numerical relations (as in differential equations) have been integrated in one modelling framework. This integration was accomplished, using the LEADSTO language as a modelling language. The variety of aspects that were found relevant in the literature, such as [4, 11, 19, 20] and are taken into account in this submodel, are: (a) use of a *theory of mind* (e.g., understanding others), (b) desires for *aggressiveness* (e.g., using violence), (c) desires to *act* (no matter which type of action) and (d) to *act safely* (e.g., avoiding risk), (e) desires for *actions with strong stimuli* (e.g., thrill seeking), (f) desires for *impulsiveness* (e.g., unplanned action), and (g) social-emotional *attitudes with respect to others* (e.g., feel pity for someone). Note that these aspects are derived on the basis of (but not exactly equal to) the characteristics as described in Table 1. Different combinations of such elements lead to different types of (composed) desires, for example:

- the desire to perform an exciting planned nonaggressive nonrisky action that harms somebody else (e.g., a pick pocket action in a large crowd)
- the desire to perform a exciting impulsive aggressive risky action that harms somebody else (e.g., killing somebody in a violent manner in front of the police department)

The following LEADSTO property (LP) is used to generate a composed desire out of some of the ingredients mentioned above; here the x1, x2, x3, x4, x5, x6, x7, x8 are qualitative labels (e.g., high, medium, low) or numerical values (integer or real numbers):

LP24 A combination of values for theory of mind, desire for aggressiveness, desire to act, desire to act safely, desire for actions with strong stimuli, desire for impulsiveness, emotional attitude towards others(pos) and emotional attitude towards others(neg) will lead to a specific composed desire, represented as d(x1, x2, x3, x4, x5, x6, x7, x8).

$\forall$x1,x2,x3,x4,x5,x6,x7,x8:SCALE
theory_of_mind(x1) $\wedge$ desire_for_aggressiveness(x2) $\wedge$ desire_to_act(x3) $\wedge$
desire_to_act_safely(x4) $\wedge$ desire_for_actions_with_strong_stimuli(x5) $\wedge$
desire_for_impulsiveness(x6) $\wedge$ emotional_attitude_towards_others(pos,x7) $\wedge$
emotional_attitude_towards_others(neg,x8)
$\twoheadrightarrow$ desire(d(x1, x2, x3, x4, x5, x6, x7, x8))

Due to space limitations, the parts of the submodel to determine each of the ingredients (a) to (g) cannot be described in detail. To give an impression, a rough sketch of part of this submodel is given. Stimuli are labeled with two aspects, indicating the strength with respect to anxiety (risk), and with respect to excitement (thrill), respectively. For both aspects, thresholds represent characteristics of the person considered. The excitement threshold depends on other aspects in the model, such as sensitivity for and use of drugs and alcohol, and basic sensitivity to stimuli. A stimulus with excitement strength below the excitement threshold leads to being bored, and being bored leads to a desire for an action with strong(er) stimuli. Similarly, a stimulus with anxiety strength above the anxiety threshold leads to

internal alarm bells, which (depending on another characteristic, the tendency to look for safety) leads to the desire to take into account anxiety.

The *submodel to determine opportunities* is based on two of the three criteria as indicated in the Routine Activity Theory by [9]. The third criterion of the Routine Activity Theory, the presence of a motivated offender, is indicated by the intention in the BDI-model. This way, the presence of the three criteria together leads to the action to perform a criminal act, in accordance with [9]. More specifically, the notion of opportunity is based on the presence of a suitable target, and the absence of social control (guardian). This was specified by the following property in LEADSTO format:

LP34 When a suitable target for a certain action is observed, and no suitable guardian is observed, then a belief is created that there is an opportunity to perform this action.

$\forall$a:ACTION
observes(suitable_target_for(a)) $\wedge$ not observes(suitable_guardian_for(a))
$\rightarrow\!\!\!\rightarrow$ belief(opportunity(a))

6 Simulated Criminal Behaviour from an Internal Perspective

The model described in the previous section has been used to generate a number of simulation traces for the different types of violent criminals addressed. In Figure 3, an example trace is depicted, which addresses the case of the criminal with IED. In this picture, time is on the horizontal axis; state properties are on the vertical axis. A dark box on top of the line indicates that the property is true during that time period, and a lighter box below the line indicates that the property is false. The lower part of the picture depicts some quantitative information: the thresholds for anxiety and excitement, and the strength of the world stimuli.

The initial state properties that have been set to model the person with IED are as follows (see time point 0): low preparedness to look for safety, low psychological self, high potential aggressiveness, medium potential positive and negative emotional attitude towards others, medium potential anxiety and excitement threshold (both value 5), a low potential sensitivity for stimuli (value 3) and (s)he drinks alcohol and is sensitive for it. Later, at time point 25, (s)he encounters a negative agent and generates an episode, which has some important consequences. Because of the episode, the person with IED generates a desire (at time point 29) that is characterised by the following elements: low theory of mind, high aggressiveness, high desire to act, low desire to act safely, high desire for actions with strong stimuli, high impulsiveness, low positive emotional attitude towards others, high negative emotional attitude towards others. As a result, the criminal generates an intention to perform a specific type of assault (denoted by assault1), and, as soon as the opportunity is there, actually performs the assault. As a result, the stimuli of the world increase, which satisfies the desires of the criminal. Note that, in order to classify these kinds of simulation traces, they can also be verified against the properties shown in Section 4. This has been performed successfully, using the TTL checker.

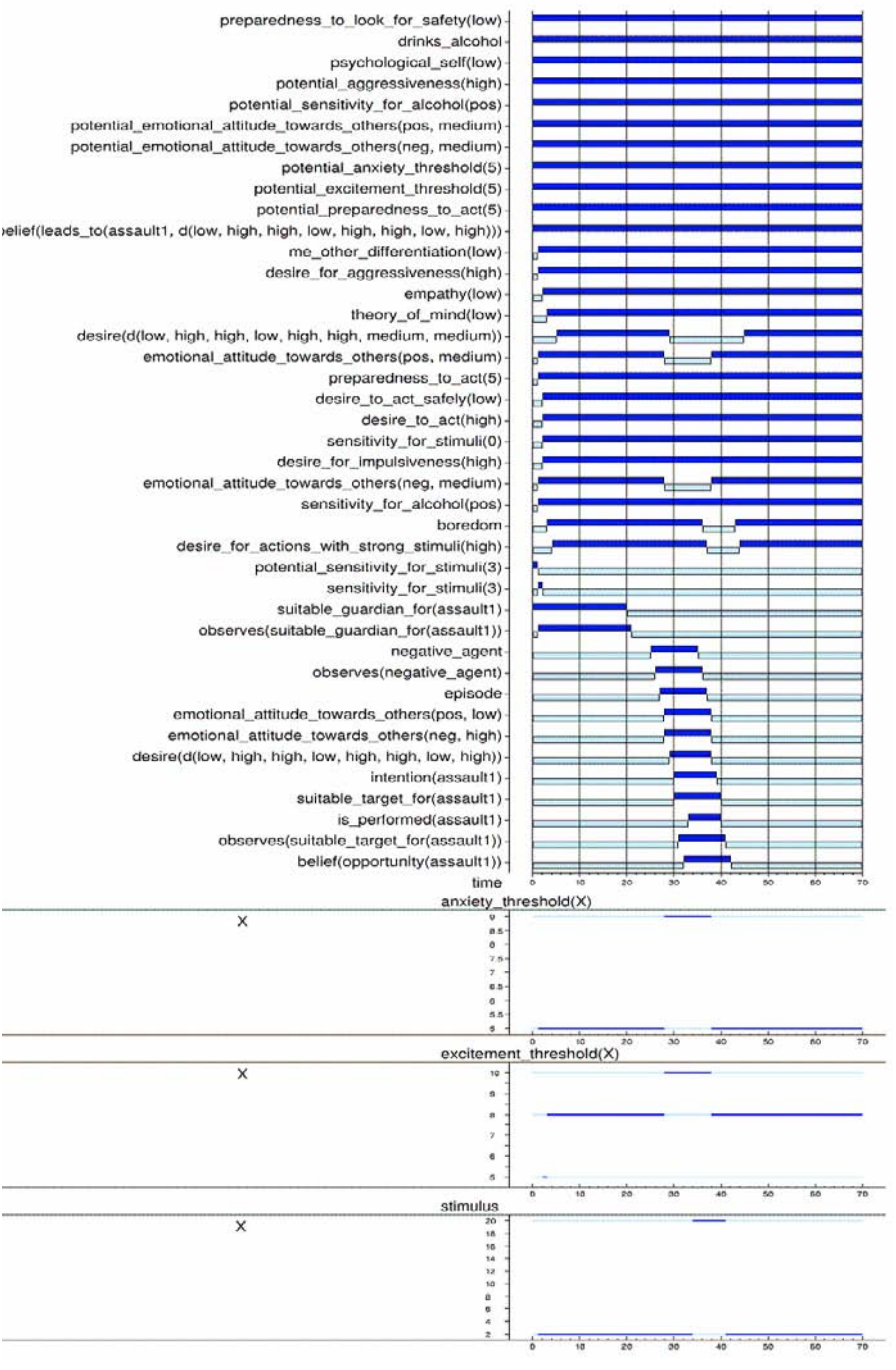

Fig. 3. Example simulation trace for a criminal with IED

7 Discussion

For the analysis of criminal behaviour computer support is more than welcome, but almost inexistent. As one of the ways to address this, a formal method to analyse crime cases against known types of criminal behaviour was presented. As a case study, this method has been applied to three types of violent criminals. It was shown how the temporal language TTL [6] can be used to specify dynamic properties that characterise the behaviour of different types of criminals from an external perspective. Moreover, it was shown how crime cases, for example as reported by the police, can be formalised. Furthermore, it was shown how the automated TTL checker can be used to verify the behavioural properties for the formal (partial) traces describing specific crime cases. Note that the properties addressed in this paper and the two cases considered are only meant as an illustration of the approach, and are therefore not too complex. However, the expressivity of TTL allows it to handle more complex properties and cases (involving, e.g., real values, or more time points). Thus, in the future the approach will be applied to such more complex realistic cases and properties as well.

In addition, from an internal perspective a model has been developed that describes the dynamics of the basic mechanisms underlying the criminal behaviour types considered. This executable model can be set with characteristics of any of these three types of criminals and used to simulate behaviour. It has been shown that, if the right characteristics are set, the model indeed shows the behaviour as known for the corresponding type of criminal.

The presented modelling approach integrates qualitative, logical aspects and quantitative, numerical aspects. This integration allows the modeller to exploit techniques from both areas, such as automated methods for logical analysis and possibilities to simulate dynamical systems using numerical methods, also incorporating qualitative elements. The model was validated by comparing it to patterns described in criminological literature.

In comparison to existing work in the formalised analysis of criminal behaviour, an important distinction is that the research presented here focuses on the dynamical aspect of criminal behaviour. Most approaches to the analysis of criminal behaviour that have been proposed are basically static and usually based on profiling. In contrast, the work reported here (1) takes the dynamical systems perspective on behaviour as a point of departure, which considers behaviour as emerging from a dynamic interplay of various components and aspects, and (2) exploits and integrates qualitative and quantitative techniques developed to model such complex dynamical systems. This is shown, for example, in the simulation of a criminal with IED, where personal characteristics may change dramatically due to events that are encountered.

Similar to the current paper, [5] also incorporates formal methods applied to criminal behaviour. However, that paper focuses only on the IED criminal, whilst the current paper addresses three types of violent criminals. Moreover, [5] does not concentrate on crime case analysis but on simulation and evaluation of simulated traces with respect to environmental properties, including some probabilistic properties.

References

1. Alison, L.J., Bennell, C., Mokros, A., Ormerod, D.: The personality paradox in offender profiling: A theoretical review of the processes involved in deriving background characteristics from crime scene actions. Psychology, Public Policy, and Law 8, 115–135 (2002)
2. van Baal, P.H.M.: Computer Simulations of Criminal Deterrence: from Public Policy to Local Interaction to Individual Behaviour. Ph.D. Thesis, Erasmus University Rotterdam. Boom Juridische Uitgevers (2004)
3. Baron-Cohen, S.: Mindblindness. MIT Press, Cambridge (1995)
4. Bartol, C.R.: Criminal Behavior: a Psychosocial Approach, 6th edn. Prentice Hall, New Jersey (2002)
5. Bosse, T., Gerritsen, C., Treur, J.: Cognitive and Social Simulation of Criminal Behaviour: the Intermittent Explosive Disorder Case. In: Proceedings of the Sixth International Joint Conference on Autonomous Agents and Multi-Agent Systems, AAMAS'07. ACM Press (in press)
6. Bosse, T., Jonker, C.M., van der Meij, L., Sharpanskykh, A., Treur, J.: Specification and Verification of Dynamics in Cognitive Agent Models. In: Nishida, T., et al. (eds.) Proc. of the 6th Int. Conf. on Intelligent Agent Technology, IAT'06, pp. 247–254. IEEE Computer Society Press, Los Alamitos (2006)
7. Bosse, T., Jonker, C.M., van der Meij, L., Treur, J.: LEADSTO: a Language and Environment for Analysis of Dynamics by SimulaTiOn. In: Eymann, T., Klügl, F., Lamersdorf, W., Klusch, M., Huhns, M.N. (eds.) MATES 2005. LNCS (LNAI), vol. 3550, pp. 165–178. Springer, Heidelberg (2005)
8. Brantingham, P.L., Brantingham, P.J.: Computer Simulation as a Tool for Environmental Criminologists. Security Journal 17(1), 21–30 (2004)
9. Cohen, L.E., Felson, M.: Social change and crime rate trends: a routine activity approach. American Sociological Review 44, 588–608 (1979)
10. Cornish, D.B., Clarke, R.V.: The Reasoning Criminal: Rational Choice Perspectives on Offending. Springer, Heidelberg (1986)
11. Delfos, M.F.: Children and Behavioural Problems: Anxiety, Aggression, Depression and ADHD; A Biopsychological Model with Guidelines for Diagnostics and Treatment. Harcourt book publishers, Amsterdam (2004)
12. Dennett, D.C.: The Intentional Stance. MIT Press, Cambridge (1987)
13. Georgeff, M.P., Lansky, A.L.: Reactive Reasoning and Planning. In: Proceedings of the Sixth National Conference on Artificial Intelligence, AAAI'87. Menlo Park, California. American Association for Artificial Intelligence, pp. 677–682 (1987)
14. Gottfredson, M., Hirschi, T.: A General Theory of Crime. Stanford University Press (1990)
15. Humphrey, N.: Consciousness Regained. Oxford University Press, Oxford (1984)
16. Jonker, C.M., Treur, J., Wijngaards, W.C.A.: A Temporal Modelling Environment for Internally Grounded Beliefs, Desires and Intentions. Cognitive Systems Research Journal 4(3), 191–210 (2003)
17. Liu, L., Wang, X., Eck, J., Liang, J.: Simulating Crime Events and Crime Patterns in RA/CA Model. In: Wang, F. (ed.) Geographic Information Systems and Crime Analysis, pp. 197–213. Singapore: Idea Group (2005)
18. Melo, A., Belchior, M., Furtado, V.: Analyzing Police Patrol Routes by Simulating the Physical Reorganisation of Agents. In: Sichman, J.S., Antunes, L. (eds.) MABS 2005. LNCS (LNAI), vol. 3891, pp. 99–114. Springer, Heidelberg (2006)

19. Moir, A., Jessel, D.: A Mind to Crime: the controversial link between the mind and criminal behaviour. Michael Joseph Ltd, Penguin, London (1995)
20. Raine, A.: The Psychopathology of Crime: Criminal Behaviors as a Clinical Disorder. Guilford Publications, New York (1993)
21. Rao, A.S., Georgeff, M.P.: Modelling Rational Agents within a BDI-architecture. In: Allen, J., Fikes, R., Sandewall, E. (eds.) Proc. of the 2nd Int. Conf. on Principles of Knowledge Representation and Reasoning (KR'91), pp. 473–484. Morgan Kaufmann, San Francisco (1991)
22. Towl, G.J., Crighton, D.A.: The Handbook of Psychology for Forensic Practitioners. Routledge, London, New York (1996)
23. Turvey, B.: Criminal Profiling: an Introduction to Behavioral Evidence Analysis. Academic Press, San Diego (1999)

Diagnosing Dependent Failures in the Hardware and Software of Mobile Autonomous Robots*

Jörg Weber and Franz Wotawa

Institute for Software Technology, Technische Universität Graz, Austria
{jweber,wotawa}@ist.tugraz.at

Abstract. Previous works have proposed to apply model-based diagnosis (MBD) techniques to detect and locate faults in the control software of mobile autonomous robots at runtime. The localization of faults at the level of software components enables the autonomous repair of the system by restarting failed components. Unfortunately, classical MBD approaches assume that components fail independently. In this paper we show that dependent failures are very common in this application domain and we propose the concept of *diagnosis environments (DEs)* in order to tackle the arising problems. We provide an algorithm for the computation of DEs and present the results of case studies.

Keywords: Model-based Reasoning, Model-based Diagnosis, Monitoring, Dependent Failures.

1 Introduction

The authors of [1] propose to detect and locate faults in the control software of mobile autonomous robots at runtime by employing model-based diagnosis (MBD) techniques. They rely on the consistency-based diagnosis paradigm [2][3]. It is assumed that the system consists of independent computational modules, the components. Faults are detected by continuously monitoring properties of the system, and the dependencies between these properties are captured by abstract behavior models of components. In case of property violations, the faults are located at the component level, and the system can be autonomously repaired by restarting failed components. The goal of this research is to improve the reliability of mobile autonomous robots and to enable them to complete their tasks even in cases when unexpected faults occur at runtime.

As usual in MBD, these approaches assume that components fail independently, i.e., the failure of one component cannot cause the failures of other components. Unfortunately, this assumption does not hold in all domains. In particular, we will show that dependent faults are quite common in hardware-software hybrid systems.

One consequence of dependent failures is that the minimal diagnoses, which are typically the base for repair actions, often do not include all components

* This research has been funded in part by the Austrian Science Fund (FWF) under grant P17963-N04. Authors are listed in alphabetical order.

H.G. Okuno and M. Ali (Eds.): IEA/AIE 2007, LNAI 4570, pp. 633–643, 2007.

which have failed. Moreover, the order of the dependent failures, which is not reflected in the minimal diagnoses, is crucial for a successful repair of the system.

Therefore, we propose the concept of *diagnosis environments (DEs)*. A DE of a diagnosis Δ contains all components in Δ and, in addition, it may contain further components which may have caused the failure of a component in Δ. Furthermore, a DE captures the order in which the components have failed. The definition of DEs is based upon the notion of diagnosis, and the computation of DEs is done after the generation of diagnoses.

To the best of our knowledge, this is the first work in the context of consistency-based diagnosis which tackles the issue of dependent failures at the level of logical reasoning. In the next section we outline previous work on the application of MBD to runtime diagnosis in mobile autonomous robots. In Sec. 3 we give examples for dependent faults in the hardware-software hybrid system of an autonomous robot, and we show that repair actions which are based on minimal diagnoses will often fail in case of dependent failures. In Sec. 4 we define the concept of diagnosis environments. Sec. 5 provides a simple algorithm for computing all minimal DEs of a diagnosis, and in Sec. 6 we present the result of case studies.

2 MBD in a Mobile Autonomous Robot

The authors of [1] introduced a technique which enables model-based runtime fault detection and localization in the control system of a mobile autonomous robot. Figure 1 depicts a fragment of the control system of a soccer robot. In addition, it also contains a hardware component, *Ca*.

This architectural view comprises largely independent components and the connections between them. The connections represent data flows over different communication channels. The software components communicate either by exchanging asynchronous events or by remote procedure calls. For example, *PG*

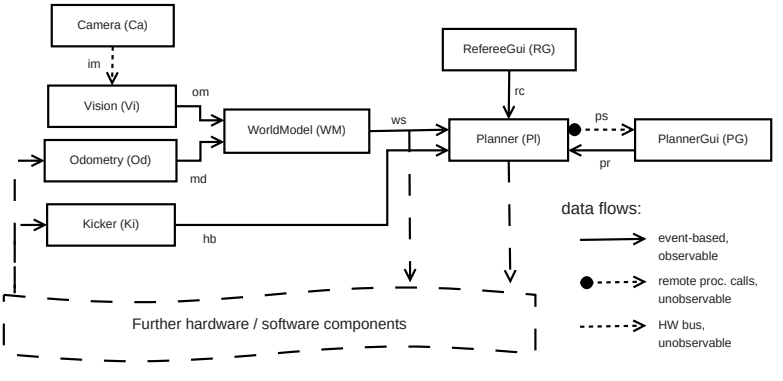

Fig. 1. Architectural view on the HW and SW of a mobile autonomous robot

receives data from *Pl* by remotely invoking *Pl* procedures, but it also sends events to *Pl*. *Vi* reads images from *Ca* which are transmitted over a bus. We assume that this channel cannot be intercepted, i.e., this connection is unobservable.

The abstract behavior model assigns arbitrary *properties* to components and connections. Properties capture invariants of the system. For example, the component property *npr* ("number of processes") expresses that a certain software component must spawn a minimal number of processes (threads). When a software component crashes, then this property will be violated. An example for a connection property is *nev* ("number of events"), indicating that a certain (minimum) number of events must occur on this connection within a certain time span. A violation of this property could be, e.g., an indication of a deadlock somewhere in the system.

In the logical model propositions of the form $ok(x, pr)$ are used, stating that the property *pr* holds for the component or connection x. At runtime, the system is continuously monitored by *rules*. For each proposition $ok(x, pr)$ there are one or more rules which monitor the system and detect violations of this property. Rules are software plug-ins, i.e., one can implement arbitrary rules and integrate them with the diagnosis system. As usual in MBD, the set OBS contains a set of literals representing the observations. If a violation of (x, pr) has been detected by a rule, then $\neg ok(x, pr)$ is added to OBS, otherwise $ok(x, pr)$ is added.

When property violations occur, the fault(s) is (are) localized by employing relationships between the properties. These relationships are reflected in the logical system description SD. For example, the component WM generates an output event for every event incoming on one of its input connections (*om* and *md*). Intuitively, if WM behaves nominally and if $ok(om, nev)$ and $ok(md, nev)$ hold, then $ok(ws, nev)$ must hold as well. Note that component properties like *npr* do not depend on any input (a component must always spawn a certain number of processes). Thus, the set SD contains the sentences

$$\neg ab(WM) \wedge ok(om, nev) \wedge ok(md, nev) \rightarrow ok(ws, nev)$$
$$\neg ab(WM) \rightarrow ok(WM, npr)$$

where *ab* denotes "abnormal".

The diagnosis candidates are computed by relying on the consistency-based MBD approach [2][3]. A *diagnosis* is a set of components Δ s.t. $SD \cup OBS \cup \{\neg ab(c) \mid c \in COMP \setminus \Delta\} \cup \{ab(c) \mid c \in \Delta\}$ is consistent, where $COMP$ is the set of components and $\Delta \subseteq COMP$. There are well-known algorithms, like Reiter's Hitting Set algorithm [2], which compute all *(subset-)minimal diagnoses*. A diagnosis Δ is minimal iff no proper subset of it is a diagnosis.

For example, suppose the rule for $ok(ws, nev)$ reports a violation – i.e., there are no or too few events on connection *ws*. Assuming that no other rules are active, we obtain a set of observations $OBS = \{\neg ok(ws, nev)\}$. From the behavior model of WM (see above) we can infer that either WM has failed or that at least one of the properties $ok(om, nev)$ or $ok(md, nev)$ is violated as well. Thus, the set of minimal diagnoses is as follows: $\{\{WM\}, \{Vi\}, \{Od\}, \ldots\}$. Moreover, suppose we activate additional rules and obtain $OBS = \{ok(om, nev),$

$ok(md, nev), \neg ok(ws, nev)\}$. Now the set of minimal diagnoses is $\{\{WM\}\}$. The reason for this misbehavior could be a crash or a deadlock.

Our goal is the autonomous repair of failed components at runtime. As described in [4], failed software components can often be "repaired" by restarting them. Although this is not a real repair, as the same fault may occur again, it often enables the robot to complete its task.

3 Dependent Failures in HW-SW Hybrid Systems

The classical approaches to MBD focus on minimal diagnoses. This strategy is well-founded if one assumes that components fail independently – an assumption which is usually made in MBD. However, as De Kleer remarks in [5], dependent failures are quite common in some domains.

Suppose that SD contains the sentence $\neg ab(Vi) \rightarrow ok(Vi, npr)$. If Vi crashes, we observe $\neg ok(Vi, npr)$ and obtain the single-fault diagnosis $\Delta = \{Vi\}$. However, from our practical experience we know that crashes of Vi are often caused by a failure of the camera, as Vi is tightly coupled to Ca because it directly accesses the camera's hardware. Since the connection im between Ca and Vi is not observable, we have no means to directly detect that Ca has failed. Thus, given the observation $\neg ok(Vi, npr)$, Ca will never be part of a minimal diagnosis.

Desirable would be a result like $\Theta(\Delta) = \{\theta_1, \theta_2\}$ with $\theta_1 = \{indf(Vi)\}$ and $\theta_2 = \{indf(Ca), df(Ca, Vi)\}$, where the predicate $indf$ means "independent failure" and df denotes "dependent failure". I.e., there are 2 possibilities: either Vi has failed independently or Ca has failed independently and Vi has failed due to Ca. The sets θ_1 and θ_2 are *diagnosis environments (DEs) of* Δ. They contain all components $c \in \Delta$ and may, in addition, contain components which have caused the failure of any $c \in \Delta$. Components which have failed independently are *primarily failed components (PFCs)*, in contrast to *secondarily failed components (SFCs)* which have failed due to another component.

The crucial point in this example is that a repair which is solely based on Δ may fail: restarting Vi is useless if the camera has caused the failure, as the restarted Vi will fail again immediately. However, a repair based on $\Theta(\Delta)$ can yield better results: after a repeated failure of the restarted Vi we can discard θ_1, i.e., θ_2 is the "right" DE, and repair the system by resetting the camera (if possible) and then restarting Vi. Even if it is not possible to repair the camera, it is still desirable to know the actual cause of the failure.

Let us look at another example: suppose both Pl and PG have failed and $\Delta = \{Pl, PG\}$. As already explained, PG makes remote procedure calls to Pl. Therefore, when Pl fails then it may be the case that PG fails as well – PG "loses" the connection to Pl, throws an exception and then terminates. Moreover, as multiple independent faults are unlikely in most domains, the diagnosis environment $\theta = \{indf(Pl), df(Pl, PG)\}$ is much more likely than the assumption that these two components have failed independently.

Unlike the previous example, where the problem was that the minimal diagnosis did not contain the PFC, in this example the candidate Δ comprises all failed

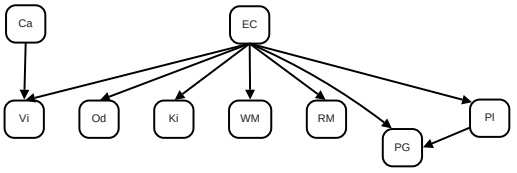

Fig. 2. The FDG of our example system

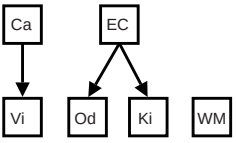

Fig. 3. A DE-DAG

components. Unfortunately, this is not sufficient in the presence of dependent faults: in order to repair the system, we also have to know the order in which the components have failed. Suppose we restart *PG* before repairing *Pl*. Clearly, *PG* will fail again, when it tries to call a *Pl* procedure. In most applications, when a component c_i causes a failure of c_j, then c_i must be repaired before c_j.

In our final example we show that components may fail dependently when they are based on a common framework. Our control system is based on CORBA, and for the asynchronous event-based communication among SW components we use a CORBA Event Channel (EC). *EC* is not contained in the model in Fig. 1. However, most of the SW components depend on *EC*: they post new events to *EC*, and/or they subscribe to events produced by other components. Our experience has shown that a failure of *EC* propagates to many other components, which typically throw exceptions and then terminate.

4 Diagnosis Environments

The notion of DE is based on the definition of diagnosis. A DE of a minimal diagnosis Δ contains all components in Δ and, in addition, it may contain further components which are assumed to have caused a failure of any $c \in \Delta$. Thus, the computation of DEs is done after computing the minimal diagnoses of $SD \cup OBS$.

The intended usage of SD is as usual in MBD: using the literal $\neg ab(\cdot)$, it contains sentences which specify the nominal behavior of components. Furthermore, we allow the usage of the fault mode *ab* in order to define conditions which must hold when a component is faulty [6]. For example, if we assume that any failure of *EC* is a total failure, then we can say that no more events can be observed on the affected connections: $ab(EC) \rightarrow \big(\neg ok(om, nev) \wedge \neg ok(md, nev) \wedge \cdots\big)$.

Our first step towards the definition of DEs is to introduce the *Failure Dependency Graph (FDG)*. The FDG is a directed acyclic graph (DAG) whose nodes are components and whose edges represent possible fault dependencies. An edge from c_i to c_j indicates that a failure of c_i may propagate to c_j. The FDG for our example system is depicted in Fig. 2. Note that *PG* is also indirectly dependent on *EC*: *EC* might cause a failure of *Pl* which propagates to *PG*.

All components in a DE are assumed abnormal. For stating the pathes of failure propagation, we use the already introduced predicates $indf(c)$ and $df(c_i, c)$. These predicates are *dependency modes (d-modes)* of *c*. If a DE contains $df(c_i, c)$, then c_i must be abnormal as well, i.e., the DE must also contain either $indf(c_i)$

or $df(\cdot, c_i)$. The set of available modes for each component is restricted by the FDG: e.g., Vi has the d-modes $indf(Vi)$, $df(Ca, Vi)$, and $df(EC, Vi)$, whereas there is no df-mode for EC, as it has no parents in the FDG.

There are 2 equivalent views at a DE: first, it can be seen as an assignment of d-modes to components. Second, it can also be regarded as a DAG, which we call DE-DAG. For example, Fig. 3 depicts $\theta = \{indf(Ca), df(Ca, Vi), indf(EC), df(EC, Od), \ df(EC, Ki), indf(WM)\}$. The DE-DAG contains all components in θ, and for all modes $df(c_i, c_j) \in \theta$ there is an edge from c_i to c_j. Obviously, a DE-DAG must be a subgraph of the FDG. However, we assume that the dependent failure of a component c is caused by a single component c_i. Hence, each node in a DE-DAG has at most one parent.

Finally, before providing a definition of DEs, we introduce the *System Dependencies Description (SDD)*. The SDD is a set of logical sentences representing addional constraints which must hold when a component c fails in dependence of c_i. These sentences typically have the form $df(c_i, c) \rightarrow [\cdots]$. For example, we know that if any component c fails due to EC, then c throws an exception and/or crashes. In the former case, the property $ok(c, no\_exc)$ will be violated. This property means that a nominally behaving component does not throw any exceptions. In the latter case, $ok(c, npr)$ is violated (see Sec. 2). This knowledge can be expressed by the sentence

$$df(EC, c) \rightarrow \big(\neg ok(c, no\_exc) \vee \neg ok(c, npr)\big)$$

Suppose that a component c has a deadlock, i.e., it neither throws an exception nor crashes. Then the assumption $df(EC, c)$ leads to a contradiction.

Now we have the necessary prerequisites to define DEs. Let $\Theta(\Delta)$ denote the complete set of DEs of a diagnosis Δ. Moreover, let $\Gamma(\theta)$ be the set containing those components which occur in θ and $\overline{\Gamma}(\theta) = COMP \setminus \Gamma(\theta)$. Then each $\theta \in \Theta(\Delta)$ is an assignment of d-modes to components s.t.:

1. $SD \cup OBS \cup \{\neg ab(c) | c \in \overline{\Gamma}(\theta)\} \cup \{ab(c) | c \in \Gamma(\theta)\} \cup SDD \cup \theta$ is consistent.
2. For all components $c \in \Delta$: either $indf(c) \in \theta$ or $df(\cdot, c) \in \theta$.
3. For all c' in θ: either $c' \in \Delta$ or there is a path in the DE-DAG from c' to any $c \in \Delta$.

Item 1 defines that all components in θ are abnormal, the remaining components are not abnormal. Furthermore, the df-assumptions in θ together with the constraints in SDD must be consistent with the observations. Item 2 says that every component in Δ must occur in θ. Item 3 ensures that only those components c' are in θ which are either in Δ or which may have (directly or indirectly) caused a failure of any $c \in \Delta$.

For example, suppose $\Delta = \{Vi, Pl, PG\}$. Then the following d-mode assignments conform to Items 2 and 3: $\{indf(Vi), indf(Pl), indf(PG)\}$, $\{indf(Ca), df(Ca, Vi), indf(Pl), indf(PG)\}$, $\{indf(Ca), df(Ca, Vi), indf(EC), df(EC, Pl), df(Pl, PG)\}$, $\{indf(Ca), df(Ca, Vi), indf(Pl), df(Pl, PG)\}$, etc.

However, $\{indf(Ca), indf(Vi), \ldots\}$ cannot be a DE, as there would be no edge in the DE-DAG from Ca to Vi.

We see that there can be quite a lot of possible DEs. The modeller has 3 possibilities to reduce the number of DEs. First, one should make use of the *ab* fault models. For example, suppose SD contains $ab(EC) \rightarrow \neg ok(om, nev)$ and we make the observation $ok(om, nev)$. Then those d-mode assignments which contain $indf(EC)$ will not conform to Item 1 of the definition of DEs. Second, the SDD should be as detailed as possible.

Finally, we should focus on those DEs which have a minimal number of PFCs (i.e., *indf*-components). The idea behind this strategy is that multiple independent failures are, in most domains, very unlikely. DEs with a minimal number of PFCs are *Minimal DEs (MDEs)*. For $\Delta = \{PG, Pl\}$, there can be at most 3 MDEs, all of them having 1 PFC: $\{indf(Pl), df(Pl, PG)\}$, $\{indf(EC), df(EC, Pl), df(EC, PG)\}$, and $\{indf(EC), df(EC, Pl), df(Pl, PG)\}$.

In general there is more than only one diagnosis candidate. The concept of DEs can be straightforwardly extended to sets of diagnoses: the DEs for a set of diagnoses are the union of the DEs for each single diagnosis candidate. Depending on the application one may choose to eliminate proper subsets from the resulting set.

5 Computing the MDEs

We outline a simple algorithm which computes all MDEs for a given diagnosis Δ. Due to space reasons, we only present a naive version which does not utilize possible optimizations which cut the search space and reduce the number of performed consistency checks. Anyway, the described algorithm is sufficient for our purpose, as the number of components is usually small in this domain.

The algorithm creates a tree, the *Diagnosis Environment Tree (DET)*. Each node n in the DET represents a possible DE: n contains a d-mode assignment $n.\sigma$ which conforms to Items 2 and 3 of the definition of DEs. A part of the DET for $\Delta = \{Vi, Pl, PG\}$ is depicted in Fig. 4. The root node contains $indf(c)$ for all $c \in \Delta$. For any node n, a child node n' is created as follows:

1. $n'.\sigma := n.\sigma$
2. Select c_i and c_j s.t. $indf(c_j) \in n'.\sigma$ and c_i is a parent of c_j in the FDG.
3. In $n'.\sigma$, replace $indf(c_j)$ with $df(c_i, c_j)$
4. If c_i is not yet in $n'.\sigma$: add $indf(c_i)$ to $n'.\sigma$.

If all components c with $indf(c) \in n.\sigma$ have no parents in the FDG, then n has no children in the DET. This is the case for nodes 6 and 7 in the depicted tree. Moreover, it is sufficient if the tree contains each possible DE only once.

For each node n, $n.\sigma$ is a DE iff Item 1 in the definition of DEs holds. Thus, by performing the corresponding consistency check, we can accept or reject $n.\sigma$ as a DE. However, only those DEs are minimal which have a minimal number of PFCs. In our example, if nodes 6 and 7 fulfill Item 1, then they are also MDEs, as EC is the only PFC in these nodes. Otherwise, all nodes with 2 PFCs are potential MDEs. Therefore, a simple algorithm is as follows:

1. Generate the DET; set $\nu := 1$.
2. Perform the consistency checks for all nodes with ν PFCs.
3. If there are consistent nodes, then they are the MDEs and we are done. Otherwise: $\nu := \nu + 1$, goto 2.

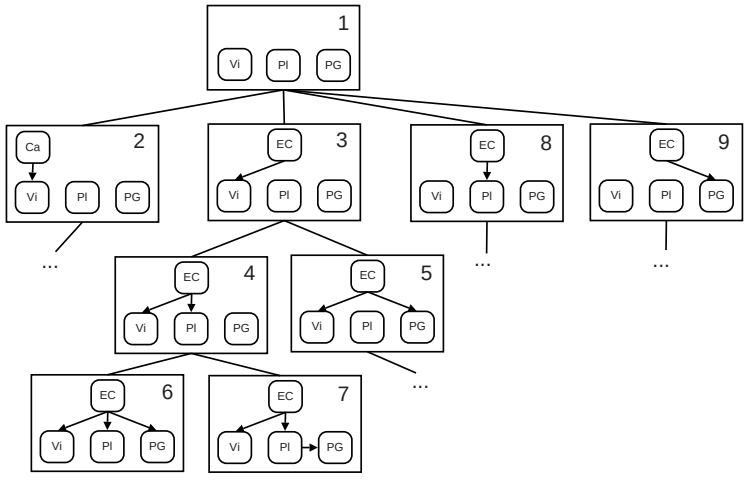

Fig. 4. A graph whose nodes are possible DEs of $\Delta = \{Vi, Pl, PG\}$. Each node is labelled with a number.

6 Case Studies

We implemented the proposed diagnosis system, partly in Java, partly in C++. For the computation of the diagnoses we used Reiter's Hitting Set algorithm [2], and the consistency checks were performed by a propositional Horn clause theorem prover [7]. The runtime monitoring algorithm works as follows: every 2 *sec* it checks if any rule has reported a violation. If yes, then it waits for a period of 2 more seconds. During this period, further rules may be violated. Then OBS is generated, and the minimal diagnoses and their MDEs are computed.

We describe 2 experiments which we conducted using the control software of our autonomous soccer robot. In scenario 1, we simulated a failure of the EC by killing its processes. As a consequence, several other components failed: PG crashed, and the following components threw exceptions: Vi, Od, Pl, and RG. The observations were $OBS = \{\neg ok(PG, npr)$, $\neg ok(Vi, no\_exc)$, $\neg ok(Od, no\_exc), \ldots\}$. We obtained a single diagnosis $\Delta = \{Vi, Od, Pl, PG, RG\}$.

Note that WM and Ki were affected as well, but they did not exhibit any symptoms. The reason is that Ki sends events only occasionally, and WM produces output only as a reaction to input events, and there were no more input events after the failure of EC. Furthermore, we assumed that there is no direct way of detecting that EC has failed, in order to demonstrate that our approach is able to determine that EC is the PFC although it is not in Δ.

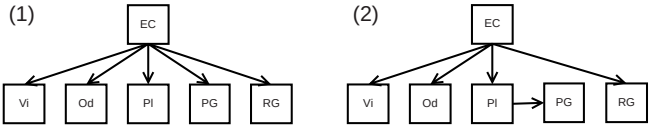

Fig. 5. The two MDEs obtained in scenario 1 (depicted as DE-DAGs)

We obtained 2 MDEs, θ_1 and θ_2, which are depicted in Fig. 5. Both contain the same components, but with different dependencies. The components were restarted according to the order in θ_2 (i.e., EC was restarted first, and PG after Pl), as the order in θ_2 is stricter than in θ_1.

After these repair actions, the component WM, which was not restarted, failed after receiving input events and trying to access the "old" instance of EC which had failed before. We obtained $\theta_3 = \{indf(WM)\}$, and the WM was restarted. After that, the largest part of the system operated as desired; the repair was successful. Only Ki would fail sometime in the future, namely after an attempt to access the EC.

This example shows that it might be better to follow a pessimistic repair strategy and reset all those components which depend, directly or indirectly, on the PFC(s). In this example, Ki and WM would be repaired immediately, although they are not contained in the MDEs.

The computational overhead imposed by the continuous monitoring which is done by the rules was negligible ($< 5\%$ of CPU usage). Due to the small size of the model, the computation of the diagnoses and the MDEs required less than $150\,ms$. The period of time between the failure of EC and the finished computation of the MDEs was about $4sec$.

In the second scenario, we killed WM and PG at the same time and obtained $OBS = \{\neg ok(WM, npr), \neg ok(PG, npr), \ldots\}$. First we did not use a fault model for EC. Thus, we got the MDE $\theta_1 = \{indf(EC), df(EC, WM), df(EC, PG)\}$. Then we improved the model by adding $ab(EC) \rightarrow (\neg ok(om, nev) \wedge \neg ok(md, nev) \wedge \cdots)$ to SD. As most of the properties on the right side of this implication were not violated, the assumption $ab(EC)$ led to a contradiction, and we obtained the desired MDE $\theta_2 = \{indf(WM), indf(PG)\}$.

7 Related Research and Conclusions

We presented a technique which tackles the issue of dependent failures of components in consistency-based MBD. Though the context of this work was runtime diagnosis in a mobile autonomous robot, our approach is very general and can be applied to other domains as well. We gave examples for dependent failures occurring in the HW-SW hybrid systems of autonomous robots and showed that a repair which is based on minimal diagnoses is insufficient in such cases. Then

we proposed to concept of minimal diagnosis environments (MDEs). We employ a Failure Dependency Graph and a logical System Dependencies Description. Moreover, we provided an algorithm which computes all MDEs of a specific diagnosis. Finally we demonstrated our approach by means of case studies.

To the best of our knowledge, this is the first work within the framework of consistency-based MBD which addresses the issue of dependent failures at the level of logical reasoning. The author of [8] proposes a method for reasoning with uncertainty in MBD which enables stochastic dependencies among components; however, dependent failures are not addressed at the logical level.

The issue of dependent failures is similar to faults in the structure of the system which lead to hidden interactions, e.g., the bridge fault [9][10]. In both cases a single *cause of failure* may lead to multiple-fault diagnoses. However, in case of structural faults there is a single *point of failure*, whereas in presence of dependent faults multiple components have actually failed.

One advantage of our approach is the fact that, similar to [10], the complexity of the computation of diagnoses is not increased. I.e., it is possible to compute the MDEs only if required (e.g., when repair actions based on the minimal diagnoses have failed). Another strength is that our work is also able to recognize failure dependencies when there are multiple primarily failed components, whereas the authors of [9] and [10] assume that there is a single cause of failure.

Our approach is very general as it is based upon Reiter's framework [2] and does not make further assumptions wrt the used diagnosis algorithms and models. However, it does not support general behavior modes [11][6]. This extension will be subject to our future research. Furthermore, we also plan to investigate the issue of minimizing the overall repair costs when there are multiple MDEs.

References

1. Weber, J., Wotawa, F.: Using AI techniques for fault localization in component-oriented software systems. In: Gelbukh, A., Reyes-Garcia, C.A. (eds.) MICAI 2006. LNCS (LNAI), vol. 4293, Springer, Heidelberg (2006)
2. Reiter, R.: A theory of diagnosis from first principles. Artificial Intelligence 32(1), 57–95 (1987)
3. de Kleer, J., Williams, B.C.: Diagnosing multiple faults. Artificial Intelligence 32(1), 97–130 (1987)
4. Steinbauer, G., Wotawa, F.: Detecting and locating faults in the control software of autonomous mobile robots. In: Proceedings of the 19$^{\text{th}}$ International Joint Conf. on Artificial Intelligence, Edinburgh, UK, pp. 1742–1743 (2005)
5. de Kleer, J.: Using crude probability estimates to guide diagnosis. Artificial Intelligence 45, 381–392 (1990)
6. Struss, P., Dressler, O.: Physical negation: Integrating fault models into the general diagnostic engine. In: Proceedings of the 11th International Joint Conf. on Artificial Intelligence, pp. 1318–1323 (1989)
7. Minoux, M.: LTUR: A Simplified Linear-time Unit Resolution Algorithm for Horn Formulae and Computer Implementation. Information Processing Letters 29, 1–12 (1988)

8. Lucas, P.J.F.: Bayesian model-based diagnosis. International Journal of Approx. Reasoning 27(2), 99–119 (2001)
9. Davis, R.: Diagnostic reasoning based on structure and behavior. Artificial Intelligence 24, 347–410 (1984)
10. Böttcher, C.: No faults in structure? how to diagnose hidden interactions. In: IJCAI, pp. 1728–1735 (1995)
11. de Kleer, J., Williams, B.C.: Diagnosis with behavioral modes. In: Proceedings of the 11^{th} International Joint Conf. on Artificial Intelligence, pp. 1324–1330 (1989)

PrDLs: A New Kind of Probabilistic Description Logics About Belief*

Jia Tao, Zhao Wen, Wang Hanpin, and Wang Lifu

School of Electronics Engineering and Computer Science, Peking Univ.,Beijing 100871,China
jiat@sei.pku.edu.cn

Abstract. It is generally accepted that knowledge based systems would be smarter if they can deal with uncertainty. Some research has been done to extend Description Logics(DLs) towards the management of uncertainty, most of which concerned the *statistical information* such as "The probability that a randomly chosen bird flies is greater than 0.9". In this paper, we present a new kind of extended DLs to describe degrees of belief such as "The probability that all plastic objects float is 0.3". We also introduce the extended tableau algorithm for Pr$\mathcal{ALC}$ as an example to compute the probability of the implicit knowledge.

Keywords: Reasoning under Uncertainty,Description Logics, Model-based Reasoning, Ontology, Probabilistic, Knowledge Representation.

1 Introduction

It has often been noted that "probability" is a term with dual use: it can be applied to the frequency of occurrence of a specific property in a large sample of objects, and to the degree of belief granted to a proposition[1]. Therefore, the probabilistic extension of Description Logics should also cover these two semantics.

Recently, several probabilistic description logics have been developed to describe uncertainty such as P-CLASSIC[2] and P-$\mathcal{SHOQ}$(D)[3]. Those probabilistic description logics focus on capturing the statistical information about the world, since given some statistical information(say, that 90% of the individuals in concept(or class) C also in concept D), then we can imagine a chance setup in which a randomly chosen individual of C has probability 0.9 of being an individual of D[4].

Such kind of probabilistic description logics inevitably cannot describe *degree of belief*[5,6] such as *the probability that class* C *is a subclass of* D *is 0.9*. In this paper, we will introduce a kind of probabilistic description logics named PrDLs which could describe and reason on such kind of information. We will use $(C \sqsubseteq D)^{\alpha}(0 < \alpha \leq 1)$ to express the degree of belief that class C is a subclass of class D is α and $(a : C)^{\alpha}$ to express the degree of belief that individual a is in class C is α. In many application domains, this kind of probabilistic subsumption semantics is more appropriate. For example,

* Supported by the National Grand Fundamental Research 973 Program of China under Grant No.2002CB312006; the National Natural Science Foundation of China under Grant Nos. 60473058.

H.G. Okuno and M. Ali (Eds.): IEA/AIE 2007, LNAI 4570, pp. 644–654, 2007.

- Dealing with conflict ontologies. On the coming semantic web, there would be a lot of ontologies on the web which are created by different people. Due to the limitation of their knowlegde or other reasons, there must be many conflict axioms and assertions such as one ontology may define the company with no more than 5 employees is *small company* and another ontology defines the company with no more than 10 employees is *small company*. How to make use of such kind of conflict knowledge? One solution is to assign each axiom a probability as degree of belief. For example, we could assign degree of belief 0.5 to the former one and 0.4 to the latter one. The remaining fraction 0.1 is left for the other possible definition about *small company*.
- Making use of knowledge not being proved yet such as Goldbach Conjecture or could not be proved such as the definition of *small company*.
- In the *information integration* domain, using PrDLs to describe the degree of the similarity of the concepts in different ontologies or schemas which is called *ontology mapping*[7] or *schema matching*[8]. For example, if there is a concept *SmallCom* in schema *A* and a concept *SCompany* in schema *B*, we may draw a conclusion that the probability $SmallCom \equiv SCompany$ is 0.9. This conclusion should follow the degree of belief semantics but not statistical semantics, because if we apply the statistical semantics, we have to admit $SmallCom \not\equiv SCompany$.

Moreover, PrDLs are different from other probabilistic description logics such as P-CLASSIC not only in semantics, but also in reasoning algorithms. For example, in PrDLs, given $(A \equiv B)^{0.9}$ and $(B \equiv C)^{0.8}$, we can infer $(A \equiv C)^{0.72}$. On the other hand, in P-CLASSIC, the statement that the probability class *A*(resp. *B*) euqals class *B*(resp. *C*) is 0.9(resp. 0.8) could be written as $Pr(A \sqcap B|A \sqcup B) = 0.9$(resp. $Pr(B \sqcap C|B \sqcup C) = 0.8$). However, we cannot draw any conclusion about $Pr(A \sqcap C|A \sqcup C)$.

In the following we will introduce PrDLs in detail. Section 2 describes the foundations of PrDLs. Section 3 introduces the reasoning algorithm of a simple probabilistic description language Pr$\mathcal{ALC}$ which is extended from the $\mathcal{ALC}$ tableaux algorithm[9]. Section 4 is the related work. Section 5 is the conclusion and future work.

2 Foundations

PrDLs are a family of logic-based knowledge representation formalisms with probabilistic extension. They are based on a common family of languages which provide a set of constructors to build concept (class) and role (property) descriptions.

2.1 Probabilistic Description Languages

PrDLs have the exact same languages with the corresponding DLs. For example, PrDLs also have $\mathcal{ALC}$ and $\mathcal{SHOQ}$, etc. distinguished by the constructors they provide but named Pr$\mathcal{ALC}$ and Pr$\mathcal{SHOQ}$. You can find more introduction in [10].

2.2 Knowledge Base

A PrDL knowledge base is also composed of two distinct part: the TBox and the ABox, but extended by the probabilistic factors.

In this paper, we separate the TBox to the C(oncept)Box and R(ole)Box which contain the axioms about concept and roles, respectively.

CBox. In A PrDL CBox C, an axiom may have the form (Mammal $\equiv$ Animal $\sqcap$ FourLegThing)$^{0.9}$ Which means the probability that the axiom is true is 0.9. Formally, let $\mathcal{L}$ be a probabilistic description language, $C, D \in$ **Cdsc**($\mathcal{L}$)$\mathcal{L}$-concepts[11], a CBox C is a finite, possibly empty, set of statements of the form $(C \sqsubseteq D)^{\alpha}, 0 < \alpha \leqslant 1$, called *concept inclusion*. **Cdsc**($\mathcal{L}$) and **Rdsc**($\mathcal{L}$) is defined as the set of concepts and roles of description language $\mathcal{L}$. α, the probabilistic weight of the statement, denotes the probability that the statement is true. $(C \equiv D)^{\alpha}$, called *concept equivalence*, is an statement denotes the probability that both $C \sqsubseteq D$ and $D \sqsubseteq C$ is true is α. Statements in C are called *concept axioms*. If $\alpha = 1$, the statements can be abbreviated to $C \sqsubseteq D$ or $C \equiv D$, called *certain concept axioms*. Otherwise, the statements are called *uncertain concept axioms*.

We can divide the CBox C into two parts C_d and C_p. C_d consists of all the certain concept axioms, while C_p consists of all the uncertain concept axioms. Here we should not treat $(C \equiv D)^{\alpha}$ as the abbreviation for $(C \sqsubseteq D)^{\alpha}$ and $(D \sqsubseteq C)^{\alpha}$, since $(C \sqsubseteq D)^{\alpha}$ and $(D \sqsubseteq C)^{\alpha}$ imply $(C \equiv D)^{\beta}, max(2\alpha - 1, 0) \leqslant \beta \leqslant \alpha$, but not $(C \equiv D)^{\alpha}$. A concept axiom without its probabilistic weight is called the *certain extension* of the concept axiom. For example, $C \equiv D$ is the certain extension of $(C \equiv D)^{\alpha}$. The certain extension of a CBox C is a new CBox C_e whose concept axioms are all coming from the certain extension of the concept axioms in C.

An interpretation $\mathcal{I}$ *satisfies* a concept inclusion $(C \sqsubseteq D)^{\alpha}$, or $\mathcal{I}$ *models* $(C \sqsubseteq D)^{\alpha}$ (written as $\mathcal{I} \models (C \sqsubseteq D)^{\alpha}$), if $\mathcal{I}$ *satisfies* its certain extension(which means $C^{\mathcal{I}} \subseteq D^{\mathcal{I}}$), and it satisfies a concept equivalence $(C \equiv D)^{\alpha}$ (written as $\mathcal{I} \models (C \equiv D)^{\alpha}$), if satisfies its certain extension (which means $C^{\mathcal{I}} = D^{\mathcal{I}}$). An interpretation $\mathcal{I}$ *possibly satisfies* a PrDL CBox C(written as $\mathcal{I} \models C$), if it satisfies all the certain concept axioms in C. We also say that $\mathcal{I}$ is a *possible model* of C.

RBox. We could give the similar definition about RBox of PrDLs. Let $\mathcal{L}$ be a probabilistic description language, $RN, SN \in \mathbf{R}$ role names, $R_1, R_2 \in$ **Rdsc**($\mathcal{L}$)$\mathcal{L}$-roles, an PrDL RBox $\mathcal{R}$ is a finite, possible empty, set of statements of the form:
- $(RN \in \mathbf{F})^{\alpha}, 0 < \alpha \leqslant 1$, where $\mathbf{F} \subseteq \mathbf{R}$ is a set of *functional roles*, or
- $(SN \in \mathbf{R}_{+})^{\alpha}, 0 < \alpha \leqslant 1$, where $\mathbf{R}_{+} \subseteq \mathbf{R}$ is a set of *transitive roles*, or
- $(R_1 \sqsubseteq R_2)^{\alpha}, 0 < \alpha \leqslant 1$, called *role inclusions*; $(R_1 \equiv R_2)^{\alpha}, 0 < \alpha \leqslant 1$, called *role equivalence*, denotes the probability that both $R_1 \sqsubseteq R_2$ and $R_2 \sqsubseteq R_1$ is true is α.

ABox. Let $\mathcal{L}$ be a probabilistic description language, $a, b \in \mathbf{I}$ individual names, $C \in$ **Cdsc**($\mathcal{L}$) an $\mathcal{L}$-concept and $R \in$ **Rdsc**($\mathcal{L}$) an $\mathcal{L}$-role. An PrDL ABox $\mathcal{A}$ is a finite, possible empty, set of statements of the form $(a : C)^{\alpha}$, called *concept assertions*, or $(< a, b >: R)^{\alpha}$, called *role assertions*. Statements in $\mathcal{A}$ are called *assertions*. If $\alpha = 1$, the assertions can be abbreviated to $a : C$ or $< a, b >: R$ and can be called *certain assertions*. Otherwise, they do not have abbreviated form and is called *uncertain assertions*.

Knowledge Base. A PrDL knowledge base $\mathcal{K}$ is a triple $< C, \mathcal{R}, \mathcal{A} >$, where C is a CBox, $\mathcal{R}$ is a RBox, and $\mathcal{A}$ is an ABox. An interpretation $\mathcal{I}$ *satisfies* a knowledge base $\mathcal{K}$, written as $\mathcal{I} \models \mathcal{K}$, iff it satisfies C, $\mathcal{R}$ and $\mathcal{A}$; $\mathcal{K}$ is *satisfiable* (*unsatisfiable*) iff there exists (does not exist) such an interpretation $\mathcal{I}$ that satisfies $\mathcal{K}$.

2.3 Semantics

We use possible worlds[12,13,14] to describe the semantics of the PrDLs. The approach is mapping a PrDL knowledge base onto a set of DL knowledge bases, where the models of each of the latter constitute the set of possible worlds(may be empty set). First, we give the definition of the DL knowledge bases related to a PrDL knowledge base.

Definition 1 (DL KBs Related to the PrDL KB). *Given a PrDL knowledge base* $\mathcal{K} =< C, \mathcal{R}, \mathcal{A} >$. C_d, $\mathcal{R}_d$ *and* $\mathcal{A}_d$ *are their certain parts, and* C_p, $\mathcal{R}_p$ *and* $\mathcal{A}_p$ *are their uncertain parts. Let* C_{pe}, $\mathcal{R}_{pe}$ *and* $\mathcal{A}_{pe}$ *be the certain extension of* C_p, $\mathcal{R}_p$ *and* $\mathcal{A}_p$.*The set of DLs* $D_\mathcal{K}$ *related to this PrDL is defined as*

$$D_\mathcal{K} = \{< C_d \cup C_i, \mathcal{R}_d \cup \mathcal{R}_i, \mathcal{A}_d \cup \mathcal{A}_i > | C_i \subseteq C_{pe} \wedge \mathcal{R}_i \subseteq \mathcal{R}_{pe} \wedge \mathcal{A}_i \subseteq \mathcal{A}_{pe}\}$$

Obviously, a model of the knowledge base of the DL in $D_\mathcal{K}$ is also a possible model of $\mathcal{K}$. All the models of the DL knowledge bases in $D_\mathcal{K}$ constitute the set of its possible worlds $\mathcal{W}_\mathcal{K}$. let $M = (\mathcal{W}_\mathcal{K}, \mu)$ denote a probability structure, where μ is a discrete probability distribution on $\mathcal{W}_\mathcal{K}$. Then we can define the notion of an extension $[t]_M$ of the term t (could be a concept description, the certain extension of an axiom in $C \cup \mathcal{R}$ or the certain extension of an assertion in $\mathcal{A}$) by means of the following rules. Let w be a world (possible model) of $\mathcal{W}_\mathcal{K}, \mathcal{K}_d$ a DL knowledge base related to $\mathcal{K}$.

1.If $\exists \alpha \in (0,1], (t)^\alpha \in C \cup \mathcal{R} \cup \mathcal{A}$, then $[t]_M = \alpha = \mu(\cup_{\mathcal{K}_d \in D_\mathcal{K} \wedge w \models \mathcal{K}_d \wedge \mathcal{K}_d \models t}\{w\})$

2.else if t is a concept, $[t]_M = 1 - \mu(\cup_{\mathcal{K}_d \in D_\mathcal{K} \wedge w \models \mathcal{K}_d \wedge \mathcal{K}_d \not\models t}\{w\})$ $\mathcal{K}_d \not\models t$ denotes concept t is not satisfiable with respect to the knowledge base $\mathcal{K}_d$.

Then, we can define the probability that a concept is satisfiable.

Definition 2 (Concept satisfiability). *Given a PrDL knowledge base* $\mathcal{K}$ *and a concept* C*, the probability that* C *is satisfiable with respect to* $\mathcal{K}$ *is* α *iff* $[C]_M = \alpha$.

Example 1. Given a PrDL knowledge base $\mathcal{K} =< C, \Phi, \Phi >$, where $C = \{(\text{Animal} \sqsubseteq \text{Creature} \sqcap \text{MovableThing})^{0.8}, (\text{Mammal} \sqsubseteq \text{Animal} \sqcap \text{FourLegThing})^{0.9}\}$, we have a possible worlds distribution $M_1 = (\mathcal{W}, \mu)$:

$$\begin{aligned}
P(\mathcal{I}_1) = 0.05 : & \Delta^{\mathcal{I}_1} = \{a,b,c\}, \text{Creature}^{\mathcal{I}_1} = \{a,b,c\}, \text{MovableThing}^{\mathcal{I}_1} = \{a,b\}, \\
& \text{Animal}_1^{\mathcal{I}} = \{a\}, \text{FourLegThing}^{\mathcal{I}_1} = \{c\}, \text{Mammal}^{\mathcal{I}_1} = \{a\} \\
P(\mathcal{I}_2) = 0.75 : & \Delta^{\mathcal{I}_2} = \{a,b,c\}, \text{Creature}^{\mathcal{I}_2} = \{a,b,c\}, \text{MovableThing}^{\mathcal{I}_2} = \{a,b\}, \\
& \text{Animal}^{\mathcal{I}_2} = \{a\}, \text{FourLegThing}^{\mathcal{I}_2} = \{a\}, \text{Mammal}^{\mathcal{I}_2} = \{a\} \\
P(\mathcal{I}_3) = 0.15 : & \Delta^{\mathcal{I}_3} = \{a,b,c\}, \text{Creature}^{\mathcal{I}_3} = \{a,b,c\}, \text{MovableThing}^{\mathcal{I}_3} = \{a,b\}, \\
& \text{Animal}^{\mathcal{I}_3} = \{b,c\}, \text{FourLegThing}^{\mathcal{I}_3} = \{b\}, \text{Mammal}^{\mathcal{I}_3} = \{b\} \\
P(\mathcal{I}_4) = 0.05 : & \Delta^{\mathcal{I}_4} = \{a,b,c\}, \text{Creature}^{\mathcal{I}_4} = \{a,b,c\}, \text{MovableThing}^{\mathcal{I}_4} = \{a,b\}, \\
& \text{Animal}^{\mathcal{I}_4} = \{b,c\}, \text{FourLegThing}^{\mathcal{I}_4} = \{b\}, \text{Mammal}^{\mathcal{I}_4} = \{c\} \\
P(\mathcal{I}_k) = 0.00 : & \mathcal{I}_k \in \mathcal{W} \wedge k \neq 1,2,3,4
\end{aligned}$$

In the possible world $\mathcal{I}_1$, only the first axiom is satisfiable and $\mathcal{I}_3$ only satisfies the second axiom. Both axioms are satisfiable in the possible world $\mathcal{I}_2$. So

$$[\text{Animal} \sqsubseteq \text{Creature} \sqcap \text{MovableThing}]_{M_1} = 0.8$$
$$[\text{Mammal} \sqsubseteq \text{Animal} \sqcap \text{FourLegThing}]_{M_1} = 0.9$$

And the probability that Mammal $\sqsubseteq$ Creature is 0.75 in this model (written as $M_1 \models (\text{Human} \sqsubseteq \text{Animal})^{0.75}$). Actually, the probability will be range from 0.7 to 0.8 with

different probability distributions. But if we assume the independence of the terms in the knowledge base, PrDL would only yield a point value 0.72.

2.4 Reasoning Tasks

The following are the main reasoning tasks related to the PrDL knowledge base:

- **Terminology** – **Satisfiability**: Given a CBox or RBox or both, decide whether their certain part are satisfiable.
- **Assertion** – **Satisfiability**: Given an ABox $\mathcal{A}$, decide whether the certain part is satisfiable.
- **Concept** – **Satisfiability**: Given a knowledge base $\mathcal{K}$ and a concept C, compute the probability that C is satisfiable with respect to $\mathcal{K}$.
- **Concept** – **Subsumption**: Given a knowledge base $\mathcal{K}$ and concepts C, D, compute the probability that C is included in D.
- **Concept** – **Membership**: Given a knowledge base $\mathcal{K}$, an individual a and a concept C, compute the probability that $a : C$.
- **Role** – **Subsumption**: Given a knowledge base $\mathcal{K}$ and roles R, S, compute the probability that R is included in S.
- **Role** – **Membership**: Given a knowledge base $\mathcal{K}$, two individuals a, b and a role R, compute the probability that $< a, b >: R$.

From their definition, we know the first two reasoning tasks are exactly same with description logics.

3 Inference Algorithm

In this section, we will introduce the probabilistic extension of tableaux algorithm for the terminologies that only contain axioms whose certain extensions contain only *unique introductions*[11] and no cycles, called Pr-Tableaux-Algorithm. We only give the Pr-Tableaux-Algorithm for Pr$\mathcal{ALC}$ which is extended from the tableaux algorithm for $\mathcal{ALC}$. First, we will introduce some relative definitions.

Definition 3 (Keys and Their Boolean Algebra). **K** *is a set of identifiers, which also contains the special elements* $\perp$ *and* $\top$ *. Given a Pr*$\mathcal{ALC}$ *knowledge base* $\mathcal{K} =< C, \mathcal{R}, \mathcal{A} >$*, whose set of possible worlds is* $\mathcal{W}$*. Let* $\varepsilon : C \cup \mathcal{R} \cup \mathcal{A} \longrightarrow \mathbf{K} - \{\perp\}$*, with constrains:1.*$\forall (t)^{\alpha} \in C \cup \mathcal{R} \cup \mathcal{A}(\alpha = 1 \Longleftrightarrow \varepsilon((t)^{\alpha}) = \top)$*;2.*$\forall (t)^{\alpha}, (t')^{\beta} \in C \cup \mathcal{R} \cup \mathcal{A}(\varepsilon((t)^{\alpha}) = \varepsilon((t')^{\beta}) \Longrightarrow (t = t' \wedge \alpha = \beta) \vee (\alpha = 1 \wedge \beta = 1))$*. We define* **KE** *to be the extension of* **K** *iff*

1.$\mathbf{K} \subseteq \mathbf{KE}$;
2.*if* $e_1, e_2 \in \mathbf{KE}$, $e_1 \wedge e_2 \in \mathbf{KE}$ *and* $e_1 \vee e_2 \in \mathbf{KE}$.

Let $\mathcal{B}(\mathbf{KE}, \perp, \top, \{\wedge, \vee\})$ *denote the boolean algebra over* **KE***. Then we can define a mapping* $\omega : \mathbf{KE} \longrightarrow 2^{\mathcal{W}}$*. For any* $e, e_1, e_2 \in \mathbf{KE}$*,we define*

1.$\omega(\top) = \mathcal{W}$
2.$\omega(\perp) = \Phi$
3.$\omega(e_1 \wedge e_2) = \omega(e_1) \cap \omega(e_2)$
4.$\omega(e_1 \vee e_2) = \omega(e_1) \cup \omega(e_2)$
5.*if* $\varepsilon((t)^{\alpha}) = e$ *and* $(t)^{\alpha} \in C \cup \mathcal{R} \cup \mathcal{A}$*, then* $\omega(e) = \{w | \ w \models (t)^{\alpha}\}$

Moreover, we define the probability of an key expression $e \in \mathbf{KE}$ as $P(e) = \mu(\omega(e))$.

Since axioms may have probabilistic factors, the unfolding rules could not just be replaced by the right side of the axioms. The new unfolding rule should add a set Θ as the suffix to each concept name called *weight set*. The elements of Θ are the keys of axioms which contribute to generating the concept related to Θ. The concept with weight set is called *weighted concept*. We consider concept name CN to be the abbreviation of $CN \wr \{\top\}$. So weighted concept is the generalization of concept. Then, we will use the weighted concepts as the basic elements during the inference. Formally

Definition 4 (Weighted Concepts). *Given a Pr$\mathcal{ALC}$ CBox C, let $CN \in \mathbf{C}$ and $\Theta \subseteq \mathbf{KE}$. $CN \wr \Theta$ is called* weighted concept name. Weighted concept descriptions *in Pr$\mathcal{ALC}$ are formed according to following syntax rule:*

$$C, D \longrightarrow CN \wr \Theta | \top \wr \{\top\} | \bot \wr \{\top\} | \neg C | C \sqcap D | C \sqcup D | \exists R.C | \forall R.C$$

Let $\mathbf{WCdsc}(\mathcal{K})$ denotes the set of all weighted concepts of knowledge base $\mathcal{K}$. Then we can define a mapping $\xi : \mathbf{WCdsc}(\mathcal{K}) \rightarrow 2^{\mathbf{K}(\mathcal{K})}$ as

$$\xi(C) = \{e | e \text{ occurs in } C\}$$

Furthermore, we define $P(C) = P(\bigwedge \xi(C)) = \mu(\{e | e \text{ occurs in } C\})$. We can see the possibility structure M will affect the value of $P(C)$. Similarly, we could define *weighted roles* by the exactly same way. So we won't describe it here.

We consider $CN \wr \Theta$ and $CN \wr \Omega$ are different weighted concepts if $\Theta \neq \Omega$ and $RN \wr \Theta$ and $RN \wr \Omega$ are different weighted roles if $\Theta \neq \Omega$.

We should also update the unfolding rule as follows:

Definition 5 (Unfold-Rule). *Given a Pr$\mathcal{ALC}$ CBox C, $CN \wr \Theta$ is a weighted concept names. If there exists an axiom $(CN \equiv C)^{\alpha} \in C$ whose key is e, we can unfold $CN \wr \Theta$ with following rules:*
1. Replace CN by C;
2. Let $\Theta' = \Theta \cup \{e\}$;
3. Replace each concept name DN appeared in C by $DN \wr \Theta'$.

Example 2. Given A CBox $C = \{(CN_1 \equiv CN_2 \sqcap CN_3)^{0.9}, (CN_2 \equiv \forall R.CN_4)^{0.3}\}$ $\varepsilon(CN_1 \equiv CN_2 \sqcap CN_3) = e_1, \varepsilon(CN_2 \equiv \forall R.CN_4) = e_2$. Concept $CN_1 \sqcup CN_4$ can be unfolded to

$$(\forall R.CN_4 \wr \{e_1, e_2\} \sqcap CN_3 \wr \{e_1\}) \sqcup CN_4 \wr \{\top\}$$

Definition 6 (Operator +). *Given a weighted concept description C and a weight set Θ, we define an operator "+" between them. The semantic of operation "+" as $C + \Theta = C'$, where C' is a weighted concept description derived from C by replacing each weighted concept name $CN \wr \Omega$ appeared in C by $CN \wr \Theta \cup \Omega$.*

Definition 7 (R-successor). *Given a completion tree, node y is called an R-Successor of node x if there exists some weighted role $R \wr \Theta \in \mathcal{L}(< x, y >)$.*

Given a concept D in NNF and a CBox C, We assign a key e_i to each axiom in C following Definition 3. We can expansion D by the expansion rules shown in Table 1(C, C_1 and C_2 are weighted concepts). *The expansion procedure won't stop until there is no rule could be applied*.Actually, we could get a set of completion tree $\mathcal{T} = \{T_1, ..., T_n\}$

by ⊔-rule. Next, we are able to compute the probability that concept description D is satisfiable according to these completion tree. First, we should redefine the *clash*.

Definition 8 (Possible Clash). *Let T be a completion tree for concept D. If for some $CN \in \mathbf{C}$ and x of T, $\{CN \wr \Theta, \neg CN \wr \Omega\} \subseteq \mathcal{L}(x)$, T is said to contain a* possible clash *c(written as $T \models_p c$).*

Let $\xi(c) = \Theta \cup \Omega$, then the probability clash c is true is $P(c) = P(\bigwedge \xi(c))$.

Given a weighted concept C of knowledge base $\mathcal{K}$, let $\mathcal{T}$ is the set of all the completion trees generated by the Table 1. If there exists a completion tree $T \in \mathcal{T}$ which has no possible clash, the probability C is satisfiable is 1(written as $[D]_M = 1$). Otherwise, 2. $[D]_M = 1-$the probability that every $T \in \mathcal{T}$ has a clash. So the equation can be rewritten to $[D]_M = \begin{cases} 1 & \exists T \in \mathcal{T}.T \text{ has no possible clash} \\ 1 - P(\bigwedge_{T\in\mathcal{T}}(\bigvee_{T\models_p c} c)) & else \end{cases}$

According to definition 8, $\bigwedge_{T\in\mathcal{T}}(\bigvee_{T\models_p c} c)$ could be translated to equivalent boolean expression of $\mathbf{KE}(\mathcal{K})$. So we could transform it to disjunction normal form(DNF) of keys. Let it be $K_1 \vee K_2 \vee \ldots \vee K_n$. If we assume the axioms are independent with each other, $P(\bigwedge_{T\in\mathcal{T}}(\bigvee\{c|T \models_p c\}))$ can be computed by the following formula

$$P(\bigwedge_{T\in\mathcal{T}}(\bigvee_{T\models_p c} c)) = P(K_1 \vee K_2 \vee \ldots \vee K_n) = \sum_{i=1}^{n}(-1)^{i-1}(\sum_{1\leqslant j_1<\ldots<j_i\leqslant n} P(e_{j_1} \wedge \ldots \wedge e_{j_i}))$$

We could change the form of $\bigwedge_{T\in\mathcal{T}}(\bigvee_{T\models_p c} c$ to $\bigvee_{i=1}^{n}\bigwedge\{c_{i1}, \ldots, c_{im}\}, m = |\mathcal{T}|, n = \prod_{T\in\mathcal{T}}|\{c|c \in T\}|$. $\{c_{i1}, \ldots, c_{im}\}$ is a set of the possible clashes and each of them comes from different completion trees in $\mathcal{T}$. The meaning of such kind of set is a clash composition that could make the concept unsatisfiable. The probability that any one of such kind of composition is true is the probability that the concept is unsatisfiable. We call such composition *possible clash composition*. Given a possible clash composition ψ, We define

$$\xi(\psi) = \bigcup_{c\in\psi} \xi(c).$$

Finally, we can prove that the probability computed by the Pr-Tableaux-Algorithm is equal to the concept extensions introduced in 2.3.

Table 1. The tableaux expansion rules for Pr$\mathcal{ALC}$

Name	Condition	Action
⊓-rule	$1.C_1 \sqcap C_2 \in \mathcal{L}(x)$, $2.\{C_1, C_2\} \nsubseteq \mathcal{L}(x)$	$\mathcal{L}(x) = \mathcal{L}(x) \cup \{C_1, C_2\}$
⊔-rule	$1.C_1 \sqcup C_2 \in \mathcal{L}(x)$, $2.\{C_1, C_2\} \cap \mathcal{L}(x) = \Phi$	$\mathcal{L}(x) = \mathcal{L}(x) \cup \{C\}$ for some $C \in \{C_1, C_2\}$
∃-rule	1. $\exists R.C \in \mathcal{L}(x)$, 2. x has no R$\wr\xi(C)$-successor with $C \in \mathcal{L}(y)$	create a new node y with $\mathcal{L}(< x, y >) = R \wr \xi(C)$ and $\mathcal{L}(y) = \{C\}$
∀-rule	1. $\forall R.C \in \mathcal{L}(x)$, 2. there is an R$\wr\Theta$-successor y of x with $C \notin \mathcal{L}(y)$	$\mathcal{L}(y) = \mathcal{L}(y) \cup \{C\}$
Unfold-rule	$1.CN \wr \Theta \in \mathcal{L}(x)$(resp. $\neg CN \wr \Theta \in \mathcal{L}(x)$), $2.(CN \equiv C)^{\alpha} \in \mathcal{C}$, $\varepsilon((CN \equiv C)^{\alpha}) = e$, and $C + \{\Theta \cup \{e\}\} \notin \mathcal{L}(x)$ (resp. $\sim C + \{\Theta \cup \{e\}\} \notin \mathcal{L}(x)$)	$\mathcal{L}(x) = \mathcal{L}(x) \cup \{C + \{\Theta \cup \{e\}\}\}$ (resp. $\mathcal{L}(x) = \mathcal{L}(x) \cup \{\sim C + \{\Theta \cup \{e\}\}\}$)

Lemma 1. *Given a Pr$\mathcal{ALC}$ knowledge base $\mathcal{K} =< C, \Phi, \Phi >$ with the probability structure $M =< \mathcal{W}, \mu >$ and the set of related $\mathcal{ALC}$ knowledge bases $D_{\mathcal{K}} = \{\mathcal{K}_1^D, ..., \mathcal{K}_n^D\}$, let $D_{\mathcal{K}}^C = \{\mathcal{K}_d =< C_d, \Phi, \Phi > | \mathcal{K}_d \not\models C \wedge \mathcal{K}_d \in D_{\mathcal{K}}\}$. Then we have*

$$[C]_M = 1 - P\left(\bigvee_{\mathcal{K}_d \in D_{\mathcal{K}}^C} \left(\bigwedge_{t \in C_d \wedge (t)^\alpha \in C} \varepsilon((t)^\alpha)\right)\right).$$

Proof. According to Definition 3, For any $\mathcal{K}_d \in D_{\mathcal{K}}^C$, we have $\omega\left(\bigwedge_{t \in C_d \wedge (t)^\alpha \in C} \varepsilon((t)^\alpha)\right) = \{w | w \models \mathcal{K}_d\}$ then,

$$\begin{aligned}
[C]_M &= 1 - \mu(\cup_{\mathcal{K}_d \in D_{\mathcal{K}}^C} \{w | w \models \mathcal{K}_d\}) \\
&= 1 - \mu\left(\cup_{\mathcal{K}_d \in D_{\mathcal{K}}^C} \omega\left(\bigwedge_{t \in C_d \wedge (t)^\alpha \in C} \varepsilon((t)^\alpha)\right)\right) \\
&= 1 - \mu\left(\omega\left(\bigvee_{\mathcal{K}_d \in D_{\mathcal{K}}^C} \left(\bigwedge_{t \in C_d \wedge (t)^\alpha \in C} \varepsilon((t)^\alpha)\right)\right)\right) \\
&= 1 - P\left(\bigvee_{\mathcal{K}_d \in D_{\mathcal{K}}^C} \left(\bigwedge_{t \in C_d \wedge (t)^\alpha \in C} \varepsilon((t)^\alpha)\right)\right)
\end{aligned}$$

For simplicity, we define $\xi(\mathcal{K}_d) = \{\varepsilon((t)^\alpha) | t \in C_d \wedge (t)^\alpha \in C\}$, then $[C]_M = 1 - P(\bigvee_{\mathcal{K}_d \in D_{\mathcal{K}}^C} (\bigwedge \xi(\mathcal{K}_d))$

Lemma 2. *Given a Pr$\mathcal{ALC}$ knowledge base $\mathcal{K} =< C, \Phi, \Phi >$ with the probability structure $M =< \mathcal{W}, \mu >$ and the set of related $\mathcal{ALC}$ knowledge bases $D_{\mathcal{K}} = \{\mathcal{K}_1^D, ..., \mathcal{K}_n^D\}$, let $D_{\mathcal{K}}^C = \{\mathcal{K}_d =< C_d, \Phi, \Phi > | \mathcal{K}_d \not\models C \wedge \mathcal{K}_d \in D_{\mathcal{K}}\}$. For any $\mathcal{K}_d \in D_{\mathcal{K}}^C$, its clash composition ψ_d generated by the $\mathcal{ALC}$ tableau algorithm has corresponding possible clash composition ψ generated by the Pr$\mathcal{ALC}$ tableau algorithm (which means each possible clash c in ψ has a corresponding clash c_d in ψ_d only without weight set) and $\xi(\psi) \subseteq \xi(\mathcal{K}_d)$*

Proof. First, we could prove that each completion tree T_d of C with respect to $\mathcal{K}_d \in D_{\mathcal{K}}^C$ which is generated by the $\mathcal{ALC}$ tableau algorithm is a "sub-tree"(with same root node) of some T generated by Pr$\mathcal{ALC}$ tableau algorithm without considering the weight set, since Pr$\mathcal{ALC}$ tableau algorithm is the extension of the $\mathcal{ALC}$ tableau algorithm. Similarly, each T generated by Pr$\mathcal{ALC}$ tableau algorithm must have a corresponding T_d of C with respect to $\mathcal{K}_d$ which is a "sub-tree" of T. So each concept D occurred in each node of T_d could be found its weighted version $D \wr \Theta$ in the corresponding node of T and $\Theta \subseteq \xi(\mathcal{K}_d)$. Then each clash c_d occurred in T_d has a corresponding possible clash c in T and $\xi(c) \subseteq \xi(\mathcal{K}_d)$. Consequently, the clash composition ψ_d of T_d has a corresponding possible clash composition ψ of T and $\xi(\psi) \subseteq \xi(\mathcal{K}_d)$.

Lemma 3. *Given a Pr$\mathcal{ALC}$ knowledge base $\mathcal{K} =< C, \Phi, \Phi >$ with the probability structure $M =< \mathcal{W}, \mu >$, a concept C and the set of related $\mathcal{ALC}$ knowledge bases $D_{\mathcal{K}} = \{\mathcal{K}_1^D, ..., \mathcal{K}_n^D\}$, let $D_{\mathcal{K}}^C = \{\mathcal{K}_d =< C_d, \Phi, \Phi > | \mathcal{K}_d \not\models C \wedge \mathcal{K}_d \in D_{\mathcal{K}}\}$. If ψ is a possible clash composition generated by Pr$\mathcal{ALC}$, then there is a related $\mathcal{ALC}$ knowledge base $\mathcal{K}_d$ with $\xi(\mathcal{K}_d) = \xi(\psi)$ and $\mathcal{K}_d \in D_{\mathcal{K}}^C$.*

Proof. According to the tableau algorithm of Pr$\mathcal{ALC}$ we have introduced, the set of the axioms $\rho = \{(t)^\alpha | (t)^\alpha \in C \wedge \varepsilon((t)^\alpha) \in \xi(\psi)\}$ is sufficient for generating the possible clash composition ψ. So the related $\mathcal{ALC}$ knowledge base $\mathcal{K}_d$ whose axioms all come from the certain extension of the axioms in ρ must be able to generate a corresponding clash

composition by the $\mathcal{ALC}$ tableau algorithm since it is the specialization of Pr$\mathcal{ALC}$ tableau algorithm. Then, $\mathcal{K}_d \in D^C_{\mathcal{K}}$.

Theorem 1 (Correctness of the Algorithm). *The probability computed by the Pr-Tableaux-Algorithm introduced in this section is equal to the concept extensions defined in section 2.3*

Proof. According to *Lemma 1*, we only need to prove that $P(\bigvee_{\mathcal{K}_d \in D^C_{\mathcal{K}}}(\bigwedge \xi(\mathcal{K}_d)) = P(\bigvee_{\text{each } \psi \text{ of } \mathcal{T}} \bigwedge \psi)$ where ψ is a possible clash composition.

According to *Lemma 2*, we could obtain $P(\bigvee_{\mathcal{K}_d \in D^C_{\mathcal{K}}}(\bigwedge \xi(\mathcal{K}_d)) \leq P(\bigvee_{\text{each } \psi \text{ of } \mathcal{T}} \bigwedge \psi)$

According to *Lemma 3*, we could get $P(\bigvee_{\mathcal{K}_d \in D^C_{\mathcal{K}}}(\bigwedge \xi(\mathcal{K}_d)) \geq P(\bigvee_{\text{each } \psi \text{ of } \mathcal{T}} \bigwedge \psi)$

4 Related Work

Halpern et al. have done much research on degree of belief(subject probability) and statistical information(object probability)[15,16]. They mainly focus on the relation ship between these two kind of uncertainty[16,17,18], belief change[19,20] and probabilistic reasoning[13,4]. For description logics, Heinsohn[21] presents a probabilistic extension of the description logic $\mathcal{ALC}$, which allows to represent generic statistical information about concepts and roles, and which is essentially based on probabilistic reasoning in probabilistic logics, similar to[14,22]. Jaeger[23] gives a probabilistic extension of the description logic, which allows for generic (resp., assertional) statistical information about concepts and roles (resp., concept instances), but does not support statistical information about role instances. The uncertain reasoning formalism in [23] is essentially based on probabilistic reasoning in probabilistic logics, as the one in [21]. The work by Koller et al. [2] gives a probabilistic generalization of the CLASSIC description logic. Like Heinsohn's work [21], it is based on inference in Bayesian networks as underlying probabilistic reasoning formalism. Giugno presents a probabilistic extension of $\mathcal{SHOQ}$(D)[3], which allows to represent generic statistical knowledge about concept and roles and the assertional statistical knowledge about concept and role instance. Baader extends Description Logics with modal operators in [24]to describe belief but not degree of belief.

5 Conclusion and Future Work

We have presented a probabilistic version of description logics–PrDLs which are used to represent the degree of belief of the axioms and assertions in the knowledge base, which are very useful in many application area. We also introduce an inference algorithm for Pr$\mathcal{ALC}$ to discover the possible implicit knowledge.

In future, we will improve our work in two aspects. First, develop the inference algorithms which are suitable for more expressive probabilistic description languages such as the knowledge bases with none empty RBox, the knowledge bases with general inclusions and so on; Second, combine PrDLs with other probabilistic description logics describing statistical information.

References

1. Jaeger, M.: A logic for default reasoning about probabilities. Uncertainty in Artificial Intelligence, 352–359 (1994)
2. Koller, D., Levy, A.Y., Pfeffer, A.: P-CLASSIC: A tractable probablistic description logic. In: AAAI/IAAI, pp. 390–397 (1997)
3. Giugno, R., Lukasiewicz, T.: P-SHOQ(D): A probabilistic extension of SHOQ(D) for probabilistic ontologies in the semantic web. In: Flesca, S., Greco, S., Leone, N., Ianni, G. (eds.) JELIA 2002. LNCS (LNAI), vol. 2424, pp. 86–97. Springer, Heidelberg (2002)
4. Halpern, J.Y.: An analysis of first-order logics of probability. In: IJCAI, pp. 1375–1381 (1989)
5. Poole, D.: Representing diagnostic knowledge for probabilistic horn abduction. In: IJCAI, pp. 1129–1137 (1991)
6. Kyburg Jr., H.E.: Higher order probabilities and intervals. Int. J. Approx. Reasoning 2(3), 195–209 (1988)
7. Noy, N.F.: Semantic integration: A survey of ontology-based approaches. SIGMOD Record 33(4), 65–70 (2004)
8. Rahm, E., Bernstein, P.A.: A survey of approaches to automatic schema matching. VLDB J 10(4), 334–350 (2001)
9. Baader, F., Nutt, W.: Basic description logics. In: Baader, F., Calvanese, D., McGuinness, D.L., Nardi, D., Patel-Schneider, P.F. (eds.) Description Logic Handbook, pp. 43–95. Cambridge University Press, Cambridge (2003)
10. Schmidt-Schauß, M., Smolka, G.: Attributive concept descriptions with complements. Artif. Intell. 48(1), 1–26 (1991)
11. Pan, J.Z.: Description Logics: Reasoning Support for the Semantic Web. PhD thesis, School of Computer Science, The University of Manchester, Oxford Rd, Manchester M13 9PL, UK (2004)
12. Fagin, R., Halpern, J.Y.: Reasoning about knowledge and probability. J. ACM 41(2), 340–367 (1994)
13. Fagin, R., Halpern, J.Y., Megiddo, N.: A logic for reasoning about probabilities. Inf. Comput. 87(1/2), 78–128 (1990)
14. Nilsson, N.: Probabilistic logic. ai 28, 71–87 (1986)
15. Halpern, J.Y.: Reasoning about knowledge: A survey. In: Gabbay, D.M., Hogger, C.J., Robinson, J.A. (eds.) Handbook of Logic in Artificial Intelligence and Logic Programming, Epistemic and Temporal Reasoning, vol. 4, pp. 1–34. Clarendon Press, Oxford (1995)
16. Bacchus, F., Grove, A.J., Halpern, J.Y., Koller, D.: From statistical knowledge bases to degrees of belief. Artif. Intell. 87(1-2), 75–143 (1996)
17. Fagin, R., Halpern, J.Y.: Uncertainty, belief, and probability. In: IJCAI, pp. 1161–1167 (1989)
18. Bacchus, F., Grove, A.J., Halpern, J.Y., Koller, D.: Generating degrees of belief from statistical information: An overview. In: Shyamasundar, R.K. (ed.) Foundations of Software Technology and Theoretical Computer Science. LNCS, vol. 761, pp. 318–325. Springer, Heidelberg (1993)
19. Friedman, N., Halpern, J.Y.: Modeling belief in dynamic systems, part I: Foundations. Artif. Intell. 95(2), 257–316 (1997)
20. Friedman, N., Halpern, J.Y.: Modeling belief in dynamic systems, part II: Revision and update. J. Artif. Intell. Res. (JAIR) 10, 117–167 (1999)

21. Heinsohn, J.: Probabilistic description logics. In: de Mantaras, R.L., Poole, D. (eds.) Proceedings of the 10th Conference on Uncertainty in Artificial Intelligence, pp. 311–318. Morgan Kaufmann, San Francisco (1994)
22. Lukasiewicz, T.: Probabilistic deduction with conditional constraints over basic events. In: KR, pp. 380–393 (1998)
23. Jaeger, M.: Probabilistic reasoning in terminological logics. In: KR, pp. 305–316 (1994)
24. Baader, F., Laux, A.: Terminological logics with modal operators. IJCAI (1), 808–815 (1995)

Multi-constraint System Scheduling Using Dynamic and Delay Ant Colony System

Shih-Tang Lo[1], Ruey-Maw Chen[2], and Yueh-Min Huang[3]

[1] Department of Information Management, Kun-Shan University, Yung-Kang City, Tainan Hsien, 710, Taiwan, ROC
[2] Department of Computer Science and Information Engineering, National Chin-yi University of Technology, Taichung, 411, Taiwan, ROC
[3] Department of Engineering Science, National Cheng-Kung University, Tainan, 701, Taiwan, ROC
edwardlo@mail.ksu.edu.tw, raymond@mail.ncut.edu.tw, huang@mail.ncku.edu.tw

Abstract. This study presents and evaluates a modified ant colony optimization (ACO) approach for the precedence and resource-constrained multiprocessor scheduling problems. A modified ant colony system, with two designed rules, called dynamic and delay ant colony system, is proposed to solve the scheduling problems. The dynamic rule is designed to modify the latest starting time of jobs and hence the heuristic function. A delay solution generation rule in exploration of the search solution space is used to escape the local optimal solution. Simulation results demonstrate that the proposed modified ant colony system algorithm provides an effective and efficient approach for solving multiprocessor system scheduling problems with precedence and resource constraints.

Keywords: Ant colony optimization, scheduling, multiprocessor.

1 Introduction

In this study, an ACO approach for the precedence and resource constrained multiprocessor scheduling problem is presented and evaluated. Hou et al. developed an efficient method, the height value of each job in graph, based on a genetic algorithm to solve the multiprocessor scheduling problem [1]. Correa et al. proposed a genetic algorithm is enhanced with some knowledge about the problem represented by the use of a list heuristic in the operators [2] [3]. Oh and Wu presented a multi-objective genetic algorithm (GA), which aims to minimize the number of processors required and the total tardiness of tasks [4]. GA generates a high quality of output schedules, but the scheduling times are generally much higher than that with the heuristic-based schemes [5][6].

ACO is a class of constructive meta-heuristic algorithms. ACO mimics the behavior of foraging ants. Ants deposit pheromones on the paths that they move along. The pheromone level deposited on a particular path increases with the number of ants passing along it. Ants adopt pheromones to communicate and cooperate with each another in order to identify the shortest paths to a destination

H.G. Okuno and M. Ali (Eds.): IEA/AIE 2007, LNAI 4570, pp. 655–664, 2007.

[7] [8]. Dorigo and Gambardella first applied the ant colony system (ACS) to solve TSP [9]. Simulation results indicate that ACS outperforms other nature-inspired algorithms, such as simulated annealing and evolutionary computation. Applications of the ACO algorithm are also involved in solving job shop scheduling problems [10]. Besten et al. presented an application of the ACO meta-heuristic to the single machine total weighted tardiness problem [11]. Gajpal et al. adopted ACO to solve the problem of scheduling in flowshop with sequence-dependent setup times of jobs [12]. Rajendran and Ziegler developed two ant-colony optimization algorithms for solving the permutation flowshop scheduling problem [13].

The resource-constrained project scheduling problem (RCPSP), which is a schedule problem to find the minimum makespan with resource and precedence constraints using ACO algorithms has recently been studied [14][15][16]. Merkle et al. presented an ACO approach for RCPSP [16]. The ACO algorithm has recently been applied to scheduling problems, such as job-shop, flow-shop, and single machine tardiness problems [17][9][18][19]. In our previous work, a multi-constraint schedule problem for a multi-processor system was solved by Hopfield neural network (HNN) [20]. Chen et al. also presented a modified neural network to solve the multiprocessor scheduling problem with inequality constraints [21]. A series of studies has been conducted using HNN and mean field annealing [22][23]. These works concentrate on each resource type has only one resource available. This work attempts to find optimal or near-optimal solutions to multiprocessor schedule problems with resource and precedence constraints and restricted scheduling times, known as resource-constrained multi-processor scheduling problems, and denoted by RCMPSP in this study. Additionally, each resource type has different available quantities.

2 Multiple Constraints Scheduling Problems and ACO Algorithm

2.1 Scheduling Problem

Suppose there are M identical processors. Jobs cannot be both segmented and preemptive. Let $J = \{1, \ldots, N\}$ denotes the set of jobs, where N is the total number of jobs. Q denotes a set of resources; total of k types, and $R_i \geq 0$ is the resource quantity for resource type i, $i \in Q$. Each job j, $j \in J$, has a predefined processing time p_j and resource requirements $r_{j,1} \ldots r_{j,k}$, where $r_{j,i}$ denotes the job j requirement for a resource type i. There is precedence relations between the jobs, and no setup time between jobs considered.

Typically, the pheromone matrix $\tau = [\tau_{ij}]$ is used to find a good solution, where τ_{ij} represents the pheromone value of job j is the ith job on the machine. The coming ants of the next generation directly use the value of τ_{ij} and heuristic function to estimate the desirability of placing job j as the ith job on the machine when obtaining a new solution [16]. Bauer et al. proposed ACO algorithms using a conventional pheromone matrix $[\tau_{ij}]$ to solve the single machine total tardiness problem and the flow-shop problem [17]. This study adopts a modified

pheromone matrix $[\tau_{tj}]$, in which the element τ_{tj}, denoting the pheromone value of job j is processed at time t on a specific machine.

Figure 1 is an example of studied problem, including a precedence graph and resources constraint with 6 jobs and 4 resource types on two machines. A two-dimensional matrix $(T \times N)$ is used to denote the scheduling result. The axes of the matrix are job and time, as denoted by j and t respectively. The state of a coordinate is represented by V_{tj} . The V_{tj} is set to 1, if job j is processed at time t; otherwise V_{tj} is set to 0.

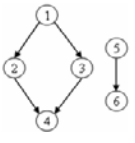

Job #	Process time	Resources required R_1=3,R_2=3,R_3=2,R_4=1
Job 1	2	2 2 1 1
Job 2	3	3 0 1 1
Job 3	4	0 2 1 0
Job 4	2	2 2 2 1
Job 5	3	1 2 2 1
Job 6	2	1 1 0 0

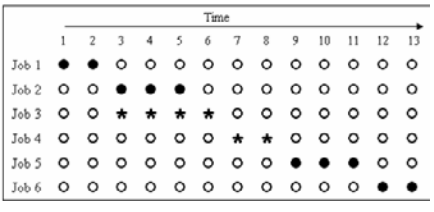

Fig. 1. The 6 jobs case and one solution matrix

2.2 Ant Colony System

Dorigo et al. proposed the ACO algorithm to solve the well-known TSP, which evolved into the ant colony system (ACS) as shown in Fig. 2 [9][24].

Initialize
Loop
  Each ant is positioned on a starting node(partial solution)
  Loop
    Each ant applies *a state transition rule* to incrementally build a solution and *a local pheromone update rule*
  Until all ants have built a complete solution
  A global pheromone updating rule is applied
Until End_condition is reached

Fig. 2. Ant Colony Systems for TSP

2.3 Local Update Rule and Global Update Rule

A graph $G = (V, E)$ comprises a set of nodes (vertex) $V = \{v_1, v_2, \ldots, v_n\}$ and a set of edges $E = \{(i, j) \mid v_i, v_j \in V\}$.The modified ACS adopts the following local updating rule to prevent succeeding ants from searching in the neighborhood of the current schedule of the current ant. The ants select job j at time t, and then modify their pheromone levels.

$$\tau(t,j)_{new} = (1-\rho) \cdot \tau(t,j) + \rho \Delta\tau(t,j), t = S_j \tag{1}$$

where $0 < \rho < 1$ denotes the evaporation rate as an input parameter, where job j progresses from S_j to f_j, where $S_j(f_j)$ is the starting (finish) processing time of job j. $\Delta\tau(t,j)$ is set to a predefined value in the proposed ACO method. Restated, $\Delta\tau(t,j) = \tau_0$ is utilized in this work. The global update rule is used to increase the pheromone τ_{tj} by applying to the best solution so far. The global update rule increases the pheromone ntj, if $V_{tj} = 1$, $t = S_j$. Otherwise, the pheromone τ_{tj} is evaporated by global pheromone evaporation rate δ, as shown in Eq. (2). This is an elitist strategy that leads ants to search near the best-found solution.

$$\tau(t,j)_{new} = (1-\delta)\cdot\tau(t,j) + \delta\Delta\tau_{gb}(t,j), t = S_j \tag{2}$$

where $0 < \delta < 1$ denotes a parameter representing the global pheromone evaporation rate, and

$$\delta\Delta\tau_{gb}(t,j) = \begin{cases} \Delta ms, \text{ if } V_{tj} = 1 \\ 0, \quad \text{if } V_{tj} = 0 \end{cases} \text{ and } \Delta ms = \frac{1 + \max\{0, ms_{old} - ms_{gb}\}}{ms_{gb}} \tag{3}$$

where $\Delta\tau_{gb}(t,j)$ is computed by the best schedule in the current iteration. The amount of pheromone added is $\delta\Delta\tau_{gb}(t,j)$ when job j is assigned to run in time period $[S_j, f_j]$. The ms_{old} and ms_{gb} denote the *makespan* of the best schedule in the previous and current iterations, respectively. For each job, pheromone is added when a job is being processed in the job schedule list of the best solution obtained in the current generation. Otherwise, the pheromone is evaporated if $V_{tj} = 0$.

2.4 State Transition Rules

The state transition rules are governed by Eq. (4) and (5) modified from [9][24]. The next job j is chosen from $J_k(t)$ when $q \leq q_0$, which flavors the choices for the next job with the highest pheromone times heuristic value (the η function is defined in Eq. (8)).

$$j = \arg \max_{l \in J_k(t)} \left\{ [\tau(t,l)]^{\alpha} \cdot [\eta(t,l)]^{\beta} \right\} \tag{4}$$

If $q > q_0$, then job j is randomly selected from $J_k(t)$ according to the probability distribution given by Eq. (7).

$$P_k(t,j) = \begin{cases} \frac{[\tau(t,j)]^{\alpha}\cdot[\eta(t,j)]^{\beta}}{\sum_{l\in J_k(t)}[\tau(t,l)]^{\alpha}\cdot[\eta(t,l)]^{\beta}}, & j \in J_k(t) \\ 0 \quad \text{otherwise} \end{cases} \tag{5}$$

where α, β denote the parameters correlating to the importance of the pheromone and heuristic, respectively.

3 Modified ACO Algorithm (DDACS) for RCMPSP

The scheduling algorithm for the precedence and resource constrained multiprocessor scheduling problem by modified ACS, which combines the dynamic rule and delay solution generation rule, is called a dynamic and delay ant colony system (DDACS).

3.1 Critical Path Method and Heuristic Function

To define the scheduling algorithm concisely, we define two auxiliary times: the *earliest* and *latest* start times of a job. First, the earliest start time of job j (E_j) is the length of the longest path from an entry job to job j. The latest start time of job j (L_j) is defined to be the latest time at which job j may start, such that job j and all successors of job j have a chance to complete as soon as possible.

$$E_j = \begin{cases} 0, & \text{if } \neg\exists i : (i,j) \in E \\ \max_{i \in Pre(j)}\{E_i + p_j\}, & \text{otherwise} \end{cases} \tag{6}$$

$$L_j = \begin{cases} \max\{E_j + p_j\} - p_j, & \text{if } \neg\exists i : (j,i) \in E \\ \max_{i \in Succ(j)}\{L_i - p_j\}, & \text{otherwise} \end{cases} \tag{7}$$

where the $pre(j)$ ($succ(j)$) is the set of immediate predecessors (successors) of job j, if $(i,j) \in E$. The earliest and latest start times of a job is applied in η function determination. The L_j is used to build the initial solution. The η function is shown in Eq. (8).

The E_j and L_j are initially computed under no resource considerations, hence there is a conservative value for each job. However, the actual starting process time of some jobs is behind the L_j when involving resource constraints. The L_j will be modified by the dynamic rule based on the best solution obtained in the current iteration.

$$\eta(t,j) = \begin{cases} \frac{1}{(d_j+1)\times \sqrt[c]{p_j+1}}, & \text{if } E_j \le t < L_j \\ \frac{1}{(2-d_j/c_1)\times \sqrt[c]{p_j+1}}, & \text{if } t \ge Lj \end{cases}, j \in J_k(t) \tag{8}$$

where $d_j = |L_j - t|$ and c, c_1 are large enough constant values.

Equation (8) demonstrates that job j with the shortest process time (shortest p_j) and near to L_j (minimum d_j) obtains the highest η value. Hence, the job with minimum d_j and shortest p_j is executed first when $E_j \le t < L_j$, or the job with maximum d_j and shortest p_j is first when $t \ge L_j$. Once one job j is selected according to the state transition rule Eq. (4), then $V_{tj} = 1$, $t \in [S_j, f_j]$, where $S_j = t$ and $f_j = t + p_j - 1$. Thus this setting ensures that the non-preemptive requirement is satisfied.

3.2 Partial Solution Initialization and Stop Condition

DDACS begins with a partial schedule containing no jobs at time 0. At each stage, a set of all eligible jobs $J_k(t)$, comprising all candidates for successors at time t. The initial jobs in $J_k(0)$ have in-degree=0 which refers to the number of eligible jobs at time 0. The following jobs selected from $J_k(t)$ are applied until $m = M$ or resource constraints are not satisfied for all job in $J_k(t)$. A job is selected by the ant from $J_k(t)$ if it satisfies resource and processor constraints. The processors number confines the most M jobs can be assigned to M processors. After allocating jobs to processors at time t, $J_k(t)$ are then updated at time $t+1$ and run until all jobs are scheduled. The algorithm runs until a certain number of generations have been performed.

3.3 Dynamic and Delay Solution Generation Rules

A schedule may contain some jobs that start to run behind L_j, which is a conservative value and is initially determined under no resource considerations. Therefore, a rule is designed to refine the latest starting time by feedback of the best solution found in current iteration. This rule is called a "dynamic" rule. For those jobs that have been scheduled later than the L_j, the new L_j is replaced by the S_j. The efficiency of estimation of the η function value rises as the accuracy of L_j increases.

The delay solution generation rule (called the delay rule for short) is enabled some jobs to be assigned later to escape the local optimal solution. The delayed job is excluded for a certain delay length, which is a uniform distribution of $[0, L_j - t]$ as demonstrated in Eq. (9).

Figure 6 depicts an example of without delay strategy, jobs 2 and 3 are schedule to run when two processors exist at $t = 1$. If jobs 2 and 3 are delayed to process, an optimal solution is obtained, since job 7 is a critical path job and can be processed earlier. The "delay" rule deliberately delays an eligible job, as shown in Eq. (9). This rule enables an undiscovered and better solution to be found.

$$\text{delay time} = \begin{cases} q \times (L_j - t), & \text{if } q > q_1 \text{ and } t \leq L_j \\ 0, & \text{otherwise} \end{cases} \tag{9}$$

where q is a random number uniformly distributed in $[0, 1]$. The q_1 $(0 < q_1 < 1)$ is a predetermined parameter that determines the probability of changing the influence on the decisions of the ants. The rules, Eq. (4) and (5) are adopted when $q \leq q_1$. Otherwise, this delay strategy is applied when $q > q_1$ and $t \leq L_j$. The q_1 value increases along with the iteration. Restated, the possibility of delaying jobs is decreased as the iteration increase.

4 Simulations and Results

The simulations involved different sets of scheduling problems with different jobs and processors. All simulation cases assumed that three or four different resource types were available and 10 ants were adopted. The $\text{iteration}_{\max} = 1000$, $\tau_0 = 0.01$, $c = 10$ and $c_1 = 50$. Moreover, $\delta = 0.1$, $\rho = 0.1$, $\alpha = 1$, $\beta = 1$, $q_0 = 0.9$ and $q_1 = 0.95$ were set in the simulation.

Figure 3 shows the simplest 10 jobs case. The *makespan* of the optimal solution in the two processors case is 10. Figures 4 and 5 indicate the scheduling results for two processors. Figures 4 show the results of the no-delay rule used in the modified ACO. Figures 5 display scheduling results of using the delay rule in the algorithm.

The following simulation cases are PSPLIB cases [25]. The PSPLIB includes project scheduling problems with no processor constraints, which are one special problem case of the studied RCMPSP. Thus, suggested DDACS can be directly applied to solve the PSPLIB problems. The following simulations were used to test the proposed DDACS whether the optimal solutions can be found as listed in PSPLIB. The other purpose of solving PSPLIB using DDACS is to verify

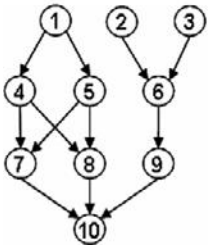

JOB#	Process time	Resource require R_1=5,R_2=6,R_3=4
1	1	2 1 2
2	2	3 5 2
3	2	3 2 2
4	1	3 3 1
5	1	2 3 3
6	1	4 1 3
7	7	1 1 1
8	1	2 4 2
9	1	0 3 3
10	1	4 3 3

Fig. 3. Simulation cases for 10 jobs with precedence and resource constraint

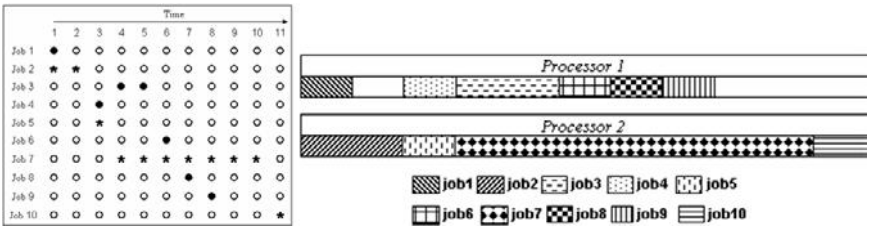

Fig. 4. The solution matrix and Gantt chart with no delay rule

the designed dynamic rule and delay solution generation rule in obtaining a near-optimal (optimal) solution.

Figure 6 shows the difference between computed *makespan* and optimal *makespan* for cases of 30 jobs with 480 instances. The total number of near-optimal solutions with dynamic and delay solution generation rules were greater than that obtained when no rule was employed. For instance, DDACS obtained about 93.3% (=448/480) cases with near-optimal solutions, in which the difference between the computed *makespan* and optimal *makespan* was no more than 2, as in Fig. 6.

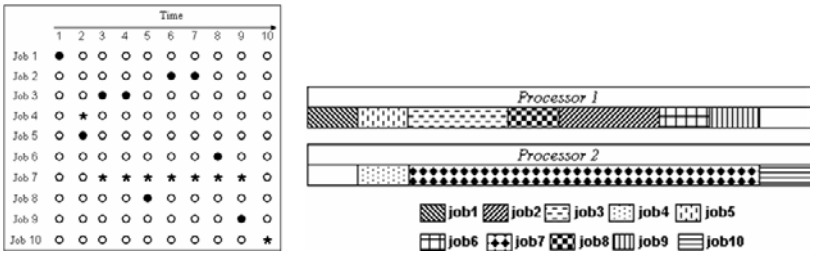

Fig. 5. The solution matrix and Gantt chart with delay rule

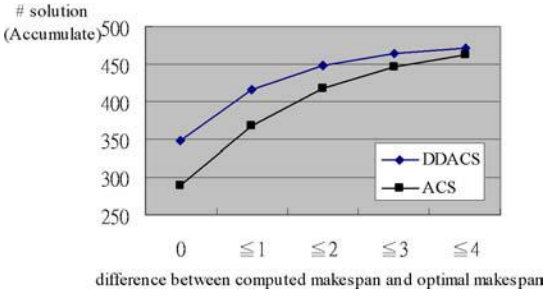

Fig. 6. The number of near optimal solutions for 480 different instances with 500 iterations

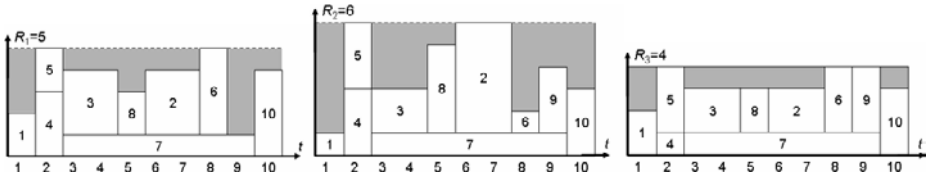

Fig. 7. Resource allocation for one simulation result

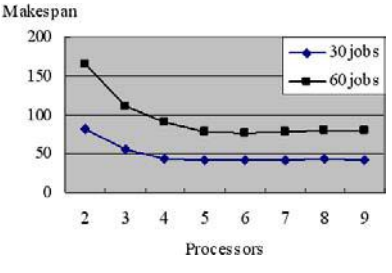

Fig. 8. The *makespan* for one 30 jobs case and one 60 jobs case after 100 iterations

Figure 7 show the corresponding optimal schedule obtained using the proposed ant approach. The allocation profiles of three types of resources are reflectively described in the schedule.

Figure 8 depicts the *makespan* of the simulation results of cases with 30 and 60 jobs with different numbers of processors. Different numbers of processors were set in the simulation. The minimum number of required processors was not considered in this study. Most of the simulations assumed that the number of processors in the multiprocessor system was sufficient. The simulation results easily reveal the requisite number of processors. The case with 60 jobs required about 5 processors, while that with 30 jobs needed 4 processors.

5 Conclusions and Discussion

This study presents a modified ACO approach named DDACS for a multi-constraint (precedence and resource constraints) multiprocessor scheduling problem. A two dimension (time and job) matrix graph is adopted to represent the scheduling problem. The proposed DDACS scheme provides an efficient method of finding the optimal schedule for the multi-constraint multiprocessor system. Meanwhile, this suggested method can be adopted to predict the minimum number of processors required in the multiprocessor system, as the results shown in Fig. 8. An important feature of the scheduling algorithm is its efficiency or performance. A fast convergence rate is a significant characteristic of an ant colony system. The execution time of the DDACS algorithm is proportional to $O(N \times T \times ant)$ for one iteration

This work focuses on investigating homogeneous multiprocessor system scheduling with precedence and resource constraints. However, the more complex conditions, such as set-up time between jobs on a particular machine, and the communication cost of jobs running on different processors and heterogeneous processors, should be further studied.

References

1. Hou, E.S.H., Ansari, N., Ren, H.: A genetic algorithm for multiprocessor scheduling. IEEE Transactions on Parallel and Distributed Systems 5(2), 113–120 (1994)
2. Correa, R.C., Ferreira, A., Rebreyend, P.: Integrating list heuristics into genetic algorithms for multiprocessor scheduling. Parallel and Distributed Processing. In: Eighth IEEE Symposium. pp. 462–469 (1996)
3. Correa, R.C., Ferreira, A., Rebreyend, P.: Scheduling multiprocessor tasks with genetic algorithms. IEEE Transactions on Parallel and Distributed Systems 10(8), 825–837 (1999)
4. Oh, J., Wu, C.: Genetic-algorithm-based real-time task scheduling with multiple goals. J. of Systems and Software 71(3), 245–258 (2004)
5. Kwok, Y.K., Ahmad, I., Gu, J.: FAST: a low-complexity algorithm for efficient scheduling of DAGs on parallel processors. Parallel Processing. In: Proceedings of the 1996 International Conference on, vol. 2, pp. 150–157 (1996)
6. Topcuoglu, H., Hariri, S., Wu, M.Y.: Performance-effective and low-complexity task scheduling for heterogeneous computing. IEEE Transactions on Parallel and Distributed Systems Publication 13(3), 260–274 (2002)
7. Maniezzo, V., Carbonaro, A.: Ant Colony Optimization: an Overview. In: Proceedings of MIC'99, III Metaheuristics International Conference, Brazil (1999)
8. Stützle, T., Hoos, H.H.: MAX-MIN Ant system. Future Generation Computer Systems 16(9), 889–914 (2000)
9. Dorigo, M., Gambardella, L.M.: Ant colony system: A cooperative learning approach to the traveling salesman problem. IEEE Transactions on Evolutionary Computation 1(1), 53–66 (1997)
10. Pierucci, P., Brandani, E.R., Sogaro, A.: An industrial application of an on-line data reconciliation and optimization problem. Computers & Chemical Engineering 20, S1539–S1544 (1996)

11. Besten, M.D., Sttzle, T., Dorigo, M.: Ant Colony Optimization for the Total Weighted Tardiness Problem. In: Deb, K., Rudolph, G., Lutton, E., Merelo, J.J., Schoenauer, M., Schwefel, H.-P., Yao, X. (eds.) Parallel Problem Solving from Nature-PPSN VI. LNCS, vol. 1917, pp. 611–620. Springer, Berlin (2000)
12. Gajpal, Y., Rajendran, C., Ziegler, H.: An ant colony algorithm for scheduling in flowshops with sequence-dependent setup times of jobs. European Journal of Operational Research 155(2), 426–438 (2004)
13. Rajendran, C., Ziegler, H.: Ant-colony algorithms for permutation flowshop scheduling to minimize makespan/total flowtime of jobs. European Journal of Operational Research 155(2), 426–438 (2004)
14. Brucker, P., Drexel, A., Möhring, R.H., Neumann, K., Pesch, E.: Resource-constraint project scheduling: Notation, classification, models, and methods. Eur. J. Oper. Res. 112(1), 3–41 (1999)
15. Herroelen, W.B., Reyck, D., Demeulemeester, E.: Resource-constrained project scheduling: A survey of recent developments. Comput. Oper. Res. 13(4), 279–302 (1998)
16. Merkle, D., Middendorf, M., Schmeck, H.: Ant colony optimization for resource-constrained project scheduling. IEEE Trans. on Evolutionary Computation 6(4), 333–346 (2002)
17. Bauer, A., Bullnheimer, B., Hartl, R.F., Strauss, C.: An ant colony optimization approach for the single machine total tardiness problem. In: Proc. 1999 Congr. Evolutionary Computation, pp. 1445–1450 (1999)
18. Iredi, S., Merkle, D., Middendorf, M.: Bi-Criterion Optimization with Multi Colony Ant Algorithms. In: Zitzler, E., Deb, K., Thiele, L., Coello Coello, C.A., Corne, D.W. (eds.) EMO 2001. LNCS, vol. 1993, pp. 359–372. Springer, Heidelberg (2001)
19. Merkle, D., Middendorf, M.: A new approach to solve permutation scheduling problems with ant colony optimization. In: Boers, E.J.W., Gottlieb, J., Lanzi, P.L., Smith, R.E., Cagnoni, S., Hart, E., Raidl, G.R., Tijink, H. (eds.) EvoIASP 2001, EvoWorkshops 2001, EvoFlight 2001, EvoSTIM 2001, EvoCOP 2001, and EvoLearn 2001. LNCS, vol. 2037, pp. 484–494. Springer, Heidelberg (2001)
20. Huang, Y.M., Chen, R.M.: Scheduling multiprocessor job with resource and timing constraints using neural network. IEEE Trans. on System, Man and Cybernetics, part B 29(4), 490–502 (1999)
21. Chen, R.M., Lo, S.T., Huang, Y.M.: Combining competitive scheme with slack neurons to solve real-time job scheduling problem. Expert Systems with Applications (In Press)
22. Chen, R.M., Huang, Y.M: Multiconstraint task scheduling in multiprocessor system by neural network. In: Proc. IEEE Tenth Int. Conf. on Tools with Artificial Intelligence, Taipei, pp. 288–294 (1998)
23. Chen, R.M., Huang, Y.M.: Competitive Neural Network to Solve Scheduling Problem. Neurocomputing 37(1-4), 177–196 (2001)
24. Dorigo, M., Maniezzo, V., Colorni, A.: The ant system: Optimization by a colony of cooperating agents. IEEE Trans. on Sys. Man & Cyber. 26(1), 1–13 (1996)
25. Kolisch, R., Schwindt, C., Sprecher, A.: Benchmark instances for project scheduling problems. In: Weglarz, J. (ed.) Handbook on Recent Advances in Project Scheduling, pp. 147–178. Kluwer, Amsterdam (1999)

Constructing Domain Ontology Using Structural and Semantic Characteristics of Web-Table Head

Sung-won Jung[1,2], Mi-young Kang[1], and Hyuk-chul Kwon[1]

[1] Pusan National University, Korean Language Processing Laboratory, Department of Computer Science Engineering
[2] Pusan National University, Center for U-Port IT Research and Education, Jangjeon-dong, Geumjeong-gu, 609-735, Busan, Korea
{swjung, kmyoung, hckwon}@pusan.ac.kr

Abstract. This study concerns the constructing of domain ontology from web tables in a specific domain. Ontology defines the common terms and their meaning (concepts) within a context. Thus only meaningful tables are our concern. The meaningful table is composed of a head and a body, which are formatted in rows and columns. The head abstracts the meaning expressed in the body. Thus, in order to obtain a table-information-extraction framework, this study extracts, as prerequisite work, the structural semantic, that is, the domain ontology that frames web-table information, from the head. We suggest a method for automatically extracting domain ontology using the structural and semantic characteristics of the web-table head. The construction of domain ontology proceeds through two steps: (a) extracting table schema as pseudo-ontology from each table from the same domain and (b) constructing domain ontology combining those extracted table schemata. The combination of schemata proceeds through splitting and clustering using (a) statistical information and (b) heuristics based on the structural and semantic characteristics of the web-table head.

Keywords: Table-information extraction; Table mining; Meaningful table; Table-head structure; Table schema; Pseudo-ontology; Domain ontology.

1 Introduction

Web-tables (we use the two terms ‘web table’ and ‘table’ interchangeably) are used mainly for structuring information, and they are the strongest means of presenting structured information. Thus, tables are the richest sources of information on the web. Each table is formatted in rows and columns, whereas it is distinguished in head and body according to meaning. In HTML documents, which are the most common form of document on the web, special tags such as <table>, <tr>, <td>, are reserved for table structure, and those such as <thead>, <tbody>, <tfoot> are reserved for table meaning. However, the latter are used for distinguishing meaning areas, not for considering the relation of those meaning areas. Furthermore, those special tags are not used systematically; in many cases <tr> and <td> are used for all components without distinction. Because of the lack of those components for machine-readable

H.G. Okuno and M. Ali (Eds.): IEA/AIE 2007, LNAI 4570, pp. 665–674, 2007.

semantic consideration, web-table information extraction, in its current state, is very limited. This study mainly focused on how to extract information while overcoming those deficiencies. The solution can be found by referring to one of the methods of extracting information from specific HTML documents, which is mapping of information to ontology. The ontology is previously constructed in such a way that it represents the structure of HTML documents. Fortunately, compared to the plain text in HTML documents, extracting ontology from web-tables is easier, because web-tables have their own structure and internal hierarchical semantic layer. Ontology is the most utilized means for structuring information [1]. Thus, this paper discusses means for structuring meaning from tables in HTML, in other words, constructing ontology from web-tables. The construction of ontology proceeds through two steps: (a) extracting table schema as a pseudo-ontology from each table among those in the same domain and (b) constructing domain ontology starting from those extracted table schemata. To achieve this objective, firstly, characteristics of web-tables are analyzed in two ways: (a) structural characteristics related to 'table-head form' and (b) semantic characteristics related to 'table contents'. The two layers together structure table information. Secondly, the table schema, as a pseudo-ontology, is extracted from each table. Finally, domain ontology is constructed combining those pseudo-ontologies using statistical information and heuristics.

Section 2 discusses related studies. Section 3 explores the means of extracting structural semantic information from a web-table via extraction of table schemata and combination of those table schemata. Section 4 examines methods for constructing a domain ontology using table schemata that are automatically extracted from various web-tables in the same domain.

2 Related Work

This study concerns table mining, which is elaborated in two directions. Firstly, tables are distinguished, and information is extracted from meaningful tables. To those ends, there is a domain-specific approach and a domain-independent approach. Domain-specific research is based on wrapper induction [2], which performs particular information extraction using extraction rules. Using these extraction rules, several studies [2, 3, 4] have extracted table information according to a special tabular form. Because these studies dealt only with the special tabular form, however, the researchers experienced difficulty in coping with the various web-document formats. Alternatively, the domain-independent approach can be found in Yang [5]. He conceives the database as being constructed with attribute-value pairs, and considers table mining as the reverse process of table publishing from a database. He extracts the attribute-value pairs using entity-patterns and extraction rules. However, Yang's method can hardly cope with new tables that contain unknown words. He needs to repetitively and manually update those rules and patterns with linguistic bias, which is rather far from domain independence. Secondly, structural characteristics of tables are analyzed and their structural semantic is extracted. Much research in this direction was contemporaneous with the beginning of the semantic-web. Notably, those researches endeavored to represent the structural semantics of tables in ontology. Yoshida [6] tried to automatically extract ontology from tables combining a statistical

method and clustering. Tijerino [7] introduced a general method of extracting ontology from tables using only heuristics. The main drawbacks of those two studies consist in not applying enough table structure, in spite of the fact that table structure offers the preeminent clue in text mining.

3 Extracting Table Schema as a Pseudo-ontology Using Characteristics of Web-Table Head

Tables on the Internet are used for both (a) the genuine purposes, that is, presenting certain types of data to users, formatted in rows and columns, and (b) helping construct the layout of a web page. Our previous work [8] classified the former as meaningful tables, the latter as decorative tables, and presented a method for distinguishing them. This paper concerns the former. Extracting information from tables begins with extracting the head. Once the head is extracted, a table schema, which corresponds to a pseudo-ontology of the table, is extracted based on the structure of that head. The following sub-sections discuss how to extract table schemata.

3.1 Extracting Head

In our previous work [8], we described two important factors that that are pertinent to separating the head from the data in a web-table while observing the editing habits of authors themselves. First, authors often use specific techniques for separating the head from the data in order that readers understand a table more clearly. Second, the head abstracts related data in a table. Therefore, the row or column related to a head contains repetition. Both of these observations concern (a) rows and columns' appearance characteristics and (b) their inter-relations. While analyzing rows and columns as parts of a head in meaningful tables and considering their appearance and relations, the features in Table 1 were formulated.

In the machine-learning step, we constructed a head extraction model. The meaningful tables are converted to an input data set for the machine-learning algorithm. The rows and columns in the tables were converted into a 14-dimensional vector using the features. From this input data, we constructed the head extraction model using a decision tree classifier, C4.5 [9]. This classifier was chosen because of the nature of our feature values and our need to observe head extraction model.

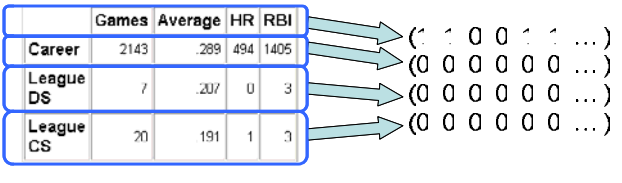

Fig. 1. Converting rows and columns to vectors

Table 1. Features for extracting head[1]

Appearance characteristics		
No.	Feature	Value
1	If a row or column is expressed by <th> tags, the feature value is 1 otherwise 0.	0 or 1
2	If a row or column contains a span tag, the feature value is 1 otherwise 0.	0 or 1
3	If a table has an empty cell in the first row, first column, the row and column that includes that empty cell is 1 otherwise 0.	0 or 1
4	The index-number of a row or column in a table.	Integer
5	The average number of characters in a cell of a row or a column	Prime number
6	The standard deviation of the number of characters in a cell of a row or a column.	Prime number
Inter-relational characteristics		
No.	Feature	Value
7	The fraction of a row's or column's representative CCT[1)] in a row or column.	Percentage
8	The fraction of TRT[2)] in a row or column.	Percentage
9	If a row's or column's CPT[3)] is different of its successive row's or column's CPT, the feature value is 1 otherwise 0. The undermost row and the rightmost column are always 0.	0 or 1
10	The fraction of a row or a column's representative CCP[4)] in a row or a column.	Percentage
11	The fraction of TRP[5)] in a row or a column.	Percentage
12	If a row's or column's CPP[6)] is different of its successive row's or column's CPP, the feature value is 1 otherwise 0. The undermost row and the rightmost column are always 0.	0 or 1
13	The degree of possibility of the presence of a head based on background color.	Prime number
14	The degree of possibility of the presence of a head based on font attributes.	Prime number

[1)] CCT : cell-contents type such as link, image, digit, and words
[2)] TRT : a table's representative CCT
[3)] CPT : contents pattern based on CCT in a row or a column
[4)] CCP : cell-contents pattern
[5)] TRP : a table's representative CCP
[6)] CPP : contents pattern based on CCP in a row or a column

3.2 Extracting Table Schemata

The table head is a unit that abstracts the data in a body. The meaning of the data, which is arranged in rows and columns, is interpreted according to the head. That is, the meaning of the data is framed by the correlation between elements in a table head. Therefore, identifying the correlation between the elements in the head that intervene to frame the meaning of the data is integral to table-information extraction. That correlation can be represented by table schemata. The extraction of table schemata can be conceived as a procedure of determining the correlation between elements in a

[1] Refer to [8] for the detail on features.

head. This table schema extraction procedure can be followed in two ways: (a) determination of the correlation between elements in a head using the structural characteristics of the table, or (b) determination of the correlation between elements in a head using the semantic characteristics of a table.

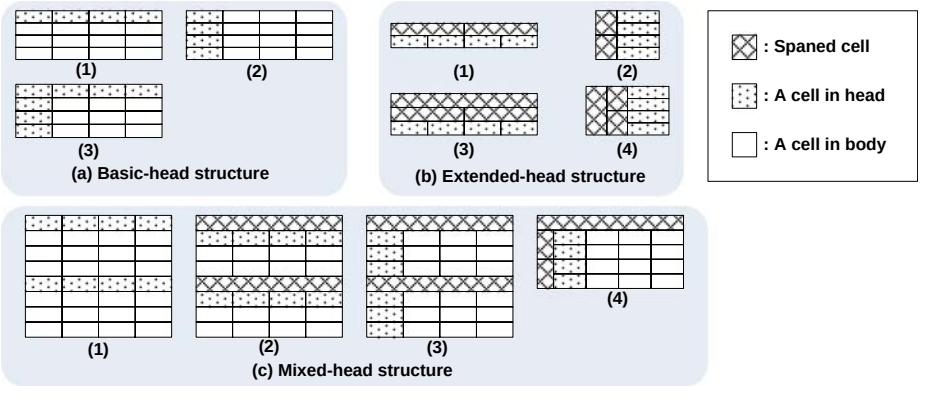

Fig. 2. Types of head structure in web-tables

3.2.1 Structure of Head in Web Tables

Heads in web tables are classified into three groups based on the location of the head and the structure of its inner elements: (a) basic-head structure, (b) extended-head structure, (c) mixed-head structure. Fig. 2.a shows basic structures, in which the head row is located in the upper-most row and the head column is located in the left-most column. Fig. 2.b shows extended table structures. They contain a higher abstraction level than a head of basic structure, which abstraction level is expressed by a spanned cell. Fig. 2.c shows the mixed or repetitive structures of those in Fig. 2.a and those in Fig. 2.b. It is difficult to extract a table schema directly from a mixed structure. However, several head areas can be extracted from a mixed-head structure. Therefore, the table heads of mixed structure must be individually distinguished before the table schema can be extracted. All mixed structures are either of basic structure or extended structure. Thus, table schema extraction proceeds only on the basis of (a) basic structure and (b) extended structure.

3.2.2 Determination of the Correlation Using Structural Characteristics

In an extended-head structure (Fig. 2.b), the spanned cell is used for representing the hierarchical semantic structure of elements in a head. The spanned cell abstracts its consecutive cells. Thus, using this characteristic, the heuristics as in Table 2 can be established. For example, if a table contains a spanned cell in the head as in an extended-head structure, it can be interpreted as the semantic hierarchy shown in Fig. 3. This semantic hierarchy corresponds to a table schema.

Table 2. Heuristics for extracting table schema based on structural characteristic of head

No.	Heuristics
1	If a $c_{i,j}$[a)] is spanned over *n* cells horizontally, the $c_{i,j}$ abstracts subcells from $c_{i+1,j}$ to $c_{i+1,\ j+n}$.
2	If a $c_{i,j}$ is spanned over *n* cells vertically, the $c_{i,j}$ abstracts subcells from $c_{i,j+1}$ to $c_{i+n,\ j+1}$.

[a)] $c_{i,j}$ is the cell that is located in the *i*-th row and the *j*-th cell.

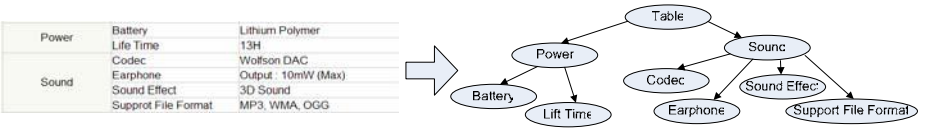

(a) Tree with 2 depths

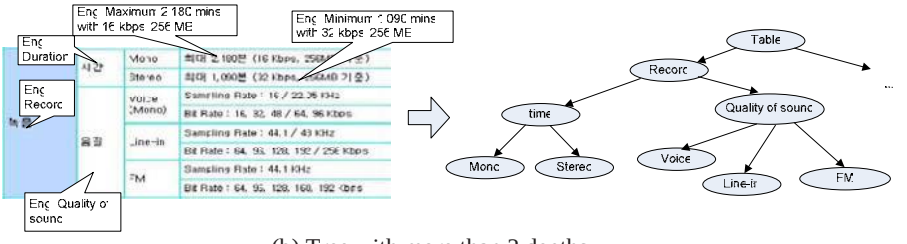

(b) Tree with more than 2 depths

Fig. 3. Table-schema extraction from mixed-head structure

3.2.3 Determination of the Correlation Using Semantic Characteristics

Contrary to extraction from the extended-head structure, it is difficult to extract table schemata from the basic-head structure (Fig. 2.a) owing to its lack of structural hierarchy. However, generally, a table provides, in a head, a semantic-core element (hereafter, SCE) that assumes the role of the 'pivot' in understanding table information. For example, in Fig. 4.a, intuitively, we first identify 'Team' as SCE, then reorganize the table structure as the hierarchical structure in Fig. 4.b. Accordingly, we interpret that 25 is W (the number of wins) and 4 is D (the number of defeats), in this case for the Chelsea soccer club.

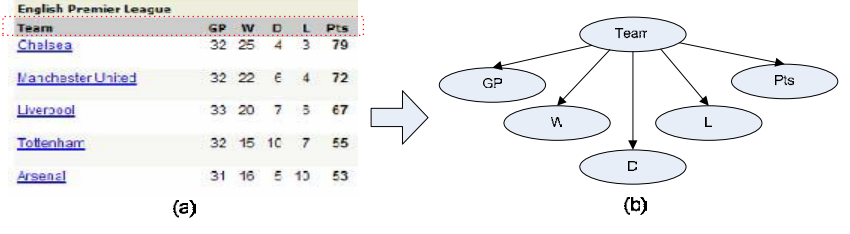

Fig. 4. Table-schema extraction using SCE

Considering this intuitive organization, we institute several heuristics for detecting an SCE, as below.

Table 3. Heuristics for detecting SCE

No.	Heuristics
1	An SCE in a head is located on the left-most side of a head row or on the upper-most side of a head column.
2	If a head cell has digit-type contents in its related body part, it has a weak possibility of being an SCE.
3	If all of the body contents in a table are the digit type, the left-most or upper-most element in a head is an SCE.
4	If a head cell is a spanned cell, it has a weak possibility of being an SCE.
5	If a head cell contains (a) word(s) which belong(s) to (an) attribute(s), it has a weak possibility of being an SCE.

For the purpose of extracting table schemata, we institute the following heuristics based on (a) the SCE that is detected by heuristics in Table 3 and (b) the characteristics of the table structure. As we mentioned above, the SCE is the core element of information and reorganizes the head by assuming the role of the pivot, as shown in Fig. 3. Accordingly, the heuristics for extracting table-schemata are formulated as below.

Table 4. Heuristics for extracting table schemata based on SCE

No.	Heuristics
1	If a $c_{m,*}$ is a head that is located in the *m*-th row, and if $c_{m,k}$ is the SCE, the $c_{m,k}$ abstracts all other $c_{m,j}$ elements in the head.
2	If a $c_{*,m}$ is a head that is located in the *m*-th column and if $c_{k,m}$ is the SCE, the $c_{i,m}$ abstracts all other $c_{i,m}$ elements in the head.

4 Constructing Domain Ontology

So far, the means of table-schemata extraction have been described. Each extracted table schema expresses the structural semantic of a table. Domain ontology can be constructed by combining table schemata extracted from tables belonging to a specific domain. This section discusses the method of constructing the domain ontology.

4.1 Evaluation of Class-Attribute Pair

Each table schema is automatically extracted in tree form. This corresponds to pseudo-ontology, though it is still far from being applied as it is in table information extraction. We can combine table schemata extracted from the same domain. However the combination cannot proceed directly. Each table schema is split into a class-attribute pair. The depth of a tree of a table schema can vary from depth 1 to more than depth 1 according to the head structure. For example, the tree of depth 2 is

extracted from table heads as in Fig. 2.b.3 and Fig. 2.b.4. Each depth forms a candidate class-attribute pair. Thus each table schema is converted into more than one class-attribute pair. Each of those candidate class-attribute pairs is estimated according to its origin. For example, a class-attribute pair belonging to a table schema extracted from an extended-head structure (Fig. 2.b) is a stronger candidate for a class-attribute pair in domain-ontology compared with that belonging to a table schema extracted from a basic-head structure (Fig. 2.a). Furthermore, class-attribute pairs belonging to a table schema extracted from a mixed-head structure with several non-uniform head areas is a weak candidate for a class-attribute pair in domain-ontology compared with those from the two other structures, because head-area detection itself in a mixed-head structure could be erroneous, and so on. The estimated values of the class-attribute pairs are shown in Table 5.

Table 5. Evaluation of candidate class-attribute pair in table schema

No.	class-attribute pair (C-A)	Value
1	C-A originated from extended-head structure: (a) class from cell with span tag located in uppermost row or in leftmost column of web-table head area and (b) attribute from its successive cell(s)	10
2	C-A originated from extended-head structure: (a) class from cell with span tag structure that is not of uppermost row or leftmost column of web-table head area and (b) attribute from its successive cell(s)	0~10 [a)]
3	C-A originated from basic-head structure with single head area, i.e. Fig. 2.a.1 or Fig. 2.a.2: (a) class extracted using SCE and (b) attribute from its successive cell(s)	6
4	C-A originated from basic-head structure with two head area, i.e. Fig. 2.a.3: (a) class extracted using SCE and (b) attribute from its successive cell(s)	5
5	C-A originated from basic-head structure, which is split from mixed-head structure with several repeated uniform head area: (a) class extracted using SCE and (b) attribute from its successive cell(s)	6
6	C-A originated from extended-head structure, which is split from mixed-head structure with several non-uniform head area: (a) class extracted using SCE and (b) attribute from its successive cell(s)	1
7	C-A originated from extended-head structure: (a) class extracted using SCE instead of cell with span tag and (b) attribute from its successive cell(s)	4

[a)] Diminish 2 per depth in table schema on the basis of 10.

4.2 Constructing Domain Ontology Using Clustering

Once class-attribute pairs are extracted from table schemata belonging to the same domain, domain ontology, starting from these pairs, can be easily constructed. The most typical agglomerative clustering method, single-link hierarchical clustering, is used for construction of the domain ontology. This method is the simplest among various clustering methods, because it begins with each data point considered to be in its own cluster and then iteratively determines to which clusters it should be combined. This clustering algorithm is a bottom-up clustering technique that will repeatedly merge clusters of similar groups until the desired number of clusters is attained [10]. The algorithm for constructing domain ontology using clustering is as the following:

```
let each element e be in a singleton group {e}
let G be the set of groups
while |G| > 1 do
  choose best Γ,Δ ∈ G according to estimation value
    e(Γ,Δ) // described in section 4.1
  remove Γ and Δfrom G
  let X= Γ∪ Δ
  insert X into G
end while
```

Algorithm 1. Domain ontology construction algorithm

4.3 Samples of Constructed Domain Ontology

Fig. 5 shows samples of domain ontologies, which are constructed in two steps: (a) extracting a table schema as pseudo-ontology from each table from the same domain and (b) constructing domain ontology combining those extracted table schemata. The combination of schemata proceeds through (a) splitting according to class-attribute pairs and (b) clustering them by applying Algorithm 1.

Table 6. Training data statistics

	Baseball Domain ontology (Fig. 5.a)	MP3 ontology (Fig. 5.b)	Weather ontology (Fig. 5.c)
Total no. of web tables of the same domain	178	127	1,105
Total no. of meaningful tables	32	10	90
Total no. of table schemata	40	12	100
Total no. of class-attribute pairs	89	32	423

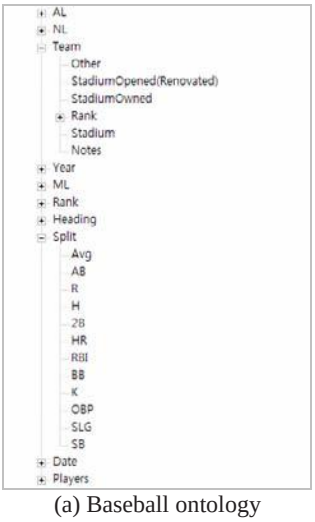

(a) Baseball ontology

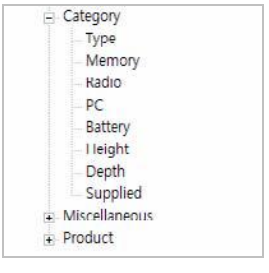

(b) MP3 ontology

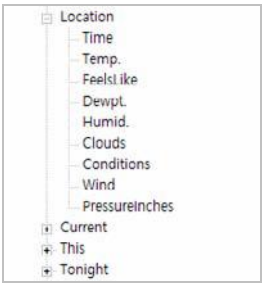

(c) Weather ontology

Fig. 5. Samples of automatically constructed domain ontologies

5 Conclusions and Further Work

This study developed a method for automatic construction of domain ontology, which is the basis for table-information extraction. As tables are themselves organized structurally and semantically, they are good resources from which we can extract ontology relatively easily. Though table schemata as pseudo-ontologies extracted from individual tables cannot be directly applicable, they offer a good basis for automatic construction of domain ontology. In addition, thanks to the proposed method, manual effort is considerably diminished in constructing domain ontology. In our future work, a more precise method for extracting table-schemata corresponding to pseudo-ontology will be developed, and we will investigate a method of extracting information using those automatically extracted domain ontologies.

Acknowledgments. This work was supported by the Korea Science and Engineering Foundation (KOSEF) through the National Research Lab. Program funded by the Ministry of Science and Technology (No. M10400000332-06J0000-33210).

References

1. Antoniou, G., Harmelen, F.: A Semantic Web Primer, pp. 10–11. MIT Press, Cambridge (2004)
2. Kushmerick, N., Weld, D.S., Doorenbos, R.: Wrapper Induction for Information Extraction. In: 15th International Joint Conference on Artificial Intelligence (IJCAI-97), Nagoya (August 1997)
3. Chen, H.H., Tsai, S.C., Tsai, J.H.: Mining Tables from Large Scale HTML Texts. In: Proceedings of 18th International Conference on Computational Linguistics, Saabrucken, Germany (July 2000)
4. Hurst, M.: Layout and Language: Beyond Simple Text for Information Interaction - Modeling the Table. In: Proceedings of the 2nd International Conference on Multimodal Interfaces, Hong Kong (1999)
5. Yang, Y.: Web Table Mining and Database Discovery. M.Sc. thesis, Simon Fraser University (August 2002)
6. Yoshida, M., Torisawa, K., Tsujii, J.: Extracting ontologies from World Wide Web via HTML tables. In: Proceedings of the Pacific Association for Computational Linguistics (2001)
7. Tijerino, Y., Embley, D., Longsdale, D., Ding, Y., Nagy, G.: Towards Ontology Generation from Tables. Springer, Heidelberg (2005)
8. Jung, S.W., Kwon, H.C.: A Scalable Hybrid Approach for Extracting Head Components from Web Tables. IEEE transaction on knowledge and data engineering 18(2), 174–187 (2006)
9. Quinlan, J.: C4.5: Programs for Machine Learning. Morgan Kaufmann Publishers, San Francisco (1993)
10. Chakrabarti, S.: Mining the Web. Morgan Kaufmann Publishers, San Francisco (2003)

Maintenance of Fast Updated Frequent Trees for Record Deletion Based on Prelarge Concepts

Chun-Wei Lin[1], Tzung-Pei Hong[2], Wen-Hsiang Lu[1], and Chih-Hung Wu[2]

[1] Department of Computer Science and Information Engineering
National Cheng Kung University
Tainan, 701, Taiwan, R.O.C.
{p78951228, whlu}@mail.ncku.edu.tw
[2] Department of Electrical Engineering
National University of Kaohsiung
Kaohsiung, 811, Taiwan, R.O.C.
{tphong, johnw}@nuk.edu.tw

Abstract. The frequent pattern tree (FP-tree) is an efficient data structure for association-rule mining without generation of candidate itemsets. It, however, needed to process all transactions in a batch way. In the past, we proposed the Fast Updated FP-tree (FUFP-tree) structure to efficiently handle the newly inserted transactions in incremental mining. In this paper, we attempt to modify the FUFP-tree maintenance based on the concept of pre-large itemsets for efficiently handling deletion of records. Pre-large itemsets are defined by a lower support threshold and an upper support threshold. The proposed approach can thus achieve a good execution time for tree maintenance especially when each time a small number of records are deleted. Experimental results also show that the proposed Pre-FUFP deletion algorithm has a good performance for incrementally handling deleted records.

Keywords: data mining, FUFP-tree, Pre-FUFP algorithm, pre-large itemsets, record deletion, maintenance.

1 Introduction

Due to the increasing usage of very large database and data warehouses, mining useful information and helpful knowledge from transactions has been evolving into an important research area. Based on the classes of knowledge derived, finding association rules in transaction databases is most commonly seen in data mining [1][2][3][5][6][11][12][14][15]. In the past, many algorithms for mining association rules from transactions were proposed, most of which were based on the Apriori algorithm [1], which generated and tested candidate itemsets level-by-level. This may cause iterative database scans and high computational costs. Han *et al*. thus proposed the Frequent-Pattern-tree (FP-tree) structure for efficiently mining association rules without generation of candidate itemsets [7]. The FP-tree [7] was used to compress a database into a tree structure which stored only large items. It was condensed and

H.G. Okuno and M. Ali (Eds.): IEA/AIE 2007, LNAI 4570, pp. 675–684, 2007.

complete for finding all the frequent patterns. The construction process was executed tuple by tuple, from the first transaction to the last one. After that, a recursive mining procedure called FP-Growth was executed to derive frequent patterns from the FP-tree. They showed the approach could have a better performance than the Apriori approach.

Hong *et al*. proposed an algorithm based on pre-large itemsets to handle the inserted transactions in incremental mining, which can further reduce the number of rescanning databases [8]. It used a lower support threshold and an upper threshold to reduce the need for rescanning original databases and to save maintenance cost. The algorithm did not need to rescan the original database until a number of new transactions have been inserted. Since rescanning the database spent much computation time, the maintenance cost could thus be reduced in the algorithm.

Hong *et al*. also proposed the Fast Updated FP-tree (FUFP-tree) structure to efficiently handle the newly inserted transactions in incremental mining [9]. The FUFP-tree structure was similar to the FP-tree structure except that the links between parent nodes and their child nodes were bi-directional. Besides, the counts of the sorted frequent items were also kept in the Header_Table of the FP-tree algorithm. In addition to record insertion, record deletion from the databases is also commonly seen in real-applications. In this paper, we thus attempt to modify the FUFP-tree maintenance algorithm based on the concept of pre-large itemsets for efficiently handling deletion of records. Based on two support thresholds, the proposed approach can effectively handle cases in which itemsets are small in an original database and also small in the deleted records. Experimental results show that the proposed FUFP-tree deletion algorithm based on pre-large itemsets could achieve a good performance for handling the deletion of records.

The remainder of this paper is organized as follows. Related works are reviewed in Section 2. The proposed Pre-FUFP deletion algorithm for deleted records is described in Section 3. An example to illustrate the proposed algorithm is given in Section 4. Experimental results for showing the performance of the proposed algorithm are provided in Section 5. Conclusions are finally given in Section 6.

2 Review of Related Works

2.1 The FUFP-Tree Structure

The FUFP-tree structure is the same as the FP-tree structure [7] except that the links between parent nodes and their child nodes are bi-directional and the items are not necessarily placed in the order of frequencies. Bi-directional linking will help fasten the process of item deletion in the maintenance process. Besides, the FUFP-tree structure has only a very small derivation from the FP-tree structure.

An FUFP tree must be built in advance from the original database before new transactions come. The counts of the sorted frequent items are also kept in the Header_Table. When new transactions are added, the FUFP-tree maintenance algorithm will process them to maintain the FUFP tree. It first partitions items into four parts according to whether they are large or small in the original database and in

the new transactions. Each part is then processed in its own way. The Header_Table and the FUFP-tree are correspondingly updated whenever necessary.

In the process for updating the FUFP tree, item deletion is done before item insertion. When an originally large item becomes small, it is directly removed from the FUFP tree and its parent and child nodes are then linked together. On the contrary, when an originally small item becomes large, it is added to the end of the Header_Table and then inserted into the leaf nodes of the FUFP tree. It is reasonable to insert the item at the end of the Headrer_Table since when an originally small item becomes large due to the new transactions, its updated support is usually only a little larger than the minimum support. The FUFP tree can thus be least updated in this way, and the performance of the FUFP-tree maintenance algorithm can be greatly improved. The entire FUFP tree can then be re-constructed in a batch way when a sufficiently large number of transactions have been inserted.

Besides, many mining methods for finding association rules based on the FP-tree structure have also been proposed [4][10][13][16], and some related researches are still in progress.

2.2 The Concept of Pre-large Itemsets

A pre-large itemset is not truly large, but may be large with a high probability in the future. Two support thresholds, a lower support threshold and an upper support threshold, are used to realize this concept. The upper support threshold is the same as that used in the conventional mining algorithms. The support ratio of an itemset must be larger than the upper support threshold in order to be considered large. On the other hand, the lower support threshold defines the lowest support ratio for an itemset to be treated as pre-large. An itemset with its support ratio below the lower threshold is thought of as a small itemset. Pre-large itemsets act like buffers and are used to reduce the movements of itemsets directly from large to small and vice-versa.

Considering an original database and some records to be deleted by the two support thresholds, itemsets may fall into one of the following nine cases illustrated in Figure 1.

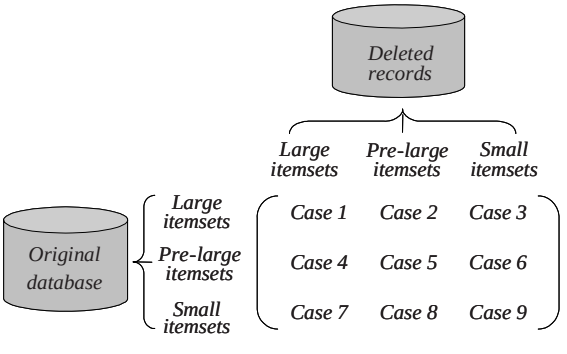

Fig. 1. Nine cases arising from and the original database and the deleted records

Cases 2, 3, 4, 7 and 8 above will not affect the final association rules. Case 1 may remove some existing association rules, and cases 5, 6 and 9 may add some new association rules. If we retain all large and pre-large itemsets with their counts after each pass, then cases 1, 5 and 6 can be handled easily. Also, in the maintenance phase, the ratio of deleted records to old transactions is usually very small. This is more apparent when the database is growing larger. It has been formally shown that an itemset in case 9 cannot possibly be large for the entire updated database as long as the number of transactions is smaller than the number f shown below [8]:

$$f = \left\lfloor \frac{(S_u - S_l)d}{S_u} \right\rfloor,$$

where f is the safety number of deleted records, S_u is the upper threshold, S_l is the lower threshold, and d is the number of original transactions.

3 The Proposed Deletion Algorithm

An FUFP tree must be built in advance from the initially original database before the records are deleted from the original databases. Its initial construction is similar to that of an FP tree. The database is first scanned to find the items with their supports larger than a predefined minimum support, which called large items. Next, the large items are sorted in descending frequency. At last, the database is scanned again to construct an FUFP tree according to the sorted order of large items. The construction process is executed tuple by tuple, from the first transaction to the last one. After all transactions are processed, an FUFP tree is completely constructed. Besides, a variable c is used to record the number of deleted records since the last re-scan of the original database with d transactions. The details of the proposed algorithm are described below.

The Pre-FUFP deletion algorithm:

INPUT: An old database consisting of (d-c) transactions, its corresponding Header_Table storing the frequent items initially in descending order, its corresponding FUFP tree, a lower support threshold S_l, an upper support threshold S_u, its corresponding pre-large table storing the set of pre-large items from the original database, and a set of t deleted records.

OUTPUT: A new FUFP tree after record deletion by using the Pre-FUFP deletion algorithm.

STEP 1: Calculate the safety number f of deleted records according to the following formula [8].

STEP 2: Scan the deleted records to get the items and their counts.

STEP 3: Divide the items in the deleted records into three parts according to whether they are large, pre-large or small in the original database.

STEP 4: For each item I from STEP 3, which is large in the original database (appearing in the Header_Table), do the following substeps (Cases 1, 2 and 3):

Substep 4-1: Set the new count $S^U(I)$ of I in the entire updated database as:

$$S^U(I) = S^D(I) - S^T(I),$$

where $S^D(I)$ is the count of I in the Header_Table (original database) and $S^T(I)$ is the count of I in the deleted records.

Substep 4-2: If $S^U(I)/(d\text{-}c\text{-}t) \geq S_u$, update the count of I in the Header_Table as $S^U(I)$, and put I in the set of *Reduced_Items*, which will be further processed to update the FUFP tree in STEP 5;
Otherwise, if $S_u \geq S^U(I)/(d\text{-}c\text{-}t) \geq S_l$, remove I from the Header_Table, connect each parent node of I directly to its corresponding child node in the FUFP tree, set $S^D(I) = S^U(I)$, and keep I with $S^D(I)$ in the pre-large table;
Otherwise, item I is small after the database is updated; remove I from the Header_Table and connect each parent node of I directly to its corresponding child node in the FUFP tree.

STEP 5: For each deleted record with an item J existing in the *Reduced_Items*, substract 1 from the count of J node at the corresponding branch of the FUFP tree.

STEP 6: For each item I from STEP 3 which is pre-large in the original database, do the following substeps (Cases 4, 5 and 6):

Substep 6-1: Set the new count $S^D(I)$ of I in the entire updated database as:

$$S^U(I) = S^D(I) - S^T(I).$$

Substep 6-2: If $S^U(I)/(d\text{-}c\text{-}t) \geq S_u$, item I will be large after the database is updated; put I in the set of *Branch_Items*, which will be further processed to update the FUFP tree in STEP 9;
Otherwise, if $S_u \geq S^U(I)/(d\text{-}c\text{-}t) \geq S_l$, set $S^D(I) = S^U(I)$ and keep I with the new $S^D(I)$ in the pre-large table;
Otherwise, remove item I from the pre-large table.

STEP 7: For each item I from STEP 3 which is neither large nor pre-large in the original database but large or pre-large in the new transactions (Cases 7 and 8), put I in the set of *Rescan_Items*, which is used when rescanning the database in STEP 8 is necessary.

STEP 8: If $t+c \leq f$ or the set of *Rescan_Items* is null, then do nothing;
Otherwise, do the following substeps for each item I in the set of *Rescan_Items*:

Substep 8-1: Rescan the original database to decide the original count $S^D(I)$ of I.

Substep 8-2: Set the new count $S^U(I)$ of I in the entire updated database as:

$$S^U(I) = S^D(I) - S^T(I).$$

Substep 8-3: If $S^U(I)/(d\text{-}c\text{-}t) \geq S_u$, item I will become large after the database is updated, put I in the set of *Branch_Items*;
Otherwise, if $S_u \geq S^U(I)/(d\text{-}c\text{-}t) \geq S_l$, set $S^D(I) = S^U(I)$ and keep I with $S^D(I)$ in the pre-large table;
Otherwise, neglect I.

STEP 9: Insert the items in the *Branch_Items* to the end of the Header_Table according to the descending order of their updated counts.

STEP 10: For each transaction in the updated database with an item J existing in *Branch_Items*, if J has existed at its corresponding branch of the FUFP tree

for the transaction, add 1 to the count of node *J*; otherwise, insert *J* at the end of its corresponding branch and set its count as 1.

STEP 11: If $t+c > f$, then set $d = d-t-c$ and set $c = 0$; otherwise, set $c = t+c$.

In STEP 5, a corresponding branch is the branch generated from the large items in a transaction and corresponding to the order of items appearing in the Header_Table. After STEP 11, the final updated FUFP tree by using the Pre-FUFP deletion algorithm to process deleted records is constructed. The records can then be deleted from the original database. Based on the FUFP tree, the desired association rules can then be found by the FP-Growth mining approach as proposed in [7].

4 An Example

In this session, an example is given to illustrate the proposed Pre-FUFP deletion algorithm for maintaining an FUFP tree when records are deleted. Table 1 shows a database to be used in the example. It contains 10 transactions and 9 items, denoted *a* to *i*.

Table 1. The original database in the example

Old database	
TID	Items
1	*a, c, d, f, h*
2	*a, h*
3	*b, c, d, e, h*
4	*c, d, f, h*
5	*a, b, c, d, g*
6	*c, d, e, i*
7	*b, e, g, f, h*
8	*a, b, c, d, f, g*
9	*a, b, f*
10	*a, c, e, f, i*

Assume the lower support threshold S_l is set at 30% and the upper one S_u at 60%. For the given database, the large 1-itemsets are *a*, *c*, *d* and *f*, from which the Header_Table can be constructed. The FUFP tree are then formed from the database and the Header_Table, with the results shown in Figure 2. Besides, the sets of pre-large items for the given database are shown in Table 2.

Assume the last four records (with TID 7 to 10) are deleted from the original database. The proposed Pre-FUFP maintenance algorithm proceeds as follows. The variable *c* is initially set at 0. The safety number *f* for deleted records is calculated as:

$$f = \left\lfloor \frac{(S_u - S_l)d}{S_u} \right\rfloor = \left\lfloor \frac{(0.6-0.3)10}{0.6} \right\rfloor = 5.$$

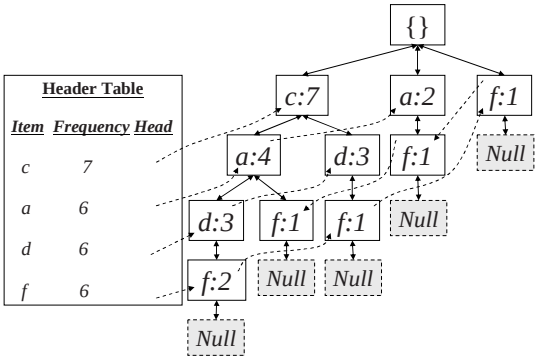

Fig. 2. TThe Header_Table and the FUFP tree constructed

Table 2. The pre-large itemset for the original database

Pre-large itemset in the original database	
Items	Count
b	5
e	4
g	3
h	5

The four deleted records are first scanned to get the items and their counts. All the items *a* to *i* of the deleted records are divided into three parts, {*a*}{*c*}{*d*}{*f*}, {*b*}{*e*}{*g*}{*h*} and {*i*} according to whether they are large (appearing in the Header_Table), pre-large (appearing in the pre-large table) or small in the original database. Each set is then processed according to the proposed algorithm. The final results after STEP 10 are shown in Figure 3.

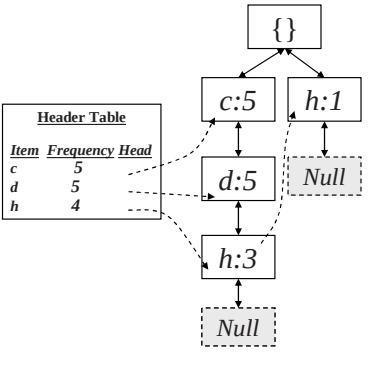

Fig. 3. The Header_Table and the FUFP tree after STEP 10

Since t (= 4) + c (= 0) < f (= 5), set c = t+c = 4+0 =4. Note that the final value of c is 4 in this example and f - c = 1. This means that one more record can be deleted without rescanning the original database for Case 9. Based on the FUFP tree shown in Figure 3, the desired large itemsets can then be found by the FP-Growth mining approach as proposed in [7].

5 Experimental Results

Experiments were made to compare the performance of the batch FP-tree construction algorithm, the FUFP-tree deletion algorithm and the Pre-FUFP deletion algorithm for record deletion. The experiments were performed in C++ on an Intel x86 PC with a 3.0G Hz processor and 512 MB main memory and running the Microsoft Windows XP operating system. A real dataset called BMS-POS [17] were used in the experiments. This dataset was also used in the KDDCUP 2000 competition. The BMS-POS dataset contained several years of point-of-sale data from a large electronics retailer. Each transaction in this dataset consisted of all the product categories purchased by a customer at one time. There were 515,597 transactions with 1657 items in the dataset. The maximal length of a transaction was 164 and the average length of the transactions was 6.5.

The transactions in the BMS-POS database were first used to construct an initial FP-tree. The minimum threshold was set at 1% to 5% for the three algorithms, with 1% increment each time. 2,000 transactions were then deleted from the database. For the Pre-FUFP deletion algorithm, the upper minimum support threshold was set at 1% to 5% (1% increment each time) and the lower minimum support threshold was set at 0.5% to 2.5% (0.5% increment each time). The execution times and the numbers of nodes obtained from the three algorithms were compared. Figure 4 shows the execution times of the three algorithms for different threshold values.

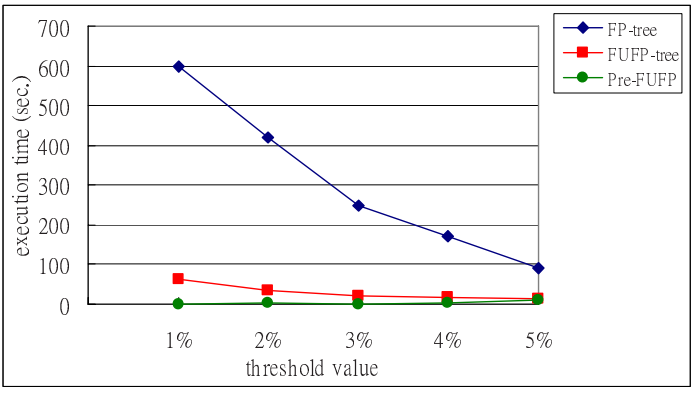

Fig. 4. The comparison of the execution times for different threshold values

It can be observed from Figure 4 that the proposed Pre-FUFP deletion algorithm ran faster than the other two. Note that the FUFP-tree deletion algorithm and the Pre-FUFP deletion algorithm may generate a less concise tree than the FP-tree

construction algorithm since the latter completely follows the sorted frequent items to build the tree. As mentioned above, when an originally small item becomes large due to deleted records, its updated support is usually only a little larger than the minimum support. It is thus reasonable to put a new large item at the end of the Header_Table. The difference between the FP-tree and the FUFP-tree structures will thus not be significant. For showing this effect, the comparison of the numbers of nodes for the three algorithms is given in Figure 5. It can be seen that the three algorithms generated nearly the same sizes of trees. The effectiveness of the Pre-FUFP deletion algorithm is thus acceptable.

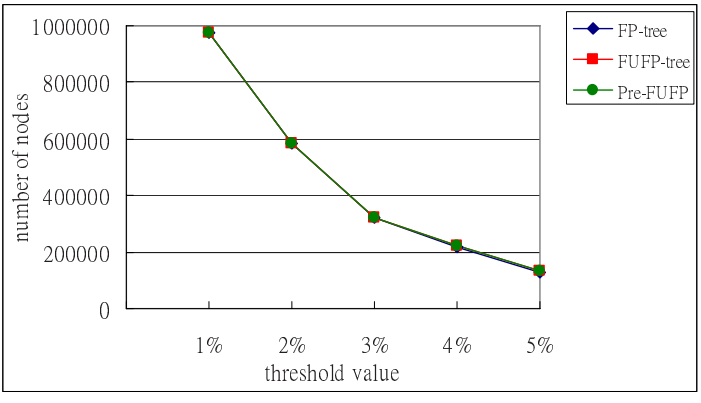

Fig. 5. The comparison of the numbers of nodes for different threshold values

6 Conclusion

In this paper, we have proposed the Pre-FUFP deletion algorithm for record deletion based on the concept of pre-large itemsets. The FUFP-tree structure is used to efficiently and effectively handle deletion of records in data mining. Using two user-specified upper and lower support thresholds, the pre-large itemsets act as a gap to avoid small itemsets becoming large in the updated database when transactions are deleted. The proposed Pre-FUFP deletion algorithm processes deleted records to maintain the FUFP tree. It first partitions items of deleted records into three parts according to whether they are large, pre-large or small in the original database. Each part is then processed in its own way. The Header_Table and the FUFP-tree are correspondingly updated whenever necessary.

Experimental results also show that the proposed Pre-FUFP deletion algorithm runs faster than the batch FP-tree and the FUFP-tree construction algorithm for handling deleted records and generates nearly the same tree structure as them. The proposed approach can thus achieve a good trade-off between execution time and tree complexity.

Acknowledgments. This research was supported by the National Science Council of the Republic of China under contract NSC 94-2213-E-390-005.

References

1. Agrawal, R., Imielinksi, T., Swami, A.: Mining association rules between sets of items in large database. In: The ACM SIGMOD Conference, pp. 207–216 (1993)
2. Agrawal, R., Srikant, R.: Fast algorithm for mining association rules. In: The International Conference on Very Large Data Bases, pp. 487–499 (1994)
3. Agrawal, R., Srikant, R., Vu, Q.: Mining association rules with item constraints. In: The Third International Conference on Knowledge Discovery in Databases and Data Mining, pp. 67–73 (1997)
4. Ezeife, C.I.: Mining Incremental association rules with generalized FP-tree. In: Proceedings of the 15th Conference of the Canadian Society for Computational Studies of Intelligence on Advances in Artificial Intelligence, pp. 147–160 (2002)
5. Fukuda, T., Morimoto, Y., Morishita, S., Tokuyama, T.: Mining optimized association rules for numeric attributes. In: The ACM SIGACT-SIGMOD-SIGART Symposium on Principles of Database Systems, pp. 182–191 (1996)
6. Han, J., Fu, Y.: Discovery of multiple-level association rules from large database. In: The Twenty-first International Conference on Very Large Data Bases, pp. 420–431 (1995)
7. Han, J., Pei, J., Yin, Y.: Mining frequent patterns without candidate generation. In: The 2000 ACM SIGMOD International Conference on Management of Data, pp. 1–12 (2000)
8. Hong, T.P., Wang, C.Y.: Maintenance of association rules using pre-large itemsets. In: Ma, Z. (ed.) Intelligent Databases: Technologies and Applications, pp. 44–60. Idea Group Inc (2006)
9. Hong, T.P., Lin, J.W., Wu, Y.L.: A fast updated frequent pattern tree. In: The 2006 IEEE International Conference on Systems, Man, and Cybernetics, pp. 2167–2172 (2006)
10. Koh, J.L., Shieh, S.F.: An efficient approach for maintaining association rules based on adjusting FP-tree structures. In: The Ninth International Conference on Database Systems for Advanced Applications, pp. 417–424 (2004)
11. Mannila, H., Toivonen, H., Verkamo, A.I.: Efficient algorithm for discovering association rules. In: The AAAI Workshop on Knowledge Discovery in Databases, pp. 181–192 (1994)
12. Park, J.S., Chen, M.S., Yu, P.S.: Using a hash-based method with transaction trimming for mining association rules. IEEE Transactions on Knowledge and Data Engineering, 812–825 (1997)
13. Qiu, Y., Lan, Y.J., Xie, Q.S.: An improved algorithm of mining from FP- tree. In: Proceedings of the Third International Conference on Machine Learning and Cybernetics, pp. 26–29 (2004)
14. Srikant, R., Agrawal, R.: Mining generalized association rules. In: The Twenty-first International Conference on Very Large Data Bases, pp. 407–419 (1995)
15. Srikant, R., Agrawal, R.: Mining quantitative association rules in large relational tables. In: The 1996 ACM SIGMOD International Conference on Management of Data, pp. 1–12 (1996)
16. Zaiane, O.R., Mohammed, E.H.: COFI-tree mining: A new approach to pattern growth with reduced candidacy generation. In: IEEE International Conference on Data Mining (2003)
17. Zheng, Z., Kohavi, R., Mason, L.: Real world performance of association rule algorithms. In: The International Conference on Knowledge Discovery and Data Mining, pp. 401–406 (2001)

Solving a Committee Formation and Scheduling Problem by Frequent Itemset Mining

Chienwen Wu

National Taipei University of Technology, Taipei 10643, Taiwan, R.O.C.

Abstract. Selecting faculty members to form a mission committee and simultaneously scheduling the corresponding committee meetings is a tough decision problem frequently encountered in every academic department. In this paper, we present a formal model of the problem. We also present an approach showing that, with simple database construction, the problem can be transformed into a constrained itemset mining problem, which is an important branch of frequent itemset mining. Thus, the problem can be exactly solved by techniques for constrained itemset mining. For high efficiency, we provide a method to convert some problem constraint into an anti-monotone constraint, which can be easily embedded into the framework of frequent itemset mining and is considered very effective for search space pruning. Experiments were performed and the results show that our approach offers very high performance.

1 Introduction

Selecting faculty members to form a mission committee and simultaneously scheduling the corresponding committee meetings is a tough decision problem frequently encountered in every academic department. For example, in my country, owing to the flexible entrance education policy, the government requires every academic department to provide multiple entrance examinations. Each entrance examination requires an entrance examination committee. Consequently, every academic department has to form several entrance examination committees. In addition, the department may have to form many other mission committees, such as the curriculum development committee, the faculty search committee, the budget auditing committee, and so on. It is estimated that the academic department has to form at least 23 different committees every year. Because of the frequentness and importance, the problem deserves serious attention.

To best realize the problem, we conduct interviews with the department staff and study the relevant university regulations. We find that the mission committees to be formed need to satisfy the following general constraints.

(1) The committee should contain a given number of faculty members in the department. For example, according to the student recruitment rules of the department, each entrance examination committee should contain five faculty members. The faculty search committee should contain three faculty members.

H.G. Okuno and M. Ali (Eds.): IEA/AIE 2007, LNAI 4570, pp. 685–695, 2007.

(2) The committee should hold at least a given number of meetings before the mission deadline. For example, the graduate entrance examination committee is required to hold five meetings, including the criteria setting meeting, the qualification evaluation meeting, the written examination meeting, the oral examination meeting, and the final ranking meeting.

(3) The committee meetings should be scheduled in the way that every committee member is available for every meeting. This is to ensure that every committee member can attend every meeting and the mission can be best accomplished. To meet this constraint, the availability schedule of every faculty member is collected. The availability schedules are collected by emails.

(4) The committee should maintain a harmonious atmosphere. For this aim, the committee should not include any two faculty members that are incompatible with each other. This is to prevent any possible conflicts that might jeopardize the mission. To meet this constraint, a list of incompatible pairs of faculty members is prepared in advance by the department staff.

(5) Faculty members are usually partitioned into groups according to their expertise. The committee should include at least a given number of faculty members from each group. For example, in our department, the entrance examination committee needs at least two committee members with manufacturing expertise and at least one committee member with information management expertise.

In this paper, we consider the problem of selecting faculty members to form a mission committee and scheduling the corresponding committee meetings so that the above constraints can be satisfied. The problem is called the committee formation and scheduling problem, or the **CFS** problem. To the best of our knowledge, the **CFS** problem has never been treated in the literature. By treating the faculty members as resources and the meetings as tasks, the **CFS** problem may be considered as a special type of the traditional resource-constrained project scheduling problem [1] with additional constraints that all the resources have to be allocated before the project begins and all the allocated resources have to get involved in every task of the project. However, this type of resource-constrained project scheduling problems bas never been considered.

In this paper, we present a formal model of the **CFS** problem. In addition, we provide an exact approach for the problem by applying frequent itemset mining [1]-[5]. Frequent itemset mining was originally proposed by Agrawal et. al [2]. It aims at discovering subsets of items that frequently occur together in a large database. We show that, with simple database construction, the **CFS** problem can be transformed into a constrained itemset mining problem [6,7], which is an important branch of frequent itemset mining. Thus, the problem can be solved by techniques for constrained itemset mining. For high efficiency, we provide a method to convert some problem constraint into an anti-monotone constraint, which can be easily embedded into the framework of frequent itemset mining and are considered very effective for search space pruning. Experiments were performed and the results show that our approach offers very high performance.

The rest of the paper is organized as follows. Section 2 presents a formal model of the problem. Section 3 introduces frequent itemset mining and con-

strained itemset mining. In Section 4, we develop a solution approach based on constrained itemset mining. Experimental results are presented in Section 5. Conclusions are given in Section 6.

2 Problem Model

Let $F = \{f_1, f_2, \ldots, f_n\}$ be a set of n faculty members in an academic department. Let $T = \{t_1, t_2, \ldots, t_m\}$ be a set of m time slots allowed to complete the mission and, for all $1 \leq i, j \leq m$, t_i happens before t_j if $i < j$. Let A: $F \rightarrow 2^T$ be a function such that $A(f_i) \subseteq T$ is the set of time slots at which the faculty member f_i is available. $A(f_i)$ can be considered as the availability schedule of the faculty member f_i.

Let $G_{inc} = (F, E)$ be an undirected graph representing the incompatibility relation between the faculty members, where $E \subseteq F \times F$. There is an undirected edge $\{f_i, f_j\}$ in E if and only if the two faculty members f_i and f_j are not compatible. G_{inc} is also called the incompatibility graph.

Let $P = \{P_1, P_2, \ldots, P_l\}$ be a partition of P, i.e., for $1 \leq i < j \leq l$, $P_i \cap P_j = \emptyset$ and $\bigcup_{1 \leq i \leq l} P_i = F$. Faculty members in the same group have the same expertise.

Let k be the number of faulty members required to form a mission committee. Let r be the minimum number of meetings required for the committee to complete the mission. Let $p = (p_1, p_2, \ldots, p_l)$ be a list of l nonnegative integers such that $p_i \leq |P_i|$ for $1 \leq i \leq l$ and $\sum_{1 \leq i \leq l} p_i \leq k$. p_i is the minimum number of faculty members in P_i required to be included in the mission committee.

Let X be a subset of F. It is easy to see that $\bigcap_{f_i \in X} A(f_i)$ contains all the time slots at which the faculty members in X are all available.

We say that X is a feasible committee if the following constraints are satisfied.

c_1: $|X| = k$.
c_2: $|\bigcap_{f_i \in X} A(f_i)| \geq r$.
c_3: For all $\{f_i, f_j\} \subseteq X$, $\{f_i, f_j\} \notin E$. That is, there is no 2-subset of X appearing in E.
c_4: $|X \cap P_i| \geq p_i$ for all $1 \leq i \leq l$.

Note that, for any feasible committee X, $\bigcap_{f_i \in X} A(f_i)$ contains all the time slots that can be scheduled for committee meetings. A pair $(X, \bigcap_{f_i \in X} A(f_i))$ is called a feasible solution if X is a feasible committee. The goal is to find all the feasible solutions. Each **CFS** problem instance is represented by $<F, T, A, G_{inc}, P, k, r, p>$.

Example 1: Consider the **CFS** problem instance $<F, T, A, G_{inc}, P, k, r, p>$, where $F = \{f_1, f_2, f_3, f_4, f_5, f_6\}$, $T = \{t_1, t_2, t_3, t_4, t_5, t_6, t_7\}$,
$A(f_1) = \{t_1, t_2, t_3, t_6\}$, $A(f_2) = \{t_1, t_2, t_3, t_4, t_5, t_7\}$,
$A(f_3) = \{t_1, t_2, t_3, t_4, t_5\}$, $A(f_4) = \{t_3, t_4, t_5, t_6, t_7\}$,

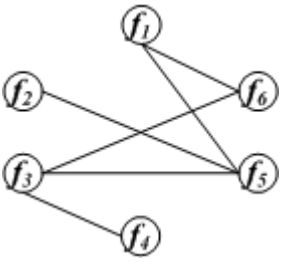

Fig. 1. The incompatibility graph G_{inc}

$A(f_5) = \{t_1, t_4, t_5, t_6, t_7\}$, $A(f_6) = \{t_2, t_4, t_5, t_6, t_7\}$,
$P = (\{f_1, f_2, f_5\}, \{f_3, f_4, f_6\})$, $k = 3$, $r = 3$, $p = (1, 2)$,
and G_{inc} is as shown in Figure 1.

It is easy to see that $\{f_2, f_4, f_6\}$ is a feasible committee because $|\{f_2, f_4, f_6\}| = 3 = k$, $|A(f_2) \cap A(f_4) \cap A(f_6)| = |t_4, t_5, t_7| = 3 \geq r$, $|\{f_2, f_4, f_6\} \cap P_1| = |\{f_2\}| = 1 \geq p_1$, $|\{f_2, f_4, f_6\} \cap P_2| = |\{f_4, f_6\}| = 2 \geq p_2$, and there is no 2-subset of $\{f_2, f_4, f_6\}$ appearing in E. Similarly, $\{f_4, f_5, f_6\}$ is a feasible committee. $\{f_2, f_3, f_4\}$ is not a feasible committee because $\{f_3, f_4\} \in E$. $\{f_1, f_2, f_3\}$ is not a feasible committee because$|\{f_1, f_2, f_3\} \cap P_2| = |\{f_3\}| = 1 < p_2 = 2$.

$(\{f_2, f_4, f_6\}, \{t_4, t_5, t_7\})$ is a feasible solution because $\{f_2, f_4, f_6\}$ is a feasible committee and $\{t_4, t_5, t_7\} = A(f_2) \cap A(f_4) \cap A(f_6)$. Similarly, $(\{f_4, f_5, f_6\}, \{t_4, t_5, t_6, t_7\})$ is a feasible solution.

3 Frequent Itemset Mining and Constrained Itemset Mining

Our approach to the **CFS** problem is based upon constrained itemset mining, which is an important branch of frequent itemset mining. Before describing our approach, we introduce frequent itemset mining and constrained itemset mining.

3.1 Frequent Itemset Mining

Frequent itemset mining was initially proposed by Agrawal et. al [2]. The aim of frequent itemset mining is to discover subsets of items that frequently occur together in a large database. The frequent itemsets reveal the associations among items and are useful in many business applications [2].

The frequent itemset mining problem is formally described as follows [5]. Let $I = \{i_1, i_2, \ldots, i_n\}$ be a set of items. An itemset is a nonempty subset of I. A transaction is a tuple $<tid, X>$, where tid is a transaction identifier and X is an itemset. A transaction database DB is a set of transactions. We say that an itemset X is contained in transaction $<tid, Y>$ if $X \subseteq Y$. Given a transaction database DB, the support of an itemset X, denoted as $sup(X)$, is the number of transactions in DB which contain X. We let min_sup be the minimum support

specified by the decision maker. We say that X is a frequent itemset in DB if $sup(X) \geq min\_sup$. The $sup(X) \geq min\_sup$ constraint is referred to as the support constraint. The goal is to find all the frequent itemsets.

Many efficient algorithms [2]-[5] for frequent itemset mining have been reported. One of the most influential algorithms for frequent itemset mining is the Apriori algorithm [2].The Apriori algorithm employs a bottom-up, breadth-first search strategy to search through all the possible itemsets and uses a pruning strategy based on the Apriori property, which states that if an itemset is infrequent, all of its supersets are infrequent. The Apriori algorithm is shown to be very effective in reducing the search space. Other examples of successful frequent itemset mining algorithms include FP-growth [3] and Mafia [4].

3.2 Constrained Itemset Mining

Constrained itemset mining [6,7] is a generalization of frequent itemset mining. It allows the user to specify the focus of mining as constraints and aims at mining all the itemsets that satisfy not only the support constraint but also the user-specified constraints. Constrained itemset mining arises from the observation that frequent itemset mining often produces an excessive number of frequent itemsets, many of which are either irrelevant to the application or uninteresting to the user. Typically, the user can utilize his knowledge of the target application to specify constraints. Constrained itemset mining focuses on utilizing the user-specified constraints to prune the search space and limit the computation to what really interests the users.

Each instance of constrained itemset mining is represented by $<I, DB, min\_sup, C>$, where I, DB and min_sup are defined the same as in frequent itemset mining and C is a set of constraints. We say that X is a constrained frequent itemset if $sup(X) \geq min\_sup$ and X satisfies every constraint in C. The problem is to find all the constrained frequent itemsets. The problem is also called the **CI** problem in this paper.

Most research works on constrained itemset mining focus on analyzing properties of constraints and devise techniques for pushing deep the constraints in the mining process in order to prune the search space as much as possible. Anti-monotone constraints [6] are considered the easiest to use and the most effective for search space pruning. A constraint c is an anti-monotone constraint if, for any $Y \subseteq X$, X satisfying c implies Y satisfying c. A famous anti-monotone constraint is the support constraint in frequent itemset mining. The support constraint is an anti-monotone constraint because any itemset meeting the support constraint implies that all its subsets do. The support constraint is used in each iteration of the Apriori-based algorithm and is reported to be effective for frequent itemset mining in search space pruning in many cases. Obviously, like the support constraint, the anti-monotone constraints can be used in each iteration of the Apriori-based algorithm and provide further pruning of the search space.

Another type of constraints that are widely considered is the monotone constraints [7]. A constraint c is a monotone constraint if, for any $Y \subseteq X$, Y satisfying c implies X satisfying c. Unlike the anti-monotone constraints, the

monotone constraints can not directly used in each iteration of the Apriori algorithm. Research works [7] have suggested the use of monotone constraints in the pre-processing phase or post-processing phase of the mining process. However, the monotone constraints are generally considered less effective than the anti-monotone constraints.

4 Our Approach

In this section, we describe our approach to solve the **CFS** problem. Given any **CFS** problem instance, our approach is to construct a **CI** problem instance such that the solutions of the original **CFS** problem instance can be easily obtained from the solutions of the constructed **CI** problem instance.

Suppose we are given a **CFS** problem instance $a = <F, T, A, G_{inc}, P, k, r, p>$. We construct a **CI** problem instance $b = <F, TDB, r, C>$, where $TDB = \{<t, S> | f \in S \text{ if } t \in A(f) \text{ for all } f \in F\}$ and $C = \{c_1, c_3, c_4\}$. We will show that, for any $X \subseteq F$, X is a solution of the **CFS** instance a if and only if X is a solution of the **CI** instance b. This suggests us a way to solve the **CFS** problem.

Lemma 1. *sup(X)* $= |\bigcap_{f_i \in X} A(f_i)|$.

Proof. $sup(X) = |\{<t, S> \in TDB|\ X \subseteq S\}|$
$= |\{<t, S> \in TDB|\ f \in S \text{ for all } f \in X\}|$
$= |\{<t, S> \in TDB|\ t \in A(f) \text{ for all } f \in X\}|$
$= |\{t \in T|\ t \in A(f) \text{ for all } f \in X\}| = |\bigcap_{f_i \in X} A(f_i)|$.

Theorem 1. *Let* $X \subseteq F$. *X is a solution of the* **CFS** *instance* $a = <F, T, A, G_{inc}, P, k, r, p>$ *if and only if X is a solution of the* **CI** *instance* $b = <F, TDB, r, C>$.

Proof. X is a solution of the **CFS** instance a.
$\Leftrightarrow$ X satisfies c_1, c_2, c_3, c_4 of the **CFS** instance a
$\Leftrightarrow$ $|\bigcap_{f_i \in X} A(f_i)| \geq r|$ and X satisfies c_1, c_3, c_4 of the **CFS** instance a
$\Leftrightarrow$ $sup(X) \geq r$ and X satisfies c_1, c_3, c_4 of the **CI** instance b
$\Leftrightarrow$ X is a solution of the **CI** instance b.

Theorem 1 implies that we can obtain all the solutions of the **CFS** problem instance $a = <F, T, A, G_{inc}, P, k, r, p>$ by finding all the solutions of the **CI** problem instance $b = <F, TDB, r, C>$.

In what follows, we seek to find an efficient way to solve the **CI** instance b. We first perform an analysis on properties of constraints, based on which we devise techniques to push the constraints as deeply as possible inside the mining process.

Constraint c_1 states that we are only interested in itemset of size k. Thus, in the Apriori algorithm, we can stop the computation of itemsets at level k.

Constraint c_3 is an anti-monotone constraint, as shown in Lemma 2, and thus can be applied at each iteration of the Apriori algorithm for effective pruining.

Lemma 2. *c_3 is an anti-monotone constraint.*

Proof. Assume that X satisfies c_3. Hence, for all $\{f_i, f_j\} \subseteq X$, $\{f_i, f_j\} \notin E$. Let Y be any subset of X. Then, for all $\{f_i, f_j\} \subseteq Y$, $\{f_i, f_j\} \subseteq X$ and thus $\{f_i, f_j\} \notin E$. This proves that c_3 is an anti-monotone constraint.

Constraint c_4 is a monotone constraint, as shown in Lemma 3, and can not be directly applied at each iteration of the Apriori algorithms.

Lemma 3. *c_4 is a monotone constraint.*

Proof. Assume that Y satisfies c_4. We have $|Y \cap P_i| \geq p_i$ for all $1 \leq i \leq l$. Let X be any superset of Y. Then, $|X \cap P_i| \geq |Y \cap P_i| \geq p_i$ for all $1 \leq i \leq l$. This proves that c_4 is a monotone constraint.

In order to use the anti-monotone property for effective prunining, we devise a new constraint $c_4^* : (|X| + \sum_{1 \leq i \leq l} max((p_i - |X \cap P_i|), 0)) \leq k$. In the next, we first show that c_4^* can be used to replace c_4 while guaranteeing the completeness of solutions because it does not add or lose any solutions. Theorem 1 and Lemma 4 are provided for this fact. Then, by Lemma 5 and Lemma 6, we show that c_4^* is an anti-monotone constraint. Thus, c_4^* can be applied at each iteration of the Apriori algorithm.

Lemma 4. *Let $X \subseteq F$ and X satisfies c_1. Then, X satisfies c_4^* if and only if X satisfies c_4.*

Proof. X satisfies $c_4^* \Leftrightarrow (|X| + \sum_{1 \leq i \leq l} max((p_i - |X \cap P_i|), 0)) \leq k$
$\Leftrightarrow \sum_{1 \leq i \leq l} max((p_i - |X \cap P_i|), 0)) \leq 0$ (because X satisfies c_1 and thus $|X| = k$)
$\Leftrightarrow$ For all $1 \leq i \leq l$, p_i - $|X \cap P_i| \leq 0$ (because $max(p_i$ -$|X_i|, 0) \leq 0$)
$\Leftrightarrow$ For all $1 \leq i \leq l$, $|X \cap P_i| \geq p_i \Leftrightarrow X$ satisfies c_4.

Theorem 2. *Let $X \subseteq F$. X is a solution of the* **CFS** *instance $<F, T, A, G_{inc}, P, k, r, p>$ if and only if X is a solution of the* **CI** *instance $<F, TDB, r, \{c_1, c_3, c_4^*\}>$*

Proof. Theorem 2 is a direct result of Theorem 1 and Lemma 4.

Lemma 5. *Let $Y \subseteq X$. For any $1 \leq i \leq l$, ($|Y \cap P_i|$ + $max(p_i$ - $|Y \cap P_i|$, 0)) $\leq$ ($|X \cap P_i|$+ $max(p_i$ - ($|X \cap P_i|$, 0)).*

Proof. We consider separately three cases.

Case 1: Assume that $p_i \leq |Y \cap P_i|$. This means that $p_i \leq |Y \cap P_i| \leq |X \cap P_i|$. We then have $(|Y \cap P_i| + max(p_i$ -$|Y \cap P_i|, 0)) = |Y \cap P_i| \leq |X \cap P_i| =$ $(|X \cap P_i| + max(p_i$ -$|X \cap P_i|, 0))$.

Case 2: Assume that $|Y \cap P_i| < p_i < |X \cap P_i|$. Thus, $(|Y \cap P_i| + \max(p_i$ - $|Y \cap P_i|, 0)) = p_i < |X \cap P_i| = (|X \cap P_i| + \max(p_i$ - $|X \cap P_i|, 0))$.

Case 3: Assume that $|X \cap P_i| \leq p_i$. This means that $|Y \cap P_i| \leq |X \cap P_i| \leq p_i$. We then have $(|Y \cap P_i| + \max(p_i - |Y \cap P_i|, 0)) = p_i = (|X \cap P_i| + \max((p_i - |X \cap P_i|, 0))$.

In all the three cases, we have $(|Y \cap P_i| + \max(p_i - |Y \cap P_i|, 0)) \leq (|X \cap P_i| + \max(p_i - |X \cap P_i|, 0))$. This concludes the proof.

Lemma 6. *c_4^* is an anti-monotone constraint.*

Proof. Assume X satisfies c_4^*. Let $Y \subseteq X$. Then, $|Y| + \sum_{1 \leq i \leq l} max((p_i - |Y \cap P_i|), 0)$
$= \sum_{1 \leq i \leq l} |Y \cap P_i| + \sum_{1 \leq i \leq l} max((p_i - |Y \cap P_i|), 0)$ (because P is a partition)
$\leq \sum_{1 \leq i \leq l} |X \cap P_i| + \sum_{1 \leq i \leq l} max((p_i - |X \cap P_i|), 0)$ (because of Lemma 5)
$= |X| + \sum_{1 \leq i \leq l} max((p_i - |X \cap P_i|), 0)$ (because P is a partition)
$\leq k$. (because X satisfies c_4^*) This proves that c_4^* is an anti-monotone constraint.

Based on the above discussions, we present an Apriori-based approach for solving the **CFS** problem. Our approach is shown in Figure 2. We follow the notations and descriptions of the original Apriori algorithm [2]. Our approach is almost the same as the Apriori algorithm with the differences that we consider the constraint c_1 at line 3 and consider c_3 and c_4^* at line 5 of Figure 2.

1. Construct $TDB = \{<t, S> | f \in S$ if $t \in A(f)$ for all $f \in F\}$.
2. $L_1 = \{$large 1-itemsets in $TDB\}$;
3. for (a=2; $(L_{a-1} \neq \emptyset)$&&$(a \leq k)$; a++) do
4. $\quad C_a = apriori Gen\ (L_{a-1})$; // candidate generation
5. $\quad Test\ (C_a, c_3$ && $c_4^*)$; // constraint test
6. $\quad$ for all transactions $< t, S > \in TDB$ do subset(C_a, S); // database scan
7. $\quad L_a = \{X \in C_a |\ X.\text{count} \geq min\_sup\}$;
8. end
9. Answer $= \{(X, \bigcap_{f_i \in X} A(f_i)\ ) | X \in L_a\}$;

Fig. 2. Our approach for the **CFS** problem

Application of our approach to the **CFS** problem is shown in Example 2.

Example 2: Consider again the **CFS** instance in Example 1. The constructed database TDB is shown in Table 1.

After applying our approach, the large itemset L_a and the candidate itemset C_a at iteration a for $1 \leq a \leq k = 3$ are shown below.

$L_1 = \{\{f_1\}, \{f_2\}, \{f_3\}, \{f_4\}, \{f_5\}, \{f_6\}\}$.
$C_2 = \{\{f_1, f_3\}, \{f_1, f_4\}, \{f_2, f_3\}, \{f_2, f_4\}, \{f_2, f_6\}, \{f_4, f_5\}, \{f_4, f_6\}, \{f_5, f_6\}\}$.
$L_2 = \{\{f_1, f_3\}, \{f_2, f_3\}, \{f_2, f_4\}, \{f_2, f_6\}, \{f_4, f_5\}, \{f_4, f_6\}, \{f_5, f_6\}\}$.
$C_3 = \{\{f_2, f_4, f_6\}, \{f_4, f_5, f_6\}\}$. $L_3 = \{\{f_2, f_4, f_6\}, \{f_4, f_5, f_6\}\}$.
The feasible solutions are $\{(\{f_2, f_4, f_6\}, \{t_4, t_5, t_7\}), (\{f_4, f_5, f_6\}, \{t_4, t_5, t_6, t_7\})\}$.

Table 1. The constructed database TDB

time slots	itemset
t_1	$\{f_1, f_2, f_3, f_5\}$
t_2	$\{f_1, f_2, f_3, f_6\}$
t_3	$\{f_1, f_2, f_3, f_4\}$
t_4	$\{f_2, f_3, f_4, f_5, f_6\}$
t_5	$\{f_2, f_3, f_4, f_5, f_6\}$
t_6	$\{f_1, f_4, f_5, f_6\}$
t_7	$\{f_2, f_4, f_5, f_6\}$

5 Experimental Results

In this section, we report our experimental results on the performance of our approach. The results shows that our approach offers very good performance.

The experiment involves a real application of the **CFS** problem in our department. For an entrance examination, the department has to select five out of 22 faculty members to form a committee. The committee has to hold five meetings. A total of 39 possible time slots are available for the committee meetings. The incompatibility relation is specified by the department staff. The faculty members are divided into three groups according to their expertise. The three groups have separately eight, eight and four faculty members. Two (one, two) faculty members from the first (second, three) group are required for the committee.

In order to see the pruning capability, we compare our approaches with two other approaches. All the three approaches transform the given **CFS** problem instance into a **CI** problem instance as previously mentioned. The first approach to compare is called the *direct_FIM* approach. The *direct_FIM* approach does not use any constraint pushing. It directly applies the frequent itemset mining algorithm to the transformed **CI** problem instance to discover all the frequent itemsets, which are committees that satisfy the c_2 constraint. All the discovered committees are then tested by constraints c_1, c_3, and c_4. The *direct_FIM* approach has the advantage of easy implementation because we can use any frequent itemset mining software to implement the approach. The second approach to compare is called the *direct_CIM* approach. Instead of directly applying frequent itemset mining, the *direct_CIM* approach pushes only constraints c_1 and c_3 at each iteration of the Apriori algorithm and discovers all the itemsets that satisfy c_1, c_2 and c_3. The discovered itemsets are then tested for the satisfaction of constraints c_4.

The experiment was performed on a 3.4 GHz PC with 1 GB of memory running Windows XP. All the three approaches were implemented by Microsoft Visual C++.

In Table 2, we show the results for running the *direct_FIM* approach, the *direct_CIM* approach and our approach. The results for each approach include: (i) the number of search nodes in the search tree required by the approach (ii) the number of database scans required by the approach (iii) the number of

Table 2. Experimental results

Approach	Number of Search nodes	Number of database scans	Constraint testing for c_3 and c_4 (or c_4^*)
direct_FIM	3070	12	2793
direct_CIM	1380	5	1695
Ours	551	5	1150

constraint tests for c_3 and c_4(or c_4^*) performed by the approach. Note that, for each approach, the number of search nodes is equal to the number of constraint tests for c_2.

The experiment shows that our approach offers better performance than the *direct_FIM* approach and the *direct_CIM* approach.

6 Conclusions

We have presented in this paper a formal model and a solution approach for a committee formation and scheduling probelm. Our approach is based on constrained itemset mining. The experimental results show that our approach offers very good performance.

Acknowledgements

The author would like to thank the anonymous referees for their helpful comments. This research was supported by the National Science Council of the Republic of China under the grant NSC 94-2213-E-027-030.

References

1. Brucker, P., Drexl, A., Mohring, R., Neumann, K., Pesch, E.: Resource-constrained project scheduling: Notation, classification, models, and methods. EUR. J. OPER. RES. 112, 3–41 (1999)
2. Agrawal, R., Srikant, R.: Fast Algorithms for Mining Association rules. In: Proceedings of the 20th International Conference on Very Large Data Bases, Santiago, Chile, pp. 487–499 (1994)
3. Han, J., Pei, J., Yin, Y., Mao, R.: Mining Frequent Patterns without Candidate Generation: A Frequent-pattern Tree Approach. DATA MIN. KNOWL. DISC. 8, 53–87 (2004)
4. Burdick, D., Calimlim, M., Gehrke, J.: MAFIA: a maximal frequent itemset algorithm for transactional databases. IEEE T. KNOWL. DATA EN. 17, 1490–1504 (2005)
5. Wang, J., Han, J., Lu, Y., Tzvetkov, P.: TFP: An Algorithm for Mining Top-K Frequent Closed Itemsets. IEEE T. KNOWL. DATA EN. 17, 652–664 (2005)

6. Ng, R., Lakshmanan, L., Han, J.: Exploratory mining and pruning optimizations of constrained associations rules. In: Proceedings of the 1998 ACM SIGMOD International Conference on Management of Data, Seattle, Washington, USA, pp. 13–24 (1998)
7. Bonchi, F., Giannotti, F., Mazzanti, A., Pedreschi, D.: ExAnte: Anticipated Data Reduction in Constrained Pattern Mining. LECT. NOTES ARTIF. INT. 2838, 59–70 (2003)

Dual Gradient Descent Algorithm on Two-Layered Feed-Forward Artificial Neural Networks

Bumghi Choi[1], Ju-Hong Lee[1], and Tae-Su Park[2]

[1,2] School of Computer Science and Engineering, Inha University, Incheon, Korea
[1]{neural,juhong}@inha.ac.kr,
[2]taesu@datamining.inha.ac.kr

Abstract. The learning algorithms of multilayered feed-forward networks can be classified into two categories, gradient and non-gradient kinds. The gradient descent algorithms like backpropagation (BP) or its variations are widely used in many application areas because of convenience. However, the most serious problem associated with the BP is local minima problem. We propose an improved gradient descent algorithm intended to weaken the local minima problem without doing any harm to simplicity of the gradient descent method. This algorithm is called dual gradient learning algorithm in which the upper connections (hidden-to-output) and the lower connections (input-to-hidden) separately evaluated and trained. To do so, the target values of hidden layer units are introduced to be used as evaluation criteria of the lower connections. Simulations on some benchmark problems and a real classification task have been performed to demonstrate the validity of the proposed method.

Keywords: Backpropagation, Dual Gradient, Local minima.

1 Introduction

Backpropagation (BP) is well known representative of all gradient descent algorithms, which is widely used technique for supervised neural networks learning in many application areas. It is used to search the feed-forward connectivity weights for a correct mapping of set of training input patterns, in order to minimize an error function that represents the difference between the targeted and obtained outputs.

We concentrate our attention just on a two-layered network such as that illustrated in Fig. 1 with notations used in this paper.

Where $z(2)_i$ is the output value of output layer unit i, $z(1)_j$ is the output value of hidden layer unit j, w_{ij}^2 is the weight from hidden unit j to output unit i, w_{jk}^1 is the weight from input unit k to hidden unit j, and ξ_k is the value of input unit k.

Our usual error measure or cost function is described as

$$E[w] = \frac{1}{2}\sum_{\mu i}\left[\zeta_i^{\mu} - g\left(\sum_j w_{ij}^2 g\left(\sum_k w_{jk}^1 \xi_k^{\mu}\right)\right)\right]^2 \quad (1)$$

Where g is a sigmoid or tangent hyperbolic function, ζ_i^{μ} is the ideal or target value of output unit i for input pattern μ.

H.G. Okuno and M. Ali (Eds.): IEA/AIE 2007, LNAI 4570, pp. 696–704, 2007.

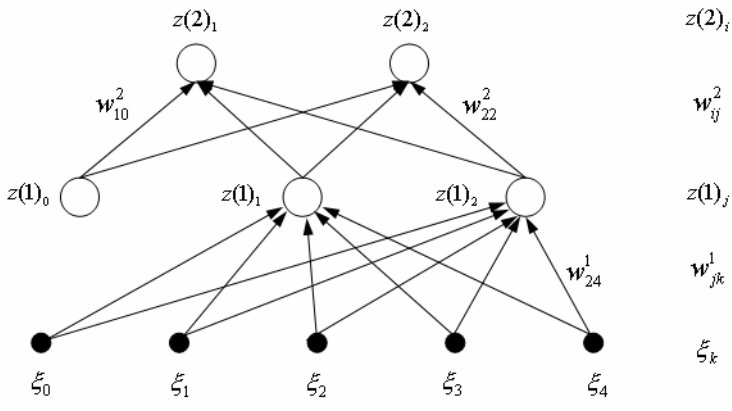

Fig. 1. Two-layered networks and notations

For the upper (hidden-to-output) connections, the gradient-descent rule gives

$$\begin{aligned}\Delta w_{ij}^{2} &= -\eta \frac{\partial E}{\partial w_{ij}^{2}} = \eta \sum_{\mu} \left[\zeta_i^{\mu} - g\left(h(2)_i^{\mu}\right)\right] g'\left(h(2)_i^{\mu}\right) z(1)_j^{\mu} \\ &= \eta \sum_{\mu} \delta(2)_i^{\mu} z(1)_j^{\mu}\end{aligned} \tag{2}$$

with

$$\delta(2)_i^{\mu} = \sum_{i} \left[\zeta_i^{\mu} - z(2)_i^{\mu}\right] g'\left(h(2)_i^{\mu}\right) \tag{3}$$

Where ηis a learning rate ranged from 0 to 1, and $h(2)_i^{\mu}$ is the input value to output unit i for input pattern μ

For the lower (input-to-hidden) connections, the error function is partially differentiated with respect to the w_{jk}

$$\begin{aligned}\Delta w_{jk}^{1} &= -\eta \frac{\partial E}{\partial w_{jk}^{1}} = \eta \sum_{\mu} \frac{\partial E}{\partial z(1)_j^{\mu}} \frac{\partial z(1)_j^{\mu}}{\partial w_{jk}^{1}} \\ &= -\eta \sum_{\mu} \frac{\frac{1}{2}\sum_{i}\left[\zeta_i^{\mu} - g\left(\sum_{j} w_{ij}^{2} z(1)_j^{\mu}\right)\right]^2}{\partial z(1)_j^{\mu}} \frac{g\left(\sum_{k} w_{jk}^{1} \xi_k^{\mu}\right)}{\partial w_{jk}^{1}} \\ &= \eta \sum_{\mu i} \left[\zeta_i^{\mu} - z(2)_i^{\mu}\right] g'\left(h(2)_i^{\mu}\right) w_{ij}^{2} g'\left(h(1)_j^{\mu}\right) \xi_k^{\mu} \\ &= \eta \sum_{\mu} \sum_{i} \delta(2)_i^{\mu} w_{ij}^{2} g'\left(h(1)_j^{\mu}\right) \xi_k^{\mu} \\ &= \eta \sum_{\mu} \delta(1)_j^{\mu} \xi_k^{\mu}\end{aligned} \tag{4}$$

with

$$\delta(1)_j^{\mu} = \sum_i \delta(2)_i^{\mu} w_{ij}^2 g'\left(h(1)_j^{\mu}\right) \tag{5}$$

Where $h(1)_j^{\mu}$ is the input value to hidden unit j for input pattern μ

BP has a great virtue of simplicity on implementation and calculation. Despite of that, there are many problems on BP. The most serious problem of BP is that the learning process can't guarantee to a global minimum, trapping into local minima or saturation points. Techniques from global optimization (GO) have been proposed to the local minima problem of BP. The GO can be classified broadly into two major groups, deterministic and stochastic. Deterministic methods [1]-[5] guarantee convergence to a global optimum only for certain classes of functions [6], and require more auxiliary calculations. Stochastic algorithms [7]-[9], guarantee convergence to global optimum only probabilistically, when the number of searches tends to be almost infinity. Among them, simulated annealing and Genetic algorithms are well known.

A local minimum is a suboptimal equilibrium point at which system error is nonzero and the hidden output matrix is singular [12]. To solve the problem of local minima, the hidden ouptut matrix has to be changed to a non-singular one by using evolutionary algorithms or random perturbation [10]-[11]. However, the random perturbations of the search direction and various kinds of stochastic adjustment to the current set of weights are not effective at enabling a network to escape from local minima and they may make the network fail to converge to a global minimum within a reasonable number of iterations [13]

Our goal is to invent a novel idea to solve the local minima problem partially while maintaining the simplicity of the gradient descent methods. The new algorithm will be called dual gradient, in which the upper connections and the lower connections separately evaluate their error functions. To do so, the target values of hidden units are newly introduced to induce the error function of the lower connections. We will explain the validity of this proposed idea in the next section.

2 Dual Gradient Learning Algorithm

In the present section, a new approach with better performance of the training speed and the ability to weaken the local minima problem will be introduced. It can be differentiated from other approaches as mentioned in that it doesn't use a random perturbation of parameters or the hidden output values. It just adopts a divide-and-conquer strategy in which a whole network is divided into two networks, the upper connections (hidden-to-output) and the lower connections (input-to-hidden), expecting them to more easily escape from local minima than the whole network. Each part is evaluated differently. Evaluating the upper connections is same as BP. But to evaluate in the lower connections, we need the target values of hidden units. The target values of hidden units are the most appropriate values of hidden units to propagate the desired values of the output units with the current weights fixed. The target values of hidden units may be calculated approximately, not accurately.

In the following sub section, we will introduce the algorithm in detail and explain why the proposed algorithm is robust to weaken the local minima problem.

2.1 Weakening the Local Minima Problem Through Separation of Networks

In the proposed algorithm the networks are separated into two parts. In the first part, the upper connections are evaluated and updated with the lower connections fixed. Then, the lower connections are differently evaluated and updated with the upper connections fixed. This process is repeated until the output values are within the allowable error from the ideal values.

If the hidden output matrix is singular, there is a strong possibility of local minima. To avoid this situation, we have to make the hidden units directed to the values at which the hidden output matrix is non-singular, thus output layer units reach the desired values. However, when all weights are updated with the same error function, hidden units are not intended to have any meaningful values. The separation of the lower connection may help the direction of the hidden units aim to deterministically designated values at which a local minima free status is expected.

At this point, the divide-and-conquer strategy clarifies the philosophy of the proposed algorithm. In supervised multilayered feed-forward networks, our goal is to find the fastest way to reach the global minimum of the cost function. At a glance, BP algorithm and its variations in which all weights are updated at the same time seems to do a lot of works at a time. However, too heavy work at a time, instead, may get the work delayed. The divide-and-conquer suggest dividing a heavy work into couple of light works.

In the next sub section, how the target values of hidden units are approximated is explained.

2.2 Approximation of the Target Values of Hidden Units

The success of the dual gradient learning depends on how accurately the target values of hidden units can be derived so that the lower connections can be directed to the target. Here a target value of a hidden unit is intended to mean the value of the hidden unit which makes a selected output has an ideal value as close as possible.

Consider the hidden-output mapping whose inputs are the output values of hidden units, and outputs are the ideal (target) values of output layer. $H = \Psi\{XW^1\}$ and $Y = \Psi\{HW^2\}$. Here what we need is to get a solution matrix of hidden space such that the matrix maps the given weight vector of the upper connections to the target values of output. That is, an inverse mapping from output layer to hidden layer have to be solved. Thus, we get $H = \Psi^{-1}(Y)(W^2)^{-1}$. Since $(W^2)^{-1}$ may not always exist, and $\Psi^{-1}(Y)$ may be out of boundary values of hidden units, we approximate the solution by Newton's method rather than a direct solution. This approximation is described as Fig. 2. The target values of hidden units, γ_j is approximately derived.

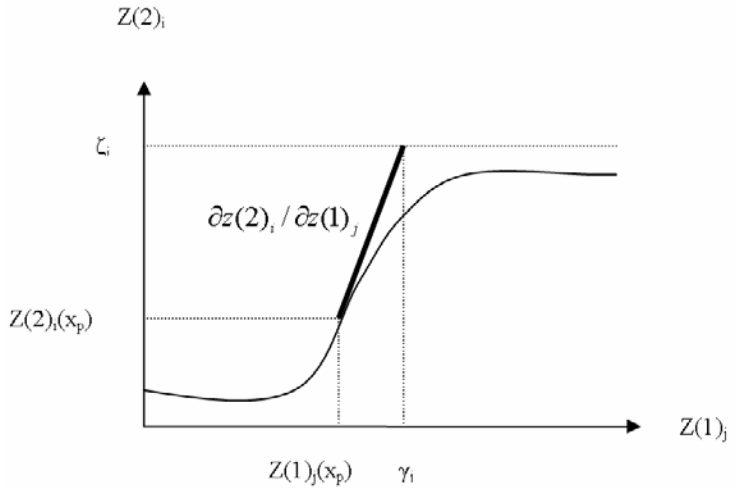

Fig. 2. The approximation of the target values of hidden units (where the x_p is the input value for input pattern p)

The approximation can be made by calculating the errors of hidden units from an output error with partial derivative. While $z(2)_i$ is a multi-variable function, not as only one variable, to derive the target value of a hidden unit $z(1)_j$, the function has to be considered as a one variable function assuming that the other hidden units are constant. In this way, the target value γ_j of $z(1)_j$ can be summed and averaged for all output units i.

We describe this procedure in terms of mathematical formulae as follows. For a single output unit, the error of hidden unit j is

$$\gamma_j - z(1)_j = \frac{\left(\zeta_i - z(2)_i\right)}{\partial z(2)_i / \partial z(1)_j} \tag{6}$$

The target value of hidden unit j is summed and averaged for all output units with total number N

$$\gamma_j = \frac{1}{N}\sum_i \frac{\left(\zeta_i - z(2)_i\right)}{g'(h(2)_i)w_{ij}} + z(1)_j \tag{7}$$

Now the evaluation function for hidden unit j of the lower connections is derived from the target value in (7)

$$E_j[w] = \frac{1}{2}\sum_\mu \left[\gamma_j^\mu - g\left(\sum_k w_{jk}^1 \xi_k^\mu\right)\right]^2 \tag{8}$$

Thus, the updating rule for the lower connections, equation (4) is replaced by the following equation.

$$\begin{aligned}\Delta w^1_{jk} &= -\eta \frac{\partial E_j}{\partial w^1_{jk}} = -\eta \sum_{\mu} \frac{\partial E_j}{\partial z(1)^{\mu}_j} \frac{\partial z(1)^{\mu}_j}{\partial w^1_{jk}} \\ &= -\eta \frac{1}{2} \sum_{\mu} \frac{\left[\gamma^{\mu}_j - z(1)^{\mu}_j\right]^2}{\partial z(1)^{\mu}_j} \frac{g\left(\sum_k w^1_{jk} \xi^{\mu}_k\right)}{\partial w^1_{jk}} \\ &= \eta \sum_{\mu} \left[\gamma^{\mu}_j - z(1)^{\mu}_j\right] g'\left(h(1)^{\mu}_j\right) \xi^{\mu}_k \end{aligned} \tag{9}$$

Thus, the updating rule (4) is replaced by equation (9) for the lower connections. Nothing is changed for the upper connections. This new updating rule calculates new hidden target values every epoch. It can help the training procedure to prevent the hidden output matrix from being stuck to a singular one.

2.3 Procedure of the Dual Gradient Learning Algorithm

The algorithm is summarized as follows.

1. Evaluate and update the upper-connections using equation (1) and (2) in the same way as BP. If converge, stop.
2. For each hidden unit, calculate the error (cost) function using (8).
3. Using (9), update the lower-connections for each hidden unit.
4. Go to 1.

3 Simulations and Evaluation

3.1 Environment of Experiments

In order to verify the performance of the DGTrain (Dual Gradient) method proposed in this paper, experiments have been performed using a computer with an AMD XP 2600+ 2.0 GB CPU and 512 MB Random Access Memory (RAM). Three types of experiments including 1) Synthetic data, 2) XOR Data, and 3) Iris Data are simulated. The Iris data set was obtained from the UCI machine learning database (http://www.ics.uci.edu/~mlearn/databases/). Synthetic data was generated as follows. An input vector X, the number of input units n, and a probability variable α are given, and each input pattern value is set to an arbitrary value between -1 and 1, the number of input patterns is set to 20, and the number of classes is set to 5. The probability variable α is assigned a value equal to or greater than 3.0 depending on the number of input units, so that an overlapping region of classes can be relatively large.

$$d_i = \|X - C_i\| = (\sum_{k=1}^{n} (x_k - \mu_k^i)^2)^{\frac{1}{2}}$$

$$t = \frac{d_j - d_i}{d_j + d_i},\ d_j > d_i,\ 0 \le t \le 1 \tag{10}$$

$$P_\alpha \langle C_i \,|\, X \rangle = \frac{1}{1 + e^{-\alpha t}},\ P_\alpha \langle C_j \,|\, X \rangle = 1 - P_\alpha \langle C_i \,|\, X \rangle$$

Where C_i is the closest class, μ_k^i is the k-th dimensional value of the center μ^i of C_i, and C_j is the next closest class. First, to find the closest class and the next closest class for a given input vector, distances (d) between the input vector and the center of each class are calculated, and a desired class is determined using a given probability.

For three types of experiments as mentioned, each experiment was performed 20 times with random weigh vectors and parameters while the number of hidden units was increased from 2 to 50 (total number of experiments is 500 for each type).

From the results, we compared and evaluated the convergence rates (SE), average total epoch (EP), average learning time (Time) and sum of squared errors (SSE) according to an increase in the number of hidden units, with respect to the DGTrain method and the BP. Also, a time limit of 60 seconds and a convergence error limit of 0.01 are set to all experiments.

3.2 Experimental Results

Summary of the results is given in Table 1. Convergence Rate is the number of experiments that have succeeded in achieving a sum of squared errors below 0.01, and EP is average epoch in successful experiments. Time represents average of the running time. SSE is the average of sum of squared errors in successful experiments. We can see that the proposed method show better performance than BP with respect to the number of convergence and average epoch, running time, sum of squared error.

Table 1. Summary of the experimental results

Problem	Backpropagation Algorithm				DGTrain Algorithm			
	SE	EP	Time	SSE	SE	EP	Time	SSE
Synthetic	144	1228	14122	0.00482	176	379	13554	0.00600
XOR	339	872	1722	0.00957	379	497	691	0.00946
Iris	95	3355	7911	0.00860	136	625	7538	0.00547

A first experimental example was performed to compare the performance of BP and DGTrain method using synthetic data in each case of the number of hidden units from 2 to 50. In the convergence rate, BP gets better results than the proposed method at a small number of hidden units. But, for the proposed method, as the number of hidden unit increases, the number of successful convergences increases. Also, in the

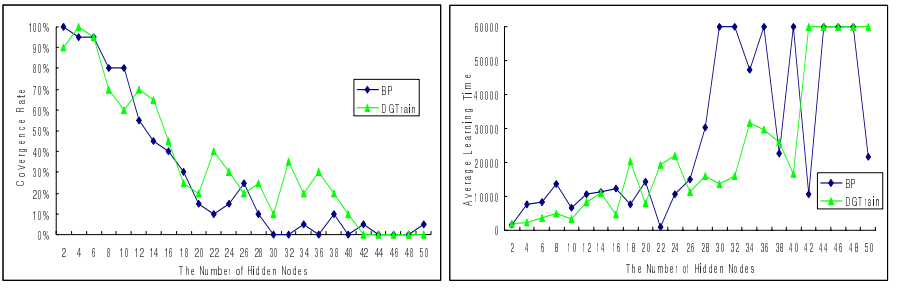

(a) Convergence Rate (b) Running Time

Fig. 3. Experimental results for synthetic data

running time, the proposed method shows better performance than BP regardless of an increase in the number of hidden units.

Iris data is composed of four variables, that is, sepal length, sepal width, petal length, and petal width. In this case, the total number of data samples is 150, and 50 data samples is provided for each class, the classes being set as setosa, versilcolor and vignica, which are three types of iris.

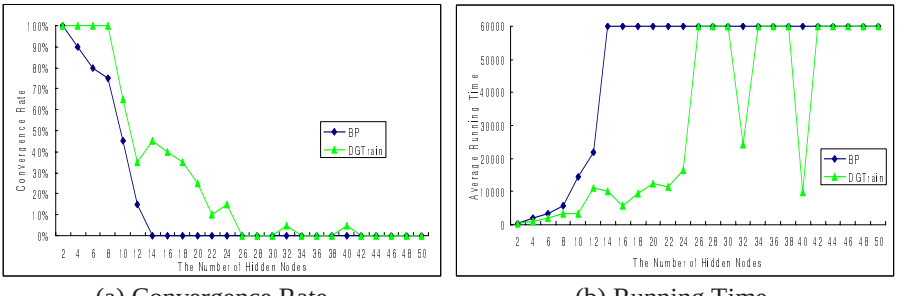

(a) Convergence Rate (b) Running Time

Fig. 4. Experiment results for the Iris Data

Fig. 4 shows the experiment results of two methods for iris data. From this figure, we can see that the proposed method shows higher convergence rate than BP. The BP did not converge with more hidden units than 14. But the proposed method can converge. Also, the running time of the proposed method is much shorter than BP regardless of an increase in the number of hidden nodes.

4 Conclusion

The proposed algorithm combines the deterministic and heuristic approach at the same time. It can't guarantee to converge to a global minimum. But it is comparatively fast, and solves the local minima problem partially. Additional virtue is that the dual gradient algorithm is so simple as to be easily understandable, constructed. The

separation of the networks is a novel idea to simplify the complexity of heavy networks, which is inevitable in the case of very complex problems in which many input patterns need to be trained, thus more hidden units are needed as we have shown in the experiments.

Acknowledgement. This research was supported by the MIC(Ministry of Information and Communication), Korea, under the ITRC(Information Technology Research Center) support program supervised by the IITA(Institute of Information Technology Assessment).

References

1. Cetin 1, B., Barhen, J.: Global descent replaces gradient descent to avoid local minima problem in learning with ANN. In: Proc. of lEEE Conf. on NN, vol. 2, pp. 836–842 (1993)
2. Hont, R., Padalos, P. (eds.): Handbook of Global Optimization. Kluwer, Dordrecht (1995)
3. Plagianakos, P., Magoulas, G.D., Vrahatis, M.: Deterministic non-monotone strategies for the effecive training of multilayer perceptrons. IEEE Trans. on N. Networks 13(6), 1268–1284 (2002)
4. Jones, D., Perttunen, C., Stuckman, B.: Lipschitzian Optimization without the Lipschitz Constant. J. of Optimization Theory and Applications 79, 157–181 (1993)
5. Vrahatis, M., Androulakis, G., Lambrinos, J., Magoulas, G.: A class of gradient unconstrained minimization stepsize. J. of Computational and Applied Mathematics 114, 367–386 (2000)
6. Jordanov, I.N., Rafik, T.A.: Local Minima Free Network Learning. In: Second lEEE International Conference On Intelligent Systems, pp. 34–39 (June 2004)
7. Bilbro, G.: Fast stochastic global optimisation. IEEE Trans. On Systems, Man, and Cybernetics 24, 684–689 (1994)
8. Huyer, W., Neumaier, A.: Global Optimization by Multilevel Coordinate Search. J. of Gl. Optimizalion 14, 331–335 (1999)
9. Tom, A., Vitanen, S.: Topographical Global Optimization Using Pre-Sampled Points. J. of Global Optimization 5, 267–276 (1994)
10. Ng, S.C., Leung, S.H., Luk, A.: A Hybrid Algorithm of Weight Evolution and Generalized Back-propagation for finding Global Minimum. In: Proceedings of IEEE International Joint Conference on Neural Networks (IJCNN'99) (1999)
11. Yu, X.H.: Can backpropagation error surface not have local minima. IEEE Transactions on Neural Networks 3(6), 1019–1021 (1992)
12. Yu, X.H., Chen, G.A.: On the local minima free condition of backpropagation learning. IEEE Transactions on Neural Networks 6(5), 1300–1303 (1995)
13. Wang, C., Principe, J.C.: Training neural networks with additive noise in the desired signal. IEEE Trans. Neural Networks 10(6), 1511–1517 (1999)

A New Hybrid Learning Algorithm for Drifting Environments

Khosrow Kaikhah

Department of Computer Science
Texas State University
kk02@txstate.edu

Abstract. An adaptive algorithm for drifting environments is proposed and tested in simulated environments. Two powerful problem solving technologies namely Neural Networks and Genetic Algorithms are combined to produce intelligent agents that can adapt to changing environments. Online learning enables the intelligent agents to capture the dynamics of changing environments efficiently. The algorithm's efficiency is demonstrated using a mine sweeper application. The results demonstrate that online learning within the evolutionary process is the most significant factor for adaptation and is far superior to evolutionary algorithms alone. The evolution and learning work in a cooperating fashion to produce best results in short time. It is also demonstrated that online learning is self sufficient and can achieve results without any pre-training stage. When mine sweepers are able to learn online, their performance in the drifting environment is significantly improved. Offline learning is observed to increase the average fitness of the whole population.

1 Introduction

Most intelligent agents do not adapt well to the changes in drifting environments. Drifting environments are environments that are dynamic over time. Evolution and learning are the two most fundamental processes of adaptation in drifting environments. The best approach for designing intelligent systems that must operate in real time drifting environments is to adopt technologies such as Artificial Neural Networks (ANNs) and Genetic Algorithms (GAs) that mimic the nature. Neural networks are massively parallel distributed processors that perform data mapping efficiently. Genetic algorithms attempt to apply evolutionary concepts to generalization capabilities of neural networks. In recent times much research has been undertaken to combine these two important and distinct areas (Yao, 1999).

There are different approaches one can take in combining the ANNs with GAs. In the supportive approach, ANNs and GAs are applied at different stages. GAs are commonly used to reduce the dimensionality of data space. In the collaborative approach, GAs and ANNs are integrated into a single system in which population of ANNs is evolved. But designing a hybrid system is not sufficient for the drifting environments. In standard hybrid algorithms, a population of networks is evolved to perform a task, and the best fit network is found. This network is fixed and is used for future instances of the problem.

H.G. Okuno and M. Ali (Eds.): IEA/AIE 2007, LNAI 4570, pp. 705–714, 2007.

Networks evolved this way do not handle dynamic environments very well (Kasabov, 2003).

The evolution of artificial neural networks can be classified according to the goals of evolution. The three basic approaches by which we can combine learning with evolution are: (a) Evolution of weights, (b) Evolution of architectures, and (c) Evolution of learning rules or transfer functions. As evolution of weights, architectures, or learning rules alone do not yield required performance, all three approaches must be combined to design a truly flexible network. This also reduces the human intervention in the network design. By combining evolutionary approaches with online learning, we have developed a hybrid algorithm that can adapt to the changing environments. In our approach, the artificial intelligent agents are equipped with a neural network (brain) which learns in two different stages, offline and online.

In the offline learning stage, we integrate network learning process with evolution. In this stage, learning is used as one of the genetic operators. We use the modified backpropagation (MBP) algorithm with all three operators of GAs on the population. The genetic operators are used only if they are required. In the online learning stage, network learning and evolution are applied at different phases. Online gradient descent method is used for learning and GA operators are used to produce a better population for learning process. Learning and evolution are applied to the entire population. In each stage, GAs are used to evolve the weights and the architecture. Online gradient descent and backpropagation use adaptive step size to evolve the learning rule.

Our algorithm mimics human evolution and development. We have successfully implemented complete evolution and online learning to achieve effective design automation of neural networks with the ability to adapt to the drifting environments. Our experimental results demonstrate the ability of our algorithm to evolve efficient neural networks with simple architectures within a few hundred generations.

2 Hybrid Learning Algorithm for Drifting Environments

Evolution and learning are the most fundamental processes of adaptation. Evolution has an ability to adapt to the internal characteristics or regularities of an environment. This area is well explored with successful results (EPNet by Yao 1999, NEAT by Stanley *et al*. 2002). From an evolutionary point of view, learning guides evolution and allows adaptation to the environmental changes which are too fast for the evolution to track. Evolution can only optimize the performance of the agents for the next generation. But when environments change from one generation to the next, the agents may not perform well in future environments since optimization is performed using the performance in the current environment. By being sensitive to environmental conditions that could not be anticipated by evolution, learning can incorporate them in the agent's behavior (Magoulas *et al*. 2001).

Over the generations, living organisms employ mutations and crossover to produce better offspring. This process of Darwinian principle is effectively used in the existing algorithms for better results. But in real life the environment surrounding the generations is not static, and if the organisms do not adapt to the changes in their lifetime, they will be extinct in a few generations. The organisms not only change from generation to

generation but learn to adapt to the changing surroundings in their lifetime. Lamarckian learning proposes the similar idea that the organisms pass on the learned knowledge, over their lifetime, to the next generations that in turn produce better offspring. For a static environment, we may choose to exclude the lifelong learning since its benefits are limited. However, this is not the case for drifting environments. To survive in dynamic environments, the artificial intelligence agents need to learn in their lifetime.

2.1 Requirements for the Proposed Algorithm

Representation, or encoding, plays an important role in evolution and affects the ease of conversion and details in mapping from genotype to phenotype. Representation influences other factors that affect the GAs and their applicability. Real value encoding is more natural and closely represents a problem space. Often real world problems have variables that are continuous over a domain rather than discrete. Hence, for our algorithm, we require real valued encoding of genotypes for the agents in drifting environments. Our algorithm attempts to combine basic types of evolutions on neural networks. Hence, the representation should be able to allow these combinations of evolution.

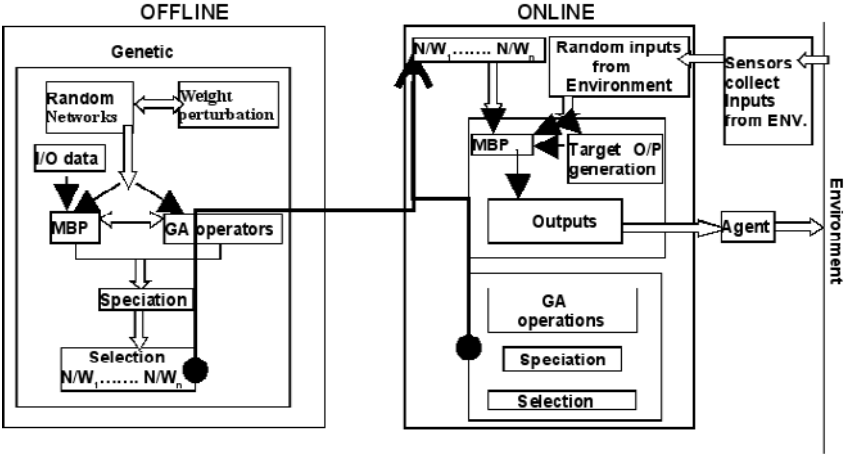

Fig. 1. Frame work of the algorithm

When we use GAs to evolve populations of ANNs, the degree of similarity or differences among the networks is an important criterion. If the population is not diverse, then the problem of crowding arises. Crowding is a problem in GAs where one individual is much more fit than the others. This makes the population concentrate on a small region of population search space. Therefore, spatially distributing the population into species preserves the diversity, thereby providing an opportunity to increase the fitness. Hence, our algorithm requires the population to be divided into several different species based on a numerical measure of the architecture. This speciation into groups mimics natural evolution.

The offline stage begins by generating the population of networks or genomes for future steps. Conceptually, our algorithm does not suggest starting with a large number of nodes and pruning them when necessary. This method seems less efficient and may result in large architectures. This problem is possible even when we have a fixed number of output and input neurons. Therefore, we start with a minimum set of nodes and add nodes when it is necessary. Our algorithm evolves random and dynamic network of neurons. We do not have layers of hidden neurons rather we have individual hidden neurons. As a result, we generate initial random networks with zero or more hidden neurons. The networks are trained using the MBP algorithm. The MBP is designed for the random neural networks with hidden nodes rather than networks with hidden layers. The crossover and mutation operators are applied to the population of networks to produce offspring. The online stage is similar to the way humans apply and update their acquired knowledge in new surroundings and passing it to the next generations for better adaptation. This is the stage where the advantage of our algorithm is observed and tested with agents in a drifting environment. The online stage follows the collaborative approach rather than the supportive approach for hybridization of evolution and learning. The online stage is the combination of two phases that toggle: (a) evolution and (b) learning online.

The learning phase generates networks that can learn continuously, rather than using pre-learned networks. The networks that can learn can adapt more efficiently to the subtleties of the environment. The evolution phase is applied between generations. GAs are used to identify the superior architecture, weight and learning rule to determine a set of best fit networks for the next generation. To preserve the diversity, we divide the population into different species. This process of speciation is similar to the speciation in offline stage. We calculate the average fitness for each species using the age and the performance of networks in the environment. Networks are sorted based on their fitness in each species, and most fit network from each species is added to the new population intact. The rest of the new population is selected from the networks generated using genetic operators and their fitness.

3 Application: Mine Sweeper

Our algorithm attempts to develop intelligent agents which can adapt to a changing environment effectively and more quickly than existing implementations. Since the algorithm is inspired by human behavior and evolution, we need an application that allows us to test and observe all aspects of our algorithm. A mine sweeper application is used to demonstrate the capabilities of our method in adapting to drifting environments. In our application, we use neural networks to control the behavior of the mine sweepers and to make them intelligent. The mine sweepers live in a drifting environment with a few different obstacles and several mines. The positions and shapes of these obstacles change from one generation to the next. The goal of the application is to evolve intelligent mine sweepers to explore as much area as possible, while avoiding the obstacles within a certain time limit.

Mine sweepers are equipped with a number of sensors, which enable them to perceive the obstacles in the world around them and to determine the distance to any

obstacle it may encounter. Equipped with only sensors, the mine sweepers can learn to avoid the obstacles in a few generations, but without guidance they cannot explore the environment efficiently. The environment is divided into a number of equal sized cells. Each cell is equipped with memory to store information about the number of time units a mine sweeper has spent in that cell. This information helps the mine sweepers to evolve the weights, architecture and learning rules of the ANNs to favor the unvisited cells. The end points of the sensors, referred to as feelers, act as antennas for the mine sweepers and retrieve the information stored in the cells.

To corroborate our claim that lifelong learning combined with evolutionary process can boost the intelligence of the agents in a drifting environment, we tested our algorithm on several different scenarios.

3.1 Performance of Only Evolutionary Genetic Algorithms

In this experiment, only genetic algorithms are responsible for the development of the networks and behavior of the mine sweepers. ANNs are merely used to generate outputs for each input. We initially start with a population of neural networks and after every generation GAs are used to generate a better population of networks using genetic operators such as mutation, crossover and selection.

For 1000 generations, each generation with 300 time units, the maximum fitness ever achieved is less than 1500 units and the average fitness is under 800 units. Also each

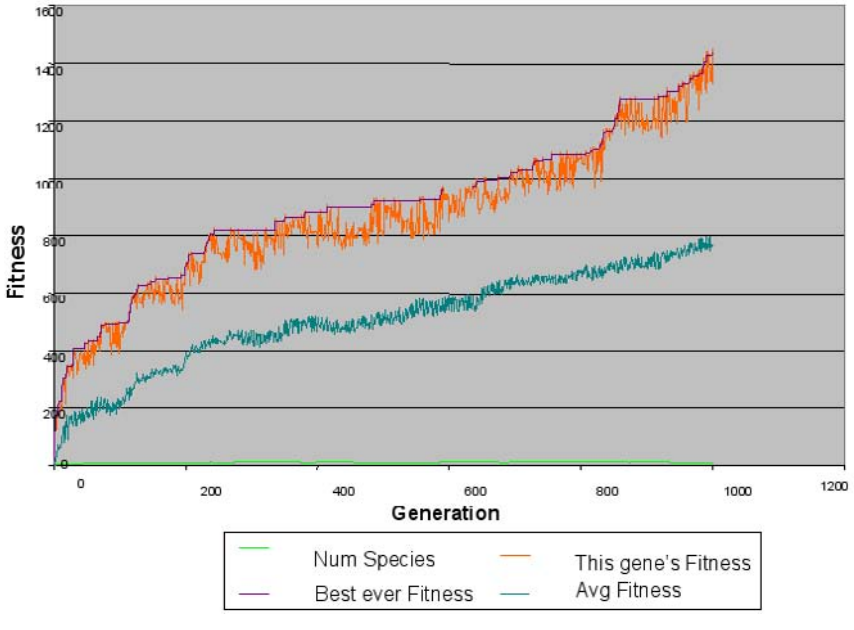

Fig. 2. The fitness of intelligent agents with only GAs

generation's fitness fluctuates across the best ever fitness. In addition, these fluctuations are random. This indicates that the GAs have failed to evolve a single best performing network. However, the performance of mine sweepers equipped with GAs alone was excellent in static environments. Within 300 and 500 generations, a best performing mine sweeper is found. But their performance in a drifting environment was not acceptable. They failed to capture the changes in the environment efficiently and in most cases they did not produce a best performing minesweeper over different generations.

3.2 Performance of Offline Learning and Evolutionary Genetic Algorithms

The offline learning is comprised of genetic algorithms and MBP algorithm. The genetic algorithms evolve weights and architecture simultaneously and MBP is used to further refine the networks. As these networks gain some knowledge about the environment, they tend to reach higher fitness values in less time when compared with only evolutionary algorithms in drifting environments. But characteristics of offline learning and evolutionary algorithms support only static environments. Therefore, offline learning may reduce the number of generations required to reach highest possible fitness, but does not really improve the performance in dynamic environments.

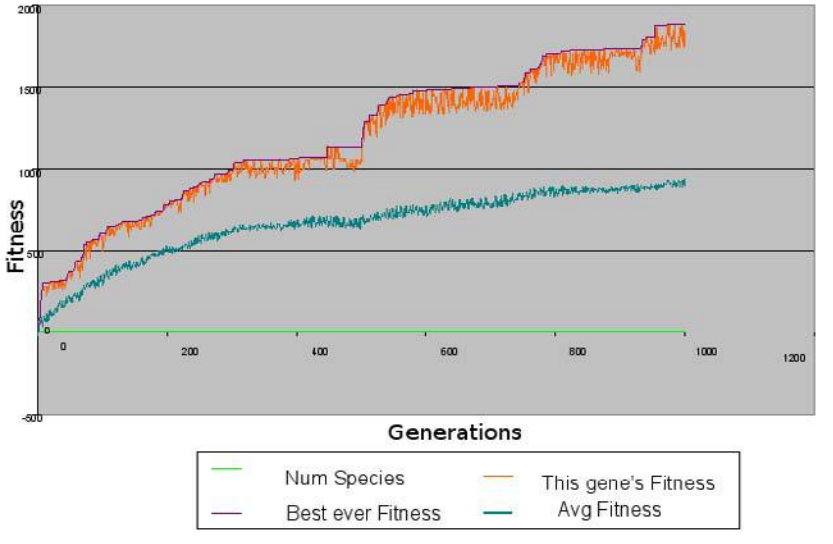

Fig. 3. The fitness of intelligent agents when offline learning is combined with GAs

Figure 3 depicts that in 1000 generations, with 300 time units for each generation, the highest ever fitness reached is below 2000 units and the average fitness is less than 1000 units. However, even with the addition of offline learning, mine sweepers were behaving similarly to those that used genetic algorithms alone. Initially the mine sweepers were performing better but as the effect of offline learning fades away their performance becomes similar to those that used only genetic algorithms.

3.3 Performance of Offline Learning with Online Learning

In this approach, the ANNs benefit from both offline and online learning. The mine sweepers are initially equipped with the neural networks that were evolved using offline learning. In the online learning phase the mine sweepers learn while they explore the environment. This helps the mine sweepers adapt to the intrinsic details of the environment. After completion of every generation in evolutionary phase, genetic algorithms are applied to generate new population from best fit networks of previous generation's population.

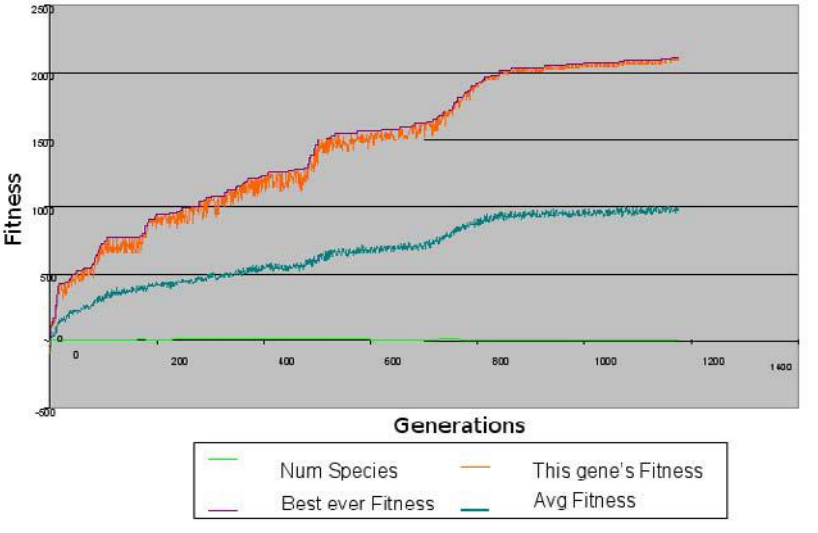

Fig. 4. The fitness of intelligent agents when offline and online learning combined

The highest ever fitness is above 2000 units and the average fitness value is near 1000 units (Figure 4). The generation's fitness variation from the best ever fitness is decreasing as generations increase. After 750 generations, the best ever fitness and the current gene's fitness are close enough to indicate a perfect evolved network i.e. a network performing best in all different environments. The mine sweepers benefit from learning while exploring the environment by adapting to the dynamics of the drifting environment. Through online learning, the mine sweepers modify their previous knowledge to adapt to the subtleties of the new environment. But they should not loose the pre-learned knowledge in the process; hence, we decrease the amount of learning over time.

3.4 Performance of Only Online Learning

The absence of offline learning slows down the fitness growth of mine sweepers. However, after a few hundred generations, mine sweepers become equally efficient to those

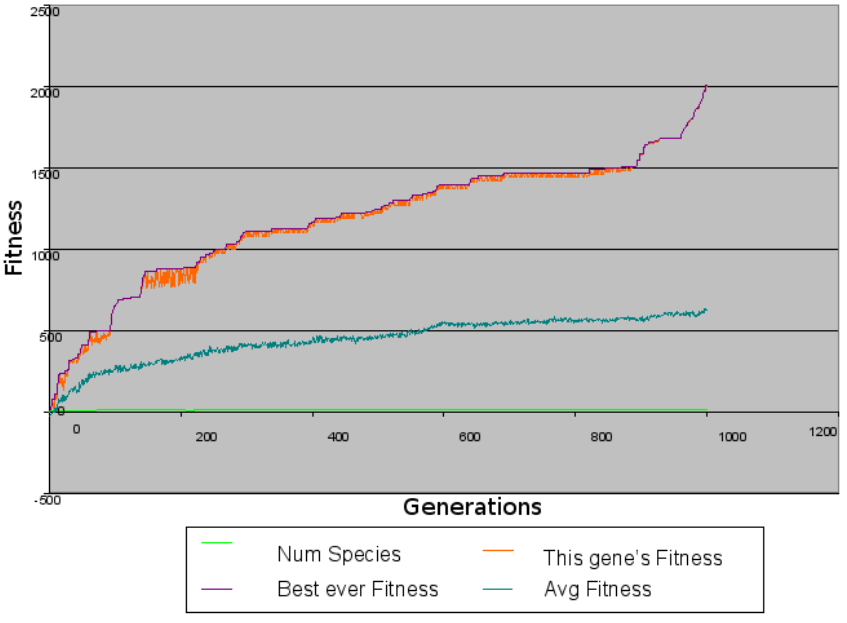

Fig. 5. The fitness of intelligent agents with only online learning

that used the combination of offline and online learning. This proves that online learning is self sufficient.

Figure 5 depicts the performance of online learning alone. For 1000 generations, with 300 time units for each generation, the best fitness ever is 2000 units, and maximum average fitness value is around 600 units. The variations between each generation's fitness and the best ever fitness decrease as the number of generations increases. Therefore, we can say that the algorithm has successfully evolved a network that can perform best in different environments. In the absence of offline learning, the initial mine sweepers are too unrefined to produce best fitness. Online learning improves their behavior as early as the first generation. After a few (200 to 300) generations, the mine sweepers' performance is as good as those that included offline learning.

3.5 Comparisons of Different Approaches

The results of all our experiments indicate that online learning is the key factor for adapting in drifting environments. The evolutionary phase combined with the online learning phase show an improved performance in drifting environments.

Figures 6 and 7 represent the architectures generated by only GAs and online learning, respectively. Whenever fitness decreases, only GAs are unable to capture the changes in the environment and, therefore, attempt to increase the complexity of the architectures in order to improve the fitness. However, GAs combined with online

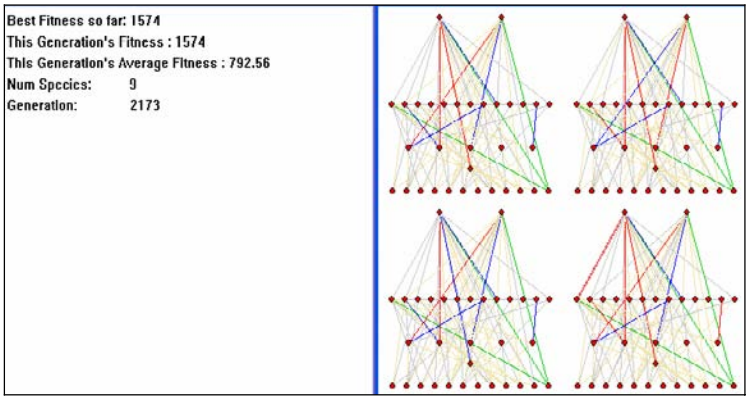

Fig. 6. A sample run of "Only GAs" showing the complex architecture generated

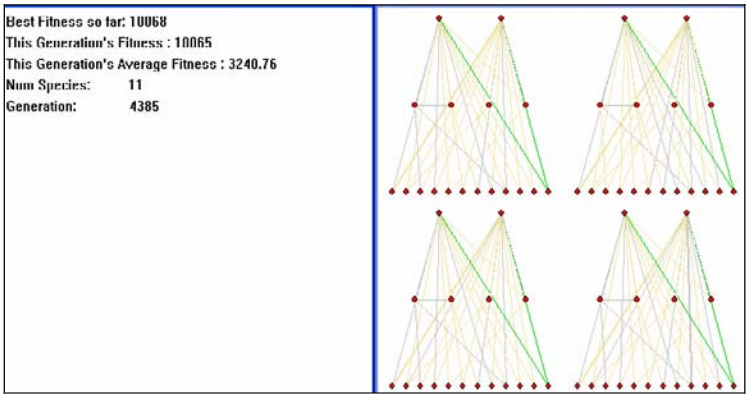

Fig. 7. A sample run of "Only Online Learning" showing the simple architectures

learning tend to generate architectures that are simpler and better tuned to the subtleties of the environment.

4 Conclusions

The design of neural networks involves three different aspects namely: connection weights, architecture, and learning rules. There are no algorithms present that can evolve a neural network using simultaneous evolution of weights, architecture, and learning rules due to the complexity of the process. Our algorithm provides an efficient approach to achieving the simultaneous evolution of all three aspects to generate neural networks for drifting environments. Our algorithm design is based on the following two evolutionary characteristics: (a) Automatic design and generation of dynamic neural networks using evolution, and (b) A continuous (life-long) learning mechanism

for these dynamic networks. Our approach is capable of evolving feedforward, as well as recurrent neural networks and focuses on a key issue: Dynamism in the environment. We provide a theoretically motivated hybrid adaptive learning algorithm for the drifting environments. With drifting environments, the nature and variables of the environment change over time, emphasizing the importance of adapting to the changes in the environments.

We have successfully used all genetic operators in the evolutionary process to evolve neural networks for mine sweepers in an environment that changes from one generation to the next. Our results indicate great improvement in the mine sweepers' behavior. In addition to evolution, we used an online learning mechanism to fine-tune the evolved networks for drifting environments. We observed that complete evolution with an online learning mechanism enables the neural networks to adapt to changing environments efficiently in a short period of time. Our experimental results demonstrate the ability of our algorithm to evolve efficient neural networks with simple architectures in a few hundred generations. In addition, our results indicate that our algorithm successfully evolved simple and easy-to-fine-tune networks in very few generations. We have used a variation of the backpropagation algorithm which can adjust the connection weights for a random and dynamic neural network without the need for re-arrangement into layers. Our modified backpropagation (MBP) algorithm can handle feedforward and recurrent networks. We successfully evolved learning rules using a simple general linear equation

Our results show the performance of the hybrid algorithm with online learning is far superior to the performance of only evolutionary algorithms, even with complete simultaneous evolution. This underlines our basic claim that life-long learning is an important mechanism in adaptation in the drifting environments. Finally, our algorithm can be effectively used with artificial life as well as artificial agents in computer games.

References

[1] Yao, X.: Evolving artificial neural networks. In: Proceedings of the IEEE 87(9) (1999)
[2] Kasabov, N.: Evolving connectionist systems: methods and applications. Bioinformatics, brain study and intelligent machines (2003)
[3] Stanley, K., Miikkulainen, R.: Evolving neural networks through augmenting topologies. Evolutionary Computation 10(2) (2002)
[4] Magoulas, G.D., Plagianakos, V.P., Vrahatis, M.N.: Hybrid methods using evolutionary algorithms for on-line training. In: Proceedings of the INNS-IEEE International Joint Conference on Neural Networks (2001)
[5] Christenson, C., Kaikhah, K.: Incremental Evolution of Trainable Neural Networks that are Backwards Compatible. In: Proceedings of the fifth IASTED International Conference on Artificial Intelligence and Applications (2006)

Solving Inequality Constraints Job Scheduling Problem by Slack Competitive Neural Scheme

Ruey-Maw Chen[1], Shih-Tang Lo[2], and Yueh-Min Huang[2]

[1] Department of Computer Science and Information Engineering, National Chin-yi University of Technology, Taichung 411, Taiwan, ROC
[2] Department of Engineering Science, National Cheng-Kung University, Tainan 701, Taiwan, ROC
raymond@mail.ncut.edu.tw, edwardlo@mail.ksu.edu.tw, huang@mail.ncku.edu.tw

Abstract. A competitive neural network provides a highly effective means of attaining a sound solution and of reducing the network complexity. A competitive approach is utilized to deal with fully-utilized scheduling problems. This investigation employs slack competitive Hopfield neural network (SCHNN) to resolve non-fully and fully utilized identical machine scheduling problems with multi-constraint, real time (execution time and deadline constraints) and resource constraints. To facilitate resolving the scheduling problems, extra slack neurons are added on to the neural networks to represent pseudo-jobs. This study presents an energy function corresponding to a neural network containing slack neurons. Simulation results demonstrate that the proposed energy function integrating competitive neural network with slack neurons can solve fully and non-fully utilized real-time scheduling problems.

Keywords: Scheduling, Real-time, Slack neuron, Competitive Hopfield neural network.

1 Introduction

Scheduling has many applications in commercial, industrial and academic fields, such as avionics, communications, signal processing, routing, industrial control, operations research, production planning, and class arrangement. Willems and Rooda translated the job-shop scheduling problem into a linear programming format, and then mapped it onto an appropriate neural network framework to obtain a solution [1]. Foo and Takefuji employed integer linear programming neural networks to solve the scheduling problem by minimizing the total starting times of all jobs with a precedence constraint [2]. Zhang et al. developed a neural network method derived from linear programming, in which preemptive jobs are scheduled based on their priorities and deadlines [3]. Silva et al. explored solving multi-processor real-time scheduling problems by a Hopfield-type neural network [4]. Hanada and Ohnishi developed a parallel algorithm based on a neural network for preemptive task scheduling problems by permitting task transfer among

H.G. Okuno and M. Ali (Eds.): IEA/AIE 2007, LNAI 4570, pp. 715–724, 2007.

machines [5]. Park et al. embedded a classical local search heuristic algorithm into the TSP optimization neural network [6].

A benefit of real-time task scheduling is owing to its ability to meet task timing constraints rather than optimize a given target. Examples of real-time scheduling include nuclear power plant control systems, traffic control systems, flight mission control systems and embedded tactical systems for military applications. Failure to meet inherent timing constraints in such systems may be dangerous.

Hopfield and Tank adopted neural networks to solve optimization problems involving constraint satisfaction [7]. Dixon et al. employed the Hopfield neural network with mean field annealing (MFA) to solve the shortest path problem in a communication network [8]. Our previous work also solved a multi-constraint schedule problem for a multiprocessor system by the Hopfield neural network with MFA [9]. Moreover, other studies have demonstrated hybrid algorithms that combine HNN with genetic algorithms (GA) [10][11][12].

Various competitive learning networks have been developed [13][14][15]. In a winner-take-all mechanism, the output neuron receiving the largest input is assigned a full value (e.g. 1), while all other neurons are set to 0. A competitive Hopfield neural network (CHNN) applies a competitive schema to update the neuron states in the Hopfield neural network. Chung et al. presented a competitive Hopfield neural network for polygonal approximation [13]. Uchiyama and Arbib utilized competitive learning in color image segmentation [14]. CHNN in the competitive learning mechanism ensures that only one neuron is activated in a column or row of a network, enforcing compliance with the 1-out-of-N constraint. The neuron has maximum net value in the Hopfield neural network is the activated neuron. A series of studies has been conducted to solve fully utilized processors scheduling problems [9][15]. Carderira and Mammeri studied multiprocessor real-time scheduling to satisfy deadline requirements by applying the k-out-of-N rule, which extends slack neurons to agree with the inequality constraints to a neural network [16]. Carderira and Mammeri then extended this methodology to handle real-time scheduling with precedence constraints [17]. Tagliarini et al. demonstrated an approach to design networks for a resources allocation task problem (the weapon-to-target assignment problem), in which a slack neuron is associated with each weapon [18]. Each slack neuron denotes the hypotheses that the associated weapon is not fired. This study extended the neural networks by adding some additional neurons to ease this restriction. The slack neurons make the tasks fully utilize the machines. The deterministic rules of the Hopfield neural networks are usually applied to update the states of slack neurons. However, this work determined neuron states by the competitive rule to cope with the inequality constraint problem. Hence, the competitive mechanism can solve non-fully utilized scheduling cases.

This work investigates the jobs schedule problem on a non-fully utilized real-time multiple identical machines system including timing and resource constraints. Extra slack neurons are added to the networks to meet the condition

of incomplete usage. An energy function is proposed to illustrate the timing and resources constraints.

2 Formulation of the Scheduling Problem

The scheduling problem assumes that a system has N jobs (or processes) and M machines (or processors). First, a job can be segmented without setup time, and the execution of each segment is preemptive. Second, no job migration is allowed between machines, implying that different segments of a job cannot be assigned to different machines. Third, each job's execution time and deadline are predetermined. Furthermore, the machine is permitted to be non-fully-utilized.

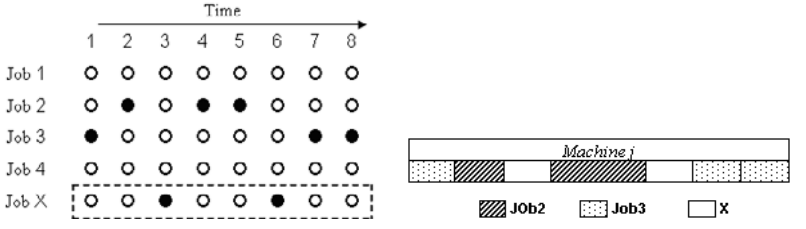

Fig. 1. Neural network with slack neurons and corresponding Gantt chart expression

The problem states that scheduling involves three variables, job, machine and time. The state variable V_{ijk} denotes whether job i is executed on machine j at a certain time k. The i represents a specific job with a range from 1 to $N+1$. The $(N+1)th$ job is a pseudo-job, i.e. a supplementary job to fulfill *1-out-of-N* rule. That is, inequality constraints can be enforced by adding neurons to the hypothesis representation neurons. The extra neurons are referred to as "slack neurons", as displayed in Fig. 1. Herein, slack neurons are neurons representing the pseudo-job. Figure 1 also shows the Gantt chart expression corresponding to the scheduling result with pseudo-job introduced for a dedicated machine j. The term j denotes a dedicated machine from 1 to M. Finally, k denotes the "time" variable bounded between 0 and T, where T denotes the job deadline. Thus, the activated neuron $V_{ijk} = 1$ indicates that job i is run on machine j at time k; otherwise, $V_{ijk} = 0$. The activated neuron $V_{(N+1)jk} = 1$ indicates that machine j at time k is free. Notably, each V_{ijk} maps to a neuron of the neural network.

The correlating energy function representing the scheduling problem is the sum of six energy terms. The first term represents the output state constraints, since machine j can only perform one job, say i or i', at time k. This term can be expressed as

$$E_1 = \sum_{i=1}^{N+1} \sum_{j=1}^{M} \sum_{k=1}^{T} \sum_{\substack{i'=1 \\ i' \neq i}}^{N+1} V_{ijk} V_{i'jk} \tag{1}$$

where N, M, T, i, j, k, i', and V_{ijk} are as defined above. The rest of this work adopts same notation. The energy term has a minimum value of zero when it meets this constraint, which arises when $V_{ijk} = 0$ or $V_{i'jk} = 0$. The second energy term confines job migration, implying that job i runs on machine j or j'. If a job is assigned on a dedicated machine, then all of its segments must be executed on the same machine. However, this term allows slack neuron of the $N+1th$ job to be activated on different machines (j and $j \neq j'$) at any time k'. The slack neurons are not considered when retrieving the problem solution. Accordingly, the energy term is defined as follows:

$$E_2 = \sum_{i=1}^{N} \sum_{j=1}^{M} \sum_{k=1}^{T} \sum_{\substack{j'=1 \\ j' \neq j}}^{M} \sum_{k'=1}^{T} V_{ijk} V_{ij'k'} \tag{2}$$

This energy term also has a minimum value of zero when $V_{ijk} = 0$ or $V_{ij'k'} = 0$. The third energy term is defined as

$$E_3 = \sum_{i=1}^{N+1} (\sum_{j=1}^{M} \sum_{k=1}^{T} V_{ijk} - P_i)^2 \tag{3}$$

where P_i denotes the total execution time required by job i. This energy term means that the time consumed by job i must equal P_i such that $\sum \sum V_{ijk} = P_i$. The processing time of the pseudo-job (the $N+1th$ job) is given by the total available time for all machines minus the total processing time needed by all N jobs. Additionally, another state constraint energy item is introduced as:

$$E_4 = \sum_{j=1}^{M} \sum_{k=1}^{T} (\sum_{i=1}^{N+1} V_{ijk} - 1)^2 \tag{4}$$

This energy term provides a supplemental constraint to ensure that a job is always executed on a specific machine at a certain time when utilizing the *1-out-of-N* rule. Thus, this energy item should also have a minimum value of zero. The following energy term is defined to meet the deadline requirement of each job i as:

$$E_5 = \sum_{i=1}^{N+1} \sum_{j=1}^{M} \sum_{k=1}^{T} V_{ijk} G_{ijk}^2 H(G_{ijk}), \text{where } H(G_{ijk}) = \begin{cases} 1, \text{if } G_{ijk} > 0 \\ 0, \text{if } G_{ijk} \leq 0 \end{cases}, G_{ijk} = k - d_i \tag{5}$$

where d_i is the deadline of the job i, and $H(G_{ijk})$ denotes the Unit step function. The energy term exceeds zero when a job is allocated with a run time greater than d_i, i.e., when $V_{ijk} = 1$, $k - d_i > 0$, and $H(G_{ijk}) > 0$. The energy value grows quadratically with the associated time lag between d_i and k, given by $k - d_i$. Conversely, this energy term has a value of zero provided that $V_{ijk} = 1$ and $k - d_i \leq 0$.

Finally, an energy term is included to reflect the prohibition on simultaneous resource preemption and resource sharing.

$$E_6 = \sum_{i=1}^{N+1}\sum_{j=1}^{M}\sum_{k=1}^{T}\sum_{\substack{i'=1\\ i'\neq i}}^{N+1}\sum_{\substack{j'=1\\ j'\neq j}}^{M}\sum_{s=1}^{F} V_{ijk}R_{is}V_{i'j'k}R_{i's} \tag{6}$$

In this term, F denotes the amount of available resource instances, while R_{is} and $R_{i's}$ represent requests by jobs i and i' for resource s, respectively. The term $R_{is} = 1$ signifies that job i requires resource s, so $R_{i's} = 1$ for job i'. Inspecting this energy term, when two distinct jobs are scheduled (say $V_{ijk} = 1$ and $V_{i'j'k} = 1$) to be executed at time k on different machines j and j', then either R_{is} or $R_{i's}$ must equal zero since machines j and j' cannot utilize the same resource at time k. Therefore, the value of the energy term becomes zero. Based on the above discussion, the derived energy function has a minimum value of zero when all constraints are satisfied. Accordingly, the total energy with all constraints can be induced as shown in Eq. (7):

$$E = \frac{C_1}{2}E_1 + \frac{C_2}{2}E_2 + \frac{C_3}{2}E_3 + \frac{C_4}{2}E_4 + \frac{C_5}{2}E_5 + \frac{C_6}{2}E_6 \tag{7}$$

Where C_1, C_2, C_3, C_4, C_5 and C_6 refer to weighting factors, which like N, M and T, are assumed herein to be positive constants.

3 Competitive Algorithm

The scheduling problem of interest and corresponding energy function are mapped onto the competitive HNN to yield solutions is presented in this section. Based on dynamic system theory, the Liapunov function shown in Eq. (8), has verified the existence of stable states of the network system [17][19]. A 3-dimentional model is as below:

$$E = -\sum_{x}\sum_{y}\sum_{z}\sum_{i}\sum_{j}\sum_{k} V_{xyz}W_{xyzijk}V_{ijk} + \sum_{i}\sum_{j}\sum_{k}\theta_{xyz}V_{xyz} \tag{8}$$

where V_{xyz} and V_{ijk} denote the neuron states; W_{xyzijk} is the synaptic weight indicating the interconnection strength among neurons, and θ_{ijk} is the threshold value representing the bias input of the neuron. Additionally, the HNN employs the deterministic rule, displayed in Eq. (9) below, to update the neuron state change

$$V_{ijk}^{n+1} = \begin{cases} 1, & \text{if } Net_{ijk} > 0 \\ V_{ijk}^{n}, & \text{if } Net_{ijk} = 0 \\ 0, & \text{if } Net_{ijk} < 0 \end{cases} \tag{9}$$

where Net_{ijk} represents the total input or net value of the neuron (i, j, k), listed as follows:

$$Net_{ijk} = -\frac{\partial E}{\partial V_{ijk}} = \sum_{x}\sum_{y}\sum_{z} W_{xyzijk}V_{xyz} - \theta_{ijk} \tag{10}$$

A Hopfield neural network that applies a winner-take-all learning mechanism is called a competitive Hopfield neural network. The competitive rule is used to build neural networks that satisfy constraints in which "exactly one neuron among $N+1$" should be activated when the network approaches a stable state. Accordingly, a machine can only execute one job at a time in a subject scheduling problem, omitting the C1 and C4 energy terms from the HNN energy function (Eq. 7) generates a simplified energy function that satisfies the competitive constraint. Restated, the C_1 and C_4 energy terms are handled implicitly. The resulting energy function is given as follows:

$$E = \frac{C_2}{2}E_2 + \frac{C_3}{2}E_3 + \frac{C_5}{2}E_5 + \frac{C_6}{2}E_6 = \frac{C_2}{2}\sum_{i=1}^{N}\sum_{j=1}^{M}\sum_{k=1}^{T}\sum_{\substack{j'=1\\ j'\neq j}}^{M}\sum_{k'=1}^{T} V_{ijk}V_{ij'k'}$$
$$+ \frac{C_3}{2}\sum_{i=1}^{N+1}(\sum_{j=1}^{M}\sum_{k=1}^{T} V_{ijk} - P_i)^2 + \frac{C_5}{2}\sum_{i=1}^{N+1}\sum_{j=1}^{M}\sum_{k=1}^{T} V_{ijk}G_{ijk}^2 H(G_{ijk})$$
$$+ \frac{C_6}{2}\sum_{i=1}^{N+1}\sum_{j=1}^{M}\sum_{k=1}^{T}\sum_{\substack{i'=1\\ i'\neq i}}^{N+1}\sum_{\substack{j'=1\\ j'\neq j}}^{M}\sum_{s=1}^{F} V_{ijk}R_{is}V_{i'j'k}R_{i's} \tag{11}$$

Hence, the synaptic interconnection strength, W_{xyzijk}, and the bias input, θ_{ijk}, can be obtained by comparing Eq. (11) with Eq. (8) as illustrated below:

$$W_{xyzijk} = -C_2 \cdot \delta(x,i) \cdot (1-\delta(y,j)) - C_3 \cdot \delta(x,i)$$
$$- C_6 \cdot (1-\delta(x,i))(1-\delta(y,j))\delta(z,k)\sum_s R_{xs}R_{is} \tag{12}$$

and

$$\theta_{xyz} = -C_3 \cdot P_i + \frac{C_5}{2} \cdot G^2 \cdot H(G) \tag{13}$$

respectively, where $\delta(a,b) = \begin{cases} 1 \text{ if } a = b \\ 0 \text{ if } a \neq b \end{cases}$ is the *Kronecker delta* function.

The CHNN imposes a competitive winner-take-all rule to update the neuron states. Neurons on the same column of a dedicated machine at a given time compete with one another to determine the winning neuron. The winner-take-all update rule of the neuron for the ith column is illustrated as follows:

$$V_{xjk} = \begin{cases} 1, \text{ if } Net_{xjk} = \max\limits_{i=1\sim N+1} Net_{ijk} \\ 0, \text{ otherwise} \end{cases} \tag{14}$$

where Net_{xjk} is the maximum total neuron input, which is equivalent to the dynamic threshold on a McCulloch-Pitts neuron [20]. This derived energy function is an appropriate Liapunov function [19][21][22].

4 Simulations

Several cases were applied in the simulation. The values of C_2, C_3, C_5 and C_6 were set to 0.35, 0.25, 1.2 and 0.3, respectively. Tables 1 and 2 list the constraints

Table 1. Timing and resource requested of 4 jobs (1a:$A = 4$, $B = 3$, $C = 3$, 1b:$A = 3$, $B = 2$, $C = 3$)

	Time Required	Time Limit	R1	R2	R3
Job 1	A	6	1	0	0
Job 2	B	4	0	0	1
Job 3	C	6	0	1	0
Job 4	2	3	1	0	0

Table 2. Timing and resource requested of 5 jobs (2a:$A = 5$, $B = 3$, $C = 4$, 2b:$A = 3$, $B = 3$, $C = 3$)

	Time Required	Time Limit	R1	R2	R3	R4
Job 1	2	3	1	0	0	0
Job 2	A	8	0	1	0	0
Job 3	B	4	0	0	1	0
Job 4	C	8	0	0	0	1
Job 5	2	5	1	0	0	1

of the simulation examples for 2 machines in cases 1-2. Tables 3 list the case for 3 machines. Cases 1a and 2a had the same conditions as in [15]. Case 3a was the case explored in [12]. These cases were included to demonstrate the full machine usage system scheduling study.[t]

Table 3. Timing and resource requested of 10 jobs (3a: $A = 5$, 3b: $A = 3$)

	Time Required	Time Limit	R1	R2	R3	R4
Job 1	A	10	1	0	0	0
Job 2	3	5	0	1	0	0
Job 3	3	9	0	0	0	0
Job 4	2	5	1	0	0	0
Job 5	3	9	0	0	1	0
Job 6	2	6	0	1	0	0
Job 7	3	10	0	0	0	1
Job 8	2	5	0	0	1	0
Job 9	3	9	0	0	0	0
Job 10	4	10	0	0	1	0

Figures 2 through 7 display the neuron states of simulation results to represent the job schedules. Figures 2, 4 and 6 illustrate the resulting schedules of cases 1a, 2a and 3a respectively. Figure 3 shows the schedule correlating with non-full usage of Cases 1b. Moreover, Fig. 5 represents the resulting schedule of case 2b. Finally, Fig. 7 presents the resulting schedule of case 3b. The job assignment of X as displayed in figures reveals that the activated neurons are the slack neurons. Restated, the machine does not do anything related to scheduled job at that time.

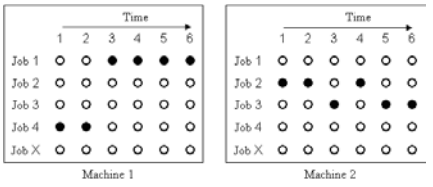

Fig. 2. Simulation results of case 1a

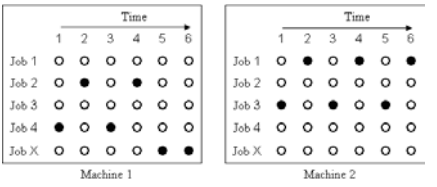

Fig. 3. Simulation results of case 1b

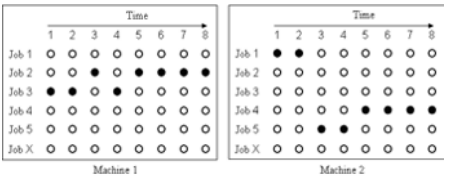

Fig. 4. Simulation results of case 1a

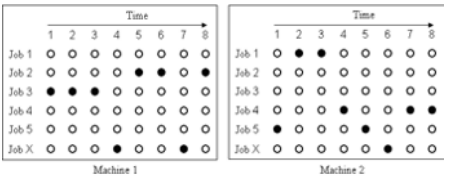

Fig. 5. Simulation results of case 1b

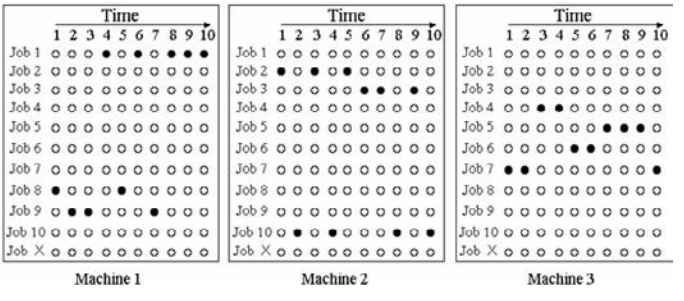

Fig. 6. Simulation results of case 3a

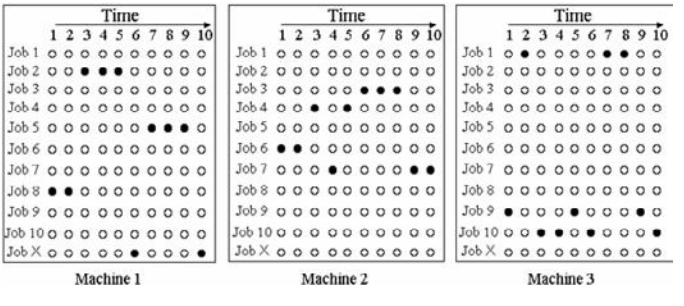

Fig. 7. Simulation results of case 3b

Table 4. Comparison of the different schemes

	HNN	MFA	CHNN	SCHNN
Energy terms	6	5	4	4
Average iterations	14	42	9	8
Non-fully utilized	$\surd$	N/A	N/A	$\surd$

Finally, Table 4 lists the comparison of the different schemes, HNN, mean field annealing, CHNN and SCHNN.

5 Conclusions

This investigation applies the competitive mechanism in neural networks to remove the constraint terms in the energy function. Hence, the competitive scheme can reduce the network complexity by decreasing the number of interconnections among neurons [13]. This study develops an approach containing extra slack neurons for solving multi-constraint schedule problems for both fully utilized and non-fully utilized systems.

The network may oscillate with the symmetric (i.e., $W_{xyzijk} = W_{ijkxyz}$) property when network is updated [19][21]. Takefuji and Lee presented a hysteresis binary neuron model, which effectively suppresses the oscillatory behaviors of neural dynamics to solve combinatorial optimization problems [23]. Table 4 indicates that the benefits of adopting the proposed scheme are: (1) elimination of the constraint terms in the energy function, decreasing the network complexity; (2) ability to discover good solutions to a scheduling problem rapidly, and (3) ability to solve both fully and non-fully utilized scheduling problems.

This work focuses mostly on solving real-time scheduling without ready time consideration. The problem can be further extended to involve the temporal relationship between ready time and priority for each job. This approach is time consuming for very large-scales problems. Cardeira and Mammeri presented the concept to lower the computation complexity by reducing the neurons [16]. Restated, the neurons are reduced using a two dimensional network, hence reduce the execution time. Future works can avoid this difficulty by mapping scheduling problems onto two dimensional neural networks instead of using proposed three dimensional networks in the work.

References

1. Willems, T.M., Rooda, J.E.: Neural Networks for Job-shop Scheduling. Control Eng. Practice 2(1), 31–39 (1994)
2. Foo, Y.P.S., Takefuji, Y.: Integer linear programming neural networks for job-shop scheduling. In: IEEE Int. Conf. on Neural Networks, vol. 2, pp. 341–348 (1998)
3. Zhang, C.S., Yan, P.F., Chang, T.: Solving Job-Shop Scheduling Problem with Priority Using Neural Network. In: IEEE Int. Conf. on Neural Networks, pp. 1361–1366 (1991)
4. Silva, M.P., Cardeira, C., Mammeri, Z.: Solving real-time scheduling problems with Hopfield-type neural networks. In: EUROMICRO 97 New Frontiers of Information Technology, Proceedings of the 23rd EUROMICRO Conference, pp. 671–678, 1–4 (1997)
5. Hanada, A., Ohnishi, K.: Near optimal jobshop scheduling using neural network parallel computing. In: Int. Conf. on Proc.Industrial Electronics, Control, and Instrumentation, vol. 1, pp. 315–320 (1993)

6. Park, J.G., Park, J.M., Kim, D.S., Lee, C.H., Suh, S.W., Han, M.S.: Dynamic neural network with heuristic. In: IEEE Int. Conf. on Neural Networks, vol. 7, pp. 4650–4654 (1994)
7. Hopfield, J.J., Tank, D.W.: Neural computation of ecision in optimization problems. Biological Cybernetics 52, 141–152 (1985)
8. Dixon, M.W., Cole, G.R., Bellgard, M.I.: Using the Hopfield network with mean field annealing to solve the shortest path problem in a communication network. In: Int. Conf. on Neural Networks, vol. 5, pp. 2652–2657 (1995)
9. Huang, Y., Chen, R.M.: Scheduling multiprocessor job with resource and timing constraints using neural network. IEEE Trans. on System, Man and Cybernetics, part B 29(4), 490–502 (1999)
10. Watanable, Y., Mizuguchi, N., Fujii, Y.: Solving optimization problems by using a Hopfield neural network and genetic algorithms combination, System Computation, Japan, vol. 29(10), pp. 68–73 (1988)
11. Sancho, S.S., Carlos, B.C., Anibal, R.: Figueiras-Vidal. A mixed Neural-Genetic Algorithm for the Broadcast Scheduling Problem. IEEE Trans. on Wireless Communication 2(2), 277–283 (2003)
12. Cheng, S.C., Huang, Y.M.: Scheduling Multi-Processor Tasks with Resource and Timing Constraints Using Genetic Algorithm. In: Chung, P. C., Tsai, C. T., Chen, E. L., Sun, Y. N. The 5th IEEE International Symposium on Computational Intelligence in Robotics and Automation (2003), [13] pp. 624–629. Polygonal approximation using a competitive Hopfield neural network, Pattern Recognition, vol. 27, pp. 1505–1512 (1994)
13. Uchiyama, T., Arbib, M.: Color Image Segmentation Using Competitive Learning. IEEE Trans. Pattern Analysis Machine Intelligence 16(12), 1197–1206 (1994)
14. Chen, R., Huang, Y.M.: Competitive Neural Network to Solve Scheduling Problem. Neurocomputing 37, 177–196 (2001)
15. Cardeira, C., Mammeri, Z.: Neural networks for multiprocessor real-time scheduling, In: IEEE Proc. 6th Euromicro Workshop on Real-Time Sys. pp. 59–64 (1994)
16. Cardeira, C., Mammeri, Z.: Handling Precedence Constraints with Neural Network Based Real-time Scheduling Algorithms. In: Proceedings of Ninth Euromicro Workshop on Real-Time Systems, pp. 207–214 (1997)
17. Tagliarini, G.A., Christ, J.F., Page, E.W.: Optimization Using Neural Networks. IEEE Transaction on Computers 40(12), 1347–1358 (1991)
18. Hopfield, J., Tank, D.W.: Computing with neural circuits: A model, Science 233, 625–633 (1986)
19. Lee, K.C., Funabiki, N., Takefuji, Y.: A parallel improvement algorithm for the bipartite subgraph problem Neural Networks. IEEE Transactions 3(1), 139–145 (1992)
20. Takeda, M.J., Goodman, W.: Neural networks for computation: number representation and programming complexity. Applied Optics 25, 3033–3046 (1986)
21. Cohen, M., Grossberg, S.: Absolute stability of goal pattern formation and parallel memory storage by competitive neural networks. IEEE Trans. On System, Man, and Cybernetics 13, 815–826 (1983)
22. Takefuji, Y., Lee, K.: An artificial hystersis binary neuron: a model suppressing the oscillatory behaviors of neuron dynamics. Biological Cybernetics 64, 353–356 (1991)

Intelligent OS Process Scheduling Using Fuzzy Inference with User Models

Sungsoo Lim and Sung-Bae Cho

Dept. of Computer Science, Yonsei University
Shinchon-dong, Seodaemun-ku,
Seoul 120-749, Korea
lss@sclab.yonsei.ac.kr, sbcho@cs.yonsei.ac.kr

Abstract. The process scheduling aims to arrange CPU time to multiple processes for providing users with more efficient throughput. Except the class of process set by user, conventional operating systems have applied the equivalent scheduling policy to every process. Moreover, if the scheduling policy is once determined, it is unable to change without resetting the operating system which takes much time. In this paper, we propose an intelligent CPU process scheduling algorithm using fuzzy inference with user models. It classifies processes into three classes, batch, interactive and real-time processes, and models user's preferences to each process class. Finally, it assigns the priority of each process according to the class of the process and user's preference through the fuzzy inference. The experimental result shows the proposed method can adapt to user and allow different scheduling policies to multiple users.

Keywords: OS process scheduling, fuzzy inference system, process classification, user's preference.

1 Introduction

Recent years there have been significant efforts in applying the reflection paradigm in system software. Reflection is widely acknowledged as a useful mechanism for facilitating the run-time adaptation and reconfiguration of software. This approach has been particularly directed at middleware systems [1], but there has also been significant work in reflective operating systems [2]. In this paper, we propose an intelligent process scheduling algorithm in operating systems.

The goal of process scheduling is to give users more efficient throughput by arranging CPU time to multiple processes. However, it is hard to arrange CPU time fairly because the purpose of each process is different. In general, there are three different purposes according to the classes of processes. The first class is batch processes such as programming language compilers, database search engines and scientific computations. They require high throughput and short turn-around time. The second one is interactive processes such as command shells, text editors and graphical applications. They interact constantly with their users and thereby spend a

H.G. Okuno and M. Ali (Eds.): IEA/AIE 2007, LNAI 4570, pp. 725–734, 2007.

lot of time waiting for key-presses and mouse operations. This makes them to require short response time to user input. The last one is real-time processes such as video and sound applications, and robot controllers. They should have a short guaranteed response time with a minimum variance [3].

Since there are different purposes according to the classes of processes and the conventional operating systems do not know the classes of processes, the research at process scheduling has proposed for a specific purpose of scheduling or for working efficiently in specific environment. In this paper, we propose a novel method of process scheduling which adapts to users' preferences. It extracts the features of processes in run time, and classifies the classes of processes. It models the preferences of users, and finally decides the priority of each process using fuzzy inference with the information of process class and user's preferences.

2 Related Works

2.1 Process Scheduling

In general, the operating systems which allow multiple processes focus on the problem of how to arrange CPU resource to processes. One of the oldest, simplest and most widely used proportional share scheduling algorithms is round robin [4]. It is the time-sharing approach in which several tasks can coexist. The scheduler gives a short time-slice to each job, before moving on to the next job, polling each task round and round. This way, all the tasks advance, little by little, on a controlled basis. There are other traditional methods, which are based on CPU resource, such as FCFS (first come first served), SJF (shortest job first), SRT (shortest remaining time), HRRN (highest response ratio next) and so on [5].

Recently, through the enhancement of CPU computational power and network bandwidth, there are some studies on CPU scheduling to support multimedia tasks. Yavatkar and Lakshman use a rate adjustable priority scheduling mechanism to provide an average frame delivery rate to a client application [6]. SMART proposed by Nieh and Monica is a hierarchical CPU scheduling algorithm that supports both hard real time and conventional time sharing applications, adjusts well to overload, and can notify applications when their deadlines cannot be met [7]. Other scheduling work has been done in supporting clients with real-time requirements [8,9] and improving the response time of interactive clients [10,11].

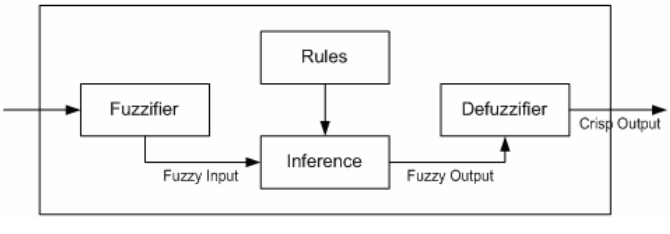

Fig. 1. Fuzzy inference system

2.2 Fuzzy Inference System

Fuzzy inference systems (FIS), which are also called fuzzy rule-based systems, are composed of 4 blocks as shown in Fig. 1. Fuzzifier transforms the crisp inputs into fuzzy inputs by membership functions that represent fuzzy sets of input vectors. In this paper, we adopt the triangular membership functions. Rule-base consists of fuzzy IF-THEN rules. Inference is an inference engine for fuzzy rules. In this paper, we use *max·min* composition rules for inference method. Defuzzifier transforms the fuzzy output into crisp output. Defuzzification process causes the most computational complexity in FIS. We apply *weighted average* for defuzzification.

$$R_l : \text{if } x_1 = F_1^l \text{ and } x_2 = F_2^l \text{ then } y = Q_k^l \tag{1}$$

For instance, let the *l*th rule as (1), where x_i denotes the input variable and F and Q denote the fuzzy set of input and output variables. Fig. 2 shows the inference process with the *l*th fuzzy rule using triangular membership functions and *max·min* composition.

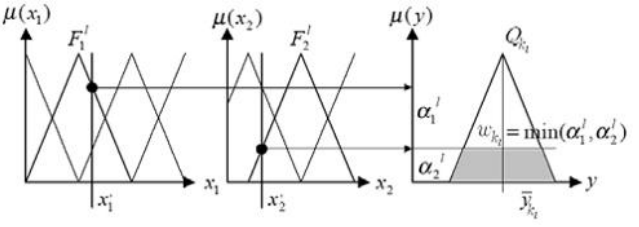

Fig. 2. The process of fuzzy inference

By the fuzzy inference with the *l*th fuzzy rule, we obtain the result through *min* operation as the shady part in Fig. 2. After applying all the rules, we can get the final result of fuzzy inference through *max* operation as follows:

$$Q_k = \max(\omega_{k_1}, \omega_{k_2}, \cdots, \omega_{k_n}) \quad (n \text{ is the total number of rules}) \tag{2}$$

This is followed by the last step of FIS, defuzzification, with *weighted average*.

$$y(x) = \frac{\sum_{k=1}^{n} \bar{y}_k \times Q_k}{\sum_{k=1}^{n} Q_k} \tag{3}$$

Here, $\bar{y}_k$ represents the value of *y*-axis when the membership value of fuzzy set Q_k is 1.0.

In this paper, we apply fuzzy inference to process classification and process priority decision. FIS has been applied to numerous engineering applications such as control, signal processing and pattern classification problems [12,13]. In pattern classification, fuzzy logic improves classification and decision systems by allowing the use of overlapping class definitions and improves the interpretability of the results by providing more insight into the classifier structure and decision-making systems [14]. Moreover, the function *schedule*() is called by OS in every brief time duration,

and we apply fuzzy inference because it requires low computational overhead comparing with other artificial intelligence methods.

3 Intelligent Process Scheduling

As shown above, although the purpose of process scheduling is different according to the classes of process, the conventional operating systems have scheduled every process equivalently because they do not know the classes of process. To overcome this limitation, we develop an intelligent process scheduling method in Linux kernel 2.4.25. The method consists of three modules as shown in Fig. 3. The process classification module classifies a process into batch, interactive and real-time processes with the type and frequency of *system call* and the amount of CPU time which the processes are used. The user modeling module models the user's preference about the three classes of processes. The process priority module decides the priority of each process using the result of classification and user models.

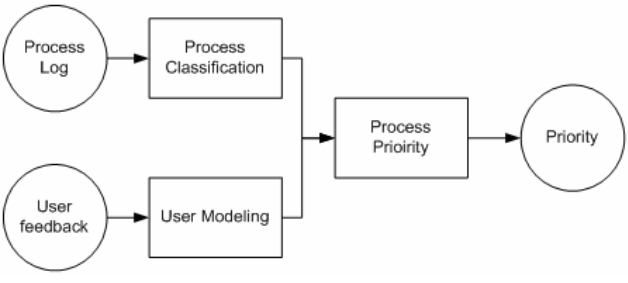

Fig. 3. Proposed process scheduling method

3.1 Process Classification

Fig. 4 shows the entire process of the process classification. For the process classification, we produce a log by pairing the occupation time of CPU and the type of *system call* together, where the occupation time of CPU denotes the CPU time which the process uses between the last log and the current one.

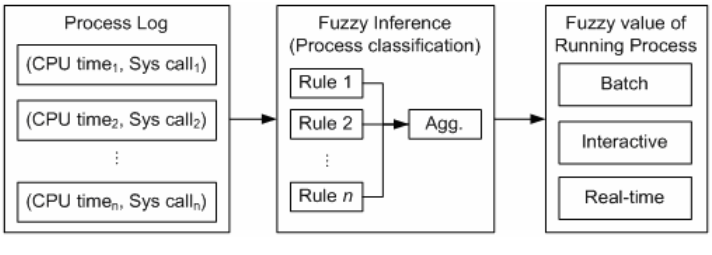

Fig. 4. Fuzzy process classifier

A *queue* is inserted in *task_struct* to record the recent *n* logs (*n* = 100). When the process is scheduled out or *system call* is occurred, a pair of logs is pushed in the *queue*. If the *queue* is full, it pops a log before pushing. When the process is scheduled out, the *null* value is inserted for the *system call* value.

To calculate CPU time, we add a variable, *bf_counter*, in *task_struct* for remembering the *counter* value before the process gets CPU control, where the *counter* variable in *task_struct* denotes the remaining arranged CPU time for the process. When the process is scheduled out or blocked by *system call*, we can get the used CPU time of the process from the difference of these two variables.

As shown in Fig. 4, we use the process log data for input value of fuzzy inference and we get the membership values about process classes through the fuzzy inference. The fuzzy rules are made by analyzing each class of processes. The batch processes, like programming language compilers and database search engines, require more CPU time than other classes of processes, and the interactive processes such as documents editors interact with humans through input and output devices they have more *system calls* related on input and output than others. The real-time processes have more *sys_nanosleep*() *system calls* than others for giving CPU control to other processes after finishing their computations. The fuzzy inference for classifying a process is conducted when a new log comes for the process in order to maintain the present condition of the process and to prevent duplicate calculations. Table 1 shows the fuzzy rules for classifying processes and Fig. 5 represents the membership functions for it.

Table 1. Fuzzy rules for classifying processes

Condition	Action
if *system call* {*sys_read*()} is many,	**then** interactive process
if *system call* {*sys_write*()} is many,	**then** interactive process
if CPU using times (per ticks) are many,	**then** batch process
if *system call* {*sys_nanosleep*()} is many,	**then** real-time process

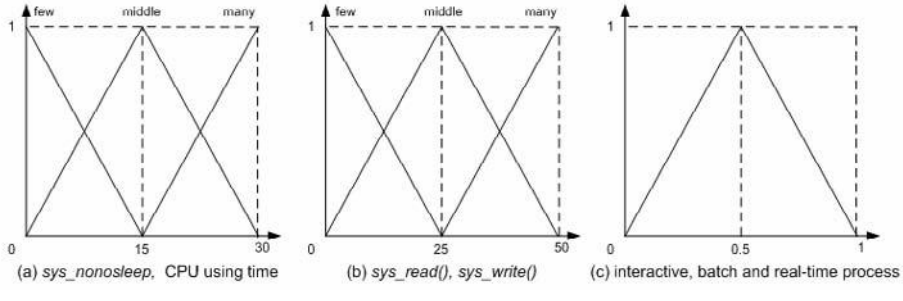

Fig. 5. Membership functions for classifying processes

3.2 Decision of Process Priority

Conventional operating systems have scheduled processes on the system level without considering user's preferences. Therefore, if user wants to change the process scheduling policy, he/she must be reset the OS which needs much time and is hard for novice.

In this section, we introduce a user adaptive process scheduling method by changing the priority of process according to the user's preferences. With this method, an operating system can satisfy multi-users' needs without resetting the operating system. It only requires modeling the user's preferences. Fig. 6 shows the process of decision of process priority based on user model and the result of process classification.

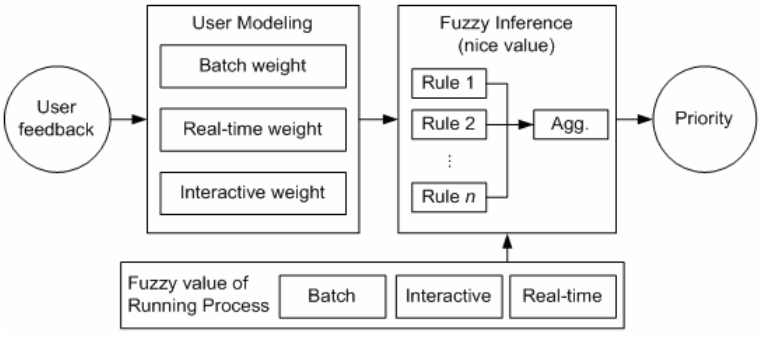

Fig. 6. Decision of process priority

In Linux, the *task_struct* has a pointer of *user_struct* to denote who the owner of this process is. Therefore, we insert variables for user's preferences in the *user_struct*. When the user is logged out after using the computer, we get the user feedback about the amount of satisfaction to each class of process. The user inputs the score from 0 to 10, and then the system calculates the preferences of the user like Table 2. We design the update method focused on four factors. First, if the feedback value of a class is low, it means that user wants to arrange more CPU time for the class of processes, and on the other hand if the feedback value of a class is high, it denotes that user wants to arrange less CPU time for the class of processes. Second, the summation of three weights ($\omega_{batch} + \omega_{inter} + \omega_{rt}$) must be 1. Third, if user inputs the same three values, the weights do not change. Last, the amount of updates depends on the relative gaps of the user's input, not the absolute gaps.

Except setting up as real-time processes by user, the processes in Linux are applied *SCHED_OTHER* schedule policy, which plays a role in round robin, and the priority of processes is deeply related on the value of *nice* in *task* structure. If the value of *nice* is high, it denotes the process has low priority, on the other hand, if its value is low, it means the process has high priority. Therefore, we determine the value of *nice* to control the priority of processes.

Table 2. Update of user's preferences from feedback

$M = \frac{f_{\text{batch}} + f_{\text{inter}} + f_{\text{rt}}}{3}$	$S = T_{\text{batch}} + T_{\text{inter}} + T_{\text{rt}}$	
$T_{\text{batch}} = \omega_{\text{batch}} \times \left(1 - \frac{f_{\text{batch}} - M}{M}\right)$	$\omega_{\text{batch}} = \frac{T_{\text{batch}}}{S}$	ω : weight,
$T_{\text{inter}} = \omega_{\text{inter}} \times \left(1 - \frac{f_{\text{inter}} - M}{M}\right)$	$\omega_{\text{inter}} = \frac{T_{\text{inter}}}{S}$	f : feedback
$T_{\text{rt}} = \omega_{\text{rt}} \times \left(1 - \frac{f_{\text{rt}} - M}{M}\right)$	$\omega_{\text{rt}} = \frac{T_{\text{rt}}}{S}$	

Table 3. Fuzzy rules for the decision of process priority

Condition	Action
if (process is interactive process) **and** (user interactive weight is high),	**then** nice is low
if (process is interactive process) **and** (user interactive weight is middle),	**then** nice is middle
if (process is interactive process) **and** (user interactive weight is low),	**then** nice is high
if (process is batch process) **and** (user batch weight is high),	**then** nice is low
if (process is batch process) **and** (user batch weight is middle),	**then** nice is middle
if (process is batch process) **and** (user batch weight is low),	**then** nice is high
if (process is real-time process) **and** (user real-time weight is high),	**then** nice is low
if (process is real-time process) **and** (user real-time weight is middle),	**then** nice is middle
if (process is real-time process) **and** (user real-time weight is low),	**then** nice is high

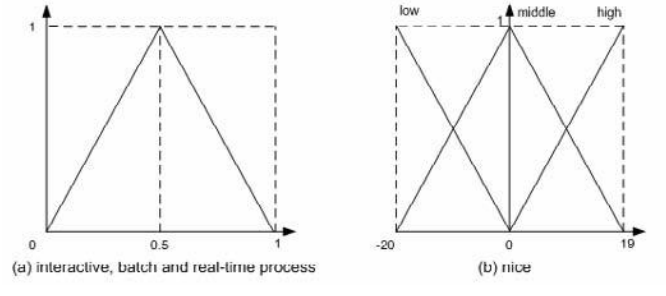

Fig. 7. Membership functions for the decision of process priority

With the user's preferences and the fuzzy membership values of process which explained at 3.1, we can determine the value of *nice* through fuzzy inference. Table 3 shows the fuzzy rules for the decision of process priority and Fig. 7 represents the membership functions for it.

4 Experimental Results

For the experiments, we set three user groups of batch user group, interactive user group and real-time user group, each of which has 10 subjects. The experiments have been conducted by typing some given sentences using *gedit*, one of interactive processes, while watching movies using *Mplayer*, one of real-time processes. Each subject performed the experiments twice in the environments: Linux kernel 2.4.25 and the environment where the proposed method is applied. When the subjects typed the sentences, we ran 10 batch processes in background to overload the CPU.

For the user model, in the experiments, we designed three models for each class. We set the user's preference values, (ω_{batch}, ω_{inter}, ω_{rt}) = (0.7, 0.15, 0.15) for batch process user group, (0.15, 0.7, 0.15) for interactive process user group and (0.15, 0.15, 0.7) for real-time process user group.

While the subjects typing sentences, we saved the logs of each process in order to analyze the difference between normal Linux kernel and the proposed method, and after typing twice, the subjects evaluated the processes of their group about how good the proposed method was compared with the normal Linux kernel (1~5 points: 1 denotes bad while 5 denotes good); the batch user evaluated only the batch processes, the interactive user evaluated only the interactive process, *gedit*, and the real-time user evaluated only the real-time process, *Mplayer*.

Fig. 8 shows the result of user evaluation. The batch users gave 3.1 points in average which are lower than the other groups, and the interactive users gave 4.1 points which means they think the proposed method is better than normal method, and the real-time users gave 4.7 points which denotes that the proposed one is much better than normal one. The batch users gave low scores because the differences in batch processes are not able to confirm the performance intuitively by humans.

Fig. 9(a) shows the number of CPU occupations per unit time and Fig. 9(b) represents the CPU usage per unit time. Although the batch user group had less CPU occupation on batch processes than normal group (see Fig. 9(a)), it used 133.52 CPU

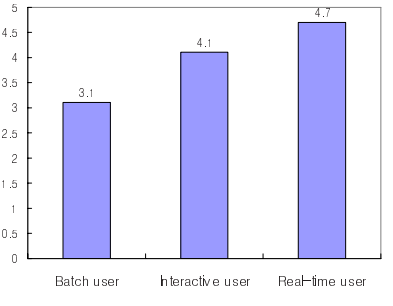

Fig. 8. The result of user evaluation

time which was more than that of normal method which used 105.2 (see Fig. 9(b)). From this result, we can confirm that the proposed method has better performance on batch processes than normal method. However, the real-time user group used up 175.44 CPU time on batch processes which was more than batch user group. The real-time user group had much lower CPU occupation than the other user groups (see Fig. 9(a)). Therefore, there were lower overhead on saving logs that gave more CPU time to the running processes compared with the other groups.

Interactive user group has the most CPU time (0.32) on interactive processes compared with other groups and the second place of the CPU occupation (43.8), next to the real-time user group (47.97). Even though the interactive user group has more CPU time and occupations number than normal method, it does not explain sufficiently because interactive processes do not need much computational power and the CPU occupation depends on the speed of subject's typing. However, through user evaluation test (see Fig. 8), we can verify the proposed method of interactive user group is better on interactive processes.

In Fig. 9(a), the real-time user group has the highest CPU occupation on real-time processes (176.92). This denotes the real-time processes can get enough CPU time when it needs computation, so the number of broken images is less than that of normal method. The result of user evaluation also verifies the performance of real-time user group.

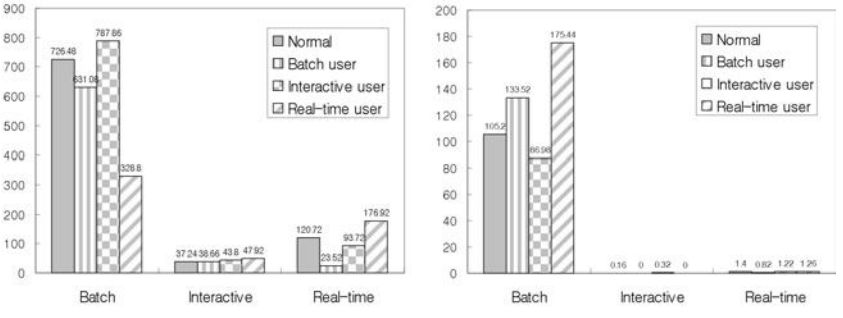

(a) No. of CPU occupations per unit time (b) CPU usage per unit time

Fig. 9. Experimental results

5 Concluding Remarks

In this paper, we have proposed a user adaptive process scheduling method using fuzzy inference. It classifies each process to batch process, interactive process and real-time process with extracted logs of processes, and it models the preferences of users. Finally it determines the *nice* value, the priority of the process, with the information of classifying processes and user preferences.

Compared with the conventional scheduling methods, the proposed method has three benefits. First, it can schedule processes according to the type of processes by classifying processes into three classes. Second, it provides adaptive scheduling method by modeling the user's preference. Third, it can provide different scheduling

method to multi users without resetting operating systems. Although there is an overload to feedback when users log out, this is easier and simpler than compiling kernels to apply other scheduling methods. Moreover, the proposed method can support different scheduling methods to different users.

Acknowledgments

This research was supported by MIC, Korea under ITRC IITA-2006-(C1090-0603-0046).

References

1. Coulson, G., Blair, G.S., Grace, P.: On the performance of reflective systems software. In: Proc. Intl. Workshop on MP2004, Satellite workshop of the IEEE IPCCC2004 (2004)
2. Fassino, J.P., Stefani, J.B., Lawall, J., Muller, G.: THINK: A software framework for component-based operating system kernels. In: USENIX Annual Technical Conference (2002)
3. Bovet, D.P., Cesati, M.: Understanding the Linux Kernel. O'REILLY (2003)
4. Nieh, J., Vaill, C., Zhong, H.: Virtual-Time Round-Robin: An O(1) proportional share scheduler. In: USENIX Annual Technical Conference, pp. 245–260 (2001)
5. Stallings, W.: Operating Systems, Internals and Design Principles. Prentice Hall, Englewood Cliffs (2001)
6. Yavatkar, R., Lakshman, K.: A CPU scheduling algorithm for continuous media applications. In: Little, T.D.C., Gusella, R. (eds.) NOSSDAV 1995. LNCS, vol. 1018, pp. 210–213. Springer, Heidelberg (1995)
7. Nieh, J., Lam, M.S.: The design, implementation and evaluation of SMART: A scheduler for multimedia applications. In: Proc. of 16th ACM symposium on operating systems principles, pp. 184–197 (1997)
8. Bollella, G., Jeffay, K.: Support for real-time computing within general purpose operating systems. In: Proc. Of the Real-Time Technology and Applications Symposium, pp. 4–14 (1995)
9. Jones, M., Rosu, D., Rosu, M.: CPU reservations and time constraints: Efficient, predictable scheduling of independent activities. In: Proc. Of the 16th Symposium on Operating Systems Principles, pp. 198–211 (1997)
10. Duda, K., Cheriton, D.: Borrowed-virtual-time (BVT) scheduling: Supporting latency-sensitive threads in a general-purpose scheduler. In: Proc. Of the 17th Symposium on Operating Systems Principles, pp. 261–276 (1999)
11. Evans, S., Clarke, K., Singleton, D., Smaalders, B.: Optimizing Unix resource scheduling for user interaction. USENIX Summer, pp. 205–218 (1993)
12. Setnes, M., Roubos, H.: GA-fuzzy modeling and classification: Complexity and performance. IEEE Trans. on Fuzzy Systems 8(5), 509–522 (2000)
13. Wu, H., Mendel, J.M.: Binary classification of ground vehicles based on the acoustic data using fuzzy logic rule-based classifiers. Technical Report 356, USC-SIPI (2002)
14. Roubos, J.A., Setnes, M., Abonyi, J.: Learning fuzzy classification rules from data. In: RASC conference (2000)

Cardinality-Based Fuzzy Time Series for Forecasting Enrollments

Jing-Rong Chang[1], Ya-Ting Lee[2], Shu-Ying Liao[2], and Ching-Hsue Cheng[2]

[1] Department of Information Management, Chaoyang University of Technology, 168, Jifong East Road, Wufong Township Taichung County 41349, Taiwan
chrischang@cyut.edu.tw
[2] Department of Information Management, National Yunlin University of Science and Technology, 123, Section 3, University Road, Touliu, Yunlin 640, Taiwan
{g9323707,g9023706,chcheng}@yuntech.edu.tw

Abstract. Forecasting activities are frequent and widespread in our life. Since Song and Chissom proposed the fuzzy time series in 1993, many previous studies have proposed variant fuzzy time series models to deal with uncertain and vague data. A drawback of these models is that they do not consider appropriately the weights of fuzzy relations. This paper proposes a new method to build weighted fuzzy rules by computing cardinality of each fuzzy relation to solve above problems. The proposed method is able to build the weighted fuzzy rules based on concept of large itemsets of Apriori. The yearly data on enrollments at the University of Alabama are adopted to verify and evaluate the performance of the proposed method. The forecasting accuracies of the proposed method are better than other methods.

Keywords: Fuzzy time series, Association rule, Weighted fuzzy rules, Forecasting.

1 Introduction

Forecasting is not only frequent activities but also an important role in our life. The traditional time series methods can predict sequential problems, but fail to deal with the problem with linguistic historical data. In 1993, Song and Chissom [6, 7] proposed the theory of fuzzy time series to solve the restrictions of the traditional time series methods.

Recently, many researchers [1, 2, 4, 8] presented their fuzzy time series methods to deal with the forecasting problems. They usually partitioned the universe of discourse into several intervals with equal length and utilized the triangular fuzzy number to fuzzify historical data. However, there is an issue of these methods is that they do not consider assigning weight to fuzzy relations. In order to solve the problem, this paper proposes a new method to calculate feasible weights for fuzzy relations, and develops step-by-step forecasting procedures to present new fuzzy time series method. Moreover, the proposed method is able to build the multiple periods weighted fuzzy rules based on concept of large itemsets of Apriori [3].

H.G. Okuno and M. Ali (Eds.): IEA/AIE 2007, LNAI 4570, pp. 735–744, 2007.

In this paper, the yearly data on enrollments at the University of Alabama is used to illustrate the steps of proposed method and utilize to evaluate the performance of proposed method. The forecasting accuracies of the proposed method are compared with other fuzzy time series methods.

2 Fuzzy Time Series

Based on Zadeh's works [9-12], Song and Chissom [6] first proposed a forecasting model called Fuzzy Time Series, which provided a theoretic framework to model a special dynamic process whose observations are linguistic values. The main difference between the traditional time series and fuzzy time series is that the observed values of the former are real numbers while the latter are fuzzy sets or linguistic values. In the following, some basic concepts of fuzzy time series are briefly reviewed [7].

Definition 1. Fuzzy time series: assume that $Y(t)(t=\ldots,0,1,2,\ldots)$, is a subset of R. Let $Y(t)$ be the universe of discourse defined by fuzzy set $f_i(t)$. If $F(t)$ consists of $f_i(t)(i=1,2,\ldots)$, $F(t)$ is defined as a fuzzy time series on $Y(t)(t=\ldots,0,1,2,\ldots)$.

Definition 2. Fuzzy time series relationship: if there is a fuzzy relationship $R(t-1,t)$, such that $F(t)=F(t-1)\times R(t-1,t)$. Where $\times$ represents an operator, then $F(t)$ is said to be caused by $F(t-1)$. (Note that the operator can be another arithmetic operator.)

When $F(t-1)=A_i$ and $F(t)=A_j$, the relationship between $F(t-1)$ and $F(t)$ (called a fuzzy logical relationship (FLR)) is denoted by $A_i \rightarrow A_j$ where A_i is called the left-hand side (LHS) and A_j the right-hand side (RHS) of the FLR.

3 Cardinality-Based Fuzzy Time Series

3.1 Data Fuzzification by MCPDA

The universe of discourse can be partitioned by mean and standard deviation (μ and σ) of the data. The cumulative probability of normal distribution is used to determine the intervals. The procedure of modified cumulative probability distribution approach (MCPDA) is as follows:

Step 1. To define the universe of discourse *U*.
Let $U=[D_{\min}-\sigma, D_{mzx}+\sigma]$, where $D_{\min}$, $D_{\max}$ and σ are the minimum value, the maximum value, and the standard deviation of the training data, respectively. Moreover, you can use more than one σ to make the universe of discourse more flexible.

Step 2. To determine the length of intervals and build membership function.
The universe of discourse is partitioned into several intervals based on cumulative probability distribution. The lower bound cumulative probability

(denoted as PLB) and upper bound cumulative probability (denoted as PUB) of each linguistic value are computed by

$$P_{LB} = (2i-3)/2m, \quad (2 \le i \le m) \tag{1}$$

$$P_{UB} = i/m, \quad (1 \le i \le m) \tag{2}$$

where i denotes the order of the linguistic values, and m denotes the total number of linguistic values, respectively.

The inverse of the normal cumulative distribution function (CDF) is computed with parameters μ and σ at the corresponding probabilities in P, where μ and σ denote the mean and standard deviation of the data, respectively. The normal inverse function in terms of the normal CDF is defined as

$$x = F^{-1}(p \mid \mu, \sigma) = \{x : F(x \mid \mu, \sigma) = p\} \tag{3}$$

where $p = F(x \mid \mu, \sigma) = \frac{1}{\sigma\sqrt{2\Pi}} \int_{-\infty^e}^{x} \frac{-(t-\mu)^2}{2\sigma^2} \; dt$

The lower bound, midpoint, and upper bound as the triangular fuzzy number of each linguistic value can be computed according to the inverse of normal CDF. In this paper, the membership values of the first and last linguistic value are modified. Fig. 1(a) is traditionally membership function, and the modified membership function such as Fig. 1(b) is more reasonable.

Step 3. To fuzzify the historical data.

If the data meets two membership functions, the max membership value is chosen and linguistic value is determined.

In order to make the calculation about cardinality of fuzzy relations more reasonable, this paper modified the first and last membership functions, as Fig. 1(b). Therefore, if data is greater than the midpoint of last linguistic or lower than the midpoint of first linguistic, then this data is assigned to last or first linguistic, and the membership value is assigned 1.

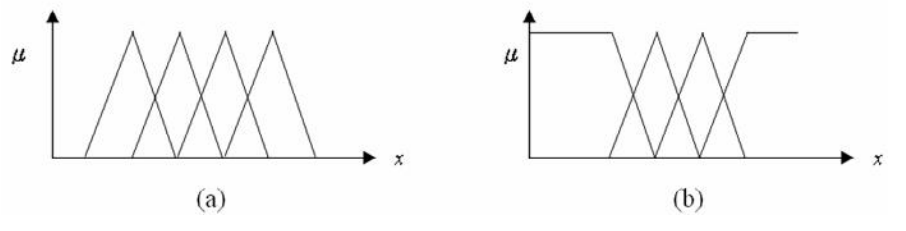

Fig. 1. Difference of membership functions

3.2 Building Cardinality-Based Fuzzy Rules and Forecasting

This section introduces the algorithm of building weighted fuzzy rules and forecasting. The steps of the weighted fuzzy rules are described as following.

Step 1. To find all one period fuzzy relations from the training data.
The one period fuzzy relations can be extracted from the historical data (i.e. training data). The one period fuzzy relation can be defined as:

$$\begin{aligned}
&\left(L_i^{o_1}, \mu\left(L_i^{o_1}\right)\right) \rightarrow \left(L_j^{o_1+1}, \mu\left(L_j^{o_1+1}\right)\right) \\
&\left(L_i^{o_2}, \mu\left(L_i^{o_2}\right)\right) \rightarrow \left(L_j^{o_2+1}, \mu\left(L_j^{o_2+1}\right)\right) \\
&\qquad\vdots \\
&\left(L_i^{o_v}, \mu\left(L_i^{o_v}\right)\right) \rightarrow \left(L_j^{o_v+1}, \mu\left(L_j^{o_v+1}\right)\right) \\
&\qquad\vdots \\
&\left(L_m^{o_n}, \mu\left(L_m^{o_n}\right)\right) \rightarrow \left(L_j^{o_n+1}, \mu\left(L_j^{o_n+1}\right)\right),
\end{aligned} \tag{4}$$

where $1 \le i \le m$, $1 \le j \le m$, $1 \le v \le n$, m denotes the total number of linguistic values, n denotes the total occurrence times of the same relation. o_v denotes v times for occurrence of the same relation. $L_i^{o_1}$ denotes the antecedent of the rule $L_i \rightarrow L_j$ for first time occurrence, and $L_j^{o_1+1}$ denotes the next linguistic value of $L_i^{o_1}$. In this paper, L_i and L_j represent the linguistic values of antecedent and consequent part for relational rules, respectively.

Step 2. To calculate the cardinality of each fuzzy relation.
First, the general equation is derived to calculate the cardinality of k-th periods fuzzy relation (by equation (5)), and when k = 1, the cardinality of each one period fuzzy relation can be computed. The cardinality of k periods fuzzy relation could be defined as:

$$W\left(L_i^{o_s-k+1}, \ldots, L_i^{o_s-1}, L_i^{t_s}, L_j^{o_s+1}\right) = \sum_{p=1}^{n} \min\left(\mu\left(L_i^{o_p-k+1}\right), \ldots, \mu\left(L_i^{o_p-1}\right), \mu\left(L_i^{o_p}\right), \mu\left(L_j^{o_p+1}\right)\right) \tag{5}$$

where n denotes the total number of the same fuzzy relations, k denotes k-th periods fuzzy relation, and s denotes sth relation, respectively.

Step 3. To compute the confidence of each fuzzy relation, and select the one period fuzzy rules. The confidence of each fuzzy relation is computed as:

$$C_{L_i \rightarrow L_j} = W\left(L_i \rightarrow L_j\right) \Big/ \sum_{k=1}^{n(L)} W\left(L_i \rightarrow L_k\right) \tag{6}$$

where $C_{L_i \rightarrow L_j}$ denotes the confidence of fuzzy rule $L_i \rightarrow L_j$, and $n(L)$ denotes the number of linguistic values. Threshold value for confidence (denoted as α) can be assigned by user. And then, the one period fuzzy rules are selected whose weights are greater than α

Step 4. To forecast data based on selecting fuzzy rules from Step 3.
From one period fuzzy rules, if $L(t) = L_i^{t_s}$, then the fuzzy rules, which antecedent equals $L_i^{t_s}$, are judged as fitting fuzzy rules, where $L(t)$ denotes the previous

linguistic value of forecasted value. The one period forecasting value can be calculated by equation (7)

$$F(t+1)=\frac{\sum_{p=1}^{n_1} W^{p}_{\left(L_i^{o_s}, L_j^{o_s+1}\right)} * D(L_j)}{\sum_{p=1}^{n_1} W^{p}_{\left(L_i^{o_s}, L_j^{o_s+1}\right)}} \tag{7}$$

where $F(t+1)$ denotes forecasted value, n_1 denotes the total number of one period fitting fuzzy rules, and W is the weight of fitting fuzzy rule. $D(L_j)$ is defuzzified value and determined by consequent of the fitted fuzzy rule (by equation (8)).

$$D(L_j)=\frac{a_{L_j}+b_{L_j}+c_{L_j}}{3} \tag{8}$$

where a_{L_j}, b_{L_j}, and c_{L_j} denote the lower bound, upper bound, and midpoint of interval of L_j, respectively.

4 Experiments and Comparison

In this section, the yearly data on enrollments at the University of Alabama is selected to illustrate and verify the proposed method.

4.1 Enrollments Data Fuzzification by MCPDA

There are 22 observations, and two attributes that year and enrollments, as listed in Table 1. $U=[11280, 21112]$ is obtained because the minimum enrollment, the maximum

Table 1. The yearly enrollments of the University of Alabama [1, 2, 7]

Year	Enrollments	Year	Enrollments
1971	13055	1982	15433
1972	13563	1983	15497
1973	13867	1984	15145
1974	14696	1985	15163
1975	15460	1986	15984
1976	15311	1987	16859
1977	15603	1988	18150
1978	15861	1989	18970
1979	16807	1990	19328
1980	16919	1991	19337
1981	16388	1992	18876

Table 2. Linguistic values and intervals of Alabama dataset by MCPDA

Linguistic value	Lower bound cumulative probability	Upper bound cumulative probability	Lower bound	Midpoint	Upper bound
L_1 (very very few)	—*	0.1429	11280	12790	14300
L_2 (very few)	0.0714	0.2857	13594	14392	15190
L_3 (few)	0.2143	0.4286	14789	15332	15875
L_4 (moderate)	0.3571	0.5714	15544	16029	16514
L_5 (many)	0.5000	0.7143	16194	16696	17199
L_6 (very many)	0.6429	0.8571	16844	17466	18089
L_7 (too many)	0.7857	—*	17599	19356	21112

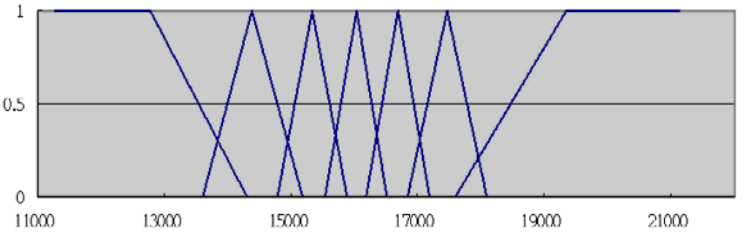

Fig. 2. Difference of membership functions

Table 3. Linguistic value of each year on Alabama

Year	Enrollments	Linguistic value	Year	Enrollments	Linguistic value
1971	13055	L_1	1982	15433	L_3
1972	13563	L_1	1983	15497	L_3
1973	13867	L_2	1984	15145	L_3
1974	14696	L_2	1985	15163	L_3
1975	15460	L_3	1986	15984	L_4
1976	15311	L_3	1987	16859	L_5
1977	15603	L_3	1988	18150	L_7
1978	15861	L_4	1989	18970	L_7
1979	16807	L_5	1990	19328	L_7
1980	16919	L_5	1991	19337	L_7
1981	16388	L_5	1992	18876	L_7

Table 4. One period fuzzy relations of the yearly enrollments

Relation No.	One period fuzzy relations	Relation No.	One period fuzzy relations
1	$(L_1, 0.82440) \rightarrow (L_1, 0.48789)$	12	$(L_3, 0.81386) \rightarrow (L_3, 0.69594)$
2	$(L_1, 0.48789) \rightarrow (L_2, 0.34237)$	13	$(L_3, 0.69594) \rightarrow (L_3, 0.65549)$
3	$(L_2, 0.34237) \rightarrow (L_2, 0.61878)$	14	$(L_3, 0.65549) \rightarrow (L_3, 0.68866)$
4	$(L_2, 0.61878) \rightarrow (L_3, 0.76411)$	15	$(L_3, 0.68866) \rightarrow (L_4, 0.90704)$
5	$(L_3, 0.76411) \rightarrow (L_3, 0.96135)$	16	$(L_4, 0.90704) \rightarrow (L_5, 0.67619)$
6	$(L_3, 0.96135) \rightarrow (L_3, 0.50063)$	17	$(L_5, 0.67619) \rightarrow (L_7, 0.31366)$
7	$(L_3, 0.50063) \rightarrow (L_4, 0.65323)$	18	$(L_7, 0.31366) \rightarrow (L_7, 0.78055)$
8	$(L_4, 0.65323) \rightarrow (L_5, 0.77974)$	19	$(L_7, 0.78055) \rightarrow (L_7, 0.98439)$
9	$(L_5, 0.77974) \rightarrow (L_5, 0.55672)$	20	$(L_7, 0.98439) \rightarrow (L_7, 0.98951)$
10	$(L_5, 0.55672) \rightarrow (L_5, 0.38594)$	21	$(L_7, 0.98951) \rightarrow (L_7, 0.72703)$
11	$(L_5, 0.38594) \rightarrow (L_3, 0.81386)$		

enrollment and the standard deviation are 13055, 19337 and 1775, respectively. Base on the concepts of Miller [5], this paper defines seven linguistic values to have better identity (From L_1 to L_7 which are assigned from "very very few" to "too many", such as Table 2). Then, the membership function is built, as shown in Fig. 2.

4.2 The Cardinality-Based Fuzzy Rules and Forecasting for Enrollments Data

On data fuzzification, the enrollment in 1973 is 13867, and this data meets two membership functions L_1 and L_2. The maximum membership value is chosen, so the linguistic value of 1973 is L_2 and the membership value is 0.34237. The linguistic value of each year is shown in Table 3. Then, according to Step 1 in Section 3.1, all one period fuzzy relations are found from Table 3, shown as Table 4.

The cardinalities of one period fuzzy relations are computed, by Section 3.2's Step 2, and shown in Table 5. For example, relation $L_3 \rightarrow L_3$ consists of one period fuzzy relations {5, 6 12, 13, 14} from Table 4. Then, cardinality of $L_3 \rightarrow L_3$ is computed by equation (5) as

$$W(L_3, L_3) = \min(0.76411, 0.96135) + \min(0.96135, 0.50063) + \min(0.81386, 0.69594) + \min(0.69594, 0.65549) + \min(0.65549, 0.68866) = 3.27167$$

The confidence of each fuzzy relation is obtained by equation (6) as listed in Table 6. For example, the confidence of $L_1 \rightarrow L_1$ is computed as follows:

$$C_{L_1 \rightarrow L_1} = \frac{0.48789}{0.48789 + 0.34237} = 0.5876$$

If we want to forecast the enrollment of 1972 by one period fuzzy rules, one period fuzzy rules {1, 2} are selected to forecast. According to equation (7), we would calculate the forecasted value as following

$$F(t+1) = \frac{0.48789 * \frac{11280 + 12790 + 14300}{3} + 0.34237 * \frac{13594 + 14392 + 15190}{3}}{0.48789 + 0.34237} = 13450$$

Table 5. Weights of one period fuzzy relations

One period fuzzy relations	Weight	Relation No.	One period fuzzy relations	Weight	Relation No.
$L_1 \to L_1$	0.48789	{1}	$L_4 \to L_5$	1.32942	{8, 16}
$L_1 \to L_2$	0.34237	{2}	$L_5 \to L_5$	0.94266	{9, 10}
$L_2 \to L_2$	0.34237	{3}	$L_5 \to L_3$	0.38594	{11}
$L_2 \to L_3$	0.61878	{4}	$L_5 \to L_7$	0.31366	{17}
$L_3 \to L_3$	3.27167	{5, 6, 12, 13, 14}	$L_7 \to L_7$	2.80562	{18, 19, 20, 21}
$L_3 \to L_4$	1.18929	{7, 15}			

Table 6. One period fuzzy rules with confidence

Rule No.	One period fuzzy rules	Weight	Confidence
1	$L_1 \to L_1$	0.48789	0.587638
2	$L_1 \to L_2$	0.34237	0.412362
3	$L_2 \to L_2$	0.34237	0.356209
4	$L_2 \to L_3$	0.61878	0.643791
5	$L_3 \to L_3$	3.27167	0.733400
6	$L_4 \to L_5$	1.32942	1.000000
7	$L_5 \to L_5$	0.94266	0.574003
8	$L_7 \to L_7$	2.80562	1.000000

4.3 Comparison with Previous Works

Previous studies on fuzzy time series often use the yearly data on enrollments at the University of Alabama to evaluate their models. The forecast accuracy is compared by average absolute error percentage and mean square error (MSE). The MSE is computed by

$$MSE = \frac{\sum_{i=1}^{n} \left(Forecasted\ Enrollment_i - Actual\ Enrollment_i \right)^2}{n} \tag{9}$$

where n denotes total number of forecasted records.

Forecasting results are compared with other fuzzy time series methods, as Table 7. It shows the proposed method gets higher forecasting accuracy than other methods in the yearly data on enrollments at the University of Alabama. Besides, the MSE value of proposed method is larger than TFA [2], which is because there are several forecasting values have higher deviation with original data. After some advanced experiments, the suggested threshold value for confidence (α) is [0.3,0.5] or by calculating the percentages of confidence for fuzzy relations.

Table 7. Comparison of forecasting accuracy

Methods	Average absolute error (%)	MSE
Song and Chissom [7]	3.22 %	423,027
Chen [1]	3.11 %	407,507
TFA [2]	2.66 %	261,142
MEPA [2]	2.75%	446,762
Proposed method	2.26 %	268,225

5 Conclusions

This paper proposes a cardinality-based fuzzy time series model. This model contains a more objective and reasonable approach for data fuzzification called modified cumulative probability distribution approach (MCPDA), and a more theoretical based method for building weighted fuzzy rules according to calculating the cardinality of fuzzy relations. The weight of each fuzzy rule is more reasonable than previous studies because it is given by calculating cardinality of the membership value with the same fuzzy relations. Experiment results of the enrollment of Alabama show that the proposed method outperforms than conventional methods. The future directions of this paper are: (1) the applications of proposed model in some other data sets; (2) the development of multiple periods fuzzy time series.

References

1. Chen, S.M.: Forecasting enrollments based on fuzzy time series. Fuzzy sets and systems 81, 311–319 (1996)
2. Cheng, C.-H., Chang, J.-R., Yeh, C.-A.: Entropy-based and Trapezoid Fuzzification-based Fuzzy time series approaches for forecasting IT project cost. Technological Forecasting and Social Change 73(5), 524–542 (2006)
3. Han, J., Kamber, M.: Data Mining: Concepts and Techniques. Morgan Kaufmann, San Francisco (2001)
4. Huarng, K.: Effective lengths of intervals to improve forecasting in fuzzy time series. Fuzzy Sets and Systems 123, 387–394 (2001)
5. Miller, G.A.: The magical number seven, plus or minus two: some limits on our capacity of processing information. The Psychological Review 63, 81–97 (1956)
6. Song, Q., Chissom, B.S.: Fuzzy time series and its models. Fuzzy Sets and Systems 54, 269–277 (1993)

7. Song, Q., Chissom, B.S.: Forecasting enrollments with fuzzy time series — Part I. Fuzzy sets and systems 54, 1–10 (1993)
8. Yu, H.K.: Weighted fuzzy time series models for TAIEX forecasting. Physica A 349, 609–624 (2005)
9. Zadeh, L.A.: Fuzzy Sets. Information and Control 8, 338–353 (1965)
10. Zadeh, L.A.: The concept of a linguistic variable and its application to approximate reasoning (I). Information Science 8, 199–249 (1975)
11. Zadeh, L.A.: The concept of a linguistic variable and its application to approximate reasoning (II). Information Science 8, 301–357 (1975)
12. Zadeh, L.A.: The concept of a linguistic variable and its application to approximate reasoning (III). Information Science 9, 43–80 (1976)

A New Fuzzy Interpolative Reasoning Method for Sparse Fuzzy Rule-Based Systems

Li-Wei Lee and Shyi-Ming Chen

Department of Computer Science and Information Engineering
National Taiwan University of Science and Technology
Taipei, Taiwan, R.O.C.
smchen@mail.ntust.edu.tw

Abstract. Fuzzy interpolative reasoning is an important research topic of sparse fuzzy rule-based systems. In recent years, some methods have been presented for dealing with fuzzy interpolative reasoning. However, the involving fuzzy sets appearing in the antecedents of fuzzy rules of the existing fuzzy interpolative reasoning methods must be normal and non-overlapping. Moreover, the reasoning conclusions of the existing fuzzy interpolative reasoning methods sometimes become abnormal fuzzy sets. In this paper, in order to overcome the drawbacks of the existing fuzzy interpolative reasoning methods, we present a new fuzzy interpolative reasoning method for sparse fuzzy rule-based systems. The proposed fuzzy interpolative reasoning method can handle the situation of non-normal and overlapping fuzzy sets appearing in the antecedents of fuzzy rules. It can overcome the drawbacks of the existing fuzzy interpolative reasoning methods in sparse fuzzy rule-based systems.

Keywords: Fuzzy interpolative reasoning, ranking values, ranking interpolative proportional coefficients.

1 Introduction

It is obvious that fuzzy interpolative reasoning is an important research topic of sparse fuzzy rule-based systems. "Fuzzy rule interpolation" is an important technique in sparse fuzzy rule-based systems, where some fuzzy rules can be derived through their neighbor fuzzy rules to reduce the complexity of fuzzy rule bases by using the fuzzy interpolative reasoning methods. In recent years, some methods have been presented for dealing with fuzzy interpolative reasoning in sparse fuzzy rule-based systems [1]-[10], [13]-[16].

However, the involving fuzzy sets appearing in the antecedents of fuzzy rules of the existing fuzzy interpolative reasoning methods must be normal and non-overlapping. Moreover, the reasoning conclusions of the existing fuzzy interpolative reasoning methods sometimes become abnormal fuzzy sets. In this paper, in order to overcome the drawbacks of the existing fuzzy interpolative reasoning methods, we present a new fuzzy interpolative reasoning method for sparse fuzzy rule-based systems. It can handle the situation of non-normal and overlapping antecedent fuzzy sets of fuzzy rules. It can overcome the drawbacks of the existing fuzzy interpolative

H.G. Okuno and M. Ali (Eds.): IEA/AIE 2007, LNAI 4570, pp. 745–755, 2007.

reasoning methods to deal with fuzzy interpolative reasoning in sparse fuzzy rule-based systems.

The rest of this paper is organized as follows. In Section 2, we present a new method for fuzzy interpolative reasoning in sparse fuzzy rule-based systems. In Section 3, we use some examples to compare the fuzzy interpolative reasoning results of the proposed method with the existing methods. The conclusions are discussion in Section 4.

2 A New Fuzzy Interpolative Reasoning Method for Sparse Fuzzy Rule-Based Systems

In this section, we present a new fuzzy interpolative reasoning method for sparse fuzzy rule-based systems. Let A_1, A_2, …, and A_n be a set of trapezoidal fuzzy sets. A trapezoidal fuzzy set A_i can be defined as $A_i = (a_{i1}, a_{i2}, a_{i3}, a_{i4}; L_{iH}, R_{iH})$, as shown in Fig. 1 [11], where a_{i1} and a_{i2} are called the left elements of the fuzzy set A_i, a_{i2} and a_{i3} are called the middle elements of the fuzzy set A_i, a_{i3} and a_{i4} are called the right elements of the fuzzy set A_i, L_{iH} and R_{iH} are called the left height and the right height of fuzzy set A_i, respectively, $L_{iH} \in [0,1]$, $R_{iM} \in [0,1]$, and $1 \le i \le n$. Let L_{iM} denote the average of the left elements a_{i1} and a_{i2} (i.e., $L_{iM} = (a_{i1} + a_{i2})/2$), M_{iM} denote the average of the middle elements a_{i2} and a_{i3} (i.e., $M_{iM} = (a_{i2} + a_{i3})/2$), R_{iM} denote the average of the right elements a_{i3} and a_{i4} (i.e., $R_{iM} = (a_{i3} + a_{i4})/2$), L_{iS} denote the standard deviation of the left elements a_{i1} and a_{i2} (i.e., $L_{iS} = \sqrt{\frac{1}{2}\sum_{j=1}^{2}(a_{ij} - \frac{1}{2}\sum_{j=1}^{2}a_{ij})^2}$), M_{iS} denote the standard deviation of the middle elements a_{i2} and a_{i3} (i.e., $M_{iS} = \sqrt{\frac{1}{2}\sum_{j=2}^{3}(a_{ij} - \frac{1}{2}\sum_{j=2}^{3}a_{ij})^2}$), and R_{iS} denote the standard deviation of the right elements a_{i3} and a_{i4} (i.e., $R_{iS} = \sqrt{\frac{1}{2}\sum_{j=3}^{4}(a_{ij} - \frac{1}{2}\sum_{j=3}^{4}a_{ij})^2}$), where $1 \le i \le n$. If $a_{i2} = a_{i3}$, then A_i is called a triangular fuzzy set, as shown in Fig. 2, where $1 \le i \le n$. In this situation, the triangular fuzzy set shown in Fig. 2 also can be represented by $A_i = (a_{i1}, a_{i2}, a_{i4;} L_{iH}) = (a_{i1}, a_{i3}, a_{i4;} L_{iH}) = (a_{i1}, a_{i2}, a_{i4;} R_{iH}) = (a_{i1}, a_{i3}, a_{i4;} R_{iH})$, where $L_{iH} = R_{iH}$ and $1 \le i \le n$. It is obvious that a crisp value x can be represented by a trapezoidal fuzzy set $A_i = (x, x, x, x; L_{iH}, R_{iH})$, where $L_{iH} = R_{iH}$, $L_{iH} \in [0, 1]$, $R_{iH} \in [0,1]$, and $1 \le i \le n$. A crisp value x also can be represented by a triangular fuzzy set $A_i = (x, x, x; L_{iH})$ or $(x, x, x; R_{iH})$, where $L_{iH} = R_{iH}$, $L_{iH} \in [0,1]$, $R_{iH} \in [0,1]$, and $1 \le i \le n$.

Let A_1, A_2, …, and A_n be a set of hexagonal fuzzy sets. A hexagonal fuzzy sets A_i can be represented as $A_i = (a_{i1}, a_{i2}, a_{i3}, a_{i4}, a_{i5}, a_{i6;} L_{iH}, LM_{iH}, RM_{iH}, R_{iH})$, as shown in Fig. 3, where a_{i1} and a_{i2} are called the left elements of the fuzzy set A_i, a_{i2} and a_{i3} are called the left-middle elements of the fuzzy set A_i, a_{i3} and a_{i4} are called the middle

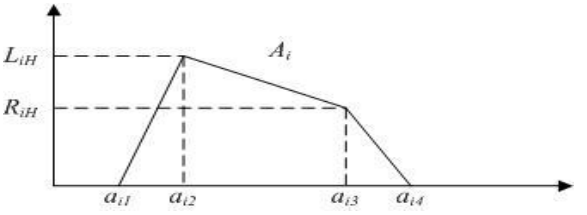

Fig. 1. A trapezoidal fuzzy set

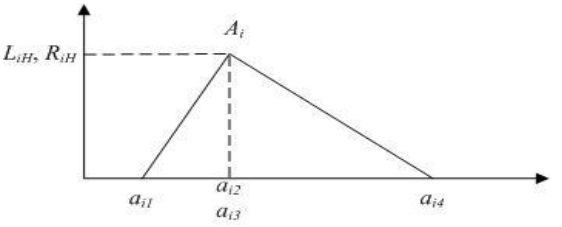

Fig. 2. A triangular fuzzy set

elements of the fuzzy set A_i, a_{i4} and a_{i5} are called the right-middle elements of the fuzzy set A_i, a_{i5} and a_{i6} are called the right elements of the fuzzy set A_i, L_{iH}, LM_{iH}, RM_{iH} and R_{iH} are called the left height, the left-middle height, the right-middle height and the right height of fuzzy set A_i, respectively, $L_{iH} \in [0,1]$, $LM_{iH} \in [0,1]$, $RM_{iH} \in [0,1]$, $R_{iH} \in [0,1]$, and $1 \le i \le n$. Let L_{iM} denote the average of the left elements a_{i1} and a_{i2} (i.e., $L_{iM} = (a_{i1} + a_{i2})/2$), LM_{iM} denote the average of the left-middle elements a_{i2} and a_{i3} (i.e., $LM_{iM} = (a_{i2} + a_{i3})/2$), M_{iM} denote the average of the middle elements a_{i3} and a_{i4} (i.e., $M_{iM} = (a_{i3} + a_{i4})/2$), RM_{iM} denote the average of the right-middle elements a_{i4} and a_{i5} (i.e., $RM_{iM} = (a_{i4} + a_{i5})/2$), R_{iM} denote the average of the right elements a_{i5} and a_{i6} (i.e., $R_{iM} = (a_{i5} + a_{i6})/2$), L_{iS} denote the standard deviation of the left elements a_{i1} and a_{i2} (i.e., $L_{iS} = \sqrt{\frac{1}{2}\sum_{j=1}^{2}(a_{ij} - \frac{1}{2}\sum_{j=1}^{2}a_{ij})^2}$), LM_{iS} denote the standard deviation of the left-middle elements a_{i2} and a_{i3} (i.e., $LM_{iS} = \sqrt{\frac{1}{2}\sum_{j=2}^{3}(a_{ij} - \frac{1}{2}\sum_{j=2}^{3}a_{ij})^2}$), M_{iS} denote the standard deviation of the middle elements a_{i3} and a_{i4} (i.e., $M_{iS} = \sqrt{\frac{1}{2}\sum_{j=3}^{4}(a_{ij} - \frac{1}{2}\sum_{j=3}^{4}a_{ij})^2}$), RM_{iS} denote the standard deviation of the right-middle elements a_{i4} and a_{i5} (i.e., $RM_{iS} = \sqrt{\frac{1}{2}\sum_{j=4}^{5}(a_{ij} - \frac{1}{2}\sum_{j=4}^{5}a_{ij})^2}$), R_{iS} denote the standard deviation of the right

elements a_{i5} and a_{i6} (i.e., $R_{iS} = \sqrt{\frac{1}{2}\sum_{j=5}^{6}(a_{ij} - \frac{1}{2}\sum_{j=5}^{6}a_{ij})^2}$), where $1 \le i \le n$. It is obvious that a crisp value x can be represented by a hexagonal fuzzy set $A_i = (x, x, x, x, x, x; L_{iH}, LM_{iH}, RM_{iH}, R_{iH})$, where $L_{iH} = LM_{iH} = RM_{iH} = R_{iH}$, and $1 \le i \le n$.

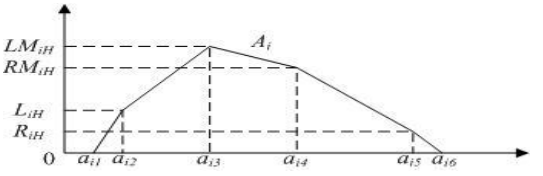

Fig. 3. A hexagonal fuzzy set

Definition 2.1: Let A_i be a trapezoidal fuzzy set, $A_i = (a_{i1}, a_{i2}, a_{i3}, a_{i4}; L_{iH}, R_{iH})$, where $1 \le i \le n$, as shown in Fig. 1. The ranking value $Rank(A_i)$ of the trapezoidal fuzzy set A_i is defined as follows:

$$Rank(A_i) = L_{iM}(A_i) + M_{iM}(A_i) + R_{iM}(A_i) - \frac{1}{3}(L_{iS}(A_i) + M_{is}(A_i) + R_{is}(A_i)) + L_{iH}(A_i) + R_{iH}(A_i), \quad (1)$$

where $1 \le i \le n$.

In Eq. (1), we take the summation of $L_{iM}(A_i)$, $M_{iM}(A_i)$, $R_{iM}(A_i)$, $L_{iH}(A_i)$ and $R_{iH}(A_i)$ and minus the average value of $L_{iS}(A_i)$, $M_{iS}(A_i)$ and $R_{iS}(A_i)$, where $1 \le i \le n$. In order to imply "the more centralized the fuzzy set, the larger the ranking value" and in order to avoid the situation that different shapes of fuzzy sets have the same ranking value, in Eq. (1), we deduct the average of $L_{is}(A_i)$, $M_{is}(A_i)$ and $R_{is}(A_i)$ form the summation of $L_{iM}(A_i)$, $M_{iM}(A_i)$, $R_{iM}(A_i)$, $L_{iH}(A_i)$ and $R_{iH}(A_i)$, where $1 \le i \le n$.

Definition 2.2: Let A_i be a hexagonal fuzzy set, $A_i = (a_{i1}, a_{i2}, a_{i3}, a_{i4}, a_{i5}, a_{i6}; L_{iH}, LM_{iH}, RM_{iH}, R_{iH})$, where $1 \le i \le n$, as shown in Fig. 3. The ranking value $Rank(A_i)$ of the hexagonal fuzzy set A_i is defined as follows:

$$\begin{aligned} Rank(A_i) = {} & L_{iM}(A_i) + LM_{iM}(A_i) + M_{iM}(A_i) + RM_{iM}(A_i) + R_{iM}(A_i) \\ & - \frac{1}{5}(L_{iS}(A_i) + LM_{iS}(A_i) + M_{is}(A_i) + RM_{iS}(A_i) + R_{is}(A_i)) \\ & + L_{iH}(A_i) + LM_{iH}(A_i) + RM_{iH}(A_i) + R_{iH}(A_i), \end{aligned} \quad (2)$$

where $1 \le i \le n$.

In Eq. (2), we take the summation of $L_{iM}(A_i)$, $LM_{iM}(A_i)$, $M_{iM}(A_i)$, $RM_{iM}(A_i)$, $R_{iM}(A_i)$, $L_{iH}(A_i)$, $LM_{iH}(A_i)$, $RM_{iH}(A_i)$ and $R_{iH}(A_i)$ and subtract the average value of $L_{iS}(A_i)$, $LM_{iS}(A_i)$, $M_{iS}(A_i)$, $RM_{iS}(A_i)$, $R_{iS}(A_i)$, where $1 \le i \le n$. In order to imply "the more centralized the fuzzy set, the larger the ranking value of the fuzzy set" and in order to avoid the situation that different shapes of fuzzy sets have the same ranking value, in Eq. (2), we deduct the average of $L_{is}(A_i)$, $LM_{is}(A_i)$, $M_i(A_i)_s$, $RM_{is}(A_i)$, and $R_{is}(A_i)$ from the summation of $L_{iM}(A_i)$, $LM_{iM}(A_i)$, $M_{iM}(A_i)$, $RM_{iM}(A_i)$, $R_{iM}(A_i)$, $L_{iH}(A_i)$, $LM_{iH}(A_i)$, $RM_{iH}(A_i)$ and $R_{iH}(A_i)$, where $1 \le i \le n$.

Definition 2.3: Let A_i and A_j be two fuzzy sets. If A_i is less than A_j (i.e., $A_i < A_j$), then $Rank(A_i) < Rank(A_j)$.

A fuzzy interpolative reasoning scheme can be described using the modus ponens model, shown as follows:

$$\begin{aligned} &\text{Observation}: X \text{ is } A^* \\ &\text{Rules}: \text{if } X \text{ is } A_1, \text{ then } Y \text{ is } B_1 \\ &\qquad\quad \text{if } X \text{ is } A_2, \text{ then } Y \text{ is } B_2 \\ &\text{Conclusion}: Y \text{ is } B^* \end{aligned}$$

where X and Y are linguistic variables, A_1, A_2, A^*, B_1, B_2 and B^* are trapezoidal fuzzy sets as shown in Fig. 4, and the following conditions must be hold:

(1) $Rank(A_1) \neq Rank(A_2), Rank(B_1) \neq Rank(B_2)$.

(2) $Rank(A^*) \in [Rank(A_1), Rank(A_2)]$.

(3) $Rank(B^*) \in [Rank(B_1), Rank(B_2)]$.

In order to perform fuzzy interpolative reasoning, we define the "ranking interpolative proportional coefficient" λ_{Rank_inter} among the fuzzy sets A_1, A^* and A_2 as follows:

$$\lambda_{Rank\_inter} = \frac{|Rank(A^*) - Rank(A_1)|}{|Rank(A_2) - Rank(A_1)|}. \tag{3}$$

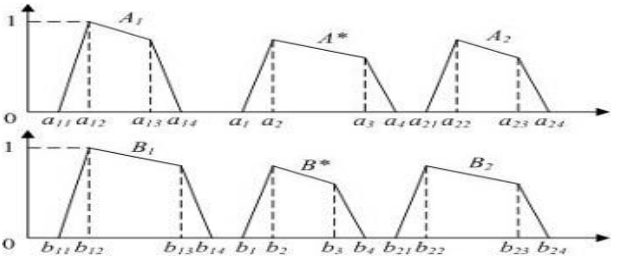

Fig. 4. Fuzzy interpolative reasoning scheme using trapezoid fuzzy sets

Assume that $A_{11}, A_{21}, ..., A_{k1} \Rightarrow B_1$ and $A_{12}, A_{22}, ..., A_{k2} \Rightarrow B_2$ are two adjacent fuzzy rules with multiple antecedent fuzzy sets, then $\lambda_{Rank\_inter} = \frac{1}{k}\sum_{i=1}^{k} \lambda_{Rank\_inter(i)}$, where k denotes the numbers of antecedent fuzzy sets of fuzzy rules and the ranking interpolative proportional coefficient $\lambda_{Rank\_inter(i)}$ among the fuzzy sets A_{i1}, A_i^* and A_{i2} is calculated as follows:

$$\lambda_{Rank\_inter(i)} = \frac{|Rank(A_i^*) - Rank(A_{i1})|}{|Rank(A_{i2}) - Rank(A_{i1})|}, \tag{4}$$

where $1 \leq i \leq n$.

Let us consider the following fuzzy interpolative reasoning scheme:

Observation : X is A^*

Rules : if X is A_1, then Y is B_1

if X is A_2, then Y is B_2

Conclusion : Y is B^*

Assume that A_1, A_2, A^*, B_1 and B_2 are triangular fuzzy sets, shown as follows:

$A_1 = (a_{11}, a_{12}, a_{13;}\ L_H(A_1)) = (a_{11}, a_{12}, a_{13;}\ R_H(A_1)) = (a_{11}, a_{12}, a_{12}, a_{13;}\ L_H(A_1), R_H(A_1))$,
$A_2 = (a_{21}, a_{22}, a_{23;}\ L_H(A_2)) = (a_{21}, a_{22}, a_{23;}\ R_H(A_2)) = (a_{21}, a_{22}, a_{22}, a_{23;}\ L_H(A_2), R_H(A_2))$,
$A^* = (a_1, a_2, a_{3;}\ L_H(A^*)) = (a_1, a_2, a_{3;}\ R_H(A^*)) = (a_1, a_2, a_2, a_{3;}\ L_H(A^*), R_H(A^*))$,
$B_1 = (b_{11}, b_{12}, b_{13;}\ L_H(B_1)) = (b_{11}, b_{12}, b_{13;}\ R_H(B_1)) = (b_{11}, b_{12}, b_{12}, b_{13;}\ L_H(B_1), R_H(B_1))$,
$B_2 = (b_{21}, b_{22}, b_{23;}\ L_H(B_2)) = (b_{21}, b_{22}, b_{23;}\ R_H(B_2)) = (b_{21}, b_{22}, b_{22}, b_{23;}\ L_H(B_2), R_H(B_2))$,

where $L_H(A_1) = R_H(A_1)$, $L_H(A_2) = R_H(A_2)$, $L_H(A^*) = R_H(A^*)$, $L_H(B_1) = R_H(B_1)$, $L_H(B_2) = R_H(B_2)$, $L_H(A_1) \in [0,1]$, $R_H(A_1) \in [0,1]$, $L_H(A_2) \in [0,1]$, $R_H(A_2) \in [0,1]$, $L_H(A^*) \in [0,1]$, $R_H(A^*) \in [0,1]$, $L_H(B_1) \in [0,1]$, $R_H(B_1) \in [0,1]$, $L_H(B_2) \in [0,1]$, $R_H(B_2) \in [0,1]$. The proposed fuzzy interpolative reasoning method for triangular fuzzy sets is now presented as follows:

Step 1: Based on Eq. (1), calculate the ranking values of the fuzzy sets A_1, A^* and A_2 appearing in the antecedents of the fuzzy rules of the fuzzy interpolative reasoning scheme, respectively.

Step 2: Based on Eqs. (3) and (4), calculate the value of the ranking interpolative proportional coefficient λ_{Rank_inter} among the fuzzy sets A_1, A^* and A_2.

Step 3: Based on the value of the ranking interpolative proportional coefficient λ_{Rank_inter} among the fuzzy sets A_1, A^* and A_2, the fuzzy interpolative reasoning conclusion B^* can be obtained, $B^* = (b_1, b_2, b_2, b_3; L_H(B^*), R_H(B^*))$, where

$$b_i = (1 - \lambda_{Rank\_inter}) \times b_{1i} + \lambda_{Rank\_inter} \times b_{2i}, \tag{5}$$

$$\begin{aligned} L_H(B^*) = R_H(B^*) &= (1 - \lambda_{Rank\_inter}) \times L_H(B_1) + \lambda_{Rank\_inter} \times L_H(B_2) \\ &= (1 - \lambda_{Rank\_inter}) \times R_H(B_1) + \lambda_{Rank\_inter} \times R_H(B_2), \end{aligned} \tag{6}$$

and $1 \le i \le 3$.

Assume that A_1, A_2, A^*, B_1 and B_2 are trapezoidal fuzzy sets, shown as follows:

$A_1 = (a_{11}, a_{12}, a_{13}, a_{14;}\ L_H(A_1), R_H(A_1))$,
$A_2 = (a_{21}, a_{22}, a_{23}, a_{24;}\ L_H(A_2), R_H(A_2))$,
$A^* = (a_1, a_2, a_3, a_{4;}\ L_H(A^*), R_H(A^*))$,
$B_1 = (b_{11}, b_{12}, b_{13}, b_{14;}\ L_H(B_1), R_H(B_1))$,
$B_2 = (b_{21}, b_{22}, b_{23}, b_{24;}\ L_H(B_2), R_H(B_2))$,

where $L_H(A_1) \in [0,1]$, $R_H(A_1) \in [0,1]$, $L_H(A_2) \in [0,1]$, $R_H(A_2) \in [0,1]$, $L_H(A^*) \in [0,1]$, $R_H(A^*) \in [0,1]$, $L_H(B_1) \in [0,1]$, $R_H(B_1) \in [0,1]$, $L_H(B_2) \in [0,1]$,

$R_H(B_2) \in [0,1]$. The proposed fuzzy interpolative reasoning method for trapezoidal fuzzy sets is now presented as follows:

Step 1: Based on Eq. (1), calculate the ranking values of fuzzy sets A_1, A^* and A_2 appearing in the antecedents of the fuzzy rules of the fuzzy interpolative reasoning scheme, respectively.
Step 2: Based on Eqs. (3) and (4), calculate the value of the ranking interpolative proportional coefficient λ_{Rank_inter} among the fuzzy sets A_1, A^* and A_2.
Step 3: Based on the value of the ranking interpolative proportional coefficient λ_{Rank_inter} among the fuzzy sets A_1, A^* and A_2, the fuzzy interpolative reasoning conclusion B^*, $B^* = (b_1, b_2, b_3, b_4; L_H(B^*), R_H(B^*))$ can be obtained, where

$$b_i = (1- \lambda_{Rank\_inter}) \times b_{1i} + \lambda_{Rank\_inter} \times b_{2i}, \tag{7}$$

$$L_H(B^*) = (1 - \lambda_{Rank\_inter}) \times L_H(B_1) + \lambda_{Rank\_inter} \times L_H(B_2), \tag{8}$$

$$R_H(B^*) = (1 - \lambda_{Rank\_inter}) \times R_H(B_1) + \lambda_{Rank\_inter} \times R_H(B_2), \tag{9}$$

and $1 \le i \le 4$.

Assume that A_1, A_2, A^*, B_1 and B_2 are hexagonal fuzzy sets, shown as follows:

$A_1 = (a_{11}, a_{12}, a_{13}, a_{14}, a_{15}, a_{16}, L_H(A_1), LM_H(A_1), RM_H(A_1), R_H(A_1))$,
$A_2 = (a_{21}, a_{22}, a_{23}, a_{24}, a_{25}, a_{26}, L_H(A_2), LM_H(A_2), RM_H(A_2), R_H(A_2))$,
$A^* = (a_1, a_2, a_3, a_4, a_5, a_6, L_H(A^*), LM_H(A^*), RM_H(A^*), R_H(A^*))$,
$B_1 = (b_{11}, b_{12}, b_{13}, b_{14}, b_{15}, b_{16}, L_H(B_1), LM_H(B_1), RM_H(A^*), R_H(B_1))$,
$B_2 = (b_{21}, b_{22}, b_{23}, b_{24}, b_{25}, b_{26}, L_H(B_2), LM_H(B_2), RM_H(B_2), R_H(B_2))$,

where $L_H(A_1) \in [0,1]$, $LM_H(A_1) \in [0,1]$, $RM_H(A_1) \in [0,1]$, $R_H(A_1) \in [0,1]$,
$L_H(A_2) \in [0,1]$, $LM_H(A_2) \in [0,1]$, $RM_H(A_2) \in [0,1]$, $R_H(A_2) \in [0,1]$,
$L_H(A^*) \in [0,1]$, $LM_H(A^*) \in [0,1]$, $RM_H(A^*) \in [0,1]$, $R_H(A^*) \in [0,1]$,
$L_H(B_1) \in [0,1]$, $LM_H(B_1) \in [0,1]$, $RM_H(B_1) \in [0,1]$, $R_H(B_1) \in [0,1]$,
$L_H(B_2) \in [0,1]$, $LM_H(B_2) \in [0,1]$, $RM_H(B_2) \in [0,1]$, $R_H(B_2) \in [0,1]$. The proposed fuzzy interpolative reasoning method for hexagonal fuzzy sets is now presented as follows:

Step 1: Based on Eq. (2), calculate the ranking values of fuzzy sets A_1, A^*, A_2 appearing in the antecedents of the fuzzy rules of the fuzzy interpolative reasoning scheme, respectively.
Step 2: Based on Eqs. (3) and (4), calculate the value of the ranking interpolative proportional coefficient λ_{Rank_inter} among the fuzzy sets A_1, A^* and A_2.
Step 3: Based on the value of the ranking interpolative proportional coefficient λ_{Rank_inter} among the fuzzy sets A_1, A^* and A_2, the fuzzy interpolative reasoning conclusion B^*, $B^* = (b_1, b_2, b_3, b_4, b_5, b_6; L_H(B^*), LM_H(B^*), RM_H(B^*), R_H(B^*))$ can be obtained, where

$$b_i = (1- \lambda_{Rank\_inter}) \times b_{1i} + \lambda_{Rank\_inter} \times b_{2i}, \tag{10}$$

$$L_H(B^*) = (1 - \lambda_{Rank\_inter}) \times L_H(B_1) + \lambda_{Rank\_inter} \times L_H(B_2), \tag{11}$$

$$LM_H(B^*) = (1 - \lambda_{Rank\_inter}) \times LM_H(B_1) + \lambda_{Rank\_inter} \times LM_H(B_2), \quad (12)$$

$$RM_H(B^*) = (1 - \lambda_{Rank\_inter}) \times RM_H(B_1) + \lambda_{Rank\_inter} \times RM_H(B_2), \quad (13)$$

$$R_H(B^*) = (1 - \lambda_{Rank\_inter}) \times R_H(B_1) + \lambda_{Rank\_inter} \times R_H(B_2), \quad (14)$$

and $1 \leq i \leq 6$.

3 Examples

In this section, we use some examples to compare the fuzzy interpolative reasoning results of the proposed method with the existing methods.

***Example 3.1*:** Let A_1, A_2, B_1, B_2 and A^* be fuzzy sets of the fuzzy interpolative reasoning scheme, where

A_1 = (2, 6, 6, 9; 0.8, 0.8),
A_2 = (5, 6, 6, 7; 0.8, 0.8),
B_1 = (1, 4, 4, 9; 0.7, 0.7),
B_2 = (3, 4, 4, 7; 0.7, 0.7),
A^* = (3, 6, 6, 8; 0.8, 0.8),

and the membership function curves of these fuzzy sets of the fuzzy interpolative reasoning scheme are shown in Fig. 5. A comparison of the fuzzy interpolative reasoning result B^* of the proposed method with the ones of the fuzzy interpolative reasoning methods [4], [7] and [8] is shown in Table 1. From Table 1, we can see that

Table 1. A comparison of fuzzy interpolative reasoning result B^* of the proposed method with that of the existing fuzzy interpolative reasoning methods

Methods	Fuzzy Interpolative Reasoning Result B^*
Koczy-and-Hirota's Method [8]	N/A
Hsiao-Chen-and-Lee's Method [4]	N/A
Huang-and-Shen's Method [7]	N/A
The Proposed Method	(1.5, 4, 4, 8.5; 0.7, 0.7)

(Note : "N/A" denotes "not applied.")

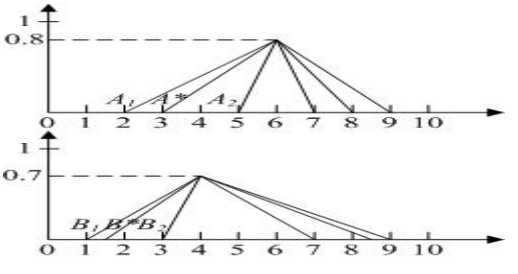

Fig. 5. The fuzzy sets of fuzzy interpolative reasoning scheme of Example 3.1

Koczy-and-Hitota's method [8], Hsiao-Chen-and-Lee's method [4] and Huang-and-Shen's method [7] can not be applied in this situation due to the fact that they can not handle non-normal and overlapping antecedent fuzzy sets of fuzzy rules. We also can see that the proposed method gets a reasonable reasoning result.

Example 3.2: Let A_1, A_2, B_1, B_2 and A^* be fuzzy sets of the fuzzy interpolative reasoning scheme, where

$A_1 = (1, 2, 3, 6; 0.8, 0.7)$,
$A_2 = (4, 5, 6, 7; 0.5, 0.4)$,
$B_1 = (2, 3, 5, 6; 0.7, 0.6)$,
$B_2 = (5, 6, 8, 10; 0.5, 0.4)$,
$A^* = (4, 4, 4, 4; 0.7, 0.7)$,

and the membership function curves of these fuzzy sets of the fuzzy interpolative reasoning scheme are shown in Fig. 6. A comparison of the fuzzy interpolative reasoning result B^* of the proposed method with the ones of the fuzzy interpolative reasoning methods [4], [7] and [8] is shown in Table 2. From Table 2, we can see that Koczy-and-Hitota's method [8], Hsiao-Chen-and-Lee's method [4] and Huang-and-Shen's method [7] can not be applied in this situation due to the fact that they can not handle non-normal and overlapping antecedent fuzzy sets of fuzzy rules. We also can see that the proposed method gets a reasonable reasoning result.

Table 2. A comparison of fuzzy interpolative reasoning result B^* of the proposed method with that of the existing fuzzy interpolative reasoning methods

Method	Fuzzy Interpolative Reasoning Result B^*
Koczy-and-Hirota's Method [8]	N/A
Hsiao-Chen-and-Lee's Method [4]	N/A
Huang-and-Shen's Method [7]	N/A
The Proposed Method	(3.64, 4.64, 6.64, 8.19; 0.59,0.49)

(Note : "N/A" denotes "not applied.")

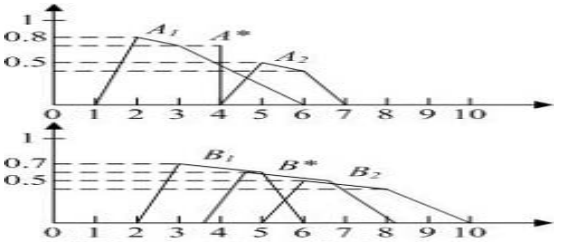

Fig. 6. The fuzzy sets of fuzzy interpolative reasoning scheme of Example 3.2

4 Conclusions

In this paper, we have presented a new fuzzy interpolative reasoning method for sparse fuzzy rule-based systems. For different types of fuzzy sets appearing in the

antecedent fuzzy sets of fuzzy rules, we use different kinds of ranking functions to calculate the ranking values of fuzzy sets. The proposed method can handle the situation of non-normal, overlapping and different types of antecedent fuzzy sets of fuzzy rules. It can overcome the drawbacks of the interpolative reasoning methods presented in [4], [7] and [8]. In the future, we will develop weighted fuzzy interpolative reasoning methods in sparse fuzzy rule-based systems.

Acknowledgements. This work was supported in part by the National Science Council, Republic of China, under Grant NSC 95-2221-E-011-116-MY2.

References

1. Baranyi, P., Gedeon, T.D., Koczy, L.T.: A General Interpolation Technique in Fuzzy Rule Bases with Arbitary Membership Functions. In: Proceedings of the 1996 IEEE International Conference on Systems, Man, and Cybernetics, pp. 510–515 (1996)
2. Baranyi, P., Tikk, D., Yam, Y., Koczy, L.T.: A New Method for Avoiding Abnormal Conclusion for α-cut Based Rule Interpolation. In: Proceedings of the 1999 IEEE International Conference on Fuzzy Systems, pp. 383–388 (1999)
3. Bouchon-Meunier, B., Marslla, C., Rifqi, M.: Interpolative Reasoning Based on Graduality. In: Proceedings of the 2000 IEEE International Conference on Fuzzy Systems, pp. 483–487 (2000)
4. Hsiao, W.H., Chen, S.M., Lee, C.H.: A New Interpolation Reasoning Method in Sparse Rule-Based Systems. Fuzzy Sets and Systems 93, 17–22 (1998)
5. Huang, Z.H., Shen, Q.: A New Fuzzy Interpolative Reasoning Method Based on Center of Gravity. In: Proceedings of the 2003 IEEE International Conference on Fuzzy Systems, vol. 1, pp. 25–30 (2003)
6. Huang, Z.H., Shen, Q.: Scale and Move Transformation-Based Fuzzy Interpolative Reasoning: A Revisit. In: Proceedings of the 2004 IEEE International Conference on Fuzzy Systems, Budapest, Hungary, vol. 2, pp. 623–628 (2004)
7. Huang, Z.H., Shen, Q.: Fuzzy Interpolative Reasoning via Scale and Move Transformations. IEEE Transactions on Fuzzy Systems 14, 340–359 (2006)
8. Koczy, L.T., Hirota, K.: Interpolative Reasoning with Insufficient Evidence in Sparse Fuzzy Rule Bases. Information Sciences 71, 169–201 (1993)
9. Koczy, L.T., Hirota, K.: Approximate Reasoning by Linear Rule Interpolation and General Approximation. International Journal of Approximate Reasoning 9, 197–225 (1993)
10. Koczy, L.T., Hirota, K.: Size Reduction by Interpolation in Fuzzy Rule Bases. IEEE Transactions on Systems, Man, and Cybernetics 27, 14–25 (1997)
11. Lee, L.W., Chen, S.M.: A New Method for Ranking Fuzzy Numbers Based on the Shapes and the Deviations of Fuzzy Numbers. In: Proceedings of the 2nd International Conference on National Computation and the Third International Conference on Fuzzy Systems and Knowledge Discovery, Xi'an, China (2006)
12. Lee, L.W., Chen, S.M.: Fuzzy Extrapolative Reasoning Based on the Ranking Values of Fuzzy Sets. In: Proceedings of the 11th Conference on Artificial Intelligence and Applications, Kaohsiung, Taiwan, Republic of China (2006)
13. Li, Y.M., Huang, D.M., Tsang, E.C., Zhang, L.N.: Weighted Fuzzy Interpolative Reasoning Method. In: Proceedings of the Fourth International Conference on Machine Learning and Cybernetics, pp. 3104–3108 (2005)

14. Qiao, W.Z., Mizumoto, M., Yan, S.Y.: An Improvement to Koczy and Hirota's Interpolative Reasoning in Sparse Fuzzy Rule Bases. International Journal of Approximate Reasoning 15, 185–201 (1996)
15. Tikk, D., Baranyi, P.: Comprehensive Analysis of a New Fuzzy Rule Interpolation Method. IEEE Transactions on Fuzzy Systems 8, 281–296 (2000)
16. Vass, G., Kalmar, L., Koczy, L.T.: Extension of the Fuzzy Rule Interpolation Method. In: Proceedings of the International Conference on Fuzzy Sets Theory Applications, pp. 1–6 (1992)

A New Multi-class Support Vector Machine with Multi-sphere in the Feature Space

Pei-Yi Hao[1] and Yen-Hsiu Lin[2]

[1] Department of Information Management, National Kaohsiung University of Applied Sciences, Kaohsiung, Taiwan
haupy@cc.kuas.edu.tw
[2] Department of Computer Science and Information Engineering, National Cheng Kung University, Tainan, Taiwan

Abstract. Support vector machine (SVM) is a very promising classification technique developed by Vapnik. However, there are still some shortcomings in the original SVM approach. First, SVM was originally designed for binary classification. How to extend it effectively for multi-class classification is still an on-going research issue. Second, SVM does not consider the distribution of each class. In this paper, we propose an extension to the SVM method of pattern recognition for solving the multi-class problem in one formal step. Contrast to previous multi-class SVMs, our approach considers the distribution of each class. Experimental results show that the proposed method is more suitable for practical use than other multi-class SVMs, especially for unbalanced datasets.

Keywords: support vector machine, SVM, multi-class pattern recognition, kernel-based learning, one-class SVM.

1 Introduction

Support vector machine (SVM) is a promising classification technique developed by Vapnik [4,13]. SVM can be seen as an approximate implementation of what Vapnik has defined as Structural Risk minimization, an inductive principle that aims at minimizing the upper bound of the generalization error of a model [13]. However, there are still some shortcomings in the original SVM approach. First, SVM was originally designed for binary classification. How to extend it effectively for multi-class classification is still an on-going research issue. There are two types of multi-class SVMs. One is by constructing and combining several binary classifiers ("one-against-all", "one-against-one", and "DAG-SVM" [2,6,8,11]); while the other is by considering directly all data in one optimization formulation [5,15]. Second, SVM does not consider the distribution, including the mean and variance, of each class. Here we propose a new multi-class SVM that considers directly all data in one optimization. The idea behind our approach comes from the Single-Class Support Vector Domain Description Machine [12], which maps data into a high-dimensional feature space via a nonlinear transform Φ, and then finds a sphere with minimal radius to enclose all

H.G. Okuno and M. Ali (Eds.): IEA/AIE 2007, LNAI 4570, pp. 756–765, 2007.

data points. In [9,14,16,17], they first combined several single-class SVMs to construct a multi-class SVM classifier. In this paper, we propose a novel extension to the single-class SVM for solving the multi-class problem in one formal step. We seek multi-spheres with minimal radius in the feature space such that the ith sphere encloses all examples from ith class but excludes all examples from the rest class. In contrast to previous multi-class SVMs, our approach considers the class distribution mean (spherical-center) and variances (spherical-radius) of each class; thus, our method resembles more the robust Bayesian classifier. The rest of this paper is organized as follows. First, we give a brief overview of the single-class support vector domain description machine. In Section 3 we address the proposed multi-class SVM with multi-spheres in the feature space, and then present the training algorithm in Section 4. Experiments are then discussed in Section 5.

2 Single-Class Support Vector Domain Description Machine

Tax and Duin introduced the use of a data domain description method [12], inspired by the SVM developed by Vapnik. Their approach is known as the support vector domain description (SVDD). In domain description the task is to give a description of a set of objects. This description should cover the class of objects represented by the training set, and should ideally reject all other possible objects in the object space.

To begin, let Φ denote a nonlinear transformation, which maps the original input space into a high-dimensional feature space. Data domain description gives a closed boundary around the data: a hypersphere. The sphere is characterized by center $\mathbf{a}$ and radius $R > 0$. We minimize the volume of the sphere by minimizing R^2, and demand that the sphere contains all training objects. The mathematical formulation of the SVDD is as follows.

$$\min_{R,\mathbf{a}} \qquad R^2 + C\sum_i \xi_i \tag{1}$$

subject to

$$\|\Phi(\mathbf{x}_i) - \mathbf{a}\|^2 \leq R^2 + \xi_i \quad \text{and} \quad \xi_i \geq 0, \tag{2}$$

where R is the radius and $\mathbf{a}$ is the center of the enclosing sphere; ξ_i is a slack variable; and C is a constant controlling the penalty of noise. Using the Lagrangian theorem, we can formulate the dual problem as

$$\max_{\alpha_i} \qquad \sum_i \alpha_i \Phi(\mathbf{x}_i) \cdot \Phi(\mathbf{x}_i) - \sum_i \sum_j \alpha_i \alpha_j \Phi(\mathbf{x}_i) \cdot \Phi(\mathbf{x}_j) \tag{3}$$

subject to

$$\sum_i \alpha_i = 1 \quad \text{and} \quad 0 \leq \alpha_i \leq C \qquad \forall i. \tag{4}$$

3 Spherical-Shaped Multiple-class Support Vector Machine

In this section, inspired by the support vector data description (SVDD), we propose a novel spherical-structured multi-class support vector machine. The proposed approach finds several class-specific spheres that each encloses all examples from one class but excludes all examples from the rest class. In addition, we proposed a new fuzzy membership function to determine the degree of a data point $\mathbf{x}$ belonging to class m.

3.1 The Quadratic Programming Problem

The proposed multi-class SVM classification is an extension of the SVDD. Assume there are ℓ training points that belong to k distinct classes. The methodology is to map training points into a high-dimensional feature via a nonlinear transform Φ, and then find k spheres in the feature space with minimal radius. The mth sphere encloses all data points in the mth classes and leaves the other data points outside it, that is

$$\|\Phi(\mathbf{x}_i) - \mathbf{a}_m\|^2 \leq R_m^2 + \xi_i^m \qquad \text{if } \mathbf{x}_i \in \text{class } m$$
$$\|\Phi(\mathbf{x}_i) - \mathbf{a}_m\|^2 \geq R_m^2 - \xi_i^m \qquad \text{if } \mathbf{x}_i \notin \text{class } m,$$

where R_m and $\mathbf{a}_m$ are the center and radius of the mth sphere respectively, and ξ_i^m are the slack variables corresponding to each training data point $\mathbf{x}_i$ in class m. We then reduce the above two inequality to

$$c_i^m(\|\Phi(\mathbf{x}_i) - \mathbf{a}_m\|^2 - R_m^2) - \xi_i^m \leq 0, \tag{5}$$

where $c_i^m = 1$ if $\mathbf{x}_i \in$class m and $c_i^m = -1$ if $\mathbf{x}_i \notin$class m. Therefore, the problem is equal to solving the following quadratic programming problem

$$\min_{R_m, \mathbf{a}_m} \qquad \sum_m R_m^2 + C \sum_i \sum_m \xi_i^m \tag{6}$$

subject to

$$c_i^m(\|\Phi(\mathbf{x}_i) - \mathbf{a}_m\|^2 - R_m^2) - \xi_i^m \leq 0 \quad \text{and} \quad \xi_i^m \geq 0 \qquad \forall i, m. \tag{7}$$

We can find the solution to this optimization problem in dual variables by finding the saddle point of the Lagrangian:

$$L = \sum_m R_m^2 + C \sum_{i,m} \xi_i^m - \sum_{i,m} \beta_i^m \xi_i^m + \sum_{i,m} \alpha_i^m (c_i^m(\|\Phi(\mathbf{x}_i) - \mathbf{a}_m\|^2 - R_m^2) - \xi_i^m) \tag{8}$$

where α_i^m and β_i^m are nonnegative Lagrange multipliers associated with the two constrains in (7), respectively. Differentiating L with respect to $\mathbf{a}_m$, R_m and ξ_i^m and setting the result to zero, we obtain:

$$\partial L / \partial R_m = 0 \rightarrow \sum_i \alpha_i^m c_i^m = 1 \tag{9}$$

$$\partial L/\partial \mathbf{a}_m = 0 \rightarrow \mathbf{a}_m = \sum_i \alpha_i^m c_i^m \Phi(\mathbf{x}_i) \tag{10}$$

$$\partial L/\partial \xi_i^m = 0 \rightarrow \alpha_i^m + \beta_i^m = C \quad \text{and} \quad 0 \leq \alpha_i^m \leq C. \tag{11}$$

Substituting (9)-(11) into (8), we obtain the following dual problem

$$\max \qquad \sum_i \sum_m \alpha_i^m c_i^m \Phi(\mathbf{x}_i) \cdot \Phi(\mathbf{x}_i) - \sum_i \sum_j \sum_m \alpha_i^m \alpha_j^m c_i^m c_j^m \Phi(\mathbf{x}_i) \cdot \Phi(\mathbf{x}_j) \tag{12}$$

subject to

$$\sum_i \alpha_i^m = 1 \quad \text{and} \quad 0 \leq \alpha_i^m \leq C \qquad \forall i, m. \tag{13}$$

The functional form of mapping Φ does not need to be known since it is implicitly defined by the choice of the kernel function $k(\mathbf{x}_i, \mathbf{x}_j) = \Phi(\mathbf{x}_i) \cdot \Phi(\mathbf{x}_i)$ where '.' represents the inner product. Throughout this paper, we used the RBF kernel function $k(\mathbf{x}_i, \mathbf{x}_j) = exp(-q\|\mathbf{x}_i - \mathbf{x}_j\|^2)$. The distance from a data point $\mathbf{x}$ to the mth sphere center, $\mathbf{a}_m$, is determined by the following equation

$$d_m^2(\mathbf{x}) = \|\Phi(\mathbf{x}) - \mathbf{a}_m\|^2 = k(\mathbf{x}, \mathbf{x}) - 2\sum_i \alpha_i^m c_i^m k(\mathbf{x}, \mathbf{x}_i) + \sum_{i,j} \alpha_i^m c_i^m \alpha_j^m c_j^m k(\mathbf{x}_i, \mathbf{x}_j) \tag{14}$$

The radius of mth sphere, R_m, can be determined from the Karush-Kuhn-Tucker (KKT) conditions:

$$\alpha_i^m (c_i^m (\|\Phi(\mathbf{x}_i) - \mathbf{a}_m\|^2 - R_m^2) - \xi_i^m) = 0$$

$$(C - \alpha_i^m)\xi_i^m = 0.$$

Therefore

$$R_m^2 = \|\Phi(\mathbf{x}_i - \mathbf{a}_m)\|^2 \quad \text{for some } \mathbf{x}_i \text{ with } \alpha_i^m \in (0, C). \tag{15}$$

To determine the membership degree of a data point $\mathbf{x}$ belonging to class m, we proposed the following equation [3]

$$\mu_m(\mathbf{x}) = \begin{cases} 0.5\frac{(1-(1/R_m))d_m(\mathbf{X})}{(1+(\lambda_1/R_m))d_m(\mathbf{X})} + 0.5 \text{ if } d_m(\mathbf{x}) \leq R_m \\ 0.5(\frac{1}{1+\lambda_2(d_m(\mathbf{X})-R_m)}) \qquad \text{otherwise,} \end{cases} \tag{16}$$

where R_m is the spherical radius in the feature space that corresponds to class m; $d_m(\mathbf{x})$ is the distance between $\mathbf{x}$ and the spherical center in the feature space; and the parameters λ_1 and λ_2 satisfy $\lambda_2 = 1/(R_m(1 + \lambda_1))$ which makes $\mu_m(\mathbf{x})$ differentiable as $d_m(\mathbf{x}) = R_m$.

Some important properties of the proposed membership function are summarized as follows. The greater the distance between a given point and the spherical center, the lower the degree of membership of the point belonging to that class is. Moreover, the membership value also takes into account the size of the corresponding sphere in the feature space. The overall membership functions become

S-type and upper-concave type when $\lambda_1 < 0$ and $\lambda_1 > 0$, respectively. It can be seen that the membership value remains higher than 0.5 if the data point is located inside the hyper-sphere in the feature space. This gives the decision function:

$$f(\mathbf{x}, \alpha) = arg \max_m \mu_m(\mathbf{x}).$$

3.2 A Comparison of Original SVM and Our Approach in Decision Curve

Unbalanced data distribution is a familiar phenomenon in a classification problem. For instance, Fig. 1 indicates two classes of Gaussian distribution with different variance and number of data. In some iterative update-based learning machines (such as back-propagation neural networks) the final decision function is deviated to the class with smaller number of data points because it takes more back-propagation update iterations in the larger class. The SVM classification does not suffer this bias. It constructs the maximum margin between the two classes, where the margin is defined as the sum of the distances of the hyperplane from the closest point of the two classes. And the hyperplane of SVM locates middleman in the maximal margin as shown in Fig. 1.

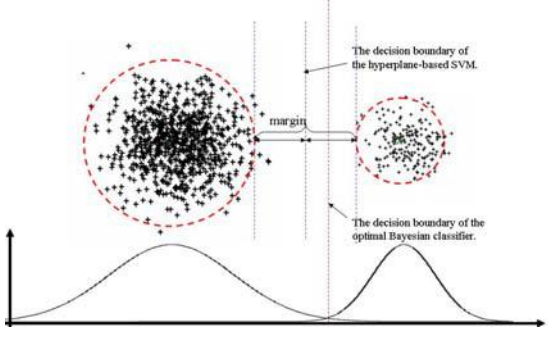

Fig. 1. An comparison of the hyperplane between the original SVM and our approach

However, the original SVM classification does not consider the distribution of each class. In the Bayesian classifier's viewpoint, the optimal decision function is defined as minimizing the error probability [7] and with location slightly deviated to the class with smaller variance. Contrast to previous multi-class SVM, our approach takes the distribution for each class into account. Therefore, taking into consideration the sphere center (mean) and the sphere radius (variance) in the feature space, our approach resembles more the optimal Bayesian classifier. Experimental results show that our approach is more suitable for practical use than other multi-class SVMs, especially for unbalanced datasets.

4 Training Algorithm

Training a SVM model using large datasets is a very difficult problem to approach without some kind of problem decomposition method [10]. The decomposition method is an iterative process where in each iteration the index set of variables are separated into two sets B and N, where B is the working set. Then in that iteration variables corresponding to N are fixed while a sub-problem on variables corresponding to B is minimized. To convert the previous description into an algorithm we need to specify the following: optimality conditions and the strategy of improvement.

4.1 Optimality Conditions

These optimality conditions allow us to decide computationally, if the problem has been solved optimally at a particular iteration of the original problem. A point is an optimality point of (12) if and only if the KKT conditions are fulfilled. Therefore, the quadratic programming (QP) problem is solved when for all i and m:

$$\alpha_i^m = 0 \rightarrow c_i^m(R_m^2 - d_m^2(\mathbf{x}_i)) \geq 0 \tag{17}$$

$$0 < \alpha_i^m < C \rightarrow c_i^m(R_m^2 - d_m^2(\mathbf{x}_i)) = 0 \tag{18}$$

$$\alpha_i^m = C \rightarrow c_i^m(R_m^2 - d_m^2(\mathbf{x}_i)) \leq 0. \tag{19}$$

The KKT conditions can be evaluated one example at a time, which is useful in the construction of the decomposition algorithm.

4.2 Strategy of Improvement

If a particular solution is not optimal, this strategy of improvement defines a way to improve the cost function and is frequently associated with variables that violate optimality conditions. Here we present a modified version of Sequential Minimal Optimization (SMO) [10]. SMO algorithm is a simple algorithm that quickly solves the SVM QP problem without any extra matrix storage and without invoking an iterative numerical routine for each sub-problem. SMO chooses to solve the smallest possible optimization problem at every step. At every step, SMO chooses two Lagrange multipliers that belong to the same class (Lagrange multipliers belonging to the different classes are independent) to jointly optimization, and finds the optimal values for these multipliers. For instance, consider optimizing over α_1^m and α_2^m with all other variables fixed. Let $\alpha_1^{m^*}$, $\alpha_2^{m^*}$ denote the values of their Lagrange parameter before the step. With the shorthand $k_{ij} := k(\mathbf{x}_i, \mathbf{x}_j)$, the updated equation for $\alpha_1^m$is

$$\alpha_i^m = \alpha_i^{m^*} + \frac{(O_1 - O_2) + \frac{1}{2}(k_{22} - k_{11})}{c_2^m(k_{11} - 2k_{12} + k_{22})}, \tag{20}$$

where $O_i := \alpha_1^{m^*} c_1^m k_{1i} + \alpha_2^{m^*} c_2^m k_{2i} + C_i$ and $C_i := \sum_{j=3}^{\ell} \alpha_j^m c_j^m k_{ij}$. Once α_2^m is found, α_1^m can be recovered from $\alpha_1^m = \alpha_1^{m^*} + (c_2^m/c_1^m)(\alpha_2^{m^*} - \alpha_2^m)$. If the point $(\alpha_1^m, \alpha_2^m)$is outside $[0, C]$, the constrained optimum is obtained by projecting α_2^m into the region allowed by the constraints, and then recomputing α_1^m.

5 Experimental Results

We present two types of experiments to demonstrate the performance of the proposed approach. First, we present a 2D artificial dataset that can be visualized in the plane. We then apply the proposed method to benchmark datasets.

5.1 Artificial Dataset

To demonstrate that the proposed algorithm can be useful for dealing with imbalance problem, we first give an artificial dataset. As shown in Fig. 2(a), we draw randomly three classes of examples from the Gaussian distribution where their class distribution means are [-0.2, -0.05], [0.3, 0.1] and [0.2, -0.15] with standard-deviations (σ) 0.2, 0.1 and 0.05, respectively. Fig. 2(b) illustrates the optimal decision boundary obtained by the Bayes decision rule according to the true probability density function of each class. We compare the proposed

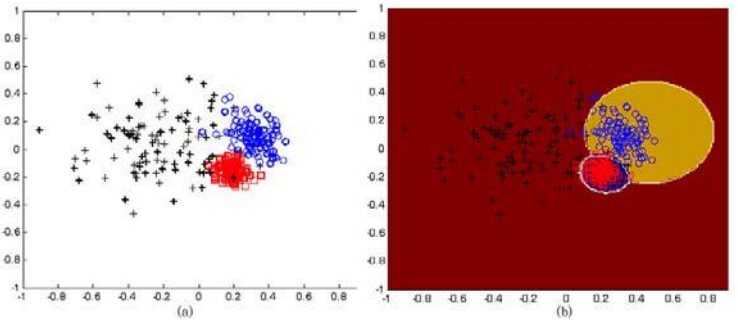

Fig. 2. An comparison of the hyperplane between the original SVM and our approach

approach with three different types of hyperplane-based multi-class SVMs. In this experiment, a half of those examples are used for training and the remaining examples are used for testing the accuracy of the resulting classifier. In Fig. 2(a) the training examples are marked with bold-face. In addition, Gaussian kernels with kernel parameter q=1 and regularization parameter C=4 were used for all algorithms. Fig. 3(a) shows the decision boundary obtained by our approach. Figs. 3 (b), (c) and (d) show the decision boundary obtained by the one-against-all, one-against-one, and directed acyclic graph SVM (DAGSVM), respectively. Note that when using the one-against-one, the problem of unclassifiable region exists. As shown in Fig. 3 (c), for any points $\mathbf{x}$ in the unclassifiable region, the votes for each class are identical. Though it may not be a good strategy, we simply say $\mathbf{x}$ belong to the class with the smallest index. The DAGSVM resolve the unclassifiable region, but the decision boundaries are changed as the order of the assignments between the binary SVM classifiers to internal nodes are changed.

We report the overall classification performance in Table 1. As can be seen, the proposed algorithm achieves better generalization ability in this artificial dataset, which demonstrates that the spherical structured SVMs is more suitable for the imbalance problem due to it deals with the distribution, characterized by the spherical center and radius, of each class. Here we should note that the radius of the hypersphere for each class in the feature space is 0.7971, 0.5675 and 0.3250, respectively. The radius of the hypersphere in the feature space are more or less proportional to the standard-deviation (σ) of the three classes in the original space. It demonstrates that we can use the radius of the hypersphere in the feature space to characterize the class variance in the original space.

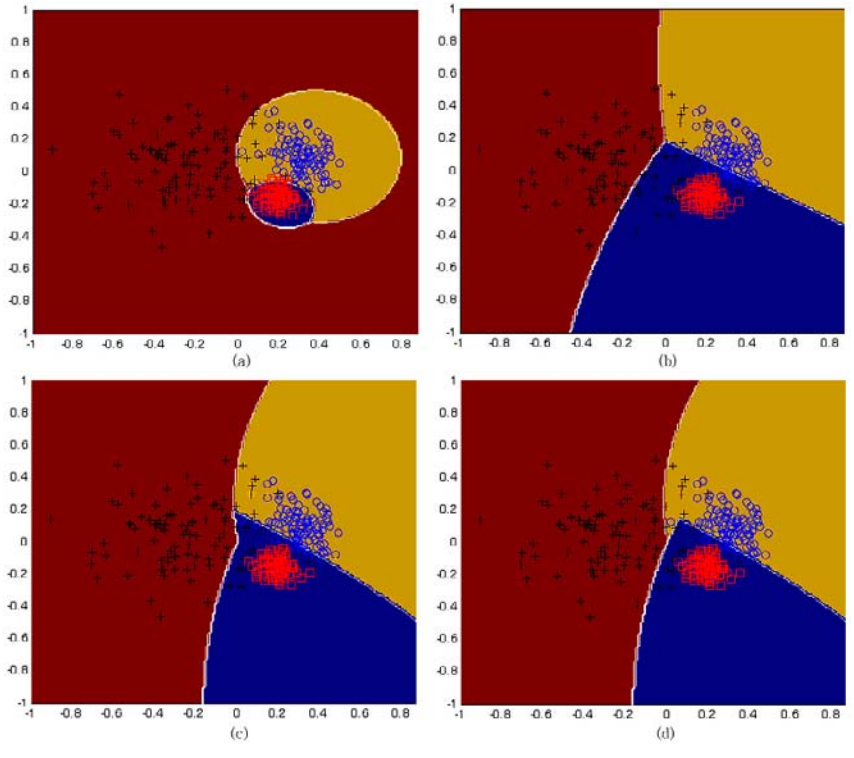

Fig. 3. An comparison of the hyperplane between the original SVM and our approach

5.2 Benchmark Datasets

We also tested the new algorithm and compared it to standard multi-class SVMs, including one-against-all method, one-against-one, DAGSVM, and SVDD. Due to the space limitation, we present the experimental results only on few real-world datasets from the UCI machine learning repository [1]. For all the datasets, we used the 5-fold cross-validation method to estimate the generalization error of the classifiers. The datasets used and the results obtained by the all algorithms

Table 1. A comparison of classification performance

	Num. of misclassified patterns	
	training data	testing data
Proposed approach	11	8
one-against-all	24	19
one-against-one	18	14
DAGSVM	17	14

are summarized in Table 2. The results of the proposed classifier and the SVM classifier both depend on the values of the kernel parameter q and the regularization parameter C. On each dataset, the values of the kernel parameter q and regularization parameter C was optimized to provide the best error rate of the SVM classifier, and the same value was used for the proposed classifier. As we can see, the proposed classifier achieves the same or slightly better results than SVMs on all datasets.

From Table 2, the SVDD classifier gives worse results than the standard multi-class SVM classifiers. However, using our proposed algorithm, which incorporated both the positive and negative examples in the training phase to improve the description, we see that the proposed classifier yields comparable results as the support vector machine, demonstrating that it is suitable for real-world classification problems.

Table 2. A comparison of classification performance

dataset	DAG	OAO	OAA	SVDD	our method
dermatology	**98.108**	**98.108**	97.297	96.756	**98.108**
german	**75.500**	**75.500**	**75.500**	72.200	**75.500**
imox	**93.500**	**93.500**	93.000	92.000	**93.500**
ionosphere	**95.211**	**95.211**	**95.211**	94.080	94.957
iris	**98.000**	**98.000**	97.333	97.333	**98.000**
sonar	66.976	66.976	66.976	61.860	**70.697**
haberman	73.548	73.548	73.225	**73.870**	**73.870**
hepatitis	87.058	87.058	87.058	85.882	**88.235**
lung cancer	83.333	83.333	83.333	**86.666**	**86.666**
new-thyroid	**97.674**	97.674	97.209	**97.674**	**97.674**

6 Discussion and Conclusions

The solution of binary classification problem using the Support Vector Machine has been well developed. Here, we propose an extension to the SVM method of pattern recognition for solving multi-class problem in one formal step. The proposed approach takes the class distribution mean and variance into account. The decision boundary of the proposed approach resembles more the Bayesian

classifier. Experimental results show that the proposed approach is suitable for real-world classification problems.

References

1. Blake, C.L., Merz, C.J.: UCI repository of Machine Learning Databases. Univ. California, Dept. Inform. Comput. Sci., Irvine, CA (1998)
2. Bottou, L., Cortes, C., Denker, J., Drucker, H., Guyon, I., Jackel, L., LeCun, Y., Muller, U., Sackinger, E., Simard, P., Vapnik, V.: Comparison of classifier methods: A case study in handwriting digit recognition. In: Proc. Int. Conf. Pattern Recognition, pp. 77–87 (1994)
3. Chiang, J.-H., Hao, P.-Y.: A new kernel-based fuzzy clustering approach: support vector clustering with cell growing. IEEE Trans. On Fuzzy Syst. 11, 518–527 (2003)
4. Cortes, C., Vapnik, V.: Support-vector network. Mach. Learn. 20, 273–297 (1995)
5. Crammer, K., Singer, Y.: On the ability and design of output codes for multiclass problems. Computational Learning Theory, 35–46 (2000)
6. Friedman, J.: Another approach to polychotomous classification. Technical report, Department of Statistics, Stanford University (1996)
7. Fukunaga, F.: Introduction to Statistical Pattern Recognition. Orlando: Harcourt Brace Jovanovich (1972)
8. KreBel, U.: Pairwise classification and support vector machines. In: Scholkopf, B., Burges, C.J.C., Smola, A.J. (eds.) Advances in Kernel Methods: Support Vector Learning, pp. 255–268. MIT Press, Cambridge, MA (1999)
9. Manevitz, L.M., Yousef, M.: One-class SVMs for document classification. J. of Machine Learning Research 2, 139–154 (2001)
10. Platt, J.C.: Fast training of support vector machines using sequential minimal optimization. In: Scholkopf, B., Burges, C.J.C., Smola, A.J. (eds.) Advances in Kernel Methods: Support Vector Learning, pp. 185–208. MIT Press, Cambridge, MA (1999)
11. Platt, J.C., Cristianini, N., Shawe-Taylor, J.: Large margin DAG's for multiclass classification. In: Advances in Neural Information Processing Systems, 12th edn., pp. 547–553. MIT Press, Cambridge, MA (2000)
12. Tax, D., Duin, R.: Support Vector Data Description. Mach. Learn. 54, 45–66 (2004)
13. Vapnik, V.: Statistical Learning Theory. Wiley, New York (1998)
14. Wang, J., Neskovic, P., Cooper, L.N.: Pattern Classification via Single Spheres. In: Hoffmann, A., Motoda, H., Scheffer, T. (eds.) DS 2005. LNCS (LNAI), vol. 3735, pp. 241–252. Springer, Heidelberg (2005)
15. Weston, J., Watkins, C.: Multi-class Support machines. In: Verleysen, M. (ed.) Proceedings of ESANN99, Brussels (1999)
16. Wu, Q., Shen, X., Li, Y., Xu, G., Yan, W., Dong, G., Yang, Q.: Classifying the Multiplicity of the EEG Source Models Using Sphere-Shaped Support Vector Machines. IEEE Trans. On Magnetics 41, 1912–1915 (2005)
17. Zhu, M.L., Chen, S.F., Liu, X.D.: Sphere-structured support vector machines for multi-class pattern recognition. In: Wang, G., Liu, Q., Yao, Y., Skowron, A. (eds.) RSFDGrC 2003. LNCS (LNAI), vol. 2639, pp. 589–593. Springer, Heidelberg (2003)

Construction of Prediction Module for Successful Ventilator Weaning

Jiin-Chyr Hsu[1], Yung-Fu Chen[2,⋆], Hsuan-Hung Lin[3], Chi-Hsiang Li[4], and Xiaoyi Jiang[5]

[1] Department of Internal Medicine, Taichung Hospital, Department of Health, Executive Yuan, 401 Taichung, Taiwan
jinchyr.hsu@msa.hinet.net
[2] Department of Health Services Management, China Medical University 404 Taichung, Taiwan
yungfu@mail.cmu.edu.tw
[3] Department of MIS, Central Taiwan University of Science and Technology 406 Taichung, Taiwan
shlin@ctust.edu.tw
[4] Department of Respiratory Care, Feng-Yuan Hospital, Department of Health, Executive Yuan, 423 Taichung County, Taiwan
regina@mail.fyh.doh.gov.tw
[5] Department of Mathematics and Computer Science, University of Muenster, D-48149 Muenster, Germany
xjiang@math.uni-muenster.de

Abstract. Ventilator weaning is the process of discontinuing mechanical ventilation from patients with respiratory failure. Previous investigations reported that 39%-40% of the intensive care unit (ICU) patients need mechanical ventilator for sustaining their lives. Among them, 90% of the patients can be weaned from the ventilator in several days while other 5%-15% of the patients need longer ventilator support. Modern mechanical ventilators are believed to be invaluable tools for stabilizing the condition of patients in respiratory failure. However, ventilator support should be withdrawn promptly when no longer necessary so as to reduce the likelihood of known nosocomial complications and costs. Although successful ventilator weaning of ICU patients has been widely studied, indicators for accurate prediction are still under investigation. Furthermore, the predication rate of successful weaning is only 35-60% based on previous studies. It is desirable to have objective measurements and predictors of weaning that decrease the dependence on the wisdom and skill of an individual physician. However, one study showed that clinicians were often wrong when predicting weaning outcome. In this study, 189 patients, who had been supported by mechanical ventilation

⋆ To whom correspondence should be addressed. 91, Hsueh-Shih Road, 404 Taichung, Taiwan; Tel: 886-4-22053366 ext. 6315; Fax: 886-4-22031108. This work was funded by Department of Health of the Executive Yuan, Taiwan, under the grant 9606, for J.C. Hsu and partially supported by 2007/2008 Project-Based Personnel Exchange Program (PPP) between the NSC of Taiwan and the DAAD of Germany for Y.F. Chen and X. Jiang.

H.G. Okuno and M. Ali (Eds.): IEA/AIE 2007, LNAI 4570, pp. 766–775, 2007.

for longer than 21 days and were clinically stable were recruited from our all-purpose ICUs. Twenty-seven variables in total were recorded, while only 8 variables which reached significant level were used for support vector machine (SVM) classification after logistic regression analysis. The result shows that the successful prediction rate achieves as high as 81.5% which outperforms a recently published predictor (78.6%) using combination of sample entropy of three variables, inspiratory tidal volume, expiratory tidal volume, and respiration rate.

1 Introduction

In the daily vernacular of intensive care unit (ICU), the process of discontinuing mechanical ventilation is typically regarded as "weaning." In the strict sense, the term weaning refers to a slow decrease in the level of support from the mechanical ventilator, with the patient gradually assuming a greater proportion of overall ventilation [1].

Previous investigations reported that 39%-40% of the ICU patients need mechanical ventilator for sustaining their lives [2]. Among them, 90% of the patients can be weaned from the ventilator in several days [3] while other 5%-15% of the patients need longer ventilator support [4,5]. Although modern mechanical ventilators are invaluable tools for stabilizing the condition of patients in respiratory failure, ventilator support should be withdrawn promptly when no longer necessary so as to reduce the likelihood of known nosocomial complications and costs [6,7].

The use of mechanical ventilator can cause two primary types of lung injury, i.e. volutrauma and atelectrauma. Volutrauma occurs when lung is overstretched, while atelectrauma is caused by repeatedly opening and closing recruitable alveoli [7]. Prolonged use of ventilator can have great risks of subglottic injury, respiratory infections, and chronic lung disease [8]. Discontinuing mechanical ventilation and removing the artificial airway as soon as possible reduces the risk of ventilator-induced lung injury (VILI), nosocomial pneumonia, airway trauma from the endotracheal tube, and unnecessary sedation. But premature ventilator-discontinuation or extubation can cause ventilatory muscle fatigue [9-11], gas exchange failure, loss of airway protection and increase patient mortality.

Recently, an automated protocol-driven mechanical ventilator has been used for more rapid extubation than the conventional protocol-driven ventilation [12]. The patients are automatically switched from mandatory to spontaneous ventilation mode if it detects two consecutive spontaneous breaths. If the patient doesn't continuously detect spontaneous breaths, it will switch back to the mandatory mode [12]. However, it still needs an indicator module which can identify the patients who can be weaned from the ventilators at the earliest time.

1.1 Ventilation Weaning

To minimize the duration of mechanical ventilation, the clinician should define and treat the underlying cause of respiratory insufficiency and discontinue machine support at the earliest possible time. The American College of Chest Physicians, the Society of Critical Care Medicine, and the American Association for Respiratory Care created evidence-based guidelines, which include the following principles. First, frequent assessment is required to determine whether ventilatory support and the artificial airway are still needed. Second, patients who continue to require support should be continually re-evaluated to assure that all factors contributing to ventilator dependence are addressed. Third, with patients who continue to require support, the support strategy should maximize patient comfort and provide muscle unloading. Fourth, patients who require prolonged ventilatory support beyond the intensive care unit should go to specialized facilities that can provide more gradual support reduction strategies. Finally, ventilator-discontinuation and weaning protocols can be effectively carried out by non-physician clinicians.

Before discontinuing ventilation for patients with acute respiratory failure, four criteria should be assessed [13]: (1) the causes inducing respiratory failure have been reversed; (2) adequate oxygenation and pH value; (3) stable hemodynamics without active myocardial ischemia and hypotension; (4) be able to initiate an inspiration.

After meeting the above criteria, ventilation weaning and extubation can be considered. A number of physiologic indexes have been described to predict the outcome of attempts at discontinuing ventilator support. Previous investigations showed that several physiological indexes, such as rapid shallow breathing index [14], maximal inspiratory pressure, maximum inspiration pressure (PImax) [15,16], vital capacity (VC) [16], minute ventilation (VE) [15,17], and pH and pCO2 values of stomach mucosa [18], etc., were proposed for the prediction of successful ventilation weaning. Scheinhorn et al. [19] believed that variables, including arterial blood gas levels, fraction of inspired oxygen, alveolar-arterial oxygen pressure difference (A-a gradient), blood urine nitrogen (BUN) level, serum creatinine level, and serum albumin level were correlated to successful weaning. In addition to BUN level and albumin level, Modawal et al. [20], on the other hand, concluded that race and reason for ventilator dependency were also major predictors. By reviewing previous published investigations, Meade et al. [6] found that rapid shallow breathing index (RSBI) is the most frequently studied and one of the most powerful index in successful weaning. An index considering rapid shallow breathing and the frequency-to-tidal volume ratio appears to be a much more accurate predictor than traditional indexes, such as maximum inspiratory pressure or minute ventilation.

1.2 Motivation and Goal

Although successful ventilator weaning of ICU patients has been widely studied [13], indexes for accurate prediction are still under investigation. Furthermore, according to previous investigations, the rate of successful weaning is only 35-60%

[20,21]. It is desirable to have objective measurements and predictors of weaning that decrease dependence on the wisdom and skill of an individual physician which are often wrong and unreliable. By identifying the earliest time that a patient is able to resume and sustain spontaneous ventilation, predictive indexes help to avoid unnecessary prolongation of the period of ventilator support. In addition, by identifying patients who are likely to fail a trial of spontaneous breathing, such indexes can prevent a premature weaning attempt and the development of severe cardiorespiratory and/or psychological decompensation.

Although there are several indexes which have been reported and used for successful weaning prediction, the specificity and sensitivity of these indexes are not consistent among different studies due to different patient groups. Unfortunately, these studies only focused on physiological variables, other disease and therapeutic progression indexes should also be considered according to our observations. On the other hand, some of these indexes are not easy to be measured clinically. Therefore, they are not widely used in ICU for assessing ventilator weaning. Since weaning failure is usually multifactorial in nature, indexes that assess a single physiologic function are frequently inaccurate predictors. The goal of this study is to find a prediction module for successful ventilator weaning using multiple variables including physiological variables and clinical syndromes, and other useful information.

2 Materials and Methods

2.1 Patients

Totally 189 patients, who had been on mechanical ventilation for longer than 21days and were clinically stable that their primary physicians considered they were ready to undergo a weaning trial, were recruited from two of the all purpose intensive care units in Taichung Hospital. Their physicians were blinded to the study design and the obtained measurements, although arterial blood gas values and routine measurements by respiratory therapists were available to them. The decision to extubate a patient or reinstitute mechanical ventilation was made solely by the primary physician. After extubation, 84 patients were successfully weaned while the other 105 patients were failed in weaning from mechanical ventilators.

2.2 Data Collection

During mechanical ventilation, the delivered volume was measured at the endotracheal tube with a calibrated spirometer. Airway pressure was measured with a differential pressure transducer attached to the endotracheal tube. PImax was measured with a calibrated differential pressure transducer. A unidirectional valve permitting expiration but not inspiration was attached to the airway, and the most negative pressure recorded during 20 seconds of airway occlusion was taken as the PImax.

In this study, sex, age, APACHE II score at the time of permission, coma scale, and the biochemistry examination variables, including blood urea nitrogen (BUN), creatinine (Cr) albumin (Alb), and hemoglobin (Hb), were collected. Pulmonary diseases were classified based on the causes of inducing the respiration failure. These causes include pulmonary, cardiac, and brain vessel (not including trauma) diseases. Other causes related to internal medicine, multiple-organ failure, historical respiratory disease, trauma, ARDS, brain surgery, and other kinds of surgeries were also considered.

The diagnosis of hospital acquired infections, including nosocomial pneumonia, ventilator associated pneumonia, blood stream infection, urinary tract infection, were according to the definition of CDC (center of disease control, USA). After the discontinuation of mechanical ventilation the patient breathed room air spontaneously under continuous positive airway pressure 5 cm H_2O for one minute, while minuet ventilation volume (VE) and respiratory frequency (f) were measured with a spirometer; the spontaneous tidal volume (VT) was calculated by dividing VE by f. The patient's base characters including the length of ICU admission, the length of ventilator use and airway type (tracheotomy tube or endotracheal tube) were also recoded. When the patient breathed spontaneously for one minute, rapid shallow breathing was quantified as the respiratory frequency (the number of breaths per minute) divided by the VT in liters.

2.3 Construction of Prediction Module Based on SVM

The goal of SVM is to separate multiple clusters with a set of unique hyperplanes with greatest margin to the edge of each cluster, where each hyperplane separating two cluster is not unique for ordinary linear classifiers. For a two-class classification example, the hyperplane separating two classes that leaves the maximum margins from both classes is represented as [22,23]

$$\mathrm{g}(\mathbf{x}) = \mathbf{w}^T\mathbf{x} + w_0 = 0 \tag{1}$$

The distance of a point from a hyperplane is given by

$$\mathrm{z}=\frac{\mathrm{g}(\mathbf{x})}{\|\mathbf{w}\|} \tag{2}$$

As shown in Fig. 1, the value of $\mathbf{w}$ and w_0 in Eq. (1) are scaled so that the values of $\mathrm{g}(\mathbf{x})$ at the nearest points in class 1 and class 2 equal to 1 and -1 respectively. Therefore, to obtain the hyperplane becomes a nonlinear quadratic optimization problem, which can be formulated as:

$$\text{Minimize } J(w) = \frac{\|\mathbf{w}\|^2}{2}, \text{ Subject to } y_i(\mathbf{w}^T\mathbf{x}_i + w_0) \ \geq 1,\ i = 1, 2, ..., N \tag{3}$$

The above minimizer must satisfy Karush-Kuhn-Tucker (KKT) condition, and the problem can be solved by considering Lagrangian duality and the problem can be stated equivalently by its Wolfe dual representation form:

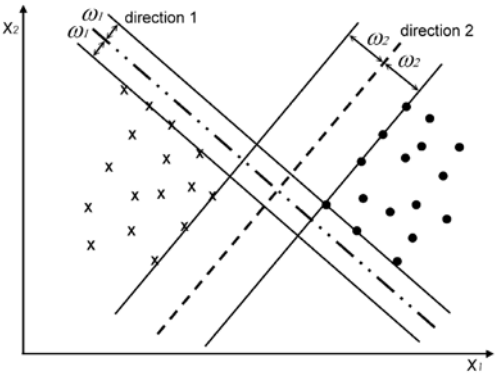

Fig. 1. The hyperplane with greatest margin. Note that the margin of direction 2 is larger than the margin of direction 1 (Modified from [22]).

$$\begin{aligned} &\text{Maximize } L(\mathbf{w},w_0,\lambda) = \tfrac{w^T w}{2} - \textstyle\sum_{i=1}^{N} \lambda_i [y_i(\mathbf{w}^T\mathbf{x}_i + w_0)\text{-}1] \\ &\text{Subject to } \mathbf{w} = \textstyle\sum_{i=1}^{N} \lambda_i y_i \mathbf{x}_i,\ \textstyle\sum_{i=1}^{N} \lambda_i y_i = 0,\ \text{and } \lambda \geq 0 \end{aligned} \tag{4}$$

where $L(\mathbf{w},\ w_0,\ \lambda)$ is Lagrangian function and λ is the vector of Lagrangian multipliers. By comparing Eqs. (3) and (4), the first two constraints in Eq. (4) become equality constraints and make the problem easier to handle. After a little bit algebra manipulation the problem in Eq. (4) becomes

$$\begin{aligned} &\max_{\lambda} \left(\textstyle\sum_{i=1}^{N} \lambda_i - \frac{1}{2} \sum_{i,j} \lambda_i \lambda_j y_i y_j \mathbf{x}_i^T \mathbf{x}_j \right) \\ &\text{Subject to } \textstyle\sum_{i=1}^{N} \lambda_i y_i = 0,\ \text{and } \lambda \geq 0 \end{aligned} \tag{5}$$

As soon as the Lagrangian multipliers have been obtained by maximizing the above equation, the optimal hyperplane can be obtained from $\mathbf{w} = \sum_{i=1}^{N} \lambda_i y_i \mathbf{x}_i$ in Eq. (4). Once the optimal hyperplane has been obtained, classification of a sample is performed based on the sign of the following equation:

$$g(\mathbf{x}) = \mathbf{w}^T\mathbf{x} + w_0 = \sum\nolimits_{i=1}^{Ns} \lambda_i y_i \mathbf{x}_i^T \mathbf{x}_i + w_0 \tag{6}$$

where Ns is the number of support vectors.

For a vector $\mathbf{x}\in\mathrm{R}_l$ in the original feature space, assume that there exists a function ϕ for mapping $\mathbf{x}\in\mathrm{R}_l$ to $\mathrm{y}=\phi(\mathbf{x})\in\mathrm{R}_k$, where k is usually much higher than l. Then it is always true that

$$\sum_r \phi_r(\mathbf{x})\phi_r(\mathbf{z}) = K(\mathbf{x},\mathbf{z}) \tag{7}$$

where $\phi_r(\mathbf{x})$ is the rth component of the mapping and $\mathrm{K}(\mathbf{x},\mathbf{z})$ is a symmetric function satisfying the following condition

$$\begin{aligned} &\textstyle\int K(\mathbf{x},\mathbf{z}) g(\mathbf{z}) d\mathbf{x} d\mathbf{z} \geq 0,\ \text{and} \\ &\textstyle\int g(\mathbf{x})^2 d\mathbf{x} \leq \infty \end{aligned} \tag{8}$$

For a nonlinear classifier, various kernels, including polynomial, radial basics function, and hyperbolic tangent, shown in Eq. (9) can be used for mapping the original sample space into a new Euclidian space with the Mercer's conditions are satisfied. The linear classifier can then be designed for classification.

$$K(\mathbf{x},\mathbf{z}) = (\mathbf{x}^T\mathbf{z} + 1)^q,\ q > 0 \tag{9a}$$

$$K(\mathbf{x},\mathbf{z}) = \exp(\frac{-\|\mathbf{x}-\mathbf{z}\|^2}{\sigma^2}) \tag{9b}$$

$$K(\mathbf{x},\mathbf{z}) = \tanh(\beta\mathbf{x}^T\mathbf{z} + \gamma) \tag{9c}$$

2.4 Classification of Weaning Outcomes for SVM Training and Testing

The successfully weaned group was consisted of patients who were able to sustain spontaneous breathing for more than 72 hours. The patients whose mechanical ventilation was reinstituted within 72 hours were classified as the failed weaning group.

All the sample data were randomly divided into n clusters (folds), in which n-1 folds were used for training while the other one for testing the accuracy of the SVM model. For example, if the data were divided into 6 folds, 5 folds would be used as the training set and the other one as the testing set. Since the number of folds affects the effectiveness of the SVM model, the data were randomly clustered into several different folds (3-8) for performance comparisons. The predictive power of the SVM is assessed by comparing with other indexes.

The free software LIBSVM2 [24], a library for SVMs, was adopted and used for classification. Since the prediction rate is highly influenced by the values of the parameters (i.e. C and γ), the method proposed by Hsu et al. [25] is useful for automatic optimal parameters selection.

3 Experimental Results

Twenty-seven variables in total were analyzed using logistic regression analysis for selecting significant variables which were then used as the training and testing data for SVM prediction model. Table 1 demonstrates the odd ratios of logistic regression analyses of 8 most significant variables. Table 2 depicts the accuracy of the prediction module for successful ventilator weaning. As shown in this table, the data are randomly grouped into 3-8 folds. For constructing the SVM model, data were divided into n folds, in which n-1 folds were used for training while the other one for testing the accuracy of the model. The procedure is repeated for several times to optimize the model parameters, i.e. C and γ. The prediction accuracy achieves values as high as 78%-81%, which outperforms other current published methods.

Table 1. Odd ratios of logistic regression analyses

Variable	Point Estimation	*P* Value	Confidence Interval (95%)
Age	1.031	0.0520	(1000, 1.063)
Coma Scale when hospitalized	1.305	0.0079	(1.072, 1.588)
Brain Surgery	0.435	0.1433	(0.143, 1.326)
Coma Scale after Weaning	0.549	$< .0001$	(0.417, 0.718)
RSBI after Weaning	1.013	0.0002	(1.006, 1.020)
Days Using Ventilator	1.033	0.0181	(1.005, 1.060)
Ventilator Induced Pneumonia	3.612	0.0123	(1.321, 9.874)
In-Hospital Urethra Infection	2.712	0.0402	(1.45, 7.034)

Table 2. Prediction rate of successful weaning using SVM

Folds	C	γ	Prediction Rate (%)
3	0.5	0.5	77.8
4	512	2^{-9}	81.0
5	512	2^{-9}	80.4
6	128	2^{-9}	81.5
7	128	2^{-9}	79.4
8	2	0.5	78.8

4 Discussion and Conclusion

The predictive power of the SVM weaning predicator modular of weaning outcome was considerably greater than that of tradition indexes and a recently published predictor (78.6%) using combination of sample entropy of three variables including inspiratory tidal volume (VTI) and expiratory tidal volume (VTE), and respiration rate (RR) [26].

A number of physiologic indexes have been described to predict the outcome of attempts at discontinuing ventilator support. Since weaning failure is usually multifactor in nature, indexes that assess a single physiologic function are frequently inaccurate predicators. Unfortunately, these studies only focused on physiological variables, according to our observation, other disease and therapeutic progression indexes should also be considered.

Certain aspects of study design become particularly important when an investigation of predictors of weaning outcome is undertaken and also when such investigations are compared. First, the study population needs to be carefully defined. We limited our study population to the patients who had been on mechanical ventilation for longer than 21days and were clinically stable. Second, the technique of making the physiologic measurements needs to be clearly stated. Third, the end point of a study needs to be well defined.

A large number of predictors were found to be of no use in predicting the results of weaning. We found few predictors that had been studied in >50 patients and for which investigators presented data that allowed estimates of the predictive power and had, at least in some studies, appreciable predictive power.

Of these predictors, none are extremely powerful, and their results are not consistent across studies.

The static data of our study are show in Table 1. We excluded the variables whose p values are greater than 0.15. The coma scale when hospitalized, coma scale when weaning tried and RSBI have significant p value with $p < 0.01$. Although the APCHE II score has no significant p vale in logistic analysis, it has $>1\%$ improvement in accuracy when used in SVM predicator module. The Brain surgery patients are more difficult to weaning because they have more complications, such as infection, low coma scale and central fever, than other disease groups.

The same data sets were also used in Artificial NeuroMolecular System for training and testing, the successful prediction rate is only 69.66%, which is lower than the SVM predicator modular.

Currently, we are recruiting more patients for blind test. Some physical examination items will also be considered as new variables, which might have great improvement in prediction of successful weaning. From our understanding, variables of physical examination have never been studied in predicator module before.

References

1. Intensive Care Society: National Guidelines: When and How to Wean. ICS, London (1995)
2. Esteban, A., Anzueto, A., Alia, I., Gordo, F., Apezteguia, C., Palizas, F., Cide, D., Goldwaser, R., Soto, L., Bugedo, G., Rodrigo, C., Pimentel, J., Raimondi, G., Tobin, M.J.: How is Mechanical Ventilation Employed in the Intensive Care Unit? An International Utilization review. American Journal of Respiratory & Critical Care Medicine 161, 1450–1458 (2000)
3. Tomlinson, J.R., Miller, K.S., Lorch, D.G., Smith, L., Reines, H.D., Sahn, S.A.: A Prospective Comparison of IMV and T-piece Weaning from Mechanical Ventilation. Chest 96, 348–352 (1989)
4. Adams, A.B., Whitman, J., Marcy, T.: Survey of Long-Term Ventilatory Support in Minnesota 1986 to 1992. Chest 103, 1463–1469 (1993)
5. Robinson, R.: Ventilator dependency in the United Kingdom. Archives in Disease of Child 65, 1235–1236 (1990)
6. Meade, M., Guyatt, G., Cook, D.J., Griffith, L., Sinuff, T., Kergl, C., Mancebo, J., Esteban, A., Epstein, S.: Predicting Success in Weaning from Mechanical Ventilation. Chest 120, 400S–424S (2001)
7. MacIntyre, N.R.: Current Issues in Mechanical Ventilation for Respiratory Failure. Chest 128, 561S–576S (2005)
8. Bancalari, E., Sinclair, J.C.: Mechanical Ventilation. In: Sinclair, J.C., Bracken, M.B. (eds.) Effective Care of the Newborn Infant, pp. 200–220. Oxford University Press, Oxford (1992)
9. Capdevila, X., Perrigault, P.F., Ramonatxo, M., et al.: Changes in Breathing Pattern and Respiratory Muscle Performance Parameters during Difficult Weaning. Crit. Care Med. 26, 79–87 (1998)
10. Jubran, A., Tobin, M.J.: Pathophysiologic Basis of Acute Respiratory Distress in Patients Who Fail a Trial of Weaning from Mechanical Ventilation. Am. J. Respir. Crit. Care. Med. 155, 906–915 (1997)

11. Vassilakopoulos, T., Zakynthinos, S., Roussos, C.: The Tension Time Index and the Frequency/Tidal Volume Ratio Are the Major Pathophysiologic Determinants of Weaning Failure and Success. Am. J. Respir. Crit. Care Med. 158, 378–385 (1998)
12. Hendrix, H., Kaiser, M.E., Yusen, R.D., Merk, J.: A Randomized Trial of Automated Versus Conventional Protocol-Driven Weaning from Mechanical Ventilation Following Coronary Artery Bypass Surgery. Euro. J. Cardio-Thor Surg. 29, 957–963 (2006)
13. MacIntyre, N.R., Cook, D.J., Ely Jr., E.W., Epstein, S.K., Fink, J.B., Heffner, J.E., Hess, D., Hubmayer, R.D., Scheinhorn, D.J.: Evidence-Based Guidelines for Weaning and Discontinuing Ventilatory Support: A Collective Task Force Facilitated by the American College of Chest Physicians; the American Association for Respiratory Care; and the American College of Critical Care Medicine. Chest 120, 375S–395S (2001)
14. Yang, K.L., Tobin, M.J.: A Prospective Study of Indexes Predicting Outcome of Trials of Weaning from Mechanical Ventilation. New Engl. J. Med. 324, 1445–1450 (1991)
15. Feeley, T.W., Hedley-Whyte, J.: Weaning from Controlled Ventilation and Supplemental Oxygen. New Engl. J. Med. 292, 903–906 (1975)
16. Sahn, S.A., Lakshminarayan, S.: Bedside Criteria for Discontinuation of Mechanical Ventilation. Chest 63, 1002–1005 (1973)
17. Stetson, J.B.: Introductory Essay. Int. Anethesiology Clinics 8, 767–779 (1970)
18. Bouachour, G., Guiraud, M.P., Gouello, J.P., Roy, P.M., Alquier, P.: Gastric Intramural PH: An Indicator of Weaning from Mechanical Ventilation in COPD Patients. European Respiratory Journal 9, 1868–1873 (1996)
19. Scheinhorn, D.J., Chao, D.C., Stearn-Hassenpflug, M., LaBree, L.D., Heltsley, D.J.: Post-ICU Mechanical Ventilation: Treatment of 1,123 at a Regional Weaning Center. Chest 111, 1654–1659 (1997)
20. Modawal, A., Candadai, N.P., Mandell, K.M., Moore, E.S., Hornung, R.W., Ho, M.L., Tsevat, J.: Weaning Success Among Ventilator-Dependent Patients in a Rehabilitation Facility. Archives of Physiological Medical Rehabilitation 83, 154–157 (2002)
21. Nava, S., Rubini, F., Zanotti, E., Ambrosino, N., Bruschi, C., Vitacca, M., Fracchia, C., Rampulla, C.: Survival and Prediction of Successful Ventilator Weaning in COPD Patients Requiring Mechanical Ventilation for More Than 21 Days. European Respiratory Journal 7, 1645–1652 (1994)
22. Theodoridis, S., Koutroumbas, K.: Pattern Recognition, 2nd edn. Academic Press, San Dieago (2003)
23. Cristianini, N., Shawe-Taylor, J.: An Introduction to Support Vector Machines and Other Kernel-Based Methods. Cambridge University Press, Cambridge (2000)
24. Chang, C.C., Lin, C.J.: LIBSVM: A Library for Support Vector Machines (2001) Software available at `http://www.csie.ntu.edu.tw/~cjlin/libsvm`
25. Hsu, C.W., Chang, C.C., Lin, C.J.: A Practical Guide to Support Vector Classification (July 2003). Available at `http://www.csie.ntu.edu.tw/~cjlin/papers/guide/guide.pdf`
26. Casaseca-de-la-Higuera, P., Martin-Fernandez, M., Alberola-Lopez, C.: Weaning from Mechanical Ventilation: A Retrospective Analysis Leading to a Multimodal Perspective. IEEE Transactions on Biomedical Engineering 53, 1330–1345 (2006)

Extension of ICF Classifiers to Real World Data Sets

Kazuya Haraguchi and Hiroshi Nagamochi

Department of Applied Mathematics and Physics
Graduate School of Informatics, Kyoto University, Japan
{kazuyah,nag}@amp.i.kyoto-u.ac.jp

Abstract. Classification problem asks to construct a classifier from a given data set, where a classifier is required to capture the hidden oracle of the data space. Recently, we introduced a new class of classifiers ICF, which is based on iteratively composed features on $\{0, 1, *\}$-valued data sets. We proposed an algorithm ALG-ICF* to construct an ICF classifier and showed its high performance. In this paper, we extend ICF so that it can also process real world data sets consisting of numerical and/or categorical attributes. For this purpose, we incorporate a discretization scheme into ALG-ICF* as its preprocessor, by which an input real world data set is transformed into $\{0, 1, *\}$-valued one. Based on the experimental studies on conventional discretization schemes, we propose a new discretization scheme, integrated construction (IC). Our computational experiments reveal that the ALG-ICF* equipped with IC outperforms a decision tree constructor C4.5 in many cases.

Keywords: classification, discretization, iteratively composed features, machine learning.

1 Introduction

Classification problem is one of the most significant issues in such fields as statistics, learning theory, machine learning, artificial intelligence, expert systems, logical analysis of data (LAD), data mining, and so on [1]. Let us denote $\mathbb{B} = \{0, 1\}$. In classification problem, we are given a *data space* $\mathbb{S}$, an *oracle* y, and a *data set* Ω. A member $\omega \in \mathbb{S}$ is called a *data element*. The oracle y is a function $y : \mathbb{S} \to \mathbb{B}$, and $y(\omega)$ is called the *class* of ω. The exact form of the oracle is not presented to us, and the classes are available only for some data elements. The data set Ω is the set of such examples, and an *example* is a member of the data set. Then classification problem asks us to find a function $c : \mathbb{S} \to \mathbb{B}$ that is an (approximately) equivalent function to y by utilizing the data set.

A typical approach to classification problem requires such a *representation model* that provides us with a framework of embodying a function by representing it as a logically structured object, called a *classifier*. There have been developed various kinds of representation models so far; e.g., neural nets, decision trees, support vector machines [2].

H.G. Okuno and M. Ali (Eds.): IEA/AIE 2007, LNAI 4570, pp. 776–785, 2007.

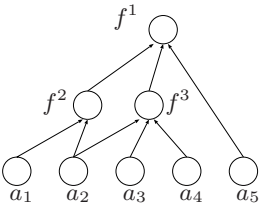

Fig. 1. The structure of an ICF classifier with the final feature f^1

Let us denote by $*$ a *missing bit*, and $\mathbb{M} = \mathbb{B} \cup \{*\}$. Recently, we proposed a new representation model ICF based on *iteratively composed features* [3]. ICF is established on an $\mathbb{M}$-valued data set, i.e., $\mathbb{S} = \mathbb{M}^n$, where n denotes the dimensionality. An *ICF classifier* $f : \mathbb{M}^n \to \mathbb{B}$ is based on functions called *features*. As a special case of feature, we introduce an *initial feature* $a_j : \mathbb{M}^n \to \mathbb{M}$ for each attribute $j = 1, 2, \ldots, n$, which is defined as $a_j(x) = x_j$ for $\forall x \in \mathbb{M}^n$.

The structure of an ICF classifier f is formulated by a directed acyclic graph (DAG). We denote by $G_f = (V_f, E_f)$ the DAG for f, where V_f and E_f denote the sets of nodes and directed edges, respectively. A node corresponds to one feature. The nodes having no incoming edges correspond to initial features. Then a feature in general is a function $f_S : \mathbb{M}^S \to \mathbb{M}$ of the set S of its fan-in features. There is only one node having no outgoing edges, which is called the *final feature*. The range of the final feature is set to $\mathbb{B}$ so that we can use the DAG as a classifier. Figure 1 illustrates an ICF classifier with the final feature $f^1 = f_{\{f^2, f^3, a_5\}}$, where $f^2 = f_{\{a_1, a_2\}}$ and $f^3 = f_{\{a_2, a_3, a_4\}}$. An ICF classifier has a hierarchical structure of features, and it is considered as an application of *concept hierarchy* [4] or *decomposable Boolean functions* [5] to classification problem.

In our previous work [3], we proposed an algorithm ALG-ICF* for constructing an ICF classifier and observed from computational experiments that it *can* construct a better classifier than a decision tree constructor C4.5 [6] or support vector machines when its parameter values are finely tuned up. Hence not only is ICF an efficient representation model but also does it display interesting knowledge representation.

In this paper, we extend ALG-ICF* so that it can process a real world data set consisting of numerical and/or categorical attributes. Let us denote by N the dimensionality of such a real world data set. For each attribute $q \in \{1, 2, \ldots, N\}$, let us denote by $\mathbb{D}_q$ the *domain* of the attribute q. We assume that $\mathbb{D}_q$ is either numerical or categorical. For a numerical attribute q, $\mathbb{D}_q$ may be a subset of the set $\mathbb{R}$ of real numbers or the set $\mathbb{Z}$ of integers. For a categorical attribute q', $\mathbb{D}_{q'}$ is a set of unordered categories, e.g., $\mathbb{D}_{q'} = \{\texttt{blue}, \texttt{red}, \texttt{white}, \texttt{black}\}$. We assume the data space $\mathbb{S}$ to be $\mathbb{S} = \mathbb{D}_1 \times \mathbb{D}_2 \times \cdots \times \mathbb{D}_N$. We denote by Ω a data set over $\mathbb{S}$ and by X an $\mathbb{M}$-valued data set.

In order to process Ω by ALG-ICF*, we equip ALG-ICF* with a *discretization scheme* as its processor, which maps Ω over $\mathbb{S}$ to X over $\mathbb{M}^n$ (where the dimensionality n is suitably determined by the discretization scheme). In the resulting algorithm, Ω is first transformed into X and then ALG-ICF* is applied to X

in order to construct an ICF classifier. Thus our purpose is to establish such a discretization scheme.

Let us denote by χ a *discretizer*, which is a mapping from $\mathbb{S}$ to $\mathbb{M}$. Our discretization scheme constructs a set $D = \{\chi_1, \chi_2, \ldots, \chi_n\}$ of n discretizers, where each χ_j $(j = 1, 2, \ldots, n)$ will be used as attribute j in the transformed $\mathbb{M}$-valued data set X. It is desirable for a discretization scheme to select discretizers so that we can construct a good ICF classifier by ALG-ICF* from the resulting X. We first introduce two conventional discretization schemes, *domain based construction* (DC) and *space based construction* (SC). DC searches the discretizer minimizing the *misclassification cost* for each attribute $q \in \{1, 2, \ldots, N\}$ based on the information of the domain $\mathbb{D}_q$, and constructs a discretizer set $D = \{\chi_1, \chi_2, \ldots, \chi_n\}$ with $n = N$. On the other hand, SC searches a set of discretizers that partitions the data space $\mathbb{S}$ into "well-separated" subspaces by a greedy algorithm.

The paper is organized as follows. In Sect. 2, we review the algorithm ALG-ICF*. In Sect. 3, with the definition on a discretizer, we introduce discretization schemes DC and SC. Then in Sect. 4, after studying the advantages and defects of DC and SC by computational experiments, we propose a new discretization scheme, *integrated construction* (IC). Let us denote by ALG-ICF$^*_{\mathrm{DC}}$ (resp., ALG-ICF$^*_{\mathrm{SC}}$ and ALG-ICF$^*_{\mathrm{IC}}$) the algorithm ALG-ICF* equipped with DC (resp., SC and IC). Our computational experiments reveal that ALG-ICF$^*_{\mathrm{IC}}$ outperforms C4.5 in a stronger sense than our previous work [3].

2 Algorithm ALG-ICF* on $\mathbb{M}$-Valued Data Sets

This section reviews the algorithm ALG-ICF* proposed to construct an ICF classifier on an n-dimensional $\mathbb{M}$-valued data set X [3]. First, let us describe how to determine function $f_S : \mathbb{M}^S \to \mathbb{M}$ for a given set S of features. For a data set X, we call an example $x \in X$ labeled as $y(x) = 1$ (resp., 0) a *true* (resp., *false*) example. Let us denote by $X^1 = \{x \in X \mid y(x) = 1\}$ (resp., $X^0 = \{x \in X \mid y(x) = 0\}$) the set of true (resp., false) examples. For a vector $s \in \mathbb{M}^S$, let us denote by $X_{S,s}$ the set of examples in X whose projections on S are s. Let $X^1_{S,s} = X^1 \cap X_{S,s}$ and $X^0_{S,s} = X^0 \cap X_{S,s}$. We write the $f_S(x|_S)$ by $f_S(x)$ for convenience.

For each $s \in \mathbb{M}^S$, the output $f_S(s)$ is determined based on the following statistical test: The hypothesis is that true and false examples in $X_{S,s}$ are generated with the same probability. If the hypothesis is accepted, we let $f_S(s) = *$ (i.e., we cannot see the bias of classes). Otherwise, we let $f_S(s) = 1$ or 0 by the major class in $X_{S,s}$. We use a parameter $\alpha \in [0, 1]$ to determine the rejection rate of the statistical test; if α is large (resp., small), then $f_S(s)$ is more likely to be 1 or 0 (resp., $*$).

Now let us describe the overview of ALG-ICF*. It consists of an iteration of *composition process* and *selection process*. In the former, a set F'' of new features are composed from the set F of maintained features, and in the latter,

promising features are selected and maintained, where a feature f_S is evaluated by the following cost function:

$$\varphi(f_S) = (E(f_S, X) + \mu U(f_S, X))(\frac{1}{\Delta(f_S)})^{\beta}, \tag{1}$$

where $\beta \in [0, 1]$ and $\mu \in [0, 0.5]$ are adjustable parameters, and

$$E(f_S, X) = \frac{|\{x \in X \mid f_S(x) \neq y(x), f_S(x) \neq *\}|}{|X|},$$

$$U(f_S, X) = \frac{|\{x \in X \mid f_S(x) = *\}|}{|X|}, \qquad \Delta(f_S) = \frac{|\{s \in \mathbb{B}^S \mid f_S(s) \in \mathbb{B}\}|}{2^{|S|}}.$$

$E(f_S, X)$ is the error rate of f_S on the data set X (i.e., *empirical error rate*), and $U(f_S, X)$ is the rate of examples on which uncertain decisions are made. The function $E + \mu U$ is called the *misclassification cost*, and is often used to evaluate a classifier with *reject option* [7]; i.e., a classifier which may output $*$ to indicate "we don't know the class" rather than 0 or 1. We hope that a feature is decisive to some extent (i.e., outputs 0 or 1 for many inputs), and thus introduce the term $(1/\Delta)^{\beta}$. $\Delta(f_S)$ is the rate of input vectors in $\mathbb{B}^S$ (not those in $\mathbb{M}^S$) for which f_S makes a decisive classification. By small E, U and large Δ, f_S should attain a small $\varphi(f_S)$ and be evaluated highly. Then ALG-ICF* is described as follows.

Algorithm ALG-ICF*

Input: An n-dimensional $\mathbb{M}$-valued data set X with n initial features $A = \{a_1, a_2, \ldots, a_n\}$.

Output: An ICF classifier $f : \mathbb{M}^n \to \mathbb{B}$.

Step 1: Let $F := A$ and $t := 1$.

Step 2: Let $F' := \emptyset$ and $h := 2$.

Step 2-1 (Composition) : Compose a set F'' of features as follows:

$$F'' \subseteq \{f_S \mid S \subseteq F, |S| = h\}.$$

(How to take the subset F'' is omitted due to the space limitation.)

Step 2-2 (Selection) : For each $x \in X$, select such a feature f_S that achieves $f_S(x) = y(x)$ and the smallest function value $\varphi(f_S)$ among all features in $(F \setminus A) \cup F' \cup F''$. Remove such features away from $F \cup F' \cup F''$ that are not selected for any $x \in X$ except those in A.

Step 2-3: If $F'' \neq \emptyset$, then let $F' := F' \cup F''$ and $h := h + 1$, and return to Step 2-1.

Step 3: If $h > 2$, then let $F := F \cup F'$ and $t := t + 1$, and return to Step 2.

Step 4: Transform the range of all features in F into $\mathbb{B}$ by setting $f_S(s) \in \mathbb{B}$ based on the major class in $X_{S,s}$. Let $f_S \in F$ denote the feature having the smallest empirical error rate. Output the ICF classifier having f_S as the final feature and halt.

3 Conventional Discretization Schemes

3.1 Discretizers

For a numerical or categorical attribute $q \in \{1, 2, \ldots, N\}$, we define a discretizer by a tuple $\chi = (q, \mathcal{P}, \ell)$, where $\mathcal{P}$ denotes a *partition* of the domain $\mathbb{D}_q$ and ℓ denotes a *label*. A partition $\mathcal{P} = \{P_1, P_2, \ldots, P_k\}$ is a family of disjoint subsets of $\mathbb{D}_q$, i.e.,

$$\bigcup_{\kappa=1,2,\ldots,k} P_\kappa = \mathbb{D}_q, \qquad P_\kappa \cap P_{\kappa'} = \emptyset \ \ (1 \leq \kappa < \kappa' \leq k). \tag{2}$$

For a numerical attribute q, we assume that $\mathbb{D}_q$ is a closed interval $[\min \mathbb{D}_q, \max \mathbb{D}_q]$, and a partition $\mathcal{P}$ is defined by *cutpoints*: For $w_1, w_2, \ldots, w_{k-1} \in \mathbb{D}_q$, we take the k intervals $[\min \mathbb{D}_q, w_1)$, $[w_1, w_2)$, $\ldots$, $[w_{k-2}, w_{k-1})$, $[w_{k-1}, \max \mathbb{D}_q]$ as the elements of $\mathcal{P}$, respectively (where we assume $\min \mathbb{D}_q < w_1 < w_2 < \cdots < w_{k-1} \leq \max \mathbb{D}_q$). For a categorical attribute, $\mathcal{P}$ is determined by a family of subsets $P_1, P_2, \ldots, P_k$ of categories satisfying (2).

A label ℓ is a mapping from $\{1, 2, \ldots, k\}$ to $\mathbb{M}$, i.e., ℓ assigns a value in $\mathbb{M}$ to each of partitioned subsets $P_1, P_2, \ldots, P_k$. Then a discretizer $\chi = (q, \mathcal{P}, \ell)$ discretizes a data element $\omega \in \mathbb{S}$ as follows: Let us denote by $\kappa \in \{1, 2, \ldots, k\}$ the index such that $\omega_q \in P_\kappa$ holds. Then ω is mapped to $\ell(\kappa)$. For convenience, we write the mapped value by $\chi(\omega)$ instead of $\ell(\kappa)$. For a set $D = \{\chi_1, \chi_2, \ldots, \chi_n\}$ of discretizers, we write $D(\omega) = (\chi_1(\omega), \chi_2(\omega), \ldots, \chi_n(\omega))$ and $D(\Omega) = \{D(\omega) \mid \omega \in \Omega\}$.

In the discretization schemes DC and SC, a discretizer $\chi = (q, \mathcal{P}, \ell)$ is determined by q and $\mathcal{P}$, which means that ℓ is determined uniquely by q and $\mathcal{P}$, but in a different way between the two schemes. How to determine ℓ and how to select q and $\mathcal{P}$ in each scheme are described in the subsequent subsections.

3.2 Discretization Scheme DC

Based on previous discretization schemes [8,9], this subsection shows the discretization scheme DC. It constructs a set $D = \{\chi_1, \chi_2, \ldots, \chi_n\}$ of discretizers with $n = N$, where each discretizer χ_j $(j = 1, 2, \ldots, n)$ is constructed from one attribute. DC has two parameters, K and μ', where K specifies the maximum cardinality of partitions for numerical attributes, and $\mu' \in [0, 1]$ denotes the cost incurred by an assignment of $*$ to a discretizer.

How to Determine a Label. Let us take a partition $\mathcal{P} = \{P_1, P_2, \ldots, P_k\}$ on attribute q. By q and $\mathcal{P}$, the data set Ω is partitioned into k subsets according to the values of attribute q as $\Omega_{q,\mathcal{P},\kappa} = \{\omega \in \Omega \mid \omega_q \in P_\kappa\}$, $\kappa \in \{1, 2, \ldots, k\}$. We denote $\Omega^1_{q,\mathcal{P},\kappa} = \Omega^1 \cap \Omega_{q,\mathcal{P},\kappa}$ and $\Omega^0_{q,\mathcal{P},\kappa} = \Omega^0 \cap \Omega_{q,\mathcal{P},\kappa}$.

For given q and $\mathcal{P}$, by regarding ℓ as a classifier with reject option, we determine the value $\ell(\kappa) \in \mathbb{M}$ for $\kappa = 1, 2, \ldots, k$ so that the misclassification

cost $E(\ell, X) + \mu' U(\ell, X)$ is minimized (see Sect. 2). The misclassification cost is minimized by the following label:

$$\ell(\kappa) = \begin{cases} * & \text{if } \mu'|\Omega_{q,\mathcal{P},\kappa}| \leq \min\{|\Omega^1_{q,\mathcal{P},\kappa}|, |\Omega^0_{q,\mathcal{P},\kappa}|\}, \\ 1 & \text{if } \mu'|\Omega_{q,\mathcal{P},\kappa}| > \min\{|\Omega^1_{q,\mathcal{P},\kappa}|, |\Omega^0_{q,\mathcal{P},\kappa}|\} \text{ and } |\Omega^1_{q,\mathcal{P},\kappa}| > |\Omega^0_{q,\mathcal{P},\kappa}|, \\ 0 & \text{otherwise.} \end{cases} \tag{3}$$

How to Select a Partition for Each Attribute. For each attribute $q \in \{1, 2, \ldots, N\}$, we select a partition $\mathcal{P}$ such that $\chi_q = (q, \mathcal{P}, \ell)$ attains the smallest misclassification cost among all candidates, by which we obtain the set $D = \{\chi_1, \chi_2, \ldots, \chi_N\}$ of N discretizers. Note that the search of a partition is independent between attributes because it is based on the domain of one attribute.

For a numerical attribute q, we examine such partitions whose cardinality is not larger than the parameter K (i.e., $|\mathcal{P}| \leq K$) in order to save computation time. Then we obtain an optimum partition $\mathcal{P}$ by solving the corresponding dynamic programming [9]. For a categorical attribute, we obtain an optimum partition as the family where each element is a singleton of a categorical value. One can easily verify that this is optimum analogously with the correctness of the Naïve-Bayesian approach [8].

3.3 Discretization Scheme SC

This subsection shows the discretization scheme SC. It constructs a set $D = \{\chi_1, \chi_2, \ldots, \chi_n\}$ of discretizers, where the dimensionality n is determined by our greedy algorithm. SC has two parameters, Γ_{SC} and $\mathbb{V}$. The parameter Γ_{SC} specifies the cost function to evaluate a discretizer set in the greedy algorithm, which is either *data space error* $\Gamma_{\mathrm{SC,ERR}}$ or *unseparated pairs* $\Gamma_{\mathrm{SC,PAIR}}$. The greedy algorithm selects discretizers based on the specified cost function, where the greedy algorithm for $\Gamma_{\mathrm{SC,PAIR}}$ was first proposed by Mii [10]. The other parameter $\mathbb{V}$ is set to either $\mathbb{B}$ or $\mathbb{M}$, and the greedy algorithm treats only such a discretizer $\chi = (q, \mathcal{P}, \ell)$ that satisfies $|\mathcal{P}| = |\mathbb{V}|$ and $\ell : \{1, \ldots, |\mathbb{V}|\} \to \mathbb{V}$.

How to Determine a Label. For a given partition $\mathcal{P} = \{P_1, \ldots, P_{|\mathbb{V}|}\}$ on attribute q, we use a bijection $\ell : \{1, \ldots, |\mathbb{V}|\} \mapsto \mathbb{V}$ as the label in order to distinguish partitioned subsets $P_1, \ldots, P_{|\mathbb{V}|}$ in the discretized data space. Under this concept, we determine ℓ so that the number of examples which are classified correctly by ℓ (as a classifier with reject option) is maximized. (The details are omitted due to the space limitation.)

How to Select an Attribute and a Partition. Let us denote by $D = \{\chi_1, \chi_2, \ldots, \chi_n\}$ a set of n discretizers ($n \geq 1$). For a vector $s \in \mathbb{V}^n$, we denote $\Omega_{D,s} = \{\omega \in \Omega \mid D(\omega) = s\}$, $\Omega^1_{D,s} = \Omega^1 \cap \Omega_{D,s}$, and $\Omega^0_{D,s} = \Omega^0 \cap \Omega_{D,s}$. Then

the data set Ω is partitioned into $\Omega = \bigcup_{s\in\mathbb{V}^n} \Omega_{D,s}$ by D. We define the data space error $\Gamma_{\mathrm{SC,ERR}}(D)$ and the unseparated pairs $\Gamma_{\mathrm{SC,PAIR}}(D)$ to be;

$$\Gamma_{\mathrm{SC,ERR}}(D) = \sum_{s\in\mathbb{V}^n} \min\{|\Omega^1_{D,s}|, |\Omega^0_{D,s}|\}, \quad \Gamma_{\mathrm{SC,PAIR}}(D) = \sum_{s\in\mathbb{V}^n} |\Omega^1_{D,s}| \cdot |\Omega^0_{D,s}|.$$

We define $\Gamma_{\mathrm{SC,ERR}}(\emptyset) = \min\{|\Omega^1|, |\Omega^0|\}$ and $\Gamma_{\mathrm{SC,PAIR}}(\emptyset) = |\Omega^1| \cdot |\Omega^0|$ for convenience. With functions $\Gamma_{\mathrm{SC,ERR}}$ and $\Gamma_{\mathrm{SC,PAIR}}$, we evaluate how D partitions the data space $\mathbb{S}$ into "well-separated" subspaces.

Let Γ_{SC} represent the cost function of either $\Gamma_{\mathrm{SC,ERR}}$ or $\Gamma_{\mathrm{SC,PAIR}}$. Now we describe the greedy algorithm for SC as follows: Starting with the empty set $D = \emptyset$, the greedy algorithm iterates selecting such χ that minimizes $\Gamma_{\mathrm{SC}}(D \cup \{\chi\})$ among N candidates from the N attributes and updating $D := D \cup \{\chi\}$; if there is no χ that attains $\Gamma_{\mathrm{SC}}(D \cup \{\chi\}) < \Gamma_{\mathrm{SC}}(D)$, then the greedy algorithm halts and outputs the final $D = \{\chi_1, \chi_2, \ldots, \chi_n\}$.

For the candidate of a numerical attribute, we select the best partition among all possible ones of cardinality of at most $|\mathbb{V}|$. For a categorical attribute, let us denote by m the number of categories, where we note that $m = O(|\Omega|)$. Then since the size $O(|\mathbb{V}|^m)$ of the search space can be extremely large, we search the candidate by a heuristic method based on local search, which is almost equivalent to the discretization scheme by Mii [10].

One can see that $\Gamma_{\mathrm{SC,ERR}}(D')$ is monotone non-increasing, while $\Gamma_{\mathrm{SC,PAIR}}(D')$ is monotone decreasing with respect to the set inclusion over all subsets $D' \subseteq D$. Hence use of $\Gamma_{\mathrm{SC}} = \Gamma_{\mathrm{SC,PAIR}}$ may construct a discretizer set including more detailed information on Ω.

4 Computational Experiments

In this section, we first examine the advantages and defects of algorithms ALG-ICF$^*_{\mathrm{DC}}$ and ALG-ICF$^*_{\mathrm{SC}}$ through computational experiments. Based on this observation, we propose another construction algorithm ALG-ICF$^*_{\mathrm{IC}}$ with a new discretization scheme IC.

Experimental Setting. For the experiments, we use data sets from UCI Repository of Machine Learning [11] as real world data sets. The summary is shown at the leftmost column of Table 1, where N_{num} (resp., N_{cat}) denotes the number of numerical (resp., categorical) attributes.

Let $\mathcal{C}$ represent a discretization scheme among DC, SC and IC. For a real world data set Ω, we evaluate the performance of the algorithm ALG-ICF$^*_{\mathcal{C}}$ as follows:

(1) We divide Ω into two halves at random, one for the training set Ω_{train} and the other for the test set Ω_{test}.
(2) We construct a discretizer set $D_{\mathcal{C}}$ by applying $\mathcal{C}$ to the training set Ω_{train}, from which we obtain an $\mathbb{M}$-valued training set $X_{\mathrm{train}} = D_{\mathcal{C}}(\Omega_{\mathrm{train}})$.

Table 1. Best (upper) and average (lower) error rates ($\times 10^2$) of classifiers

Data $(\lvert\Omega\rvert, N_{\rm num}, N_{\rm cat})$	ALG-ICF$^*_{\rm DC}$ $K=3$ $u=0.3$	ALG-ICF$^*_{\rm SC}$ $\Gamma_{\rm SC}=\Gamma_{\rm SC,ERR}$ $\mathbb{V}=\mathbb{B}$	ALG-ICF$^*_{\rm SC}$ $\Gamma_{\rm SC}=\Gamma_{\rm SC,ERR}$ $\mathbb{V}=\mathbb{M}$	ALG-ICF$^*_{\rm SC}$ $\Gamma_{\rm SC}=\Gamma_{\rm SC,PAIR}$ $\mathbb{V}=\mathbb{B}$	ALG-ICF$^*_{\rm SC}$ $\Gamma_{\rm SC}=\Gamma_{\rm SC,PAIR}$ $\mathbb{V}=\mathbb{M}$	ALG-ICF$^*_{\rm IC}$	C4.5
BCW	⋆**3.71**	**4.18**	**4.26**	**4.73**	**4.18**	**4.12**	5.00
(683,9,0)	**4.78**	**4.85**	**4.98**	**5.2**	⋆**4.62**	**4.63**	5.21
BUPA	**36.82**	**34.10**	**36.35**	**36.12**	**35.66**	⋆**33.81**	37.12
(345,6,0)	39.90	**36.42**	**37.48**	**37.81**	38.24	⋆**36.27**	38.18
HABER	27.21	27.14	27.61	⋆**25.91**	26.66	27.34	26.27
(294,3,0)	⋆**27.64**	**28.26**	29.31	29.10	29.27	**28.17**	28.40
IONO	**11.59**	**11.42**	12.44	13.86	13.63	⋆**10.85**	12.32
(351,34,0)	**12.50**	**12.32**	13.53	15.89	16.13	⋆**12.27**	12.64
PIMA	⋆**24.60**	26.17	27.42	26.64	26.45	26.04	25.52
(768,8,0)	⋆**25.75**	28.41	29.43	29.22	29.81	28.04	27.90
AUS	**15.42**	**15.21**	**15.68**	**15.42**	⋆**15.13**	⋆**15.13**	15.95
(690,6,8)	⋆**16.61**	17.70	18.72	18.45	18.15	**17.35**	17.48
CRX	**13.45**	**13.11**	**13.79**	**13.45**	**13.66**	⋆**12.87**	14.33
(666,6,9)	⋆**14.76**	**16.65**	17.32	17.15	17.13	**16.46**	16.74
FLAG	10.92	⋆**9.69**	12.47	**10.51**	12.88	**10.00**	10.51
(194,10,18)	**12.61**	⋆**11.01**	14.93	14.75	15.10	**12.30**	12.77
HEART	⋆**18.88**	**22.29**	25.77	**19.99**	25.55	**20.66**	24.45
(435,0,16)	⋆**20.42**	**25.27**	28.37	**23.06**	29.44	**22.89**	25.50
CAR	7.02	6.94	6.55	⋆**1.12**	**1.38**	⋆**1.12**	2.36
(1728,0,6)	7.28	8.17	7.76	2.87	⋆**2.68**	2.88	2.73
MUSH	⋆**0.00**	0.23	0.23	**0.01**	⋆**0.00**	⋆**0.00**	0.01
(8124,0,22)	0.02	0.23	0.23	0.01	0.01	⋆**0.00**	0.01
TTT	24.80	8.18	13.84	**5.26**	13.96	⋆**5.11**	8.08
(958,0,9)	26.58	12.11	17.51	9.01	17.34	9.17	⋆8.54
VOTES	4.35	4.49	4.49	4.77	4.26	4.40	⋆3.98
(435,0,16)	5.04	5.42	5.42	5.73	5.72	5.86	⋆4.66
BEST	15.29	**14.08**	15.45	**13.67**	14.87	⋆**13.18**	14.30
AVG	16.45	15.90	17.30	16.01	17.20	⋆**15.09**	15.44

(3) We construct an ICF classifier f by applying the original ALG-ICF* to $X_{\rm train}$, and measure its error rate $E(f, X_{\rm test})$ on an $\mathbb{M}$-valued test set $X_{\rm test} = D_{\mathcal{C}}(\Omega_{\rm test})$.

We repeat the process of (1) to (3) 10 times for a set of given parameter values (i.e., α, β, μ for ALG-ICF* and ones for discretization scheme $\mathcal{C}$), and we use the average of error rates on test sets as the performance evaluator.

Results on ALG-ICF$^*_{\rm DC}$ and ALG-ICF$^*_{\rm SC}$. Now we show the experimental results in Table 1. (The column on ALG-ICF$^*_{\rm IC}$ will be described later.) The parameters for discretization schemes are written at the top of the table; e.g., as to ALG-ICF$^*_{\rm DC}$, we show only the result of $K=3$ and $\mu'=0.3$ in the table, which was fairly better than all other tested values of $K \in \{2,3,\ldots,6\}$ and $\mu' \in \{0.1, 0.2, \ldots, 0.5\}$.

For each data set, an indicated value in an upper (resp., lower) entry denotes the best (resp., average) true error rate in all combinations of parameters: For ALG-ICF$^*_{\mathrm{DC}}$ and ALG-ICF$^*_{\mathrm{SC}}$, we take $\alpha \in \{0.01, 0.05, 0.1, 0.25, 0.5\}$, $\beta = 0.3$, $\mu \in \{0.1, \ldots, 0.5\}$, and $\pi = 0.3$. For C4.5 [6], we use 1%, 5%, 10%, 25%, 50%, 75%, 100% as its *confidence level*, considered as the most influential parameter. For ICF algorithms, an error rate smaller than C4.5 is indicated by boldface. For each data set, a sign $\star$ shows the best error rate among all construction algorithms.

At the bottom of the table, the row Best represents the average of the best error rate for each data set, among those realized by adjusting parameters as above. On the other hand, the row Avg represents the average of error rates observed in all data sets and in all tested parameter values. We observe that ALG-ICF$^*_{\mathrm{DC}}$ and ALG-ICF$^*_{\mathrm{SC}}$ outperforms C4.5 in Best but does not in Avg. It means that, with the discretization schemes DC or SC, ALG-ICF* retains its high performance even on real world data sets in the same sense as our previous work [3]. In the following, we consider how to improve the discretization schemes so that ICF algorithms has a better performance in Avg.

We consider that ALG-ICF$^*_{\mathrm{DC}}$ has a good performance in data sets with numerical attributes partly because an effective discretizer for a numerical attribute can be constructed by dynamic programming.

For ALG-ICF$^*_{\mathrm{SC}}$, use of $\mathbb{V} = \mathbb{B}$ outperforms $\mathbb{V} = \mathbb{M}$ regardless of Γ_{SC}. We consider that this is because the discretization process with $\mathbb{V} = \mathbb{M}$ partitions the data space into rather too small subspaces and the resulting data set X may include misleading information for classifier construction.

As to evaluation function, use of $\Gamma_{\mathrm{SC}} = \Gamma_{\mathrm{SC,PAIR}}$ is effective particularly for the data sets consisting only of categorical attributes. It is empirically known that these data sets contain enough information to produce good classifiers. As mentioned in Sect. 3.3, use of $\Gamma_{\mathrm{SC}} = \Gamma_{\mathrm{SC,PAIR}}$ may construct a discretizer set containing more detailed information on Ω than $\Gamma_{\mathrm{SC,ERR}}$, which may explain the above phenomena.

Algorithm ALG-ICF$^*_{\mathrm{IC}}$. We consider combining plural discretizer sets constructed by different discretization schemes. From the above observation, we introduce a discretization scheme IC. Let us denote by $D_{\mathcal{C}}$ a discretizer set constructed by discretization scheme $\mathcal{C}$. Then we integrate DC and SC as follows:

- If the data set consists only of categorical attributes (i.e., $N_{\mathrm{num}} = 0$), then we use $D = D_{\mathrm{DC}(3,0.3)} \cup D_{\mathrm{SC}(\Gamma_{\mathrm{SC,PAIR}},\mathbb{B})}$ as the discretizer set.
- Otherwise, we use $D = D_{\mathrm{DC}(3,0.3)} \cup D_{\mathrm{SC}(\Gamma_{\mathrm{SC,ERR}},\mathbb{B})}$.

As seen from Table 1, ALG-ICF$^*_{\mathrm{IC}}$ outperforms C4.5 not only in Best but also in Avg. This indicates that ALG-ICF$^*_{\mathrm{IC}}$ is better than C4.5 in a stronger sense than the original ALG-ICF* is. It is interesting to see that the performance is enhanced by integrating two discretization schemes of different concepts; in other words, either of DC and SC may not provide enough information with ICF learning by itself.

We do not observe that, however, integration of more discretization schemes always enhances ICF classifiers. For example, we construct a discretizer set by the scheme IC′ as $D_{\mathrm{IC}'} = D_{\mathrm{DC}(3,0.3)} \cup D_{\mathrm{SC}(\Gamma_{\mathrm{SC,ERR}},\mathbb{B})} \cup D_{\mathrm{SC}(\Gamma_{\mathrm{SC,PAIR}},\mathbb{B})}$ for any data set, the result is 13.19 for Best, and 15.35 for Avg, which is slightly worse than ALG-ICF$^*_{\mathrm{IC}}$. Also, an integration method of this type increases the size of discretizer set. It can increase the computation time of classifier construction process.

5 Concluding Remarks

In this paper, we considered how to extend ICF classifiers so that it can handle real world data sets. In order to process such data sets by ICF, we apply a discretization scheme to the given data set, and construct a classifier from the discretized data set. We proposed a new discretization scheme IC based on experimental studies on DC and SC. We observed that ALG-ICF$^*_{\mathrm{IC}}$ outperforms C4.5 in a stronger sense than our previous work.

References

1. Fayyad, U., Piatetsky-Shapiro, G., Padhraic, S.: From data mining to knowledge discovery in databases. AI Magazine 17(3), 37–54 (1996)
2. Weiss, S.M., Kulikowski, C.A.: Computer Systems that Learn: Classification and Prediction Methods from Statistics, Neural Nets, Machine Learning, and Expert Systems. Morgan Kaufmann, San Francisco (1991)
3. Haraguchi, K., Ibaraki, T.: Construction of classifiers by iterative compositions of features with partial knowledge. IEICE Trans. Fund. Elec. Comm. and Comp. Sci. E89-A(5), 1284–1291 (2006)
4. Bohanec, M., Zupan, B.: A function-decomposition method for development of hierarchical multi-attribute decision models. Dec. Supp. Sys. 36(3), 215–233 (2004)
5. Boros, E., Gurvich, V., Hammer, P.L., Ibaraki, T., Kogan, A.: Decomposability of partially defined boolean function. Disc. Appl. Math. 62, 51–75 (1995)
6. Quinlan, J.R.: C4.5: Programs for Machine Learning. Morgan Kaufmann, San Francisco (1993)
7. Chow, C.K.: On optimum recognition error and reject tradeoff. IEEE Trans. Inf. Th. 16(1), 41–46 (1970)
8. Domingos, P., Pazzani, M.J.: Beyond independence: Conditions for the optimality of the simple bayesian classifier. In: Saitta, L. (ed.) Proc. 13th Int'l Conf. Mach. Learn. pp. 105–112 (1996)
9. Elomaa, T., Rousu, J.: Fast minimum training error discretization. In: Sammut, C., Hoffmann, A. (eds.) Proc. 19th Int'l Conf. Mach. Learn, pp. 131–138 (2002)
10. Mii, S.: Feature determination algorithms in the analysis of data. Master's thesis, Department of Applied Mathematics and Physics, Graduate School of Informatics, Kyoto University (2001)
11. Hettich, S., Blake, C.L., Merz, C.J.: UCI Repository of Machine Learning Databases. University of California, Department of Information and Computer Science (1998) `http://www.ics.uci.edu/~mlearn/MLRepository.html`

Hierarchical Visualization for Chance Discovery

Brett Bojduj and Clark S. Turner

Department of Computer Science
California Polytechnic State University, San Luis Obispo, CA 93407, USA
{bbojduj, csturner}@calpoly.edu

Abstract. Chance discovery has achieved much success in discovering events that, though rare, are important to human decision making. Since humans are able to efficiently interact with graphical representations of data, it is useful to use visualizations for chance discovery. KeyGraph enables efficient visualization of data for chance discovery, but does not have provisions for adding domain-specific constraints. This contribution extends the concepts of KeyGraph to a visualization method based on the target sociogram. As the target sociogram is hierarchical in nature, it allows hierarchical constraints to be embedded in visualizations for chance discovery. The details of the hierarchical visualization method are presented and a class of problems is defined for its use. An example from software requirements engineering illustrates the efficacy of our approach.

1 Introduction: Chance Discovery

Chance discovery is the realization of an opportunity or a risk in a decision-making environment. Ohsawa [1] defines a chance as "an event significant for decision making." Chance discovery does not stop at the realization of a chance, but rather is concerned also with explaining the chance [2]. The process of chance discovery excels at and depends on creating a collaborative environment with a human user [3]. Since visualization of information can be more efficient than textual information [4], visual representations of data for chance discovery are required. Several visualizations for chance discovery have been developed [5,6]. For the scope of this work, we will be mainly concerned with one of those visualization methods - KeyGraph.

KeyGraph [6] is both an algorithm and an application. It is used to display a graph of data as clusters of "islands" connected by "bridges." To build this graph, data about a domain is delimited by major changes, such as a period at the end of a sentence or a new requirement in a software requirements document. Islands of data are grouped by their co-occurrence (e.g. spatial, temporal, or conceptual co-occurrence), such as related requirements being grouped to form one island. Bridges between islands are formed by the co-occurrence of a piece of data with islands, such as the co-occurrence of a non-functional software requirement with islands of related requirements. Bridges that connect multiple islands have potentially greater importance and Ohsawa [6] refers to them as "hubs."

H.G. Okuno and M. Ali (Eds.): IEA/AIE 2007, LNAI 4570, pp. 786–795, 2007.

KeyGraph has been shown to work well at finding previously undiscovered concerns critical to decision making for a variety of problems and domains, from earthquake prediction [7] to understanding desires of consumers [8]. However, using the KeyGraph method to visualize chance discoveries is not ideal in domains in which multiple domain-specific constraints must be preserved in order to make rational decisions. This is due to the fact that KeyGraph emphasizes the relationships between data points and does not model constraints of the problem domain. In many domains, such as economics, hierarchical constraints must be explicitly considered to preserve the context of events. Thus it is proposed to instead turn to a modification of the target sociogram to visualize chance events in such domains.

2 Visualization Framework

In order to allow visualization of chance discoveries in domains where hierarchical constraints are important, a hierarchical visualization framework is presented that builds on the concepts of the target sociogram from sociology. A target sociogram is a way of visualizing social networks on a graph of concentric rings, with each ring representing a different level of sociometric status [9]. Target sociograms are inherently hierarchical in nature, since "one may observe each person's sociometric status in terms of his proximity to the center of the circumference of the target." [10] This hierarchical structure can be extended from being only related to sociometric status among people to work with any domain, since arbitrary scales can be imposed on the graph and related to the proximity to the center.

Extending the hierarchical structure of the target sociogram is our point of entry to chance discovery. To apply the target sociogram to chance discovery, two options present themselves:

1. Display data hierarchically, based upon estimated priority or importance
2. Display data hierarchically, based upon the constraints of the problem domain

Hierarchical display is defined as with the target sociogram: with respect to proximity to the center. Note that for option 2, the human collaborator will not be able to rely upon proximity to the center for importance, as in option 1, but will have to search through the entire graph. This is desirable because basing the event importance on proximity to the center, as in option 1, could potentially cause rare, but significant chances to be overlooked. Since option 2 bases the hierarchy on the constraints of the problem domain, it does not have this problem. It is the position of this paper that option 2 should be favored over option 1, for this reason. However, searching the entire graph does have certain implications regarding scalability. If there are many potential chances on the same graph, it could take a significant amount of time to find and evaluate each chance. For now, it is left to future work to study and solve this open problem of scalability for large systems.

Thus the target sociogram can be adapted to display data hierarchically, with the hierarchical constraint(s) (but not the importance!) defined by the proximity to the center of the target. An example of our suggested visualization is shown in Figure 1.

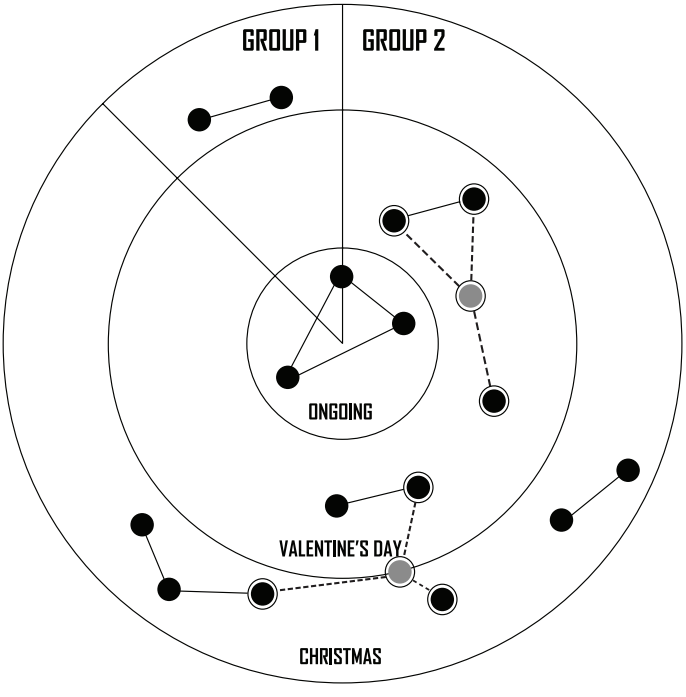

Fig. 1. Visualization of Seasonal Shopping Events Solid black nodes are frequently bought items. Nodes connected by solid black lines are items frequently bought together. Clusters of nodes linked with solid black lines form islands. Nodes in gray are bridges connecting islands together with dashed lines. The nodes with the outer rings are boundaries to nodes that link to other islands.

2.1 Structural Considerations

The importance of Figure 1 is not the data it displays, but rather the structure it illustrates. Multiple constraints can be visualized by dividing the target into regions, such as the "GROUP 1" and "GROUP 2" divisions in Figure 1. Nodes on regional boundaries are contained in both regions. If the division between boundaries is not equal, the greater regional association lies with the region that contains more of the node.

It should be noted that by region, we mean the area of the graph defined by the plane between an arc and two connecting radii. Having too many regions will cause the graph to become unduly cluttered. Finding a heuristic for a maximum number of regions is an open problem and is left to future work.

The division into regions is a major deviation from the design of the target sociogram. Another major difference is that the approach recommended here allows any number of concentric rings, whereas the target sociogram specifically requires four rings [9]. These changes allow the visualization method to be more readily adapted to a variety of problem domains.

It is true that data in KeyGraph could be arbitrarily structured to impose hierarchical relationships. However, unless this is defined explicitly through constraints on the diagram, this could be confusing to the user. The advantage of the visualization method presented here is that the constraints on the graph are explicitly imposed. This lends itself to a situation that Shimojima [11] calls a "free ride." A "free ride" situation exists when the constraints of the spatial representation cause the realization of a conclusion, without any additional computation. Thus including constraints in a graph of events may lend itself to the realization of chance discoveries. An example of a "free ride" is shown in Figure 2. The merits of "free ride" situations for chance discovery is left to future work.

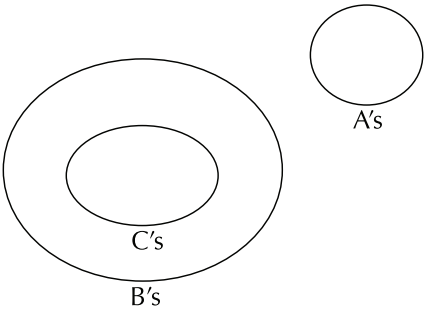

Fig. 2. Example of a "Free Ride" Using Euler Diagrams Euler diagrams can be used to show set intersections, as in this example. This figure is adapted from Shimojima's [11] example. Shimojima shows the proposition, "no C's are A's," can be automatically inferred based on the constraints of these Euler diagrams.

3 Visualization Method as a Modification of KeyGraph

Figure 1 shows fictional data of the shopping habits of two arbitrary groups. The idea is to show how shopping habits that occur only during specific times of the year can be modeled together with ongoing shopping habits. As in KeyGraph [6], the solid black nodes are frequently bought items and the nodes connected by solid black lines are items frequently bought together. These clusters of nodes connected with black lines form islands. The nodes in gray, are bridges linking one island to another with dashed lines. The nodes with the outer rings are boundaries to nodes that link to other islands. In all cases, the syntax of the nodes and lines is the same as in KeyGraph. The only difference is the placement of nodes within the hierarchical target.

3.1 Implications of Modifying KeyGraph

Applying the visualization method based on the target sociogram to KeyGraph is a significant modification with several important implications:

- Domain-specific constraints can be modeled directly in the visualization.
- Constraints can be explicitly incorporated in the chance discovery process.
- The incorporation of constraints provides context for the process of chance discovery.

Modeling domain-specific constraints provides a significant opportunity for chance discovery to branch into areas where domain-specific constraints are important. It also provides a possible means for further automation of the chance discovery process. Further study of these implications are left as future work.

Explicitly incorporating constraints into our visualization method for chance discovery allows several human collaborators to more readily work together. This is because the constraints of the system are explicit, and thus readily apparent to each collaborator.

Finally, providing constraints directly in the model allows context to be preserved. The context of the situation is especially important for a human collaborating with a computer because if we can improve "the computer's access to context, we increase the richness of communication in human-computer interaction and make it possible to produce more useful computational services." [12]

4 Class of Applicable Problems

The visualization framework presented here is applicable to tracking chance events in domains where constraints that are fundamental to that domain must be preserved in order to make sense of the events. For example, in the field of military supply distribution, there exists strategic, operational, and tactical levels of planning [13]. Strategic planning is concerned with planning between theaters of operation, operational planning is within a theater, and tactical planning is concerned with distribution to individual units within a theater. Thus these three levels of planning form constraints that are inherent in the domain of military supply distribution. Therefore, when visualizing events for chance discovery in this domain, it is useful to consider the structure of the domain.

Generalizing this concept to any problem domain, the visualization method presented here will work best with constraints that have a structure that can be viewed as hierarchical. This is because hierarchical constraints can naturally be imposed based upon distance to the center of the diagram. For example, time is a common constraint that has a structure that can be viewed as hierarchical, since earlier times can be thought of has having a higher (or lower) hierarchical level than later times.

For the example in Figure 1, the hierarchical arrangement is somewhat arbitrary, since the seasonal shopping divisions could be rearranged and still represent the same information. In this case, you could say the constraints form

a flattened hierarchy, with each element relating to the ongoing events at the center. The inclusion of domain-specific constraints for chance discovery is a leitmotif of this work.

5 Example of Application to Software Requirements Engineering

Software engineering can be defined as the "application of a systematic, disciplined, quantifiable approach to development, operation, and maintenance of software." [14]

Related to software engineering is software requirements engineering, which Zave [15] defines as follows:

> Requirements engineering is the branch of software engineering concerned with the real-world goals for functions of and constraints on software systems. It is also concerned with the relationship of these factors to precise specifications of software behavior, and to their evolution over time and across software families.

The "evolution over time" that Zave [15] speaks of is software maintenance, which is the evolution of requirements (and thus the software system) over time. Jackson [16] defines a requirement to be a "property of the application domain that the system must enforce." Thus software requirements engineering deals with the empirical reality of a software system.

Software requirements engineering would not be so hard if reality was static. Unfortunately our world is not static, so requirements will change and software must be maintained [17]. Gibson and Senn [18] discuss that changing a system requires three steps:

1. understanding the system
2. implementing the change(s)
3. validating the system after change(s)

It is our position that understanding the system is the most important step, since without proper understanding, changes cannot be properly made and validated. As Bohner and Arnold [19] point out:

> Experience over the last three decades shows that making software changes without visibility into their effects can lead to poor effort estimates, delays in release schedules, degraded software design, unreliable software products, and the premature retirement of the software system.

Thus if greater visibility of changes in software were to be achieved, then it would help decrease production expenses by allowing more reliable work estimates, mitigating delays in release schedule, and improving the reliability of software systems. This visibility of changes can easily be obtained once the software system is understood.

Without proper understanding of the system, the rest of the software change process cannot proceed. That is because changing random segments of code will most likely not be able to satisfy new requirements. Instead, only specific sections of code should be changed, in order to change the functionality of the system. Specific changes can only be made once the system is understood. In order to understand the state of software under maintenance it is useful to track requirements evolution over time. It is this purpose that we turn to chance discovery for.

5.1 Capturing Requirements for Chance Discovery

In order to use chance discovery for software requirements engineering, a method must be developed to capture requirements as islands and bridges. For our work here we capture requirements by looking at groups of requirements and how they relate to a specific component.

For example, if you have requirements for a radiation therapy machine, one requirement could be to limit the dosage to a specific maximum amount. This requirement, in turn, could lead to requirements to have software check dosage levels, as well as hardware interlocks to prevent overdosing a patient (overdosing patients has actually happened before, due to improper analysis of the requirements [20]). It could also lead to requirements to formally prove the correctness of the system. Thus one requirement could lead to several other related requirements, which in turn are grouped together as sets of related requirements. It is the requirements that bridge multiple groups of requirements that we will consider the bridge nodes.

An outcome of defining requirements in this way is that nonfunctional requirements may often be categorized as bridges, since nonfunctional requirements typically have several functional implications. To better illustrate this, an example is given.

5.2 Example of Visualization

As shown in Figure 3, you can represent software requirements evolution for chance discovery. In the case of software requirements, requirements related to a specific section of software code are considered islands, which are represented as nodes connected by solid black lines. Requirements that relate one component to another are bridges, shown as gray nodes. As in KeyGraph, these bridge nodes may be important to the software maintenance process, since they span multiple components. Additionally, the hierarchical structure (based on time grouped together as software development phases) of the target graph allows the suggestion that the requirement node “Must Run on a Single Machine” may be important, since it affects much of the latter requirements. In fact, since that development path ends with a requirement to deprecate that feature, it can be inferred that the “Must Run on a Single Machine” requirement was the root cause of that failure. Indeed, if you look elsewhere on the graph, you see that a conflicting requirement for a “Distributed Architecture” occurs right before the

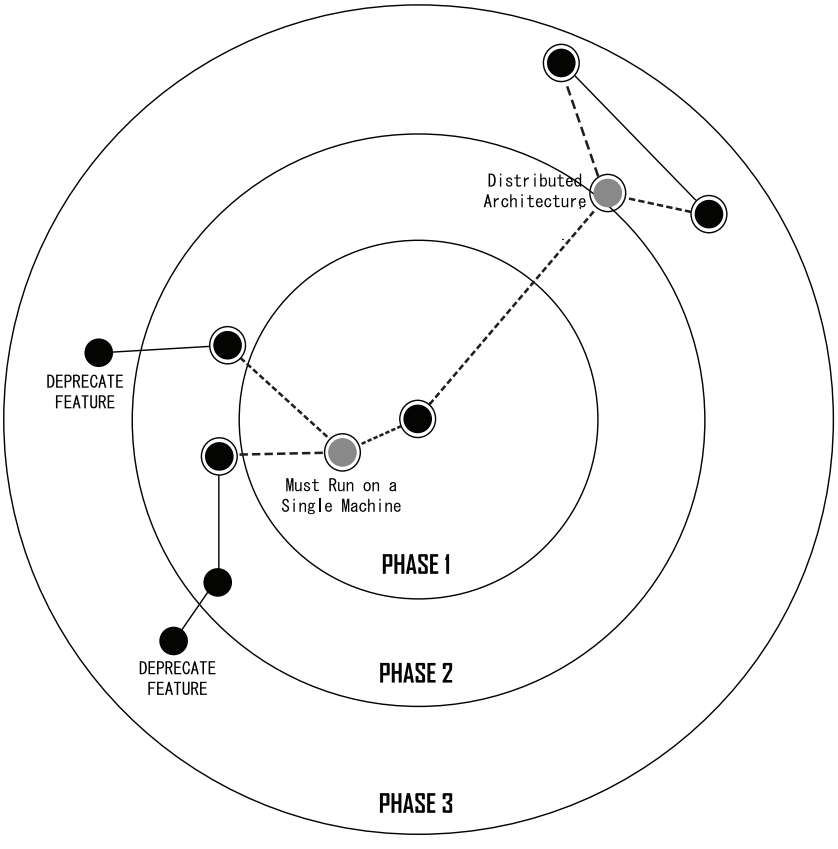

Fig. 3. Requirements Across Software Development Phases

deprecation of the features related to the "Single Machine" requirement. Thus this representation method lends itself to understanding the status of software development.

6 Conclusions and Future Work

Much of chance discovery depends on collaboration with a human user [3]. In collaboration with humans, visualization is the sine qua non of chance discovery. Thus any improvement in visualization could be of great potential benefit to the chance discovery process.

In order to develop an improved visualization for chance discovery, a method for visualizing social networks in borrowed from sociology. This method allows for the inclusion of domain-specific constraints directly in the visualization. The implications of this for chance discovery is that it helps to aid human decision

making since the human collaborator is able to view potential chances in the context of the problem domain.

Future work includes practical application of this approach to chance discovery, in order to test the efficacy of this approach. Towards this end, the development of visualization software based on the method presented here is a next step for this work.

References

1. Ohsawa, Y.: Data crystallization: chance discovery extended for dealing with unobservable events. New mathematics and natural science 1(3), 373–392 (2005)
2. Ohsawa, Y.: Chance discoveries for making decisions in complex real world. New Generation Computing 20, 143–163 (2002)
3. Ohsawa, Y.: Modelling the process of chance discovery. In: Ohsawa, Y., McBurney, P. (eds.) Chance Discovery, pp. 2–15. Springer, Heidelberg (2003)
4. Larkin, J., Simon, H.: Why a diagram is (sometimes) worth ten thousand words. Cognitive Science 11, 65–99 (1987)
5. Matsumura, N.: Topic diffusion in a community. In: Ohsawa, Y., McBurney, P. (eds.) Chance Discovery, pp. 84–97. Springer, Heidelberg (2003)
6. Ohsawa, Y.: Keygraph: Visualized structure among event clusters. In: Ohsawa, Y., McBurney, P. (eds.) Chance Discovery, pp. 262–275. Springer, Heidelberg (2003)
7. Ohsawa, Y.: Detection of earthquake risks with keygraph. In: Ohsawa, Y., McBurney, P. (eds.) Chance Discovery, pp. 339–350. Springer, Heidelberg (2003)
8. Fukuda, H.: Application to understanding consumers' latent desires. In: Ohsawa, Y., McBurney, P. (eds.) Chance Discovery, pp. 383–396. Springer, Heidelberg (2003)
9. Northway, M.: A method for depicting social relationships obtained by sociometric testing. Sociometry 3(2), 144–150 (1940)
10. Northway, M.L.: A Primer of Sociometry. University of Toronto Press (1967)
11. Shimojima, A.: Operational constraints in diagrammatic reasoning. In: Allwein, Barwise (eds.) Logical Reasoning with Diagrams, pp. 27–48. Oxford University Press, Oxford (1996)
12. Dey, A., Abowd, G.: Towards a Better Understanding of Context and Context-Awareness. In: CHI 2000 Workshop on the What, Who, Where, When, and How of Context-Awareness (2000)
13. Weber, B., Bojduj, B.: Tabu search for military supply distribution. In: InterSymp-2006, Focus Symposium on Advances in Intelligent Software Systems, Baden-Baden, Germany, August, 2006, pp. 87–91 (2006)
14. Geraci, A.: IEEE Standard Computer Dictionary: Compilation of IEEE Standard Computer Glossaries. Institute of Electrical and Electronics Engineers Inc. (1991)
15. Zave, P.: Classification of research efforts in requirements engineering. ACM Comput. Surv. 29(4), 315–321 (1997)
16. Jackson, M.: Software requirements and specifications. ACM Press, New York (1995)
17. Welty, C.A., Selfridge, P.: Artificial intelligence and software engineering: Breaking the toy mold. Automated Software Engineering 4(3), 255–270 (1997)

18. Gibson, V.R., Senn, J.A.: System structure and software maintenance performance. Commun. ACM 32(3), 347–358 (1989)
19. Bohner, S., Arnold, R.: An introduction to software change impact analysis. In: Bohner, S., Arnold, R. (eds.) Software Change Impact Analysis, pp. 1–26. IEEE Computer Society Press, Los Alamitos (1996)
20. Leveson, N., Turner, C.: An investigation of the therac-25 accidents. IEEE Computer 26(7), 18–41 (1993)

Episodic Memory for Ubiquitous Multimedia Contents Management System*

Kyung-Joong Kim, Myung-Chul Jung, and Sung-Bae Cho

Dept. of Computer Science, Yonsei University
134 Shinchon-dong, Sudaemoon-ku, Seoul 120-749, South Korea
kjkim@cs.yonsei.ac.kr, mcjung@sclab.yonsei.ac.kr,
sbcho@cs.yonsei.ac.kr

Abstract. Recently, mobile devices are regarded as a content storage with their functions such as camera, camcorder, and music player. It creates massive new data and downloads contents from desktop or wireless internet. Because of the massive size of digital contents in the mobile devices, user feels difficulty to recall or find information from the personal storage. If it is possible to organize the storage in a style of human-memory management, it could reduce user's effort in contents management. Based on the evidence that human memory is organized as an episodic-style, we propose a KeyGraph-based reorganization method of mobile device storage for better accessibility to the data. It can help user not only find useful information from the storage but also expand his/her memory by adding user's contexts such as location, SMS, call, and device status. User can recall his/her memory from the contents and contexts. KeyGraph finds rare but relevant events that can be used as a memory landmark in the episodic memory. Using artificially generated logs from a pre-defined scenario, the proposed method is tested and analyzed to check the possibility.

1 Introduction

Personal information management is one of the hottest issues because huge number of sensors is available at this moment and they can collect all the information about users [1]. Everything about users including photo, e-mail, movie clip, computer usage, TV watching, and contexts can be stored in a unified manner [2]. However, it requires a special-purpose equipment and software to do that and has difficulty to be used generally.

Though we cannot collect everything about users, relatively easy method such as using personal mobile devices can be a partial solution for the problem. Advances in mobile computing devices have led to digital convergence. Recent mobile phones provide many functions such as MP3, camera, game, PIMS (Personal Information Management System) and so on. Using logging software [3], the user's interaction data on the phone can be stored in the inside of device or remote server and retrieved for future use. Such information can be used to enhance user's access to the contents on the phone and expand limited human's memory.

* This research was supported in part by MIC, Korea under ITRC IITA-2006-(C1090-0603-0046).

H.G. Okuno and M. Ali (Eds.): IEA/AIE 2007, LNAI 4570, pp. 796–805, 2007.

Chance discovery is to recognize a chance which is a very rare event, but with significant impact on decision making or future change [4][5]. Also, although it is not rare, finding an event implying an uncertainty of the future is important. It gives not only an awareness of chances but also an explanation about chances. This approach has been applied to various applications domains such as predicting earthquake [6], discovering new topics from WWW [7], and identifying intrusions for computer security [8].

KeyGraph is one of the most frequently used methods for chance discovery [9]. Originally, it is proposed to index terms in a set of documents and its purpose is to find the main point of the documents, not frequent terms. Because the KeyGraph is only based on the information within documents, it does not rely on the domain-specific corpus. If we can expand the meaning of sentence and documents to the more general one, it is possible to detect chance in many practical areas.

The purpose of this research is applying the chance discovery method to the organization of information stored in the personal database. Because the size of information is huge, efficient organization of information is critical to find information quickly and accurately. The idea is to organize the information similar to human's memory structure. Studies on human memory support the assertion that people use special landmarks for recall and the memory is organized by episodes of significant events [10]. Chance discovery algorithm is used to find landmark events among daily events and the whole memory is reorganized by episodes with landmarks identified. Figure 1 shows an episodic memory of personal databases.

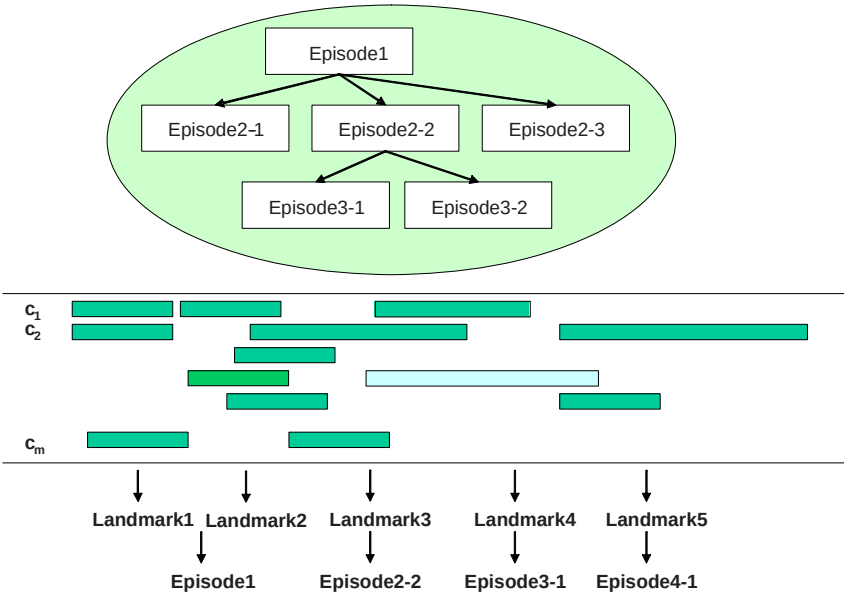

Fig. 1. Episodic memory of personal database (*c* means context and multimedia in the personal database)

In this paper, we propose a novel method to manage user's information in smartphone. User's logs such as call logs, SMS logs, multimedia logs, GPS logs and so on are recorded and combined into an integrated log format. The logs follow the prearranged procedure to find the key events and the relationship of each pair of events applying KeyGraph algorithm which detects rare but very important event based on event sequences and major changes of event environment. Because the key is unique and memorable thing, it can be used as landmarks. Each cluster is regarded as an episode. A user can explore the personal databases using the provided landmark identifiers.

2 Related Works

The initial work for the episodic memory is done by Miikkulainen who proposes an episodic memory that has functions of classifying, storing and retrieving user's memory recorded in scripts using hierarchical SOM (Self-organizing Feature Maps) [11]. Hierarchical structure enables the system to reduce time for recalling the memory.

At Microsoft research, there are many papers about personal information management. Eric Horvitz *et al.* attempt to re-organize personal information storage in desk top PC into an episodic style memory [10]. He learns Bayesian networks to detect landmark event from the data stored in outlook scheduler. Given schedule information, the Bayesian network provides the probability of landmarks of events. Bayesian networks are used for chance discovery and it can easily deal with uncertainty in the data [12]. However, Bayesian network requires relatively high computational cost compared to other simple models and it is the main reason of difficulty in the use of the model in computationally poor environments.

Bayesphone uses client-server communication for Bayesian network, its inference is done on server-side, and the results are transmitted to device through network [14]. It causes communication cost and the device must be always online. SMILE (Structural Modeling, Inference, and Learning Engine) is a Bayesian network library for mobile device [13]. Though it supports a way to implement Bayesian network inference in mobile device easily, it cannot handle inference of large Bayesian networks. KeyGraph is relatively simple model for predicting landmark and it provides a natural view on the episodic memory because each cluster can be regarded as an episode. Useful services using the well-organized personal information are very important for the success of personal information management. E. Horvitz *et al.* develop LifeBrowser and MemoryLens for more efficient access for the information on desktop [15][16]. They exploit the landmark probability inferred from the learned Bayesian networks to visualize the structure of information (stored desktop files).

MIT reality mining group develops serendipity service using the ContextPhone software [18]. The group collaborates with MIT common sense reasoning group to generate diary automatically. Because the research is at early stage, there is no concrete result about that. Only visualization tool for collected log is available in their paper. However, their work shows a new way to generate more interpretable high-level diary (interpretation) using common sense. Basic details about the common sense knowledge can be found in [19].

Recently, Sumi *et al*. develop a ubiquitous system to summarize user's experience on conference tour in a video, but his work requires too many sensors and devices to do that [17].

3 Contents Management Using KeyGraph

The framework of the proposed method consists of log collection, log integration, KeyGraph generation, KeyGraph analysis and information search. Figure 2 shows the overview of the system.

Log collection module continuously gathers application usage, call & SMS, location, device status, and public web information. The logs for several sources are sorted based on the time. The sorted log is called as integrated log. Then, KeyGraph is generated from the new log and key events are extracted. The whole memory is reorganized based on the keys and clusters. By clicking the key, user can access to the related information easily.

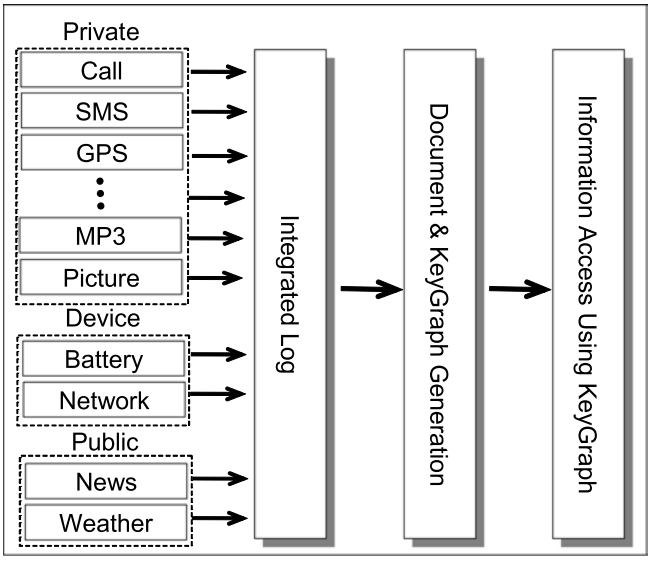

Fig. 2. System overview of the proposed method

3.1 Log Preprocessing

Time, GPS, call, SMS, photo, MP3, e-book, device status and web information can be logged into personal store. Figure 3 shows log preprocessing procedure in detail. Because GPS information is just a pair of longitude and latitude, it is required to convert them into semantic label such as name of building, street and landmark place. Pre-stored mapping table is used to do that. Other log data except location are sorted based on the time and each event is labeled as a unique ID. The naming is the

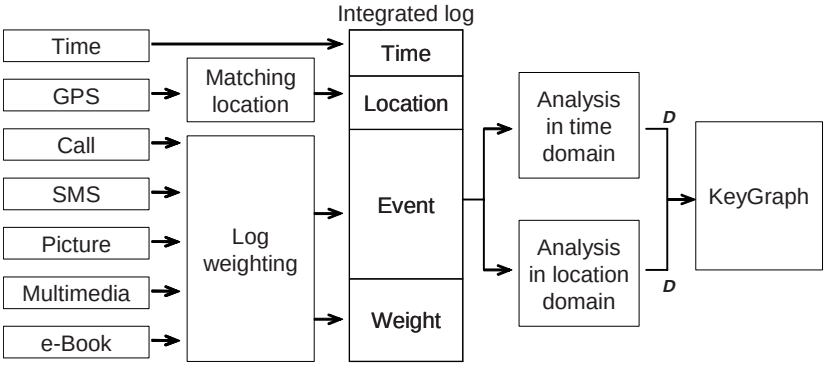

Fig. 3. Details of log preprocessing and KeyGraph generation

combination of log type and event ID. If the event is for calling and it is the 5th event of the day, the ID is Call5.

3.2 Document and Sentence Separation

Because input of the KeyGraph is a set of documents, it is required to reorganize the logs into sentences and documents. The separation of logs is done based on pre-defined rule. 24 hour data are regarded as a separated document. If the data are collected for 7 days, it means that there are 7 documents. Each document contains each day's log. Let's define the total document set as *D*.

$$D = \{d_1, d_2, ..., d_N\} \tag{1}$$

Each document is defined as follows.

$$d_i = \{e_{i1}, e_{i2}, ..., e_{iM}\} \tag{2}$$

e_{ij} means the j th event in the document. A sentence is defined as a group of events. Based on the grouping rule, there are many different ways to form the sentence. The rule set is defined as R_i.

$$R_i = \{r_{i1}, r_{i2}, ..., r_{iP}\} \tag{3}$$

Let's define a set of sentences generated from each rule as S_{ij}. The sentence set S_i for the document d_i is defined as the union of all S_{ij}.

$$S_i = S_{i1} \cup S_{i2} \cup \cdots \cup S_{ip} \tag{4}$$

Table 1 summarizes all sentence separation rules. If time is used as a rule and the threshold is 1 hour, there could be 24 sentences for a day.

Table 1. Sentence separation rule

Log	Sentence separation rules
Time	T < Time < T+δ, T+δ < Time < T+2×δ, …
Location	**If** (L_new ≠ L_old) **then** new_sentence

3.3 KeyGraph Generation

KeyGraph extracts the important events and the causal structures among them from such an event sequence [9]. A document example is given in Eq.(5).

$$\begin{aligned} &\text{Call20\#Pic2\#Pic7\#SMS11\#.}\\ &\text{EB24\#MM12\#Pic7\#Call20\#SMS11\#.}\\ &\text{MM5\#SMS11\#.}\\ &\text{EB24\#MM5\#.} \end{aligned} \tag{5}$$

It is composed of 4 sentences. Figure 4 shows an example of KeyGraph based on the document. Each cluster is composed of co-occurring frequent events. That is, events appearing frequently in *D* are extracted, and each pair of events that often occur in the same sentence unit is linked to each other. 'Call20, Pic7, SMS11' forms a cluster as shown in the figure. The events that are not frequent but co-occurring with multiple clusters, e.g., 'MM5' are a key event. It is rare but very important events.

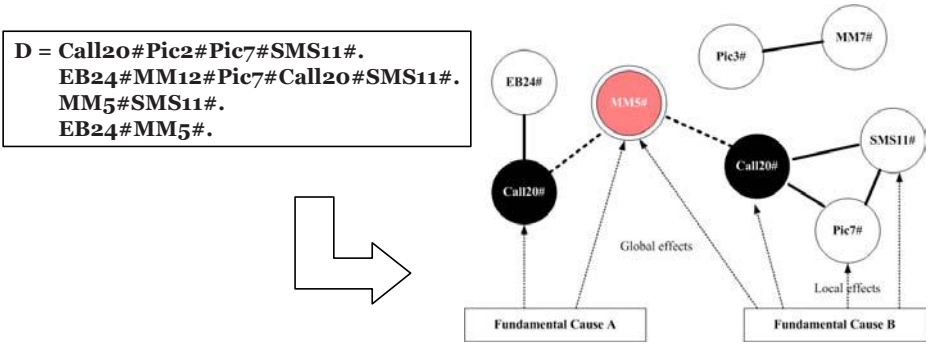

Fig. 4. An example of KeyGraph

The details of the KeyGraph generation are as follows. First, highly frequent events in the document are listed. Then, pairs of the events that are often co-occurred are extracted based on $local(e_i, e_j)$ in Eq.(6), and their link is drawn by the solid line in Figure 5. e means each event and g means the cluster that is composed of e linked by solid lines. $|e|_s$ means the count of e in sentence *S*.

$$local(e_i, e_j) = \sum_{S \in d} \min(|e_i|_S, |e_j|_S) \tag{6}$$

$global(e_i, g)$ in Eq.(7) calculates the strength between event and cluster. Event e that has the highest value summed by $global(e_i, g)$ from every cluster is extracted as key event described as Eq. (8). Links with key events is drawn by dot lines. $|g|_s$ means the count of cluster g in sentence *S*.

$$global(e_i, g) = \frac{\sum_{S \in d} |e_i|_S |g - e_i|_S}{\sum_{S \in d} \sum_{e_i \in S} |e_i|_S |g - e_i|_S} \tag{7}$$

$$where\ |g - e_i|_S = \{ \begin{matrix} |g|_S - |e_i|_S & if\ w \in g \\ |g|_S & if\ not\ w \in g \end{matrix} \}$$

$$key(e_i) = 1 - \prod_{g \in G} (1 - global(e_i, g)) \tag{8}$$

3.4 Information Access

Every key event arranges in order of time. User can simply search for his/her key events of a day and get access to their sub-events quickly. For each key event, associated contents are linked and user can access them hierarchically from the keys. If user did not know much about the detailed contents, he would only search the keys and attempt to remember about the contents. If he thinks that the contents are related to the specific key event, he can expand the searching by following the linked contents from the keys.

4 Experimental Results

The target of a scenario is daily life of an undergraduate student with smartphone, which is summarized in Table 2. The logging software of the smartphone records the events when user's activity changes. When the schedule of the day finishes, contents management software lets user know the key events and the sub-events based on their co-occurrence analysis.

Table 2. User's daily life

Time	Location	Works	Main Events
-9:00	Home		Call
9:00-10:00	Bus	To college	Mp3
10:00-12:00	Engineering hall II	A major	SMS
12:00-13:00	Cafeteria	Lunch with friend	Picture
13:00-14:00	General classroom bui lding	Liberal arts	SMS
14:00-15:00	Bench in front of engi neering building	Rest	E-book, MP3
15:00-17:00	Engineering hall I	A major	E-book
17:00-18:00	Central library	Study	Movie Clip
18:00-21:00	Sinchon	Meeting with frie nds	Call, Picture
21:00-22:00	Bus	To home	MP3
22:00-	Home		SMS

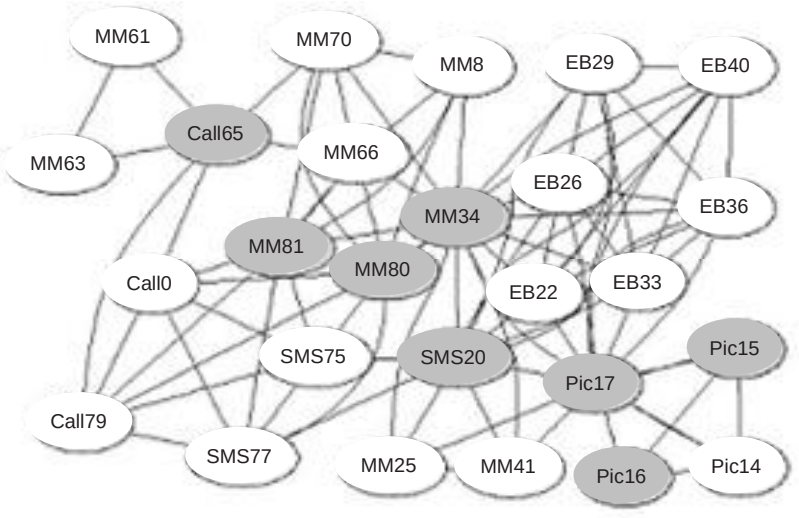

Fig. 5. KeyGraph from the scenario

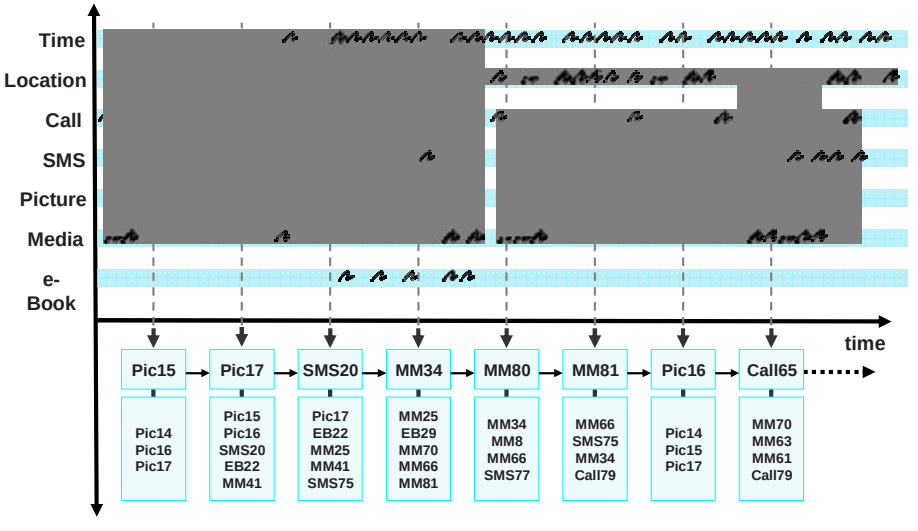

Fig. 6. The key events and the sub-events based on user's logs in time order

Figure 5 shows a part of KeyGraph based on the user's events of the scenario. The black nodes denote key events of the graph and the white nodes denote highly frequent events. "Pic15," "Pic16," and "Pic17" mean the pictures taken by smartphone with his friends in cafeteria. "SMS20" denotes friend's SMS to notify the important meeting with club friends. "MM34," "MM80," and "MM81" are impressive songs to the user. "Call65" means the events that user call to his girlfriend

when the meeting is over. At this time, “Call65” is strongly linked to MP3 events because he goes home as listening MP3.

Figure 6 is a part of the results of analyzing KeyGraph. The key events are extracted on time axis, and the sub-events linked with the key events are displayed. At this stage, the performance of the system is tested using synthetic data because collecting real data requires much time. It takes more than one month to get useful statistics.

5 Conclusions and Future Works

In this paper, we propose the method that can find rare but very important events based on event sequences from smartphone using KeyGraph. We define available logs in smartphone and build the integrated logs and transform them into documents using sentence generation rules. Analyzing the results of KeyGraph, user's information is arranged by key events. The usefulness of the system is evaluated based on scenario and artificially generated data. KeyGraph results show the possibility of the proposed method. As a future work, real logging software needs to be used for collecting user’s data. Based on them, the system can be evaluated and tested in a systematic way. Also, it is required to define a way to handle large-scale KeyGraphs in the limited resource environment.

References

[1] Teevan, J., Jones, W., Bederson, B.B.: Personal information management. Communications of the ACM 49(1), 40–43 (2006)
[2] Gemmell, J., Bell, G., Lueder, R.: MyLifeBits: A personal database for everything. Communications of the ACM 49(1), 88–95 (2006)
[3] Raento, M., Oulasvirta, A., Petit, R., Toivonen, H.: ContextPhone: A prototyping platform for context-aware mobile applications. IEEE Pervasive Computing 4(2), 51–59 (2005)
[4] Ohsawa, Y.: Chance discoveries for making decisions on complex real world. New Generation Computing 20(2), 143–164 (2002)
[5] Ohsawa, Y., McBurney, P.: Chance Discovery. Springer, Heidelberg (2003)
[6] Ohsawa, Y.: KeyGraph as risk explorer from earthquake sequence. Journal of Contingencies and Crisis Management 10(3), 119–128 (2002)
[7] Ohsawa, Y., Soma, H., Matsuo, Y., Matsumura, N., Usui, M.: Featuring web communities based on word co-occurrence structure of communications. In: Proceedings of the 11th International Conference on World Wide Web, pp. 736–742 (2002)
[8] Koo, J.-M., Cho, S.-B.: Interpreting chance for computer security by viterbi algorithm with edit distance. New Mathematics and Natural Computation 1(3), 421–433 (2005)
[9] Ohsawa, Y., Benson, N.E., Yachida, M.: KeyGraph: Automatic indexing by co-occurrence graph based on building construction metaphor. In: Proc. Of Advanced Digital Library Conference (IEEE ADL’98), pp. 12–18 (1998)
[10] Horvitz, E., Dumais, S., Koch, P.: Learning predictive models of memory landmarks. In: 26th Annual Meeting of the Cognitive Science Society (2004)
[11] Miikkulainen, R.: Script recognition with hierarchical feature maps. Connection Science 2, 83–101 (1990)

[12] Kim, K.-J., Cho, S.-B.: Uncertainty reasoning and chance discovery. In: Chance Discovery in Real World Decisions, Springer, Heidelberg (2006)
[13] GeNIe & SMILE, http://genie.sis.pitt.edu
[14] Horvitz, E., Koch, P., Sarin, R., Apacible, J., Subramani, M.: Bayesphone: Precomputation of context-sensitive polices for inqury and action in mobile devices. User Modeling, pp. 251–260 (2005)
[15] Ringel, M., Cutrell, E., Dumais, S., Horvitz, E.: Milestones in time: The value of landmarks in retrieving information from personal stores. In: Proceedings of Interact 2003, the Ninth IFIP TC13 International Conference on HCI, pp. 228–235 (2003)
[16] Cutrell, E., Dumais, S.T., Teevan, J.: Searching to eliminate personal information management. Communications of the ACM 49(1), 58–64 (2006)
[17] Sumi, Y., Ito, S., Matsuguchi, T., Fels, S., Mase, K.: Collaborative capturing and interpretation of interactions. In: Pervasive 2004 Workshop on Memory and Sharing of Experiences, pp. 1–7 (2004)
[18] Eagle, N.: Machine Perception and Learning of Complex Social Systems. Ph. D. Thesis, Program in Media Arts and Sciences, Massachusetts Institute of Technology (2005)
[19] Singh, P., Barry, B., Liu, H.: Teaching machines about everyday life. BT Technology Journal 22(4), 227–240 (2004)

Catalyst Personality for Fostering Communication Among Groups with Opposing Preference

Yoshiharu Maeno[1], Yukio Ohsawa[2], and Takaichi Ito[3]

[1] Graduate School of Systems Management, Tsukuba University,
3-29-11 Otsuka, Bunkyo-ku, Tokyo 112-0012, Japan
maeno.yoshiharu@nifty.com
[2] School of Engineering, University of Tokyo,
7-3-1 Hongo, Bunkyo-ku, Tokyo 113-8563, Japan
[3] Graduate School of Media and Governance, Keio University,
5322 Endo, Fujisawa-shi, Kanagawa 252-8520, Japan

Abstract. The activity of an organization is excited by introducing new persons. Understanding such catalyst personality is an important basis for fostering communication among groups with opposing preference. In the prior understanding, the groups are independent segments. Cognition, resulted from seeing the overlaps revealed between the segments, is not the same as the prior understanding. This gap is a clue. We demonstrate an experiment using questionnaire on the preference of art pieces.

1 Problem

The activity of an organization is often excited by introducing new persons. For example, in a company, a development unit and a sales unit often overcome sectionalism and start dense discussion together with the aid of a product manager as a catalyst personality. Understanding such catalyst personality is an important basis to invent scenarios on fostering communication, and on creating active interactions among groups with opposing preference, tendency, or objectives.

Complex network is an active research area [Barabási 1999], [Watts 1998]. In particular, a model for contemporary inter-working terrorists, a model for a self-organizing community, and a model for a purposefully organized business team are of much interest [Singh 2004]. Such social networks are studied with centrality measures [Borgatti 1997], matrix decomposition techniques [Keila 2006], cognitive social structure analysis [Krackhardt 1987], etc. These studies, however, focus on description of the network, rather than on actively changing the network with use of scenarios invented to acquire opportunity.

In this paper, we present an approach to a catalyst personality for fostering communication among groups with opposing preference. In the prior understanding, the groups are independent segments. Cognition, resulted from seeing the overlaps revealed between the segments, is not the same as the prior understanding. We believe that this gap and its origin are a clue to the catalyst. The clue

H.G. Okuno and M. Ali (Eds.): IEA/AIE 2007, LNAI 4570, pp. 806–812, 2007.

is grown up into a scenario on opportunity, or threat. This process is formulated into the human-interactive annealing process [Maeno 2007], [Maeno 2006b]. We demonstrate an experiment using questionnaire on art pieces.

2 Process

The human-interactive annealing process [Maeno 2007] aims at discovery from the understanding gap with a scenario map [Ohsawa 2005]. The gap lies between internal construct of the mind (prior understanding) and external artifact supporting decision making resulting cognition to observation). The scenario map evolves in the iteration of interpretation and an algorithm [Maeno 2006b] as illustrated in Fig.1. In the scenario map, clusters are connected with dummy events to form a single construct. The dummy events correspond to a latent structure hidden behind observation.

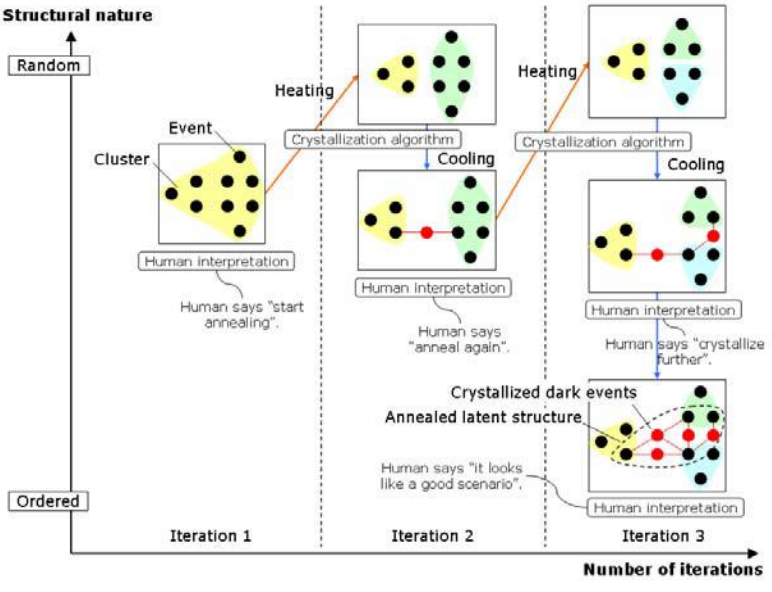

Fig. 1. Scenario map evolving in the iteration of interpretation and algorithm in the human-interactive annealing process (Copyright, IEEE 2007)

The algorithm is as follows. Market basket data equivalent to a bipartite graph structure (eq.(1)) is the input to the algorithm. The market basket consists of a subject and a set of events, which occur simultaneously, or related strongly under a given subject. The events are clustered into groups based on co-occurrence (Jaccard coefficient in eq.(2)) as a measure of similarity between

events [Maeno 2006a]. K-medoids (an EM algorithm similar to k-means for numerical data), hierarchical clustering, self-organization mapping, etc. are employed.

$$b_i = s_i : \{e_{ij}\}\ (0 \leq i \leq B-1, 0 \leq j \leq |b_i|-1). \tag{1}$$

$$\mathrm{J}(e_i, e_j) = \frac{\mathrm{Freq}(e_i \cap e_j)}{\mathrm{Freq}(e_i \cup e_j)}. \tag{2}$$

A dummy event DE_i, representing a latent structure, is inserted into b_i, that results in b'_i (eq.(3)) [Ohsawa 2005]. The index i can be used to identify the market basket where the corresponding dummy event was inserted.

$$b'_i = s_i : \{e_{ij}\} \cup \mathrm{DE}_i. \tag{3}$$

The clusters which a dummy event connect to are derived with a measure in eq.(4). The primary and secondary clusters for the dummy events are determined according to eq.(5), and eq.(6). The secondary cluster is either one that the dummy event is associated next to the primary cluster, or the least.

$$\mathrm{C}(\mathrm{DE}_i, c_n) = \max_{e_m \in b_i, c_n} \mathrm{J}(\mathrm{DE}_i, e_m). \tag{4}$$

$$c_{\mathrm{P}}(i) = \arg\ \max_n \mathrm{C}(\mathrm{DE}_i, c_n). \tag{5}$$

$$c_{\mathrm{S}}(i) = \arg\ \max_{c_n \neq c_{\mathrm{P}}(i)} \mathrm{C}(\mathrm{DE}_i, c_n),\ c'_{\mathrm{S}}(i) = \arg\ \min_n \mathrm{C}(\mathrm{DE}_i, c_n). \tag{6}$$

The primary and secondary clusters are connected with the subject, and its corresponding dummy event, resulting in a scenario map as shown in Fig.2.

3 Experiment

We prepared 50 art pieces ranging from portraits, landscapes to abstract paintings. In a questionnaire, 30 subject persons are asked to pick up the art pieces as many as they like. Their answers are configured to the input market basket data, b_i = art piece ID: person IDs who picked up this piece.

The data is visualized in a scenario map as described in 2. Nodes are persons. The persons expressing similar preference form a group. Groups have, therefore, opposing preference. We focus on three scenarios on catalyst personality who is suitable for [a] persons among most groups, [b] persons between the two groups potentially associated the most strongly, and [c] persons in the most isolated clique group. The corresponding three scenario maps are shown in Fig. 3. The dummy event and the corresponding art piece (like DE_3, s_3 in Fig.2) are represented by a single node. Four persons including three subject persons discussed on scenarios on the catalyst personality indicated by dummy events.

At first, the characteristics of the persons in the individual clusters are interpreted. They are summarized in Table 1. Then, they invented scenarios. In

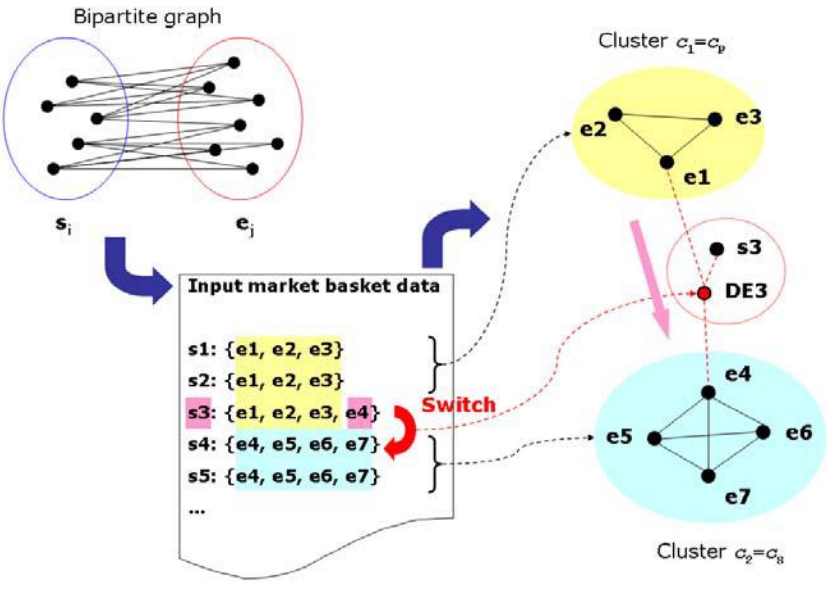

Fig. 2. Algorithm to convert a bipartite graph (corresponding market basket data) to a scenario map where dummy events are identified and placed to connect clusters (Copyright, Springer-Verlag 2007)

Fig. 3 [a], the dummy events which have the largest nodal degree are picked up. Deer standing still just by the woods (DE_{38}) and flowers in bases in a monochrome tone (DE_{39}) indicates tendency toward quietness. A catalyst personality who has mental maturity to share such loneliness or tendency toward quietness can be effective. In Fig. 3 [b], the dummy events which bridges two groups (4 and 6) most strongly are picked up. A colorful mountain (DE_{15}) and a human-like abstract painting (DE_{25}) convey vivid and spectacular feeling. Uniquely smiling countenance (DE_{23}) and a lion staring at elephants and zebras (DE_{24}) are stimulating. A catalyst personality who is unique and spectacularly strong enough to stimulate and encourage persons can be effective. In Fig. 3 [c], the dummy events which bridge the most independent clique group (3) to other groups are picked up. The catalyst can foster communication from the group 3 in three directions. A catalyst personality who looks luxurious, strong, and lively (DE_{16}, DE_{20}) can be effective toward the group 4. A catalyst personality who has, or loves feminine attractiveness (DE_{27}, DE_{46}) can be effective toward the group 8.

Finally, they evaluated the three scenarios in terms of propoeability (possibility to be a concrete action plan), unnoticeability (difficulty to notice), and growaility (feasibility to carry out). The evaluation score is summarized in Table 2. The scenario [c] is of particular interest. Gentle persons in the groups 3 and 8 interact together with vivid personality. Commonsense persons in the group 3 and unique scholars in the group 5 are activated together with feminine attractive

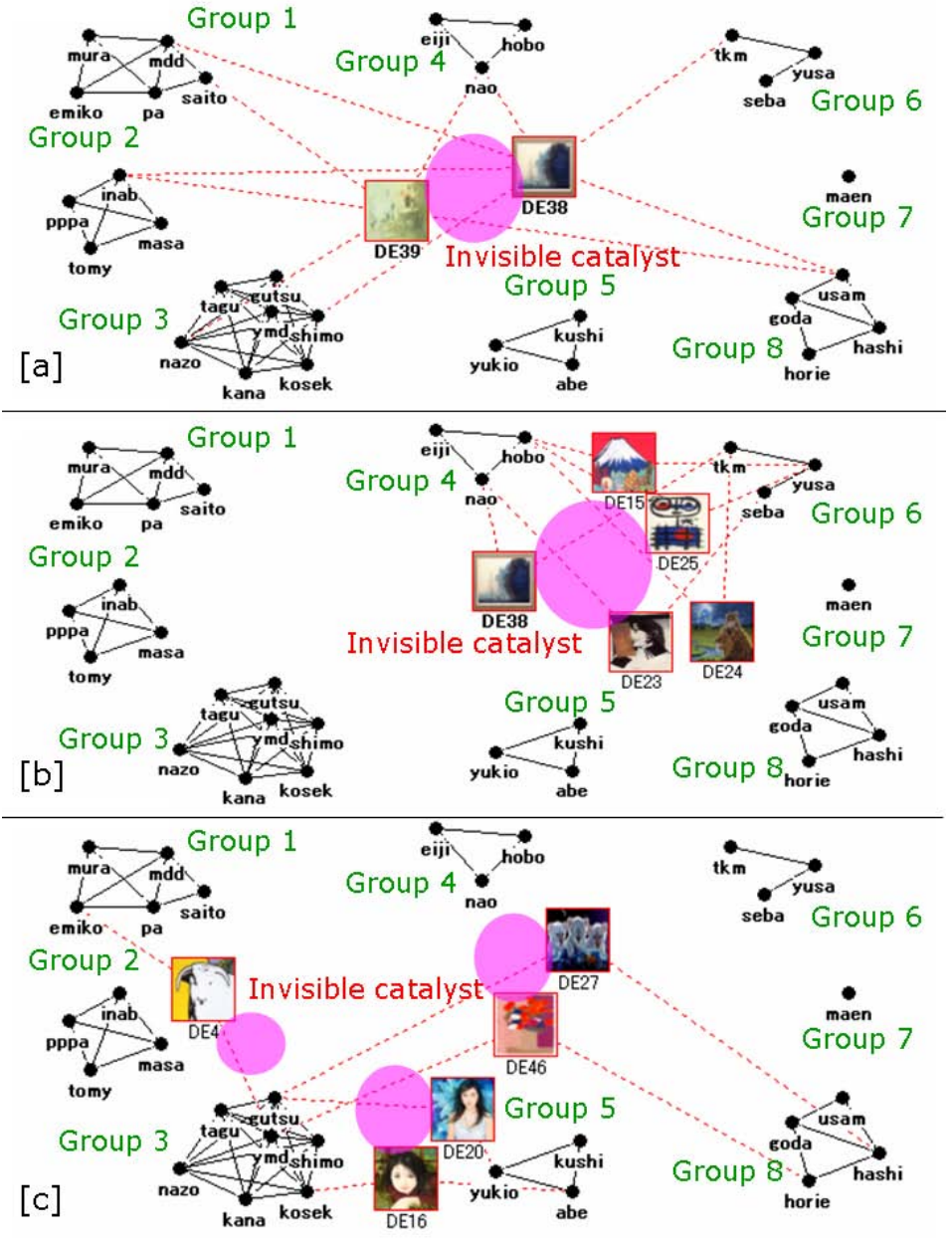

Fig. 3. Eight groups having opposing preference and a catalyst personality. The catalyst personality is collectively indicated by dummy events, DE_i, and associated with corresponding art piece graphics, s_i. [a] Catalyst who has the largest nodal degree. [b] Catalyst who bridges two groups most strongly. [c] Catalysts who bridge the most independent clique group to other groups.

Table 1. Interpretation of the clusters

Cluster	Keywords for the member persons
1	Fashion, trendy, lowbrow, imitation
2	Health, brave, independent, non group-oriented
3	Commonsense, balance
4	Cheerful, hidden abnormality
5, 6	Autonomous, scholar, abnormal, dark
7	Premature, growing, talent
8	Calm, adult, businessperson

Table 2. Evaluation of the three scenarios

Scenario	Proposability	Unnoticeability	Growability	Total
a	Moderate	Moderate	Bad	Bad
b	Good	Moderate	Moderate	Moderate
c	Good	Good	Moderate	Good

personality. These are unexpected, but agreed as relevant. Concreteness, as well as novelty as a hypothesis, increases in the order from the scenario [a], [b] to [c]. They indicate that it leads to less noticeable, but more relevant scenarios to pay attention to a particular fine structure than to overlook the whole structure.

References

[Barabási 1999] Barabási, A.L., Albert, R., Jeong, H.: Mean-field theory for scale-free random networks. Physica A 272, 173–187 (1999)

[Borgatti 1997] Borgatti, S.P., Evarett, M.G.: Network analysis of 2-mode data. Social Networks 13, 155–168 (1997)

[Krackhardt 1987] Krackhardt, D.: Cognitive social structures. Social Networks 9, 109–134 (1987)

[Keila 2006] Keila, P.S., Skillicorn, D.B.: Structure in the Enron email dataset. J. Computational & Mathematical Organization Theory 11, 183–199 (2006)

[Maeno 2007] Maeno, Y., Ohsawa, Y.: Human-computer interactive annealing for discovering invisible dark events. IEEE Trans. Industrial Electronics 54 (to appear)

[Maeno 2006a] Maeno, Y., Ohsawa, Y.: Stable deterministic crystallization for discovering hidden hubs. In: Proc. IEEE Int'l. Conf. Systems, Man & Cybernetics, Taipei (2006)

[Maeno 2006b] Maeno, Y., Ito, K., Horie, K., Ohsawa, Y.: Human-interactive annealing for turning threat to opportunity in technology development. In: Proc. IEEE Int'l. Conf. Data Mining, Workshops, Hong Kong, pp. 714–717 (2006)

[Ohsawa 2006] Ohsawa, Y. (ed.): Chance discovery in real world decision making. Springer, Heidelberg (2006)

[Ohsawa 2005] Ohsawa, Y.: Data crystallization: chance discovery extended for dealing with unobservable events. New Mathematics and Natural Computation 1, 373–392 (2005)

[Singh 2004] Singh, S., Allanach, J., Haiying, T., Pattipati, K., Willett, P.: Stochastic modeling of a terrorist event via the ASAM system. In: Proc. IEEE Int'l. Conf. Systems, Man & Cybernetics, Hague, pp. 6/5673–6/5678 (2004)

[Watts 1998] Watts, D.J., Strogatz, S.H.: Collective dynamics of small-world networks. Nature 398, 440–442 (1998)

On Using Learning Automata to Model a Student's Behavior in a Tutorial-*like* System

Khaled Hashem[1] and B. John Oommen[2]

[1] School of Computer Science, Carleton University, Ottawa, Canada, K1S 5B6
khaled_hashem@external.mckinsey.com
[2] Chancellor's Professor; Fellow: IEEE and Fellow: IAPR
School of Computer Science, Carleton University, Ottawa, Canada, K1S 5B6.
Also an Adjunct Professor with Agder University College in Grimstad, Norway
oommen@scs.carleton.ca

Abstract. This paper presents a new philosophy to model the behavior of a Student in a Tutorial-*like* system using Learning Automata (LA). The model of the Student in our system is inferred using a higher-level of LA, referred to *Meta-LA*, which attempt to characterize the learning model of the Students (or Student Simulators), while the latter use the Tutorial-*like* system. To our knowledge, this is the first published result which attempts to infer the learning model of an LA when it is treated externally as a black box, whose outputs are the only observable quantities. Additionally, our paper represents a new class of Multi-Automata systems, where the *Meta-LA* communicate with the Students, *also modelled* using LA, in a synchronous scheme of interconnecting automata.

Keywords: Student Modelling, Tutorial-*like* Systems, Learning Automata.

1 Introduction

The Student is the focal point of interest in any Tutorial system. The latter is customized to maximize the learning curve for the Student. In order for the Tutorial system to achieve this, it needs to treat every student according to his[1] particular skills and abilities. The system's model for the Student permits such a customization.

The aim of this paper is to present a new philosophy to model how a Student learns while using a Tutorial-*like* system, that is based on the theory of stochastic Learning Automata (LA). The LA will enable the system to determine the learning model of the Student, which, consequently, will enable the Tutorial-*like* system to improve the way it "deals" (i.e., presents material, teaches and evaluates) with the Student to customize the learning experience.

In this paper, we propose what we call a *Meta-LA* strategy which can be used to examine the Student model. As the name implies, we have used LA as

[1] For the ease of communication, we request the permission to refer to the entities involved (i.e. the Teacher, Student, etc.) in the masculine.

H.G. Okuno and M. Ali (Eds.): IEA/AIE 2007, LNAI 4570, pp. 813–822, 2007.

a learning tool/mechanism which steers the inference procedure achieved by the *Meta-LA*. To be more specific, we have assumed that a Student can be modelled as being one of the following types: slow learner , normal learner , or fast learner.

In order for the system to determine the learning model of the Student, it monitors the consequent actions of the Student and uses the *Meta-LA* to unwrap the learning model. The proposed *Meta-LA* scheme has been tested for numerous (benchmarks) environments, and the results obtained are remarkable.

Indeed, to our knowledge, this is the first published result which attempts to infer the learning model of an LA when it is treated externally as a black box, whose outputs are the only observable quantities. This paper is necessarily brief; more details of all the modules and experimental results are found in [4].

Using machine learning in Student modelling was the focus of a few previous studies (a more detailed review is found in [4]). Legaspi and Sison [5] modelled the tutor in ITS using reinforcement learning with the temporal difference method as the central learning procedure. Beck [3] used reinforcement learning to learn to associate superior teaching actions with certain states of the student's knowledge. Baffes and Mooney implemented ASSERT [2], which used reinforcement learning in student modelling to capture novel student errors using only correct domain knowledge. Our method is distinct from all the above.

1.1 Stochastic Learning Automaton

The stochastic automaton tries to reach a solution to a problem without any information about the optimal action. By interacting with an Environment, a stochastic automaton can be used to learn the optimal action offered by that Environment [6]. A random action is selected based on a probability vector, and then from the observation of the Environment's response, the action probabilities are updated, and the procedure is repeated. A stochastic automaton that behaves in this way to improve its performance is called a Learning Automaton (LA).

In the first LA designs, the transition and the output functions were time invariant, and for this reason these LA were considered "fixed structure" automata. Later, a class of stochastic automata known in the literature as Variable Structure Stochastic Automata (VSSA) was introduced. In the definition of a VSSA, the LA is completely defined by a set of actions (one of which is the output of the automaton), a set of inputs (which is usually the response of the Environment) and a learning algorithm, T. The learning algorithm [6] operates on a vector (called *the Action Probability vector*)

$\mathrm{P(t)} = [\mathrm{p_1(t)}, \ldots, \mathrm{p}_r\mathrm{(t)}]^{\mathrm{T}}$,

where $\mathrm{p}_i\mathrm{(t)}$ ($\mathrm{i} = 1, \ldots, \mathrm{r}$) is the probability that the automaton will select the action α_i at time 't',

$\mathrm{p}_i\mathrm{(t)} = \Pr[\alpha(\mathrm{t}) = \alpha_i]$, $\mathrm{i} = 1, \ldots, \mathrm{r}$, and it satisfies

$\sum_{i=1}^{r} \mathrm{p}_i\mathrm{(t)} = 1 \; \forall \; \mathrm{t}$.

Note that the algorithm $T : [0,1]^r \times \mathrm{A} \times \mathrm{B} \rightarrow [0,1]^r$ is an updating scheme where $\mathrm{A} = \{\alpha_1, \alpha_2, \ldots, \alpha_r\}$, $2 \leq \mathrm{r} < \infty$, is the set of output actions of the automaton, and B is the set of responses from the Environment. Thus, the updating is such that

$P(t+1) = T(P(t), \alpha(t), \beta(t))$,
where $P(t)$ is the action probability vector, $\alpha(t)$ is the action chosen at time t, and $\beta(t)$ is the response it has obtained.

If the mapping T is chosen in such a manner that the Markov process has absorbing states, the algorithm is referred to as an absorbing algorithm [6]. Ergodic VSSA have also been investigated [6,8]. These VSSA converge in distribution with the asymptotic distribution being independent of the initial vector. Thus, while ergodic VSSA are suitable for non-stationary environments, automata with absorbing barriers are preferred in stationary environments.

In practice, the relatively slow rate of convergence of these algorithms constituted a limiting factor in their applicability. In order to increase their speed of convergence, the concept of discretizing the probability space was introduced [8,10]. This concept is implemented by restricting the probability of choosing an action to a finite number of values in the interval [0,1].

Pursuit and Estimator-based LA were introduced to be faster schemes, since they pursue what can be reckoned to be the *current* optimal action or the set of current optimal schemes [8]. The updating algorithm improves its convergence results by using the history to maintain an estimate of the probability of each action being rewarded, in what is called the *reward-estimate* vector.

LA have been used in systems that have incomplete knowledge about the environment in which they operate [1]. They have been used in telecommunications and telephone routing, image data compression, pattern recognition, graph partitioning, object partitioning, and vehicle path control [1].

1.2 Contributions of This paper

This paper presents a novel approach for modelling how the Student learns in a tutoring session. We believe that successful modelling of Students will be fundamental in implementing the task of effective Tutorial-*like* systems. Thus, the salient contributions of this paper (clarified extensively in [4]) are:

- The concept of *Meta-LA*, in Student modelling, which helps to build a higher-level learning concept, that has been shown to be advantageous for customizing the learning experience of the Student in an "efficient" way.
- The Student Modeler, using the *Meta-LA*, will observe the action of the Student concerned and the characteristics of the Environment. It will use these observations to build a learning model for each Student and see whether he is a slow, normal, or fast learner.
- Unlike traditional Tutorial systems, which do not consider the "psychological" perspective of the Students, we model their cognitive state. This will enable the Tutorial-*like* system to customize its teaching strategy.

2 Intelligent Tutorial and Tutorial-*like* Systems

Intelligent Tutorial Systems (ITSs) are special educational software packages that involve Artificial Intelligence (AI) techniques and methods to represent the knowledge, as well as to conduct the learning interaction [7].

An ITS mainly consists of three modules, the domain model (knowledge domain), the student model, and the pedagogical model, (which represent the tutor model itself). Self [9] defined these components as the tripartite architecture for an ITS – the *what* (domain model), the *who* (student model), and the *how* (tutoring model). More details of these differences are found in [4].

2.1 Tutorial-*like* Systems

Tutorial-*like* systems share some similarities with the well-developed field of Tutorial systems. Thus, for example, they model the Teacher, the Student, and the Domain knowledge. However, they are different from "traditional" Tutorial systems in the characteristics of their models, etc. as will be highlighted below.

1. **Different Type of Teacher.** In Tutorial systems, as they are developed today, the Teacher is assumed to have perfect information about the material to be taught. Also, built into the model of the Teacher is the knowledge of how the domain material is to be taught, and a plan of how it will communicate and interact with the Student(s). The Teacher in our Tutorial-*like* system possesses different features. First of all, one fundamental difference is that the Teacher is uncertain of the teaching material – he is stochastic. Secondly, the Teacher does not *initially* possess any knowledge about "How to teach" the domain subject. Rather, the Teacher himself is involved in a "learning" process and he "learns" what teaching material has to be presented to the particular Student.
2. **No Real Students.** A Tutorial system is intended for the use of *real-life* students. Its measure of accomplishment is based on the performance of these students after using the system, and it is often quantified by comparing their progress with other students in a control group, who would use a *real-life* Tutor. In our Tutorial-*like* system, there are no *real-life* students who use the system. The system could be used by either:
   (a) Students Simulators, that mimic the behavior and actions of *real-life* students using the system.
   (b) An artificial Entity which, in itself, could be another software component that needs to "learn" specific domain knowledge.
3. **Uncertain Course Material.** Unlike the domain knowledge of "traditional" Tutorial systems where the knowledge is, typically, well defined, the domain knowledge teaching material presented in our Tutorial-*like* system contains material that has some degree of uncertainty. The teaching material contains questions, each of which has a probability that indicates the certainty of whether the answer to the question is in the affirmative.
4. *School* **of Students.** Traditional Tutorial Systems deal with a Teacher who teaches Students, but they do not permit the Students to interact with each other. A Tutorial-*like* system assumes that the Teacher is dealing with a *School* of Students where each learns from the Teacher on his own, and can also learn from his "colleagues" if he desires.

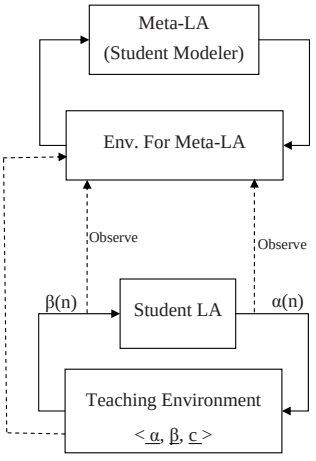

Fig. 1. Modelling Using a Network of LA

3 Network Involving the LA/*Meta-LA*

Our Tutorial-*like* system incorporates multiple LA which are, indirectly, interconnected with each other. This can be perceived to be a system of interconnected automata [11]. Since such systems of interconnecting automata may be one of two models, namely, synchronous and sequential, we observe that our system represents a synchronous model. The LA in our system and their interconnections are illustrated in Figure 1.

In a traditional interconnected automata the response from the Environment associated with one automaton represents the input to another automaton. However, our system has a rather unique LA interaction model. While the Student LA is affecting the *Meta-LA*, there is no direct connection between both of them. The *Meta-LA* Environment monitors the "performance" of the Student LA over a period of time, and depending on that, *its* Environment would penalize or reward the action of the *Meta-LA*.

This model represents a new structure of interconnection which can be viewed as being composed of two levels: a higher-level automaton, i.e., the *Meta-LA*, and a lower-level automaton, which is the Student LA. The convergence of the higher-level automaton is dependent on the behavior of lower-level automaton. Based on these differences, and additional ones listed in [4], the reader will observe the uniqueness of such an interaction of modules, as:

1. The *Meta-LA* has no Environment of its own.
2. The Environment for the *Meta-LA* consists of observations, which must be perceived as an Environment after doing some processing of the signals observed.
3. The *Meta-LA* has access to the Environment of the lower level, including the set of the penalty probabilities that are unknown to the lower-level LA.

4. The *Meta-LA* has access to the actions chosen by the lower-level LA.
5. Finally, the *Meta-LA* has access to the responses made by the lower-level Environment.

In conclusion, we observe that items (3)-(5) above collectively constitute the Environment for the *Meta-LA*. Such a modelling is unknown in the field of LA.

4 Formalization of the Student Model

To simplify issues, we assume that the learning model of the Student is one of these three types[2]:

1. A FSSA model, which represents a Slow Learner.
2. A VSSA model, which represents a Normal Learner.
3. A Pursuit model LA, which represents a Fast Learner.

The Student model will use three specific potential LA, each of which serve as an action for a higher-level automaton – (i.e., a *Meta-LA*).

In our present instantiation, the *Meta-LA* which is used to learn the best possible model for the Student Simulator is a 4-tuple: $\{\underline{\alpha}, \underline{\beta}, \mathrm{P}, T\}$, where:

$\underline{\alpha} = \{\alpha_1, \alpha_2, \alpha_3\}$, in which
  α_1 is the action corresponding to a FSSA model (Slow Learner).
  α_2 is the action corresponding to a VSSA model (Normal Learner).
  α_3 is the action corresponding to a Pursuit model LA(Fast Learner).

$\underline{\beta} = \{0, 1\}$, in which
  $\beta = 0$ implies a Reward for the present action chosen, and
  $\beta = 1$ implies a Penalty for the present action chosen.

$\mathrm{P} = [\mathrm{p}_1, \mathrm{p}_2, \mathrm{p}_3]^{\mathrm{T}}$, where
  $\mathrm{p}_i(\mathrm{n})$ is the current probability of the Student Simulator being represented by α_i.

T is the probability updating rule given as a map as:
  T: $(\mathrm{P}, \underline{\alpha}, \underline{\beta}) \rightarrow \mathrm{P}$.

Each of these will now be clarified.

1. $\underline{\beta}$ is the input which the *Meta-LA* receives (or rather, infers). For a fixed number of queries, which we shall refer to as the "Window", the *Meta-LA* assumes that the Student Simulator's model is α_i. Let $\theta(\mathrm{t})$ be the rate of learning of the lower LA at time 't'. By inspecting the way by which the Student Simulator learns within this Window, it infers whether this current model should be rewarded or penalized. We propose to achieve this by using two thresholds, which we refer to as $\{\theta_j | 1 \leq j \leq 2\}$ where the Student is considered to be a slow learner if his learning rate is less than θ_1, a fast learner if his learning rate is greater than θ_2, and a normal learner if his learning rate is between θ_1 and θ_2.

[2] Additional details of such a modelling phenomenon are included in [4], and omitted here in the interest of brevity. Also, extending this to consider a wider spectrum of learning models is rather straightforward.

2. P is the action probability vector which contains the probabilities that the *Meta-LA* assigns to each of *its* actions. At each instant t, the *Meta-LA* randomly selects an action $\alpha(t) = \alpha_i$. The probability that the automaton selects action α_i, at time t, is the action probability $p_i(t) = \Pr[\alpha(t) = \alpha_i]$, where $\sum_{i=1}^{r} p_i(t) = 1 \quad \forall\, t$, i=1, 2, 3.
   Initially, the *Meta-LA* will have an equal probability for each of the three learning models as:
   $$[1/3 \quad 1/3 \quad 1/3]^{\mathrm{T}}$$
   By observing the sequence of $\{\theta(\mathrm{t})\}$, the *Meta-LA* updates $\mathrm{P}(t)$ as per the function T, described presently. One of the action probabilities, p_j, will, hopefully, converges to a value as close to unity as we want.
3. T is the updating algorithm, or the reinforcement scheme used to update the *Meta-LA*'s action probability vector, and is represented by:
   $\mathrm{P}(t{+}1) = T[\mathrm{P}(t), \alpha(t), \beta(t)]$.

5 Experimental Results

This section presents the experimental results obtained by testing the prototype implementation of the *Meta-LA*. The simulations were performed for two different types of Environments, two 4-action Environments and two benchmark 10-action Environments. These Environments represent the teaching "problem", which contains the uncertain course material of the Domain model associated with the Tutorial-*like* system. In all the tests performed, an algorithm was considered to have converged, if the probability of choosing an action was greater than or equal to a threshold $T(0 < T \leq 1)$. In our simulation, T was set to be 0.99 and the number of experiments (NE) was set to be 75.

The *Meta-LA* has been implemented as a Discretized LA, the DL_{RI} scheme, with a resolution parameter N=40. The Student Simulator was implemented to mimic three typical types of Students as follows:

- Slow Learner: The Student Simulator used a FSSA, in the form of a Tsetlin $\mathrm{L}_{N,2N}$ automaton, which had two states for each action.
- Normal Learner: The Student Simulator used a VSSA, in the form of a L_{RI}, with λ=0.005.
- Fast Learner: The Student Simulator utilized the Pursuit PL_{RI}, with λ=0.005.

The rate of learning associated with the Student is a quantity that is difficult to quantify. For that, the *Meta-LA* Environment calculates the loss-function of the Student Simulator LA. For a "Window" of n choice-response feedback cycles of the Student Simulator, the loss-function is defined by:
$\frac{1}{n} \sum \mathrm{n}_i \; \mathrm{c}_i$,
where n_i is the number of instances an action α_i is selected inside the "Window" and, c_i is the penalty probability associated with action α_i of the lower-level LA.

We consider the rate of learning for the Student to be a function of the loss-function and time, as illustrated in Figure 2. This reflects the fact that the loss function for any learning Student, typically, decreases with time (for all types of learners) as he learns more, and as his knowledge improves by time.

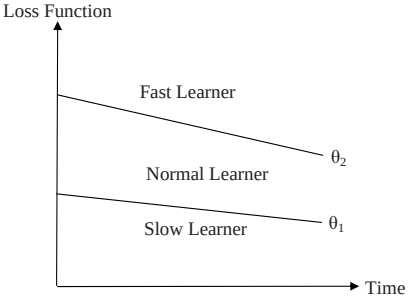

Fig. 2. Loss Function and θ

5.1 Environments with 4-Actions and 10-Actions

The 4-action Environment represents a Multiple-Choice question with 4 options. The Student needs to learn the content of this question, and conclude that the answer for this question is the action which possesses the minimum penalty probability. Based on the performance of the Student, the *Meta-LA* is supposed to "learn" the learning model of the Student. The results of this simulation are presented in Table 1.

Table 1. Convergence of *Meta-LA* for Different Student's Learning Models in Four-Action Environments

Env.	θ_1	θ_2	PL_{RI}		L_{RI}		Tsetlin	
			# of Iter.	% correct convergence	# of Iter.	% correct convergence	# of Iter.	% correct convergence
$\mathbf{E_A}$	0.50-0.31	0.60-0.35	607	100%	1037	87%	1273	91%
$\mathbf{E_B}$	0.28-0.17	0.37-0.24	790	97%	1306	89%	1489	85%
Reward probabilities are:			$\mathbf{E_A}$: 0.7 0.5 0.3 0.2 $\mathbf{E_B}$: 0.1 0.45 0.84 0.76					

To be conservative, the simulation assumes that when the Student starts using the system, the results during a transient learning phase, are misleading and inaccurate. Therefore, the first 200 iterations are neglected by the *Meta-LA*.

The results obtained were quite remarkable. Consider the case of $\mathrm{E_A}$, where the best action was α_1. While an FSSA converged in 1273 iterations[3], the L_{RI} converged in 1037 iterations and the Pursuit PL_{RI} converged in 607 iterations. By using the values of θ_1 and θ_2 as specified in Table 1, the *Meta-LA* was able to characterize the true learning capabilities of the Student 100% of the time when the lower-level LA used a Pursuit PL_{RI}. The lowest accuracy of the *Meta-LA*

[3] The figures include the 200 iterations involved in the transient phase.

for Environment E_A was 87%. The analogous results for E_B were 97% (at its best accuracy) and 85% for the Slow Learner. The power of our scheme should be obvious !

On the other hand, the 10-action Environment represents a Multiple-Choice question with 10 options. Table 2 show the results of this simulation.

Table 2. Convergence of *Meta-LA* for Different Student's Learning Models in Ten-Action Environments

Env.	θ_1	θ_2	PL_{RI}		L_{RI}		Tsetlin	
			# of Iter.	% correct convergence	# of Iter.	% correct convergence	# of Iter.	% correct convergence
$\mathbf{E_A}$	0.55-0.31	0.65-0.40	668	95%	748	93%	1369	96%
$\mathbf{E_B}$	0.41-0.17	0.51-0.26	616	100%	970	85%	1140	96%
Reward probabilities are:								
$\mathbf{E_A}$:	0.7	0.5	0.3	0.2	0.4	0.5	0.4	0.3	0.5	0.2
$\mathbf{E_B}$:	0.1	0.45	0.84	0.76	0.2	0.4	0.6	0.7	0.5	0.3

Similar to the 4-action Environments, the results obtained for the 10-action Environments were very fascinating. For example, we consider the case of E_A, where the best action was α_1. While an FSSA converged in 1369 iterations, the L_{RI} converged in 748 iterations and the Pursuit PL_{RI} converged in 668 iterations. By using the values of θ_1 and θ_2 as specified in Table 2, the *Meta-LA* was able to determine the true learning capabilities of the Student 95% of the time, when the lower-level LA used a Pursuit PL_{RI}. The lowest accuracy of the *Meta-LA* for Environment E_A was 93%. By comparison, for E_B, the best accuracy was 100% for the Fast Leaner and the worst accuracy was 85% for the Slow Learner. The details of more simulation results can be found in [4], and are omitted here in the interest of brevity.

We believe that the worst-case accuracy of 15% (for the inexact inference) is within a reasonable limit. Indeed, in a typical learning environment, the Teacher may, incorrectly, assume the wrong learning model for the Student. Thus, we believe that our *Meta-LA* learning paradigm is remarkable considering that these are the first reported results for inferring the nature of an LA if it is modelled as a black box.

6 Conclusion and Future Work

This paper presented a novel strategy for a Tutorial-*like* system inferring the model of a Student. The Student Modeler itself uses a LA as an internal mechanism to determine the learning model of the Student, so that it could be used in the Tutorial-*like* system to customize the learning experience for each Student. To achieve this, the Student Modeler uses a higher-level automaton, a so-called

Meta-LA, which observes the Student Simulator LA's actions and the teaching Environment, and attempts to characterize the learning model of the Student (or Student Simulator), while the latter uses the Tutorial-*like* system.

From a conceptual perspective, the paper presents a new approach for using interconnecting automata, where the behaviorial sequence of one automaton affects the other automaton. From the simulation results, we can conclude that this approach is a feasible and valid mechanism applicable for implementing a Student modelling process. The results shows that the Student Modeler was successful in determining the Student learning model in a high percentage of the cases – sometimes with an accuracy of 100%.

We believe that our approach can also be ported for use in traditional Tutorial Systems. By finding a way to measure the rate of learning for *real-life* Students, the Student Modeler should be able to "approximate" the learning model for these Students. This would decrease the complexity of implementing Student models in these systems too. The incorporation of all these concepts into a Tutorial-*like* system is the topic of research which we are currently pursuing.

References

1. Agache, M., Ooommen, B.J.: Generalized pursuit learning schemes: New fam- ilies of continuous and discretized learning automata. IEEE Trans. Syst. Man. Cybern. 32(6), 738–749 (2002)
2. Baffes, P., Mooney, R.: Refinement-based student modeling and automated bug library construction. J. of AI in Education 7(1), 75–116 (1996)
3. Beck, J.: Learning to teach with a reinforcement learning agent. In: Proceedings of The Fifteenth National Conference on AI/IAAI, p. 1185, Madison, WI (1998)
4. Hashem, K., Oommen, B.J.: Modeling a student's behavior in a tutorial-like system using learning automata. Unabridged version of this paper
5. Legaspi, R.S., Sison, R.C.: Modeling the tutor using reinforcement learning. In: Proceedings of the Philippine Comp. Sc. Congress (PCSC), pp. 194–196 (2000)
6. Narendra, K.S., Thathachar, M.A.L.: Learning Automata: An Introduction. Prentice-Hall, New Jersey (1989)
7. Omar, N., Leite, A.S.: The learning process mediated by ITS and conceptual learning. In: Int. Conference On Engineering Education, Rio de Janeiro (1998)
8. Oommen, B.J, Agache, M.: Continuous and discretized pursuit learning schemes: Various algorithms and their comparison. IEEE Trans. Syst. Man. Cybern. SMC 31(B), 277–287 (2001)
9. Self, J.: The defining characteristics of intelligent tutoring systems research: ITSs care, precisely. International J. of AI in Education 10, 350–364 (1999)
10. Thathachar, M.A.L., Oommen, B.J.: Discretized reward-inaction learning automata. Journal of Cybernetics and Information Science 24–29, Spring (1979)
11. Thathachar, M.A.L., Sastry, P.S.: Varieties of learning automata: An overview. IEEE Trans. Syst. Man. Cybern. 32(6), 711–722 (2002)

Test-Sheet Composition Using Immune Algorithm for E-Learning Application

Chin-Ling Lee[1], Chih-Hui Huang[2,⋆], and Cheng-Jian Lin[2]

[1] Dept. of Applied Foreign Languages
Chaoyang University of Technology
168 Gifeng E. Rd., Wufeng
Taichung County 413, Taiwan, R.O.C.
[2] Dept. of Computer Science and Information Engineering
Chaoyang University of Technology
168 Gifeng E. Rd., Wufeng
Taichung County 413, Taiwan, R.O.C.
Tel.: +886-4-23323000 Ext. 7633; Fax: +886-4-23742375
chh@cyut.edu.tw, s9367601@cyut.edu.tw

Abstract. In this paper, a novel approach Immune Algorithm (IA) is applied to improve the efficiency of composing near optimal test sheet from item banks to meet multiple assessment criteria. We compare the results of immune and Genetic Algorithm (GA) to compose test-sheets for multiple assessment criteria. From the experimental results, the IA approach is desirable in composing near optimal test-sheet from large item banks. And objective conceptual vector (OCV) and objective test-sheet test item numbers (M) can be effectually achieved. Hence it can support the needs of precisely evaluating student's learning status. We successfully extend the applications of artificial intelligent - Immune to the educational measurement.

1 Introduction

In recent years, the development of internet in teaching and learning fields has overcome the time and space limitation no matter in teaching or learning environment. Therefore some researchers have developed various computer-assisted testing systems to more precisely evaluate student's learning status [1]-[3]. Most of the existing systems construct a test-sheet by manually or randomly selecting test items, which are inefficient and unable to help with the diagnosis of students learning problems. A well-constructed test-sheet can help evaluation of the learning status of the students, and improve the diagnosis of any problems students encounter during their learning process [6]. However, the quality of a test is not only dependent upon the quality of the item bank, but also how the test-sheet is constructed [1]. Further, it is important to select appropriate test items when constructing a test-sheet that meets multiple assessment requirements, such as

⋆ Corresponding author.

H.G. Okuno and M. Ali (Eds.): IEA/AIE 2007, LNAI 4570, pp. 823–833, 2007.

an objective conceptual weight and objective test-sheet test item numbers. To facilitate a well-constructed test-sheet, some special techniques have emerged, such as Hwang et al. (2003) proposed a multiple-criteria where the test-sheet composing problem is formulated as a dynamic programming model [11] to minimize the distance between the parameters (e.g., discrimination, difficulty, etc.) of the generated test-sheet and the objective values subject to the distribution of concept weights. For the evolutionary algorithms (EAs), genetic algorithm (GA) has currently provided a method for constructing a test-sheet. GA represents effective techniques for evaluating system parameters and finding global solutions while optimizing the overall structure. Chen (2003) proposed an applying greedy-genetic algorithm to select test items [2]. Sun (1999) and Hwang (2003) used a genetic algorithm to construct a test-sheet [3]-[4]. Hwang (2002) using Grey Theory on test items selection[5]. However, GA is defeated by the low rate of convergence during the evaluation process and the above-mentioned methods usually may not achieve the anticipated objectives.

The immune system algorithm uses the clonal selection principle to cancel antibodies between others of high similar degree, and these antibodies, after the process, will be of higher quality, accelerating the search and increasing the global search capacity [8]. Because the number of test items in an item bank is usually large and the number of feasible combinations to form test-sheet thus grows exponentially, an optimal test-sheet takes enormous time to build up. Therefore, to deal with the problem in order to compose an optimal test-sheet from large item banks, we employ a novel approach immune algorithm (IA) [10] to optimize selection of test items which can highly effectively achieve special instructional objectives. The IA use not only clonal selection principle to deal with the high similar antibodies but also an elitism selection in order to ensure the best composition of the antibody (test-sheet) could be kept to next generation for the optimal test-sheet.

This paper is organized as follows. Section 2 describes the application of the immune algorithm (IA) for the test-sheet composition, the structure of test-sheet composition and the definition of two conditions OCV and M (In section 2.1). And the proposed TSCIA in section 2.2 expresses how to use TSCIA to construct the optimal test-sheet from large item banks. Finally, the experimental results and conclusions are summarized in the last section 4 and 5.

2 An Immune Algorithm (IA) for the Test-Sheet Composition

In the field of testing, the test-sheet constructing usually depends on specific objectives defined by the teacher according to instructional objectives, such as difficulty degree, concept weight, discrimination degree and number of test items in the test-sheet. Therefore we defined the instructional objectives parameter based on concept weights and number of test items, and the composition of test-sheet must achieve objective conceptual vector (OCV) and objective test-sheet test item numbers (M). In this paper, the test test-sheet composition with

immune algorithm (TSCIA) aims to generate an optimal test-sheet that fits for objective conceptual vector (OCV) and objective test-sheet test item numbers (M).

2.1 Structure of Test-Sheet Composition

First, the test items in TSCIA are coded into an antibody, one antibody regarded as a test-sheet, and the other as an antigen shown in Fig. 1. Where L is the size of an antibody and where i and j represent the ith test item in jth test-sheet respectively.

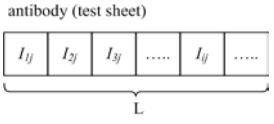

Fig. 1. Coding a test-sheet into an antibody

In a test-sheet the I_{ij} expresses as 0 and 1, 1 represents the ith test item selected in jth test-sheet, otherwise not (see Fig. 2). In order to reach the op-

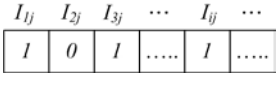

Fig. 2. Represent the selection in a test-sheet (antibody)

timization, two conditions, objective conceptual vector (OCV) and objective test-sheet test item numbers (M), must be accordance with each other, which will be described by the following.

A. The Objective Conceptual Vector (OCV)
The objective conceptual vector (OCV) used to evaluate the effectiveness of the test-sheet component where is varied over the range [0, 1] and the vector of OCV represents as below:

$$OCV = [C_1, C_2, \ldots, C_{n-1}, C_n]$$

where n expects the number of objective conceptual group, C represents of objective conceptual group weights, for example OCV = $[C_1, C_2, C_3, C_4, C_5, C_6]$ = [0, 0.1, 0.4, 0.4, 0.1, 0], there n=6 objectives conceptual group and relative weights represent [0, 0.1, 0.4, 0.4, 0.1, 0]. The first priority is the objective conceptual vector (OCV). In TSCIA, first the calculation of an antibody (test-sheet) average conceptual vector (o_{jk}) is applied to compare with the OCV, and each gene (test item) has its concept weights fitting to specific concept group. The (o_{jk}) represents the jth antibody (test-sheet) with the kth concept group, and the calculating method is illustrated as below:

$$o_{jk} = \frac{\sum_{i=1}^{L} c'_{ijk}}{\sum_{i=1}^{L} I_{ij}} \tag{1}$$

where o_{jk} is average concept weight, o'_{ijk} is concept weight, $I_{ij}$is test item, i is ith test item, j is jth test-sheet, k is kth concept.

B. The Objective Test-Sheet Test Item Numbers (M)

In TSCIA, the second condition m should be approximate to objective test-sheet test item numbers (M), and m can be calculated by below equation:

$$m = \sum_{i=1}^{L} I_i \tag{2}$$

where m represents the summation of the chosen times and L is the number of test items.

2.2 Test-Sheet Composition with Immune Algorithm (TSCIA)

This section describes the test-sheet composition using Immune algorithm (TSCIA) to construct the optimal test-sheet from item bank. Analogous to the biological immune system, the proposed algorithm has the capability of seeking feasible solutions while maintaining diversity. In order to effectively approach two conditions (OCV and M), the *clonal selection principle* is used to guarantee and improve the quality of antibodies (test-sheet) with high similar degree are canceled principle, and the *elitism selection* in reproduction stage is used to ensure keeping the best antibody (test-sheet) in next generation. The whole TSCIA process is illustrated as follows.

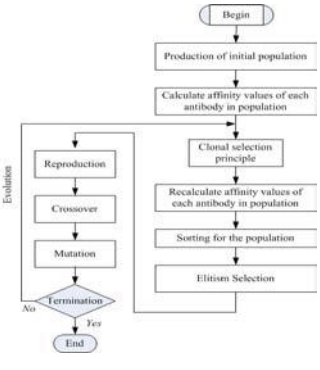

Fig. 3. Flowchart of the proposed TSCIA

A. Production of Initial Population

In this section, the initialization process is demonstrated which antibodies utilize binary-code string. And the antibodies (test-sheet) are generated by randomly in order to cope with the antigens (test items) in the population size.

B. Evaluation Affinity Value in TSCIA

In this subsection, the TSCIA presents a novel approach immune algorithm (IA) to optimize selection of test items, which can effectively achieve special instructional objectives (objective conceptual vector (OCV) and objective test-sheet test item numbers (M)). In TSCIA, *affinity* refers to the binding strength between a single antigenic determinants and an individual antibody-combining site. The process of recognizing antigens is to search for antibodies with the maximum affinity with antigens. In this paper, the *affinity value* is designed according to the following formulation:

$$Affinity\ value = \frac{1}{1 + (1 - w)E_{OCV} + wE_{ME}} \tag{3}$$

where E_{OCV} represents the mean square error between the antibodys concept weight and the objective conceptual vector (OCV), and E_{ME} represents the mean square error between the antibodys test items numbers and the objective test-sheet test items numbers (M). The objectives are minimum errors of sum of the E_{OCV} and the E_{ME}, and parameter w, which is a weight value that influences the results of the E_{OCV} and the E_{ME}. We need to adjust w at the same time, then let E_{OCV} and E_{ME} can archiving as above objectives. The affinity value approximate 1 represents the test-sheet approximate to objectives: objective conceptual vector (OCV) and objective test-sheet test items numbers (M)). The E_{OCV} is given by the following formula:

$$E_{OCV} = \sqrt{\sum_{j=1}^{ps} (o_j - O)^2} \tag{4}$$

where O represents the objective conceptual vector (OCV), o_j is the average conceptual vector in jth antibody, and ps is the population size.

The E_{ME} is given by the following formula:

$$E_{ME} = \sqrt{\sum_{j=1}^{ps} (m_j - M)^2} \tag{5}$$

where M represents the objective test-sheet test item numbers (M), m is the test-sheet test item number in jth antibody, and ps is the population size.

C. Clonal Selection Principle

The antibodies of this immune system that eliminate the antigen should exhibit at least a minimal threshold of diversity. Accordingly, the *diversity operator* is applied to these antibodies such as those between others of highly similar degree

are canceled, guaranteeing and improving in quality. This process is called *clonal selection principle*. Therefore, if the affinity between two antibodies exceeds the suppression threshold Th_{aff}, then these two antibodies are similar. Now, the population is assumed to be composed of ps antibodies with L genes, as shown in Fig. 4.

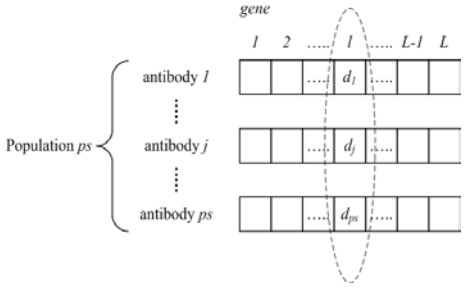

Fig. 4. Composition of population with these antibodies

An information theory yields the entropy value $EV_l(ps)$ of the ith gene in this jth antibody:

$$EV_l(ps) = \sum_{j=1}^{ps} -P_{ij}\ logP_{ij} \tag{6}$$

where P_{ij} is the probability of the jth allele from the ith gene, and $p_{ij} = 1/(1 + ||d_j - d_{j'}||)$ is defined, where dj and dj' are the genes of the jth and the j'th antibody, respectively. The diversity of the genes is calculated using Eq. (6). If all alleles of the ith gene are of the same form, then the entropy value $EV_l(ps)$ will be zero. The average entropy value $EV(ps)$ of the diversity is also given as follows;

$$EV(ps) = \frac{\sum_{l=1}^{L} EV_i(ps)}{L} \tag{7}$$

where L is the size of an antibody. Equation (7) yields the diversity of the antibody pool in terms of the entropy. Two affinity expressions are considered in the proposed approach. The first one explains the relationships between the antibody and the antigen, and is given by Eq. (3). The second one describes the degree of association between antibodies. The following equation computes the affinity between antibodies;

$$Affinity_Ab_{ij'} = \frac{1}{1 + EV(2)} \tag{8}$$

where $Affinity\_Ab_{jj'}$ is the affinity between two antibodies j and j', and $EV(2)$ is the entropy of only the antibodies j and j'. This affinity is constrained from

zero to one. When $EV(2)$ is zero, the genes of the jth antibody and the j'th antibody are the same. Therefore, the clonal selection principle is that if the $Affinity\_Ab_{jj'}$ exceeds Th_{aff}, then the antibody should be canceled. Reproduction, crossover and mutation steps follow, according to the flowchart presented in Fig. 5.

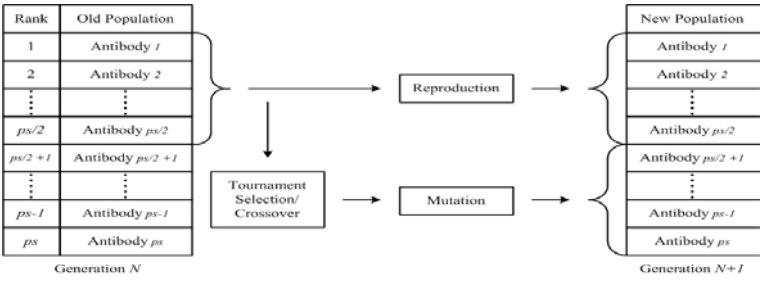

Fig. 5. Flowchart of reproduction, crossover and mutation steps

D. Reproduction Step

In the reproduction step, when creating a new generation, there is always a risk of losing most fit individuals. In this step, we keep the top half of antibodies into the next generation by *elitism selection* in the population. Using elitism, the antibodies are ranked in ascending order to their affinity value. The most fit individuals are kept as the parent for the next generation. Elitism selection improves the efficient of TSCIA considerably, as it prevents losing the best results. The other half is generated to perform crossover on antibodies in the top half of the parent generation.

E. Crossover Step

Reproduction directs the search toward the best existing antibodies but does not create any new antibodies. The new antibodies are principally generated by crossover. In this process, the first step is to select two antibodies for crossover. Two antibodies for crossover are selected by tournament selection [9] on the top half of the best-performing antibodies. Tournament selection shown in Fig.6 randomly selects three antibodies, and the antibody with the best affinity is adopted as the designated antibody. The other designated antibody is selected in the same way. Two new antibodies are generated by performing crossover on the selected designated antibodies. In the second step, the two designated antibodies are crossed and separated using a one-point crossover, as shown in Fig. 7, in which new antibodies are created by exchanging the gene between the selected sites of the two designated antibodies. Thereafter, the two new antibodies replace the two designated antibodies.

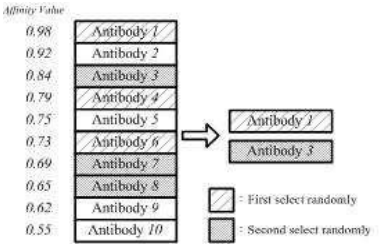

Fig. 6. Tournament selection

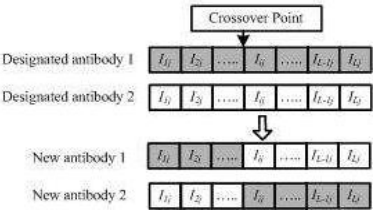

Fig. 7. One-point crossover

F. Mutation Step

The operation of a mutation for the antibody avoids the result falling in a local optimal solution and to ensure the searching capacity of approximate global optimal solution. First, we randomized a value as the mutation site. If the randomized value is smaller than the mutation rate, then we will select a gene to replace by 0 to 1 or 1 to 0, and selection gene side by means of randomly generating a value.

3 Experimental Results

To efficiently determine the performance of the proposed TSCIA, experiments were conducted to compare to GA. The item bank consists of 1000 Chinese test items on the subject of *"Introduction to Computers"*. The initial parameters of population size (ps)=200, crossover rate=0.5, mutation rate=0.2, iteration=100 and object test-sheet test item numbers (M) 10.

3.1 Comparison Example of Objective Conceptual Value

In order to prove the performance of proposed TSCIA, we compared TSCIA and GA with different objective conceptual vector (OCV). The Table 1 shows that the GA and TSCIA select the best value after 10-time operation, and compare to different case of OCV. The results show, the TSCIA is more approximate objective conceptual vector (OCV) then to GA. At the same time TSCIA totally achieve objective test-sheet test item numbers (M) but GA did not have. For example, in Table1 of the case 4 OCV= [0.3 0.4 0.2 0.1 0 0], TSCIA affinity value is close to 1 that approximate to optimal solution. And test-sheet test item numbers m is also fulfilled object test-sheet test items number ($M = 10$). The TSCIA nearly reaches two limiting conditions (OCV and M). The affinity value curves are represented in Fig. 8.

Table 1. Comparison results from different OCV

Case1	OCV						M	Affinity value
Object	0	0	0.2	0.1	0.3	0.4	10	
GA	0.048436	0.089191	0.17031	0.072582	0.2578	0.36168	12	0.94357
TSCIA	**0**	**0**	**0.2**	**0.12029**	**0.27971**	**0.4**	**10**	**0.98854**
Case2	**OCV**						**M**	**Affinity value**
Object	**0**	**0.1**	**0.4**	**0.4**	**0.1**	**0**	**10**	
GA	0.028808	0.1051	0.33333	0.36731	0.082117	0.083333	12	0.93704
TSCIA	**0.03457**	**0.08014**	**0.4**	**0.38675**	**0.09854**	**0**	**10**	**0.98329**
Case3	**OCV**						**M**	**Affinity value**
Object	**0**	**0.1**	**0.5**	**0.3**	**0.1**	**0**	**10**	
GA	0.088845	0.10561	0.44304	0.26741	0.0951	0	11	0.9481
TSCIA	**0.02838**	**0.11211**	**0.5**	**0.26376**	**0.09575**	**0**	**10**	**0.98105**
Case4	**OCV**						**M**	**Affinity value**
Object	**0.3**	**0.4**	**0.2**	**0.1**	**0**	**0**	**10**	
GA	0.26972	0.34661	0.16667	0.13367	0	0.083333	12	0.93808
TSCIA	**0.30004**	**0.39996**	**0.2**	**0.1**	**0**	**0**	**10**	**0.99998**

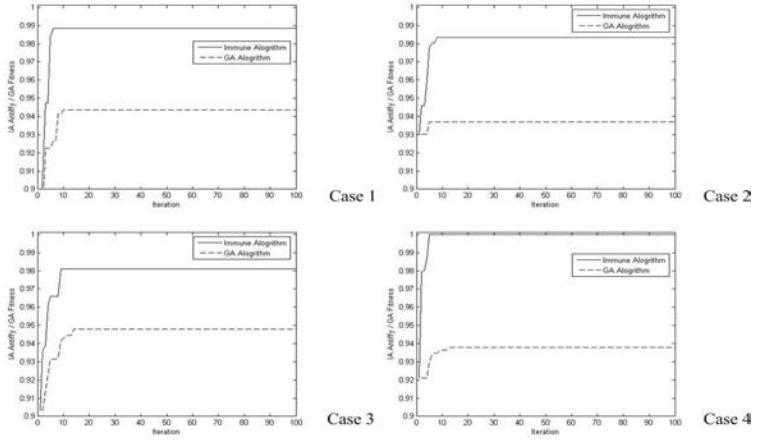

Fig. 8. The comparison curves of TSCIA and GA

3.2 Comparison Example of the Performance and Stably

Table 2 represents the comparison results of TSCIA and GA, which is based on OCV= [0 0.1 0.5 0.3 0.1 0], M=10 by 10-time operation. The results show that even the fitness value of GA can approximate 0.96048 (in the column 4) but test-sheet test item numbers of m still can't approximate objective M. The TSCIA average affinity value is 0.975519 exceed to GA, and produced test items m every time can achieve objective M perform that represent TSCIA is very stable. In column 1, the TSCIA affinity value approximate 1 and at the same time satisfies $m = M$ which almost approximate to an optimal solution. The performance of comparison results with worse, best and average values show in Table 3.

Table 2. The TSCIA and comparison results by 10-time operation

		1	2	3	4	5	6	7	8	9	10	Average
TSCIA	Affinity	0.99908	0.99612	0.95352	0.96749	0.96704	0.99784	0.98039	0.96704	0.96983	0.98684	**0.975619**
	m	10	10	10	10	10	10	10	10	10	10	**10**
GA	Affinity	0.93824	0.95337	0.91929	0.96048	0.95536	0.93813	0.93979	0.95539	0.94507	0.95523	**0.945735**
	m	13	11	12	11	11	11	11	12	11	12	**11.5**

Table 3. The results of affinity/fitness values and m

		Best	Worst	Average
TSCIA	*Affinity value*	0.99908	0.95352	0.975519
	m	10	10	10
GA	*Affinity value*	0.96048	0.91929	0.945735
	m	11	13	11.5

4 Conclusion

In this paper, a novel approach TSCIA is proposed. This approach uses the clonal selection principle to promote the quality of test-sheet (antibody) with the function of canceling the antibodies with highly similar degrees. And accelerating the search and increasing the global search capacity improve the efficiency of composing near optimal test-sheet in an item bank. According to the experimental results, the TSCIA approach is a desirable and stable approach composing near optimal test-sheet from large item banks. Manifesting the results satisfyingly, the TSCIA is effectively approximate to objective conceptual vector (OCV) and stably reaches to objective test-sheet test item numbers (M). Base on the quality of the results, the TSCIA could be suitably applied to evaluate the students learning, and to practice in actual evaluation system in the future work.

Acknowledgement

This research is supported by the National Science Council of the R.O.C. under grant NSC 95-2221-E-324-028-MY2.

References

1. Hwang, G.J., Zen, S.H.: On the development of a computer-assisted testing system with genetic test sheet generating approach. IEEE Transactions on Systems, Man, and Cybernetics XPart C: Applications and Reviews 35, 590–594 (2005)
2. Chen, C.Y.: Study of applying greedy-genetic algorithm to select test items. The unpublished masters dissertation of Information Management of National Chi Nan University (2003)
3. Sun, K.T., Lai, Y.H., Day, B.C.: A study on the test-sheet-generating strategy using genetic algorithm. National Computer Symposium (NCS 99), pp. 379–386 (1999)
4. Hwang, G.J.: A test-sheet-generating algorithm for multiple assessment requirements. IEEE Transactions on Education 46, 329–337 (2003)

5. Hwang, J.H.: The applications of grey theory on test items selection. The unpublished masters dissertation of Department of Information Engineering I- Shou University (2002)
6. Yin, P.Y., Chang, K.C., Hwang, G.J., Hwang, G.H., Chan, Y.: A particle swarm optimization approach to composing test sheets for multiple assessment criteria. Educational Technology and Society 9, 3–15 (2006)
7. Zhenguo, T., Yong, L.: A robust stochastic genetic algorithm (StGA) for global numerical optimization. IEEE Transactions on Evolutionary Computation 8, 456–470 (2004)
8. De Castro, L.N., Von Zuben, F.J.: Learning and optimization using the clonal selection principle. IEEE Transactions on Evolutionary Computation 6, 239–251 (2002)
9. Cordon, O., Herrera, F., Hoffmann, F., Magdalena, L.: Advances in fuzzy systems-applications and theory. In: Genetic Fuzzy Systems Evolutionary Tuning and Learning of Fuzzy Knowledge Bases, vol. 19, World Scientific Publishing, NJ (2001)
10. Jerne, N.K.: The immune system. Scientific American 229, 52–60 (1973)
11. Hwang, G.J.: A test-sheet-generating algorithm for multiple assessment requirements. IEEE Transactions on Education 46, 329–337 (2003)

PDA Plant Search System Based on the Characteristics of Leaves Using Fuzzy Function

Shu-Chen Cheng[1], Jhen-Jie Jhou[2], and Bing-Hong Liou[3]

Department of Computer Science and Information Engineering, Southern Taiwan University of Technology, Tainan 710, Taiwan
kittyc@mail.stut.edu.tw[1],tatajay@gmail.com[2],blueangel5112200@yahoo.com.tw[3]

Abstract. In view of the fact that most people do not know the names of the plants which can be seen everywhere, a plant search system with artificial intelligence on PDA devices is developed. In this study, users need to input the classified characteristics of leaves by observing plants' leaves. After calculating the centroid-contour distance (CCD) and fuzzy function for all characteristics, the search results are displayed and arranged according to their ranks. Thus there is no need to consult all kinds of correlative books about plants. With the help of the plant search system on PDA devices, users can broaden their knowledge by mobile learning and the observation of plants.

Keywords: centroid-contour distance, fuzzy sets, PDA, artificial intelligence.

1 Introduction

Plants are everywhere. But most of us are not familiar with plants. Because there are so many varieties of plants, which can also be subdivided into flowers, grass and trees. It is really difficult for us to identify the plant with limited knowledge. If someone wants to inquire the plant he sees, the first move for him is to get the scientific name or the name of this plant, which would waste much of his time on searching. The leaves of plants are different in shape and vary a lot in kind, so we use leaves as the characteristics in this study.

In the related researches, some of them provide image retrieval techniques on personal computers, not on PDA devices[1][2][3][6][7][9][10][11]. Some of them implement fuzzy approach.[4][12][13]Some of them provide mobile learning on PDA devices, however, the computation tasks are performed on a internet server [5][8][12][13]. For mobile learning users, the internet service may not be provided in some areas. In this study, a plant search system with artificial intelligence on PDA devices is developed.

This fuzzy sets defines the degree of membership of each characteristic. But in order to figure out the relationship between the characteric of leaves clicked by users and that of other leaves, fuzzy value is utilized. With triangular and trapezoidal fuzzy functions, we can grade the matching degree of selected characteristics. Thus users can choose each classified characteristic through observing the leaf characteristics.

H.G. Okuno and M. Ali (Eds.): IEA/AIE 2007, LNAI 4570, pp. 834–844, 2007.

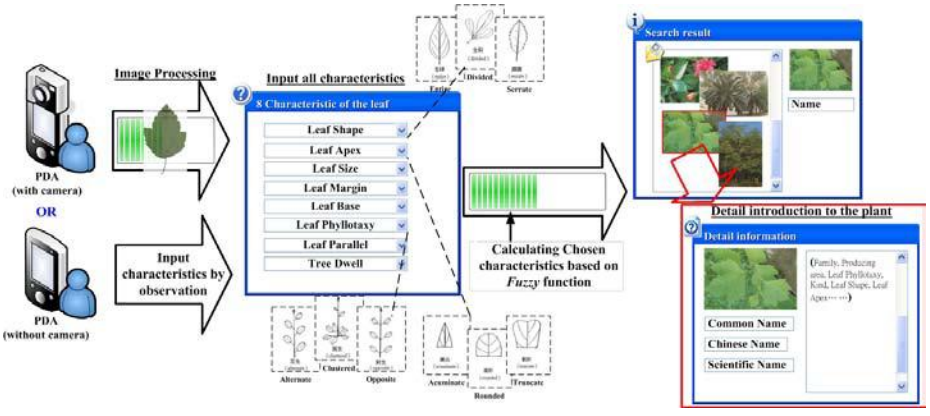

Fig. 1. The system architecture

Fig. 1 shows the system architecture in this research.. After users select certain characteristics of leaves on a PDA, the values can be computed through the Centroid-contour distance, the matching degree is given according to fuzzy theory and the leaves with the highest points would be found. Finally, the results are shown to users. In this way, the users knowing little about plants can select the characteristics by observation and easily find out the answer.

In the following section, we will introduce the quantitative method of the leaf characteristics, explaining how to calculate the characterics of leaves and providing different quantitative values. Section 3 will discuss the strategy of search, explaining how to calculate and grade the quantitative values of all characteristics obtained in Section 2 and taking the highest value as the result of search. Section 4 is about the experiment and evaluation, introducing the implementation interface in this research, analyzing and exploring all kinds of data and results. Finally, we draw a conclusion and propose the future research in Section 5.

2 The Quantitative Method of Characterics

The method for search presented in this paper mainly depends on the characterics of leaves, including leaf shape, leaf Apex, leaf base, leaf margin, leaf phyllotaxy, leaf vein and leaf size. In this section, we will explain how to take out the obvious characterics of leaves, individually give them different quantitative values, and provide the data needed in search.

2.1 The Leaf Shape

Among the landscape plants in the color photo album, the author has sorted the common leaf shapes into the following groups. As shown in Fig. 2:

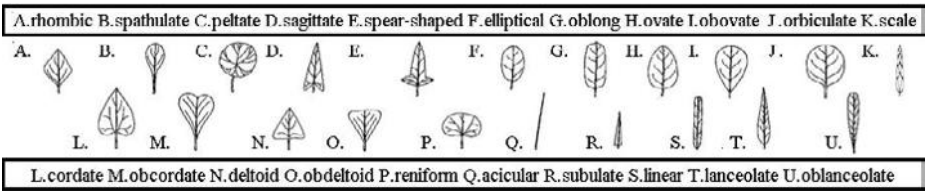

Fig. 2. Classification of the leaf shape

On the basis of these basic leaf shapes, the centroid-contour distance of the leaf shapes is calculated. The calculating process is as follows: Firstly, we took out the edge of the original shape, and then worked out the center point with the average value of all points on the edge. We first lengthwise scanned the original shape and found out the maximum and minimum values on Y_{axis}, and next transversely scanned it and found out the maximum and minimum values on X_{axis}. These points that are found out set the edge of the original shape. Then we calculated the average value of all points on the edge. As shown in *equation* 1:

$$(X_{center}, Y_{center}) = \left(\frac{\sum_{p=1}^{N} X_{axis_p}}{N}, \frac{\sum_{p=1}^{N} Y_{axis_p}}{N} \right) \tag{1}$$

In the above equation, X_{center} and Y_{center} are respectively the center points on X-axis and Y-axis; N stood for the total number of points on the edge; X_{axis} and Y_{axis} respectively referred to X coordinate and Y coordinate of the Pth point on the edge.

Then we worked out the distance from the center point to the edge according to along 0°–360°. But before this step, we decided the variable of X_{axis} and Y_{axis} with *equation* 2:

$$Y_{axis} = X_{axis} \times \tan(\theta) \tag{2}$$

The accumulation with X_{axis} as the baseline value can help to solve the variable of Y_{axis}. The scanning along the beeline at cXextended up to the farmost edge. In implementation, we individually dealt with the four polar coordinates (0°, 90°, 180°, 270°) to avoid the problem that the denominator is 0 or $\tan(\theta)$ is 0. The centroid-contour distance is calculated with Euclidean Distance. As shown in *equation* 3:

$$Dis_\theta = \sqrt{{DisX_{axis_\theta}}^2 + {DisY_{axis_\theta}}^2} \tag{3}$$

In *equation* 3, disc is the distance from the center point to the farmost edge at $\theta°$; $DisX_{axis_\theta}$ and $DisY_{axis_\theta}$ respectively stood for the differences between the X_{axis} of the center point and the X_{axis} of the edge and between the Y_{axis} of the center point and the Y_{axis} of the edge at $\theta°$. By calculating the centroid-contour distance, we can get the quantitative values of all kinds of leaves, but it is impossible to obviously differentiate the different degrees with the direct use of the sum of the centroid-contour distance. Moreover, the sizes of each original image are not always the same. So in this research we use the square sum of the centroid-contour distance, which is then divided by the square of the maximum value of the centroid-contour distance of this leaf. Thus we can differentiate the difference in the sizes of the centroid-contour distance. Meanwhile, there had been normal standards serving this comparison.

$$ShapeSqureDis = \frac{\sum_{\theta=0}^{359} Dis_\theta^2}{\max(Dis_\theta^2)} \tag{4}$$

It is designed in this research that these values can be compared with each other in the degree of similarity, so finally all types are figured out in turn and accumulated. The ratio of these types to the whole is taken as the quantitative value and the segmentation of all types is increased.

2.2 The Leaf Apex and the Leaf Base

The method for quantifying the characterics of leaf shapes is used to calculate the quantitative values of the leaf Apex. What is needed to notice is that the characterics of the leaf Apex highlighted the shape of the front part of the leaf. The leaf Apex can be divided into the following types. As shown in Fig. 3-1:

In the calculation of the centroid-contour distance of the leaf Apex in *equation* 3, only the upper half (i.e. the threshold of θ is limited to 0°–180°) is computed; on the contrary, the leaf base highlighted the shape of the bottom part of the leaf, so in the calculation of the leaf base, the threshold of θ in *equation* 3 is limited to 180°–360°. The leaf base is divided into the following types. As shown in Fig. 3-2:

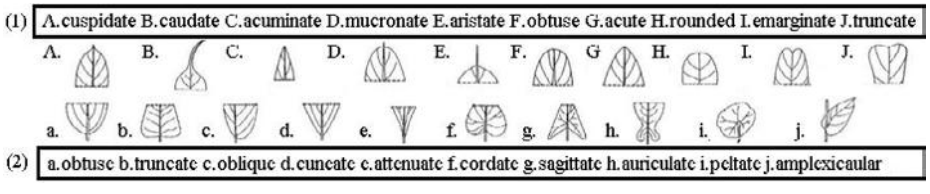

Fig. 3. (1)Classification of the leaf apex.(2)Classification of the leaf base.

2.3 The Leaf Margin

The leaf margin refers to the growth condition of the outer region on the leaf. It can be divided into palmately parted leaf and pinnately parted leaf. These two kinds of leaves can also be subdivide into lobed, cleft, parted and divided leaves. As shown in Fig. 4:

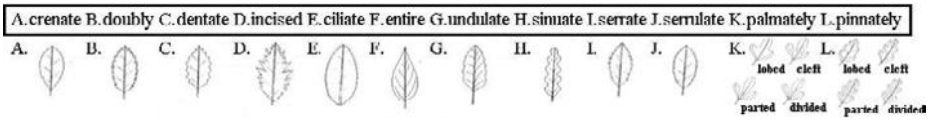

Fig. 4. Classification of the leaf margin

The characteristic of the leaf margin contains two quantitative values: the times and the total amount of leaf margin's ascending and falling. We first computed in turn the centroid-contour distance according to all the points on the edge and then analyzed the maximum and minimum values in the region from which the curve of the centroid-contour distance is taken out. Thereinto, the times of the ascending and falling are the sum of the times of the appearance of the maximum and minimum values in the region. While the total amount of the ascending and falling equals to that the sum of differences between the maximum and minimum values in each interval is divided by the number of points on the edge and the maximum centroid-contour distance.

2.4 The Leaf Vein, the Leaf Phyllotaxy and the Living Habits of Plants

The characteric of the leaf vein shows the distribution situation of the veins on the leaf surface. It includes parallel venation, palmate venation, reticular venation and plannate venation, as shown in Fig. 5-1 Moreover, there are other six situations with obvious costa and fuzzy leaf vein.

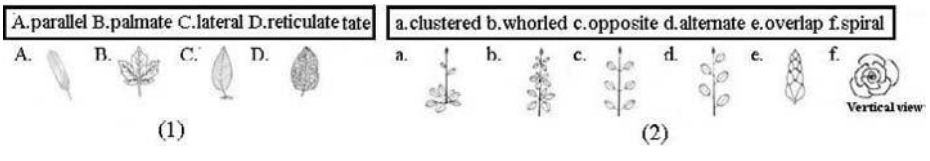

Fig. 5. (1)Classification of the leaf vein. (2)Classification of the leaf phyllotaxy.

The leaf phyllotaxy referrs to the six methods in ranking that leaves grew on the branches, such as clustered, whorled, opposite, alternate, alternate-over, and spiral phyllotaxes.

The living habits of a plant meant the growth condition of the plant. This research used arbor, shrub, liane and herbage to represent the characteristics of the living habits of the plant.

For the three characterics, there is no the relation showing the degree of membership among all varieties and it is not easy to cause incorrect choice in observation and judgment, so boolean values are adopted to stand for the leaf vein and the leaf phyllotaxy of all plants.

2.5 The Leaf Size

The leaf size is the range of a common mature leaf, recorded in the database of the plant. The characteric of the leaf size is given two fields, respectively storing the minimum and maximum values of the leaf size; while the input item provided for users is singular value, so the trapezoidal membership function in fuzzy process is adopted. The vertical axis is the degree of membership and the horizontal axis is the quantitative value of the leaf size.

3 The Strategy of Search

In Section Two, we illustrated how to get the quantitative values of all characteristics. In this section, we will explain how to grade each characteric of each plant in the plant database and further work out the highest value that is taken as the result of search. The three characterics, like the leaf shape, the leaf Apex and the leaf base are all fuzzified with triangular membership function. This definition is shown in *equation* 5:

$$score = \begin{cases} 0 & \text{if } x < a \\ \dfrac{x-a}{c-a} & \text{if } x \in [a, c] \\ \dfrac{b-x}{b-c} & \text{if } x \in [c, b] \\ 0 & \text{if } x > b \end{cases} \tag{5}$$

In *equation* 5, c is the quantitative value of the characteristics chosen by users, and x is the quantitative value of the characteristics of all kinds of plants in the database. It is set that $a = c-1$, $b = c+1$. the fuzzy quantitative values designed in this research are all within the range of 0–1, so the situation of $x < a$ and $x > b$ would not appear. Thus the above equation can be simplified as:

equation 6 can be obtained by combining the two situations in *equation* 5:

$$score = 1 - |c - x| \tag{6}$$

In *equation* 6, c is the quantitative values represented by one leaf shape that users chose from the previous 20 kinds of leaf shapes after actually observing the leaves; while x is the quantitative values represented by the leaf shapes of each plant in all plant databases. With this calculation method, we can work

out the scores of the leaf shapes' attribute of all plants. In addition, the quantitative values hadn't been given to the bud scale shape because this shape is so peculiar that it can be easily identified with direct observation. Thus we individually treats this leaf shape with Boolean values. If users chose the the bud scale shape and the plants in the database are also the bud scale shape, these plants can obtain one score, while the plants with other leaf shapes cann't get any score. The partial characteristics of Boolean values also included the peltate and amplexicaul shapes of the leaf base and the fimbriate shape of the leaf margin.

In Fig. 6, five items of the leaf shape attributes are taken out to describe the relation between the leaf shapes users chose and all kinds of leaf shapes in the database. In this figure, it is assumed that users chose rhombic leaves after observing the leaves. The red representing the items users chose expanded towards the left and the right from the highest point. When it moved downwards at 45° and intersected all kinds of leaf shapes, we can get the scores of this leaf shape. In Fig. 6, the vertical axis is the degree of membership and the horizontal axis is the quantitative values of all leaf shapes.

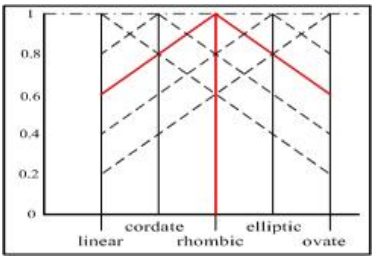

Fig. 6. The fuzzy function of the characteristics of the leaf shape

For the leaf vein and the leaf phyllotaxy, we use Boolean values. In search and comparison, we compared the items chosen by users with all plants in the database.

The same items can get one point for the score, while the different items cannot get any. The leaf margin had two quantitative values: the times and the total amount of the ascending and falling. Their score can be calculated with *equation* 7:

$$\max\left(0, 1 - \frac{\Delta X}{\max(X)} - \frac{\Delta Y}{\max(Y)}\right) \tag{7}$$

In the above equation, ΔX stood for the difference of the times of the ascending and falling of the variety of the leaf margin chosen by users and of the variety of the leaf margin in a certain piece of datum of the database. Then this difference can be normalized through being divided by the maximum value of the times of the ascending and falling in all varieties. While ΔY represented the difference of the total amount of the ascending and falling. Likewise it is also normalized through being divided by the maximum of the total amount of the

ascending and falling. The score of the leaf margin is 1 minus these two differences. In order to avoid negative score, finally we took the maximum value in the result and 0. In grading the leaf size, we use triangular membership function. The definition is shown in *equation* 8:

$$score = \begin{cases} 0 & \text{if } x < a \\ \dfrac{x-a}{c-a} & \text{if } x \in [a,c] \\ 1 & \text{if } x \in [c,d] \\ \dfrac{b-x}{b-d} & \text{if } x \in [d,b] \\ 0 & \text{if } x > b \end{cases} \tag{8}$$

In *equation* 8, c is the minimum value of the attribute of the leaf size; d is the maximum value of the attribute of the leaf size. In addition, $a = c - \frac{d-c}{2}$ and $b = d + \frac{d-c}{2}$, and x is the x value inputted by users. With equation 9, we can figure out the score of the leaf size.

Finally, we added up the scores of all characterics. The higher the score is, the closer to the leaved users observed the characteristics of this plant are. Except the leaf vein, the leaf phyllotaxy and the peculiar leaf shape, leaf base and leaf margin, the score would still be given according to the difference in the degrees of the fuzzy theory even if users chose improper characteristics, which is in more accord with the situation of actual operation.

4 Experimental Results

4.1 PDA Interface

Fig. 7-1 shows the situation of the implementation in PDA. The classified characteristics of leaves helped users make choices, for example: The alternate, opposite, imbricate etc. leaf phyllotaxy can be chosen. Here the clicked leaf characteristics would be accompanied by the corresponding pictures or descriptions, which made users, with observation, easily click the characteristics of plants according with what they saw. Moreover, the characteristics of plants we let users click are arranged in the descending order of their measured importance. Thus users can make choices according to the importance of the characteristics of plants. After users made choices and started to search, here the characteristics chosen by them would be calculated. While five pieces of the calculation results with higher scores would be shown on PDA.

Fig. 7-2 displayed the plants that are searched out with the characterics users clicked in the above figure. We can see that on the left of the figure are listed the names of the first five plants with the highest scores and their specific scores. If feeling like knowing more about the data of this plant, users can choose the plant they wanted to observe in Fig. 7-2 and then click to look through the detailed data.

Fig. 7-3 shows that users clicked the detailed data of a certain plant. Here all kinds of data about this plant would be displayed. For example: the scientific

name of the plant, all characteristics of the leaves, the related information etc., which provided users with detailed information about the plant.

The searching results are shown in Fig. 7-2: Dragon juniper, with the score of 800, ranked first; Flame tree, with the score of 763, ranked first, too. It can be learned that in Fig. 7-2, Dragon juniper and Flame tree cypress had got the same score of 800, which meant that in the database, the characterics of these two plants are very similar to each other. They can be differentiated according to these characterics. In spite of the similar characterics, these two plants are quite different in appearance, so users can identify them by observing the pictures shown on PDA. In Fig. 7-2, users clicked similar characteristics: The leaf shape is elliptical, but the oblong leaf is mistakenly clicked. In this situation, although the inputted characteric is improper, the score wouldn't have too much difference through the calculation with the fuzzy theory.

Fig. 7. (1)The input interface of the characteristics.(2)Click to look through the detail data.(3)The detail data of a certain plant.

4.2 The Experimental Results

We have created 150 pieces of data about the common plants in Taiwan in our database. All the records in the database have been transferred to PDA and tested. The plants of top five highest scores would be displayed on PDA. From the data with wrong test results, we summarized the following three causes often resulting in errors: 1. When the leave grew densely, users tended to mistakenly thought the alternate or opposite leaf phyllotaxy for clustered one. 2. When there are folds on the leaf surface, it is also difficult to differentiate the entire leaf margin from the undulate margin. 3. In the choice of the leaf parallel, it is not easy to tell plannate venation and palmate venation apart.

4.3 Analysis of the Accuracy

When examining the accuracy, two kinds of rules are used. The hard rule means the correct answer must get the highest score, while the soft rule means that the

correct answer must appear among the top 5 highest scores. When users input the characterics, they can skip any characteric they don't know the right value. Certainly, the more characterics values are provided, the higher accuracy can be obtained. The following figure illustrates the influence of different number of used characterics on the accuracy.

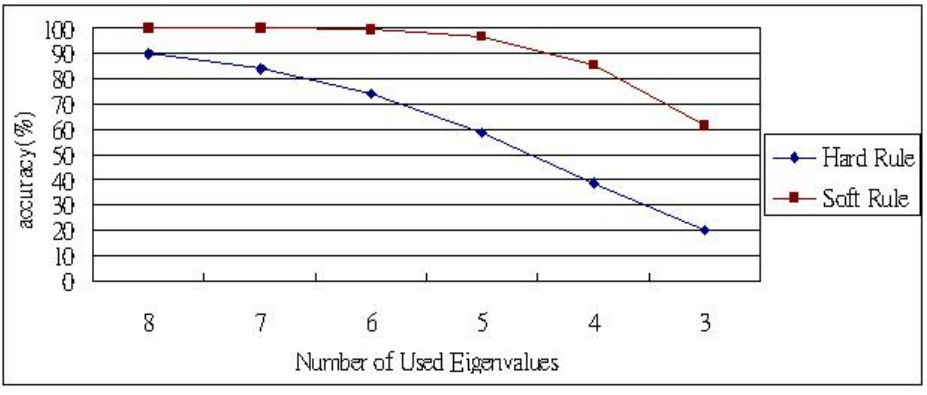

Fig. 8. The accuracy for different number of used characterics

In Fig. 8, the horizontal axis shows the number of the used characterics and the vertical axis stands for the average accuracy (%) of the test results in various combinations. As we can see in Fig. 8, the accuracy when using 8 characterics is 90% when hard rule is applied, while the accuracy is 100% when soft rule is applied. Especially when soft rule is applied, the accuracy is high enough even only 4 characterics are entered.

According to all the experimental conditions, we can conclude the significance of characterics in the following order: the leaf Apex, the leaf shape and the leaf size, and the less important characterics into the leaf parallel, the living habits, the leaf phyllotaxy and the leaf base. Therefore, we can arrange the order of these characterics appearing on PDA interface.

5 Conclusions

Based on all kinds of characteristics of leaves, this research constructed a mobile learning system allowing users to input all the observed attributes of leaves on PDA without knowing the name of the plant. According to all the experimental conditions, we can arrange the characterics in the proper order on PDA interface according to their significance. Meanwhile, we successfully improved the fault tolerance of the system, combining the calculation of the centroid-contour distance and the quantification process of the fuzzy theory. The accuracy when using all of the characterics is 90% when hard rule is applied. Especially when

soft rule is applied, the accuracy is high enough even only half of the characterics are entered.

References

1. Zhang, D., Lu, G.: Study and evaluation of different Fourier methods for image retrieval. Image and Vision Computing 23, 33–49 (2005)
2. Zhang, D., Lu, G.: Review of shape representation and description techniques. Pattern Recognition 37, 1–19 (2004)
3. Zhang, D., Lu, G.: Content-Based Shape Retrieval Using Different Shape Descriptors: A Comparative Study. In: Multimedia Conference on, pp. 1139–1142 (2001)
4. Wang, Z., Chi, Z., Feng, D.: Fuzzy Integral for Leaf Image Retrieval. In: Proceedings of the 2002 IEEE International Conference on Fuzzy Systems (FUZZ-IEEE2002), pp. 372–377 (May 12-17, 2002)
5. Chen, Y.-S., Kao, T.-C., Yu, G.-J., Sheu, J.-P.: A Mobile Butterfly-Watching Learning System for Supporting Independent Learning. In: The 2nd IEEE International Workshop on Wireless and Mobile Technologies in Education, pp. 11–18 (2004)
6. Wang, Z., Chi, Z., Feng, D., Wang, Q.: Leaf image retrieval with shape features. In: Laurini, R. (ed.) VISUAL 2000. LNCS, vol. 1929, pp. 477–487. Springer, Heidelberg (2000)
7. Wang, Z., Chi, Z., Feng, D.: Leaf image retrieval using a two-step approach with shape features. In: Proceedings of 2000 IEEE Pacific-Rim Conference on Multimedia (PCM2000), pp. 380–383 (December 12-15, 2000)
8. Nam, Y., Hwang, E., Kim, D.: CLOVER: A Mobile Content-Based Leaf Image Retrieval System. In: Fox, E.A., Neuhold, E.J., Premsmit, P., Wuwongse, V. (eds.) ICADL 2005. LNCS, vol. 3815, pp. 139–148. Springer, Heidelberg (2005)
9. Mokhtarian, F., Abbasi, S.: Matching Shapes With Self-Intersections: Application to Leaf Classification. IEEE Transactions On Image Processing 13(5), 653–661 (2004)
10. Wang, Z., Chi, Z., Feng, D.: Shape based leaf image retrieval. IEE Proceedings - Vision, Image and Signal Processing 150(1), 34–43 (2003)
11. An-xiang, H., Gang, C., Jun-li, L., Zhe-ru, C., Dan, Z.: A flower image retrieval method based on ROI feature. Journal of Zhejiang University SCIENCE, 764–722 (2004)
12. Huang, Y.-P., Tsai, T.: A Fuzzy Semantic Approach to Retrieving Bird Information Using Handheld Devices. Intelligent Systems, IEEE 20, 16–23 (2005)
13. Huang, Y.-P., Tsai, T.: Bird information retrieval using fuzzy semantic concepts. IEEE Publication 24(3), 26–28 (2005)

Stochastic Point Location in Non-stationary Environments and Its Applications*

B. John Oommen[1,**], Sang-Woon Kim[2,***], Mathew Samuel[1], and Ole-Christoffer Granmo[3]

[1] School of Computer Science, Carleton University, Ottawa, Canada
oommen@scs.carleton.ca
[2] Dept. of Computer Science and Engineering, Myongji University, Yongin, Korea
kimsw@mju.ac.kr
[3] Dept. of ICT, Agder University College, Grimstad, Norway
ole.granmo@hia.no

Abstract. This paper reports the first known solution to the Stochastic Point Location (SPL) problem when the Environment is non-stationary. The SPL problem [12,13,14] involves a general learning problem in which the learning mechanism attempts to learn a "parameter", say λ^*, within a closed interval. However, unlike the earlier reported results, we consider the scenario when the learning is to be done *in a non-stationary setting*. The Environment communicates with an intermediate entity (referred to as the Teacher) about the point itself, advising it where it should go. The mechanism searching for the point, in turn, receives responses from the Teacher, directing *it* how *it* should move. Therefore, the point itself, in the overall setting, is moving, delivering possibly incorrect information about its location to the Teacher. This, in turn, means that the "Environment" is itself non-stationary, implying that the advice of the Teacher is both uncertain and *changing with time* - rendering the problem extremely fascinating. The heart of the strategy we propose involves discretizing the space and performing a controlled random walk on this space. Apart from deriving some analytic results about our solution, we also report simulation results which demonstrate the power of the scheme.

1 Introduction

The SPL problem [12,13,14] considers a general learning problem in which the learning mechanism (which could be a robot, a Learning Automaton (LA), or in general, an algorithm) attempts to learn a "parameter", say λ^*, within a closed interval. Consider the problem of a learning mechanism moving around on the

* The first author was partially supported by NSERC, the Natural Sciences and Engineering Research Council of Canada. This work was generously supported by KOSEF, the Korea Science and Engineering Foundation (F01-2006-000-10008-0).

** *Chancellor's Professor* ; *Fellow : IEEE* and *Fellow : IAPR*. This Author also holds an *Adjunct Professorship* with the Dept. of ICT, Agder University College, Norway.

*** *Senior Member, IEEE*.

H.G. Okuno and M. Ali (Eds.): IEA/AIE 2007, LNAI 4570, pp. 845–854, 2007.

real line attempting to locate a particular point. To assist the mechanism, it communicates with an Environment which provides it with information regarding the direction in which it should go. If the Environment is deterministic, the problem is the "Deterministic Point Location Problem" and this has been studied rather thoroughly [4].

This problem is akin to the field of LA [11,16], in which the learning mechanism attempts to learn from a *stochastic Teacher*. More specifically, unlike the traditional LA model in which the LA attempts to learn the optimal action offered by the Environment, we consider the following learning problem : The learning mechanism is trying to locate an unknown *point* on a real interval by interacting with the stochastic Environment through a series of informed guesses.

Unlike the deterministic problem alluded to above, in the SPL, rather than receive deterministic responses as to where it should go, the learning mechanism is given, at every time step, a stochastic (i.e., possibly erroneous) response. Thus, when it should really be moving to the "right" it may be advised to move to the "left" and vice versa. However, to render the current study even more challenging, unlike the results currently available [12,13,14], we generalize the problem even more to consider the scenario when the Environment is *non-stationary*. We thus refer to the problem being studied as the *Non-Stationary SPL* (or NS-SPL).

The main contribution of this paper is to present a formal strategy, which we believe is the first reported method, to solve the NS-SPL problem for a specific type of non-stationarity. Besides formulating a solution, we also show how such a solution can be analyzed, and demonstrate its applicability by simulating it on benchmark learning problems. More specifically, the novel scheme which we propose uses the principle of discretizing the parameter space [1], and performing a controlled random walk on this space. However, the way that this random walk is motivated and analyzed is also rather novel to the theory and application of Markov chains [11,16].

To present our solution in the right perspective, we first formalize the SPL and NS-SPL problems.

Problem Formulation: We assume that there is a learning mechanism whose task is to determine the optimal value of some variable (or parameter), λ. We assume that there is an optimal choice for λ - an unknown value, say $\lambda^* \in [0, 1]$. The question which we study here is the one of learning λ^*. Although the mechanism does not know the value of λ^*, we assume that it has responses from an intelligent "Environment" E (via a Teacher) which is capable of informing it whether the current value of λ is too small or too big. To render the problem both meaningful and distinct from its deterministic version, we would like to emphasize that the response from this Environment is assumed "faulty." Thus, E may tell us to increase λ when it should be decreased, and vice versa. However, to render the problem tangible we assume that the probability of receiving an intelligent response is $p > 0.5$. Finally, to render the problem distinct from SPL, we shall assume that the Environment is non-stationary. We shall presently explain how this non-stationarity (by means of the Teacher) is modelled.

Observe that the quantity "p"reflects on the "effectiveness" of the Environment, E. Thus, whenever the current $\lambda < \lambda^*$, the environment correctly suggests that we increase λ with probability p. It simultaneously could have incorrectly recommended that we decrease λ with probability $(1-p)$. Similarly, whenever $\lambda > \lambda^*$, the Environment tells us to decrease λ with probability p, and to increase it with probability $(1-p)$. The crucial issue that we have to address is that of determining how to change our guess of λ^*. SPL-related problems : state of the art are omitted here in the interest of brevity, but can be found in [17].

Applications of SPL and NS-SPL: As mentioned in [12,13,14], apart from the problem being of importance in its own right, it also has potential applications in solving optimization problems. Besides these fairly generic applications, with a little insight, it is easy to see how an efficient solution to the SPL can be used to assist in solving (by determining the associated parameters) the stochastic sampling problem in computer graphics [8], the problem of determining roads in aerial images by using geometric-stochastic models [5], and various location problems [7]. Such an SPL solution can also be used to analyze the stochastic properties of the random waypoint mobility model in wireless communication networks [6], to achieve spatial point pattern analysis codes for GISs [15], and to analyze spatial point patterns [3]. Thus, seeking for a good and efficient solution for such a fundamental problem can be quite rewarding.

Philosophy and Advantages of Discretization: Our proposed solution to NS-SPL works in a discretized manner, by subdividing the unit interval into N steps $\{0, \frac{1}{N}, \frac{2}{N} \cdots, \frac{(N-1)}{N}, 1\}$, where N is the resolution of the learning scheme[1]. A larger value of N will ultimately imply a more accurate convergence to the unknown λ^*. This involves discretizing the parameter space and performing a controlled random walk on this space. The beauty of a discrete LA is that it does not ignore the limitations of practical implementations - on the contrary, this limitation is used to its advantage. Philosophically, discrete machines represent a hybrid of the fixed and variable structured families.

Some of the existing results about discretized automata are found in [1,10]. Indeed, the fastest reported learning automata are the discretized pursuit and estimator algorithms [1]. The advantages of using discretized LA are omitted here in the interest of brevity, but can be found in [17].

2 Proposed Solution to the NS-SPL Problem

Modeling Non-Stationarity: The first issue that we have to confront is that of modeling non-stationarity. This has been done in the literature and in the field of LA, using one of few possible mechanisms.

1. The Non-Stationary Environment is modelled using a Markov chain [11,16]; which means that there is a set of Environments, and the non-stationarity is achieved by the system switching between environments in a Markovian manner.

[1] Whenever we refer to the state whose index is i, we imply the state which has an associated discretized value of λ as $\frac{i}{N}$.

2. The Non-Stationary Environment is modelled using a scheme where the penalty probabilities of the environment are themselves random variables with known/unknown distributions [9,11].

3. In certain application domains (as in list organizing) [2] the non-stationarity is modelled using "locality of reference" concepts. Such a modeling is (in our opinion) not appropriate in this present context.

Approaching the problem from the perspectives of (1) and (2) above is really rather straightforward applications of the results already available in the literature to the specific application domain (of SPL). Rather, we shall propose a new model of non-stationarity, which we refer to as *Meta-Level* non-stationarity. This model works as follows : We are interested in locating a point which is constantly (stochastically) moving. Although the point is stochastically moving, the mechanism searching for the point is receiving deterministic responses from the point itself, telling it where it should go. Therefore, the point itself, in the overall setting, is delivering possibly incorrect information on where the mechanism should go so as to reach it. Thus conceptually, the moving point that is being searched for can be perceived to be the "Non-Stationary Stochastic Teacher" and the mechanism doing the searching can be perceived to be the "Student". We thus formalize the solution to the NS-SPL as follows.

Solution NS-SPL: From a modelling perspective, first of all, we assume there is some unknown parameter λ^*, and a Teacher (T) who wants to teach the Student (S) the value of λ^*. Unfortunately this two stage process is flawed. The Teacher itself is initially ignorant and only obtains noisy information about λ^*. So if it is at a value $T(n)$ less than λ^* it could itself be told to move right with probability p and to move to the left with probability $(1-p)$. Notice that this corresponds exactly to the SPL Problem studied in [12]. The Teacher in turn gives deterministic responses to the Student who will now move left or right depending on these responses.

When we have to study the properties of *Solution NS-SPL*, the questions to be analyzed are two-fold: (1) How close will the Teacher get to λ^*, and, (2) How close will the Student be to the Teacher, and in turn to λ^*. Using this model, we prove the fundamental theoretical contribution of this paper.

Theorem 1. Solution NS-SPL *is ϵ-optimal whenever it interacts with a meta-level non-stationary environment.*

Proof. We intend to show that the value of $\lambda(n)$ learned by the Student, converges to λ^* as the time index $n \to \infty$, and the resolution parameter $N \to \infty$.

Since $\lambda^* < 1$, as in [12], we will let Z be the index where: $Z/N < \lambda^* < (Z+1)/N$. As shown in [12], the steady state probabilities of the Markov chain associated with the Teacher, $\Pi = [\pi_0, \pi_1, \ldots \pi_N]^T$, can be expressed recursively[2] using the notation that $e = p/q$, where $q = 1-p$:

$$\pi_i = e(\pi_{i-1}) \quad when\ i \leq Z,$$

[2] The arguments for this are exactly the same as in [12] and are omitted in the interest of brevity.

$$\pi_i = \pi_{i-1}/e \quad when\ i > Z+1,$$
$$\pi_{Z+1} = \pi_Z,$$

The π_i's are normalized to render Π to be a probability vector.

When we now consider the case of the Student, we see that *Solution NS-SPL* dictates that its transitions (which, in turn determine the Markov Chain) is as follows. If $S(n)$ and $T(n)$ are the "states" of the Student and Teacher respectively at time 'n', then, if $S(n) = i$,

$$S(n+1) = i+1; \quad if\ T(n) > i,$$
$$S(n+1) = i-1; \quad if\ T(n) < i,$$
$$S(n+1) = i; \quad if\ T(n) = i.$$

To obtain the matrix for *this* Markov Chain, we observe the following. The first row represents the scenario when the Student is in state 0 and the probabilities that the Student will stay there or move to the other states, and in particular, to state 1. The second row represents the scenario when the Student is in state 1 and the probabilities that the Student will stay in that state, or move to the other states, and again, in particular, to either states 0 or 2 etc. We also observe that these probabilities, for the Student matrix, can be determined from the vector Π. Since the Student's transition matrix uses only the Teacher's vector, Π, as a guide, the former would have the form:

$$\Theta = \begin{bmatrix} \pi_0 & \beta_1^N & 0 & 0 & \cdot & \cdot & \cdot & \cdot \\ \pi_0 & \pi_1 & \beta_2^N & 0 & \cdot & \cdot & \cdot & \cdot \\ 0 & \beta_0^1 & \pi_2 & \beta_3^N & \cdot & \cdot & \cdot & \cdot \\ \cdot & \cdot & \cdot & \cdot & \cdot & \cdot & \cdot & \cdot \\ \cdot & \cdot & \cdot & \cdot & \cdot & \cdot & \cdot & \cdot \\ \cdot & \cdot & \cdot & \cdot & \beta_0^{N-3} & \pi_{N-2} & \beta_{N-1}^N & 0 \\ \cdot & \cdot & \cdot & \cdot & 0 & \beta_0^{N-2} & \pi_{N-1} & \pi_N \\ \cdot & \cdot & \cdot & \cdot & 0 & 0 & \beta_0^{N-1} & \pi_N \end{bmatrix}, \tag{1}$$

where $\beta_i^j \equiv \sum_{k=i}^{j} \pi_k = \pi_i + \cdots + \pi_j, \quad i < j$.

Our task is to compute the steady state probabilities of Θ. Because this cumbersome computation can be found in [17], in the interest of brevity, we will here only provide an *outline* of the resulting proof.

We first have to get the equilibrium value of $E[\lambda_T(n)]$ for any finite N for the Teacher. This argument can be separated into three different cases as in [12]:

1. The first case is when Z/N is close to zero. In this case the maximum is quickly reached and then geometrically falls away.

2. When Z/N is close to 1, the value of π_i geometrically increases but when the maximum is reached it quickly falls away. For both these cases when $N \to \infty$, most of the probability mass will be centered in a small interval around Z.

3. The third case is slightly more complex because it involves Z/N being away from either end. This case must be broken down into two distinct geometric series, one representing the geometric series from π_0 to π_Z and the other from

π_{Z+1} to π_N. The first series increases geometrically (or rather, exponentially as $N \to \infty$) until it reaches the maximum at π_Z. The second series starts at the maximum at the value π_{Z+1} and then decreases geometrically (i.e., exponentially as $N \to \infty$) until π_Z is reached. In this case the probability mass will be centered within a small interval around Z/N and $(Z+1)/N$ as $N \to \infty$.

As for the Student, since it follows the Teacher it can be shown that the average value of the Students' equilibrium position will be arbitrarily close to the Teacher's. The argument for the Students' equilibrium value can be divided into two separate parts for any finite N.

1. The first part consists of the interval between state 0 and state Z. When dealing with this interval, the probability mass of the Student will be concentrated on the states closest to Z as $N \to \infty$. Since the Teacher will be arbitrarily close to state Z (as shown above) because of the exponential growth of the probabilities with the state index, and the fact that the Student is receiving deterministic responses informing it to proceed closer to the Teacher, its state will be arbitrarily near the Teacher's state, which implies that it will be close to state Z.

2. The second part consists of the interval between state Z+1 and state N. In this case, the probability mass of the Student will be concentrated near state $Z+1$ as $N \to \infty$, and will decay exponentially with the state index. Because the Teacher is arbitrarily close to state $Z+1$ and since the Student is receiving deterministic responses from the Teacher, the Student will move closer to the state where the Teacher is located. This implies that the majority of the probability mass of the Student will lie close to state $Z+1$.

A consequence of these two cases implies that the probability mass of the Student will also be centered within an interval around Z/N and $(Z+1)/N$ as $N \to \infty$. The theorem follows.

2.1 Some Clarifying Examples

To clarify the actual learning process, we present two rather straightforward examples.

Example 1. Consider the case when $\lambda^* = 0.725$ and when $N = 10$. This implies that for the Teacher we partition the interval into 10 sub-intervals between $[0, 1]$ as: $\{0, 0.1, 0.2, \ldots, 1\}$. Thus:

1. When the Teacher is in a state between 0 and 0.7 inclusive, it will move to the right with a probability p, and move to the left with a probability q.

2. When the Teacher is in a state between 0.8 and 1 inclusive, it will move to the left with a probability p, and move to the right with a probability q.

In this case, there is a normalizing constant K which yields: $\pi_i = K(e^i) \;\; 0 \leq i \leq 7; \pi_8 = K(e^7); \pi_i = K(e^{15-i}) \;\; 9 \leq i \leq 10$. Thus, π_i increases geometrically from π_1 to π_7 and decreases geometrically from π_8 to π_{10}. Also, π_7 and π_8 are exactly the same. So, as N goes towards infinity, the probability mass for the Teacher will be concentrated in states Z and $Z+1$. In this case, for any N, Z and $Z+1$ will satisfy $\frac{Z}{N} < 0.725 < \frac{Z+1}{N}$ because λ^* is in between these two

states. Due to the exponential growth of π_i for $0 \leq i \leq Z$, and the exponential decay for $(Z+1) \leq i \leq N$, $E[\lambda_T(\infty)]$ will be arbitrarily close to λ^*.

While the Teacher is moving closer to λ^*, the Student is trying to track it. To determine the actual probabilities of the Student moving right, moving left, or remaining static, the steady state probabilities of the Teacher would have to be calculated. In this way, we will know the actual asymptotic probability of the Teacher being in a particular state. As N goes to infinity, the Teacher will be arbitrarily close to the two states that neighbour λ^*, and since the Student will be arbitrarily close to the Teacher, the Student will also be arbitrarily close to the neighbouring states of λ^*. Therefore, the probability mass will be concentrated between these two states and $E[\lambda_S(\infty)]$ will be arbitrarily close to λ^* for the Student as well.

Example 2. It is interesting to note how the transitions change when the point sought for is close to one of the boundaries of the unit interval (for example, when $\lambda^* = 1$). We illustrate this by examining the probabilities for a simple 4×4 matrix (i.e, when $N = 3$) when $\lambda^* = 1$. The corresponding matrix for the Teacher can be easily written down, and the steady state probabilities can be seen to obey the following:

$$\begin{bmatrix} q & p & 0 & 0 \\ q & 0 & p & 0 \\ 0 & q & 0 & p \\ 0 & 0 & q & p \end{bmatrix}^T \begin{bmatrix} \pi_0 \\ \pi_1 \\ \pi_2 \\ \pi_3 \end{bmatrix} = \begin{bmatrix} \pi_0 \\ \pi_1 \\ \pi_2 \\ \pi_3 \end{bmatrix}$$

The solution to the vector Π (where $e = p/q$) is:

$$\Pi = 1/(e^0 + e^1 + e^2 + e^3) \begin{bmatrix} e^0 \\ e^1 \\ e^2 \\ e^3 \end{bmatrix}.$$

The matrix for the Student can then be seen to be:

$$S = 1/(e^0 + e^1 + e^2 + e^3) \begin{bmatrix} e^0 & e^1 + e^2 + e^3 & 0 & 0 \\ e^0 & e^1 & e^2 + e^3 & 0 \\ 0 & e^0 + e^1 & e^2 & e^3 \\ 0 & 0 & e^0 + e^1 + e^2 & e^3 \end{bmatrix}.$$

This matrix obeys $S^T \Xi = \Xi$, where $\Xi = [\xi_0,\ \xi_1\ \xi_2\ \xi_3]^T$. Solving the above, we obtain the following values for ξ_i's: $\xi_0 = k$, $\xi_1 = \frac{a}{b}\xi_0$, $\xi_2 = (\frac{b+c}{d})\xi_1 - \frac{a}{d}\xi_0$, and $\xi_3 = (\frac{d+e}{f})\xi_2 - \frac{c}{f}\xi_1$, where k is some normalizing constant, $a = (e + e^2 + e^3)/(1 + e + e^2 + e^3)$, $b = 1/(1 + e + e^2 + e^3)$, $c = (e^2 + e^3)/(1 + e + e^2 + e^3)$, $d = (1+e)/(1+e+e^2+e^3)$, $e = (e^3)/(1+e+e^2+e^3)$, and $f = (1+e+e^2)/(1+e+e^2+e^3)$.

3 Experimental Results

The parameter learning mechanism, *Solution NS-SPL*, described in this paper, was experimentally evaluated to verify the validity of our analytic results and

Table 1. True value of $E[\lambda(\infty)]$ for a varying number of states when $\lambda^* = 0.725$

Number of States (N)	$E[\lambda(\infty)]$ for Teacher	$E[\lambda(\infty)]$ for Student
10	0.6767	0.7034
20	0.7065	0.7171
30	0.7117	0.7151
40	0.7355	0.7370
50	0.7294	0.7299

to examine its rate of convergence[3]. To verify the power of the scheme and to study its effectiveness for various conditions, simulation experiments were conducted for various values of λ^*, for various values of p, the probability of the Environment correctly providing the feedback. The experiments were also conducted for various values of the resolution parameter N. We present the following experimental results to verify the mathematical validity of the above analytic results, and to examine the convergence rates.

We conducted two types of experiments. The first type of experiments was done to obtain results that have been calculated using the closed form expression. The results from that set of experiments could then be compared to the second type of experiments which involved simulating what is actually happening over time. Examining how the learning mechanisms converged (as time progressed) thus gave us a better understanding of what was happening and of how the systems behaved.

Each simulation consisted of one hundred experiments. The ensemble average of these experiments were taken to avoid extreme results. The simulations were done so that after every 5 time intervals, the average was taken and then recorded so that we would be able to see the convergence with respect to time. In each simulation the value of λ^* was unknown to the mechanisms representing the Teacher and the Student, and the simulations were carried out for various values of p and N while λ^* remained constant.

In Table 1, we report the results from the first type of experiments. These results are the true values of $E[\lambda(\infty)]$ calculated from the closed expression for assorted values of N and with p and λ^* being constant at 0.6 and 0.725 respectively. As can be seen by Table 1, as the number of states increases, the values of $E[\lambda(\infty)]$ for both the Teacher and the Student approach $0.725(\lambda^*)$. When there are 10 states, the value of $E[\lambda(\infty)]$ is 0.6767 for the Teacher and 0.7034 for the Student, but when the number of states reaches 50, the values are 0.7294 and 0.7299 for the Teacher and the Student respectively.

We now look at results from the second type of experiments which will show the convergence of $\hat{E}[\lambda(n)]$ with respect to time. Figure 1 shows the convergence of $\hat{E}[\lambda(n)]$ when the number of states remains constant at 10, but with the

[3] The simulations were conducted for a large number of values of p, λ^* and N. In the interest of brevity, we present here only a few results . But we do emphasize that the results are representative - the scheme always converged to a value arbitrarily close to the true unknown value.

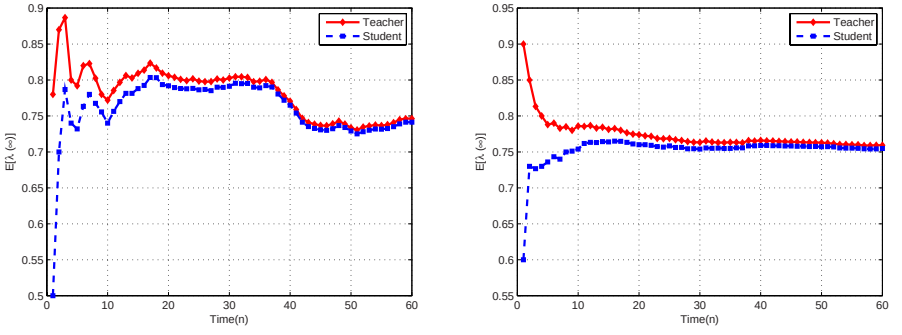

Fig. 1. Plots of $\hat{E}[\lambda(\infty)]$ for both the Student and the Teacher when p is 0.6 (left) and p is 0.9 (right). In both pictures, the parameter λ^* is 0.725 and N is 10.

probability p being different in each of the figures. In these plots, one unit of time corresponds to 5 steps.

By examining these two pictures, we see that the Student finds the Teacher very quickly, and so the convergence occurs rather rapidly. Of course, while the Student learns the value proposed by the Teacher, they both simultaneously converge to the value of λ^* in the pictures. For example, before the time index reaches 300, both the Student and the Teacher have almost converged. It is interesting to note that even by the 35^{th} time step, the values of $\hat{E}[\lambda(\infty)]$ for the Student and the Teacher are within 0.5 percent of each other in each of the three figures. For $N = 20$ and $N = 50$, however, the values of $\hat{E}[\lambda(\infty)]$ for the Student and Teacher are within 0.5 percent of each other, only by the 125^{th} step and by 200^{th} step respectively. In these cases, while the Student converges to the value suggested by the Teacher, they both converge quite slowly to the unknown λ^* value. The details of this type of experiments are omitted here in the interest of brevity, but can be found in [17].

4 Conclusions

In this paper we have reported the first known solution for the Stochastic Point Location (SPL) problem when the Environment is non-stationary. Unlike the results available in the literature [12,13,14], we consider the fascinating case when the point sought for is *itself* moving stochastically, while the mechanism searching for the point is receiving responses from a Teacher about the point itself, which advises the learning mechanism where it should go. We have presented a solution which involves discretizing the space and performing a controlled random walk on this space. Apart from deriving some analytic results about our solution, we also report simulation results which demonstrate the power of the scheme, and state some potential applications. We are currently working on utilizing the various SPL schemes in some of the application domains cited.

References

1. Agache, M., Oommen, B.J.: Generalized pursuit learning schemes: New families of continuous and discretized learning automata. IEEE Trans. on Systems, Man and Cybernetics SMC-32(B), 738–749 (2002)
2. Amer, A., Oommen, B.J.: A novel framework for self-organizing lists in environments with locality of reference: Lists-on-Lists. The Computer Journal (to appear)
3. Baddeley, A., Turner, R.: Spatstat: An R package for analyzing spatial point patterns. Journal of Statistical Software 12, 1–42 (2005)
4. Baeza-Yates, R.A., Culberson, J.C., Rawlins, G.J.E.: Searching with uncertainty. In: Karlsson, R., Lingas, A. (eds.) SWAT 1988. LNCS, vol. 318, pp. 176–189. Springer, Heidelberg (1988)
5. Barzohar, M., Cooper, D.B.: Automatic finding of main roads in aerial images by using geometric-stochastic models and estimation. IEEE Transactions on Pattern Analysis and Machine Intelligence 7, 707–722 (1996)
6. Bettstetter, C., Hartenstein, H., Pérez-Costa, X.: Stochastic properties of the random waypoint mobility model. Journal Wireless Networks 10, 555–567 (2004)
7. Brandeau, M.L., Chiu, S.S.: An overview of representative problems in Location Research. Management Science 35, 645–674 (1989)
8. Cook, R.L.: Stochastic sampling in computer graphics. ACM Trans. Graph. 5, 51–72 (1986)
9. Kim, S.-W., Oommen, B.J.: Prototyype reduction schemes applicable for nonstationary data sets. Pattern Recognition 39(2), 209–222 (2006)
10. Lancôt, J.K., Oommen, B.J.: Discretized estimator learning automata. IEEE Trans. on Systems Man and Cybernetics SMC-22, 1473–1483 (1992)
11. Narendra, K.S., Thathachar, M.A.L.: Learning Automata. Prentice-Hall, Englewood Cliffs (1989)
12. Oommen, B.J.: Stochastic searching on the line and its applications to parameter learning in nonlinear optimization. IEEE Trans. on Systems, Man and Cybernetics SMC-27B, 733–739 (1997)
13. Oommen, B.J., Raghunath, G.: Automata learning and intelligent tertiary searching for stochastic point location. IEEE Trans. on Systems, Man and Cybernetics SMC-28B, 947–954 (1998)
14. Oommen, B.J., Raghunath, G., Kuipers, B.: Parameter learning from stochastic teachers and stochastic compulsive liars. IEEE Trans. on Systems, Man and Cybernetics SMC-36B, 820–836 (2006)
15. Rowlingson, B.S., Diggle, P.J.: SPLANCS: Spatial point pattern analysis code in S-Plus. University of Lancaster, North West Regional Research Laboratory (1991)
16. Thathachar, M.A.L.T., Sastry, P.S.: Networks of Learning Automata: Techniques for Online Stochastic Optimization. Kluwer Academic, Boston (2003)
17. Oommen, B.J., Kim, S.-W., Samuel, M., Granmo, O-C.: A Solution to the Stochastic Point Location Problem in Meta-Level Non-Stationary Environments. Unabridged version of this paper

Quick Adaptation to Changing Concepts by Sensitive Detection

Yoshiaki Yasumura, Naho Kitani, and Kuniaki Uehara

Graduate School of Science and Technology, Kobe University,
1-1 Rokkodai, Nada-ku, Kobe 657-8501, Japan
{yasumura,naho,uehara}@ai.cs.kobe-u.ac.jp

Abstract. In mining data streams, one of the most challenging tasks is adapting to *concept change*, that is change over time of the underlying concept in the data. In this paper, we propose a novel ensemble framework for mining concept-changing data streams. This algorithm, called QACC (Quick Adaptation to Changing Concepts), realizes quick adaptation to changing concepts using an ensemble of classifiers. For quick adaptation, QACC sensitively detects concept changes in noisy streaming data. Empirical studies show that the QACC algorithm is efficient for various concept changes.

Keywords: data streams, classifier ensemble, concept change.

1 Introduction

Mining data streams has become important for many application fields such as credit card fraud detection, target marketing and information filtering. A classification problem for data streams is not a trivial task because the data are often not stable but change over time. For example, in information filtering that automatically extracts user's interested documents, the interest of the user may change over time. The underlying concept that we try to learn is time-varying and the filtering system needs to adapt to such changes. This problem is known as *concept change*. Since conventional classification models target at static data, it is difficult for them to handle the problem of changing concepts.

Recently, a variety of algorithms for handling streams with concept changes have been proposed [1,3,4,5,8,9,10,12]. These algorithms can be classified into two approaches, i) incremental methods and ii) ensemble methods. The incremental methods successively refine a model whenever a new instance arrives. Hulten et al. [3], for example, proposed the CVFDT system that learns a single decision tree. It adapts to concept changes by discarding outdated instances or re-growing sub-trees. However, the system cannot properly respond to recurring concepts such as seasons of the year. On the ohter hand, the ensemble methods use an ensemble of classification models instead of updating a single model. This approach divides the stream into data chunks of a fixed size (*ChunkSize*), and builds a classifier from each of the chunks. Wang et al. [9] give each classifier a weight based on its expected prediction accuracy on the current instances.

H.G. Okuno and M. Ali (Eds.): IEA/AIE 2007, LNAI 4570, pp. 855–864, 2007.

To classify future instances, the approach uses a weighted vote of all classifiers. According to [9], the weighted ensemble has lower error rate than a single classifier. However, the ensemble approach cannot quickly adapt to concept changes because the approach updates the learning model on a per-chunk basis. That is, it cannot deal with concept changes in a chunk. In order to solve the problem, the system needs to detect concept changes and revise the model.

For quick adaptation, we propose a novel ensemble approach which can deal with changes at short intervals. This approach detects concept changes using an ensemble of classifiers based on the AdaBoost algorithm [2]. The two key ideas of this approach are duplication of training data and sensitive detection of concept changes. **(1) Duplication of training data:** The existing ensemble approaches do not take into account changes in a chunk. In order to cope with them, we propose to update the learning model before new data of *ChunkSize* are stored. In this method, a classifier is built from the dataset which includes some instances in the previous chunk and new instances. This framework can quickly adapt to changing concepts. **(2) Sensitive detection of concept changes:** We detect concept changes using the difference between the prediction result of the previous classifiers and that of the latest classifier, however noise causes lower reliability of change-detection. We also suggest sensitively detecting concept changes by reducing noise influence. This method uses the weights of instances in AdaBoost procedure to derive the measure for rates of change. AdaBoost assigns noise a higher weight and the inverse weight of noise is small. We use this aspect to suppress noise influence.

Integrating these techniques, we propose a novel ensemble framework. This approach tries to handle various concept changes such as gradually changing (*concept drift*) and suddenly changing (*concept shift*). The difference in the rate of change requires the difference way to deal with change. Our approach detects concept shifts which need substantial revision of the model. When concept shift is detected, the system re-chooses the classifiers for next time. Concept drifts are resolved by weighting classifiers and discarding the outdated classifiers. In addition, we tackle recurring concept problem. When a concept reappears, the old classifier built from the similar concept will help prediction. In order to use historical data efficiently, we compute similarity of classifiers and we store the diverse classifiers.

2 Concept Change

Data mining from time-varying data streams poses new challenges unlike traditional data mining. We consider peculiarities of the concept-changing problem and review existing approaches for it.

2.1 Types of Concept Change

Concept change can be roughly divided into two types. One is to really change the underlying concept of the data. The other is to change the data distribution even when the concept remains the same. The latter is known as *virtual concept*

change [11] or *sampling change* [6]. However, it is not important which kind of concept change occurs, because both cases need to revise the current model.

More importantly, there is a problem of rates of change. The gradual change, so-called *concept drift*, is very small. There is not much difference between the current concept and the oncoming one. Since it is difficult to detect concept drifts, the model for handling drifts should continuously evolve to reflect the current concept. On the other hand, *concept shift* is big change which happens abruptly. This case requires the system to quickly revise the learning model because the new concept is substantially different from the previous one.

2.2 Related Work

In this section, we introduce existing approaches for the time-varying data environment. To adapt to concept changes, typical methods often use time windows of fixed or adaptive size on the training data. For instance, Klinkenberg et al. [4] proposed an error minimization framework for adaptive time windows using support vector machines (SVMs). It does not require complicated parameterization. However, many of these approaches cannot deal with recurring concepts and cannot directly apply most-advanced learning methods.

Ensemble methods are also effective approaches to handle concept changes. The SEA [8] uses an ensemble of decision trees. It divides the stream into data chunks of a fixed size, and trains a decision tree from each of the chunks. To make a prediction, the trees are combined by an unweighted majority-vote. The SEA adapts to concept changes by discarding trees based on heuristic measure in constant time. In contrast, the ensemble approach presented by Wang et al. [9] constructs a weighted ensemble of classifiers (WCE). The WCE assigns the inverse estimated error rate on the latest chunk to the classifier's weight. Fan [1] provides sensible candidates, including (a) the new model trained from new data, (b) the model trained from new data combined with carefully selected old data, (c) the old model updated with new data and (d) the old model itself. The system statistically compares these plausible optimal models, and chooses the one with the highest accuracy. The AddExp [5] is the ensemble method using online learners. It steadily updates the weight of predictive models, referred to as *experts*, and adds a new expert if the overall prediction is incorrect. There are various other ensemble methods to set different goals, such as reducing model update cost [10], effective utilization of concept history [12].

A lot of ensemble algorithms have been proposed to cope with concept changes, nevertheless, concept changes in a chunk and concept changes at short intervals are not addressed properly. If the changes are addressed properly, adaptation to concept changes can be more quickly.

3 Quick Adaptation Method for Changing Concepts

Here we propose a novel ensemble framework to quickly adapt to various concept changes even in noisy streaming data.

3.1 Duplication of Training Data

In the streaming data environment, instances incrementally become available. Each instance $(\boldsymbol{x}, y)$ consists of a feature vector $\boldsymbol{x}$ and a class label y. The basic idea of ensemble approaches is to divide the incoming data stream into data chunks of a fixed size (*ChunkSize*) and build a classifier from each of the chunks. Traditional ensemble approaches store instances until data of *ChunkSize* are available, so they cannot handle changes in a chunk. One potential solution for handling changes in a chunk is to use the only most recent data. However, only new data cannot be enough to build a stable classifier. In order to address the issue, we propose to build a classifier from some instances in the previous chunk and incoming instances as shown in Fig. 1. A new chunk is formed by the union of new instances and the previous instances excluding older instances of the same size. We call the size *SlideSize*. This framework enables to quickly adapt to concept changes.

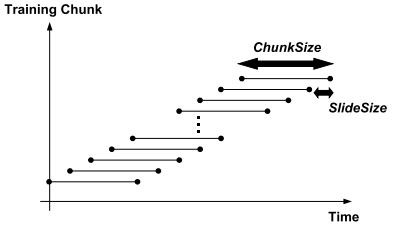

Fig. 1. Duplication of training data

3.2 Sensitive Detection of Concept Changes

The second key idea in this paper is to sensitively detect concept changes by suppressing noise influence. Concept shifts require a significant revision of the classification model. For quick adaptation to concept shifts, the system should detect them. To detect concept shifts, we compare the prediction result of the previous classifiers to that of the latest classifier. If they are significantly different, concept shift should occur. One measure of the difference is the number of differently classified instances by the two. However, the measure is susceptible to noise. For more accurate detection, we define a new measure for rates of change. We call the measure *RCC* (rates of concept change).

In order to derive the *RCC* measure, we use the weights of instances in the AdaBoost algorithm [2]. This ensemble framework repeatedly builds classifiers based on AdaBoost from the same chunk. AdaBoost assigns each instance a weight. At the beginning, all weights are equal. In every round, the weights of all misclassified instances are increased. As a result, the difficult instances are focused on. We use the weights of instances to suppress noise influence. Noise is one of the most difficult instances, so it should be assigned a higher weight. The inverse weight of noise is small. From this assumption, we use the inverse weights to derive the *RCC* measure.

The procedure to derive the *RCC* measure is as follows. First, the assigned weights of instances in each round of AdaBoost procedure are sumed up. Each sum of weights is denoted by $sum_{weight}(i)$ $(i = 1, \cdots, ChunkSize)$. Second, the method finds the instances which are differently classified by the previous generated classifiers $C_{previous}$ and the latest classifier C_{latest} in the most recent chunk S. Then the method totalizes the inverse $sum_{weight}(i)$ corresponding to the instances. Finally, the method calculates the difference between the sum and the average of the sum in the past N times, denoted by ave_N. The difference is the *RCC* measure. If *RCC* is higher than a threshold, the method detects a concept change. *RCC* is described as follows, where $I(\pi)$ is 1 if π holds and 0 otherwise:

$$RCC = \left| ave_N - \sum_{(\boldsymbol{x}_i, y_i) \in S} \left(\frac{1}{sum_{weight}(i)} \right) I(C_{previous}(\boldsymbol{x}_i) \neq C_{latest}(\boldsymbol{x}_i)) \right| \quad (1)$$

3.3 Algorithm

We describe the QACC (Quick Adaptation for Changing Concepts) algorithm. As in Fig. 2, whenever a new chunk has arrived, the algorithm first builds classifiers from the chunk using the AdaBoost algorithm. Let c denote a classifier and C denote a weighted combination of classifiers generated in T rounds of AdaBoost, that is $C(\boldsymbol{x}) = \arg\max_{y \in Y} \sum_{t=1}^{T} \left(\log \frac{1}{\alpha}\right) I(c_t(\boldsymbol{x}) = y)$. In the AdaBoost procedure, the weights assigned to each instance are totalized. Second, QACC calculates the *RCC* measure as noted in Section 3.2. Based on *RCC*, it determines whether the current model should be modified or not. If *RCC* is higher than a $threshold_{modify}$, QACC modifies the model to reflect the current concept. In this step, the system chooses the combination of classifiers in use for next time. The feasible classifier is similar to the latest classifier, so QACC compares the expected prediction error rate of each C to that of the latest combination of classifiers C'. If the difference from C' is smaller than a $threshold_{use}$, the combination of classifiers will be used for next time. When the error rate is calculated, we assign a decreasing weight to older instances. That is because later instances are likely to belong in the new concept and the weighted error rate is closer to real error rate on the new concept. Finally, the weights for all Cs are updated based on their expected error rates on the most recent chunk.

To classify an unknown instance, we use the following equation, where α is a weight assigned to a classifier c and β is a weight assigned to a combination of classifiers C:

$$C_{fin}(\boldsymbol{x}) = \arg\max_{y \in Y} \sum_{C \in \mathrm{Cs}_{use}} \left(\log \frac{1}{\alpha} \right) \left(\log \frac{1}{\beta} \right) I(C(\boldsymbol{x}) = y) \quad (2)$$

Only combinations of classifiers in use Cs_{use} are combined with these two weights.

Input: S: a dataset of *ChunkSize*
T: the number of iterations in AdaBoost procedure
N: the number of averaging to derive the RCC measure
Output: Cs_{use}: the combinations of classifiers in use for next time
Initialize: $w_1(i) = \frac{1}{ChunkSize}$ for $i = 1, \cdots, ChunkSize$

1. build classifiers from S using the AdaBoost algorithm:
for $t = 1, \cdots, T$
(1) build a classifier c'_t from S with the weight w_t.
(2) calculate the error of c'_t: $\epsilon_t = \sum_{(\boldsymbol{x}_i, y_i) \in S} w_t(i) I(c'_t(\boldsymbol{x}_i) \neq y_i)$.
(3) set $\alpha_t = \epsilon_t / (1 - \epsilon_t)$.
(4) update weights w_t: $w_{t+1}(i) = \frac{w_t(i)}{z_t} \times \begin{cases} \alpha_t \text{ if } c'_t(\boldsymbol{x}_i) = y_i \\ 1 \quad \text{otherwise} \end{cases}$
where z_t is a normalization constant.
(5) add updated weights: $sum_{weight}(i) = sum_{weight}(i) + w_{t+1}(i)$.
2. derive the RCC measure using Eq. (1).
3. modify a model:
if $RCC > threshold_{modify}$,
(1) calculate the weighted error of all combinations of classifiers:
$\epsilon = \sum_{(\boldsymbol{x}_i, y_i) \in S} w(i) I(C(\boldsymbol{x}_i) \neq y_i)$.
update classifiers in use:
$Cs_{use} = \{C |$ a difference from ϵ of $C' < threshold_{use}\}$.
(2) set $\beta = \epsilon / (1 - \epsilon)$.
else,
(1) calculate the error of C' and C_{use}: $\epsilon = \sum_{(\boldsymbol{x}_i, y_i) \in S} I(C(\boldsymbol{x_i}) \neq y_i)$.
(2) set $\beta = \epsilon / (1 - \epsilon)$.

Fig. 2. The QACC algorithm

Ensemble pruning: QACC stores historical classifiers for recurring concepts. However, retaining all classifiers causes high cost, so we discard similar classifiers to the latest classifier. We define a measure for diversity as the following equation. QACC discards the combination of classifiers whose *diversity* is smaller than a $threshold_{discard}$.

$$diversity(C) = \sum_{(\boldsymbol{x}_i, y_i) \in S} \left(\frac{1}{sum_{weight}(i)} \right) I(C(\boldsymbol{x}_i) \neq C'(\boldsymbol{x}_i)) \tag{3}$$

4 Experiments

We conducted experiments on three types of synthetic data stream to estimate the performance of the QACC algorithm.

4.1 Streaming Data and Experimental Setup

We create synthetic data to simulate three types of concept change, i) concept drift, ii) concept shift (the rate of change is small) and iii) concept shift (the rate of change is big). The dataset based on **a moving hyperplane** simulates the first two types. A hyperplane in d-dimensional space is denoted by the equation: $\sum_{i=1}^{d} a_i x_i = a_0$. We generate random instances uniformly distributed in $[0,1]^d$. Instances satisfying $\sum_{i=1}^{d} a_i x_i \geq a_0$ are labeled as positive, and otherwise negative. Weights $a_i (1 \leq i \leq d)$ are randomly initialized in $[0,1]^d$. We always set $a_0 = \frac{1}{2}\sum_{i=1}^{d} a_i$ so that the hyperplane cuts the space in two parts of the same volume. In this experiment, we use $d = 5$. Concept drift is simulated by changing weights a_i slightly per 10 instances and concept shift (the rate of change is small) is simulated by more strongly changing them per 2500 instances. As for concept shift, the rate of change is gradually-increased. **STAGGER** [7] can simulate concept shift (the rate of change is big). Each instance has three features, $color \in \{green, blue, red\}$, $shape \in \{triangle, circle, rectangle\}$ and $size \in \{small, medium, large\}$. STAGGER consists of three target concepts, (a) $color = red \wedge size = small$, (b) $color = green \vee shape = circle$ and (c) $size = medium \vee size = large$. We change the target concept per 2500 instances to simulate concept shift (the rate of change is big). It also simulates recurring concepts.

We demonstrate the efficiency of the QACC algorithm by comparing to the weighted classifier ensemble (WCE) [9] and QACC without sensitive detection process. Based on a prior experiment, we choose $ChunkSize = 200$, $SlideSize = 50$ and set parameters as follows: the total number of classifiers $K = 10$ for WCE; $T = 10$, $N = 5$, $threshold_{modify} = 2.0$, $threshold_{use} = 1.0$, $threshold_{discard} = 0.05$ for QACC. The base learner used by all algorithms is the C4.5 decision tree. The tests are performed on a dataset in a next chunk.

4.2 Experimental Results

We first verify that the *RCC* measure is efficient for measuring rates of concept change. Fig. 3 shows temporal transition of two different measures on a moving hyperplane dataset with concept shift (the rate of change is small). The noise level is set to 5%. The X-axis represents the number of arrived instances. Fig. 3(a) shows the *RCC* measure and Fig. 3(b) shows the number of differently classified instances by the previous generated classifiers and the latest classifier. Comparing the two measures, *RCC* suppresses noise influence and bursts more clearly when concept changes occur. The differences between the averaged Z-score of the concept change point and that of otherwise are (a) 1.59, (b) 1.28. The result indicates the efficiency of *RCC* as a criterion for rates of change.

Next, we compare the QACC algorithm to the other approaches using three types of synthetic data. Each type of synthetic data is introduced 5% and 10% noise. For all types, we averaged the results over 10 runs. Fig. 4, 5 and 6 show temporal transition of the expected prediction accuracy. In Fig. 4, a moving hyperplane simulates concept drift. All approaches can adapt to changes without decreasing the accuracy because they build classifiers incrementally. Among

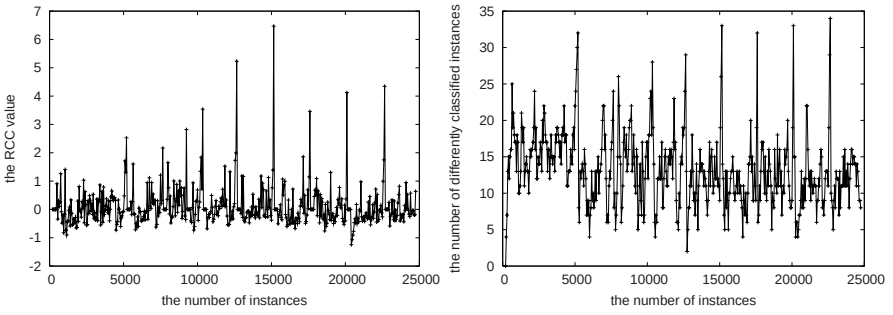

(a) The RCC measure. (b) The num. of differently classified instances.

Fig. 3. The RCC measure and the number of differently classified instances

Table 1. The averaged prediction accuracy

Dataset		WCE	QACC w/o SD	QACC
moving hyperplane (drift)	no noise	91.54	93.34	93.74
	noise 5%	90.50	93.45	**95.00**
	noise 10%	88.95	91.19	**92.87**
moving hyperplane (shift)	no noise	88.47	90.16	**91.98**
	noise 5%	87.28	90.83	**91.76**
	noise 10%	85.29	89.14	**89.77**
STAGGER (shift)	no noise	93.70	95.42	95.90
	noise 5%	93.39	95.40	95.54
	noise 10%	93.21	94.99	95.30

them, QACC keeps higher accuracy. The reason is that it modifies the model at short intervals and incorporates AdaBoost. In Fig. 5, a moving hyperplane simulates concept shift whose rate of change is small. We can see obvious decline of accuracy after concept changes in this case. It should be noted that QACC is more resilient to the decline. WCE stores instances until data of *ChunkSize* are available, so it delays a response to concept changes in a chunk. In contrast, QACC can address them by overlapping training data. Moreover, it detects concept shifts and modifies the current model substantially. As a result, QACC gives the best performance of the three. In Fig. 6, STAGGER simulates concept shift whose rate of change is big. As in the result of Fig. 5, QACC adapts to concept shifts quickly. However, Fig. 6(b) shows that the accuracy of QACC drops a little in phases without concept changes. This is due to that noise affects AdaBoost procedure adversely.

Table 1 shows that the averaged prediction accuracy of each approach on all datasets. They are averaged until 25000 instances arrive. We use **bold** font for significantly different results from WCE. QACC achieves higher prediction accuracy than other approaches in all datasets.

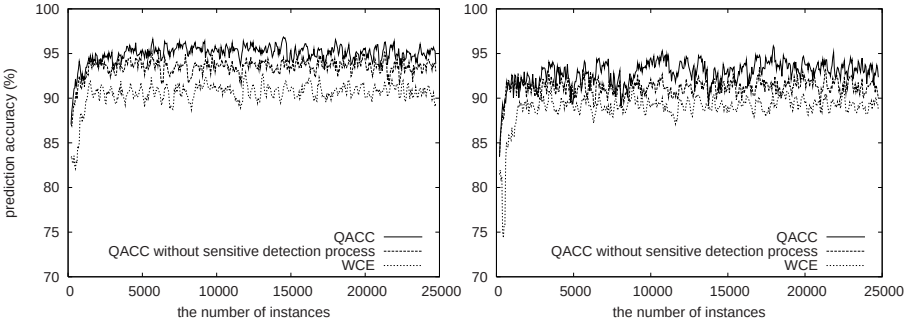

(a) including 5% noise. (b) including 10% noise.

Fig. 4. The prediction accuracy on a moving hyperplane dataset (concept drift)

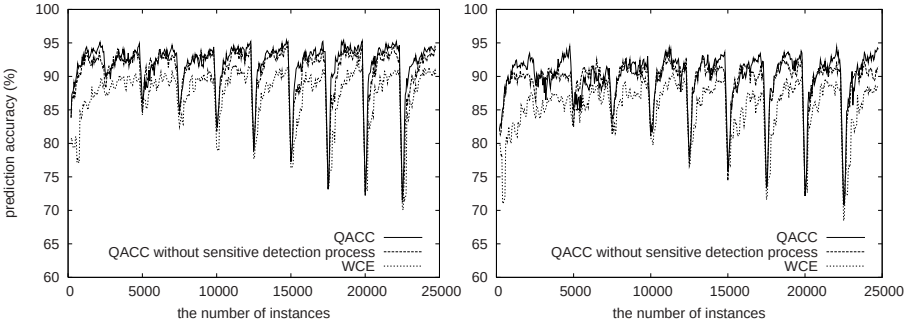

(a) including 5% noise. (b) including 10% noise.

Fig. 5. The prediction accuracy on a moving hyperplane dataset (concept shift)

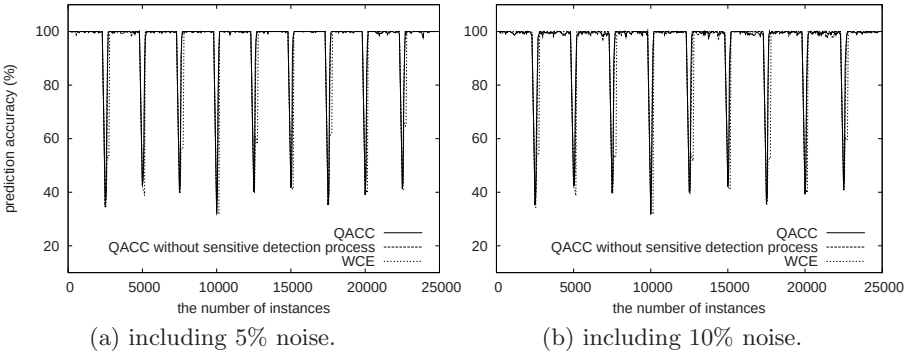

(a) including 5% noise. (b) including 10% noise.

Fig. 6. The prediction accuracy on a STAGGER dataset (concept shift)

5 Conclusion

In mining data streams, classification models are required to quickly adapt to time-varying concepts. For quick adaptation, this paper proposed the QACC algorithm, which is able to deal with concept changes at short intervals and sensitively detect concept shifts. Empirical studies show that QACC is more efficient for both concept drift and concept shift than WCE. Moreover, sensitive detection method improves ability to adapt to concept changes. In future work, we plan to investigate a strategy for dynamically adjusting the parameters of the QACC algorithm and consider the time complexity.

References

1. Fan, W.: Systematic data selection to mine concept-drifting data streams. In: Proc. of the 10th ACM Int. Conf. on Knowledge Discovery and Data Mining, pp. 128–137 (2004)
2. Freund, Y., Schapire, R.E.: A decision-theoretic generalization of on-line learning and an application to boosting. Journal of Computer and System Sciences 55, 119–139 (1997)
3. Hulten, G., Spencer, L., Domingos, P.: Mining Time-Changing Data Streams. In: Proc. of the 7th ACM Int. Conf. on Knowledge Discovery and Data Mining, pp. 97–106 (2001)
4. Klinkenberg, R., Joachims, T.: Detecting concept drift with support vector machines. In: Proc. of the 17th Int. Conf. on Machine Learning, pp. 487–494 (2000)
5. Kolter, J., Maloof, M.: Using Additive Expert Ensembles to Cope with Concept Drift. In: Proc. of the 22nd Int. Conf. on Machine Learning pp. 449–456 (2005)
6. Salganicoff, M.: Tolerating concept and sampling shift in lazy learning using prediction error context switching. Artificial Intelligence Review, Special Issue on Lazy Learning 11(1–5), 133–155 (1997)
7. Schlimmer, J., Granger, R.: Beyond incremental processing: Tracking concept drift. In: Proc. of the 5th National Conf. on Artificial Intelligence, pp. 502–507 (1986)
8. Street, W.N., Kim, Y.: A Streaming Ensemble Algorithm (SEA) for Large-Scale Classification. In: Proc. of the 7th ACM Int. Conf. on Knowledge Discovery and Data Mining, pp. 377–382 (2001)
9. Wang, H., Fan, W., Yu, P., Han, J.: Mining concept-drifting data streams with ensemble classifiers. In: Proc. of the 9th ACM Int. Conf. on Knowledge Discovery and Data Mining, pp. 226–235 (2003)
10. Wang, P., Wang, H., Wu, X., Wang, W., Shi, B.: On reducing classifier granularity in mining concept-drifting data streams. In: Proc. of the 5th IEEE Int. Conf. on Data Mining, pp. 474–481 (2005)
11. Widmer, G., Kubat, M.: Effective learning in dynamic environments by explicit context tracking. In: Brazdil, P.B. (ed.) Machine Learning: ECML-93. LNCS, vol. 667, pp. 227–243. Springer, Heidelberg (1993)
12. Yang, Y., Wu, X., Zhu, X.: Combining proactive and reactive predictions for data streams. In: Proc. of the 11th ACM Int. Conf. on Knowledge Discovery and Data Mining, pp. 710–715 (2005)

ACIK：Association Classifier Based on Itemset Kernel*

Yang Zhang[1], Yongge Liu[2], Xu Jing[1,**], and Jianfeng Yan[3]

[1] College of Information Engineering, Northwest A&F University, Yangling, P.R. China
[2] Dept. Computer Science, Anyang Normal University, Anyang, P.R. China
[3] Intel Asia-Pacific Research & Development Ltd, Shanghai, P.R. China

Abstract. Considering the interpretability of association classifier, and high classification accuracy of SVM, in this paper, we propose ACIK, an association classifier built with help of SVM, so that the classifier has an interpretable classification model, and has excellent classification accuracy. We also present a novel family of Boolean kernel, namely itemset kernel. ACIK, which takes SVM as learning engine, mines interesting association rules for construct itemset kernels, and then mines the classification weight of these rules from the classification hyperplane constructed by SVM. Experiment results on UCI dataset show that ACIK outperforms some state-of-art classifiers, such as CMAR, CPAR, L^3, DeEPs, linear SVM, and so on.

Keywords: Association Classifier, Support Vector Machine, Kernel Function.

1 Introduction

Nowadays, many successful association classifiers have been proposed, such as CBA[1], CMAR[2], CPAR[3], DeEPs[4], L^3[5], CSFP[7], and so on. They either select one association rule (itemset), or select a set of association rules (itemsets) for classification. Hence, their classification models are interpretable to human experts. However, the way they select one rule (itemset) for classification, or set weight to the rules (itemsets) for classification, is heuristic, lacking strong mathematical background, which also limits the accuracy of the classifier.

SVM classifier, which is based on the structural risk minimization theory [10], is an excellent classifier. However, its classification model is non-interpretable, while for some applications, an interpretable classification model is very helpful.

In this paper, we are trying to build an association classifier with help of SVM, so that the classifier has an interpretable classification model, and has excellent classification accuracy. In order to fulfill this task, we propose itemset kernel, a novel family of Boolean kernel, and we give the algorithm for mining the structure of itemset kernel by borrowing ideas form research community of association rule mining. SVM, which is applied with an itemset kernel, is used as a learning engine, and an easy algorithm is proposed to mine the weight of association rules from the

* This work is supported by Talent Fund of Northwest A&F University (01140402, 01140401) and Young Cadreman Supporting Program of Northwest A&F University.
** Corresponding author.

H.G. Okuno and M. Ali (Eds.): IEA/AIE 2007, LNAI 4570, pp. 865–875, 2007.

hyperplane constructed by SVM. In this way, we build our association classifier, ACIK (Association Classifier based on Itemset Kernel). Experiment results on UCI datasets show that ACIK has better classification accuracy than some state-of-art classifiers, such as CMAR, CPAR, L^3, DeEPs, linear SVM, and so on.

2 Related Works

Current methods to build association classifiers could be divided into 3 categories.

1. Mining frequent itemsets. This is also the traditional way to build association classifiers. CBA, CMAR, CPAR, L^3, L^3_M, and CSFP are classifiers belong to this category. They either mine frequent itemsets[7], or mine rules with left part only made up of attribute information, and right part only made up of category information for classification [1][2].
2. Mining EPs (Emerging Pattern). EPs are defined as event associations whose supports change significantly from one dataset to another. CAEP, iCAEP [11], and DeEPs belong to this category.
3. Mining associations with help of SVM. To the best of our knowledge, only DRC-BK [8][9] and ACIK belongs to this category.

For CBA and L3, their algorithms for selecting one rule for classification are heuristic. For CPAR, L^3_M, CSFP, DeEPs, and so on, the algorithms to set weight to association rules (EPs), and the algorithm for classification, are also heuristic. These algorithms lack strong mathematical background, which limits their accuracy.

ACIK takes SVM with itemset kernel as learning engine, which means that ACIK is also based on structural risk minimization theory, and that ACIK also makes classification decision by the optimal hyperplane in the feature space.

3 Itemset Kernel

Suppose $U \in R^n$, $V \in R^n$, $\phi(U): R^n \to R^m$, $a \in R^+$, K_1 and K_2 are kernels over $R^n \times R^n$, K_3 is kernel over $R^m \times R^m$. In [10], N. Cristianini etc. proves that the functions satisfy formula (1)~(4) are all kernels over $R^n \times R^n$:

$$K(U,V) = K_1(U,V) + K_2(U,V) \ . \tag{1}$$

$$K(U,V) = aK_1(U,V) \ . \tag{2}$$

$$K(U,V) = K_1(U,V)K_2(U,V) \ . \tag{3}$$

$$K(U,V) = K_3(\phi(U),\phi(V)) \ . \tag{4}$$

Kernels which take $\{0,1\}^n$ as input space are known as **Boolean kernel**. Let $U \in \{0,1\}^n$, $V \in \{0,1\}^n$, it is obviously that we can get lemma 1 by formula (4).

Lemma 1. $K(U,V)=U_iV_i$, $(1\le i\le n)$ is a Boolean kernel.

By formula (2), (3) and lemma 1, we can get:

Lemma 2. $K_{j-itemset}(U,V)=a_jU_{i1}V_{i1}U_{i2}V_{i2}...U_{ij}V_{ij}$, ($1\le i_k\le n$, $1\le k\le j$, $j\le n$, $a_j>0$) is a Boolean kernel.

Taking $\{0,1\}^n$ as input space, each dimension in the input space could be looked as a Boolean attribute. Let's borrow the term ***item*** and ***itemset*** from the research of association rule mining. If each Boolean attribute is looked as an item, then there are j items in kernel $K_{j-itemset}$, which means that $K_{j-itemset}$ represents a *j*-itemset. The weight a_j represents our knowledge of the importance of this *j*-itemset for classification. For simplicity, in this paper, we set $a_j=1$.

By formula (1) and lemma 2, we get:

Theorem 1. $K_{itemset}(U,V)=\sum_k K_{j-itemset,k}(U,V)$ is a Boolean kernel.

Since each term in $K_{itemset}$ represents a *j*-itemset, we name $K_{itemset}$ **itemset kernel**.

If we have $K_{j-itemset,k}(U,V)=U_kV_k$, ($1\le k\le n$), then, we get $K_{itemset}(U,V)=\sum_{k=1}^{n}U_kV_k=<U,V>$. Therefore, when taking $\{0,1\}^n$ as input space, linear kernel is an example of itemset kernel. It is also easy to prove that the Boolean kernels used in [8][9][12] are all examples of itemset kernel.

4 Building ACIK Classifier

There are 4 steps for building ACIK classifier.

1. Mining interesting association rules from training dataset.
2. Constructing itemset kernel from the association rules.
3. Learning hyperplane for classification with help of SVM that is applied with itemset kernel.
4. Mining the classification weight of association rules from the hyperplane.

4.1 Mining Association Rules

When mining association rules, if we set the parameter minimal support *MinSup* and minimal confidence *MinCon* close to 1, then some important rules will be filtered, and hence decrease the classification accuracy. However, if we set these parameters close to 0, then huge amount of rules could be mined out. Among these rules, most are redundant rules, which can also decrease the accuracy and efficiency of the classifier. Hence, we need to filter the redundant rules.

For association rule r, we write $Con(r)$ for the confidence of r, $Left(r)$ for the left part of r. For association feature r_i and r_j, if $Con(r_j) > Con(r_i)$, then we say that r_j has greater discriminative ability than r_i. If we have $Left(r_j) \subset Left(r_i)$, then r_j is more generalized than r_i, and this means that the probability that we observe r_j in testing samples is higher than the probability that we observe r_i in testing samples. If we have both $Con(r_j) > Con(r_i)$ and $Left(r_j) \subset Left(r_i)$, this means that r_i is a redundant rule and could totally be replaced by r_j. We define redundant rule as:

Definition 1. For association rule r_i and r_j, we say that r_i is redundant rule with respect to r_j if and only if $Left(r_j) \subset Left(r_i) \wedge Con(r_j) > Con(r_i)$.

Definition 2. The length of association rule r_i is defined as the number of items in $Left(r)$.

Fig. 1 gives our algorithm for selecting association rules.

Currently, there are many algorithms for mining association rules, such as Apriori[13], FPtree, and so on. Here, we simply use an Apriori-like algorithm, which is not discussed in detail here for lacking of space, for mining association rules in step 1 of Fig.1. Please note that in step 1, we only mine out association rules with maximal length *MaxLen*. Previous approaches for building association classifiers, such as CBA, CMAR, and CPAR mines out rules with arbitrary length. The reason we only mines out rules with maximal length *MaxLen* is that we prefers to more generalized association rules, as more generalized rules are expected to be observed in testing samples again with high probability. Step 2 in this algorithm is used to speed up the running of step 3. Step 4 ensures that all 1-itemset rules are included in R, and this will further ensures that all the original dimensions in the input space will be copied into the feature space by the itemset kernel. If we set bad values to parameter *MinCon*, *MinSup*, or *MaxLen*, then this algorithm will produce an association rule set R with bad quality. We hope to preserve the classification accuracy of linear kernel inside the itemset kernel by step 4 under the condition that R has bad quality.

4.2 Constructing Itemset Kernel

From the association rule set R, we get a set of itemsets $\{itemset \mid itemset = Left(r), r \in R\}$. Each itemset in this set is mapped into a term in $K_{itemset}$, and for a certain itemset, each item in it is mapped into a factor in the corresponding term. Hence, the structure of $K_{itemset}$ is totally defined by R.

The detailed algorithm for constructing itemset kernel is given in Fig.2.

Here we illustrate this algorithm by an example. Suppose association rule set R is:

$$I_1 I_2 \to C_+ \quad I_1 I_2 I_3 \to C_- \quad I_1 \to C_+ \quad I_2 \to C_+ \quad I_3 \to C_+$$

then, the resulted itemset kernel is :

$$K_{itemset}(U,V) = U_1V_1U_2V_2 + U_1V_1U_2V_2U_3V_3 + U_1V_1 + U_2V_2 + U_3V_3$$

Algorithm 1: Association Rule Selection
Input: Training dataset D (with its attribute set I)
Minimal support *MinSup*
Minimal confidence *MinCon*
Maximal length *MaxLen*
Output: The set of association rules after rule selection
1. Mine out the set of association rules R from D with minimal support *MinSup*, minimal confidence *MinCon*, and maximal length *MaxLen*;
2. Sort R into a sequence according to the length of the rule in ascending order;
3. Filter out redundant rules from R according to definition 1;
4. $R = R \cup \{r \mid r = I_i \to C_+, I_i \in I\}$;

Fig. 1. Association Rule Selection Algorithm

Algorithm 2: Constructing Itemset Kernel
Input: Association rule set R
Output: The itemset kernel
1. $K_{itemset}(U,V) = 0$;
2. for each r in R
3. $K_r(U,V) = 1$;
4. for each item I_i in $Left(r)$
5. $K_r(U,V) = K_r(U,V) \cdot U_i V_i$;
6. end for;
7. $K_{itemset}(U,V) = K_{itemset}(U,V) + K_r(U,V)$;
8. end for;
9. output $K_{itemset}(U,V)$;

Fig. 2. Constructing Itemset Kernel Algorithm

4.3 Mining Classification Weight for Association Rules

Please note that each dimension in the feature space corresponds to an association rule in R, so, the weight of the dimension is exactly the classification weight of the corresponding association rule.

Let's suppose there are $|D|$ samples in the training dataset $D=\{X_i, y_i\}$, $i=1, 2, ..., |D|$. Here, $X_i \in \{0,1\}^n$, represents a sample; and $y_i \in \{+1, -1\}$, represents the class label of the sample. For the testing sample $X \in \{0,1\}^n$, the classifier learned by SVM could be represented as:

$$f(X) = \text{sgn}(\sum_{i=1}^{|D|} \alpha_i y_i K_{itemset}(X_i, X) + b) \ . \quad (5)$$

Here, $\alpha \in R^n$, $b \in R$ are knowledge learned by SVM; sgn() is the sign function.

It is obvious in formula (5) that the contribution to classification made by the itemset of rule r, say, $Left(r)$, is $\sum_{i=1}^{|D|} \alpha_i y_i$. As we have $\alpha_i \neq 0$ for support vectors, and $\alpha_i = 0$ for other samples, we only need to calculate $\sum \alpha_i y_i$ on the set of support vectors. Fig.3 gives the algorithm to mine classification weight of association rules from the optimal hyperplane built by SVM.

Algorithm 3: Mining Classification Weight for Association Rules
Input: Support vector set SV
Weight vector
Association rule set R
Output: ACIK Classifier
1. $classifier =$;
2. for each rule r_i in R
3. $weight_i = 0$;
4. for each SV_j in SV
5. if $Left(r_i)$ matches SV_j then $weight_i = weight_i +$ $_j y_j$;
6. end for;
7. $classifier = classifier \cup \{< Left(r_i), weight_i >\}$;
8. end for;
9. output $classifier$;

Fig. 3. Algorithm for Mining Classification Weight for Association Rules

In Fig.3, step 4 to step 6 mines the classification weight of rule r_i from the hyperplane constructed by SVM. In step 7, the itemset of r_i, and the classification weight of r_i together form a new classification rule.

Compared with to use only one rule for classification, to use a set of rules for classification could utilize more knowledge learned from training dataset, and this could possibly leads to better classification accuracy [6].

5 Classification Algorithm for ACIK

The classification algorithm of ACIK follows formula (5), and it is shown in Fig.4. In this figure, parameter b is the knowledge learned by SVM.

Let's look the feature space as linear space. The classification decision here is made by the linear sum of the weights of all matched rules. And this is shown in step 2 to step 4 in Fig.4.

Algorithm 4: Classification Algorithm
Input: ACIK classifier $classifier$
Sample $sample$
Parameter b
Output: The category of $sample$
1. $f = b$;
2. for each $< itemset_i, weight_i >$ in $classifier$
3. if $itemset_i$ matches $sample$, then $f = f + weight_i$;
4. end for;
5. output $\mathrm{sgn}(f)$;

Fig. 4. Classification Algorithm of ACIK

Suppose there are p rules in the association rule set, and maximal length of the rules is q, then the time complexity and space complexity of this algorithm is $O(pq)$.

6 Experiment Result

In this section we report our experiment results for measuring the classification accuracy of ACIK. The algorithms were implemented in C language, and we modified SVM-light[1] by implementing our itemset kernel. Our experiment is made on a PC with Pentium 4 3.0 GHz CPU and 512M memory.

UCI[2] dataset is often used in experiments for classification analysis research. 16 binary datasets from UCI dataset are used in our experiment as their classification

[1] URL: http://svmlight.joachims.org/
[2] URL: http://www.ics.uci.edu/~mlearn/MLRepository.html

accuracy on several state-of-art classifiers is available in the literature for comparison. We made our experiment in the 10-fold cross validation way, and report the average classification accuracy (%). The pre-processing is made following the steps reported in [8][9].

Table 1(A). Classification Results on UCI Dataset

Dataset	#Sam	#Att	#Bool	ACIK	Rule	Time	DeEPs	C5.0	RIPPER	CBA
AUSTRA	690	14	50	86.52	1102.0	0.096	88.41	85.94	87.3	84.9
DIABETES	768	8	15	76.57	86.4	0.006	76.82	73.03	74.7	74.5
GERMAN	1000	200	60	75.40	999.7	0.128	74.40	71.30	69.8	73.4
HEART	270	13	18	82.96	244.6	0.006	82.22	77.06	80.7	81.9
IONO	351	34	143	92.29	8945.2	0.660	91.24	91.92	91.2	92.3
PIMA	768	8	15	76.82	87.1	0.002	77.08	73.03	73.1	72.9
SONAR	208	60	42	86.17	2068.2	0.156	86.97	70.20	78.4	77.5
TIC-TAC	958	9	27	98.86	535.9	0.036	99.06	-	98.0	99.6
BREAST	699	10	30	96.86	263.0	0.028	96.42	95.43	95.1	96.3
CLEVE	303	13	29	83.16	501.8	0.024	84.21	77.16	82.2	82.8
CRX	690	15	61	86.52	1301.0	0.092	88.11	83.91	84.9	84.7
HEPATIC	155	19	46	85.00	623.5	0.076	82.52	74.70	76.7	81.8
HORSE	368	22	78	85.30	2839.0	0.268	85.31	84.81	84.8	82.1
HYPO	3163	25	57	99.05	200.2	0.388	98.26	99.32	91.2	98.9
LABOR	57	16	41	95.00	313.1	0.064	87.67	83.99	84.0	86.3
SICK	2800	29	63	97.75	356.1	0.726	96.63	98.78	97.7	97.0
Average	828	30.9	48.4	87.76	1279.2	0.172	87.21	82.71	84.36	85.43
Improvement	-	-	-	-	-	-	0.55	5.05	3.40	2.33
Win	-	-	-	-	-	-	8	13	15	14

After our pilot experiment, we fond that we could get best average performance of ACIK when we set parameter to *MinSup*=0.02, *MinCon*=0.7, *MaxLen*=3. We report our experiment results with this parameter setting in table 1(A) and table 1(B).

In table 1(A), column 1 lists the name of the datasets. Column 2, 3, and 4 gives the number of samples, the number of attributes in the original dataset, and the number of attributes after pre-processing, respectively. Column 5, 6, and 7 gives the classification results, the size of rule set, and the totally running time needed by algorithm 1, 2 and 3 for ACIK classifier (in second), respectively. Column 8 and 9 gives the classification results of DeEPs and C5.0, respectively. These results are copied from [4]. Column 10 and 11 gives the classification results of RIPPER, and CBA, respectively. These results are copied from [3].

In table 1(B), column 1 lists the name of the datasets. Column 2 and 3 gives the classification results of CMAR, and CPAR, respectively. These results are copied

from [3]. Column 4 and 5 gives the classification results of linear SVM and DRC-BK that is applied with MPDNF kernel, respectively. These results are copied from [8]. Column 6 and 7 gives the classification result of SVM with polynomial kernel $(\langle U,V\rangle+1)^d$. Column 8 and 9 gives the classification results of L^3 and L^3_M, respectively. These results are copied from [6]. Column 10 gives the classification results of CSFP, and these results are copied from [7].

Table 1(B). Classification Results on UCI Dataset

Dataset	CMAR	CPAR	SVM	DRC-BK	POLY d=2	POLY d=3	L^3	L^3_M	CSFP
AUSTRA	86.1	86.2	84.49	84.64	84.35	85.942	85.7	86.4	86.5
DIABETES	75.8	75.1	77.73	78.13	76.31	76.70	75.8	79.0	76.9
GERMAN	74.9	73.4	74.90	75.70	75.70	76.30	73.8	74.7	71.4
HEART	82.2	82.6	81.48	82.59	84.08	84.07	84.4	84.4	81.5
IONO	91.5	92.6	90.03	91.74	91.44	92.58	93.2	93.2	89.4
PIMA	75.1	73.8	77.21	76.82	76.95	77.73	78.4	79.2	76.7
SONAR	79.4	79.3	87.02	87.98	84.74	86.17	78.9	81.7	77.9
TIC-TAC	99.2	98.6	98.33	98.33	95.10	98.33	98.4	100.0	99.0
BREAST	96.4	96.0	96.42	96.71	96.85	96.71	95.9	96.7	94.7
CLEVE	82.2	81.5	83.17	84.16	84.50	83.50	82.5	86.4	84.4
CRX	84.9	85.7	86.24	85.80	85.51	86.09	84.4	85.9	86.9
HEPATIC	80.5	79.4	85.81	86.45	86.37	84.46	81.9	83.2	87.0
HORSE	82.6	84.2	82.34	83.97	84.76	83.68	82.9	83.2	80.7
HYPO	98.4	92.6	99.34	99.24	99.27	99.27	95.2	97.5	95.0
LABOR	89.7	84.7	92.98	94.74	91.33	94.67	91.2	96.5	95.0
SICK	97.5	96.8	97.29	97.25	97.32	97.43	94.7	94.7	94.3
Average	86.03	85.16	87.17	87.77	87.16	87.73	86.08	87.67	86.08
Improvement	1.74	2.60	0.59	-0.01	0.6	0.03	1.68	0.09	1.68
Win	15	15	10	10	10	9	13	9	10

The three rows at the bottom of both table 1(A) and table 1(B) give the average accuracy over the 16 datasets, the accuracy improvement of ACIK with respect to the corresponding classifier, and the number of datasets that ACIK wins with respect to the corresponding classifier, respectively.

From table 1(A) and table 1(B), it is obviously that ACIK outperforms polynomial kernel, and that ACIK outperforms CBA, CMAR, L^3, and CSFP, which are association classifiers built by mining frequent itemsets. Among all the association classifiers built by mining frequent itemsets, L^3_M has the best classification accuracy. ACIK outperforms L^3_M on 9 datasets of the 16 datasets used. ACIK also outperforms

DeEPs, an association classifiers build by mining EPs. It is also shown that ACIK outperforms linear SVM, C5.0, and RIPPER.

It is obviously that ACIK and DRC-BK outperform other classifiers in table 1(A) and table 1(B). ACIK and DRC-BK both builds association classifiers with help of SVM. The success of ACIK and DRC-BK may suggest that to study association classifier or decision rule classifier with help of structural risk minimization theory is a good research direction.

7 Conclusion and Future Work

In this paper, we present ACIK classifier, an association classifier based on structural risk minimization theory. We also present itemset kernel, a novel family of Boolean kernel. ACIK mines association rules to construct itemset kernel, taking SVM which is applied with itemset kernel as learning engine, and mines the weight of the association rules from the hyperplane constructed by SVM. The experiment results on UCI dataset show that ACIK has better classification performance than some state-of-art classifiers, such as CMAR, CPAR, L^3, DeEPs, linear SVM, and so on.

In the future, we will study itemset kernels with better structure, so as to further improve the classification accuracy of association classifiers built with help of SVM.

References

[1] Liu, B., Hsu, W., Ma, Y.: Integrating Classification and Association Rule Mining. In: Proc. the 4th International Conference on Knowledge Discovery and Data Mining (KDD 98), NY (1998)

[2] Li, W., Han, J., Pei, J.: CMAR: Accurate and Efficient Classification Based on Multiple Class-Association Rules. In: IEEE International Conference on Data Mining (ICDM'01) (2001)

[3] Yin, X., Han, J.: CPAR: Classification Based on Predictive Association Rules. In: Proc. 2003 SIAM Int'l Conf. Data Mining (SDM '03) (2003)

[4] Li, J., Dong, G., Ramamohanarao, K., Wong, L.: DeEPs: A New Instance-Based Lazy Discovery and Classification System. Machine Learning 54(2), 99–124 (2004)

[5] Baralis, E., Garza, P.: A lazy approach to pruning classification rules. In: Proc. of the IEEE 2002 International Conference on Data Mining (ICDM'02), Maebashi City, Japan, pp. 35–42 (2002)

[6] Baralis, E., Garza, P.: Majority Classification by Means of association Rules. In: Lavrač, N., Gamberger, D., Todorovski, L., Blockeel, H. (eds.) PKDD 2003. LNCS (LNAI), vol. 2838, Springer, Heidelberg (2003)

[7] Sucahyo, Y.G., Gopalan, R.: Building a More Accurate Classifier Based on Strong Frequent Patterns. In: Webb, G.I., Yu, X. (eds.) AI 2004. LNCS (LNAI), vol. 3339, Springer, Heidelberg (2004)

[8] Yang, Z., Zhanhuai, L., Kebin, C.: DRC-BK: Mining Classification Rules by Using Boolean Kernels. In: Gervasi, O., Gavrilova, M., Kumar, V., Laganà, A., Lee, H.P., Mun, Y., Taniar, D., Tan, C.J.K. (eds.) ICCSA 2005. LNCS, vol. 3480, Springer, Heidelberg (2005)

[9] Yang, Z., Zhanhuai, L., Yan, T., Kebin, C.: DRC-BK: Mining Classification Rules with Help of SVM. In: Dai, H., Srikant, R., Zhang, C. (eds.) PAKDD 2004. LNCS (LNAI), vol. 3056, Springer, Heidelberg (2004)
[10] Cristianini, J., Shawe-Taylor.: An Introduction to Support Vector Machines. Cambridge Press, Cambridge (2000)
[11] Zhang, X., Dong, G., Kotagiri, R.: Information-Based Classification by Aggregating Emerging Patterns. In: Lecture Notes in Computer Science, Hong Kong, pp. 48–53 (2000)
[12] Sadohara, K.: Learning of Boolean functions using support vector machines. In: Abe, N., Khardon, R., Zeugmann, T. (eds.) ALT 2001. LNCS (LNAI), vol. 2225, pp. 106–118. Springer, Heidelberg (2001)
[13] Agrawal, R., Imielinski, T.: Mining association rules between sets of items in large databases. In: Proc. ACM international conference on Management of data (SIGMOD'93) (1993)

Risk Discovery Based on Recommendation Flow Analysis on Social Networks

Jason J. Jung and Geun-Sik Jo

Intelligent E-Commerce Systems Laboratory,
Department of Computer and Information Engineering, Inha University,
253 Yonghyun-dong, Incheon, Korea 402-751
j2jung@intelligent.pe.kr, gsjo@inha.ac.kr

Abstract. Social networks have been working as a medium to provide cooperative interactions between people. However, as some of users take malicious actions, the social network potentially contains some risks (e.g., information distortion). In this paper, we propose a robust information diffusion (or propagation) model to detect malicious peers on social network. Especially, we apply statistical sequence analysis to discover a peculiar patterns on recommendation flows. Through two experimentation, we evaluated the performance of risk discovery on social network.

Keywords: Social network; Recommendation; Risk discovery.

1 Introduction

Chance discovery methods have been studied to analyze events (or situations) that affect human decision making [1]. In particular, social network analysis is an emerging field to deal with supporting efficient interactions (e.g., Q&A, discussion, recommendation, and dissemination) between people. It means that people can have a "chance" to communicate with potential neighbors of whom they are not currently aware on the same social network.

On the other side, risk discovery (e.g., information distortion and network failure) is also an important challenge to make the social interactions more reliable. We want to devise a novel facilities to detect malicious users (or groups) who might cause the harmful effects on social network. Thereby, information flows on social network have to be analyzed to discover rare (or unusual) patterns. The main goal of this paper is to find out noise-free propagation paths with optimal stabilization performance for reaching equilibrium state.

As proposed in earlier work [2,3], we have investigated socialized recommender systems based on sharing information with only acquaintances (these entities can be a set of people, groups, or software agents) in order to overcome privacy issues on centralized recommender systems. This system is capable of not only exchanging the rating dataset (meaning the corresponding entities' preference), but also reinforcing the propagated recommendation with the user's subjective opinion. However, the problem is that the information sources on social network are assumed to be completely trustworthy with each other.

H.G. Okuno and M. Ali (Eds.): IEA/AIE 2007, LNAI 4570, pp. 876–885, 2007.

In this paper, we focus on "open" social networks, which means that there possibly exist some risks (particularly, malicious users) of recommendation distortion. The malicious users are "intentionally or unintentionally" involved in a social network and spreading biased and fraud (or deceitful) information to other people. Outlier detection method is thereby exploited to find out the specific positions in a given sequential datasets. Eventually, the social network is able to be refined as filtering out the malicious people.

The remainder of this paper is as follows. In the following Sect. 2, we formulate a social network for distributed recommender systems, and define a flow of recommendation. Sect. 3 will describe how to analyze a set of sequential datasets and detect some anomaly patterns indicating malicious behaviours. Sect. 4 will show experimental results obtained by simulations and discuss some issues. Finally, Sect. 5 draws the conclusions of this paper.

2 Recommendation Flow

Socialized recommender system is motivated by epidemic process on a social network. Basically, a social network $\mathcal{S}$ is represented as $\mathcal{S} = \langle N, E \rangle$ where N is a set of entities $N = \{n_1, \ldots, n_{|N|}\}$ (i.e., in this paper, users), and E is a set of links between two entities $E \subseteq |N| \times |N|$ (i.e., affinity). These social links are easily represented as an adjacency matrix. Along to the social links, users can send (or receive) a set of rating information to (or from) their neighbors. Then, they can individually build the so-called *recommendation*, and spread it to their neighbors with respect to the estimated interested model of receivers [4,3]. In case of sending recommendation, we have to consider three patterns of spreading behavior, mentioned by Borgatti [5];

1. Broadcast, i.e., to firstly invoke a new recommendation,
2. Serial replication, i.e., to reflect his opinion, and
3. Transfer, i.e., to hand over some received recommendation as a broker.

Especially, in order to select some neighbors to whom they occur the recommendation, user interests should be modeled by using the shared rating datasets[1].

Definition 1 (User interest). *Assume that a user u_i can design his neighbor's interest model $\mathcal{I}_i$ by using vector-space model with a set of topics C. Given a set of normalized rating information D_j from n_j, his interest model by user n_i is defined as*

$$\mathcal{I}_i(n_j) = [w_1, \ldots, w_{|C|}]^T \tag{1}$$

where $E_{ij} = 1$, and $w_k = \frac{|\{d_h | label(d_h) = c_k, d_h \in D_j\}|}{|D_j|}$ means a weighting value about topic $c_k \in C$.

[1] We exploit model-based recommendation method like [6], rather than collaborative filtering methods like item-based [7] using statistical analysis.

We regard that user n_i can makes recommendation to his neighbors n_j by the following subjective evaluation process (it will be discussed later)

$$\phi_i(\mathcal{I}_i(n_j), x) = \psi_i(x) \tag{2}$$

where x is a certain item, and ϕ_i is a function to reflect user u_i's subjective opinion. Now, the recommendation is formulated as follows.

Definition 2 (Recommendation). *A recommendation r_{ij} is a message from user n_i to n_j where $E_{ij} = 1$. It consists of*

$$r_{ij}^x = \langle x, \Gamma(\psi_i(x), \alpha) \rangle \tag{3}$$

where x indicates the recommended item, and $\psi_i(x) \in [0, 1]$ is a rating information attached by sender n_i. The recommendation in previous step (i.e., item x was transfered to n_i from n_{i-1}) is influenced with a certain decaying coefficient α, and it is given by

$$\Gamma(\psi_i(x), \alpha) = \alpha \times \psi_i(x) + (1 - \alpha)\psi_{i-1}(x) \tag{4}$$

where $\alpha \in (0, 1)$.

Particularly, in case of simple transfer-based propagation, we assume that the rating information ψ should be consistently kept as previous one.

As collecting the recommendation interactions between both persons in a centralized server, we can build a sequential path of the corresponding interactions. It is called a *recommendation flow*.

Definition 3 (Recommendation flow). *Given a set of recommendations, a recommendation flow rf^x for an item$_x$ is a subnetwork, which is containing a set of all possible paths piecing the recommendations together $rf^x = \{rf_{st}^x | \langle r_{s,s+1}^x, \ldots, r_{t-1,t}^x \rangle, n_s \in N, n_t \in N\}$. It is a sequence of recommendations $r_{\alpha,\alpha+1}^x \rightarrow r_{\alpha+1,\alpha+2}^x \rightarrow \cdots \rightarrow r_{\alpha+\Delta-1,\alpha+\Delta}^x$ in which $n_\alpha = n_s$ and $n_{\alpha+\Delta} = n_t$. The length of a recommendation flow is its number of edges (here, Δ_{st}). Finally, a recommendation flow rf_{st}^x is represented as a set of the recommendation paths, i.e., a subnetwork of the original social network $\mathcal{S}$.*

Here, we show two possible examples. Let five users $\{A, B, C, D, E\}$ be *involved* in a social network as shown in Fig. 1.

Example 1. A recommendation x is invoked by user A. He can *broadcast* this recommendation to his neighbors B, C, and D. User D can *transfer* the recommendation to user E (i.e., $\psi_A(x) = \psi_D(x)$). Finally, user E can *propagate* it to user B with attaching his opinion $\psi_E(x)$. Consequently, two paths of recommendation flow for item x are built as $rf_{AB}^x = \{r_{AB}, r_{AD} \rightarrow r_{DE} \rightarrow r_{EB}\}$.

Example 2. By a certain set of malicious effects, user B may be received either "high-rated" recommendation of irrelevant items or "low-rated" recommendation or relevant items. If he is interested in item x, user C should have recommended the item as user E did. Otherwise, user E should not have sent "high-rated" recommendation to him.

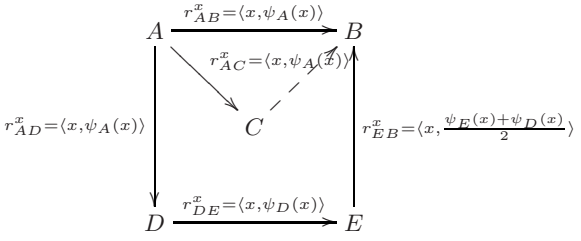

Fig. 1. Recommendation flows with multiple paths ($\alpha = 0.5$)

3 Refinement of Collaborative Network

In this paper, we have been focusing on the second example, and overcoming the problem by refining the social network. In order to protect the people in the society from potentially harmful consequences of naively (or poorly) designed feedback mechanisms, the malicious nodes should be identified. There are two kinds of *malicious* patterns, as previously mentioned in Example 2.

- False-negative error; a user who makes "high-rated" recommendation about irrelevant items
- False-positive error; a user who makes "low-rated" recommendation about relevant items

These malicious results are caused by the corresponding user's subjective model ϕ (shown in Eq. 2), including internal comparison process and recommendation utility. Of cause, we are not interested in formulating this model (this model can be left as a black box), but comparing a model ϕ_i with others $\phi_j \in \{\phi_j | E_{ij} = 1\}$.

3.1 Consensus Recommendation

We exploit a consensus-based approach to compare and merge their opinions. Basically, social consensus theory is an approach taken by social institutions and it may be called truth by social agreement [8,9]. From seven postulates designed to deal with a certain conflict among distributed information systems in [10], our study takes into account *maximal similarity* postulate[2].

Definition 4 (Consensus recommendation). *Given a set of conflicted recommendations $r^x = \{r^{x_s} | r^{x_1}, r^{x_2}, \dots\}$ about an item x, a consensus recommendation $\mathcal{CR}_i(r^x)$ of user n_i is given by*

$$\mathcal{CR}_i(r^x) = \arg\max_{r^{x_s}} \frac{|\{r^{x_s}_{ki} | \psi_k(x_s) \geq \tau\}|}{|nghb(n_i)|} \tag{5}$$

where $nghb(n_i) = \{n_k | E_{ik} = 1\}$ meaning a set of neighbors of n_i. Finally, recommendation r^{x_s} is established as consensus recommendation, the others conflicted with it are denoted as $\mathcal{CR}_i^-(r^x) = r^x - \mathcal{CR}_i(r^x)$.

[2] A full detail of this consensus postulate is described in [10].

3.2 Detecting Malicious Nodes

From the conflicts (i.e., $\mathcal{CR}_i^-(r^x) = \{r^{x_s^-} | r^{x_1^-}, r^{x_2^-}, \dots\}$) between recommendations, we have to investigate whether a certain set of malicious (or noisy) effects have intruded into the social network. If so, where are the patterns from? (which node is a source of the pattens?) The malicious patterns can be traced backward along the recommendation flow. We can figure out the most malicious recommendation $r^{x_p^-}$ by

$$\arg\max_s \left[\mathcal{CR}_i(r^x) - \mathcal{CR}_i(r^x - r^{x_p^-})\right], \tag{6}$$

so that we can obtain all possible paths on which the recommendation was traveling from the recommendation flow $rf^{x_p^-}$, as shown in Def. 3.

Here, we extend the outlier detection method from a sequential dataset proposed in [11]. Given a sequence of the recommendation flow $rf_{st}^{x_p^-} \in rf^{x_p^-}$ of which length is Δ_{st}. A diagonal distance matrix $\Lambda_{st}^{x_p^-}$ is given by

$$\Lambda_{st}^{x_p^-} = \begin{bmatrix} \dots & \dots & \dots \\ \dots & \delta(r_i^{x_p^-}, r_j^{x_p^-}) & \dots \\ \dots & \dots & \dots \end{bmatrix} \tag{7}$$

where (i, j)-th element is computed by

$$\delta(r_i^{x_p^-}, r_j^{x_p^-}) = |\Gamma(\psi_i(x), \alpha) - \Gamma(\psi_j(x), \alpha)| \tag{8}$$

and, the size of this matrix is $\Delta_{st} \times \Delta_{st}$, meaning the length of the recommendation flow. Of cause, the diagonal elements are all zero. Based on $\Lambda_{st}^{x_p^-}$, the mean $\mu_{st}^{x_p^-}$ is given by

$$\mu_{st}^{x_p^-} = \frac{2\sum_{i=1}^{\Delta_{st}} \sum_{j=i}^{\Delta_{st}} \Lambda_{st}^{x_p^-}(i,j)}{\Delta_{st}(\Delta_{st} - 1)} \tag{9}$$

where $\Lambda_{st}^{x_p^-}(i,j)$ is the (i,j)-th element of the distance matrix. This is the mean value of upper triangular elements except diagonals. Then, with respect to the given length of the recommendation flow, the deviation $\sigma_{st}^{x_p^-}$ is derived as shown by

$$\sigma_{st}^{x_p^-} = \sqrt{\frac{2\sum_{i=1}^{\Delta_{st}} \sum_{j=i}^{\Delta_{st}} \left(\Lambda_{st}^{x_p^-}(i,j) - \mu_{st}^{x_p^-}\right)^2}{\Delta_{st}(\Delta_{st} - 1)}}. \tag{10}$$

These factors are exploited to quantify the distances between two random logs, and statistically discriminate outliers such as the most distinct or the N distinct data from the rest in the range of over preset threshold, with respect to a given sequential data.

By using the statistical measures, the malicious nodes can be detected by two-step evaluation process; *i*) monotonicity testing and *ii*) minimization of the

summation of deviation. Firstly, monotonicity testing figures out whether the malicious patterns is existing or not. We assume that a given recommendation flow $r_{st}^{\bar{x_p}}$ is *monotone* (in three cases, monotonically decreasing, increasing, and constant), if and only if $\sigma_{st}^{\bar{x_p}} \leq \tau$. As next step, more importantly, in case of $\sigma_{st}^{\bar{x_p}} > \tau$, the malicious patterns are discovered through *bottom-up merging process* establishing the most optimal partitioning of given dataset. We want to obtain the best combination of the patterns, which is making the sum of partial deviation $\mu_{st}^{\bar{x_p}}$ for each segment (or subsequence) minimized. Thereby, the principle segment identifiers

$$PSI = \{psi_a | a \in [1, \ldots, S-1], psi_a \in [1, \ldots, T-1]\} \tag{11}$$

is defined as the set of boundary positions, where the variables S and T are the required number of segments and the interval of sliding window, respectively. The malicious pattern analysis segmenting the sequential dataset SOA_S as objective function with respect to PSI is given by

$$SOA_S(PSI) = \sum_{i=1}^{S} \mu_i^{\bar{x_p}} \tag{12}$$

where $\mu_i^{\bar{x_p}}$ means partial deviation of i^{th} segment. In order to minimize this objective function, we scan the most distinct pairs, in other words, the largest value in the distance matrix $\Lambda_{st}^{\bar{x_p}}$, as follows:

$$\delta_{\max}(r_{T_a}^{\bar{x_p}}, r_{T_b}^{\bar{x_p}}) = \arg \max_{i=1,j=1}^{T} \Lambda_{st}^{\bar{x_p}}(i,j) \tag{13}$$

where $\arg\max_{i=1}^{T}$ is the function returning the maximum values during a given interval $[T_a, T_b]$. When we obtain $\Lambda_{st}^{\bar{x_p}}(p,q)$ as the maximum distance, we assume there must be at least a principle segment identifier between p-th and q-th recommendations. Then, the initial time interval $[T_a, T_b]$ is replaced by $[T_p, T_q]$, and the maximum distance in reduced time interval is scanned, recursively. Finally, when two adjacent recommendations are acquired, we evaluate this candidate *psi* by using $SOA_S(psi)$. If this value is less than $\sigma_{st}^{\bar{x_p}}$, this candidate *psi* is inserted in PSI. Otherwise, this partition by this candidate *psi* is cancelled. This segmentation process is top-down approaching, until the required number of segments S is found. Furthermore, we can also be notified the over-segmentation, which is a failure caused by overfitting segmentation, detected by the evaluation process $SOA_S(PSI)$.

For example in Fig. 2, let a recommendation flow composed of two segments S_A and S_B, and $A^(2)$ be a malicious user in two cases. We assume that the distances between $\mathrm{A}^{(i)}$s (or $\mathrm{B}^{(i)}$s) is much less than between each other. The four largest distances $\Lambda_{st}^{\bar{x_p}}(A^{(1)}, B^{(1)})$, $\Lambda_{st}^{\bar{x_p}}(A^{(2)}, B^{(2)})$, $\Lambda_{st}^{\bar{x_p}}(A^{(2)}, B^{(0)})$, and $\Lambda_{st}^{\bar{x_p}}(A^{(2)}, B^{(1)})$ are 0.86, 0.85, 0.81, and 0.79, respectively. We want to segment

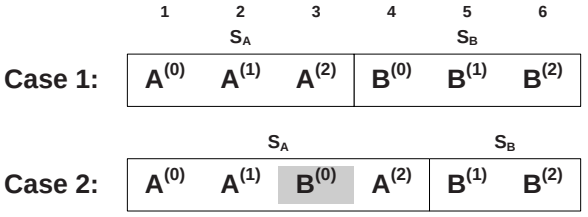

Fig. 2. Example for top-down approaching segmentation

them into two parts. In Case 1, due to the maximum distance $\Lambda_{st}^{x_p^-}(A^{(1)}, B^{(1)})$ in the initial time interval $[1, 6]$, time interval is reduced to $[2, 5]$, and then, $\Lambda_{st}^{x_p^-}(A^{(2)}, B^{(0)})$ in updated time interval determines that psi_3 can be a candidate. Finally, the evaluation $\sigma_{st}^{x_p^-}(1,3) + \sigma_{st}^{x_p^-}(4,6) < \sigma_{st}^{x_p^-}(1,6)$ makes a candidate psi_3 inserted to PSI. This case is clear to find the candidate psi and prove this segmentation to be validate. More complicatedly, in Case 2, a heterogeneous recommendation $B^{(0)}$ is located in the segment S_A. The first candidate psi_3 is generated by $\Lambda_{st}^{x_p^-}(B^{(0)}, A^{(2)})$ in time interval firstly refined by $\Lambda_{st}^{x_p^-}(A^{(1)}, B^{(1)})$. By the evaluation $\sigma_{st}^{x_p^-}(1,3) + \sigma_{st}^{x_p^-}(4,6) \geq \sigma_{st}^{x_p^-}(1,6)$, however, this candidate psi_3 is removed. Finally, because the second candidate psi_4 by $\Lambda_{st}^{x_p^-}(A^{(2)}, B^{(1)})$ meets the evaluation $\sigma_{st}^{x_p^-}(1,4) + \sigma_{st}^{x_p^-}(5,6) < \sigma_{st}^{x_p^-}(1,6)$, a candidate psi_4 can be into PSI.

4 Experiments and Discussion

For evaluate the proposed approach, we have conducted simple simulations. We chose NetLogo 3.1.3[3], which is is a cross-platform multi-agent programmable modeling environment.

As a first testing, QAP (quadratic assignment problem) correlation ratio [12] has been measured to evaluate the precision of malicious node discovery. One hundred legitimate agents with ten ($P_{100/10}$), twenty ($P_{100/20}$), thirty ($P_{100/30}$), and forty ($P_{100/40}$) malicious agents could interact with each other (decaying coefficient $\alpha = 0.4$). As shown in Fig. 3, $P_{100/30}$ and $P_{100/40}$ have shown almost same discovery performance (0.43). They were converged into a certain level quickly, as the malicious population got increased.

The second experimentation was to measure the convergence ratio, as changing the decaying coefficient α. The agents were allowed to communicate with each other, after a certain time delay (we set 2 second.). Using $P_{100/30}$, we have measured the time taken until all malicious agents were detected. When $\alpha = 0.4$, it took only 36 second to detect the malicious. We found out the relationship between the decaying coefficient and the performance of risk discovery. For the high

[3] NetLogo 3.1.3, http://www.ccl.sesp.northwestern.edu/netlogo/

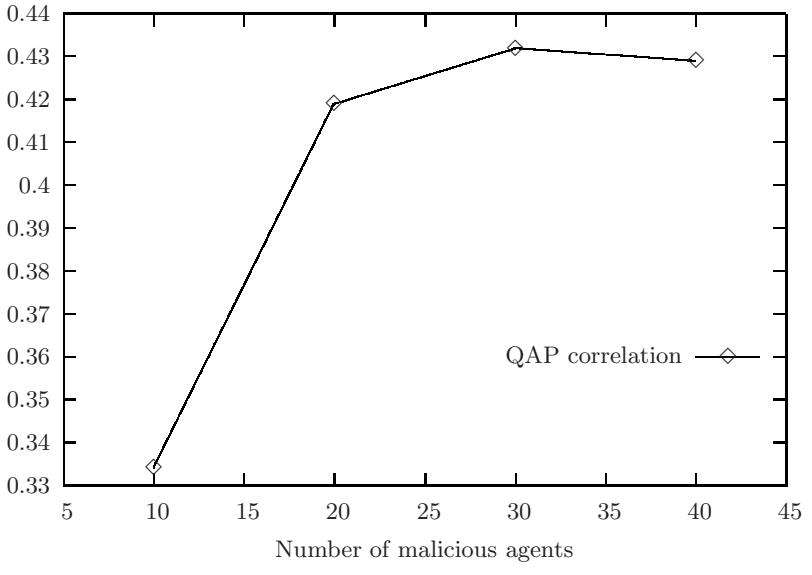

Fig. 3. QAP correlation over α

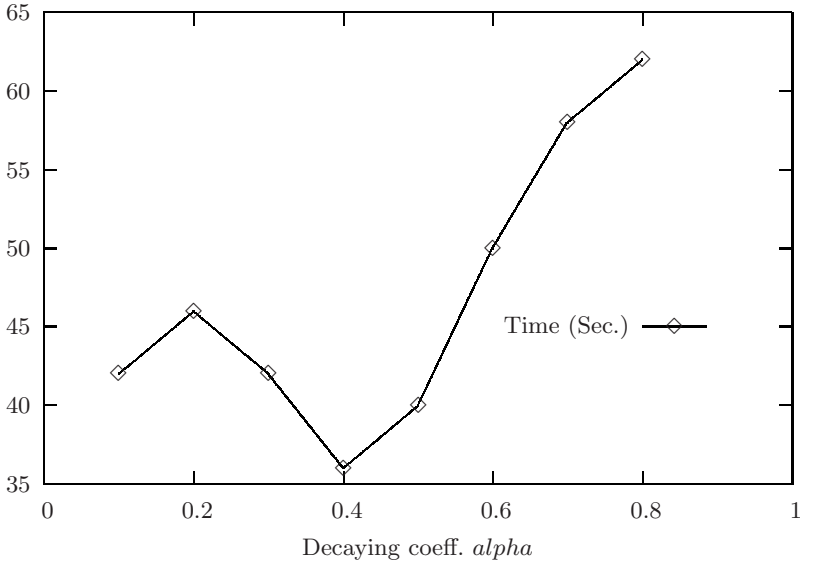

Fig. 4. Time taken to detect the malicious agents, as changing α

decaying efficient, the recommendation flow has shown over-segmented, because it was very sensitive the neighbors.

We want to discuss two main drawbacks of the proposed approach;

1. Batch process; For building the consensus recommendation, we had to wait for a certain number of recommendation from the neighbors. We have been planning to deal with real-time consensus builder module.
2. We have assumed that the majority of neighbors is fair and trustworthy, because the consensus recommendation should be anyhow safe. However, we have to consider that the most of neighbors are malicious, and the consensus recommendation will be contaminated.

As the related work, there have been various approaches to put new values on the social networks [13]. Representatively, trust and reputation can be efficiently computed, but they need to collect explicit rating information, which is fully trustworthy [14].

5 Conclusions and Future Work

Dissemination and delivery for rapidly changing information in large user communities remains a serious challenge. Obviously, noisy information is an obstacle decreasing the performance of efficient collaborations on social network. In conclusion, We have been attempting to model "word-of-mouth" recommendation propagation process in real world, as filtering out the noisy (malicious) recommendation. Particularly, we focus on on privacy-enhanced platform for socialized recommender systems to keep the privacy of users. We found out the optimal decaying coefficient and relationship with the discovery performance.

As future work, we have planned to work on the following issues;

- exploiting important social features, e.g., centralities, hub and authoritative measurements
- detecting circulation patterns on social networks

One of the most serious drawbacks in this paper is to pile up the recommendation flows until they are saturated on the whole social network. Thereby, we have to investigate how to detect the malicious users on real time. Furthermore, in the context of semantic web, multiple agents (or crawlers) have been investigated to collaboratively build semantic space [15]. Thus, the proposed approach needs to be applied to trustworthy semantic collaborations.

References

1. Ohsawa, Y.: Chance discoveries for making decisions in complex real world. New Generation Computing 20(2), 143–164 (2002)
2. Kim, H.J., Jung, J.J., Jo, G.: Conceptual framework for recommendation system based on distributed user ratings. In: Li, M., Sun, X.-H., Deng, Q.-n., Ni, J. (eds.) GCC 2003. LNCS, vol. 3032, pp. 115–122. Springer, Heidelberg (2004)
3. Jung, J.J.: Visualizing recommendation flow on social network. Journal of Universal Computer Science 11(11), 1780–1791 (2005)

4. Vidal, J.M.: A protocol for a distributed recommender system. In: Falcone, R., Barber, S., Sabater-Mir, J., Singh, M.P. (eds.) Trusting Agents for Trusting Electronic Societies. LNCS (LNAI), vol. 3577, pp. 200–217. Springer, Heidelberg (2005)
5. Borgatti, S.P.: Centrality and network flow. Social Networks 27(1), 55–71 (2005)
6. Good, N., Schafer, J.B., Konstan, J.A., Borchers, A., Sarwar, B.M., Herlocker, J.L., Riedl, J.: Combining collaborative filtering with personal agents for better recommendations. In: Proceedings of the AAAI/IAAI, pp. 439–446 (1999)
7. Sarwar, B.M., Karypis, G., Konstan, J.A., Riedl, J.: Item-based collaborative filtering recommendation algorithms. In: Proceedings of the World Wide Web Conference, pp. 285–295 (2001)
8. Arrow, K.J.: Social Choice and Individual Values. Wiley, New York (1963)
9. Goguen, J.A., Rosu, G.: Institution morphisms. Formal Aspects of Computing 13(3-5), 274–307 (2002)
10. Nguyen, N.T.: Consensus system for solving conflicts in distributed systems. Information Science 147(1-4), 91–122 (2002)
11. Jung, J.J.: Semantic preprocessing of web request streams for web usage mining. Journal of Universal Computer Science 11(8), 1383–1396 (2005)
12. Garey, M.R., Johnson, D.S.: Computers and Intractability: A Guide to the Theory of NP-Completeness. W. H. Freeman & Co (1979)
13. Jordan, K., Hauser, J., Foster, S.: The augmented social network: Building identity and trust into the next-generation internet. First Monday 8(8) (2003)
14. O'Donovan, J., Smyth, B.: Trust no one: Evaluating trust-based filtering for recommenders. In: Kaelbling, L.P., Saffiotti, A. (eds.) Proceedings of the Nineteenth International Joint Conference on Artificial Intelligence (IJCAI-05), Professional Book Center, pp. 1663–1665 (2005)
15. Jung, J.J.: Ontological framework based on contextual mediation for collaborative information retrieval. Information Retrieval 10(1), 85–109 (2007)

Using Conceptual Scenario Diagrams and Integrated Scenario Map to Detect the Financial Trend

Chao-Fu Hong[1], Tzu-Fu Chiu[2], Yu-Ting Chiu[3], and Mu-Hua Lin[4]

[1] Department of Information Management, Aletheia University, NO.32 Chen-Li St., Tamsui, Taipei County, 25103, Taiwan (R.O.C.)
cfhong@email.au.edu.tw
[2] Department of Industrial Management, Aletheia University, NO. 32 Chen-Li St., Tamsui, Taipei County, 25103, Taiwan (R.O.C.)
chiu@email.au.edu.tw
[3] School of Computing, University of Leeds, U.K
gloch2004@yahoo.com
[4] MIS Dept., National Chengchi University, NO. 64, Sec. 2, ZhiNan Rd., Wenshan District, Taipei, 116, Taiwan (R.O.C.)
95356503@nccu.edu.tw

Abstract. In order to visualise the decision making process, the data association diagram is prepared to show the relationships or scenarios extracted from data, and provide a way for designing or discovering alternatives. However, managers are not easy to design alternatives if the collected data is large and complex. Thus, this study provides an approach for extracting the concepts from association diagrams to create the conceptual scenario diagrams. Afterward, variant diagrams are generated from the conceptual scenario diagrams for easily visualising and explaining the variation of financial status within a firm. Finally, the integrated scenario map is produced for managers to understand the financial manipulations of the firm.

Keywords: Chance Discovery, Conceptual Scenario, Decision Making.

1 Introduction

Bankruptcy of a firm would affect stakeholders associated with the firm and even the whole community. Thus, detecting financial distress of a firm becomes an important topic nowadays. According to Lensberg et al., "The social costs incurred by various stakeholders associated with bankrupt firms have spurred searches for better theoretical understanding and prediction capability." [1]

"Values are principles for evaluating the desirability of any possible alternatives or consequences." [2] In this study, the value of describing financial status is used to analyze whether a company has financial distress comparing to the well performed period. The relevant intelligence is determined as gathering descriptive rules of financial distress. Thus, this study aims at providing a stable and usable approach to detect the scenario of financial trend within a firm using the integrated scenario map.

H.G. Okuno and M. Ali (Eds.): IEA/AIE 2007, LNAI 4570, pp. 886–895, 2007.

2 Literature Review

In order to obtain the basis of this study, this section will introduce the financial distress and traditional prediction models; the scenario map in chance discovery; and the process of decision making.

2.1 Financial Distress and Prediction Models

Financial failure is defined, by Beaver, as the inability of a firm to pay its financial obligations as they mature [3]. According to Blum, financial failure could be defined as an inability to pay due debts, entrance into a bankrupt proceeding, or an agreement with creditors to reduce debts [4]. Moreover, pursuant to Article 49, 50, and 50-1 of the *Operating Rules of the Taiwan Stock Exchange Corporation*[5], if a listed company satisfies any of the conditions such as unable to pay for the bonds matured, that company should change its listed securities to altered-trading-method category or apply to terminate its listing.

Since 1960s, prediction models with different analysis methods had been proposed to forecast financial distress of companies. Those are, for instance, Single ratio analysis model [3]; Multiple discriminant analysis (MDA) model [4,6]; Logit model [7,8]; Neural network model; Generic programming model. However, the traditional statistic models only explain the static state of the given data, and can not be good detective tools for dynamic financial status.

2.2 Scenario Map in Chance Discovery

A chance in chance discovery means to understand a rare event or unnoticed situation which can be significant for making a decision [9]. A chance in the scenario map means an emerging scenario bringing across the existing scenarios. The double-helical model, which was presented by Ohsawa to demonstrate the interactions between humans and computers [10], is used in the scenario communication helping experts to extract the emerging scenario from their mind [9]. Nevertheless, the scenario map in chance discovery is recently utilised to find static chances but is not applied well to discover the variation in a dynamic period of time.

2.3 Decision Making Process

According to Keeney [11], Normative, Descriptive, and Prescriptive theories are used interactively for decision making. In the Descriptive theory, it is concerned with explaining the way people making-decisions and predicting the decisions they may make [11]. In 1994, the Value-focused thinking (VFT) model [2], a value-oriented approach to generate alternatives, was proposed by Keeney and is able to generate better alternatives and identify decision situations more appealingly. In addition, Simon presented four phases of decision making, which are intelligence, design, choice, and review [12]. That is, managers can define problems using intelligence; then design alternatives for solving the problems;

choose the best alternative; and finally review the result. Therefore, intelligence phase in decision making will be employed in this study as a knowledge guider to refine the data association diagram.

3 Research Design and Experiment

Since discovering a rare event or a chance could aid the detection of financial trend, it is useful to find rare events from the given data. However, the importance of rare events is not always the same in different social phenomena. For instance, in the marketing study, a chance might occur while the sales volume of a product is increased. In the finance study, a rare event might emerge while the profitability of a firm is decreased. Thus, it is important to utilise directions to distinguish rare events in the financial domain. This study will use "+" and "-" to denote status of features.

In order to detect the financial status of a company, financial analysis could be introduced to extract information for investors and stakeholders. Thus, the research experiment is designed for understanding the phenomena of a firm via a series of association diagrams and conceptual scenario diagrams, and for identifying financial status via the variant diagrams. In addition, the integrated scenario map of each target firm will be applied to understand the trend of the company.

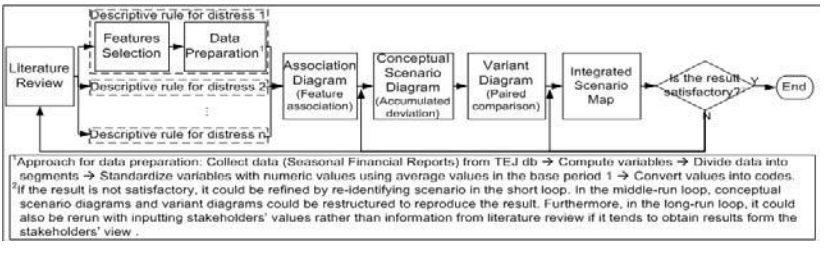

Fig. 1. Experiment process of this study

The experiment process through this study is shown as in Fig. 1. The details of executing the experiment will be described in the following sub-sections.

3.1 Descriptive Rules

From the literature, several descriptive rules were collected for depicting financial status, especially financial distress. In each descriptive rule, an event occurs while the features exist, and each feature is influenced by its corresponding financial activities.

Considering a business firm as a reservoir of financial resources, distress might occur if the income of the reservoir is less than the outcome of it [3,4]. Lee et al. also indicated that financial distress means that a firm's short-run operating and financial cash inflows are less than its outflows [13]. Consequently, the first

descriptive rule would be that a distressed firm has high financial leverage, poor ability of refunding liabilities, and poor ability of liquidity.

The second descriptive rule is: a financial failure means that the firm's assets are smaller than its liabilities [13].

According to Lee et al., a firm which sells assets and doesn't make any investment for future operations will be failed [13]. Therefore, the third descriptive rule could be that a firm might fail while the firm size decreased by selling assets and the performance of current capital, which represents operating ability of a firm, remained poor.

Furthermore, Lensberg et al. indicated the interaction of the features, which is: companies with low profits can remain non-bankruptcy with high levels of liquidity, and companies with low profits can decrease bankruptcy risk with increased size [1]. Thus, the forth descriptive rule is that a firm might bankrupt because of low profits and poor ability of refunding liabilities as low levels of long-term liquidity. Accordingly, the fifth descriptive rule is that a firm might bankrupt because of low profits and small size.

Finally, the sixth descriptive rule of financial distress is that a firm with weak ability of liquidity, with inefficiency of using assets or performing current capital, and with great extent of using financial leverage, would fail.

Features Selection. According to Levy [14], the financial ratios analysis can be divided into four categories, which are Liquidity ratios, Financial Leverage ratios, Activities ratios, and Profitability ratios. Besides, in accordance with Article 19 and Table 23 of the *Criteria Governing Information to be Published in Annual Reports of Public Companies* [15] in Taiwan, the overview of the financial status for a company should include the aspects of financial structure, solvency, operating performance, profitability, cash flow, and leverage. Because the situation of cash flow and leverage could be covered in analyzing solvency, profitability and financial structure, analyzing the cash flow and leverage would be proper to be combined and then omitted.

Therefore, features representing these four aspects and related to the above descriptive rules were selected as: the firm size, the extent of using financial leverage, the efficiency of using assets, the inverse of liquidity, and the extent of profit. These features can be calculated using the financial ratios shown in Table 1. Additionally, these financial ratios were appeared in Ohlson's model and proved to be distinct and significant [7]. Although it might be argued about using financial ratios to detect or predict financial distress, the predictive abilities of financial-statement data are well accepted in general consensus [3]. Financial ratios calculated from the financial-statement data would also be useful as predicting elements.

Data Preparation. This study aims at investigating financial situation in the disk industry, which is contained in the electronic industry and consists of optical storage media firms and CD-ROM drive firms. Within the study, distressed and non-distressed firms in the disk industry have been selected for the experimental purpose, and a distressed firm is defined as which terminates its listing. The non-distressed and distressed firms are CMC Magnetics Corporation and Megamedia

Feature and Formulac	Description	Pref.
$F1 = \log(TotalAsets/GNP)$	the firm size	H[1]
$F2 = TotalLiabilities/TotalAssets$	the debt ratio, and the extent of using financial leverage	L[2]
$F3 = WorkingCapital/TotalAssets$	the efficiency of using assets or the performance of current capital	H
$F4 = Cur.Liabiilties/Cur.Assets$	the reciprocal of current ratio or the inverse of liquidity	L
$F5 = 1$ while total liabilities exceeds total assets; and $F5 = 1$	the relationship between liabilities and assets or the amount of equity	Z[3]
$F6 = NetIncome/TotalAssets$	the return of assets or the extent of profit	H
$F7 = OperationFunds/TotalAssets$	the ability for refunding total liabilities by cash	H
$F8 = 1$ while net income was negative and last for two seasons; and $F8 = 0$ otherwise	the amount of net income	Z
$F9 = (NI_t - NI_{t-1}/\|NI_t\| + \|NI_{t-1}\|)$ where NI_t is netincome of the nearest period t	the growth of net income	H

Corporation accordingly. It is planned to gather the seasonal financial reports of these companies during 1996 to 2005 from the Taiwan Economic Journal (TEJ) Data Bank to extract financial data.

The time frame of raw data from the database was divided into three periods in sequence. Every period was assumed to last for three years, and consist of twelve seasonal financial reports. However, the data period of the 2^{nd} and the 3^{rd} period might be shortened if the seasonal financial reports could not be available. Afterward, raw data were calculated for obtaining every ratio and the ratio were then standardized against the basis of the first period. After standardization, the initial values would be converted into codes using the scale of every 0.5 standard deviation. Besides, non-numeric values were converted into codes using "1" to represent true and "0" to represent false. All features were coded with different levels so as to generate a meaningful association diagram.

3.2 Feature Association and Association Diagram

After features selection and data preparation, the original data association diagrams with all the co-occurred links were generated for each company in every period. However, the collected descriptive rules were used as guidance for neglected the meaningless relations between each pair of features and refine the original data association diagrams. After refinement, the modified association diagrams were produced.

For instance, data of CMC were converted into association diagrams shown in Fig. 2. Every node in the diagram indicates the position of a feature with a

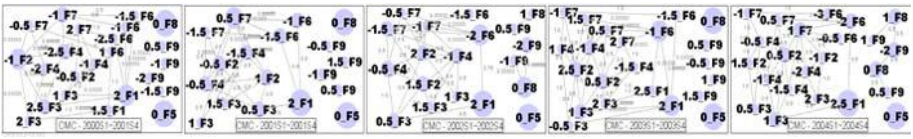

Fig. 2. Association diagrams of CMC Magnetics Corporation

specific level. While drawing diagram, every 0.5 standard deviation is defined as a unit in the level scale. That is, "1.5-F9" denotes that the feature F9 is greater than 1.0, and less than or equal to 1.5 standard deviation. For example, if the original value of feature F3 is 1.6, 1.7, or 1.9, all of them will be transformed into "2-F3", and so forth.

Features with different levels were drawn on the association diagram, but it is difficult to detect the financial situation from this complex diagram. In addition, it is even harder to observe the trend of a company in a long period of time by reading a series of association diagrams simultaneously. Besides, the association diagram is not very suitable for presenting the result of time series analysis. The accumulated deviation will be introduced to improve the performance of visualised diagrams.

3.3 Accumulated Deviation and Conceptual Scenario Diagram

In order to get an overview of the financial state or phenomena of a company annually, conceptual scenario diagrams (as in Fig. 3) would be generated according to their association diagrams. In the analysis of financial distress, the features with median levels could be ignored and those with extreme levels should be concentrated upon. Thus, the accumulated deviation is calculated as:

$$AD_{F_j} = \sum_{k=1}^{4} stdev_k \tag{1}$$

where AD (on F_j) is the accumulated deviation of summation of *stdev*, which is the sum-up standard deviation of the j^{th} Feature, across k (i.e., from 1 to 4) seasons.

In the conceptual scenario diagram, each cell represents a concept rather than data itself. The green cells mean the features with positive value or strong ability, and the red cells mean the features with negative value or weak ability. Using

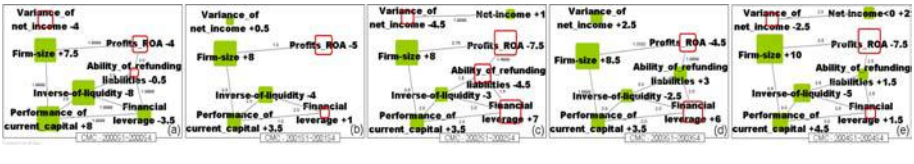

Fig. 3. Conceptual scenario diagrams of CMC Magnetics Corporation

a series of conceptual scenario diagrams in Fig. 3 as an example, CMC has good performance during the period in (a) because there are more cells in green color and the green cells are larger than red ones. Furthermore, the cell named financial leverage (in red color) is getting larger through (b), (c), (d), and (e), that means CMC beginning to use financial leverage to keep itself remaining in a better status. In other words, most scenarios in CMC are similar and can be viewed as using financial leverage for investing in machine and equipments to enlarge the firm size.

3.4 Paired Comparison and Variant Diagram

In order to understand the migration of the financial status of a company upon the time series, the accumulated diagrams were compared in pairs successively. After paired comparison, the variant diagram would be drawn according to the set of variant scores. The variant score is calculated as:

$$VS_{F_j}(t_{i+1}) = AD_{F_j}(t_{i+1}) - AD_{F_j}(t_i) \tag{2}$$

where VS (on F_j) of t_{i+1} is the variant score (on the j^{th} Feature) of the difference of accumulated deviation between the time period t_i and t_{i+1}; t_i denotes the time period i (e.g., t_1 is the first time period).

The variant score of period t_{i+1} is derived by subtracting the AD (on t_i and F_j) from the AD (on t_{i+1} and F_j) successively. The higher the variant score is, the greater the extent of difference is. Furthermore, the company might have negative status while most features are with red cells, and might have positive status while most features are with green cells in the variant diagram. Thus, it is easier to observe the financial status through this visualised variant diagram.

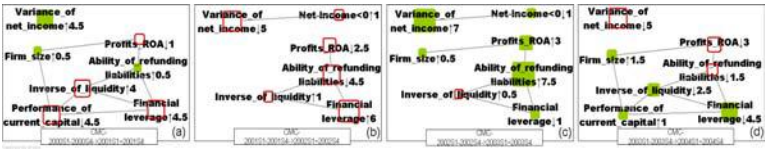

Fig. 4. Variant diagrams of CMC Magnetics Corporation

According to the variant diagram of CMC in Fig. 4(a), the firm might manipulate the financial leverage to enlarge its firm size. In Fig. 4(b), all variant scores are growing negatively and every feature turns to the distress-like direction. However, a lot of long-term loans and investments of machinery and equipment has been found in the annual financial report of CMC. In Fig. 4(c), the firm size of CMC keeps growing, the profits increasing, and the ability of refunding liabilities uplifting. CMC is still enlarging its firm in Fig. 4(d) while the financial structure became strengthened. Thus, a low-profit company would reduce distress probability with increasing firm size.

3.5 Integrated Scenario Map and Experimental Results

The integrated scenario map, formed by combining variant diagrams of a specific company, can be read to find out a trend whether the company is running improvingly, performing steadily, or approaching distress. The difference of each feature between every two year can be viewed as the action of decision-making. The actions during the inspected years can be explained via this integrated scenario map. While the variant score of a feature increased or decreased continuously, a company might be experiencing a good or bad situation. Moreover, comparing maps which represent different companies can see the abnormal actions. These abnormal actions might be clues for observing financial distress.

On the map of CMC in Fig. 5(a), the states vary from one another. The financial manipulation is raising financial leverage by making a long-term loan and purchasing new machines and equipments. Thus, CMC is a company with improving status. However, the states of Megamedia on the map in Fig. 5(b) are inactive, and the performance and profitability are bad. That is, Megamedia might not good at investment, production, or selling during 1999 to 2004. Thus, Megamedia is a company in the approaching distress state.

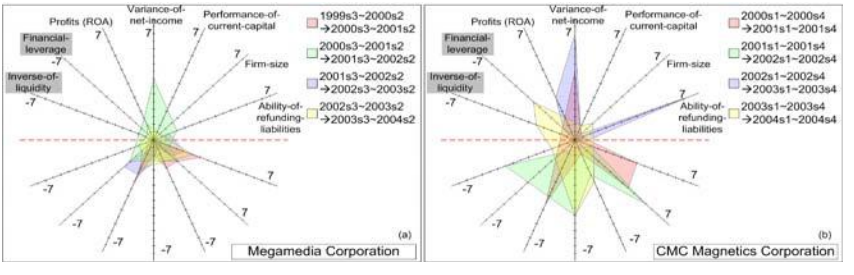

Fig. 5. Integrated scenario map of Megamedia Corporation and CMC Magnetics Corporation

On the other hand, the variant diagram of several companies can be read comparatively to obtain which company stands in a better position than the others. For instance, comparing the steady company to the distressed one, the steady and succeeded pattern in the disk industry could be conjectured that larger firm would survive while its products only have a slight profit.

4 Conclusion

In this study, a new approach has been proposed: The association diagram was used to analyze the appearance of financial features and the relationships between these features; The accumulated diagram was generated to estimate the static situation or phenomena in every time period (i.e., t_i); The variant diagram was produced to identify the dynamic difference between every two periods (i.e.,

t_i to t_{i+1}); Finally, the integrated scenario map was utilised to integrate the dynamic differences of a company to identify the strategic value and recognize the managerial behavior of a company. Using the target firm in the experiment as an example, the integrated scenario map of Megamedia pointed out that even the company decreased its firm size and increased the financial leverage to improve the liquidities, Megamedia still suffered in distress. Besides, in the integrated scenario map of CMC, the company adopted different financial strategies every year according to the market needs to obtain sufficient profits.

Therefore, the graphic diagrams generated in this study could help managers to discover the status of their own company more easily. The association diagram could be used to recognize possible alternatives of financial manipulations and the selected alternatives would provide advice for managers during strategic planning. Furthermore, the trend discovered from the integrated scenario map could guide managers to do proper actions and financial manipulations.

One of the future works would be to derive descriptive rules from the relevant literature more comprehensively and to make the descriptive rules more convincible. Moreover, this approach could be refined by adding expertise from specialists or applying methods from social association networks.

References

1. Lensberg, T., Eilifsen, A., McKee, T.M.: Bankruptcy theory development and classification via genetic programming. European Journal of Operational Research. 169, 677–697 (2006)
2. Keeney, R.L.: Creativity in Decision Making with Value-Focused Thinking. Sloan Management Review. Summer, pp. 33–41 (1994)
3. Beaver, W.H.: Financial Ratios as Predictors of Failure. Journal of Accounting Research 4, 71–111 (1966)
4. Blum, M.: Failing company discriminant analysis. Journal of Accounting Research 12, 72–102 (1974)
5. Securities and Futures Bureau. Operating Rules of the Taiwan Stock Exchange Corporation. Law Source Retrieving System of Stock and Exchange and Futures Trading [05-Norvember-2006] (2006) URL: `http://eng.selaw.com.tw/FLAWDAT01.asp?LSID=FL007304`
6. Altman, E.I.: Financial Ratios, Discriminant Analysis and the Prediction of Corporate Bankruptcy using Capital Market Data. Journal of Finance 589–609 (September 1968)
7. Ohlson, J.A.: Financial Ratios and the Probabilistic Prediction of Bankruptcy. Journal of Accounting Research, 109–131 (1980)
8. Mensah, Y.M.: An Examination of the Stationarity of Multivariate Bankruptcy Prediction Models: A Methodological Study. Journal of Accounting Research 22(1), 380–395 (1984)
9. Ohsawa, Y.: Chance Discovery: The Current States of Art. In: Ohsawa, Y., Tsumoto, S. (eds.) Chance Discovery in Real World Decision Making, pp. 3–20. Springer, Heidelberg (2006)
10. Ohsawa, Y.: Modeling the process of Chance Discovery. In: Ohsawa, Y., McBurney, P. (eds.) Chance Discovery, pp. 2–15. Springer, Heidelberg (2003)

11. Keeney, R.L.: On the Foundations of Prescriptive Decision Analysis. In: Edwards, W. (ed.) Utility Theories: Measurements and Applications, pp. 57–72. Kluwer Academic Publishers, Boston (1992)
12. Simon, H.A.: The New Science of Management Decision, 3rd edn. Prentice-Hall, Englewood Cliffs (1977)
13. Lee, C.F., Finnerty, J.E., Norton, E.A.: Foundations of Financial Management. West Publishing Company, MN (1997)
14. Levy, H.: Principles of Corporate Finance. South-Western College Publishing, Ohio (1998)
15. Securities and Futures Bureau: Criteria Governing Information to be Published in Annual Reports of Public Companies. Law Source Retrieving System of Stock and Exchange and Futures Trading. URL: [05-Norvember-2006] (2006) http://eng.selaw.com.tw/FLAWDAT01.asp?LSID=FL007032

Chance Discovery in Credit Risk Management

Estimation of Chain Reaction Bankruptcy Structure by Directed KeyGraph

Shinichi Goda and Yukio Ohsawa

School of Engineering, The University of Tokyo, 113-8656 Japan
sgoda@mwa.biglobe.ne.jp

Abstract. Credit risk management based on portfolio theory becomes popular in recent Japanese financial industry. But consideration and modeling of chain reaction bankruptcy effect in credit portfolio analysis leave much room for improvement. That is mainly because method for grasping relations among companies with limited data is underdeveloped. In this article, chance discovery method with directed KeyGraph is applied to estimate industrial relations that are to include companies' relations that transmit chain reaction of bankruptcy. The steps for the data analysis are introduced and result of example analysis with default data in Kyushu, Japan, 2005 is presented.

Keywords: chance discovery, credit risk, chain reaction, bankruptcy.

1 Introduction

Credit risk management based on portfolio theory becomes popular in recent Japanese financial industry promoted by introduction of BIS regulation and increasing use of model-based loan decision making. Simulation method comes to be common tool for analysis of credit portfolio and simulation models have been developed for credit risk management [1,2,3,4]. However, there still remain major areas for improvement. Analysis on chain reaction bankruptcies is one of these areas.

2 Effect of Chain Reaction Bankruptcy

Chain reaction bankruptcies are common phenomenon. Its general definition is like "bankruptcy triggered by a preceding default of a company that has trade and other relations with the bankrupting company".

Most of industry experts regard it necessary to take the effect of chain reaction bankruptcy into accounts when they analyze profile of their credit risk portfolio. By introducing chain reaction factor into analysis, we can expect to better grasp the risk profile of credit risk portfolio since amount of loss caused by a default can be larger if there are other bankruptcies triggered by the default.

H.G. Okuno and M. Ali (Eds.): IEA/AIE 2007, LNAI 4570, pp. 896–904, 2007.

However, majority of simulation models actually used in business do not fully take the chain reaction into account. That is mainly because it is difficult to directly grasp relations among companies since available data is limited as;

1. Background information about bankruptcies publicly available is very limited, and it is not organized in way that can be used for statistical analysis.
2. Corporate data related to relations among corporation is very limited to public. Few companies make trade, financial and technological relations public, but very few with numbers.

3 Current Methods to Grasp Relations

Adjustments have been devised in models and simulators to include relation effect, but there is much room for improvement. A major method to take the effect into account is to grasp relations among companies by measuring co-relations among movements of the security price of the companies (In this method, a company's security price is regarded as representative of default probability of the company). But this method is applicable only to security issuing large companies whose number is very small. On the other hand, most of companies in a credit risk portfolio are non-security-issuing and small-mid size.

Another way is to make industry groups represent companies that belong to them, and to estimate relations among companies by grasping relations among the industries. Co-relations are measured among indexes of securities issued by companies in the industry groups and are applied to non-security-issuing ones in the groups. But the idea to estimate relations among industries with co-relations among security prices seems to be unreasonable. The most of Japanese companies are non-security-issuing ones and there does not not seem to be enough evidence of the relations among security-issuing companies being same as that of non-issuing ones.

4 Grasp Chain Reaction Bankruptcy Structure by Chance Discovery Method

We proposed a method that detects relationship among bankrupted companies, without direct information of trade relations i.e., by chance discovery method in our previous work [5]. (The basic idea of this method follows the method that used for the chance discovery of earthquake by Ohsawa, Y. [6,7]).)

In this method, we estimate trade and/or other relations among companies defaulted in a geographical area within a certain time period, by visualizing relations among industry groups that include the defaults with KeyGraph. The method is based on the assumptions as follows;

1. There should be relations that transmitted factors causing defaults among companies that defaulted in a geographical area within a certain time period.

2. The default transmitting relations among companies should be mainly based on and represented by relations among industry groups. As seen in the above definition of chain reaction bankruptcy, "trade relation" is generally regarded as one of the most influential relations. Trade relation between a pair of industry is generally universal among companies in the paired industries.
3. Default transmitting relations among industries could be paths to transmit default of a company in an industry to other companies in other industries.

Suppose that cloth retailer A and cloth wholesaler B defaulted within a month successively in Kansai district. Suppose other sets of cloth retailer and wholesaler those located in same districts defaulted successively within a month repeatedly. We can estimate with high confidence that there were sets of trade relation between the cloth retailer and the wholesaler defaulted successively and that the sets of trade relation between the two companies caused the successive default, even if there is no public information of sets of trade relations between the two companies. We can estimate so based on expert's knowledge about cloth trading industry and on the observed default patterns analyzed with KeyGraph.

5 Methodology

5.1 Original Method

First, we explain the original method proposed in our previous work [5] and introduce its basic idea. Steps are as follows (see Table 1);

Step1. Preparation of data

1. Data of defaults: each default event has attributes of default date, geographical area in which the defaulted company is located and an industry to which it belongs.
2. Sorting: group the defaults by area and sort the events in each area by default dates.
3. Select companies that seemed to have triggered chain reaction.

Step2. Transformation of company data to industry data

Transform company data prepared in Step1. to industry data by replacing a company's name to a code of an industry to which the company belongs.

Step3. Transformation of data to sentence form

1. Make the default events grouped by area in sentence form by order of their default dates. Each event is denoted by industry name and spaced.
2. Form one sentence starting from a triggering company and ending at a company whose default date is after the default date of the starting company.

Step4. Discovery of relations among industries by KeyGraph

1. Extract co-occurrence of default events by using KeyGraph with sentences formed default data.

2. Interpret a result of KeyGraph and estimate relations among industries. It is important to read relations expressed in a KeyGraph with experts' knowledge.

Examples of experts' knowledge about factors that are supposed to work behind relations extracted by KeyGraph are as listed below.

a. Technological and business relations among industries
(example) An automobile is made of steel, glass, tires and electronic parts.
b. Commonality of customers among industries
(example) Consumers living in Kyushu region shop at cloth/food retailers and eat restaurant both located in Kyushu.
c. Ownership relation:

Table 1. Example of data and sentence

Step1. Data (1) sorted by date

No.	date of default	comp.	ind. code	area
1	2005/1/4	A	101	north
2	2005/1/15	B	210	south
3	2005/1/30	C	303	east
	⋮			
N	2005/12/28	ZZZ	330	north

Step2. Data (2) grouped by area, and sorted by date

No.	date of default	comp.	ind. code	area
3	2005/1/30	C	303	east
8	2005/3/20	H	440	east
	⋮			
1	2005/4/1	A	101	north
	⋮			
N	2005/12/28	ZZZ	330	north
	⋮			
9	2005/3/29	I	211	west

Step3. Transform to sentence form
Series starting from D1 = 101 110 418 ...
Series starting from D2 = 210 105 330 ...
Series starting from D3 = 303 240 440 ...
⋮

5.2 Time Order Method (with Directed KeyGraph)

The original method had two points to be improved;

1. Time order among defaults is not captured. That makes the estimation of causal relation among defaults difficult.
2. The criteria for selecting trigger defaults were not clear enough.
In our previous work [5], we made a sentence with default events in a month that starts from a hypothetical trigger default that were selected from a list of defaults that was made by Japanese SME Agency, based on the size or impact of defaults.

We newly introduce time order method to deal with above points. The basic idea of the new method is to try to better distinguish the causal relations among defaults with the time order among them.

With time order method, by making a sentence include only a pair of defaults with distinction of earlier event of the two, the time order among defaults can be expressed by KeyGraph with direction – we name it as "directed KeyGraph". Detailed steps are as follows (see Table 2);

1. Make a sentence of a pair of defaults.
2. Put "S" to industry code of the earlier default in a pair to distinguish it as a starting default.
3. Make series of pairs with a selected starting default indicated by "S", and ending defaults each of which follows the starting default within a set period.
4. Select another default that occurred next to the first default as the second starting event and take step 3.
5. Repeat step 3. and 4. until all the defaults in the analyzed period are selected as starting events.
6. Make and include linking pairs to link the nodes those are captured as ending events but at the same time are starting ones. For example, in Table 2, default E, that is coded as 10, is included in pair "S20_10", "S30_10", "S40_10" as an ending default and also included in pair "S10_30", "S10_20" as a starting one.

When the paired data is analyzed with directed KeyGraph, starting defaults are indicated by "S" put on the industry code. When a node, "S20" for example, is linked to another node, "10", it means that defaults in the industry 20 occurred before defaults in 10, indicating that defaults in 20 trigger the defaults in 10. In case two nodes of same industry are linked, like "10 – S10", it means ending defaults in "10" are at the same time starting defaults.

Table 2. Method for making time ordered pair of defalts

Default date		1/1	1/10	1/20	2/1	2/5	2/25	2/28		12/1	12/20	12/30
Name of company		A	B	C	D	E	F	G	···	X	Y	Z
Industry code		10	20	30	40	10	30	20		40	10	50
Pair	Start from 10(A)		S10_20	S10_30								
	Start from 20(B)			S20_30	S20_40	S20_10						
	Start from 30(C)				S30_40	S30_10						
	Start from 40(D)					S40_10	S40_30	S40_20				
	Start from 10(E)						S10_30	S10_20	···			
	···									···		
	Start from 20(W)									S20_40	S20_10	
	Start from 40(X)										S40_10	S40_50

5.3 Charcteristics and Merits of Time Order Method

Characteristics and possible merits of our new method, when we compare it to Bayesian network that is one of methods to express causal relations among nodes by directed arch[8-12], are as follows;

1. Our new method decides a direction of an arch based on time order of events, whereas Bayesian network decides a direction basically based on information criterion. Time order is generally regarded as one of the most basic information for estimating causal relations. It is especially important for causal estimation of time series event like chain reaction.
2. Our new method is able to express bidirectional/cyclic relations among industries, which might imply cyclic chain reaction of bankruptcies. Suppose the defaults in industry A cause defaults in industry B. Then, due to the defaults in industry B, the other companies in industry A may get defaulted. This positive feedback may trigger the non-linear growth of the defaults in both industries. This kind of non-liner effect is out of the scope of Bayesian network since basic method of Bayesian network is for handling one-direction/noncyclic structure.

6 Case Study – Analysis of Chain Reaction Structure of Bankruptcies in Kyushu, 2005

As a case study, we applied time order method described above to data of bankruptcies in Kyushu district, Japan, 2005. The reason for limiting area for analysis only to Kyushu district is simply to make the size of data controllable.

A. Contents of data

Samples are 343 defaults in Kyushu, a local part of the Japanese samples described below. About 10,400 pairs are made from the above selected 343 default samples.

1. Japanese samples, about 3,400 defaults, are randomly selected from the all defaulted companies that defaulted based on bankruptcy laws and published in the official gazette in Japan, 2005. The area consists of 9 districts including Kyushu. Samples are categorized in about 200 mid-level industry groups by author, based on the industry categories defined by Teikoku Databank, Ltd.
2. Period for pairing one starting default with ending ones is set to one month.
3. About 6,200 linking pairs are added.

B. Analysis

First, the data was analyzed by original method and then by time order method.

(1) Original method (see Fig. 1 for result)

With this KeyGraph by original method, we can understand that defaults in linked industries occurred in a close time period. But it is difficult to estimates whether the co-occurrence is based on chain reaction. That is partly because this graph lacks of information about causal relation estimated by time order among defaults.

For example, there is a group of linked black nodes - C60s and C77 - those represent civil engineering/construction related industries. Although we can understand that defaults in C60s and C77 occurred in a close time period, it is

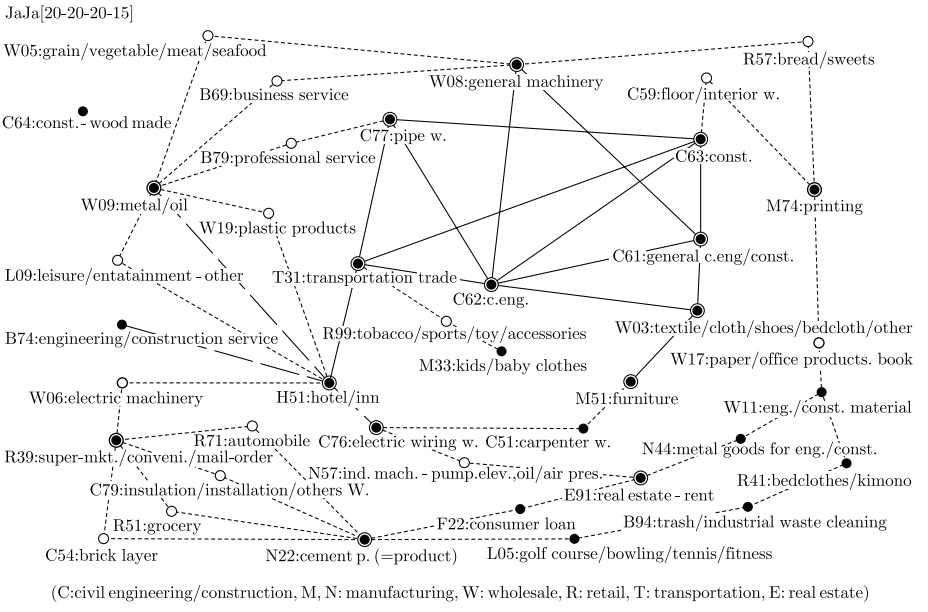

Fig. 1. KeyGraph by original method

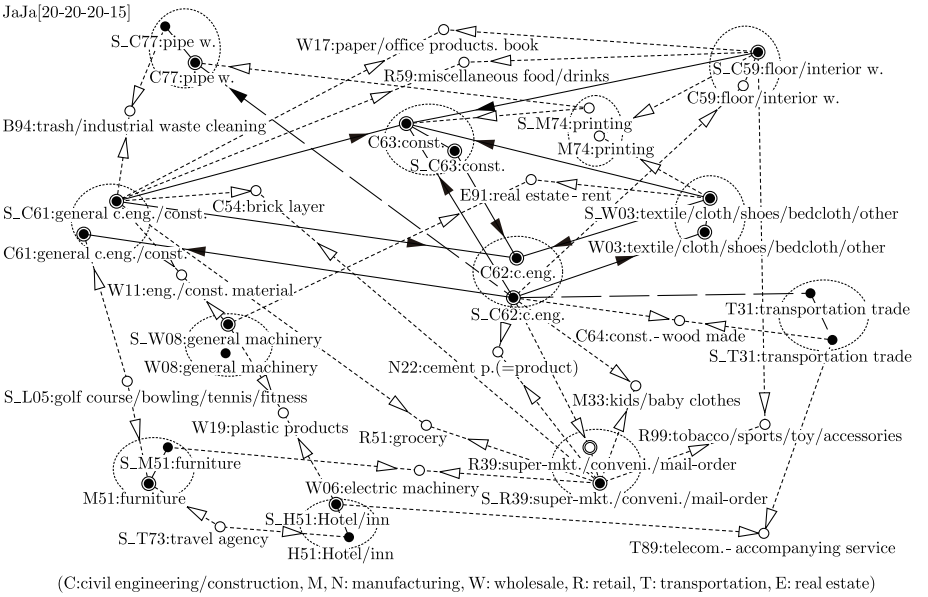

Fig. 2. KeyGraph by time order method ("S_" indicates starting default)

difficult to estimate whether the co-occurrence is based on chain reaction or on a common economic fundamental like overall decrease of construction work in Kyusyu. C60s are also linked to T31 (transportation_trade) and W03 (textile/cloth/others wholesale). But it is difficult to estimate whether defaults in C60s cause the defaults in T31 and in W03 or vice versa. The links may contain both case, but by distinguishing two directions - "from C62 to W03" and "from W03 to C62", i.e. - based on time order among defaults, we can better estimate causal relation among them.

(2) Time order method with directed KeyGraph (see Fig. 2 for result)

In Fig. 2, time orders among defaults in the industries are shown by arrows indicating causal relations among them. Nodes consist of starting defaults are indicated by "S_" put on industry codes. Time order is expressed by arrows from a node with "S_" to another node without "S_". Circled pair of two nodes, one with "S_", are in same industry. For example, an arrow from S_C61 goes to C63, showing defaults in C61 occurred before defaults in C63 in major case, not vice versa. C63 is linked to S_C63 and two nodes are circled. An arrow then goes from S_C63 to C62. It shows that defaults in C63 those occurred after defaults in C61 are, at the same time, defaults those occurred before those in C62. It indicates that defaults in C63 caused by those in C61 then triggered defaults in C62.

When we see Fig. 2 this way, we can better estimate causal relations among defaults. The number of arrows go out from C61 (= S_C61) and C62 (= S_C62) are greater than those go into C61 and C62, that indicates defaults in civil engineering/construction and civil engineering industry caused defaults in other industries in major case, not vice versa. The defaults in C61, C62 might then trigger defaults in variety of related industries like C54 (brick layer work), C77 (pipe work), T31 (transportation_trade), i.e. Arrows from S_W03 (textile/cloth/others wholesale) go to C62 and to C63, indicating defaults in W03, caused by depressed consumer spending for cloth, were source of defaults in C62 and in C63 other than decreased public construction work. Many arrows go out from R39, indicating defaults of super markets, caused by depressed consumer spending, triggered defaults of groceries, toy/accessory shops in the super markets and of electric machinery wholesalers who trade with the market.

7 Conclusion

In this article, we applied chance discovery method to estimate structure of industrial relations that are to transmit chain reaction of bankruptcy. We introduced time order method with directed KeyGraph to capture/express time order of defaults and to better estimate causal relations among defaults. The result of the analysis of default data in Kyushu 2005 was promising. With further accumulation of analyses and improvement of method, a structure estimated by chance discovery method will sufficiently be a base for risk analysis and risk management of a credit portfolio.

The areas for further improvements are;

1. techniques for extracting appropriate time range between start/end of defaults
2. measurement of influence over a default probability of an industry/company of a default event to be transmitted through estimated industrial relations
3. modeling of estimated industrial relations in network structure for the use for risk analysis and risk management of a credit portfolio

References

1. Saunders, A.: Credit Risk Measurement (Japanese). Kinyu Zaisei Jijo Press (2001)
2. FISC: Working Report on Risk Management Model (1999)
3. Nakabayashi, A., Sasaki, M.: Models for credit risk measurement and its application to Japanese bank. FRI Review 2(2) (1998)
4. Torii, H.: Portfolio based credit risk management models – its effectiveness and limit. Weekly Kinyu Zaisei Jijo Magazine (June 1998)
5. Goda, S., Ohsawa, Y.: Chance Discovery in Credit Risk Management – Estimation of chain reaction bankruptcy structure by chance discovery method. In: Proceedings of the 2006 IEEE International Conference on Systems, Man, and Cybernetics, vol. 6 (October 8–11, 2006)
6. Ohsawa, Y.: Discovering risky subduction zones of earthquake. Information Technology for Chance Discovery, pp. 314–325. Tokyo-Denki University Press (2005)
7. Ohsawa, Y.: Visualizing relations between chances and surrounding events. Information Technology for Chance Discovery, pp. 121–153. Tokyo-Denki University Press (2005)
8. Shigematsu, K., Ueno, M., Motomura, Y.: An Introduction to Bayesian Networks, Baifukan (2006)
9. Motomura, Y.: Modeling with large scale data by Bayesian networks. JSAI Technical Report SIG-CII-9707-04 (1997)
10. Motomura, Y.: Bayesian Network that Learns Conditional Probabilities by Neural Networks. In: Workshop on Information-Based Induction Sciences(IBIS) (1998)
11. Cooper, G., Herskovits, E.: A Bayesian methods for the induction of probabilistic Networks from data. Machine Learning 9, 309–347 (1992)
12. Mathematical Systems, Inc.: BayoNet 4.0 manual, `http://www.msi.co.jp/BAYONET/files/manual.pdf`

The Design of Phoneme Grouping for Coarse Phoneme Recognition

Kazuhiro Nakadai[†], Ryota Sumiya[‡,⋆], Mikio Nakano[†],
Koichi Ichige[‡], Yasuo Hirose[‡], and Hiroshi Tsujino[†]

†Honda Research Institute Japan Co., Ltd.,
8-1 Honcho, Wako-shi, Saitama 351-0114, Japan
‡Faculty of Engineering, Yokohama National University,
79-5 Tokowadai, Hodogaya-ku, Yokohama, Kanagawa 240-8501, Japan
nakadai@jp.honda-ri.com

Abstract. Automatic speech recognition for real-world applications such as a robot should deal with speech under noisy environments. This paper presents coarse phoneme recognition which uses a phoneme group instead of a phoneme as a unit of speech recognition for such a real-world application. In coarse phoneme recognition, the design of the phoneme group is crucial. We, thus, introduce two types of phoneme groups – exclusive and overlapping phoneme groups, and evaluate coarse phoneme recognition with these two phoneme grouping methods under various kinds of noise conditions. The experimental results show that our proposed overlapping phoneme grouping improves the correct phoneme inclusion rate by 20 points on average.

1 Introduction

Half a century has passed since Artificial Intelligence (AI) was born. We could see a lot of achievements in the last fifty years, which have been applied into many practical systems. However, we still have a lot of issues facing AI. One of the most important issues for the next fifty years is sound processing such as computationary auditory scene analysis (CASA), music recognition/retrieval, and automatic speech recognition (ASR). Actually, ASR systems have been developed for many years, and HMM-based ASRs with high recognition accuracy are now available as both commercial products [1] and free software [2]. An interesting application of ASR is a service robot, because recently there is burgeoning interest in such a robot and it is expected to listen to and recognize human speech by using its own microphones[3,4]. However, it is a challenging research topic to apply conventional ASR to real-world applications such as robots as described in [5]. We are focusing on two issues in realizing such a real-world application as follows:

1. ASR does not deal with out-of-vocabulary (OOV) words, out-of-grammar (OOG) phrases such as grammatically incorrect sentences and fillers well.

⋆ Currently with Nippon Telegraph and Telephone East Corp.

H.G. Okuno and M. Ali (Eds.): IEA/AIE 2007, LNAI 4570, pp. 905–914, 2007.

2. The performance of ASR deteriorates when signal-to-noise ratio (SNR) of input speech becomes low.

In real-world applications, it is difficult to avoid occurrence of OOV and OOG, because the size of vocabulary and grammar patterns in the language model is limited. This means that ASR should be extended to be able to deal with such a situation. A common way to cope with spontaneous speech is the use of phoneme recognition, but the accuracy of phoneme recognition is lower than that of word recognition since the language model contributes less to recognition. To solve this problem, subword representations based on a lattice of phonemes have been reported [6,7], and their effectiveness is shown through the retrieval of spoken documents including OOV words.

However, in the case of robots, SNR input is basically quite low (often less than 0 dB), since it is inevitable to mix robot noises from robot's actuators which are much closer to the microphones than a target sound source. Because even humans feel difficulties in speech recognition under such a noisy condition, we think that phoneme-based speech recognition for ASR would be more difficult. To address this problem, we propose coarse phoneme recognition. It uses a phoneme group consisting of a set of phonemes instead of a phoneme as a unit of speech recognition. Because a phoneme group has multiple phonemes, the accuracy of correct phoneme inclusion in recognition results is expected to improve. As related work of phoneme group, Sugamura *et al* reported ASR using a phoneme-like template which was formed by clustering acoustic features of input speech signals [8]. Some researchers used hierarchical phoneme classes which were structured according to the similarity of articulation [9,10]. Although they showed the improvement in the noise-robustness of phoneme grouping, they did not discuss what kind of design for phoneme grouping is appropriate.

In this paper, we discuss how we should design a phoneme group, and propose overlapping phoneme grouping which allows one phoneme to belong to multiple phoneme groups. We show that it is more suitable for coarse phoneme recognition by applying two types of designs for overlapping phoneme grouping to noisy speech recognition. In addition, by introducing a word dictionary, we try to resolve the ambiguity that a phoneme group has multiple phoneme candidates.

The rest of this paper is organized as follows: Section 2 introduces coarse phoneme recognition using phoneme groups. Section 3 describes the design for exclusive phoneme grouping in detail, and discusses a problem in the exclusive phoneme grouping. Section 4 introduces overlapping phoneme grouping to solve the problem. Section 5 evaluates the overlapping phoneme grouping and the last section gives conclusions and future works.

2 Coarse Phoneme Recognition

Coarse phoneme recognition outputs a sequence of phoneme groups for a speech input. It is inspired by auditory confusion [11], which appears in human speech recognition under a noisy environment. The auditory confusion shows that perceptually-close phonemes are perceived as a phoneme group when humans

perform phoneme recognition under a noisy environment. The higher the noise level is, the larger the number of phonemes which are unified into a phoneme group is. This indicates that it is reasonable for phoneme recognition by ASR to output a phoneme group which includes multiple phoneme candidates rather than to estimate a phoneme for the corresponding input forcefully. On the other hand, the result of coarse phoneme recognition includes an ambiguity in applying it to word recognition, because the result is not a sequence of phonemes, but that of phoneme groups. We consider that this ambiguity can be resolved by using other modalities like visual speech recognition and higher-level knowledge.

2.1 Phoneme Grouping

The main issue of coarse phoneme recognition is how phoneme groups are designed. We can consider two types of phoneme grouping ways – exclusive and overlapping phoneme grouping. The exclusive phoneme grouping does not assume any shared phoneme between phoneme groups. In this case, two phonemes in a phoneme group do not belong to any other phoneme group. Therefore, we call it exclusive phoneme grouping. The exclusive phoneme grouping was used in related work. For example, clustering of acoustic features [8,12] and perceptual similarity based on articulation [9,10] have been reported to design an exclusive phoneme group. On the other hand, overlapping phoneme grouping allows a phoneme to belong to multiple phoneme groups. When two phonemes belong to a phoneme group, another phoneme group which has one of these two phonemes does not always have the other phoneme. Therefore, we call it overlapping phoneme grouping. When we use overlapping phoneme grouping, more flexible phoneme groups can be represented. However, this type of phoneme grouping has not been reported as far as we know.

3 Exclusive Phoneme Grouping

We designed two types of exclusive phoneme grouping methods. One is based on Japanese phoneme confusion obtained by a psychological experiment [13]. The other is phoneme grouping based on acoustic model distance. To calculate the distance between two acoustic models, the Kullbuck-Leiber distance can be used [14]. However, its computational cost is expensive. We, thus, assume 3-state and 16-mixture monophones, and used $L(P_a, P_b)$ which denotes the distance between two acoustic models P_a and P_b defined by Eqs. (1) and (2). The phoneme groups are clustered with a group average method from an acoustic model trained by using 216 ATR phonetically-balanced words.

$$L(P_a, P_b) = -\frac{D(P_a, S_c, P_b, S_c) + D(P_b, S_c, P_a, S_c)}{2} \tag{1}$$

$$D(P_a, S_i, P_b, S_j) = \sum_{k=1}^{K} w(k, S_i, P_a) f_{S_j, P_b}(\mu(k, S_i, P_a)) \tag{2}$$

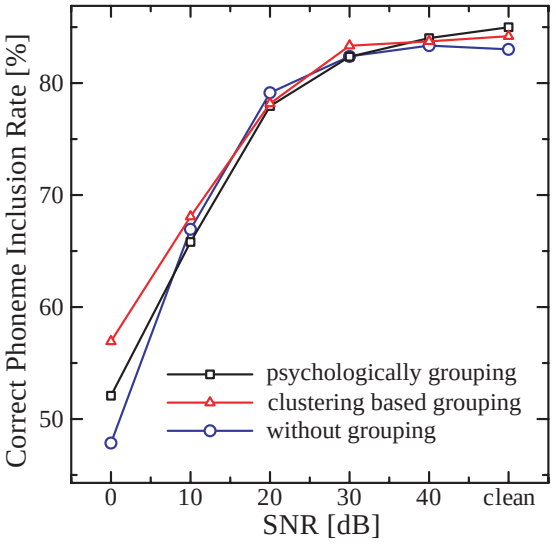

Fig. 1. Coarse Phoneme Recognition Using Exclusive Phoneme Grouping

where K is the number of the mixture. $\mu(k, S_i, P_a)$ and $w(k, S_i, P_a)$ are the mean value and the weight of k-th Gaussian in state S_i of acoustic model P_a, respectively. $f_{S_j,P_b}(x)$ is a probability density function for the a Gaussian mixture in state S_j of acoustic model P_b. S_c is fixed to 2. Finally, we obtained the following phoneme groups.

- Phoneme groups based on a psychological experiment
  a, i, u, e, o, a:, i:, u:, e:, o:, w, f, q, N, d, dy, g, gy, z, j, {b,by,r,ry,y}, {h,hy,k,ky,p,py,t,ch}, {m,my,n,ny}, {s,sh,ts}
- Phoneme groups based on acoustic model distances
  n, u, N, m, r, y, u:, w, {o,o:}, {a,a:}, {e,e:}, {gy,py}, {hy,ky}, {s,j,b,h,f,q,z}, {ts,ch,sh}, {k,p,t}, {g,d,dy}, {my,ny,i,ry,by,i:}

3.1 Problem in Exclusive Phoneme Grouping

The effectiveness of exclusive phoneme grouping was examined by performing coarse phoneme recognition for the phonetically-balanced words. The acoustic models were trained using 23 sets of 216 ATR phonetically-balanced words as 3-state and 16 mixture monophones according to these phoneme groups and ASR was configured as a speech typewriter. Another two sets of the phonetically-balanced words were used as test data. The input SNRs varied from 0 dB to 40 dB at an interval of 10 dB, and clean speech input was also examined. Figure 1 shows word recognition results. The horizontal and the vertical axis are input SNR and correct phoneme inclusion rate, respectively. The correct phoneme inclusion rate, $CPIR$ is defined by

$$CPIR = PG_{Correct}/P_{total} \cdot 100 \tag{3}$$

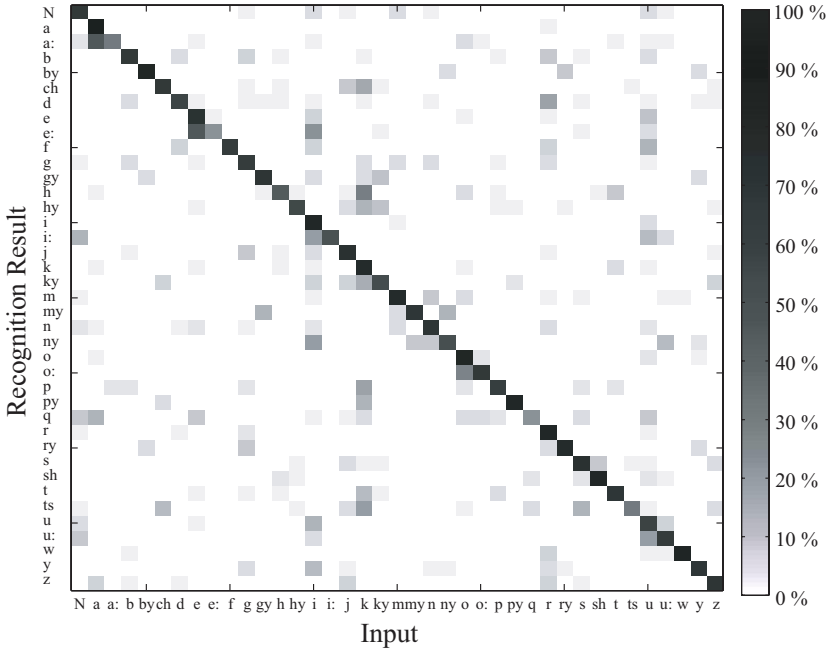

Fig. 2. Phonetic Confusion Matirix in Phoneme Recognition (SNR:10dB, white noise)

where $PG_{Correct}$ is the number of recognized phoneme groups which include the correct phoneme, P_{total} is the total numner of phonemes of input speech.

White noise was used as the noise source. The result showed that the performance of phoneme grouping is almost equivalent to that of the speech typewriter without using phoneme grouping. This indicates that these designs for phoneme grouping were not suitable for ASR.

To know why the above designs of phoneme grouping did not improve the performance, we analyzed the phoneme recognition errors in detail when phoneme grouping was not adopted. We made a phonetic confusion matrix in each noise level. Figure 2 shows a phonetic confusion matrix when SNR is 10 dB. We found that the confusion matrix was *asymmetric*. For example, "i" was easily misrecognized as "y", "ny", "i:" and "e:", while the opposite directions of misrecognition rarely appeared. In every noise level, we found a similar tendency in the confusion matrices. This is also true of human phonetic confusion reported in [13]. This means that the asymmetricity in the phonetic confusion matrix should be considered in designing a phoneme group, that is, overlapping phoneme grouping is necessary.

4 Overlapping Phoneme Grouping

In overlapping phoneme grouping, an acoustic model has to support shared phonemes when we want to make overlapping phoneme groups on the level for

an acoustic model. However, it is difficult to train such an acoustic model. Thus, we implemented overlapping phoneme grouping by applying a phoneme group to a recognition result. We proposed two types of designs for overlapping phoneme grouping. One was based on the phonetic confusion matrix, and the other was based on phoneme N-best (hereafter, *CM-based and NB-based phoneme grouping*, respectively).

4.1 Overlapping Phoneme Grouping Based on Phonetic Confusion Matrix

Table 1 shows an example of CM-based phoneme grouping which was obtained from a phonetic confusion matrix by allowing 5% of confusion errors when SNR was 20 dB. In Table 1, the phoneme groups for "y" and "i:" have "i". A phoneme, thus, can be included in multiple overlapping phoneme groups. To control phoneme grouping, we introduced the average number of phonemes included in a phoneme group, m, instead of using the confusion error allowance, because it is convenient to control the degree of ambiguities included in phoneme groups. In Table 1, m was 2.2 when confusion error allowance was 5%.

4.2 Overlapping Phoneme Grouping Based on *N*-Best

In NB-based phoneme grouping, a speech typewriter without phoneme grouping was performed at first. From the recognition result, N-best phonemes were then selected by using a phoneme alignment of the best recognition result. The selected phonemes formed a phoneme group and a sequence of phoneme groups became the system output. Because N-best phonemes are obtained after recognition, we cannot prepare a phoneme group corresponding to a phoneme in advance. It is possible that N phonemes are not obtained when the acoustic likelihood score of the best phoneme is high. Thus, we introduced the average number of phonemes included in a phoneme group as $\bar{N}$.

5 Evaluation

To evaluate the effectiveness of overlapping phoneme grouping, we performed coarse phoneme recognition for 216 ATR phonetically-balanced words by using a speech typewriter with proposed overlapping phoneme grouping and without phoneme grouping. Training data for acoustic models included 23 sets of the phonetically-balanced words as 3-state and 16 mixture monophones, and another two sets of the phonetically-balanced words were used as test data. We used three types of noise sources – white noise, car noise and elevator hall noise. The overlapping phoneme groups were constructed on the condition of $\bar{N} \geq m \cong 3$. A phonetic confusion matrix for CM-based phoneme grouping was generated from phoneme recognition results of two sets selected from the 23 training data sets.

First, we assumed that the noise level was known, that is, an acoustic model for each SNR was separately trained by using the speech data with the SNR.

Table 1. An Example of CM-based Overlapping Phoneme Grouping

(SNR: 20 dB, confusion error allowance: 5%, $m = 2.2$)

N →N,u:	hy →hy	py→py,y
a →a	i →i	q →a,e,i,q,t,u
a: →N,a,a:,o	i: →i,i:	r →r
b →b	j →j	ry →by,g,ry
by→by,i,ry	k →k	s →s,z
ch→ch,j,k	ky →k,ky	sh→k,sh
d →d,e,r	m →m	t →k,p,t
e →e	my→gy,my	ts →ch,h,k,s,ts
e: →e,e:,i	n →m,n	u →N,i,u,u:
f →f,k	ny →gy,ny,y	u: →u,u:
g →g,m	o →o	w →w
gy→e,gy,k	o: →o,o:	y →i,y
h →a,h,k,t	p →k,o,p	z →a,ch,d,j,z

(Recognition result → the corresponding phoneme group)

The input SNRs of -10 dB, 0 dB, 10 dB, and 20 dB as well as clean speech input were examined for each noise source.

We, then, tried the coarse phoneme recognition with overlapping phoneme grouping when the noise level was unknown. An acoustic model which was trained using clean speech data was used in every case. As input SNRs, 10 dB and 20 dB were selected for the cases of white noise and elevator hall noise, and -10 dB and 0 dB for car noise.

Figures 3–5 show the recognition results in the cases of white noise, car noise, and elevator hall noise, respectively. The horizontal and the vertical axis denote an input SNR in dB and a correct phoneme inclusion rate. The left graph in each figure corresponds to the case where the noise level is known, and the right graph is the case of unkown noise levels.

Figures 3a), 4a), and 5a) prove that overlapping phoneme grouping improves phoneme inclusion rates at every noise level. From Figures 3a) and 5a), we can say that NB-based phoneme grouping is superior to CM-based in the case where there is a high SNR (> 0 dB), and vice versa. The performance deterioration of NB-based phoneme grouping at a low SNR is caused by degradation of recognition reliability, that is, all N-best results are unreliable at such a low SNR. On the other hand, in CM-based phoneme grouping, phoneme groups are extracted from the phonetic confusion matrix in advance. Since each extracted phoneme group is reliable, performance deterioration of CM-based phoneme grouping is slower than that of NB-based phoneme grouping. When dealing with car noise, NB-based is better than CM-based regardless of SNR shown in Figure 4a). This indicates that the effect of car noise is weaker than the other noises at the same SNR. If a stronger power car noise is used, we think that CM-based grouping would be superior to NB-based.

Figures 3b), 4b), and 5b) show that overlapping phoneme grouping works successfully even when the noise level is unknown. The improvement in correct phoneme inclusion rates was about 20 points on average. The tendency that

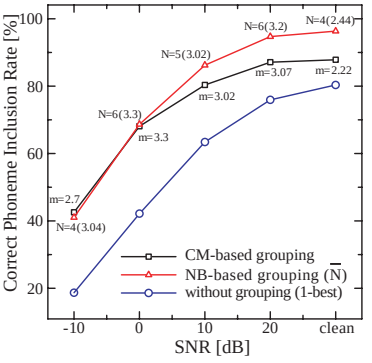

a) Acoustic model trained for each noise level

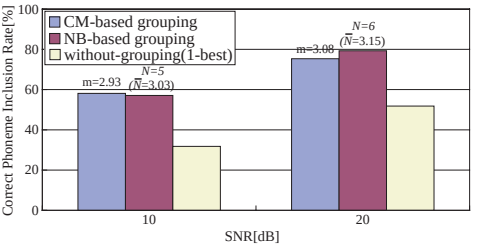

b) Clean acoustic model

Fig. 3. Coarse Phoneme Recognition under White Noise

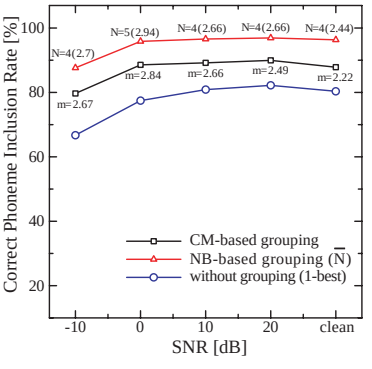

a) Acoustic model trained for each noise level

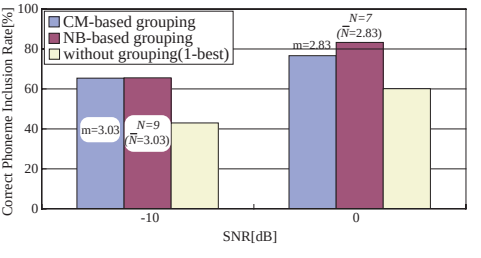

b) Clean acoustic model

Fig. 4. Coarse Phoneme Recognition under Car Noise

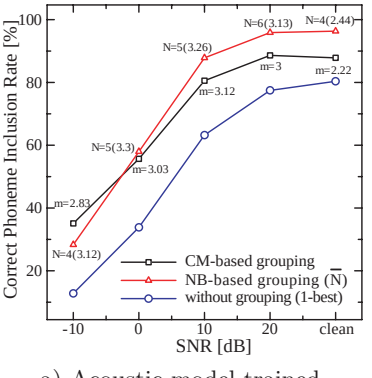

a) Acoustic model trained for each noise level

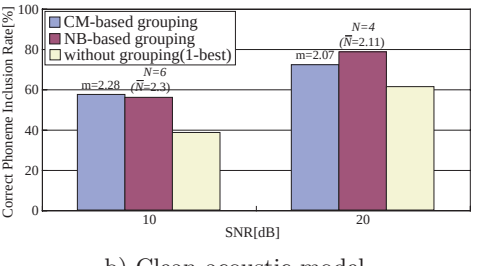

b) Clean acoustic model

Fig. 5. Coarse Phoneme Recognition under Elevator Hall Noise

NB-based grouping is superior at a high SNR, and CM-based at a low SNR was also observed.

5.1 Towards Disambiguation of A Sequence of Phoneme Groups

We showed that overlapping phoneme grouping improved correct phoneme inclusion rates regardless of noise level. The proposed method does not use any temporal relationship between phonemes such as a word dictionary and grammar. This means that the proposed method can help to cope with an unknown word and grammar. Indeed, the recognition result of coarse phoneme recognition included an ambiguity that the recognition result has multiple hypotheses, because the result was not a sequence of phoneme groups but that of phonemes. Therefore, it is difficult to solve OOV and OOG completely when we use only speech signals. However, multimodal integration with other information from visual speech recognition can solve these problems. As the first trial to disambiguate a sequence of phoneme groups, we performed a preliminary experiment to disambiguate the ambiguity by using a word dictionary. We used a dictionary of 10 Japanese words, and each word consisted of a sequence of six phonemes. First, a speech typewriter without grouping recognized 10-word speech input with a SNR of 10 dB. Secondly, CM-based overlapping phoneme groups obtained by using clean speech data were applied to the recognition results, and then the Hamming distance between the obtained sequence of phoneme groups and each word in the dictionary was calculated. Finally, we confirmed that the best matched word which has the minimum Hamming distance for each speech input was correct.

6 Conclusions

We proposed coarse phoneme recognition, which used phoneme groups instead of phonemes as a unit of recognition, to improve the noise-robustness of speech recognition for real-world applications like robots. We discussed how we should design the phoneme group, and finally designed overlapping phoneme grouping. We showed that our proposed overlapping phoneme grouping improved the correct phoneme inclusion rate. In addition, to disambiguate the ambiguity included in the result of coarse phoneme recognition, we showed that the use of a word dictionary was effective in the case of a small vocabulary as a preliminary experimental result. We have a lot of future work such as the use of other modalities such as visual speech recognition to disambiguate the ambiguities, the use of triphones to improve the robustness, and a hybrid system using multiple phoneme grouping methods.

Acknowledgements

We thank Prof. Hiroshi G. Okuno, Kyoto University for his advice, and also thank Shunichi Yamamoto for his help.

References

1. http://www.nuance.com/viavoice/
2. http://julius.sourceforge.jp/
3. Nakadai, K., Hidai, K., Mizoguchi, H., Okuno, H.G., Kitano, H.: Real-time auditory and visual multiple-object tracking for robots. In: Proc. of the 17th Int. Joint Conf. on Atificial Intelligence (IJCAI-01), pp. 1424–1432. MIT Press, Cambridge (2001)
4. Yamamoto, S., Takeda, R., Nakadai, K., Nakano, M., Tsujino, H., Valin, J.M., Komatani, K., Ogata, T., H.G., O.: Recognition of simultaneous speech by estimating reliability of separated signals for robot audition. In: Yang, Q., Webb, G. (eds.) PRICAI 2006. LNCS (LNAI), vol. 4099, pp. 484–494. Springer, Heidelberg (2006)
5. Nakadai, K., Lourens, T., Okuno, H.G., Kitano, H.: Active audition for humanoid. In: Proc. of 17th National Conference on Artificial Intelligence (AAAI- 2000) AAAI, pp. 832–839 (2000)
6. Srinivasan, S., Petkovic, D.: Phonetic confusion matrix based spoken document retrieval. In: Proc. of 23rd Annual ACM Conference on Research and Development in Information Retrieval (SIGIR'00), pp. 81–87. ACM, New York (2000)
7. Ng, K.: Towards robust methods for spoken document retrieval. In: Proc. of International Conference on Spoken Language Processing (ICSLP-98), vol. 3, pp. 939–942. ISCA (1998)
8. Sugamura, N., Shikano, K., Furui, S.: Isolated word recognition using phoneme-like templates. In: Proc. of IEEE International Conference on Acoustics, Speech, and Signal Processing (ICASSP 83), pp. 723–726. IEEE, Los Alamitos (1983)
9. Hansen, J.H.L., Arslan, L.: Markov model based phoneme class partitioning for improved constrained iterative speech enhancement. IEEE Trans. on Speech & Audio Processing 3(1), 98–104 (1995)
10. Arslan, L., Hansen, J.: Minimum cost based phoneme class detection for improved iterative speech enhancement. In: Proc. of IEEE International Conference on Acoustics, Speech, and Signal Processing (ICASSP 94), vol. II, pp. 45–48. IEEE, New York (1994)
11. Miller, G., Nicely, P.: An analysis of perceptual confusions among some english consonants. Journal of the Acoustical Society of America 27, 338–352 (1955)
12. Ishihara, K., Hattori, Y., Nakatani, T., Komatani, K., Ogata, T., Okuno, H.: Disambiguation in determining phonemes of sound-imitation words for environmental sound recognition. In: Proc. of International Conference on Spoken Language Processing (ICSLP-2004), ISCA, pp. 1485–1488 (2004)
13. Hoshino, M., Ito, M., Kimura, M.: M., N.: The effect of visual information for japanese syllables recognition. In: IEICE Techinical Report (in Japanese), SP 2005-129, IEICE, pp. 109–114 (2005)
14. Shozakai, M., Nagino, G.: Analysis of speaking styles by two-dimensional visualization of aggregate of acousticmodels. In: Proc. of International Conference on Spoken Language Processing (ICSLP- 2004), ISCA, pp. 717–720 (2004)

An Improved Voice Activity Detection Algorithm for GSM Adaptive Multi-Rate Speech Codec Based on Wavelet and Support Vector Machine

Shi-Huang Chen[1], Yaotsu Chang[2], and T.K. Truong[2]

[1] Department of Computer Science and Information Engineering, Shu-Te University, Kaohsiung County, 824, Taiwan, R.O.C
shchen@mail.stu.edu.tw
[2] Department of Information Engineering, I-Shou University, Kaohsiung County, 840, Taiwan, R.O.C
ytchang@isu.edu.tw, truong@isu.edu.tw

Abstract. This paper proposes an improved voice activity detection (VAD) algorithm for controlling discontinuous transmission (DTX) of the GSM adaptive multi-rate (AMR) speech codec. First, based on the wavelet transform, the original IIR filter bank and the open-loop pitch detector are implemented via the wavelet filter bank and the wavelet-based pitch detection algorithm, respectively. The proposed wavelet filter bank divides the input speech signal into 9 frequency bands so that the signal level at each sub-band can be calculated. In addition, the background noise can be estimated in each sub-band by using the wavelet de-noising method. The wavelet filter bank is also derived to detect correlated complex signals like music. Then one can apply support vector machine (SVM) to train an optimized non-linear VAD decision rule involving the sub-band power, noise level, pitch period, tone flag, and complex signals warning flag of input speech signals. By the use of the trained SVM, the proposed VAD algorithm can produce more accurate detection results. Various experimental results carried out from the Aurora speech database show that the proposed algorithm gives considerable VAD performances superior to the AMR VAD Option 1 and comparable with the AMR VAD Option 2.

Keywords: GSM AMR, VAD, Wavelet, Support Vector Machine.

1 Introduction

Voice activity detection (VAD) that can detect voice and non-voice periods in speech signal is an important process in improving the channel capacity for voice communication systems. For example, the GSM adaptive multi-rate (AMR) speech codec makes use of a VAD module to control the discontinuous transmission (DTX) and to reduce power consumption [1]. VAD is also useful in other applications such as speech recognition [2] and speech enhancement [3]. Various types of different approaches to VAD have been proposed and most of the conventional VAD algorithms are accomplished by applying several parameters extracted from the input speech signal to compare with the predetermined thresholds. If the measured

H.G. Okuno and M. Ali (Eds.): IEA/AIE 2007, LNAI 4570, pp. 915–924, 2007.

parameters exceed the thresholds, a voice-active decision is made. The decision parameters used in these VAD algorithms are based on the averages over the windows of fixed length, *e.g.*, short time energy levels, zero-crossing rates, and pitch period. There is only a limited flexibility being allowed by these methods in the choice of the time-frequency resolution. It is well known that speech signals are non-stationary and contain lots of transient components. Using a fixed time-frequency resolution method to extract parameters for VAD is not suitable and is not appropriate for noisy environments. Although GSM AMR applies filter bank to improve the performance of noise level estimation, it remains another problem, that is, the use of preset fixed threshold values. It is difficult to derive fixed threshold values for accurate VAD under variable pronunciation conditions. Furthermore, the threshold values used in some of traditional VAD algorithms are calculated in the silence intervals and are improper for noisy conditions.

Because of these, this paper proposes an improved VAD algorithm for GSM AMR speech codec using wavelet transforms and support vector machine (SVM). The wavelet transform is acknowledged as a powerful tool for the nonlinear filtering of speech signals corrupted by noises. In addition, the SVMs proposed by Vapnik [4], have been regarded as a new learning algorithm for various applications such as audio classification [5]. Since VAD can be regarded as a classification of voice and non-voice speech, SVM could be one of the solutions of VAD problem. In addition, this paper modifies the wavelet-based de-noising method [6] with Stein's unbiased risk estimate (SURE) [7] to estimate the background noise in the input speech. The wavelet filter band is also derived to detect correlated complex signals like music. Then one can apply SVM to train an optimized non-linear VAD decision rule involving the sub-band power, noise level, pitch period, tone flag, and complex signals warning flag of input speech signals. In this paper, the exponential radial basis function (ERBF) is selected as a kernel for SVM. By the use of the trained SVM, the proposed VAD algorithm can achieve accurate voice detection results. Using speech signals corrupted by various real noises, the experimental results show that the proposed VAD algorithm performs better than that of AMR VAD Option 1 and is comparable with the AMR VAD Option 2 [1].

The remainder of this paper is organized as follows. The VAD algorithm for GSM AMR speech codec is briefly reviewed in Section 2. Section 3 gives the description of the wavelet-based VAD feature extraction schemes. Then the SVM is described in Section 4. Section 5 illustrates experimental results and compares to other methods. Finally, conclusion is given in the last Section.

2 VAD Algorithm of GSM AMR Speech Codec

In the GSM AMR speech codec, the VAD module is applied to indicate whether each 20 ms speech frame contains signals that should be transmitted, i.e. speech, music or information tones. The output of the AMR VAD module is a Boolean flag (VAD_flag) indicating presence of such signals. There are two types of VAD algorithm, namely Option 1 and Option 2, proposed in the GSM AMR VAD standard [1]. The VAD Option 1 is mainly an energy detector based on the sub-band level estimation whereas the VAD Option 2 is based on the channel energy. The block

diagrams of the VAD Option 1 and Option 2 are shown in **Figs. 1** and **2**, respectively. For simplification, this paper focuses on the VAD Option 1. For more information, see [1].

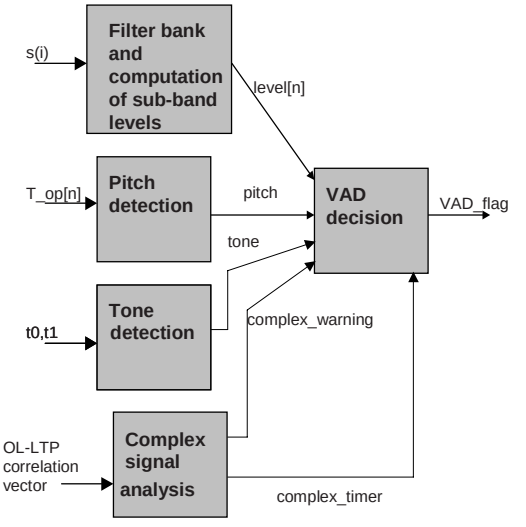

Fig. 1. Block diagram of the VAD algorithm: Option 1 [1]

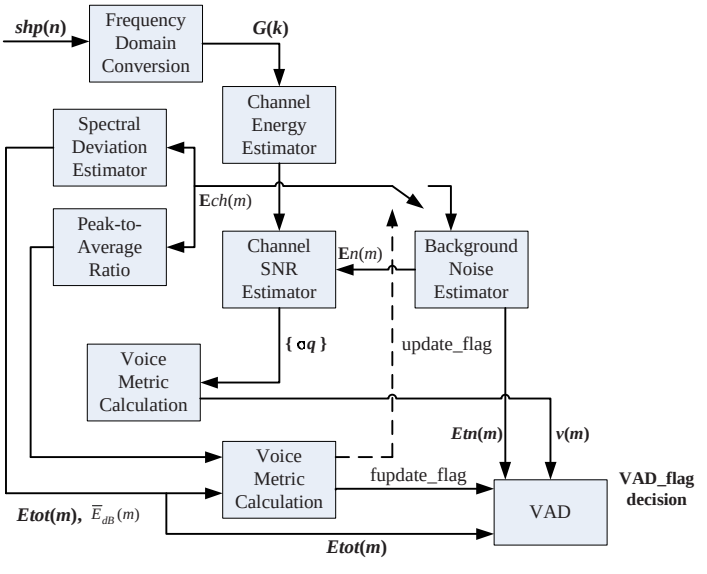

Fig. 2. Block diagram of the VAD algorithm: Option 2 [1]

In the VAD Option 1, samples of the input frame (s(i)) are divided into sub-bands. The VAD uses 160 samples long frames like the AMR speech codec. This is usually done by using a filter bank because it can be implemented with low complexity. The filter bank is based on a critically decimated IIR-filter bank as shown in **Fig. 3** where filter blocks of the 5th and the 3rd order are utilized. Each filter block divides the input into high-pass and low-pass parts and decimates the sampling frequency by two. The filter bank divides the signal into 9 sub-bands, where the lower bands are narrower.

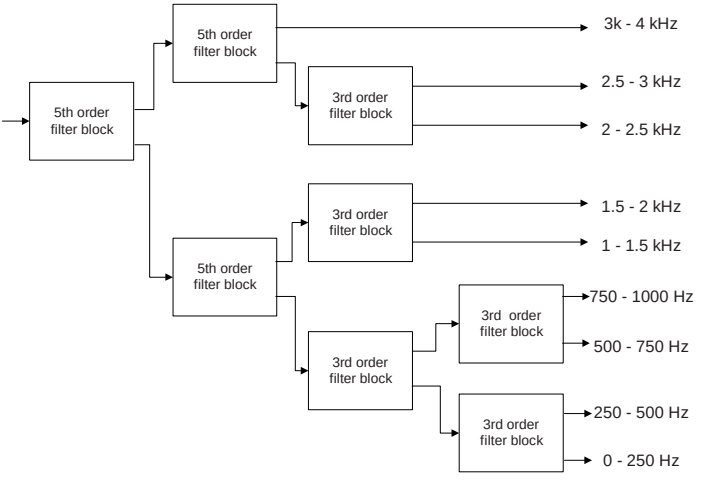

Fig. 3. The filter bank used in the VAD algorithm: Option 1 [1]

After the samples of a frame have been divided into sub-bands, the signal level (level[*n*]) at each sub-band is calculated by summing absolute values at each band where *n* is the index for the frequency bank. Then, the pitch and tone detections are to detect stationary signals including vowel sound and signaling tones. Input for the pitch detection function are open-loop lags (T_op[*n*]), which are calculated by open-loop pitch analysis of the speech encoder. The pitch detection is implemented by comparing lag values of consecutive sub-frames. If the difference of the consecutive lag values is small enough, pitch is detected and pitch_flag (pitch) is set. Tone detection function calculates a flag (tone), which indicates presence of an information tone. Tone detection is done by comparing the open-loop pitch gain of the open-loop pitch analysis to a threshold. The pitch gain is estimated using autocorrelation values (t0 and t1) received from the pitch analysis. If the gain is high, the tone_flag is set.

In order to increase the discrimination between background noise and music signals, a complex signal detection function is used. Complex signal detection calculates a flag (complex_warning), which indicates presence of a correlated complex signal such as music. Correlate complex signals are detected based on analysis of the correlation vector available in the open-loop pitch analysis. The complex_warning flag will adjust the stationary assumption in the background noise estimation processes if the pitch flag and tone flag would fail to do so. A complex_timer flag is also used to initiate a long-term hangover when the filtered complex-correlation values have been consistently large for a considerable time.

The VAD decision function estimates background noise levels. Intermediate VAD decision is calculated based on the comparison of the background noise estimate and levels of the input frame. That is,

$$snr\_sum = \sum_{n=1}^{9} MAX(1.0, \frac{level[n]}{bckr\_est[n]})^2 \tag{1}$$

In (1), the background noise estimate (*bckr_est*[*n*]) is updated using amplitude levels of the previous frame. The noise estimate is updated as follows:

$$bckr\_est_{m+1}[n] = (1.0 - alpha) * bckr\_est_m[n] + alpha * level_{m-1}[n] \tag{2}$$

where *m* is index of the frame. The VAD decision is made by comparing the variable *snr_sum* to a threshold. The threshold is tuned to get desired sensitivity at each background noise level. The higher the noise level the lower is the threshold. Finally, the VAD flag is calculated by adding hangover to the intermediate VAD decision. The hangover addition improves detection of low power endings of speech bursts, which are subjectively important but difficult to detect.

3 Wavelet-Based Speech Features Extraction for VAD

In this paper, the speech features used for VAD are the same as those of VAD Option 1. The main modification is that the signal level, pitch flag, tone flag, and complex warning flag are calculated via wavelet transform.

3.1 Wavelet Filter Bank and Sub-band Signal Level

The wavelet transform mentioned here is implemented via filter bank structure, i.e., the fast discrete algorithm proposed by Mallat [8]. **Fig. 4** is the basic structure of wavelet analysis filter bank where $h(n)$ and $g(n)$ are the analysis low-pass and high-pass filters, respectively. Also, the symbol $\downarrow 2$ denotes the downsampling by 2. Let $a_{j+1}(m)$ be the input to the analysis filter bank. Then the outputs of the analysis filter bank are given by

$$a_j(k) = \sum_m h(m-2k)a_{j+1}(m) \tag{3}$$

$$d_j(k) = \sum_m g(m-2k)a_{j+1}(m) \tag{4}$$

where $a_j(k)$ and $d_j(k)$ are called the approximation and detail coefficients of the wavelet decomposition of $a_{j+1}(m)$, respectively.

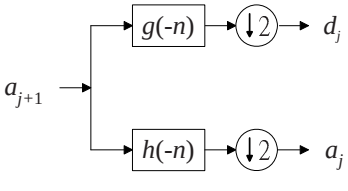

Fig. 4. The basic wavelet analysis filter bank

The splitting, filtering, and decimation shown in **Fig. 4** can be repeated on the approximation and detail coefficients to give the VAD filter bank shown in **Fig. 3**. It follows from [5] that the Daubechies length-8 wavelet filter is select for the proposed VAD algorithm. Therefore, the signal level (*level*[*n*]) at each sub-band can also be calculated as

$$level[n] = \sum_{k} |w_n(k)| \tag{5}$$

where $w_n(k)$ is the corresponding approximation or detail coefficients.

3.2 Detect Pitch and Tone Flags by Using Wavelet

The pitch information is extracted by using a noise-robust wavelet-based pitch detection method [9] instead of an open-loop algorithm. The first stage of the pitch detection method [9] is to apply the wavelet transform with aliasing compensation to decompose the input sound into three sub-bands (approximation and detail signals). Then this method makes use of a modified spatial correlation function, which was determined from the approximation signals obtained in the previous stage to extract the pitch frequency. It was shown [9] that this algorithm is capable of outperforming other time-, frequency- and wavelet-domain pitch detection algorithms.

The tone detection is done by comparing the pitch frequency and the energy of spatial correlation function of the wavelet-based pitch detection method to a threshold. If pitch frequency is higher than 100 Hz and the energy of spatial correlation function is larger than that of total sum of *level*[*n*], the tone_flag is set.

3.3 Complex Signal Detection Using Wavelet

In the original VAD Option 1 algorithm, correlated complex signal detection is used to detect correlated signals in the high-pass filtered weighted speech domain, since the pitch and tone detection functions cannot always detect these signals [1]. A flag of complex_warning will be set when the statistics of the correlation value of a high pass filtered input signal indicates the presence of a correlated complex signal. In this paper, the correlate complex signal is detected based on analysis of the spatial correlation function in the wavelet-based pitch detection algorithm [9]. If the energy of spatial correlation function is greater than that of the sub-band signal in the level-3 wavelet decomposition, the flag *complex_warning* is set.

3.4 Wavelet-Based Background Noise Estimation

The estimation of background noise is by the use of wavelet-based de-noising method. One of the most popular schemes for wavelet-based de-noising is proposed by Donoho and Johnstone [6]. This scheme is based on thresholding the wavelet coefficients of the noise-corrupted signal and can be easily applied to speech de-noising. It has been shown [10] that the wavelet de-noising scheme has a better performance than other traditional methods. The wavelet-based speech de-noising algorithm can be summarized in the following three steps:

(a) Decompose the noisy speech signal into wavelet coefficients.
(b) Employ a threshold method to the wavelet coefficients obtained in (a).
(c) Synthesize these thresholded wavelet coefficients obtained in (b) to achieve the enhanced speech signal.

In this paper, the threshold selection procedure is based on SURE [7] and the soft shrinkage is used. Let $x(n)$ and $y(n)$ be the original and the de-noised speech signals, respectively. Then the background noise can be estimated via calculating the energy of $\{x(n) - y(n)\}$, namely the different between the original and the de-noised speech signals.

4 Support Vector Machine

It is well known that SVM use a known kernel function to define a hyperplane in order to separate given points into two predefined classes. An improved SVM called soft-margin SVM can tolerate minor misclassifications [5] and use in this paper.

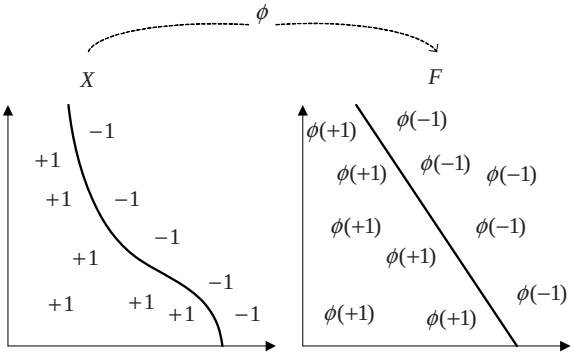

Fig. 5. A feature map simplifies the classification task

Let $x_i \in X \subseteq R^n$ and $y_i \in Y = \{1,-1\}$ be the input vector and the target variable, respectively, where R^n denotes the n-dimensional real space. Suppose a training set $S = \{(x_1, y_1), \cdots, (x_l, y_l)\}_{i=1}^{l} \subseteq (X \times Y)^l$ and a kernel function $K(x_i, x_j) = <\phi(x_i), \phi(x_j)>$ on $X \times X$ is given, where $<\cdot,\cdot>$ denotes the inner product and ϕ maps the input space X to another high dimensional feature space F. With suitably chosen ϕ, the given nonlinearly separable samples S may be linearly separated in F, as shown in **Fig. 5.**

Many hyperplanes can achieve the above separation purpose but the SVM used in this paper is to find the one that maximizes the margin (the minimal distance from the hyperplane to each points). The soft-margin SVM, which includes slack variables $\xi_i \geq 0$, is proposed to solve non-separable problems. The slack variables $\xi_i = \max(0, \gamma - y_i(< w, x_i > + b))$, shown in **Fig. 6**, measure the amount by which the training set fails to have margin γ, and take into account any misclassification of the training data. Consequently, the training process tolerates some points misclassified

and is suitable in most classification cases. The kernel function of exponential radial basis function (ERBF) that is defined as $K(x,\bar{x}) = \exp(-|x-\bar{x}|/2\sigma^2)$ where parameter σ^2 is the variance of the Gaussian function is used in this paper. The parameter σ^2 is set to be 60.

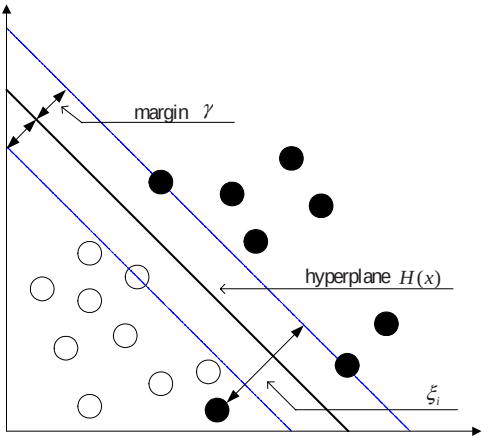

Fig. 6. The margin and the slack variable for a classification problem

5 Experimental Results

This paper selects 320 different sentences from the Aurora database [11] for evaluating the VAD performances. In which 160 sentences are used for SVM training and the remaining 160 sentences are applied for VAD testing. Furthermore, three types of noise, *i.e.*, train station, street, and car, with 5 different SNRs are added to the test speech signal to simulate noisy environments. The original speech signals in Aurora database were sampled at 8000 Hz with 16-bit resolution. Each sound is divided into frames with 256 samples (32ms) frame length and 128 samples (50%) overlap between adjacent frames. The software simulations were performed using Matlab® 7.0 on a Pentium® IV 2.0, Windows® XP PC.

In this paper, the probabilities of detection P_d and false-alarm P_f for a number of noisy speech signals are utilized to evaluate the VAD performances. To obtain P_d and P_f, the active and inactive regions of the clean speech signals are first marked manually. P_d is calculated as the percentage of test cases when the hand-marked speech regions are correctly detected by the VAD algorithm while P_f is the percentage of test cases when hand-marked noise regions are erroneously identified as speech. Using three types of noise with different SNRs, the P_d and the P_f of the proposed VAD algorithm are compared with those of the VAD Option 1 and Option 2 of AMR codec [1]. These experimental results are summarized in Table 1.

Table 1. *Pd*'s(%) and *Pf*'s(%) of the proposed VAD, AMR Option 1 and Option 2 VAD under various noisy environments

Proposed VAD						
Noise	Train station		Street		Car	
SNR	P_d	P_f	P_d	P_f	P_d	P_f
Clear	99.61	5.86	--	--	--	--
20dB	98.43	6.17	99.15	8.24	98.83	7.83
15dB	98.13	7.81	98.97	8.48	98.24	8.51
10dB	97.78	8.48	98.14	8.94	97.54	8.82
5dB	97.23	9.48	97.38	9.09	95.62	9.31
0dB	96.12	9.87	94.32	9.36	90.71	9.73
AMR VAD Option 1						
Noise	Train station		Street		Car	
SNR	P_d	P_f	P_d	P_f	P_d	P_f
Clear	99.44	11.42	--	--	--	--
20dB	99.30	16.82	98.18	26.44	98.46	20.01
15dB	98.66	25.24	98.28	31.76	97.45	21.32
10dB	97.84	32.14	96.84	33.25	96.20	39.87
5dB	96.13	45.34	95.82	40.87	94.78	54.53
0dB	93.72	57.47	94.42	49.15	94.08	54.32
AMR VAD Option 2						
Noise	Train station		Street		Car	
SNR	P_d	P_f	P_d	P_f	P_d	P_f
Clear	99.76	11.32	--	--	--	--
20dB	88.37	19.69	78.74	19.36	83.96	22.18
15dB	84.37	20.02	82.78	18.72	86.42	23.29
10dB	90.93	22.56	88.73	19.18	93.58	25.18
5dB	96.79	30.45	94.96	27.27	95.69	30.35
0dB	96.39	39.57	98.46	40.37	98.09	41.42

From Table 1, one observes that although the probabilities of detection P_d of AMR VAD Option 1 and Option 2 are fine, their probabilities of false-alarm P_f are somewhat unsatisfied. This means that most noisy sounds have been classified as speech frames using AMR VAD Option 1 and Option 2. The proposed VAD scheme provides a good alternative to these standardized algorithms. In addition to the well average probabilities of detection, the proposed VAD scheme has lower probabilities of false-alarm P_f than all the mentioned standardized algorithms over a variety of noise environments.

6 Conclusion

An improved VAD algorithm based on the wavelets and SVMs is proposed in this paper. By the use of wavelet transform, the signal level at each sub-band can be calculated. In addition, the background noise can be estimated in each sub-band via

the wavelet de-noising method with SURE thresholding. The wavelet filter bank is also derived to detect correlated complex signals like music.

Then one applies SVM with ERBF kernel function to train an optimized non-linear VAD decision rule involving the sub-band power, noise level, pitch period, tone flag, and complex signals warning flag of input speech signals. It is shown in this paper that the trained SVM offers accurate VAD under noisy environments. Various experimental results reveal that the proposed VAD algorithm performs better than those of VAD Option 1 of AMR and is comparable with the AMR VAD option 2. Moreover, the proposed VAD algorithm can operate reliably in real noisy environments.

References

1. 3GPP TS 26.094 V6.1.0, Voice Activity Detector (VAD) for Adaptive Multi-Rate speech codec (2006)
2. Ramírez, J., Segura, J.C., Benítez, C., de la Torre, Á., Rubio, A.J.: A New Kullback-Leibler VAD for Speech Recognition in Noise. IEEE Signal Processing letters 11(2), 266–269 (2004)
3. Garner, N.R., Barrett, P.A., Howard, D.M., Tyrrell, A.M.: Robust noise detection for speech detection and enhancement. Electron. Lett. 33(4), 270–271 (1997)
4. Vapnik, V.N.: Statistical Learning Theory. Wiley, Chichester (1998)
5. Lin, C.-C., Chen, S.-H., Truong, T.K., Chang, Y.: Audio Classification and Categorization Based on Wavelets and Support Vector Machine. IEEE Trans. on Speech and Audio Processing 13(5), 644–651 (2005)
6. Donoho, D.L., Johnstone, I.M.: Adapting to unknown smoothness via wavelet shrinkage. Journal of the American Statistical Association 90, 1200–1224 (1995)
7. Stein, C.: Estimation of the mean of a multivariate normal distribution. Annals of Statistics 9(6), 1135–1151 (1981)
8. Mallat, S.: Multifrequency channel decomposition of images and wavelet model. IEEE Trans. Acoustic, Speech and Signal Processing 68, 2091–2110 (1980)
9. Chen, S.-H., Wang, J.-F.: Noise-robust pitch detection method using wavelet transform with aliasing compensation. IEE Proc. Vision, Image and Signal Processing 149(6), 327–334 (2002)
10. Hu, Y., Loizou, P.C.: Speech enhancement based on wavelet thresholding the multitaper spectrum. IEEE Trans. on Speech and Audio Processing 12(1), 59–67 (2004)
11. Aurora 2 Database (2000) http://www.elda.org/article52.html

The PICA Framework for Performance Analysis of Pattern Recognition Systems and Its Application in Broadcast News Segmentation

Xiangdong Wang[1,2], Meiyin Li[1,2],
Shouxun Lin[1], Yueliang Qian[1], and Qun Liu[1]

[1] Institute of Computing Technology, Chinese Academy of Sciences, Beijing 100080, China
[2] Graduate University of Chinese Academy of Sciences, Beijing 100085, China
{xdwang,limeiyin,sxlin,ylqian,liuqun}@ict.ac.cn

Abstract. In this paper, the performance influencing class analysis (PICA) framework is proposed for performance analysis of pattern recognition systems dealing with data with great variety and diversity. Through the PICA procedure, the population of data is divided into subsets on which the system achieves different performances by means of statistical methods. On basis of the division, performance assessment and analysis are conducted to estimate the system performance on the whole data population. The PICA framework can predict true performance in real application and facilitate comparison of different systems without the same test set. The PICA framework is applied to the analysis of a broadcast news segmentation system. The procedure is presented and experimental results were given, which verified the effectiveness of PICA.

Keywords: performance analysis, PICA, PIFA, pattern recognition, speech recognition, broadcast news segmentation.

1 Introduction

In the field of pattern recognition, the variance and diversity of input data poses great challenge to performance assessment, since a system can achieve quite different performances on different test data. This makes it difficult to assess the overall performance of a system considering all possible test data and to compare the performances between different systems. As a resolution, the evaluation scheme is popular adopted, in which test database is collected with variability in some basic data properties (e. g. speaker gender for speech data) and all systems are tested with the same data. Though this makes comparison possible, the performances obtained are still highly dependant on the test data. In most evaluations [1,2,3] and other researchers work, the test data are collected randomly or arbitrarily despite the coverage of some basic data properties, so they are not representative of all data and the performances are not representative, either.

In this paper, we present the Performance Influencing Class Analysis (PICA) framework of performance assessment for applied pattern recognition systems. It

H.G. Okuno and M. Ali (Eds.): IEA/AIE 2007, LNAI 4570, pp. 925–934, 2007.

aims to estimate the overall performance on the set of all possible input data (the population) for a given task, making the performance assessment more reliable and performance comparison between different systems feasible. The main idea of PICA is to divide the data population into some subsets, and estimate the performance on the data population with performances on the subsets and the proportions of each subset in the data population.

The rest of the paper is organized as follows. In Section 2, the basic logic and procedure of PICA are presented. In Section 3, we describe the application of PICA to the performance assessment of a broadcast news segmentation system. Experimental results and analysis for the application in broadcast news segmentation are given in Section 4. Finally, conclusions are drawn in Section 5.

2 The Framework of PICA

2.1 The Basic Logic of PICA

To further explore the PICA framework, some terms are proposed as follows.

Population: the set of all possible input data for a specific task, denoted by Ω. Each element of the population is a *basic unit of data*, which can be decided according to the features of data and the task performed. For example, for a speech recognition task, the basic unit of data may be decided as one utterance.

Data property: the feature or characteristic of each basic unit of data, e. g. the gender of speaker, or the signal-noise ratio for the speech recognition task. For a basic unit of data d, its data properties are denoted as $d.P_i$, where $i = 1, 2, \ldots$

Levels of a data property: values or classes of a data property. In PICA, only discrete levels are used, so levels of data properties with continuous values are decided by dividing the value domain into intervals. We defined that for basic unit of data d, $d.P_i$ refers to the level of the data property instead of the value.

Performance metric: a value as the measurement of performance. For example, word error rate for the continuous speech recognition task.

PIF and PIC. The main idea of PICA is to divide the population into subsets satisfying that performances are significantly different on different subsets and close on data in the same one. These subsets are referred to as performance influencing classes (PICs). To achieve the division, the method of ANOVA (analysis of variance) [4,5] is introduced from statistics, which is a powerful method of hypothesis test. For data with n data properties, when not considering interaction between data properties, the statistical model of ANOVA is written as

$$F_{l_1 l_2 \ldots l_n m} = \mu + \sum_{i=1}^{n} \tau_{l_i} + \varepsilon_{l_1 l_2 \ldots l_n m} \tag{1}$$

where l_i $(i = 1, \ldots, n)$ stands for a level of the i^{th} data property, $F_{l_1 l_2 \ldots l_n m}$ denotes the performance metric value on the m^{th} data with specific data property levels, τ_{l_i} denotes the effect of the l_i level on the performance, and ε denotes

experimental error. The purpose of ANOVA is to test statistically that for a data property with K levels, whether the following hypothesis is accepted or rejected.

$$\tau_1 = \tau_2 = \ldots = \tau_K = 0 \tag{2}$$

Definition 1. *If for a data property, the hypothesis in (2) is rejected through ANOVA, the data property is called a performance influencing factor (PIF).*

Definition 2. *For a PIF P_i, if for each two levels l_1, l_2 of it, $\tau_{l_1} = \tau_{l_2}$ is rejected through ANOVA, then P_i is called a level-complete PIF.*

Only PIFs are considered when dividing the population into PICs, since other data properties bring no significant difference in performance. Though not all PIFs are level-complete ones, in practice, most PIFs can be modified to be level-complete PIFs by adjusting the definition of levels.

Theorem 1. *Let P_i be a level-complete PIF, whose levels are $l_1, l_2, \ldots, l_K$, and set A_j is defined as $A_j = \{d | d.P_i = l_j, d \in \Omega\}$, $j = 1, 2, \ldots, K$, then $S_i = \{A_j, j = 1, 2, \ldots, K\}$ is a partition of Ω.*

Proof. S_i is a partition of Ω because A_j, $j = 1, 2, \ldots, K$, satisfying

$$A_{j_1} \cap A_{j_2} = \Phi, j_1 \neq j_2, \text{ and } \bigcup_{j=1}^{K} A_j = \Omega \tag{3}$$

□

Definition 3. *The partition $S_i = \{A_j, j = 1, 2, \ldots, K\}$ in Theorem 1 is called the performance influencing partition of Ω for P_i, and $A_j \in S_i, j = 1, 2, \ldots, K$ is called a performance influencing class (PIC) for P_i.*

Definition 4. *Let $P_1, P_2, \ldots, P_n$ be level-complete PIFs, whose performance influencing partitions are $S_1, S_2, \ldots, S_n$, then the product of the partitions $S = S_1 \cdot S_2 \cdot \ldots \cdot S_n$ is called the performance influencing partition of Ω for $P_1, P_2, \ldots, P_n$, and each $B \in S$ is called a performance influencing class for $P_1, P_2, \ldots, P_n$.*

It can be seen from the definitions that when many data properties are considered, the performances on different PICS are quite likely to be different due to different levels of PIFs. And when enough data properties are considered and not too few data are used, performances on subsets in the same PIC are likely to be similar for few factors may influence the performance in a PIC.

Estimation of Performance on the Population. Once the PICs are determined, performance metric value on each PIC can be obtained by testing the system using corresponding data. These performances as a whole can give more information than simply test the system using a randomly selected test set. But sometimes, only one metric value is needed to represent the overall performance on population or to compare with other systems. In the following theorem, it is proved that for metrics such as precision or error rate, the metric value on the population equals to a weighted sum of metric values on all PICs.

Theorem 2. *Assume that for a data set D, a performance metric is defined as*

$$R = f(D)/q(D) \tag{4}$$

where f and q are functions of D, satisfying that for two data sets D_1, D_2,

$$f(D_1 \cup D_2) = f(D_1) + f(D_2), q(D_1 \cup D_2) = q(D_1) + q(D_2), \text{ if } D_1 \cap D_2 = \Phi \tag{5}$$

Then for a partition $S = \{A_1, A_2, \ldots, A_n\}$ of the data population Ω, letting R_i be the metric for the subset A_i, the following holds true.

$$R = \sum_{i=1}^{n} c_i R_i, \text{ where } c_i = q(D_i)/q(\Omega), i = 1, 2, \ldots, n \tag{6}$$

Proof. According to (4) , for each subset, we have $R_i = f(D_i)/q(D_i)$, and according to (5), $f(\Omega) = \sum_{i=1}^{n} f(D_i)$, $q(\Omega) = \sum_{i=1}^{n} q(D_i)$. Let $Q = q(\Omega)$, we have $R = f(\Omega)/Q = [\sum_{i=1}^{n} f(D_i)]/Q = [\sum_{i=1}^{n} R_i q(D_i)]/Q = \sum_{i=1}^{n} [q(D_i)/Q]R_i = \sum_{i=1}^{n} c_i R_i$ □

In fact, in most metrics used in the pattern recognition area, the function $q(D)$ in the above theorem usually stand for the amount of data, such as the number of basic units of data or the whole duration of speech. So the proportion $q(D_i)/Q$ stands for the proportion of amount of D_i in the population.

Design of Test Data. For performance metrics that do not satisfy (4) or (5), there is a more direct way for estimating overall performance on the population. That is, to design and collect a test set in which the proportion of each PIC is equal to that in the population. For cases that levels of all PIFs can be controlled when collecting data, this can be easily done. However, for most cases, the data are just collected with little control, so a selection approach is proposed, as described in the following.

Let Ω be the data population for a specified task. Suppose that there are K PICs. If there are n sets of data already collected, denoted by $D_1, D_2, \ldots, D_n$. The data amount of D_i is N_i, the proportion of the j^{th} PIC in D_i is a_{ij}, and the proportion of the j^{th} PIC in the population is b_j. So the problem can be described as forming a test data set D of data amount N by selecting sets from $D_1, D_2, \ldots, D_n$, satisfying that the proportion of PICs are most close between D and Ω. The *Euclid distance* is used as the measurement of similarity between the proportions of PICs in D and Ω, so this can be transformed into the problem of finding $X_0, X_1, \ldots, X_n$ that minimizes

$$d(D, \Omega) = [\sum_{j=1}^{K} (\frac{1}{N} \sum_{i=0}^{n} a_{ij} N_i X_i - b_j)^2)]^{1/2} \tag{7}$$

under the restriction of

$$\sum_{i=0}^{n} N_i X_i = N, \ \mathrm{X}_i \in \{0, 1\}, \ i = 1, \ldots, n \tag{8}$$

This is a problem of *integer programming* and can be solved using classical algorithms such as the *branch and bound method* [10].

2.2 The Procedure of PICA

The whole procedure of PICA is shown in Figure 1.

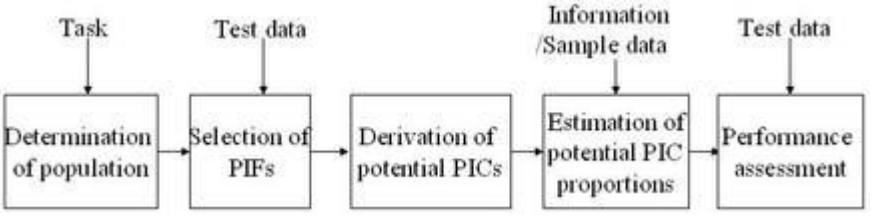

Fig. 1. The procedure of PICA

First, the data population should be determined according to the task, which includes deciding the basic unit of data and the coverage range of the population.

Once the population is fixed, data properties under examination should be decided because it is impossible to study all of them. Then the framework of PIFA [8] is incorporated into PICA to select PIFs from the data properties. The main idea of PIFA is to design the experiments using orthogonal design and test for significant differences of performance between levels using ANOVA.

After the PIFs are chosen, their levels may be slightly adjusted to become level-complete PIFs. Then, PICs for each PIF and all PIFs are derived according to Defination 3 and 4. The product of multiple partitions is computed as [9]

$$S = S_1 \cdot S_2 \cdot \ldots \cdot S_n = \{\bigcap_{i=1}^{n} A_i | \bigcap_{i=1}^{n} A_i \neq \Phi, A_i \in S_i\} \tag{9}$$

To decide whether $\bigcap_{i=1}^{n} A_i \neq \Phi$, all $\bigcap_{i=1}^{n} A_i$ are maintained as *potential PICs*, and after the proportions of all potential PICs are estimated, the sets with proportion less than a threshold will be eliminated as approximate null set.

As for estimating the proportions, information from other researchers may be useful. If such information is not available, the sampling method can be used to draw a sample from the population and compute the proportions in the sample set as substitution. Sampling theory supports that if the sampling method is appropriate, the sample set may be good miniature of the population [6,7].

When PICs are determined and their proportions are know, an overall performance metric is calculated as estimation of performance on the population. There are two ways for such assessment—-estimating the metric on the population using (6) or designing a test set by solving (7) and (8).

3 Application of PICA to Broadcast News Segmentation

To verify the effectiveness of the PICA, we applied it to the performance assessment of a broadcast news segmentation system. The aim of broadcast news segmentation is to segment the audio stream into homogeneous regions (referred to

as *segments*) according to speaker identity, environmental condition and channel condition. It can also be seen as detection of change points which are the positions in the audio where change occurs in speaker identity or recording conditions.

Considering the cost of experiment, the system task is narrowed to segmentation of broadcast news from one radio channel (China National Radio). Segmentation result of the system is compared to the reference to yield performance metrics of rejection rate (RJ) and false alarm rate (FA), as defined in the following, where N_{miss}, N_{fa}, and N_{ref} denote the number of missed, false alarm and reference change points.

$$RJ = N_{miss}/N_{ref} \tag{10}$$

$$FA = N_{fa}/(\text{Duration of the audio stream}) \tag{11}$$

The PICA framework is applied respectively to RJ and FA. Since the procedures are quite similar, only details for the FA metrics are described in this paper.

Determination of Population. First, decision should be made about the basic unit of data. In our work, when investigating false alarm rate, each segment (speech between two change points) is considered as a basic unit of data, since data properties such as recording condition usually keep the same within one segment and varies much between different ones. Then, population is defined as the set of all segments in broadcast news from China National Radio.

Selection of PIFs. Once the basic unit of data is chosen, data properties of a unit are also determined. Since there could be innumerous data properties, only those that may influence system performance and can be measured in practice are involved in the selection of PIFs. In our work, data properties about the speaker, recording condition and channel condition are chosen, and their levels are decided, as listed and explained in table 1.

When selecting PIFs from these data properties, the PIFA (performance influencing factor analysis) framework [8] is adopted. In our work, because the data properties such as speaker gender are only related to speech segments, a hierarchical approach is utilized: The two levels of the data property "content" is analyzed first using a 1-way ANOVA, and the orthogonal design (the orthogonal table $L_8(2^7)$ is adopted) is used for the other data properties. Then a data set (referred to as the *PIFA set*) of 6 hours is collected and used as input of the segmentation system. With the result and reference, statistical data of performance are generated for each group according the method presented in [8], the main idea of which is to divide the group into subgroups and consider metric on each subgroup as one observation. The results of ANOVA shows that content, speech background and speech scene influence system performance significantly ($\Pr < 0.05$). So three PIFs are selected, which is content, background, and speech scene.

Derivation of Potential PICs. When PIFs are determined, PICs can be derived according to (9). As mentioned in section 2.2, potential PICs are first derived and tested later for whether it can be eliminated as a null set. For our work, the potential PICs are listed in table 2.

Table 1. Data properties and their levels

Data property	Level	Explanation
Content	Speech	Speech by human
	Non-Speech	Music, noise, etc.
Speaker gender	Male	Male speaker
	Female	Female speaker
Speaker accent	Yes	With dialectal accent
	No	Without dialectal accent
Speech mode	Planned	Reading planned text
	Spontaneous	Speaking spontaneously
Background	Yes	Speech with music or noise
	No	Speech in silent environment
Speech scene	Studio	Speech in studio
	Live	Speech in open environment

Table 2. Potential PICs and their proportions

	Content	Background	Speech scene	Proportion
1	Speech	No	Studio	0.566
2	Speech	Yes	Studio	0.028
3	Speech	No	Live	0.247
4	Speech	Yes	Live	0.083
5	Non-speech	—	—	0.060

Estimation of Potential PIC Proportions. Since no information of the potential PICs is available from other researchers, the approach of sampling is adopted, as explained in section 2.2. In our work, the sampling frame is defined as all broadcast news from China National Radio in 2005, and sampling unit is defined as one section. A procedure similar to stratified sampling [6,7] is performed: the sampling frame is divided into 12 strata according to the month (from Jan. to Dec.) and broadcast news of 2 hour is draw from each stratum using simple random sampling method. Notice that what is needed for these data is the information of the duration of the PICs, so full speech data is unnecessary. So with the sample data of 24 hours, the proportion of a PIC is calculated as the quotient of the duration of all segments in the PIC and the total duration of the sample set. The result is shown in table 2. Since the proportion of the 2nd potential PIC is less that 0.05 which is the threshold in our work, so it is eliminated. Therefore, there are only 4 PICs and the proportions are re-estimated, as shown in part of table 3.

Performance Assessment. Once the PICs are fixed, the system is tested with a test set of 2 hours in which total duration of each PIC is about 30 minutes and the FA metric is calculated for each PIC. The results are shown in Table 3. From the definition of FA, it can be seen that (6) is suitable. So FA metric on the population is estimated using (6), and the result is 3.213.

Table 3. Proportion and FA values of PICs

	Content	Background	Speech scene	Proportion	FA
1	Speech	No	Studio	0.592	2.348
2	Speech	No	Live	0.258	4.313
3	Speech	Yes	Live	0.087	4.944
4	Non-speech	—	—	0.063	4.427
Estimated FA on population = Proportion(i)*FA(i) = 3.213					

The method of test data designing is also used. A data set of 30 hours are divided into 90 clips each with the duration of 10 minutes, from which 12 clips are selected according to (7) and (8) resulting in a test set of 2 hours. The proportions of PICs in the selected data set are shown in Table 4. The system is tested with this set, and the FA metric obtained is 3.115, which is close to the estimation in Table 3.

Table 4. Details of the selected test set

PIC	1	2	3	4
Proportion in population	0.592	0.258	0.088	0.063
Proportion in the selected set	0.586	0.251	0.081	0.060
$d(D, \Omega)$	0.0014			
FA	3.115			

4 Experiments and Analysis

Test of PICs. It is expected that performance be similar when on data within the same PIC, and be significantly different on data from different PICs. So for each PIC, we collected 10 data sets of 20 minutes, and for comparison, ten random sets are also selected randomly without any consideration of PIC. The FA metrics were calculated on all 5 data sets, as shown in Figure 2(a). The result indicates that performance is consistent in one PIC and varies much for different ones. And for random sets with the same size, performance also varies much, which implies that testing the system using one or few random sets is unreliable.

Test of Performance Assessment. The main advantage of PICA is that it can achieve performance approximate that on the population. So we test the system using 5 difference test sets: the test set designed and the sample set described in Section 3, and 3 random selected test sets. Sizes and FAs for those test sets are listed in Table 5, which shows that performance on the test set designed is most similar to that on the sample set of larger size, while metrics on sample sets varies considerably for different sets. It is also favorable that the FA value estimated in Table 3 is quite close to the metric on the sample set, which means the estimation is reliable, too.

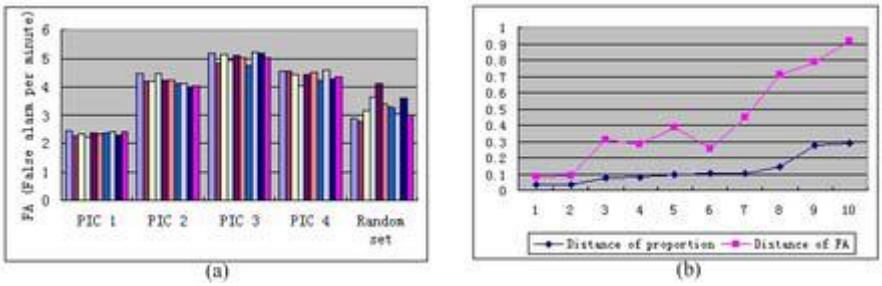

Fig. 2. Experiments results: (a) Result of test of PICs; (b) Result of test of performance assessment

Table 5. Result of experiment on different test sets

	Designed set	Sample set	Random set1	Random set2	Random set3
Size	2 hrs	24 hrs	2 hrs	2 hrs	2 hrs
FA	3.115	3.223	2.933	3.318	3.581

Figure 2(b) shows the result of another experiment: the system was tested using 10 test sets, each is of 2 hours. For each test set D_i, the PIC proportion distance between D_i and Ω is calculated as the Euclid distance, and distance of FA is calculated as

$$\text{FA distance for } D_i = |(\text{FA on } D_i) - (\text{FA on } \Omega)| \tag{12}$$

The figure indicates that the less the distance D_i, the closer the performance on D_i to the performance estimated for the population, implying that when the distance is small enough, the performance on the designed test set is close to that on population.

5 Conclusions

In this paper, the PICA (performance influencing class analysis) framework is presented. Under the framework, performance on the population of all possible data is estimated to analyze the system. By means of the analysis, difference in performance caused by different test data can be avoided, performance in real application can be predicted, and comparison between different systems tested with different data can be easily realized.

Also in this paper, the application of the PICA framework to the analysis of a broadcast news segmentation system was described. The whole procedure was presented and experimental results were given, which verified the effectiveness of PICA.

Actually, the PICA framework can be applied to any pattern recognition task with complex input data. So in the future, we are planning to apply PICA in other task of speech recognition and wider fields.

References

1. Vandecatseye, A., et al.: The COST278 pan-European Broadcast News Database. In: Procs. LREC 2004, Lisbon, pp. 873–876 (2004)
2. Paul, D.B., Baker, J.M.: The Design for the Wall Street Journal-based CSR Corpus. In: Proceedings of Second International Conference on Spoken Language Processing, pp. 899–902 (1992)
3. Pearce, D., Hirsch, H.-G.: The Aurora Experimental Framework for the Performance Evaluation of Speech Recognition Systems under Noisy Conditions. In: Proceedings of 6th International Conference on Spoken Language Processing, pp. 29–32 (2000)
4. http://www.statsoft.com/textbook/stanman.html
5. Shen, Q.: SAS Statistical Analysis, pp. 84–107. Higher Education Press, Beijing (2005)
6. Renssen, R.: A Course in Sampling Theory. http://www.cs.vu.nl/~stochgrp/aionetwerk/course.doc
7. Friel, C.M.: Sampling Theory. http://www.shsu.edu/~icc_cmf/cj_787/research11.doc
8. Wang, X., Xie, F., et al.: DOE and ANOVA based Performance Influencing Factor Analysis for Evaluation of Speech Recognition Systems. In: ISCSLP, Proceedings (companion volume), pp. 431–442 (2006)
9. Jiao, Z.-y., Hu, Y.-p.: Quotient Set and Fundamental Operation of Quotient Set. Journal of Xi'an University of Science and Technology 24(3), 372–375 (2004)
10. Kaufmann, A.: Pure and Mixed Integer Programming (1997)

The Theory of Maximal Social Welfare Feasible Coalition

Laor Boongasame[1], Veera Boonjing[2], and Ho-fung Leung[3]

[1] Department of Computer Engineering,
King Mongkut University of Technology Thonburi,
Bangkok, Thailand
[2] Department of Mathematics and Computer Science,
King Mongkut's Institue of Technology Ladkrabang,
Bangkok, Thailand
[3] Department of Computer Science and Engineering,
The Chinese University of Hong Kong,
Sha Tin, Hong Kong, P.R. China
laor.b@bu.ac.th,kbveera@kmitl.ac.th,lhf@cse.cuhk.edu.hk

Abstract. This paper proposes a new theory for forming a maximum-value-cooperation coalition known as *the Maximal Social Welfare Feasible Coalition*. This theory can give such solution because it does not assume that each player requesting to join a coalition knows information of other players. However, all players' private information requesting to join the coalition is known by an honest coordinator. This allows the coordinator to select a coalition structure with maximal value of cooperation among successful players so as they get at least at their required minimum values. Not only this maximal value is shown to be equal to or larger than the value of a core coalition but also the value allocation is shown to be Pareto optimal.

Keywords: cooperative game theory, coalition formation, Pareto optimality, the core, group buying.

1 Introduction

Cooperative game theory, with solution concepts such as *the core* [2], *the Shapley value* [4] , *the bargain set* [1], *the private core* [6], and *the fine core* [5], is one important branch of *n-person* game theory which deals with situations where the players in a coalition can make binding agreements. The primary aim of the theories is to investigate the conditions under which players in a coalition receive sufficiently large payoffs that they will not break away from the coalition. This means that they seek for a coalition maximizing payoffs of successful players. Therefore, they might not give a maximum-value-cooperation coalition.

This paper proposes a new theory of *Maximal Social Welfare Feasible Coalition* for forming a maximum-value-cooperation coalition. The theory assumes that each player in a coalition does not know the private information of other

H.G. Okuno and M. Ali (Eds.): IEA/AIE 2007, LNAI 4570, pp. 935–942, 2007.

players. The assumption agrees with the situation of forming a coalition in the real world environment, i.e., each player in the coalition has some private information and is not assumed to exchange his private information with other players. However, all players' private information requesting to join the coalition is known by an honest coordinator. This allows the coordinator to select a coalition structure with maximal value of cooperation among successful players so as they get at least at their required minimum values. The value of this coalition is known to be equal to or larger than the core coalition formed using *the core theory.*

The rest of paper is organised in four sections. Section 2 describes the core theory. Section 3 elaborates *the maximal social welfare feasible coalition theory.* Section 4 evaluates the theory. Lastly, section 5 concludes the paper.

2 The Core Theory

The core theory is one of the most popular solution concepts. The coalition structure, called C, can be found as follows. Let $N = \{1, 2, ..., n\}$ be a set of players, $C \subseteq N$ be a subset of players in N, $Tv(|C|)$ be the value of cooperation among players in a coalition C, $\frac{Tv(|C|)}{|C|}$ be the value of each player in a coalition C which is an ascending function of the number of players in the coalition C, mv_i be the required minimum value of player i, and $Ts(|C|) = Tv(|C|) - \sum_{i \in C} mv_i$ be the surplus of cooperation among players in a coalition C. Then, let

$\beta = \{C \subseteq N : Tv(|C|) \geq \sum_{i \in C} mv_i\}$,
$\chi = \{C \in \beta : Ts(|C|) \geq Ts(|C^{'}|), \forall C^{'} \in \beta\}$,
$\ell = \{C \in \chi : |C| \geq |C^{'}, \forall C^{'} \in \chi\}$

Example 1. The purchasing office of a university obtains a discount on items purchased for all departments in the university. Consequently, when any departments in the university order the same item, the purchasing office combines these orders to purchase the item with a larger discount. Suppose some departments in the university want to purchase computers of a particular model. The price schedule for the particular model of computer is shown in Table 1. For instance, if three or four units are purchased, the unit price is $900 each. The departments' reservation prices, that is, the maximum price which a department is willing to pay for a unit of the particular model of computer, are shown in Table 2. For instance, the Economics Faculty wants to purchase a unit of the computer at $921 or less.

Let $U = \{u_1, u_2, ..., u_k\}$ be the set of departments in the university. A coalition C is a subset of the departments $C \subseteq U$ which can join together to purchase computer of a particular model with a larger discount. R_k is the reservation price of department u_k. $P(|1|)$ is the price that one needs to pay when he buys only one unit of the particular model of computer and $P(|C|)$ is the unit price of the particular model of computer when the computers are sold to the departments in coalition C. Let $RD_i = P(|1|) - R_i$ be the required minimum discount of

Table 1. The price schedule for a particular model of computer

Number of units sold	Unit price ($)
1	940
2	920
3-4	900
5-6	890
7-8	880
9-10	870

Table 2. Departments' reservation prices of this example

Department	R_k	RD_k
Economics Faculty (Econ)	$921	$19
Library (Lib)	$920	$20
Computer Center (Com)	$899	$41
Business Faculty (Bus)	$879	$61
Engineering Faculty (Eng)	$870	$70

Table 3. The total discount and the total required minimum discount of any subsets in these departments in this example

Coalition	$TD(\|C\|)$	$\sum_{i\in C} RD_i$	$TD(\|C\|) - \sum_{i\in C} RD_i$
{Econ,Lib,Com,Bus,Eng}	$(940 - 890) \times 5 = 250$	211	250-211=39
{Econ,Lib,Com,Bus}	$(940 - 900) \times 4 = 160$	141	160-141=19
{Econ,Lib,Com}	$(940 - 900) \times 3 = 120$	80	120-80=40
{Econ,Lib}	$(940 - 920) \times 2 = 40$	39	40-39=1
{Econ}	$(940 - 940) \times 1 = 0$	19	0-19=-19

department i, and $TD(|C|) = (P(|1|) - P(|C|)) \times |C|$ be the total discount of coalition C. We define β, χ and ℓ of this example based on the core theory.

$\beta = \{C \subseteq U : TD(|C|) \geq \sum_{i\in C} RD_i\}$,
$\chi = \{C \in \beta : TD(|C|) - \sum_{i\in C} RD_i \geq TD(|C'|) - \sum_{i\in C'} RD_i, \forall C' \in \beta\}$, and
$\ell = \{C \in \chi : |C| \geq |C'|, \forall C' \in \chi\}$

The coalition C is found as follows. First, we find the set β which is {{Econ, Lib}, {Econ, Lib, Com}, {Econ, Lib, Com, Bus}, {Econ, Lib, Com, Bus, Eng}}. Then, we find the set χ which is {{Econ, Lib, Com}}. The total discount and the total required minimum discount of any subsets in these departments are shown in Table 3. Finally, we find the set ℓ which is $\{\{Econ, Lib, Com\}\}$.

In summary, the number of departments in the coalition C is 3, and the purchasing office saves \$120 = (\$940 - \$900) ×3 in total for the university.

3 The Maximal Social Welfare Feasible Coalition Theory

3.1 Basic Terms

Let $N = \{1, 2, ..., n\}$ be a set of players, and $C \subseteq N$ be a subset of players in N.

Definition 1: The value of each player in a coalition C is an ascending function of the number of players in the coalition C. That is, $\frac{Tv(|C_1|)}{|C_1|} \geq \frac{Tv(|C_2|)}{|C_2|}$ if $|C_1| > |C_2|$, and $\frac{Tv(|C_1|)}{|C_1|} = \frac{Tv(|C_2|)}{|C_2|}$ if $|C_1| = |C_2|$ where $Tv(|C|)$ be the value of cooperation among players in a coalition C.

Definition 2: Let $Tv(|C|)$ be the value of cooperation among players in a coalition C. *An Allocation of Value in Coalition* C is defined as $(v_i)_{i \in C}$ such that $\sum_{i \in C} v_i \leq Tv(|C|)$, where v_i is *the allocated value of player* i.

Definition 3: Let v_i be the allocated value of player i. $(v_i)_{i \in C}$ is a *Feasible Allocation* if $\forall i \in C(v_i \geq mv_i)$, where $mv_i \geq 0$ is called *the required minimum value of player* i.

Definition 4: Let $Tv(|C|)$ be a value of cooperation among players in a coalition C, mv_i be the required minimum value of player i. The surplus of cooperation among players in a coalition C is defined as $Ts(|C|) = Tv(|C|) - \sum_{i \in C} mv_i$.

3.2 The Maximal Social Welfare Feasible Coalition Theory

In conventional coalitional game theory, *the core* [2] is one of the most important solution concepts. This theory selects a coalition that gives the maximal surplus of cooperation among players in a coalition C to give incentive for players not to leave the coalition if each player in a coalition completely knows all other players' information. However, the assumption is seldom practical in forming a coalition in the real word and the solution may decrease the value of cooperation among players in the coalition.

We define that a coalition is a *maximal social welfare feasible coalition* if (1) the value of cooperation among players in the coalition is more than or equal to the sum of the required minimum values of players in the coalition, (2) the coalition is the largest among such coalitions, and (3) the surplus of cooperation among players in the coalition is the highest among all these largest coalitions. We do not make the assumption that each player has complete information of all other players. Instead, we assume that each player's private information is not known to other players. Since all players' private information in the coalition is known by an honest coordinator and each player does not know other players' information, a coalition structure that give maximal value of cooperation among players is selected by the honest coordinator.

Without knowing other players' private information, each player is satisfied with a payoff that is higher than his minimum required value. *The maximal social welfare feasible coalition* is thus one in which there are maximum number of players receiving a satisfactory payoff in a Pareto optimal manner. An outcome

of players in a coalition is *Pareto optimal* if there are no choices of outcome which can make at least one player in the coalition better off, without making any other player worse off [3].

Definition 5: Let mv_i be the required minimum value of player i, $\rho = \{C_{max} \subseteq N : Tv(|C_{max}|) \geq \sum_{i \in C_{max}} mv_i\}$, $\lambda = \{C_{max} \in \rho : |C_{max}| \geq |C'_{max}|, \forall C'_{max} \in \rho\}$, and $\gamma = \{C_{max} \in \lambda : Ts(|C_{max}|) \geq Ts(|C'_{max}|), \forall C'_{max} \in \lambda\}$. Then, C_{max} is a *maximal social welfare feasible coalition* if and only if $C_{max} \in \gamma$.

We show existence of a Pareto optimal feasible payoff allocation of a coalition in this theory.

Theorem 1. *If $\gamma \neq \emptyset$ and $C_{max} \in \gamma$, then there exists a Pareto optimal feasible allocation $(v_i)_{i \in C_{max}}$ of coalition C_{max}.*

Proof. Consider the feasible allocation $X = (v_i)_{i \in C_{max}} = (mv_1, mv_2, ..., mv_{n-1}, Tv(|C_{max}|) - \sum_{i=1}^{n-1} mv_i)$. Therefore, X satisfies $\sum_{i \in C_{max}} v_i = Tv(|C_{max}|)$ and is consequently Pareto optimal. To prove that X satisfies $\forall i \in C_{max}, v_i \geq mv_i$, we only need to prove that $Tv(|C_{max}|) - \sum_{i=1}^{n-1} mv_i \geq mv_n$, or $Tv(|C_{max}|) \geq \sum_{i=1}^{n} mv_i$. Since $C_{max} \in \gamma$, therefore $C_{max} \in \rho$ and trivially $Tv(|C_{max}|) \geq \sum_{i=1}^{n} mv_i$.

Theorem 1 shows that the allocation of value in the coalition is a Pareto optimal. Then, we show a concept of a *maximal social welfare feasible coalition* in selecting members into a coalition.

Theorem 2. *If $D \subseteq N$, and $D \notin \rho$, then either there is no $C_{max} \subseteq D$ such that $C_{max} \in \gamma$, or there exists $C_{max} \subseteq D \backslash \{P_{highest}\}$ such that $C_{max} \in \gamma$ where $P_{highest} = argmax_{i \in D} mv_i$.*

Proof. Let $mv_{highest} \geq mv_{highest-1} \geq ... \geq mv_{lowest-1} \geq mv_{lowest}$ be the required minimum values of players $P_{highest}, P_{highest-1}, ..., P_{lowest-1}, P_{lowest}$ in D, respectively. Since $D \notin \rho$, therefore, $(Tv(|D|) - \sum_{i \in D} mv_i) < 0$, or $\sum_{i \in D} (\frac{Tv(|D|)}{|D|} - mv_i) < 0$. The term $(\frac{Tv(|D|)}{|D|} - mv_{highest})$ on the left hand side of the inequality is the smallest and must be negative. Denote $D^{(-1)} = D \backslash \{P_{highest}\}$, then we find that $\sum_{i \in D^{(-1)}} (\frac{Tv(|D^{(-1)}|)}{|D^{(-1)}|} - mv_i) \geq \sum_{i \in D \backslash \{P_j\}} (\frac{Tv(|D \backslash \{P_j\}|)}{|D|-1}) - mv_i, \forall j \in D$; that is, the set $D^{(-1)}$ has the highest $Tv(|D|) - \sum_{i \in D} mv_i$ among all subsets of D of size $|D| - 1$. Therefore, $D^{(-1)} \in \lambda$ if and only if $D^{(-1)} \in \gamma$. Next, if $\sum_{i \in D^{(-1)}} (\frac{Tv(|D^{(-1)}|)}{|D^{(-1)}|} - mv_i)$ is less than zero and $D^{(-1)} \neq \emptyset$, then we repeat this process until we find the smallest k such that the subset $D^{(-k)} \subseteq D$, of size $|D| - k$, satisfies $(Tv(|D^{(-k)}|) - \sum_{i \in D^{(-k)}} mv_i) \geq 0$; or $D^{(-k)} = \emptyset$. Note that for each $k' = 1, 2, ..., k$, the set $D^{(-k')}$ has the highest $Tv(|D|) - \sum_{i \in D} mv_i$ among all subsets of D of size $|D| - k'$. Therefore $D^{(-k')} \in \lambda$ if and only if $D^{(-k')} \in \gamma$.

If we find the smallest k such that the nonempty subset $D^{-k} \subseteq D$ that satisfies $(Tv(|D^{(-k)}|) - \sum_{i \in D^{(-k)}} mv_i) \geq 0$, $D^{(-k)} \in \rho$, then $D^{(-k)} \in \lambda$ because $D^{(-k)}$

is among the largest coalitions that satisfies $(Tv(|D^{(-k)}|) - \sum_{i \in D^{(-k)}} mv_i) \geq 0$. Consequently, $D^{(-k)} \in \gamma$, because $D^{(-k)} \in \lambda$ if and only if $D^{(-k)} \in \gamma$. The theorem is proved with $C_{max} = D^{(-k)} \in \gamma$ and $C_{max} \subseteq D \backslash \{P_{highest}\}$.

If we do not find the smallest k such that the nonempty subset $D^{(-k)} \subseteq D$ that satisfies $(Tv(|D^{(-k)}|) - \sum_{i \in D^{(-k)}} mv_i) \geq 0$, then there is no $C_{max} \subseteq D$ such that $C_{max} \in \gamma$, because if there is a $C^{'}_{max} \subseteq D$ such that $C^{'}_{max} \in \gamma$, where $|C^{'}_{max}| = |D| - l \neq 0$, then $C^{'}_{max}$ is a coalition of size $|D| - l \neq 0$ that satisfies $(Tv(|D^{(-l)}|) - \sum_{i \in D^{(-l)}} mv_i) \geq 0$. However, we know that $D^{(-l)}$ is the coalition that does not satisfy $(Tv(|D^{(-l)}|) - \sum_{i \in D^{(-l)}} mv_i) \geq 0$. Thus they are contradictions.

Theorem 3. *Given a set N of players, then either $N \in \gamma$; or if $N \notin \gamma$ then there exists $C_{max} \subset N$ and $C_{max} \in \gamma$ only if $C_{max} \subseteq N \backslash \{P_{highest}\}$, where $P_{highest} = argmax_{i \in N} mv_i$.*

Proof. We note that either $N \in \rho$ or $N \notin \rho$. If $N \in \rho$, then $N \in \lambda = \{N\}$ and hence $N \in \gamma$. Otherwise, if $N \notin \rho$, then by Theorem 2, either there is no $C_{max} \subseteq N$ such that $C_{max} \in \gamma$, or there exists $C_{max} \subseteq N \backslash \{P_{highest}\}$ such that $C_{max} \in \gamma$ where $P_{highest} = argmax_{i \in N} mv_i$.

Theorem 3 shows that if a set of players is not a member of γ, the set of players can become a member of γ by using a concept as follows. The player with the highest require minimum value is removed from the set of players one by one until the surplus of cooperation among players in the coalition is non-negative, or the set of players is empty. Then, if the set of players is not empty, the set of players is a member of γ. Otherwise, the set of players can not become a member of γ.

3.3 Example1 Revisited

Consider the scenario in Example 1 again.
We define ρ, λ and γ of this example based on *the maximal social welfare feasible coalition theory.*

$\rho = \{C_{max} \subseteq U : TD(|C_{max}|) \geq \sum_{i \in C_{max}} RD_i\}$,
$\lambda = \{C_{max} \in \rho : |C_{max}| \geq |C^{'}_{max}|, \forall C^{'}_{max} \in \rho\}$, and
$\gamma = \{C_{max} \in \lambda : TD(|C_{max}|) - \sum_{i \in C_{max}} RD_i \geq TD(|C^{'}_{max}|) - \sum_{i \in C^{'}_{max}} RD_i$,
$\forall C^{'}_{max} \in \lambda\}$

The coalition C_{max} is found as follows. First, we find the set ρ which is {{Econ, Lib}, {Econ, Lib, Com}, {Econ, Lib, Com, Bus}, {Econ, Lib, Com, Bus, Eng}}. Then, we find the set λ which is {{Econ, Lib, Com, Bus, Eng}}. Finally, we find the set γ which is {{Econ, Lib, Com, Bus, Eng}}.

In summary, the number of departments in the coalition C_{max} is 5, and the purchasing office saves \$250 = (\$940 - \$890) $\times$5 in total for the university. The total discount and the number of departments of the coalition in *the maximal social welfare feasible coalition theory* are larger than or equal to those in the core theory.

4 Evaluation

The primary aim of this theory is to generate the maximal value of cooperation among players in a coalition. This theory guarantees that a value of cooperation among player in a coalition in *the maximal social welfare feasible theory* is larger than or equal to that in the core theory.

Proposition 1. *Let* $\beta = \rho = \{C \subseteq N : Tv(|C|) \geq \sum_{i \in C} mv_i\}$,
$\chi = \{C \in \beta : Ts(|C|) \geq Ts(|C^{'}|), \forall C^{'} \in \beta\}$,
$\ell = \{C \in \chi : |C| \geq |C^{'}|, \forall C^{'} \in \chi\}$,
$\lambda = \{C_{max} \in \rho : |C_{max}| \geq |C^{'}_{max}|, \forall C^{'}_{max} \in \rho\}$,
$\gamma = \{C_{max} \in \lambda : Ts(|C_{max}|) \geq Ts(|C^{'}_{max}|), \forall C^{'}_{max} \in \lambda\}$
$C \in \ell$ be a coalition that is formed by using concepts of the core theory, and $C_{max} \in \gamma$ be a coalition that is formed by using concepts of the maximal social welfare feasible theory. We have $|C_{max}| \geq |C|$.

Proof (Number of players in a coalition). Let $C_{max} \in \gamma$ and $C \in \ell$. Therefore $C_{max} \in \lambda$ and $C \in \chi$. Since λ contains only all the largest coalitions in ρ, and elements of χ are all chosen from ρ as well, we have $|C_{max}| \geq |C|$.

Corollary 1. *Let $C \in \ell$ be a coalition that is formed by using concepts of the core theory, and $C_{max} \in \gamma$ be a coalition that is formed by using concepts of the maximal social welfare feasible theory. We have $\frac{Tv(|C_{max}|)}{|C_{max}|} \geq \frac{Tv(|C|)}{|C|}$.*

Proof. Since $|C_{max}| \geq |C|$ by Preposition 1, the Corollary follows trivially from the fact that $\frac{Tv(|\bullet|)}{|\bullet|}$ is an ascending function.

Proposition 2. *Let $C \in \ell$ be a coalition that is formed by using concepts of the core theory, and $C_{max} \in \gamma$ be a coalition that is formed by using concepts of the maximal social welfare feasible theory. We have $Tv(|C_{max}|) \geq Tv(|C|)$.*

Proof (Value of cooperation among players in a coalition). Since $|C_{max}| \geq |C|$ by Preposition 1, and by Corollary 1, $\frac{Tv(|C_{max}|)}{|C_{max}|} \geq \frac{Tv(|C|)}{|C|}$, therefore, $\frac{Tv(|C_{max}|)}{|C_{max}|} \times |C_{max}| \geq \frac{Tv(|C|)}{|C|} \times |C|$ or $Tv(|C_{max}|) \geq Tv(|C|)$.

Proposition 2 shows that there is a larger value of cooperation for all players in the coalition to share.

5 Conclusion

In this paper, we propose a new theory for forming a coalition known as *the maximal social welfare feasible coalitions*. The theory assumes that each player in a coalition does not know other players' information. It gives each player a payoff at least his minimum required value. Thus, it achieves the maximal value of cooperation among players in the coalition by forming a coalition that gives the number of players as large as possible (when the value of each player in the

coalition is an ascending function of the number of players). We show that the value of cooperation among players in a coalition in this theory is equal to or larger than that in the core theory and its payoff allocation of the coalition is Pareto optimal.

References

1. Aumann, R.J., Maschler, M.: The bargaining set for cooperate games. In: Advances in Game Theory (Annals of Mathematics Studies 52), pp. 443–477. Princeton University Press, Princeton (1964)
2. Gillies, D.B.: Solutions to general non-zero-sum games. In: Contributions to the Theory of Games 5 (Annals of Mathematics Studies 40), pp. 47–85. Princeton University Press, Princeton (1959)
3. Straffin, P. D.: Game Theory and Strategy. The Mathematical Association of America (1993)
4. Shapley, L.S.: A value of n-person games. In: Contributions to the Theory of Games 2 (Annals of Mathematics Studies 28), vol. 2, pp. 307–317. Princeton University Press, Princeton (1953)
5. Wilson, R.: Information, efficiency and the core of an economy. Econometrica 46, 807–816 (1978)
6. Yannelis, N.C.: The core of an economy with differential information. Economic Theory 1, 183–198 (1991)

Recommender Agent Based on Social Network

Heng-Li Yang and Hsiao-Fang Yang

Department of MIS, National Cheng-Chi University,
64, Sec. 2, Chihnan Rd., Mucha Dist, Taipei 116, Taiwan
{yanh, 94356507}@nccu.edu.tw

Abstract. Conventional collaborative recommendation approaches neglect weak relationships even when they provide important information. This study applies the concepts of chance discovery and small worlds to recommendation systems. The trust (direct or indirect) relationships and product relationships among customers are to find candidates for collaboration. The purchasing quantities and feedback of customers are considered. The whole similarities are calculated based on the model, brand and type of purchased product.

Keywords: recommender system, social network, chance discovery, trust.

1 Introduction and Related Work

Internet technology is changing day by day, and has becomes an important media channel of enterprises in the twenty-first century. By transcending the limits of time and space, electronic commerce (EC) has changed business marketing and people life-style. However, high growth rates are difficult to obtain in highly competitive and turbulent environments. Maintaining the loyalty of current customers and further attracting new customers are challenges for business.

To attract customers to purchase products, recommendation systems are often embedded into EC web sites [14]. Common approaches include content-based approach [2,6] and collaborative filtering [1,4,13,15,16]. The content-based approach analyzes the content of item description documents, compares customer profiles, then recommends highly-related items to the customer. InforFiner [5] and NewsWeeder [6] are some examples of content-based systems. This approach has some limitations, e.g., the difficulties of analyzing multimedia documents, generating serendipitous finding, and filtering items based on criteria other than those disclosed [16].

Collaborative filtering is an alternative approach, which recommends items that other similar users have liked. It calculates the similarity of users rather than the similarity of items. Ringo [16] is an collaborative filtering application for recommending music.

To judge similarity, some clusters of customers with the same characteristics (e.g., shared experiences, location, education or interests have to be found. However, this study argues that the clustering approach has some blind spots in. First, a customer might not trust the recommendations of customers in a cluster assigned by the system. Second, two customers in different clusters could still reference each other recommending *A* based on *B*'s preferences. This is the kernel spirit of chance

H.G. Okuno and M. Ali (Eds.): IEA/AIE 2007, LNAI 4570, pp. 943–952, 2007.

discovery: chances occur while mining low relationships but important information [9]. This study applies the idea of chance discovery to the recommendation approach.

However, the problem is locating these weak but important relationships. As shown in Fig. 1, relationships among customers of a commercial web site can be categorized into two groups. The first class of relationship, namely product, occurs because customers purchased the same product(s), e.g., the same model, brand or type. The second class of relationship is trust. Some previous studies have recommended trust-based recommendation systems [3,7,8,10,11,12]. For example, Pitsilis and Marshall [11,12] recommended establishing a direct trust link between two people with common experiences (i.e., purchased the same items), and deriving indirect trusts through a chain. Battiston et al. [3] suggested that when purchasing an item, consumers could query their neighborhood for recommendations. O'Donovan and Smyth [8] proposed a system that automatically infers trust values from ratings between users and movie producer. Massa et al. [7] suggested that consumer *A* could assert a trust statement toward *B* if *A* consistently found the product reviews and ratings of *B* valuable. Integrating the concepts of the above works, this study proposes checking the list of trustful customers, which are explicitly established by same customers. The listing of trustful customers might already exist before becoming the customers of the web. Alternatively, customers could provide names by searching product reviews or the forum discussions at this web site. People may consult the suggestions from others that they directly or indirectly trust when buying something.

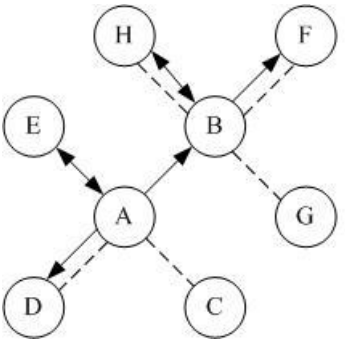

Fig. 1. Two kinds of networks among members: dotted line is product connection (purchase the same product), solid line is trust connection, A→B implies A trusts B

The number of relationships that should be consulted could be determined by the small world theory of developed by Watts [17]. The small world theory claims that the distance between any two people is no more than six degrees. People can be clustered into groups based on characteristics. A person may belong to several clusters simultaneously at the same time. Because of such overlap, a target person can be found by consulting only six persons. In the proposed model, the indirect trust listing could be constructed from the direct trust listing: *A* trusts *C* because *A* trusts *B*, and *B* trusts *C*. However, for efficiency, this study only considers three layers of trust.

The rest of this study is organized as follows. Section 2 explains the main idea of the proposed approach. Section 3 describes a scenario to explain how such an approach would help customers. Section 4 draws conclusions.

2 The Proposed Approach

The web site is assumed to maintain basic profiles of its members. The past year of detailed transaction data should be kept. A proper product type hierarchy should be maintained. These data enable the system to determine the product model, brand and type bought by each member. The granularity of type classification, fine or coarse, depends on management decisions. For example, the chain of ancestors of model "Nokia model N90" could be "Nokia model N-series", "Nokia 3G cellular phone", "3G cellular phone", "cellular phone", "telephone", "communication product", "electronic product". The website should also maintain the evaluation scores of bought products for each customer. If a customer bought a product for one month, then the website would e-mail him (her) to ask for his (her) evaluation score ("1" to "7"). The website might give some bonus to encourage the replies. If the customer did not reply within some specified period, then a default score "4" would be assigned.

Additionally, the trustfulness listing of each member is obtained. It could be established at the time that a person became the member of the website, and could be updated anytime later by the member. The website has a forum for customer discussions and product reviews. The persons on the trustful list are also members of the website. They may be friends before in real world or have become acquainted in the virtual world. Alternatively, customers could pick up the member names after reading their product reviews. A member could only provide five names (IDs) for all products, or could give five names for each product type. However, even if the website already had the name listing, the system would ask when a member requesting a recommendation to confirm his trust rating.

The proposed approach has two phases. Based on the two relationships mentioned above, the first phase searches all candidate persons with similar purchasing experience. The second phase calculates the similarities of each candidate, and recommends the candidate with the most similar experience.

2.1 Candidate Search Phase

As shown in Fig. 2, the first phase would attempt to find candidates from trust and product relationships. Users are then requested to clarify the recommendation task: specifying product model series (e.g., "Nokia N-series cellular phone", product brand (e.g., "Nokia 3G cellular phone") or product type (i.e., "3G cellular phone" or "cellular phone"). As shown in Fig. 3, at most three layers of trust are consulted. In the first derivative (i=1), the direct trustful list (five persons at most), is applied. The transitive trusts are derived from the direct trusts: the second derivative (i=2) consists of 25 persons at most, while the third derivative (i=3) consists of 125 persons at most. The expansions stop once any candidates are found. As shown in Fig. 4, when consulting with the trusted persons, the system checks whether these trusted persons have purchased any related product model (e.g., any "Nokia", "3G cellular phone" or "cellular phone" model) based on the product type hierarchy.

```
Procedure Search_Candidate

Step1: Initialize i=1 // i denotes the expanding times
of trustful relationship

Step2: Initialize TL0 and Candidate to be {} // TLi
denotes a trust list; TL0, the initial set, is empty;
Candidate store all candidates who purchased the
specified product

Step3: Set r as some specified product model series,
brand, or type specified by the user or automatically
recommended by the system.

Step4: Ask the user to confirm or provide the trustful
list TL1

Step5: Do while (i <= 3) and Candidate ={} // at most
search 3 derivatives of trust list

Setp6: Merge TLi-1 into TLi; sort the result, and delete
any duplicates

Setp7:   for k = 1 to length(TLi) // the number of
trusted name are length(TLi)

Step8(check-loop): for all sub-layers j of r in the
type hierarchy

Step9: if purchased (k,j) = true then insert k into
Candidate and exit the check-loop // k-th person
purchased

Step10:    end //end of steps 8-10 to check person k

Step11:   end//end of steps 7-11 to check persons in TLi

Step12:  i= i+1 // advance to next derivative

Step13:  end //end of steps 5-13, the while loop

Step14: End //end of the procedure
```

Fig. 2. The candidate search algorithm

If no candidate is found, then the system automatically relaxes the specification constraint to climb up one level of the type hierarchy, and calls the procedure *Search_Candidate* again. For example, if the website cannot find any trusted person who purchased “Nokia 3G cellular phone”, then it relaxes the constraint to “3G cellular phone”. If any candidate is found, after relaxing the constraints, then the system provides the information to the user, and discusses with the user whether to confirm such a constraint relaxation.

The procedure *Search_Candidate* has three loops. The outer loop (steps 5-13) is iterated at most three times. The middle loop (steps 7-11) is iterated 125 times in the worst case. The worst case of iteration in the inner loop (steps 8-10) depends on the

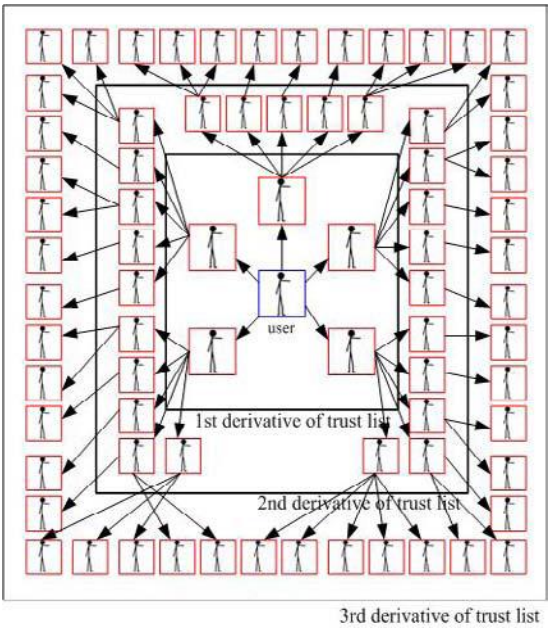

Fig. 3. The expansion of trustful list consultation

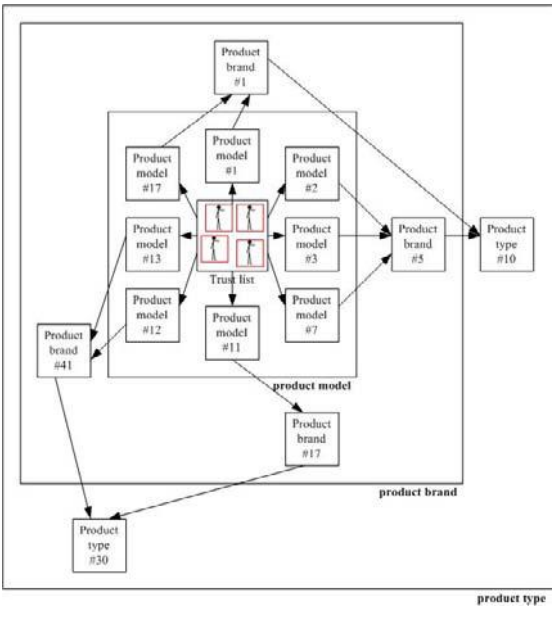

Fig. 4. The product hierarchy consultation

number of sub-items belonging to an item in the type hierarch. In the real case, this number is small. The merge-sort in Step 6 also takes a short time, because the maximal number of the list is only 125. Therefore, this algorithm is efficient with a good data structure.

The density of the social network is related to the performance of recommendation system [3]. If the network is dense enough, i.e., has "small-world" properties [17], then the recommender agent could reach all nodes in a few hops, enabling the customer to obtain a recommendation. This study ran a simulation by assuming 10 product types, where each type had 100 brands, each brand had 100 models, and there were 10000 members. Each member was given a purchasing record by randomly assigning the product models. Finally, the recommender agent was found to be able to give recommendations if each member had purchased two product models and provided one trusted member, or even better if they had purchased one product model and provided two trusted members.

2.2 Similarity Computation Phase

In the second phase, the website calculates the similarity between the query person and the candidates. The website would suggest the best product item evaluated by the person who is most similar to the query person. The similarity would be based on the whole purchase experiences — not only items, but also the quantities of the items, and the evaluation feedback from users. Furthermore, with regard to the product items, three levels (model, brand, primitive type) are considered together. The similarity of two users is certainly high if they purchased the same product models, but is also high even if they bought the same brands, but different models.

Assume that in the website the numbers of product model, brand and primitive types are M, B and T, respectively. The primitive types are those with one level higher than product brands in the type hierarchy. Additionally, suppose that the number of members is N. For efficiency, the website may periodically construct three feedback matrices, *FM*, *FB*, and *FT*. The dimensions of these matrices, *FM*, *FB*, and *FT* are $N \times M$, $N \times B$, $N \times T$, respectively. These matrices store the weighted average evaluation feedback scores of all members on all product models, brands and primitive types in this recent year, respectively. For example, if a user *u* purchased product model *d* three times, in quantities of 15, 20, 32, and gave the evaluation scores 6, 4, 5, respectively, then his weighed evaluation score on this product model is 4.9, i.e., (6*15+4*20+5*32)/67.

Formula (1), (2), (3) are used to compute the similarities between the query member *x* and any candidate *u* on the dimensions of product model, brand, and primitive type, respectively. Formula (4) determines the total similarity between these two users. The weighs *w1*, *w2*, and *w3* are applied to product model, brand, and type, respectively. If two persons bought the same product model, then they would buy the same brand and type consequently. Therefore, this study recommends assigning values such that $w1 > w2 > w3$. The max function would return the maximal values of all values of SM, SB, or ST.

$$SM(x,u) = \sum_{m=1}^{M} \left| FM[x,m] - FM[u,m] \right| \tag{1}$$

$$SB(x,u) = \sum_{b=1}^{B} \left| FB[x,b] - FB[u,b] \right| \tag{2}$$

$$ST(x,u) = \sum_{t=1}^{T} \left| FT[x,t] - FT[u,t] \right| \tag{3}$$

$$S(x,u) = w1 \times \frac{SM(x,u)}{\max(SM)} + w2 \times \frac{SB(x,u)}{\max(SB)} + w3 \times \frac{ST(x,u)}{\max(ST)} \tag{4}$$

3 A Scenario

A person, James, is currently unsure about what notebook he should purchase for his work. He has not used any notebook before. Additionally, he is not familiar with the technology market. He is worried about the notebook price, performance and future possible repair support. If he is a member of the website, then he can use it to help him choose a suitable notebook. The user could first browse the product items and read the descriptions on the website. Suppose that he has good previous impressions of IBM products and has become interested in the *Z*-series after reading the product descriptions. The IBM notebooks are available in several series, such as, *X*, *T*, *R* and *Z*. The *Z*-series has a number of models, such as *Z60t* and *Z60m*.

The user makes a recommendation request. The website first asks him to provide a list of names of trusted users, at most five members. If he cannot provide such a listing, then the website can only recommend the best *Z*-series model as evaluated by all of the members who had purchased before. Suppose that he provides the names of three members. In the candidate searching phase, the website checks whether these members have purchased any *Z*-series model. If no directly trusted member has such purchase records, then the system searches the indirect trustful member listings in at most two iterations. If neither direct nor indirect members have such experiences, then the website relaxes the constraints to set the search target to the higher level of product items (e.g., any series of IBM notebook). If the system can find any suitable candidate after relaxing constraints, then it gives the user a message such as "No members whom you trust directly or indirectly have purchased any IBM *Z*-series model notebook, but some have purchased IBM *R*-series models. Would you agree to relax your original constraints?"

If more than one candidate exists, then the system calculates the similarity, and recommends the purchase experiences of the candidate (say Tom), who was most similar to James from past experience. For example, the system would give the user a message such as "Based on the previous records, the system has found that among those your directly (or indirectly) trusted persons, as the whole, Tom, had purchase behaviors most similar to you. Among those IBM *Z*-series models, which Tom

purchased, he gave *Z60m* the highest feedback evaluation. Therefore, we suggest you consider *Z60m*". If James were a new member without any purchase records, then the system could not calculate the similarity. In that case, the system would suggest him the best *Z*-series model, which was evaluated by all of the members whom James trusted (of course, the directly trusted would be given first priority).

Figure 5 shows the GUI of a proposed recommendation system. On the left side, a user can browse product descriptions, input/modify trust lists and request recommendation via type hierarchy.

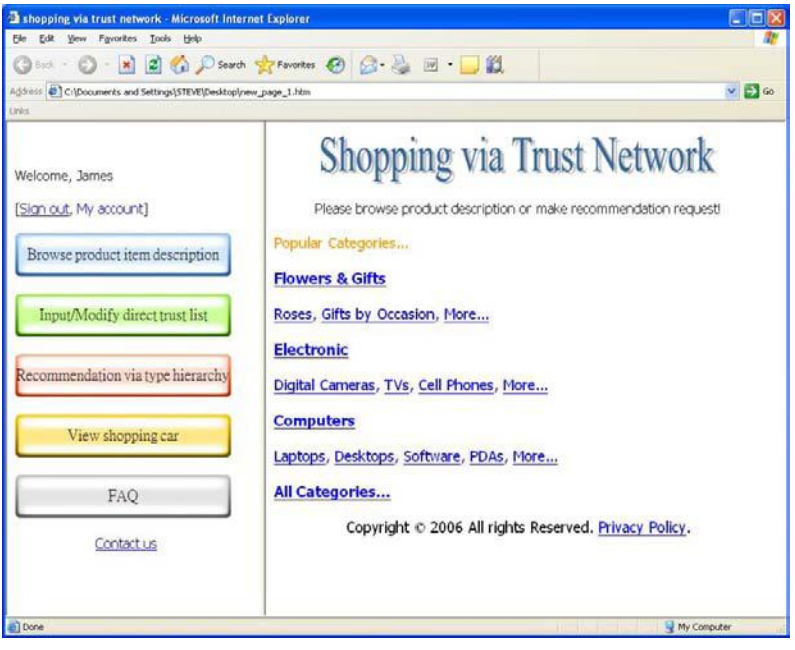

Fig. 5. The proposed recommendation system

4 Conclusions

Integrating the ideas of the literature, this study applies the ideas of chance discovery and small world to recommendation systems. The proposed approach has the following characteristics of our approach. (1)The explicit trust relationships are respected. The indirect trusts are derived beginning from the direct trust listing. The theory of chance discovery means that indirect trust relationships might imply low relationships, but provide important [9]. Watts [17] reported that in a world consisting of hundreds of thousands of individuals, every actor could be connected to every other actor within an average of less than six steps. This study uses three layers of trustful lists. Customers should feel comfortable because the consulted persons are within their trust networks, had all purchased the requested product, had the most similar purchasing experiences. Therefore, the recommender would pay attentions to

psychological status as well as the actual behaviors of the consumers. Suppose that a consumer John chooses a particular product brand because it has been purchased by Mary whom he trusts. However, upon consumption, he discovers that this brand does not match his taste and gives low evaluation feedback. In this case, the similarity score between John and Mary is lowered. John would be less likely to follow the recommendations of Mary the next time he goes shopping, although Mary remains in his list of trusted members. (2) In case the customer does not know any other members, he could pick up the professionals as the trusted persons after querying some of the product reviews and judging who are “best” buyers. Notably, trustful persons must first be selected to enable the customers to refer to their experiences. (3) The concept of product type hierarchy is used to allow the recommendation to climb up or drill down to search the "same" product purchases. The system relaxes the user's specification and provides more intelligent suggestions. (4) The similarities between customers are based on overall pictures of their purchase behaviors: purchasing quantities, feedback of customers, the whole chain of product model, brand, and type. Therefore, the similarity would be integrated and holistic. Future work will be to implement the proposed approach, and perform experiments to evaluate its performance.

References

1. Balabanovic, M., Shoham, Y.: Fab: Content-Based, Collaborative Recommendation. Communications of the ACM. 40(3), 66–72 (1997)
2. Basu, C., Hirsh, H., Cohen, W.: Recommendation as Classification: Using Social and Content-Based Information in Recommendation. In: Proceedings of AAAI Symposium on Machine Learning in Information Access (1998)
3. Battiston, B., Walter, F.E., Schweitzer, F.: Impact of Trust on the Performance of a Recommendation System in a Social Network. In: W Proceedings of the Fifth International Joint Conference on Autonomous Agents and Multi-Agent Systems (AAMAS’06). Hakodate, Japan (2006)
4. Goldberg, D., Nichols, D., Oki, B., Terry, D.: Using Collaborative Filtering to Weave an Information Tapestry. Communications of the ACM. 35(12), 61–70 (1992)
5. Krulwich, B., Burkey, C.: Learning User Information Interests through Extraction of Semantically Significant Phrases. In: Proceedings of the AAAI Spring Symposium on Machine Learning in Information Access (1996)
6. Lang, K.: Newsweeder: Learning to Filter Nnetnews. In: Proceedings of the 12th International Conference on Machine Learning, pp. 331–339. Morgan Kaufmann, San Francisco (1995)
7. Massa, P., Bhattacharjee, B.: Using Trust in Recommender Systems: An Experimental Analysis. In: Jensen, C., Poslad, S., Dimitrakos, T. (eds.) iTrust 2004. LNCS, vol. 2995, pp. 221–235. Springer, Heidelberg (2004)
8. Montaner, M., Lopez, B., de la Rosa, J.L.: Developing Trust in Recommender Agents. In: Proceedings of the First International Joint Conference on Autonomous Agents and Multi-agent Systems (AAMAS’02). Palazzo Re Enzo Italy, pp. 304–305 (2002)
9. Ohsawa, Y., McBurney, P.: Chance Discovery, Advanced Information Processing. Springer, Heidelberg (2003)

10. Pitsilis, G., Marshall, L.: Trust as a Key to Improving Recommendation System. In: Herrmann, P., Issarny, V., Shiu, S.C.K. (eds.) iTrust 2005. LNCS, vol. 3477, pp. 210–223. Springer, Heidelberg (2005)
11. Pitsilis, G., Marshall, L.: A Proposal for Trust-enabled P2P Recommendation Systems. Technical Report Series (CS-TR-910). University of Newcastle upon Tyne (2005)
12. O'Donovan, J., Smyth, B.: Trust in Recommender Systems. In: Proceedings of the 10th International Conference on Intelligent User Interfaces, pp. 167–174 (2005)
13. Resnick, P., Iacovou, N., Suchak, M., Bergstrom, P., Riedl, J.: GroupLens: An Open Architecture for Collaborative Filtering of Netnews. In: Proceedings of the ACM Conference on Computer Supported Cooperative Work, pp. 175–186. ACM Press, New York (1994)
14. Resnick, P., Varian, H.: Recommender Systems. Communications of the ACM 40(3), 56–58 (1997)
15. Sarwar, B., Karypis, G., Konstan, J., Riedl, J.: Item-based Collaborative Filtering Recommendation Algorithms. In: Proceedings International WWW Conference, pp. 285–295 (2001)
16. Shardanand, U., Maes, P.: Social Information Filtering: Algorithms for Automating 'Word of Mouth'. In: Proceedings of the Conference on Human Factors in Computing Systems (CHI95), pp. 210–217 (1995)
17. Watts, D.J.: Six Degrees: The Science of a Connected Age. W.W. Norton & Company, New York (2003)

A New Pooled Buying Method Based on Risk Management

Tokuro Matsuo

Department of Informatics,
Faculty of Engineering,
Yamagata University,
4-3-16, Jonan, Yonezawa, Yamagata, 992-8510, Japan
matsuo@yz.yamagata-u.ac.jp
http://veritas.yz.yamagata-u.ac.jp/

Abstract. In this paper, we handle a negotiation method in which a main negotiation consists of multiple sub-negotiations. In items allocation for commerce, there are some risks on the trade because the market balance is determined by supply and demand. The result of main negotiation is also determined by the order of sub-negotiations and agents' behaviors since agents' budgets have limitations on the actual commercial trading. However, it is difficult to decide the order of negotiations, such as simultaneous decisions and rotations. In this paper, we give the trading model in such cases, that is, agents purchase items by pooled buying. In actual trading as pooled buying, items are sold by the volume discount. Concretely, we discuss joint-stock company and private limited partnership on the web. In the negotiation phase, an agent proposes pooled buying based on the number of items and their prices considering their budgets. The degree of risks is calculated. All agents can see the risks with each item. Agents cooperate to the proposing agent based on the degree of risks. In this paper, we give two scenarios for trading. One is to avoid free riders who get surplus without risks. Another one is to promote agents' participation to increase social surplus. For risk aversion and promoting cooperation, we employ the side-payment policy, that is, cooperative agents' risks are preserved to a minimum. Further, we give some discussions where agents must pay the negotiation costs and charge for storage.

1 Introduction

In recent years, one of important research issues in agent-mediated negotiations is to support multiple users when users use the system such as e-commerce [1][4][5][6]. There are some researches concerned with negotiations and decision making for agents including multiple utility function-based negotiations, realistic decision support systems and several others. To solve the problems in many situations, most of researches should be integrated to support us as intelligent systems. In the most of agent researches, many B2C/C2C-based negotiations and trading methods are proposed as commercial activities like an agent-mediated auctions [2][7]. In this paper, we handle an integrated both B2B and B2C trading case where agents purchase items from sellers as pooled buying to sell the end buyers.

H.G. Okuno and M. Ali (Eds.): IEA/AIE 2007, LNAI 4570, pp. 953–962, 2007.

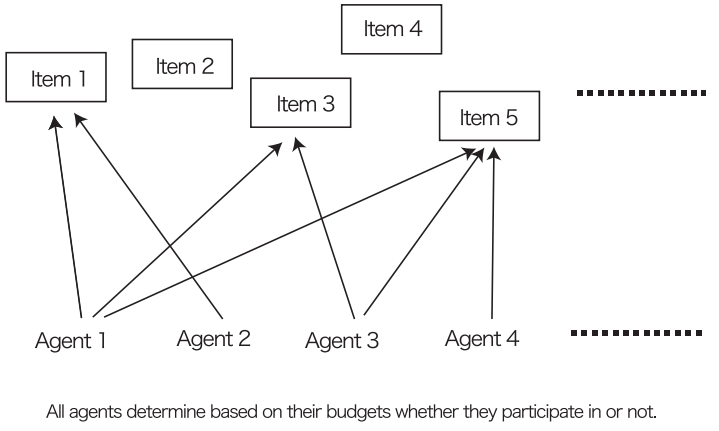

Fig. 1. Overview of the marketplace

Generally, in electronic commerce, agents who negotiate with other agents, have a certain limitation concerned with their budgets and they cannot spend money over their budgets. Using this realistic condition, we consider that one negotiation consists of multiple sub-negotiations such as pooled buying. Figure 1 shows an example in which multiple traders select items with cooperatively. Agents ante up to pay to purchasing at low price. All agents cannot determine whether they stock in the item or not without other agents' behaviors. For example, there are 3 items and each item's cost is $\{\$5, \$3, \$4\}$ and the market price of each item is $\{\$6, \$4.8, \$4.8\}$. When an agent's budget is 7 dollars and he/she gets the first item for five dollars, he/she cannot stock in the other items even though second and third items' surpluses are larger than the first item's surplus. Agent's utility is just $\$1$. On the other hand, if agent purchase items 2 and 3 with other agent's joint payment $\$1$, the agent's utility is $\$1.4$ and another agent's utility is $\$0.2$ even though we simply divide the surplus. Let me give more complex situations. In actual commercial activities, agents are sometimes cooperate with each other and make a collusion to purchase items at a low price. Moreover, when agents purchase items for pooled buying, a seller sometimes discounts the items' prices if a lot of items are traded. In these situations, an agent may not increase his/her total utilities even though he/she gets a lot of utilities in sub-negotiations. Concretely, we discuss the situation where multiple sole proprietorships exist in the marketplace. Although each agent's transaction volume is not heavy, agents can buy-in the items at a low price when they cooperate with each other. If all agents know players' preference distributions, the cooperation performs easily. However, it is difficult for agents to know other agents' preferences, values, intentions and strategies. Further, pooled buyers have some risks in which they stock in the items since the items might not be purchased by end-buyers. Cooperative agents might pin the blame for the dismal outcome on the proposing agent in actual tradings.

To solve the problems, we give a new negotiation process and property of our proposed issues. In our proposed pooled buying, first, an agent proposes buying-in of items to all agents who participate in the association. All agents can know the discount rates

with number of items. Agents who want to participate in the buying group declare to the proposing agent. Then, agents negotiate about allocations and costs. Agent a_i gathers money from agents who participate in the group. After that, items are allocated to the agents. Finally, each agent deals in the item of self-discipline. In this paper, we give two scenarios for trading. One is to avoid free riders who gets surplus without risks. Another one is to promote agents' participation to increase social surplus.

The rest of this paper consists of the following six parts. In Section 2, we show preliminaries on several terms and concepts of tradings. In Section 3, we give a simple trading model. In Section 4, we consider an example based on the trading model. In Section 5, we discuss and give a trading rule to modify the dry hole of tradings. Further, we give an experiment to compare between some cases and show related work. Finally, we present our concluding remarks and future work.

2 Preliminaries

In this section, we give some definition of model used in our proposed mechanism. There are agents who have multiple preferences based on their trading history. Here, we give the model for the mechanism.

2.1 Model

- Agent a_i is ith agent in a set of agents $\{a_1, ..., a_i, ..., a_n\}$ who participate in a trade.
- Seller b_j is jth seller in a set of sellers $\{1, ..., j, ..., m\}$ who sells items to an agent.
- Item j is an item sold by the seller b_j.
- C_h is an agent group formed as coalition. If agents $\{a_1, a_2, a_3\}$ participate in the group, C_h is $C_{\{a_1,a_2,a_3\}}$.
- π_{ij} is an expected price of item j for agent i when the agent deals in item j.
- $\mathit{\Pi}_{ij}$ is a cost price in which an agent stocks up items from sellers.
- p_{ij} is an actual price sold in the market.

Assumption 1. *All sellers can deal in the sets of items at price on volume discount.*

Assumption 2. *Each agent has enough money to purchase much number of items at one time.*

2.2 Overview

We consider a model about broking business and intermediate business on both B2B and B2C. Figure 2 shows the overview of the trading model of intermediate traders. The intermediate agent stocks in the item from sellers such as producers on the B2B. The items are sold to buyers on the price added some yields. However, in some cases, the agent might not have any ability of buying in the items because he/she is nothing but a small trader. If traders can cooperate with each other, they can get some opportunities for enlargement of the trading. In such case, multiple agents ante up to pay for stocking in the items form sellers. Then, how the items are allocated ?

We consider a simple case of the allocation by agent i and i'. The set of allocations is $X = \{(x_i, x_{i'})|x_i + x_{i'} = 1, x_i \geq 0, x_{i'} \geq 0\}$. x_i is the allocation to agent i and $x_{i'}$ is the allocation to agent i'.

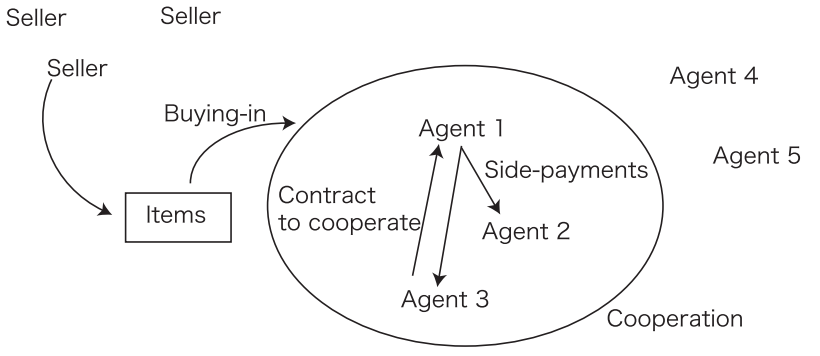

1. Agent 1 proposes buying-in the items.
2. Negotiation whether they stock-in the items or not.
3. Agents decides appropriate an allocation based on risk managements.

Fig. 2. Overview of trading

Number of items	Price
1 - 4	$ 7
5 - 9	$ 5
10 - 50	$ 4.5

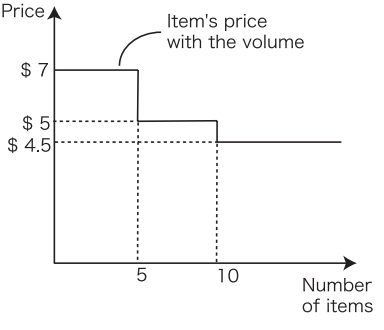

Fig. 3. Volume discount

2.3 Volume Discount

Volume discount is one of trading scheme used in some commercial situations. Company called as ”Co-op” employs volume discount trading based on number of items. Generally, when items increase sold in a trading, item’s price decreases. For example, in volume discount, item’s price is decided based on the number of items as shown in the Figure 3. If the buyer purchases each item individually, each item is sold for $7. When a buyer purchases 5 items simultaneously, the item is dealt in for $5. Trading in volume discount can provide items at a lower price compared with individual purchasing. Buyer’s utility is calculated as $35 - 25 = 10$.

3 Trading Model

In this section, we give a trading model for intermediaters.

3.1 Risk Management

In actual trading, items are not dealt in to the buyers on the expected price. Each item has a risk on the cost. Figure 4 shows an example of the graph of a risk function. The left figure in Figure 4 shows an example of reasonable price for general buyers. The right figure in Figure 4 shows an example of relationship of price and number of items purchased by buyers. When expected price π_{ij} is a lower price than item's price p_{ij}, items may end up on the shelf. If $p_{ij} > \pi_{ij}$, much number of items are sold comparing with above case. The inside area of the curve is the number of potential buyers who want to purchase the items. Thus, if item's price drops-off as the right figure in Figure 4, many items are purchased by buyers. When sellers deals in the items on the volume discount price, the stable solution is on the cooperations. However, it is difficult to know how agents should cooperate effectively.

Simply, we assume the following situation about the reasonable price and relationships between number of items and its price.

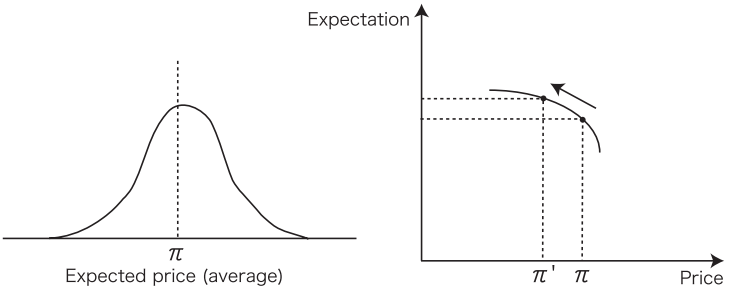

Fig. 4. Trading risks

3.2 Trading Scheme

The difference between general cooperation purchasing and the trading on this paper is the order of making a coalitions. In general volume discount, it is difficult for each agent to negotiate with each other. Agents must anticipate how many agents join in the group. If no agents participate in the cooperation group, the agent who declares an intention to purchase must purchase the items at an expensive rate. On the other hand, the cooperation of this paper gives the opportunity of negotiation with each agent. Based on the result of negotiations, agents can determine whether items are stocked in or not.

Then, What is the appropriate negotiation for this situation ? First, we consider the simple negotiation model except for the order of negotiations. We assume that agents make the traders association to cooperate when they stock in items.

Protocol
(1) Agent a_i proposes buying-in of items b_j to all agents who participate in the association. All agents can know the discount rates with number of items.
(2) Agents who want to participate in the buying group declare to agent a_i.
(3) Agents negotiate about allocations and costs.

(4) Agent a_i gathers money from agents who participate in the group.
(5) Items are allocated to the agents.
(6) Finally, each agent deals in the item of self-discipline.

Demand of items determines the risk if there are some items as shown in the area in Figure 5. Even though the distribution of expected price is different, the risk is shown as essentially same as the area. In microscopic point of view, the agent in which a lot of items are allocated may suffer latent losses. Thus, even though some agents participate in the buying group, the agent a_i who propose making coalition should be secure the remained items if no agent want to stock in a lot of items.

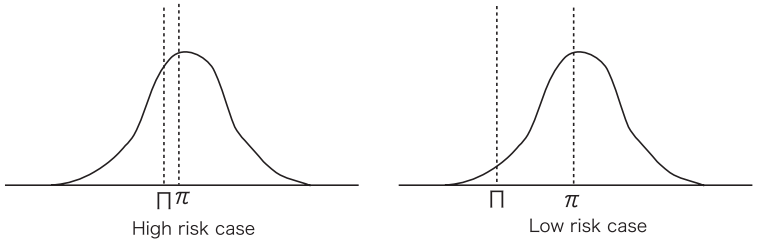

Fig. 5. Trading risks

4 Examples

First, we give a simple example of determination of price and allocations. Agent 1 proposes buying-in the item, which is sold for the price as same as Figure 3. In this case, we assume p in the Figure 3 is 1. Agent 1's budget is 7.5. Agent 2 declares that he/she can cooperate with agent 1's project. Agent 2's budge is 3. Here, if agent 2 does not participate in the group, agent 1 purchases 8 items for 7.2. Since agent 2 joins in the group ($C_{\{1,2\}}$), they can buy-in the items at the lowest price. Agent 2 can purchase 3 items for 2.4. Each items price for agent 1 is 0.8. Table 1 shows the total price of each case where agent 2 does not join in and he/she joins in.

Agent 1's risk reduce as $7.2 - 6.4 = 0.8$. Here, side-payment from agent 1 to agent 2 is calculated. It is determined in the value 0 to 0.8 because agent 1 can buy-in the item at low price for 0.8 comparing with individual purchasing.

Then, we give another example of generalized formations. There are n agents in the marketplace and a proposing agent is a_1. There is a seller who deals in the item for buyers' pooled buying. We assume, in this case, that only one item is sold for the

Table 1. Examples

	Number of items	Agent 2 does not cooperate	Agent 2 cooperates
Agent 1	8	0.9 * 8 = 7.2	0.8 * 8 = 6.4
Agent 2	3	-	0.8 * 3 = 2.4

price π. The seller gives an item's price level as $\{\Pi_{ij}^1, \Pi_{ij}^2, ..., \Pi_{ij}^k ..., \Pi_{ij}^{k'}\}$. Π_{ij}^1 is the cheapest price in the table like 3. Π_{11}^1 shows that item 1 is sold to the agent a_1 at the lowest price. The following shows the some situations on the cooperations.

- If $\Pi_{11}^k < p_{11}$, agent a_1 needs not searching for cooperative agents. However, agent a_1 can get more utilities if he/she can cooperate with agents holding $\Pi_{11}^1 < p_{11}$. In this case, agent a_1's expected utility is $p_{11} - \Pi_{11}^1$ without side-payments. Side-payments should be defined between 0 to $(\Pi_{11}^k - \Pi_{11}^1) * l$ (l is number of items whom cooperative agents can stock in).
- If $p_{11} < \Pi_{11}^k$, agent a_1 should make coalitions with other agents because expected utility is minus.

Then, we consider there are multiple items in the market-place. We assume there are 2 items $\{b_1, b_2\}$ and 3 agents $\{a_1, a_2, a_3\}$. Each item's price table is 2 levels, that is, for example, item b_1's price is $\{\Pi_{i1}^1, \Pi_{i1}^2\}$. Each agent has his/her budget. In this case, how agents cooperate with each other. If is difficult to determine allocations because each agent has a certain strategy to increase his/her utilities. If agent a_1's expected utility for item b_1 is $p_{11} - \Pi_{11}^1 > 0$ when he/she has enough amount of budgets, the agent may not propose cooperations because he/she can get the maximized utility. On the other hand, we consider agent a_1's budget has a limitation and he/she can not stock in the item at the lowest price. If agent a_1's expected utilities for item b_1 and b_2 are $p_{11} - \Pi_{11}^2 < 0$ and $p_{12} - \Pi_{12}^2 < 0$, agent a_1 should make coalitions with other agents. Otherwise, the agent never trades.

Under the above situation, we consider there is a certain distributions of expected price like Figure 4. If a relationship of expected price and cost price for item b_1 is $\pi_{i1} < \Pi_{i1}$, no agent proposes and cooperates because the expected utility is below zero. On the other hand, a relationship of expected price and cost price for item b_1 is $\pi_{i1} >> \Pi_{i1}$, agents can propose and cooperate easily. Here, we consider the case, that is, a relationship of expected price and cost price for item b_1 is $\pi_{i1} > \Pi_{i1}$. In this case, some agents may make a loss when each agent deals in the items. Agents who have a lot of items have a higher chance of making a loss even through the rate of selling items assumed on the uniformed distributions. There are less proposing agents like this situation. Most of agents might consider getting a lot of utilities with a low risk.

5 Discussion

5.1 Safty or Efficiency

In our protocol, there are 2 scenarios/options set up by a system manager, that is, the mechanism can avoid free riders who gets surplus without risks or can promote agents' participation to increase social surplus. If the manager employ our mechanism for secured e-commerce system, the former is selected. Otherwise, if the manager uses our mechanism to be an efficient marketplace, the latter is employed. Particularly, in the economical point of view, the latter is selected to increase traders' utilities.

Table 2. Result

	Individual Purchasing	Mechanism 1	Mechanism 2
Total Utilities	$1737	$1260	$2905

Avoiding Free Rider. In our mechanism, proposing agents must buy-in some number of items in which they selected. Moreover, if the proposing agents' payment amounts are decrease due to the participation of cooperative agents, they pay the sided-payment to the cooperator. In this situation, if all agents are rational, no agents propose their intentions to select and purchase items. They can increase their utilities to be a cooperative agent rather than to be a proposing agent. In this case, the allocation might never determine for a long, long time because free-rider agents can come off more gainers than proposing agents. Some agents may not propose the pooled buying. Instead, they participate in the cooperation to get the high utilities. Thus, we give one rule for trading to avoid free riders. Agents who participate in the marketplace must be proposing agents. If the agents propose purchasing items, they have rights to be cooperative agents. Further, agents propose simultaneously. When the negotiation should be conducted simultaneously in the mechanism, agents should give proposals of pooled buying to get item j, which is $\max(\pi_{ij} - \Pi_{ij})$ if there are not any risks. If agents are rational, they search for the allocations for pooled buying in which agents' utilities are maximum.

Efficiency. On another hand, if the system manager wants to hold the efficiency of trading. The simultaneous proposings from agents are removed. If agent can forecant that the items price goes down by participating other cooperative agents, proposing agents can propose the purchasing easily. Cooperative agent participate group buyings as funds permit sequentially. In this mechanism, the social surplus for agents increases.

5.2 Experiment

To show the difference between general volume discount, the mechanism for avoiding free riders, and the mechanism for efficiency, we conducted an experiment by a simulation. We prepares the three items and five agents. Each item has a price with number of items. In this experiment, we set that there are three sorts of price with the number of items. Each price is set up based on the uniform distribution from $\$1$ to $\$100$. First, the lowest price is defined. The middle rank of price is defined from the lowest price to $\$100$. Finally, the highest price is defined from middle price to $\$100$. Each agent's budget also set up based on the uniform distribution from $\$200$ to $\$1,000$. Market price of each item is defined as 2(the highest price) - the lowest price. We conducted 100 trial simulations. As the result, the averages of agents surplus show in Table 2 Mechanism 1 is the protocol of avoiding free riders and mechanism 2 is the protocol of increasing efficiency.

5.3 Related Work

In this section, we present an overview of the work of others related to our study.

eMediator [8] is an electronic commerce server and consists mainly of eAuctionHouse and eCommitter. eAuctionHouse is a configurable auction place that supports many auction types, while eCommitter is a leveled commitment contract optimizer that can solve the Nash equilibrium thresholds. The above systems do not handle volume discount.

GroupBuyAuction [9] is an agent-based electronic market on which agents automatically negotiate with each other on behalf of their users. In particular, in the GroupBuyAuction, buyer agents can form coalitions to buy goods at a volume discount price.

Li and Sycara considered an e-market where each buyer places a bid on a combination of items with a reservation cost, and sellers offer price discounts for each item based on volumes [4]. By artificially dividing the the reservation cost of each buyer among the items, optimal coalitions with respect to each item are constructed. These coalitions satisfy the complementarity of the items by reservation cost transfers, and induce the optimal solution.

The $BiddingClub$ [3] is proposed by Layton-Brown, Shoham and Tennenholtz. In the $BiddingClub$, agents conduct a pre-auction. After the pre-auction, monetary transfers take place.

The $G - Commerce$ [1] is an agent-mediated electronic commerce system which seller agents and buyer agents negotiate with each other. In the model, seller agents cooperatively negotiate in order to sell goods in stock. Buyer agents cooperatively form coalitions in order to buy goods based on discount prices. Seller agents' negotiations are completed by using an exchanging mechanism for selling goods. Buyer's multi-attribute preferences are not referred to in these researches.

Matsuo proposed the effective cooperation methods based on group buying [6]. Buyers cannot always purchase goods at a lower price, because buyers' sub-groups are distributed. Matsuo proposed three methods for group integration. First, buyers trades on simple group buying. Second, all buyers are integrated. Third, some buyers are integrated.

6 Conclusion

In this paper, we proposed negotiation mechanism where a certain negotiation consists of multiple sub-negotiations. In items allocation for commerce, there are some risks on the trade because the market balance is determined by supply and demand. The result of main negotiation is also determined by the order of sub-negotiations and agents' behaviors since agents' budgets have limitations on the real commercial trading. We also discussed joint-stock company and private limited partnership on the web. In the negotiation phase, an agent proposes pooled buying based on the number of items and their prices considering their budgets. If we employ the model based on same preference distributions among all agents, the allocation might never determine because free-rider agents can come off more gainers than proposing agents. On the other hand, we give some property under the realistic situations. In discussion, we give 2 types of protocols. One is to avoid free riders who gets surplus without risks. Another one is to promote agents' participation to increase social surplus. In experiments, avoiding free riders, social surplus decreases a lot of degrees.

Our future work includes how side-payments are calculated and determined. In real commercial activities, side-payments are one of most important issues to give incentives to cooperations among agents. Further, we apply our mechanism to the real electronic commerce marketplace.

References

1. Ito, T., Hattori, H., Shintani, T.: A cooperative exchanging mechanism among seller agents for group-based sales. The International Journal of Electronic Commerce Research and Applications (ECRA) 1(2) (2002)
2. Ito, T., Yokoo, M., Matsubara, S.: A combinatorial auction protocol among versatile experts and amateurs. In: Proc. of the 3rd International Joint Conference on Autonomous Agents and Multi-Agent Systems (AAMAS04), pp. 481–488 (2004)
3. Layton-Brown, K., Shoham, Y., Tennenholtz, M.: Bidding clubs: Institutionalized collusion in auction. In: the proceeding of the ACM Conference on Electronic Commerce(EC'00), pp. 253–259. ACM Press, New York (2000)
4. Li, C., Sycara, K.: Algorithms for combinational coalition formation and payoff division in an electronic marketplace. In: the proceedings of International Joint Conference on Autonomous Agents and Multi-agent Systems, pp. 120–127 (2002)
5. Matsuo, T., Ito, T.: A decision support system for group buying based on buyers' preferences in electronic commerce. In: the proceedings of the Eleventh World Wide Web International Conference (WWW-2002), pp. 84–89 (2002)
6. Matsuo, T., Ito, T., Shintani, T.: A buyers integration support system in group buying. In: the proceedings of EEE International Conference on Electronic Commerce Technology (2004)
7. Parkes, D.C, Ungar, L.H: An ascending-price generalized vickrey auction. In: The SITE Workshop on The Economics of the Internet (2002)
8. Sandholm, T.: emediator: A next generation electronic commerce server. In: Proceedings of the Sixteenth National Conference on Artificial Intelligence (AAAI99), pp. 923–924. AAAI Press, Stanford (1999)
9. Yamamoto, J., Sycara, K.: A stable and efficient buyer coalition formation 40 scheme for e-marketplaces. In: the proceedings of International Joint Conference on Autonomous Agents and Multi-agent Systems(AAMAS-2001) (2001)

The Representation of e-Contracts as Default Theories*

Georgios K. Giannikis and Aspassia Daskalopulu

Department of Computer and Communications Engineering,
University of Thessaly, Gklavani 37, 38221 Volos, Greece
{ggiannik,aspassia}@inf.uth.gr

Abstract. It is widely acknowledged that a temporal representation of e-contracts is essential in order to support e-contract execution and performance monitoring. One possibility that has been explored by many researchers is to represent e-contracts in Event Calculus. Although such representations are intuitive and facilitate temporal reasoning about actions/events and their factual and normative effects, they fall short in situations where domain knowledge cannot be assumed to be complete. Moreover, it is not clear how dynamic normative conflict resolution can be achieved, without resorting to unintuitive representations for conflict resolution strategies. In order to maintain the benefits of an underlying Event Calculus representation, and incorporate assumption-based reasoning and dynamic conflict management capability, we propose a representation of e-contracts as Default Theories, which are constructed by translating Event Calculus representations dynamically. Finally, we discuss how the resulting Default Theory representation enables a software agent to address various reasoning problems.

Keywords: Multi-agent systems, E-commerce, Reasoning with incomplete knowledge, Event Calculus, Circumscription, Default Logic, Default reasoning.

1 Introduction

This paper reports on work conducted within a broader project that is concerned with the development of open electronic markets. It is envisaged that such e-markets will be offering a variety of services to software agents, to seek potential partners, negotiate and establish agreements and subsequently monitor whether the business exchanges that they perform comply with the established agreements. During the conduct of a business transaction regulated by an e-contract, an agent will need to establish at a given time point, among other things:

(i) What state the business exchange is in, that is, given a history of events, what factual information is established and what norms are active for each party. This calls for some kind of temporal reasoning and reasoning about actions and their effects. Moreover, if the history of events is incomplete, or if the agent

* This work was supported by the European Commission and the Greek Secretariat for Research and Technology (PENED 2003 – 03EΔ466).

H.G. Okuno and M. Ali (Eds.): IEA/AIE 2007, LNAI 4570, pp. 963–973, 2007.

possesses incomplete domain knowledge, such reasoning will need to employ assumptions; should more information become available later, rendering some of these assumptions false, any conclusions drawn will need to be retracted. Hence, some kind of temporal default reasoning is required.

(ii) Whether normative conflicts arise for the agent, that is, whether it finds itself in a situation where it bears norms that it cannot fulfill simultaneously. In such cases, the agent needs some way to resolve such conflicts: perhaps resolution may be achieved through planning, where the agent can identify a course of action that makes it possible to fulfill all the norms it bears; alternatively resolution may amount to choice, where there is really no plan that could satisfy all the active norms. Then, the agent must accept that some violation is inevitable and the question for it is which norm to sacrifice. This kind of reasoning calls for some way to detect and manage normative conflicts.

In order to support temporal reasoning and reasoning about actions and their effects, many researchers (for example, [1, 2, 3, 4] among others) have adopted Event Calculus (EC) [5] for contract representation. However, EC representations cannot support assumption-based reasoning. In order to enhance the EC representation of an e-contract and support default reasoning one might use the Closed World Assumption (CWA) [6] or McCarthy's Circumscription [7], both of which seem problematic for our purposes. In the first case, under the CWA, an atomic formula is assumed false, unless it is known to be true. The agent using a (possibly incomplete) EC contract representation essentially admits into its knowledge base negative literals that correspond to assumptions it makes under CWA, about the falsity of certain atomic formulae. In many realistic scenarios, however, the agent will need to make assumptions about the truth of certain atomic formulae. In the second case, we might use Circumscription, a generalization of the CWA. Here, we use special predicates to denote abnormal (unexpected) events and effects of actions, and our inference strategy attempts to minimize abnormality. The agent essentially admits into its knowledge base explicit information about abnormality and the conclusions derived are those contained in the minimal models of the augmented knowledge base. Yolum and Singh [8] work in this direction. However, this approach presents some problems for realistic scenarios: First, it requires that we define abnormal events, effects of actions and the like, explicitly, and, also, that we explicitly distinguish each abnormal from other individuals. Second, in order to decide which individuals to characterize as abnormal, we are required to anticipate the conclusions that we want to be able to derive.

There are two other approaches to support default reasoning with e-contracts that do not, however, employ some underlying temporal logic. Grosof's SweetDeal [9] represents contract rules via Logic Programs. Governatori *et al.* [10] use Nute's Defeasible Logic [11] in their DR-Contract architecture. Both of these address conflict detection and management, by ascribing priorities to contract norms. However, the ascription of priorities is static, and hence, the agent's conflict handling mechanism cannot evolve and adapt as circumstances change. Finally, a third approach to e-contract representation is Paschke's ContractLog [12], developed for Service Level Agreements, which represents contracts via event-condition-action rules. ContractLog also adopts Nute's Defeasible Logic and conflict management is possible, again through the explicit, static, ascription of priorities to norms.

In order to maintain the benefits afforded by Event Calculus and address its limitations, we propose a representation of e-contracts in Reiter's Default Logic (DfL) [13], which may be constructed from an EC representation.

2 e-Contracts in Event Calculus

Consider a 3-party business transaction that takes place in an electronic marketplace populated by software agents. A retailer agent (RA) communicates with a wholesaler agent (WA) and establishes an agreement for purchasing a certain product. Consequently, WA communicates with a carrier agent (CA) and establishes another agreement for the timely and safe delivery of goods from WA to RA.

The first agreement (between RA and WA) is to be conducted on the following terms: WA should see to it that the goods be delivered to RA within 10 days from the date RA's order happens. RA, in turn, should see to it that payment be made within 21 days from the date it receives the goods. The agreement specifies sanctions in case the two agents do not comply with their obligations, but we do not need to refer to them explicitly here. In the same spirit, the second agreement (between WA and CA) defines obligations, deadlines and possible sanctions/reparations in case of violations.

Following [14], we may take an informal, process view of the business transaction that is regulated by the two agreements. Each state offers a (possibly partial) description of the factual and normative propositions that hold true in it. A transition between states corresponds to an event that takes place, i.e., an action that one of the parties performs or omits to perform. Initially, at time point T0, the transaction is in state S0 where the two agreements have been established and no events have occurred yet. If RA places an order at some time after T0, the transaction will move to a state S1, where WA is obliged towards RA to deliver goods within 10 days. Also, CA's obligation towards WA, to deliver goods to RA on WA's behalf within 10 days, is active. If CA delivers within the specified time bounds, then the business exchange will move to a state S2, where CA's obligation (and WA's obligation towards the RA for delivery, which is related to it) is successfully discharged, and RA's obligation towards WA to pay becomes active (as does WA's obligation to pay CA). If, when the transaction is at state S1, CA does not deliver on time, then the transaction will move to some state S3, where WA must compensate RA as specified by their agreement (and CA must compensate WA as specified by their agreement). In the same manner we may discuss other states of the business exchange.

To establish the state of the business exchange, given the actions that parties perform or omit to perform, we may employ a representation of the two agreements in Event Calculus [5]. The basic elements of the language are *time points*, *fluents* and *actions* or *events*. Fluents are factual and normative propositions whose truth-value alters over time, as a result of the occurrence of an action or an event. For our example we adapt the simple EC formalism presented in [15]. In its original form, the formalism does not distinguish between events that are brought about through agents' actions, and events that are brought about independently of the agents. We preserve the distinction and use the term 'action' to refer to the former, and 'event' to refer to the latter. We use terms, such as Order(agent1, agent2), for fluents that become true as a result of specific actions (here ordering AOrder(agent1, agent2)). We use terms of the form Op(agent1, agent2, action, time) for fluents that describe normative propositions and their

intended reading is "agent1 is in legal relation Op towards agent2 to perform action by time". The legal relation Op may be obligation, prohibition or permission; although these notions are typically formalized in some system of Deontic Logic, we merely use them as descriptive names for fluents, and do not adopt any specific Deontic Logic axiomatization. As [16, 2] note, the effects of an action apply only when the action is considered valid, and this, in turn depends on whether its agent has the legal and practical ability to perform it. An agent's legal and practical ability with respect to certain actions may be time-dependent, so we use the fluents IPower(agent, action) and PAbility(agent, action) respectively, and the fluent Valid(agent, action) to denote that an action performed by an agent is valid. We employ the six basic predicates of [15]; of those, Initiates and Terminates are used along with Happens in the specific description of a particular contract, to represent causal relations between fluents and actions/events. The other three are defined in domain-independent manner. We have modified the original definition of the HoldsAt predicate to take into account action validity, and have extended the Happens predicate to include the agent of an action as an argument (for events, though, we use the original form of Happens).

Table 1. Basic Event Calculus Predicates

Initiates(action, fluent, time) / Terminates(action, fluent, time)	fluent starts/stops to hold after action occurs at time.
Initiates(event, fluent, time) / Terminates(event, fluent, time)	fluent starts/stops to hold after event occurs at time.
HoldsAt(fluent, time)	fluent holds at time.
Happens(agent, action, time) Happens(event, time)	agent performs (instantaneous) action at time. event occurs (instantaneously) at time.
Clipped(time1, fluent, time2) / Declipped(time1, fluent, time2)	fluent is terminated/activated between time1 and time2.

Some of the domain-independent definitions are shown below:

$$\text{Clipped}(t_1, f, t_2) \leftarrow (\text{Happens}(a, act, t) \wedge t_1 \leq t < t_2 \wedge \text{Terminates}(act, f, t) \wedge \text{HoldsAt}(\text{Valid}(a, act), t))$$

$$\text{HoldsAt}(f, t_2) \leftarrow (\text{Happens}(a, act, t_1) \wedge \text{Initiates}(act, f, t_1) \wedge t_1 < t_2 \wedge \neg\text{Clipped}(t_1, f, t_2) \wedge \text{HoldsAt}(\text{Valid}(a, act), t_1))$$

$$\text{HoldsAt}(f, t_2) \leftarrow (\text{HoldsAt}(f, t_1) \wedge t_1 < t_2 \wedge \neg\text{Clipped}(t_1, f, t_2))$$

Note that the first definition for HoldsAt above reflects the establishment of a fluent as a result of an action, while the second one reflects the common sense law of inertia[1].

The specific representation of our example e-contract is given via the Initiates, Terminates and Happens predicates. Note that this information may be incomplete; this is a crucial point raising limitations for the EC representation and we shall return to it in the next section. For the moment, here is an extract of the EC representation for the agreement between RA and WA:

[1] Due to space restrictions, we do not show, here, the definitions of Declipped and of ¬HoldsAt, and the definitions of all the predicates with respect to event (rather than action) occurrence; a reader familiar with EC may easily see what form they take.

Initiates(AOrder(RA, WA), Obligation(WA, RA, ADelivery(WA, RA), time+10), time)←
Happens(RA, AOrder(RA, WA), time)

Initiates(ADelivery(WA, RA), Obligation(WA, RA, APayment(RA, WA), time+21), time)←
(Happens(WA, ADelivery(WA, RA), time) ∧
HoldsAt(Obligation(WA, RA, ADelivery(WA, RA), time′), time) ∧ time≤ time′)

Terminates(ADelivery(WA, RA), Obligation(WA, RA, ADelivery(WA, RA), time′), time)←
(Happens(WA, ADelivery(WA, RA), time) ∧
HoldsAt(Obligation(WA, RA, ADelivery(WA, RA), time′), time) ∧ time≤ time′)

Terminates(APayment(RA, WA), Obligation(RA, WA, APayment(RA, WA), time′), time)←
(Happens(RA, APayment(RA,WA), time) ∧
HoldsAt(Obligation(RA, WA, APayment(RA, WA), time′), time) ∧ time≤ time′)

3 Benefits and Limitations of the EC Representation

An EC representation of a contract allows us to establish what factual and normative fluents are true at a given time point, through appropriate queries on the HoldsAt predicate. For example, given a history of actions that record that RA placed an order at time T and that CA performed delivery at time T+4, we may infer that at a time point T′, after T+4, RA's obligation to pay WA by time T′+25 becomes active, as does WA's obligation to pay CA by whatever time is specified in the agreement between them. Such inference can be performed on other temporal frameworks (e.g. [17]) that have been developed for legal reasoning. This representation, though, presents several problems, which we discuss below, illustrating them with examples.

Inference Limitations: An agent may establish the factual and normative state of the transaction only in the presence of complete domain-specific information: if it does not have complete explicit causal knowledge (i.e., Initiates and Terminates relations), or a complete history of actions/events (i.e., Happens facts), or complete explicit knowledge about the validity of actions performed by agents, then it cannot derive certain conclusions. Yet, we can think of two reasons why it may be useful for an agent to be able to reason on a *hypothetical* basis.

First, the agent may wish to plan its future activities on the assumption that certain events/actions will occur, and that certain causal relations will be effected, or that its partners' actions will be valid, i.e., the agent has incomplete knowledge because it does not (indeed, cannot) know the future. For example, suppose that RA orders from WA at time point T. A reasonable query that RA might have is "when will I, potentially, have to pay for this order, assuming all goes well and I receive the goods in due time, so that I plan to have adequate available funds?" To derive an answer RA needs to perform *best-guess reasoning*. This may be achieved in EC, if the agent asserts any information it lacks at a given time point, and poses queries on the HoldsAt predicate for subsequent time points. These assertions may be viewed as analogous to assumptions that certain propositions are true. Note, however, that to perform best-guess reasoning in such a manner, the agent must know what assumptions are appropriate to make, and since these are determined by the desired conclusion, the agent must know *a priori* what conclusion it is hoping to derive. Also, making assumptions in this manner commits the agent to the truth of certain propositions, which is too strong a requirement; a more natural way to make assumptions would be for the agent to require that the assumptions are not inconsistent with its current knowledge.

Second, an agent may not know everything about the past and present, i.e., the history so far. Consider the case where, at time point T′, RA does not know that CA has performed delivery, yet it needs to plan its business activity so that it may be able to fulfill an obligation to pay WA in due time, should it later be informed that CA delivered at T+4. This situation corresponds to *no-risk reasoning*, i.e., an agent should be able to derive a conclusion even though this is based on assumptions, because alternatively it might find itself in an undesirable situation. One might argue that this case is not problematic, because we can insist that the history of actions/events be complete, for an agent to perform reasoning.

But, generally, is it reasonable to insist on complete domain-specific knowledge? An agent may not have complete information about all the circumstances under which it, and other agents, are practically and legally able to perform actions. Consider the case where RA knows that CA performed a delivery, and should, therefore, infer that its obligation to pay is active. Such inference requires that RA knows that CA's delivery is valid, i.e., that CA is practically and legally able to perform it. The fact that the product has been received may be taken as proof that CA is indeed practically able to perform delivery. But, how, without resorting to an assumption, can RA infer that CA is also legally empowered to perform delivery? It is, therefore, clear that an agent should be able to reason non-monotonically and establish potential conclusions on the basis of assumptions.

In EC, we may incorporate assumptions that refer to the occurrence of actions/events straightforwardly, through assertions. Assumptions that refer to causal relations, though, are tricky. It is impractical to require an agent to foresee all fluents that are established by the hypothetical occurrence of an action/event, even more so when there are exceptions. For example, consider the case where RA, on the assumption that it pays, wants to establish the conclusion that its obligation towards WA to pay is discharged. That is, RA also assumes that its action of payment terminates its obligation to pay. However, to be realistic, RA must foresee that this will be the case, provided that no abnormalities arise (e.g., provided that its intended on-line banking system works as expected, or that WA can receive the funds). RA essentially performs *prototypical reasoning* in assuming that normally, most instances of its payment action will terminate its obligation to pay. Even if RA could foresee all possible situations that would constitute exceptions to such a causal relation, it is debatable whether it would be able to establish each such condition, and so it would inevitably need to make assumptions. We could resort to Circumscription (as indeed others do, e.g. [8]), and only focus on particular kinds of exceptions of interest. This presents two problems: all abnormal individual cases must be explicitly distinguished from others so that potentially useful conclusions are not missed, and to choose the exceptions of interest one must know *a priori* what the desired conclusions are.

Conflict Management Limitations: The representation enables us to detect that an agent bears conflicting norms, again through queries on the HoldsAt predicate. For example, consider the case where two agents RA and RA′ have established separate agreements with WA[2]. Assume that RA and RA' order at times T and T' (T<T') respectively. Consequently, CA, bears two obligations for delivery at time T1, which is

[2] Let us assume that the terms of the agreements are identical, for convenience, so that we do not describe yet another contract; this assumption does not affect the discussion that follows.

after T'. If CA can perform only one action at a time, it has two conflicting obligations to satisfy. Somehow, CA should be able to infer a plan that might enable it to fulfill both of these obligations, if this is possible; if fulfillment of both obligations is not possible, CA has to choose which one to fulfil, based on some criterion. A reasonable way to resolve the conflict might be to prioritize the norms temporally, and meet the obligation that was initiated first, i.e., towards RA. The EC representation can be extended with appropriate rules for priority ascription that determine criteria for conflict resolution[3]. However, realistically, an agent might want to change its criteria over time, to adapt its conflict resolution strategy. For example, CA might normally prioritize its obligations to its customers temporally, unless some customer is considered privileged for some reason, in which case it is served first, regardless of the time it placed its order. In this case the priority that CA ascribes to the obligations it bears towards RA and RA′ should be rearranged dynamically. One might argue that priorities between norms can be treated as fluents in EC. This requires that they be viewed as action/event-driven, and this seems unintuitive to us.

The other approaches to normative conflict handling, mentioned in the introduction [9, 10, 12] use explicit priority assignment; [8] does not address conflict management — perhaps it can be extended to prioritized Circumscription, but this, again, would rely on explicit priority assignment.

To summarize, although EC representations for e-contracts are intuitive and facilitate temporal and causal reasoning, they fall short when domain knowledge may be incomplete. Moreover, it is not clear how dynamic conflict resolution strategies can be accommodated, without resorting to unintuitive representations.

4 e-Contracts in Default Logic

We propose a representation of e-contracts as default theories in Reiter's Default Logic [13] for various reasons: it is arguably the most notable formulation for default reasoning (cf. [18, 19]) and addresses general issues, such as negation by default, the frame problem and causal reasoning, satisfactorily. Also, it is suitable for prototypical, no-risk, and best-guess reasoning, all of which interest us.

A default rule (henceforth default) has the form $P:J_1,J_2,\ldots J_n/C$, where P is the prerequisite, $J=\{J_1,J_2,\ldots J_n\}$ is a set of justifications, and C is the derived consequent. The semantics of this rule is: If P holds and the assumption J is consistent with the current knowledge, then C may be inferred. Defaults of the form $P:C/C$ are called normal. A Default Theory (DfT) is a pair of the form (W, D), where W is a set of predicate logic formulae that represent currently available knowledge, and D is a set of defaults. A default is applicable to a deductively closed set of formulae $E \supseteq W$, iff $P \in E$ and $\neg J_1 \notin E,\ldots,\neg J_n \notin E$. The set E is the *extension* of the DfT. We consider closed default theories, and derive extensions in the manner presented in [18], i.e., by maintaining syntactically consistent sets of formulae.

[3] E.g. based on the temporal ordering of events and deadlines, or based on the normative strength of the particular conflicting norms, the severity of the penalty associated with the violation of each norm, etc.

An e-contract can be represented as a $DfT \equiv (W, D)$ by translating its EC representation. The currently available knowledge W is constructed from the domain-specific part of the EC representation, i.e., it contains all currently available information about HoldsAt, ¬HoldsAt, Happens, and causal relations Initiates and Terminates.

The set of defaults D of the theory is constructed from the domain-independent definitions of the EC representation, i.e., from the definitions for the predicates HoldsAt, ¬HoldsAt, Clipped and Declipped. The conclusion of each such definition is mapped to the consequent part of each default, while its conditions may be mapped to the prerequisite or the justification part of each default, depending on what information is defined in W: conditions that can be derived from W are mapped to the prerequisite, while conditions that cannot be derived from W are candidates for assumptions, and are mapped to the justification. That is, each EC domain-independent axiom does not correspond uniquely to a default. Although this may seem unsettling, it affords an agent flexibility in the construction of the DfT, as it can identify the set of candidate assumptions for its reasoning, dynamically, depending on the knowledge W it possesses. We present a more detailed example illustrating the various different defaults that may be obtained with varying W in [20], where no formal characterization of the construction of the DfT is given. Here we rectify this.

Let the EC representation of an e-contract be characterized as a triple (H, R, A), where H is a (possibly empty/incomplete) set of definitions for predicates H_L={Happens, HoldsAt, ¬HoldsAt}, R is a (possibly empty/incomplete) set of definitions for R_L={Initiates, Terminates}, and A is the (non-empty) set of Horn definitions for the domain–independent predicates A_L={HoldsAt, ¬HoldsAt, Clipped, Declipped}, that is, $A=\{Y \leftarrow X_1 \wedge \ldots \wedge X_k \mid Y \in A_L$ and $X_i \in A_L \cup H_L \cup R_L \cup T_L\}$. Note that T_L contains the first-order-logic predicates used to express temporal relations, i.e., $T_L=\{<, =, >, \geq, \leq\}$. The DfT of an e-contract is then (W, D), where $W=H \cup R$ and D contains, for each definition $(Y \leftarrow X_1 \wedge \ldots \wedge X_k) \in A$, (possibly semi-grounded) defaults of the form $P_1 \wedge \ldots \wedge P_n : J_1, J_2, \ldots J_m \; / \; C$, such that $n+m=k$ and $P_i = SUBST(\theta, X_i)$ if $W \vdash SUBST(\theta, X_i)$, $J_i = SUBST(\theta, X_i)$ if $W \nvdash SUBST(\theta, X_i)$, and $C=SUBST(\theta, Y)$.

To illustrate this, let us return to our example scenario. RA orders from WA at time point T, and let us assume that RA's current knowledge is:

W_{RA} ={ Happens(RA, AOrder(RA, WA), T),
Initiates(AOrder(RA, WA), Obligation(WA, RA, ADelivery(WA, RA), time+10), time)← Happens(RA, AOrder(RA,WA), time),
Initiates(ADelivery(WA, RA), Obligation(RA, WA, APayment(RA, WA), time+21), time)← (Happens(WA, ADelivery(WA, RA), time) ∧ HoldsAt(Obligation(WA, RA, ADelivery(WA, RA), time′), time) ∧ time≤ time′) }

RA constructs the following defaults, amongst others:

$$D1_{RA} \equiv \frac{\begin{array}{c}\text{Happens(RA, AOrder(RA, WA), T)} \wedge \\ \text{Initiates(AOrder(RA, WA), Obligation(WA, RA, ADelivery(WA, RA), T+10), T)} \\ \vdots \\ \neg\text{Clipped(T, Obligation(WA, RA, ADelivery(WA, RA), T+10), time2),} \\ \text{HoldsAt(Valid(RA, AOrder(RA, WA)), T),} \\ \text{T<time2}\end{array}}{\text{HoldsAt(Obligation(WA, RA, ADelivery(WA, RA), T+10), time2)}}$$

and

$$D2_{RA}\equiv \frac{\begin{array}{c}:\\ \text{Happens}(WA, \text{ADelivery}(WA, RA), time3),\\ \text{Initiates}(\text{ADelivery}(WA, RA), \text{Obligation}(RA, WA, \text{APayment}(RA, WA), time3+21), time3),\\ \neg\text{Clipped}(time3, \text{Obligation}(RA, WA, \text{APayment}(RA, WA), time3+21), time4),\\ \text{HoldsAt}(\text{Valid}(WA, \text{ADelivery}(WA, RA)), time3),\\ time3<time4\end{array}}{\text{HoldsAt}(\text{Obligation}(RA, WA, \text{APayment}(RA,WA), time3+21), time4)}$$

Now, RA is able to perform both no-risk and best-guess reasoning by employing these defaults. In the absence of information to the contrary, it assumes that its order is a valid action and that WA's obligation to deliver is not unexpectedly terminated. And on the assumption that WA's delivery will happen at some time point, and that such delivery will be valid, and that its effect will be an obligation for it to pay, and finally that such obligation will not be terminated by some other action, RA may infer what its potential payment period will be, relative to the time point of its assumption[4].

Remarks

An agent that derives conclusions on the basis of assumptions, by applying defaults, constructs the extension of its DfT incrementally. At each step i of the reasoning process, i.e. after the application of each default $P:J_1,\ldots,J_n/C$, the extension computed is a set of ground sentences $In(i)=In(i-1)\cup\{C\}$, and the set of assumptions employed, which should not turn out to be true, is $Out(i)=Out(i-1)\cup\{\neg J_1,\ldots, \neg J_n\}$. For the first step of the process, i.e. for $i=1$, $In(0)=W$ and $Out(0)=\varnothing$.

At first glance, this may seem to suggest that the agent computes possible world models that are counter-intuitive: for instance, in our example above, RA would compute, after applying $D1_{RA}$ and $D2_{RA}$, the extension

$$In(2)= W_{RA} \cup \{\ \text{HoldsAt}(\text{Obligation}(WA, RA, \text{ADelivery}(WA, RA), T+10), time2),\ \text{HoldsAt}(\text{Obligation}(RA, WA, \text{APayment}(RA, WA), time3+21), time4)\ \}$$

This extension seems to suggest that RA infers a possible version of the world, in which it bears an obligation to pay WA although no delivery from WA is explicitly recorded in this world, and similarly that WA bears an obligation to deliver, although this world does not explicitly record that RA's order is valid. This view of extensions, separated from assumptions, as possible world models is clearly undesirable. To overcome this problem which arises in "forward in time" temporal reasoning, Turner [21] suggests that all available knowledge about fluents that hold initially be represented as justification-free defaults of the form $\neg\text{HoldsAt}(fluent, T0) / False$; also, for each fluent of the domain, two prerequisite-free normal defaults are constructed of the form $: \neg\text{HoldsAt}(fluent, T0) / \neg\text{HoldsAt}(fluent, T0)$ and $: \text{HoldsAt}(fluent, T0) / \text{HoldsAt}(fluent, T0)$. In this way, Turner notes, "each fluent is either true or false in the initial situation, by forcing each consistent extension of the default theory to include, for each fluent, [either that it is true or that it is false]"; we agree that in this way, undesirable extensions are

[4] Naturally, if RA's initial knowledge contains less information (e.g. it is empty, or it only contains information about what initially Happens/HoldsAt but nothing about causal relations), the defaults that RA constructs are different from those shown above: they contain additional justifications and, consequently, fewer conjuncts in their prerequisites. Also note that the defaults are grounded before they are applied, and so the actual conclusions derived are also grounded. We show them here in semi-grounded form for generality.

eliminated, while assumption making is facilitated. It seems to us, though, that there is no need to resort to such a measure, since there is a simpler solution to the problem, offered by Schaub [22]: we may employ Constrained Default Logic and require joint consistency of default assumptions. The possible world model that the agent infers, in this view, is the consistent set $In(i) \cup \neg Out(i)$. This is tantamount to saying that the possible world models inferred by the agent contain both the consequents and the assumptions of the applied defaults.

Finally, we should note that Turner also suggests that domain-specific rules expressing causal relations be represented via defaults, so that reasoning "backwards in time" (i.e. temporal explanation) does not produce counter-intuitive results. We agree with him on this point, for the additional reason that it is likely that an agent may not have complete causal information or indeed any causal information at all!

5 Conclusions and Future Work

We discussed the benefits that an Event Calculus representation of e-contracts affords in order to support e-contract execution and performance monitoring, and noted its two main limitations with respect to inference and conflict management, in realistic scenarios, where agents reason with incomplete knowledge. We discussed the former in detail and argued for the construction of a default theory representation for an e-contract from its Event Calculus formulation. We do not present here a detailed account of how dynamic conflict management may be achieved by employing a representation in Default Logic; we refer an interested reader to our previous work [20]. Our current work focuses on the computational implementation of the default theory construction and its use for the computation of extensions: the DfT constructed by an agent relative to some currently available knowledge, may contain defaults that are prerequisite-free; if the agent applies these it may derive potential conclusions on a purely hypothetical basis. This may be undesirable in certain application domains, where we would prefer more cautious agents that, as much as possible, avoid purely or largely hypothetical conclusions. In these cases, perhaps the construction of the DfT must be interleaved with the reasoning process of the agent, to enable it to modify the defaults that it will employ, after it has revised its knowledge as a result of the application of some defaults.

References

1. Marín, R.H., Sartor, G.: Time and norms: A formalisation in the event-calculus. In: 7th International Conference on Artificial Intelligence and Law, New York, NY, USA, pp. 90–99. ACM Press, New York (1999)
2. Artikis, A., Pitt, J., Sergot, M.J.: Animated specifications of computational societies. In: 1st International Joint Conference on Autonomous Agents & Multiagent Systems, pp. 1053–1061. ACM Press, New York (2002)
3. Farréll, A.D.H., Sergot, M.J., Sallé, M., Bartolini, C.: Using the event calculus for tracking the normative state of contracts. Int. J. Cooperative Inf. Syst. 14, 99–129 (2005)

4. Rouached, M., Perrin, O., Godart, C.: A contract-based approach for monitoring collaborative web services using commitments in the event calculus. In: Ngu, A.H.H., Kitsuregawa, M., Neuhold, E.J., Chung, J.-Y., Sheng, Q.Z. (eds.) WISE 2005. LNCS, vol. 3806, pp. 426–434. Springer, Heidelberg (2005)
5. Kowalski, R.A., Sergot, M.J.: A logic-based calculus of events. New Generation Comput. 4, 67–95 (1986)
6. Reiter, R.: On closed world data bases. Logic and Data Bases 55–76 (1977)
7. McCarthy, J.: Circumscription - a form of non-monotonic reasoning. Artif. Intell. 13, 27–39 (1980)
8. Yolum, P., Singh, M.P.: Reasoning about commitments in the event calculus: An approach for specifying and executing protocols. Ann. Math. Artif. Intell. 42, 227–253 (2004)
9. Grosof, B.N.: Representing e-commerce rules via situated courteous logic programs in RuleML. Electronic Commerce Research and Applications 3, 2–20 (2004)
10. Governatori, G., Hoang, D.: A semantic web based architecture for e-contracts in defeasible logic. In: 1st International Conference on Rules and Rule Markup Languages for the Semantic Web, pp. 145–159 (2005)
11. Nute, D.: Defeasible logic. In: Gabbay, D., Hogger, C.J., Robinson, J.A. (eds.) Handbook of Logic in Artificial Intelligence and Logic Programming, Nonmonotonic Reasoning and Uncertain Reasoning, vol. 3, pp. 353–395. Oxford University Press, Oxford (1994)
12. Paschke, A., Bichler, M., Dietrich, J.: ContractLog: An approach to rule based monitoring and execution of service level agreements. In: 1st International Conference on Rules and Rule Markup Languages for the Semantic Web, pp. 209–217 (2005)
13. Reiter, R.: A logic for default reasoning. Artif. Intell. 13, 81–132 (1980)
14. Daskalopulu, A.: Modeling legal contracts as processes. In: Legal Information Systems Applications, 11th International Workshop on Database and Expert Systems Applications, pp. 1074–1079. IEEE Computer Society Press, Los Alamitos (2000)
15. Miller, R., Shanahan, M.: The event calculus in classical logic - alternative axiomatisations. Electron. Trans. Artif. Intell. 3, 77–105 (1999)
16. Makinson, D.: On the formal representation of rights relations. Journal of Philosophical Logic 15, 403–425 (1986)
17. Vila, L., Yoshino, H.: Time in automated legal reasoning. Technical Report ICS-TR-96-57 (1996)
18. Antoniou, G.: A tutorial on default logics. ACM Computer Surveys 31, 337–359 (1999)
19. Lifschitz, V.: Success of default logic. In: Levesque, H., Pirri, F. (eds.) Logical Foundations for Cognitive Agents: Contributions in Honour of Ray Reiter, pp. 208–212. Springer, Heidelberg (1999)
20. Giannikis, G.K., Daskalopulu, A.: Defeasible reasoning with e-contracts. In: IEEE/WIC/ACM International Conference on Intelligent Agent Technology, Hong Kong, China, pp. 690–694. IEEE Computer Society, Los Alamitos (2006)
21. Turner, H.: Representing actions in logic programs and default theories: A situation calculus approach. J. Log. Program. 31, 245–298 (1997)
22. Schaub, T.: On constrained default theories. In: 17th European Conference on Artificial Intelligence, pp. 304–308 (1992)

Competitive Ant Colony Optimisation

Marcus Randall

School of Information Technology
Bond University, QLD 4229, Australia
Ph: +61 7 55953361
mrandall@bond.edu.au

Abstract. The usual assumptions of the ant colony meta-heuristic are that each ant constructs its own complete solution and that it will then operate relatively independently of the rest of the colony (with only loose communications via the pheromone structure). However, a more aggressive approach is to allow some measure of competition amongst the ants. Two ways in which this can be done are to allow ants to take components from other ants or limit the number of ants that can make a particular component assignment. Both methods involve a number of competitions so that the probabilistic best assignment of component to ant can be made. Both forms of competitive ant colony optimisation outperform a standard implementation on the benchmark set of the assignment type problem, generalised assignment.

Keywords: heuristic search, ant colony optimisation.

1 Introduction

The premise of ant colony optimisation (ACO) is that cooperating agents each construct a single solution to a problem in a single iteration [4]. Cooperation (i.e., the sharing of information) is achieved implicitly via a pheromone mechanism. However, this should be balanced with more aggressive competitive strategies to realise greater search effectiveness. It is believed that this is in part may be achieved by allowing ants to compete amongst the members of the colony for the right to use specific solution components.

Merkle and Middendorf [10] describe another form of competitive behaviour for ACO. In their model, solutions (ants) within an iteration compete with one another to determine the relative strength with which they can update the pheromone repository for their individual component decisions. Working with the simple test permutation problem showed that the competitive control pheromone system could outperform a standard ACO implementation.

There have been some other attempts that have moved away from standard ACO algorithms and challenged the notion of always having a colony of constructive solution producing ants. The most notable of these are the hybrid ant systems. HAS-QAP (Hybrid Ant Systems for the QAP) uses pheromone information to manipulate complete solutions, applying standard local search

H.G. Okuno and M. Ali (Eds.): IEA/AIE 2007, LNAI 4570, pp. 974–983, 2007.

operators [7] rather than a constructive process. The local search operator used is to swap the facilities at two locations. The first location is chosen at random. The second is chosen such that either the combined pheromone levels of both locations are maximum (corresponding to exploitation) or probabilistically according to the second pheromone amount (exploration). Another hybrid ant system (for the sequential ordering system, HAS-SOP [6]) differs slightly from HAS-QAP. It retains the normal constructive component, but combines this with a sophisticated local search procedure that is tailored to the sequential ordering problem. Gambardella and Dorigo [6] found that this new ACO derivative outperforms one of the best available heuristics for the problem.

The paper is organised as follows. Section 2 describes assignment type problems with particular regard to the test problem, the generalised assignment problem (GAP) while Section 3 shows how ACO may be applied to this problem. Section 4 gives an account of how competitive ant colonies differ from standard versions of the algorithm. This description is given in terms of the GAP. Finally, Sections 5 and 6 give the computational results and conclusions respectively.

2 Assignment Type Problems

The competitive approaches described herein are particularly suitable for assignment optimisation problems. Therefore this paper focuses on solving the generalised assignment problem (GAP) as it is the prototypical assignment problem and very suitable for this first implementation. Costa and Hertz [3] refer to these problems as "Assignment Type Problems" (ATPs). These include such problems as graph colouring, quadratic assignment, set covering and generalised assignment.

2.1 ACO for ATPs

There has been a relatively small amount of work on using ACO based techniques specifically for ATPs. The major problems of this type that have been solved are graph colouring and GAP.

Lourenço and Serra [8] present hybrid meta-heuristic search techniques for solving the GAP. The two base meta-heuristics they use are greedy randomised adaptive heuristic (GRAH) and the ant system heuristic (ASH) – based on $\mathcal{MAX} - \mathcal{MIN}$ Ant System. Both of these have their native internal local search phases removed. The local search methods are replaced by descent and tabu search components having move and ejection chain neighbourhoods. A total of seven methods are tested which include the original $\mathcal{MAX} - \mathcal{MIN}$ Ant System and GRASP (greedy randomised adaptive search procedures). The methods are differentiated on constructive meta-heuristic, local search technique and neighbourhood operator. On the whole, the ant-based search techniques outperformed the greedy methods on small GAP instances.[1] In particular, ASH combined with

[1] These instances correspond to the problem sets gap1 to gap12 (5,15 to 10,60 jobs/agents) developed by Chu and Beasley [2].

tabu search based on ejection chains performed the best overall. A further exploration of ACO mechanisms for the GAP was undertaken by Randall [11]. This work examined the use of different component selection heuristics as well as local search strategies. It was concluded that provided there is a powerful local search mechanism, it is more important to select solution components (i.e., assignments of jobs to agents) based on satisfying capacity constraints rather than optimising the objective function.

Costa and Hertz [3] solve ATPs by generalised evolutionary approaches (based on ACO). The two parts of such generalised algorithms are the self adaptation phase and the cooperation phase in which members of a population build/modify a solution and learn from the other members respectively. Using ant colony optimisation, the authors could satisfactorily solve various instances of the graph colouring problem.

2.2 The Generalised Assignment Problem

The generalised assignment problem [9] is a problem in which jobs are assigned to agents for these agents to perform subject to capacity constraints. Each job may be performed by one agent only. The aim is to minimise the total cost of assigning the jobs to the set of agents. Equations 1-4 give the integer linear programming model of the problem.

$$\text{Minimise} \sum_{i=1}^{N}\sum_{j=1}^{M} c_{ij}x_{ij} \tag{1}$$

$$\text{s.t.} \sum_{i=1}^{N} a_{ij}x_{ij} \leq b_j \quad \forall j \quad 1 \leq j \leq M \tag{2}$$

$$\sum_{j=1}^{M} x_{ij} = 1 \quad \forall i \quad 1 \leq i \leq N \tag{3}$$

$$x_{ij} \in \{0,1\} \quad \forall i \quad 1 \leq i \leq N \quad \forall j \quad 1 \leq j \leq M \tag{4}$$

Where:

c_{ij} is the cost of assigning job i to agent j,
a_{ij} is the resource required by agent j to perform job i,
x_{ij} is 1 if job i is assigned to agent j, 0 otherwise,
b_j is the capacity of agent j,
M is the number of agents and
N is the number of jobs.

Benchmark problem instances are provided by Beasley [1]. In this study, large and tightly constrained instances are solved. These correspond to the A, B, C and D type problem sets and have the following definitions (reproduced from Chu and Beasley [2]):

Type A: a_{ij} are integers from $U(5,25)$, c_{ij} are integers from $U(10,50)$ and $b_i = 0.6(\frac{n}{m})15+0.4R$ where $R = \max_{i \in I} \sum_{j \in J, I_j = i} a_{ij}$ and $I_j = \min[i \mid c_{ij} \leq c_{kj}, \forall k \in I]$.

Type B: a_{ij} and c_{ij} are the same as Type A and b_i is set to 70% of the value given in Type A.

Type C: a_{ij} and c_{ij} are the same as Type A and $b_i = 0.8 \sum_{j \in J} \frac{a_{ij}}{m}$.

Type D: a_{ij} are integers from $U(1,100), c_{ij} = 111 - a_{ij} + e$ where e are integers from $U(-10,10)$ and $b_i = 0.8 \sum_{j \in J} \frac{a_{ij}}{m}$.

where $U(a,b)$ represents a uniform random number, I is the set of agents and J is the set of jobs. Note that n and m correspond to N and M respectively given in Equations 1-4.

As can be seen from the above, each problem type is more tightly constrained than the preceding problem type. Each category of problem instances ranges in size from 5 agents, 100 jobs to 20 agents, 200 jobs.

3 Applying Standard ACO to ATPs

The algorithm described here follows the ant colony system (ACS) implementation of the ACO meta-heuristic. The GAP is used to illustrate the algorithm mechanics. In discrete time steps, allow each ant to uniquely assign agents to successive jobs until all have been allocated. After adding a job to the solution, the amount of pheromone on the job-agent assignment is modified. Pheromone is a scalar quantity that allows ants to communicate with one another about the utility of assigning an agent to a job. The accumulated strength of pheromone of job i and agent j is denoted by $\tau(i,j)$. The heuristic measure of the suitability of assigning agent j to job i is given by $\eta(i,j)$. This could either correspond to the resource (the a matrix) or the cost (the c matrix) of assigning agent j to job i.

At the beginning of each time step, Equation 5 is used to select agent j for job i. The agents that ensure that the partial solution satisfies the capacity constraints are given by the set $J_k(i)$, where k represents the ant and i is the job/step. If $J_k(i)$ becomes an empty set at any step of an iteration (i.e., there is no agent to which job i can be assigned, as they do not have sufficient capacity), ant k terminates. It is no longer considered for the duration of the iteration.

Equation 5 is a selection technique that favours the best combination of pheromone level and the heuristic measure. In order to allow for other combinations of agents and jobs, Equation 6 selects the agent probabilistically. This is essential to avoid premature convergence to a small group of elite solutions. The use of each equation is governed by the q_0 parameter. q is a uniform random number that is generated at each step of the ACS process. β governs the relative importance of the heuristic. It is set as a negative value for minimisation problems such as the GAP.

$$j = \begin{cases} \arg\max_{s \in J_k(i)} \left\{ \tau(i,j)[\eta(i,j)]^{\beta} \right\} & \text{if } q \leq q_0 \\ \text{Equation 6} & \text{otherwise} \end{cases} \tag{5}$$

$$p_k(i,j) = \begin{cases} \frac{\tau(i,j)[\eta(i,j)]^\beta}{\sum_{u \in J_k(i)} \tau(i,u)[\eta(i,u)]^\beta} \text{ if } j \in J_k(i) \\ 0 \qquad\qquad\qquad\qquad\quad \text{otherwise} \end{cases} \tag{6}$$

The pheromone level of the selected agent for a particular job is modified according to the local updating rule in Equation 7 (while the other pheromone values are left unaltered). The equation slightly decreases the amount of pheromone on the job-agent combination so that ants have a measure of diversity between their solutions within a particular colony.

$$\tau(i,j) \leftarrow (1-\rho) \cdot \tau(i,j) + \rho \cdot \tau_0 \tag{7}$$

Where:

ρ is the local pheromone decay parameter, $0 < \rho < 1$,
τ_0 is the initial pheromone amount,
i is the job and
j is the agent.

Lourenço and Serra [8] initialise the pheromone level as $\tau(i,j) = \frac{1}{c_{ij}}$, where i is the job and j is the agent. Once all ants have assigned an agent to each job and have hence completed an iteration of the algorithm, the components of the best solution are rewarded with an increase in their pheromone level while other component values are decayed/evaporated (Equation 8).

$$\tau(i,j) \leftarrow (1-\gamma) \cdot \tau(i,j) + \gamma \cdot \begin{cases} \frac{Q}{L} \text{ if } (i,j) \in S \\ 0 \quad \text{otherwise} \end{cases} \tag{8}$$

Where:

γ is the global pheromone decay parameter, $0 < \gamma < 1$,
L is the cost of the best solution found to date,
Q is a constant [5] and
S is the set of job-agent pairings of the best solution found since the beginning of the optimisation process.

4 Competitive Ants

In traditional ant colony meta-heuristics, ants are treated as cooperative agents that generate solutions to solve combinatorial optimisation problems. To increase solution quality, it is possible to allow ants to compete for solution components. This will increase the likelihood that the final assignments of components will optimise the objective function. Two approaches to achieve this are outlined.

Compete 1: Ants creating partial solutions: In assignment type problems, a solution value is typically assigned to a group. For the GAP each job is assigned to only one agent. Therefore allow each ant in the colony to

represent a single agent (corresponding to a partial solution). The combination of the ants' partial solutions gives a complete solution. Defining ants in this way allows them to compete for component values (i.e., jobs). Thus in terms of the target application, the number of ants would equal the number of agents (M).

At each step of the revised algorithm, each ant chooses a component value to assign to its group (e.g., a job to an agent). In the first instance an ant evaluates all solution components to work out the best value at this time. This component value must be drawn from either the unallocated values or from those that have been assigned to other ants/agents. In the case of the latter, the ant cannot just reallocate the value to itself. It must be won by means of a competition between the two ants. Given that k represents the current ant/agent and v is the agent to which the job belongs. The probability of ant k winning the competition is given by Equation 9. Of course, the probability of ant/agent v retaining the job is $(1 - p_k)$.

$$p_k = \frac{\tau_{kj} \times c_{kj}}{(\tau_{kj} \times c_{kj}) + (\tau_{vj} \times c_{vj})} \tag{9}$$

Where:

τ_{ij} is the pheromone strength on the assignment of ant/agent j to job i and

c is as defined in Section 2.2.

A uniform random number is then generated to determine the winner. If the original ant wins, it keeps the component and the current ant must go through the process again with the next value on its list. Conversely, the value is reassigned to the current ant and the next ant is then allowed to select a component. If an ant at any stage is unable to choose a value (because it does not have the spare capacity to accommodate any assignable value), nothing is assigned. In case of the GAP, this allows agents to have variable length job lists while ensuring they utilise the available capacity. The pseudocode for one iteration is given in Algorithm 1.

Compete 2: Ants competing for solution component assignments: Ants that construct full problem solutions may also use the idea of competition. In the case of ATPs, competition can be used to achieve intra-colony diversification (see Randall [12]) by restricting how often an assignment can be made between the ants. For instance, a particular job and agent combination may be permitted to be used by more than one ant (in a single iteration) with a given probability.[2] If this fails and the current ant is not automatically allowed to make the assignment, a competition for it (as per Equation 9) must be held. The competition is between the current ant and the ant for which the assignment is of the highest cost (i.e., the weakest ant). The loser will be given a blank assignment instead. At the end of each

[2] In the experiments, the probability is given as $\frac{1}{n}$ where n is the number of the same assignment across the other ants.

Algorithm 1. The competitive ant colonies algorithm

```
1: while the size of the unallocated pool is not 0 do
2:   for each ant do
3:     Generate the candidate list of components a in decreasing order of fitness
4:     while a component is not chosen and a is not exhausted do
5:       v = Choose a candidate component value from a
6:       if v is part of another ant's partial solution then
7:         if the current ant wins the competition for v then
8:           Add v to the current ant's partial solution
9:           Remove v from the former ant
10:        end if
11:      else
12:        Remove v from the unallocated pool
13:      end if
14:    end while
15:  end for
16: end while
```

iteration, jobs that have a blank assignment will be allocated an agent by a greedy heuristic. This heuristic and the competitive mechanism add very little computational overhead to the algorithm.

4.1 Local Search

As with all ant colony techniques, it is unlikely that the constructed solutions of the colony will be locally optimal, thus a form of descent or local search is necessary. The two local search operators that have been found to be effective for ACO and the GAP [11] are:

`swap`: Given two jobs, the agent assignments of the two jobs are swapped.
`change`: The agent of a particular job is changed to another agent.

Exhaustive neighbourhood searches, terminating when an improved solution cannot be obtained, can be used for both operators.

5 Computational Experiments

The computing platform used to perform the experiments is a 3GHz Pentium 4 based PC. Each problem instance is run across ten random seeds. The experimental programs are coded in the C language and compiled with `gcc`. Ant Colony System (ACS) [5] is used as the ACO meta-heuristic. The ACS parameter settings are given by the set $\{\beta = -2, \gamma = 0.1, \rho = 0.1, m = 10, q_0 = 0.9\}$. These values have been found to be robust by Dorigo and Gambardella [5]. The test suite of problems is the large-sized set of Chu and Beasley [2].

Both of the new solvers and a standard implementation are run using local search based on swap and change neighbourhoods (see Section 4.1). The standard

Table 1. Cost results of running the three solvers. These are represented as relative percentage differences (RPDs) from the optimal cost. RPD is given as $\frac{a-b}{b} \times 100$ where a is the best cost achieved in a run and b is the optimal cost of the problem instance. Note that 'Min', 'Med' and 'Max' denote minimum, median and maximum respectively. Bolded items indicate the best result for the combination of problem and measure.

	Optimal	Compete 1			Compete 2			Control		
Problem	Cost	Min	Med	Max	Min	Med	Max	Min	Med	Max
A5-100	1698	**0**	**0**	**0**	**0**	**0**	**0**	**0**	**0**	**0**
A5-200	3235	**0**	**0**	**0**	**0**	**0**	**0**	**0**	**0**	**0**
A10-100	1360	**0**	**0**	**0**	**0**	**0**	**0**	**0**	**0**	**0**
A10-200	2623	**0**	**0**	**0**	**0**	**0**	**0**	**0**	**0**	**0**
A20-100	1158	**0**	**0**	**0**	**0**	**0**	**0**	**0**	**0**	**0**
A20-200	2339	0.04	0.04	**0.04**	**0**	**0**	**0.04**	**0**	**0**	**0.04**
B5-100	1843	**0.43**	**0.71**	**0.92**	0.65	1	1.14	3.36	4.72	6.02
B5-200	3553	**0.51**	**0.65**	**0.79**	0.53	0.66	0.87	0.73	0.89	1.04
B10-100	1407	0.07	0.28	0.43	**0**	**0**	**0.07**	0.07	0.14	0.36
B10-200	2831	1.31	**1.45**	1.66	**1.27**	1.54	**1.62**	1.38	1.7	2.08
B20-100	1166	0.69	1.03	1.11	0.34	**0.6**	**0.77**	**0.26**	0.69	0.94
B20-200	2340	0.64	0.75	0.81	**0.43**	**0.56**	**0.64**	0.51	0.68	0.81
C5-100	1931	**0.31**	**0.57**	**0.73**	0.67	0.85	1.04	0.62	1.09	1.35
C5-200	3458	0.52	0.67	0.81	**0.35**	**0.64**	**0.75**	0.49	0.78	1.01
C10-100	1403	1.14	1.43	**1.57**	**0.93**	**1.18**	**1.57**	1.5	1.75	2.07
C10-200	2814	**0.92**	**1.33**	**1.46**	1.39	1.58	1.78	1.46	1.74	1.92
C20-100	1244	1.69	1.89	2.49	**0.88**	**1.17**	**1.53**	1.53	1.65	2.25
C20-200	2397	1.63	1.98	2.13	**1.34**	**1.81**	**2**	1.88	2.07	2.17
D5-100	6373	**1.99**	**2.38**	**2.51**	2.97	3.21	3.4	3.36	3.88	4.14
D5-200	12796	**2.31**	**2.5**	**2.79**	3.17	3.26	3.39	3.4	3.56	3.74
D10-100	6379	**3.45**	**3.66**	**3.87**	4.04	4.37	4.61	4.33	4.45	4.73
D10-200	12601	**2.77**	**3.02**	**3.18**	3.56	3.84	3.95	3.4	3.92	4.03
D20-100	6269	**3.51**	**3.55**	**3.96**	3.53	3.88	4.15	3.73	4.07	4.4
D20-200	12452	**3.17**	**3.48**	**3.7**	4.09	4.26	4.41	4.14	4.33	4.49

implementation of ACS (herein referred to as 'control') is the same used in Randall [11]. The two solvers for which ants complete full solutions used three thousand iterations per run. As the other competitive approach only produces one solution per iteration, a larger number of iterations (twenty thousand) are allotted to it per run as being roughly equivalent. A Kruskal-Wallis comparison will be used to determine if there is any discernable difference in solution quality across the approaches.

5.1 Results

The results of running the three solvers are given in Table 1 and graphically in Figure 1. Three trends from this table are evident. All solvers can more or less solve the A type instances to optimality. Compete 2 often finds the best solutions to the middle B and C problems. Compete 1, however, consistently find better solutions on the tightly constrained D problems.

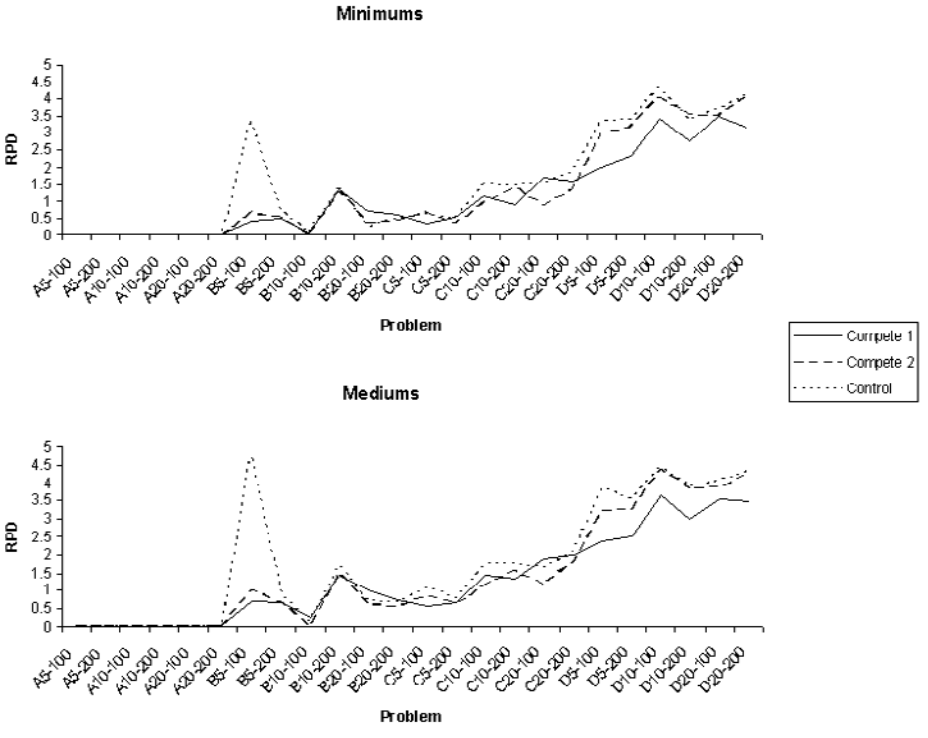

Fig. 1. Graphical form of the minimum and maximum RPD results

A statistical analysis shows that there is a significant difference between the methods. It was found that the two competitive ant colony approaches produced statistically significantly better results than the control solver (at the 0.05 level). This therefore represents an improvement on the results for the same test problems used in Randall [11]. There was no significant difference between the two solvers. Additionally, there was little variation in the overall computational runtimes used by the solvers.

6 Conclusions

The balance between competitive and cooperative approaches is an important part of multi-solution (particularly evolutionary) optimisation algorithms. Given the test cases presented herein, two forms of competition added to ACO showed that significantly improved solutions could be found compared to a standard implementation. The nature of the competitions in this paper was quite simple and could be more sophisticated. This will need to be done if a greater variety of problem types are to be solved in this manner. It will also be interesting to see how these notions extend to other multi-solution (population) heuristics, particularly genetic algorithms.

References

[1] Beasley, J.: OR-Library (2007) http://people.brunel.ac.uk/mastjjb/jeb/info.html

[2] Chu, P., Beasley, J.: A genetic algorithm for the generalised assignment problem. Computers and Operations Research 24, 17–23 (1997)

[3] Costa, D., Hertz, A.: Ants can colour graphs. Journal of the Operational Research Society 48, 295–305 (1997)

[4] Dorigo, M., Di Caro, G.: The ant colony optimization meta-heuristic. In: Corne, D., Dorigo, M., Glover, F. (eds.) New Ideas in Optimization, pp. 11–32. McGraw-Hill, London (1999)

[5] Dorigo, M., Gambardella, L.: Ant Colony System: A cooperative learning approach to the traveling salesman problem. IEEE Transactions on Evolutionary Computation 1(1), 53–66 (1997)

[6] Gambardella, L., Dorigo, M.: HAS-SOP: An hybrid ant system for the sequential ordering problem. Technical Report IDSIA-11-97, IDSIA (1997)

[7] Gambardella, L., Taillard, E., Dorigo, M.: Ant colonies for the quadratic assignment problem. Journal of the Operational Research Society 50, 167–176 (1999)

[8] Lourenco, H., Serra, D.: Adapative search heuristics for the generalized assignment problem. Mathware and Soft Computing 9, 209–234 (2002)

[9] Martello, S., Toth, P.: An algorithm for the generalised assignment problem. In: Proceedings of the 9th IFORS Conference, Hamburg, Germany (1981)

[10] Merkle, D., Middendorf, M.: Competetition controlled pheromone update for ant colony optimization. In: Dorigo, M., Birattari, M., Blum, C., Gambardella, L.M., Mondada, F., Stützle, T. (eds.) ANTS 2004. LNCS, vol. 3172, pp. 95–105. Springer, Heidelberg (2004)

[11] Randall, M.: Heuristics for ant colony optimisation using the generalised assignment problem. In: Proceedings of the Congress on Evolutionary Computing 2004, Portland, Oregon, pp. 1916–1923 (2004)

[12] Randall, M.: Maintaining diversity within individual ant colonies. In: Abbass, H., Bossamaier, T., Wiles, J. (eds.) Recent Advances in Artificial Life. Advances in Natural Computation, vol. 3, pp. 227–238. World Scientific, New Jersey (2005)

Optimization of Dynamic Combinatorial Optimization Problems Through Truth Maintenance

Brett Bojduj[1], Dennis Taylor[1], and Franz Kurfess[2]

[1] CDM Technologies, Inc.
2975 McMillan Ave. Suite 272
San Luis Obispo, CA 93401
{bbojduj,djtaylor}@cdmtech.com
[2] Department of Computer Science
California Polytechnic State University
San Luis Obispo, CA 93407
fkurfess@csc.calpoly.edu

Abstract. Combinatorial optimization problems are embedded in dynamic environments, spanning many domains. As these problem environments may change repeatedly, agents that attempt to solve problems in such environments must be able to adapt to each change that occurs. We present a technique for a Tabu Search-based meta-heuristic agent that collaborates with a truth maintenance agent to maximize reuse of generated solutions that may become partially inconsistent when a change occurs in the problem space. By allowing the truth maintenance agent to perform partial plan repairs, we hope to mitigate the effect that a change has on the performance of the planning agent. Such a system is discussed in a global logistics scheduling program. The performance of our approach is analyzed with respect to a dynamic constrained vehicle routing problem. Our results show that partial plan repairs increase the stability of solutions in dynamic domains.

1 Motivation

A common definition of combinatorial optimization problems are those problems that deal with the efficient allocation of finite resources to meet desired objectives when the values of some or all of the variables are restricted to be integral [1]. For our work we have found it best to take the following definition of combinatorial optimization:

> Given a set S = {a_1, a_2, ..., a_n } where a_i is an atomic entity, find an ordering or subset of S such that the objective criteria is minimized or maximized.

This definition can be applied to dynamic combinatorial optimization problems by considering that atomic entities can be added, changed, or removed

H.G. Okuno and M. Ali (Eds.): IEA/AIE 2007, LNAI 4570, pp. 984–991, 2007.

from the solution set. From this definition, you can clearly see that combinatorial optimization is an exponential process, since the number of subsets of the set S is equal to 2^n and the number of possible orderings of the set S is n!. Thus finding an optimal solution set is not feasible for many problems. Fortunately, the idea of finding "good enough" or "satisficing" [2] solutions can be applied to develop heuristics that find satisfactory solutions to combinatorial optimization problems [3].

Taylor et al. [4] provide a framework for finding "good enough" solutions using a Dynamic Tabu Search. Their Dynamic Tabu Search extends the standard Tabu Search [5,6], a meta-heuristic algorithm used to explore large solution spaces. By identifying the invalid parts of a solution when a change in the environment takes place, the dynamic approach is able to re-use the valid portions of the previous solution; the Dynamic Tabu Search was able to adapt to changes faster than a static Tabu Search using the Open Tabu Search framework (http://www.coin-or.org/OpenTS/). This shows that solution reuse can help increase the stability of solutions in a dynamic environment, allowing the algorithm to converge to "good enough" solutions quicker. Thus it can be inferred that the more of a solution that is reused, the more the solution stability is retained. It should be noted that this does not necessarily imply that solution stability is in any way related to solution optimality. As shown in Taylor et al.'s [4] "Marching Grid" example, a Dynamic Tabu Search that attempts to reuse as much of the solution as possible does not necessarily mean that better solutions will be found, but rather that the quality of the solution is likely to be similar to the previous one. This is essential in real-world planning problems since if a proposed plan changes rapidly it is very difficult for human planners to identify the necessary course of action.

2 Truth Maintenance Agent for Optimization of Dynamic Tabu Search

As shown by Taylor et al. [4], a Dynamic Tabu Search can be used to efficiently solve dynamic combinatorial optimization problems. It achieves its performance by only invalidating the portion of a solution affected by a change in the problem. Additionally, Bojduj et al. [7], show that breaking the problem of truth maintenance into aspects, enables a truth maintenance agent to make explicit which aspects become inconsistent when information comes into the knowledge base that invalidates a solution. It does this by running a series of tests on each aspect, such that if a test fails, the aspect that fails the test is clearly inconsistent. Aspectualizing the problem domain through truth maintenance frees up the resources of the planning agent, since it no longer has to identify what has become invalid and can continue planning. Combining domain knowledge with an ontology allows related aspects to be identified.

Bringing together the concepts of a truth maintenance agent to provide feedback to a Dynamic Tabu Search allows the Dynamic Tabu Search to not only

invalidate the portion of its solution that has become inconsistent, but also enables the resolution of the inconsistency. Since a solution generated by the Dynamic Tabu Search may contain many different aspects that are unrelated to each other, it makes sense to try to resolve only the aspects that are inconsistent, rather than recomputing the entire solution.

The division of the problem space into aspects is a leitmotif of this work and is based on Bertel et al.'s [8] work on aspectualization of a design problem. Bertel et al. show how in a design process, related aspects are selected and other aspects are filtered out. As shown by Bojduj et al. [7], this concept can be extended to other problem domains in a strategy similar to the divide and conquer paradigm in artificial intelligence, which Bertel et. al. [8] call "aspectualize and conquer":

> As with divide and conquer, [aspectualize and conquer] does not provide a solution to a specific problem. Rather, it offers a framework to accommodate different classes of processes, such as those that aspectualize a problem, that provide solutions with respect to selected aspects, and those that based on a partial ordering of aspectualizations serve to integrate the partial solutions with one another.

Thus decomposing a problem domain into related aspects allows each related aspect to be solved in turn, without disturbing other parts of a solution. Maintaining the consistency of each aspect is the *sine qua non* of the truth maintenance agent.

For our definition of consistency, we maintain the definition given by Bojduj et al. [7]:

$$C_{KB} = F_V(O, C) \tag{1}$$

where the consistency of a knowledge base, C_{KB}, is a function of the objects, O, and the constraints on those objects, C. The verification function, F_V, checks that all constraints are satisfied by the set of objects. The knowledge base is thus defined as inconsistent only when constraints in the problem definition exist that are not satisfied.

When an event occurs, part of a solution may become inconsistent. If this happens, the truth maintenance agent will catch the invalidation and can repair the inconsistent aspect. Then all solutions that are dependent on the current solution can be updated. The truth maintenance agent then submits the repaired solution(s) to the planning agent. The planning agent can then merge the changes into its current solution as a basis for further optimization or just replace the current solution outright.

This approach is cognitively motivated, since humans generally do not completely restart solving a solution if it fails, but rather adapt the solution and fix inconsistent parts of it [9]. This may not yield as good a solution as if the problem-solving had restarted, but it is much more efficient in dynamic domains and provides solutions that do not vary wildly, thus making them easier to understand by human planners.

3 Applications

As this technique is designed to find feasible solutions to dynamic combinatorial optimization problems, there are many applications of this approach. One domain with many applicable problems is logistics. In particular the logistical dynamic vehicle routing and scheduling problem with time windows, is a difficult problem to solve, as it is embedded in a dynamic domain that can change continuously.

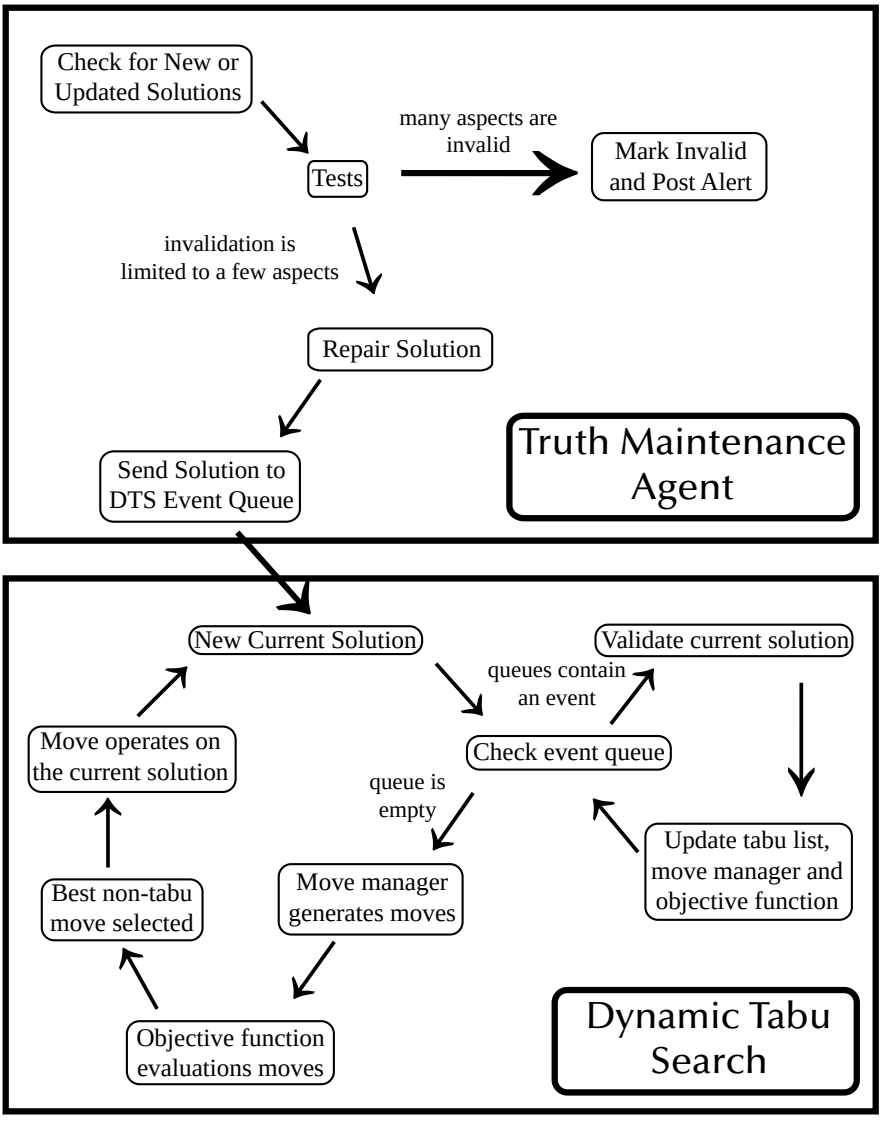

Fig. 1. Optimization Process

For example, in a real-world vehicle routing problem, bridges can fail or weather can make certain routes impassible, and thus the vehicles must be routed around such obstructions. In such cases, much of a logistical plan can still be reused (e.g. cargo manifests, point of departure, etc.), but the aspects of the plan related to departure and arrival times, as well as the routes which are to be taken, must be changed to accommodate the changes in the environment. In this case, the truth maintenance agent can determine that the route the vehicle is scheduled to traverse has failed the consistency check and so portions of the plan using that route must be repaired. If no other tests fail than the route traversability test, then the truth maintenance agent can decide to repair the solution by either calculating a route on its own or contacting the Dynamic Tabu Search and requesting a new route to traverse. Then the related aspects of the problem, namely the start and end times of the solution, must be updated to account for differences in the distance between the previous route and the new route. The Dynamic Tabu Search can then take the updated solution that the truth maintenance agent planned and use that as a basis for further optimization. Figure 1 shows the process of optimization through the interplay of the truth maintenance agent and the Dynamic Tabu Search.

4 TRANSWAY

We designed a truth maintenance agent such that it works in conjunction with a Dynamic Tabu Search-based planning agent in TRANSWAY[1], a global scheduling and logistics program developed by CDM Technologies, Inc. TRANSWAY is comprised of multiple agents that work together to solve a global-scale logistical problem. For more information, please see Nibecker et al. [10]. As TRANSWAY is a multi-agent system, the Tabu Search planning agent was designed to interface with other agents in the system to accomplish its reasoning tasks. To better illustrate the design of the TRANSWAY system, an example is given:

> A request for delivery of cargo comes into the system. The planning agent then creates a solution which schedules the delivery of the requested cargo via a truck driving across one of many paved road routes connected to the request location. Then information about a change in the earliest time of delivery (ETD) and latest time of delivery (LTD) of the request comes to the truth maintenance agent, which then sees that the current solution is now inconsistent. Since changes in the request time only affect one aspect of the problem, namely the departure time of the truck, the truth maintenance agent can then attempt to repair the solution by shifting the scheduled missions accordingly, so that it can deliver within the new request times. The truth maintenance agent

[1] The TRANSWAY project was funded by the U.S. Department of Defense, Joint Chiefs of Staff (J4), via USTRANSCOM under contract DAMT01-02-D-0024 (Delivery Order 0021).

then saves the repaired solution to the shared knowledge base. The planning agent can then take this new solution and merge it with its current solution, and use that solution as the basis for further improvement.

In order to quantify the results of our framework, we created a similar scenario in TRANSWAY that can show how repairing plans can improve the stability of logistical solutions in a dynamic problem domain.

5 TRANSWAY Test Methodology and Results

To illustrate the efficacy of our solution, we created a request for six pallets of cargo, with a time window sufficient to deliver all the cargo. We distributed the cargo within a theater such that we knew the planning agent could reach an optimal planning configuration within a few seconds. We arranged that after some time the ETD of the request would be changed - shifted forward by two days - such that the current solution would become invalid. We ran this test two different ways with the Dynamic Tabu Search (DTS) planning agent - once in conjunction with the truth maintenance agent (TMA), and once without.

After the change is made with the DTS and TMA, the TMA catches the event, repairs the part of the current solution based on the aspect that failed, and

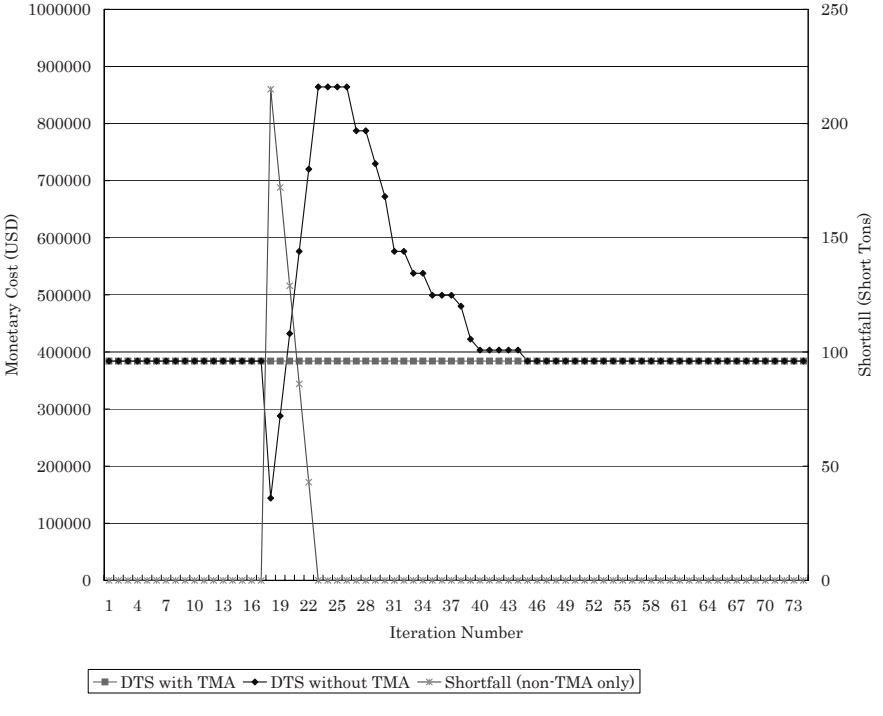

Fig. 2. TRANSWAY Results

replaces the current best solution the DTS has with the repaired solution. This is visible by the straight line in the graph of Figure 2, since the solution is optimal before and after the event. However, the line for the DTS by itself, without the TMA, does not display this behavior. Instead, when the event occurs, the cost of the best solution currently drops, due to the fact that the event causes the solution to be replanned from the start. The reason the costs drops is because most of the cargo is not being delivered, which is shown by a shortfall of 215 short tons. As the DTS continues to solve, the shortfall drops to zero and the cost levels off. Eventually, the DTS reaches the optimal cost again. To give a sense of time, the DTS took on average 5.2 seconds to replan the change, whereas the DTS with the TMA required no replanning, since the solution was already at optimality.

In Figure 2, the values of the best known solution at each iteration is plotted. On the left y-axis is the monetary cost of the best plan. The cost is the dollar cost per hour for a conveyance, multiplied by the usage time of that conveyance in hours. The values on the right y-axis correspond to the amount of shortfall in short tons. The DTS with the TMA has no shortfall, since it keeps the optimal plan by repairing the plan and overwriting the best plan the DTS has with the repaired plan.

6 General Analysis

The previous section shows empirical evidence of the effectiveness of this approach on a specific case. Determining when to use the truth maintenance repair system in a more general sense involves several trade offs. The comparison is between the standard optimization solution, that just invalidates parts of a solution when a change occurs, and using the truth maintenance agent to perform repairs on the previous best solution. In the standard optimization approach, the time it takes to converge from an invalidation event to a new best solution is the only time that needs to be measured to determine the stability of the solution. However, in the truth maintenance approach, the time it takes to repair the solution and the network latency time of transferring the new solution to the planning agent (assuming a distributed system like TRANSWAY) needs to also be considered. The truth maintenance repair will only provide faster convergence if it is able to repair and transfer the solution faster than the search is able to compensate for an invalidation. To mitigate the risk of one approach taking significantly longer than the other the system should always be set up to run both methods in parallel and take the faster of the two. This can be done by comparing the planning agent's current solution with the repaired solution and continuing with the best of the two.

7 Conclusions and Future Work

We have presented a framework for maximizing stability of solutions to dynamic combinatorial optimization problems. Through the use of a truth maintenance

agent, plans representing solutions for the problem can be repaired by modifying those aspects that have lead to inconsistencies. The more that is known about the problem domain, the better the aspects of the problem can be repaired for plan reuse. The feasibility of the approach has been demonstrated within the context of the TRANSWAY logistics system. Our initial results show that the use of the truth maintenance agent in combination with the Dynamic Tabu Search agent can lead to significant improvements in the quality of the solution, measured in terms of the monetary cost and shortfall in short tons, and compared against a Dynamic Tabu Search without truth maintenance. For a comparison of the Dynamic Tabu Search without truth maintenance to a static Tabu Search, please see Taylor et al. [4]. While we believe that this approach can be applied to other problems and domains that require dynamic combinatorial optimization, additional experiments will be conducted to further explore it.

References

1. Hoffman, Padberg, Manfred.: Combinatorial and Integer Optimization. George Mason University, New York University (2005)
2. Simon, H.: The Sciences of the Artificial. MIT Press, Cambridge (1996)
3. Eracar, Y.A.: Negotiating Solutions to Multiobjective Combinatorial Optimization Problems. PhD thesis, Northeastern University (2005)
4. Taylor, D., Weber, B., Bojduj, B.: A tabu search framework for dynamic combinatorial optimization problems. In: Proceedings, Integrated Design and Process Technology, IDPT-2006, Society for Design and Process Science, pp. 663–668 (2006)
5. Glover, F., Laguna, M.: Tabu search. In: Reeves, C.R. (ed.) Modern Heuristic Techniques for Combinatorial Problems, pp. 71–140. Blackwell Scientific Publishers, Oxford, England, Oxford, England (1993)
6. Glover, F., Laguna, M.: Tabu Search. Kluwer Academic Publishers, Norwell, Massachusetts (1997)
7. Bojduj, B., Weber, B., Taylor, D.: A framework for truth maintenance in multiagent systems. In: Proceedings of Operations Research 2006 (to appear)
8. Bertel, S., Freksa, C., Vrachliotis, G.: Aspectualize and conquer in architectural design. In: Gero, J.S., Tversky, B., Knight, T. (eds.) Visual and Spatial Reasoning in Design III, Key Centre of Design Computing and Cognition; University of Sydney, pp. 255–279 (2004)
9. Anderson, J.: Cognitive psychology and its implications. Worth Publishers (2005)
10. Nibecker, J., Taylor, D., Chambers, R., Larsen, H., Cudworth, K., Warren, C., Porczak, M., Pohl, J.: Transway: Planning with the tabu search algorithm. In: InterSymp-2006, Focus Symposium on Advances in Intelligent Software Systems, Baden-Baden, Germany, August, 2006, pp. 63–86 (2006)

A Microcanonical Optimization Algorithm for BDD Minimization Problem*

Sang-Young Cho, Minna Lee, and Yoojin Chung

Computer Science & Information Communications Engineering Division
Hankuk University of Foreign Studies, Yongin, Kyeonggi, Korea
{sycho,mnlee,chungyj}@hufs.ac.kr

Abstract. Reduced ordered binary decision diagrams (ROBDDs) have become widely used for CAD applications such as logic synthesis, formal verification, and etc. The size of RDBDDs for a Boolean function is very sensitive to the ordering choices of input variables and the problem of finding a minimum-size variable ordering is known to be NP-complete. In this paper, we propose a new ROBDD minimization algorithm based on the microcanonical optimization (MO). MO iteratively applies an initialization phase and a sampling phase to combinatorial optimization problems. In the proposed MO-based algorithm, the initialization phase is replaced with the existing Sifting algorithm known to be a very fast local search algorithm to find a minimum-size ROBDD. We derived equations for the proposed MO-based algorithm parameters empirically. The algorithm has been experimented on well known benchmark circuits and the experiments show that, even with slightly better solutions, the run time of the algorithm is 24% and 48% of the Genetic and SA algorithms', respectively, on average. The proposed MO-based algorithm is a good candidate for the large size problems that cannot be attacked by exact algorithms when a near-optimal solution is required.

1 Introduction

Boolean function manipulation is an important component of many logic-related applications such as logic synthesis, logic optimization, and logic verification for combinational and sequential circuits. Reduced ordered binary decision diagrams (ROBDDs) have been used in these applications as efficient canonical data structures for the representation and manipulation of Boolean functions[1,2].

The size of ROBDDs depend crucially on the order in which the variables occur, i.e., the sizes may vary from linear to exponential, depending on the ordering of the variables[3]. Therefore, it is very important to find a good variable ordering that minimizes the size of ROBDDs. Unfortunately, the problem of computing an optimal variable ordering for a ROBDD is NP-complete[4]. Due to the great importance of finding good orderings, many heuristic and exact algorithms have been proposed for the ROBDD minimization problem.

* This work was supported by Hankuk University of Foreign Studies Research Fund 0f 2006.

H.G. Okuno and M. Ali (Eds.): IEA/AIE 2007, LNAI 4570, pp. 992–1001, 2007.

The heuristic algorithms based on structural information[5] or on dynamic reordering of ROBDDs[6] cannot guarantee an optimal result, and experimental studies have shown that they yield ROBDDs up to twice the size of the best known solution frequently. However, the Rudell's Sifting algorithm[6] based on variable exchange scheme and its variances[7,8] are used in many ROBDD-based applications in which execution time is an important issue.

To overcome the poor qualities of heuristic algorithms based on variable exchange scheme, the exact algorithms have been suggested under the framework of [9].The exact algorithms[10,11] find the optimal orderings for ROBDDs but suffer from the exponential time and space complexity in the worst case even though the algorithms are improved continuously and are achieving considerable search space reduction. The algorithms are well applied to small-size problems in which optimal solutions are required.

Other heuristic algorithms using probability-based Simulated Annealing (SA) and Genetic Algorithm (GA) have been proposed and they find very good solutions[12,13]. These algorithms consume long execution times and suitable for large-size problems to find near-optimal solutions regardless of time.

Microcanonical optimization (MO) is another combinatorial optimization scheme derived from statistical physics[14,15]. MO is based on the Creutz algorithm[16] that generates sample states of a uniform state distribution in an thermally isolated system. Generally, MO consists of an initialization phase and a sampling phase that are iteratively applied. Initialization phase is to find a local-minimum solution fast. From there, the sampling phase creates new solutions at the same cost level through the Creutz algorithm in order to climb out from the local minimum. These cycles proceed until no further improvement is made.

In this paper, we propose a modified MO algorithm for the ROBDD minimization problem by changing the initialization phase with the Sifting algorithm[6]. To run the modified MO algorithm, We derived equations for the modified MO algorithm parameters empirically. Experiments show that the modified algorithm found slightly better solutions compared with the Genetic and SA algorithms and the run time is 24% and 48% of the Genetic and SA algorithms's, respectively, on average.

The remainder of This paper is organized as follows: Sect. 2 explains fundamental concepts of ROBDD, sifting algorithm, and MO. The modified MO algorithm for the ROBDD minimization problem is proposed in Sect. 3. Section 4 will present the derived equations for algorithm parameters and the analysis and discussion for experimental results. We conclude with some final remarks in Sect. 5.

2 Background

2.1 Reduced Ordered Binary Decision Diagram

In [3], Bryant introduced ROBDDs as data structures for Boolean function and circuit manipulation. Let $f : \{0,1\}^n \rightarrow \{0,1\}$ be a Boolean function over

the variable set $X_n = \{x_1, \ldots, x_n\}$ and π be a permutation of X_n, i.e., $\pi : \{1, \ldots, n\} \rightarrow X_n$ The function f is represented by a binary decision diagram that is a directed acyclic graph where a Shannon decomposition

$$f = x_i f_{x_i=1} + \overline{x_i} f_{x_i=0} \quad (1 \leq i \leq n) \tag{1}$$

into two cofactors in x_i is applied to each node $v \in X_n$ with the order specified by π. Each Shannon decomposition yields 1-successor via a 1-edge and 0-successor via a 0-edge. v is connected to the first decomposition node among 1-successor (resp. 0-successor) via 1-edge (resp. 0-edge). Therefore, the root node is $\pi(1)$ and terminal nodes are 1 and 0. The generated graph is ordered because each variable is encountered at most once on each path from the root to a terminal and the variables are encountered in the same order on all such paths.

A ordered binary decision diagram is called reduced if it contains no vertex v without coincidence of 1-edge and 0-edge, nor contain distinct vertices v and v' such that the subgraphs rooted by v and v' are isomorphic[3]. In the following, only ROBDD is considered and for briefness these graphs are called BDD. (BDDs are defined analogously for multi-output functions $f : \{0,1\}^n \rightarrow \{0,1\}^m$, using a graph for each of the m single-output functions and reducing by the sharing of subgraphs.)

The BDD is a canonical representation for a given Boolean function, given an ordering on its variables. This property enables the BDDs to be widely used for CAD applications such as logic synthesis, formal verification, and etc. However, a serious drawback of BDD's is that the size of the BDD for a given function is extremely sensitive, from linear to exponential, to the choice of an ordering on the variables. It is very important to find a good ordering to apply the BDDs to CAD applications efficiently. The problem of computing an ordering that minimizes the size of a BDD graph is itself a NP-complete problem[4].

2.2 Sifting Algorithm

The Sifting algorithm[6] has emerged so far as the most successful algorithm for dynamic reordering of variables and is used in many BDD-based applications when execution time is an important issue. This algorithm is based on finding an optimum position for a variable x_i, assuming all other variables remain fixed. If there are n variables in a BDD (excluding the constant level which is always at the bottom), then there are n potential positions for x_i, including its current position. Among these n positions, the algorithm finds the position which minimizes the size of the BDD and fixes x_i to the position. When checking the sizes of all the potential positions, the algorithm repeatedly shifts x_i to the next positions and calculates the BDD sizes. This swap scheme can reduce the computation burden to calculate the BDD sizes because the difference of sizes by shifting can be easily calculated. And the same procedure is applied for the remained $n - 1$ variables.

Although the algorithm produces good results on average, it has a limitation of usually finding local optimal solutions because the absolute position of a variable

is used as the primary objective when shifting. The Sifting algorithm is used in our proposed algorithm as an initialization phase.

2.3 Microcanonical Optimization (MO)

The microcanonical optimization is a procedure derived from statistical physics for thermally isolated systems. An isolated system does not interact with its environment, and so has constant energy. Any available state compatible with this fixed energy condition can then be found with equal probability. The Creutz algorithm[16] simulates an isolated system and generates samples of a uniform state distribution. In the Creutz algorithm, the sampling energy range is from $E_S - E_{DMAX} + E_D$ to $E_S + E_D$, where E_S is a system energy, E_D is a demon energy, and E_{DMAX} is the maximum demon energy ($E_S + E_D = const$). A new transition from the current system state to new one is accepted if the $0 \leq E_D \leq E_{DMAX}$.

MO was proposed to solve combinatorial optimization problems[14,15] and have shown that it finds good solutions. MO adapts iterative application of Creutz's simulation with an annealing feature. Figure 1 shows the MO algorithm.

```
Algorithm MO
Variables
  best_sol    : solution_instance;  // best solution
  cur_sol     : solution_instance;  // current solution
begin
  best_sol = ∞;
  cur_sol = Get_Initial();
  while (stop-criterion)
  begin
    Initialzation();
    if ( Cost(cur_sol) < Cost(best_sol) ) then
      best_sol = cur_sol;
    endif
    Sampling();
  endwhile
end
```

Fig. 1. The microcanonical optimization algorithm

The MO algorithm consists of an initialization and a sampling phases that are repeatedly applied. The goal of the initialization phase is to implement a fast local search, rapidly converging to a local-minimum solution: from there, the sampling phase generates alternative solutions at the same cost level through a Creutz simulation in order to climb out from the local minimum previously attained. After the sampling, a new initialization is run, and the initialization/sampling cycle thus proceeds, until stop criterion.

3 Modified MO Algorithm for BDD Minimization

Given a variable ordering, the BDD size should be calculated by time-consuming BDD construction and counting the nodes of the constructed BDD. In the initialization and sampling phases of the MO algorithm shown in Fig. 1, candidate solutions are repeatedly generated and each cost of the solutions should be calculated to determine the acceptance of the new one.

The goal of the initialization phase is to implement a fast local search. We adapted the Sifting algorithm as the initialization phase of our proposed MO algorithm so that the burden of the size calculation can be reduced. (We call the proposed MO algorithm as the modified MO (MMO) algorithm.) As the size of variables becomes larger, the calculation time of a BDD may increases more than linear. This incurs a rapid increasing in execution time if we directly use the initialization method of the MO algorithm.

Also we applied the Sifting algorithm to finding an initial ordering before entering the main loop of the MMO algorithm because, given a random ordering for a large number of variables, a BDD may not be found in the worst case. The initialization and the sampling steps in the main loop are exchanged to remove redundancy of the algorithm. Figure 2 shows the MMO algorithm.

```
Algorithm  Modified MO for BDD minimization
Input    : Boolean function of {x_1, ..., x_n}
Output   : variable ordering
Variables
  rejected       : integer;   // iteration number
  best_sol[1,n]  : integer;   // best ordering
  cur_sol[1,n]   : integer;   // current ordering
  Stop_Num       : integer    // the number of out loop
begin
  rejected = 0;
  Sifting();   // get initial ordering
  while (rejected < Stop_Num)
  begin
    Sampling();  // sampling phase
    Sifting();       // initialization phase
    if ( Size(cur_sol) < Size(best_sol) ) then
      best_sol = cur_sol;
      rejected = 0;
    else
      rejected++;
    endif
  endwhile
end
```

Fig. 2. The proposed MMO algorithm

The MMO algorithm finds an initial variable ordering by Sifting() and stores it into *cur_sol* with an associated BDD size. The initial size of *best_sol* is assumed to be infinite. The main **while** loop of the MMO algorithm consists of Sampling() and Sifting(), and these two phases will repeat until it satisfies some stop criterion. After the completion of sampling and sifting phases for each iteration, the best ordering is updated with the current ordering if the size of current ordering is smaller than the the size of the best one so far. To check out the stop criterion, we maintain a variable *rejected* that remembers the rejection number of the orderings found by iterations after every successful acceptance. The algorithm parameter $Stop\_Num$ is determined empirically as shown in Sect. 4.

Figure 3 shows the sampling algorithm that generates alterative orderings within the range from $E_S + E_D - E_{DMAX}$ to $E_S + E_D$, where E_S is an initial energy, E_D is an initial demon energy, and E_{DMAX} is a maximum demon energy. Generating alterative orderings makes the MMO algorithm escape from a local optimum obtained in the Sifting() procedure.

```
Algorithm Sampling
Input    : variable ordering
Output : variable ordering
Variables
  iter          : integer;    // iteration number
  new_sol[1,n] : integer;   // generated new ordering
  cur_sol[1,n]  : integer;   // current ordering
  Samp_Num  : integer    // the number of sampling
begin
  cur_sol = Input_ordering;
  E_S = Size(cur_sol); // initial system energy
  E_D = E_S × B; // initial demon energy, B is demon constant
  E_DMAX = E_D × 2;
  iter = 0;
  while ( iter < Samp_Num )
  begin
    new_sol = Perturb(cur_sol);
    if ( (E_S + E_D − E_DMAX) ≤ Size(new_sol) ≤ (E_S + E_D) ) then
      cur_sol = new_sol;
    endif
    iter++;
  endwhile
end
```

Fig. 3. The sampling phase for the MMO algorithm

The sampling algorithm requires the algorithm parameters, E_D, E_{DMAX}, and $Samp\_Num$. Usually, the performance of the algorithm is less dependent on the $Samp\_Num$ value because the purpose of the sampling phase is to escape

from a local optimum. The $Samp\_Num$ value is assigned with a logarithmic proportional value of the initial BDD size with Eqn. (3) in Sect. 4. However, the size of E_D is largely influencing to the algorithm performance. As the initial demon energy becomes bigger, the search space becomes wider and, thus, the probability to make Sifting() useless becomes higher. A comparatively small demon energy may not enable the sampling phase to escape from a local optimal ordering found at Sifting(). The initial demon energy is set to the value of $E_S \times B$, where E_S is the initial BDD size and B is a demon constant. So the demon constant B should be precisely determined by parameter experiments as shown in Sect. 4.

To generate a random ordering in Perturb(), the algorithm uses three perturbation methods that are exchange, jump-up, and jump-down trasitions[12]. Exchange transition exchanges the locations of two randomly selected variables. Jump-up transition moves the rear variable of randomly selected two variables to the front of the other variable, and jump-down transition moves the front variable to the right after position of the rear variable. These methods are implemented with the swapping of neighborhood valuables. The Perturb() procedure uses the three transitions with 40% exchange, 30% jump-up, and 30% jump-down as recommended in [12].

4 Experimental Results

The MMO algorithm was implemented with C language and CUDD package[17] from Colorado State University and executed on 248MHz SUN SPARC-II.

With several experiments, we established three equations for the algorithmic parameters such as $Stop\_Num$, $Samp\_Num$, and B. $Stop\_Num$ is calculated using the following equation.

$$loop\_func = Initial\_BDD\_Size \times 0.92^k \tag{2}$$

$Stop\_Num$ is the maximum integer k that makes the $loop\_func$ be less than 1. This method is used in SA algorithms frequently. And by experiments, the value 0.92 is determined. The performance of the MMO algorithm is not sensitive to the value of $Samp\_Num$. The value of $Samp\_Num$ is determined with the following equation.

$$Samp\_Num = 10 \times log_{10}(Initial\_BDD\_Size) \tag{3}$$

The initial demon size E_D of Sampling() has the biggest impact on the MMO algorithm performance. By experiments, we determined the demon constant B as 0.3. Therefore E_D is calculated with the following equation.

$$E_D = Initial\_BDD\_Size \times 0.3 \tag{4}$$

Experiments are performed for Sifting algorithm[6], SA algorithm[12], Genetic algorithm[13], and the MMO algorithm with IWLS91 benchmark circuits[18]. We

Table 1. Experimental results of Sifting, SA, Genetic, and MMO algorithms

Circuit			Sifting		SA		Genetic		MMO	
Name	In	Out	Node	Time	Node	Time	Node	Time	Node	Time
c1355	41	32	30775	26.99	25866	9089.79	25866	24792.05	25866	3741.85
c3540	50	22	39780	62.85	23831	6385.48	23828	8981.15	23828	2435.90
c1908	33	25	7153	21.52	5652	874.68	5832	1843.09	5526	1065.65
c880	60	26	7064	41.14	4054	1674.86	4065	3344.00	4053	303.95
des	256	245	3054	26.13	3037	665.90	2969	1220.61	2947	506.30
i8	133	81	2182	4.18	1300	215.78	1277	316.48	1277	107.81
k2	45	45	1394	9.24	1264	133.73	1256	170.10	1259	74.67
c432	36	7	1210	1.36	1209	96.22	1095	452.40	1164	40.11
apex	135	99	641	1.81	555	113.96	511	168.93	500	55.89
vda	17	39	507	2.50	481	15.53	478	12.15	478	12.19
x1	51	35	479	1.39	409	72.67	423	100.87	409	44.33
x4	94	71	532	1.37	363	62.63	340	97.39	336	35.17
too_large	38	3	652	6.29	315	66.62	306	130.71	304	41.61

used the CUDD package that contains the implementations of Sifting algorithm, SA algorithm, and Genetic algorithm. The algorithmic parameters for the SA and Genetic algorithms are set to the values recommended in CUDD package.

Table 1 shows the experimental results and the table lists only the circuits that the best BDD size, found by algorithms, of each circuit is over 200, i.e., each circuit listed has an appropriate problem size to compare heuristic algorithms. The first three columns list the name, the number of input variables, and the number of output functions of each circuit. The other eight columns list the best BDD sizes and execution times of each algorithm.

For clear view of the MMO algorithm's behavior, we classified the input circuits into three types according to the best BDD sizes found by experiments: Type 1 consists of c1355, c3540, c1908, and c880 and all of them have the best BDD size over 4000. Type 2 has des, i8, k2, and c432 with the range of the best BDD size from 1000 to 4000. The circuits that have the best BDD sizes below 1000 are classified into Type 3. We calculated the ratios of all the Node and Time data of each algorithm with respect to the MMO's Node and Time data. Then, we calculated the averages of Node ratios and Time ratios (R_{Node} and R_{Time}) of three types. Table 2 shows the summary of experiments data of Table 1.

The Sifting algorithm finds very poor variable orders and thus the BDD sizes obtained are 139% of the MMO algorithm's on average even though it executes very fast. It cannot be directly applied to practical applications that have to deal with large circuits.

The MMO algorithm is slightly better solutions than the SA and Genetic algorithms. But it found the best orderings for 11 circuits among 13 circuits. The SA algorithm performs poorly on the Type 3 circuits but it becomes comparative to the Genetic algorithm as the problem size becomes larger.

Table 2. Summary of experimental results

Circuit	Sifting		SA		Genetic		MMO	
Type	R_{Node}	R_{Time}	R_{Node}	R_{Time}	R_{Node}	R_{Time}	R_{Node}	R_{Time}
Type 1	1.47	0.05	1.01	2.85	1.01	5.76	1.00	1.00
Type 2	1.22	0.06	1.02	1.88	0.99	4.73	1.00	1.00
Type 3	1.45	0.09	1.05	1.67	1.01	2.44	1.00	1.00
All	1.39	0.07	1.03	2.09	1.01	4.17	1.00	1.00

When considering the execution times, the MMO algorithm overwhelms the SA and Genetic algorithms. The MMO algorithm consumes 24% of the Genetic algorithm's execution time and 48% of the SA algorithm's on overall average even with slightly better solutions. The execution time gab between the MMO algorithm and the SA or Genetic algorithms becomes larger as the problem size becomes larger. For Type 3 case, the MMO algorithm consumes just 17% of the Genetic algorithm's execution time and 34% of the SA algorithms's. This means that the MMO algorithm is a good candidate algorithm for large-size problems that cannot be attacked by exact algorithms when a near-optimal solution is required.

5 Conclusion

In this paper, a new heuristic algorithm (the MMO algorithm) is proposed for the BDD minimization problem that is known to be NP-complete. The proposed algorithm is based on the MO algorithm that iteratively applies an initialization phase and a sampling phase for a combinational problem.

In the MMO algorithm, the initialization phase uses the Sifting algorithm known to find a local optimal variable ordering efficiently. By this, the execution time of the initialization phase of the MMO algorithm can be reduced and find a better local optimum compared with the MO algorithm's.

The MMO algorithm requires the values for algorithm parameters such as the number of iterations in the main loop, the initial demon size, and the sampling number in the sampling phase. We derived equations for the required parameters empirically. With the algorithmic parameters determined by the derived equations, experiments were performed on IWLS91 benchmark circuits.

The experimental results show that the MMO algorithm's execution time is 24% of the Genetic algorithm's and 48% of the SA algorithm's on average even with slightly better solutions compared with the Genetic and SA algorithms. The execution time gab between the MMO algorithm and the SA or Genetic algorithms becomes larger as the problem size becomes larger. When a near-optimal solution is required, the MMO algorithm is a good candidate algorithm for a large-size problem that cannot be attacked by a exact algorithm due to its execution time or by a heuristic based on dynamic reordering due to its solution quality.

References

1. Scholl, Christoph, Drechsler, Rolf, Becker, Bernd.: Functional Simulation using Binary Decision Diagrams. In: ACM/IEEE International Conference on Computer Aided Design (ICCAD'97), pp. 8–12 (1997)
2. Yang, C., Ciesielski, M.: BDS: A BDD-based logic optimization system. IEEE Trans. Comput.-Aided Des. Integr. Circuits Syst. 21(7), 866–876 (2002)
3. Bryant, R.E.: Graph-Based Algorithms for Boolean Function Manipulation. IEEE Transaction on Computers C-35, 667–691 (1986)
4. Bollig, B., Wegener, I.: Improving the variable ordering of OBDDs in NP-complete. IEEE Trans. Comput. 45(9), 993–1002 (1996)
5. Fujii, H., Otomo, G., Hori, G.: Interleaving Based Variable Ordering Methods for Ordered Binary Decision Diagrams. ICCAD 1993, pp. 622–627 (1993)
6. Rudell, R.: Dynamic Variable Ordering of Ordered Binary Decision Diagrams. ICCAD 1993, pp. 42–47 (1993)
7. Moller, D., Molitor, P., Orechsler, R.: Symmetry based variable ordering for OBDDs. In: IFIP Workshop on Logic and Architecture Synthesis (1994)
8. Panda, S., Somenzi, F.: Who are the variables in your neighborhood. ICCAD 1995, pp. 74–77 (1995)
9. Fredman, S.J., Supowit, K.J.: Finding the Optimal Variable Ordering for Binary Decision Diagrams. IEEE Transaction on Computers C-39(5), 710–713 (1990)
10. Ebendt, R., Gunther, W., Drechsler, R.: An improved branch and bound algorithm for exact BDD minimization. IEEE Trans. on CAD Integr. Circuit Syst. 22(12), 1657–1663 (2003)
11. Ebendt, R., Gunther, W., Drechsler, R.: Combining Ordered Best-First Search With Branch and Bound for exact BDD minimization. IEEE Trans. on CAD Integr. Circuit Syst. 24(10), 1515–1529 (2005)
12. Bollig, B.M., Lobbing, M., Wegener, I.: Simulated Annealing to improve variable orderings for OBDDs. In: International Workshop on Logic Synthesis vol. 5B, pp. 5.1–5.10 (1995)
13. Drechsler, Rolf, Beckern, Bernd, Gockel, Nicole.: A Genetic Algorithm for Variable Ordering of OBDDs. In: International Workshop on Logic Synthesis, vol. 5C, pp. 5.55–5.64 (1995)
14. Linhares, A., Yanasse, H.H., Torreao, J.R.A.: Linear Gate Assignment: A Fast Statistical Mechanics Approach. IEEE Transaction on Computer-Aided Design of Integrated circuits and system 18(12) (1999)
15. Linhares, A., Torreao, J.A.: Microcanonical optimization applied to the traveling salesman problem. Int. J. Modern Phys. C 9, 133–146 (1998)
16. Creutz, M.: Microcanonical Monte Carlo simulation. Phys. Rev. Lett. 50, 1411–1413 (1983)
17. Somenzi, F.C.: Decision Diagram Package Release 2.3.1. University of Colorado (2002)
18. Yang, S.: Logic Synthesis and Optimization Benchmarks User Guide Version 3.0. Distributed as part of the IWLS91 benchmark distribution (1991)

A Lot Size Model for Deteriorating Inventory with Back-Order Cancellation

Peng-Sheng You[1] and Yi-Chih Hsieh[2]

[1] Graduate Institute of Transportation & Logistics, National ChiaYi University
300 Shiue-Fu Road, Chia-Yi 600, Taiwan
psyuu@mail.ncyu.edu.tw
[2] Department of Industrial Management, National Formosa University
Huwei, Yunlin 632, Taiwan
yhsieh@nfu.edu.tw

Abstract. This paper investigates a production planning problem in which the inventory is deteriorating at a constant rate, demand is price dependent and back-order is allowed. It is assumed in most previous works that back-ordering customers may not cancel their orders. However, in reality, many customers may withdraw or cancel their orders before receiving their orders. Tacking the cancellation phenomenon into account, this paper develops a continuous-time model to simultaneously determine the production decision and the selling price. A simple algorithm is used to obtain the optimal solutions. Numerical examples are also used to illustrate the solution searching procedure and the characteristics of the optimal decisions.

Keywords: Planning and Scheduling, Heuristic Search, Inventory.

1 Introduction

In a conventional economic production quantity model, several conditions should be satisfied. These conditions include non-perishable, price-independent demand rate, no back-order and so on. Such assumptions may not always true. Because, in reality, many products such as vegetables, medicines, as well as bloods are perishable and may deteriorate with time; demand can evidently be affected by sale price ,and back-orders are accepted by many customers. The conventional economic production model thus can not be applied to this problem.

Research on production policy for deteriorating inventory can be dated back to Ghare and Schrader [4]. In their paper, inventories' decaying rate is assumed to be exponential. Recently, Balkhi and Benkherouf [1] dealt with a production lot size model for deteriorating items. They used the numerical analysis to find the optimal replenishment schedule. Kim and Hong [5] developed an EMQ model for determining an optimal production run length under the condition that the production process is subject to a random deterioration. Wee and Law [9] dealt with a deteriorating inventory model in which the cash flow is considered. Since the developed model is very complicated, it is difficult to obtain analytical result.

H.G. Okuno and M. Ali (Eds.): IEA/AIE 2007, LNAI 4570, pp. 1002–1011, 2007.

Thus, the numerical analysis is used to illustrate how to develop decision. Balkhi [2] developed a finite time lot size inventory model for deteriorating items. In this paper, shortages are allowed and completely backlogged. The conditions for obtaining the minimum total cost was developed. Balkhi [3] dealt with a infinite time production lot size models for deteriorating items. A closed form that leads to minimum total cost was introduced. Skouri and Papachristos [8] investigated a production model in which production rate, demand rate, deterioration rate and backlogging are time dependent. Pal et al. [7] investigated the problem of determining the lot size decision for a deteriorating item. A solution procedure was developed for finding the optimal decision. Lin et. at. [6] dealt with a economic lot size model for deteriorating items. A near optimal production cycle time is found under the condition of continuous review, deterministic demand and no shortage.

Many models have considered the back-ordering situation. However, these models have rarely considered a situation in which back-ordering customers may cancel their orders before receiving their orders. By incorporating the cancellation phenomena, this paper addresses the simultaneous determination of production policy and sale price. The purpose of this paper is to find the optimal decision for maximizing the unit time profit. The decision rules include (1) production policy, specifying the duration of production and shortage, and (2) pricing policy, specifying the sale price.

2 Modeling Assumption and Formulation

The following notation is used through this paper.

L = the production lead time;
T = the cycle time, $T = T_1 + L + T_4$;
$I(t)$ = the inventory level at time t;
I_{max} = the maximum inventory level;
I_b = the maximum stock-out demand;
s = the selling price;
$d(s)$ = the demand rate when a sale price is set at s (the demand rate $d(s)$ is assumed to be a linear function of $d(s) = a - bs$ where a and b are constant values);
p = the production rate per unit time;
θ = the inventory deteriorating rate per unit time;
β = the fraction of the number of cancellation;
λ = the fraction of revenue from penalty for cancellation to the selling price s (the revenue from penalty for cancellation is λs);
c_s = the setup cost per production run;
c_b = the unit back-ordering cost per unit time;
c_d = the deteriorated cost per unit;
c_h = the unit inventory carrying cost per unit time;

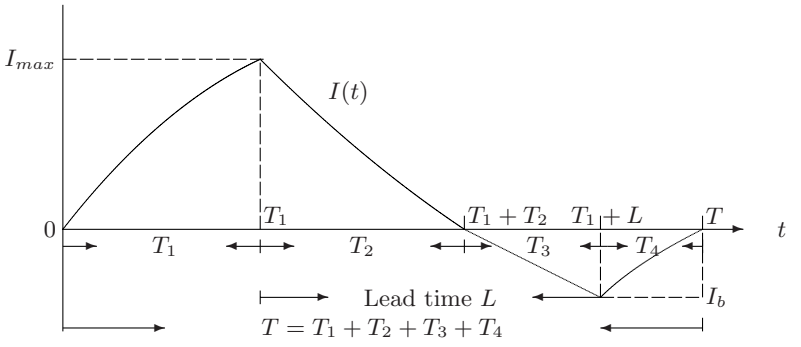

Fig. 1. Behavior of deteriorating inventory level with time

In this section, we will develop the mathematical model for this problem. Figure 1 depicts the inventory level at any time for a given cycle. At time $t = 0$, the inventory level is zero and production runs from time $t = 0$ to $t = T_1$. Production runs at a constant rate, p, during the production period. Suppose the selling price is set at s. Then, since there is demand at rate, $d(s)$, and deterioration at a constant rate, θ, the inventory increases at a rate $p-d(s)-\theta I(t)$ during the production period. The inventory level will be at its maximum, I_{max}, at the time, $t = T_1$, where product stops.

After time, $t = T_1$, no production run until time $t = T_1 + L$. During the time period from time $[T_1, T_1 + T_2]$, the inventory level decreases at a rate $d(s) + \theta I(t)$ due to demand and deterioration. At time $t = T_1 + T_2$, the inventory level becomes zero. During period from $[T_1 + T_2, T_1 + L]$ no inventory on hand, demand should be back-orders. In addition, since back-ordering customers may withdraw or cancel their orders, the number of back-orders may decrease. This paper assume that the number of cancellations is proportional to the number of back-orderings. The cancellation rate is assumed to be a constant rate β. Then, since back-ordering customers may cancel their orders at a rate β, the inventory level during this period changes at a rate $-d(s) - \beta I(t)$. After time $t = T_1 + L$, another production runs and back-orders will be made up during the period from $[T_1 + L, T]$. At time $t = T$, the inventory level becomes zero again and another cycle starts. During the period $[T_1 + L, T]$, production runs at a constant rate, p, demand occurs at a rate $d(s)$, and cancellations take place at a rate β, thus the inventory increase at a rate $p - d(s) - \beta I(t)$. Now, we will develop the mathematical model. The inventory level $I(t)$ can be divided into four segments $I_1(t_1)$ during period $[0, T_1]$, $I_2(t_2)$ during period $[T_1, T_1 + T_2]$, $I_3(t_3)$ during period $[T_1 + T_2, T_1 + T_2 + T_3](= [T_1 + T_2, T_1 + L])$ and $I_4(t_4)$ during period $[T_1 + L, T_1 + L + T_4]$. For notation convenience, let $t_1 = t$, $t_2 = t - T_1$, $t_3 = t - T_2$ and $t_4 = t - T_1 - L$. Then, the inventory level $I(t)$ can be reexpressed as follows

$$I(t) = \begin{cases} I_1(t_1), 0 \le t_1 \le T_1, \\ I_2(t_2), 0 \le t_2 \le T_2, \\ I_3(t_3), 0 \le t_3 \le T_3, \\ I_4(t_4), 0 \le t_4 \le T_4, \end{cases} \tag{1}$$

with $I_1(T_1) = I_2(0)$, $I_2(T_2) = I_3(0)$, $I_3(T_3) = I_4(0)$, and $T_3 = L - T_2$. Suppose the selling price is set at s, then the inventory level of the system at any time t can be described by the following differential equations.

$$\frac{dI_1(t_1)}{dt} = p - d(s) - \theta I_1(t_1), \quad 0 \le t_1 \le T_1, \tag{2}$$

$$\frac{dI_2(t_2)}{dt} = -d(s) - \theta I_2(t_2), \quad 0 \le t_2 \le T_2, \tag{3}$$

$$\frac{dI_3(t_3)}{dt} = -d(s) - \beta I_3(t_3), \quad 0 \le t_3 \le T_3, \tag{4}$$

$$\frac{dI_4(t_4)}{dt} = p - d(s) - \beta I_4(t_4), \quad 0 \le t_4 \le T_4. \tag{5}$$

Solving the above equations by using the boundary conditions $I_1(0) = 0$, $I_2(T_2) = 0$, $I_3(0) = 0$ and $I_4(T_4) = 0$ yields the following form.

$$I_1(t_1) = (p - d(s))(1 - e^{-\theta t_1})/\theta, \quad 0 \le t_1 \le T_1, \tag{6}$$

$$I_2(t_2) = d(s)(e^{\theta(T_2 - t_2)} - 1)/\theta, \quad 0 \le t_2 \le T_2, \tag{7}$$

$$I_3(t_3) = d(s)(e^{-\beta(t_3 - T_2)} - 1)/\beta, \quad 0 \le t_3 \le T_3, \tag{8}$$

$$I_4(t_4) = (p - d(s))(1 - e^{\beta(T - t_4)})/\beta, \quad 0 \le t_4 \le T_4. \tag{9}$$

Using (6)-(9), we will develop the profit function. The components of profit function include the production cost, holding cost, back-ordering cost, deteriorating cost, revenues from cancellation and sales revenue.

Production cost: The total production cost within a cycle time, K_s, is

$$K_s = c_s. \tag{10}$$

Inventory holding cost: The total inventory holding cost within a cycle time, K_h, is

$$K_h = c_h\Big(\int_0^{T_1} I_1(t)dt + \int_0^{T_2} I_2(t)dt\Big). \tag{11}$$

Using the Taylor-series approximation for the exponential term in $I_1(t)$ and $I_2(t)$ and neglecting second or higher order of θ, we have

$$K_h \approx \frac{c_h}{6}\Big((p - d(s))(3 - \theta T_1)T_1^2 + d(s)(3 + \theta T_2)T_2^2\Big). \tag{12}$$

Back-ordering cost: The total back-order cost within a cycle time, K_b, is

$$\begin{aligned} K_b &= c_b\Big(-(\int_0^{T_3} I_3(t)dt + \int_0^{T_4} I_4(t)dt)\Big) \\ &= c_b\frac{(d(s)e^{-\beta T_3} + \beta d(s)T_3 - \beta pT_4 + \beta d(s)T_4 - p + (p - d(s))e^{\beta T_4})}{\beta^2}. \end{aligned} \quad (13)$$

Using the relationship of $(p-d(s))e^{\beta T_4} = p-d(s)e^{-\beta T_3}$ due to $I_3(T_3) = I_4(0)$, we can simplify K_b as follows.

$$K_b = c_b(d(s)(T_3 + T_4) - pT_4)/\beta. \quad (14)$$

Deteriorating cost: Let I_{max} be the maximum inventory level. Then, the number of units deteriorated during $[0, T_1]$ and $[T_1, T_1 + T_2)$ are $(p - d(s))T_1 - I_{max}$ and $I_{max} - d(s)T_2$, respectively. Thus, the total deteriorating cost within a cycle time, K_d, is

$$\begin{aligned} K_d &= c_d\Big((T_1(p - d(s)) - I_{max}) + (I_{max} - d(s)(T_2 - T_1))\Big) \\ &= c_d((p - d(s))T_1 - d(s)T_2). \end{aligned} \quad (15)$$

Revenue from cancellation: The total number of cancellations is

$$d(s)(T_3 + T_4) - pT_4. \quad (16)$$

Thus, the revenue from cancellation, R_c, is

$$R_c = \lambda s(d(s)(T_3 + T_4) - pT_4). \quad (17)$$

Sales revenue: The total number of sales is $d(s)(T_1 + T_2)$ during the period $[0, T_1 + T_2]$ and pT_4 during the period $[T_1 + T_2, T]$. Thus, the total sales revenue, R_s is

$$R_s = s(d(s)(T_1 + T_2) + pT_4)). \quad (18)$$

Objective function: The total revenues, TR, can be obtained from summing the revenues from sales and cancellations. That is, $TR = (R_c + R_s)$. The total cost, K, can be obtained by summing the productions cost, holding cost, back-ordering cost and the deterioration cost. That is $K = (K_s + K_h + K_b + K_d)$. Accordingly, the profit per unit time is given as follows:.

$$R = TR/T = (R_s + R_c - K_s - K_h - K_d - K_b)/T \quad (19)$$

where $T = T_1 + L + T_4$ is the cycle time.

3 Analysis

There are 4 unknown variables, T_1, T_2, T_4 and s in the objective function. In order to solve this problem, we will reduce the number of unknown variables. We will express the unit time profit function in terms of T_2 and s only. First, we will derive the relationship between T_1 and T_2. Note that $I_1(T_1) = I_2(0)$, thus we have

$$\frac{p - d(s)}{\theta}(1 - e^{-\theta T_1}) = \frac{d(s)}{\theta}(e^{\theta(T_2)} - 1) \tag{20}$$

from which we obtain

$$T_1 = \frac{-1}{\theta} ln\Big(\frac{p - d(s)e^{\theta T_2}}{p - d(s)}\Big). \tag{21}$$

Similarly, since $I_3(T_3) = I_4(0)$, we have

$$\frac{d(s)}{\beta}(e^{-\beta(t-T_2)} - 1) = \frac{p - d(s)}{\beta}(1 - e^{\beta(T-t)}). \tag{22}$$

Solving the above equation yields

$$T_4 = \frac{1}{\beta} ln\Big(\frac{p - d(s)e^{-\beta T_3}}{p - d(s)}\Big) \tag{23}$$

where

$$T_3 = L - T_2. \tag{24}$$

From (21) and (23), we see that T_1 and T_4 can be expressed in terms of T_2 and s, thus the number of unknown variables in the objective function can be reduced from 4 to 2. Then, the unit time profit function can be rewritten as

$$R(T_2, s) = \frac{TR(T_2, s)}{T(T_2, s)} \tag{25}$$

where

$$\begin{aligned} TR(T_2, s) = {} & s(d(s)(T_1(T_2, s) + T_2) + pT_4(T_2, s)) + \lambda s(d(s)(L - T_2 + T_4(T_2, s)) \\ & - pT_4(T_2, s)) - c_s - \frac{c_h}{6}\Big(3T_1(T_2, s)^2 p - T_1(T_2, s)^3 \theta p \\ & - 3T_1(T_2, s)^2 d(s) + T_1(T_2, s)^3 d(s)\theta + T_2^3 d(s)\theta + 3T_2^2 d(s)\Big) \\ & - c_d((p - d(s))T_1(T_2, s) - d(s)T_2) \\ & - c_b \frac{(d(s)(L - T_2 + T_4(T_2, s)) - pT_4(T_2, s))}{\beta}, \end{aligned} \tag{26}$$

$$T(T_2, s) = T_1(T_2, s) + L + T_4(T_2, s). \tag{27}$$

For given parameters $\omega = \{a, b, p, \theta, \lambda, \beta, L, c_s, c_d, c_b, c_h\}$ and a solution set (T_2^1, s^1), $R(T_2^1, s^1)$ is a maximum if the following necessary and sufficient conditions are satisfied.

(1) Necessary conditions:

$$\frac{\partial R(T_2, s)}{\partial T_2} \Big]_{(T_2,s)=(T_2^1,s^1)} = 0, \tag{28}$$

$$\frac{\partial R(T_2, s)}{\partial s} \Big]_{(T_2,s)=(T_2^1,s^1)} = 0. \tag{29}$$

(2) Sufficient conditions:

$$H = \frac{\partial^2 R(T_2, s)}{\partial T_2^2} \frac{\partial^2 R(T_2, s)}{\partial s^2} - \frac{\partial^2 R(T_2, s)}{\partial T_2 \partial s} \Big]_{(T_2,s)=(T_2^1,s^1)} > 0 \tag{30}$$

and either one of the following

$$\frac{\partial^2 R(T_2, s)}{\partial T_2^2} \Big]_{(T_2,s)=(T_2^1,s^1)} < 0, \tag{31}$$

$$\frac{\partial^2 R(T_2, s1)}{\partial s^2} \Big]_{(T_2,s)=(T_2^1,s^1)} < 0. \tag{32}$$

is satisfied. The first derivatives for the unit time profit function are given as follows:

$$\frac{\partial R(T_2, s)}{\partial T_2} = \frac{1}{T(T_2, s)} \frac{\partial TR(T_2, s)}{\partial T_2} - \frac{TR(T_2, s)}{T(T_2, s)^2} \frac{\partial T(T_2, s)}{\partial T_2}, \tag{33}$$

$$\frac{\partial R(T_2, s)}{\partial s} = \frac{1}{T(T_2, s)} \frac{\partial TR(T_2, s)}{\partial s} - \frac{TR(T_2, s)}{T(T_2, s)^2} \frac{\partial T(T_2, s)}{\partial s} \tag{34}$$

where

$$\begin{aligned}
\frac{\partial TR(T_2, s)}{\partial T_2} = {} & s\Big((\frac{\partial T_1(T_2, s)}{\partial T_2} + 1)d(s) + p\frac{\partial T_4(T_2, s)}{\partial T_2}\Big) \\
& + \lambda s\Big((-1 + \frac{\partial T_4(T_2, s)}{\partial T_2})d(s) - p\frac{\partial T_4(T_2, s)}{\partial T_2}\Big) \\
& - \frac{c_h}{6}\Big(- 6T_1(T_2, s)\frac{\partial T_1(T_2, s)}{\partial T_2}d(s) + 3T_1(T_2, s)^2\theta\frac{\partial T_1(T_2, s)}{\partial T_2}d(s) \\
& + 3T_2^2\theta d(s) + 6T_2 d(s) + 6T_1(T_2, s)p\frac{\partial T_1(T_2, s)}{\partial T_2} \\
& - 3T_1(T_2, s)^2\theta p\frac{\partial T_1(T_2, s)}{\partial T_2}\Big) \\
& - c_d\frac{\partial T_1(T_2, s)}{\partial T_2}(p - d(s)) - d(s)) - \frac{c_b}{\beta}\Big((-1 + \frac{\partial T_4(T_2, s)}{\partial T_2})d(s) \\
& - p\frac{\partial T_4(T_2, s)}{\partial T_2}\Big),
\end{aligned} \tag{35}$$

$$\begin{aligned}\frac{\partial TR(T_2,s)}{\partial s} &= (T_1(T_2,s)+T_2)d(s)+s\Big(\frac{\partial T_1(T_2,s)}{\partial s}d(s)+(-T_1(T_2,s)-T_2)b\\ &\quad +p\frac{\partial T_4(T_2,s)}{\partial s}\Big)+\lambda\Big((L-T_2+T_4(T_2,s))d(s)-pT_4(T_2,s)\Big)\\ &\quad +\lambda s\Big(\frac{\partial T_4(T_2,s)}{\partial s}d(s)+(-L+T_2-T_4(T_2,s))b-p\frac{\partial T_4(T_2,s)}{\partial s}\Big)\\ &\quad -\frac{c_h}{6}\Big(-6T_1(T_2,s)\frac{\partial T_1(T_2,s)}{\partial s}d(s)+3T_1(T_2,s)^2\theta\frac{\partial T_1(T_2,s)}{\partial s}d(s)\\ &\quad +(3T_1(T_2,s)^2-T_1(T_2,s)^3\theta-T_2^3\theta-3T_2^2)b\\ &\quad +6T_1(T_2,s)p\frac{\partial T_1(T_2,s)}{\partial s}-3T_1(T_2,s)^2\theta p\frac{\partial T_1(T_2,s)}{\partial s}\Big)\\ &\quad -c_d\Big(\frac{\partial T_1(T_2,s)}{\partial s}(p-d(s))+b(T_1(T_2,s)+T_2)\Big)\\ &\quad -\frac{c_b}{\beta}\Big(\frac{\partial T_4(T_2,s)}{\partial s}d(s)+(-L+T_2-T_4(T_2,s))b-p\frac{\partial T_4(T_2,s)}{\partial s}\Big)\\ &\quad +pT_4(T_2,s), \end{aligned} \tag{36}$$

$$\frac{\partial T(T_2,s)}{\partial T_2}=\frac{\partial T_1(T_2,s)}{\partial T_2}+\frac{\partial T_4(T_2,s)}{\partial T_2}, \tag{37}$$

$$\frac{\partial T(T_2,s)}{\partial s}=\frac{\partial T_1(T_2,s)}{\partial s}+\frac{\partial T_4(T_2,s)}{\partial s}, \tag{38}$$

$$\frac{\partial T_1(T_2,s)}{\partial T_2}=\frac{e^{\theta T_2}d(s)}{p-d(s)e^{\theta T_2}}, \tag{39}$$

$$\frac{\partial T_1(T_2,s)}{\partial s}=\frac{p(e^{\theta T_2}-1)b}{\theta(-p+d(s)e^{\theta T_2})(p-d(s))}, \tag{40}$$

$$\frac{\partial T_4(T_2,s)}{\partial T_2}=-\frac{e^{-\beta(L-T_2)}d(s)}{p-d(s)e^{-\beta(L-T_2)}}, \tag{41}$$

$$\frac{\partial T_4(T_2,s)}{\partial s}=\frac{p(e^{-\beta(L-T_2)}-1)b}{\beta(-p+d(s)e^{-\beta(L-T_2)})(-p+d(s))}. \tag{42}$$

Set

$$\frac{\partial R(T_2,s)}{\partial T_2}=0, \tag{43}$$

$$\frac{\partial R(T_2,s)}{\partial s}=0 \tag{44}$$

and let (T_2^*,s^*) be the solutions to the above nonlinear equation system. Then, $R(T_2^*,s^*)$ can be a maximum if sufficient conditions are satisfied. Note that the equation system of (43) and (44) can be solved by using the Newton procedure. To confirm whether $R(T_2^*,s^*)$ is a maximum, we need to derive the second derivatives for the unit time profit function. The second derivatives for the unit time profit function are

$$\frac{\partial^2 R(T_2,s)}{\partial T_2^2} = \frac{1}{T(T_2,s)}\frac{\partial^2 TR(T_2,s)}{\partial T_2^2} - \frac{2}{T(T_2,s)^2}\frac{\partial TR(T_2,s)}{\partial T_2}\frac{\partial T(T_2,s)}{\partial T_2} + \frac{2TR(T_2,s)}{T(T_2,s)^3}\frac{\partial T(T_2,s)}{\partial T_2}^2 - \frac{TR(T_2,s)}{T(T_2,s)^2}\frac{\partial^2 T(T_2,s)}{\partial T_2^2}, \tag{45}$$

$$\frac{\partial^2 R(T_2,s)}{\partial T_2 \partial s} = \frac{1}{T(T_2,s)}\frac{\partial^2 TR(T_2,s)}{\partial T_2 \partial s} - \frac{1}{T(T_2,s)^2}\frac{\partial TR(T_2,s)}{\partial T_2}\frac{\partial T(T_2,s)}{\partial s} - \frac{1}{T(T_2,s)^2}\frac{\partial TR(T_2,s)}{\partial s}\frac{\partial T(T_2,s)}{\partial T_2} + \frac{2TR(T_2,s)}{T(T_2,s)^3}\frac{\partial T(T_2,s)}{\partial T_2}\frac{\partial T(T_2,s)}{\partial s} - \frac{TR(T_2,s)}{T(T_2,s)^2}\frac{\partial^2 T(T_2,s)}{\partial T_2 \partial s}, \tag{46}$$

$$\frac{\partial^2 R(T_2,s)}{\partial T_2 \partial s} = \frac{1}{T(T_2,s)}\frac{\partial^2 TR(T_2,s)}{\partial s^2} - \frac{2}{T(T_2,s)^2}\frac{\partial TR(T_2,s)}{\partial s}\frac{\partial T(T_2,s)}{\partial s} + \frac{2TR(T_2,s)}{T(T_2,s)^3}\frac{\partial T(T_2,s)}{\partial s}^2 - \frac{TR(T_2,s)}{T(T_2,s)^2}\frac{\partial^2 T(T_2,s)}{\partial s^2}. \tag{47}$$

Since the profit function is very complicated, it is difficult to verify the above sufficient conditions analytically. Therefore, we analyze the optimal decisions by numerical analysis.

4 Numerical Example

In this section, the preceding approach is used to derive the optimal decisions. We consider the cases in which the demand rate decreases according to the equation $d(s) = 20 - 1.5s$. The unit time production rate is $p = 25$, the production lead time is $L = 5$ unit times, the production cost per production run is $c_s = \$50$, the back-order cost per unit per unit time is $c_b = \$1$, the cost per deteriorating unit is $c_d = 1$, and the carrying cost per unit per unit time is $c_h = \$1$. Additionally, the unit time deteriorating rate θ, the fraction of cancellation to the number of back-order β and the fraction of revenue from cancellation to the selling price λ are assumed to be 0.03, 0.03 and 0.5, respectively.

Using the Newton procedure, we find that the solution to the nonlinear equation system 43 and 44 is $(1.565, 7.105)$. Substituting this solution into 38 40 obtains $H = 11.90124 > 0$ and $\frac{\partial^2 R(T_2,s)}{\partial T_2^2} = -4.0069 < 0$, thus the optimal solutions are $T_2^* = 2.469$, $s^* = 7.105$. Thus, The production time T_1 and T_4 should be set at 1.565 and 1.424, respectively. Additionally, the non-production period T_2 and T_3 is expected to be 2.469 and 2.531, respectively. The maximum unit time profit is $R(2.469, 7.105) = 47.65$.

5 Conclusion

This paper studied a production and pricing problem for a deteriorating inventory under the condition that back-order is allowed. Numerous inventory models

have addressed this problem. However, these models have rarely considered a situation in which back-ordering customers may cancel their orders. Tacking the cancellation phenomenon into account, this paper developed a continuous-time model to deal with this problem. The sales price and production period are jointly derived by a simple approach studied in this paper.

The proposed model can be extended to cases with changeable price and stochastic demand, such extensions would be worthy of future research.

Acknowledgment

The author would like to thank the National Science Council of the Republic of China for financially supporting this research under Contract No. NSC 94-2213-E-415-003.

References

1. Balkhi, Z.T., Benkherouf, L.: A production lot size inventory model for deteriorating items and arbitrary production and demand rates. European Journal of Operational Research 92, 302–309 (1996)
2. Balkhi, Z.T.: On a finite horizon production lot size inventory model for deteriorating items: An optimal solution. European Journal of Operational Research 132, 210–223 (2001)
3. Balkhi, Z.T.: The effects of learning on the optimal production lot size for deteriorating and partially backordered items with time varying demand and deterioration rates. Applied Mathematical Modelling 27, 763–779 (2003)
4. Ghare, P.M., Schrader, G.P.: A model for exponentially decaying inventory. Journal of Industrial Engineering 32, 137–142 (1963)
5. Kim, C.H., Hong, Y.: An optimal production run length in deteriorating production processes. International Journal of Production Economics 58, 183–189 (1999)
6. Lin, G.C., Kroll, D.E., Lin, C.J.: Determining a common production cycle time for an economic lot scheduling problem with deteriorating items.pdf. European Journal of Operational Research 173, 669–682 (2006)
7. Pal, A.K., Bhunia, A.K., Mukherjee, R.N.: Optimal lot size model for deteriorating items with demand rate dependent on displayed stock level (DSL) and partial backordering. European Journal of Operational Research 175, 977–991 (2006)
8. Skouri, K., Papachristos, S.: Optimal stopping and restarting production times for an EOQ model with deteriorating items and time-dependent partial backlogging. International Journal of Production Economics 81–82, 525–531 (2003)
9. Wee, H.M.: Economic production lot size for deteriorating items taking account of the time-value of money. Computers and Operations Research 26, 545–558 (1999)

An Intermodal Transport Network Planning Algorithm Using Dynamic Programming

Jae Hyung Cho[1], Hyun Soo Kim[2], Hyung Rim Choi[2], Nam Kyu Park[3], and Moo Hong Kang[2]

[1] School of International Business and Area Studies, Pusan University of Foreign Studies
55-1 Uam-dong, Nam-gu, Busan 608-738, South Korea
chojh@pufs.ac.kr
[2] Department of Management Information Science, Dong-A University
840 Hadan2-dong, Saha-gu , Busan 604-714, South Korea
{hskim,hrchoi,mongy}@dau.ac.kr
[3] Department of Distribution Management, Tongmyong University
Yongdang-dong 535, Nam-gu, Busan 608-711, South Korea
nkpark@tit.ac.kr

Abstract. This paper presents a dynamic programming algorithm to draw optimal intermodal freight routing with regard to international logistics of container cargo for export and import. This study looks into the characteristics of intermodal transport using two or more modes, and presents a Weighted Constrained Shortest Path Problem (WCSPP) model. This study draws a Pareto optimal solution that can simultaneously meet two objective functions by applying the Label Setting algorithm, one of the Dynamic Programming algorithms, after setting feasible area using the objective function values drawn in the model. To improve the algorithm performance, pruning rules have also been presented. The algorithm is applied to real transport paths from Busan to Rotterdam. This study quantitatively measures the savings effect of transport cost and time by comparing single transport modes with existing intermodal transport paths. Lastly, this study applies the multiple Pareto optimal solutions drawn, to a mathematical model and MADM model, and compares the two evaluation methods as a means to evaluate the solutions.

Keywords: Intermodal Freight Routing Problem, Dynamic Programming, WCSPP Model, Label Setting Algorithm.

1 Introduction

In general, ordinary transport means a single transport mode by carrier. However, intermodal transport refers to usage of two or more transport modes to deliver goods from a point of departure to the point of arrival. Third party logistics companies are playing important roles in the intermodal transport [1, 8, 12]. A third party logistics company is required to be armed with NPS (Network Planning System), NOS (Network Optimization System) and DSS (Decision Support System). However, most companies are unable to provide enough information, because they lack such systems.

H.G. Okuno and M. Ali (Eds.): IEA/AIE 2007, LNAI 4570, pp. 1012–1021, 2007.

That can cause increasing cost to consignors[2, 6]. Transport network planning by manual work is therefore likely to pose problems when cargo volume carried by intermodal transport is increasing.

To solve this problem, i.e. to support the common interests of the consignors and the third party logistics companies, it is necessary to build systems that can integrate the modes of transport, routing and scheduling for intermodal transport planning. Therefore, developing an efficient algorithm for intermodal transport planning is very necessary. This study suggests such algorithm using Dynamic Programming(DP). We suggest a Dynamic Programming algorithm for Pareto optimal transport paths among many routing paths so consignors can minimize transport cost and time simultaneously. As a Dynamic Programming algorithm, this study has selected the Label Setting algorithm for constrained shortest path problem. And to simplify the numerous routing paths, pruning rule have also been presented. To test their efficacy, we have applied them to the actual intermodal transport path from Busan a Korean port to Rotterdam in the Netherlands.

2 International Intermodal Freight Routing Problem

Macharis et al. [6] and Jang et al. [5] pointed out that Intermodal Freight Routing Problem (IFRP) was not actively studied in the optimization research field. Even worse, the studies dealing with International Intermodal Freight Routing Problem (IIFRP) were scanty. In the Min' study, (a representative study dealing with IIFRP), a chance-constraint objective planning model was presented to select the most effective transport mode in terms of service cost among trucks, airlines, and ships, but used virtual data[8]. Jang et al. [5] studied IIFRP to achieve the efficiency in transport cost and time using genetic algorithms. However, it was limited to domestic intermodal freight routing problem considering ship as the only international transport mode.

For the transport modes studied previously, Min [8] considered truck, airline and ship, Barnhart et al. [1] considered truck and ship and Boardman et al. [2] considered truck, train and airline. All these focused on trucks because they concerned domestic(inland) transport modes more than international ones. On the contrary, this study focuses on international intermodal transport modes. It is realistic for a consignor to decide international intermodal transport modes first, and then inland transport modes second, because the schedules of international transport modes are operated with fixed schedules while the schedule of inland transport modes such as trucks are flexible by request.

This study considers the ship, train, and airline as international intermodal transport, and has developed an intermodal transport network planning algorithm, based on real intermodal freight routing from Busan to Rotterdam.

We have assumed following conditions to define our problem of intermodal transport network planning. During cargo loading, all cargo needs to be loaded together in the mode of transport. If there is a mode of transport that cannot load the cargo as a whole, it will be precluded in the route generation. Each port, airport, and station becomes a node. Transshipment between different transport modes can be made at a 'location'. One location includes multiple nodes. Transshipment can be made only once

in the same location. Transshipment into the other transport modes may be allowed only by land. The transport cost and time by land are proportional to the distance.

3 Optimal Intermodal Transport Network Planning Algorithm

3.1 Pruning Rules

Major transit points between Busan and Rotterdam are exhibited in Fig. 1. Only the nodes where transshipment is possible between other transport modes have been indicated as Transit points.

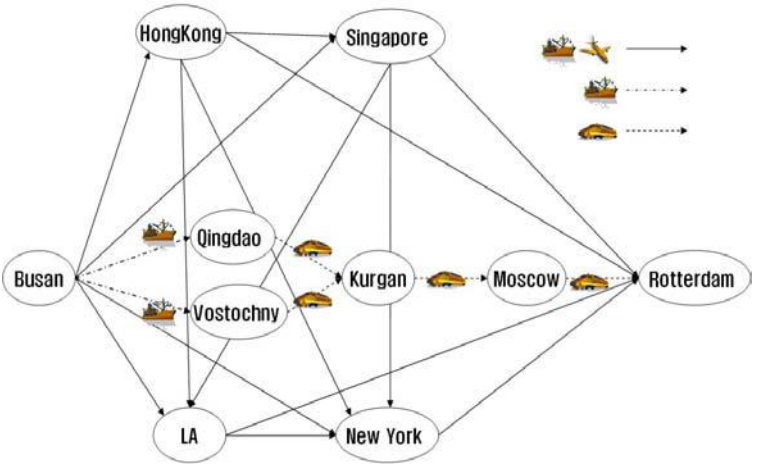

Fig. 1. Major Intermodal Transport Nodes between Busan and Rotterdam

About 850,375 paths have been drawn between Busan and Rotterdam, based on schedule information by transport modes secured in this study. However, more schedules for transits exist in reality. This study has used a pruning rule which serves to upgrade performance and efficacy while seeking an optimal path from among the numerous available paths for intermodal transport to operate. If there are two arcs of "k" and "l" in one node (n), the transport cost (C) and transport time (T) comprise of one pair (C_n^k, T_n^k) and (C_n^l, T_n^l). Also, if one is in a dominant position, the other arc will be eliminated by the pruning rules. The pruning rules are as follows.

Rule 1. The arc with a higher cost and time in one node will be eliminated.

If $C_n^l > C_n^k$ *and* $T_n^l > T_n^k$, (C_n^l, T_n^l) is eliminated by (C_n^k, T_n^k)

Rule 2. If the cost of both arcs is the same in one node, but the time taken is different, then, the arc with the longer time is eliminated. Also, if the time taken is the same, but their cost is different, the higher cost arc is to be eliminated.

If $(C_n^l = C_n^k \quad and \quad T_n^l > T_n^k)$ *or* $(T_n^l = T_n^k \quad and \quad C_n^l > C_n^k)$,
(C_n^l, T_n^l) is eliminated by (C_n^k, T_n^k)

Rule 3. If an arc in a node has an arrival date later than the latest departure date, it is to be eliminated.

$$\max(S_n^{\delta^+}) < (A_n^{\delta^-})$$

If there is a departure arc (δ^+) and arrival arc (δ^-) in a node, and the departure time of the departure arc is represented as $S_n^{\delta^+}$ and the arrival time of the arrival arc is represented as $A_n^{\delta^-}$, the arc $A_n^{\delta^-}$ is larger than the maximum value of $S_n^{\delta^+}$ so it is to be eliminated.

3.2 Mathematical Formulation of WCSPP

The constrained shortest path problem which is an extended shortest path problem, is generally known as the NP-hard problem. Taking account of the trade-off relationship between time and cost, Martins discovered multiple Pareto optimal paths, solving the problem by way of combination and optimization[7]. However, he also proved that it was impossible to test all of Pareto optimal solutions. Due to this, there is only one objective function, and the other considerations are constraints. Based on this proposition, the research is active on the shortest path problem. These studies are known as WCSPP (Weighted Constrained Shortest Path Problem)[3, 9, 11]. The objective function of WCSPP Linear Program Formulation based International Intermodal Transport, its constraints, and variables are defined as follows.

$$\min \sum_{a \in A} (c_a^m \cdot q_a \cdot x_a^m + q_a \cdot lc_n^a + q_a \cdot uc_n^a) \quad \cdots (1)$$

$$\text{such that} \sum_{a \in \delta^+(i)} x_a - \sum_{a \in \delta^-(i)} x_a = \begin{cases} 1, \text{if i = s} \\ -1, \text{if i = t} \\ 0, \text{if i} \in \text{V} \setminus \{\text{s, t}\} \end{cases} \quad \forall i \in V$$

$$\sum_{a \in A} w_a x_a \le W_t$$

$$x_a \in \{0,1\} \ \forall a \in A$$

$$\min \sum_{a \in A} (t_a^m \cdot x_a^m + lt_n^a + ut_n^a) \quad \cdots (2)$$

$$\text{such that} \sum_{a \in \delta^+(i)} x_a - \sum_{a \in \delta^-(i)} x_a = \begin{cases} 1, \text{if i = s} \\ -1, \text{if i = t} \\ 0, \text{if i} \in \text{V} \setminus \{\text{s, t}\} \end{cases} \quad \forall i \in V$$

$$\sum_{a \in A} w_a x_a \le W_c$$

$$x_a \in \{0,1\} \ \forall a \in A$$

c_a^m : Transport cost of transport mode m at the arc a
x_a^m : When transported from arc a by transport mode m, 1 or 0
q_a : Quantity of Cargo at the arc a
lc_n^a : Loading cost of arc a at node n
uc_n^a : Unloading cost of arc a at node n
lt_n^a : Loading time of arc a at node n
t_a^m : Transport time of transport mode m at the arc a
lt_n^a : Loading time of arc a at node n
ut_n^a : Unloading time of arc a at node n
w_a : Constraint at the arc a
W_c : Cost constraint
W_t : Time constraint

3.3 Dynamic Programming for WCSPP

The Formula 1 and Formula 2 can bring the points Z_1 and Z_2 as shown in the Fig. 2 respectively. Z_3 at the intersection of these two points seems to be an optimal solution for the two objective functions. But Z_3 is not feasible as a solution. Accordingly, we have defined the area (area in the shade) in the three points as feasible area. So if the solution of DP algorithm lies in the feasible area, it will become a feasible solution. The distance from T_1 and T_2 in the feasible area is defined as an 'effective time range', which becomes a constraint scope to cost of DP algorithm.

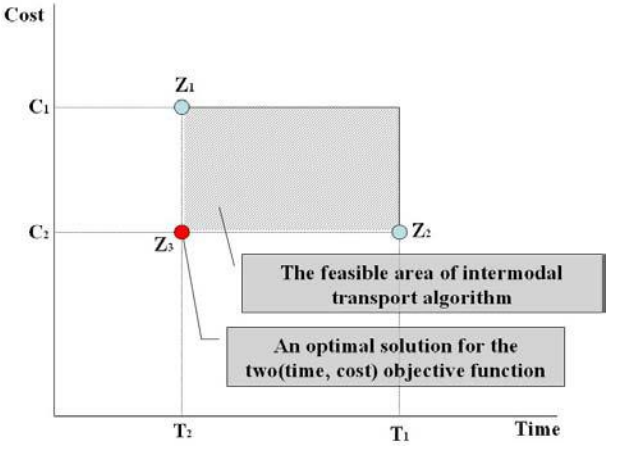

Fig. 2. The Feasible Area of WCSPP Algorithm

As a solution for DP algorithm, this study has used Label Setting algorithm which is a dynamic programming. Label Setting algorithm was developed by Descrochers et al. [4]. This method attaches labels to each node, and the labels are composed of a pair {weight, objective function}. In the Label Setting algorithm, time was weighted as a constraint and cost was expressed as the objective function. Although we need to minimize cost, the consignor's desired date of arrival needs to be considered, rather than minimization of transport time. This is because earlier arrival than scheduled arrival date will incur warehousing or inventory costs, and if transport time is later than the scheduled arrival date, penalty will be imposed due to breach in agreement. Therefore, effective time range obtained in the WCSPP LP model is made the weight constraint of the Dynamic Programming algorithm.

In the label $\{W_i^q, C_i^q\}$, W_i^q refers to the q^{th} weight in the node i, and C_i^q refers to the q^{th} cost in the node i. w_{ij} and c_{ij} respectively refer to the weight and cost from node i to node j. The Label Setting algorithm is generally performed as follows.

Step 0: Initialization
Set $Label_s = \{(0, 0)\}$ and set $Label_i = \Phi$ for all $i \in V \setminus \{s\}$.

Step 1: Selection of the label to be extended
If all Labels have been marked, then TERMINATE; all efficient labels have been generated;

Else choose i∈ V such that there's unmarked label in $Label_i$ and W_i^q is minimal, where q is the path that attains this weight value

Step 2: Extend label (W_i^q, C_i^q)

For all (i,j)∈ $\delta^+(i)$ with $W_i^q + w_{ij} \leq W$ do

If $(W_i^q + w_{ij}, C_i^q + c_{ij})$ is not dominated by (W_j^k, C_j^k) for any existing label at node j

Then set $Label_j = Label_j \cup \{(W_i^q + w_{ij}, C_i^q + c_{ij})\}$

Mark label (W_i^q, C_i^q)

Goto Step 1.

4 Experiment

4.1 Results and Analyses of Experiment

The routing path leaving Busan and arriving in Rotterdam is representative of the transport paths between Asia and Europe. The experiment's data was composed of schedule information, provided between transit points of major intermodal transport paths. The schedule and cost information was calculated based on tariff rates provided by shipping companies and airlines. Primarily, pruning rules have been applied to 850,375 paths, which were set as basic data of the experiment. About 100 paths are drawn between Busan and Rotterdam, considering single transport and intermodal transport modes. However, multiple schedules exist between transit points in one path, and the transits' schedules are then multiplied; thus, 850,375 paths have been drawn. Due to the application of the pruning rules to the schedules in the same path, all except for 512 paths have been removed. The pruning rules have been executed through Structured Query Language (SQL) of the Data Management System, which is currently under way in this study.

As a next step, a WCSPP LP model was applied to 512 paths. As a result, a ship and an airline were drawn incurring minimum cost and taking the shortest time, respectively. Table 1 exhibits the results.

Table 1. Transport Time and Cost of Single Transport Modes between Busan and Rotterdam

Classification	Transport Mode	Transport Time	Transport Cost
Min. Cost	Ship	792 hours	$325
Shortest Time	Airplane	11 hours	$1854

The feasible area has been defined, based on the results drawn in the WCSPP LP model. Lastly, Label Setting algorithm was carried out for 512 paths. Due to the execution of the Label Setting algorithm, the paths deviating from the feasible areas have been removed again. The number of the paths that deviated was 461. Most of them executed four or more transshipments, and those dealing in cargo transshipped by air twice if not more, were removed. This is because loading and unloading costs and

time have relatively increased, due to frequent transshipments. Fig. 3 indicates the solutions included in the feasible area based on the time-cost coordinates by applying a Label Setting algorithm. The paths exhibited in the coordinates are 51, and these are the values included in the feasible area in Fig. 2.

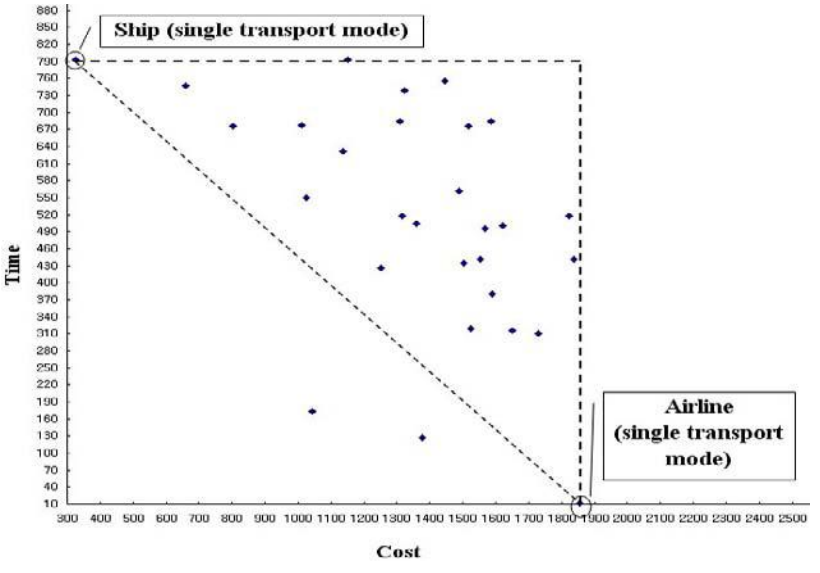

Fig. 3. Results of Label Setting Algorithm Experiment

As presented above, minimum transport cost was US$325, when cargo was transported by ship in single transport mode, and the transport time took 792 hours. In the intermodal transport format, drawn through the experiment, the path departing Busan (Ship) – Hong Kong (Airline) – Singapore (Ship) and arriving in Rotterdam cost US$660, the minimum cost, and the transport time took 747 hours. As a result of carrying out the Label Setting algorithm, intermodal transport path did not draw a cheaper path compared to single transport by ship. However, when considering the transport cost along with transport time, the intermodal transport path had the competitive edge.

When transport time was 700 hours or less, a total of 40 Pareto optimal solutions have been drawn, when it was 600 hours or less, 31 Pareto optimal solution have been drawn, when 500 hours or less, 25 Pareto optimal solutions have been drawn. When transport time was 400 hours or less, a total of 16 Pareto optimal solutions have been drawn, and when it was 200 hours or less, 7 Pareto optimal solutions (Same number of Pareto optimal solutions in the case of 300 hours or less), and when 100 hours or less, 3 Pareto optimal solutions have been drawn. The Pareto paths from which minimum transport costs by transport time have been drawn are exhibited in Table 2.

Table 2. Results of Label Setting Algorithm Application

Transport time	Departure	Transit(1)	Transit(2)	Transit(3)	Transport cost	Transport time
792 hours or less	Busan(S)	Hong Kong(A)	Singapore(S)	Rotterdam	660	747
700 hours or less	Busan(A)	Hong Kong(S)	Singapore(S)	Rotterdam	802	676
600 hours or less	Busan(S)	LA(S)	Rotterdam		1025	550
500~200 hours or less	Busan(S)	Singapore(A)	Rotterdam		1042	173
100 hours or less	Busan(A)	Hong Kong(A)	Rotterdam		1752	13

4.2 Evaluation of Pareto Optimal Solutions

A user(shipper or consignor) can select one from among the 5 Pareto optimal solutions. Each user can have a different preference in terms of time and cost. However, in order to enable effective selection, we can use the evaluation method by means of user's value satisfaction of the optimal solution. To this end, this study has suggested two kinds of evaluation methods.

The first is a mathematical model. Among the values of the straight lines connecting the Z_3 point of a discretionary optimal solution and 5 Pareto optimal solutions, the shortest value has been evaluated as the optimal alternative. To this end, the value of time and cost has been normalized as in Table 3. Table 3 shows the normalized values of discretionary optimal solution Z_3 and the 5 alternatives. As time and cost have a different size, its relative distribution is denoted as the values between 0 and 1. By using these values, the user's value satisfaction for the 5 Pareto optimal solutions has been generated, and the results are shown in the Table 3. By using the mathematical model, the Table 3 shows that the highest degree of value satisfaction is (1042, 173).

Table 3. Normalization Value Results of Time and Cost & Value Satisfaction Evaluation Results of Pareto Optimal Solutions through the Mathematical Model

Pareto optimal solutions	Normalized Value	Pareto Optimal Solutions	Distance with Z_3
(660,747)	(0.00, 0.35)	(660,747)	0.122
(802,676)	(0.07, 0.32)	(802,676)	0.107
(1025,550)	(0.18, 0.26)	(1025,550)	0.100
(1042,173)	(0.19, 0.08)	(1042,173)	0.042
(1752,13)	(0.55, 0.00)	(1752,13)	0.302
Z_3	(0.00, 0.00)		

The second evaluation method is MADM(Multi-Attribute Decision Making). By using MADM, many negotiation items with different measuring criterion can be normalized by the same criterion, so that each negotiation item will be compared. MADM can not only show the evaluation values of each alternative, but also give a subjective weight to the items, consequently helping to seek an optimal solution.

MADM method is mainly used for the solution of the problems having many alternatives and attributes, thus aiming to decide the order of preference for many alternatives. At his point in time, the weight carrying the significance of many attributes has a critical influence upon the final result. Because of this, an easy and convenient

method should be used for a decision maker. In this respect, the entropy measure is widely used in many fields to confirm and check the difference between given data. Accordingly, the entropy measure concept is being used in the MADM in order to confirm, check, and evaluate the items in the MADM problem. But in case that a certain attribute among many alternatives has the same evaluation value, it will be eliminated because it cannot contribute to the selection of the alternatives.

Table 4. Value Satisfaction Evaluation Results of Pareto Optimal Solutions through MADM

Pareto Optimal Solutions	MADM Evaluation Results
(660,747)	0.104
(802,676)	0.120
(1025,550)	0.153
(1042,173)	0.311
(1752,13)	0.312

According to the results 0.312 of the MADM evaluation, (1752, 13) has been generated as an optimal alternative. However, this result is different from the result of the mathematical model. The reason being in case of MADM evaluation, the entropy denoting the weight and co-relationship degree of each alternative is determined first, and then each alternative is evaluated by means of the entropy value.

5 Conclusion

This study has suggested an optimal transport algorithm for intermodal transport that can practically be used by third party logistics. A WCSPP LP model has been presented first to apply the revised Label Setting algorithm, one of the Dynamic Programming algorithms, to the path from Busan to Rotterdam in line with the proposition in this study. Pareto feasible area was set by using the minimum cost and shortest time drawn by the WCSPP LP model, through which a new model, which can apply the Label Setting algorithm to realistic problems, has been presented. The performance of algorithm improved furthermore by carrying out the pruning rules side by side. A mathematical model and MADM model have been applied to evaluate multiple Pareto optimal solutions. The significance of this study lies in that feasibility has been verified by applying the algorithm to the real intermodal transport path from Busan and Rotterdam. In the future study, we will develop a third party logistics transportation network system mounted with the algorithm used in this study and present the system.

Acknowledgments. "This work was supported by the Korea Research Foundation Grant funded by the Korean Government(MOEHRD)" (The Regional Research Universities Program/Research Center for Logistics Information Technology).

References

1. Barnhart, C., Donald, H.R.: Modeling Intermodal Routing. Journal of Business Logistics. 14(1), 205–223 (1993)
2. Boardman, B.S., Malstrom, E.M., Butler, D.P., Cole, M.H.: Computer Assisted Routing of Intermodal Shipments. Computers and Industrial Engineering. 33(1-2), 311–314 (1997)
3. Chen, Y.L., Chin, Y.H.: The Quickest Path Problem. Computer Operations Research. 17(2), 153–161 (1990)
4. Descrochers, M., Soumis, F.: A Generalized Permanent Labeling Algorithm for the Shortest Path Problem with Time Windows. INFOR 26, 191–212 (1988)
5. Jang, Y., Kim, E.: Study on the Optimized Model of Intermodal Transport Using Genetic Algorithm. Shipping Logistics Research (45), 75–98 (2005)
6. Macharis, C., Bontekoning, Y.M.: Opportunities for OR in Intermodal Freight Transport Research: A Review. European Journal of Operational Research 153, 400–416 (2004)
7. Martins, E.Q.V.: On a Multicriteria Shortest Path Problem. European Journal of Operational Research. 1, 236–245 (1984)
8. Min, H.: International Intermodal Choices via Chance-constrained Goal Programming. Transportation Research Part A: General 25(6), 351–362 (1991)
9. Moore, M.H.: On the Fastest Route for Convey-type Traffic in Flowrate-contrained Networks. Transportation Science 10, 113–124 (1976)
10. Pasquale, A., Maurizio, B., Antonio, S.: A Penalty Function Heuristic for the Resource constrained Shortest Path Problem. European Journal of Operational Research 142, 221–230 (2002)
11. Rosen, J.B., Sun, S.Z., Xue, G.L.: Algorithm for the Quickest Path Problem and the Enumeration of Quickest Paths. Computer Operations Research 18(6), 579–584 (1991)
12. Yu, I., Kim, J., Cho, G., So, S., Park, Y.: Study on the Evaluation Standards to Select Third Party Logistics Firms. Journal of Korea Information and Strategy Society 8(1), 579–584 (2004)

Immune Inspired Optimizer of Combustion Process in Power Boiler

Konrad Świrski[1] and Konrad Wojdan[2]

[1] Institute of Heat Engineering
Warsaw University of Technology, Nowowiejska 15/19, 00-665 Warsaw, Poland
swirski@itc.pw.edu.pl
[2] Institute of Radioelectronics
Warsaw University of Technology, Nowowiejska 15/19, 00-665 Warsaw, Poland
kwojdan@ire.pw.edu.pl

Abstract. The article presents an optimization method of combustion process in a power boiler. This solution is based on the artificial immune systems theory. A layered optimization system is used, to minimize CO and NOx emission. Immune inspired optimizer SILO is implemented in each of three units of Ostroleka Power Plant (Poland). The results from this implementation are presented. They confirm that presented solution is effective and usable in practice.

Keywords: Adaptive Control, Bio-informatics, Intelligent Systems, Systems for Real Life Applications, Artificial Immune Systems, Optimization.

1 Introduction

Optimization and decision support systems enjoy great popularity in power stations and thermal power stations in the last few years. From the economical point of view plant's work management is complicated without such systems because of big amount and variety of problems connected with electric energy production process. Lots of research institutes and companies develop this type of systems. Most of them are focused on the combustion process. Reasons for such research's direction are obviously. Successful implementation of combustion process optimization in a boiler leads to reduction in fuel consumption and in deleterious gases emission, what brings considerable economic profits. Although there is a big amount of successful implementations of such systems all solutions which are known by authors have two basic disadvantages:

- in each case implementation of technologies, mentioned above, is connected with high implementation cost. While computer cost is low, the cost of work of high qualified engineers staff is the significant load to power plant budget;
- fuel parameters, which are usually analyzed in laboratory once a day, are not taking into account during defining quality indicator for optimization problem.

There is no possible to eliminate those disadvantages using standard methods. This tends us forward to search for new techniques. It seems that SILO system, which is a

H.G. Okuno and M. Ali (Eds.): IEA/AIE 2007, LNAI 4570, pp. 1022–1031, 2007.

stochastic optimizer inspired by artificial immune system theory, is a good method to solve such problem.

2 Biological and Artificial Immune Systems

Dąbrowski in [2] noticed, that immune system, like the nervous system, is the particular structure, which is able to gather and develop qualification during learning and testing process. Moreover this system has the memory. It can develop new or lost old abilities, according to external conditions. The immune system's features mentioned by Dąbrowski come in useful in solving diverse technical problems.

The main goal of immune system is to protect organism against pathogens. Term pathogens means viruses, bacteria, parasites and other microorganisms, which are dangerous for live organism. Therefore immune system has to detect properly and effectively eliminate pathogens. Pathogens has antigens, which induce immune response. Antigens are detected by detectors – lymphocytes, which structure represents directly the knowledge of immunological system. There are two types of lymphocytes in immune system - B cells and T cells. In our article we will concentrate on the B cells and Th cells (sub-group of T cells). Each B cell could have different combination of tools to destroy pathogens. Thus lymphocytes could have variety level of effectiveness in fighting with the particular sort of pathogens. Indeed those tools are the antibodies, which are produced by B cells ([1], [2] ,[5]). New B cells are created in bone marrow without antigens' stimulation or during clonal selection process, which is caused by antigen stimulation [13].

Continuously learning is characteristic feature of immune system. This process is connected with so-called primary response ([1], [7]). It's organism's reaction to new, unknown pathogen. Primary response of the immune system is usually slow. System needs time to eliminate unknown pathogen. It should be noticed that information about pathogen is remembered after successful defense action. It causes faster and more effectiveness organism's reaction to renewed pathogen's attack. It is secondary response ([1], [7]) which testify to adaptability feature of immune system.

Nowadays knowledge about immune system is base for artificial immune systems theory. This theory could inspire to construct efficient information processing systems, which is able to learn continuously and adapt to new environment.

3 Combustion Process in a Boiler

Combustion process in a boiler is presented in this chapter. Of course the process is described superficially. This chapter describes combustion process from the immune point of view ([3], [4]). Diagram of the power boiler is shown in Fig. 1. Control signals, disturbances signals and process outputs are marked.

We define health level of the organism as the deviation from the optimal parameters [15]. Immune optimizer wants to assure the best health level. Therefore he

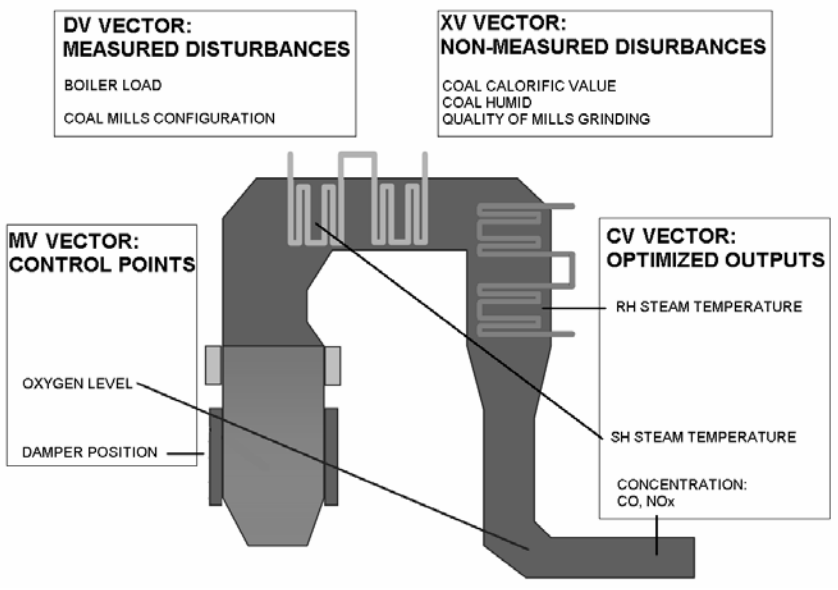

Fig. 1. Power plant boiler in the context of combustion process control

minimizes deviation from the optimal parameters ([3], [4]). In more formal notation optimization algorithm minimize indicator (1):

$$J = \sum_{k=1}^{N} \left[a_k \cdot \left| K_l (ap_k - sp_k) \right| + b_k \cdot \left(K_k (ap_k - sp_k) \right)^2 \right] \tag{1}$$

where:

N *total number of points from MV and CV group.*
ap_k *current value of k-th point*
sp_k *set point value for k-th point*
a_k, *weight for the Linear Penalty Coefficient for k-th point from MV or CV group*
b_k *weight for the Square Penalty Coefficient for k-th point from MV or CV group*
K_l *linear insensitivity zone operator*
K_k *square insensitivity zone operator*

4 Problem Representation

In this chapter combustion process optimization problem representation in the context of immune systems will be described. Structure of immune inspired optimizer SILO will be compared with real immune system.

4.1 Pathogen

Pathogen represents the disturbances (measured and non-measured), which have effect on boiler work. In some points this approach is similar to Krishnakumar and Neidhoefer ([6], [8], [9], [10]) idea. They also represent system disturbances as an antigen.

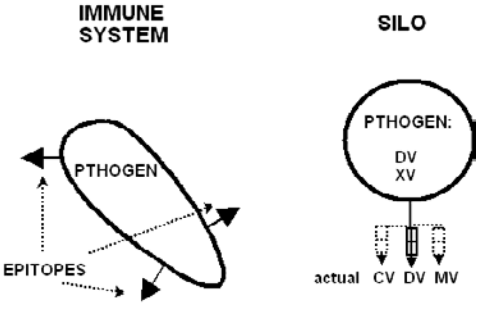

Fig. 2. Pathogen representation

Pathogen is recognized by antibody thanks to the epitopes, which are located on the pathogen's surface. Thus epitopes present the pathogen to immune system. In the case of combustion process, disturbance's influence is expressed by process state ({CV, DV, MV} vector) changes. Thus in SILO system pathogen represent disturbance and pathogen is presented to immune system in process' state form.

4.2 Antibody

Antibodies are created by B cells. The task of antibody is to bind the antigen. Each antibody is able to recognize only one sort of epitopes. Antibody consist of antigen binding part and effector part [12].

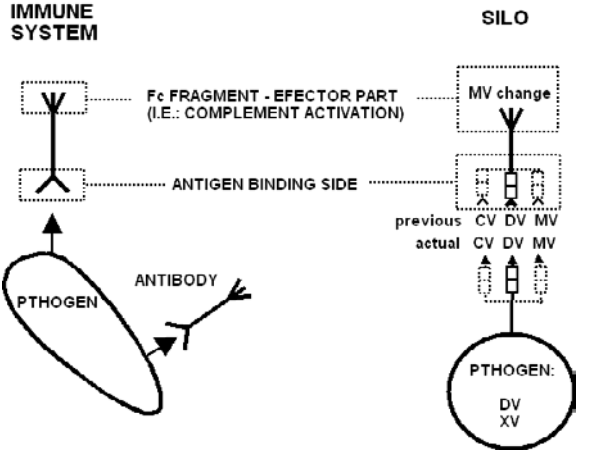

Fig. 3. Antibody representation

In SILO system antibody effector part is a vector of MV points' increments, which minimize indicator (1). Thus setting new control vector to the object should compensate disturbance's influence on combustion process. This approach is similar to those proposed by Fukuda ([6], [11]). He also treats best solution vector as antibody.

There are many propositions of defining antibody binding strength (lymphocyte affinity). Measure to calculate lymphocytes' affinity is determinated by lymphocyte's representation ([7]). In most optimizations problem affinity is evaluated with use of optimized quality indicator [14]. In SILO other solution was proposed. We assumed that antibody binds antigen only when actual process points' values are similar to process points' values stored in lymphocyte, which created an antibody. Set of process points can be limited only to points which represent disturbances. In the case when process characteristics are strong non-linear it is possibility to compare also an actual (antigen) and previous (antibody) values of MV and CV points. One should noticed, that if previous and actual MV, DV and CV vectors are similar, then elements of previous and actual XV (non-measured disturbances) vector are also similar. This correlation has simple explanation. If XV vectors are distinctly different, then process response {CV} for the same input signals {MV, DV} will be different. Thus lymphocytes will represent different pathogens. Therefore information of rarely or non-measured disturbances is indirectly taking into consideration while evaluating affinity level.

4.3 Lymphocyte - B Cell and Th Cell

B cells produces certain type of antibodies. B cells also take part in immune memory creation process. When antibody, which is located on the surface of the B cell, binds the antigen, then the pathogen is presented on the surface of the lymphocyte in the

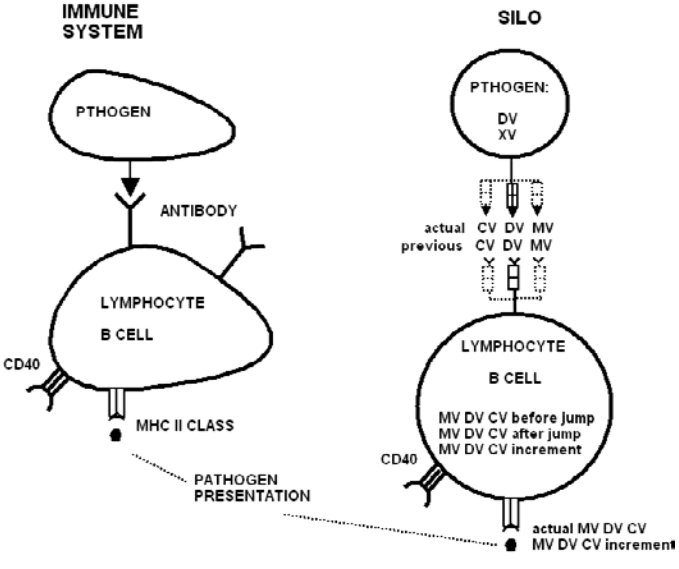

Fig. 4. B cell representation

context of MHC class II particle. When Th cell recognizes the presented antigen, then it activates B cell to intensive proliferation and differentiation (clonal selection mechanism). B cell receives activation signal through CD40 receptor.

In SILO system lymphocyte represent process state before and after control change. Each pair *process state* and *object's outputs response to control variables' change* represents one lymphocyte. Antigen presentation on the surface of the B cell, consists of *actual process state* and *MV points (input) influence on CV points values (output)*. Th cell takes a decision about B cell activation, based on indicator (1).

4.4 Complement

When antibody binds antigen, effector part activates complement system to pathogen lysis. In SILO system effector part consist of demand increment of MV points' values. Complement system consists of real control devices (boiler's dampers, oxygen controller) which realize SILO instructions.

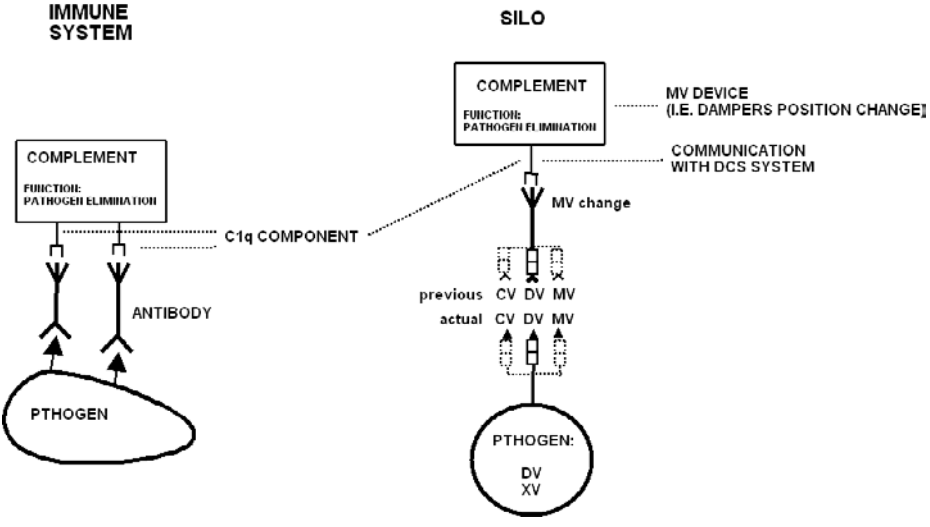

Fig. 5. Complement representation

5 Layer Optimization Algorithm

Optimization algorithm's layers are shown at Fig. 6. Function of each layer is described below.

5.1 Layer 1 - Direct Application of Lymphocyte

In this layer whole immune memory is searched for B cells which represent a process state similar to the current one. Only one B cell is activated from obtained lymphocytes' subset, the one with has antibodies (MV increments) which cause the

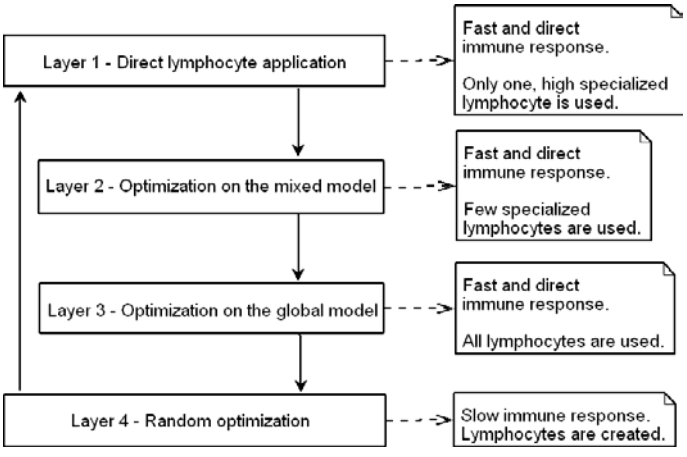

Fig. 6. Optimizer layers

biggest drop of the indicator (1). Each lymphocyte activation cause generation of new lymphocyte which is very similar to parent's B cell. Combustion process safeties not allows for big increments of MV vector values. Because of this fact, in most cases, lymphocytes needs to be applied few times, before he neutralized pathogen. Thus we obtain a few new clones of the parent's B cell. The real process inputs and real process outputs will never be exactly the same (devices inaccuracy, other parameters influence), what causes a lymphocytes mutations. This mechanism is very similar to clonal selection mechanism.

If the solution found in this layer turns out unsuccessful, the program is switched to layer 2.

5.2 Layer 2 - Optimization on Mixed Model

In this layer all B cells, which fulfill affinity conditions are activated. An incremental mathematical model is constructed based on that B cells. This is so-called local model. Apart from a local model, a global model is also constructed. A global model is constructed from all B cells saved in immune memory. Then on the basis of these two model, a mixed model is constructed. This model represent MV vector increment's influence on CV vector increment (constant disturbances DV vector). The weight of the global model is small. Global model is used only for improve a SILO robust. If the process is strongly nonlinear, global model could be disable.

Th cell searches for solution which minimizes indicator (1) based on mixed model . Then Th cell activates new B cell which has the optimal demand MV vector. New B cell is the descendant of the B cells, which fulfill affinity conditions.

If the solution found in this layer turns out unsuccessful, the program is switched to layer 4.

5.3 Layer 3 - Optimization on Global Model

This layer is similar to layer 2. The main difference is that only global model is build.

5.4 Layer 4 - Random Optimization

Since during the initial stage of program operation, the immune memory is relatively small, it frequently happens that the system is attacked by unregistered so far pathogens (new mills configuration, new boiler load). In this layer random movements of MV class signals are performed (damper positioning, O2 content). Thus, we can see that the main task of this layer is to generate new lymphocytes which will constitute the immune memory. Apart from generating new lymphocytes, thanks to applying special heuristic, this algorithm also causes a reduction of the quality indicator (1). This layer has similar function to bone marrow.

5.5 Innate Immune System

Thanks to innate immune system body is born with the ability to recognize certain pathogens and immediately destroy them [5]. After SILO installation, before launching the program, user (power station's engineer with some experience) can also define (in very easy way) some defense scenarios, against some well known pathogens' attacks

6 Results from Ostroleka Power Station

Results from the SILO implementation in Ostroleka Power Station (Poland) will be presented in this chapter. SILO was implemented on each of three units (max. boiler load - 240 MW). SILO works in range 110-240 MW. Table 1 contains information about MV, CV and DV vector size. Disturbances, which are not taken under consider, should be treated as elements of XV vector.

Table 1. MV, DV and CV vectors' size

	Unit 1	Unit 2	Unit 3
MV vector size	11	11	9
CV vector size	6	6	6
DV vector size	5	5	5

Main goals of SILO was to keep:

- SH (super-heat) steam temperature on 540 ^{o}C +/- 7 ^{o}C;
- average CO emission below 250 mg/nm^3;
- average NOx emission below 500 mg/nm^3.

Table 2. Results obtained in Ostroleka Power Station

duration of test – one week		Unit 1	Unit 2	Unit 3
NOx emission: 500 mg/nm^3 level exceed (one hour average)	SILO ON	0.0 %	11.1 %	7.1 %
	SILO OFF	6.7 %	33.5 %	42.5 %
CO emission: 250 mg/nm^3 level exceed (5 minute averages)	SILO ON	0.0 %	0.0 %	1.6 %
	SILO OFF	0.2 %	1.3 %	5.1 %

Six month analyzes of SILO operation in Ostroleka Power Station, allows us to formulated following conclusions. On each of three unit:

- SILO is able to continuously control combustion process. SILO was turned off only in the case of coals mills failure.
- SILO is able to effective react for disturbances changes without operators' interventions.
- SILO distinctly reduces NOx and CO emission without deterioration of boiler efficiency and super-heat steam temperature.

7 Conclusions

Stochastic Immune Layer Optimizer uses in practice Artificial Immune Systems theory. Main goal of this solution is power station's variable costs optimization, achieved by combustion process optimization, especially by CO and NOx emission minimization. Main advantages of this solution are presented below:

- decrease cost of electric plant work achieved by optimizing combustion process with indirect use of information about non-measured or rarely measured disturbances (fuel parameters, quality of mills grinding);
- implementation cost decrease achieved by highly qualified engineers staff work time reduction (there is no need to build complex models after SILO installation);
- on-line learning and adaptation to new environment.

SILO was implemented in Ostroleka Power Plant. Very good results obtained on this plant induce Power Plant management to order new SILO application to flue-gases desulphurization process' optimization. Transition Technologies company, which distribute SILO system, is going to implement next SILO's in USA. Results obtained on new power stations will be successively published in branch press and on scientific and technical conferences.

References

1. Wierzchoń, S.: Artificial Immune Systems – theory and application, Exit, Warsaw (2001)
2. Dąbrowski, M.: Immune system: your personal doctor, Sanmedia, Warsaw (1994)
3. Chomiak, T., Jarmoszewicz, G., Świrski, K., Wojdan, K.: Optimization of combustion in a boiler using immune system. In: conference materials Scientyfic Problems of Thermal Energy 2005, Warsaw, pp. 53–62 (2005)
4. Wojdan, K.: Immune optimizer SILO – user manual, Transition Technologies S.A. materials (unpublichied)
5. De Castro, N., Von Zuben, F.J.: Artificial Immune Systems: Part I – Basic Theory and Applications, Technical Report – RT DCA 01/99
6. De Castro, N., Von Zuben, F.J.: Artificial Immune Systems: Part II – A Survey of Applications, Technical Report – RT DCA 01/99
7. De Cstro, L.N., Timmis, J.I.: Artificial Immune Systems as Novel Soft Computing Paradigm. Soft Computing Journal 7(7) (2003)

8. KrishnaKumar, K., Neidhoefer, J.: Immunized Adaptive Critics for Level 2 Intelligent Control. In: Proc. Of the IEEE SMC' 97, pp. 856–860
9. KrishnaKumar, K., Neidhoefer, J.: Immunized Neurocontrol. Expert Systems with Applications, 201–214
10. KrishnaKumar, K., Neidhoefer, J.: An Immune System Framework for Integrating Computational Intelligence Paradigms with Applications to Adaptive Control. In: Palaniswami, M., Attikiouzel, Y., Marks, R.J., Fogel, I.D., Fukuda, T. (eds.) Computational Intelligence A Dynamic System Perspective, pp. 32–45. IEEE Press
11. Fukuda, T., Mori, K., Tsukiama, M.: Parallel Search for Multi-Modal Function Optimization with Diversity and Learning of Immune Alghorithm. In: Dasgupta, D. (ed.) Artificial Immune Systems and Their Applications, pp. 210–22, Springer, Heidelberg
12. Lydyard, P.M., Whelan, A., Fanger, M.W.: Instant Notes in Immunology, BIOS Scientific Publishers Limited (2000)
13. Solomon, E.P., Berg, L.R., Martin, D.M., Villee, C.A.: Biology, Saunders College Publishing, USA (1993)
14. Wierzchoń, S.T.: Immune algorithms in action: Optimization of nonstationary functions, SzI-16'2001: XII Ogólnopolskie Konwersatorium nt. Sztuczna Inteligencja - nowe wyzwania (badania - zastosowania - rozwój), Warsaw (2001)
15. Wojdan, K., Świrski, K., Jarmoszewicz, G.: Stochastic Immune Layer Optimizer - efficient tool for optimization of combustion process in a boiler, accepted on Bionetics 2006 conference, Italy, 2006 (unpublished)

Dynamic Search Spaces for Coordinated Autonomous Marine Search and Tracking

Benjamin Lavis and Tomonari Furukawa

ARC Centre of Excellence for Autonomous Systems
School of Mechanical and Manufacturing Engineering
The University of New South Wales, Sydney 2052, Australia
benjamin.lavis@student.unsw.edu.au

Abstract. This paper presents a technique for dynamically determining search spaces in order to enable sensor exploration during autonomous search and tracking (SAT) missions. In particular, marine search and rescue scenarios are considered, highlighting the need for exploration during SAT. A comprehensive method which is independent of search space representation is introduced, based on exploration frontiers and reachable set analysis. The advantage of the technique is that recursive Bayesian estimation can be performed indefinitely, without loss of information. Numerical results involving multiple search vehicles and multiple targets demonstrate the efficacy of the approach for coordinated SAT. These examples also highlight the added benefit for human mission planners resulting from the technique's simplification of the search space allocation task.

1 Introduction

A common marine search and rescue scenario involves the crew of ship in distress and with failing navigation systems dispatching a final mayday signal and boarding life rafts. The crew can then only wait for discovery and rescue, all the while being buffeted by strong winds and waves, and drifting due to ocean currents. The objective for authorities is to rescue the crew before their survival expectancy vanishes, requiring an efficient search for the life rafts and the prompt and safe rescue of the victims.

The use of a team of fast autonomous unmanned aerial vehicles (UAVs) together with a team of autonomous helicopters bearing rescue crews has been presented as a implementable robotics approach to marine search and rescue (SAR) [1]. In such an application the use of multiple autonomous agents can produce a significant reduction in search times. If the UAVs have the additional ability to track the found life rafts as they drift, to provide high powered lighting and/or gather environmental information, then the safety of the rescue operation may be improved.

For extensive or complex rescue operations the UAVs may be required to track the life rafts well beyond the boundary originally designated for the search task. The focus of this paper is the introduction of a method which allows a team

H.G. Okuno and M. Ali (Eds.): IEA/AIE 2007, LNAI 4570, pp. 1032–1041, 2007.

of autonomous agents to explore the region beyond the boundary of the initial search space, whilst satisfying the objectives and constraints of a time critical SAR operation.

Many of the fundamental issues of search theory were posed by the Antisubmarine Warfare Operations Research Group (ASWORG) during World War II [2]. Initial studies simplified the search problem to an area coverage problem, however the introduction of the probability of detection lead to an expansion of search theory and to considerations of optimal allocation of search effort [3], [4], [5]. Bayesian approaches to search for a moving target with a prior distribution and a motion model have been formulated [6] and generalized for search with multiple vehicles [7].

Target tracking was initially considered independently of search theory and began as simple feedback motion tracking. However as a result of a general interest in multi-objective missions, in particular amongst the UAV community, several approaches to unified search and tracking (SAT) have recently appeared [8]. The majority of these approaches have consisted of collections of independent search and tracking techniques, however a general, unified SAT technique was presented in [9]. Whilst this most recent work successfully showed multiple coordinated SAT within a fixed search space, the inclusion of moving targets in the search space over indefinite mission horizons is not guaranteed.

Exploration is the field of robotics that is concerned with garnering information about that which is beyond those regions already known to the robot. Frontier based exploration is a well established approach to exploration and has been extended to encompass exploration with multiple agents [10]. Frontier based exploration is generally associated with occupancy grid maps, but as a concept can be applied to other useful representations such as topological maps [11] or manifolds [12], provided the representation allows for a distinction between known areas and unknown areas [13].

This paper introduces a modified frontier, defined on the basis of reachable set analysis, in order to produce a dynamic search space, thus enabling a more comprehensive approach to SAT. The proposed technique may be applied independently of search space representation, and has been formulated such that the established objective function for coordinated Bayesian SAT requires no alteration.

This paper is organized as follows. Section 2 covers the unified approach to SAT using recursive Bayesian estimation. Section 3 describes the modified frontier, based on reachable set analysis, and its use in defining dynamic search spaces for SAT. Section 4 presents a number of numerical examples which demonstrate the efficacy of the proposed technique. Conclusions and future considerations are discussed in the final section.

2 Recursive Bayesian Search and Tracking

Recursive Bayesian estimation (RBE) is a basis for estimating nonlinear non-Gaussian models. Implementation of RBE requires computationally expensive

numerical integration and has only recently gained popularity as a result of general increases in computing power. A number of techniques exist which enable the use of RBE, including grid based methods, Gauss Quadrature methods and Sequential Monte Carlo methods [14].

2.1 Target and Sensor Platform Models

In order to successfully apply RBE for autonomous SAT it is essential to have accurate models of both the target of the SAR operation (the lost entity) and of the autonomous sensor platforms conducting the operation. The motion of a target, t, is given by the following discrete time equation

$$\mathbf{x}_{k+1}^t = \mathbf{f}^t(\mathbf{x}_k^t, \mathbf{u}_k^t, \mathbf{w}_k^t) \tag{1}$$

where $\mathbf{x}_k^t \in \mathcal{X}^t$ is the state of the target at time k, $\mathbf{u}_k^t \in \mathcal{U}^t$ describes the target's control inputs and $\mathbf{w}_k^t \in \mathcal{W}^t$ represents the 'system noise', which includes environmental influences on the target. In general, the state of the target describes its two-dimensional location, but may also include other variables such as velocity.

An autonomous agent, s, used to perform the SAR operation is assumed to accurately know its own state via global sensors such as a combination of GPS, a compass and an inertial measurement unit (IMU). The motion of the search vehicle with state $\mathbf{x}_k^s \in \mathcal{X}^s$ and control inputs $\mathbf{u}_k^s \in \mathcal{U}^s$ is therefore given by

$$\mathbf{x}_{k+1}^s = \mathbf{f}^s(\mathbf{x}_k^s, \mathbf{u}_k^s). \tag{2}$$

The observation made from the vehicle s at time k is ${}^s\mathbf{z}_k \in \mathcal{X}^t$ and is subject to observation noise, $\mathbf{v}_k^s$. The observation model is given by the formula

$${}^s\mathbf{z}_k = \mathbf{h}^s(\mathbf{x}_k^s, \mathbf{v}_k^s). \tag{3}$$

Note that if the autonomous search vehicle only carries a single sensor for observation then the terms 'sensor platform' and 'autonomous search vehicle' may be used interchangeably.

2.2 Recursive Bayesian Estimation

In general RBE is concerned with maintaining two probability density functions (PDFs), known as the posterior distribution and the prediction. Two distinct stages are used: the update stage and the prediction stage. The update stage calculates the posterior distribution of the current state given a prior estimation of the state (based on the sequence of previous observations) and a new observation at the present time. The prediction stage calculates the PDF of the next state using the posterior density of the current state and a probabilistic Markov motion model.

Before these stages are discussed in greater detail, a number of terms must first be defined. The PDF of a continuous random variable X in n_x dimensional Euclidean space is $p(\mathbf{x})$, and by definition satisfies the following two conditions

$$\Pr(\mathbf{x} \in \mathcal{X} \subset \mathbb{R}^{n_x}) = \int_{\mathcal{X}} p(\mathbf{x}) d\mathbf{x} \tag{4}$$

and

$$\Pr(\mathbf{x} \in \mathbb{R}^{n_x}) = \int p(\mathbf{x}) d\mathbf{x} \equiv 1. \tag{5}$$

The sequence of states of a sensor platform s from time step 1 to k is given by the term $\tilde{\mathbf{x}}^s_{1:k} \equiv \{\tilde{\mathbf{x}}^s_i | \forall i \in \{1, \ldots, k\}\}$. The tilde is used here to indicate an instance $\tilde{(\cdot)}$, of a variable $(\cdot)$. Additionally, let the sequence of observations made by sensor platform s from time step 1 to k be given by ${}^s\tilde{\mathbf{z}}_{1:k} \equiv \{{}^s\tilde{\mathbf{z}}_i | \forall i \in \{1, \ldots, k\}\}$.

It is possible to estimate the posterior distribution of the target at any time step k, $p(\mathbf{x}^t_k | {}^s\tilde{\mathbf{z}}_{1:k}, \tilde{\mathbf{x}}^s_{1:k})$, given a prior distribution of the target, $p(\tilde{\mathbf{x}}^t_0)$, and the sequences of sensor platform states and observations, $\tilde{\mathbf{x}}^s_{1:k}$ and ${}^s\tilde{\mathbf{z}}_{1:k}$. This is achieved via the recursive application of the two stages of RBE, update and prediction, described below.

Update. The update stage considers a new observation ${}^s\mathbf{z}_k$ in light of the corresponding estimation of state based on the observations up to the previous time step, $p(\mathbf{x}^t_k | {}^s\tilde{\mathbf{z}}_{1:k-1}, \tilde{\mathbf{x}}^s_{1:k-1})$, and calculates the posterior density $p(\mathbf{x}^t_k | {}^s\tilde{\mathbf{z}}_{1:k}, \tilde{\mathbf{x}}^s_{1:k})$. The update equation is given by

$$p(\mathbf{x}^t_k | {}^s\tilde{\mathbf{z}}_{1:k}, \tilde{\mathbf{x}}^s_{1:k}) = \frac{p({}^s\tilde{\mathbf{z}}_k | \mathbf{x}^t_k, \tilde{\mathbf{x}}^s_k) p(\mathbf{x}^t_k | {}^s\tilde{\mathbf{z}}_{1:k-1}, \tilde{\mathbf{x}}^s_{1:k-1})}{\int p({}^s\tilde{\mathbf{z}}_k | \mathbf{x}^t_k, \tilde{\mathbf{x}}^s_k) p(\mathbf{x}^t_k | {}^s\tilde{\mathbf{z}}_{1:k-1}, \tilde{\mathbf{x}}^s_{1:k-1}) d\mathbf{x}^t_k} \tag{6}$$

where $p({}^s\tilde{\mathbf{z}}_k | \mathbf{x}^t_k, \tilde{\mathbf{x}}^s_k)$ is the observation likelihood given knowledge of the current state, or the sensor model defined by (3). It is important to note that when $k = 1$ the update is carried out using $p(\mathbf{x}^t_k | {}^s\tilde{\mathbf{z}}_{1:k-1}, \tilde{\mathbf{x}}^s_{1:k-1}) = p(\tilde{\mathbf{x}}^t_0)$.

Prediction. The prediction step applies the Total Probability Theorem to the target's probabilistic Markov model, $p(\mathbf{x}^t_{k+1} | \mathbf{x}^t_k)$ defined by (1), and the posterior distribution (6), in order to compute the PDF for the next time step, $p(\mathbf{x}^t_{k+1} | {}^s\tilde{\mathbf{z}}_{1:k}, \tilde{\mathbf{x}}^s_{1:k})$. The prediction is performed using the Chapman-Kolmogorov equation

$$p(\mathbf{x}^t_{k+1} | {}^s\tilde{\mathbf{z}}_{1:k}, \tilde{\mathbf{x}}^s_{1:k}) = \int p(\mathbf{x}^t_{k+1} | \mathbf{x}^t_k) p(\mathbf{x}^t_k | {}^s\tilde{\mathbf{z}}_{1:k}, \tilde{\mathbf{x}}^s_{1:k}) d\mathbf{x}^t_k. \tag{7}$$

2.3 Coordinated Control for Search and Tracking

Sensor data fusion is one form of coordination for multiple sensor platforms. The conditional independence of observations from n_s sensors leads to the multiple-sensor observation likelihood

$$p({}^s\tilde{\mathbf{z}}_k | \mathbf{x}^{t_j}_k, \tilde{\mathbf{x}}^s_k) = \prod_{i=1}^{n_s} p({}^{s_i}\tilde{\mathbf{z}}_k | \mathbf{x}^{t_j}_k, \tilde{\mathbf{x}}^{s_i}_k) \tag{8}$$

where $\tilde{\mathbf{x}}^s_k = \{\tilde{\mathbf{x}}^{s_i}_k | \forall i \in \{1, \ldots, n_s\}\}$ and ${}^s\tilde{\mathbf{z}}_k = \{{}^{s_i}\tilde{\mathbf{z}}_k | \forall i \in \{1, \ldots, n_s\}\}$ represent the states of the n_s platforms at time k, and their corresponding observations respectively, and $p({}^{s_i}\tilde{\mathbf{z}}_k | \mathbf{x}^{t_j}_k, \tilde{\mathbf{x}}^{s_i}_k)$ is the observation likelihood for sensor platform

s_i given the state of target t_j. For fully connected sensors with lossless and delay free communication, each platform i can receive $p({}^{s_q}\tilde{\mathbf{z}}_k|\mathbf{x}_k^{t_j}, \tilde{\mathbf{x}}_k^{s_q}), \forall q \neq i$ and decentrally construct (8). Substitution of (8) into (6) gives the update equation for multiple sensors. Prediction using (7) completes the general decentralized data fusion approach to RBE as presented in [7]. Within this framework a sensor model and a control objective for SAT were formulated in [9].

3 Exploration Using Dynamic Search Boundaries

There exists a case when the result of the prediction equation (7), that is $p(\mathbf{x}_{k+1}^t|{}^s\tilde{\mathbf{z}}_{1:k}, \tilde{\mathbf{x}}_{1:k}^s)$, the probability density of the target's state in the next time step, is not a valid PDF. Namely, when

$$\Pr(\mathbf{x}_{k+1}^t \in \mathcal{X}^t) = \int_{\mathcal{X}^t} p(\mathbf{x}_{k+1}^t|{}^s\tilde{\mathbf{z}}_{1:k}, \tilde{\mathbf{x}}_{1:k}^s) d\mathbf{x}_{k+1}^t < 1 \tag{9}$$

(5) is not satisfied. In this case there is some probability that the target will no longer be within the search space at time step $k+1$ since,

$$\Pr(\mathbf{x}_{k+1}^t \notin \mathcal{X}^t) = 1 - \Pr(\mathbf{x}_{k+1}^t \in \mathcal{X}^t). \tag{10}$$

Therefore, in order to maintain an accurate estimate of the target's state at time step $k+1$, a new search space $\mathcal{X}_{k+1}^t$ must be defined such that $\Pr(\mathbf{x}_{k+1}^t \in \mathcal{X}_{k+1}^t) = 1$. A comprohensive approach to SAT must therefore be able to recognize the potential for the target to move beyond the search space, before it occurs, and adapt the search space accordingly.

3.1 Forward Reachable Sets

The state space that a target can reach within a certain time frame is called the target's reachable set. Of particular interest is the target's *forward reachable set* (FRS) which is the state space reachable forwards in time given an initial target state. The forward reachable set for target t from time $k+1$ to $k+n_k$, is denoted $\mathcal{A}_{k+1:k+n_k}^{\tilde{\mathbf{x}}^t}$. There are a number of methods for determining a vehicle's FRS, the most common being kinematic analysis. It is also possible to describe a target's FRS in terms of its probabilistic motion model, (1). The FRS evaluated at a point $\tilde{\mathbf{x}}^t \in \mathcal{X}_k^t$ may therefore be expressed as

$$\mathcal{A}_{k+1:k+n_k}^{\tilde{\mathbf{x}}^t} = \{\mathbf{x}_{k+1:k+n_k}^t | p(\mathbf{x}_{k+1:k+n_k}^t|\tilde{\mathbf{x}}_k^t) > 0\}. \tag{11}$$

3.2 Frontier Based Exploration

In its usual sense, frontier based exploration involves robots moving to a frontier in order to gain some additional information about the environment, where a frontier consists of those areas of the search space about which some information is known and which are adjacent to unknown space. In this work a frontier, $\mathcal{F}_k$,

is defined as the set of points from which the target is able to, in the next time step, reach beyond the boundaries of the current search space:

$$\mathcal{F}_k = \{\mathbf{x}_k^t | \mathcal{A}_{k+1:k+1}^{\mathbf{x}_k^t} \not\subseteq \mathcal{X}_k^t\}. \tag{12}$$

For any frontier node, $\tilde{\mathbf{x}}_k^t \in \mathcal{F}_k$, if the value of the posterior distribution is greater than zero,

$$p(\tilde{\mathbf{x}}_k^t | {}^s\tilde{\mathbf{z}}_{1:k}, \tilde{\mathbf{x}}_{1:k}^s) > 0 \tag{13}$$

then application of the prediction equation (7) will always result an invalid PDF, as described by (9), implying $\Pr(\mathbf{x}_{k+1}^t \notin \mathcal{X}_k^t) > 0$. In such cases, a new search space ${}^f\mathcal{X}_k^t$ should be defined, based on the present search space $\mathcal{X}_k^t$ and the target's FRS evaluated at those frontier nodes described by (13),

$${}^f\mathcal{X}_k^t \equiv \mathcal{X}_k^t \cup \mathcal{A}_{k+1:k+1}^{\tilde{\mathbf{x}}_k^{t+} \in \mathcal{F}_k} \tag{14}$$

where $\mathbf{x}^{t+} \in \{\mathbf{x}^t | p(\mathbf{x}^t | {}^s\tilde{\mathbf{z}}_{1:k}, \tilde{\mathbf{x}}_{1:k}^s) > 0\}$. Before it can be used for RBE, the posterior distribution must be redefined in order to fit this new search space. However this is made straightforward by observing that at time k, $\Pr(\mathbf{x}_k^t \notin \mathcal{X}_k^t) = 0$. Therefore put

$$p(\mathbf{x}_k^t | {}^s\tilde{\mathbf{z}}_{1:k}, \tilde{\mathbf{x}}_{1:k}^s) = \begin{cases} p(\mathbf{x}_k^t | {}^s\tilde{\mathbf{z}}_{1:k}, \tilde{\mathbf{x}}_{1:k}^s) \text{ if } \mathbf{x}_k^t \in \mathcal{X}_k^t \\ 0 \qquad\qquad \text{otherwise} \end{cases} \tag{15}$$

for $\mathbf{x}_k^t \in {}^f\mathcal{X}_k^t$. Using this newly defined search space and posterior distribution function the prediction stage may now be performed without loss of information using

$$p(\mathbf{x}_{k+1}^t | {}^s\tilde{\mathbf{z}}_{1:k}, \tilde{\mathbf{x}}_{1:k}^s) = \int_{{}^f\mathcal{X}_k^t} p(\mathbf{x}_{k+1}^t | \mathbf{x}_k^t) p(\mathbf{x}_k^t | {}^s\tilde{\mathbf{z}}_{1:k}, \tilde{\mathbf{x}}_{1:k}^s) d\mathbf{x}_k^t. \tag{16}$$

The update stage should then be applied using $\mathcal{X}_{k+1}^t = {}^f\mathcal{X}_k^t$.

It should be noted that this approach may be applied independently of the method chosen for implementing RBE. Furthermore, as there is no loss of information, the technique requires no change to the established objective function for coordinated SAT.

4 Numerical Examples

This section presents three examples in order to demonstrate the use of FRS frontier based exploration for autonomous SAT. The first example considers only a single target and a single sensor whilst the second and third consider two lost targets and the use of three UAVs. The targets in each of the examples share a common model. They move in the horizontal plane according to

$$\begin{aligned} x_{k+1}^{t_j} &= x_k^{t_j} + \Delta t \cdot v_k^{t_j} \cos \gamma_k^{t_j} \\ y_{k+1}^{t_j} &= y_k^{t_j} + \Delta t \cdot v_k^{t_j} \sin \gamma_k^{t_j} \end{aligned} \tag{17}$$

where $v_k^{t_j}$ and $\gamma_k^{t_j}$ are, respectively, the speed and direction of the target's motion due to external disturbances such as wind and current, subject to Gaussian noise. A time increment, $\Delta t = 100s$, was used in each example. The sensors also move in the horizontal plane, and share the following model

$$\begin{aligned} x_{k+1}^{s_i} &= x_k^{s_i} + \Delta t \cdot v_k^{s_i} \cos(\theta_k^{s_i} + \gamma_k^{s_i}) \\ y_{k+1}^{s_i} &= y_k^{s_i} + \Delta t \cdot v_k^{s_i} \sin(\theta_k^{s_i} + \gamma_k^{s_i}) \\ \theta_{k+1}^{s_i} &= \theta_k^{s_i} + \gamma_k^{s_i} \end{aligned} \tag{18}$$

where $v_k^{s_i}$ is the speed of the sensor platform and $\gamma_k^{s_i}$ is the angle through which the platform turns. Table 1 shows the sensor platform and target control limits used during each of the simulations.

Table 1. Vehicle Model Control Limits

	Sensor Platform	Target
Maximum Speed [m/s]	30	20
Minimum Speed [m/s]	10	0
Maximum Turn Rate [deg/s]	3	60

The probability of detection was given by a zero mean Gaussian distribution with constant covariance. The observation likelihood was given by a zero mean Gaussian distribution with covariance proportional to the distance between the sensor platform and the target. A five step lookahead with receding horizon was used for control optimization.

In each of the simulations the sensors are indicated with a cyan circular marker, the targets with a yellow triangular marker. The search space is shown as a colored surface, representing the posterior distribution, against a grey background.

4.1 Single UAV, Single Target

In this example a single UAV searches for and tracks a single lost target over a 20 km × 20 km search space. Figure 1 shows a comparison between static and dynamic search spaces. The top row shows the result of using a static search space. The second row shows the result of using a dynamic search space.

When the target was within 1 km of the UAV it was detected by the sensor. The true distance between the sensor and target for each case can be seen in Fig. 1(d). This example clearly highlights the limitations of SAT over static search spaces: once the target drifted beyond the boundary of the search space, Fig. 1(c), the UAV was incapable of maintaining an appropriate PDF of the target, leading to mission failure. The use of a dynamic search space allowed the UAV to keep the detected target within 1 km and therefore within its sensor range for the remainder of the 3 hour mission.

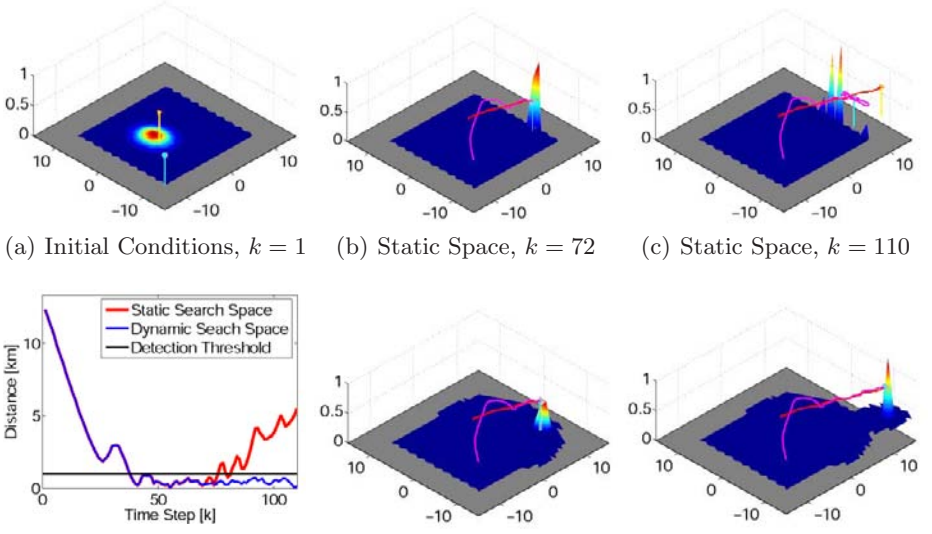

(a) Initial Conditions, $k = 1$ (b) Static Space, $k = 72$ (c) Static Space, $k = 110$

(d) Distance, Sensor to Target (e) Dynamic Space, $k = 72$ (f) Dynamic Space, $k = 110$

Fig. 1. Comparison of Static and Dynamic Search Spaces

4.2 Coordinated Search and Tracking - Multiple Targets

In this example three UAVs cooperatively search for and track two lost targets, see Fig. 2. The exploration method was again implemented, with each of the UAVs decentrally determining the required changes in the search space. Both targets were located by $k = 30$, that is, within 50 minutes. Again the technique allowed the sensors to continuously track the targets over a period of more than 4 hours, even after the targets drifted beyond the initial search boundary. This example shows the ease with which the proposed method can be scaled to include multiple targets and multiple sensor platforms. It should also be noted that the exploration method operates regardless of whether the targets have been detected or not, see Fig. 2(b). This advantage is exploited in the final example.

4.3 Coordinated Search and Tracking - Reduced Initial Space

In this example the initial target locations and PDFs from the previous example were used, however the initial search space was reduced such that its boundary only barely includes the extremities of the PDFs. Figure 3 shows that regardless of this the UAVs were still able to successfully locate and track the two lost targets. Furthermore, a comparison of Figs. 3(b) and 2(b) reveals that as a result of the smaller initial search space, the time taken to locate both of the targets is less than in the previous example (both targets were located by $k = 25$, under 42 minutes, when the reduced search space was used).

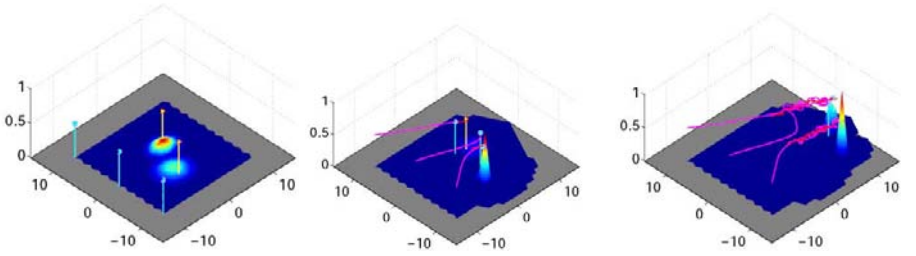

(a) Searching, $k = 1$ (b) Target found, $k = 25$ (c) Tracking, $k = 150$

Fig. 2. Dynamic Search Spaces for Coordinated Search and Tracking

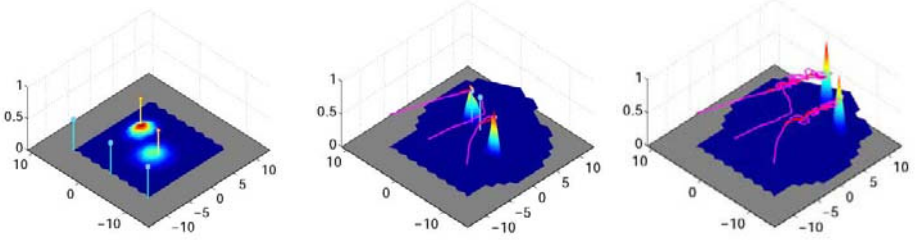

(a) Searching, $k = 1$ (b) Targets found, $k = 25$ (c) Tracking, $k = 150$

Fig. 3. Search and Tracking Using Reduced Initial Search Space

This example highlights the advantage of the proposed technique, in that a complete representation of the PDFs can be maintained for all time steps, so long as the initial search boundaries completely enclose the initial distributions. This greatly reduces the burden on human mission planners, who when using static search spaces must consider not only the initial PDFs, but also the possible duration of the mission. Also, the reduction in time required to locate the missing targets may be a life saving factor in real marine search and rescue scenarios.

5 Conclusion

A general theoretical approach was presented which enables sensor exploration during recursive Bayesian SAT. This approach may be applied decentrally and independently of the method of Bayesian estimation. It was demonstrated through a number of examples that a sensor with the ability to explore during SAT has an improved chance of succeeding in its mission compared with a sensor with no exploration capabilities, especially over extended time periods. Another advantage of the technique is that the sensor's ability to explore reduces the burden on mission planners when specifying the initial boundaries of the search space, as the presented technique maintains a complete representation of the target's PDF for all time steps, provided the prior distribution is complete. Future work focussing

on search space reduction for areas of low probability density, will aim to reduce the computational burden associated with the increased search space sizes.

Acknowledgements

This work is partly supported by the US Air Force Office of Scientific Research (AFOSR) and the ARC Centre of Excellence programme, funded by the Australian Research Council (ARC) and the New South Wales State Government.

References

1. Wong, E.-M., et al.: Multi-vehicle Bayesian search for multiple lost targets. In: Proc. IEEE Int. Conf. Robot. Autom (ICRA 2005) pp. 3180–3185 (2005)
2. Le Cadre, J.-P.: Search and Screening: General Principle with Historical Applications. Alexandria, VA: MORS Heritage Series (1999)
3. Stone, L.D.: Search theory: a mathematical theory for finding lost objects. Mathematics Magazine 50(5), 248–256 (1977)
4. Stone, L.D.: What's happened in search theory since the 1975 Lanchester prize? Operations Research 37(3), 501–506 (1989)
5. Stone, L.D.: Theory of Optimal Search, Arlington, VA: Operations Research Society of America (ORSA) Books (1989)
6. Bourgault, F., et al.: Process Model, constraints and the coordinated search strategy. In: Proc. IEEE Int. Conf. Robot. Autom (ICRA 2004), vol. 5, pp. 5256–5261 (2004)
7. Bourgault, F., et al.: Coordinated decentralized search for a loast target in a Bayesian world. In: Proc. IEEE/RSJ Int. Conf. Intel. Robot. Sys. pp. 48–53 (2003)
8. Butenko, S., et al.: Recent Developments in Cooperative Control and Optimization. Kluwer Academic Publishers, Boston (2005)
9. Furukawa, T., et al.: Recursive Bayesian search-and-tracking using coordinated UAVs for lost targets. In: Proc. IEEE Int. Conf. Robot. Autom., pp. 2521–2526 (2006)
10. Yamauchi, B.: Frontier-based exploration using multiple robots. In: Proc. 2nd Int. Conf. Autonomous Agents, pp. 47–53 (1998)
11. Choset, H., Nagatani, K.: Topological simultaneous localization and mapping (SLAM): toward exact localization without explicit localization. IEEE Trans. Robot. Autom. 17(2), 125–137 (2001)
12. Howard, A., et al.: Multirobot simultaneous localization and mapping using manifold representations. Proc. IEEE 94(7), 1360–1369 (2000)
13. Burgard, W., et al.: Coordinated multi-robot exploration. IEEE Trans. Robot. 21(3), 376–386 (2005)
14. Arulampalam, M.S., et al.: A tutorial on particle filters for on-line non-liner/non-Gaussian Bayesian tracking. IEEE Trans. Sig. Proc. 50(2), 174–188 (2002)

Composite Endoscope Images from Massive Inner Intestine Photos

Eunjung Kim[1], Kwan-Hee Yoo[2], Je-Hoon Lee[1], Yong-Dae Kim[1], and Younggap You[1]

[1] Dept. of Computer and Communication Eng., Chungbuk Nat'l Univ, San 12, Gaeshin-dong, Cheongju, Chugnbuk, Korea
ejkim@hbt.cbnu.ac.kr
[2] Dept. of Computer Education, Chungbuk Nat'l University, San 12, Gaeshin-dong, Cheongju, Chugnbuk, Korea

Abstract. This paper presented an image reconstruction method for a capsule endoscope. The proposed method constructs a 3–D model of the intestine using massive images obtained from the capsule endoscope. It merges all images and yields a complete 3-D model of the intestine. This 3-D model is reformed as a 2-D plane image showing the inner side of the entire intestine. The proposed image composition has been evaluated using the OpenGL 3-D simulator. The composite image provides an easy-to-understand view for examining the intestine. In addition, it provides fast track-and-check diagnosis using the 3-D model implementation.

Keywords: Capsule endoscope, image composition, 3-D modeling, bio-informatics.

1 Introduction

There are two types of endoscopes to examine the GI (gastrointestinal) track; a wired endoscope and a capsule endoscope. The wired endoscope can easily diagnose the GI track using the real image and catch the biopsy sample. It causes discomfort to the patient when a physician pushes the cable into the patient body. Further, it is difficult to reach the small intestine using the wired endoscope. However, the capsule endoscope can directly examine the entire gastrointestinal tract, including the small intestine. And the capsule endoscope is easier to swallow [1–2]. It observes the inside of the small intestine and transfers the pictures obtained from the capsule [3–6].

There has been a substantial amount of technical improvements to make the capsule endoscope complete. The captured images may suffer substantial nonlinear spatial distortion, which obstructs accurate medical examination. The calibration will help to restore the original image. There are many researchers devoted to improving image quality [7–12]. S. Pongnumkul et al. proposed an image reconfiguration method to change the video stream captured by the endoscope to a 2-D image, to reduce the time required for diagnosis [10].

H.G. Okuno and M. Ali (Eds.): IEA/AIE 2007, LNAI 4570, pp. 1042–1051, 2007.

The main goal of a capsule endoscope is to form accurate diagnosis in a short time. The capsule endoscope transfers the image data to the diagnose system at a rate of two frames per second. The capsule transmits about 50,000 images for each patient. This causes some problems for fast diagnosis. The images are reviewed by video at speeds of about 20 [frame/second]. The time spent watching the video is over 42 minutes. It takes a long time for the physician to diagnose a patient, because only a fraction of this video is needed.

This paper proposes an image reconstruction method. The intestine model is similar to that of the patient model. This 3-D model is reformed as a 2-D plane image. We generate a dissection image of an intestine from the image sequence, where the dissection image looks like an image obtained by cutting the intestine lengthwise and opening its inside. The physician can diagnose this image at a glance and thereby saves time.

This paper is organized as follows. Section 2 describes the modeling environment. Section 3 describes the transformation method from a photo image into a planar image. Section 4 introduces 3-D image reconstruction from a planar image. Section 5 presents the experimental results. Section 6 concludes this paper.

2 Modeling Environment

This section explains the three dimensional modeling of the intestine based on the pictures from the capsule camera. The position and attitude data are attached to the images captured by the endoscope, which will help formulate precise diagnosis. A cylindrical intestine model utilizes the information on the camera location and attitude for each intestine image from the capsule.

The small intestine of a human being is about 6 meters in length, including duodenum, jejunum, and ileum as shown in Fig. 1. The average diameter is about 20 mm for adults. The small intestine is constantly in motion, for digestion and absorption.

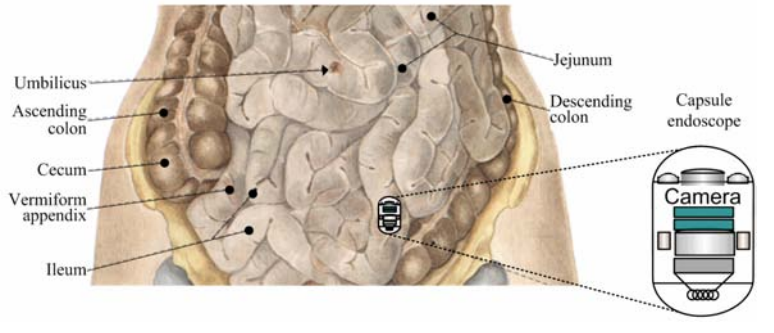

Fig. 1. The capsule endoscope and the intestine

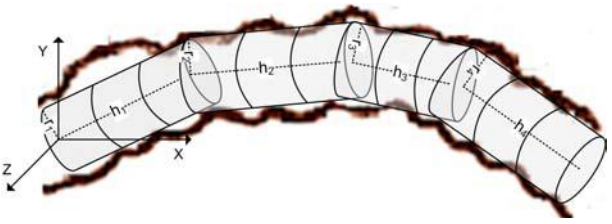

Fig. 2. Cylindrical model of an intestine

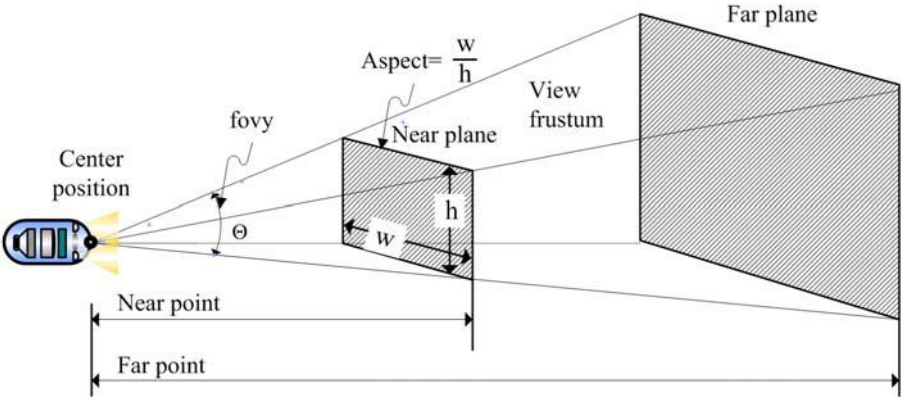

Fig. 3. The parameters for cylindrical modeling

The three dimensional model of the intestine image leads to a composite image representing massive capsule photos. An intestine is assumed to be a series of piecewise cylindrical pieces as shown in Fig. 2, with each cylindrical piece of differing radius and height. The i_{th} piece has a radius of r_i and a height of h_i. The process of three dimensional modeling begins with photo images from the capsule endoscope. Each image carries the position and attitude information of a capsule endoscope in the human body. Each image experiences a different camera setting of image center position, direction vector, fovy, near and far point, and aspect ratio, as shown in Fig. 3. The coordinate of the capsule endoscope is (x, y, z) in the Cartesian coordinate system. The center position represents the coordinate of the capsule camera lens. The rotation angle (α, β, γ) changes with capsule movement. We use the position and orientation tracking method proposed by Wang and Meng [13]. The radius and total height of the 3D model cylinder are assumed 30.0 mm and 200.0 mm, respectively. The fovy is assumed 100°. The near and far points are 4.5 mm and 25 mm, respectively. The camera focuses on objects between 4.5 mm and 25 mm. The aspect ratio is the ratio of the height and the width of an image. This model assumes an aspect ratio of 1. The default direction vector is defined (0.0, 0.0, -1.0).

3 Transformation from a Photo Images into a Planar Images

The photos from a capsule camera are the raw data for constructing a three dimensional cylindrical model, which is then transformed into a two dimensional planar composite image. The image is equivalent to the inner wall of the cylinder model inside the view frustum of the capsule camera. The camera's view frustum can be obtained from the fovy, aspect ratio, near and far planes. The view frustum with their values is shown in Fig. 4a. Here x_{min}, y_{min}, and -near values are coordinates of a lower left corner point and also x_{max}, y_{max} and -far values are coordinates of a higher right corner point.

Let Int(V,C) be the intersection area of the original view frustum and the given cylinder. In order to compute Int(V,C) efficiently, we use the transform matrix, $M_{pers \to cv}$ like Eq. 1, by which the original view frustum is transformed into a canonical view volume as shown in Fig. 4b. Clearly, the problem to compute Int(V,C) is equivalent to the clipping problem of the transformed line segments with respect to the canonical view volume, where the used line segments are obtained from multiplying $M_{pers \to cv}$ to end points of each line segment modeling the given cylinder. By applying the 3D clipping algorithm proposed by Cyrus and Back [14], we can identify a portion of the transformed line segments inside the canonical view volume.

$$M_{pers \to cv} = \begin{pmatrix} \frac{2(-near)}{x_{max}-x_{min}} & 0 & \frac{x_{max}+x_{min}}{x_{max}-x_{min}} & 0 \\ 0 & \frac{2(-near)}{y_{max}-y_{min}} & \frac{y_{max}+y_{min}}{y_{max}-y_{min}} & 0 \\ 0 & 0 & -\frac{far+near}{far-near} & -\frac{2far+near}{far-near} \\ 0 & 0 & 1 & 0 \end{pmatrix} \begin{pmatrix} x \\ y \\ z \\ 1 \end{pmatrix} \quad (1)$$

The identified line segments are projected orthogonally on the normalized view rectangle as shown in Fig. 4b, which is a rectangle on the near plane of the canonical view volume. With the orthogonally projected line segments, we can determine the corresponding positions of the captured image, through the mapping function between the normalized view rectangle and the captured image rectangle. Clearly, we can apply the methods so that the mapped texture, MT_i, on Int(V_i,C) is computed efficiently.

Finally, we have to decide where the mapped texture is mapped into the portions of the composite image. Let S = (S_1, S_2, $\cdots$, S_k), S_i=(CL_i, CH_i) be the set of line segments of Int(V, C) on the cylinder surface. CL_i and CH_i are the (x, y, z) coordinate values of the low point and the high point, respectively. The reconstruction of the image employs a set of foregoing line segments S. It is used to find a place corresponding to an intersected line segment S_i=(CL_i, CH_i) as Eq. 2. The foregoing transformation method solves this problem, by transforming the cylindrical coordinate into a texture coordinate.

$$CL_i = (\frac{k}{n}, \frac{CL_{iy}}{h}), CH_i = (\frac{k}{n}, \frac{CH_{iy}}{h}) \quad (2)$$

Here, k is the sequence of the line segment that belongs to the intersection area of the original cylinder and the view frustum. A captured image is obtained

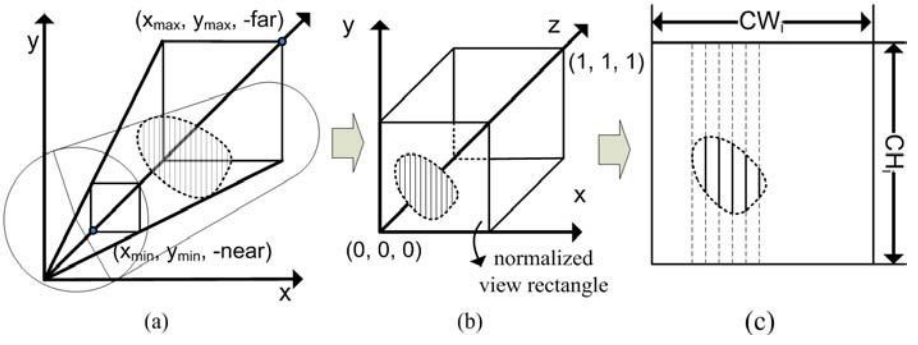

Fig. 4. Projection normalization

by projecting the photo corresponding to the normalized view angle and the texture coordinate.

The pinnacle points p=(nucx, nucy) of each line segment corresponds to the point of (CW_i × nucx, CH_i × nucy) for the two dimensional image size of (CW_i, CH_i). Here, nucx and nucy are the x and y coordinates in the canonical view volume, respectively. Figure 4 shows the correspondence between them. Figure 4b shows the line segments within the normalized view rectangle. Figure 4c shows the line segments mapped on the captured image. (CW_i, CH_i) is the captured image from the i_{th} photo.

4 3-D Image Reconstruction from a Planar Image

A composite image is formed by mapping captured images on a two-dimensional plane. A two-dimensional planar image is obtained from the massive intestine photos, from a capsule endoscope employing the foregoing transformation scheme. It is possible to perform a texture mapping of the photos from the capsule camera on the two dimensional planar image. The intersected areas are filled with the best quality pixels or interpolated data.

The piecewise cylindrical model described in the previous section becomes the basis of the three dimensional modeling of the intestine. The model of the intestine leads to the reconstruction of a two dimensional composite image. Figure 5a shows the cylindrical model of the intestine. The first step of the transformation is the conversion of cylindrical images into planar images. The origin of a Cartesian coordinate is the center of the cylinder, where its radius is r. The top and bottom of the cylinder are h/2, -h/2, respectively. The high and low points denote the points on the top and the bottom circumferences of the cylinder, respectively. The Eq. 3 of (H_{xi}, H_{yi} ,H_{zi},) and (L_{xi}, L_{yi} ,L_{zi},) define traces of high and low points of the i_{th} cylinder, respectively. The angle value, Θ_i of the equation represents the angle between the vector from the center to the high

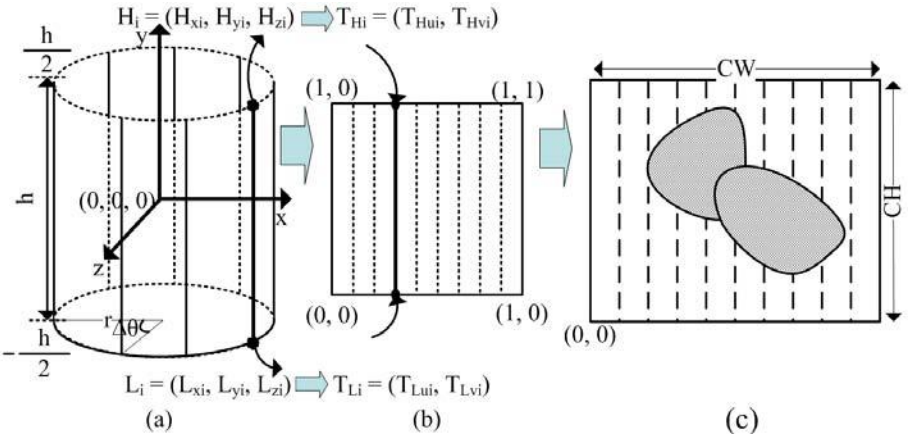

Fig. 5. Reconstruction method: (a) the 3-D cylinder model; (b) the normalized texture coordinate; (c) the composite image

or low point and the reference vector when the circumference is divided into n pieces.

$$\begin{gathered}\Theta_i = i \times \Delta\Theta, \Delta\Theta = \frac{2\pi}{n} \\ H_{xi} = 2\pi r \times \cos(\Theta_i), H_{yi} = \frac{h}{2}, H_{zi} = 2\pi r \times \sin(\Theta_i) \\ L_{xi} = 2\pi r \times \cos(\Theta_i), L_{yi} = -\frac{h}{2}, L_{zi} = 2\pi r \times \sin(\Theta_i) \\ (where, i = 0, 1, \ldots, n)\end{gathered} \tag{3}$$

An image on the inner cylinder wall is transformed into normalized coordinate values of the two dimensional planar form through a mapping defined by Eq 3.

The second step is the mapping of the three dimensional cylindrical image into the two dimensional image as shown in Fig. 5b. The coordinates of points on the high and low points of the two dimensional image are represented as T_{Hi} and T_{Li}, respectively. The points H_i and L_i on the three dimensional cylinder are mapped on T_{Hi} and T_{Li}, respectively. T_{Hui} and T_{Hvi} represent the x and y coordinate values of a point (H_{xi}, H_{yi}, H_{zi}) on high points after normalization and mapping on the two dimensional image, respectively.

T_{Lui} and T_{Lvi} represent the x and y coordinates of a point (L_{xi}, L_{yi}, L_{zi}) on low points after normalization and mapping on the two dimensional image, respectively. The coordinate values of T_{Hui} and T_{Lui} are obtained from Eq 4.

$$\begin{gathered}T_{Hui} = \frac{i}{n}, T_{Hvi} = 1 \\ T_{Lui} = \frac{i}{n}, T_{Lvi} = 0\end{gathered} \tag{4}$$

The third step is to perform texture mapping on the normalized coordinate values of Fig. 5b, yielding the result shown in Fig. 5c. The size of the output image is obtained by multiplying the width, CW and height, CH values on the normalized x and y values of the two dimensional image, respectively, as shown in Fig. 5c.

5 Simulation Results

The proposed scheme was implemented using the OpenGL three dimensional simulator of MS Visual Studio. Figure 6 shows the transformation process of generating a composite image. Figure 6a shows the mapping of a series of two dimensional consecutive photos on a three dimensional cylinder. The parallel dotted lines represent the intersected area of a view frustum and the cylinder. This area contains all the image data captured by the capsule camera. Figure 6b shows the two dimensional image from the capsule camera. Figure 6c describes the capsule information on the center position, direction vector, fovy, near and far point and aspect ratio. Figure 6d shows the partial composite image projected on the intersection areas of the cylinder and the view frustum.

Figure 7a shows the eye point of (4.00, 22.20, -1.00), and the center position of (0.30, -0.20, 0.00). Figure 7b shows the eye point of (4.60, 26.10, -3.10), and the center position of (-0.30, -5.60, 0.00). Figure 7c shows the eye point of (30.10, 10.30, 6.90), and the center position of (-0.00, -1.30, 0.80). The resultant composite image obtained by overlapping Figures 7a, 7b and 7c is shown in Fig. 7d. The photos are reconstructed as a two–dimensional planar image.

Figure 8 shows the photo taken inside the intestine after the three dimensional cylindrical modeling. The doctors can examine modeling photos by moving camera positions down to the outside areas of Fig. 9. This single composite image

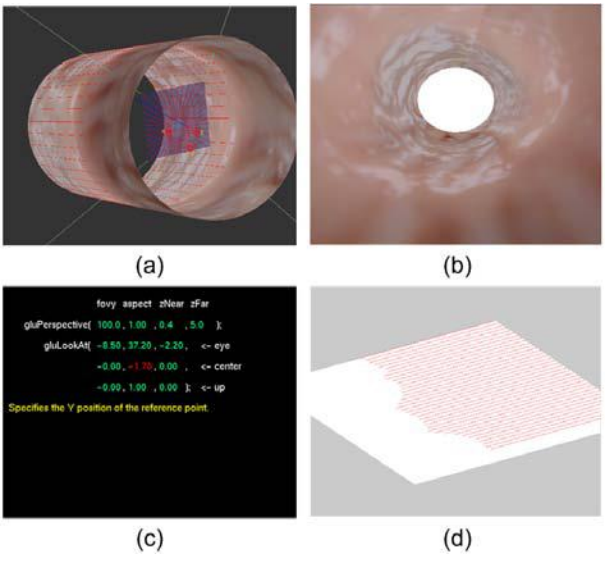

Fig. 6. The 3-D model for a small intestine and reconstructed 2-D image: (a) 3-D Cylinder Modeling, (b) Captured 2-D Image, (c) Capsule Endoscope Position and Camera Parameter, (d) Composite Image

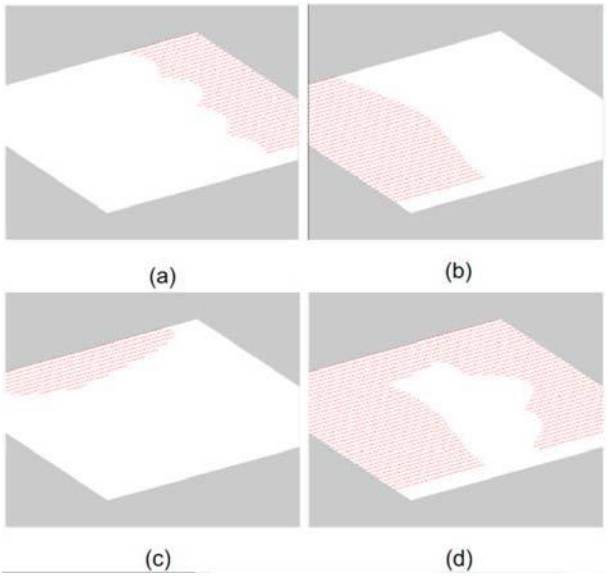

Fig. 7. Process of a composite image construction

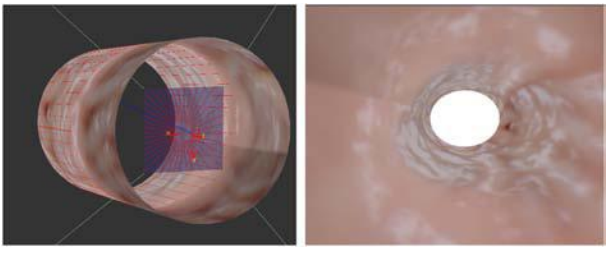

Fig. 8. The picture captured at the front of a small intestine

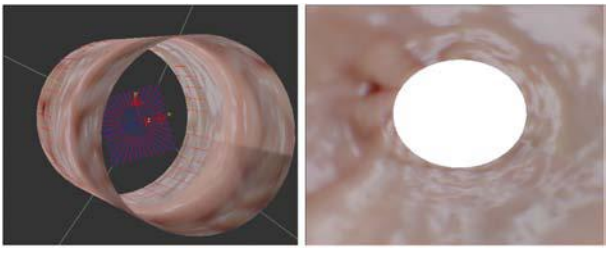

Fig. 9. The picture captured at the end of a small intestine

can save a substantial amount of diagnosis time to find the location of a lesion inside the intestine.

6 Conclusion

This paper presents an image reconstructing method for a capsule endoscope. The capsule endoscope transmits about 50,000 images. A physician spends almost 2 hours to examine a patient's intestine because he looks at only one small fragment at a time. The proposed method creates a three-dimensional model of a small intestine that includes all images obtained from the capsule endoscope. We assume that the shape of a small intestine consists of a series of consecutive cylinders. The photos obtained from the capsule endoscope contain the image information of the intersection between the cylinder model and the view frustum. The clipping algorithm is used to get the image information from the intersection. We use the perspective transformation method to reconstruct the planar image. It generates a three dimensional model and a planar image. The proposed image composition is evaluated using the OpenGL three dimensional simulator. This simulation result shows that a composite endoscope image is obtained from the massive inner intestine photos. The physician can diagnose this two dimensional image at a glance. They can freely track and check the location using the implemented three-dimensional model if they find an abnormal section in a planar image. This result allows a physician to diagnose a patient over a short time period. In future work, we will make an improved model to overlap each cylinder model of a small intestine.

Acknowledgments. This work was supported by the Regional Research Centers Program of the Ministry of Education & Human Resources Development in Korea. And Dr. J. H. Lee participated in this work is supported by the Second Phase of the Brain Korea 21 Project at Chungbuk National University.

References

1. Iddan, G., Meron, G., Glukhovsky, A., Swain, P.: Wireless capsule endoscopy. Nature 405, 417–420 (2000)
2. Ginsberg, G.G., Barkun, A.N., Bosco, J.J., Isenberg, G.A., Nguyen, C.C., Petersen, B.T., Silverman, W.B., Slivka, A., Taitelbaum, G.: Wireless capsule endoscopy. Gastrointestinal Endoscopy 56(5), 621–624 (2002)
3. Tang, T.B., Johannessen, E.A., Wang, L., Astaras, A., Ahmadian, M., Murray, A.F., Cooper, J.M., Beaumont, S.P., Flynn, B.W., Cumming, D.R.S.: Toward a miniature wireless integrated multisensor microsystem for industrial and biomedical application. IEEE Sensors Journal 2(6), 628–635 (2002)
4. Lin, M.C., Dung, L R, Weng, P.K.: An ultra–low–power image compressor for capsule endoscope. BioMedical Engineering Online , 1–8 (2006)
5. Park, H.J., Park, J.C., Lee, J.H., Moon, Y.K., Song, B.S., Won, C.H., Choi, H.C., Lee, J.T., Cho, J.H.: New method of moving control for wireless endoscopic capsule using electrical stimulus. In: Proc. of Int'l Technical Conference on Circuits, Systems, Computers and Communications, pp.7E1L–1–1–7E1L–1–4 (2004)

6. Shahidi, R., Bax, M.R., Maurer, C.R., Johnson, J.A., Wilkinson, E.P., Wang, B., West, J.B., Citardi, M.J., Manwaring, K.H., Khadem, R.: Implementation, calibration and accuracy testing of an image–enhanced endoscopy system. IEEE Trans. on Medical Imaging 21(12), 1524–1535 (2002)
7. Hu, C., Meng, M., Liu, P.X., Wang, X.: Image distortion correction for wireless capsule endoscope. In: Proc. IEEE Int'l Conference on Robotics and Automation, pp. 4718–4723 (2004)
8. Asari, K.V., Kumar, S., Radhakrishnan, D.: A new approach for nonlinear distortion correction in endoscopic images based on least squares estimation. IEEE Trans. On Medical Imaging 18(4), 345–354 (1999)
9. Kim, B., Lee, S., Park, J.H., Park, J.O.: Design and fabrication of a locomotive mechanism for capsule–type endoscopes using shape memory alloys (SMAs). IEEE Trans. on Mechatronics 10(1), 77–86 (2005)
10. Pongnumkul, S., Sagawa, R., Echigo, T., Yagi, Y.: Deformable registration for generating dissection image of an intestine from annular image sequence. In: Liu, Y., Jiang, T., Zhang, C. (eds.) CVBIA 2005. LNCS, vol. 3765, pp. 271–280. Springer, Heidelberg (2005)
11. Smith, W.E., Vakil, N., Maislin, S.A.: Correction of distortion in endoscope image. IEEE Trans. on Medical Imaging 11(1), 117–122 (1992)
12. Mranda-Luna, R., Blondel, W.C.P.M., Daul, C., Hermandez-Mier, Y., Posada, P., Wolf, D.: A simplified method of endoscopic image distortion correction based on grey level registration. In: Proc. 2004 Int'l Conf. on Image Processing, pp. 3383–3386 (2004)
13. Wang, X., Meng, M.Q.H.: Study of a position and orientation tracking method for wireless capsule endoscope. Int'l Journal of Information acquisition 2(2), 113–121 (2005)
14. Cyrus, M., Back, J.: Generalized two–and three–dimensional clipping. Computer and Graphics 3, 23–28 (1978)

Using Trust in Collaborative Filtering Recommendation

Chein-Shung Hwang and Yu-Pin Chen

Department of Information Management, Chinese Culture University,
55, Hwa-Kang Road, Yang-Ming-Shan, Taipei, Taiwan, R.O.C.
cshwang@faculty.pccu.edu.tw, speedft@yahoo.com.tw

Abstract. Collaborative filtering (CF) technique has been widely used in recommending items of interest to users based on social relationships. The notion of trust is emerging as an important facet of relationships in social networks. In this paper, we present an improved mechanism to the standard CF techniques by incorporating trust into CF recommendation process. We derive the trust score directly from the user rating data and exploit the trust propagation in the trust web. The overall performance of our trust-based recommender system is presented and favorably compared to other approaches.

Keywords: Trust, Collaborative Filtering, Recommender System.

1 Introduction

The ever-increasing popularity of the Internet has led to an explosive growth of the sheer volume of data. Recommender systems are emergent to solve the information overload problem by suggesting users items that they might like or find interested. Collaborative filtering (CF) [1][2][3] is one of the most successful and widely used recommender systems. The main idea behind CF model is to automate the process of 'word-of-mouth' by which people recommend items to one another. For each user, CF model uses historical information to identify a neighborhood of people who have shown similar behavior in the past and then predicts the interest of new items by analyzing the neighborhood. The formation of neighborhood requires the computation and comparison between current user and every other user based on their ratings data. However, the number of ratings already collected is very small compared to the number of ratings needed to provide a prediction. As a result, CF model often has difficulty in finding a sufficient number of similar neighbors for a user and providing an effective recommendation.

Recently, several researches have suggested that the incorporation of a notion of *trust* into the standard CF model can effectively solve the sparsity problem and thus provide better recommendations. A user can build his personalized *web of trust* by specifying those friends or users he trusts. The trust web can be constructed through the explicit trust ratings provided by users. For example, Massa et al. [4] build a trust model directly from users' direct feedbacks.

H.G. Okuno and M. Ali (Eds.): IEA/AIE 2007, LNAI 4570, pp. 1052–1060, 2007.

This trust model is incorporated into the recommendation process for recommending various items (such as books, movie, music, software etc.) to on-line users. Users can express their personal *web of trust* by identifying those reviewers whose reviews and ratings are consistently found to be valuable. Massa et al. argue that it is possible to predict trust in unknown users by propagating trust even there were no direct connection between them. They also show, in their subsequent experiment [5], that the incorporation of trust metric and similarity metric can increase the coverage of recommender systems while maintaining the recommendation accuracy. Due to the limitation on trust value representation, in their experiments, the webs of trust are built on binary relationships among users and the propagating trusts are computed simply based on the distances between them. Avesain et al. [6] apply the trust model into the ski mountaineering domain. They present a community-based website in which users can share their opinions about the snow conditions of different ski routes and also express their trust on others' opinions. The trust score of a user depends on the trust statements of other users on him/her and their trust scores. However, the trust model requires the direct feedback of users and the effectiveness of the trust model on the skiing community has not been validated. Golbeck et al. [7] describe an E_mail filtering system based on trust ratings. The predicted trust of a user is given by a weighted average of her neighbors' trust ratings. They have shown that the weighted average metric can provide better results than other metrics. However they still need the explicit trust ratings from users and do not use any mail ratings information.

The explicit user participation for providing his trustworthiness to one another suffers from some limitations such as *additional user effort* and *cold start* that new users have to build up their trust webs before the filtering is effective. Alternatively, the trust web can be implicitly and directly derived from the item ratings data. Pitsilis et al. [8] view trust as a form of opinions which are always subjective and uncertain. Every opinion is expressed as a three-dimensional metric comprising *belief*, *disbelief* and *uncertainty*. The uncertainty is modeled from prediction error and the levels of belief and disbelief are derived based on correlation between every pair of users. The system presents a comparative performance to Beta distribution approach. However, no comparison to the traditional CF has been performed and reported. Donovan et al. [9] claim that the reliability of a user profile to deliver accurate recommendation in the past is an important factor for influencing recommendation and prediction. A user is viewed as more trustworthy if he has made more accurate predictions in the past than other users. The trust metrics are calculated at both the *Item* and *Profile* levels. Essentially these metrics summarize the relative number of correct recommendations that a given user has made, according to a predefined error bound. They have shown that the incorporation of trust metric into a standard CF has a positive impact on the prediction quality. However, this system only uses a global trust metric and provides neither any personalization nor trust propagation.

In general, while local trust metrics can be more precise and personalized than global trust metrics, they are also computationally more expensive. In this paper, we present an improved mechanism to the existing trust-based CF techniques. In particular, we will discuss how the local trust metrics can be incorporated into CF process and be efficiently propagated in the trust web. Formally, we aim to tackle the following problems:

1. How to directly derive trust ratings score from item ratings data?
2. How to define the global trust metric and the local trust metric?
3. How to propagate the trust score in the trust web?

2 System Architecture

The main goal of our study is to design an effective recommender system by integrating trust metric into the traditional CF process. The proposed system consists of three modules: Trust Computation (TC) module, Similarity Computation (SC) module, and Rating Prediction (RP) module as shown in Fig. 1.

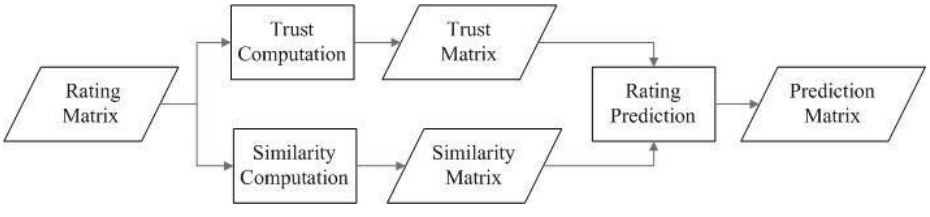

Fig. 1. System Architecture

The overall system can be viewed as a blackbox which takes as input the rating matrix and produces, as output, a prediction matrix. The ratings matrix R contains the rating scores $r_{i,k}$ standing for the rating of user u_i for item i_k, which can be either a numerical scale (representing his opinion) or $\perp$(representing no rating). The TC module derives the trust score directly from rating data and computes the propagated trust. The SC module computes the correlation coefficient between each pair of users. The RP module integrates the trust matrix and the similarity matrix to produce predictions for unseen items.

2.1 Trust Computation Module

The TC module involves a lot of works as shown in Fig. 2. Trust derivation module takes as input the rating matrix and computes the direct trust score of each pair of users. For every user, two trust metrics are computed. Global trust metric measures every user's global trust score reflecting the trustworthiness of all other users with the target user. The global trust score of a user is the same for every user. Local trust metric computes a user's trustworthiness with

respect to another user. Local trust metric takes as input the direct trust relationships resulting from the Trust derivation module and exploits the indirect trust relationships through trust propagation and path composition.

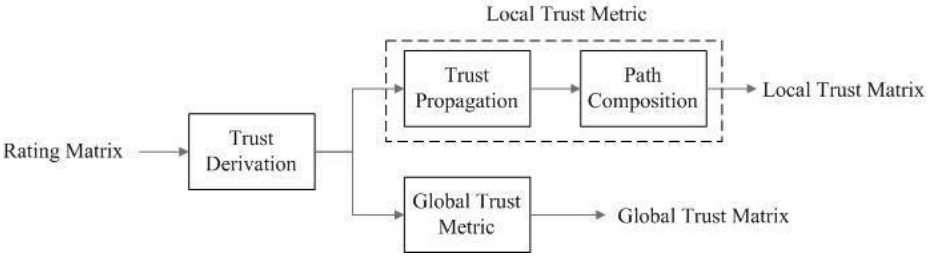

Fig. 2. Trust Computation Module

Trust Deviation. We believe that prediction accuracy of a user in the past is an important factor for measuring the trustworthiness of him. Therefore if a user delivers high accurate recommendations to another user in the past, then he is trustworthy and should obtain a high trust score from that user. Our system uses a simple version of Resnick's prediction formula [10] to compute the predicted rating. The predicted rating of item i for user u_a by another user u_b is given as follow:

$$p^b_{a,i} = \overline{r}_a + (r_{b,i} - \overline{r}_b)\,, \tag{1}$$

where $\overline{r}_a$ and $\overline{r}_b$ refer to the mean ratings of u_a and u_b, respectively, and $r_{b,i}$ is the rating of item i given by u_b. The trust score of u_a with respect to u_b is then derived by averaging the prediction error of co-rated items between them.

$$t_{a\to b} = \frac{1}{n(I_a \cap I_b)} \sum_{i\in(I_a\cap I_b)} \left(1 - \frac{|p^b_{a,i} - r_{a,i}|}{m}\right), \tag{2}$$

where I_a and I_b refer to the set of rated items of u_a and u_b, respectively, and m is the size of the rating range. It should be noted that the computation of the trust score is performed based on the co-rated items.

Global Trust Metric. A user's global trust with respective to another user combines the local trust with recommendations received from other users. We define the global trust score of a user u_a as the average of the local trust scores given by neighbors who are directly connected to u_a in the trust web.

$$gt_a = \frac{1}{n(NB(u_a))} \sum_{j\in NB(u_a)} t_{j\to a}, \tag{3}$$

where $NB(u_a)$ is the neighborhood of u_a.

Trust Propagation Metric. Due to the large number of items existing in a recommender system, the ratings matrix is very sparse. The sparsity of rating matrix often makes two users have no co-rated items, which results in no direct trust relationships between them. The problem can be handled by means of trust propagation to infer the indirect relationships. Trust propagation implies that, in the trust web, there exists a trust path between a source user u_s and a target user u_t. Suppose that there is an intermediate user u_m in the trust path connected u_s and u_t. The inferred trust score of u_t given by u_s through u_m is computed by the weighted average of the two direct relationships of $u_s \rightarrow u_m$ and $u_m \rightarrow u_t$ [11].

$$t_{s \underset{m}{\rightarrow} t} = t_{s \rightarrow m} \oplus t_{m \rightarrow t} = \frac{n(I_s \cap I_m) t_{s \rightarrow m} + n(I_m \cap I_t) t_{m \rightarrow t}}{n(I_s \cap I_m) + n(I_m \cap I_t)}, \tag{4}$$

The rational behind this computation is that if two users have more co-rated items then their direct relationship should be more reliable and desiring more weight. The propagation operator can be repetitively applied for computing the indirect trust relationship between any two users in the trust web.

Path Composition. It is possible that there are multiple paths between two users in the trust web. Each path contributes its own inferred trust score. The inferred trust score in each path is independent of each other. We need to decide how to combine these trust scores to give a single composite measure. In our current study, we simply compute the average of all the inferred trust scores contributed by each of the alternative paths.

2.2 Similarity Computation Module

The SC module is one of the standard steps in the standard CF algorithms. SC module computes the similarity between users. Recent studies [12][13] have shown a strong and significant correlation between trust and similarity. The more similar the two users are the higher trust they have. We take the ratings matrix as an input and produce a similarity matrix containing the similarity value of any user against every other user. We calculate the similarity as Pearson correlation coefficient [14].

$$sim_{a,b} = \frac{\sum_{i \in (I_a \cap I_b)} (r_{a,i} - \overline{r}_a)(r_{b,i} - \overline{r}_b)}{\sqrt{\sum_{i \in (I_a \cap I_b)} (r_{a,i} - \overline{r}_a)^2 \sum_{i \in (I_a \cap I_b)} (r_{b,i} - \overline{r}_b)^2}} \ . \tag{5}$$

2.3 Rating Prediction Module

The RP module is the final step in the standard CF algorithms. A common used algorithm is Resnick's standard prediction formula [10]. The predicted rating of item i for a user u_a is the weighted sum of the ratings given by users in his neighborhood.

$$p_{a,i} = \overline{r}_a + \frac{\sum_{k \in NB(u_a)} (r_{k,i} - \overline{r}_k) w_{a,k}}{\sum_{k \in NB(u_a)} w_{a,k}}, \tag{6}$$

where, $w_{a,k}$ represents the weight of user u_a assigned to his neighbor u_k. $w_{a,k}$ can be taken either from the similarity score $sim_{a,k}$, the local trust score $t_{a\to k}$ or the global trust score gt_k.

3 Experimental Evaluation

3.1 Data Sets

We use the *movielens* dataset collected by the GroupLens Research at the University of Minnesota. It contains 100,000 ratings from 943 users for 1628 movies. Each user has rated at least 20 movies, and each movie has been rated at least once. The original data set was converted into a new user-movie matrix R that had 943 rows (i.e. 943 users) and 1682 columns (i.e. 1682 movies). We employ the 5-fold cross-validation approach. First, we randomly divide the dataset into five groups. Then we run five rounds of tests, each time choosing one group of data as test data and the other four groups as training data. The training set is used to generate the recommendation model. For each user in the test data, we employ the AllButOne protocol in which one item is selected at a time as the predicated item; all other ratings are used as input to the system. Our recommender system is then evaluated by comparing the predicted ratings with the actual ratings of the selected items.

3.2 Evaluation Metrics

To measure the accuracy of the recommendations we computed the standard Mean Absolute Error (MAE) between ratings and predictions in the test data. MAE is a measure of the deviation of recommendations from their actual ratings. Specifically, given the set of actual/predicted pairs ($r_{a,i}$,$p_{a,i}$) for all the movies rated by user u_a, the MAE for user u_a is computed as:

$$MAE_a = \frac{\sum_{i \in R(u_a)} |r_{a,i} - p_{a,i}|}{n(R(u_a))}, \tag{7}$$

where $R(u_a)$ represents the set of items that are rated by u_a. The overall MAE is computed by averaging these individual MAEs over all users in the test data.

Another important measure for discriminating between different recommendation approaches is coverage. Coverage is a measure of percentage that a recommender system can provide predictions. A prediction is impossible to be computed only when very people rated the movie or the active user has no correlation with other users. So a movie is predictable even only two users have rated it. Our pilot study reveals a near perfect coverage (around 99% in all experiments). To make a reasonable comparison,we examine the change of coverage with respect to different sparsity of user rating data.

3.3 Performance Results

Table 1 shows the prediction accuracy of different trust settings in our recommender system in contrast to those produced by standard CF technique. In all experiments, we compare the recommendation quality of different trust settings in our recommender system with those produced by standard CF technique. We compare the global trust model to local trust model with different maximum propagation distance, precisely, 1, 2, 3, and 4. We define as global-CF the method that employs the global trust metric in the CF process. Local-CF-n represents the method in which the local trust metric with maximum propagation distance n is used. The MAE is expressed with respect to different neighborhood sizes.

Table 1. MAE of trust-based CFs vs.standard CF recommendation

Size of NB	Standard CF	Global-CF	Local-CF-1	Local-CF-2	Local-CF-3	Local-CF-4
10	0.893	0.879	0.870	0.864	0.861	0.862
20	0.861	0.845	0.831	0.822	0.816	0.816
30	0.832	0.829	0.802	0.794	0.790	0.790
50	0.801	0.805	0.776	0.769	0.767	0.768
70	0.763	0.784	0.752	0.744	0.742	0.742
90	0.763	0.782	0.753	0.746	0.744	0.744
120	0.764	0.785	0.755	0.749	0.745	0.745
150	0.767	0.786	0.757	0.752	0.750	0.750

In all approaches, the prediction accuracy improves as the number of neighbors increases but they reach the maximum performance at around 70 neighbors and any further increment makes no better or even worse results. However, the trust enhanced approaches result in an overall improvement in accuracy. Specifically, the local trust CFs perform the best under all cases and the global trust CF is slight better than the standard CF in a small neighborhood, but performs worse with increasing number of neighbors. The performance of the local trust CF varies with the propagation distances and reaches the best when the distance is 3.

As discussed earlier, sparsity of ratings is one of the common problems that collaborative recommender system may encounter. The sparsity problem is one major reason causing poor prediction quality. In this experiment, we examine the effectiveness of trust in solving the sparsity problem. To evaluate the coverage of different approaches, we relax the size of neighborhood to all users, and perform an experiment with different sparsity levels. Table 2 shows the result of coverage for different CF approaches. As expected, when the sparsity level increases, the coverage drops gradually. The global-CF has the highest coverage as all users are involved for recommendations. Local-CF-1 gains a slight improvement in coverage compared with the standard CF. The coverage increases when the maximum propagation distance increases. Local-CF-2 provides a large improvement over Local-CF-1, but the improvement starts to converge to 0 with increasing propagation distance.

Table 2. Coverage of different CF approaches

Sparsity (%)	Standard CF	Global-CF	Local-CF-1	Local-CF-2	Local-CF-3	Local-CF-4
96.0	0.942	0.998	0.961	0.991	0.993	0.993
96.5	0.934	0.996	0.956	0.990	0.992	0.993
97.0	0.932	0.994	0.951	0.990	0.992	0.992
97.5	0.922	0.991	0.948	0.988	0.990	0.990
98.0	0.913	0.989	0.933	0.982	0.984	0.985
98.5	0.804	0.984	0.846	0.953	0.958	0.959
99.0	0.597	0.977	0.627	0.925	0.928	0.929
99.2	0.437	0.962	0.474	0.875	0.881	0.883
99.5	0.277	0.968	0.372	0.785	0.789	0.791

4 Discussion and Future Work

In this paper we have presented a trust-based CF recommender system which incorporates the trust notion into the standard CF process. We derive the trust score directly from the ratings data based on users' prediction accuracy in the past. We investigate the effects of both the local trust metric and the global trust metric in the standard CF recommendation. The global metric has shown to have an advantage over other approaches in prediction coverage. The local metrics provide more accurate recommendations than those provided by standard CF technique. Experimental results verify that the incorporation of trust into CF process can indeed improve the prediction accuracy while maintain satisfactory prediction coverage.

We have described the proposed trust-based CF approach in the context of the movie domain. A further application to a range of other domains would be investigated. In fact, we would suggest that any social community network could benefit from the web of trust, assuming that the ratings data are available.

References

1. Shardanand, U., Maes, P.: Social Information Filtering: Algorithms for Automating 'Word of Mouth'. In: Proceedings of Human Factors in Computing Systems, pp. 10–217 (1995)
2. Breese, J.S., Heckerman, D., Kadie, C.: Empirical Analysis of Predictive Algorithms For Collaborative Filtering. In: Proceedings of the 14th Conference on Uncertainty in Artificial Intelligence, pp. 43–52 (1998)
3. Herlocker, J., Konstan, J.A., Terveen, L., Riedl, J.: Evaluating Collaborative Filtering Recommender Systems. ACM Transactions on Information Systems 22, 5–53 (2004)
4. Massa, P., Bhattacharjee, B.: Using Trust in Recommender Systems: An Experimental Analysis. In: Proceedings of the 2nd International Conference on Trust Management, Oxford, England, pp. 221–235 (2004)
5. Massa, P., Avesani, P.: Trust-Aware Collaborative Filtering for Recommender Systems. In: Proceedings of the International Conference on Cooperative Information Systems (CoopIS), Agia Napa, Cyprus, pp. 492–508 (2004)

6. Avesani, P., Massa, P., Tiella, R.: Moleskiing: A Trust-Aware Decentralized Recommender System. In: Proceedings of the First Workshop on Friend of a Friend Social Networking and the Semantic Web, Galway, Ireland (2004)
7. Golbeck, J., Hendler, J.: Reputation Network Analysis for Email Filtering. In: Proceedings of the First Conference on Email and Anti-Spam, Mountain View, California (2004)
8. Pitsilis, G., Marshall, L.: A Model of Trust Derivation from Evidence for Use in. Recommendation Systems. Technical Report, University of Newcastle Upon-Type (2004)
9. O'Donovan, J., Smyth, B.: Trust in recommender systems. In: Proceedings of the 10th international conference on Intelligent user interfaces, pp. 167–174 (2005)
10. Resnick, P., Iacovou, N., Suchak, M., Bergstrom, P., Riedl, J.: Grouplens: An Open Architecture for Collaborative Filtering of Netnews. In: Proceedings of ACM CSCW'94 Conference on Computer-Supported Cooperative Work, Sharing Information and Creating Meaning, pp. 175–186. ACM Press, New York (1994)
11. Papagelis, M., Plexousakis, D., Kutsuras, T.: Alleviating the sparsity problem of collaborative filtering using trust inferences. In: Herrmann, P., Issarny, V., Shiu, S.C.K. (eds.) iTrust 2005. LNCS, vol. 3477, pp. 224–239. Springer, Heidelberg (2005)
12. Ziegler, C., Georg, L.: Analyzing Correlation Between Trust and User similarity in Online Communities. In: Proceedings of Second International Conference on Trust Management, pp. 251–265 (2004)
13. Abdul-Rahman, A., Hailes, S.: Support Trust in Virtual Communities. In: Proceedings of the 33rd Hawaii International on System science. Maui, Hawaii, USA, pp. 1769–1777 (2000)
14. Pearson, K.: Mathematical contribution to the theory of evolution: VII, on the correlation of characters not quantitatively measurable. Phil. Trans. R. Soc. Lond. A 195, 1–47 (1900)

AdaptRank: A Hybrid Method for Improving Recommendation Recall

Maciej Kiewra[1] and Ngoc Thanh Nguyen[2]

[1] Fujitsu Spain Services, C/ Camino Cerro de los Gamos, 128224 Pozuelo de Alarcon, Madrid, Spain
mkiewra@mail.fujitsu.es
[2] Institute of Information Science & Engineering, Wroclaw University of Technology, Poland
thanh@pwr.wroc.pl

Abstract. A hybrid recommendation method is presented in this paper. Its main goal is to improve recommendation recall maintaining high recommendation precision and adaptive ability. The formal model is used to define the method and to analyze how the measures known from traditional Information Retrieval may be adapted to recommendation. The presented theorems show that the method is able to adapt to changing user's needs and achieve the maximal effectiveness if the component methods work properly.

1 Introduction

Hundreds of recommender systems have appeared during more than ten years of investigations related to recommendation in hypertext environment [6], [9], [14]. Their main goal is to select from a set of items, a subset of them that are relevant for the user needs. The selection process is usually iterative and it is based on observing user behavior and characteristics of visited items.

Researchers noticed relatively early that combining two or more methods of recommendation had a lot of benefits [2], [11]. There are two main types of component methods that can be used to obtain a new hybrid method: content-based filtering and collaborative filtering. The former assumes that the recommended items should be "somehow similar" to the items that have been seen or rated as valuable by the current user. The latter recommends such items that were interesting for the users whose behavior or features are similar to the current user's counterparts.

Many different algorithms of component methods integration have been presented including interesting surveys [1], [4]. All of them can be divided in seven groups (following the classification presented in [4]). First of them known as *weighted integration* assumes that component methods assign the number that reflects estimated relevance to each item. The hybrid method combines these numbers by means of weighted sum. The items that possess the highest value of the total number are recommended to the user. The second approach labeled as *switching* uses only one component method in each iteration, replacing it by the other if the user has not found interesting initial recommendation. The third type of hybrid methods, known as

H.G. Okuno and M. Ali (Eds.): IEA/AIE 2007, LNAI 4570, pp. 1061–1071, 2007.

mixed, presents *m* the best items of each component method simultaneously. The remaining four types mentioned in [4] (feature combination, cascade approach, feature augmentation and meta-level integration) do not integrate component methods but rather create a single method using different source of data. In our opinion, only weighted integration can increase recommendation precision significantly, because neither switching nor mixed approach can avoid recommending irrelevant items if one of the component methods is not able to find any relevant item (e.g. due to well-known sparsity problem in case of collaborative filtering or over-specialization in case of content based filtering [1]).

The main contribution of this paper consists in defining an original formal model and a method for hybrid recommendation. The novelty of this method is based on using modified weighted integration not only to enhance recommendation precision, but also to improve diversity of recommended items (diversity of recommendation is measured by means of recall). Since information retrieval research has revealed that increase in recall usually causes decrease in precision and vice versa (this phenomena is known as the recall-precision curve [13]), we will try to demonstrate that our method permits the maximal precision and recall to be achieved.

This paper presents in short the results worked out by the authors in [7]. In this non-published thesis the recommendation model has been defined in detail and the AdaptRank method has been analysed and verified by experiments.

2 The Recommendation Model

The model, presented in this paper, permits recommendation in a hypertext system to be formalized. The hypertext system (e.g. a web site) is a system that manages and provides access to a set of hypertext documents $D = \{d_1, d_2, \ldots, d_n\}$.

Definition 1. *A hypertext document* $d \in D$ *is a quadruple* $d = (u_d, F_d, L_d, \mathbf{v}^d)$, *where*: u_d *is the unique document's identifier*; F_d *is the set of statistical features of the document d*; L_d *is the set of hyperlinks located inside the document d that point to the documents from the set D and* $\mathbf{v}^d = (v^d_1, v^d_2, \ldots, v^d_{n_w})$ *is the descriptor vector. Each coordinate* $v^d_j \in [0,1]$ *for* $j = 1, 2, \ldots, n_w$ *is a number that determines importance of the* j^{th} *descriptor in the document d.*

The detailed algorithm for calculation of the $\mathbf{v}^d$ vector depends on a recommendation method. Statistical features of documents may vary for each hypertext system. The most popular magnitudes used in web environments are document visit frequency and opening rate (the ratio of the sessions' number in which the document *d* was visited as the first to the total number of sessions in which the document *d* was visited) [8].

Once the user establishes connection with the hypertext system, he or she sends requests in order to obtain documents. Each request is related to exactly one document from the set *D*. A session is a sequence of requests sent during one connection. Each sent request together with the response will be denominated a step of the session (see Fig. 1).

As it can be appreciated in Fig. 1, the system sends as the response to the single request not only the requested document, but also the set of hyperlinks to recommended documents that can (but does not have to) be requested in the next step.

If the document recommended in the i^{th} step is not requested in the next step, it will be considered as ignored in the i^{th} step. The session ends when the user closes the connection with the hypertext system.

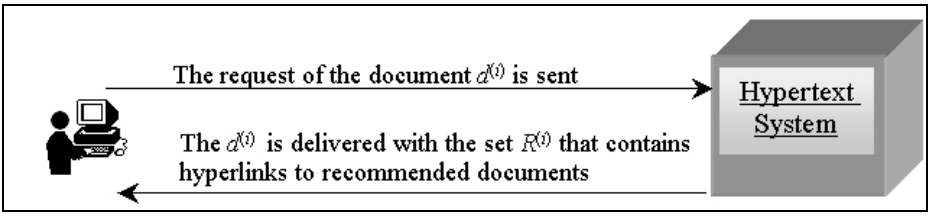

Fig. 1. A single step of the current session

There are two types of sessions in the recommendation model: current sessions and historical sessions. The current session is a session that has not been closed yet (the recommender system is performing recommendation for this session).

Definition 2. *Let* $s_b = (s_b^{(1)}, s_b^{(2)}, ..., s_b^{(n_{sb})})$ *be the current session, where* n_{sb} *is the session's length and* $s_b^{(i)} = <R^{(i)}, \mathbf{z}^{(i)}, \mathbf{g}^{(i)}>$ *for* $i = 1,\ldots, n_{sb}$, *is the state of the session* s_b *in the* i^{th} *step, where*:

- $R^{(i)}$ *is the set of documents recommended in the* i^{th} *step* ($R^{(i)} \subseteq D$),
- $\mathbf{z}^{(i)} = (z_1^{(i)}, z_2^{(i)},\ldots,z_n^{(i)})$ *is the vector of documents visited till the* i^{th} *step of the current session. Each coordinate* $z^{(i)}_j \in [0, 1]$ *for* $j = 1,\ldots,n$ *determines how long ago the document* $d^{(j)}$ *has been visited in the session* s_b (0 - *it has not been visited*, 1- *it is visited just now*). *The detailed algorithm of coordinate's calculation varies for the particular method.*
- $\mathbf{g}^{(i)} = (g_1^{(i)}, g_2^{(i)},\ldots,g_n^{(i)})$ *is the vector of ignored documents. The coordinate* $g^{(i)}_j \in [0, 1]$ *for* $j = 1,\ldots,n$ *determines how long ago the document* $d^{(j)}$ *has been ignored in the session* s_b (0 - *it has not been ignored*, 1- *it has been ignored in the previous step*). *The detailed algorithm of coordinate's calculation varies for the particular method.*

Let $R = \bigcup_{i=1}^{n_{sb}} R^{(i)}$ be the set of all documents recommended during the session. Once the session is finished it is converted in a historical session.

Definition 3. *Let* $\mathbf{s} = (s_1,s_2,\ldots,s_n)$ *be a historical session vector, where* $s_j = 1$ *when the document* d_j *has been visited in the session*; $s_j = 0$ *– otherwise*

Let S be the set of all historical sessions available in the system. Data related to a single historical session are very limited comparing with the current session, because even a medium hypertext system can possess millions of sessions. We have decided to restrict the historical data in order to avoid possible performance problems.

The component of the hypertext system that is responsible for recommendation will be denominated *recommender system.*

Definition 4. *Let RS = <D, S, f> be a recommender system where D is the set of available documents, S is the set of historical sessions and f is the recommendation function that in every step of the current session s_b assigns for each document from the set D a real number that represents relevance of the document in the current step of the session s_b.*

For example, $f(d,s_b^{(4)}) = 0.9$ means that in the 4th step of the current session s_b relevance to the user's needs is equal 0.9. The recommendation function is the most important element of every recommender system. It is similar to the retrieval status value that estimates degree of document relevance to the given query and it is widely used in information retrieval [3]. In case of the recommendation function the query is replaced with the current session. Although recommendation and search processes are similar (in both cases the relevant documents are presented) the recommendation process does not require the implicit user intervention and is more iterative.

Obviously, the user's needs can change during the same session (e.g. due to the recommendation content), therefore document relevance should be estimate in every session step separately. Let $DR^{(i)}$ be the subset of the set D that contains documents considered by the system as relevant for the user in the i^{th} step of the current session and the rest of the documents ($D \backslash DR^{(i)}$) as irrelevant ones.

Precision and recall – two measures known from Information Retrieval [13] can be successfully adapted to evaluate the quality of recommender systems. Due to possible changes in user's needs, recommendation precision in the current session is slightly more complex than search precision in the given query.

Definition 5. *Recommendation precision of the system RS in the session s_b is the ratio of the number of relevant documents recommended by the system RS during the session s_b to the total number of documents recommended by the system RS during the session s_b*:

$$prec(RS, s_b) = \frac{\sum_{i=1}^{n_{s_b}} card(R^{(i)} \cap D_R^{(i)})}{\sum_{i=1}^{n_{s_b}} card(R^{(i)})}. \tag{1}$$

The difference between recommendation recall definition and its counterpart from searching is more significant, because recommender systems tend to recommend only a few documents in each step, therefore the standard recall definition (the ratio of the number of relevant documents retrieved by the system to all relevant documents available) would promote the long sessions (sessions with many steps).

Definition 6. *Recommendation recall of the system RS in the session s_b is the ratio of the number of different relevant documents recommended by the system RS during the session s_b to the total number of different relevant documents that would have been recommended by the system RS during the session s_b assuming that up to m documents could be recommended in a single step*:

$$rec(RS, s_b) = \frac{card\left(\bigcup_{i=1}^{n_{s_b}} \left(D_R^{(i)} \cap R^{(i)}\right)\right)}{n_r} \tag{2}$$

where n_r can be obtained from the following formula:

$$n_r = \min\left(m, card\left(D_R^{(1)}\right)\right) + \sum_{i=2}^{n_{s_b}} \min\left(m, card\left(D_R^{(i)} \setminus \bigcup_{i=1}^{i-1} R^{(j)}\right)\right) \quad (3)$$

As it can be deduced from Definition 6, n_r expresses the number of relevant documents that would have been recommended during the session s_b. The left part of the formula (3) – $\min(m, card(D^{(1)}{}_R))$ corresponds to the first step. Obviously, there is no document recommended in the session s_b before the first step therefore the number of relevant documents that can be recommended to the user in the first step according to the conditions from Definition 6 is equal to m, except for the situation in which $m > card(D^{(1)}{}_R)$ (the set D would not contain m relevant documents).

The number of relevant documents that can be recommended in the next steps is calculated iteratively in a similar way. Obviously, only the number of not recommended relevant documents is compared with m.

Recall and precision can be expressed as effectiveness. This measure is also widely used in Information Retrieval and its calculation formula differs according to the authors [5], [10], [13]. We have chosen the definition proposed in [15]:

$$E(RS, s_b) = \sqrt{prec(RS, s_b \cdot rec(RS, s_b)}\,. \quad (4)$$

This definition is simple, intuitive and it promotes recommender systems that are able to keep balance between high recall and high precision. It is important to underline that it is relatively easy to obtain high recall by recommending different documents neglecting their relevance and as a consequence recommendation precision. Similarly, if a recommender system proposed the same very relevant documents in each step of the current session, the recommendation precision would be very high but the recall would decrease drastically for medium and long sessions. The effectiveness from the formula (4) will be relatively low in both cases.

3 AdaptRank – A Hybrid Recommendation Method

The model defined in the previous section will be used to present a hybrid recommendation method denominated AdaptRank that integrates two method of recommendation. The first is based on collaborative filtering (recommended documents are selected comparing the current session s_b with the set of historical sessions - S) and the second on content based filtering (the documents similar to the visited documents are obtained using the $\mathbf{v}^d$ vector). The detailed definitions of the both methods are beyond the scope of this paper (their examples may be find in [7] or [11]). Let f_u be a recommendation function that estimates document relevance using a collaborative filtering method (usage component) and let f_c be a recommendation function that estimates document relevance using content based filtering method (content component).

Additionally, let q be a quality function that for each document from the set D assigns the real number from [0, 1] that describes quality of every document. The value of the q function may vary for each implementation. It can depend on the statistical features of documents (the set F_d from Definition 1) [8]. Similarly, the

value of the q function may be determined by hyperlink structure (see the set L_d from Definition 1). Obviously, the value of the q should not depend on user interactions because it does not measure the relevance of documents to particular user's needs. It rather expresses contextless value of documents. Its main goal is to promote the documents that are objectively valuable and it should have more impact at the beginning of the current session when the user's needs have not been transmitted to the system yet.

Definition 2 has left to a particular method the way in which the coordinates of the **z** and **g** vectors are obtained. The (5) formula presents the value of the **z** vector coordination in the first step of the AdaptRank method:

$$z_j^{(1)} = \begin{cases} 0 & \text{for} \quad d^{(1)} \neq d_j \\ 1 & \text{for} \quad d^{(1)} = d_j \end{cases} \tag{5}$$

The values of the **z** vector in the next steps can be calculated recursively from the following formula:

$$z_j^{(i+1)} = \begin{cases} \rho_s \cdot z_j^{(i)} & \text{for} \quad d^{(1)} \neq d_j \\ 1 & \text{for} \quad d^{(1)} = d_j \end{cases}. \tag{6}$$

where $d^{(i)}$ is the document visited in the i^{th} step of the current session and $\rho_s \in (0, 1)$ is a parameter that determines how fast the fact of the document's visit will be "forget" by recommender system (the visited documents are almost treated as no visited ones when their $z_j^{(i)}$ values are close to 0).

As it can be noticed the value of the coordinate that corresponds to the document visited in a given step decreases geometrically in next steps. It was shown in [7] that the increase of the ρ_s value may improve recommendation recall and decrease recommendation precision.

The **g** vector is obtained in the following way:

$$g_j^{(1)} = 0;$$

$$g_j^{(i+1)} = \begin{cases} \gamma - \alpha & for \quad d^{(i)} \neq d_j \wedge g_j^{(i)} = 1 \\ 1 & for \quad d_j \in R^{(i)} \wedge d^{(i+1)} \neq d_j \\ \gamma \cdot g_j^{(i)} & otherwise \end{cases}. \tag{7}$$

where $d^{(i)}$ is the document visited in the i^{th} step of the current session, $\alpha \in (0, 1)$ and $\gamma \in (\alpha, 1)$. The α parameter will be used in the f function definition (see below) to regulate the influence of the values of the function f in previous steps on the current one. Although the formulas 5, 6 and 7 are similar (the γ parameter is the counterpart of the ρ_s) there are three differences that should be explained.

The explanation of the first difference is obvious the $\mathbf{g}^{(1)}$ vector has 0 values for all its coordinates because before the first step any document cannot be recommended and as a consequence ignored.

The second difference is the value of the coordinate that corresponds to the document that was ignored two steps ago: $\gamma - \alpha$. If this value was equal to γ, there

would be cases in which the fact of ignoring the document d_j in the i^{th} step would have more impact in the step i+2 that in the step i+1 (see the theorem 5.1.6 from [7]). The third difference - $\gamma \in (\alpha, 1)$ - is a consequence of the second one ($\gamma > \alpha$ would drive to $\gamma - \alpha < 0$ that would be contrary to the condition $z^{(i)}_j \in [0, 1]$ from Definition 2).

Definition 7. *The value of the recommendation function f for the document* d_j ($d_j \in D$) *in the* i^{th} *step of the current session* s_b *can be obtained from the following formula*:

$$f(d_j, s_b^{(1)}) = \left(0.5 \cdot (\beta + \delta) \cdot \alpha \cdot q(d_j) + \beta \cdot f_u(d_j, s_b^{(1)}) + \delta \cdot f_c(d_j, s_b^{(1)})\right) \cdot (1 - z_j^{(1)})$$
$$f(d_j, s_b^{(i+1)}) = \left(\alpha \cdot f(d_j, s_b^{(i)}) + \beta \cdot f_u(d_j, s_b^{(i)}) + \delta \cdot f_c(d_j, s_b^{(i)}) - g_j^{(i+1)}\right) \cdot (1 - z_j^{(i+1)}) . \quad (8)$$

where $\beta, \delta \in (0, 1]$ *and* $\alpha \in (0;1)$ *are parameters that regulate the influence of the both component functions and the previous step function's value respectively.*

As it can be seen in Definition 7 the value of the function *f* in the first step is a linear combination of the quality function and two component functions for all documents from the set *D* except for the document $d^{(1)}$ for which it is equal to 0. In the rest of the steps the quality function is replaced by the function's value from the previous step. Additionally, the function value is decreased for the documents that have been ignored or visited in the current session. Analyzing the formulas 5, 6 and 7 it is easy to notice that this decrease tends to be weaker and weaker in the next steps after the document's visit or ignoring. The main goal of the lower function's values for recommended documents is to increase recommendation recall.

Table 1 contains description of the parameters used in the AdaptRank method. Their impact on precision and recall presented in the table was deeply analyzed in [7].

Table 1. Parameters' description. The characters "+" and "–" determine if the increase of the parameter value will improve/decrease the corresponding measure.

Parameter	*Description*	*Precision*	*Recall*	*Proposed value*
α	Regulates the influence of the recommendation function from the previous step	–	–	0.25
β, δ	Controls the influence of the usage and component method respectively	+	–	1
γ	Determines how fast the system "forgets" that a given document has been ignored	–	+	0.9
ρ_s	Determines how fast the system "forgets" that a given document has been visited.	–	+	0.75
m_r	The total number of relevant documents	+	–	
m	The number of documents recommended in one step	–	+	2

Table 1 shows that high values of the α parameter deteriorate both measures, but it does not mean that its value should be close to 0. The very small value of α would cause that recommendation would be based only on the last visited document.

The algorithm of the AdaptRank method is simple: the value of recommendation function f is calculated in each step of the current session s_b for each document from the set D and m documents with the highest value of the function f are recommended.

4 The Characteristics of AdaptRank

The theorems presented in this section reflect the most important characteristics of the AdaptRank method. Their proofs can be found in [7].

Theorem 1. *The document d_{max} that*:

$$\underset{n_{s_b}\geq i'>i}{\forall}\left(\underset{d_j\in D}{\forall}\left(f_u(d_{\max},s_b^{(i')})\geq f_u(d_j,s_b^{(i')})\ \wedge\ f_c(d_{\max},s_b^{(i')})\geq f_c(d_j,s_b^{(i')})\right)\right). \tag{11}$$

it will be recommended in at most st *steps where* st *is the smallest natural number that holds the inequality*:

$$st>\log_{\alpha}\left(\frac{c}{c+1-0.5\cdot\alpha^{i}-0.5\cdot\alpha^{i+1}}\right). \tag{12}$$

where c is the greatest positive real number that holds the following:

$$\underset{i'>i}{\forall}\left(\underset{d_j\in D\setminus\{d_{\max}\}}{\forall}\left(f_u(d_{\max},s_b^{(i')})-f_u(d_j,s_b^{(i')})\geq c\ \wedge\ f_c(d_{\max},s_b^{(i')})-f_c(d_j,s_b^{(i')})\geq c\right)\right) \tag{13}$$

This theorem illustrates the adaptive character of the method. It shows that the d_{max} document (the document that possesses the highest value of two component functions since the i^{th} step) will be recommended, even if the component functions' values for this document have been the smallest before the i^{th} step. In other words, if the component functions are able to identify properly the relevant documents, the document that has been irrelevant to initial user's needs, but it converts in relevant when the user has changed the interests will be recommended in the limited number of steps. For example, if α=0.5, c=0.4 and i=10, then $st\approx1.81$.

The next theorem needs four auxiliary variables to be introduced. Let r_{cmin}, r_{umin}, be the minimum values of the component functions f_c and f_u obtained by the relevant documents in the current session:

$$\begin{aligned} r_{cmin} &= \min\left\{f_c(d,s_b):0<i\leq n_{sb}\ \wedge\ d\in D_R^{(i)}\right\}.\\ r_{umin} &= \min\left\{f_u(d,s_b):0<i\leq n_{sb}\ \wedge\ d\in D_R^{(i)}\right\}. \end{aligned} \tag{14}$$

Similarly, let n_{cmax}, n_{umax}, be the maximal values of the component functions f_c and f_u obtained by the irrelevant documents in the current session:

$$\begin{aligned} n_{cmax} &= \max\left\{f_c(d,s_b):0<i\leq n_{sb}\ \wedge\ d\in D\setminus D_R^{(i)}\right\}.\\ n_{umax} &= \max\left\{f_u(d,s_b):0<i\leq n_{sb}\ \wedge\ d\in D\setminus D_R^{(i)}\right\}. \end{aligned} \tag{15}$$

Theorem 2. *Effectiveness of the recommender system RS will be maximal in the current session* $s_b - E(RS,s_b) = 1$ *independently from the session's length, if the user visits one of the m documents recommended in the previous step in each* i^{th} *step* ($i = 2,..,n_{sb}$) *of the current session* s_b (*i. e.* $d^{(i)} \in R^{(i-1)}$) *and the recommender system RS possesses* m_r ($m_r > m$) *relevant documents that do not change during the session* s_b $D_R^{(1)} = D_R^{(2)} = ... = D_R^{(n_{s_b})}$ *and the following conditions hold in the first* $\lfloor m_r / m \rfloor$ *steps:*

$$\begin{matrix} r_{c\min} > 0.5 \cdot \alpha + \frac{n_{c\max}}{1-\alpha}, & r_{c\min} > (1-\rho_s) \cdot \frac{1-\alpha^{[m_r/m]}}{1-\alpha^2} \\ r_{u\min} > 0.5 \cdot \alpha + \frac{n_{u\max}}{1-\alpha}, & r_{u\min} > (1-\rho_s) \cdot \frac{1-\alpha^{[m_r/m]}}{1-\alpha^2} \end{matrix}. \quad (16)$$

and in the next steps the following inequalities are fulfilled:

$$r_{cmin} > \frac{0.5 \cdot \alpha}{1-\rho_s^{[m_r/m]}} + \frac{n_{cmax}}{(1-\rho_s^{[m_r/m]}) \cdot (1-\alpha)}, \; r_{umin} > \frac{0.5 \cdot \alpha}{1-\rho_s^{[m_r/m]}} + \frac{n_{umax}}{(1-\rho_s^{[m_r/m]}) \cdot (1-\alpha)} \quad (17)$$

Theorem 2 shows that AdaptRank guarantees the maximal effectiveness, if there is a significant difference between the values of the component functions for relevant and irrelevant documents (i. e. component methods behave properly). For example, the AdaptRank method would obtain the maximal effectiveness with the following parameter: α=0.25, ρ_s=0.8, m_r=20 (there was 20 relevant documents), m=2 (two documents were recommended in each step), n_{cmax}=n_{umax}=0.2 (values of the component functions for irrelevant documents did not exceed 0.2), r_{cmin}=r_{umin}=0.4 (values of the component functions for relevant documents did exceed 0.4).

The inequalities presented in the theorem 2 guarantee only the maximal precision of the component methods, but not recall. The most important contribution of the AdaptRank method illustrated in the theorem 2 is the achievement of maximal recall maintaining maximal precision.

5 Experiments

Effectiveness of the presented method has been also measured and verified by means of *AdaptRank Simulator* program. Its main purpose is to simulate the AdaptRank method and its component behaviour in hypothetical random current sessions. The all method parameters presented in Table 1 can be configured. Additional variables that can be established on configuration level are presented in Table 2.

All performed experiments consist of generating 100 sessions for each iteration defined in Table 3. The principal goal of the experiments is to analyze the method's effectiveness when the component function value for relevant documents is only slightly greater than for irrelevant ones: *rmin*=0.49 and *rmax*=0.5 (please note that Theorem 2 requires that the difference between *rmin* and *rmax* is significant).

AdaptRank has obtained the highest effectiveness in all cases. The condition *rmin*>*nmax* guarantees maximum precision of the component methods, so the better effectiveness of AdaptRank has been achieved by recall increase.

Table 2. Additional variables that can be established in AdaptRank Simulator

Parameter	*Description*	*Established Value*
n	Cardinality of the set *D*	100
nr	Number of relevant documents	20
sessionLen	The length of the session	Random [5,30]
rmin	The value of r_{cmin} and r_{umin} presented in the formula 14	0.49
nmax	The value of n_{cmax} and n_{umax} presented in the formula (15)	0.5

Table 3. Designed experiments and their results

Changing parameter	*Minimal Value*	*Maximal Value*	*Increase per step*	*Mean AdaptRank Effect.*	*Mean Usage Component Effect.*	*Mean Content component Effect.*
n	20	100	1	0.93	0.85	0.82
nr	20	100	1	0.97	0.94	0.89
rmin	0.5	1	0.01	0.97	0.95	0.9
nmax	0	0.49	0.01	0.97	0.95	0.89

6 Conclusions

A hybrid recommendation method has been presented in this paper. The method has introduced integration mechanisms that permit the method to adapt to user's needs very quickly and to increase recommendation recall. Although recall improvement can deteriorate recommendation precision, formal analysis and the experiments have demonstrated that AdaptRank can achieve the maximal effectiveness, if the component methods work correctly. Moreover, the parameters of the method permit the system administrators to adjust recommendation to local needs (it is possible to increase recommendation recall at the expense of precision and vice versa).

References

1. Adomavicius, G., Tuzhilin, A.: Recommendation technologies: Survey of current methods and possible extensions. MISRC working paper 0329. University of Minnesota (2003)
2. Balabanovic, M., Shoham, Y.: Fab: content-based, collaborative recommendation. In: Communications of the ACM, vol. 40(3), pp. 66–72. ACM Press, New York (1997)
3. Bookstein, A.: Relevance. Journal of the American Society for Information Science 30(5), 269–273 (1979)
4. Burke, R.: Hybrid Recommender Systems: Survey and Experiments. In: User Modeling and User-Adapted Interaction, vol. 12(4), pp. 331–370. Springer, Netherlands (2002)
5. Heine, M.H.: Distance between sets as an objective measure of retrieval effectiveness. Information Storage and Retrieval 9, 181–198 (1973)
6. Kazienko, P., Kiewra, M.: ROSA - Multi-agent System for Web Services Personalization. In: Menasalvas, E., Segovia, J., Szczepaniak, P.S. (eds.) AWIC 2003. LNCS (LNAI), vol. 2663, pp. 297–306. Springer, Heidelberg (2003)

7. Kiewra, M.: A Hybrid Method of Document Recommendation in Hypertext Environment. Ph.D. Thesis. Wroclaw University of Technology (Advisor: Nguyen, N.T. in Polish) (2006)
8. Kiewra, M., Nguyen, N.T.: Non-textual Document Ranking Using Crawler Information and Web Usage Mining. In: Khosla, R., Howlett, R.J., Jain, L.C. (eds.) KES 2005. LNCS (LNAI), vol. 3682, pp. 520–526. Springer, Heidelberg (2005)
9. Lieberman, H.: Letizia: An Agent that Assists Web Browsing. In: Proc. of IJCAI'95, pp. 924–929. Morgan Kaufmann publishers Inc., San Mateo (1995)
10. Meadow, C.T.: Text Information retrieval Systems. Academic Press, Orlando (1992)
11. Mobasher, B., Dai, H., Luo, T., Sun, Y., Zhu, J.: Integrating Web Usage and Content Mining for More Effective Personalization. In: Proc. of 1st International Conference on Electronic Commerce and Web Technologies, pp. 165–176. Springer, London, UK (2000)
12. Montaner, M.: Collaborative Recommender Agents Based on Case-Based Reasoning and Trust. Ph.D. Thesis. Universitat de Girona (2003)
13. van Rijsbergen, C.J.: Information Retrieval. Dept. of Computer Science, University of Glasgow (1979)
14. Schafer, J.B., Konstan, J., Riedl, J.: Recommender Systems in E-Commerce. In: Proc. of ACM Conference on Electronic Commerce, pp. 156–158. ACM Press, New York (1999)
15. Voiskunskii, V.G.: Evaluation of search results: a new approach. Journal of the American Society for Information Science 48(2), 133–142 (1997)

Combinatorial Auction with Minimal Resource Requirements

Fu-Shiung Hsieh

Department of Computer Science and Information Engineering
Chaoyang University of Technology
41349 Taichung County, Taiwan, R.O.C.
apistech@ms14.hinet.net

Abstract. Although combinatorial auction has been studied extensively, it is difficult to apply the existing results to a problem with minimal resource requirements. In this paper, we consider a combinatorial auction problem in which an auctioneer wants to acquire resources from a set of bidders to process the tasks on hand. Each task requires a minimal set of resources for executing the operations. Each bidder owns a set of resources to bid for the tasks. The problem is to determine the resource assignment to minimize the total cost to perform the tasks. The main results include: (1) a problem formulation for combinatorial auction with minimal resource requirements; (2) a solution methodology based on Lagrangian relaxation; (3) an economic interpretation and a proposed structure for implementing our solution algorithms.

1 Introduction

Auctions are popular, distributed and autonomy preserving ways of allocating items or tasks among multiple agents to maximize revenue or minimize cost. An excellent survey on combinatorial auctions can be found in [3]. In a combinatorial auction [1], bidders may place bids on combinations of items or tasks. This allows the bidders to express complementarities between items instead of having to speculate into an item's valuation about the impact of possibly getting other, complementary items or tasks. The combinatorial auction problem can be modeled as a set packing problem (SPP), a well-known NP-complete problem [4]-[8]. Many algorithms have been developed for combinatorial auction problems. For example, in [2], the authors proposed a Lagrangian Heuristic for a combinatorial auction problem. Exact algorithms have been developed for the SPP problem, including a branch and bound search [8], iterative deepening A* search [7] and the direct application of available CPLEX IP solver [4]. However, in real world, a task may require a minimum number of resources for processing. In this case, it is difficult to apply the existing combinatorial auction algorithms to allocate the resources.

Motivated by the deficiency of the existing methods, we consider a combinatorial auction problem in which an auctioneer wants to acquire resources from a set of bidders to process the tasks on hand. Each task requires a minimal set of resources for executing the operations. Each bidder owns a set of identical resources to bid for the tasks. The problem is to determine the winners to minimize the total cost to perform

H.G. Okuno and M. Ali (Eds.): IEA/AIE 2007, LNAI 4570, pp. 1072–1077, 2007.

the tasks. The remainder of this paper is organized as follows. In Section 2, we present the problem formulation. In Section 3, we propose the solution algorithms. We give an economic interpretation for our solution approach in Section 4. Finally, we address our future research direction for this paper.

2 Combinatorial Auction with Minimal Resource Requirements

Suppose an auctioneer has a set $\boldsymbol{J}$ of tasks to be performed. Each task consists of a set of operations which rely on a minimum set of resources for processing. There are a set of potential bidders in the system. Each bidder holds a set of resources that can be used to process the operations of the tasks. Depending on the operations involved, the costs of using different resources for conducting the same operation vary. The problem is to distribute the tasks among a set of bidders such that the total cost is minimized. In this paper, we first formulate the above combinatorial optimization problem as an integer programming problem. We then develop solution algorithms based on Lagrangian relaxation.

Let $\boldsymbol{B}$ denote the set of bidder agents in the system. A bidder $b \in \boldsymbol{B}$ holds a set $\boldsymbol{R}_b$ of resources. The set of all resources is denoted by $\boldsymbol{R} = \bigcup_{b \in \boldsymbol{B}} \boldsymbol{R}_b$. Let A_j denote the set of operations in task $j \in \boldsymbol{J}$. The set of all operations is denoted by $A = \bigcup_{j \in \boldsymbol{J}} A_j$, where $A_i \neq A_k \ \forall i \neq k$. Let x_{ra} be the decision variables for allocating resource $r \in \boldsymbol{R}$ to process operation $a \in A$. The decisions variables x_{ra}, $r \in \boldsymbol{R}$, $a \in A$ must satisfy the following constraints $x_{ra} = \begin{cases} 1 \ if \ \ resource \ r \ is \ allocated \ to \ operation \ a \\ 0 \ otherwise \end{cases}$

$$\sum_{a \in \boldsymbol{A}} x_{ra} \leq 1, x_{ra} \in \{0,1\}.$$

Let w_{ra} denote the cost of applying resource r to process task a. For a given resource allocation x_{ra}, $r \in \boldsymbol{R}$, $a \in A$, the total cost is $\sum_{r \in \boldsymbol{R}} \sum_{a \in \boldsymbol{A}} w_{ra} x_{ra}$. To completely process a task, a minimum set of resources is required. Let ω_a denote the minimum number of resources required for operation $a \in A$. The following constraints must hold

$$\sum_{r \in \boldsymbol{R}} x_{ra} \geq \omega_a \ \forall a \in A.$$

The combinatorial auction with minimal resource requirements (CAMRR) optimization problem can be formulated as follows

$$\begin{aligned} &\min_{x_{ra}} f(x) = \sum_{r \in \boldsymbol{R}} \sum_{a \in \boldsymbol{A}} w_{ra} x_{ra} \\ &\text{s.t.} \sum_{r \in \boldsymbol{R}} x_{ra} \geq \omega_a \ \forall a \in A \\ &\sum_{a \in \boldsymbol{A}} x_{ra} \leq 1 \ \forall r \in \boldsymbol{R}, \\ &x_{ra} \in \{0,1\} \ \forall r \in \boldsymbol{R} \ a \in A. \end{aligned} \tag{2-1}$$

In the CAMRR problem, we observe that the coupling among different operations is caused by the contention for resources through the minimal resource requirement constraints (2-1). Applying Lagrangian relaxation to these coupling constraints, we form a Lagrangian function

$$
\begin{aligned}
L(\pi) &= \min_{x}\{[\sum_{r\in R}\sum_{a\in A} w_{ra}x_{ra}] - [\sum_{a\in A}\pi_a(\sum_{r\in R}x_{ra} - \varpi_a)]\} \\
&= \min_{x}\{[\sum_{r\in R}\sum_{a\in A} x_{ra}[w_{ra} - \pi_a]] + (\sum_{a\in A}\pi_a\varpi_a)\} \\
&= [\sum_{r\in R}\min_{x_{ra},a\in A}\sum_{a\in A} x_{ra}[w_{ra} - \pi_a]] + (\sum_{a\in A}\pi_a\varpi_a) \\
&= \sum_{r\in R} L_r(\pi) + (\sum_{a\in A}\pi_a\varpi_a), \textit{where}
\end{aligned}
$$

$$
L_r(\pi) =
$$

$$
\min_{x_{ra},a\in A}\sum_{a\in A} x_{ra}[w_{ra} - \pi_a]
$$

$$
s.t.\ \sum_{a\in A} x_{ra} \le 1, x_{ra} \in \{0,1\}
$$

For a given Lagrange multiplier π, the relaxation of constraints (2-1) decomposes the original problem into a number of resource assignment (RA) subproblems. These subproblems can be solved independently. That is, the Lagrangian relaxation results in subproblems with a highly decentralized decision making structure. Interactions among subproblems are reflected through Lanrange multipliers, which are determined by solving the following dual problem.

$$
\max_{\pi\ge 0} L(\pi)
$$

3 Solution Algorithms

Our methodology for finding a near optimal solution of the CAMRR problem is developed based on the result of Lagrangian relaxation and decomposition. It consists of three parts: (1) an algorithm for solving subproblems by exploiting their individual structures; (2) a subgradient method for solving the non-differentiable dual problem; (3)a heuristic algorithm for finding a near-optimal, feasible solution based on the solution of the relaxed problem. The structure of our algorithms is depicted in Fig. 1.

(1) An algorithm for solving subproblems

Given Lagrange multiplier π, the RA subproblem to be solved for resource r is as follows. $L_r(\pi) =$

$$
\min_{x_{ra},a\in A}\sum_{a\in A} x_{ra}[w_{ra} - \pi_a]
$$

$$
s.t.\ \sum_{a\in A} x_{ra} \le 1, x_{ra} \in \{0,1\}
$$

As $\sum_{a\in A} x_{ra} \le 1$ and $x_{ra} \in \{0,1\}$, the above RA subproblem can be solved by finding the a with the minimum $w_{ra} - \pi_a$ and setting x_{ra} =1and setting $x_{ra'} = 0$ for $a' \ne a$.

(2) A subgradient method for solving the dual problem

Let x^l be the optimal solution to the subproblems for given lagrange multipliers π^l of iteration l. We define the subgradient of $L(\pi)$ as

$$g_a^l = \left.\frac{\partial L(\pi)}{\partial \pi_a}\right|_{\pi_a^l} = -(\sum_{r \in R} x_{ra}^l - \varpi_a), \text{ where } a \in A.$$

The subgradient method proposed by Polak [9] is adopted to update π as follows

$$\pi_a^{l+1} = \begin{cases} \pi_a^l + \alpha^l g_a^l \ \textit{if} \ \pi_a^l + \alpha^l g_a^l \geq 0; \\ 0 \ \textit{otherwise.} \end{cases}$$

where $\alpha^l = c\frac{\overline{L} - L(\pi)}{\sum_a (g_a^l)^2}$, $0 \leq c \leq 2$ and $\overline{L}$ is an estimate of the optimal dual cost. The iteration step terminates if α^l is smaller than a threshold. Polyak proved that this method has a linear convergence rate.

Iterative application of the algorithms in (1) and (2) may converge to an optimal dual solution (x^*, π^*).

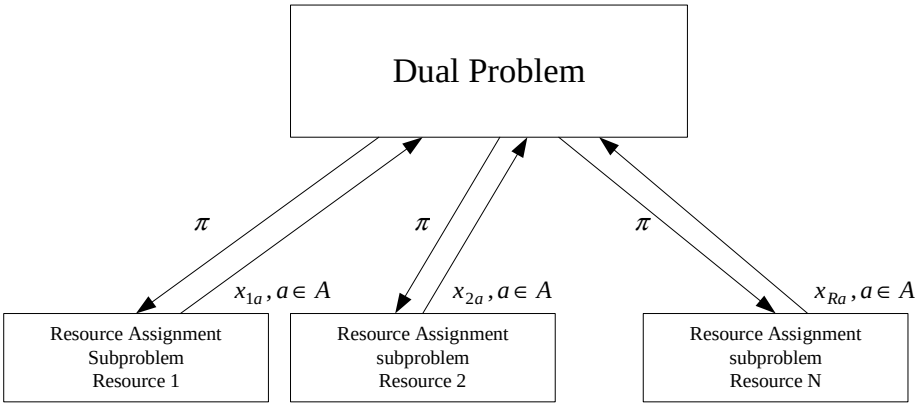

Fig. 1. Structure of solution algorithms

(3) A heuristic algorithm for finding a near-optimal, feasible solution based on the solution of the relaxed problem

The solution (x^*, π^*) may result in one type of constraint violation due to relaxation: assignment of resources less than the minimal resource requirements. Our heuristic scheme first checks all the operations that have been allocated with excessive resources. We then move these excessive resources to the operations without sufficient resources to fix the violation. If the violation cannot be completely resolved, all the

remaining operations without sufficient resources will be allocated the remaining available resources according to their cost.

$$\max_{\pi \geq 0} L(\pi)$$

4 Economic Interpretation

Decomposition of the original problem into RA subproblems provides us a different viewpoint of the original problem. Decision making of the original problem is composed of those of RA subproblems. RA subproblems can be regarded as the decision making problem to acquire the required resources and benefits from utilizing the acquired resources. The decision processes of each entity are just like the ones made by sellers in a real business environment. That is, a seller is willing to sell a good only when its utility is at least equal to its market price. The buyer will raise the market price in case of resource shortage. Such processes occur in the decision making of the RA subproblems. Lagrange multipliers can often be given the economic interpretation as marginal costs for using the resources when they are used to relax resource constraints. In our relaxation procedure above, the Lagrange multipliers π_a is used to relax the minimal resource constraints of an activity a. Lagrange multipliers π_a can be interpreted as the marginal benefit of using an additional unit of resources in activity a. If the constraint $\sum_{r \in \boldsymbol{R}} x_{ra} \geq \varpi_a$ is violated, that is, $\sum_{r \in \boldsymbol{R}} x_{ra} < \varpi_a$. In this case, adding an additional unit of resources in activity a reduces the total cost by π_a. On the other hand, if the constraint $\sum_{r \in \boldsymbol{R}} x_{ra} \geq \varpi_a$ holds. In this case, adding an additional unit of resources in activity a increases the total cost by π_a.

The effectiveness of the solution algorithms can be evaluated based on the duality gap, which is the difference between primal and dual objective values. That is, duality gap is defined by $f(x^*) - L(\pi^*)$.

Example: Consider a problem with $\boldsymbol{J} = \{1,2\}$, $A = \{1,2\}$, $A_1 = \{1\}$, $A_2 = \{2\}$, $\varpi_1 = 2$, $\varpi_2 = 2$, $\boldsymbol{R} = \boldsymbol{R}_1 \cup \boldsymbol{R}_2 = \{1,2,3,4,5,6\}$, where $\boldsymbol{R}_1 = \{1,2,3\}$ and $\boldsymbol{R}_2 = \{4,5,6\}$. Let $w_{11} = 1, w_{12} = 2,\ w_{21} = 2, w_{22} = 4,\ w_{31} = 3, w_{32} = 6,\ w_{41} = 2, w_{42} = 1,\ w_{51} = 4, w_{52} = 2,\ w_{61} = 6, w_{62} = 3$. For this example, our algorithms yield an optimal solution in which $x_{11}^* = 1, x_{21}^* = 1, x_{42}^* = 1, x_{52}^* = 1$. The duality gap for this example is less than 3%.

5 Future Research Direction

We formulate an optimization problem for combinatorial auction with minimal resource requirements on the tasks. The minimal resource requirements for tasks impose additional constraints on determination of the winners. By applying Lagrangian relaxation technique, the original optimization can be decomposed into a number of

resource assignment subproblems. Our methodology consists of three parts: (1) an algorithm for solving subproblems by exploiting their individual structures; (2) a subgradient method for solving the non-differentiable dual problem; (3) a heuristic algorithm for finding a near-optimal, feasible solution. Numerical results indicate that our proposed algorithms yield near optimal solutions for small problems. Our future research direction is to study the optimality of the near optimal solutions obtained from our algorithms for large problems.

Acknowledgement

This paper was supported in part by the National Science Council of Taiwan, R.O.C. under Grant NSC95-2416-H-324-009-MY2.

References

[1] de Vries, S., Vohra, R.V.: Combinatorial Auctions:A Survey. INFORMS Journal on Computing 3, 284–309 (2003)
[2] Guo, Y., Lim, A., Rodrigues, B., Tang, J.: Using a Lagrangian heuristic for a combinatorial auction proble. In: Proceedings of the 17th IEEE International Conference on Tools with Artificial Intelligence (2005)
[3] de Vries, S., Vohra, R.V.: Combinatorial Auctions: A Survey. INFORMS Journal on Computing 15(3), 284–309 (2003)
[4] Andersson, A., Tenhunen, M., Ygge, F.: Integer programming for combinatorial auction winner determination. In: Proceedings of the Seventeenth National Conference on Artificial Intelligence, pp. 39–46 (2000)
[5] Fujishima, Y., Leyton-Brown, K., Shoham, Y.: Taming the computational complexity of combinatorial auctions:Optimal and approximate approaches. In: Sixteenth International Joint Conference on Artificial Intelligence, pp. 548–553 (1999)
[6] Hoos, H.H., Boutilier, C.: Solving combinatorial auctions using stochastic local search. In: Proceedings of the Seventeenth National Conference on Artificial Intelligence, pp. 22–29 (2000)
[7] Sandholm, T.: Algorithm for optimal winner determination in combinatorial auctions. Artificial Intelligence 135(1-2), 1–54 (2002)
[8] Sandholm, T., Suri, S., Gilpin, A., Levine, D.: CABOB: A fast optimal algorithm for combinatorial auctions. In: IJCAI, pp. 1102–1108 (2001)
[9] Polyak, B.T.: Minimization of Unsmooth Functionals. USSR Computational Math. and Math. Physics 9, 14–29 (1969)

Effectiveness of Autonomous Network Monitoring Based on Intelligent-Agent-Mediated Status Information

Susumu Konno, Sameer Abar, Yukio Iwaya, and Tetsuo Kinoshita

Tohoku University, 2–1–1 Katahira, Aoba-ku, Sendai, Miyagi, 980–8577, Japan
skonno@isc.tohoku.ac.jp
http://www.ka.riec.tohoku.ac.jp/ka/menber.index.en.html

Abstract. The growing complexity of communication networks and their associated information overhead have made network management considerably difficult. This paper presents a novel Network Management Scheme based on the novel concept of Active Information Resources (AIRs). Many types of information are distributed in the complex network, and they are changed dynamically. Under the AIR scheme, each piece of information in a network is activated as an intelligent agent: an I-AIR. An I-AIR has knowledge and functionality related to its information. The I-AIRs autonomously detect run-time operational obstacles occurring in the network system and specify the failures' causes to the network administrator with their cooperation. Thereby, some network management tasks are supported. The proposed prototype system (AIR-NMS) was implemented. Experimental results indicate that it markedly reduces the network administrator workload, compared to conventional network management methods.

1 Introduction

In recent years, computer communication networks have grown dramatically both in size and complexity. Moreover, they comprise heterogeneous multi-vendor environments. Traditionally, network management activities have been performed by network managers. However, these activities are becoming more demanding and data-intensive because of the rapid growth of modern networks. For those reasons, automation of network management activities has become necessary. For managing these huge distributed network systems, manual procedures have become tedious.

A typical approach to network management is centralized, static, polling-based management that involves high-capacity computing resources at the centralized platform including commercially available management tools. As managed components become more numerous, the amount of network traffic, which should be managed, have increased accordingly. Consequently, in centralized management systems, the management traffic might eventually oppress the network bandwidth. Even where the management platform uses several distributed

H.G. Okuno and M. Ali (Eds.): IEA/AIE 2007, LNAI 4570, pp. 1078–1087, 2007.

management stations, the huge bulk of management traffic remains concentrated around those stations [1]. The overwhelming volume and complexity of the information involved in network management imparts a terrible load [2].

Furthermore, in view of the dynamic nature of evolving networks, future network management solutions need to be flexible, adaptable, and intelligent without increasing the burden on network resources. The rapid of network systems has posed the issues of flexibility, scalability, and interoperability for the centralized paradigm. Even though failures in large communication networks are unavoidable, quick detection and identification of the causes of failure can fortify these systems, making them more robust, with more reliable operations, thereby ultimately increasing the level of confidence in the services they provide [3]. Motivated by these considerations, the proposed approach is intended to provide an intelligent, adaptive and autonomous network monitoring support paradigm for communication network systems.

A network monitoring support method based on the activated information is proposed in this paper. In this method, the distributed information in a computer network is activated using the concept of Active Information Resource (AIR). In the AIR scheme, each unit of distributed information has knowledge and functionalities related to utilization of the information resource as well as its information. In our experiment network system, each activated information AIR (I–AIR) is developed as an intelligent agent. The proposed framework simplifies network monitoring for the administrator. Experiments were performed to investigate the effectiveness of the proposed method.

The remainder of the paper is organized as follows. Section 2 presents an overview of the AIR concept and conversion of the dynamic status information as I-AIRs. The detailed design and implementation considerations of I-AIRs in the proposed prototype system are discussed in Section 3. Experimental results, along with the system's performance evaluations are outlined in Section 4. Finally, the conclusions and future issues are presented in Section 5.

2 Automated Network Monitoring Based on Activated Information

For monitoring of communication network by an administrator, much status information distributed in a network is required, such as network traffic, conditions of service processes, and application server logs. Commonly, the information is static; furthermore, an administrator must investigate them one by one, which places a necessary physical and mental load on the administrator.

In this study, therefore, this static information is activated to reduce the administrator's workload. For activation of status information, a concept of an active information resource (AIR) [4] [5] [6] is employed. Each unit of status information is wrapped as an AIR for activation; it is called I-AIR. An I-AIR has its original information resources along with related knowledge and functionalities. Several I-AIRs can cooperate autonomously based on their status information and knowledge. Consequently, our scheme can reduce network management loads

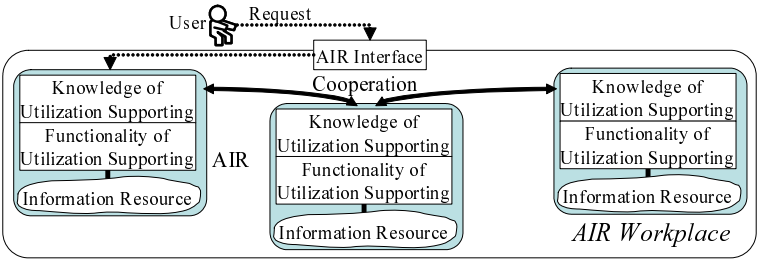

Fig. 1. Active Information Resource

by presenting the dynamic status information of the network resources during automatic detection and specification of network failures.

2.1 AIR Concept

An AIR is defined as the distributed information resource enhanced with its knowledge as well as functionality to facilitate its resources. Figure 1 shows a conceptual model of an AIR with its support knowledge and functionality. The knowledge of an AIR typically consists of metadata of the information contents and their processing descriptions. The functionality of AIR is about how to analyze and process the users' query as well as defining the cooperation strategy among the multiple AIRs.

An AIR can be implemented using the multi-agent-based approach. Agent-based computing is known as a complementary way to manage the resources of distributed systems because of the increased flexibility in adapting to the dynamically changing requirements of such systems [7].

Essential features of AIRs include:

- To extract and process the information contents in response to the query from user (or another AIR) in a knowledge-based manner.
- To interact actively and mutually to make full use of the information contents, the embedded support knowledge, and functionality.

The effectiveness of AIR has been employed in the context of diverse web-based information retrieval techniques. The prototype systems have exhibited very promising results.

2.2 Applying the AIR Concept to Network Monitoring

Generally, the status information of the communication network is classifiable into two types: static information and dynamic information. For example, the relationship between IP addresses and Mac addresses, host names, domain names, IP-routing, etc., are included as static network information. On the other hand,

the dynamic information includes number of packet traffic, RMON-MIB, SNMPv2-MIB, logs of network services, etc. To apply the concept of AIR to both types of information for network monitoring, each unit of information is converted to an AIR to form a so-called I-AIR.

Conventionally, an administrator collects various status information through periodical polling. She aggregates the data and decides the status of the network system using her know-how. This task can be disaggregated into three stages, such as detection, recognition, and specification of the failure. This task requires much experience as a network manager; therefore, a beginner cannot be employed as an administrator.

To support the empirical task of the administrator, an I-AIR includes diverse knowledge and functionality in addition to its original data. For example:

- meta-knowledge about information resources
- knowledge about failure condition (threshold)
- knowledge about cooperation with another I-AIR
- functionality to handle original data

Using this additional knowledge and functionality, I-AIRs can mutually cooperate. The following tasks can be partially supported by AIR:

- distributed and effective monitoring of network system
- detection of network failure using a threshold
- processing of information resources according to the failure with its functionality
- improvement of reliability of detection, recognition, and specification of the failure through cooperation among AIRs

These features can reduce the overall workload of the administrator.

3 Design and Implementation of I-AIR

In this section, the design of an I-AIR is discussed. The design comprises three vital ingredients: internal support knowledge, functionality for sharing the information contents, and specifications of the information resource itself.

3.1 Design of Knowledge in I-AIR

The support knowledge for sharing information contents is the empirical knowledge of network management which inspects the status information of the network for occurring faults. Essential components of this knowledge are as follows:

- I-AIR Identification Knowledge (ID):
  The ID includes an identification number, task number of I-AIR, etc.
- Knowledge about Information Resource (IR):
  The IR includes a type, an update-time, a format type, etc.

- Knowledge about Failure Inspection (FI)
  The FI includes two types of knowledge to inspect the failure: text information to be detected in logs, and a threshold of packets, etc.
- Knowledge about Network Periodic Investigation - Control Method (CM):
  The CM includes the polling time and other conditions for updating of the information resource.
- Knowledge about Cooperation Protocol (CP):
  The CP includes protocol sequences for cooperation with other AIRs.

The knowledge contained in an I-AIR as ID, IR, and CP is required mainly in order to operate on the information resource and facilitate communication and cooperation among the I-AIRs. The preeminent characteristic of I-AIR is its autonomous monitoring mechanism, which is supported via FI and CM for the inspection and investigation of the obstacles that hinder the normal network operation. Thus, the performance of I-AIRs in the proposed technique relies heavily on the design of various types of internal support knowledge.

3.2 Design of Functionality of I–AIR

I-AIRs' functionality deals with the sharing and processing of the information resource for cooperative problem solving during the active fault monitoring and detection phases. In this regard, the design of some essential features is crucial as follows:

- Functionality as an Interface to I-AIR internal support knowledge
- Functionality for processing the information resource
- Functionality for transmitting the processed results to other I-AIRs
- Functionality for inspecting the obstacle with respect to the pre-defined threshold

3.3 Design of Information Resource

Two I-AIR information resource types are described here.

- Simple text format
- RDF/XML syntax specification

The RDF/XML language is a W3C-recommended framework for describing information resources using machine-readable metadata, which brings about an unprecedented level of automation for the representation and retrieval of information. The plain-text format consists of log-information that is acquired through the syslog (a standard logging solution on Unix and Linux systems). In the proposed approach, the I-AIR functionality extracts a diverse type of log-information during operational management scenarios and converts it to RDF/XML format specifications.

Table 1. Examples of implemented I-AIRs for network monitoring

I-AIR No.	Function	I-AIR No.	Function
1	Network Disconnection detector	11	DNS server process checker
2	NIC config failure detector	12	SMTP server process checker
3	SPAM mail detector	13	POP server process checker
4	MSBlaster attack detector	14	DNS connection checker
5	Mail send/receive error detector	15	Network route to host checker
6	TCP/IP stack failure checker	16	Kernel information checker
7	NIC config failure checker	17	Lease IP address checker
8	HUB failure checker	18	Mail server error checker
9	Ruter failure checker	19	Number of SPAM mail
10	Communication failure checker		

3.4 Implementation of I-AIR

A multi-agent-based approach was adopted for implementation of I-AIRs in the proposed technique. For the effective realization of I-AIR support knowledge and functionality, the multi-agent system is a highly pragmatic choice. The I-AIRs realized with the software agents render the I-AIRs active, which, after being invoked by an outside event, can autonomously perform the task of cooperative problem-solving. The proposed system architecture is supported by an Agent-based Distributed Information Processing System (ADIPS) framework [8], which is a flexible computing environment for designing multi-agent systems. Table 1 illustrates the I-AIRs developed in this study.

4 Evaluate the Effectiveness of I-AIR in Actual Monitoring Task

To evaluate the prototype system's effectiveness, an experimental NMS system, called AIR-NMS, was set up in the laboratory. The network administrator per-

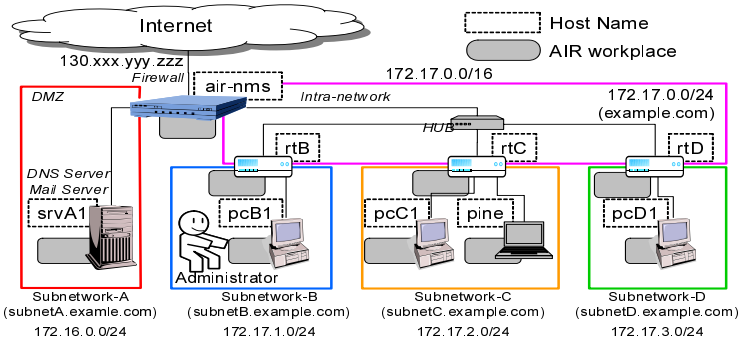

Fig. 2. Construction of Network Systems and AIR-NMS

forms the management task according to the conventional manual method, as well as with the I-AIRs based proposed system. He also measures the performance of the proposed approach adopted for the automation of network functions. In the experiment, the time and the number of procedures executed to correct the obstacle were measured after a network obstacle was reported to a subject.

4.1 Experimental Network

Figure 2 demonstrates the practical setup of the environment for experimenting with the I-AIRs. The network system comprises a 100BASE-TX Ethernet with a firewall configured as a Network Address Translation (NAT) firewall, a router, and various personal computers (PCs) arranged in four subnetworks. Subnetwork A is configured as a DeMilitarized Zone range 172.16.0.0/24. The server (sevA1) DNS and Mail application settings are configured. The other three subnetworks (B, C, D) have IP-addresses in the order given as 172.17.1.0/24, 172.17.2.0/24, and 172.17.3.0/24. Moreover, the network management console for managing the whole setup resides in pcB1 of subnetwork B. In subnetwork C, there is a desktop-type PC system (pcC1) with a fixed IP address from the DNS server, and a notebook computer (pine) which acquires the IP-addresses through the DHCP. In addition, Fig. 2 depicts the nodes (PCs, routers, firewall etc.) of the experimental network system. Each node shows the corresponding AIR workplace where the I-AIRs operate actively. For each node, about 15 AIRs were implemented. This implies that nearly 140 I-AIRs were incorporated within the experimental setup. A Linux operating system was used in each PC.

4.2 Experiment I: Various Application Scenarios

In this experimentation technique, several obstacle circumstances are generated and then inspected with and without I-AIR based system. These obstacles might occur by various causes. The task of a subject is to determine only one cause of a failure.

1. Cannot Connect to the Specific Host: In this case, file-transfer from pcD1 to pcB1 is not possible. A rare cause has been presumed, that is, a problem with the settings of Network Interface Card (NIC) of the host computer (pcB1).
2. Transmission of Spam Mail: In this case, a spam mail is transmitted from pcD1. However, the originating location of spam is concealed, so it is required to detect accurately the host that sends out the illicit message.
3. Slow Network: This delinquency is reported in the case of accessing World Wide Web (WWW) connection. The notebook PC (pine) was infected through an attack (from MSBlaster from outside source) at the port 135, thereby hindering its access to the Internet.
4. Mail Sending/Receiving Error: Here, the client network encounters the problem in sending/receiving email because the reason that the SMTP server process is down.

Table 2. Experimental results (Exp.1)

1. Cannot Connect to the Specific Host

	A		B		C		D		E		Average	
	Time	Step	Time	Step	Time	Step	Time	Step	Time	Step	Time	Step
no I-AIR	1056	20	756	20	680	22	771	20	282	40	709.0	24.4
I-AIR	99	5	51	2	125	4	226	5	52	2	110.6	3.6
$\frac{\text{I-AIR}}{\text{no I-AIR}}$(%)	9.4	25.0	6.7	10.0	18.4	18.2	29.3	25.0	18.4	5.0	15.6	14.8

2. Transmission of SPAM Mail

	A		B		C		D		E		Average	
	Time	Step	Time	Step	Time	Step	Time	Step	Time	Step	Time	Step
no I-AIR	1096	24	221	4	901	23	1155	26	92	5	693.0	16.4
I-AIR	49	3	93	3	83	4	129	2	40	2	78.8	2.8
$\frac{\text{I-AIR}}{\text{no I-AIR}}$(%)	4.5	12.5	42.1	75.0	9.2	17.4	11.2	7.7	43.5	40.0	11.4	17.1

3. Slow Network

	A		B		C		D		E		Average	
	Time	Step	Time	Step	Time	Step	Time	Step	Time	Step	Time	Step
no I-AIR	208	3	205	3	330	9	323	3	682	35	349.6	10.6
I-AIR	528	4	53	1	61	1	63	1	94	1	159.8	1.6
$\frac{\text{I-AIR}}{\text{no I-AIR}}$(%)	253.8	133.3	25.9	33.3	18.5	11.1	19.5	33.3	13.8	2.6	45.7	15.1

4. Mail Sending / Receiving Error

	A		B		C		D		E		Average	
	Time	Step	Time	Step	Time	Step	Time	Step	Time	Step	Time	Step
no I-AIR	996	31	369	16	680	22	565	7	1499	49	821.8	25.0
I-AIR	98	4	59	2	125	4	81	2	73	2	87.2	2.8
$\frac{\text{I-AIR}}{\text{no I-AIR}}$(%)	9.8	12.9	16.0	12.5	18.4	18.2	14.3	28.6	4.9	4.1	10.6	11.2

Management experience: A. 1 year, B. 2 year, C. 2 year, D. 3 year, E. 7 year

Results. The experimental results were compiled into Table 2. The results show that, for each failure situation, with the inclusion of I-AIRs, the management load related to the time taken to resolve a certain fault as well as the number of steps necessary to locate the cause of failure was reduced to an average 20%.

4.3 Experiment II: One Obstacle from Various Causes

An application scenario is tested against various causes for the occurrence of a specific failure condition to demonstrate the flexibility of the proposed approach using I-AIRs. Furthermore, these causes do not occur necessarily in any fixed pattern. The checks to detect these causes are performed randomly. However, using I-AIRs is advantageous because every check is done only once during the course of the fault-localizing process. The failure cause is detected and the main cause behind the failure is reported to the network operator actively.

Table 3. Assumed failure causes: Mail Sending/Receiving Error (Exp.2)

Problem	causes
Cable problem	a. Cable was disconnected.
Port problem	b. The 25th port was closed.
	c. The 110th port was closed.
DNS Server problem	d. DNS Server process was downed.
	e. Config was not available.
Mail Server problem	f. Mail Server process was down.

Table 4. Experimental results among individual administrators (Exp.2)

	F			G			H			I			J		
		Time	Step		Time	Step		Time	Step		Time	Step		Time	Step
no I-AIR	d	158	9	b	566	8	e	929	23	f	235	5	a	655	19
	e	743	24	d	871	12	b	339	9	c	615	9	f	182	5
I-AIR	a	51	1	f	104	2	c	82	3	a	40	1	b	86	2
	f	85	4	c	106	2	d	52	3	e	74	2	e	128	6
$\frac{\text{I-AIR}}{\text{no I-AIR}}$(%)		151.1	15.2		14.6	20.0		10.6	18.8		13.4	21.4		25.6	33.3

Management experience: F. 2 year, G. 2 year, H. 3 year, I. 3 year, J. 7 year

Table 5. Experimental results among individual failures (Exp.2)

	a		b		c		d		e		f	
	Time	Step	Time	Step	Time	Step	Time	Step	Time	Step	Time	Step
no I-AIR	655	19	566	8	615	9	158	9	743	24	235	5
	–	–	339	9	–	–	871	12	929	23	182	5
I-AIR	51	1	86	2	106	2	52	3	74	2	85	4
	40	1	–	–	82	3	–	–	128	6	104	2
$\frac{\text{I-AIR}}{\text{non I-AIR}}$(%)	6.9	5.3	19.0	23.5	15.3	27.8	10.1	28.6	12.1	17.0	45.3	60.0

Table 3 depicts the failure situation "Mail Sending/Receiving Error" with some possible causes underlying the occurrence of this anomaly. The task of the subject is to determine the cause of this error.

Results. Experimental results computed by each manager while resolving the mail sending/receiving anomaly were compiled into Table 4. Additionally, the results corresponding to each failure cause were accumulated into Table 5. The results demonstrate that the network management overhead regarding the time taken to resolve a certain fault, along with the number of steps necessary to locate the cause of failure, were reduced to 20% on average, which concurs exactly with the results of Experiment 1.

5 Summary

This paper presented a novel technique for the automation of management tasks for communication network systems. The foundation of the proposed framework is the use of I-AIRs, which, through active mutual interaction and with the functional network system, can resolve various network-failure situations. A part of the I-AIR knowledge is modified dynamically and frequently according to the operational characteristics of the network. Moreover, experimental results demonstrated a marked reduction in the administrator workload through the use of the proposed automated network monitoring and fault detection functions.

Acknowledgement. The authors thank Mr. Satoshi YOSHIMURA for his contribution to this study.

References

1. Stephan, R., Ray, P., Paramesh, N.: Network management platform based on mobile agent. International Journal of Network Management 14, 59–73 (2003)
2. Consens, M., Hasan, M.: Supporting network management through declaratively specified data visualizations. In: IEEE/IFIP 3rd International Symposium on Integrated Network Management, pp. 725–738 (1993)
3. Bouloutas, A.T., Calo, S., Finkel, A.: Alarm correlation and fault identification in communication networks. IEEE Transactions on Communications 42(2,3,4), 523–533 (1994)
4. Kinoshita, T.: A method for utilizing distributed information resources effectively: Design of active information resource (in japanese). In: Technical Report of IEICE (Japan) AI99-54, 13–19 (1999)
5. Li, B., Abe, T., Sugawara, K., Kinoshita, T.: Active information resource: Design concept and example. In: The 17th International Conference on Advanced Information Networking and Applications, pp. 274–277 (2003)
6. Li, B., Abe, T., Kinoshita, T.: Design of agent-based active information resource. In: The 1st International Conference on Agent-Based Technologies and Systems, pp. 233–244 (2003)
7. Papavassiliou, S., Puliafito, A., Tomarchio, O., Ye, J.: Mobile agent-based approach for efficient network management and resource allocation: Framework and applications. IEEE Journal on Selected Areas in Communication 20(4), 858–872 (2002)
8. Fujita, S., Hara, H., Sugawara, K., Kinoshita, T., Shiratori, N.: Agent-based design model of adaptive distributed systems. Journal of Applied Intelligence 9(1), 57–70 (1998)

Design and Implementation of Interactive Design Environment of Agent System

Takahiro Uchiya[1], Takahide Maemura[2], Xiaolu Li[2], and Tetsuo Kinoshita[3]

[1] Research Institute of Electrical Communication, Tohoku University
[2] Graduate School of Information Science, Tohoku University
[3] Information Synergy Center, Tohoku University
2-1-1 Katahira, Aoba-ku, Sendai, 980-8577 Japan
uchiya@riec.tohoku.ac.jp, maemura@ka.riec.tohoku.ac.jp,
littledeer@ka.riec.tohoku.ac.jp, kino@riec.tohoku.ac.jp

Abstract. The agent-based systems have been designed and developed using the latest agent technologies. However, the design and the debugging of these systems contain some difficult problems due to the situational and nondeterministic nature of the agents, and the effective design-supporting technologies have not been proposed so far. In order to make efficient design process of agent system, we propose an interactive development method of agent system based on the agent-repository-based multiagent framework which focuses on an essential feature of agent system design, i.e., the reuse of existing agents stored in the agent repository. In this paper, we propose an Interactive Design Environment of Agent system called IDEA and demonstrate the effectiveness of the proposed method.

Keywords: agent design method, repository-based agent framework.

1 Introduction

Agent technology is one of the primary technologies for the next-generation information processing system. Generally speaking, software with new characteristics such as autonomy and sociality is called an agent and a knowledge information system which uses agents as its components is called an agent system. Many kinds of agent systems have been designed and developed using latest agent technologies. However, the design and debugging of agent systems contains some difficult problem due to not only the situational and nondeterministic nature of the agents, but also the lack of effective design-supporting technologies.

So far, we have proposed an agent-repository-based agent framework [1, 2], which accumulates the developed agent systems in the agent-repository and enables dynamic organization and reorganization of agent systems by using agent-repository. Using this framework, we designed and developed various agent systems in our previous work [3, 4, 5, 6]. Hereafter, we simply call the agent-repository as the repository. In this paper, in order to provide an efficient and systematic design process of agent system for agent system designers, we propose a new method for developing agent systems in an interactive way, based on the repository-based agent framework. This

H.G. Okuno and M. Ali (Eds.): IEA/AIE 2007, LNAI 4570, pp. 1088–1097, 2007.

method focuses on the important features of agent system development such as the reuse of existing agent system and the cooperation between designers and agent systems. Moreover, an Interactive Development Environment of Agent system called IDEA is proposed and implemented to show the effectiveness of the proposed method.

2 Problems in Agent System Development

2.1 Problems in Agent Design

An agent system is composed of various agents that perform the required information processing. In the design of agent system, the design targets should be the agents equipped with various functions and the organization of agents that deal with the problem solving. In a design of an agent of the target agent system, several types of agents can be considered. For example, the following four types of agents can be introduced, i.e., (a) Basic type, (b) Reactive type, (c) Deliberative type, and (d) Composite type, on the basis of the structure and functions of the agent.

A designer determines an agent type and implements the functions and knowledge of an agent based on the requirements and usage of the target agent in the design process. Here, we can find a problem such that (P1) the volume of descriptions of the target agent increases according to the volume of functions and knowledge required for both the problem solving and the behavioral control of the agent.

On the other hand, from the point of view of the design method of agent, there are two kinds of approaches, i.e., (i) Programming Approach and (ii) Framework Approach.

(i) Programming Approach
An agent is designed and implemented in a top-down way, by using the existing programming languages such as Java. Since the flexibility of design can be kept in the design process, the agents such as basic type and reactive type can easily be implemented. However, in case of deliberative type and composite type agents, the burden of designer increases due to the design and implementation of knowledge processing mechanisms embedded in all of the agents.

(ii) Framework Approach
Since this approach provides an agent design support environment based on the specific agent architecture for the designers, the design and implementation of the agents can be done systematically and efficiently. Such an environment is called a framework that provides the facilities such as the knowledge representation scheme, the problem solving function and the agent communication function. In recent years, a lot of frameworks such as ADIPS/DASH [1, 2], JADE [7], AgentBuilder [8], JATLite [9], ZEUS [10] and JACK [14] had been proposed and implemented. These frameworks provide many functions for designing and implementing various agents to designers, where we will encounter the second problem, i.e., (P2) the designers need to learn a lot of know-how about specific agent framework.

2.2 Problems in Agent System Design

Development of an agent system that consists of many agents can be done by two types of design, i.e., top-down design and bottom-up design.

(1) Top-down design
A top-down design process consists of the following stages, i.e., problem definition, requirements definition, design, implementation, test and verification, as same as the conventional software system. To realize the target agent system, a lot of design processes of both the agents and the organization of agents have to be carried out sequentially or concurrently. To fulfill top-down design, the design methods/tools such as ZEUS [10], MaSE [11], Tropos [12], GAIA [13] and JACK [14], have been proposed. Using these methods, the designers can promote the consistent design of an agent system as well as its component agents systematically; therefore, the unexpected result such as the competitive situations among agents may easily be detected and removed at the design phase. However, it become difficult to deal with the changes of the architecture and functions of the whole system after the development has been finished.

(2) Bottom-up design
In the bottom-up design, it is assumed that the required agents can be selected from a set of the existing agents and assigned them as the components of the target agent system, without the design and implementation of new agents. It is difficult to find out all needed agents for the target system. However, the designers can concentrate on the design of new agents that realize the required new functions, if some of the existing agents could be reused as a part of the target agent system according to the given requirements. Moreover, in the bottom-up design, the function of autonomous and dynamic organization based on the existing agents can be expected at the runtime. Although the new functions are required to support the designers, the bottom-up design is useful method for the agent system development. But useful design-supporting tools have not been provided for the designers.

Although the design and implementation of an agent system can be done in the top-down or bottom-up manner, as one of the existing problem in both methods that (P3) it is hard to test and debug the target agent system due to the non-deterministic and situation-dependent nature of the multiagent organization. The generate-and-test cycle in an explorative design process of agent system should be supported effectively.

As mentioned above, there are three problems in order to overcome the difficulties of design and implementation both for the agent and the agent system. Therefore, in this paper, we focus on the bottom-up design based on the framework approach, an interactive development method is proposed and a prototype of design-supporting environment is also demonstrated to show the effectiveness of the proposed method.

3 Concept of Interactive Development of Agent System

3.1 Overview of Interactive Development Method

In this section, we propose an interactive development method of agent system. At first, we explain the fundamental idea of the proposed method.

- **Reuse of existing agents:** To support a bottom-up design process, the agents and the agent systems that have already been designed and utilized as applications, are stored and managed to reuse them in the design process for new agent system. For instance, the repository of the repository-based agent framework explained in section 3.2 can be utilized as one of the essential mechanisms.

- **Interaction between designer and agent system:** To support the generation-and-test cycle in the bottom-up design process, some supporting functions are provided for the designers. For instance, an interactive simulation of agents' behavior over a virtual distributed environment may be useful for the test and debugging of agents.

3.2 Repository-Based Agent Framework

The repository-based agent framework ADIPS/DASH [1, 2], as shown in Fig.1, has a mechanism called the repository that is responsible to manage and control the lifecycle of agents in ADIPS/DASH framework. The agents developed by designers are accumulated in the repository in order to generate at runtime and construct the organization at runtime according to the requests given by users or other agents. The repository of ADIPS/DASH framework is one of unique mechanisms compare with other framework mentioned in section 2.1.

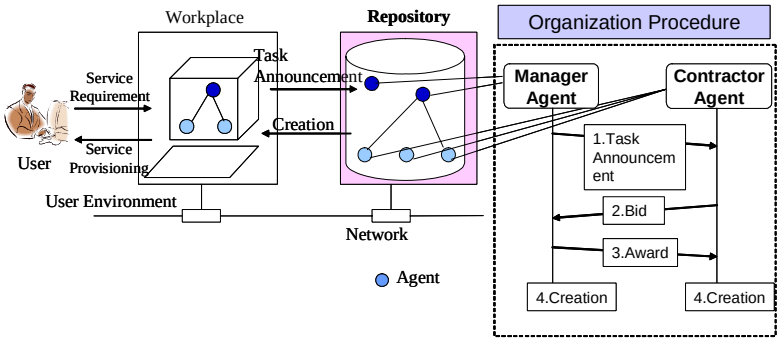

Fig. 1. Repository-based agent framework

3.3 Interactive Design Process of Agent System

Let's explain an interactive design process of agent system. In the following design stages, we focus on the design and implementation stage on a basis of the bottom-up design.

A. Problem Definition
A problem is defined in this stage, for instance, by using a design specification language and natural language.

B. Requirements Definition
The requests from users are defined and described as the requirement specifications of the target agent system. For instance, a state transition diagram or an agent knowledge

description language of ADIPS/DASH framework can be used to represent the specifications. Some simple examples of requirement are shown as below.

Example1:
(task :name XYZ :attribute1 value1 :attribute2 value2 ...)

Example2:
(task :name www-browser :window-system X11
:width ?width :height ?height :color ?color
:input url :output (graphic-image text-image audio) ...)

Example3:
(task :name TownGuide :city Sendai :country Japan ...)

C. Design and implementation
An agent system is designed and implemented based on the following secondary processes.

C-1. Trying to reuse the existing agent system
A designer sends a requirement of the necessary function to the repository to reuse the existing agents and agent system. According to the requirement, each agent in the repository examines whether the given specification is fulfilled or not by itself. As a result, the designer receives the responses from the agents in the repository and selects a suitable agent to be used in the design.

C-2. Programming of agent knowledge and function
Using an agent knowledge representation language of ADIPS/DASH framework, a designer describes the behavioral knowledge as a set of rules (it is called an agent program in ADIPS/DASH framework). Some parts of functions will be designed and implemented by using the conventional programming language. These are combined with the agents by using the wrapping mechanism of ADIPS/DASH agent. To make the agent programming process simply, a knowledge template such as the extended contract net protocol of ADIPS/DASH agent, are provided for the designers.

C-3. Interactive simulation
As mentioned in section 3.1, an interactive simulation function of agents' behavior is provided for a designer to support the generate-and-test cycle in the bottom-up design process. Using a virtual distributed environment defined by the designer, the designer can generate the agents from the repository and observe their behaviors. The behavioral simulation of an organization of agents can also be done, and the same as a single agent. Moreover, a function to exchange messages between designer and agents is provided to test the agent behavior at development phase. Using this function, for instance, the designer can run a part of an agent, which is under development, to simulate its cooperation behavior in the virtual distributed environment. Through the interactive simulation, the designers can detect and modify the deficits of knowledge and functions of agents quickly by returning to the stage C-2.

C-4. Registration of agent system to the repository
The results of design for the target agent systems can be stored in the repository at any stage of the design process, in order to support a step-wise refinement in the agent system development.

D. Test and Verification
The functions of the target agent system should be verified in the real environment.

4 Design and Implementation of IDEA

According to the proposed method explained in the chapter 3, we design and implement a prototype of the Interactive Design Environment of Agent system called IDEA. In order to support the design stage C explained in chapter 3, the following four functions are introduced in the IDEA, as shown in Fig.2.

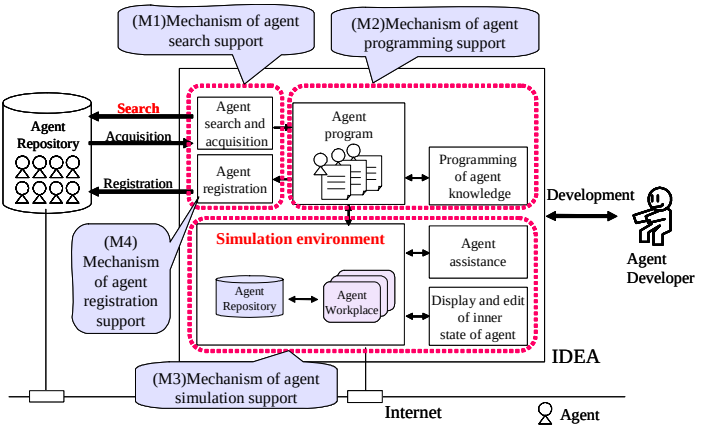

Fig. 2. Construction of the IDEA

(M1) Mechanism of agent search support
Fig.3 shows an interface of the agent search phase. There are main three parts, that is, the search condition input field for searching the agents from the repository, the search result display tab and the preview window of the agent knowledge.

In the search condition input filed, a designer inputs the requirement specification of a candidate agent, such as an agent name and a function name. When a candidate agent detected in the repository sends a message as its response, the received message is displayed in the search result display tab. Then, the designer can take an agent into the developer's environment by choosing the agent from this tab.

(M2) Mechanism of agent programming support
Fig.4 shows a mechanism for agent programming support. This mechanism has an agent-programming editor based on the rule-based knowledge representation of ADIPS/DASH framework. Using this editor, the designer can describe and test the agent programs.

(M3) Mechanism of agent simulation support
Fig.5 shows an agent monitor for observing the behavior of the agents and the agent organization. The agent inspector shows the inner states of an agent. Using these tools, the designer can browse and modify the agent behavioral knowledge during the

interactive simulation. Moreover, an ACL editor supports the interactive communication between the designer and the agents under development by the ACL message of ADIPS/DASH framework.

(M4) Mechanism of agent registration support
This mechanism offers an interface to store the completed agent system to the repository.

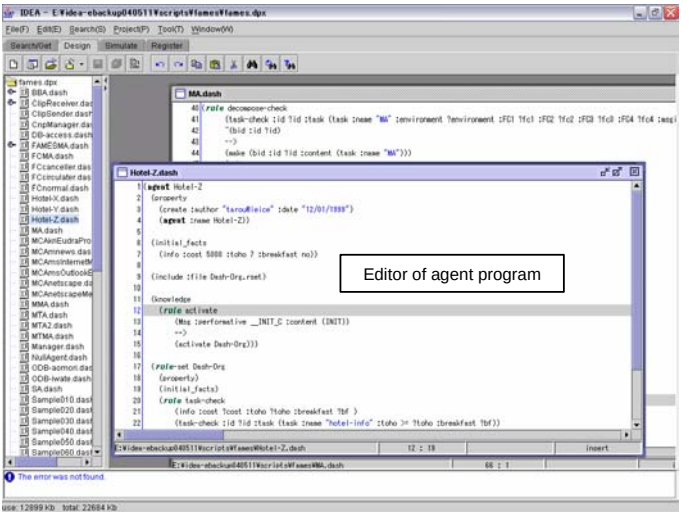

Fig. 3. Supporting function of agent search phase

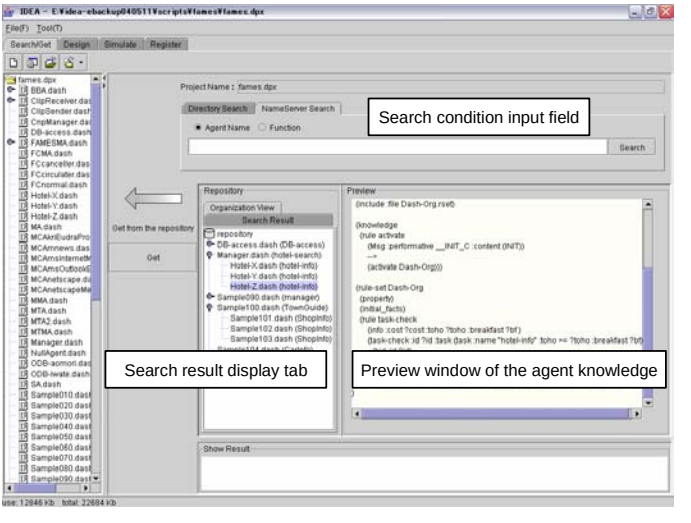

Fig. 4. Supporting function of agent programming phase

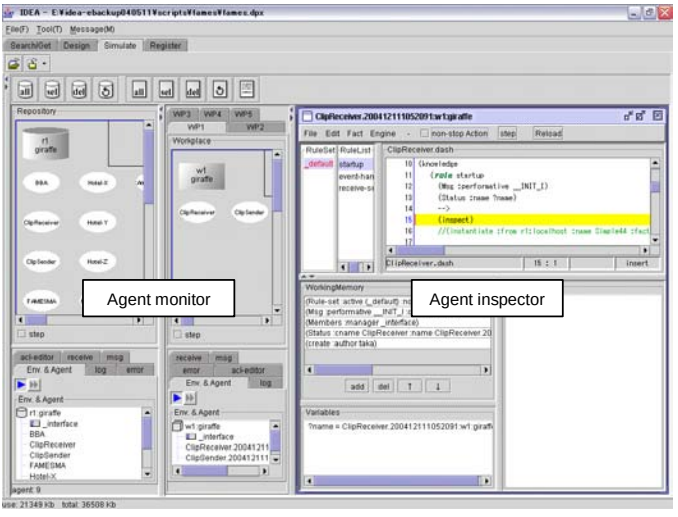

Fig. 5. Supporting function of agent simulation phase

5 Experiment and Evaluation

5.1 Evaluation of Agent Programming Support

Using a prototype of the IDEA system, we evaluated the amount of agent knowledge description in the bottom-up development. Two cases of the agent system development have been measured, i.e., (1) without reuse the existing agent system in the repository, and (2) reuse the existing agent system by using the IDEA system.

In the case (1), the designers created the protocol, the rule set and the agent knowledge from the scratch. Test and debug had been repeated and the burden of the designers became large.

On the other hand, in case (2), the designers can search the reusable agents from the repository, and assign the selected agents as a part of agents of the target system. The knowledge templates such as the contract net protocol template could be utilized effectively. Table.1 shows the results of experiment. We confirmed that the amount of agent knowledge descriptions is reduced to 54% on the average.

5.2 Evaluation of Simulation Support

The amount of workload had been measured to evaluate the simulation support function of IDEA. The following measures are introduced, i.e.,

- The number of fact used as the start conditions :N
- The number of times of error :k
- The time required by the completion of correction of the i-th error from a cooperation operation start :Ti ($i \leq k$)

- The required time from the operation start to the end in the case of being errorless :T*min*
- The required time from the operation start to the end using IDEA :T*a*

The result of this experiment is shown in Table 2.

By using the [Ex.2] in the section 5.1 we set up the agent system so that three errors may occur at the beginning, middle stage and the end of operation. The results are as follows.

First, T*min* was about 75 seconds. Next, we measured the time of debugging without IDEA. The total time is about 291 seconds. This is because whenever the designer corrects the agent knowledge in the simulation phase, the designer has to reboot the agent system and input the initial fact again and again. Then, the debugging time increases according to the number of errors.

Finally, we measured the time of debugging with IDEA. The total time of this condition is about 137 seconds. This is because the rebooting of the system is no longer necessary and the designer can set the initial facts by using IDEA.

Table 1. Evaluation of agent programming support

		Ex.1 Hotel Selection System	Ex.2 Meeting Schedule Adjustment System	Ex.3 Hotel Reservation System	Ex.4 Retrieval System of Manual of UNIX Command	Ex.5 Retrieval System of Presence Information	Ex.6 Ad-hoc Communication Service	Ex.7 Network Management System	Ex.8 Asynchronous Messaging System
No reuse	Total number of description lines	655	385	266	1863	839	12991	15479	35927
Reuse	Total number of developed agents	9	4	5	60	8	11	89	23
	Number of agents that developer reused using the repository	3	1	4	60	7	10	84	23
	Number of agents which is developed newly	6	3	1	0	1	1	5	0
	Total number of description lines[n]	655	385	266	1861	839	13018	15479	35996
	Number of reused lines [n-r]	316	107	107	1331	419	6894	12596	24635
	Number of lines which is newly written [r]	339	278	159	530	420	6124	2883	11381
	The rate of description curtailment 【((n-r)/n)×100】	**48%**	**28%**	**40%**	**71%**	**50%**	**53%**	**81%**	**68%**

Table 2. Evaluation of reduction of debugging work

	The number of times of starting of agent system	The number of times of input the fact	Execution time
Without IDEA	k + 1	(k + 1)× N	ΣTi + Tmin
IDEA	**1**	**N**	**Ta (Tmin < Ta << ΣTi + Tmin)**

6 Conclusion

In this paper, we propose the interactive development method of agent system that supports the bottom-up design based on the repository-based agent framework. A prototype of the Interactive Design Environment of Agent system called IDEA is implemented based on the proposed method and the results of experiment are also demonstrated to show the effectiveness of the proposed method.

References

1. Fujita, S., Hara, H., Sugawara, K., Kinoshita, T., Shiratori, N.: Agent-Based Design Model of Adaptive Distributed System. Applied Intelligence 9(1), 57–70 (1998)
2. Hara, H., Sugawara, K., Kinoshita, T., Uchiya, T.: Flexible Distributed Agent System and Its Application. In: Proceedings of the Fifth Joint conference of Knowledge-based Software Engineering, pp. 72–77. IOS Press, Amsterdam (2002)
3. Suganuma, T., Imai, S., Kinoshita, T., Sugawara, K., Shiratori, N.: A Flexible Videoconference System Based on Multiagent Framework. IEEE Trans. on Systems, Man, and Cybernetics - Part A: Systems and Humans 33(5), 633–641 (2003)
4. Kitagata, G., Matsushima, Y., Hasegawa, D., Kinoshita, T., Shiratori, N.: An Agent-Based Middleware for Communication Service on Ad Hoc Network. In: Proceedings of the 19th International Conference on Advanced Information Networking and Application, pp. 363–367 (2005)
5. Konno, S., Iwaya, Y., Abe, T., Kinoshita, T.: Design of Network Management Support System Based on Active Information Resource. In: Proceedings of the 18th International Conference on Advanced Information Networking and Application, pp. 102–106 (2004)
6. Kitagata, G., Sekiba, J., Suganuma, T., Kinoshita, T., Shiratori, N.: Communication Mechanism of Loose Coupled Agents in FAMES. In: Proceedings of the 1st International Workshop on Flexible Networking and Cooperative Distributed Agents (FNCDA2000), pp. 467–472 (2000)
7. Bellifemine, F., Poggi, A., Rimassa, G.: JADE - A FIPA -compliant Agent Framework. In: Proceedings of Practical Application of Intelligent Agents and Multi Agents (PAAM '99), pp. 97–108 (1999)
8. Reticular Systems: AgentBuilder - An Integrated Toolkit for Constructing Intelligence Software Agents, available at http://www.agentbuilder.com/
9. Jeon, H., Petrie, C., Cutkosky, M.: JATLite: A Java Agent Infrastructure with Message Routing. IEEE Internet Computing 4(2), 87–96 (2000)
10. Nwana, H.S., Ndumu, D.T., Lee, L.C., Collis, J.C.: ZEUS: A Toolkit for Building Distributed Multi-Agent Systems. Applied Artificial Intelligence Journal 13(1), 129–186 (1999)
11. DeLoach, S.A., Wood, M., Sparkman, C.H.: Multiagent Systems Engineering. The International Journal of Software Engineering and Knowledge Engineering 11(3), 231–258 (2001)
12. Mylopoulos, J., Kolp, M., Giorgini, P.: Agent Oriented Software Development. In: Proceedings of the 2nd Hellenic Conference on Artificial Intelligence (SETN-02) (2002)
13. Zambonelli, F., Jennings, N., Wooldridge, M.: Developing Multiagent Systems: The Gaia Methodology. ACM Transactions on Software Engineering and Methodology 12(3), 317–370 (2003)
14. Howden, N., Rnnquist, R., Hodgson, A., Lucas, A.: Jack - summary of an agent infrastructure. In: 5th International Conference on Autonomous Agents (2001)

An Agent-Based Approach to Knapsack Optimization Problems

Sergey Polyakovsky[1] and Rym M'Hallah[2]

[1] Department of Computer Science and Robotics, Ufa State Aviation Technical University, Ufa, Russia
maxles@yandex.ru
[2] Department of Statistics and Operations Research, Kuwait University, P.O. Box 5969, Safat 13060, Kuwait
mhallah@kuc01.kuniv.edu.kw

Abstract. This paper proposes a new artificial intelligence framework that solves knapsack related problems (a class of complex combinatorial optimization problems). This framework, which is pseudo-parallel and stochastic, uses an agent based system to approximately solve the optimization problem. The system consists of active agents interacting in real time. They mimic the behavior of the parameters of the optimization problem while being individually driven by their own parameters, decision process, and fitness assessment. The application of the framework to the two-dimensional guillotine bin packing problem demonstrates its effectiveness both in terms of solution quality and run time.

Keywords: heuristics, agent-based systems, artificial intelligence.

1 Introduction

Agent based systems have recently been applied to various types of optimization problems [4,8] ranging from modeling the stock market to predicting the spread of epidemics. Despite their time consuming design, these systems offer an intrinsic paradigm for modeling complex problems while being problem independent and having a low cost adaptability.

Agent based systems are comprised of autonomous, interacting agents characterized by an emergent behavior and a self-organization. They reflect most real life systems where a large number of agents interact locally while individually seeking a set of specific objectives. This interaction determines the overall system dynamics and the evolution of its characteristics. At each time epoch, each agent makes an observation and takes an action that obeys the constraints of the system. Each adopted action affects the system's objective function and influences the agents' future decisions. The system reaches steady state when its objective function is optimized.

Formally, the system can be represented by a set of agents, a finite set of pure actions available to the agents at each time epoch, the decision process or strategy of each agent, and the reward an agent obtains when opting for

H.G. Okuno and M. Ali (Eds.): IEA/AIE 2007, LNAI 4570, pp. 1098–1107, 2007.

a specific strategy at a given time. Agents select their actions according to a greedy policy; that is, an agent assesses the potential of each of the feasible available actions, chooses the action that optimizes its reward, and subsequently readjusts its decision process and characteristics. Results of agents' activities are disseminated in the system, and fed back to the agents [7]. The process is reiterated until the system reaches steady state.

Different structures have been adopted in the design of agent based modeling systems. These include domain-based hierarchical structure (DBHS), cascading agent structure (CAS), proximity relation structure (PRS), and bus-based network structure (BNS). In DBHS, static agents act as domain, resources, user interface, and gateway agents whereas mobile agents -which move around the network domains taking advantage of the resources to fulfill their goals- act as task brokers. In CAS, agents obey a hierarchical structure. In PRS, agents are located by function and abilities, and obey the agent announcing the tasks. Communication occurs only among relational agents. In BNS, some agents execute jobs while others negotiate and inform the group of the results of their negotiation activities.

Four kinds of communication channels are used in agent-based modeling: changing medium (agents communicate if and only if they share a common physical location), addressing (agents send messages via a star or a bus network), persistence (transmitted messages persist for a period of time after they are sent as in ant colonies), and proximity (an agent sends a request to its neighboring agents which may accept the request if they fulfill the constraints; if none of them does, the agent sends its request to agents belonging to a wider neighborhood).

This paper develops a multi-agent modeling framework for a class of complex combinatorial optimization problems, and illustrates its implementation to the NP hard guillotine two-dimensional bin packing problem. The proposed agent based modeling system adopts a CAS where agents obey a hierarchical structure. Agents use the Foudation for Intelligent Physical Agents (FIPA) descriptive protocols [3] to communicate while obeying the proximity principle of communication. All system's activities are abstracted through agents [9].

This paper is organized as follows. Section 2 details the proposed agent based (AB) modeling system. Section 3 illustrates its application to an NP hard combinatorial optimization problem: the guillotine two dimensional bin packing problem and assesses its performance. Finally, Section 4 discusses the extension of AB and its application to more complex problems.

2 Agent Based Modeling

The proposed AB system assimilates the items of a knapsack-type problem to agents. Each agent is characterized by its fitness, behavioral rules, and parameters. These characteristics determine the agent's decision making process.

Agents co-existing in the system proclaim themselves *agent-initiators* or *individual agents*. Agent initiators strive toward the global optimization goal of the knapsack problem. Each of them creates a group and strives to attract to

it the "best" individual agents. Individual agents, on the other hand, strive to maximize their own objectives which may or may not concord with the global goal of the problem. An individual agent is *free* if it does not belong to any agent-initiator's group, and *busy* otherwise. A free individual agent tries to join a group which will maximize its purpose parameter. An individual agent that attaches itself to an agent initiator is no longer free to participate in other system's activities unless the agent initiator that invited it undertakes a group breaking activity. In such a case, the two types of agents may swap their roles if the system's dynamics requires so.

AB's design mimics the behavior of agents in economic systems. These systems are geared toward organizing the interaction between institutions and individuals. Their input consists of participants in a free, unorganized state whereas their output is the same agents but connected via a set of relationships. The lifetime of these relationships may be short or long resulting respectively in the break up (death) or survival of the relationship. For example, consider a free market (system) where a group of college graduates are seeking employment. A subset of these graduates may decide to create firms, and proclaim themselves managers (agent-initiators). The remaining graduates (individual agents) will be seeking to join one of the created firms. Evidently, each firm's manager tries to attract the most competent graduates, and every graduate will opt to join the firm that best fits his/her own objectives (be them career advancement or salary or working hours, etc.). Since the market is dynamic, graduates can move from firm to firm, and/or create their own firms. Similarly, firms may merge, expand, break up into two or more firms, hire/fire individual agents, etc.

In the proposed AB system, the interaction of agent-initiators with free individual agents and vice versa is undertaken simultaneously (not sequentially). Thus, the adopted implementation can be assimilated to a working environment where agent-initiators and individual agents interact in real time; however, the system simulates this interaction using a pseudo-parallel environment.

In addition, the interaction between agents is a direct informational exchange where only agents from different types can communicate. Subsequently, tools - such as informational streams, information gathering and processing- known for their effectiveness are used in AB. The information is spread gradually within the system. Indeed, the system's information space is represented by a series of theoretical zones; each defined by source remoteness, speed of information spread, and speed of agents' states change. The gradual spread of information offers AB a better control of the search process. The use of speed and remoteness during informational exchange influences the speed of convergence of AB to a steady state solution and the quality of this solution.

In the proposed AB, the concept of distance or remoteness between two different agents is achieved through the adopted data structure and its coding. The remoteness of an agent is directly deduced from its position in the data structure. This implicitly implies the existence of a metrics for distance measurement; with the metrics depending on the data structure.

The space P of interacting agents consists of the set N of all agents and of the set Z of all external factors that influence AB. Each agent $i \in N$ has its own perception $O\{i, P\}$ of P; i.e., i can picture P totally or partially. When the system has a large number of agents, i does not need to view the whole system as the feedback may be useless. To avoid unnecessarily searching P, i dynamically updates its field of vision $O\{i, P\}$ by considering the part of P that is relevant to its decision process. To update $O\{i, P\}$, i redefines the distances that separate it from the remote agents that are within $O\{i, P\}$, and simulates the speed of information spread. Subsequently, the search is intensified in high potential areas and halted in less promising ones. Good quality solutions are therefore obtained during the early stages of the search.

The proposed AB system proceeds as follows. Initially, the n items of the knapsack-type problem are entered into the system as free individual agents whereas the set A of agent-initiators is set to the empty set. m agent-initiators are chosen according to a search strategy, with $1 \leq m \leq n$ and m initialized to M. The m items are removed from N, and entered into A. Each agent-initiator $j \in A$ creates its own group: $J_j = \{j\}$, and defines its capacity C_j.

Having been initialized, $j \in A$ undertakes **group formation action**s which are directed toward inviting a subset of the free individual agents (i.e., items of N) to join J_j. It examines its $O\{j, P\}$, identifies the best free individual agents that it can attach, and invites them to join J_j by sending each of them an attachment offer. The attachment of any of these free individual agents to J_j increases the group's purpose parameter; thus, improves the fitness of j.

When receiving an offer from agent-initiator $j \in A$, free individual agent $i \in N$ processes it and decides whether to reject it or accept it. To reach its decision, i analyzes the offer and considers the potential offers that may emanate from other agent-initiators in its vision spectrum $O\{i, P\}$. To determine these alternatives, i undertakes **group-joining action**s. It sends potential agent-initiators $j' \in A \setminus \{j'\}$ a request of subscription which asks for information regarding their suitability to receive i. Upon receipt of the request from i, agent-initiator $j' \in A \setminus \{j'\}$ processes the request by sending the appropriate information back to i. Agent i analyzes this information, computes its profit for each case, and reaches a decision. If its profit when joining J_j is highest, i accepts the invitation of j; else, it rejects it. Upon undertaking a decision, i relates it to j.

Agent-initiator j records the response of each of the free individual agents it invited, analyzes the responses, chooses the most eligible free individual agent i^*, and notifies all the free individual agents it invited about its decision. The free individual agents that j considered but did not finally choose do not change their state: each of them remains free, and pursues group-joining actions. The free individual agent i^* that j invited and chose receives -along with the confirmation notification - the parameters of j. i^* changes its state from free to busy, leaves N, and updates its attributes. Subsequently, j attaches i^* to its group: $J_j = J_j \bigcup \{i^*\}$, and updates its capacity C_j.

The process described above is reiterated until none of the m agent-initiators can extend an invitation. In this case, when there are free non-attached individual

agents in the system, m individual agents of N proclaim themselves (additional) agent-initiators, and build their own groups. On the other hand, when there is no free individual agent in the system, the current solution is feasible.

When a feasible solution is at hand, the system investigates its neighborhood in search for a local optima. It decreases m by 1, and undertakes **group breaking** actions. These actions are geared toward breaking low fitness groups and offering high fitness groups the opportunity to further improve their performance. Specifically, the busy agents in J_j ask agent-initiator j if it intends to undertake a group breaking action. To reach a decision, j compares its group's fitness to a threshold fitness coefficient $\alpha \in [0, 1]$. J_j remains grouped if its fitness is larger than α; and disassembles its group otherwise. An agent-initiator j that reaches a decision to disassemble relays the information to the elements of J_j. These elements change their state from busy to free, and append themselves to N. Furthermore, j changes its role from an agent-initiator to a free individual agent; thus leaves A. The freed agents initiate group joining / group formation actions. Meanwhile, a surviving agent-initiator seizes this opportunity to increase its performance: It invites freed agents that are in its field of vision to join its group.

Group breaking activities are equivalent in a socio-economic context to the death of a firm due to competition. Subsequently, the firm's employees -including the manager- undertake group joining / group formation actions oriented toward joining one of the existing firms or creating new firms, respectively.

Every time a feasible solution is obtained, m is decreased by 1 and the process is reiterated. The process stops when $m = 1$. The best solution among the m feasible solutions is viewed as a local optimum.

To explore a wider spectrum of the solution space and intensify the search around the current solution, A-B investigates, for every feasible solution, $M-1$ neighbors. When it obtains a feasible solution, A-B initiates group breaking activities: It tags the freed agents into N, and let them initiate group formation / group joining activities. The actions to be undertaken by these freed agents depend mainly on their relative position in N. Therefore, AB assigns these freed agents to random positions in N -in lieu of their original relative positions- and lets them interact in the system. Thus, each of the $M-1$ neighbors corresponds to the solution obtained given a random permutation of the freed agents. A summary of the proposed AB system is given in Table 1.

3 Illustrative Example

The proposed agent based system is applied herein to the NP hard guillotine two dimensional bin packing (2BP|$\star$|G). The 2BP|$\star$|G consists of allocating, without overlap, a set of n small rectangles, each defined by a length l_i and a width w_i, $i \in N = \{1, ..., n\}$, into the minimum number of identical large rectangular bins of length L and width W, such that $\max\{l_i, w_i\} \leq \max\{L, W\}$ and $\min\{l_i, w_i\} \leq \min\{L, W\}$, $i \in N$. In addition, each piece is to be extracted using guillotine

Table 1. The Proposed AB system

```
// Initialization of the A-B System //
    Create n free individual agents; each corresponding to an item of N.
    Set m = M, and A = ∅.
// Iterative Step //
    While ((m ≥ 1) and (there are free agents in the system))
        Let m free individual agents of N initialize themselves as agents-initiators;
        append them to A; and remove them from N;
        Flag:=True;
        While (Flag=True)
            Flag:=False;
            Set j := 1; //j is the index of the current agent initiator being examined. //
            While (j ≤ m)
                Find a free individual agent to be attached to j;
                If (candidate for attachment is found) then
                    Flag:=True;
                End if;
                Update the capacity C_j.
                Set j:=j+1;
            End while;
        End while;
        If (there is no free agent in the system) and (m > 1) then
            Set m = m − 1; j = 1
            while (all agents-initiators are not examined)
                Attempt a group breaking activity of agent initiator j;
                Set A = A \ {j}, and N = N ⋃ {j};
                Set j = j + 1;
            End while;
        Set j = 1
        While (all agents-initiators are not examined)
            Find free individual agents to be attached to j;
            Set j = j + 1;
        end while;
    end if;
end while;
```

cuts. The technological constraints may impose a fixed orientation on the items (2BP|O|G) or allow the items to be *rotated by* 90° (2BP|R|G).

The adaptation of AB to the 2BP|O|G is given in Table 2. The goal of an *agent initiator* is to pack as efficiently as possible the individual agents of its group into a bin while respecting the guillotine, orientation, and capacity constraints. The goal of a *free individual agent* is to position itself in the bottom left most position of the unused area or vacancy -among all agent initiators' vacancies- that maximizes its occupancy ratio.

AB creates n free individual agents corresponding to the n items of N, and sets $A = \emptyset$. It initializes the priority list $U = I \bigcup \overline{I}$ (where the elements of $I = \{i \in N : l_i > L/2, w_i > W/2\}$ and $\overline{I} = N \setminus I$ are ordered in non-ascending order of their areas). It chooses the first m items of U as agent-initiators, removes them from U, and appends them to A.

Agent-initiator $j \in A$ sets $J_j = \{j\}$, and positions itself in the bottom-left most position of the bin; i.e., in position $(x_j, y_j) = (0, 0)$. It chooses the cut type by favoring the one that leaves the largest unused area. Consequently, it enters, into its queue of vacancies C_j, the two unused areas $\{S_1, \overline{S}_1\}$ if the cut is horizontal and $\{S_2, \overline{S}_2\}$ if the cut is vertical (cf. Figures 1.a and 1.b, respectively); with each element of C_j being characterized by its attributes which are its dimensions and relative coordinates with respect to its bin. C_j is a first-in- first-out queue; so the first element of C_j is processed first whereas newly created vacancies are tagged to the end of C_j.

Having been initialized, j undertakes **group formation** actions which are directed toward inviting a subset of U to join J_j. It sets its current unused area $S_j = (L_j, W_j)$ to the first vacancy queued in C_j. It then identifies the best free

Table 2. The AB system adapted to the 2BP|O|G

```
// Initialization of the AB System //
Create n free individual agents; each corresponding to an item of N.
Set m = M, and A = ∅.
Construct the priority list U of free individual agents.
// Iterative Step //
While ((m ≥ 1) and (there are free agents in the system))
    Let the first m individual agents of U initialize themselves as agents-initiators; append
    them to A; and remove them from U;
    Flag=True;
    while (Flag=True)
        Flag=False;
        Set j = 1;   //j is the index of the current agent initiator being examined. //
        While (j ≤ m)
            Set i = 1;   //i is the counter of vacancies. //
            While (i ≤ 2)
                Find a free individual agent to be attached to j
                (i.e., to be packed in S_j, the first vacancy in C_j);
                if (candidate for attachment is found) then
                    Flag=True;
                    Remove S_j from C_j;
                else
                    transfer S_j to C̄_j;
                end if;
                Set i=i+1;
            end while;
            Set j=j+1;
        end while;
    end while;
    if (there is no free agent in the system) and (m > 1) then
        Set m = m − 1; j = 1
        while (all agents-initiators are not examined)
            Attempt a group breaking activity of agent-initiator j;
            Set A = A \ {j}, and U = U ⋃ {j};
            Set j = j + 1;
            end while;
        Set j = 1
        while (all agents-initiators are not examined)
            Find free individual agents to be attached to j for every S_j ∈ C̄_j;
            Set j = j + 1;
        end while;
    end if;
end while;
```

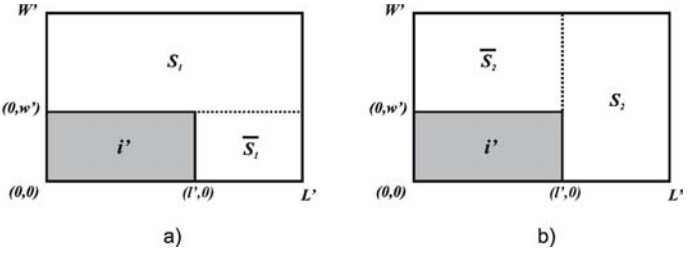

Fig. 1. Illustrating the cut type and the resulting vacancies

individual agents that can be positioned in S_j, and invites each of them to join its group by sending it an attachment offer. The attachment of any of these free individual agents to J_j increases the packing coefficient of the bin; thus, improves the fitness of j.

When receiving an offer from agent initiator $j \in A$, a free individual agent $i \in U$ decides whether to reject or accept it by undertaking a **group joining** action. It sends each potential agent initiator $j' \in A \setminus \{j\}$ a request of subscription asking for the attributes of the vacancies of $C_{j'}$ that can fit i. Upon receipt of the request from i, agent initiator $j' \in A \setminus \{j\}$ processes the request by sending

the suitable elements of its $C_{j'}$ back to i. Then, i computes its occupancy ratio for each vacancy, and reaches a decision. The occupancy ratio r_{ij} of agent i in area S_j is the ratio of the area of i to the area of S_j. If r_{ij} is close to 1 and is the highest ratio among all potential agent initiators' vacancies, i accepts the invitation of j; else, it rejects it. Upon undertaking a decision, i relays the information to j.

Agent initiator j records the response of each individual agent it invited; analyzes the responses; chooses the best free individual agent i^*, and notifies all the free individual agents it invited about its decision. i^* changes its state from *free* to *busy*, and leaves U and N. Subsequently, j attaches i^* to its group J_j; and chooses the type of cut to undertake by comparing the areas of $S_1 = (L_j, W_j - w_{i^*})$ and $S_2 = (L_j - l_{i^*}, W_j)$. It updates C_j by removing S_j from C_j and tagging the two newly created unused areas to the end of C_j. Finally, it updates the attributes of i^* (i.e., orientation and coordinates relative to the left bottom corner of the bin).

If no free individual agent is attached to J_j, $S_j = (L_j, W_j)$ is removed from C_j. S_j is permanently removed from the agent initiator's memory if none of the n items fits S_j; that is, $L_j < \min_{i=1,n}\{l_i\}$, or $W_j < \min_{i=1,n}\{w_i\}$. On the other hand, if there are items that fit into S_j but these items are currently busy individual agents or agent initiators, then S_j is appended into the queue of non-filled vacancies $\overline{C}_j$. By joining $\overline{C}_j$, S_j will later be reconsidered for possible filling (with some of these items) when group breaking activities take place.

Thereafter, the process proceeds as described in Section 2 with agent initiator j undertaking a group breaking action if its group's fitness is less than a prefixed threshold level.

The data structure adopted in this problem is a special modification of the basic matrix structure (two-dimensional array). It is a $V \times V$ matrix, where V is the number of partitions such that $V \in N$, and $1 \leq V \leq min\{W, H\}$. Thus, each cell of the matrix contains a set of items whose sizes belong to the range of the cell; i.e., the agents of N are distributed among the cells of this matrix. The proposed matrix data model describes the space of interacting agents. When searching for a suitable free individual agent, an agent initiator residing in one of the matrix cells dynamically updates its individual vision of the matrix to few cells (which satisfy the required parameters). It then explores them starting from the cell, corresponding to the agent whose priority is highest.

The adopted data structure speeds the computation time over all instances by 10%. Figure 2 illustrates the variation of run time as V increases. When $V = 1$, the matrix model reduces to a linear array.

The performance of AB when applied to the 2BP|O|G is assessed in terms of runtime and solution quality. AB is compared to the tabu-based heuristics of [5]. AB is coded in `Borland Delphi 6.0 with Object Pascal`, and run on an `Athlon XP 2800`.

AB's runtime varies between 10 milliseconds for 40-item instances and 1400 milliseconds for 1000-item instances. It is less than 14 minutes for 100000 items.

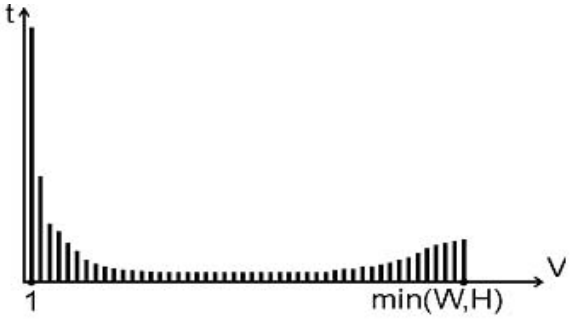

Fig. 2. Run time t as the number of partitions V varies

(No comparable heuristic is known to handle such large problems.) These run times are obviously negligible; thus, will not be further discussed.

AB is tested on the instances of [1,6]. For each class, five problem sizes are considered: $n = 20, 40, 60, 80,$ and 100. Each problem type is replicated ten times. The analysis of the results reveals that AB performs on average better than TS for the 2BP|O|G. For all classes, the average ratio of AB is less than TS's: it is 1.055 for AB versus 1.080 for TS. For the 2BP|R|G, AB is consistently as good or better than TS. Its average ratio is 1.035 versus 1.065 for TS.

AB has several advantages in comparison to traditional heuristic approaches [2]. First, its interacting agents strive continuously towards increasing their groups' fitness. Second, decisions are revokable since agent initiators' groups can be disassembled, and agents can be reassigned to new groups. Third, the pseudo-parallelism of the approach helps it perform better in terms of solution quality. Fourth, its reconstruction process maintains the "good" part of the solution and rebuilds the "weaker" part; thus, mimics path relinking based heuristics. Last, its stochastic nature allows it to investigate a larger part of the solution space; thus, ends up getting a high quality solution.

4 Conclusion

This paper proposes a general distributed artificial intelligence framework for complex combinatorial optimization problems. It uses a dynamic pseudo-parallel stochastic AB system of active interacting agents; each with its own characteristic (parameters), fitness, and decision process (or rules or logic of work). It applies the principle of self organization of the agents to build solutions, and intensifies the search around their neighborhoods till reaching a local optimum. When the system reaches steady state, AB diversifies the search looking for a near global optima.

In this paper, the implementation of AB is illustrated via the NP hard guillotine two dimensional bin packing problem. However, AB, which is modular,

can be easily adapted to any knapsack-type optimization problem such as early tardy scheduling, districting and timetabling problems. The agents for any new problem are directly inherited from the already developed agents, and adapted to the new problem via the modification of their decision processes and properties.

Even though it can be assimilated to a meta-heuristic, AB is not a traditional approach: it is not oriented to solving a particular problem; thus, does not require any major modification to reflect the constraints and the particularity of the problems. Differently stated, AB can be viewed as a new way to design adaptive algorithms. The application of the agent based modeling to complex combinatorial problems will lead to better informed decision making, and to the resolution of large scaled problems.

References

1. Berkey, J.O., Wang, P.Y.: Two-dimensional finite bin packing algorithms. Journal of the Operational Research Society 38, 423–429 (1987)
2. Mukhacheva, E.A., Valeeva, A.F., Kartak, V.M., Filippova, A.S.: Models and methods for orthogonal packing and cutting problems: analytical review. Application to Journal of Information Technologies 5, 1–17 (2004)
3. FIPA Request Interaction Protocol Specification `http://www.fipa.org/specs`
4. Jedrzejowicz, J., Jedrzejowicz, P.: Agent-Based Approach to Solving Difficult Scheduling Problems. In: Ali, M., Dapoigny, R. (eds.) IEA/AIE 2006. LNCS (LNAI), vol. 4031, pp. 24–33. Springer, Heidelberg (2006)
5. Lodi, A., Martello, S., Vigo, D.: Heuristic and metaheuristic approaches for a class of two-dimensional bin packing problems. INFORMS Journal on Computing 11, 345–357 (1999)
6. Martello, S., Vigo, D.: Exact solution of the two-dimensional finite bin packing problem. Management Science 44, 388–399 (1998)
7. Parinov, S.I.: Toward a theory and agent based model of the networked economy (July 1999) `http://rvles.ieie.nsc.ru/parinov/theory/eng/index.htm`
8. Parunak, H.V.D.: Agents in Overalls: Experiences and Issues in the Development and Deployment of Industrial Agent-Based Sytems, Intern. J. of Cooperative Information Systems 9(3), 209–228 (2000)
9. Polyakovsky, S., M'Hallah, R.: An agent-based approach to the two-dimensional guillotine bin packing problem. European Journal of Operational Research (submitted 2006)

Constraint-Based Approach for Steelmaking–Continuous Casting Rescheduling

Tieke Li[1] and Dongfen Guo[1,2]

[1] University of Science and Technology Beijing, Beijing
30 Xueyuan Road, Haidian District Beijing 100083, P.R. China
[2] Shijiazhuang Post and Telecommunication Technical College, Shijiazhuang, China, 050021
guodf640@hotmail.com

Abstract. Steelmaking-continuous casting rescheduling problem is an NP-hard problem. In this paper, we present a constraint-based approach for steelmaking–continuous casting rescheduling problem in integrated steel production environment. We treat the steelmaking–continuous casting rescheduling problem as a dynamic constraint satisfaction problem. To maintain the production stability and the material flow continuity after rescheduling, the perturbation measure function of the model is defined as the summation of the absolute deviation between the new start times and the original start times of operations in continuous casting stage, the variable selection and value selection heuristics is designed based on the resource slackness to minimize the change extent of the rescheduling solution. The resource conflicts in the original schedule are incrementally repaired by the variable selection and value selection heuristics. The validity of the proposed model and approach are demonstrated by the computational examples.

Keywords: steelmaking-continuous casting; rescheduling; dynamic constraint satisfaction problem; constraint propagation.

1 Introduction

Steelmaking-continuous casting is the critical process in steel production, it consists of three stages: steelmaking, refining and continuous casting. Pig iron is transformed into steel liquid by convert furnace (CF) and refining furnace (RF) in steelmaking and refining stages, the steel liquid is then continuously cast into slabs on continuous caster (CC) in casting stage, these slabs will supply to hot rolling stage according to the slab rolling sequence defined by hot rolling schedule.

In practical steelmaking-continuous casting process, each stage usually has identical parallel machines, steelmaking-continuous casting scheduling problem has the general characteristic of hybrid flow shop. In addition, steelmaking-continuous casting process has many special constraints, such as the basic job unit in steelmaking and refining stages is Heat, while the basic job unit in casting stage is Cast, which consists of a range of Heats they must continuously cast on casters, i.e., in the last stage of steelmaking-continuous casting process, jobs (Heats) must be divided into

H.G. Okuno and M. Ali (Eds.): IEA/AIE 2007, LNAI 4570, pp. 1108–1117, 2007.

different groups (Cast) and there are precedence constraint and no-break casting constraint within these groups. These special constraints make the scheduling for steelmaking-continuous casting production much more difficult to attack than general hybrid flow shop.

Most of the literature on steelmaking-continuous casting scheduling focused on the static problems [1~4]. However, these scheduling systems may not be effective in a dynamic manufacturing environment. During the execution of steel production, machine failure is one of the most frequently occurring unexpected events which can disturb the existing schedule and interrupt the current production, a revised schedule must be arranged in a short time to restore the production. However, fewer research works have addressed the dynamic scheduling problem. LI[5] set up a dynamic scheduling model based on Petri net for steelmaking-continuous production system, given a heuristic algorithm to shorten the total flow time. Cowling[6] proposed a dynamic scheduling method based on real time information, he reduced the continuous casting rescheduling problem to a $n/1//\overline{C}$ single machine sequencing problem, given the rescheduling strategy against the disturbance events of jobs' processing time changing from p_k to $p_k^{'}$. These researches considered the rescheduling problem in the traditional cold charge situation, where a slab yard exists between steelmaking-continuous casting and hot rolling stages, the material flow continuity and the production stability can be maintained by adjusting the intermediate storage of the slabs, the highlight of the rescheduling is the utility of the machine.

In modern steel production factory, steelmaking-continuous casting process and hot rolling process are directly connected at high temperature and form an integrated and synchronized production environment, there is a higher requirement for material flow continuity, steel liquid temperature dropping, and job's waiting time between adjacent stages. Since there are no intermediate storage areas for buffering between continuous casting and hot rolling stages, any great changes in continuous casting plan may result in great disturbance on its downstream. The goal of steelmaking-continuous casting rescheduling is not only to restore the consistency in a schedule disturbed by unexpected events, but also to reduce the disruption on downstream so as to maintain the material flow continuity and the production stability.

This paper investigates the constraint-based approach for steelmaking-continuous casting rescheduling problem in integrated steel production environment. Section 2 presents the DCSP model of the steelmaking-continuous casting rescheduling problem. Section 3 describes the constraint-based approach for steelmaking-continuous casting rescheduling. Section 4 presents the experimental results of the computational examples. Finally, conclusions are presented in section 5.

2 The DCSP Model of the Rescheduling Problem

2.1 Dynamic Constraint Satisfaction Problem

A constraint satisfaction problem (CSP) is a 3-tuple: $CSP\Theta = (V, D, C)$ where V is a set of variables $\{v_1, v_2, \cdots, v_n\}$, D is a function mapping the variables to n

corresponding domains of values $d_1, d_2, \cdots, d_n$, and C is a set of constraints on subsets of the variables in V. Let α_Θ be a complete assignment, mapping each variable $v_i \in V$ to a value in its corresponding domain d_i. α_Θ is a solution to Θ, if and only if each constraint in C holds under α_Θ.

A dynamic constraint satisfaction problem (DCSP) is a sequence of CSP which evolves by time, where each one differs from its predecessor by constraint additions or deletions[7]. Consider the case of a CSP Θ transformed into a new CSP Θ^1, the transformation is captured in terms of two sets C_{add} and C_{del} respectively standing for the set of constraints about to be removed from, and added to the constraint C_Θ, $C_{\Theta^1} = C_\Theta \cup C_{add} \backslash C_{del}$. An optimal solution to a DCSP is a solution to the altered CSP that is minimally different to a previously satisfaction solution. This solving idea has important meaning to many practical rescheduling problems.

Sakkout[8]treated the job shop dynamic scheduling problem as a dynamic constraint satisfaction problem, given a probe-based backtrack search approach to minimize the perturbation in dynamic scheduling. Wang[9] modeled the scheduling of the product development projects as a dynamic constraint satisfaction problem, proposed the meta-heuristic approaches including simulated annealing and genetic algorithms to repair the disrupted schedule with the minimum cost of resource constraint violation. In this paper, we model the steelmaking–continuous casting rescheduling problem as a dynamic constraint satisfaction problem, and propose a constraint-based approach to minimize perturbation of the rescheduling solution.

2.2 DCSP Model of Steelmaking-Continuous Casting Rescheduling Problem

Notations

The notations used in model and approaches are defined as follows:

i –index of Heat; q – index of Cast;

j – index of stage (j =1 denotes steelmaking stage, j =2 denotes refining stage, j =3 denotes continuous-casting stage);

m –index of machine; I – set of Heats, $I = \{1,2,\cdots N\}$;

K_q –set of Heats in q*th* Cast; K –set of Cast, $K = \{1,2,\cdots Q\}$;

M_j –set of machines in stage j; o_{ij} –operation of ith Heat in stage j;

$cap\_r(o_{ij})$ –the number of capacity demanded by o_{ij};

$cp(m)$ –the capacity of machine m; $M(o_{ij})$ –the machine used by o_{ij};

$AO(m)$ –set of operations using machine m; $st(o_{ij})$ –start time of o_{ij};

$et(o_{ij})$ –end time of o_{ij}; $p(o_{ij})$ –processing time of o_{ij};

$Init\_st(o_{ij})$ –start time of o_{ij} in relaxation problem;

$FH(q)$ –the first Heat of the qth Cast;

δ_j –the allowed value of the Heat's waiting time between stages;

DCSP model

The CSP model of steelmaking-continuous casting scheduling problem is defined as follows:

$$\min \varepsilon = \sum_{i\in I, j=1} \max(0, Init\_st(o_{ij}) - st(o_{ij})) + \sum_{i\in I, j=3} \max(0, st(o_{ij}) - Init\_st(o_{ij})) \ . \quad (1)$$

Subject to:

$$st(o_{ij}) \geq 0 \ , \forall i \in I, \ j = 1,2,3 \ . \quad (2)$$

$$st(o_{i,j+1}) \geq st(o_{ij}) + p(o_{ij}) \ , \forall i \in I, \ j = 1,2,3 \ . \quad (3)$$

$$\sum_{o_{ij}\in AO(m) \mid st(o_{ij}) \leq t \leq st(o_{ij}) + p(o_{ij})} cap\_r(o_{ij}) \leq cp(m) \ , \forall i \in I, \mathrm{m} \in \mathrm{M_j}, \ j = 1,2,3 \ . \quad (4)$$

$$et(o_{ij}) = st(o_{ij}) + p(o_{ij}) \ , \forall i \in I, \ j = 1,2,3 \ . \quad (5)$$

$$st(o_{i+1,j}) \geq et(o_{ij}), \forall i, i+1 \in K_q, q \in K; \ j = 3 \ . \quad (6)$$

$$st(o_{FH(q),3}) \geq T_q, \forall q \in K \ . \quad (7)$$

$$0 \leq st(o_{ij+1}) - et(o_{i,j}) \leq \delta_j \ , \forall i \in I; \ j = 1,2 \ . \quad (8)$$

$$K_1 \cap K_2 \cap K_3 \cdots \cap K_Q = \phi \ (\text{Null}) \ . \quad (9)$$

$$K_1 \cup K_2 \cup K_3 \cdots \cup K_Q = I \ . \quad (10)$$

The objective function (1) is to minimizes the Heat's waiting time and the tardiness of Casts production; (2) ensures the operation's start time should be greater than zero; (3) is the precedence constraints of operations which are defined by processing route; (4) is the resources capacity constraint; (5) ensures the operation's processing cannot be interrupted; (6) is the precedence and the no-break constraints within a Cast; (7) means the start time of the Cast q should match up with the hot rolling production plan; (8) ensures the Heat's waiting time should be less than the allowed value; (9) and (10) ensure that one Heat can only be assigned to one Cast.

The unexpected machine failures can be viewed as additions or deletions of constraints to the original problem. Steelmaking-continuous casting rescheduling problem can be regarded as a dynamic constraint satisfaction problem. This provides a mechanism for minimizing the change extent in the solution of the redefined

problem. The DCSP model of steelmaking-continuous casting rescheduling problem is a 6-tuple:

$$\Theta^{n+1} = (\Theta^n, \alpha_{\Theta^n}, C_{add}, t_{invalid}, m, \delta). \tag{11}$$

Where Θ^{n+1} denotes the redefined problem, Θ^n denotes the original problem; α_{Θ^n} denotes the solution of Θ^n. $t_{invalid}$ denotes the period of machine failure, during this period, the resource's capacity $cp(m)$ changes , this can be viewed as the fact that add a new constraint $C_{add}: cp(m) = 0, \forall t \in t_{invalid}$ to the original problem Θ^n, the constraints of redefined problem becomes $C_{\Theta^{n+1}} = C_{\Theta^n} \cup C_{add}$. δ is a perturbation measure function that evaluates the difference between two complete assignments to Θ^n and Θ^{n+1}.

In integrated steel production environment, continuous casting production plays an important part of supplying slabs to hot rolling production. Great changes in start times of the operations in casting stage will heavily affect the material flow continuity and the hot rolling production stability. In addition, the start times of operations in original schedule are the optimal start times under considering the constraints of steelmaking-continuous casting production and matching up with the hot rolling production. In the revised schedule, the start times of the operations in casting stage should keep changes to a minimum. So the perturbation measure function of the model is defined as the summation of the absolute deviation between new start times and original start times of operations in continuous casting stage.

$$\delta(\alpha_{\Theta^n}, \alpha_{\Theta^{n+1}}) = \sum_{o_{ij} \in O, j=3} \left| st^{new}(o_{ij}) - st^{original}(o_{ij}) \right|. \tag{12}$$

3 Rescheduling Approach

Modern steel production factory has adopted the automatic control system and computer information management system. The real-time data acquisition system based on the industrial control computers and sensors can monitor the state of machine resource, supply real-time feedback information to production scheduling system. This advanced automation and information production environment not only brings challenges to dynamic production scheduling, but also provides a feasible implementation environment for dynamic production scheduling system.

This research is based on the real-time feedback information system. The occurring time and recovering time of machine failure events can be predicted in advance by real-time data acquisition system.

3.1 Basic Idea of the Rescheduling Approach

We build the rescheduling approach based on dynamic constraint satisfaction and repair-based technology. Firstly, the operations related to the failed machine form the

minimal rescheduling task set A'. During the solving process, any operation that loses its value will be added to A'. The inconsistencies in the original schedule are repaired by variable selection and value selection heuristics. The temporal constraint propagation and resource constraint propagation are implemented to enhance the consistency of temporal and resource constraint. When the rescheduling task set A' becomes null, the approach computes the perturbation measure function value of the current solution, then compares it with the one of current best solution, selects the better solution as the current best solution.

3.2 Formula Used in Rescheduling Approach

(a) The resource capacity slackness

Let $slack\_cap(m, t_1, t_2)$ denotes the resource capacity slackness of machine m in time window $[t_1, t_2]$. Let $cap(m, t_1, t_2)$ denotes the available capacity of machine m in time window $[t_1, t_2]$. Let $demand(o_{ij}, m, t_1, t_2)$ denotes the capacity quantity demanded by operation o_{ij} in time window $[t_1, t_2]$. The resource capacity slackness is defined as follows:

$$slack\_cap(m, t_1, t_2) = cap(m, t_1, t_2) - \sum_{o_{ij} \in AO(m)} demand(o_{ij}, m, t_1, t_2) \ . \tag{13}$$

$$\text{Where} \quad cap(m, t_1, t_2) = cp(m) \times (t_2 - t_1) \ .$$

$$demand(o_{ij}, m, t_1, t_2) = overlap(o_{ij}, m, t_1, t_2) \times cap\_r(o_{ij}) \ .$$

$$overlap(o_{ij}, m, t_1, t_2) = \begin{cases} 0, & \text{iff } [st(o_{ij}), et(o_{ij})] \cap [t_1, t_2] = 0 \\ \min\{et(o_{ij}), t_2\} - \max\{st(o_{ij}), t_1\}, & \text{otherwise} \end{cases} .$$

(b) The resource conflict value

Let Δf_m denotes the resource conflict value , if $M(o_{ij}) = M(o_{rj})$

$$\Delta f_m = p(o_{ij}) + p(o_{rj}) - (\max\{et(o_{ij}), et(o_{rj})\} - Min\{st(o_{ij}), st(o_{rj})\}) \ . \tag{14}$$

(c) The variable selection and value selection heuristics

Variable selection rule: Select an operation o_{ij} with the earliest start time from A' as the next scheduling variable.

Value selection rule: Firstly, compute the slackness of resource capacity of m ($m \in M_j$)in time window $[st(o_{ij}), et(o_{ij})]$; Secondly, select a machine with the maximal slackness of resource capacity as value to assign to the selected o_{ij} , i.e.,

$M(o_{ij}) = m \mid m = \max\{slack\_cap(m, st(o_{ij}), et(o_{ij})), m \in M_j\}$. if more than one machine have the same maximal slackness, then randomly select one machine as value to allocate to operation o_{ij}.

(d) The feasible start time window

Let $[\, est(o_{ij}), lst(o_{ij}) \,]$ denotes the feasible start time window of operation o_{ij}

$$lst(o_{ij}) = lst(o_{i,j+1}) - p(o_{ij}), j = 1,2. \tag{15}$$

$$est(o_{ij}) = est(o_{i,j+1}) - p(o_{ij}) - \delta_{j,j=1,2}. \tag{16}$$

(e) The temporal constraint propagation and resource constraint propagation

$$st(o_{ij}) \le st(o_{i,j+1}) - p(o_{ij}), j = 1,2. \tag{17}$$

$$st(o_{r+1,j}) \ge st(o_{rj}) + p(o_{rj}), \text{ where } o_{rj} \prec o_{r+1,j}, M(o_{rj}) = M(o_{r+1,j}), j = 1,2,3. \tag{18}$$

3.3 Description of the Rescheduling Approach

Step0: Let $sche\Phi 1$ denotes the initial revised solution, $sche\Phi 2$ denotes the current best solution, $sche\Phi 3$ denotes the current solution. δ^0 is the perturbation measure function of $sche\Phi 2$. Maxstart is the maximal number of restarting, M is a very large positive number, C is the counter of restarting number, let $sche\Phi 2 = sche\Phi 1$, $\delta^0 = M$

Step1: Determine the rescheduling tasks in original schedule and adding them into A'

Step2: Variable selection and value selection

If $A' \neq \phi$, select an operation from A' according to the variable selection rule, then select a machine according to the value selection rule, allocate this machine to the selected operation, go to Step3; if $A' = \phi$, save this current solution to $sche\Phi 1$, go to Step5.

Step3: Resource conflict checking and eliminating

According to (14), compute Δf_m. If $\Delta f_m > 0$, there is a resource conflict, add a precedence constraint between the operations related to this conflict, prune the start time of the operation o_{ij}, $st(o_{ij}) = \max\{est(o_{ij}), st(o_{ij}) - \Delta f_m\}$, go to Step4; If $\Delta f_m \le 0$, keep the start time of o_{ij} no change, go to Step4.

Step4: Constraint propagation

After reassigning a value to the selected operation, the temporal and resource constraint propagation are performed, the start times of other operations are updated

in their feasible start time window, the precedence constraint consistency and resource constraint consistency are enhanced, go to Step2.

Step5: Let $\text{sche}\Phi 3 = \text{sche}\Phi 1$.

Step6: Check if there are resource conflicts in $\text{sche}\Phi 3$, if no conflicts exist, go to Step8; else, go to Step7.

Step7: First, randomly select a conflict; relax the right bound of the feasible start time window of the operations related to this conflict. Then search a new start time for these operations to eliminate this conflict. Next, implement temporal and resource constraint propagation go to Step6.

Step8: Compute the perturbation measure function value δ of the $\text{sche}\Phi 3$. If $\delta < \delta^0$, then $\text{sche}\Phi 2 = \text{sche}\Phi 3$, $\delta^0 = \delta$, $C = C + 1$. If $C > \text{Maxstart}$ or $\delta^0 = 0$, go to Step9; else, go to Step5.

Step9: Output the final rescheduling solution $\text{sche}\Phi 2$.

4 Computational Examples

To demonstrate the validity of the proposed rescheduling approach, 10 groups of practical production data are used to test the performance of it. The propose approach has been implemented using C++ and run on Pentium 1.4GHZ computer. Table 1 is one group of practical production dada. Table2 is the original schedule;

Table 1. Practical production data

			q =1, τ_1 =95						q =2, τ_2 =160					
j	M_j	i	1	2	3	4	5	6	7	8	9	10	11	12
1	3		50	50	50	50	50	50	45	45	45	45	35	35
2	3	$p(o_{ij})$	45	45	45	45	40	40	40	40	40	40	30	30
3	2		35	35	35	35	35	35	35	35	35	35	40	40

We randomly generate 4 machine failure events and use the proposed rescheduling approach to cope with these five real-time disturbance events.

Table 3 summarizes the rescheduling results and lists the operations their processing plans have been changed in the revised schedule, the numbers or letters with the star symbol on their right corner express the start time or processing machine have been changed. The operations they are not shown in Table3 keep the start time and processing machine no change. δ^0 is the perturbation measure function value of the final revised schedule.

Table 2. Original scheduling results

Index of Heats	Steelmaking stage		Refining stage		Continuous casting stage	
	st(o_{i1})-et(o_{i1})	Processing machine	st(o_{i2})-et(o_{i2})	Processing machine	st(o_{i3})-et(o_{i3})	Processing machine
1	0-50	1#CF	50-95	1#RF	95	1#CC
2	35-85	2#CF	85-130	2#RF	130	1#CC
3	60-110	3#CF	120-165	1#RF	165	1#CC
4	85-135	2#CF	155-200	3#RF	200	1#CC
5	145-195	1#CF	195-235	2#RF	235	1#CC
6	180-230	3#CF	230-270	1#RF	270	1#CC
7	75-120	1#CF	115-155	3#RF	160	2#CC
8	110-155	3#CF	155-195	2#RF	195	2#CC
9	135-180	2#CF	190-230	1#RF	230	2#CC
10	180-225	2#CF	225-265	3#RF	265	2#CC
11	235-270	1#CF	270-300	2#RF	300	2#CC
12	275-310	3#CF	310-340	3#RF	340	2#CC

Table 3. Rescheduling results

Real-time events			Operation's processing plan have been changed in the revised schedule			δ^0
Index	$t_{invalid}$	machine failure	o_{ij}	st^{new}	Processing machine	
1	t=50-100	1#RF	o_{12}	t=50	**3#RF***	0
2	t=90-125	2#RF	o_{21}	**t=20***	2#CF	0
			o_{22}	**t=70***	**3#RF***	
3	t=155-190	3#RF	o_{32}	**t=100***	1#RF	0
			o_{42}	**t=145***	**1#RF***	
4	t=155-190	2#CF	o_{31}	**t=40***	3#RF	0
			o_{51}	**t=130***	1#CF	
			o_{81}	**t=90***	3#CF	
			o_{91}	t=135	**3#CF***	
			$o_{10,1}$	t=180	**1#CF***	

5 Conclusions

In this paper, we modeled the steelmaking-continuous casting rescheduling problem in integrated steel production environment as a dynamic constraint satisfaction problem, proposed a constraint-based approach to repair the inconsistency introduced

by the machine failure events. The computational results show the proposed approach can minimize the deviation between new start times and original start times of operations in continuous casting stage, reduce the disturbance on hot rolling production and then keep the material flow continuity and production stability. In the future research, we will improve the proposed approach to cope with the rescheduling problem initiated by other unexpected events, such as the uncertain processing times, uncertain due date of slabs, as well as the ill quality of slabs etc.

References

1. Tang, L., Liu, J., Rong, A.: A mathematical programming model for scheduling steelmaking-continuous casting production. European Journal of Operational Research 120, 423–435 (2000)
2. Harjunkoski, I., Grossmann, I.E.: A decomposition approach for the scheduling of a steel plant production. Computers and Chemical Engineering 25, 1647–1660 (2002)
3. Guanghang, L.I.U., Tieke, L.: A steelmaking-continuous casting production scheduling model and its heuristic algorithm. System engineering 6, 44–48 (2002)
4. Pacciarelli, D., Pranzo, M.: Production scheduling in a steelmaking-continuous casting plant. Computers and Chemical Engineering 28, 2823–2835 (2004)
5. Xiaofeng, L.I., Liyun, X.U., Huihe, S., et al.: Dynamic model of steelmaking and continuous casting system and heuristics algorithm of dynamic scheduling. Journal of Shanghai Jiaotong University 35(11), 1659–1662 (2001)
6. Cowling, P.I., Johansson, M.: Using real time information for effective dynamic scheduling. European Journal of Operational Research 139(2), 230–244 (2002)
7. Dechter, R., Dechter, A.: Belief maintenance in dynamic constraint networks. In: Proceedings of the AAAI, pp. 37–42 (1988)
8. Sakkout, H.E., Wallace, M.: Probe backtrack search for minimal perturbation in dynamic scheduling. Constraints 5(4), 359–388 (2000)
9. Wang, J.: Constraint-based schedule repair for product development projects with time-limited constraints. International Journal of Production Economics 95, 399–414 (2005)

Study on Loop Problem in Opening Database for Chinese Chess Programs

Shi-Jim Yen[1], Tai-Ning Yang[2], Jr-Chang Chen[3], and Shun-Chin Hsu[4]

[1] Department of Computer Science and Information Engineering, National Dong Hwa University, Hualien, Taiwan
sjyen@mail.ndhu.edu.tw
[2] Department of Computer Science, Chinese Culture University, Taipei, Taiwan
tnyang@faculty.pccu.edu.tw
[3] Department of Applied Mathematics, Chung Yuan Christian University, Chung Li, Taiwan
jcchen@cycu.edu.tw
[4] Department of Information Management, Chang Jung Christian University, Tainan, Taiwan
schsu@mail.cju.edu.tw

Abstract. A Chinese chess program systematically constructs a large tree-based opening database by collecting knowledge from chess masters, books and game records in the opening phrase. However, those games with loops are not managed properly in the database. The perpetual situations are not recorded correctly in the database, and therefore the program will play a draw in an advantageous position and a loss in a draw position. This study describes a solution to the loop problem in opening database.

Keywords: heuristic search, computer Chinese chess, opening database, loop problems.

1 Introduction

Chinese chess (Xiang Qi) is one of the most popular board games worldwide, being played by approximately one billion people in China, Taiwan and wherever Chinese have settled. Having a long history, the modern form of Chinese chess was popular during the Southern Song Dynasty (1127AD-1279AD). Chinese chess is a two-player, zero-sum game with complete information. Chinese chess expert knowledge was developed 800 years ago. The world has many excellent human players. The skill of a Chinese chess program can be compared to that of human players. Table 1 shows the space states complexity and the game tree complexity of chess, Chinese chess, Shogi and Go. The space states complexity of Chinese chess was estimated by Allis [1]. The game tree complexity is based on a branching factor of 38 and an average game length of 95 plies [12]. The complexity of other games was estimated by Bouzy and Cazenave [3] and Iida et.al. [6]. The complexity of Chinese chess is between that of chess and

H.G. Okuno and M. Ali (Eds.): IEA/AIE 2007, LNAI 4570, pp. 1118–1126, 2007.

Shogi. Now that Deep Blue has beaten Kasparov, Chinese chess may become the next popular board game at which a program will defeat a top human player. In fact, Chinese chess programs ELP and SHIGA have beaten some 7-dan players in some human tournaments in Taiwan. A program is expected to defeat a top human player before 2012.

Table 1. Space states complexity and game tree complexity of chess, Chinese chess, Shogi and Go

Game	Space states complexity	Game tree complexity
Chess	10^{50}	10^{123}
Chinese Chess	10^{48}	10^{150}
Shogi	10^{71}	10^{226}
Go	10^{160}	10^{400}

The opening phase of Chinese chess refers to the first 8 12 rounds after a game begins. During this phase, the main objective is to occupy better positions, to establish an advantageous position for later combat, and furthermore, to achieve command over the pieces of opponents and thus a strong battle array. Thus, the opening phase is the foundation of the game [12]. How well the opening phase is played will directly and strongly influence the mid-game and endgame.

The current design of the opening phase of Chinese chess is based on an effective and sound opening database system. The database is constructed by gathering games from numerous books and game records, and by extracting and adjusting the abundant master knowledge [4]. Based on the opening database, each move is statistically analyzed, and the optimal move is thus identified. Combined with mid-game programs, the opening database can clearly improve the strength of Chinese chess programs [5]. Certain methods of designing chess programs automatically increase the quality of opening databases [7], take the habitual behaviors of opponents into consideration, and then adopt an appropriate response strategy [10].

In game records of Chinese chess, the same boards frequently appear. Loops due to repetitive boards affect the opening database structure, and create difficulty in gathering statistics about moves. In this study, we develop an efficient data structure and update algorithm to maintain database integrity. This data structure and algorithm solve the problem in gathering statistics about moves in a tree-structured opening database.

The organization of this paper is as follows. Section 2 describes the basic concept of a Chinese Chess opening database. Section 3 discusses the influence of the loop problem. Section 4 gives a data structure for of loop. Section 5 shows how to process loop in the opening database. Three key findings of this paper are given in Section 6. A simple repetition rule of Chinese chess is provided in Appendix A.

2 Opening Database

Computers simulate human thinking in order to get the best move to attack and defend based on the current situation, and create a game tree during the process. When a game tree expands to a specific depth, each leaf node is assigned a score calculated from an evaluation function, and the best move is identified by the mini-max method [9]. Because the main task during the opening phase is to move pieces to advantageous positions, no obvious fighting occurs, and thus the limited difference between the two sides produces a blind spot in the evaluation function. [12]

To overcome this problem, an opening database system was designed using techniques such as framework, tree structure and hash function [4]. Mass good quality games records played by masters from internet are collected and analyzed to retrieve statistical information, including the usage rate and winning rate of each move from each board. The strength of each move can now be compared, and this information can be used as a reference during mid-game play [5].

The architecture of the proposed knowledge-base system has a hash area and an overflow area. The hash function calculates a hash address using move plies and piece positions on board as keys. The address corresponds to a specific slot in the hash area if the slot is available. Otherwise, the board is saved in a slot in the overflow area, and this slot and the specific slot in the hash area are linked.

Each node in the database is assigned a specific board status, which has three types of information - position, statistics and links. The position records the ply and the distribution of all pieces used by a hash function. The statistical information includes winning ratio, usage rate, and the differences among win, draw and lose. The links maintain the connection between the hash and overflow areas, and record all moves but alter the board from its previous to its current status [4].

3 Influence of the Loop Problem

In Chinese chess, a repetition occurs when the same position reappears for the third time. The rules that govern perpetual moves (moves repeated in the same situation) vary among in China, Hong Kong and Taiwan. In this paper, this problem will be discussed based on Asian rules [2]. An English translation of part of the Asian rules can be found in [11]. Forty rules govern perpetual situations in Asian rules, some of which are complex for an amateur player.

Some simplified repetition rules are listed in [8][12]. A repetition is said to have occurred when the same position is repeated on the board for the third time. Sometimes this occurs when both players are making non-attacking moves (perhaps aimless ones), in which case the game is a draw. More commonly a repetition occurs because one side is perpetually attacking (threatening) a specific opponent piece (e.g. the King, but could be almost any piece). Here these perpetually attacking moves will be called forcing, and any the third-time attacking move is "forbidden". Appendix A lists a simple and almost complete summary of repetition rules.

The loop resulting from repetitions deeply influences the way that opening databases operates. While updating scores using the mini-max method or gathering statistics of game information related to the node, the program will get an inaccurate result, or even worse, will run into an infinite loop. Therefore, loops must be fully recorded in the database so that programs can suggest the correct move.

To simplify the process of updating the score using the mini-max method, we delete loops in the opening database in our previous Chinese chess program. When a game contains a loop, the same positions, nodes A and B, are identified; then all nodes between A and B are deleted, and all descendent of B now become those of A. Therefore, before a game is added to the database, all loops in the game are deleted, and the structure of the database becomes a tree without any loop. Although the loop-deletion method simplifies the loop problem, if the program uses scores as a guide in choosing moves, the result will be a draw which actually should be a win, and a loss which actually should be a draw, because loops are not recorded in the database.

4 Data Structure of Loop

To record a loop accurately and completely, a mark is made on each node of the loop with the shortest distance to the leaf. The marked nodes can not have any other child nodes besides those belonging to the loop.

Figure 1 indicates that the node sequence ABCDA exists in the database, in which nodes BCDA form a marked loop, and the two As nodes are repetitive nodes with the same position. If a loop node has a child node whose position is different from all of the loop nodes, then the same board with different plies appears on different nodes. Figure 1 shows that nodes E and G are the child nodes of the two nodes As, respectively. This situation affects the operation of the database in two ways:

First, when updating score using the mini-max method, one node will have two different scores representing the scores of a loop node and that of a non-loop node respectively. The program must design another mechanism to choose between the two different scores. Figure 1 shows that node A chooses the best score based on three scores from child node G (score 60), loop node B (score -20), and loop ABCDA (score 0, the score can not be shown in Figure 2 because it is an infinite loop since both players repeat the same moves.).

Second, the move the opponent chooses will affect the score obtained with mini-max method. An ancestor node in the tree shadows a descendent node such that the nodes with the same position have inconsistent scores. Figure 2 shows that nodes E and G are both child nodes of the two As nodes by playing different moves, and have scores of 100 and 60 respectively. When updating the score, since node B chooses the move to node F, which has a score of -20, the ancestor node A must choose the move to node G which has a score of 60. Hence, although both E and G are child nodes of node A, worse move to node G (score 60) is chosen rather than that to node E (score 100), which is wrong.

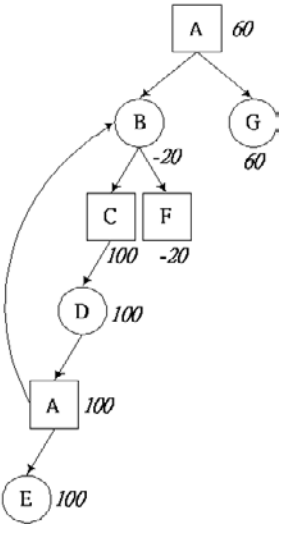

Fig. 1. An example of a loop in the opening database

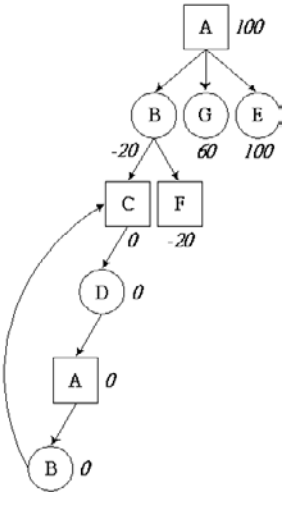

Fig. 2. Solution of loop problem in the example in Fig. 1

In the tree structure of the database system designed here, all loop nodes are stored at the lowest level of the game tree, and child nodes of loop nodes are moved to upper corresponding nodes with identical positions. Figure 2 shows that loop nodes CDAB have no other child node, and the ancestor node A can choose the better move to node E whose score is 100.

In order to make the most of limited time, or achieve a draw when in an inferior situation, a player adopts repetitive plays to repeat among several positions, for

example through circulated checking and freeing. Such games will have loops that are not in the end of a game. To allow all loops to only exist in the lowest level of the database, we adopt the following steps: Before adding a game to the database, we split the game containing loops into multiple games, including a game without the loops, and games whose positions are from the beginning to the loop position and let the loop to be the last moves of the game. After this procedure, these derivative games are added to the database.

5 Implementation

A new game can be added to the database as follows. First, we flip the first move according to the symmetry of the board. Second, we transform the following moves according to the move order relation. Then, we add the game into the hash area of the database if the specific slot is available, or add it to the overflow area if the slot is occupied. Because each node records the relation between the parent nodes and child nodes, the tree structure is maintained. Finally, we update the score of each node with the mini-max method, and gather statistical information on winning ratio, usage rate, and the difference among the frequencies of wins, draws and losses.

If the game being added contains loops, the loops must be stored in the lowest level of the tree structure. First, the loops inside a game must be removed, and the game must be added into the database, as mentioned in section 4.2. Next, the combination of loop nodes must be processed with the nodes existing in the database. This section adopts the method of extending the loop nodes, and then duplicating all the non-loop nodes of the lower level to the upper level. This approach avoids the situation in which the program must choose between loop moves and non-loop moves. Incidentally, if loop nodes are ignored, the database itself is a complete tree structure, making it easy to update scores using the mini-max method. Figure 3 shows three situations about the combination of loop nodes and non-loop nodes.

1. A loop exists in the database, and we want to add a game containing no loops, as shown in Figure 3(a).
2. No loop exist in the database, and we want to add a game containing no loops, as shown in Figure 3(b).
3. A loop exists in the database, and we want to add a game containing a loop, as shown in Figure 3(c).

To maintain the architecture that no loops are within the tree structure, when nodes of a new game intersect with existing loop nodes in the database, the loop nodes must be extended into an independent branch that contains only one child, and the branch must be duplicated to the upper node with the same position as the loop nodes.

Let LOOP represent the set of nodes whose move results in the same board appearing repeatedly. Let loop_head represent the last node in LOOP whose board is the same as that of leaf in the game. If the game is a draw due to

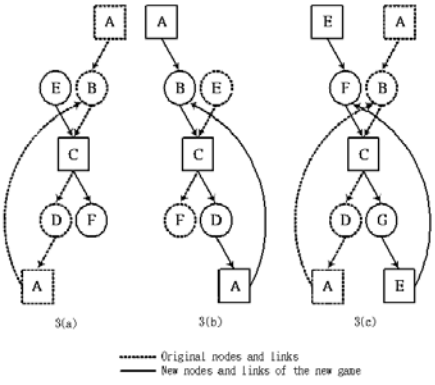

Fig. 3. Three situations about the combination of loop nodes and non-loop node

repetitive boards, and if the loop nodes exist in the database, we take the following steps. First, nodes in database downward whose positions are the same as those of loop nodes recursively are found, and these nodes then are joined to the LOOP set, with the last one being set as a new leaf. Then, the intersect node upwards from which an independent loop must be extended is identified. Finally, all nodes between loop_head and the intersect node are duplicated to those below the leaf node. After an extension is done, if the extended nodes still collide with another node in the database, the above procedure is repeated. Ultimately, only one branch of the loop exists at the bottom of the game tree.

After an independent branch of the game is extended, the situation in which the game nodes collide with the loop nodes in the database must be extended. Besides, let the upper loop nodes reserve child nodes and statistic information more completely, making it necessary to duplicate all descendent nodes of a lower node to the upper node with the same position. As this point, the nodes are scanned from leaf to root, and loop nodes are encountered before non-loop nodes, and each node is processed depending on whether it is a loop node or not, as shown below. Loop nodes are processed in the first step. First, because adding a new game result in the loop nodes (say LOOP_A) which contained in the database no longer form a complete and independent branch, LOOP_A must be extended.

Loop nodes (say LOOP_B) of the new game are then extended to the child nodes of the corresponding upper loop node in LOOP_A. Finally, all child nodes of the last extended node in LOOP_A are duplicated to the child nodes of the corresponding upper loop node in LOOP_B. Non-loop nodes are encountered in the second step. Because only non-loop nodes of the new game collide with the loop nodes in the database, all that have to do is to duplicate the nodes of the new game to the child nodes of the uppermost loop node after extending the spoiled structure of the loop nodes.

6 Conclusions

This study offers a method of managing the loop problem created by playing repetitive moves so as to cause the same board to appear reiteratively in Chinese chess opening database. This study reaches three key findings, as following.

1. If loop nodes are ignored, the database is a complete tree structure, and is compatible with the previous system we developed.
2. While updating statistical information using the mini-max method, this method does not trap into an infinite loop because no loop nodes exist inside the game tree.
3. Nodes with the same board in a lower level are moved to an upper level, so complete information is stored in upper level nodes, and the mid-game program can rapidly retrieve the optimum move.

The opening database stores loops in the leaf of the database such that repetitive boards could be completely contained and correct scores can be obtained using the mini-max method. The program does not result in draws that should be wins, or in losses that should be draws.

References

1. Allis, L.V.: Searching for Solutions in Games and Artificial Intelligence. Ph.D. Thesis, University of Limburg, Maastricht, The Netherlands (1994) ISBN 90-9007488-0
2. Asian Xiangqi Federation (in Chinese) (2003) `http://tysung.cjb.net/xq/index.html`
3. Bouzy, B., Cazenave, T.: Computer Go: An AI oriented survey. Artificial Intelligence 132, 39–103 (2001)
4. Huang, S.L.: Strategies of Chinese Chess Opening. World Culture Inc. Press (1991)
5. Hsu, S.C., Tsao, K.M.: Design and Implementation of an Opening Game Knowledge-Base System for Computer Chinese Chess (in Chinese). Bulletin of the College of Engineering, N.T.U., (53), 75–86 (1988)
6. Iida, H., Sakut, M., Rollason, J.: Computer Shogi. Artificial Intelligence 134, 121–144 (2002)
7. Lincke, T.R.: Strategies for the Automatic Construction of Opening Books. In: Marsland, T., Frank, I. (eds.) CG 2001. LNCS, vol. 2063, pp. 74–86. Springer, Heidelberg (2002)
8. Marsland, T.A.: A Review of Game-Tree Pruning. ICCA Journal 9(1), 3–19 (1986)
9. Shannon, C.E.: Programming a Computer for Playing Chess. Philosophical Magazine 41, 256–257 (1950)
10. Walczak, S.: Improving Opening Book Performance through Modeling of Chess Opponents. In: ACM Conference on Computer Science, 53–57 (1996)
11. Wu, E.: English Translation Drafts of Asian Rules (2002) `http://www.clubxiangqi.com/rules/`
12. Yen, S.J., Chen, J.C., Yang, T.N., Hsu, S.C.: Computer Chinese Chess. ICGA Journal 27(1), 3–18 (2004)

Appendix A: A Simple Repetition Rule of Chinese Chess

The following is a simple and almost complete summary of repetition rules as they pertain to forcing moves.

1. If only one side attempts to repeat a position with a forbidden move, then they are judged to have lost (i.e., a forbidden move is illegal).
2. If both sides repeat the position using forcing moves, the game is ruled a draw at the third repetition.
3. If both sides repeat non-forcing (non-threatening) moves, the game is ruled a draw at the third repetition.
4. Sometimes a move can be judged in two ways (as, for example, being both a threat move and a threat to checkmate by continual checks in following moves), the move that is forbidden is selected.
5. A side can ask the referee to adjudicate a draw if no piece has been taken, and no more than ten checks have been made by the opponent within the last 40 moves.

Forbidden forcing moves are defined as follows.

1. Perpetual checks on the King are forbidden.
2. Perpetual threats on an unprotected piece (except on a Pawn that has not crossed the River) are forbidden.
3. Perpetual threats on a Rook by Cannons and/or Horses are forbidden.

Job Shop Scheduling Optimization Using Multi-modal Immune Algorithm

Guan-Chun Luh and Chung-Huei Chueh

Department of Mechanical Engineering, Tatung University, Taipei, Taiwan, R.O.C.
gluh@ttu.edu.tw

Abstract. A multi-modal immune algorithm is utilized for finding optimal solutions to job-shop scheduling problem emulating the features of a biological immune system. Inter-relationships within the algorithm resemble antibody molecule structure, antibody-antigen relationships in terms of specificity, clonal proliferation, germinal center, and the memory characteristics of adaptive immune responses. In addition, Gene fragment recombination and several antibody diversification schemes were incorporated into the algorithm in order to improve the balance between exploitation and exploration. Moreover, niche scheme is employed to discover multi-modal solutions. Numerous well-studied benchmark examples were utilized to evaluate the effectiveness of the proposed approach.

Keywords: multi-modal immune algorithm, job-shop scheduling problem, clonal proliferation, Gene fragment recombination, antibody diversification.

1 Introduction

Scheduling problems exist almost ubiquitously in real-world applications including distribution, transportation, management, and manufacturing, especially in the industrial engineering world. Many scheduling problems on manufacturing industries are quite complex and very difficult to solve using conventional optimization techniques. It has been the subject of extensive research and captured the interest of researchers from different research communities such as operation research, management science, and industrial engineering since the early 1950s. Its main focus is concerned with the allocation of finite resources to tasks to improve the resource utilization. It is well known that the job-shop scheduling problem (JSSP) is one of the most complicated and typical production scheduling problems. The purpose is to improve the production efficiency and reduce the processing duration to gain profits.

The JSSP may be described as follows: given n jobs, each composed of several operations that must be processed on m machines. Each operation uses one of the m machines with a deterministic processing time and each machine can process at most one operation at a time. Once an operation initiates processing on a given machine it must complete processing on that machine without interruption. Each job consists of a specific set of operations, which have to be processed according to a given technical precedence order. The operation sequences on the machines are usually scheduled to

H.G. Okuno and M. Ali (Eds.): IEA/AIE 2007, LNAI 4570, pp. 1127–1137, 2007.

minimize makespan, the total time required to complete all jobs. The total number of all possible schedules including feasible and infeasible solutions is $(n!)^m$. A comprehensive survey of job shop scheduling techniques can be found in [1]. In the last decade, numerous biological-inspired methods have been employed to solve practical size JSSP. Among these include simulated annealing [2], tabu search [3], ant colony optimization [4], genetic algorithms [5], and immune algorithm, and [6-10].

Genetic algorithms (GAs), powerful tools based on biological evolution mechanisms and natural selection theory, have received considerable attention as the optimal design efforts. Methods based on GAs have become a popular and effective way for solving large-scale combinational optimization problems, including job shop scheduling. GAs are considered powerful in terms of global optimization, nevertheless, they have several drawbacks regarding local searches. Tazawa *et al*. [11] has identified two of them as lack of local search ability, and premature convergence. Consequently, a number of researches utilized biological immunity-based optimization approaches [12, 13] to overcome these two drawbacks implicit in genetic algorithms. Xu and Li [6] combined the immune theory and the GAs for solving theJSSP. Similarly, Miyahita [7] applied modified immune algorithm for the JSSP and showed that the calculate time was less than employing GAs. Coello *et al.* [8], Chandrasekaran *et al.* [9] and Zhou *et al*. [10] applied artificial immune system to the JSSP. Two main principles were included in these immune algorithms: clonal proliferation and affinity maturation. Obviously, their immune algorithms did not utilize the whole feature of the biology immune system. To highlight the significant features and completeness of the immune system, a multi-modal immune algorithm (MMIA) [13] is adopted in this study to solve JSSP. Inter-relationships within the algorithm resemble antibody molecule structure, antibody-antigen relationships in terms of specificity, clonal proliferation, germinal center, and the memory characteristics of adaptive immune responses. In addition, Gene fragment recombination and several antibody diversification schemes were incorporated into the algorithm. Moreover, it is intuitive that there exist many different operations with equal makespan as the number of jobs and machines increase. This suggests that with the increase in sizes of the job shop, the resulting JSSP becomes to have multiple solutions and hence a niche scheme is essential to find all the possible solutions.

2 Biological Immune System

The immune system protects living bodies from the invading of foreign substances, called antigens, including viruses, bacteria, and other parasites. Lymphocytes float freely in blood and lymph nodes, and patrol everywhere for antigens, then gradually drift back into the lymphatic system, to begin the cycle all over again. There are mainly two types of lymphocytes, namely B-cells and T-cells, which play an important role in immunities. The former takes part in the humoral immunity that secretes antibodies by clonal proliferation, and the latter takes part in cell mediated immunity. One class of T-cells, called Killer T-cell, destroys the infected cell whenever they recognize the infection. The other class which triggers clonal expansion and stimulate/suppress antibody formation is called Helper T-cell.

The basic unit of an antibody molecule is composed of four polypeptide chains: two identical light chains and two identical heavy chains. The grouping of two different types of gene fragments constructs the light chains and the combination of three different types of gene fragments forms the heavy chains. Additionally, antibody gene fragments could move and rearrange themselves within the genome (inherited DNA) of a differentiating cell. The set of rearranged gene fragments is then transcribed and translated into a complete heavy or light chain. Consequently, the gene fragments required to produce an antibody are encoded in a set of antibody library named germ-line DNA library, each library containing a set of components or fragments of antibodies. An antibody's paratope can bind with an antigen's epitope according to their affinity value. In terms of affinities, the immune system self-regulates the production of antibodies and diverse antibodies.

After binding to antibody receptors, an antigen stimulates the B cell to proliferate and mature into plasma cells and memory antibodies through the process known as clonal proliferation or clonal selection. In clonal proliferation, random changes (e.g. hypermutation) are introduced to the variable region genes, and occasionally one such change will lead to an increase in the affinity of the antibody. These higher-affinity matured cells are then selected to enter the pool of memory cells. The antibody is not only diversified through a hypermutation process but mechanisms whereby rare B-cells with high affinity mutant receptors can be selected to dominate the immune response (donor of B-cell). On the contrary, those cells with low affinity receptors, or the self-reaction cells, must be efficiently eliminated. Three major categories are reported to increase the diversity of antibodies.

3 Job Shop Scheduling Using MMIA

Several different representations have been employed for chromosome-based optimization for JSSP [14-16]. This study utilizes operation-based representation [17] for JSSP in that it guarantees feasible solutions although it is not a one-to-one mapping between the coding space and solution space. Corresponding to the JSSP, the antigen and antibodies serve as objective and associated solutions (*i.e.* schedules) in a computational model and are expressed as follows:

$$\begin{aligned} Ab_i \equiv \mathbf{x}_i &= \text{possible schedules},\ i = 1,2,..., N_{Ab} \\ AgAb_i &\equiv f(\mathbf{x}_i) \end{aligned} \tag{1}$$

where Ab_i (or $\mathbf{x}_i$) indicates the *ith* antibody/schedule while $AgAb_i$ indicates the affinity between an *ith* antibody and antigen/objective, N_{Ab} is the number of antibodies. The antibody continuously evolves until a match is found with the specific antigen. The whole procedure is described below:

[**Step 1**] ***Random initialization of antibody population***
Similar to the genetic algorithms, the initial integer-string antibody population is randomly generated. An operation-based representation is used in this study. This representation names all operations for a job with the same number and then interprets it according to the order of occurrence in the given antibody. Consequently, an antibody contains $n \times m$ genes for an n jobs and m machines problem. Each job appears

in the antibody *m* times, and each repeating gene/integer number does not indicate a concrete operation of a job but refers to a unique operation.

[Step 2] ***Gene classification and makespan computation***
Imitating the biological immune system, each locus of antibody/schedule is classified into two kinds of genes: heavy-chain gene (**H**) and light-chain gene (**L**) according to a predefined light/heavy chain-length ratio γ and a job/gene order of occurrence appearing in the identical machine. For an *n*-job *m*-machine problem, the number of light-chain genes n_L in each antibody is calculated using equation $n_L = \textbf{\textit{round}}(\gamma \times n)$, where operator "***round***" means rounded to integer. In addition, the components of light chains are assigned to the latest n_L jobs appearing in the same machine.

A 3-job and 3-machine scheduling problem is presented here to explain how the encoding scheme operates. Table 1 indicates the normal format showing the processing time and the routing for these three jobs on three machines, respectively. Fig. 1 illustrates the antibody representation and Gantt chart of an antibody [3 1 2 2 1 3 1 2 3], where numbers 1, 2, and 3 stand for jobs 1, 2, and 3, respectively. Each job appears exactly three times in an antibody since it needs three operations/machines. Corresponding to the machine sequence and processing time given in Table 1, the order of machine processing for job 1 is 1-2-3 while 1-3-2 and 2-1-3 are machine orders for job 2 and job 3, respectively. Consequently, the related machine list and time list for this schedule are [2 1 1 3 2 1 3 2 3] and [3 3 1 5 3 2 2 3 3] as Fig. 1 shown. If the light/heavy chain-length ratio γ is set to 0.3, then the number of light-chain genes n_L equals to 1 since n_L=***round***(0.3×3)=1. Consequently, the genes (3, 2, 3) located at the last locus of each machine are assigned to light chain as the black blocks illustrated in Fig. 5. As a result, the structural representation of the antibody

Table 1. Processing time t_{ij} and job routing *k* of a 3×3 scheduling data

t_{ij}	O_1	O_2	O_3
J_1	3	3	2
J_2	1	5	3
J_3	3	2	3

k	O_1	O_2	O_3
J_1	1	2	3
J_2	1	3	2
J_3	2	1	3

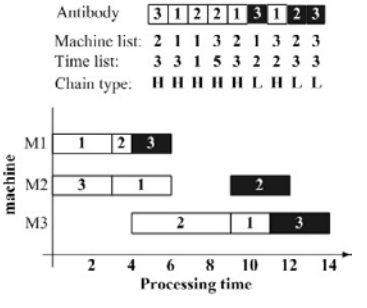

Fig. 1. Antibody representation and corresponding schedule (Gantt chart)

[3 1 2 2 1 3 1 2 3] is defined as [H H H H H L H L L] since the light-chain genes (3, 2, 3) are located at the 6th, 8th, and 9th locus of the antibody, respectively. Finally, the makespan of this antibody/operation is 14 as the Gantt chart demonstrated.

[Step 3] ***Calculating antibody-to-antigen affinity***

The antibody-to-antigen affinity value ($AgAb_i$) is utilized to illustrate the combinatorial intensity between antigen/objective and the *ith* antibody/schedule and the resemblance among antibodies expressed as follows:

$$AgAb_i = \frac{obj_i}{SC_i} \text{ with } obj_i = \frac{\min\{makespan_i \mid i = 1, 2, \cdots, N_{Ab}\}}{makespan_i} \tag{2}$$

where $makespan_i$ indicates the makespan value of the *i*th antibody/schedule and obj_i is its associated normalized value. In addition, similar to the sharing or niching schemes implemented in multi-modal genetic algorithms, the relationship among antibodies is evaluated according to the similarity count SC_i expressed as:

$$SC_i = \frac{\sum_{j=1}^{N_{Ab}} \text{count}_{ij}}{N_{Ab}}, \qquad i = 1,2,\cdots,N_{Ab}; \quad j = 1,2,\cdots,N_{Ab} \tag{3}$$

with

$$\text{count}_{ij} = \frac{\sum_{k}^{n \cdot m} Ab_{ij}^{k}}{n \cdot m} \tag{4}$$

where the similarity count at the *k*th locus among antibodies Ab_i and Ab_j is

$$Ab_{ij}^{k} = \begin{cases} 1 & \text{if the jobs at the } k \text{ locus of } Ab_i \text{ and } Ab_j \text{ are identical} \\ 0 & \text{else} \end{cases} \tag{5}$$

A higher affinity value means that an antibody has a higher activation with an antigen and a lower similarity with the other antibodies. Therefore, the higher the affinity value, the higher the probability that the antibody may be selected as the donor to enter the germ-line DNA library for gene fragment rearrangement. After affinity values of all antibodies are calculated, the best (highest affinity) antibody will be placed into the germinal center for clonal proliferation with the remaining antibodies proceeding to Step 5 awaiting donor selection.

[Step 4] ***Clonal proliferation of the most matched antibody***

In biological immune systems, only antibodies stimulated by antigens enter the germinal center. In the proposed MMIA, the most-matched (maximum affinity value) antibody derived from the earlier step is chosen for hypermutation with a user-defined rate and proliferation number. To prevent excessive discrepancies, hypermutation only takes place in the locus of light-chain genes (**L**). Note that hypermutation is a kind of local search operator since it only occurs in the light-chain genes. To avoid yielding illegal or infeasible schedule after hypermutation operation, the associated gene with job *j* of the same machine has to mutate to job *i* at the same time (*i.e.* reciprocal exchange within the same machine number) when a light-chain gene of an antibody mutates from job *i* to job *j*.

After the hypermutation process, mature antibodies that have a greater affinity than un-proliferated antibody are differentiated into plasma and memory antibodies preserved and updated in the memory pool. Further, the resulting bad antibodies are deleted as immature antibodies imitating the cell apoptosis process in natural immune system. Resulting plasma antibodies combined with the remaining antibodies derived from Step 3 are then proceed to next step for donor antibody selection.

As to the memory pool, only the most diverse antibodies with high affinity survive. On the other hand, those antibodies with low affinity and high similarity will be removed from the memory pool (cell apoptosis). In this step, diversity is evaluated by checking the similarity count for each memory antibody. In addition, a part of memory antibodies are induced into the germ-line DNA library (as per Step 6) according to a user-defined inducing rate.

[Step 5] ***Tournament selection for donor antibodies***

Emulating to the construction of germ-line DNA libraries in biological immune system, this study uses a tournament selection scheme to select donor antibodies exhibiting higher affinity values to assemble germ-line DNA libraries. According to the predefined tournament size, antibodies/schedules are chosen randomly for competition with the surviving winner being turning into a donor antibody.

[Step 6] ***Germ-line DNA library construction***

As described in the previous section, the genetic material used to produce antibody molecules is stored in germ-line DNA libraries, each one containing a fragment of an antibody gene. Components from the memory antibodies and the donor antibodies construct the germ-line DNA library.

[Step 7] ***Gene fragment rearrangement***

In natural immune system, antibodies are produced through a random recombination of selected fragments from a germ-line DNA library. In MMIA, new antibodies/schedules are created via gene fragments rearrangement process. For simplicity, a 3×3 scheduling example is employed to explain the procedure as Fig. 2 illustrates.

First, a seed antibody is chosen randomly form the gene library. Then its genes/jobs of the 1^{st} machine located at the 2^{nd}, 3^{rd}, and 4^{th} loci are replaced by the associated genes/jobs (1^{st}-, 3^{rd}-, and 6^{th}-bit) of the donor antibody randomly selected from the gene library. Next, another donor antibody is chosen randomly and its genes/jobs belonging to the 2^{nd} machine take place the corresponding components of the newly generated seed antibody. Similar processes are repeated to create new seed antibody until the genes/jobs of all machines are rearranged.

[Step 8] ***Antibody diversification***

Matching a large variety of antigens requires an equal level of diversity in antibody type. In the proposed MMIA, this was achieved by mimicking the following six diversification mechanisms found in biological immune systems: *Somatic point mutation* (Fig. 3), *Somatic recombination* (Fig. 4), *Gene conversion* (Fig. 5), *gene inversion* (Fig. 6), and *gene shift* (Fig. 7), *Nucleotide addition* (Fig. 8).

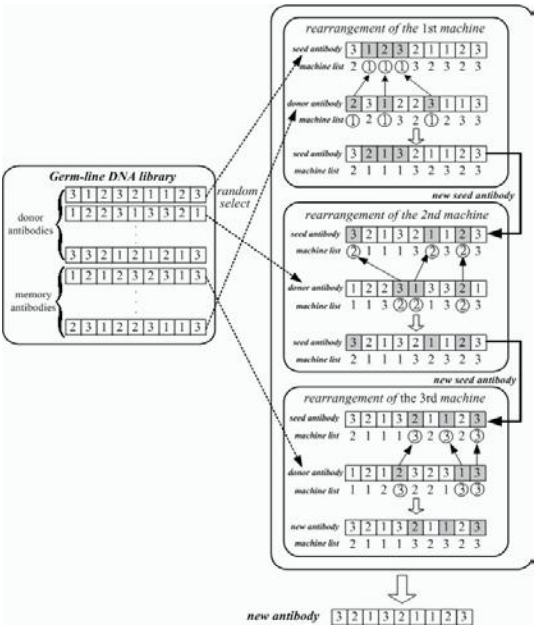

Fig. 2. Illustration of fragmental rearrangement

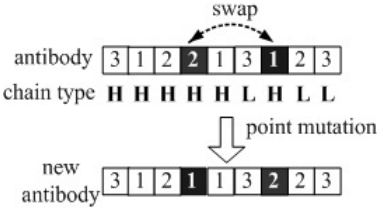

Fig. 3. Somatic point mutation illustration

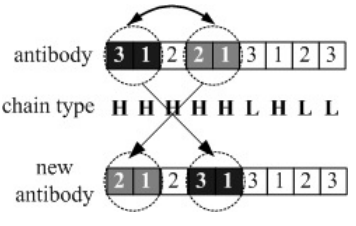

Fig. 4. Somatic recombination illustration

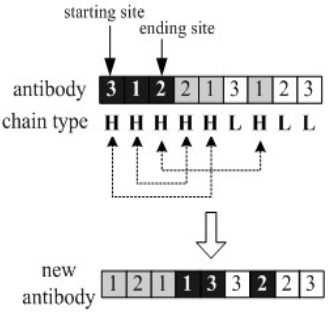

Fig. 5. Gene conversion

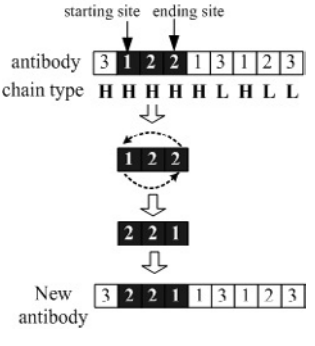

Fig. 6. Gene inversion

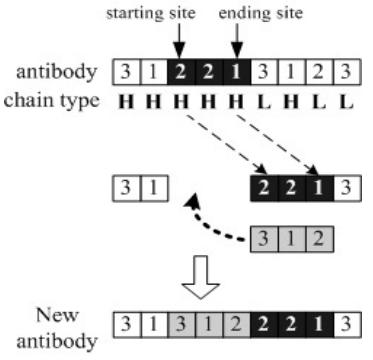

Fig. 7. Gene shift

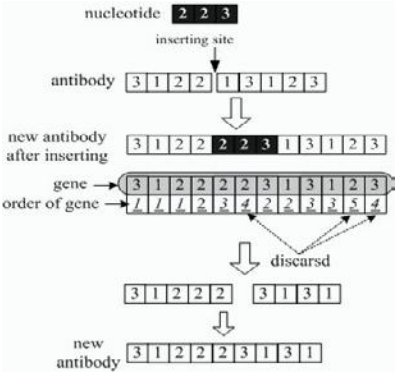

Fig. 8. Nucleotide addition illustration

It should be noted that the six diversification mechanisms described in [Step 8] are selected to implement randomly in the antibody diversity process.

[Step 9] ***Stopping criterion***
The whole process will stop when the generation equals to a pre-defined number. Otherwise the process reverts to [Step 2] for iteration. In the final stage, the best and most diverse solutions are stored in the memory pool.

4 Computation Results and Discussion

For carrying out the necessary computations and evaluating the performance of the proposed immune algorithm, the program for computing JSSP was developed using C++ language. Table 2 lists the associated parameters adopted in the proposed MMIA for scheduling optimization. These parameters were determined through numerical experiments after multiple simulation runs.

Table 2. Immune algorithm parameters for solving JSSP

Instance size ($n \times m$)	6x6	10x5	15x5	20x5	30x10
Iteration number	100			500	1000
Antibody population size	$n \times m$			$2 \times (n \times m)$	
Antibody length	36	50	75	100	200
Diversity probability (somatic point mutation)	0.1			0.1	0.1
Hypermutation rate	0.5			0.5	0.5
Light/heavy chain-length ratio	6:4			5:5	5:5
Number of proliferation	6			8	10
Inducing ratio	0.1			0.2	0.2
Bit number in Gene shift	2-bit			2-bit	
Bit number of nucleotide	random number between 1 to n				
Tournament size	$(n \times m)/10$			$(n \times m)/5$	

Eighteen benchmark instances from two classes of standard JSSP test problems were employed to illustrate the effectiveness of the proposed algorithm. One problem prefixed by FT is from Fisher & Thompson [17] while the other 17 problems prefixed by LA are from Lawrence [18]. Problem dimensions vary from 6 to 30 jobs and 5 to 10 machines. All test instances can be downloaded from the OR-Library at http://mscmga.ms.ic.ac.uk. Table 3 lists, for each test problem, its dimension (number of jobs and number of machines), name, the best-known solution, and the computation results found by MMIA. It shows that the proposed MMIA discovers optimal and near-optimal solutions (LA19 and LA21) in all instances. As expected, a set of multiple solutions derived for each benchmark instance, respectively. Table 4 lists the schedules derived for the case FT06, respectively. It should be noted that the last three optimal schedules are identical to the results derived by separate researchers in [9, 19-21]. The results show that MMIA is an effective and efficient algorithm for solving JSSP.

Table 3. JSSP instances and the computation results derived using MMIA

Instance	Size	Best known solution	MMIA	Instance	Size	Best known solution	MMIA
FT06	6x6	55	55	LA01	10x5	666	666
LA02	10x5	655	655	LA03	10x5	597	597
LA04	10x5	590	590	LA05	10x5	593	593
LA06	15x5	926	926	LA07	15x5	890	890
LA08	15x5	863	863	LA09	15x5	951	951
LA10	15x5	958	958	LA11	20x5	1222	1222
LA13	20x5	1150	1150	LA15	20x5	1207	1207
LA17	10x10	784	784	LA19	10x10	842	**857**
LA21	15x10	1046	**1088**	LA31	30x10	1784	1784

Table 4. Multiple optimal schedules derived for FT06 problem

Multiple optimal schedules (5 solutions)
[3 2 3 1 4 6 2 3 6 2 5 6 4 3 3 2 4 5 1 4 5 6 4 1 2 1 3 5 1 5 4 2 5 6 1 6]
[3 2 3 1 4 6 2 3 6 6 1 2 5 4 3 5 3 2 4 5 1 1 5 6 4 1 2 2 5 3 4 5 4 6 1 6]
[3 2 3 1 4 6 2 3 6 6 4 2 5 5 3 2 4 5 1 1 5 6 4 1 2 1 3 2 5 3 4 5 4 6 1 6]
[3 2 3 1 4 6 2 3 6 6 4 2 5 5 3 2 4 5 1 1 1 6 4 1 2 5 3 2 5 3 4 5 4 6 1 6]
[3 2 3 1 4 6 2 3 6 6 4 2 5 5 1 2 4 5 3 1 1 6 4 1 2 5 3 2 5 4 3 5 4 6 1 6]

5 Conclusion

In this study, a novel concept for handling multi-modal job-shop scheduling optimization has been presented by using an immune algorithm to imitate the features of a biological immune system. Operation-based representation is adopted to guarantee feasible schedules and the goal is to minimize the makespan of a scheduling. The exploration and exploitation of solutions within a search space are realized through the antibody molecule structure, integration of clonal proliferation, germ-line gene library, gene fragment rearrangement, and memory antibodies, further

assisted by six diversification schemes. The proposed methodology enhances accuracy and diversity via the procedures of clonal proliferation and schemata recombination implemented through the process of gene fragment rearrangement. Also, niche antibody is utilized to find multiple solutions. The computation results of the 18 benchmark instances demonstrate the effectiveness of the proposed immune algorithm. The capability of discovering multiple schedules illustrates the flexibility and diversity of the proposed MMIA.

References

1. Jain, A.S., Meeran, S.: A State-of-the-Art Review of Job-Shop Scheduling Techniques. European Journal of Operations Research 113, 390–434 (1999)
2. Steinhöfel, K., Albrecht, A., Wong, C.K.: Two Simulated Annealing-Based Heuristics for the Job Shop Scheduling Problem. European Journal of Operational Research 118, 524–548 (1999)
3. Ponnambalam, S.G., Aravindan, P., Rajesh, S.V.: A Tabu Search Algorithm for Job Shop Scheduling. The International Journal of Advanced Manufacturing Technology 16, 765–771 (2000)
4. Blum, C.: An Ant Colony Optimization Algorithm to Tackle Shop Scheduling Problems. Technical Report TR/IRIDIA/2003-01, IRIDIA, Université Libre de Bruxelles, Belgium
5. Wang, L., Zheng, D.-Z.: An Effective Hybrid Optimization Strategy for Job-Shop Scheduling Problems. Computers & Operations Research 28, 585–596 (2001)
6. Xu, X.-D., Li, C.-X.: Research on Immune Genetic Algorithm for Solving the Job-Shop Scheduling Problem. International Journal Advanced Manufacturing Technology DOI 10.1007/s00170-006-0652-x
7. Miyahita, M.: An application of immune algorithms for job-shop scheduling problems. In: Proceedings of the 5th IEEE International Symposium on Assembly and Task Planning, Besancon, France, pp. 146–150 (2003)
8. Coello Coello, C.A., Rivera, D.C., Cortés, N.C.: Use of Artificial Immune System for Job Shop Scheduling. In: Timmis, J., Bentley, P.J., Hart, E. (eds.) ICARIS 2003. LNCS, vol. 2787, pp. 1–10. Springer, Heidelberg (2003)
9. Chandrasekaran, M., Asokan, P., Kumanan, S., Balamurgan, T., Nickolas, S.: Solving Job Shop Scheduling Problems Using Artificial Immune System. International Journal Advanced Manufacturing Technology 31, 580–593 (2006)
10. Zhou, Y., Li, B., Yang, J.: Study on Job Shop Scheduling with Sequence-Dependent Setup Times Using Biological Immune Algorithm. International Journal Advanced Manufacturing Technology 30, 105–111 (2006)
11. Tazawa, I., Koakutsu, S., Hirata, H.: An Immunity Based Genetic Algorithm and its Application to the VLSI Floorplan Design Problem. In: Proceedings of 1996 IEEE International Conference on Evolutionary Computation, pp. 417–421 (1996)
12. Luh, G.-C., Chueh, C.-H., Liu, W-W.: MOIA: Multi-objective immune algorithm. Engineering Optimization. 35, 143–164 (2003)
13. Luh, G.-C., Chueh, C.-H.: Multi-Modal Topological Optimization of Structure Using Immune Algorithm. Computer Methods in Applied Mechanics and Engineering 193, 4035–4055 (2004)
14. Park, L.-J., Park, C.H.: Genetic algorithm for job shop scheduling problems based on two representational schemes. Electronics Letters 31, 2051–2053 (1995)

15. Gonçalves, J.F., de Magalhães Mendes, J.J., Resende, M.G.C.: A Hybrid Genetic Algorithm for the Job Shop Scheduling Problem. Technical Report, TD-5EAL6J. AT&T Labs (2002)
16. Yamada, T., Nakano, R.: Genetic algorithms for job-shop scheduling problems. In: Proceedings of Modern Heuristic for Decision Support, London, UK, pp. 67–81 (1997)
17. Fisher, H., Thompson, G.L.: Probabilistic Learning Combinations of Local Job-Shop Scheduling Rules. In: Muth, J.F., Thompson, G.L. (eds.) Industrial Scheduling, pp. 225–251. Prentice-Hall, Englewood (1963)
18. Lawrence, S.: Resource constrained project scheduling: an experimental investigation of heuristic scheduling techniques. Technical Report, Carnegie Mellon University, Pittsburgh (1984)
19. Ventresca, M., Ombuki, B.M.: Meta-heuristics for the job shop scheduling problem. Technical report, CS-03-12. Department of Computer Science, Brock University (2003)
20. Yang, S., Wang, D.: A new adaptive neural network and heuristics hybrid approach for job-shop scheduling. Computers & Operations Research 28, 955–971 (2001)
21. Yu, H., Liang, W.: Neural network and genetic algorithm-based hybrid approach to expanded job-shop scheduling. Computers & Industrial Engineering 39, 337–356 (2001)

Simulated Annealing Algorithm for Solving Network Expanded Problem in Wireless ATM Network

Der-Rong Din*

Department of Computer Science and Information Engineering,
National ChangHua University of Education, Taiwan, R.O.C.
deron@cc.ncue.edu.tw

Abstract. In this paper, the *network expanded problem* (NEP) which optimally assigns new adding and splitting cells in *PCS* (Personal Communication Service) network to switches in an *ATM* (Asynchronous Transfer Mode) network is studied. In NEP, the locations of cells (or Base Stations, BSs) in PCS network are fixed and known, but new switches should be installed to ATM network and the topology of the backbone network may be changed. Given some potential sites of new switches, the problem is to determine how many switches should be added to the backbone network, the locations of new switches, the topology of the new backbone network, and the assignments of new adding and splitting cells in the PCS to switches of the new ATM backbone network in an optimal manner. The goal is to do the expansion in an attempt to minimize the total communication cost under budget and capacity constraints. The NEP is modelled as a complex integer programming problem. Since finding an optimal solution to this problem is Impractical. A simulated annealing (SA) algorithm is proposed to solve this problem. In the proposed SA, several heuristics are encoded into the perturbation to generate good solutions. Experimental results indicate that the proposed simulated annealing algorithm can get better performance than heuristic algorithm.

1 Introduction

The rapid worldwide growth of digital wireless communication services motivate a new generation of mobile switching networks (such as *wireless ATM*[1]) to serve as infrastructure for such services. In the architecture which based on wireless ATM presented in [1], the base stations (BSs or *cells*) were directly connected to the ATM switches. In the process of designing PCS (Personal Communication Service) network, first, the telephone company determined the global service area(GSA) and divided the GSA into several smaller coverage areas. For each area, a BS was established and connected to a switch of the backbone network to

* This work was supported in part by National Science Council (NSC) of R.O.C. under Grant NSC-95-2221-E-018-012.

H.G. Okuno and M. Ali (Eds.): IEA/AIE 2007, LNAI 4570, pp. 1138–1147, 2007.

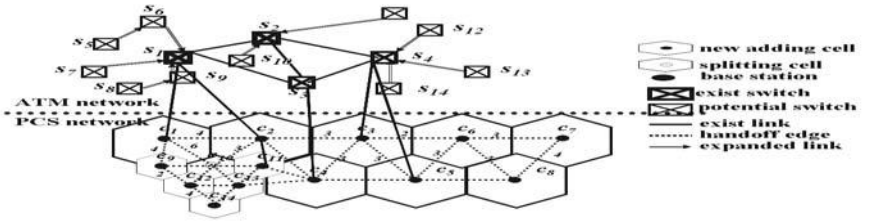

Fig. 1. Example of the network expanded problem in the two layers wireless ATM network

form a two-level wireless ATM network. This topology may be out of date since more users may joint and use the PCS. Some areas not been covered may have users needed to be served. The service demands of some areas may increase and exceed the capacities provided by the BSs and switches. Though, the wireless ATM system should be expanded so that the PCS can provide better quality of services to users. Two methods can be used to expand the capacities of system: (1) adding new cells to the wireless ATM network so that those non-covered areas can be covered by new cells; (2) reducing the size of the cell so that the capacity of the system can be increased. In practice, this can be achieved by using *cell splitting*[2] process. The cell splitting process establishes new BSs at specific points in the PCS and reduces the cell size by a factor of 2 (or more).

For the given two-level wireless ATM network, cells in PCS are divided into two sets. One is the set of cells which are built originally and assigned to fixed switches on the ATM network. The other is the set of cells which are newly added or established by performing the cell splitting process. Moreover, the locations of all cells in PCS network are fixed and known, but the number of switches in ATM network may be increased. Given some potential sites of new switches, the capacity of the switch, and the designing budget, the problem is to determine the number of switches should be added to the backbone network, the locations of the new switches, the connections between the new switches and original backbone network, and the assignment of new and splitting cells in the PCS to switches in an optimal manner. The goal is to do the expansion in an attempt to minimize the objective cost under budget and capacity constraints.

For the *cell assignment problem (CAP)*, Merchant and Sengupta [3] considered the CAP problem. In [4,5], this model of CAP was extended. Moreover, in [6], the *extended cell assignment problem (ECAP)* has been investigated and formulated. In ECAP, the new adding and the splitting cells were assigned to the switches of the ATM network so that the objective cost can be minimized. In ECAP, the number of new and splitting cells were not greater than the remaining capacities provided by the original ATM network. The objective cost considered in this paper has two components: one is the LU (location update or handoff) cost that involve two switches, and the other is the cost of *cabling* (or *trucking*) [3,4,5,6,7]. Assume that the LU costs of intra-switch handoffs involving only one switch are negligible. In this paper, each new or splitting cell is to be connected to only one

switch. The budget constraint is used to constrain the sum of following costs: (1) the sum of the switch setup cost, (2) the backbone link setup cost between two switches, and (3) the local link setup cost between cells and switches.

In this paper, a more complex problem is considered. Following the objective function formulated in [3,4,5,6,7], new cells and new switches should be introduced into the two-level network. In this paper, the locations of new switches, the connections between switches, and the assignments of new and splitting cells should be determined so that the objective cost can be minimized under budget and capacity constraints. This problem is denoted as *network expanded problem* (NEP) in wireless ATM environment. Obviously, finding an optimal solution for it is impractical due to exponential growth in execution time. *Simulated annealing* (*SA*) is a stochastic computational technique derived from statistical mechanics for finding near globally-minimum-cost solutions to large optimization problems. In this paper, a simulated annealing algorithm is developed to find an approximate solution of the NEP problem.

2 Problem Formulation

For the backbone network, assume that: (1) each cell is connected to a switch through a *local link*, (2) the switches are interconnected with a specified topology through *backbone links*, (3) the number of cells can be handled by a new switch cannot exceed CAP, (4) at most one switch can be installed at a given potential site, (5) all links of the current backbone network are kept in place, (6) a switch site in the current network is also a switch site in the expanded network, and (7) the backbone network topologies are preserved in the expanded backbone network. Moreover, assume the information described below are fixed and known: (1) the location of the new cells and the handoff frequency between cells, (2) the potential switch sites, (3) the setup cost of switch at a particular site, (4) the local link setup cost between cells and switches, and (5) the backbone link setup cost between switches. The goal is to find the minimum-cost expanded network subject to all of the above assumption, facts and constraints (described later).

Let $CG(C, L)$ be the PCS network, where C is a finite set of cells and L is the set of edges such that $L \subseteq C \times C$. Assume $C^{new} \cup C^{old} = C$, $C^{new} \cap C^{old} = \emptyset$, C^{new} be the set of new and splitting cells where $|C^{new}| = n'$, and C^{old} be the set of original cells where $|C^{old}| = n$. Without loss of generality, cells in C^{old} and C^{new} are numbered from 1 to n and $n+1$ to $n+n'$, respectively.

If cells c_i and c_j in C are assigned to different switches, then an inter-switch handoff cost is incurred. Let f_{ij} be the frequency of handoff per unit time that occurs between cells c_i and c_j. All edges in C are undirected and weighted; cells c_i and c_j in C are connected by an edge $(c_i, c_j) \in L$ with weight w_{ij}, where $w_{ij} = f_{ij} + f_{ji}$, $w_{ij} = w_{ji}$, and $w_{ii} = 0$[4,5]. Let $G^{old}(S^{old}, E^{old})$ be the currently exist ATM network, where S^{old} is the set of switches with $|S^{old}| = m$, $E^{old} \subseteq S^{old} \times S^{old}$ is the set of edges, s_k, s_l in S^{old}, (s_k, s_l) in E^{old}, and G^{old} is connected. The topology of the ATM network $G^{old}(S^{old}, E^{old})$ will be expanded to $G(S, E)$. Let S^{new} be the set of potential sites of switches. Without loss of

generality, switches in S^{old} and S^{new} are indexed from 1 to m and $m+1$ to $m+m'$, respectively. Let (X_{s_k}, Y_{s_k}) be the coordinate of switch s_k, $s_k \in S^{old} \cup S^{new}$, k=1, 2, ..., $m+m'$, (X_{c_i}, Y_{c_i}) be the coordinate of cell c_i, i=1, 2, ..., $n+n'$; and d_{kl} be the minimal communication cost between the switches s_k and s_l on network $G(S,E)$, $s_k, s_l \in S$; k,l=1, 2, ..., $m+m'$.

The total communication cost has two components, the first is the cabling cost between cells and switches, and the other is the handoff cost which occurred between two switches. Let l_{ik} be the cabling cost per unit time between cell c_i switch s_k, (i=1, 2, ..., $n+n'$; k=1, 2, ..., $m+m'$) and assume l_{ik} is the function of Euclidean distance between cell c_i and switch s_k. Assume the number of calls that can be handled by each cell per unit time is equal to 1 and CAP denotes the cell handling capacity of each new switch $s_k \in S^{new}$, ($k = m+1, m+2$, ..., $m+m'$). Let Cap_k be the number of remaining cells that can be used to assigned cells to switch $s_k \in S^{old}$,(k=1, 2, ..., m). Let q_k =1, (k = 1, 2, ..., $m+m'$) if there is a switch installed on site s_k; q_k=0, otherwise (as known, q_k =1, for k= 1, 2, ..., m). Let $setup_k$ be the setup cost of the switch at site $s_k \in S$, k=1, 2, ..., $m+m'$ (as known $setup_k = 0$, for k=1, 2, ..., m). Let $x_{ik} = 1$ if cell c_i is assigned to switch s_k; $x_{ik} = 0$, otherwise; where $c_i \in C$, i= 1, 2, ..., $n+n'$, $s_k \in S$, s=1, 2, ..., $m+m'$. Since each cell should be assigned to one switch, the constraint $\sum_{k=1}^{m+m'} x_{ik} = 1$, for i=1, 2, ..., $n+n'$ should be satisfied. Further, the constraints on the call handling capacity is that: for the new switch s_k, $\sum_{i=n+1}^{n+n'} x_{ik} \le CAP,\ k = m+1, m+2, ..., m+m'$, and for the existing switch s_k, $\sum_{i=n+1}^{n+n'} x_{ik} \le Cap_k, k = 1, 2, ..., m$.

If cells c_i and c_j are assigned to different switches, then an inter-switch handoff cost is incurred. To formulate handoff cost, let y_{ij} take a value of 1, if both cells c_i and c_j are connected to a common switch; $y_{ij} = 0$, otherwise. The cost of handoffs per unit time is given by

$$Handoff\ Cost = \sum_{i=1}^{n+n'} \sum_{j=1}^{n+n'} \sum_{k=1}^{m+m'} \sum_{l=1}^{m+m'} w_{ij}(1-y_{ij}) q_k q_l x_{ik} x_{jl} D_{kl}, \qquad (1)$$

where D_{kl} is the minimal communication cost between switches s_k and s_l on $G(S,E)$. The objective function is :

$$\textbf{Minimize}\ Total\ cost = Cabling\ Cost + \alpha \times Handoff\ Cost \qquad (2)$$
$$= \sum_{i=1}^{n+n'} \sum_{k=1}^{m+m'} l_{ik} x_{ik} + \alpha \sum_{i=1}^{n+n'} \sum_{j=1}^{n+n'} \sum_{k=1}^{m+m'} \sum_{l=1}^{m+m'} w_{ij}(1-y_{ij}) q_k q_l x_{ik} x_{jl} D_{kl},$$

where α is the ratio of the cost between cabling communication cost and inter-switch handoff cost. Let e_{kl} be the variable that represents the link status between two switches s_k and s_l. If e_{kl}=1 then there is a link between two switches s_k and s_l ($s_k, s_l \in S^{old} \cup S^{new}$); e_{kl}=0, otherwise. Let u_{ik} be link setup cost of constructing the connection between cell c_i,($i = n+1, n+2$, ..., $n+n'$) and switch s_k(k=1, 2, ..., $m+m'$), and assume u_{ik} is the function of Euclidean distance between cell c_i and switch s_k. Let v_{kl} be link setup cost of constructing the

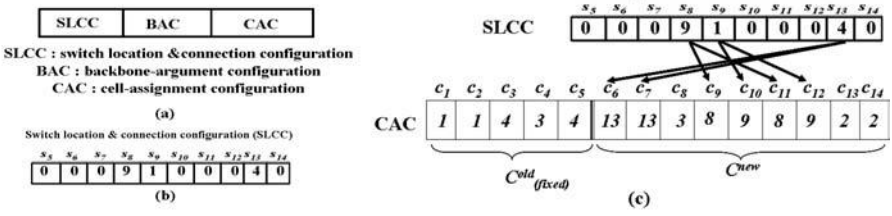

Fig. 2. (a) Configuration of the SA, (b) SLCC, (c) Configuration used to represent the relation between the locations of switches and the assignments of cells

connection between switch s_k and switch s_l,(k, l=1, 2, ..., $m + m'$), and assume v_{kl} is the function of Euclidean distance between switch s_k and switch s_l. Define e_{kl}^{old} =1 if there is a backbone link in G^{old}; e_{kl}^{old} =0, otherwise for k, l =1, 2, ...,m.

The following constraints must be satisfied:

$$EC = \sum_{k=m+1}^{m+m'} q_k setup_k + \sum_{i=n+1}^{n+n'} \sum_{k=1}^{m+m'} u_{ik} x_{ik} q_k \tag{3}$$

$$+ \Big(\sum_{k=m+1}^{m+m'} \sum_{l=1}^{m+m'} (e_{kl} - e_{kl}^{old}) v_{kl} q_k q_l \Big)/2 \leq Budget$$

$$x_{ik} \leq q_k, \ \ for \ k = 1, 2, ..., m + m^{'}. \tag{4}$$

$$e_{kl} \leq q_k \quad and \quad e_{kl} \leq q_l, \quad for \ k = 1, 2, ..., m^{'}; l = 1, 2, ..., m + m^{'}. \tag{5}$$

3 Simulated Annealing Algorithm for NEP

3.1 Configuration Space

The object of NEP problem is to find the location of the new switch, the topology of backbone network, and the assigning switch of cell, so that the objective function is minimized under the capacity and budget constraints. To do this, the configuration space is designed to be the set of possible solutions. To solve the network expanded problem in wireless ATM network, three types of configurations, known as *switch location and connection configuration* (SLCC), *backbone-augment configuration* (BAC), and *cell-assignment configuration* (CAC) are introduced and illustrated in Fig. 2(a). The switch location and connection configuration in the form of nonnegative integer decides the activation or deactivation of the new switch and the connection of the corresponding new switches. The number of switches with positive integer in the SLCC is assumed to be equal to $\lceil (|C^{new}| - \sum_{k=1}^{m} Cap_k)/CAP \rceil$, that is, base on the assumption that the cost of setup a new switch is more expensive than the cost of establishing several backbone links. The SLCC can also be used to represent the backbone links between new switches and other (new or old) switches. To make the design of backbone network simply, the links and switches selected in SLCC together with

the network G^{old} will form a base connected backbone network G^B. The network G^B can be improved by adding backbone links described in backbone-augment configuration (BAC) if the budget not yet been use up. The cell-assignment configuration (CAC) defines the assigning switches of cells. The new cell can only be assigned to old switches with unused capacity or the new switch whose value in SLCC is greater than zero.

The detail information of three types of configurations are described as follows: (1) *Switch location and connection configuration* (SLCC): Since there are m' potential sites for the choice of news switches, a nonnegative integer encoding method is used to represent whether the site is selected or not. An integral array $SLCC[m+1, ..., m+m']$ is used to represent the choice. If $SLCC[k] > 0$ $(m+1 \leq k \leq m+m')$ then a new switch is located at potential site s_k; $SLCC[k] = 0$, otherwise. Moreover, the content of the element in SLCC is used to represent the connections between switches. Since the existing ATM network is connected. Thus, to form a new connected backbone network, the only thing should be done is to keep the information of how the new switch is connected to another switches. The value of $SLCC[m+1, ..., m+m']$ is used to represent the connections of new switches to another switches. If $SLCC[k] = l(m+1 \leq k \leq m+m', 1 \leq l \leq m+m')$ then there is a backbone link between switches s_k and s_l. (2) *Backbone-augment configuration* (BAC): The network G^B formed by G^{old} and the link described in $SLCC$ can be improved by adding backbone links to the backbone-augment configuration (BAC) if the budget not yet been use up. The implementation of the BAC is a linked list, which consists of nodes used to represent the link of backbone link, is used. (3) *Cell-assignment configuration* (CAC): A coding scheme that uses positive integer numbers is used to represent the assigning switches of cells. The cell–assignment configuration is shown in Fig. 2(c), where the i^{th} cell belongs to the $CAC[i]$-th switch. It should be noticed that, the cell-assignment configuration can be divided into two sets, the first set of cells which represents the assignment of cells in C^{old} is fixed in running of SA. Thus, the first set of cells can be ignored since it is unchanged during experiments.

3.2 Initial Configuration Generation

Since the content of $SLCC$ does effect the contents of the BAC and CAC. The number of switches to be selected is equal to $\lceil (|C^{new}| - \sum_{k=1}^{m} Cap_k)/CAP \rceil$ and the switch is randomly selected. Once the location of new switches have been selected, the connections of switches should be updated according to the selection of new switches. To do this, let *switch-pool for connection* (SPC) be the set of numbers indicated switches which will be used to determine $SLCC$. Thus $SPC = \{1, 2..., m\} \cup \{i \mid SLCC[i] > 0, m+1 \leq i \leq m+m'\}$. To generate the connection of new switches, the value of element of array $SLCC$ is randomly selected from SPC. This process will guarantee that each new switch will be connected to an exist switch. Similarly, the assignments of cells to switches should be updated according to the selection of new switches. Let *switch-pool for assignment (SPA)* be the set of numbers indicated switches which can be

used in choosing of $SLCC$. For switch s_k, $1 \leq k \leq m$, Cap_k "k" are inserted into set SPA. For switch s_k, if $m+1 \leq k \leq m+m'$, if $SLCC[k] > 0$, CAP "k" are inserted into set SPA. Note that, the SPC should be updated if the a new switch is selected. To assign cells to switches, the value of element in array CAC is randomly selected a number from SPA and removed it from SPA. After performing the cell assignment, if the budget not yet been use up the link which connected two switches in SPC is randomly selected to argument the backbone network.

The objective cost defined in (2) is used as the cost function. In the proposed SA, only the feasible solution can be generated, thus there is no need for designing the penalty function. Only generating feasible solutions can expedite the converge and improve the performance of the proposed SA.

3.3 Perturbation Mechanism

Simulated annealing algorithm uses perturbation to change the configuration from one state to another state. After perturbation, the resulted configuration still a constraint-satisfied one after performing perturbation. In the following, several types of perturbations are introduced into the SA algorithm for solving the NEP problem.

(1) **P1:** *Cell exchanging perturbation* (CEP): Random selected two cells in C^{new}, say c_i and c_j which assigned to switch s_k and s_l, respectively. The assignment of these cells are exchanged, that is, c_i assigned to s_l and c_j assigned to s_k. (2) **P2:** *Switch exchange perturbation* (SEP): Random selected two switches s_k and s_l in S^{new}, all cells assigned to these switches are exchanged. (3) **P3:** *Switch migrating perturbation* (SMP): The perturbation randomly selected switch s_k in SLCC with positive value and change it to 0 and another switch s_l ($k \neq l$) from "0" to the original value of $SLCC[k]$. All cells assigned to switch s_k are reassigned to s_l, all backbone links which connected to s_k should be deleted and new backbone links connected to s_l should be established. (4) **P4:** *Backbone link perturbation* (BLP): Randomly selected a backbone link in current backbone remove it and random selected a new backbone link to added.

Let p_i be the probability of transforming current configuration to a new one by applying the perturbation **Pi**, i=1, 2, ..., 4, respectively. Assume that $\Sigma_{i=1}^{4} p_i = 1$. Let $AP_0 = 0$ and $AP_i = \Sigma_{j=1}^{i} p_j$ be the accumulated probability of p_i, i=1, 2, ..., 4.

3.4 Cooling Schedule

The parameters of the SA are described as follows. (1) *Decrement of the control parameter*: The decrement rule in SA is defined as follows: $T_{k+1} = \gamma T_k$, where γ is empirically determined and discussed in Section 4.(2) *The final value of the control parameter*: The iterative procedure is terminated when there is no significant improvement in the solution after a pre-specified number of iterations. (3) *The length of Markov Chains*: In this paper, the chain length is empirically determined and discussed in Section 4.

3.5 Simulated Annealing Algorithm of NEP Problem

The details of the simulated annealing is described as follows:

Algorithm: Simulated Annealing

Step 1. For a given initial temperature T, perform initial configuration generation algorithm to generate initial configuration IC. The currently best configuration (CBC) is IC, i.e. $CBC = IC$, and the current temperature value (CT) is T, i.e. $CT = T$. Determine $p_i, i = 1, 2, ..., 10$, $AP_0 = 0$ and $AP_i = \Sigma_{j=1}^{i} p_j$, i=1,2,...,12.
Step 2. If $CT = 0$ or the stop criterion is satisfied then go to **Step 7**.
Step 3. Generate a random number p in $[0, 1)$, if $AP_{i-1} \leq p \leq AP_i, (i = 1, 2, ..., 4)$ then new configuration (NC) is generated by applying the Pi perturbation schema.
Step 4. The difference of the costs of the two configurations, CBC and NC is computed, i.e. $\Delta C = E(CBC) - E(NC)$.
Step 5. If $\Delta C \geq 0$ then the new configuration NC becomes the currently best configuration, i.e. $CBC = NC$. Otherwise, if $e^{-(\Delta C/CT)} > random[0, 1)$, the new configuration NC becomes the currently best configuration, i.e. $CBC = NC$. Otherwise, go to **Step 2**.
Step 6. The cooling schedule is applied, in order to calculate the new current temperature value CT and go to **Step 1**.
Step 7. End.

4 Experimental Results

In order to evaluate the performance of the proposed algorithm, the simulated annealing algorithm is implemented and applied to solve problems that were randomly generated. The results of these experiments are reported below. In all the experiments, the implementation language was C^{++}, and all experiments were run on a Windows XP with a Pentium IV 3.0Ghz CPU and 512MB RAM. A hexagonal system in which the cells were configured as an H-mesh is simulated. The handoff frequency f_{ij} for each border was generated from a normal random number with mean 100 and variance 20. The CAP of new switch is set to be 5, the potential sites of the new switch are assumed be the same as the locations of the switches in S. The GSA is assumed in the 2-D plane, with width and length equal to 1000 (unit). The cabling cost of the local link is equal to the distance between cell and switch multiplied by 1 and the cabling cost of the backbone link is equal to the distance between switches multiplied by 10. The setup cost of the each switch is assumed to be equal to 100. Assume $|C^{old}|$=50, $|C^{new}|$=50. Total budget is assumed to be 6000. The backbone network is randomly generated with 100 backbone links. Assume $|S^{old}|$=12, α=0.001, the cell assignment of the set of cells C^{old} to switches S^{old} is determined be the simulated annealing algorithm proposed in [4]. After performing cell assignment, the remaining capacity of each switch can be obtained.

In this section, first, the effects of the various parameters of each simulated annealing algorithm are discussed. All simulations are run ten times and the average result is presented. (1) Effect of the chain length: In Fig. 3(a), the average result of 10 runs with the different chain length is presented. In this experiment, assume chain length is in $\{10x | 1 \leq x \leq 10 \wedge x \in N\}$. It can be found that the algorithm can get better result when the chain length is set to 60. The CPU time in seconds also showed in Fig. 3(b). (2) Effect of accepted ratio: In Fig. 3(c), the average result of 10 runs with the different values of accepted ratio is presented. In this experiment, assume accepted ratio (γ) is in $\{0.05x | 13 \leq x \leq 20 \wedge x \in N\}$.

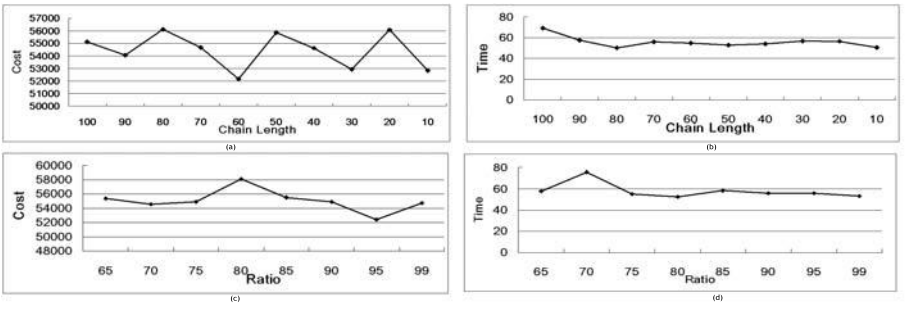

Fig. 3. Results of the network expanded problem in different values of parameter

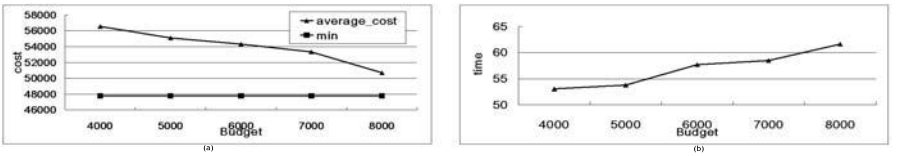

Fig. 4. Results of the network expanded problem in different values of Budget

It can be found that the algorithm can get best result for (γ=0.95). The CPU time in seconds also showed in Fig. 3(d).

Effect of budget: In Fig. 4(a), the effect of the budget is presented. In this experiment, assume *Budget* is in {4000, 5000, 6000, 7000, 8000}. It can be found that as the budget increase, the total cost of the NEP can be reduced. The CPU time in seconds also showed in Fig. 4(b). The "min" in Fig. 4(b) be the cost obtained by designing backbone network as a complete graph.

The performance of the proposed simulated annealing algorithm is examined and compared here. Let $|C^{old}|$=50, $|C^{new}|$= 50, 100, or 150, $|S^{old}| = 12$, the value of CAP is in {5, 6, 7, 8, 9, 10}. $\alpha = 0.001$, the best results of the simulated annealing algorithm after running 10 times are compared with the greedy

Table 1. Comparison of SA and HA

$\|C^{old}\|$	$\|C^{new}\|$	CAP	HA Cost	SA Cost	$ratio = SA/HA \times 100\%$	HA Time	SA Time
50	150	5	66575	56157	84.35%	611.08	152.5
50	100	5	53524	45052	84.17%	190.54	102.8
50	50	5	58125	41526	71.44%	7.87	51.3
50	150	6	66179	55231	83.46%	611.08	152.5
50	100	6	52600	44188	84.01%	190.54	107.8
50	50	6	56759	43361	76.39%	7.03	51.2
50	150	7	65471	54537	83.30%	611.08	152.5
50	100	7	51689	43493	84.14%	190.54	105.7
50	50	7	55020	45312	82.36%	5.78	51.3
50	150	8	65100	53736	82.54%	611.08	152.5
50	100	8	51554	42984	83.38%	190.54	107.8
50	50	8	54886	44167	80.47%	4.28	51.8
50	150	9	64150	53551	83.48%	611.08	152.5
50	100	9	50865	42834	84.21%	190.54	105.7
50	50	9	41977	33288	79.30%	3.6	51.1
50	150	10	63266	52656	83.23%	611.08	152.5
50	100	10	50577	42765	84.55%	190.54	105.7
50	50	10	38182	32548	85.24%	2.21	51.5

heuristic algorithm HA[8]. The results were shown in Table. 1. It is easy to find that the SA gets better results then HA.

5 Conclusions

In this paper, the *network expanded problem* (NEP) which optimally assigns new and splitting cells in *PCS* network to switches on an ATM network is investigated. This problem is currently faced by designers of mobile communication service and in the future, it is likely to be faced by designers of PCS. Since finding an optimal solution of the NEP is NP-hard, a stochastic search method based on the simulated annealing approach is proposed to solve it. Simulation results showed that simulated annealing algorithm is robust for this problem. Experimental results indicate that the algorithm can run efficiently.

References

1. Cheng, M., Rajagopalan, S., Chang, L.F., Pollini, G.P., Barton, M.: PCS mobility support over fixed ATM networks. IEEE Communication Magazine 35(11), 82–91 (1997)
2. Rappaport, T.S.: Cellular radio and personal communications, vol. 1. IEEE Press, New York (1995)
3. Merchant, A., Sengupta, B.: Assignment of cells to switches in PCS networks. IEEE/ACM Trans. on Networking 3(5), 521–526 (1995)
4. Din, D.R., Tseng, S.S.: Simulated annealing algorithms for optimal design of two–level wireless ATM network. Proceeding of NSC 25(3), 151–162 (2001)
5. Din, D.R., Tseng, S.S.: Heuristic algorithm for optimal design of two-level wireless ATM network. Journal of Information Science Engineering 17(4), 665–674 (2001)
6. Din, D.R., Tseng, S.S.: Heuristic and simulated annealing algorithms for solving extended cell assignment problem in wireless ATM network. International Journal of Communication Systems 15(1), 47–65 (2002)
7. Din, D.R., Tseng, S.S.: A solution model for optimal design of two-level wireless ATM network. IEICE Transactions on Communications, IEICE Trans. Commun., E85-B(8), 1533–1541 (2002)
8. Din, D.R.: A heuristic algorithm for the network expanded problem on wireless ATM environment. Technical Report, NCUE-2004-04-01, Taiwan, R. O. C

An Intrusion Detection Based on Support Vector Machines with a Voting Weight Schema

Rung-Ching Chen and Su-Ping Chen

Department of Information Management, Chaoyang University of Technology,
168, Jifgong E. Rd., Wufong Township, Taichung County, 41349, Taiwan, R.O.C.
{crching,s9414638}@cyut.edu.tw

Abstract. Though IDS (Intrusion Detection System) have been used for many years, the large number of returned alert messages leads to management inefficiencies. In this paper, we propose a novel method based on SVM (Support Vector Machines) with a voting weight schema to detect intrusion. First, TF (Term Frequency), TF-IDF (Term Frequency-Inverse Document Frequency) and entropy features are extracted from processes. Next, these three features are sent to the SVM model for learning and then for testing. We then use a general voting schema and a voting weight schema to test attack detection rate, false positive rate and accuracy. Preliminary results show the SVM with a voting weight schema combines low the false positive rates and high accuracy.

Keywords: Intrusion Detection System, TF-IDF, Entropy, Support Vector Machine.

1 Introduction

The Internet plays an increasingly important role in communications in modern society. However, attacks on network security are a common problem, and network security is critical for many organizations. Firewalls, widely used, are a good way to prevent attacks, but cannot monitor packets in real time on the network. Intrusion detection, which monitors the network in real time, has been studied by many researchers. However, Intrusion Detection Systems (IDS) generally produce high false positive rates, making them unattractive to information technology managers [13, 18, 4].

The major difference between firewall and IDS system is that firewall is a manual, passive defense system. By contrast, the IDS collects packets online from the network. After collecting them, the IDS will monitor and analyze these packets, acting as the "second line of defense". It provides the results of its detection analysis, either attacks or normal behaviors, to managers.

An ideal IDS system has a 100% attack detection rate along with a 0% false positive rate, but attaining those goals is difficult. Detecting illegal behaviors on the host or network is the major object of IDS. The IDS monitors the network and sends a warning message to the managers if it detects an attack.

H.G. Okuno and M. Ali (Eds.): IEA/AIE 2007, LNAI 4570, pp. 1148–1157, 2007.

Briefly, the aim of intrusion detection is to identify malicious attacks. There are two main methods of identifying intrusion detection in IDS systems: misuse (signature-based) and anomaly (behavior-based) [20].

Misuse detection establishes a pattern or a signature form so that similar attacks can be detected. It may be used in personal computers, like an antivirus program. The main drawback of misuse detection is it cannot detect new attacks, though new forms of attack are constantly being generated. Misuse detection is based on patterns stored in a database that contains possible signature of attacks. If the system matches the data with the attack pattern, the IDS regards it as an attack. Consequently, misuse detection provides a lower false positive rate. Currently, misuse detection systems such as Snort, developed by Marty Roesch [14], are being produced for network security.

Anomaly detection is a behavior-based method based on statistical theory that establishes a normal activity profile for system detection. Anomaly detection can detect new attacks, but has higher false positive rates. Behavior-based methods focus on later attacks, and ignore earlier attacks. In general, the majority of attacks will be detected in the later period, and the greatest damage will occur in the later period as well. Thus, anomaly detection not only detects attacks but also prevent intrusions.

Entropy has been used in intrusion detection for a long time. B. Balajinath et al. used entropy in a learning behavior model of intrusion detection in 2001 [2]. TF-IDF has often been applied to IDS, too. For example, Wun-Hwa Chen et al. compared SVM to ANN for intrusion detection using a TF-IDF-based method [22].

Previously, researchers commonly used ANN for intrusion detection [7, 16] but in recent years SVM has been increasingly applied in intrusion detection [22, 21]. According to experimental results, in most cases SVM has outperforms the ANN method.

In this paper, we propose a classification method based on SVM with a voting weight schema to detect intrusion [17]. The operations of the SVM include two phases: a learning phase and a testing phase. In the learning phase, three SVM learning models are constructed based on TF, TF-IDF and entropy features. In the testing phase, five types of SVM models, TF feature based SVM, TF-IDF feature based SVM, Entropy based SVM, voting SVM and voting weight SVM are tested.

The remainder of the paper is organized as follows. We give a system overview in section 2. Section 3 introduces the support vector machine and the features of the VW-SVM. In Section 4, we present details of voting policy. Experimental results are given in section 5. Conclusions are presented in section 6.

2 The System Overview

Our framework is shown in Figure 1. First, KDD Cup 1999 Data is transferred to a matrix [15]. Then the system extracts TF, TF-IDF and entropy features

from the matrix. Three SVM models are then constructed to detect intrusions. Finally, a VW-SVM method is utilized to detect intrusion. It is briefly described as follows:

(1) Preprocessing: A process can be composed of many system calls. A system call is a text record [10]. In this phase, useless data will be filtered and modified. For example, it is necessary to convert some text items into numbers.
(2) Features selection: The system regards the processes and system calls as a two dimensional matrix. The system maps system calls to keywords and processes to documents, so the TF and TF-IDF values can be obtained from the matrix. The system also calculates the entropy of each process from the matrix.
(3) SVM classification: The system uses TF, TF-IDF and entropy features to train the SVM models. The three SVM category models will then be utilized to predict the category of a given process.
(4) Voting weight policy: After the three SVM models classify the process, the output of each SVM will be utilized for a hybrid system using voting weight to determine which category the process should be placed in.

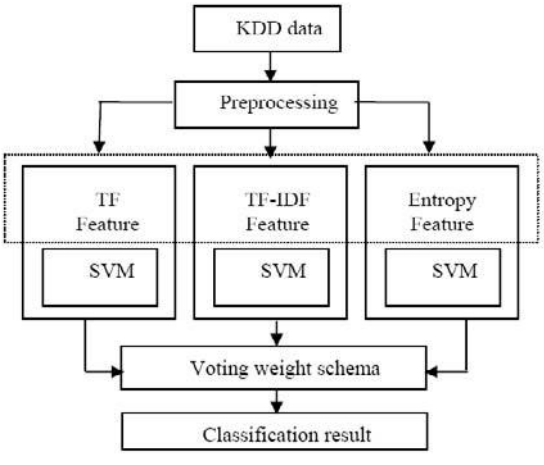

Fig. 1. The framework of VW-SVM

3 The Input Features of the SVM

In our system, the processes and system calls are regarded as a two dimensional matrix. System calls are mapped to keywords and processes are mapped to documents. Thus, the TF and TF-IDF values for the features can be obtained from the matrix. In this section, we will introduce the operations of the SVM and how the TF, TF-IDF and entropy feature values are extracted.

3.1 Support Vector Machine

The SVM uses a high dimension space to find a hyper plane in order to perform binary deviation, where the error rate is minimal [21]. The SVM can handle the problem of linear inseparability.

The SVM uses a portion of the data to train the system and finds several support vectors that represent training data. These support vectors will be formed into a model by the SVM, representing a category. According this model, the SVM will classify a given unknown document by the following classification decision formula:

$$(x_i, y_i), \ldots, (x_n, y_n), x \in R^m, y \in \{+1, -1\} \tag{1}$$

Where (x_i,y_i), ... ,(x_n,y_n) are training samples, n is the number of samples, m is the input dimension, and y belongs to the category of +1 or -1 respectively.

In a linear problem, a hyper plane is divided into two categories. Figure 2 shows a high dimension space divided into two categories by a hyper plane. The hyper plane formula is: (w • x)+b=0

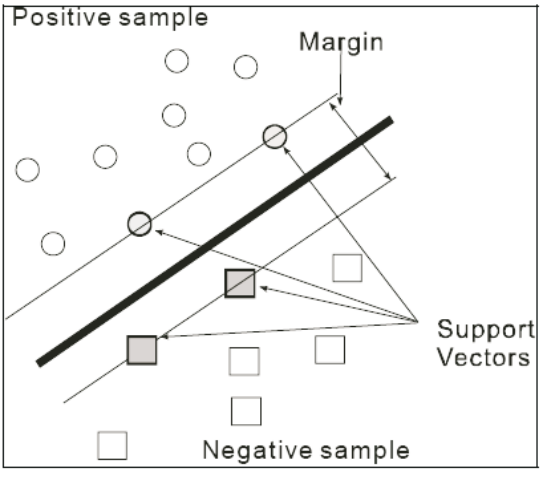

Fig. 2. The hyper-plane of SVM

The classification formula is:

$$(w \bullet x_i) + b > 0 \quad if \quad y_i = +1 \qquad (w \bullet x_i) + b < 0 \quad if \quad y_i = -1 \tag{2}$$

However, for many problems it is not easy to find a hyper plane to classify the data. The SVM has several kernel functions that users can apply to solve different problems. Selecting the appropriate kernel function can solve the problem of linear inseparability.

3.2 TF and TF-IDF Feature

In general, the importance of system calls is determined by two factors in the collected processes. The first factor is the relative frequency of the appearance of the system calls in the processes, called Term Frequency (TF). We used the TF features for SVM training samples. The second factor is the quantity of processes containing the system call, or Document Frequency (DF). TF shows the relative frequency of a given system call appearing in processes. If the appearance frequency of a system call in the process is higher than in other processes, it means that this system call is able to represent the current process better than other processes. We can thus use the product of TF and Inverse Document Frequency (TF-IDF) to represent the importance of a system call in the process [19, 10, 24, 8]. The formula for calculating TF-IDF for our system is:

$$w_i = \log(\frac{N}{n_i}) \times \frac{f_i}{\sqrt{\sum_i f_i^2}} \tag{3}$$

w_i : The component of the process vector corresponding to system call i
n_i : The number times of system call i appear in the whole data set
f_i : The number times of system call i appears in the process
N : The number of processes appears in the whole data set

3.3 Entropy Feature

In recent years, entropy has been utilized in intrusion detection research [2, 6]. Shannon proposed that entropy is related to the uniform distribution [3, 11]. Entropy values represent whether the information is sparse or not, and the probability of terms. Here, entropy is applied to calculating the weight of processes. By the definition, the entropy can be expressed as follows.

$$P_T = -\sum_{i=1}^{n} s_i \log s_i \tag{4}$$

s_i is the probability of Uniform Distribution of the system calls i in process T, while n is the number of system calls. Each process has an entropy value.

4 The Voting Policy

The original concept of multiple recognizers selects greater than one recognizer to perform the classification. One classification result is determined by these recognizers. In our system, only SVM is used as the classification tool. The idea is to choose different features to construct SVM models because different features have different characteristics. In the hybrid system, many different kinds of pattern classifiers have their own strengths and weaknesses. The most direct form of voting is when all the individual recognizers must agree; otherwise the pattern is rejected. However, this condition is too strict. More common operators

and less strict forms of voting are more useful where substitution errors are not lethal [1,17]. The majority voting rule states as follows:

$$T_k(x \in C_i) = \begin{cases} 1 & e_k(x) = i, \ i \in \Lambda \\ 0 & Otherwise \end{cases} \tag{5}$$

$$E(x) = \begin{cases} 1 & if \ T_E(x \in C_i) > \frac{K}{2} \\ -1 & Otherwise \end{cases} \tag{6}$$

where

$$T_E(x \in C_i) = \sum_{k=1}^{K} (x \in C_i), \ \ i = 1, \ldots, M \tag{7}$$

The combined interpretation of equations 5 and 6 is that the pattern is classified as class C_i if over half of the recognizers say pattern x $\in C_i$. e_k(x) is the output of SVM model and Λ is the range of normal. In our system, the value of M is 2, and a given process is classified as either normal or as an intrusion. In this case, each recognizer has the same weight in deciding the results. The output value of each SVM is either +1 or 0, meaning that when the value of T_E(x) is greater than half of the number of SVM models, the decision is that the process is a normal operation. Because the precision of the different SVM models varies, we use different voting weights in each of the different SVM models when making voting decisions. We modify the equations 6 and 7 as follows.

$$E(x) = \begin{cases} 1 & if \ \ f(T_E(x \in C_i)) > \Theta_T \\ -1 & Otherwise \end{cases} \tag{8}$$

where

$$T_E(x \in C_i) = \sum_{k=1}^{K} W_k \times T_k(x \in C_i), \quad i = 1, \ldots, M \tag{9}$$

W_k is the weight of a SVM model k and the value of K is 3 (which are TF SVM, TF-IDF SVM and entropy SVM) in our system. However, the formula only considers the positive value outcome of a vote, but in many cases, the vote results in a negative value, also an important attribute. Thus, we let the Tk value be 1 or -1, replacing "0" with "-1". Even in the SVM model, the output values of the weight for positive 0 and negative 1 are different, as we found in our experiments. So we modified formula 5 as follows:

$$T_k(x \in C_i) = \begin{cases} 1 & e_k(x) = i, \ i \in \Lambda \\ -1 & Otherwise \end{cases} \tag{10}$$

$$E(x) = \begin{cases} 1 & if \ \ f(T_E(x \in C_i)) > \Theta_T \\ -1 & Otherwise \end{cases} \tag{11}$$

where

$$T_E^k(x \in C_i) = W_k^s \times T_k(x \in C_i), \quad k = 1, \ldots, M; \ S \in \{-1, 1\} \tag{12}$$

$$f(T_E(x \in C_i)) = \alpha \times T_E^1 + \beta \times T_E^2 + \gamma \times T_E^3 \tag{13}$$

If the value of T_k is 1, the system selects weight value W_k^1, but if T_k is -1, the system selects a weight value W_k^{-1} for system operations. M is the number of SVM models. In the system, the value of M is 3. The function f summarizes the voting weights (α,β,γ), multiplexing the weighting output of the SVM models. Θ_T is a threshold for detecting the output of the intrusion system.

5 Experiment and Discussion

The experiments were implemented on a Windows XP Professional operating system using the Pentium-4 2.4G MHz of computer with 512 MB RAM in Java language. The data were collected from the KDD Cup 1999 Data, originally from the 1998 DARPA Intrusion Detection Evaluation Program [15]. This dataset was used in the third international knowledge discovery and data mining tools competition. The data include "bad" connections and "good" connections. In "bad" connections, attacks fall into four main categories:

(1) DOS: denial-of-service
(2) R2L: unauthorized access from a remote machine
(3) U2R: unauthorized access to root privileges
(4) probing: surveillance and other probing

60,000 processes used as training data, while 60,094 processes were used for testing data. The system has 41 system calls, whose frequency in this dataset has been presented and calculated. Libsvm was used as our classification tool [12]. The experimental materials and results output to a website [23].

Three important formulas are utilized to evaluate the performance of the system [24], the attack detection rate, false positive rate and system accuracy listed as follows.

$$Attack\ Detection\ Rate = \frac{Total\ number\ of\ detected\ attacks}{Total\ number\ of\ attacks} \times 100\% \tag{14}$$

$$FPR = \frac{Total\ number\ of\ misclassified\ processes}{Total\ number\ of\ normal\ processes} \times 100\% \tag{15}$$

$$Accuracy = \frac{Total\ number\ of\ corrected\ detected}{Total\ number\ of\ processes} \times 100\% \tag{16}$$

While the system finds the TF, TF-IDF and entropy feature values, the system uses them to train three SVM models. Before running the SVM, we used a scaling step to reduce the range of the input data. Scaling increases the accuracy of SVM [9] by avoiding a large range of for the input numbers, and reducing calculation complexity. The kernel values are determined by inner feature vectors. In the experiment, the kernel used was RBF. Table 1 shows the number

of testing results using TF-SVM, TF-IDF SVM, Entropy SVM, a general voting schema (Voting-SVM) and a voting weight schema(VW-SVM). In a general voting schema, if more than two SVM models present the same decision, the system chooses this result for the final output of the Voting-SVM. The voting weight approach classifies a process into a given category after calculating the weight.

In the experiment, the three models (TF, TF-IDF and entropy features) in turn yielded three types of classification results. Based on the results of the three models, we determined the classification strength of the feature. Because judgments may not be consistent, a voting weight schema determines the category of processes [16]. The threshold of T here we set as -0.18. Table 2 illustrates each parameter value in the experiment. The weight w upper index "1" means normal behavior, a "-1" means abnormal behavior. For example in TF-SVM, is set to 0.4; is equal to 0.3 but is equal to 0.7. The two weight values in TF-SVM are different. Though we focus on the false positive rate of TF in Table 3, it has the better performance. As a result we increased the weight value of .

Table 1. Output of testing data

Method	Attacks		Normal sessions	
	Discovered	Real	Misclassified	Real
TF-IDF-SVM	52293	53649	504	6445
TF-SVM	51876	53649	150	6445
Entropy-SVM	52396	53649	2213	6445
Voting-SVM	53423	53649	935	6445
VW-SVM	52983	53649	336	6445

Table 2. Parameter table

SVM model	Voting Weight	SVM output weight
TF-IDF-SVM	$\beta = 0.3$	$W_2^1 = 0.5$, $W_2^{-1} = 0.5$
TF-SVM	$\alpha = 0.4$	$W_1^1 = 0.3$, $W_1^{-1} = 0.7$
Entropy-SVM	$\gamma = 0.3$	$W_3^1 = 0.5$, $W_1^{-1} = 0.5$

Table 3 summarizes the testing results. They include attack detection rate, false positive rate, and accuracy. The attack detection rate of the TF-IDF SVM is 97.47%, while that of the entropy-SVM is 97.66%. The TF-SVM has an attack detection rate of 96.70%. However, when we use the Voting-SVM framework, the Attack Detection Rate rises to 99.58%. The accuracy of the TF-IDF-SVM is 96.91% that of the Entropy-SVM is 96.80%, while the TF-SVM is 94.23%. However, when we use the VW-SVM framework, the total accuracy rises to 98.35%. Further, the TF-SVM has a 2.3% false positive rate, while the Voting-SVM method has a 14.50% false positive rate. The Voting-SVM has the best attack detection rate, but its false positive rate is poor by comparison with other methods.

When the experiment uses TF-SVM to learn and test, performs well on false positives but its accuracy is poor. The TF feature calculates the relative frequency of system calls that appear in the processes. The TF-IDF adds one property to its analysis: system calls are the most important feature of the processes. The Entropy-SVM model performs poorly, generating unacceptable numbers of false positives. When we train the Entropy-SVM, each process only uses a entropy value to represent the process. If the weight method is not used, Voting-SVM also performs poorly, generating unacceptable numbers of false positives. From the overall view, the VW-SVM has the best false positive rate and accuracy. In addition, its attack detection rate is close to that of the Voting SVM. The voting weight is thus the best choice for intrusion detection among the systems studied in this research.

Table 3. Performance of the five methods in detecting attacks

Method	Attack Detection Rate	False Positive Rate	Accuracy
TF-IDF-SVM	97.47%	7.8%	96.91%
TF-SVM	96.70%	2.3%	94.23%
Entropy-SVM	97.66%	34.33%	96.80%
Voting-SVM	99.58%	14.50%	98.06%
VW-SVM	98.76%	5.21%	98.35%

6 Conclusions

In this paper, we have proposed an intrusion detection method using an SVM based on a voting weight schema, whose feature vectors include the TF, TF-IDF and entropy of the processes. The TF-IDF represents common relations between system calls and processes, while the entropy values represent the distribution of system calls in a given process. The TF-SVM, TF-IDF-SVM, entropy-SVM, Voting-SVM and VW-SVM were then compared.

The VW-SVM results have higher accuracy than the other methods. In addition, its attack detection rate is nearly as high as that of Voting SVM, while its false positive rate is nearly as low as that of TF-IDF-SVM. Based on these considerations, the voting weight method is the best choice for the intrusion detection. In future research, we will incorporate domain ontology into the IDS to improve its accuracy.

References

1. Pandya, A.S., Macy, R.B.: Pattern Recognition with Neural Networks in C++. IEEE Press, New York (1995)
2. Balajinath, B., Raghavan, S.V.: Intrusion detection through learning behavior model. Computer Communications 24, 1202–1212 (2001)
3. Shannon, C.: Bell System Tech. J. (1948)

4. Denning, D.E.: An intrusion-detection model. IEEE Trans. Software Eng. SE-13, 222–232 (1987)
5. Naiman, D.Q.: Statistical anomaly detection via httpd data analysis. Computational Statistics & Data Analysis 45, 51–67 (2004)
6. Yeung, D.Y., Ding, Y.: Host-based intrusion detection using dynamic and static behavioral models. Pattern Recognition 36, 229–243 (2003)
7. Giacinto, G., Roli, F., Didaci, L.: Fusion of multiple classifiers for intrusion detection in computer networks. Pattern Recognition 24, 1795–1803 (2003)
8. Salton, G., Buckley, C.: Term-weighting approaches in automatic text retrieval. Information Processing & Management, pp. 513–523 (1988)
9. Guide of LIBSVM.: http://www.csie.ntu.edu.tw/~cjlin/papers/guide/guide.pdf
10. Feng, H., Kolesnikov, O., Fogla, P., Lee, W., Gong, W.: Anomaly detection using call stack information. In: Proceedings of the 2003 IEEE Symposium on Security and Privacy, p. 62. IEEE Computer Society Press, Los Alamitos (2003)
11. Kao, H.Y., Lin, S.H., Ho, J.M., Chen, M.S.: Mining web informative structures and contents based on entropy Analysis. IEEE Trans. on Knowledge and Data Engineering 16, 41–55 (2004)
12. LIBSVM – A Library for Support Vector Machines. Chih-Chung Chang and Chih-Jen Lin http://www.csie.ntu.edu.tw/~cjlin/libsvm
13. Botha, M., Solms, R.V.: Utilising fuzzy logic and trend analysis for effective intrusion detection. Computers & Security 22, 423–434 (2003)
14. Roesch, M.: Snort-lightweight intrusion detection for network. In: Proceedings of LISA'99: 13th System Administration Conference, Seattle, Washington, pp. 229–238 (1999)
15. MIT.: http://www.ll.mit.edu/IST/ideval/data/1998/1998_data_index.html
16. Depren, O., Topallar, M., Anarim, E., Kemal Ciliz, M.: An intelligent intrusion detection system (IDS) for anomaly and misuse detection in computer networks. Expert Systems with Applications 29, 713–722 (2005)
17. Chen, R.C., Hsieh, C.H.: Web page classification based on a support vector machine. Expert System with Applications 31, 427–435 (2006)
18. Mukkamala, S., Sung, A.H., Abraham, A.: Intrusion detection using an ensemble of intelligent paradigms. Computer Application 28, 167–182 (2005)
19. Rubin, S., Jha, S., Miller, B.: Automatic generation and analysis of NIDS attacks. In: Proceedings of 20th Annual Computer Security Application Conference, vol. 00, pp. 28–38. IEEE Computer Society, Los Alamitos (2004)
20. Verwoerd, T., Hunt, R.: Intrusion detection techniques and approaches. Computer Communications 25, 1356–1365 (2002)
21. Vapnik, V.N.: The nature of statistical learning theory. Springer, New York (1995)
22. Chen, W.H., Hsu, S.H., Shen, H.P.: Application of SVM and ANN for intrusion detection. Computers & Operations Research 32, 2617–2634 (2005)
23. Website, http://163.17.27.154/cyut.jsp
24. Liao, Y., Rao Vemuri, V.: Use of K-Nearest Neighbor classifier for intrusion detection. Computer & Security 21, 439–448 (2002)

An Ontology-Supported and Fully-Automatic Annotation Technology for Semantic Portals

Sheng-Yuan Yang

Department of Computer and Communication Engineering, St. John's University, 499, Sec. 4, TamKing Rd., Tamsui, Taipei County 25135, Taiwan
ysy@mail.sju.edu.tw

Abstract. We employ the techniques of ontology and linguistics to develop a fully-automatic annotation technique, which, when coupled with an automatic ontology construction method, can play a key role in the development of semantic portals. Based on this technique, we also demonstrate a semantic-portal prototype which defines how a semantic portal is interacting with the user by providing five different types of interaction patterns, including keyword search, synonym search, POS (Part-of-Speech)-constrained keyword search, natural language query, and semantic index search. Our primarily demonstrations show that it can indeed retrieve better semantic-directed information to meet user requests.

Keywords: Automatic Webpage Annotation, Ontology, Semantic Portal, Internet Applications, Intelligent Interfaces.

1 Introduction

The Web has been drastically changing the availability of electronically available information. An information portal, which can help people effectively use this voluminous repository, is becoming ever important. Tim Berners-Lee visions "Semantic Web" as the next generation of web by allowing the web pages on the Semantic Web to be machine-readable [11]. Techniques to realize this vision include the techniques centered on domain ontology [11], which help domain knowledge conceptualization. Webpage annotation is another important technique, which adds relevant domain knowledge and meta-information into a web page to enhance its semantics [1]. Logic inference is yet another important technique, which allows the development of various web services. These techniques can effectively relieve the bottlenecks of the current Web [6,18]. Automatic webpage annotation can even reduce the high cost of pre-processing of web pages into a semantic web by humans [4,9]. We conjecture that these techniques can equally help us overcome the problems associated with general portals and develop a fully-automatic annotation technique, which, when coupled with an automatic ontology construction method, can play a key role in the development of semantic portals. Based on this technique, we also demonstrate a semantic-portal prototype [5] which defines how a semantic portal is interacting with the user by providing five different types of interaction patterns, including keyword search, synonym search, POS (Part-of-Speech)-constrained keyword search, natural language query, and semantic index search. Our primarily demonstrations show that it can indeed retrieve better semantic-directed information

H.G. Okuno and M. Ali (Eds.): IEA/AIE 2007, LNAI 4570, pp. 1158–1168, 2007.

to meet user requests. The "Einstein" domain is chosen as the target application of our semantic portal and will be used for explanation in the remaining sections.

2 Semantic Portal Architecture

Fig. 1 illustrates the architecture of our semantic-portal prototype. Pre-Processor is responsible for removing HTML tags and punctuations from the original web pages, and storing them in "Pre-Processed WebPages Database." Semantic Webpages Generator then bases on the database to produce three supporting knowledge bases. The first knowledge base is "Stemmed WebPages Database" created by Stemmer, which stems words and removes stop and noisy words on a pre-processed web page. The second is "POS-attached WebPages Database" created by the POS Tagger, which analyzes the parts-of-speech (POS) of the words on a web page and transforms the web page into a list of words with POS. The third is "Annotated WebPages Database" created by Automatic Annotator, which automatically identifies the concepts and relationships contained in a web page, derives a content summary for the web page, and constructs a semantic index for the web page. These knowledge bases, along with Ontology Database, support Portal Interface (Fig. 2) to provide a better semantic portal. In other words, Portal Interface applies these five knowledge bases during the interaction with the user by providing five different types of search mechanisms (described before). The user can choose one of the five patterns to input his/her queries. Answer Generator finally produces semantic-directed answers to respond to the user query. Finally, Ontology Database provides the most fundamental semantics, as illustrated in Fig. 3, developed based on the method described in [20] using

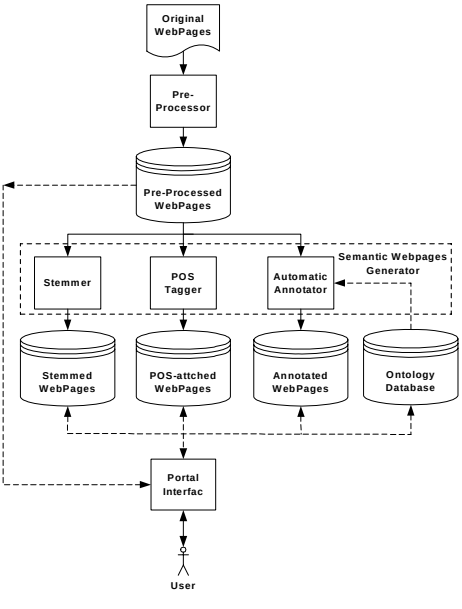

Fig. 1. Semantic portal architecture

Protégé2000 [13]. In the figure, nodes represent ontology concepts; links labelled with “isA” denotes the parent-child relationship between concepts, which allows inheritance of features from parent classes to child classes; links labelled otherwise represent some reference relationships from a concept to another concept, where ”*” denotes multiple instance reference [5].

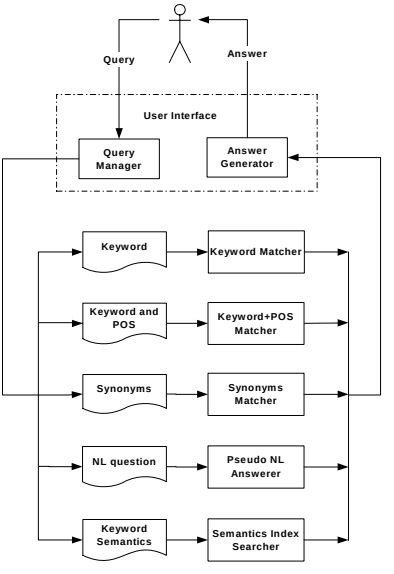

Fig. 2. Portal interface workflow

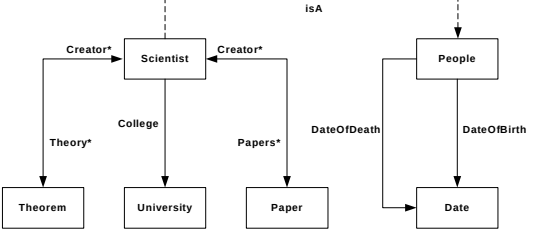

Fig. 3. Part of Scientist Ontology hierarchy

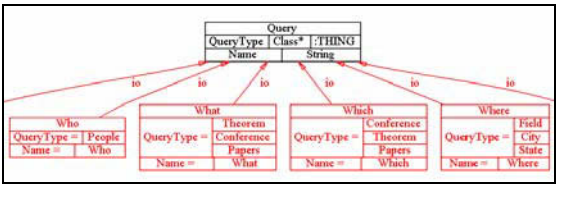

Fig. 4. Query Ontology

In addition to the scientist ontology, we also defined a query ontology to facilitate the description of queries. Fig. 4 shows the query ontology, where the root node represents class "Query" which contains a set of fields defining the semantics of the class, each field representing one attribute of "Query," e.g., QueryType, Name, etc. The links labelled with "io" represent relationship "instance_of", relating an instance to the Query class. The figure shows four query instances, including Who, What, Which, and Where, each standing for a specific solution pattern. For example, query instance "Who" has "People" as the value of its QueryType attribute, which means the answer to the query instance must belong to the People class. Finally, we have used Protégé's APIs to develop a set of ontology services, which provide primitive functions to support the applications of the ontologies. The ontology services currently available include transforming query terms into canonical ontology terms, finding definitions of specific terms in ontology, finding relationships among terms, finding compatible and/or conflicting terms against a specific term, etc.

3 Semantic Webpages Generator

3.1 Stemmer

Fig. 5 illustrates the workflow of Stemmer. Qtag is used here to help remove stop words, passing only major terms to WordNet-based Stemmer. Specifically, Qtag

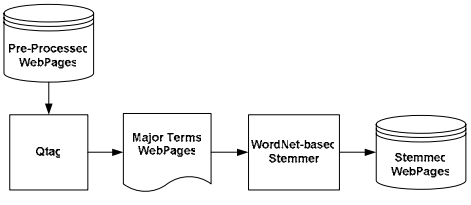

Fig. 5. Workflow of Stemmer

Table 1. Part of POS tags used by Stemmer and POS Tagger

	POS Tag	Meaning
1	BE	be
2	BEDR	were
3	BEDZ	was
4	BEG	being
5	BEM	am
6	BEN	been
7	BER	are
8	BEZ	is
9	CC	conjunction, coordinating (and)
10	DO	do
11	DOD	did
12	DON	Done
13	DOG	Doing
14	DOZ	Does
15	DT	determiner, general (a, the, this, that)
16	IN	preposition(on, of)
17	MD	modal auxiliary (might, will)
18	TO	infinitive marker (to)
19	WDT	det, wh- (what, which, whatever, whichever)
20	WP	pronoun, wh- (who, that)
21	WP$	pronoun, possessive wh- (whose)
22	WRB	adv, wh- (how, when, where, why)

employs probability with a sliding window [19] to determine POS of the words in a web page. The output of Qtag contains detailed POS tags (Examples shown in Table 1), which are further categorized into five categories, namely, noun, verb, adjective, adverb, and DC (for Don't Care) for the purpose of removing stop words. Finally, WordNet-based Stemmer employs WordNet, which is a comprehensive vocabulary [21], to transform the major terms into their stems and stores them in Stemmed WebPages Database.

3.2 POS Tagger

Fig. 6 illustrates the workflow of POS Tagger, which is very similar to the Stemmer. Qtag is used here to actually produce a POS for each word of a web page. WordNet-based Stemmer is then used as in Stemmer to do word stemming.

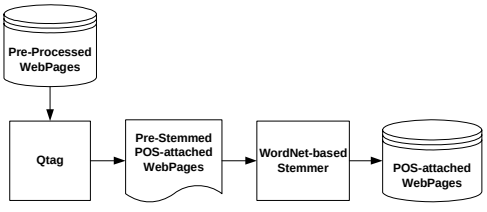

Fig. 6. Workflow of POS Tagger

3.3 Automatic Annotator

Fig. 7 illustrates the architecture of Automatic Annotator. Concept Identifier and Relationship Identifier work together to extract the concepts and relationships contained in a web page, supported by the domain ontology. Text Summarizer

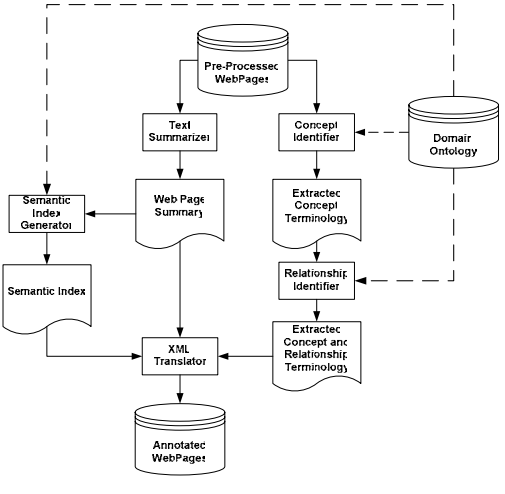

Fig. 7. Automatic Annotator architecture

employs Text-Miner, developed by IBM [8], to identify important sentences in order to derive a summary for the web page. Semantic Index Generator identifies the most important sentence in the summary as the semantic index, supported by the domain ontology again. Once the semantic index is identified, it is treated as the center theme of the webpage and we can use it to refine the summary. Basically, we employ the vector space model [15] to calculate the correlations between the semantic index and the sentences in the webpage summary, and accordingly adjust their appearance order or remove some less relevant sentences. This helps us develop a summary which contains sentences that are not only highly-weighted but also highly relevant to the center theme. Finally, XML Translator adds all of these into a web page and transforms it into an annotated web page. Note that Automatic Annotator not only annotates a web page, but also adds relevant synonyms into the annotated web page, with the help of Concept Identifier and the domain ontology [5].

4 System Demonstrations

First, suppose the user chooses to query by keywords, Query Manager will directly invoke Keyword Matcher, which uses full-text search to compare the keywords with the words in all of the web pages stored in Pre-Processed WebPages Database. This process is the same as the classical keyword match employed by most general portals. Two major issues are associated with the keyword-based query method, however. First, it only retrieves web pages which contain syntactically the same keywords. Second, keywords of different parts of speech may represent different meanings. The second issue can be easily coped with by allowing the user to use the Word+POS

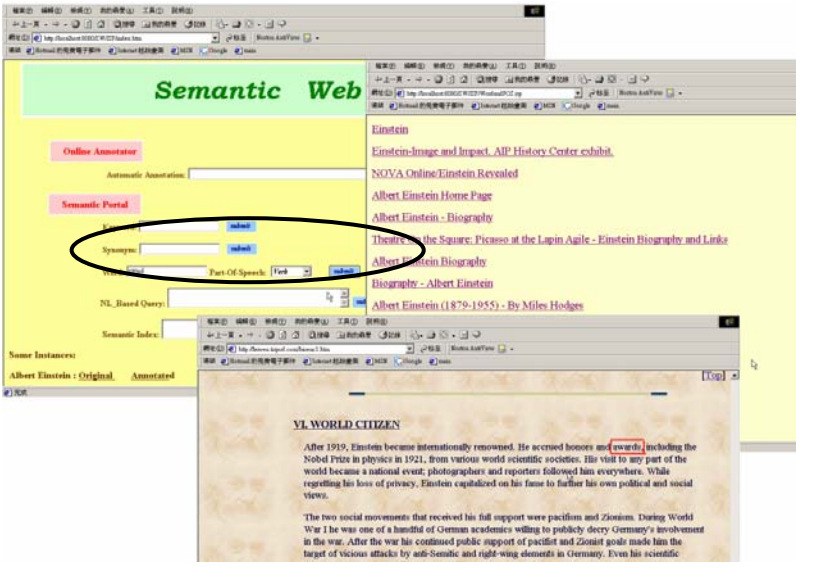

Fig. 8. Search result of keyword+POS match

Match method, which requires the user to associate a part-of-speech with each input keyword. Query Manager then invokes Keyword+POS Matcher to search in POS-attached WebPages Database for web pages which contain the keywords appearing in the correct part of speech, as illustrated in Fig. 8.

We employ two methods to cope with the first issue in our system. The first method not only invokes Synonyms Matcher to search in Annotated WebPages

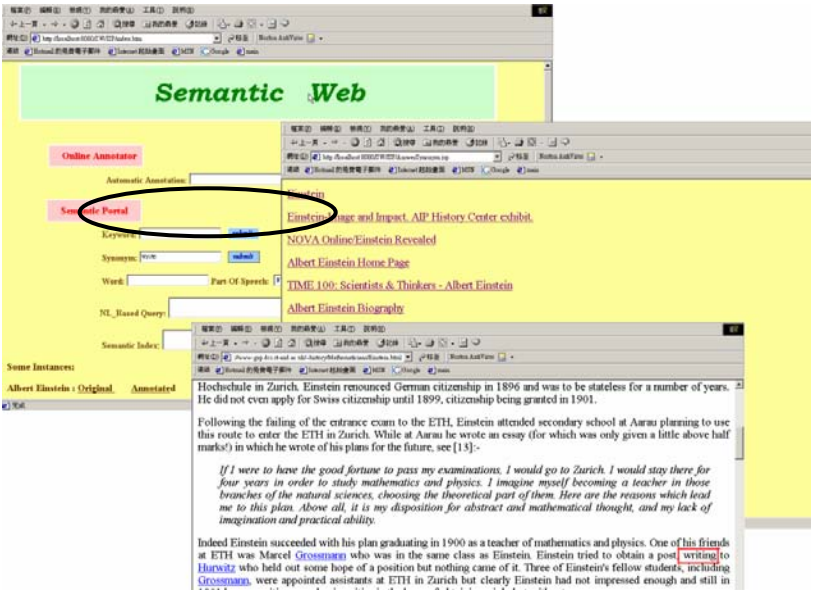

Fig. 9. Search results in response to stemmed keywords

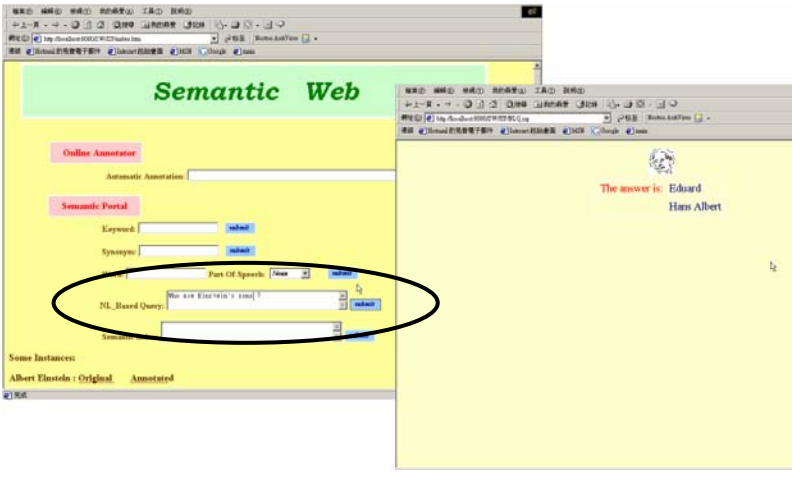

Fig. 10. Search results in response to a natural language query

Database for web pages containing the synonyms of the entered keywords, but also tackles morphological changes by returning a web page containing "writing," given input keyword "wrote," as shown in Fig. 9.

Alternatively, we allow the user to post natural language query in order to deal with the first issue. The user can place a natural language query by using NL-Based Query method, when Query Manager invokes Pseudo NL Answerer to propose answers. Fig. 10 shows an example of NL question "Who are Einstein's sons?"; Query Manager answers "Edward (Albert)" and "Hans Albert."

In addition to the above four user interface methods, we define a new keyword query method called semantic index match. The user can choose the method and enter usual keywords; Query Manager will invoke Semantic Index Searcher to search in Annotated Webpages Database for all web pages whose semantic index contains the keywords and accordingly displays the semantic indices for the user, as illustrated in Fig. 11. Note that the return page contains a list of URLs, each followed by its semantic index. This approach is different from general keyword-based search engines, which usually return the title and the first sentence of each web page.

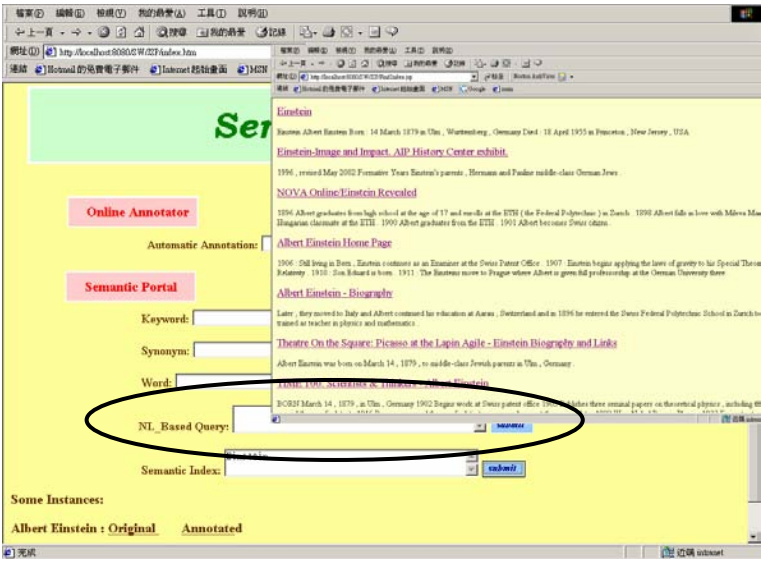

Fig. 11. Search results in response to semantic index search

5 Related Works and Comparisons

The Semantic Web or semantic portals heavily rely on webpage annotation, which inevitably becomes one of the hottest research topics. SHOE (Simple HTML Ontology Extension) is equipped with a manual Knowledge Annotator [17], which is a Java program allowing the user to annotate web pages graphically. OntoMat-Annotizer [14] is a user-friendly interactive webpage annotation tool. It supports the user with the task of creating and maintaining ontology-based DAML+OIL markups,

e.g., creation of DAML-instances, attributes and relationships. Annotea [3] in LEAD (Live and Early ADoption) uses special RDF annotation schema to add comments (a kind of annotation) as metadata. S-CREAM (Semi-automatic CREAtion of Metadata) [7] allows creation of metadata and is trainable for a specific domain. The above annotation mechanisms are either manual or semi-automatic, which impose heavy labor on humans facing a voluminous amount of web pages.

Some automatic annotation mechanisms appeared in the literature. For instance, [12] describes two algorithms which use redundancies in the content of table and detail pages to help information extraction. [16] proposes a strategy based on active recommendation to support the semantic annotation of contested knowledge to promote annotators' interest. [10] devises conflict detection patterns based on different data, ontology at different inference levels and proposes the corresponding automatic conflict resolution strategies for image annotation.

Amilcare [2] is an information extraction system which helps automatic annotation with learning capability. Its power of linguistic analysis stems from Gate, which performs tokenization, sentence identification, POS tagging, gazetteer lookup and named entity recognition. Gate functions virtually in the same way as the combination of Qtag, Concept/Relationship identifier, and Text-Miner in our system during automatic annotation. However, since Gate is easier to be used, it will be planned to employ in our future semantic-based systems. In addition, Amilcare is salient in employing the $(LP)^2$ algorithm, a supervised algorithm that falls into a class of Wrapper Induction System using LazyNLP. $(LP)^2$ can induce rules which help insert annotations in the texts and rules which correct mistakes and imprecision in the annotations generated by the former rules. We reckon that as an information extraction system, Amilcare works very similarly to part of our system. Its adaptive feature, supported by the underlying learning capability, however, provides yet another level of automation in webpage annotation and deserves more attention.

6 Conclusions and Discussions

We have developed a fully-automatic annotation technique, which employs the techniques of ontology and linguistics. It supports the five patterns of interaction of the portal interface by generating annotated webpages, stemmed webpages, and POS-attached webpages with the help of domain ontology. Our technique is an interesting contribution in terms of the following features. First, it is a fully automatic annotation tool. The tool not only helps develop annotated web pages during the construction of the portal, but also provides the user with an automatic online annotation process. The user can use the process to annotate the web pages specific to his/her interests. Second, it enriches webpage annotation by content summary and semantic index as two facets of representative semantics of a web page. Finally, it improves the traditional keyword-based retrieval mechanism by providing word-stemming, parts-of-speech, natural language processing, and semantic index search. These extensions help capture the true intention of the user and return better information.

For easy demonstration of the techniques in our semantic-portal prototype, the current implementation runs on a very simple "scientist" domain. However, we believe even if the domain is scaled up, our techniques still be applicable. The idea is this: we are not directly scaling up our ontology. Instead we can create a complex

system by integrating a set of simple systems through a multi-agent architecture which is supported by a set of simple domain ontologies. By exploiting the capability of Protégé2000, which supports the creation, extension and cooperation of a set of domain ontologies, we really need not make much change to our ontology-supported semantic portal in order to transform it into a complex portal. What we really need to focus on is how to make a set of ontology-supported systems cooperate effectively, which is under our investigation.

The ontology plays a very important role in our annotation technique. One major difficulty is its construction, which currently still relies on the help of domain experts. We are planning to investigate the technique of automatic ontology construction in the future. We believe our automatic annotation technique, when coupled with the automatic ontology construction technique, can help proliferate the techniques of Semantic Web and in turn promote the development of better Semantic Portals.

Acknowledgments. The author would like to thank Y.H. Chang for her assistance in system implementation. This work was supported by the National Science Council, R.O.C., under Grants NSC-89-2213-E-011-059, NSC-89-2218-E-011-014, and NSC-95-2221-E-129-019.

References

1. Albanese, C., Calabrese, A., D'Amico, A., Mele, F., Minei, G., Kostakopoulos, L.: Web-pages Annotation and Adaptability: A Semantic Portal on the International Space Station. In: Proc. of the 2nd Italian Semantic Web Workshop: Semantic Web Applications and Perspectives, Trento, Italy (2005)
2. Amilcare.: (2002) Available at http://nlp.shef.ac.uk/amilcare/amilcare.html
3. Annotea.: (2001) Available at http://www.w3.org/2001/Annotea/
4. Benjamins, V.R., Contreras, J., Corcho, O., Gomez-Perez, A.: Six Challenges for the Semantic Web. In: Proc. of the KR2002 Workshop on Semantic Web, Toulouse, France (2002)
5. Chang, Y.H.: Development and Applications of Semantic Webs. Master Thesis, Dept. of Computer Science and Information Engineering, National Taiwan University of Science and Technology, Taipei, Taiwan (2003)
6. Fensel, D., Hendler, J., Lieberman, H., Wahlster, W.: Creating of Semantic Web. Available at http://informatik.uibk.ac.at/users/c70385/ftp/paper/mit.introduction.pdf (2000)
7. Handschuh, S., Staab, S., Ciravegna, F.: S-CREAM: Semi-automatic CREAtion of Metadata. In: The 13th International Conference on Knowledge Engineering and Knowledge Management, Siguenza, Spain, pp. 358–372 (2002)
8. IBM Intelligent Miner for Text (1998) Available at http://www.searchtools.com/tools/ibm-imt.html
9. Kiyavitskaya, N., Zeni, N., Cordy, J.R., Mich, L., Mylopoulos, J.: Semi-Automatic Semantic Annotation for Web Documents. In: Proc. of the 2nd Italian Semantic Web Workshop, Trento, Italy (2005)
10. Lee, C.Y., Soo, V.W.: The Conflict Detection and Resolution in Knowledge Merging for Image Annotation. Information Processing and Management 42(4), 1030–1055 (2006)
11. Lee, T.B., Hendler, J., Lassila, O.: The Semantic Web. Scientific American 284(5), 35–43 (2001)

12. Lerman, K., Getoor, L., Minton, S., Knoblock, C.: Using the Structure of the Web Sites for Automatic Segmentation of Tables. In: Proc. of the 2004 ACM SIGMOD International Conference on Management of Data, Paris, France, pp. 119–130 (2004)
13. Noy, N.F., Sintek, M., Decker, S., Crubezy, M., Fergerson, R.W., Musen, M.A.: Creating Semantic Web Contents with Protégé-2000. IEEE Intelligent Systems 16(2), 60–71 (2001)
14. OntoMat.: Available at http://annotation.semanticweb.org/tools/ontomat (2003)
15. Salton, G., Wong, A., Yang, C.S.: A Vector Space Model for Automatic Indexing. Communications of the ACM 18(11), 97–107 (1975)
16. Sereno, B., Shum, S.B., Motta, E.: Semi-Automatic Annotation of Contested Knowledge on the World Wide Web. In: Proc. of the 2004 International World Wide Web Conference, New York, USA, pp. 276–277 (2004)
17. SHOE.: (2000) Available at http://www.cs.umd.edu/projects/plus/SHOE/KnowledgeAnnotator.html
18. Stollberg, M., Thomas, S.: Integrating Agents, Ontologies, and Semantic Web Services for Collaboration on the Semantic Web. In: Proc. 2005 AAAI Fall Symposium Series on Agents and the Semantic Web, Arlington, Virginia, USA (2005)
19. Tufis, D., Mason, O.: Tagging Romanian Texts: a Case Study for QTAG, a Language Independent Probabilistic Tagger. In: Proc. of the 1st International Conference on Language Resources & Evaluation, Granada, Spain, pp. 589–596 (1998)
20. Uschold, M., Gruninger, M.: Ontologies: Principles, Methods and Applications. The Knowledge Engineering Review 11(2), 93–136 (1996)
21. WordNet 2.1.: Available at http://wordnet.princeton.edu/ (2005)

Development and Evaluation of an Intelligent Colour Planning Support System for Townscapes

Yuichiro Kinoshita[1], Eric W. Cooper[2], and Katsuari Kamei[1]

[1] Department of Human and Computer Intelligence,
Ritsumeikan University, Kusatsu, Shiga 525-8577, Japan
kino@spice.ci.ritsumei.ac.jp, kamei@ci.ritsumei.ac.jp
[2] Department of Computer Science,
Ritsumeikan University, Kusatsu, Shiga 525-8577, Japan
cooper@is.ritsumei.ac.jp

Abstract. Aesthetics of townscapes have been a main factor in urban development. This paper introduces *IroKage*, an intelligent colour planning support system. The system offers improved colour schemes for existing townscapes based on three elements: colour harmony, impressions of the townscape, and cost for the change of colours. The system is constructed using an evolutionary algorithm and the *Kansei* engineering approach. After the construction, system evaluation is conducted. The subjects evaluate fifteen colour schemes output from the system in terms of colour harmony and the ideal impressions for the townscapes using the semantic differential method introduced by Osgood et al. The results of the evaluation demonstrate that the system has sufficient ability to propose appropriate colour schemes for the ideal town impressions.

1 Introduction

The problem of how to live in a comfortable environment has attracted attention with the changing expectation of residents, and the townscape is a central factor in urban-development problems. Aesthetics of townscapes have been studied in various fields [1, 2], and the colour scheme of the buildings is one of the most influential factors. In considering colours of the buildings, each nearby colour in the row is a key point. Proper evaluation of colours has to consider the whole street, not only individual buildings. Several colour studies have been reported as colour harmony principles [3]. Using one of those principles may enable evaluation of the colours in the whole street and allow a better colour scheme for the townscape to be found. However, characteristics of the target town also need to be respected throughout the colour planning process. In addition to the form and material of the buildings in the town, the climate and the historical background of the town are also elements affecting the characteristics, and these elements evoke particular impressions as well. Although several previous colour plans have included characteristics and impressions of towns, most of them have been based on anecdotal reports or experience and have been conducted for individual localities.

H.G. Okuno and M. Ali (Eds.): IEA/AIE 2007, LNAI 4570, pp. 1169–1179, 2007.

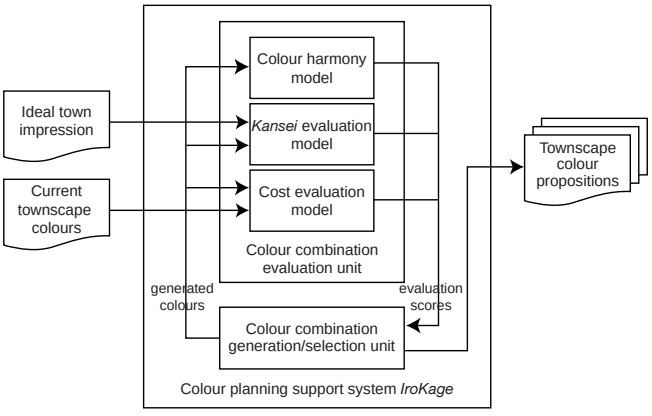

Fig. 1. Block diagram of the colour planning support system

In our studies, an intelligent colour planning support system for townscapes, called *IroKage*, was developed [4]. The system helps to improve existing townscapes by considering colour harmony as well as the town impressions. This paper focuses on the system evaluation based on townscape colour schemes output from the system.

2 System Overview

The inputs to the colour planning support system are the current townscape colours and ideal town impressions expressed by adjectives. The system offers several colour propositions for the townscape, as shown in Fig. 1. In the system, the colour combination generation/selection unit generates a large number of colour combinations. The colour combination evaluation unit evaluates the colour combinations generated from the generation/selection unit one by one.

First, the colour combination generated is evaluated from the approach of colour harmony. Moon and Spencer brought together the concepts in previous colour harmony principles and proposed equations to calculate aesthetic measure for colour harmony [5–7]. We expanded their aesthetic measure for townscape colours and constructed a colour harmony model [4] using Takagi-Sugeno type fuzzy reasoning [8]. The inputs to the model are townscape colours and the output is the aesthetic measure.

In addition to colour harmony, impressions of the generated colour combination are evaluated in respect of their suitability when compared to the ideal impressions of the townscape. The differences between the ideal impressions of the townscape and the psychological response for the generated colour combination is calculated. The combination having the smallest difference is evaluated as the appropriate combination. Handling the impressions of the townscape requires quantification of psychological responses. A *Kansei* evaluation model to quantify the human responses is constructed by linking town impressions and

townscape colours [9]. *Kansei* is a Japanese term which means human sensibility or impression.

The targets of this system are mostly townscapes that already exist. A critical issue is finding the most effective colour scheme changes at the lowest cost. The cost evaluation model calculates the cost to convert the current townscape colours to the generated colours. In terms of the colour changing cost, the repaint cost is assumed to be almost the same even if the new colour is similar to the original colour. The number of colour changes is therefore simply applied for the cost evaluation.

Based on scores obtained by the evaluation unit, the generation/selection unit selects several colour propositions for the output of the system.

3 Quantification of Town Impressions

3.1 Evaluation Experiments of Town Impressions

In order to manage town impressions in the system, psychological responses to townscape colours are quantified from the *Kansei* engineering approach [10]. This technique translates target psychological responses into perceptual design elements.

First, evaluation experiments were conducted to investigate the relationship between town impressions and townscape colours. Adjectives allow expression of the psychological responses. In this study, adjectives express the impressions of the townscape. Approximately 470 adjectives related to the town impressions were collected from dictionaries and previous studies. After the collection, similar adjectives were combined and they were paired with opposite meanings. Finally, the number of adjectives was reduced to sixteen pairs. One hundred colour picture samples were prepared for the evaluation experiments. The pictures show the front side of a row of houses. The samples were made by altering the same picture while maintaining all the other conditions. The wall and roof colours of the houses were selected from a wide variety of chromatic and achromatic colours, and the window frame colours were selected from a set of achromatic colours.

Computer-based evaluation experiments were conducted for 20 subjects, four females and sixteen males, using the semantic differential (SD) method [11]. One picture sample and the sixteen adjective pairs are placed on the computer screen. In the experiments, the subjects select a suitable response on the five-step SD scale for each pair of adjectives. The subjects evaluated all of the 100 picture samples, which were shown at random.

3.2 Selection of Adjectives

After the experiments, appropriate adjectives were selected based on the results of the above experiments. An evaluation in the centre of the SD scale implies that the adjective was evaluated as neutral. The adjectives with many neutral evaluations may be irrelevant for expressing town impressions. Four adjectives

Table 1. Pairs of adjectives related to townscape impressions

adjective No.	adjectives
1	cold – warm
2	unrefined – refined
3	restless – calm
4	unfriendly – friendly
5	uncomfortable – comfortable
6	artificial – natural
7	typical – individualistic
8	conservative – progressive
9	quiet – lively
10	old-fashioned – modern
11	awkward – elegant
12	western – eastern

were excluded for this reason. Variance of evaluation scores is also a factor to be considered. We checked the variance for each sample but every pair of adjectives showed low variance. No adjective was excluded in this process. Consequently, the twelve adjectives shown in Table 1 were selected.

3.3 Construction of *Kansei* Evaluation Model

With the selected adjectives, a *Kansei* evaluation model is constructed. The behaviour of *Kansei* response is usually non-linear and it is difficult to manage *Kansei* data using conventional methods. Some previous studies adopted neural networks for *Kansei* data [12, 13]. Neural networks are one of the best methods for modelling non-linear data. The model was constructed using a neural network for each pair of adjectives. Sixty-two experimental results were selected as the training data for the neural networks and 20 results were selected as the testing data for the model validation. Both training and testing data were selected to consist of various, dissimilar colour combinations. Each colour in the data was selected to have unique hue, brightness or saturation attributes.

The input items to each neural network are the wall colours, roof colours, and window frame colours of the houses in the picture samples. Every colour is expressed in the CIELAB colour system [14]. The three CIELAB values, L^*, a^* and b^*, are used for the wall colours and roof colours, and only L^* is used for the window frame colours because the use of chromatic colours is generally limited. Since there are three buildings in the sample picture, the input data becomes 21 values. The output from each neural network is the SD scale response for the town impression. Every value is given in [0, 1]. Each neural network has three layers and the numbers of units are 21, 30, and 1 on the input, hidden, and output layers, respectively. Every network was trained using back-propagation learning to an accuracy of 3.125×10^{-4} mean square error, which is equivalent to 0.1 on the SD scale of 1 to 5.

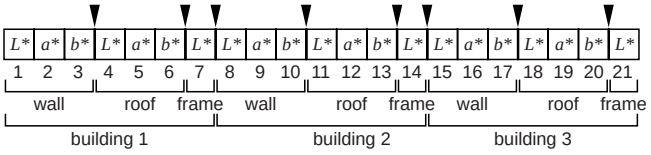

Fig. 2. Encoding of individuals. Black arrows represent candidate crossover points.

3.4 Performance Test

After the model construction, a performance test was conducted. The 20 testing data were input into the constructed model, and the errors between the output from the model and the average of the experimental results were calculated. The average accuracy of the twelve neural networks was 7.321×10^{-3} mean square error, 0.374 on the SD scale of 1 to 5. This result indicates that our *Kansei* model has adequate ability to evaluate the town impressions.

4 Townscape Colour Generation and Selection

4.1 Approach

For the implementation of the colour combination generation/selection unit in the system, the problem is the method to select appropriate combinations under the evaluation scores with the three different objectives: colour harmony, impression and cost. For selecting appropriate colour combinations to output from the system, we focuse on Pareto optimal solutions.

In a maximization problem, a is said to *dominate* b when

$$f_e(a) \geq f_e(b) \quad (\forall e \in \{1, 2, \ldots, n\},\ a \neq b) \tag{1}$$

where f_e represents a vector function, and a and b represent two decision vectors. The decision vectors that are not *dominated* by any other vector are called Pareto optimal solutions. In this study, those solutions are searched from an evolutionary algorithm approach [15].

4.2 Encoding

The system uses wall, roof and window frame colours of three buildings, nine colours in total. In the evolutionary algorithm, the colours are expressed in the CIELAB colour system and encoded by value encoding. Each wall colour and roof colour consists of the three CIELAB values, L^*, a^* and b^*. Each window frame colour consists of L^* value only. Seven values therefore express the colour scheme of one building. In total, one individual includes 21 values, as shown in Fig. 2. Every L^* value is given in [10, 90] while a^* and b^* values are given in [-40, 40].

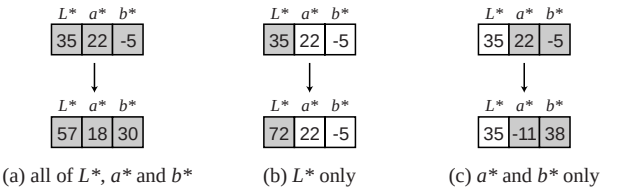

Fig. 3. Wall colour alteration patterns in the initialization and mutation processes. Pattern (a) alters all attributes of the target colour while pattern (b) only alters the lightness attribute. Pattern (c) alters the hue and saturation attributes.

Table 2. Candidate roof colours

colour	L^*	a^*	b^*
grey	45	0	0
brown	35	20	25
green	30	−15	10
red	45	40	25
blue	45	0	−35

Fig. 4. Configuration of the townscape samples

4.3 Colour Search Algorithm

The generation/selection unit generates the population of the first generation by altering several colours in the current townscape input. First, up to three colours are chosen as the target(s) for alteration. When a wall colour is chosen as the alteration target, one of the three alteration patterns shown in Fig. 3 is randomly applied. When a roof colour is chosen as the target, the colour is randomly replaced with one of the five candidate roof colours shown in Table 2. For a window frame colour, the target L^* value is randomly replaced with either '10' or '90.'

The individuals generated are evaluated based on the three evaluation models. Based on the evaluation scores, individuals are selected as the parents of the next generation. For the selected parents, single point crossover is executed at one of the eight crossover points shown in Fig. 2. After that, each of nine colours in an individual mutates with a given probability. The target colours are altered in the same manner as the initialization processes. Finally, those individuals will be the population of the next generation.

The system stores all individuals through all generations and selects the highest-ranking individuals for output.

5 System Evaluation

5.1 Townscape Colour Development

Townscape colour development is conducted using our system, *IroKage*. Three townscape samples are prepared as the targets of the colour development. Every

Table 3. Colours in the townscape samples

sample No.	building No.	wall			roof			frame
		L^*	a^*	b^*	L^*	a^*	b^*	L^*
1	1	80	0	−10	45	0	0	10
	2	50	20	−20	45	0	0	90
	3	80	0	15	30	−15	10	10
2	1	80	−10	−10	45	0	0	90
	2	45	0	0	45	0	0	90
	3	30	0	−20	45	0	0	90
3	1	80	0	0	45	0	0	10
	2	75	20	20	45	0	0	90
	3	65	0	0	45	0	0	90

Table 4. Parameters for the evolutionary algorithm

population size	100
crossover probability	0.9
mutation probability	0.03
number of generations	300

sample consists of three buildings in a row. Fig. 4 shows the configuration of the samples and Table 3 shows colours in the samples. Here, *natural*, *warm* and *lively* are selected as the ideal impressions for Samples 1, 2 and 3, respectively. The system searches for Pareto optimal solutions using the evolutionary algorithm with the parameters shown in Table 4.

Tables 5, 6 and 7 show examples of the system output for Samples 1, 2 and 3, respectively. The bold face numbers in the tables indicate modified colours. For Sample 1, the system modified the wall colour of Building 1, light blue, and/or the wall colour of Building 2, purple, in most cases. Those colours were replaced with brownish, greenish and yellowish colours. For Sample 2, the system output warm colours, yellowish and reddish colours. These match to the ideal impression *warm*. For Sample 3, the system mainly output colour schemes with high saturation and high lightness colours.

5.2 Evaluation Methods

In order to make sure that the system output is appropriate, evaluation experiments are conducted. The participants of the experiments evaluate colour schemes output from the system in respect of colour harmony and the ideal impressions using the SD method. As the targets of evaluation, a set of samples is prepared. The sample set consists of fifteen samples repainted in the output colour schemes shown in Tables 5, 6 and 7 and three original colour schemes shown in Table 3. However, the participants are not informed that the sample set includes the original colour schemes. For the evaluation of colour harmony, a pair of adjectives, disharmonious—harmonious, is used. For the evaluation of impression, one pair of adjectives is selected from Table 1 depending on the ideal impressions (e.g., artificial—natural for Sample 1). In total, the participants therefore evaluate eighteen samples with the two pairs of adjectives.

The experiments were conducted in a computer-based environment. The participants sit 70 cm away from a CRT display. The participants sit 70cm away from a CRT display. Fig. 5 shows the screen appearance of the experiments. One of the samples is placed at the centre of the screen with a black background, and one pair of adjectives is placed on the lower part. There is a five-step scale

Table 5. System output examples for Sample 1 with the ideal impression *natural*

result No.	building No.	wall			roof			frame
		L^*	a^*	b^*	L^*	a^*	b^*	L^*
1A	1	80	0	−10	45	0	0	10
	2	50	**4**	**30**	45	0	0	90
	3	80	0	15	30	−15	10	10
1B	1	80	0	−10	45	0	0	10
	2	**39**	**16**	**13**	**30**	**−15**	**10**	90
	3	80	0	15	30	−15	10	10
1C	1	80	**−12**	**13**	45	0	0	10
	2	50	**−1**	**15**	45	0	0	**10**
	3	80	0	15	**45**	**0**	**0**	10
1D	1	80	0	−10	45	0	0	10
	2	**40**	**−9**	**27**	45	0	0	90
	3	80	0	15	**45**	**0**	**0**	10
1E	1	**62**	**1**	**37**	45	0	0	10
	2	**46**	**11**	**30**	45	0	0	90
	3	80	0	15	30	−15	10	10

Table 6. System output examples for Sample 2 with the ideal impression *warm*

result No.	building No.	wall			roof			frame
		L^*	a^*	b^*	L^*	a^*	b^*	L^*
2A	1	80	**13**	**15**	45	0	0	90
	2	45	0	0	45	0	0	90
	3	30	0	−20	45	0	0	90
2B	1	**81**	**1**	**19**	45	0	0	90
	2	45	0	0	45	0	0	90
	3	**67**	**7**	**27**	45	0	0	90
2C	1	80	**8**	**16**	45	0	0	90
	2	**68**	**15**	**30**	45	0	0	90
	3	30	0	−20	45	0	0	90
2D	1	**86**	**2**	**2**	45	0	0	90
	2	45	0	0	45	0	0	90
	3	**67**	**23**	**24**	45	0	0	90
2E	1	**78**	**11**	**22**	45	0	0	90
	2	45	**19**	**19**	**35**	**20**	**25**	90
	3	**68**	**15**	**28**	45	0	0	90

between the adjectives and one value is highlighted as the current selection. The participants move the selection and choose a suitable response using arrow and space keys on a keyboard. The samples and adjectives are shown in random sequence to reduce influence from the order of the presentation.

5.3 Results and Discussion

The experiments were conducted for seventeen participants, fourteen males and three females. Figs. 6, 7 and 8 show the average evaluation scores of the experiments for Samples 1, 2 and 3, respectively.

Table 7. System output examples for Sample 3 with the ideal impression *lively*

result No.	building No.	wall			roof			frame
		L^*	a^*	b^*	L^*	a^*	b^*	L^*
3A	1	**87**	**10**	**−7**	45	0	0	**90**
	2	75	20	20	45	0	0	90
	3	65	**−33**	**12**	45	0	0	90
3B	1	80	0	0	45	0	0	**90**
	2	75	20	20	45	0	0	90
	3	65	**−33**	**2**	45	0	0	90
3C	1	80	0	0	45	0	0	10
	2	75	20	20	45	0	0	90
	3	65	**11**	**34**	45	0	0	90
3D	1	80	0	0	45	0	0	10
	2	**34**	**22**	**−12**	45	0	0	90
	3	**71**	**8**	**29**	45	0	0	90
3E	1	80	0	0	45	0	0	**90**
	2	**74**	**−23**	**−17**	**45**	**0**	**−35**	90
	3	**42**	**−32**	**−4**	45	0	0	90

In Fig. 6, Sample 1, with the original colour scheme, was evaluated as 1.88 for colour harmony (standard deviation 1.05) and 1.35 for the *natural* impression (standard deviation 0.49). Those scores indicate that the sample had poor colour harmony and no ideal impression. This kind of townscape is the main target of our system. Compared to the original sample, all the results output from the system, 1A–1E, achieved good evaluation scores for both colour harmony and the *natural* impression. Especially, Result 1E was evaluated as 4.12 for colour harmony (standard deviation 0.78) and 3.71 for the *natural* impression (standard

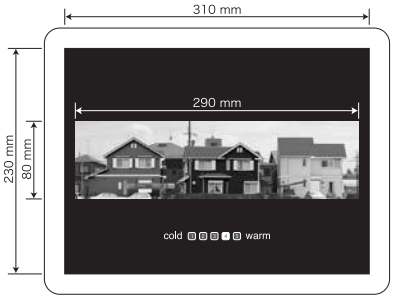

Fig. 5. Screen appearance of the experiments

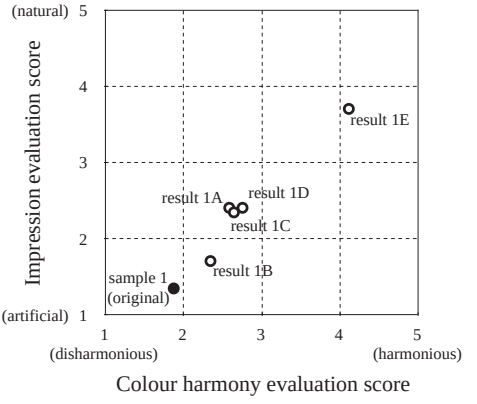

Fig. 6. Evaluation results for Sample 1

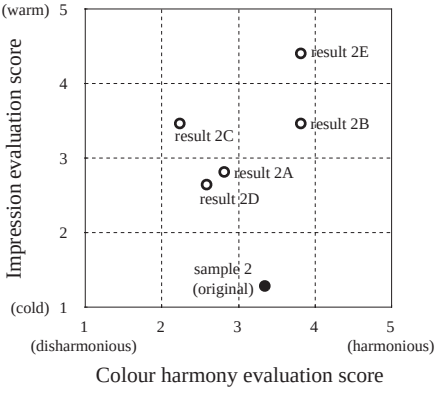

Fig. 7. Evaluation results for Sample 2

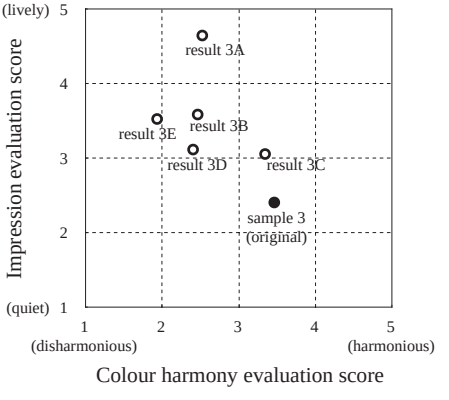

Fig. 8. Evaluation results for Sample 3

deviation 1.05) with the two colour changes. The system successfully improved colour harmony and realized the ideal impression.

In Fig. 7, Sample 2 was evaluated as 3.35 for colour harmony (standard deviation 1.27) and 1.29 for the *warm* impression (standard deviation 0.47). It represents that the original sample already had good colour harmony. Although this kind of townscape is not the target of our system, the results from the system, 2A–2E, showed high scores for the *warm* impression. Not only for the impression, Results 2B and 2E even achieved better colour harmony. The colour harmony score for Result 2E was 3.82 (standard deviation 1.01) while the impression evaluation score was 4.41 (standard deviation 0.62). For some results, colour harmony scores were somewhat decreased. However, the decreases were not significant compared to the improvements in the *warm* impression.

Like Sample 2, Sample 3 also had good colour harmony but did not have enough *lively* impression. For this sample, colour harmony score was getting decreased concurrently with increasing of the impression score. Here, the

relationship between colour harmony and the *lively* impression can be considered a *trade-off* where it is difficult to improve the two objectives at the same time. In this case, the system is expected to output the optimal colour schemes with variety. The output from the system included *lively* impression samples, such as Result 3A as well as harmonious samples, such as Result 3C, as shown in Fig. 8. The use of the evolutionary algorithm helped to obtain a variety of results as Pareto optimal solutions.

6 Conclusions

In this paper, the intelligent colour planning support system for townscape, *IroKage*, was introduced. The system was constructed using an evolutionary algorithm with colour harmony, impression and cost evaluations. The evaluation of *IroKage* demonstrated that the system has sufficient ability to improve colour harmony and realize ideal impressions. The system successfully proposed appropriate colour schemes.

References

1. Lynch, K.: The Image of the City. MIT Press, Cambridge, MA (1960)
2. Nasar, J.L.: The Evaluative Image of the City. Sage Publications, Thousand Oaks, CA (1998)
3. Judd, D.B., Wyszecki, G.: Color in Business, Science and Industry. Wiley, New York, NY (1975)
4. Kinoshita, Y., Sakakura, Y., Cooper, E.W., Hoshino, Y., Kamei, K.: Townscape colour planning system using an evolutionary algorithm and Kansei evaluations. In: Proc. IEEE Int. Conf. Fuzzy Syst. pp. 931–938 (2006)
5. Moon, P., Spencer, D.E.: Geometric formulation of classical color harmony. J. Opt. Soc. Am. 34(1), 46–59 (1944)
6. Moon, P., Spencer, D.E.: Area in color harmony. J. Opt. Soc. Am. 34(2), 93–103 (1944)
7. Moon, P., Spencer, D.E.: Aesthetic measure applied to color harmony. J. Opt. Soc. Am. 34(4), 234–242 (1944)
8. Takagi, T., Sugeno, M.: Fuzzy identification of systems and its applications to modeling and control. IEEE Trans. Syst., Man, Cybern. 15(1), 116–132 (1985)
9. Kinoshita, Y., Cooper, E.W., Hoshino, Y., Kamei, K.: Kansei and colour harmony models for townscape evaluation. Proc. Inst. Mech. Eng., I J. Syst. Control Eng. 220(8), 725–734 (2006)
10. Nagamachi, M.: Kansei Engineering: A new ergonomic consumer-oriented technology for product development. Int. J. Ind. Ergonomics 15(1), 3–11 (1995)
11. Osgood, C.E., Suci, G.J., Tannenbaum, P.H.: The Measurement of Meaning, University of Illinois Press, Urbana, IL (1957)
12. Hsiao, S.W., Huang, H.C.: A neural network based approach for product form design. Design Studies 23(1), 67–84 (2002)

13. Kosaka, H., Watanabe, K.: A Kansei product design system using neural network. Kansei Engineering International 3(4), 31–36 (2003)
14. Agoston, G.A.: Color Theory and Its Application in Art and Design. Springer, Berlin (1987)
15. Coello Coello, C.A.: An updated survey of GA-based multiobjective optimization techniques. ACM Comput. Surv. 32(2), 109–143 (2000)

A Testing Device for the Human Ability to Utilise Beneficial Environmental Features

Blagovest Vladimirov, Hiromi Mochiyama, and Hideo Fujimoto

Nagoya Institute of Technology, Nagoya, Japan
vesko@vier.mech.nitech.ac.jp

Abstract. In this paper, we propose a device for testing the human ability to utilise, even unconsciously, beneficial environmental features. An important characteristic of the proposed testing device is that additional stimuli, correlated to the correct task outcome, are introduced during the test without informing the subject. The device tests whether the subject will notice the subtly provided stimuli and use them, consciously or not, to improve the task performance. The use of these additional stimuli is confirmed by observing a sudden drop in the subject's performance (slump-like effect) when the additional stimuli are reversed, i.e., correlate to the wrong task outcome. We present several facts suggesting that the ability tested by the proposed device supports the human skill acquisition. An illustrative example of a specific implementation of the proposed device, based on a visual alternative choice task with additional audio stimuli, is presented to explain the testing process.

1 Introduction

Many high-quality products and services rely on the availability of skilled professionals. The competitiveness and the success of product or service companies depend on the ability to find skilled employees, emphasising the need of better understanding and reliable assessment of the desired employee characteristics.

The purpose of this research is to develop a device for testing human skill acquisition potential (Fig. 1). Such device could help identifying prospective employees.

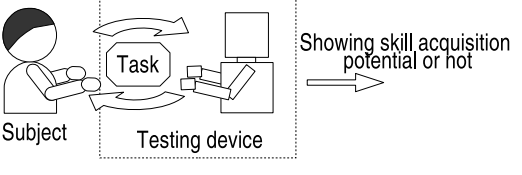

Fig. 1. A testing device for identifying subjects that show skill acquisition potential

In practice, general personality aspects of potential employees have been assessed with various tests like Synthetic Personality Inventory (SPI)[1], etc. In

[1] http://www.recruit-ms.co.jp

H.G. Okuno and M. Ali (Eds.): IEA/AIE 2007, LNAI 4570, pp. 1180–1189, 2007.

addition to general cognitive abilities, Ackerman [1] investigated also the relation between perceptual speed and psycho-motor abilities, and performance in Air Traffic Control task, which is representative of the class of short term skill acquisition tasks. However, compared to the general abilities mentioned above, abilities that are more closely related to the skill acquisition process itself have not received enough attention. In this paper, we propose a device for testing the human ability to utilise, even unconsciously, task relevant, beneficial environmental features for performance improvement.

A specific implementation of the proposed device is presented in the next section, together with an example illustrating the testing process. A discussion of the idea behind the proposed device and its relation to the human skill acquisition process follows in the third section. The last section concludes with comments on the current results and directions for further development.

2 Testing Device and Illustrative Example

Here, we describe a specific implementation of the proposed testing device based on an alternative choice task, and present an illustrative example of the test. First, the device and the task are described as seen from the tested subject's point of view. Then, follows an explanation of the behind-the-scene part that shows the actual idea of the test. Finally, we give an example illustrating the testing process and interpretation of the results.

2.1 Device and Task from the Subject's Point of View

Device. Figure 2a shows the configuration of the proposed device as seen by the tested subject. The device consists of a computer with a program implementation of an alternative choice task, a visual display (monitor) and a keyboard.

Task. The task to be performed is Bounce-or-not task, in which one of two possible motion patterns is presented on the visual display. The subject is asked to guess which pattern was shown and to reply with a key-press.

The two possible motion patterns, *Bouncing* and *Not Bouncing*, are shown in the left part of Fig. 2b. Each motion pattern is illustrated with drawings showing the positions of the moving objects.

In the top row, at time t_0, two discs are shown in the upper corners of the screen. Then, these two discs move at the same speed along the diagonal lines toward the opposite corners. The numbers and arrows are added here only to illustrate the discs' trajectories, and are not shown to the subject. In the middle row, at time t_c, the discs overlap at the centre of the screen. In the bottom row, at time t_f, the final positions of the discs are different for the two motion patterns. In the *Bouncing* pattern, after bouncing off one another at time t_c, the discs end in the corners on the same side of the screen as their initial positions. In the *Not Bouncing* pattern, the discs stream through at time t_c and end in the corners on the opposite side of the screen.

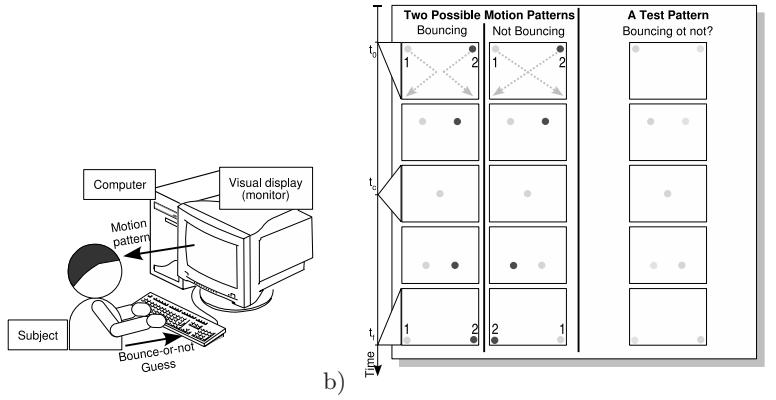

Fig. 2. a) The testing device, as seen by the subject, is a computer implementation of an alternative choice task. The subject has to recognise the motion pattern presented on the video display and to respond with a key-press. b) Explanation of the Bounce-or-not task, given to the subject. The two possible motion patterns, shown on the left, are *Bouncing* and *Not Bouncing*. A typical test pattern uses similar colours for the discs, as shown on the right. The task is to recognise whether the discs in the test patterns have bounced or not.

The two discs are displayed in colour. When the difference between the discs' colours is large, as shown in the two patterns on the left in Fig. 2b, distinguishing bouncing from not bouncing is easy. The actual patterns presented in the test, as the one illustrated on the right in Fig. 2b, use small distance between the disc's colours, making the task much more challenging.

Procedure. During the test, randomly selected motion patterns are presented in a sequence and the subject is asked to guess correctly as many as possible. At the end of each sequence, the proportion of correct answers is calculated and shown to the subject.

2.2 Behind-the-Scene Part of the Device and the Task

Device. Figure 3a shows the full configuration of the testing device. This configuration includes an audio display (speakers) that is placed away from the subject's view. The subject is not informed about the speakers and their role in the test.

Task. The Bounce-or-not task also contains details that are hidden from the subject. As shown in Fig. 3b, besides the motion patterns presented on the display, for some patterns a barely audible beep sound is introduced at time t_c without informing the subject. Thus, task relevant information is communicated to the subject in two ways: openly and subtly. The openly provided information is presented through the visual display, and the subtly introduced information is presented through the audio display.

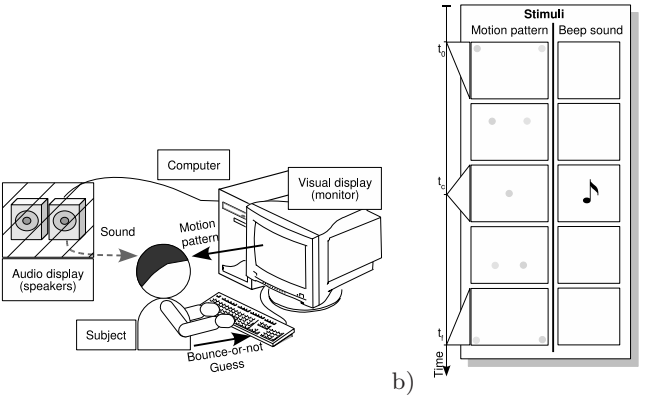

Fig. 3. a) An audio display, placed away from the subject's view, is added to the testing device. b) In some trials, an additional beep sound is introduced to the Bounce-or-not task at time t_c.

Procedure. The actual idea is to test whether or not the subject will notice the subtly introduced beep sound among the various other background stimuli coming from the environment and utilise it to improve the task performance.

Initially, the subject is tested only on motion patterns, without using the beep sound, until the task performance is stabilised, i.e., three consecutive performance measurements are within certain small interval. Then, without informing the subject, a beep sound is added only when the discs bounce and again the test continue until the performance is stabilised.

In the testing device, a t-test is used to compare these two task performances. A statistically significant improvement of the performance after adding the sound leads to the assumption that the subject has used the additional sound information. To confirm this assumption, again without informing the subject, the test continues with a beep sound only when the discs stream through. If this results in significantly below chance level task performance, then the assumption that the subject has used the beep sound information is correct. In this case, the testing device *accepts* the subject, i.e., classifies the subject as having shown ability to utilise beneficial environmental features without being explicitly instructed to do so. Such subject is considered as having skill acquisition potential.

On the other hand, if the subject's performance doesn't improve after adding a beep sound when the discs bounce, the conclusion is only that the subject didn't show the above ability and not that the subject doesn't possess it. In this case, the testing device *rejects* the subject.

2.3 Illustrative Example

Test Parameters. The colour of the disc starting from the top right corner was held constant yellow with RGB value of (255/255/0). The colour of the other disc was varied between RGB (250/250/0) and RGB (210/210/0) by

changing the red and green components in steps of 10, obtaining five levels of task difficulty. The colour distances corresponding to each difficulty level were $d = (0.02, 0.06, 0.1, 0.14, 0.18)$ after normalisation. The significance level of the t-test was set to $P = 0.01$.

One female and two male subjects in their early 20's participated in the test. The tested subjects were instructed to watch the displayed motion patterns and to answer with a key-press whether the discs had bounced or not.

The test consisted of several sessions, each one having 10 blocks of trials. In one block, 60 or 30 trials were performed sequentially, with one trial consisting of displaying a motion pattern and receiving an answer. In each block of trials, the task difficulty was held constant. Each session started with the minimum task difficulty level, gradually increasing it to the maximum level, and decreasing it again to the minimum. The proportion of correct answers was calculated for each block of trials and was shown to the subject at the end of the block.

Test Results. Figure 4 shows the task performance of the subject that was accepted by the testing device. The three lines in the graph represent the proportion of correct answers in the three cases of the task: when no beep sound is used (*no sound*), with beep sound only when the discs bounce (*with sound*), and with beep sound only when the discs stream through (*reversed sound*). The points show the mean value of the proportion of correct answers and the bars show the standard deviation. The horizontal axis shows the distance d between the colours of the two discs, which corresponds to the task easiness.

Compared to the case without sound, in the case in which similarly to the physical phenomenon there is a beep sound when the discs bounce, the proportion of correct answers significantly ($P < 0.01$) increased. This suggests that the subject has used the beep sound information even though it was not explicitly mentioned in the task instructions and was introduced without informing the subject. In other words, this is an example of the skill related ability to utilise beneficial environmental features to improve the task performance.

In the case in which there is a beep sound only when the discs stream through, for the most difficult level $d = 0.02$, the proportion of correct answers is significantly ($P < 0.003$) below the chance level. This result confirms that the performance improvement in the previous case is due to the beep sound information.

The test settings are such that if the subject consciously perceives the sound and relies on it, the maximum proportion of correct answers can be achieved. But from Fig 4 we can see that the subject's performance in the *no sound* case is not the maximum possible. This and the observed below chance-level performance suggest that the beep sound information may have been used at a level below the conscious experience.

Figure 5 shows the task performance of the subjects that were rejected by the testing device. For these two subjects, there are no significant differences between the proportion of correct answers in the two cases: *no sound* and *with sound*. Also, there was no significant decrease of the task performance in the *reversed sound* case. These results suggest that the subjects didn't use the beep sound information in their decisions.

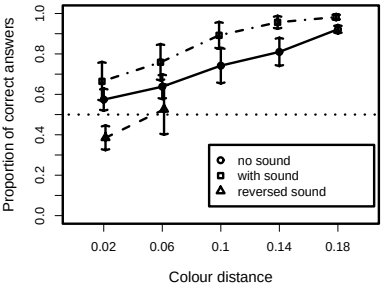

Fig. 4. Task performance of the subject that passed the test successfully, i.e, was accepted by the testing device

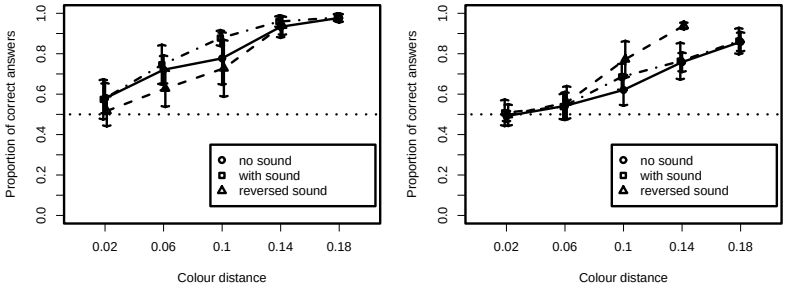

Fig. 5. Task performance of the subjects that failed the test, i.e, were rejected by the testing device

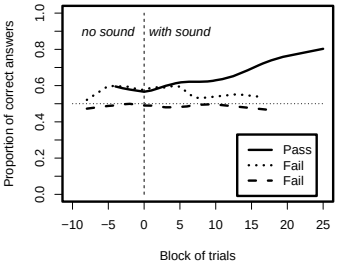

Fig. 6. Performance of the accepted (pass) and the rejected (fail) subjects in the *no sound* and *with sound* cases for colour distance $d = 0.02$

We can see from Fig. 4 and Fig. 5 that one of the rejected subjects has shown similar performance level to that of the accepted subject for colour distance $d >= 0.06$ in the *with sound* case. If the testing device relied only on the absolute task performance, both subjects should have been accepted. But since we are interested in the subject's skill acquisition ability, the testing device is based on detecting specific improvements of the task performance. Thus, to be

accepted by the testing device, the subject has to show significant improvement of the performance in the *with sound* case compared to *no sound* case, i.e., to show ability to utilise beneficial environmental features to improve the task performance without being instructed to do so.

Figure 6 gives another view of the subjects' performance in the *no sound* and *with sound* cases for colour distance $d = 0.02$. The horizontal axis shows the number of block of trials and the vertical axis shows the proportion of correct answers in the corresponding block. We can see an improvement of the accepted subject's performance starting after 10 block of trials, while the performance of the rejected subjects doesn't improve. The accepted subject was able to utilise the additional sound information to overcome the initial asymptotic task performance.

2.4 Generalised Form of the Device

The device implementation presented above was based on Bounce-or-not task and used visual and audio stimuli. Other implementations can be obtained using different tasks and different stimuli, providing that the following essential characteristics of the device and the task are retained.

Generally, the device serves as an interface through which the subject performs a given task. There are two or more task relevant stimuli that are necessary to achieve good performance. In its role as an interface, the device gives us control over the relevant stimuli that are presented to the subject. We should be able to control which stimuli are presented and their intensity level. The device, also, computes appropriate task performance based on the presented stimuli to the subject and the subject's response.

Using the device, we prepare three test cases: *normal*, *enhanced* and *reversed*. In the *normal* task case, only a part of the relevant stimuli are presented to the subject. In the *enhanced* task case we add in a subtle manner some or all of the task stimuli that were held out in the *normal* case. In the *reversed* task case the stimuli added in the *enhanced* case are reversed so that they would trigger incorrect responses to the task.

The testing procedure is similar to that in the illustrative example. At the beginning, the subject is tested with the *normal* test case until the performance stabilises. Then, without informing the subject, the test continues with the *enhanced* case. The performance in these two test cases is compared. If there is statistically significant improvement of the performance in the *enhanced* case, the test continues with the *reversed* case to confirm that the observed improvement is due to the use of additional information provided by the subtly introduced task stimuli. A drop in the performance after reversing these stimuli confirms that the subject indeed used them. Because of the observed sudden drop in the subject's performance, we call this a slump-like effect. This effect is more pronounced when the additionally introduced stimuli is used unconsciously. Finally, the device accepts a subject that is able to improve his task performance by utilising these additional stimuli.

The decision for including beep sound in the Bounce-or-not task is based on the effect of sound on visual perception discussed by Sekuler [2] and Shimojo [3].

Due to our experience with bouncing as a physical phenomenon, where bouncing is often correlated with a sound, we have already acquired the relation between sound and bouncing. This reduces the time requirements of the experiment, since the subjects don't have to learn this relation but only to notice and use, consciously or not, the subtly introduced sound information.

3 Discussion on the Idea Behind the Proposed Testing Device

This section presents a discussion on the idea behind the proposed testing device in relation to the implicit part of the skill acquisition process, a stepwise character of the performance improvement, and a general difference between humans and machines.

3.1 Implicit Learning

Children learn to speak their mother tongue without any formal understanding of its grammar. They can speak more or less correctly, as if they follow the language rules, while at the same time they are not aware of the rules themselves. This kind of knowledge and its acquisition are subjects of the research on implicit learning [4].

Similar observation can be made in the case of skilled practitioners. They perform very well on given tasks but sometimes have difficulties to state explicitly how they achieve it. This suggests that implicit learning also plays a role in the skill acquisition process. In the proposed testing device, we address an important aspect of the learning process, namely, noticing and utilising relevant information that helps to improve the task performance. Further experiments with testing device based on different tasks are considered to investigate the implicit part of the skill acquisition process.

3.2 Skill Acquisition as Stepwise Performance Improvement

Posner [5] distinguishes "cognitive", "associative", and "autonomous" phases in the skill acquisition process. In the initial "cognitive" phase, the individuals acquire understanding of the task, which information is important and which is not, what actions are appropriate, etc. In the second "associative" phase, a coherent strategy and behaviour are formed, that result in acceptable level of performance. In the third "autonomous" phase, the individuals achieve a level in which the skill performance require little or no conscious control. Usually, the initial phases are associated with major performance improvements, while at the last phase, an asymptotic performance level is achieved with little further improvements.

The Ericsson's theory of expertise [6,7,8] explains the role of deliberate practice in avoiding full automaticity and overcoming the asymptotic performance level. The deliberate practice is characterised with active attempts to go

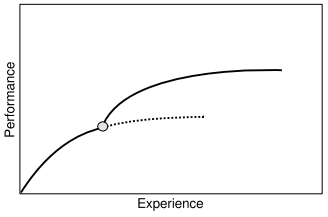

Fig. 7. Overcoming asymptotic performance

beyond the current performance level and often with the use of specific training situations. This results in refining the existent and forming new mental representations, improving the control over the task performance.

Based on the above positions, we view the skill acquisition process, as a repeating cycle of finding new or improved mental representations, adjusting the task related decisions and actions to utilise the new information, rehearse the newly created associations, and look again for another possibility for improvement. This can be illustrated with the curve in Fig. 7, showing a point of overcoming an asymptotic performance with initial accelerated performance improvement and setting for another asymptotic level. The human abilities that facilitate and maintain this process of stepwise improvements are essential for the skill acquisition. We consider individuals as having skill acquisition potential if they are able to overcome such asymptotic performance levels on their own, i.e, without being explicitly instructed how to do so.

Based on the idea that the ability to notice and utilise beneficial environmental features among the information coming through our senses is a general factor for task performance improvement, we can use the proposed testing device for testing skill acquisition potential.

3.3 Intelligence in Humans and Devices

If we consider using the proposed testing device to test robots instead of human subjects, an important advantage of humans comes to attention. This advantage is related to the frame problem [9], or more precisely to that, unlike robots, humans are able to overcome this problem. The frame problem arises from the need to be able to distinguish which information is important for achieving a given task and which is not. Even if we consider robots with learning capabilities, currently it is the humans that have to decide which sensory inputs and in what form should be fed to the learning algorithm to achieve good results in acceptable time limits. In that context, the proposed testing device doesn't attempt to overcome the frame problem but to test for human abilities that allow them to overcome that problem, in this case, the ability to find and utilise task related information that supports better performance.

4 Conclusion

In this paper we proposed a device for testing the human ability to utilise beneficial environment features for skill improvement. We presented a device implementation based on Bounce-or-not task, using combinations of visual and audio stimuli. An illustrative example of the testing process shows the device capturing successfully the ability to utilise beneficial environmental features for task performance improvement. The importance of that ability for skill acquisition suggests that the proposed device can be used for testing skill acquisition potential.

The presented device implementation gives one possibility to test for skill acquisition potential. Further experiments with adapting the generalised form of the proposed device to different tasks and sensory modalities are necessary to investigate the reliability and the feasibility for practical application. Device variants for both cognitive and motor skills are also considered.

References

1. Ackerman, P.L., Cianciolo, A.T.: Cognitive, perceptual speed, and psychomotor determinants of individual differences during skill acquisition. Journal of Experimental Psychology: Applied 6, 259–290 (2000)
2. Sekuler, R., Sekuler, A.B., Lau, R.: Sound alters visual motion perception. Nature 385, 308 (1997)
3. Watanabe, K., Shimojo, S.: When sound affects vision: Effects of auditory grouping on visual motion perception. Psychological Science 12, 109–116 (2001)
4. Cleeremans, A., Destrebecqz, A., Boyer, M.: Implicit learning: news from the front. Trends in Cognitive Sciences 2(10), 406–416 (1998)
5. Fitts, P.M., Posner, M.I.: Human performance. Brooks/Cole (1967)
6. Ericsson, K.A., Krampe, R.Th., Tesch-Römer, C.: The role of deliberate practice in the acquisition of expert performance. Psychological Review 100(3), 363–406 (1993)
7. Ericsson, K.A., Charness, N.: Expert performance: Its structure and acquisition. American Psychologist 49(8), 725–747 (1994)
8. Ericsson, K.A.: Attaining excellence through deliberate practice: Insights from the study of expert performance. In: Ferrari, M. (ed.) The pursuit of excellence in education, pp. 21–55. Erlbaum, Hillsdale, N.J (2002)
9. McCarthy, J., Hayes, P.: Some philosophical problems from the standpoint of Artificial Intelligence. In: Meltzer, B., Michie, D. (eds.) Machine Intelligence 4, pp. 463–502. Edinburgh University Press (1969)

Author Index